A THREE-COLOUR PHOTOMETRIC SURVEY OF VIRGO 'CORE' LENTICULAR GALAXIES

Gordon J. Malcolm

A Thesis Submitted for the Degree of PhD
at the
University of St Andrews

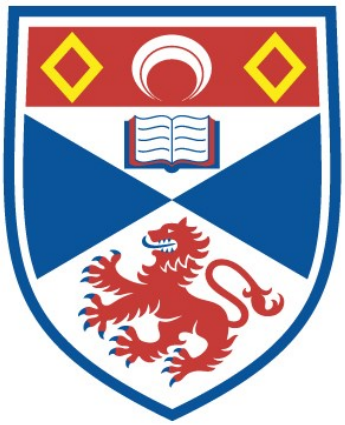

1987

A THREE-COLOUR PHOTOMETRIC SURVEY OF VIRGO 'CORE' LENTICULAR GALAXIES

by Gordon J. Malcolm

Thesis submitted to the Faculty of Science in candidature for the degree of Ph.D in the University of St. Andrews.

VOLUME ONE

Dedication

This work is dedicated to my parents, Alan and Doreen, whose sacrifices gave me two gifts beyond price: my home and my education.

DECLARATION

I, Gordon J. Malcolm, hereby certify that this thesis, which is approximately 45,000 words in length, has been written by me, that it is the record of work carried out by me, and that it has not been submitted in any previous application for a higher degree.

Date 5th May 1986 Signature of Candidate

I was admitted as a research student under Ordinance No. 12 on 1st October 1981 and as a candidate for the degree of Ph.D on 1st October 1982 the higher study for which this is a record was carried out in the University of St. Andrews between 1981 and 1984.

Date 5th May 1986 Signature of Candidate

In submitting this thesis to the University of St. Andrews I understand that I am giving permission for it to be made available for use in accordance with the regulations of the University Library for the time being in force, subject to any copyright vested in the work not being affected thereby. I also understand that the title and abstract will be published, and that a copy of the work may be made and supplied to any bona fide library or research worker.

CERTIFICATE

I certify that Mr. Gordon J. Malcolm has spent nine terms in research in the Department of Astronomy, University of St. Andrews, that he has fulfilled the conditions of Ordinance General No. 12 and Senate Regulations under Resolution of the University Court, 1967, No. 1, and that he is qualified to submit the accompanying thesis in application for the degree of Ph.D.

Prof. D.W.N. Stibbs

SUPERVISOR

ERRATA

Abstract, title			for:	"GALAXY"	read: "GALAXIES"
Acknowledgements				tunure	tenure
				Coulsen	Coulson
				Herstmonsieux	Herstmonceux
List of contents				Dilemnas	Dilemmas
I page 1	line	4		Elliptical	Disk
		5		Disk	Elliptical
I-4		10		"as"	"and"
I-9		4		asymmetrics	asymmetries
I-10		6		recombinaton	recombination
I-33		20		Force PV^2	Force = PV^2
I-57		4		concensus	consensus
II-22		11		"of any"	"of the centre of any"
II-32		16		chapter 3	chapter III
II-36		3-4	delete excess phrase	"and the convection of momentum from the hot gas will become turbulent"	
III-2		3		Jonhson	Johnson
IV-5		25		sytem	system
IV-8		22		stronge	strong
VI-6		1		tabulate	tabulates
		11		characterstic	characteristic
		21		Tinsely	Tinsley
VI-8		bottom		a	an
VI-10		bottom		profile	profiles
VI-11		line 1	delete 'were'		
VI-52			for:	"prior"	read: "priori"
VI-71	Table xxiii			Sprial	Spiral
VII-10		line 19		similarlity	similarity

Acknowledgements

Academic

The work described in this thesis was carried out at the University Observatory in the University of St. Andrews during the period of tunure of an S.E.R.C. research studentship. I am indebted to the members of staff of the Department of Astronomy and Astrophysics for many helpful discussions throughout my time as a student. Dr. C.W. Fraser encouraged my interest in galaxy photometry and is acknowledged, in due measure, for his supervision of the early stages of this thesis. Prof. D.W.N. Stibbs is acknowledged for his supervision of the remainder of my thesis and for invaluable encouragement and advice given in numerous discussions.

Acknowledgement is also due to the staff of the Royal Observatory at Edinburgh for their hospitality and help during many visits to use the STARLINK reduction facilities. Dr. A.C. Davenhall is especially thanked for his generous hospitality, helpful advice and extremely patient software maintainance.

Drs. D. Kilkenny and I. Coulsen of the South African Astronomical Observatory are similarly thanked for their hospitality during two visits in 1983, and for valuable advice on observational techniques of photo-electric photometry.

The assistance of staff of the Royal Greenwich Observatory at Herstmonsieux in demonstrating the P.D.S. micro-densitometer control system is also gratefully acknowledged.

Personal

This work would not have been possible without the continual support and encouragement provided by my family throughout my education. Colleagues at St. Andrews University, who are too numerous to mention, are warmly thanked for their interest and friendship. Lastly I would like to thank my wife Elaine for her fortitude and patience in putting up with seven years of Astronomy !

Production

Jenny Merriman is thanked for her stalwart typing of Volume One in the face of what must have been a rather esoteric manuscript. Elaine Malcolm annotated all the Figures and Data Appendices, and shared the dreary task of proofreading the typed draft.

ABSTRACT

A THREE-COLOUR PHOTOMETRY SURVEY OF VIRGO 'CORE' LENTICULAR GALAXY, by Gordon J. Malcolm. A thesis submitted in candidature for the degree of Ph.D in the University of St. Andrews.

Photographic Surface photometry in the Johnson B, R and I passbands of eighteen galaxies within 3^{o} of the Virgo cluster 'core' is presented in this work. U.K. National facilities and STARLINK common-user software were used to produce major and minor-axis luminosity profiles, colour-difference profiles, isophotal maps, equivalent profiles, and standard luminosity parameters for each galaxy in each passband. Standard techniques have been applied to the equivalent profiles to produce decomposed bulge and disk components for each galaxy. Solutions which are demonstrated to be realistic representations of the programme galaxies are amalgamated with previously-published independent data to construct homogeneous data sets.

Nearly all the lenticular systems surveyed display vestigial disk structure or unusual features in the colour-difference profiles. Statistical analysis of the constructed data sets reveals no significant structural differences in the bulge components of disk systems as a function of morphological type, in contradiction with the earlier results of Dressler (1980). Significant differences in the disk components as a function of morphological type are found in the B-band data, but not the I-band data, in agreement with the results of Hamabe (1982) and Boroson et al. (1983b) respectively.

The primary objections to the production of lenticular galaxies from spiral progenitors appear to have been discredited, together with several intrinsic-formation theories, and the results presented in this survey are considered strongly supportive of the hypothesis of a common origin of disk systems of all morphological types. The conclusion that at least some fraction of lenticular systems must have looked like spiral galaxies at some time in their history seems almost inescapable.

Volume 1: List of contents

Chapter I: Theoretical and Observational Dilemnas

CHAPTER I

INTRODUCTION

Theoretical and Observational Dilemmas

Introductory Remarks

Within the past decade several profound changes have been made to the conventional theory of galaxy formation, which was comprehensively reviewed by Gott (1977). The picture of Elliptical galaxies being formed by dissipational (gaseous) collapse and Disk galaxies by dissipationless (stellar) collapse has been particularly embarrassed by the observations of low rotational velocities and extended mass distributions respectively. Even more important has been the growing realization of the crucial importance of a galaxy's environs, both during the epoch of formation and subsequent aeons, in the determination of its currently observed state. Galaxies are not inviolate units marooned in an empty void, but under close scrutiny often appear to nearly overlap (e.g.: the enhanced image of the Virgo cluster 'core' presented by Malin (1981)). Moreover, in our expanding Universe we can be certain that even currently isolated systems will have been juxtaposed with their now distant neighbours at the epoch of formation.

It has become clear that attempts to explain the formation and evolution of galaxies are implicitly related to an understanding of the development of large-scale structure in the Universe, as the various theories describing this development present very different scenarios for the environs and composition of proto-galaxies.

Grossly over-simplified, the theories divide into those which predict that very large structures form first and subsequently fragment into smaller and smaller units, and those which argue that small objects form first and later amalgamate into larger structures. In the former case, one would expect the local conditions in the very early history of a galaxy to determine its present-day properties. In the latter case, one might expect the processes that profoundly influence a galaxy's evolution to operate in later epochs.

Potentially, one of the most powerful discriminants between these types of theory is provided by the detailed study of lenticular galaxies which are suspected to be specimens of environmentally modified spiral systems. If lenticulars are demonstrated to be the end product of some agent acting on previously 'normal' disk systems and the mechanism can be successfully identified, or if it can be shown that lenticular systems have been different from the epoch of formation, then a coherent theory that explains the evolution of the present-day structure of galaxies and clusters may be isolated from its competitors.

The rationale of this thesis is to contribute to this goal by undertaking a detailed photometric study of the Lenticular systems in the relatively-dense environment of the Virgo cluster 'core' and to compare their observed structure with previous studies of lenticular and 'normal' disk systems.

The remainder of this chapter will be devoted to expanding the important aspects of the discussion outlined above. Firstly, theories describing the development of large-scale structure in the Universe will be reviewed, together with their implications for the formation and evolution of galaxies. Secondly, the environmental mechanisms that may be important in determining galaxy structure and content will be examined. Thirdly, the observed properties of lenticular systems and the observational evidence for and against the environmental modification of spiral systems to form lenticular galaxies will be discussed. Finally, the selected programme of observation and analysis, together with the aims and intention of this work, will be defined.

I-1 The Formation of Matter Agglomerates in the Universe

"Big Bang" cosmological theories, postulating that the Universe originates from a primordial extreme temperature and density regime, are currently the only theories that can directly explain three cosmological observations: the expansion of the Universe, the ubiquitous $3^{\circ}K$ background radiation field and the cosmic abundance of elements heavier than Hydrogen.

These theories predict that at early epochs the Universe was dominated by a slowly cooling radiation field and only at a redshift of approximately $Z = 1000$ will the mass density of matter exceed the radiation equivalent mass density. Before this time the domination of ordinary matter by radiation will preclude matter from clumping by mutual gravitational attraction, due to

the dissociation of zones of enhanced electron density by the random scatterings produced by the intense background radiation field. Once the radiation temperature drops to about 3000 ^{o}K neutral hydrogen can form from the combination of protons and electrons. Helium nucleii created by nucleosynthesis very early in the lifetime of the Universe would have become neutral slightly before this epoch. The formation of neutral hydrogen will effectively remove almost all free electrons from the Universe rendering it transparent to electro-magnetic radiation, as from this time radiation field photons will no longer suffer electron scattering.

Currently popular theories for the formation of matter agglomerates after the time of recombination can be divided into three groups. The first, and perhaps simplest, group of theories postulate that isothermal density perturbations on many scales were present in the Universe at the time of recombination. The typical formation time of objects is determined by the size of the density perturbations, with dissipative processes having negligible effect on the evolution of the larger perturbations. The environment in which galaxies form is relatively peaceful although interactions become important as clusters form by gravitational amalgamation. The second class of theories proposes that adiabatic perturbations dominate any inhomogeneities in the Universe at the time of recombination and lead only to the formation of very-large condensations of matter. These then collapse and fragment into sub-units which themselves subsequently condense to form galaxies. Since the environment of

galaxy formation forms first, the interactions between the forming galaxies at these early epochs may profoundly influence their subsequent evolution. The final class of theory, most recently advocated, suggests that galaxies and clusters need not derive directly from primordial fluctuations, but from an early generation of relatively-small pregalactic objects. The pregalactic objects currently most popular are either massive stars or black holes, and although many details of these theories are controversial and uncertain, recent attention has been focussed on the subject because of the number of theoretical routes from which pregalactic objects might arise and because of the number of associated astrophysical processes consequently available for the subsequent creation of large-scale density fluctuations.

Each of these classes of theory may be modified to some degree by the currently-popular proposal that much of the mass of the Universe may be in some invisible non-gaseous form (e.g. Faber and Gallagher (1979)); the implications of 'dark' matter and the current state of these theories has been extensively reviewed recently (e.g. White (1982) and Carr and Rees (1984,a,b)). A synopsis of each of these classes of theory will now be presented together with their implications for the formation and evolution of galaxies.

1.1 Isothermal Density Perturbations

Isothermal perturbations in the early Universe may be produced by

locally varying the relative numbers of particle classes (e.g. baryons and photons) provided that the total energy density is maintained (White (1982)). Perturbations of total mass less than the Jeans mass at the time of recombination (10^5 - 10^6 $M_\odot$, Peebles (1974)) will not become bound systems due to internal pressure, but perturbations larger than this limit should collapse to form bound systems and cannot be routinely dissipated by any known physical process.

Numerical simulations of the subsequent evolution of isothermal perturbations (e.g. Peebles (1970), White (1976b), Aarseth et al. (1979) and Efstathiou et al. (1979)) have collectively demonstrated the heirarchical growth of structure: groups of objects condense out of the general expansion with the total population of condensing groups increasing as time progresses. The condensations occur in zones of enhanced density, and each large condensation usually contains sub-units that have previously collapsed because of their initially higher densities. Clustering of these groups of objects subsequently takes place by gravitational amalgamation on larger and larger scales; at some judiciously chosen point the general pattern of clustering obtained is similar to the cosmologically-observed galaxy distribution.

Several criticisms may be levelled at these types of simulation. Firstly, the point masses used in these experiments must be very high, since the total mass of the system of particles must represent the total mass of the Universe. In addition, the test

particles cannot destructively interact to produce mergers or disruption as might be expected in the real Universe. Thus the analogy between the dynamics of the real Universe and dense groups of massive test particles must necessarily be considered rather loose.

From studies of these numerical simulations of clustering and some simple scaling arguments, it is possible to deduce the implications of this scheme for the formation and evolution of galaxies. The currently observed clustering structure should have been preceded by a generation of smaller clusters, of higher local density and lower average velocity dispersion, in which the rate of interactions between galaxies would be much higher than is currently observed; during this epoch, the majority of environmental 'damage' would be inflicted on member galaxies. Thus one would expect currently to observe clusters whose members display a variety of types of modification, dependent upon the previous history of local mass density in the cluster; indeed, one would expect sparse clusters to be still in the process of forming (dynamically 'young') with little or no environmental effects yet apparent.

At present, it is difficult to be more precise about the rate of galaxy interaction during the growth of structure from an initially weakly-clustered distribution because of the lack of agreement amongst authors whose numerical simulations allow some interaction between model galaxies. For example, Aarseth and Fall (1980) find that model clusters frequently coalesce rapidly

into large objects due to the continual merging of their galaxy populations, whereas Roos (1981) obtains a clustering distribution similar to that commonly observed.

The growth of structure by heirarchical clustering, in an analogous fashion, is also a consequence of some pregalatic 'seed' theories. Some aspects (particularly the role of 'dark' matter) will be dealt with in more detail subsequently.

In addition to the question as to whether the observed heirarchy of clustering can be satisfactorily modelled by the progressive growth of structure by gravitational amalgamation, there is the problem of the production of an Intra-Cluster Medium in sparse clusters. Many galaxy clusters have a hot X-ray emitting gas located at or near the cluster core, which is commonly termed the Intra-Cluster Medium (hereafter ICM). In regions of high local density, interactions between collapsing proto-galaxies should remove diffuse gas from the systems (White (1976)a) after some early stellar population has formed (Silk (1977a,c)). The removed gas should then settle into the cluster potential well, become heated and hence observable as an X-ray source. However, this process should be much less efficient in regions of low local density, as interactions will be less frequent and galaxies have time to form more stars, reducing the amount of material available for removal. Thus low-density irregular clusters should never produce a significant ICM and X-ray luminosity, whereas this has been observed (e.g. A119, Dressler (1980)).

The entire consideration of isothermal perturbations may be profoundly affected by recent theoretical advances in the realm of particle physics (e.g. Weinberg (1979)) which have given new insight as to how baryon/antibaryon asymmetrics may have arisen but may also prohibit variations in the Baryon/Photon ratio and hence preclude the formation of isothermal perturbations. If the predictions of the so-called Grand Unified Theories (e.g.: the Weinberg-Salam-Glashow (WSG) theory) continue to be verified by collisional high-energy experiments, then isothermal perturbations must be increasingly unlikely in the early Universe. Although some of the predictions of the WSG theory have been accurately verified, such as the discovery of W and Z intermediate vector bosons at CERN, Geneva (e.g.: Science News (1983) 123, No 6, p. 84), some unexpected discoveries have also been reported from CERN (e.g. Science News (1984) 125, No 18, p.276). Even more recently the discovery of the so-called 'zeta' particle has been reported from the DESY laboratory at Hamburg (e.g. Science News (1984) 126, No 6, p. 84). This particle is very energetic (about 8.3 GeV) but appears not to display the properties of the long-sought 'Higgs' particle predicted by the WSG theory. These unexpected discoveries stress that important modifications to the WSG theory may still have to be made (particularly if the 'zeta' particle were to be identified as the fundamental 'Higgs' particle) and it may be premature to rule out all consideration of isothermal perturbations.

1.2 Adiabatic Density Perturbations

If the perturbations later responsible for the formation of matter agglomerates originate at some very early epoch, then adiabatic density fluctuations, in which the matter and radiation fields are similarly compressed, should be completely dominant by the time of recombinaton (Z = 1000).

These perturbations will remain essentially unchanged throughout the majority of the radiation-dominated epoch of the Universe (when 'exotic' massive particles are absent) until the time of recombination when the photon mean-free-path increases rapidly as almost all free electrons are removed from the Universe. As the photon mean-free-path increases, perturbations can be dissipated by thermal damping as energy is transported away from the regions of enhanced density, leading to the dissipation of all perturbations below some (large) limiting size.

The study of adiabatic density perturbations was pioneered by Zel'dovich (1970) and Sunyaev and Zel'dovich (1972), and has subsequently been part of a long programme of study in Russia (see e.g.: Doroshkevich et al. (1980) for details and references). The main features of this model are that only very large perturbations corresponding to galaxy cluster masses ($\sim 10^{15} M_{\odot}$) survive the epoch of recombination to condense out of the expanding background, with the subsequent collapse of these masses being highly anisotropic and typified by the formation of sheetlike surfaces or 'pancakes' sandwiched between strong gaseous shocks. The existence of galaxies within clusters which

are in turn within superclusters is explained by the subsequent fragmentation of the cooling shocked gas of the pancakes.

Numerical simulations of the development of structure from the fragmentation of large density perturbations has been performed by Frenk et al.(1983), who also contrasted the results with simulations of the growth of structure from an initially weakly clustered beginning (i.e.: isothermal perturbations). Comparison of the simulated clustering with the observed clustering distribution in a large volume of nearby space shows that the structure predicted by the adiabatic picture is in much better agreement with observation.

The observation of extensive voids of comparatively empty space (e.g. Bahcall and Soneira (1982) or Zel'dovich et al. (1982)) between superclusters is predicted in a straightforward manner as the spacing between collapsed pancakes, which is expected to be large (Doroshkevich et al. (1980)).

The implications of this theory for the formation and evolution of galaxies are clearly different from those of the heirarchical clustering scenario because the forming galaxies are already clustered together and interactions between these gaseous fragments should be a far more frequent occurrence. This subject has been extensively studied by Silk (1977a) and (1978), who argues that adiabatic perturbations can break up into galaxy-sized fragments ($\sim 10^{11} - 10^{12}\ M_{\odot}$) with early interactions between these collapsing gaseous proto-galaxies both

frequent and highly inelastic, leading to the construction of a galaxy mass function (and hence luminosity function) which is similar to that observed by Schechter (1976). The proto-galaxies should also acquire higher velocities in a shorter time than predicted by gravitational clustering theories (as crossing times will be much shorter) implying that 'supersonic' interactions should happen much earlier; these interactions are efficient in heating and removing interstellar gas from the forming galaxies leading to the possibly-rapid production of a hot ICM, which can itself interact with the forming galaxies (as discussed subsequently in section 2.2). The interactions may also stimulate star-formation (Silk (1978) via mechanisms described by Silk (1977a,b,c). The general picture is of significant environmental interaction being common at much earlier epochs than predicted by most gravitational clustering theories.

The 'pancake' scenario should thus naturally predict that many properties of galaxies should be quite strongly related to their initial environment, and the rather modest variation of galaxy luminosity function (Schechter (1976)) and morphological type (Dressler (1980)) with local mass density may be embarrassing, as it is not obvious why the same characteristic parameters should describe galaxies formed in both dense and sparse regions of a pancake. On the other hand, it can be argued (Silk (1978)) that the very similarity of 'field' and rich cluster luminosity functions (e.g.: equal relative numbers of dwarf systems) demonstrates that most systems originate from a clustered state.

Several problems assail the standard adiabatic perturbation theory. Firstly, Sunyaev and Zel'dovich (1972) themselves admit that only about one-third of the gas in a 'pancake' can cool sufficiently to be able to collapse and fragment; one might expect the remainder to exist as a hot gas but this is not observed in the required quantities. It is difficult to explain why this material is not visible or what form it now takes. Secondly, the characteristic size of fragments forming in the pancake is controversial (e.g. Jones et al.(1981)); if they are small (e.g. White (1982) $\sim 10^8 - 10^9$ $M_\odot$) then very considerable merging within the pancake is necessary to produce galactic mass-objects (e.g. Burbidge and Burbidge (1969) $\geq 10^{10} - 10^{11}$ $M_\odot$). This mixing process is not conducive to the production of the segregated distributions of dark and luminous material implied by observation (e.g. White and Rees (1978), White (1982) and Gilmore and Hewett (1983)).

Potentially the most serious problem assailing the standard adiabatic scenario is that the adiabatic perturbations which are large enough to ensure pancake formation and evolution by the present epoch cannot be reconciled with the currently-observed galaxy covariance function and the apparent isotropy of the microwave background. (e.g. Silk and Wilson (1981), Peebles (1981)). These difficulties can only be overcome by rather contrived conditions, in particular when $\Omega = 1$ (i.e. the Universe is marginally bound as the actual mass density of the Universe is close to the critical 'closure' mass density). However, a baryonic density corresponding to $\Omega = 1$ is much greater than the

maximum mass density deduced from widely-accepted nucleosynthesis arguments concerning the cosmic abundances of Helium, Deuterium and Lithium (e.g. Gott et al. (1974), Olive et al.(1981)).

Many of these problems may be largely circumvented if a substantial function of the mass of the Universe consists of dark matter from a very early epoch. In order to permit the segregation of dark and luminous mass distributions, it is usually postulated that the dark matter is in the form of some massive stable-particle species, which interacts only gravitationally with luminous matter. The current choice in vogue is neutrinos with a rest mass of tens of electron-volts (e.g. Schramm and Steigman (1981), Mellot (1983)), and this topic has been the subject of much recent attention particularly since a non-zero neutrino rest-mass is predicted by many of the Grand Unified Theories discussed in the previous sub-section. A synopsis of the currently available conclusions now follows.

Massive neutrinos can dominate the total mass density (allowing $\Omega \simeq 1$) without constraining the total mass density to exceed the limits set by nucleosynthesis calculations. The essential features of the standard adiabatic scenario, together with the implications for galaxy formation and evolution, are retained in a neutrino-dominated treatment. It turns out that collisionless damping dissipates all perturbations below a critical size which corresponds to a supercluster mass of $10^{15} - 10^{16}$ $M_{\odot}$ and dimensions equivalent to tens of megaparsecs when viewed at the present epoch. The physical size of these fluctuations is

particularly interesting when compared to the observations of large filaments or 'strings' of galaxies on scales of 10 - 100 Mpc reported by Davis et al.(1982) and others. Perturbations in the baryonic density do not have to be large at the time of recombination (they may be zero, for example, and be subsequently induced by neutrino-density fluctuations) so that no large anisotropies in the background radiation field need be produced.

The formation of galaxies within the context of a neutrino-dominated adiabatic scenario has been extensively studied by Shapiro et al.(1983), who present three-dimensional numerical simulations demonstrating that the post-recombination growth of large-scale adiabatic fluctuations is characterized by the formation of a number of sheetlike structures quite analogous to the conventional 'pancakes'. Moreover, a number of more complex structures form at the intersections of two pancakes, strongly reminiscent of the filamentary structure reported earlier, with the densest structures forming at the intersection of three or more pancake sheets. When these results are considered along with the simulations of Frenk et al.(1983), it is very tempting to identify much of the observed large-scale structure in the Universe with the predictions of a neutrino-dominated adiabatic perturbation theory.

Shapiro et al. further investigate the viability of galaxy formation within this rationale by means of a simplified numerical solution of the hydrodynamical problem, choosing the initial conditions of their treatment to maximise the possibility

of galaxy formation whilst agreeing with all observational and theoretical constraints. They conclude that if 90% of the matter in the Universe is non-baryonic, only 10-15% of the remaining baryons can constitute the relatively cool pancakes by recent epochs, leaving the remaining 85-90% of baryons in the form of a hot diffuse intergalactic gas of characteristic temperature 10^6 - 10^7 ^{o}K. Thus, even if the formation of galaxies within the pancake is highly efficient, only a few percent of all the matter in the Universe will be in the form of luminous material, in quite good agreement with the observational conclusions of Faber and Gallagher (1979). The conversion of pancake material into galaxies could be highly efficient, particularly in the pancake intersection zones, if gas-dynamical effects are important (e.g.: the Ostriker-Cowie mechanism discussed later in section 1.3). Shapiro et al. maintain that their predicted end results, namely Ω(TOTAL) $\simeq$ 1, Ω (GALAXIES) $\simeq$ 0.01 and Ω(IGM) $\simeq$ 0.1, do not conflict with the available observational data which they summarize.

Several areas of uncertainty remain to be resolved. Firstly, the 'canonical' parameters chosen by Shapiro et al. must be varied systematically to assess their individual impact on the viability of galaxy formation. More fundamentally, detailed modelling of the actual baryon gas cooling and fragmentation must be carried out, with particular reference to the subsequent dynamical evolution of the proto-galaxies. Lastly, the rest masses of the various species of neutrino must be determined, as the currently allowed range ($o \lesssim m \lesssim 100$ eV) is very large.

Despite these remaining problems, it is encouraging to note that studies of the neutrino-dominated adiabatic perturbation theory appear to resolve some of the shortcomings of the standard picture while retaining many attractive observational predictions. The agreement of these predictions, at least qualitatively, with many observed features in the Universe is largely responsible for the current popularity of this type of model.

One final point worth emphasizing is that the neutrino-dominated scenario is still controversial (e.g. compare the conclusions of White et al. (1983) with those of Bond and Szalay (1983)) and other, more 'exotic' particles may have a cosmologically significant rest mass. The probable effect of these particles (Shapiro et al. (1983)) would be to allow pancakes with a wide variety of sizes and masses to form, with the smaller pancakes having the most efficient cooling and so presumably the most efficient conversion of material into galaxies (or pre-galactic objects). This suggestion is especially intriguing in view of the observations of Press and Davis (1982) reporting that the mass/luminosity ratios of galactic systems increases as the clustering scale of these galactic systems increases.

1.3 Galaxy Formation triggered by Pregalactic 'seed' Objects

Theorists have disliked the imposition of adiabatic or isothermal density fluctuations on the initial conditions of the Universe;

obviously it would be preferable if these could be shown to arise naturally from mechanisms operating in an initially-homogeneous Universe. A compendium of scenarios which leads to the spontaneous production of fluctuations is given by Carr and Rees (1984b). Unfortunately, these mechanisms generally produce fluctuations which are minute compared to galactic dimensions and cannot be successfully amplified to produce the much larger perturbations required without considerable modification to the conventional Hot Big Bang (hereafter HBB) conditions of the early Universe (e.g. the 'tepid' Universe of Carr and Rees (1977)). However, these spontaneous fluctuations can generate small bound objects of characteristic size dependent upon the initial environment of the Universe, and a number of additional theoretical routes are available for the formation of pregalactic objects (see e.g. Carr and Rees (1984a) for a review).

In the standard HBB model of the Universe dominated by baryonic matter and adiabatic perturbations, the formation of pregalactic objects is inhibited by thermal diffusion and the standard adiabatic theory results, as previously detailed, unless primaeval 'black holes' are formed by some agency. Although these are postulated to have low individual mass, they could cluster together to produce much larger units capable of stimulating significant statistical fluctuations in density.

In the standard HBB model dominated instead by isothermal perturbations, pregalactic objects of low mass can form, but radiative damping and other effects will nullify the importance

of condensations much below $\sim 10^6$ $M_\odot$ leading to the standard isothermal scenario.

However, the formation of an early generation of massive stars is quite feasible in either of these theories (Silk (1977a)) and the evolution of these stars could have a profound effect upon their surroundings and modify these theories very substantially.

If the HBB model is dominated by non-baryonic matter, then the formation of pregalactic objects depends upon the nature of this material: if it provides a homogeneous gravitational background then the formation of pregalactic objects is severely inhibited, regardless of whether there are adiabatic or isothermal fluctuations. If the gravitational background is not constrained to be homogeneous (i.e. the dark matter can cluster) then the statistical fluctuations generated by these inhomogeneities can promote the formation of pregalactic objects with a resulting heirarchical growth of structure analogous to that expected in the standard isothermal theory.

If the early history of the Universe is described by 'tepid' or 'cold' models then the situation is even more complicated and pregalactic objects can form from a variety of circumstances. As mentioned previously, Carr and Rees (1984a,b) also point out a host of opportunities for the spontaneous formation of small bound objects by 'phase transitions' at theoretically significant epochs irrespective of any perturbations that might exist.

Some of the mechanisms which utilize these pregalactic objects to account for the formation of clusters and galaxies will now be discussed in more detail.

White and Rees (1978) address the problem of the formation and evolution of matter in the Universe by considering the process of gravitational amalgamation, with particular reference to the role of dissipative processes and the formation of 'dark' matter. The existence of 'dark' matter is postulated to explain why only about 20-30% of the mass needed to virialize rich clusters (e.g. Coma) is in an observable luminous form such as gas or stars. White and Rees prefer the view that this dark matter took the form of small pregalactic objects such as low-mass stars (or 'brown' dwarfs and 'Jupiters') or the remnants of earlier generations of high-mass stars, but they acknowledge that their treatment is valid for any mass constituent that behaves as an assembly of point masses of individual mass $\lesssim 10^6$ $M_\odot$, which could include more exotic objects such as massive particles (e.g.: neutrinos) or black holes which formed before the epoch of recombination.

White and Rees argue convincingly that it is difficult to produce both low and high-luminosity material by constructing larger and larger structures from smaller units by purely dissipationless processes, as one would then expect the material to be thoroughly mixed rather than segregated. In addition, the survival of internal structure (galaxies) within larger systems (clusters) of 'short' crossing times argues against the dissipationless

clustering of luminous matter as the numerical simulations of White (1976b) and Aarseth et al. (1979) predict that the violent interaction and destruction of all internal structure within a system proceeds rapidly via the agencies of tidal interaction, collisional mergers and dynamical friction. Hence it is inferred that dissipative processes were important in the formation of luminous matter in the Universe.

The crux of the treatment of White and Rees is that most of the matter in the Universe has been in the form of dark matter since early times and has subsequently undergone dissipationless heirarchical gravitational clustering (from some epoch prior to $z = 100$) forming associations on ever larger scales. At any given instant 't' during this process, the Universe would thus contain dark matter clustered on some particular scale, with very little substructure evident as it would have been eradicated within a few crossing times via the processes noted previously (White (1976b) and Aarseth et al. (1979). At the time '2t' the dark matter would display a similar appearance at the next level of heirarchical clustering. The present-day distribution of collapsed cluster masses would thus correspond to the largest heirarchical level currently formed with the bulk of the matter of the Universe consisting of dark matter distributed smoothly on smaller mass scales, thus giving possible explanations for both cluster 'missing mass' and galaxy 'massive-halo' observations.

It is further suggested that all luminous matter has formed from gas which initially shared the same distribution as the dark

matter, but later cooled and settled into the potential wells provided by the dark matter at each stage of the clustering process. If cooling can proceed long enough, the gas can condense to become self gravitating and is able to fragment to form stars once its self-gravity dominates the effect of the surrounding dark matter. As these luminous cores condense during their cooling and star-formation phases of evolution, they become increasingly compact and hence much 'harder' dynamical units than the surrounding 'halo' of dark matter.

When the first low-mass haloes are disrupted to form a larger unit, residual gas (left over from the formation of the small luminous remnants of the previous stage) may be able to settle again into the new (larger) potential well to cool and collapse to form a larger central system. Thus the theory might naturally account for groups of small satellite systems surrounding larger central galaxies, as is commonly observed. These small groups may themselves be able to interact (e.g. Tremaine (1976)), and to boost the luminosity of the central system at the expense of its neighbours, in the time available before the amalgamation of the central halo into the next, still larger, scale of structure.

White and Rees also note that as the residual gas is 'effectively recycled at each stage of the heirarchy', it may be enriched by this process, leading to the prediction that the most massive galaxies (which should be the most recently formed) should have the highest metal abundance.

The formation of galaxy morphological type within this scenario

is studied by Kashlinsky (1982) who presents an explanation in terms of several critical parameters (e.g. angular momentum) affecting the accumulation of luminous material within the gravitational potential wells.

Black holes of large individual mass have also been invoked (e.g. Carr (1975)) as pregalactic objects capable of explaining cluster 'missing-mass' observations and stimulating the formation of matter agglomerates in a manner analogous to that described by White and Rees (1978) by providing condensation nucleii. The massive holes provide the 'seed' fluctuations in the matter density which can grow after the decoupling of matter and radiation to give rise to bound units of galactic mass by recent epochs. These theories have been considered since Lynden-Bell (1969) proposed that quasars and active galaxies might contain massive ($\sim 10^8$ $M_\odot$) black holes, and interest has been more recently fueled by claims that the nucleii of M 87 (Sargent et al. (1978) and our own galaxy (Lacy et al. (1982)) may contain massive black holes.

Various scenarios utilizing swarms of primaeval solar-mass black holes to statistically generate the density perturbations that later form galaxies have been proposed (e.g. Meszaros (1975), Carr (1977)), but it can be demonstrated that if the holes have a significant mass spectrum then the clustering scenario rapidly reduces to the 'seed' theory mentioned above. A recent modification (Carr and Rees 1984,b) observes that, if the formation of individual black holes commonly involves asymmetry in the collapse phase, then individual black holes might have

quite significant peculiar velocities (10^2 - 10^3 kms^{-1}). They go on to show that large-scale density fluctuations can be generated (leading to the subsequent formation of galactic mass condensations at recent epochs) purely as a result of these peculiar velocities.

Generally, all the models described in this section follow the pattern of the White and Rees (1978) scenario, which is itself analogous to the standard isothermal perturbation theory, so the implications for the formation of galaxies and the evolution of structure in the Universe will be similar to those previously discussed in section 1.1.

The final class of pre-galactic objects to be discussed leads to very different conclusions about the nature of the environment encountered by forming galaxies and in some aspects is almost the reverse of the standard adiabatic picture discussed in section 1.2. Ostriker and Cowie (1981) first proposed this scenario in which an early generation of massive stars formed at some epoch around Z = 100. Massive stars in the range 10 - 200 $M_\odot$ would have a cosmologically-brief lifetime characterized by an explosive end to their stellar evolution as supernovae; the energy output from the deaths of these stars might induce the formation of much larger structure. The essential part of Ostriker and Cowie's theory is that the spherical shock front generated by each individual supernova would expand adiabatically, sweeping up any surrounding gas to form a shell of shocked material. This shell can cool by inverse Compton scattering of background photons or by gas radiative processes at

more recent epochs, and then fragment to form a new generation of stars which themselves may subsequently explode. If this process can occur efficiently, then a progressively-larger fraction of the Universe will consist of stellar material at the completion of each cycle. Eventually, in more recent times ($Z \simeq 5$), a collapsing shell can only fragment into galactic-mass objects, instead of another generation of stars, with such formation predicted to decrease rapidly after $Z \simeq 4$.

Unfortunately, such critical parameters as: the typical masses of stars forming in each cycle; the efficiency of stellar-formation in each cycle; and (most crucially) the amount of material which can be swept up into gas shells; are all currently uncertain and the subject of considerable controversy.

An interesting variation of the Ostriker and Cowie mechanism is discussed by Freese et al. (1983): if swarms of primordial planetary-mass black holes form in the Universe, then as they subsequently cluster, zones of gaseous baryonic material may settle into the gravitational potential wells provided by the inhomogeneous distribution of primordial planetary-mass black holes. Pregalactic objects in the mass range $10^4 - 10^7$ $M_\odot$ forming in the period $100 \lesssim Z \lesssim 5$ can cool to form an early generation of massive stars. The subsequent evolution of these objects can then form galaxies via the Ostriker-Cowie mechanism. As pointed out by White (1982), the supernovae-driven blast waves could also compress the dense regions of the surrounding gas compontent, resulting in the immediate formation of luminous galaxies via shock-induced star-formation. The mechanism is

analogous to that described in detail by Elmegreen and Lada (1977), but operating on a much larger scale to produce a more energetic version of the White and Rees (1978) scheme.

As mentioned previously, the Ostriker and Cowie mechanism must also be considered within the larger context of isothermal or adiabatic density perturbations, as the formation of an early generation of stars is feasible in either scheme (Silk (1977 a)). However, if the stars form within an already collapsing proto-galaxy the lifetime of a massive star and the 'crossing-time' for the blast waves are both much shorter than the collapse time of the system. The problem is then that, if the gas-sweeping process is as efficient as Ostriker and Cowie suggest, then the proto-galaxy will be blown apart by the first supernovae explosions unless most of the gas is already in quite dense clouds that can be triggered into shock-induced star-formation. If the gas-sweeping process is less efficient (to preserve the proto-galaxy) then the whole mechanism may not be self-propagating. In either case, one would expect a great deal of enriched material to be ejected into the intergalactic medium, so a natural prediction of the Ostriker and Cowie theory is that galaxies are surrounded by a hot, diffuse, relatively metal-rich intergalactic gas. This medium could itself interact with the galaxies during their subsequent evolution in the usual manner (described in more detail in section 2.2)

The precise implications of this scheme for the growth of structure in the Universe and for the formation and evolution of galaxies are rather enigmatic because of uncertainties in the

crucial parameters already mentioned. These difficulties are unlikely to be resolved until the inherent complex theoretical problems are mastered and detailed numerical simulations are undertaken. What is qualitatively clear is that the Ostriker and Cowie theory suggests that the environment at the time of galaxy formation was very turbulent and probably dominated by violent non-gravitational processes.

I - 2 Environmental Mechanisms Influencing Galaxy Structure and Content.

As may be appreciated from the previous section, a variety of models are available for the formation of matter agglomerates in the Universe, with each yielding separate predictions about the nature of a galaxy's environs at various redshift epochs and the corresponding influence of the environment on galaxy evolution. Various interaction mechanisms have been alluded to, and it seems pertinent to review these in more detail. A number of environmental mechanisms capable of influencing galaxy structure and content have been proposed, and it is convenient to divide them into three classes: 'galaxy-galaxy' interactions, 'galaxy-environment' interactions and 'internal' galaxy mechanisms. Each of these classes will now be considered in turn.

2.1 Galaxy-Galaxy Interactions

The environmental modification of galaxies by direct collision was first proposed by Spitzer and Baade (1951), who viewed Lenticular (SO) systems as the outcome of colliding 'normal' disk systems. During a direct collision the dynamically 'hard' stellar populations typically do not suffer major disruption (see Toomre and Toomre (1972) for damaging criterea), but the gaseous component of each disk will become heated at the collisional interface and subsequently escape from both galaxies. The net effect is the removal of the majority of gas from both galaxies, which are then characterized by a rapid evolution towards

gas-poor red disk systems. While the efficiency of this mechanism is undoubted, direct collisions between galaxies should be very rare except in the densest cluster environments, and only for regions such as the Coma cluster core (Rood et al. (1972)) is the collision time less than a Hubble time. Hence, this mechanism is not thought to be yet important for theories that involve progressive gravitational clustering, although collisional interactions and merging clearly must be considered within the framework of adiabatic scenarios where proto-galaxies form in an already clustered environment. A number of observational arguments have led to a recent resurgence of the idea that some fraction of elliptical galaxies, and particularly cD galaxies, are formed by collisional merging (e.g. White (1978)). Hoessel (1980) presented observations showing that nearly 30% of the brightest cluster members had more than one nucleus and thus provided strong evidence for the importance of merging processes in the core of rich clusters. Faber and Gallagher (1979) draw attention to the paucity of elliptical components in suspected binary systems, and further concluded from statistical analysis that only a small proportion of the ellipticals in suspected binary systems formed actual physical associations. It is tempting to attribute the dearth of ellipticals in binary systems, despite the ubiquitous association of ellipticals and spirals in groups and clusters, to the collisional merging of neighbouring systems, but the available observational evidence is somewhat contradictory and reviewed in a following section of this chapter.

"Grazing" encounters between galaxies, at larger interaction

distances, should be far more common than direct collisions. The possible importance of tidal effects during grazing collisions has been recognized for over twenty years, since King (1962) discussed the tidal truncation of a small system by a larger unit and later developed an approximate dynamical model (King (1966)). This model appears to agree well with observations of globular clusters and dwarf galaxies (e.g.: Hodge and Michie (1969)) and may also apply to some larger ellipticals (Faber (1973)). More recent studies (e.g. Kormendy (1977a)) have shown that tidal effects "heat" the outer halo causing expansion of the outer regions of both interacting galaxies, with material removed only from small victims interacting with much more massive systems, or by many encounter repetitions. The tidal distension effect is confirmed by numerical simulations such as Albada and van Gorkum (1977), White (1978) and Miller and Smith (1980). Theoretical arguments (e.g.: White (1982)) indicate that the majority of tidal damage will be done to any galaxy by the few closest encounters it suffers, especially if the interaction speeds are low or the perturbing galaxy is massive. These general conclusions are vividly supported by the simulations of Toomre and Toomre (1972) which demonstrate the large disrupting effects of close encounters between spiral systems.

However, the efficiency of the tidal mechanism in stripping material from the outer parts of real galaxies in realistic cluster environments is rather controversial. Gallagher and Ostriker (1972) calculate the amount of luminosity collisionally removed from an elliptical galaxy during a Hubble time of motion in a rich cluster and, despite quite generous collision

probabilities, conclude that tidal encounters will not have a significant influence on the observed luminosity profiles of galaxies in rich clusters. These calculations did not include any effects modelling the presence of massive dark haloes, but these were included in the studies of Richstone (1975), (1976) who concluded that tidal effects would limit the extent of such haloes to about 50 kpc for galaxies near the cluster core. These general conclusions are confirmed by Merritt (1983), who concludes that the tidal stripping of dark haloes should have relatively little effect on the distribution of luminous material in a galaxy. Merritt also adds that if most of the cluster mass was in a collisionless form (e.g. neutrinoes) from early times, then tidal stripping should be unimportant within a Hubble time. Despite these theoretical arguments against the importance of the tidal mechanism, there is a considerable body of direct observational effects on the luminosity profiles of galaxies in some rich clusters (see Kormendy (1980) for review). The observational evidence is, however, subject to a variety of interpretation and a more detailed discussion will be given in a later section of this chapter.

2.2 Galaxy - Environment Interactions

A galaxy will be tidally limited to some degree by the mean field of the cluster of which it is a member, in a manner analogous to the galaxy-galaxy tidal interactions described previously. A simplified treatment is given by White (1982), who shows that the tidal limits imposed are much larger than the typical luminous extent of galaxies, even for a rich cluster where the mean field

effects should be strongest. Keenan (1981), in a more detailed study of a dynamically analogous problem, demonstrates that the simple treatment (following King (1962)) underestimates the strength of tidal effects and that the tidally limited extent of galaxies should be reduced by about 30%. Although this new limit is still not likely to significantly affect the visible parts of most galaxies, it seems increasingly likely that any massive dark haloes surrounding the cluster members would be severely truncated. This conclusion agrees well with the numerical experiments of White (1976 a, 1977), which demonstrate that if galaxies in rich clusters had large massive haloes then dynamical friction would quickly produce an observable mass segregation within the cluster. Since little segregation is apparent, it follows that the galaxies do not have massive haloes and hence the majority of any dark matter must be distributed throughout the cluster. A more useful observational prediction is that spiral systems in rich clusters should not have the large, diffuse envelopes of hydrogen gas that have been observed around some nearby (low-density environment) spirals (e.g. Rubin et al. (1978)), as these should be removed by tidal effects.

Miller (1984) presents a series of numerical experiments which investigate the effect of the cluster mean field on orbiting galaxies. Although galaxies far from the cluster core will be relatively unaffected, those passing close to the centre can be severely distorted or destroyed altogether. If cluster tidal effects are as powerful as those of the models, then clusters must be dynamically young, particularly the spiral population. Arguments in favour of the unevolved nature of many rich clusters

are also presented by Forman and Jones (1982).

If a galaxy interacts with a large, gaseous entity then a number of physical processes may significantly alter the content and structure of the intruding galaxy, depending upon the interaction parameters. As many of the theories discussed in section I naturally predict the existence of a pervasive Intra-cluster Medium (ICM), and such a hot medium has been detected as an X-ray source in many clusters (e.g. Jones et al. (1979), Henry et al. (1979)), these mechanisms have been the subject of considerable recent attention. Modelling of the X-ray data (e.g.: White and Silk (1980)) implies that the X-ray gas in the core of rich clusters is typically at some high temperature (10^6 - 10^7 ^oK) and at a nearly constant pressure between ten to fifty times that of the interstellar medium in the solar neighbourhood.

If a galaxy moves through the ICM, a dynamic force will be applied to any interstellar medium in the galaxy since this will provide a barrier around which the hot gas must flow. The force exerted on any interstellar gas will be approximated by the ram-pressure applied to its cross-section, so the following result applies : Force pv^2, where 'p' is the ICM density and 'V' is the velocity of the galaxy; if this force exceeds the gravitational force binding the gas in the galaxy, then the interstellar gas will be 'swept' out (Gunn and Gott (1972)). The Gunn-Gott treatment naturally leads to the concept of critical sweeping thresholds so that for any ICM density there will be a critical velocity above which gas removal should be highly efficient. Using typical galaxy and ICM parameters, it is

apparent that gas ablation should be efficient near the core of a rich cluster but less significant in the low-density environments far from the cluster centre or in groups with a small dispersion of relative velocities. In the majority of interactions, the gas near the galactic centre will be difficult to sweep out (Zasov (1975)), although much more vulnerable in the outer regions of a galaxy. The Gunn-Gott treatment is clearly a simplification as it neglects any hydrodynamical effects in the problem; as the galaxy motion is almost always supersonic with respect to the ICM, one can expect a 'leading-edge' shock to form and some density enhancement of the ICM along the 'wake' of motion (e.g.: Rephaeli and Salpeter (1980)).

For disk systems, the sweeping efficiency will also depend on the orientation of the galaxy as it moves through the ICM (e.g. Bothun (1982); galaxies moving in a face-on manner should be more easily swept of gas due to the low restoring force in the direction perpendicular to the disk. Although ram-pressure effects cannot significantly perturb the dynamically-'hard' stellar population, the stellar content of a galaxy could be significantly influenced by this mechanism (Silk (1977 a)) if the gas content was compressed sufficiently to generate shock-induced star-formation (analogous to that described by Elmegreen and Lada (1977)) before it could be swept out of the galaxy.

Even if the ICM density were too low, or a galaxy has insufficient velocity, for viable ram-pressure sweeping, it seems probable that many galaxies will spend considerable periods immersed in the ICM near the cluster core and that several other

agents might operate in these circumstances. The hot ICM will be thermally coupled to some degree with the cooler interstellar gas of the galaxy and two processes compete in this situation: an inward conductive heat flux will be set up from the ICM into the interstellar gas which will be countered by radiative losses from collisional processes (e.g. bremsstrahlung) which will be more efficient in the denser gas zones near the centre of the galaxy. If conduction dominates, then the cooler interstellar gas in the galaxy will be lost as a result of thermal evaporation onto the ICM (e.g. Cowie and McKee (1977), Cowie and Songaila (1977)). If the radiative cooling dominates, then galaxies can accrete by trapping and refridgerating the gaseous ICM (e.g. Gunn and Gott (1972)). Evaluating the efficiency of these processes is difficult because of the complexities involved. The conduction efficiency is critically dependent on the magnetic field in the hot gas, which can act either as a conductor or as a shield depending upon its structure. The efficiency of the collisional processes, which provide the radiative cooling of the interstellar gas, are dependent upon a number of uncertain parameters, and especially on the interstellar gas density.

Nulsen (1982) presented a detailed examination of the transport processes involved with a flow of hot gas over a galaxy. He concluded that the viscous transport of momentum across the boundary layer between the hot ICM and the interstellar gas is efficient when the electron mean-free-path in the hot gas is long and the gas flow is smooth. This mechanism was termed as the Laminar Viscous Stripping of the interstellar medium of the galaxy. If the Reynolds number of the gas flow is very high

(due, for example, to magnetic field effects reducing the effective ionic mean-free-paths in the hot ICM gas) then the interface between the hot gas will become turbulent and the convection of momentum from the hot gas will become turbulent and the convection of momentum from the hot-gas flow and the surface layers of the interstellar medium will be effective as viscosity is now negligible. This process was termed by Nulsen as Turbulent Viscous Stripping.

It is clear (Nulsen (1982), White (1982)) that these stripping mechanisms provide gas removal efficiencies comparable to the effects of thermal conduction for quite different values of particle mean-free-paths within the media. Moreover, together with thermal conduction, these mechanisms operate with very little regard for galaxy orientation during motion through the hot ICM (unlike ram-pressure sweeping), and these three mechanisms will operate independently of, and additively to, ram-pressure sweeping.

On the basis of the above considerations, it is therefore evident that a variety of agents exist which should efficiently remove the interstellar gas from galaxies which become immersed for any significant period in the hot ICM observed in many rich clusters. The rate at which these various agents are extinguished at larger distances from the cluster core, as the ICM density falls, is still uncertain as so many parameters are involved. The complexity of the situation and the efficiency of gas-removal from an idealized galaxy is reinforced by the simulations of Takeda et al. (1984).

2.3 Internal Gas-Removal Mechanisms

All the mechanisms described in the previous sub-sections depend upon the galaxy interacting with some external entity, either another galaxy, the cluster potential itself or an Intra-cluster Medium. There are also available a number of internal agents capable of modifying galaxy content and structure which can operate largely independently of the external environment.

It has been argued (e.g. Faber and Gallagher (1976)) that some sweeping agent must be responsible for the low level of hydrogen gas observed in the elliptical (and lenticular) galaxies found in low density environments (where external effects would be minimised), as gas replenishment should naturally result from the mass lost by evolving stars well within a Hubble time.

Mathews and Baker (1971) proposed that the heating effects of supernovae-driven blast waves could act as galactic 'winds' sweeping out any hydrogen built up in an elliptical galaxy. Bregman (1978) proposed that these galactic winds could operate in disk systems, with an efficiency proportional to the Bulge to Disk luminosity ratio, as the bulge components of disk systems approximate to elliptical galaxies. Although such a simple model would be attractive (as a clear relationship between morphological type and Bulge to Disk ratio is observed) the efficiency of this process in removing significant amounts of hydrogen is controversial, particularly since the same agent is invoked as an efficient star-producing mechanism (Ostriker and

Cowie (1981)).

Gorbatskij (1982) has revived the suggestion that the gas content of a galaxy could be removed by the radiation pressure generated by an active nucleus, concluding that typical outbursts of activity could keep a galaxy essentially gas-free if they persist for about 10^6 years and continually recur within about 10^8 years. Although Gorbatskij acknowledges that his treatment makes simplified assumptions about the momentum transfer to the interstellar medium for a non-variable active nucleus, this mechanism could have been significant in the past as it is widely accepted that violent nuclear activity was more prevalent in previous epochs. A remaining difficulty (e.g. Faber and Gallagher (1976)) is the known correlation of radio activity with absolute luminosity for elliptical and lenticular systems, and the lack of optical evidence for past violent activity in these fainter systems which appear to be as gas-poor as the larger galaxies. Due to the lack of radio or optical evidence for violent activity in the fainter systems, the mechanism seems incapable of operating systematically for all gas-poor systems, which rather undermines the mechanism's credibility as a dominant sweeping agent.

The final mechanism which remains to be discussed is perhaps the simplest and most obvious method of altering galactic structure and gas content, namely via star-formation. A review of the current complex theories of star-formation and associated problems will not be presented here, as it is sufficient to point out three parameters that are uncertain, yet probably critical to

the evolution of star-formation in a galaxy. These are: the efficiency of the initial burst of star-formation which determines the amount of hydrogen 'fuel' left for subsequent star-formation and dynamical evolution (e.g.: disk formation); the initial mass function (hereafter IMF) of any star-formation; and the star-formation rate (hereafter SFR). These three parameters were used by Bothun (1982), together with a number of associated variables, to construct simplified models of galaxy evolution in terms of the observable colour and gas content. Although the number of free parameters involved rendered the solutions non-unique, a number of significant results are suggested. The basic conclusion reached is that proto-galaxies which efficiently convert a large fraction of their available hydrogen into a bulge component should naturally evolve into a red gas-poor system well within a Hubble time unless the SFR is very low. On the other hand, proto-galaxies which have an inefficient burst of star-formation have a large amount of hydrogen 'fuel' available for subsequent star-formation and dynamical evolution (e.g.: disk formation); these galaxies should unavoidably remain gas-rich and have blue observable colours over a Hubble time unless influenced by external processes. Bothun concludes that although these galaxies are evolving towards the red, gas-poor 'galactic graveyard', the Universe is not yet old enough for the small Bulge to Disk ratio systems to have exhausted their hydrogen 'fuel' supply. Bothun further notes that the evolutionary history of galaxy models with an initial burst of star-formation intermediate in efficiency between the two cases just described is dominated by the interaction of the various free parameters, particularly the SFR.

The importance of Bothun's work is that he convincingly demonstrates that the evolution of a disk system will be largely dictated by the processes driving the SFR, and that a galaxy's structure and gas content after a Hubble time could be largely predestined by the amount of hydrogen gas remaining after the formation of the bulge component (c.f. Sandage et al. (1970)).

This concept of predestination from an early epoch echoes the 'birth defect' scenario examined in detail by Larson et al. (1980), in which the current morphological appearance of a galaxy is determined by the amount of primordial hydrogen removed by local interactions during its formation. Larson et al. consider that only disk systems which retain a gas-rich outer envelope (consisting of gas-rich satellite galaxies, the debris of any tidal interactions and primordial gas) can avoid the exhaustion of available gaseous 'fuel' and the subsequent inevitable evolution to a red, gas-poor state. Elliptical galaxies are identified in this scheme as those systems which have lost their gas supply at a very early stage before the formation of any significant disk component. The 'birth-defect' scenario can thus naturally account for the observed trend, namely ellipticals being preferentially found in the most-highly clustered environs, lenticulars being more widely distributed, and spirals preferentially populating the least-dense regions.

Thus there exists a variety of purely internal mechanisms which could determine the currently observed content and structure of a galaxy, particularly when coupled to the various physical parameters which may be determined 'at birth', without recourse

to any external environmental agents since the epoch of formation.

I - 3 Observed Properties of Lenticular Galaxies

It is clear from the previous section that the available modes whereby a disk galaxy can become gas-poor within a Hubble time are legion. Moreover, it is quite possible that each of the myriad operates with different efficiency amongst the various cluster environments, with the cumulative effects producing lenticular galaxies and perhaps elliptical systems in addition. Alternatively, one agent may dominate over all the rest, but the identification of any controlling mechanism is problematic as the observable differences between the systems produced by the various mechanisms are obscure. In addition, the fundamental question of whether any evidence of widespread environmental modification is observed is both complex and controversial. Before embarking upon a critical analysis of the evidence, it is perhaps appropriate, at this juncture, to briefly review those observed properties of lenticular systems which are essentially uncontroversial but are responsible for much of the interest in this class of object.

3.1 Galaxy content

Lenticular systems generally have very red (Johnson) colours almost indistinguishable from those of elliptical galaxies (de Vaucouleurs (1977a), Sandage and Visvanathan (1977)),

particularly the bulge component (Griersmith et al. (1982)).

Lenticular galaxies display a further similarity with elliptical systems in that they have gas and dust contents much lower than spiral galaxies of later morphological type. The visually obvious shortage of dust, in the form of prominent absorption lanes, has been known since the first revisions of the Hubble classification scheme (Sandage (1961)), and the low hydrogen (HI) abundance has been confirmed since the first radio surveys (e.g. Roberts (1971)). The radio observations have been complemented by spectroscopic surveys, generally employing forbidden oxygen ([OII], 3727 A) as a tracer of gas content, which also demonstrate the systematic trend of increasing gas content along the Hubble sequence from elliptical to late-type spriral (e.g. Morgan and Osterbrock (1969)).

3.2 Galaxy Structure

Lenticular systems are defined (e.g. Sandage (1961)) as recognisable disk galaxies which exhibit no obvious trace of spiral structure, in contrast with all other disk systems which are primarily classified on the prominence, openness and resolution displayed by these features (e.g. Hubble (1936), Sandage (1961)). Excluding the absence of spiral arms, lenticular systems appear to have similar disk structure to that of spiral galaxies (Freeman (1970)). The more modern analyses of Boroson (1981) and Burstein (1978) indicate that subtle, but significant, differences may exist between the disks of lenticulars and spirals, although the old-disk stellar population

distributions may be very similar for spiral and lenticular systems (Boroson et al. (1983b)). In addition, Dressler (1980) contends that the bulges of lenticular systems are absolutely larger and more diffuse than those of normal spirals, although the intrinsic scatter in the extracted parameters (Davenhall (1984a)) makes analysis difficult. More significantly, Dressler and Sandage (1983) find clear evidence that the bulges of lenticular systems rotate far more rapidly than those of normal spiral systems. Several authors (e.g. Yoshizawa and Wakamatsu (1975), Burstein (1979b), Dressler (1980) and Boroson (1981)) have convincingly demonstrated that the luminosity ratio of the Bulge and Disk components (hereafter termed the 'Bulge to Disk' ratio) is generally much larger for lenticular galaxies than for spiral systems, indicating the dynamical dominance of the bulge component in lenticular galaxies.

3.3 Galaxy Distribution

Numerous authors (e.g. Oemler (1974), Davis and Geller (1976), Dressler (1980) and Sadler and Sharp (1984)) have also demonstrated, beyond reasonable doubt, that lenticular (and elliptical) galaxies are found preferentially in clusters of galaxies rather than in low density environments. The implication naturally arises that these galaxies are the end products of processes operative with an efficiency dependent on local density. Since the population ratio of lenticulars to spiral systems also increases with local density the further suggestion, namely, that lenticulars are formed by some modification of normal disk systems, naturally follows.

I - 4 Observational Arguments For and Against Environmental Modification

Introductory Remarks

The dramatic resurgence in the past decade of theoretical interest in theories of galaxy formation and evolution has been matched by a similar burgeoning of observational research in the field. Unfortunately, as outlined in section I - 3, this has resulted in a plethora of contradictory analyses fuelling debate over the fundamental question of whether the environmental modification of galaxies has been ubiquitous or unimportant in previous epochs. An exhaustive critique of all the available work is clearly beyond the scope of this section, but a synopsis of the most fundamental and relevant evidence will be presented (see also e.g. Bothun (1981), White (1982), Kormendy (1982), Dressler (1984) and Haynes et al. (1984)) together with some concluding remarks.

4.1 Modification by Inter-Galaxy Interactions

Direct observational evidence of collisional merging is presented by Schweizer (1980, 1982) in which NGC 7252 and 1316 are presented as candidates of on-going or recent mergers. Malin (1979) and Malin and Carter (1980) have presented observations of large-scale low-luminosity shells surrounding a substantial fraction of a sample of isolated and apparently normal elliptical galaxies. These shells may consist of stars

(Carter et al. (1982)) and represent the remnants of a merger between an elliptical and a disk galaxy.

Indirect evidence for the formation of ellipticals by collisional merging is also presented in the statistical treatment of Faber and Gallagher (1979) and has been mentioned in section 2.1.

The most serious objection to this scheme of collisional merging to form elliptical systems is provided by the general continuity of the properties of elliptical systems over the entire range of observed luminosity, which is about four orders of magnitude. Size, colour (Visvanathan and Sandage (1977)), metallicity (Faber (1977)), and central velocity dispersions (Faber and Jackson (1976), Tonry and Davis (1981)) all appear to scale, to first order, with luminosity, but dwarf ellipticals cannot form by merger because the required encounter velocities are implausibly high (Kormendy (1982)).

Moreover, Harris (1981) points out that ellipticals have a much higher number of globular clusters per unit luminosity than late-type spiral systems; unless globular clusters are a by-product, merging cannot be responsible for the formation of elliptical systems.

This objection may be weakened, particularly for prominent central systems, by the numerical simulations of Muzzio et al. (1984) which indicate that the larger cluster systems gradually denude smaller galaxies of their globular clusters by tidal interaction.

The observational evidence for tidal interactions between cluster members seems somewhat contradictory, since both an enlargement or a reduction in galaxy size can be ascribed to tidal effects (Kormendy (1980)). The tidal distension of the outer parts of Virgo ellipticals with close companions is reported by Kormendy (1977), whereas Strom and Strom (1978a,b,c,d,e) convincingly demonstrate that ellipticals observed in dense environments are generally smaller than those of equivalent luminosity found in less-dense spiral-rich clusters. Moreover, they present evidence that a similar size gradient is observed for the ellipticals within the dense clusters as a function of radial distance (and thus local density), and for lenticular galaxies in the Coma cluster.

Further optical evidence for the truncation of disks is provided by Peterson et al. (1979), who report that Virgo spirals are ~20% smaller at a given luminosity than those of Holmberg's (1958) sample.

The body of evidence presented by Strom and Strom is certainly highly suggestive, but it must be borne in mind that the technical difficulties of photographic surface photometry are considerable (see Chapters 2 and 3), particularly for objects of small angular extent. Furthermore, the data display considerable scatter in the results, some of which is almost certainly intrinsic to the populations studied.

Tidal interaction between galaxies may also produce gas depletion

of the smaller 'victim'; Appleton (1983) presents radio and optical observations which he interprets as showing the tidal distortion of the companion galaxies UGC 6956 and 6922 by the more massive lenticular NGC 4026, and in particular that UGC 6956 is being stripped of gas.

Possibly the most compelling evidence for the existence of dynamical evolution via galaxy-galaxy interaction is provided by the class of bright elliptical galaxies surrounded by an extensive outer envelope which are found in some clusters. These systems are termed cD galaxies (for historical reasons) and have been the subject of a great deal of study over the past two decades. The kernel of the surrounding debate has been whether cD galaxies are merely the brightest members of the cluster luminosity distribution or the products of their environment. The consensus which has emerged is based upon three key observations. Firstly, those cD galaxies with the more extreme properties (i.e.: the largest and most luminous) are never found in field density environments, but always in clustered surroundings. Secondly, these objects are located very close to the local density maxima (Oemler (1974), Leir and van den Bergh (1977), Beers and Geller (1983)) and very often exactly in the centre of an X-ray emitting ICM (Jones et al. (1979), Jones and Forman (1982)). Thirdly, a substantial fraction of cD galaxies are observed to have multiple nucleii (Hoessel (1980)), whereas other bright ellipticals display this phenomena far less frequently.

However, although the evidence for galactic 'cannibalism' - in

which cD galaxies grow by destroying their smaller neighbours via tidal stripping and dynamical friction - seems well-established, it may be argued that this process is irrelevant to the evolution of most galaxies: many clusters are not dominated by a central galaxy or ICM, and many galaxies within a dominated cluster should have orbits precluding interaction with the cluster core. The heirarchical clustering scenario predicts earlier generations of smaller clusters with higher interaction rates, but presumably only a few groups coalesce since clusters are generally dominated by only one system. Galactic 'cannibalism' cannot have been spectacularly effective as we do not observe cluster-mass amorphous systems. In addition, X-ray observations of clusters have been interpreted (e.g. Canizares et al. (1979), Fabian et al. (1981), Stewart et al. (1984)) as showing widespread evidence for cooling flows of ICM gas at the centre of the cluster. The deduced mass infall rates vary between approximately 10 - 400 $M_{\odot}$ per year, which could build a massive central object (such as a cD galaxy) well within a Hubble time without recource to dynamical interactions. This scheme is attractive, but optical observations do not indicate strong star-formation in cD systems, and a very substantial modification of the initial mass function of star-formation is required to preserve the gas-infall model (White (1982)).

4.2 Galaxy-Environment Interactions

Within the last few years, the first direct observational evidence for the gas depletion of several individual galaxies by a hot ICM has been presented by several groups of investigators.

Longmore et al. (1979) present a comprehensive radio and optical investigation of NGC 5291 which reports the presence of $\sim 10^{11} M_{\odot}$ HI extending up to 100 kpc from the main body of the galaxy in association with emission-line optical knots. An explanation in terms of galaxy-galaxy interactions is demonstrated to be implausible and the observations are explained in terms of a massive gas-rich disk system undergoing compression and gas sweeping by an ICM.

Sullivan et al. (1981) present radio observations of the disk system UGC 6697 which display an unusual 'head-tail' morphology; they further note that the galaxy is optically distorted along both major and minor luminosity axes, has very blue colours, and shows [OIII] emission lines indicating high excitation. X-ray observations indicate a large ICM density gradient coincident with the radio emission, and the situation is interpreted by Sullivan et al. as the on-going gas depletion of UGC 6697 via ICM interaction with associated shock-induced star-formation.

Shostak et al. (1982) have examined the peculiar Sb galaxy NGC 1961 and observe the radio continuum and X-ray emission coincident with the distortion of optical structure. The data is convincingly interpreted as the on-going stripping from this massive galaxy by an ICM of temperature $\sim 10^7$K and density $\lesssim 10^{-3}$ cm^{-3}.

The X-ray observations of the Virgo cluster core reported by Forman et al. (1979) showed that the elliptical galaxy

NGC 4406 (M86) displayed unusual source characteristics; further analysis by Fabian et al. (1980) confirmed that the most plausible explanation was ram-pressure stripping by the ICM at the centre of the cluster.

Further graphic evidence of the environmental modification of galaxies in the Virgo cluster is provided by Kotanyi end Ekers (1983) and Kotanyi et al. (1983) who present X-ray, optical, and radio observations of the peculiar disk galaxy NGC 4438. The optical morphology of NGC 4438 shows severe distortion of the outer regions (e.g. Arp (1966)) with a ridge of dust West of the nucleus which coincides with the reported maxima of both the radio and X-ray emission. Tidal interactions with its nearest neighbours, NGC 4435 and 4406, are discounted as causes of the distortion because of the lack of counter-tide damage (e.g. isophotal twisting) displayed by these systems and the high relative velocity of NGC 4435. Once again, the most plausible mechanism responsible for the gas displacement is shown to be interaction with the ICM. NGC 4438 is also studied by Chincarini and de Souza (1985) who present a rotation curve and H_{α} imagery. They interpret various H_{α} features as strongly suggestive of a bow shock generated by the galaxy motion through the ICM and associated shock-induced star-formation. The characteristic shock parameters are calculated and the model shows very good agreement with the observations. (NGC 4438 is discussed in more detail in section I - 5 and Chapter 4).

X-ray observations of the cluster A1367, which is morphologically similar to Virgo, are presented by Bechtold et al. (1983), who report several galaxies with hot X-ray coronae near the cluster

core which itself displays X-ray emission signifying a hot ICM. All the X-ray galaxies which also have radio observations display HI deficiency, indicating that the normally cool disk gas is being heated and removed by ICM interaction. Bechtold et al. also calculate that there is more gas in the ICM than can readily be accounted for via depletion of the cluster population, implying that much of it must be of primordial origin (i.e. left over from cluster formation).

Thus the evidence for the environmental modification of some galaxies, particularly gas-rich disk systems, via interaction with an ICM appears well-established, and provides strong circumstantial support for the production of lenticular systems from normal spiral progenitors.

However, several authors have amassed an equally imposing body of observational evidence to argue against this conclusion. Dressler (1980) argues that the bulges of lenticular systems are intrinsically larger than those of normal spiral systems, whereas no difference should be observable if spirals are swept of gas via ICM interactions. The bulge should also be the most dynamically resistant component to tidal disruption, so this evidence argues against any external agency being responsible for the production of lenticulars. Furthermore, as mentioned in section I - 3, numerous authors (e.g. Yoshizana and Wakamatsu (1975), Burstein (1979b), Dressler (1980) and Boroson (1981)) have demonstrated that the Bulge: Disk luminosity-ratio distribution for lenticulars is very different to that of spirals, so lenticulars have far more dominant bulges.

Farouki and Shapiro (1980) conclude that ICM-galaxy interactions cannot appreciably alter the Bulge:Disk ratio, so if lenticulars are formed from spirals, where are the stripped late-type spirals ?

To explain this dearth of small Bulge:Disk ratio lenticulars, Kent (1981) proposed that disks could fade after sweeping due to the termination of star-formation, but comparison of the observed luminosity functions of lenticulars and spirals fails to support the disk-fading model (Bothun (1982), Dressler (1984)).

Boroson et al. (1983b) report that the near-infra-red characteristic disk parameters of spiral and lenticular populations in the Virgo cluster are very similar, and conclude that this is strong evidence against 'congenital' environmental modification (e.g. Larson et al. (1980)).

Lastly, Sandage and Visvanathan (1978) conclude from a substantial body of observational data that the colours of lenticular systems in clusters are indistinguishable from those in low-density environments, some of which are unlikely <u>ever</u> to have been in an environment where ICM interactions could be important.

Once again, although the case for some environmental modification by galaxy-ICM interactions seems proven, argument centers over the importance of this process in the evolution of the majority of galaxies.

Supplementary Evidence

In addition to searches for observational evidence favouring some particular mechanism of modification, considerable effort has been made to assess the general properties of cluster populations for signs of environmental modification without particular regard for the mechanism involved.

4.3 Cluster Luminosity Functions and Population Ratios

The cluster luminosity function (hereafter CLF) is defined as the population distribution as a function of luminosity for a volume-limited sample (to minimise Malmquist bias). Clearly, the mechanisms of environmental modification outlined in section I - 2 should produce some evolution of the CLF, and one might expect to observe CLFs related in some way to cluster morphology. Moreover, since adiabatic-perturbation models of the Universe predict that galaxies form in an already structured environment, some initial variation of CLFs as a function of environment might be expected. Both those predictions are apparently refuted by observations (e.g. Austin et al. (1975), Schechter (1976)) which demonstrate that CLFs show remarkably little variation, even between very-different local-density environments, and display some characteristic luminosity above which the abundance of galaxies falls rapidly with increasing luminosity, and below which the number distribution is relatively flat.

The homogeneity of CLFs has, however, been weakened by subsequent investigations of rich clusters (e.g. Dressler (1978) and

numerous contributions from the Oxford group of researchers: Austin and Peach (1974), Austin et al. (1975), Godwin and Peach (1977), Bucknell et al. (1979), Carter and Godwin (1979) and Godwin and Peach (1982)). These investigations show some CLFs to have high gradient at high luminosities (i.e. the number of luminous systems falls rapidly with luminosity) and others with a much lower gradient than the average; the slope at low-luminosity also displays considerable variation, and for some clusters is quite flat considerably below the characteristic luminosity. These differences may be correlated with the cluster morphology and population ratios (Thomson and Gregory (1980)), and are suggestive of environmental modification via galaxy-galaxy interaction (Dressler (1984)).

The population ratios of 55 rich clusters were analysed by Dressler (1980) who confirmed the well-known relationship between local density and morphological type (i.e. the richer clusters have higher proportions of elliptical and lenticular systems), but presents three arguments against the environmental modification of disk galaxies. Firstly, the relation between local density and cluster population is so slow that a considerable fraction of lenticulars are observed in low-density environments where interaction mechanisms should have little power. Secondly, the relationship between local density and cluster population appears very similar in clusters of very different morphology (i.e. independent of cluster concentration). Lastly, the absolute sizes of lenticular bulges and bulge:disk luminosity ratios are larger than those of normal spirals in all density regimes. (This final point has been mentioned in section

I - 3 and will be discussed in more detail later in this section.) Dressler goes on to interpret the data as supportive of a long time-scale for disk formation and the truncation of disk development via proto-galaxy interactions as envisaged by Larson et al. (1980).

Dressler's analysis has been challenged by White (1982) who criticizes the technique used to calculate the local galaxy density and reiterates the point that the currently observed environment of lenticulars may be irrelevant in many cases if modification occurred in previous epochs when conditions were very different. Secondly, White maintains that a significant dependence of the population density with cluster morphology and X-ray emission is contained in Dressler's data. Furthermore, Wirth and Gallagher (1980) convincingly demonstrate the vulnerability of photographic morphological classification to systematic error, which must cast doubts on the accuracy of the population ratios determined in Dressler's study. Dressler's conclusions appear somewhat weakened, and to rest in particular on his third line of argument: structural differences between lenticular and spiral galaxies.

4.4 The Hydrogen Content of Cluster Populations

Attempts to compare the hydrogen content of cluster populations with the hydrogen content of field galaxies began over ten years ago (Davis and Lewis (1973)) but recent years have seen a spectacular growth in the amount of observational material available, (see e.g. Haynes et al. (1984) for a review) and this area of research provides perhaps the most compelling evidence for the environmental modification of galaxies, although controversy still exists (c.f. the conclusions of Kennicutt et al. (1984) and Giovanelli and Haynes (1985). A significant proportion of the investigations have concentrated on the Virgo cluster and have been published during the completion of the survey described in this thesis, which is especially fortuitous.

The hydrogen gas content of galaxies is primarily determined by radio observations (λ: 21 cm) measuring the flux and distribution of the neutral gas, which might typically comprise half of the interstellar medium of the target galaxies. The observed HI content can be compared with optical colour or associated with parameters such as luminosity or optical diameter to try and formulate distance-independent ratios (e.g. M_H/L or M_H/D^2); formulae have been defined (e.g. Sullivan and Johnson (1978)) to compare cluster and 'control' samples. All these procedures are fraught with difficulties, (see e.g. Bottinelli and Gouguenheim (1974), Bothun (1982) and Dressler (1984)) and care must be exercised in their application and subsequent statistical analysis. Despite these problems, the

weight of observational evidence for the deficiency of hydrogen gas in cluster disk systems with respect to field disks, regardless of the particular analysis employed, is forcing concensus and acceptance of the data.

The HI-deficiency of galaxies in the core of five out of the ten best-studied clusters seems well-established, and these are: A1656 (Coma) and A1367 (Sullivan and Johnson (1978), Sullivan et al. (1981), Chincarini et al. (1983a,b)), A2147 (Schommer et al. (1981), Giovanelli et al. (1981) and Giovanelli and Haynes (1985)), A262 (Giovanelli et al. (1982)) and Virgo (discussed below in more detail).

All these five systems have extended X-ray sources associated with them, whereas the clusters with no reported deficiency such as Cancer, Pegasus I or ZW 1400 + 0949 (e.g. Chincarini et al. (1979), Schommer et al. (1981), Giovanelli et a l. (1981), Bothun et al. (1982), and Kennicutt et al. (1984)) are 'X-ray quiet' (Giovanelliand Haynes (1983)). Giovanelli and Haynes (1985) intercompare the data on the HI-deficient and non-deficient clusters and further suggest a relationship between the fraction of HI-deficient systems in a cluster and the cluster X-ray luminosity, in the sense that the most X-ray luminous clusters (i.e. those with the most substantial ICM) have the largest fraction of HI-deficient galaxies. In addition, three of these clusters: A262, 1656 and 2147 display HI-deficiency as a function of radial distance from the cluster core, in the sense that central systems are the most deficient (Haynes et al. (1984) and Giovanelli and Haynes (1985)).

The Virgo cluster is a particularly favourable target for radio astronomers because its relative proximity allows complete samples to be made to quite faint magnitudes, even for early-type systems of low gas content; this proximity also facilitates the resolution of detected sources, permitting the sizes of gaseous disks within the cluster to be studied. These opportunities have resulted in a host of investigations of generally increasing sophistication (Davis and Lewis (1973), Huchtmeir et al. (1976), Krumm and Salpeter (1979a,b), Charmaraux et al. (1980), Giovanardi et al. (1983a,b) and Giovanelli and Haynes (1983)) which have demonstrated three important results. Firstly, a substantial fraction of the Virgo population is significantly HI-deficient with respect to control samples; secondly, detection/non-detection statistical analyses indicate that early-type galaxies are more deficient within 6^{o} of the cluster centre; lastly, the sizes of HI-disks are generally smaller near the cluster centre than in the outer regions (see e.g. Haynes et al. (1984) Fig. 5).

The results of these radio surveys of the neutral hydrogen content have been complemented by optical studies of the ionised gas content of Virgo systems. Stauffer (1983) finds that there is no difference between the H_{α} + [NII] emission line strengths of a sample of the Virgo population and a control sample. He also shows that many of the HI-deficient Virgo spirals have red optical colours consistent with gas depletion more than about 10^{9} years ago, although several blue HI-deficient candidates for

recent depletion are reported. This work is complemented by that of Kennicutt (1983) who measured the H_α + [NII] flux from the entire disk of spirals in Virgo, and showed that those systems within 6^o of the cluster centre had lower H_α + [NII] luminosities than those further from the cluster core. One may deduce from the results of Stauffer and Kennicutt that the depletion mechanism is preferentially operating on the outer parts of the disks of those spirals near the cluster core, exactly as expected for galaxy-ICM interactions (see section I - 2). Gisler (1978) reaches a similar conclusion from an archival survey of galaxy spectra, in which he finds that the observed frequency of nuclear emission lines is far lower in dense clusters than in the general field.

However, Kennicutt (1983) goes on to argue that the observed properties of Virgo spirals are identical with field galaxies of slightly earlier type, and concludes that recent rapid gas depletion is unlikely. He cites the most extreme examples of this dilemma, NGC 4571 and 4689, as galaxies with the morphology of late-type spirals but less than half the normal HI content, half the normal H_α emission and redder optical colours. It is interesting to note that examination of photographs of these systems reveals highly complex spiral structure reminiscent of flocculent spirals, and which may be a signature of shock-induced star-formation (Kormendy (1982)). Thus these galaxies may have an optical morphology consistent with a recent mild environmental interaction which triggered global star-formation rather than removing the gas. This suggestion could be tested by inspection of high-resolution I-band images as the flocculent spiral pattern

appears to have a less pronounced red stellar component than the 'global' spiral pattern attributed to density-wave theory (Kormendy (1982)).

Although the evidence for the environmental modification of the HI content of several cluster populations (particularly Virgo) with a substantial ICM is convincing, it is by no means clear that this vindicates the conclusion that lenticulars are environmentally 'processed' spirals. The problem is that the observed gas deficiencies are relatively modest (typically less than a factor of five), whereas the lenticulars are typically over twenty times more deficient. The relative absence of intermediate deficiencies is embarrassing; it may be partially due to selection effects and difficulties in measuring the low gas content of early-type systems, but a more convincing explanation is probably required.

Concluding Remarks

Unfortunately, observational evidence can be presented in favour of almost all the theoretical mechanisms for depleting the gas content of those disk galaxies unfortunate enough to reside in crowded surroundings. Although the evidence is mainly circumstantial, it may be enough to 'convict' the environment as guilty of some modification of cluster populations, and it is worth examining in detail the main arguments against modification in order to try and assess how ubiquitous the effects may have been.

The apparent 'universal' nature of CLFs may indicate that the processes determining galaxy luminosity are relatively insensitive to local conditions of density, temperature and turbulence at the time of formation (or the conditions of formation for all galaxies were very similar) and that environmental processes do not have gross effects on the luminosity population distribution over the observable timescale. Thus the evolution of a gas-depleted disk system will certainly be to optically redder colours, but it may not dim drastically enough to distort the CLFs more than the observed differences mentioned in the previous sub-section. Galaxy mergers may be as yet similarly incapable of boosting large galaxy luminosities (at the expense of their smaller neighbours) to distort the CLFs. (These competing mechanisms also distort the CLFs in approximately opposite senses, which may further reduce apparent evolution of the CLFs).

The idea that the conditions of galaxy formation may be irrelevant to its currently observable luminosity may not be such a surprising result as there are only two types of grossly dissimilar galaxies produced in any case: one-component systems (ellipticals) and two-component systems (bulge plus disk galaxies). One can argue that bars are relatively easily produced in numerical simulations of disks and that these can drive the evolution of many other morphological features (see Kormendy (1982) for a detailed discussion), including spiral structure.

The observation that population ratios are a very slow function of local density, and that many lenticulars are found in the low-density field, is certainly strong evidence for the production of some of these systems via internal gas-removal processes or birth-defect scenarios. However the residual correlation of population ratios with both cluster morphology and X-ray emission (together with the mass of evidence in favour of modification) suggests that some galaxies, and particularly lenticulars, are indeed the product of their environment.

The strongest arguments which remain to refute the production of lenticular systems from normal disk systems are those based on the structural differences of the luminosity components. Dressler's (1980) result that the bulges of lenticulars are absolutely larger than those of spirals is based on a technique of visual estimation; since the determination of luminosity component parameters is inherently complex even with well-determined luminosity distributions (see e.g. Kormendy (1982)), Dressler's subjective data must be viewed with scepticism because of the difficulties involved in disentangling the contributions of the luminosity components. Apart from Dressler's visually-estimated data very little photometric data is available, the most relevant being that of Burstein (1979b), and hence one has the usual problem of selection effects and the attendant dangers of erroneously extrapolating conclusions to much larger populations.

The observation that lenticulars have much more dominant bulges than most spiral systems is much more definitely established, but may simply reflect a very long formation time for disk components. If early-type spirals completed their disk formation long ago, some of them could be swept of gas to form large Bulge:Disk ratio lenticulars; if the late-type spirals (with more prominent disks) have only recently finished forming then dynamical depletion processes will have had little opportunity to work upon them as yet.

Evidence in favour of cluster lenticulars being made up of both congenital and environmentally-processed populations is still tentative, mainly due to the subtlety of observational differences between the end-results.

Bothun (1982) reports that a population of small bulge:disk ratio lenticulars may be observed in the core of the Coma cluster, which would represent unequivocal evidence for the production of some lenticulars from spirals, at least in very-dense environments.

Pacheco et al. (1983) analyse the flattening distribution of galaxies as a function of environment, and find an excess of flat lenticulars in regions of high local density. Their interpretation of such systems as gas-depleted Sa galaxies is certainly intriguing, and will be compelling evidence for widespread environmental modification if confirmed.

I - 5 Aims and Objectives in the Observational Programme

It is clear from the previous section that lenticular galaxies provide a critical test of the power of environmental modification: if many lenticulars can be shown to be 'processed' spirals then we can expect the majority of any cluster core population to have been influenced by the external agencies listed in section I - 2.

The Virgo cluster is generally thought to be a dynamically unevolved cluster in the early stages of collapse and virialization (e.g. Forman and Jones (1982)), representative of the environment experienced by a substantial proportion of all observable galaxies. In addition, it seems to have: a well-defined core containing a population of ellipticals and lenticulars in close proximity with an X-ray emitting ICM, indications of widespread gas depletion of disk systems, and several candidates for on-going dynamical interaction. An examination of the available literature in 1981 suggested that a detailed photometric survey of all the lenticulars in the inner core of the Virgo cluster would provide an excellent opportunity to discriminate between "intrinsic-formation" and 'modification' theories for the production of these systems.

The observational programme undertaken was constrained to be one that could be realistically undertaken during the tenure of an S.E.R.C. research studentship with the facilities available to U.K. astronomers. A conscious decision was made at the outset to make the fullest possible use of national facilities to maximise

the time that could be devoted to the production of the survey. The development of a common-user reduction and analysis package for photographic photometry, as part of the STARLINK programme, together with the availability of excellent photographic material for the United Kingdom Schmidt Telescope Unit, and a reliable computerized microdensitometer at the Royal Greenwich Observatory, naturally suggested a programme of photographic surface photometry; the practical techniques were already familiar to the author from undergraduate studies at St. Andrews University.

Detailed inspection of the inner Virgo cluster core (defined for this work as within 3^{o} of the cluster centre, i.e. the inner half of the HI-deficient core) revealed 15 systems of interest which were suitable for analysis: NGC 4267, 4371, 4377, 4419, 4425, 4429, 4435, 4438, 4459, 4461, 4474, 4477, 4503, 4531 and 4550, which were classified as lenticular systems by de Vaucouleurs et al. (1976) (or appeared to meet the classification criteria) and were listed as probable members of the cluster by de Vaucouleurs (1961). Two additional systems were also selected: NGC 4501 is the brightest normal spiral in close proximity to the cluster centre, and NGC 4552 is classified as lenticular by Sandage and Tammann (1981) and has anomalous low surface brightness features described by Malin (1979).

In order to maximize the usefulness of the survey it was decided to attempt photometry of each of these 17 systems in three colour passbands (Johnson B, R and I) and to present luminosity profiles, isophotal maps and standard luminosity parameters for

each system in each passband. This was felt to be the largest amount of reduction and analysis that could be undertaken in the time available.

The principal aim of this survey was to provide, for the first time, high-precision photometric data on all the lenticulars in the inner core of a cluster in the early stages of dynamical evolution, and to enable the evaluation of the properties of the class as a whole by comparison with previously published observations of disk systems of later morphological type. The survey would also provide the first absolutely-calibrated 'R' and 'I' photographic photometry of lenticular systems, and thus make available the first wide-baseline colour profiles of early-type disk galaxies (see Chapter 4 for a further discussion).

If evidence for the environmental modification of these lenticulars from normal spirals emerged from the analysis, then this would provide clear evidence that dynamical processes were important in determining galaxy evolution from early epochs since Virgo is relatively unevolved. If the structural differences reported by Dressler (1980) were confirmed, then it could be convincingly argued that environmental influences are probably not yet significant modifiers of galaxy evolution, since the majority of observable galaxies inhabit environments of similar, or lower, local galaxian density.

CHAPTER II

PROCEDURES FOR DATA REDUCTION AND ANALYSIS

II - 1 Programme Data-Base

The United Kingdom Schmidt Telescope Unit (UKSTU) at the Royal Observatory of Edinburgh (ROE) provides a nationally available facility optimized for photographic survey projects which do not require a small platescale. The United Kingdom Schmidt Telescope, located on Siding Spring Mountain near the Anglo-Australian Telescope, is of classical Schmidt design. Functioning as a Schmidt camera it has the following parameters:

Telescope Focal Length:	3.07 metres
Primary Mirror Diameter:	1.83 metres
Photographic Aperture (Diameter):	1.24 metres
Photographic platescale:	67.12 arcseconds per millimetre
Plate size:	356 x 356 millimetres
Plate field:	6.4 x 6.4 degrees

All photographic plates are processed in a standard procedure: an automatic plate-rocking machine is used for developing, followed by a stop bath, two fixer baths using nitrogen bubble-burst agitation, rinse, hypo-clearing agent, wash and photoflo. The plates are then dried in a laminar flow of filtered air.

The system is designed to yield highly uniform processing results with minimal ageing effects of the plate emulsion.

As mentioned in Chapter 1, the survey was intended to cover the three Johnson passbands B, R and I, and so three sky-limited plates were obtained from the UKSTU with their centres close to the centre of the Virgo cluster at R.A. = 12^{H} $25^{M}.4$, DEC = $+12^{o}$ 40' (Van den Bergh (1977)). The 'B' plate (B 7675) was formed from an exposure through a GG 385 filter on to IIaO emulsion, the 'R' plate (R 4891) from the combination of an RG 630 filter and IIIaF emulsion, and the 'I' plate (I 6867) was formed from the combination of an RG 715 filter and IV - N emulsion.

Unfortunately, the long exposure 'R' plate, obtained by the UKSTU especially for this project, was marred by an extensive emulsion flaw which probably resulted from a manufacturing error. The loan of an older UKSTU 'R' plate (R 4891) from the A.P.M. unit of the Institute of Astronomy at the University of Cambridge was kindly arranged by Dr. G. Stewart.

The Relative Intensity calibration of the UKSTU photographic plates is obtained from two uniformly-illuminated stepwedges projected on to each photograph through the filter used for the exposure. The projector bodies themselves mask off the region of plate onto which the calibration marks are impressed, ensuring an area of otherwise clear plate. This follows the universal practice which guarantees that there is no contamination from stars or nebulae and the calibration will be well determined to a

level below the lowest sky density on the plate. The calibration illumination is automatically switched on and off when the telescope shutter is opened and closed, ensuring that the calibration exposure is equal to the plate exposure and made under identical conditions of temperature and humidity. These arrangements make sure that the calibration impressed represents as nearly as possible the true Density/Intensity transformation appropriate for the entire photographic plate.

The 'B' and 'I' plates (B 7675 and I 6867) were calibrated with both a seven-step projector (North edge of field) and a sixteen step Kitt Peak National Observatory (KPNO) type projector (South East corner). The seven-step projector provides a strip arrangement of steps, with illumination from tungsten filament bulbs. The KPNO projector provides sixteen steps arranged in a square, with illumination from a Quartz-Halogen lamp through a BG 34 colour correction filter. The older 'R' plate (R 4891) was calibrated by two seven-step projectors as it predates the installation of the KPNO device on the telescope.

Full details of the UKSTU, concerning plates, developing procedures, hypersensitizing techniques and so forth are detailed in the UKST Handbook published by the ROE.

II - 2 Scanning Procedures

The digitization of the density information available on each photographic plate was performed using the PDS microdensitometer at the Royal Greenwich Observatory (RGO). The details of this computer-controlled microdensitometer have been reported many times (e.g. Davies (1981)), and so only a summary will be presented here.

The density or transmission of areas on a photographic plate is measured by passing illumination from a Quartz-Iodine lamp through the selected apertures, the photographic plate and on to a photomultiplier tube. The output from this PM tube is digitized and sent to the controlling computer, a Digital Equipment PDP 11/34. The density range that can be accommodated is approximately 5.0 which corresponds to an encoded digital range of 4096 units.

An extensive range of options is available to a user via FORTH command procedures which are detailed in the PDS Users Manual, available from the RGO. In particular, the user may interactively specify the following: the co-ordinates of areas to be scanned, the number of pixels in the X and Y directions of scan, the pixel separation, scanning speed and the eventual data storage medium (which is usually nine-track magnetic tape).

The level of light reaching the PM tube is governed by selecting neutral density filters, mounted in two filter wheels, at the start of each scanning session. The output of the Quartz-Iodine

lamp is continuously monitored throughout the scanning session. The humidity and temperature of the room housing the PDS microdensitometer and associated hardware is controlled by a filtered air-conditioning system.

Small periodic variations in measured density reported previously by some users (e.g. Penny (1982), Curry (1982)) have been traced to the cycling period of the air-conditioning system. Modifications to the system had been introduced before the current programme was undertaken and no evidence for periodic density variations has been found on any scan array (hereafter referred to as 'frame') obtained for this work.

For the sake of uniformity, and subsequent advantages in the data-reduction procedures, every programme galaxy on each photographic plate was scanned using a 24 micron aperture and a 24 micron stepsize between pixels, with each frame consisting of 512 rows of 512 data points. Thus each frame contained 262,144 information pixels. The choice of pixel size is nearly identical to the optimum value for Schmidt plates calculated by Okamura et al. (1982). The frame size was sufficient to ensure that each programme galaxy image was surrounded by a large region of sky.

Following Blackmann (1982), the scanning speed adopted was 20 PDS velocity units (or 4.7 millimetres per second) in order to avoid the well-known effect (e.g. Fraser (1977)) of high-density smear at scanning speeds that are too high. In fact, this effect is just discernible on the innermost (densest) isophotes of some of

the 'I' passband contour maps, but will have no measurable effect on any luminosity parameters extracted from the frames in this work.

In addition to the sixteen chosen scan fields on each plate, the Relative-Intensity calibration marks impressed on each plate were scanned at the beginning and end of each scanning session in an identical fashion to the galaxy scan fields.

II - 3 Data-Reduction Procedures

As part of the STARLINK programme of developing common-user data reduction facilities available to all U.K. astronomers, the R.O.E. Image and Data Processing Unit (IDPU) has developed a number of routines designed to perform photometric reductions on the digitized images of bright galaxies. These routines form part of the ASPIC set of two-dimensional image-processing programs and may be used in conjunction with these, as appropriate. The routines have been optimized for bright galaxy photometry where the intention is primarily to reduce a relatively small number of detailed images in a meticulous manner. Hence these programs are highly interactive in operation and employ a Sigma Advanced Raster Graphics System (ARGS) for displaying the image frame being reduced.

The ARGS consists essentially of a high-resolution (1024 x 1024) colour monitor plus a controlling computer which can store up to four images and display them in user-defined 'false' colour. The term 'false' colour, as is normal practice, refers to the fact that the colours chosen do not in any way represent the true appearance of the image; the colours are deliberately chosen to represent different ranges of density (or intensity) information and to maximize the image contrast. A user may select from a large variety of ASPIC 'false' colour tables or define one interactively. The colour-graphics facility adds a new dimension to image inspection so that by careful choice of a suitable false-colour table low-contrast image features, which are inconspicuous or invisible to monochromatic inspection, become

clearly discernible.

As with all STARLINK software, the ASPIC routines developed by the IDPU are written in Vax-specific FORTRAN-77, which means essentially that the programs will run only on a Digital Equipment VAX series computer linked to a sigma ARGS, and thus will not run on alternative computers or drive alternative graphics display systems.

The routines developed follow the general precepts of previous schemes for the computerized reduction of bright-galaxy images pioneered by Jones et al. (1967) and followed by others, such as Benacchio (1975), Godwin (1976) and Okamura (1977). The various stages involved in transforming raw data into a form suitable for analysis are as follows:

1) Removal of Artifacts such as stars or plate defects;
2) Smoothing;
3) Polynomial Background Fitting;
4) Conversion from Density to Intensity;
5) Absolute Calibration of Intensity using available photo-electric photometry.

3.1 Object Removal

An image frame will include many features in addition to the galaxy image, e.g. stars, faint galaxies and nebulae, asteroid or satellite trails and plate blemishes of numerous types. For the

purposes of galaxy photometry, these phenomena are regarded as contaminating the galaxy image and surrounding sky and must be removed before further reductions can proceed. The STAREMASP routine was developed to meet this requirement: the image frame is displayed using an ARGS terminal and object removal is totally interactive.

No automatic removal procedure was used, as these routines always carry the implicit risk of damaging the galaxy image features, as, for example, in the work of Romashin et al. (1983).

Objects that are far from the galaxy image are removed by defining a rectangular-box region around the object and replacing all the data points contained therein by the mean value of a local (user-defined) rectangular patch of sky. Care was always taken to ensure that the local sky regions were large compared with the blemish zone, and uncontaminated by faint stars.

Stars embedded in the galaxy image are removed by defining a circular region around the star and replacing all the data points enclosed with a polynomial fitted to the periphery of the region. Care was always taken to ensure that a realistic substitution was being made, as the choice of aperture size for the circular region surrounding the star is crucial to the success of the replacement. It is equally vital to ensure that only faint stellar images, rather than nebulosities (e.g. HII regions) associated with the programme galaxy, are selected for removal but experience facilitates the visual discrimination between these two classes of objects.

These procedures were repeated until subsequent inspection of each 'cleaned' image frame did not reveal any obviously-undesirable features, at which point the process of object removal was terminated.

3.2 Smoothing

It is desirable to reduce the level of noise in the image frame, particularly at low light levels close to the sky background. A simple smoothing algorithm uniformly applied to the entire image frame would be inappropriate at the high density levels close to the galaxy nucleus where the Signal/Noise level is relatively large because such smoothing would degrade the image quality.

A more sophisticated approach is described by Jones et al. (1967) and discussed by de Vaucouleurs (1976), where the amount of smoothing to which any data point (or 'pixel') is subjected is dependent upon its intensity. Bright pixels close to the galaxy nucleus are unsmoothed, pixels of moderate brightness are subjected to a 9-point smoothing procedure and low-brightness pixels (the faint outer regions of the galaxy and surrounding sky) are subjected to 25-point smoothing.

The smoothing algorithms consist of weighted gaussian grids as detailed below:

9 POINT GRID:

1/16	1/8	1/16
1/8	1/4	1/8
1/16	1/8	1/16

25 POINT GRID:

1/256	1/64	3/128	1/64	1/256
1/64	1/16	3/32	1/16	1/64
3/128	3/32	9/64	3/32	3/128
1/64	1/16	3/32	1/16	1/64
1/256	1/64	3/128	1/64	1/256

These smoothing procedures are implemented in the JONESASP routine, which allows the user interactively to specify the upper thresholds for 9-point and 25-point smoothing appropriate for each image frame. These thresholds were determined for every image frame by the interactive inspection of one-dimensional sections ('cuts') through each image, and the JONESASP routine was applied to each frame individually using the appropriate parameters.

The smoothing operations were carried out on density data rather than intensity data since the noise in Density-space follows a normal distribution, whereas the noise in Intensity-space is generally non-gaussian as the conversion from Density to Intensity is very rarely linear. Thus the use of numerical gaussian-smoothing grids is only rigorously justified in density-space, although in practice (Davenhall (1983)) any systematic errors introduced are usually small.

This type of smoothing technique reinforces faint stellar images and plate blemishes which are previously inconspicuous, allowing them to be identified during subsequent careful examination of the smoothed image frame. All such features were removed using the interactive object-removal procedure (STAREMASP) described previously.

3.3 Background Fitting

The sky background measured on a photographic plate will almost invariably exhibit significant density fluctuations over scales of a few centimetres. The cause of these density fluctuations is usually attributed to variations in the emulsion sensitivity, probably inherent in the manufacturing process. The situation is analogous to the 'flat-field' corrections which must be applied with solid-state detectors, and these density fluctuations must be systematically evaluated and removed from the image frame before data reduction can proceed.

The FITBAKASP routine follows the principles detailed in Jones et al. (1967) where a low-order polynomial is fitted to the surrounding sky background and interpolated across the galaxy image.

The galaxy image frame was displayed using an ARGS terminal, and regions that completely contained the galaxy image were designated; due care was always taken to ensure that a generous margin was left around the faintest discernible extent of each galaxy image. These image regions are excluded from the subsequent fitting process where the remaining sky regions are divided up into cells of interactively specified size, from each of which the median background-density value will be extracted. In this programme, cell sizes were chosen as 32 x 32 pixels for the majority of the image frames, with 16 x 16 pixels chosen for those frames with the largest image zones.

The polynomial fitting order for X and Y co-ordinates is interactively specified and a least-squares fit is made to the cell-centroid co-ordinates and extracted median background-density values. It is essential to use the lowest order polynomial which will fit the background data (Capaccioli and de Vaucouleurs (1983)) in order to avoid instabilities in the interpolation across the image zone. After experimentation, a third order polynomial was found to be optimal and so this order-of-fit was applied to each image frame.

To facilitate evaluation of the fit, contour plots of the fitted polynomial and listings of the fit residuals were automatically

produced, and the best-fitting polynomial was saved as an image frame. Examination of each background polynomial frame excluded any possibility of 'humping' across the interpolated region, which would be symptomatic of the erroneous inclusion of faint-galaxy nebulosity in the background zone.

The best-fit background polynomial frames generally had a low total amplitude, typically corresponding to much less than a 1% variation in density across the galaxy image region, with many of the fitted polynomials being nearly mono-directional (i.e. a simple tilted surface with few irregularities). The total amplitude of the background polynomial frames tended to increase in the sense from 'B' through 'R' to 'I' frames, implying that sensitivity variations are more pronounced as the photographic emulsion becomes more red-sensitive.

3.4 Conversion from the Photographic Density Distribution to a Normalized Intensity Distribution.

The relative-intensity calibration procedures used by the UKSTU have been described in Section II-1 and the fiducial marks impressed on each plate were scanned in the manner detailed in Section II-2. The recommended values of log(Relative Intensity) appropriate for each stepwedge, provided by the UKSTU and detailed in Data Appendix 'J', were used throughout this programme. More comprehensive details of the UKSTU calibration procedures are described in Dawe and Metcalfe (1981).

Each frame corresponding to a scan of calibration marks was displayed, using an ARGS terminal, and the mean density (and standard error on the mean) for each mark was determined interactively using the MEAN routine.

A data file was constructed containing the log(Relative Intensity) values and the uncertainty in these values (provided by the UKSTU) together with the corresponding measured mean step heights and standard errors previously determined interactively.

The CALIB routine allows the user to determine interactively the best-fitting polynomial relation between Baker Density, as defined by de Vaucouleurs (1968) following Baker (1925), and log(Relative Intensity) appropriate for the calibration marks scanned. The CALIB routine accesses the data file previously constructed and also requires the density step per encoder value appropriate for the microdensitometer used (0.0012488 for the PDS) as well as the fog level in encoder units appropriate for the plate in question, as determined in the scanning session.

The user can interactively fit polynomials of arbitrary order to the calibration-spot data points, deleting aberrant points if required, and then display the quality of each fit. The lowest-order polynomial that gave a satisfactory fit to the calibration-spot data values was adopted as defining the transformation from density to intensity. The UKSTU calibration techniques provided similar transformations for all the plates used in this programme, with a third-order polynomial typically giving the preferred fit to the calibration data points. Once a

satisfactory fit was obtained, the polynomial coefficients were stored in a user-defined data file. This file can be used by the DILUT routine to generate a "look-up-table" (hereafter LUT) relating each encoder density value to the appropriate intensity value using the polynomial relationship previously determined.

Each density frame, and associated background density polynomial frame, was then converted to an intensity frame using the CONVERT routine and the appropriate LUT. Division of each intensity image frame by the appropriate background intensity polynomial frame, performed using the DIV routine, produced a 'flat-fielded' intensity frame normalized to the background sky level.

3.5 Absolute Calibration of the Normalized Intensity Distribution.

The final stage of data reduction is the calibration of the relative intensity data to an absolute brightness scale in magnitudes. This was achieved by using the multi-aperture photo-electric photometry available for each galaxy to determine the sky background (in magnitudes per square arcsecond) corresponding to a normalized sky intensity of 1.0. All the available photometry appropriate for each image was collected in a set of data files, each containing a list of aperture diameters (in arcseconds) and the observed brightness of the galaxy (in magnitudes) through each aperture. This photometry is listed in Data Appendix 'J'.

The PECALBASP routine allows the user to interactively determine the value of sky brightness appropriate for each image frame by specifying the data file containing the available multi-aperture data, the stepsize used to digitize the image frame (in microns) and the platescale (in arcseconds per millimetre). The luminosity of the galaxy within circles of radii corresponding to each of the available multi-aperture measures is then computed and compared with the magnitude measured through each aperture.

Although in principle each of the apertures should give an independent value for the frame sky brightness, which could then be averaged together to give a final value, in practice the observational errors in the published photometry preclude this straightforward procedure. Large aperture photometric measures may contain errors due to the inclusion of faint stars in the sky-level determinations, whereas small aperture galaxy photometry often suffers from centering difficulties or only covers areas where the photographic emulsion is saturated. These effects, together with transformation errors in converting older photometry to the standard Johnson system, often produce aberrant values for the sky background determined for some apertures. Such discrepant values can be interactively rejected using PECALBASP, and the best estimate of the sky background can be determined from the remaining apertures.

The crucial hindrance to programmes of galaxy surface photometry is the almost total lack of 'R' and 'I'-band multi-aperture photo-electric photometry currently available in the published literature.

An alternative technique for the determination of the absolute sky background is based upon the existence of faint photometric sequences in the desired image fields (e.g. Feitzinger et al. (1983), Fong et al. (1981), Dixon (1981)). In principle, this technique should allow more accurate determination of the sky background utilizing the higher precision of stellar photo-electric photometry, but in practice the dearth of suitable photo-electric sequences precludes the use of this method.

To alleviate these deficiencies for the 'core' of the Virgo cluster, the author proposed, together with Prof D.W.N. Stibbs, to undertake a programme of Johnson (B, R, I) photo-electric multi-aperture photometry of selected galaxies and to extend and improve some of the photometric sequences of Hanes et al. (1976).

The U.K. P.A.T.T. allocated observing time in April 1983 on the 0.5 m telescope at the S.A.A.O. for the brighter portion of this programme, but due to the pressure of allocations were unable to award time in March 1984 for the completion of the programme. Dr D. Kilkenny of the S.A.A.O expressed interest in this programme and collaborated extensively with the author; the observational procedures and results are detailed in Kilkenny and Malcolm (1984). The multi-aperture photometry obtained in this programme is detailed in Data Appendix 'J', and was subsequently converted from the Kron-Cape to the Johnson 'RI' system following Cousins (1980).

As only the bright end of the sequences could be obtained, the sky background could not be determined from the stellar sequences because there were insufficient unsaturated stellar images available in the image fields. The absolute intensity calibration was done using the available 'R' and 'I' multi-aperture galaxy photometry with the adopted sky brightness for each image frame listed in Table II-1. Those galaxies for which no calibration photometry was available, were awarded the mean of those frames which had a determined sky brightness. As the dispersion of these values can be nearly as much as 0.2 magnitudes from the mean, the sky-brightness levels adopted for those frames with no calibration photometry must be presumed to be similarly uncertain. The standard deviation of the 'B' frames about the mean 'B' sky brightness is 0.07 magnitudes, so the likely error for those frames with adopted 'R' and 'I' sky brightnesses is likely to be less than 0.1 magnitudes, assuming similar dispersions.

With the absolute calibration of the intensity data accomplished, the data reduction stages are complete, and the intensity data is ready for analysis.

II - 4 Data-Analysis Procedures

Once the image frames are in the form of absolutely-calibrated intensity data, "flat-fielded" and normalized to a sky intensity of 1.0, ASPIC data-analysis routines may be used to produce the major and minor-axes luminosity profiles, colour-difference

profiles, equivalent luminosity profiles, standard luminosity parameters and isophotal maps which are the objective of this survey programme.

4.1 Major and Minor-Axes Luminosity Profiles

The standard practice in surface photometry is to extract the major and minor-axes luminosity profiles for each galaxy image, with most workers "folding" the luminosity axes about the centre of the image to produce averaged profiles. This procedure has the advantage of reducing noise in the data and typically produces smooth luminosity profiles even at low light levels far from the galaxy-image centre. However, this may destroy information, if the galaxy image is not closely symmetric, by smearing out local structure in the luminosity profile. Moreover, galaxy luminosity profiles very commonly exhibit 'periodic' variations at low light levels (e.g. Watanabe (1983) Fig. 4 or Bingelli et al. (1984) Fig. 1) which are often asymmetric in origin. These 'periodic' variations may be due to small-scale emulsion sensitivity variations (Blackmann (1982)) or they may represent intrinsic fluctuations in the image luminosity distribution. Only by repetition of the entire data acquisition and reduction procedures on another set of photographic plates could this uncertainty be resolved, but time restrictions on most research projects render this approach impracticable. The "folding" around luminosity axes, regardless of galaxy symmetry, largely circumvents this problem by smoothing out most of the low-light variations in the luminosity profile. However, unlike most elliptical systems, it is an obvious fact that many disk

galaxies are not symmetrical, so the author was prompted to try and preserve the asymmetry of any extracted luminosity profiles by not "folding" the data, following some previous workers (e.g.: Burkhead and Kalowinski (1974) and Blackmann (1983)), and to use alternative smoothing methods to reduce profile noise.

The PRIAXEASP routine was used to extract interactively the major and minor-axes from each image frame using an ARGS terminal. The program allows the interactive determination of the image centre, constraining the major and minor-axes extracted to be perpendicular and to intersect at this point. The program extracts the axes along "pie-slice" sectors, of interactively-specified length, thickness and orientation, with data averaged in circular arcs along the sector. The axes were then interactively inspected to ensure they had been correctly extracted and stored as STARLINK image frames.

The "pie-slice" extraction has the advantage of reducing noise at large radii from the image centre, due to the averaging of additional data pixels, thus making the extracted profile more reliable at faint light levels. Care was always taken to ensure that the "pie-slices" were not so wide as to produce systematic dimming of the extracted major-axis due to the inclusion of pixels far from the major-axis; a sector width of between 5 and 10 degrees was determined as optimal after systematic experimentation.

The extracted luminosity axes were then smoothed in a manner analogous to the technique of Jones et al. (1967) in that the

degree of smoothing used is dependent upon the local signal-to-noise ratio. All profile data points with intensities above the frame sky intensity were unsmoothed; data points with intensities between the sky intensity and 20% of the sky intensity were subjected to a three-point running-mean smoothing, while intensity values between 20% and 2% of sky were five-point smoothed. No data was extracted below 2% of the sky intensity after consideration of both the precision to which the sky background could be determined and the strictures of Capaccioli and de Vaucouleurs (1983). No data was analysed within 4.5 arcseconds of any galaxy image as this regime will be dominated by seeing-convolution effects (Capaccioli and de Vaucouleurs (1983)) for the seeing estimates provided by the U.K.S.T.U. for the plates used in this survey.

An evaluation of the reliability of the extracted luminosity profiles is detailed subsequently in Chapter 3, and the smoothing program "AXES" written by the author is detailed in Data Appendix 'J'. Graphs of the extracted profiles along the major and minor axes are detailed in Data Appendix 'A', with the tabular listings of the profiles given in Data Appendix 'I'.

4.2 The Generation of Colour-Difference Profiles

The extraction of colour-difference profiles from galaxies is complicated by the cumulative effects of noise from each colour profile and uncertainties in the determination of the sky background appropriate for each profile. In view of the

difficulties in producing precise colour-difference profiles, it was decided to follow previous workers (e.g. Strom et al. (1976), Strom et al. (1978) and Boroson et al. (1983a)) and produce 'folded' colour-difference profiles with data points averaged in 'bins' a few arcseconds wide.

The 'COLOUR' program was developed by the author to facilitate the extraction of colour-difference profiles from the extracted luminosity profiles listed in Data Appendix 'A'. The program compares two specified luminosity axes and calculates the colour difference between matching radius values, terminating whenever either luminosity profile falls below 10% of the relevant sky background. The colour profile generated in this manner is smoothed in three-point 'bins', the data folded about the image centre (r = 0) and the final profile written out to an interactively specified file.

A discussion of the colour-difference profiles extracted for this survey programme will be presented in Chapter 4 and the COLOUR program is detailed in Data Appendix 'J'. The extracted colour-difference profiles are shown graphically in Data Appendix 'B' and tabulated in Data Appendix 'H'.

4.3 Production of Isocontour Maps

Absolutely-calibrated isocontour maps of the programme galaxies were generated using the ASPIC MAGCNTASP routine. A user must interactively specify the area of an intensity-normalized image frame for which a map is required using an ARGS terminal. A user

must then specify the absolute sky brightness (in magnitudes per square arcsecond) appropriate for the image frame, the faintest isophote to be contoured and the increment between brightness contours. The routine then calculates the required contours using the standard ASPIC function CONTOUR and produces a hardcopy on the plotter, which at the R.O.E. STARLINK node is a Versatek unit.

In order to produce maps which are easily inter-comparable and free from isophotal "crowding" and extraneous background features, a standard increment of one magnitude between contours was adopted with the faintest isophote extracted being 25^{th} magnitude for the 'B' frames, 24^{th} magnitude for the 'R' frames and 23.5^{th} magnitude for the 'I' frames.

As previously mentioned, the extreme innermost isophotes of some of the 'I' isocontour maps exhibit the phenomenon of high-density "smear" due to the adopted scanning speed being slightly too high for this plate. It is reiterated that this should have no effect on any of the luminosity parameters extracted for this programme.

The 'B, 'R' and 'I' contour maps of the programme galaxies are presented in Data Appendix 'D'.

4.4 The Equivalent Profile and Standard Luminosity Parameters.

The equivalent profile for some galaxy image, following de Vaucouleurs (1962), may be constructed by considering a number of

isophotal levels and calculating the area bounded within these arbitrarily shaped isophotes, including isolated "islands". The equivalent radius is defined for each specified intensity level as the radius of a circle whose area is equal to the area bounded by the isophotal contour being considered. That is,

$$r_i^* = (A_i/\pi)$$

where A_i is the area under the i^{th} isophote, and r_i^* is the i^{th} equivalent radius.

The equivalent profile I(r) can be calculated by simply counting the number of pixels in the image frame above each of a set of intensity levels. At low light levels, the profile will be distorted by the erroneous counting of random sky-noise pixels. The contribution of sky noise at faint light levels to an equivalent profile may be calculated using the technique developed by Blackmann (1979).

In brief, consider a scan containing Z_i pixels enclosing the galaxy image in which a number 'n_i' pixels are detected at some specified faint intensity level. This number will be larger than the true number 'n' due to the erroneous counting of some sky pixels. If one defines:

$$f = (n_i - n) \;/\; (Z_i - n)$$

then if two scans i and j completely enclose the galaxy image, then $f_i = f_j$ = constant if the sky noise is truly random. Hence

Hence one may immediately obtain

$$n = (Z_j\, n_i - Z_i\, n_j) \;/\; (Z_j - Z_i + n_i - n_j)$$

The examination of successively-larger scan areas surrounding the galaxy image allows evaluation of 'f' and hence calculation of 'n'.

Compensation for the effects of random sky noise by this procedure should make the equivalent profile (and hence the total apparent magnitude) reliable to much fainter light levels, as in practice the equivalent profile can be dominated by the effects of random sky noise below 5% of the night-sky intensity (Blackmann (1982)). Blackmann's technique relies on the sky noise being truly random, and may introduce a spurious cut-off in the equivalent profile at very low light levels below approximately 1% of the sky intensity. The random nature of the sky noise in the scan frames processed in this survey programme, was kindly confirmed by Stobie (1982) utilizing Fourier techniques used by the Cosmos unit at the R.O.E.

The EQPROFASP routine allows an ASPIC user to determine interactively the equivalent profile for some normalized-intensity galaxy image using an ARGS terminal. A user may extract the equivalent profile by either simple pixel counting or using the Blackmann sky correction technique, in which case the EQPROFASP automatically terminates the profile calculation if a spurious cut-off at low light levels is detected. A standard procedure was adopted for this programme of

data analysis whereby the equivalent profile was calculated in steps of 0.1 in log(Intensity) down to 1% of the sky intensity, unless automatically terminated due to the detection of the low-light artificial cut-off previously mentioned.

The calculation of the equivalent profile allows the calculation of the characteristic photometric image parameters first introduced by de Vaucouleurs (1948) and described more fully later (e.g. de Vaucouleurs and Page (1962)). The standard definitions of the parameters are as follows:

The integrated luminosity within some given equivalent radius is given by

$$L_r = 2\pi \int_0^{r^*} I(r^*)\, r^*\, dr^*$$

Hence the Total Apparent Luminosity is given by

$$L_t = 2\pi \int_0^{\infty} I(r^*)\, r^*\, dr^*$$

The Relative Integrated Luminosity profile k(r) is defined as the fraction of the total luminosity contained within the radius 'r^*', and so

$$k(r^*) = {}^{L_r}{}^*/L_t$$

The quartiles of the Relative Integrated Luminosity profile are denoted:

$$k(r_1^*) = 0.25; \quad k(r_2^*) = 0.5; \quad k(r_3^*) = 0.75$$

The quantity r_2^* is often termed the "Effective Radius" and denoted as "r_e". The intensity at r_e is denoted by I_e.

The ratios of these quartiles are termed the "Concentration Indices" and defined as:

$$C_{21} = r_2^*/r_1^* \; ; \quad C_{32} = r_3^*/r_2^* \; ; \quad C_{31} = r_3^*/r_1^*$$

The luminosity distribution in a galaxy image may be further expressed in terms of dimensionless variables by setting:

$$J = I/I_e \text{ and } \quad \rho = r^*/r_e$$

The areal quantity 'P' is defined for the i^{th} isophote (with bounded area A_i and intensity I_i) and as:

$$P_i = 1/2\ (I_i - I_{i-1})\ (A_i - A_{i-1})$$

The quantity 'Σ P' is defined as the sum of P for all isophotes brighter than, and equal to 'i'.

The calculated equivalent profile and characteristic parameters are conventionally presented in a standard format termed the "Integration Table". This table contains for each specified

Log I value in the equivalent profile (relative to the frame sky background intensity) the appropriate values of Area 'A' bounded within this contour, P, Σ P, k, r , φ , log J and the surface brightness 'μ' in magnitudes per square arcsecond.

The ASPIC EQPROFASP routine allows the user to calculate the characteristic luminosity parameters from the extracted equivalent luminosity profile and automatically produces a hardcopy output listing the total apparent magnitude, r_1^*, r_2^*, r_3^* (in arcseconds) and the concentration indices c_{21}, c_{32} and c_{31}. The Integration Table is also printed in the conventional layout described above with the Area 'A', P and Σ P given in units of square minutes of arc. The equivalent radius for each isophotal level is given in arcseconds and the surface brightness 'μ' represented by each isophotal level is given in units of magnitudes per square arcsecond. Integration Tables for each programme galaxy in each passband are presented in Data Appendix 'E'.

4.5 The Extrapolation Correction for Total Apparent Magnitude.

The calculation of the total apparent magnitude (via the total apparent luminosity) by totalling the intensity of all pixels within some isophotal contour must terminate at the faintest measured isophote. This must underestimate the true total luminosity since the contribution of regions fainter than the limiting isophote is necessarily neglected. The necessity of correcting for this deficiency has been recognised since the work of Redman (1936) and de Vaucouleurs (1948). de Vaucouleurs

(1960) presented an empirical method for correcting the total apparent luminosity of light beyond the faintest measured isophote, formulated during his investigations of the Magellanic Clouds. The technique is discussed in more detail by Head et al. (1976) who emphasise the necessity of making this form of correction, even for equivalent profiles extending down to a few percent of the sky intensity, in order to avoid the introduction of serious errors in the derivation of total apparent magnitudes.

Davenhall (1984a) has demonstrated that the extrapolation correction used must be appropriate to the morphological type of the galaxy being studied, as suggested by Okamura (1977) who derived analytical expressions for the total luminosity contributed beyond a limiting isophote by exponential and $R^{1/4}$ luminosity distributions. The de Vaucouleurs extrapolation should be valid for disk systems, since it was founded on the low light distribution of the Magellanic Clouds but it is inappropriate for elliptical systems. As all the systems in this survey programme are disk systems, with the exception of NGC 4552, the de Vaucouleurs extrapolation correction was applied throughout to calculate the total apparent magnitude.

NGC 4552 is classified as E0 (de Vaucouleurs et al. (1976)), a classification supported by the photometry of King (1978). For this system the extrapolation correction of Okamura (1977) was applied in the calculation of the total apparent magnitude.

In the later stages of data reduction it was suggested that NGC 4552 deviated from the $R^{1/4}$ law at faint light levels (supporting the SO classification of Sandage in the "Revised Shapely-Ames Catalogue") and this point is discussed in greater detail in Chapters 4 and 6.

The corrected total apparent magnitudes, produced using the EOPROFASP routine, are tabulated in Data Appendix 'E' together with the characteristic radii and concentration indices for each galaxy in each passband.

CHAPTER III

ESTIMATION OF THE ACCURACY OF THE PHOTOMETRIC SURVEY

III - 1 The 'B'-band Photometry

It is widely recognised that the subject of galaxy surface photometry is pervaded with numerous sources of error, which have been discussed by divers authors, e.g.: Redman and Shirley (1937), de Vaucouleurs (1948), Jones et al. (1967), Kormendy (1977), Fraser (1977), Burstein (1978, 1979 a), Carter and Dixon (1978) and in depth by Capaccioli and de Vaucouleurs (1983).

Capaccioli and de Vaucouleurs (1983) conclude from their detailed analysis of the effects of all sources of error that these combine "to restrict the domain of meaningful surface photometry of galaxies to $\mu_B \leq 28$ magnitudes per square arcsecond ... at brighter levels, $18 \leq \mu_B \leq 28$, true mean errors less than 0.1 magnitudes are difficult to achieve". They also note "the very poor agreement of many of the luminosity profiles of multiply observed galaxies" which is notorious, and has been discussed in detail by Carter and Dixon (1978) and Burstein (1979 a).

It is thus imperative that the results of any programme of surface photometry be vindicated by comparison with independent data produced by other authors. The published data of Burstein (1979 a) and Watanabe (1983) provide by far the best opportunity for critical comparison with the results obtained in this survey programme. These authors have applied independent modern digital

techniques analagous to those used in this programme in their investigations of photographic surface photometry.

Burstein (1979 a) presents surface photometry in the Jonhson 'B' passband, consisting of the major and minor-axes profiles for eighteen SO galaxies and the Elliptical luminosity standard NGC 3379, and critically compares his photometry with that of Liller (1960, 1966); van Houten (1961); Markarian et al. (1965); Benedict (1971); Burkhead and Kalowinski (1974); Fraser (1977); Tsikoudi (1977); Kormendy (1977a) and King (1978) for those galaxies in common with the respective authors. Neglecting zero-point differences due to differently defined photographic passbands, Burstein reports as follows:

(1) High levels of agreement (within 0.1 magnitude per square arcsecond) between his data and that of Burkhead and Kalowinski (1974), Kormendy (1977a) and King (1978);

(2) Good agreement (systematic differences averaging less than 0.2 magnitudes per square arcsecond and nowhere worse than 0.5 magnitudes per square arcsecond) is reported between his work and that of Van Houten (1961), Markarian et al. (1965) and Tsikoudi (1977);

(3) Large systematic differences between his work are that of Fraser (1977), Benedict (1971) and Liller (1960, 1966), although the data of Liller exhibits much better agreement at faint light levels ($\mu_B \geq 21$).

Burstein considers that the best external estimate will be found via comparison with the photo-electric data of Burkhead and Kalowinski (1974), and concludes that his own photometry is accurate to within 0.1 magnitudes per square arcsecond (hereafter 'μ') from $18.5 \leq \mu \leq 25$.

Watanabe (1983) presents major and minor-axis profiles in the 'V' passband for 261 galaxies of all morphological types in the Virgo and Ursa Majoris regions. Watanabe compares his photometry with the profiles of Fraser (1977), Kormendy (1977), Tsikoudi (1977), Barbon et al. (1978), Carter and Dixon (1978), King (1978), Burstein (1979 a), Boroson (1981) and Send (1982) for those galaxies in common with the respective authors. Watanabe finds:

(1) Systematic differences between his work and that of Fraser (1977) for many of the galaxies they have in common, in the same sense as previously reported by Burstein (1979 a);

(2) Systematic differences between his work are that of Carter and Dixon (1978) at surface brightness greater than 24 magnitudes per square arcsecond;

(3) Systematic differences between his work and all the other compared sources are less than 0.2 μ for $19 \leq V \leq 24$, and within 0.5 μ for $24 \leq V \leq 25.5$.

Hence, comparison of the present survey work with the results of Burstein (1979 a) and Watanabe (1983) immediately allows indirect comparison with the work of Liller (1960, 1966); Van Houten

(1961); Markarian et al. (1965); Benedict (1971); Burkhead and Kalowinski (1974); Fraser (1977); Tsikoudi (1977); Kormendy (1977), King (1978), Barbon et al. (1978), Carter and Dixon (1978), Boroson (1981) and Send (1982).

The current photometry is then also linked to the standard luminosity profile of NGC 3379 (de Vaucouleurs and Capaccioli (1979)) via the photometry of Kormendy (1977).

It was decided to present a direct graphical comparison of major-axis profiles (following Watanabe (1983)) rather than the graphical displays of residuals (as in Burstein (1979 a)) in the interests of clarity. Individual graphs are presented in Data Appendix 'C' and reproduced for convenience on pages III-14 to 23, for every galaxy where comparison with the work of Burstein and Watanabe is possible, as Burstein (1979, figures 3(e) and (f)) has demonstrated the need to make any comparison comprehensive by considering all galaxies in common in order to evaluate possible random errors in addition to systematic effects.

The convention is adopted that the author's profiles are represented by solid-diamond symbols, Watanabe's profiles by open circles, and Burstein's profiles by open squares when plotted against this author and solid squares when plotted against Watanabe. The plots were prepared using the GIPSY common-user graphics package written by A. Bridger (formerly of St. Andrews but now at the R.O.E) which utilized the St. Andrews University VAX computer and a Sigma graphics terminal linked to a Tektronix

hardcopy unit. The profiles of Watanabe and Burstein have been shifted in ordinate with respect to the author's major-axis profiles (presented in Data Appendices 'A' and 'I') in order to give the best coincidence since the colour band varies amongst the data sets, and to allow for errors in zero-point determination.

It is important to remember that the comparison is not strictly between equivalent forms of data: the profiles of Burstein and Watanabe have been folded and smoothed by interpolation and running-mean techniques respectively. The comparisons presented are between the author's unfolded major-axis profiles and the profiles of Burstein and Watanabe reflected through the origin r = 0. The ordinate shifts are tabulated at the end of Data Appendix 'C'.

Inspection of the graphs intercomparing the current photometry with that of Watanabe (1983) reveals a level of agreement which is encouraging, averaging to within 0.2 magnitudes in the interval $19 \leq B \leq 24\ \mu$ are within 0.5 magnitudes in the interval $24 < B < 26\ \mu$. The profiles in best agreement are generally those for the largest and brightest systems (e.g.: NGC 4429, 4477 and 4552) which is to be expected since more information pixels are available for these images. The good agreement also displayed by fainter systems (e.g.: NGC 4377, 4461 and 4550) is particularly gratifying. The asymmetry of the present author's major-axis profiles is very obvious (e.g. NGC 4371 or 4501).

Examination of the graphs intercomparing the current photometry with that of Burstein (1979a) reveals a similar level of agreement, averaging to within 0.2 magnitudes in the interval $20 < B < 24\ \mu$ and within 0.5 magnitudes in the interval $24 < B < 26$, although the number of comparison galaxies is reduced to four. A tendency is discernible, however, for the photometry of Burstein to be systematically slightly fainter than this author's photometry at higher brightness levels for $B < 20$, a trend also discernible from his own comparison (Burstein (1979a, figure 3(b)) with the data of Kormendy (1977). The photometry of Kormendy (1977) is certainly reliable at high surface brightnesses (de Vaucouleurs and Capaccioli (1979), figure 21) and hence it can be inferred that the error is probably intrinsic to Burstein's photometry.

As a test of this, the photometry of Watanabe and Burstein was intercompared in the same manner as each was compared with the author, the graphs being presented in Data Appendix 'C' and reproduced for convenience on pages III-24 and 25. If the profiles are matched to give the best fit at faint light (as in NGC 4377) Burstein's profile is systematically fainter near the galaxy centre. If the profiles are constrained to match at bright light levels (NGC 4429, 4459 and 4474) then Burstein's profiles are systematically too bright at fainter light levels. It is therefore concluded that since a number of independent workers all show systematic differences (in the same sense) with the profiles of Burstein in the regime $B \lesssim 20$, then the photometry of Burstein is affected by systematic error in this regime.

The size of the systematic error is difficult to quantify definitively because there is not an extensive overlap with the current photometry, but as it would appear to average less than 0.3 magnitudes the effect is probably not excessive. The bulge luminosity parameters which Burstein extracts (Burstein (1979 b)) from these major-axis profiles may be more significantly affected. In particular, his conclusion that lenticular bulges are more diffuse than elliptical systems is likely to be weakened, as he anticipates in his own caveat (Burstein (1979 b), Section IV).

It is impossible to isolate unambiguously the cause of the systematic error at high surface brightnesses which appears to affect Burstein's photometry, but intuitive speculation is possible. The general procedures of data reduction and analysis followed in the current work and that of Watanabe (1983) are completely independent but quite similar, particularly the Density/Intensity conversion techniques. Burstein combined data from both large and small scale plates and used "combined characteristic curves" to define the Density/Intensity transformation. The technique of combining characteristic curves should, in principle, increase the accuracy of the Density/Intensity transformation, but as Burstein (1978, p. 134) warns: "if a mistake is made in fitting the CC (characteristic curve) of one plate, that mistake will probably be made on all plates of the same emulsion batch ". It may well be that such a mistake was made in the determination of the characteristic curve for the Crossley (large-scale) plates used by Burstein.

1.1 Intercomparison of the Data Sets for NGC 4474

For one galaxy, NGC 4474, the agreement of high surface brightness is quite poor among all three data sets, in the sense that the profile of Burstein (1979 a) is systematically fainter than the profile of Watanabe (1983) which in turn is systematically fainter than the major-axis profile produced in this current work. The disagreement between Burstein and the other data sets has already been discussed, but the question remains why the agreement between the current work and that of Watanabe should be poorer for this galaxy than for the other systems. The good agreement for the other systems implies that this is a random effect, and one may note that the systematic difference between Burstein and Watanabe appears roughly similar for both NGC 4377 and 4474 whereas the agreement between the current work and that of Watanabe is much better at high surface brightness for NGC 4377 than for NGC 4474. The implication would seem to be that the major-axis profile of NGC 4474 extracted in the current work is systematically too bright by several tenths of a magnitude at $B \geq 20$. However, the most obvious source of random error, namely misalignment of the extracted major-axis, would produce a major-axis that is systematically too faint rather than too bright. The only other source of random error in the data would seem to be the introduction of a set of erroneously bright pixels by the scanning microdensitometer, although this would seem most unlikely. An alternative external source of the disagreement could be that the nuclear brightness of NGC 4474 varies with an amplitude of at least several tenths

of a magnitude. Burstein (1978) points out that NGC 4474 is classified as a peculiar SØ by de Vaucouleurs et al. (1976) and notes that the bulge luminosity profile appears unusual for this galaxy, so there may be circumstantial evidence for believing that the source of disagreement in the bulge photometry of NGC 4474 could be due to intrinsic light variation. Other than these speculations, the discrepancy between the current work and that of Watanabe (1983) for the bulge profile of NGC 4474 cannot be clearly understood. The disagreement between the three data sets is illustrated on page 14 of Data Appendix 'C' and reproduced for convenience on page III-26, where the North East wing of the 'B' major-axis profile presented in this work is plotted against the major-axis profiles of Burstein and Watanabe.

In conclusion, it has been demonstrated by comparison with previously published independent photometry that the 'B'-passband profiles calculated in this survey programme are free from systematic error and appear at least as reliable as any comparable published photometry over a wide range of surface brightness. The success of this comparison vindicates the scanning, data reduction and data-analysis procedures used to produce the current photometry.

III-2 The 'R' and 'I'-band photometry

There is a great dearth of published surface photometry in the 'R' and 'I' passbands; until recently the author was not aware of any photometry in the current literature available for

comparison with the galaxies studied in this programme. However, since the 'R' and 'I' photometry presented in this survey programme has been reduced in a completely homogeneous fashion with the 'B'-band photometry, there seems no reason to think that it should be any less reliable than the 'B' photometry. For the reasons discussed previously (Chapter 2) the zero-point of the 'R' and 'I' profiles is necessarily less well defined than for the 'B'-band photometry, and more 'R' and 'I' multi-aperture photometry is urgently needed for the vast majority of bright galaxies.

Complete vindication of the 'R'-band photometry will have to await publication of independent surface photometry, although indirect checks are discussed subsequently in section IV-2. Hamabe (1983) has confirmed that the KISO galaxy-photometry group at the University of Tokyo (which includes Hamabe, Okamura, Kodaira and Watanabe) may extend their automated programme of surface photometry to cover the Virgo cluster in the 'R' passband which would certainly provide, at some future date, the data necessary for a critical evaluation of the 'R'-band photometry presented in this thesis.

Towards the end of his fellowship at the R.O.E, Dr C. Blackmann was attempting to examine the infra-red ('I'-band) light distribution of selected galaxies, one of which was NGC 4501. After he had left the R.O.E, Dr Blackmann very kindly provided the author with some of his preliminary results for NGC 4501 in the form of absolutely calibrated major and minor-axis profiles. The photometry of Blackmann was produced using completely

independent scanning, data analysis and reduction procedures but the data source was the same as this programme, UKSTU plate no. I6867, so the photometry is not ideally independent. The data was in a fairly raw form from which the author extracted points at selected intensity intervals, the profiles being presented in Data Appendix 'J'. Graphical comparison of Blackmann's data with the author's major-axis 'I'-band photometry of NGC 4501 is shown in Data Appendix 'C' and reproduced for convenience on page III-27. No zero-point adjustment of the ordinate has been made. Since the data of Blackmann has been processed only in a simple manner by the author the agreement between the two data sets is surprisingly good and suggests that the 'I'-band photometry presented in the current programme is free from any substantial systematic errors.

More recently, the 'I'-band data of Boroson et al. (1983b) (hereafter in this chapter denoted as BSS) became available for comparison with nine of the galaxies included in the current survey. Unfortunately, although the data-base and scanning procedures of BSS are analogous to those described in Chapter II, the data reduction procedures used by BSS to calculate luminosity profiles are very different to those traditionally used in galaxy photometry. In essence, the luminosity profiles presented by BSS are equivalent profiles "corrected" to the major-axis via the ellipticity-ratio of the galaxy at various isophotal levels. A very similar technique is discussed in detail in Chapter VI, with particular reference to the intercomparison of extracted major-axis luminosity profiles and "corrected" equivalent profiles.

The profiles presented by BSS are compared graphically with the author's 'I'-band photometry in the same fashion as described previously in section III-1. Individual graphs are presented in Data Appendix 'C' and reproduced for convenience on pages III-28 to 32. The convention adopted is for the author's profiles to be represented by open squares, and those of BSS by solid squares. The profiles presented by BSS have been shifted in ordinate, with respect to the author's data, to provide the best coincidence since the colour band differs slightly between the data sets and to allow for errors in the zero-point determinations.

It is important to note that the comparison of "corrected" and true major-axis profiles is not strictly valid and will only be a good approximation for featureless galaxies of well-determined ellipticity, as the azimuthal smoothing will obliterate virtually all detailed structure in an image. Although this point is also stressed by BSS, it should be noted that their comparison with independent photometry (BSS Fig. I) uses unpublished major and minor-axis data and not the azimuthally smoothed profiles presented in their paper.

Inspection of the graphs intercomparing the current photometry with that of BSS reveals good agreement for the most "featureless" galaxies (NGC 4267 and 4459), and demonstrates that both sets of data are free from any significant systematic errors in the range $18 \leq I \leq 23\,\mu$. Galaxies with discernible major-axis structure (e.g. the spiral arms of NGC 4429) show predictable differences between the profiles, but there are no

suggestions of photometric errors.

Serious and unexpected differences between the data sets are visible only in the inner regions of NGC 4477, where the photometry of BSS is considerably fainter than the author's profile. In an attempt to identify which data set is in error the 'V'-band photometry of Watanabe (1983) (open squares) was compared with the data of BSS (solid squares), and the resultant graph is shown on page III-32. The photometry of Watanabe has been shifted in ordinate to achieve the best coincidence of the profiles. It is apparent from inspection of the two data sets that the level of agreement in the disk of NGC 4477 is reasonable, considering the large colour-difference, but the profile presented by BSS is systematically fainter in the bulge. Since the photometry of BSS is systematically faint in the inner regions of NGC 4477 with respect to two independent data sets, it seems highly likely that their data is affected by some source of random error, such as the use of invalid ellipticity ratios within 30 arcseconds radius of the galaxy centre.

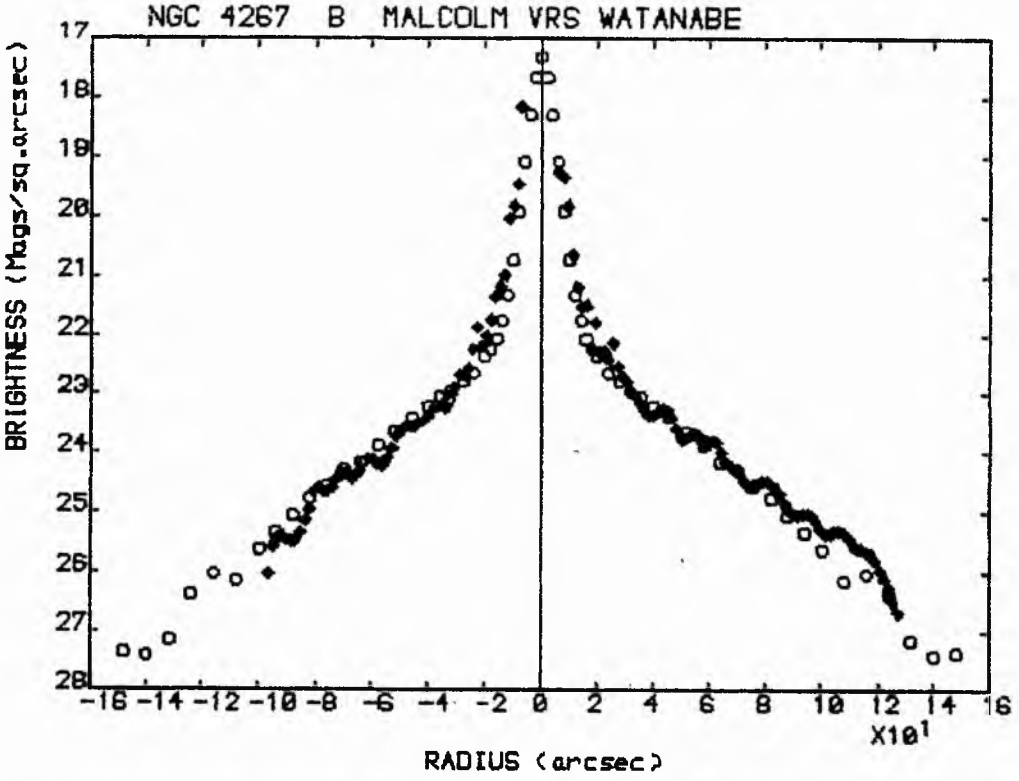
NGC 4267 B MALCOLM VRS WATANABE
BRIGHTNESS (Mags/sq.arcsec)
17
18
19
20
21
22
23
24
25
26
27
28
-16 -14 -12 -10 -8 -6 -4 -2 0 2 4 6 8 10 12 14 16
X10¹
RADIUS (arcsec)

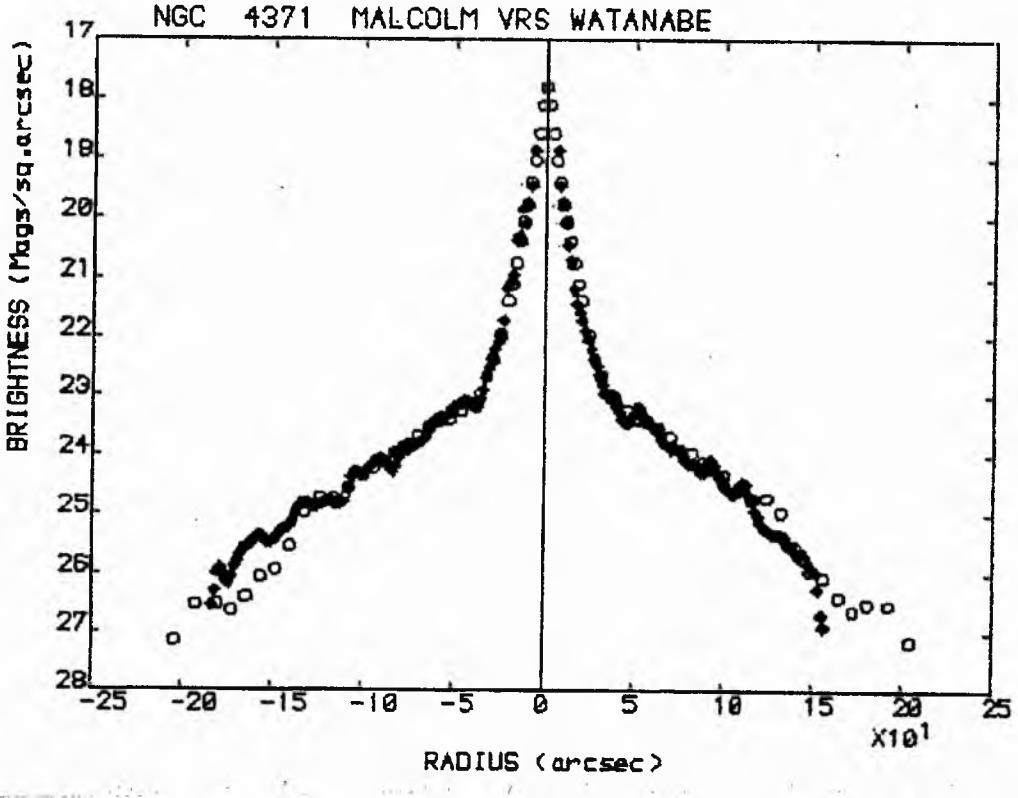
NGC 4371 MALCOLM VRS WATANABE
BRIGHTNESS (Mags/sq.arcsec)
17
18
19
20
21
22
23
24
25
26
27
28
-25 -20 -15 -10 -5 0 5 10 15 20 25
X10¹
RADIUS (arcsec)

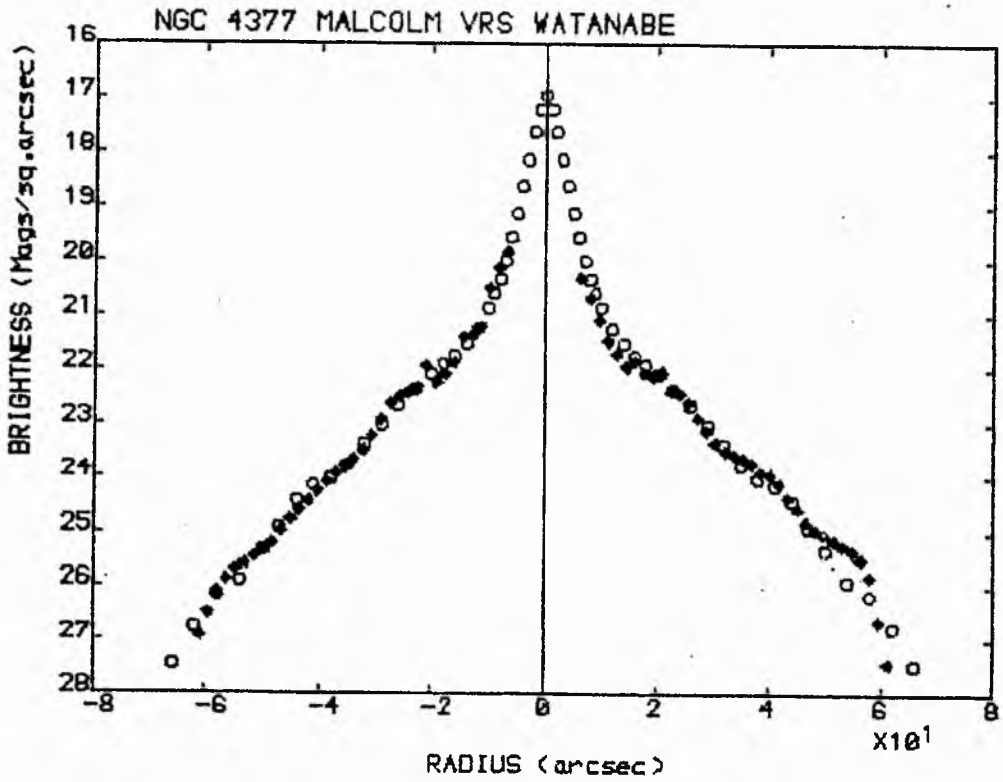
NGC 4377 MALCOLM VRS WATANABE
BRIGHTNESS (Mags/sq.arcsec)
16
17
18
19
20
21
22
23
24
25
26
27
28
-8
-6
-4
-2
0
2
4
6
8
X10¹
RADIUS (arcsec)

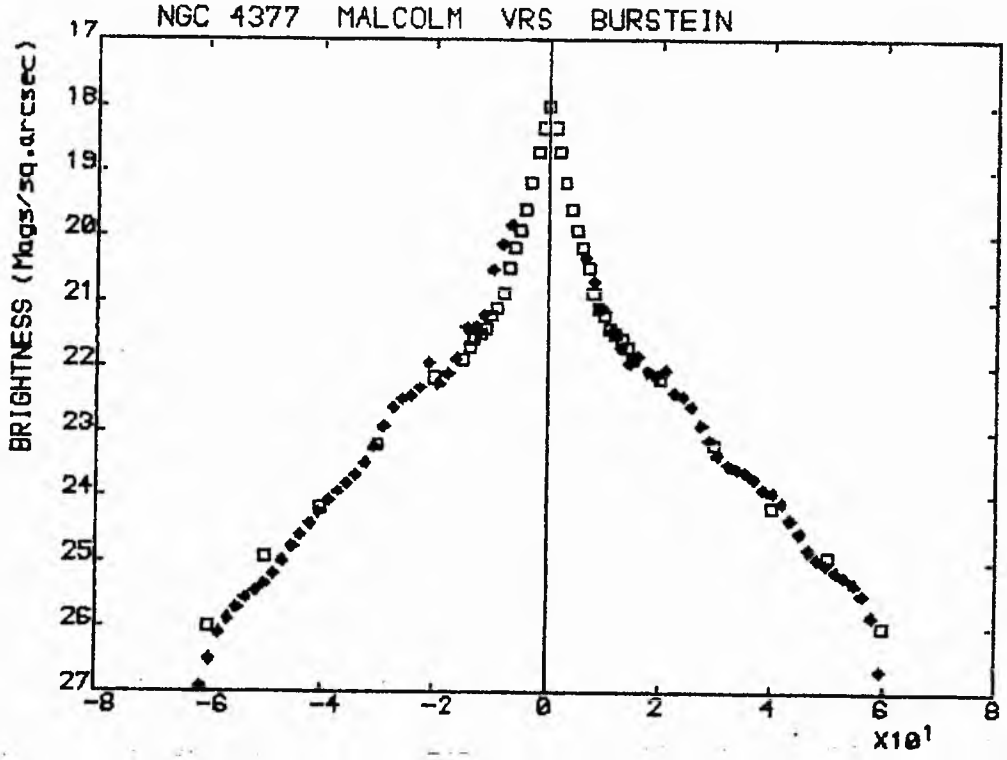
NGC 4377 MALCOLM VRS BURSTEIN
BRIGHTNESS (Mags/sq.arcsec)
17
18
19
20
21
22
23
24
25
26
27
-8
-6
-4
-2
0
2
4
6
8
X10¹

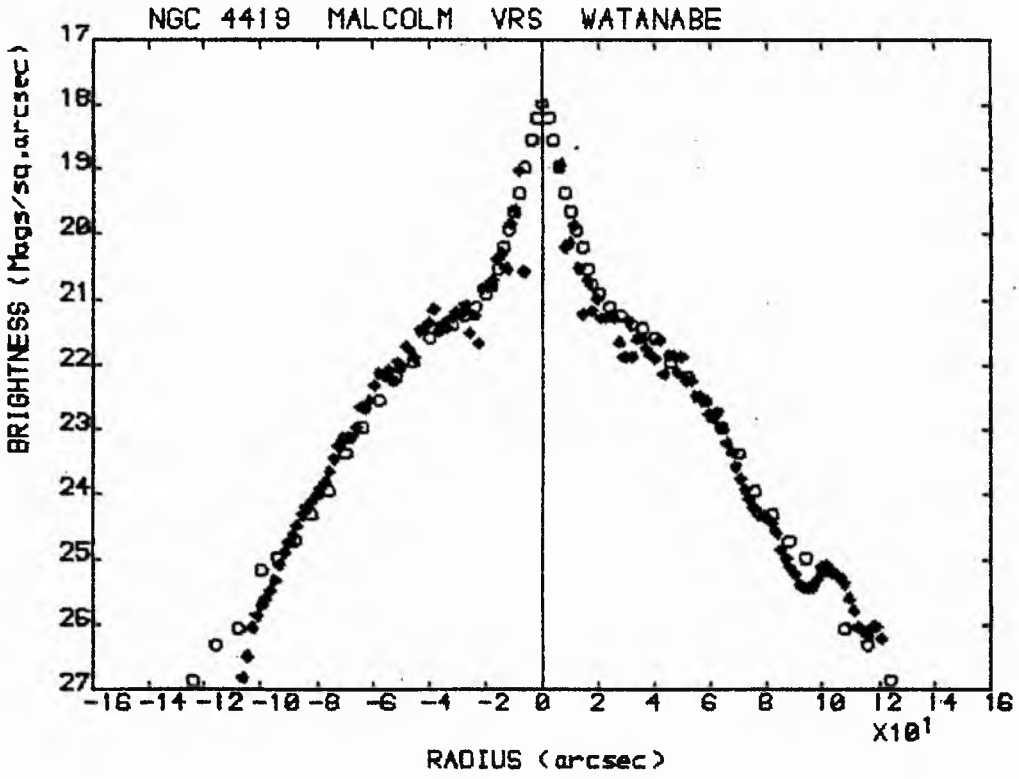
NGC 4419 MALCOLM VRS WATANABE
BRIGHTNESS (Mags/sq.arcsec)
17
18
19
20
21
22
23
24
25
26
27
-16 -14 -12 -10 -8 -6 -4 -2 0 2 4 6 8 10 12 14 16
X10¹
RADIUS (arcsec)

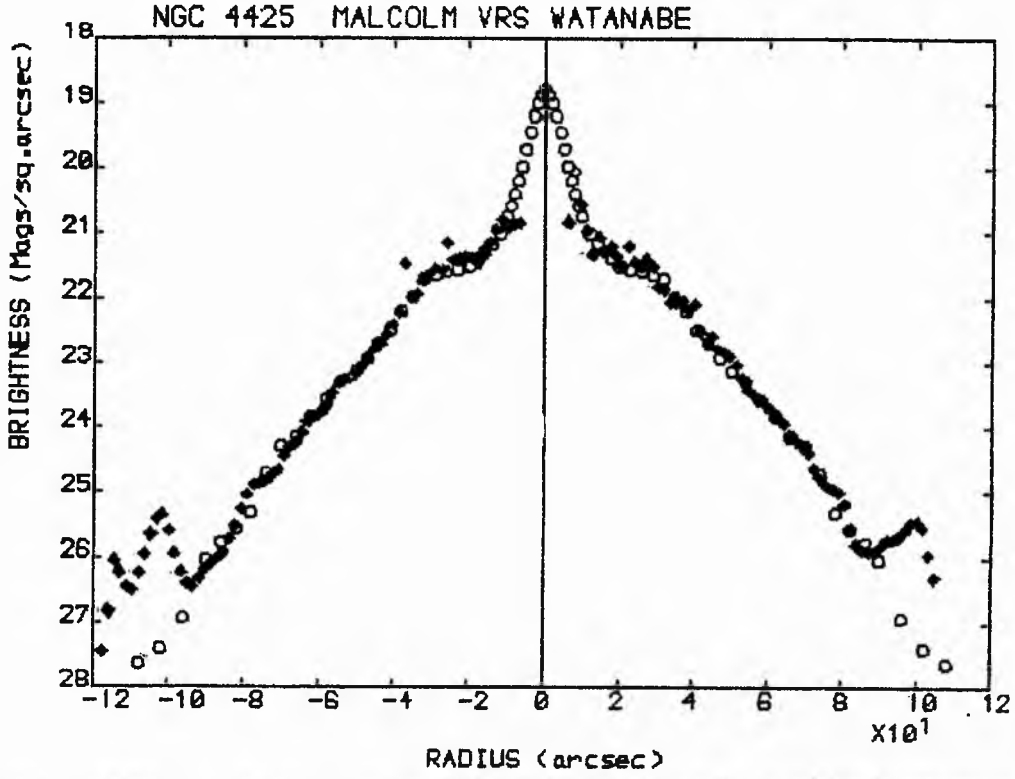
NGC 4425 MALCOLM VRS WATANABE
BRIGHTNESS (Mags/sq.arcsec)
18
19
20
21
22
23
24
25
26
27
28
-12 -10 -8 -6 -4 -2 0 2 4 6 8 10 12
X10¹
RADIUS (arcsec)

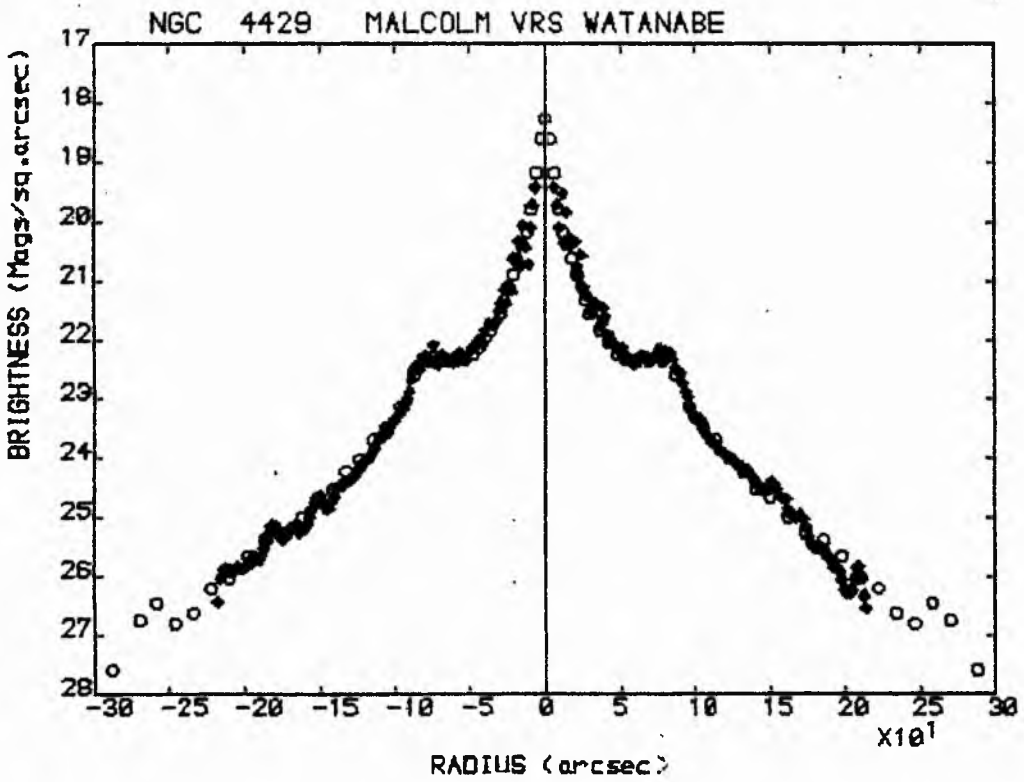
NGC 4429 MALCOLM VRS WATANABE
BRIGHTNESS (Mags/sq.arcsec)
17
18
19
20
21
22
23
24
25
26
27
28
-30 -25 -20 -15 -10 -5 0 5 10 15 20 25 30
X10¹
RADIUS (arcsec)

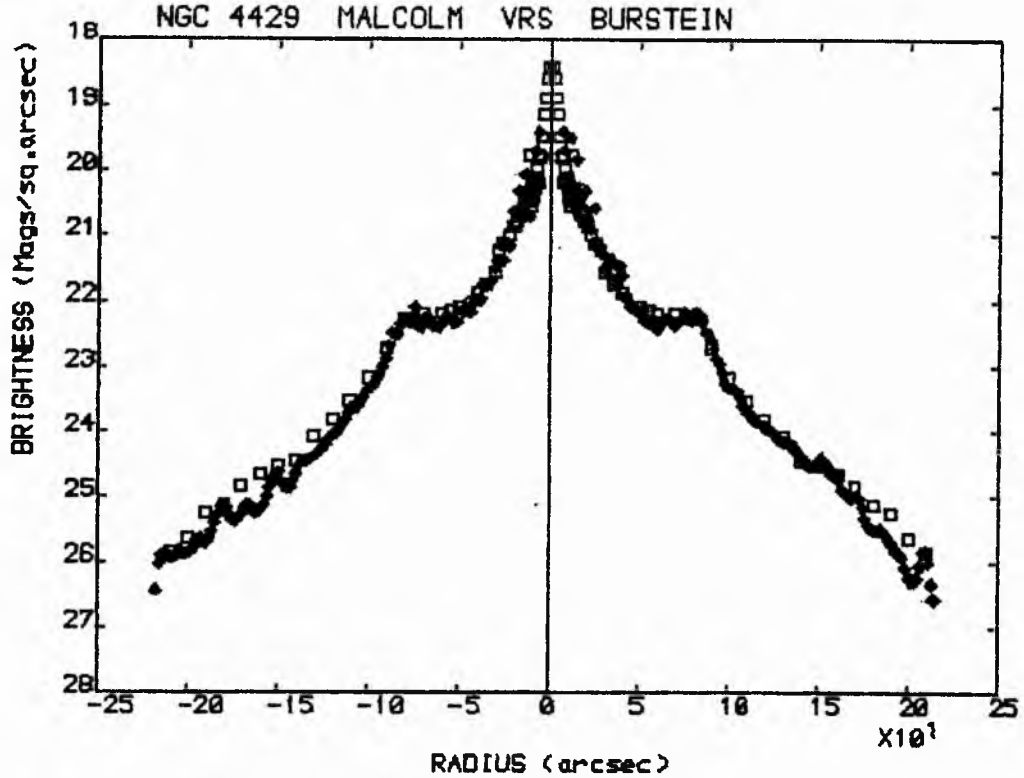
NGC 4429 MALCOLM VRS BURSTEIN
BRIGHTNESS (Mags/sq.arcsec)
18
19
20
21
22
23
24
25
26
27
28
-25 -20 -15 -10 -5 0 5 10 15 20 25
X10¹
RADIUS (arcsec)

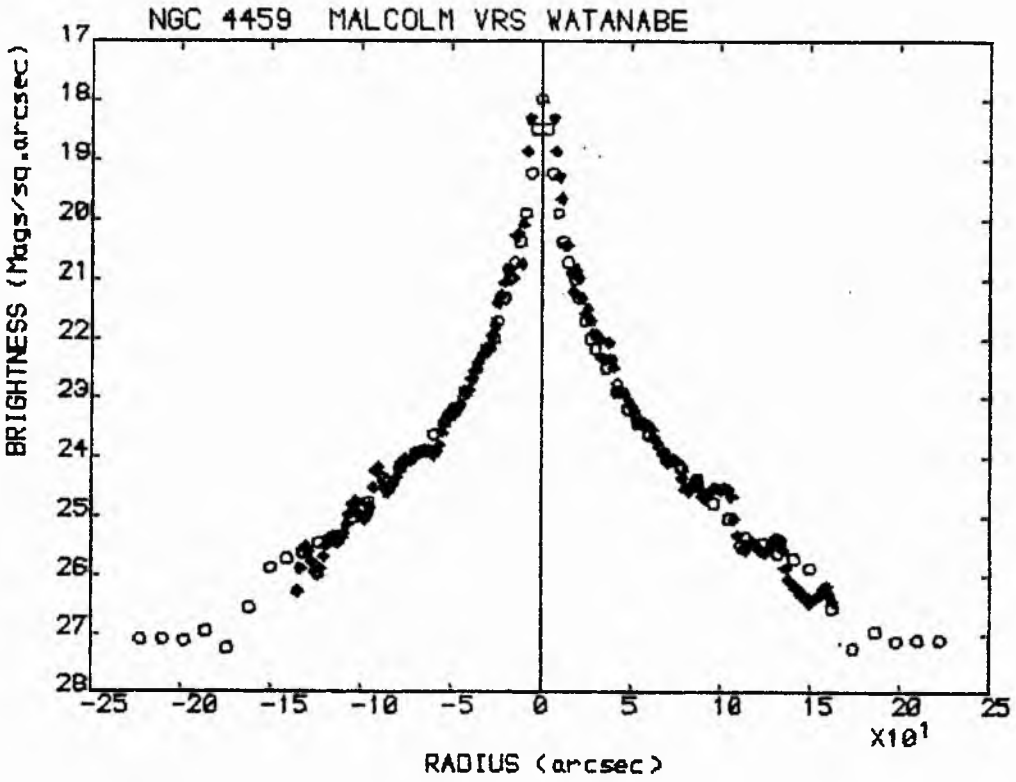
NGC 4459 MALCOLM VRS WATANABE
BRIGHTNESS (Mags/sq.arcsec)
17
18
19
20
21
22
23
24
25
26
27
28
-25 -20 -15 -10 -5 0 5 10 15 20 25
X10¹
RADIUS (arcsec)

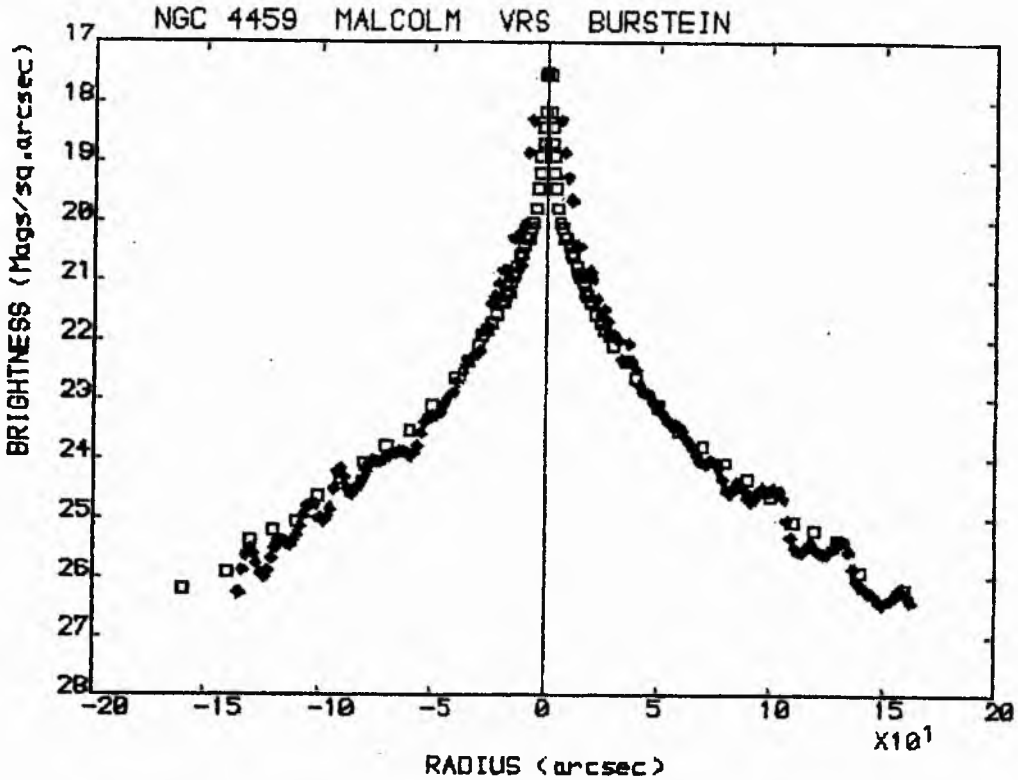
NGC 4459 MALCOLM VRS BURSTEIN
BRIGHTNESS (Mags/sq.arcsec)
17
18
19
20
21
22
23
24
25
26
27
28
-20 -15 -10 -5 0 5 10 15 20
X10¹
RADIUS (arcsec)

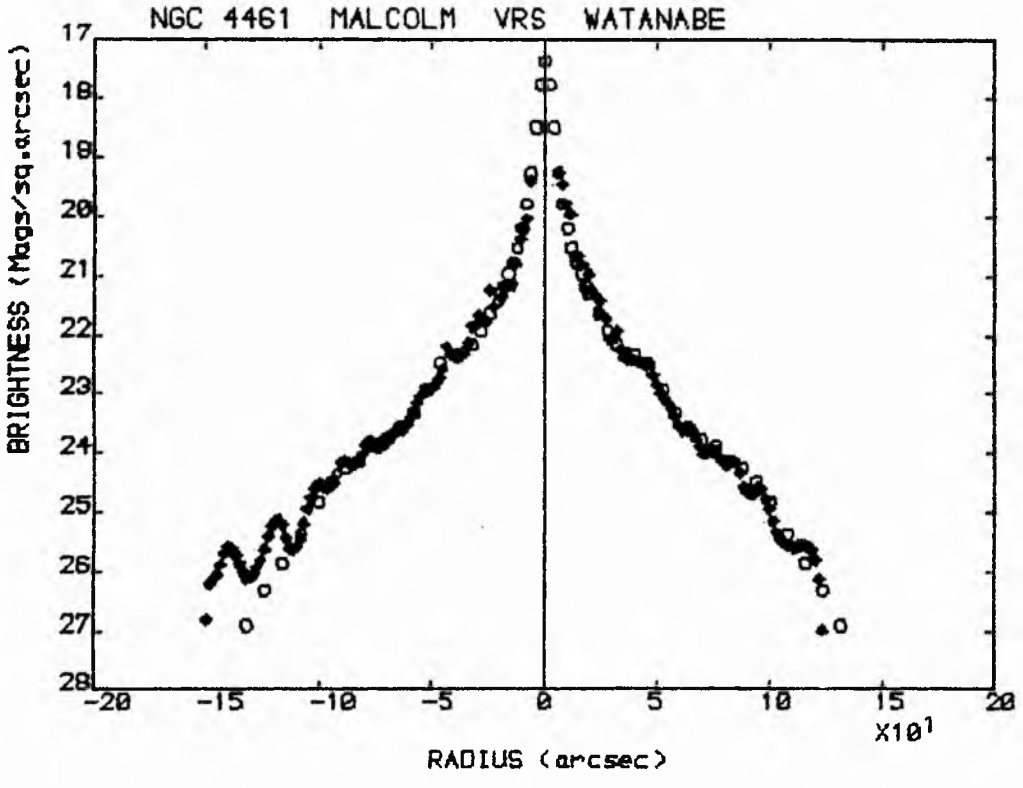
NGC 4461 MALCOLM VRS WATANABE
BRIGHTNESS (Mags/sq.arcsec)
17
18
19
20
21
22
23
24
25
26
27
28
-20
-15
-10
-5
0
5
10
15
20
X10¹
RADIUS (arcsec)

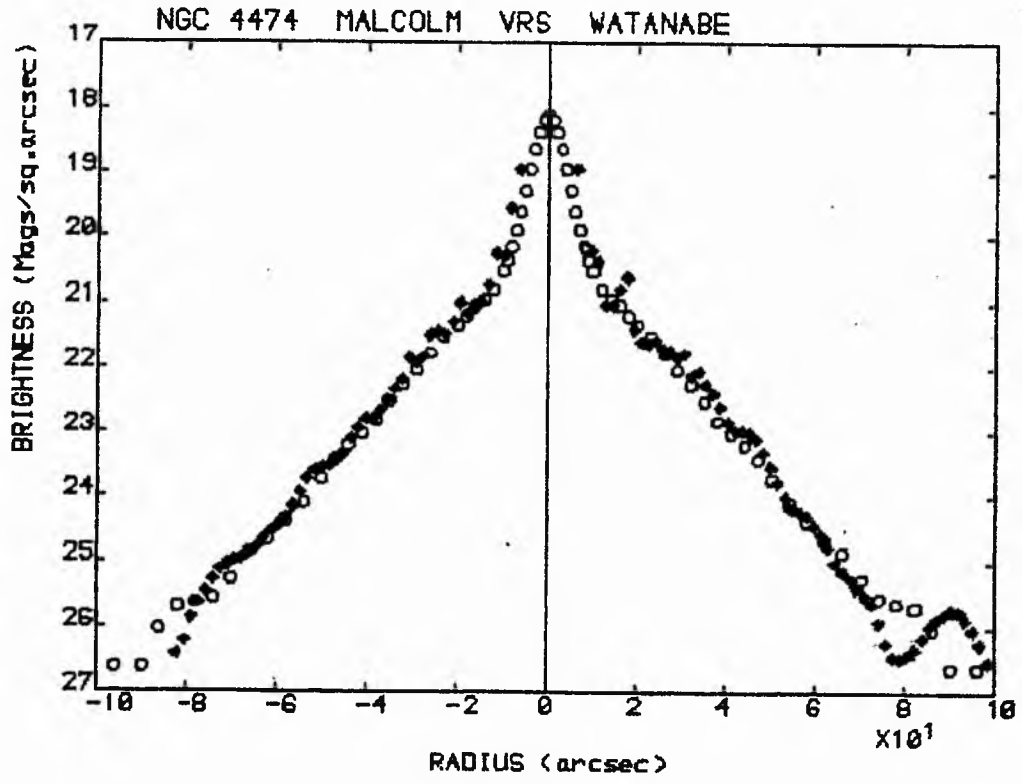
NGC 4474 MALCOLM VRS WATANABE
BRIGHTNESS (Mags/sq.arcsec)
17
18
19
20
21
22
23
24
25
26
27
-10 -8 -6 -4 -2 0 2 4 6 8 10
X10¹
RADIUS (arcsec)

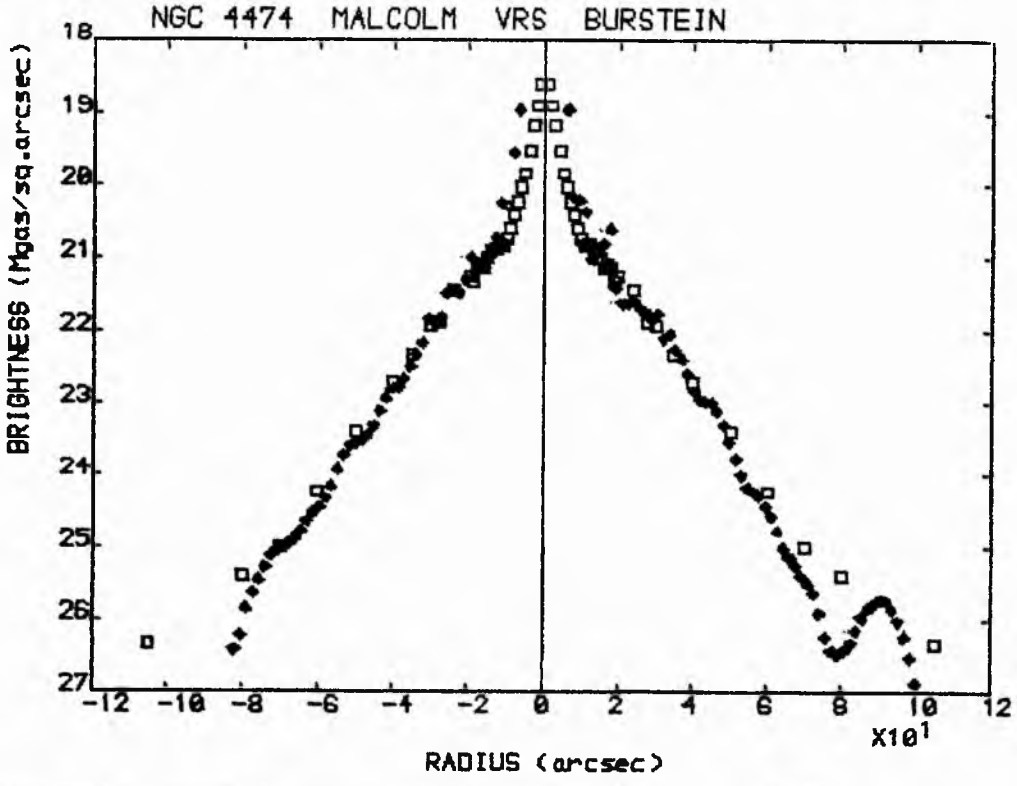
NGC 4474 MALCOLM VRS BURSTEIN
BRIGHTNESS (Mgas/sq.arcsec)
18
19
20
21
22
23
24
25
26
27
-12 -10 -8 -6 -4 -2 0 2 4 6 8 10 12
X10¹
RADIUS (arcsec)

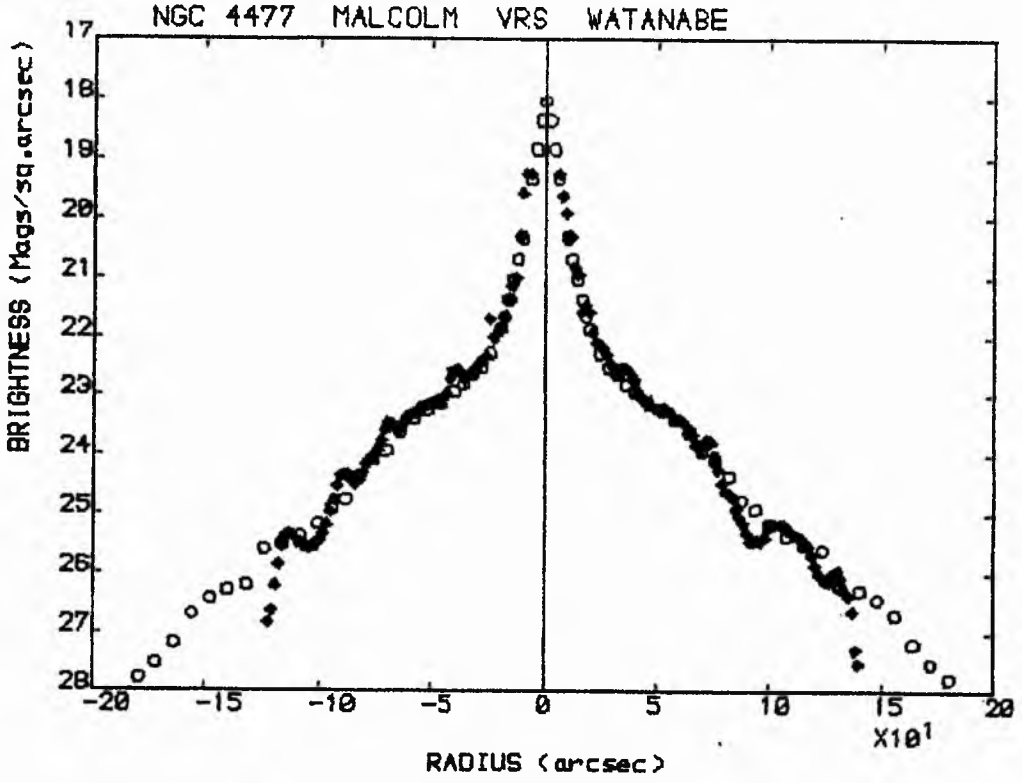
NGC 4477 MALCOLM VRS WATANABE
BRIGHTNESS (Mags/sq.arcsec)
17
18
19
20
21
22
23
24
25
26
27
28
-20
-15
-10
-5
0
5
10
15
20
X10¹
RADIUS (arcsec)

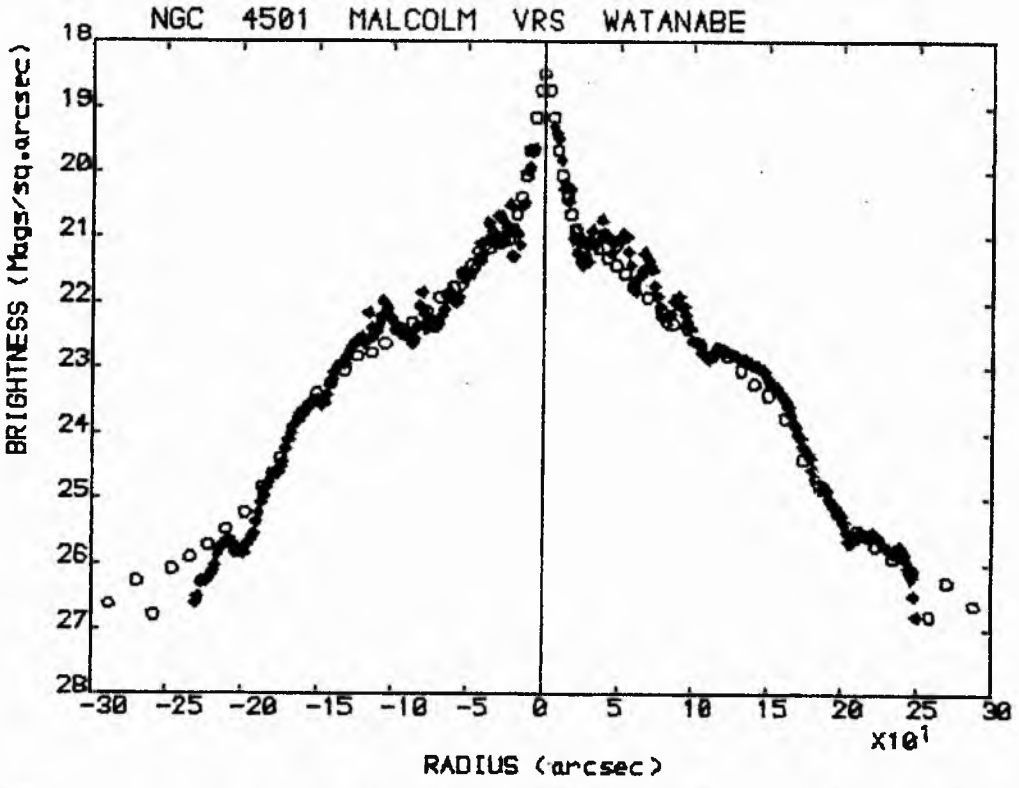
NGC 4501 MALCOLM VRS WATANABE
BRIGHTNESS (Mags/sq.arcsec)
18
19
20
21
22
23
24
25
26
27
28
-30
-25
-20
-15
-10
-5
0
5
10
15
20
25
30
X10¹
RADIUS (arcsec)

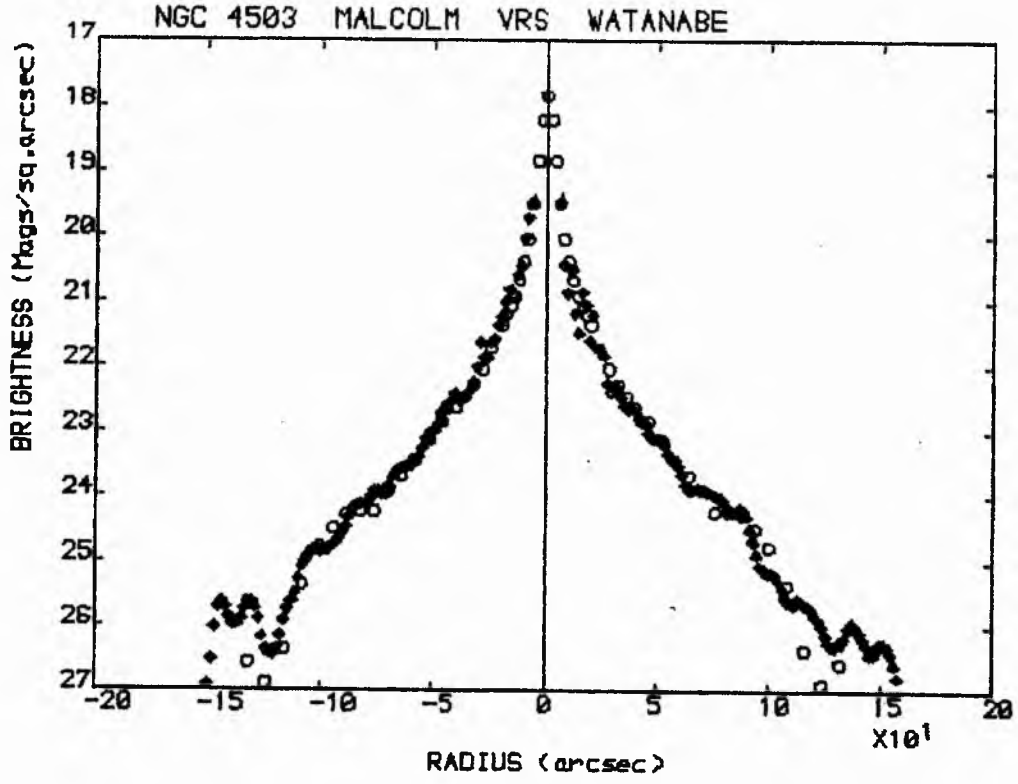
NGC 4503 MALCOLM VRS WATANABE
BRIGHTNESS (Mags/sq.arcsec)
17
18
19
20
21
22
23
24
25
26
27
-20
-15
-10
-5
0
5
10
15
20
X10¹
RADIUS (arcsec)

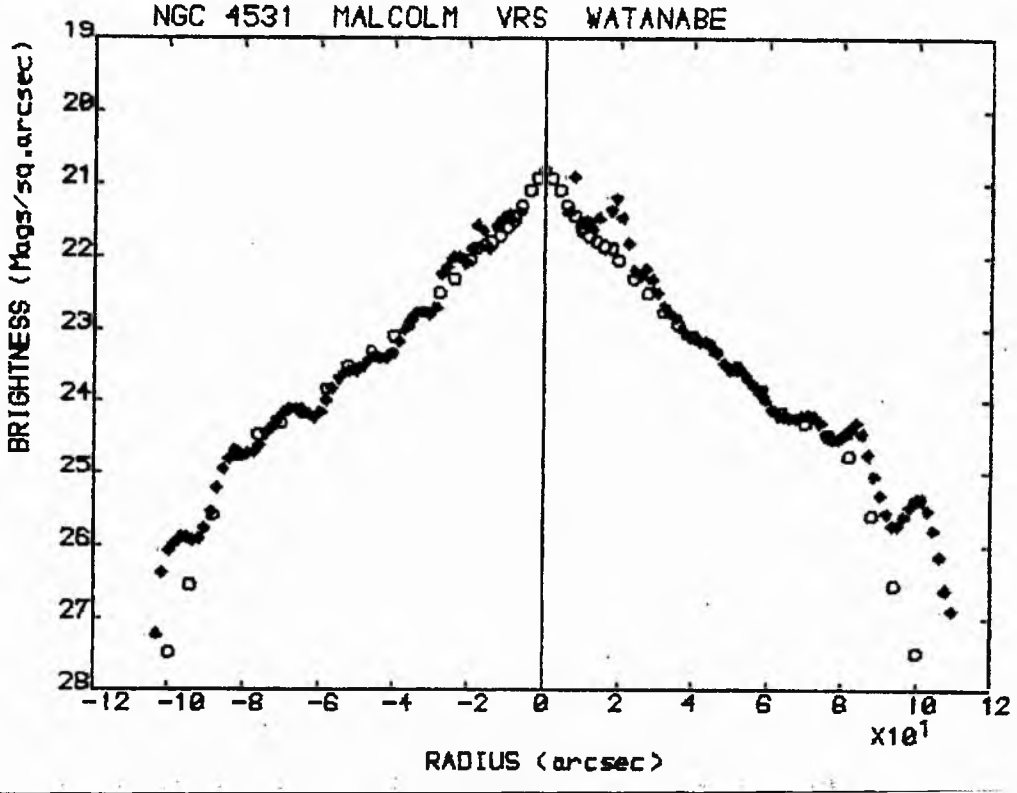
NGC 4531 MALCOLM VRS WATANABE
BRIGHTNESS (Mags/sq.arcsec)
19
20
21
22
23
24
25
26
27
28
-12
-10
-8
-6
-4
-2
0
2
4
6
8
10
12
X10¹
RADIUS (arcsec)

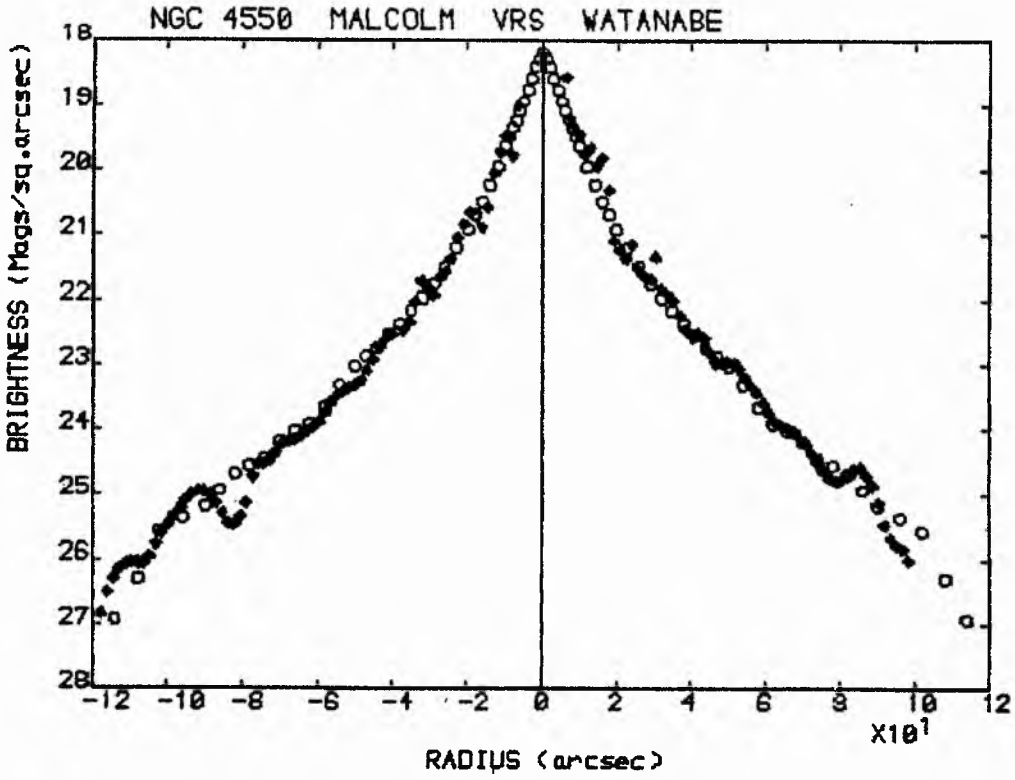
NGC 4550 MALCOLM VRS WATANABE
BRIGHTNESS (Mags/sq.arcsec)
18
19
20
21
22
23
24
25
26
27
28
-12 -10 -8 -6 -4 -2 0 2 4 6 8 10 12
X10¹
RADIUS (arcsec)

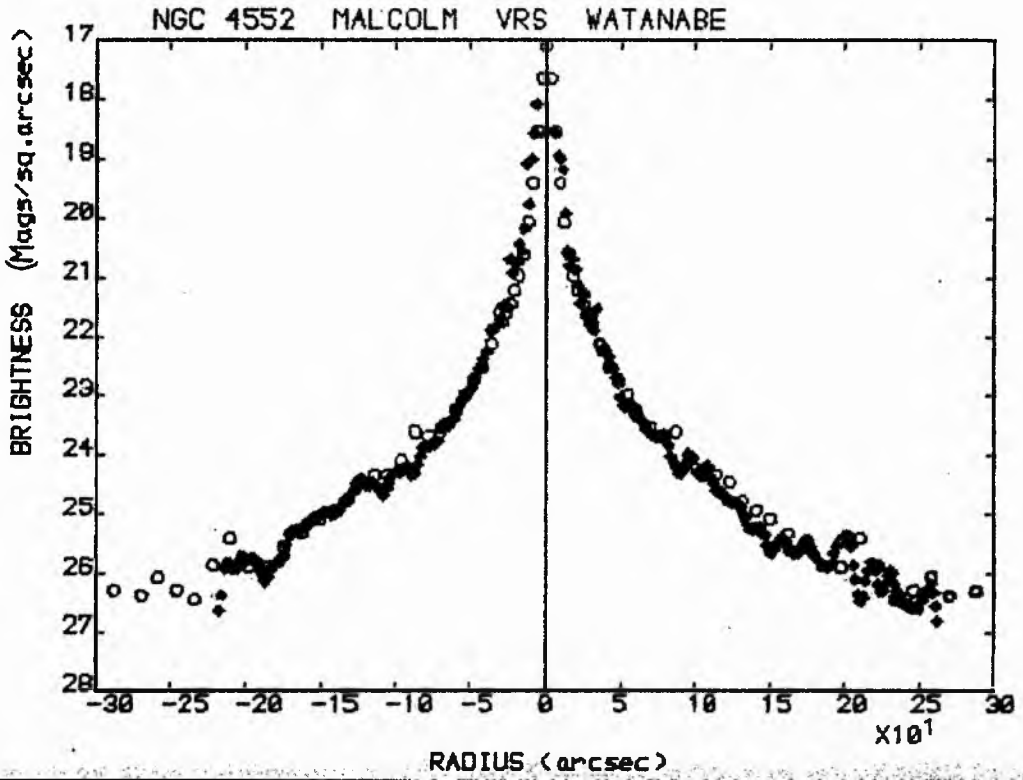
NGC 4552 MALCOLM VRS WATANABE
BRIGHTNESS (Mags/sq.arcsec)
17
18
19
20
21
22
23
24
25
26
27
28
-30 -25 -20 -15 -10 -5 0 5 10 15 20 25 30
X10¹
RADIUS (arcsec)

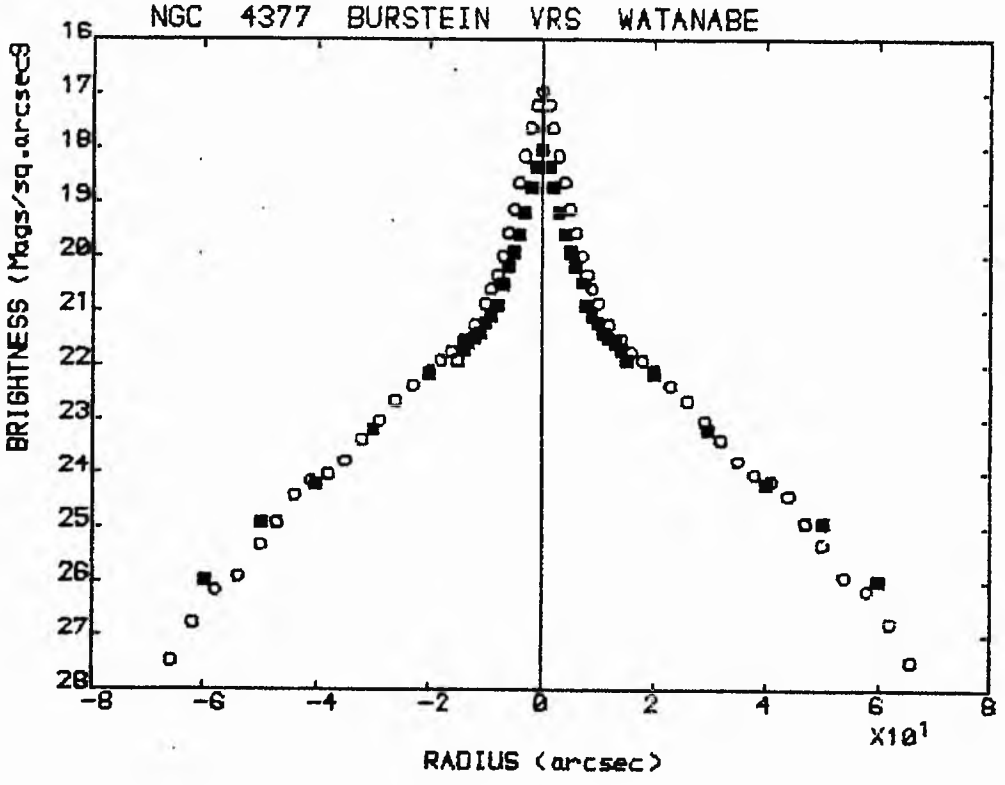
NGC 4377 BURSTEIN VRS WATANABE
BRIGHTNESS (Mags/sq.arcsec)
16
17
18
19
20
21
22
23
24
25
26
27
28
-8
-6
-4
-2
0
2
4
6
8
X10¹
RADIUS (arcsec)

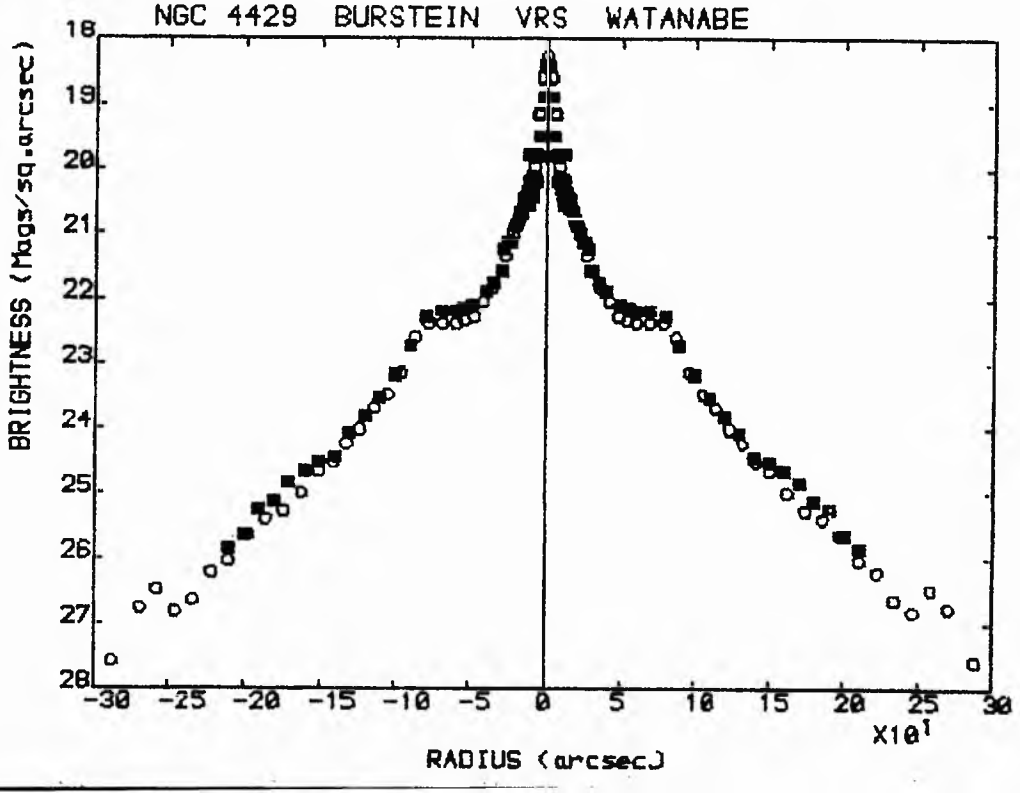
NGC 4429 BURSTEIN VRS WATANABE
BRIGHTNESS (Mags/sq.arcsec)
18
19
20
21
22
23
24
25
26
27
28
-30
-25
-20
-15
-10
-5
0
5
10
15
20
25
30
X10¹
RADIUS (arcsec)

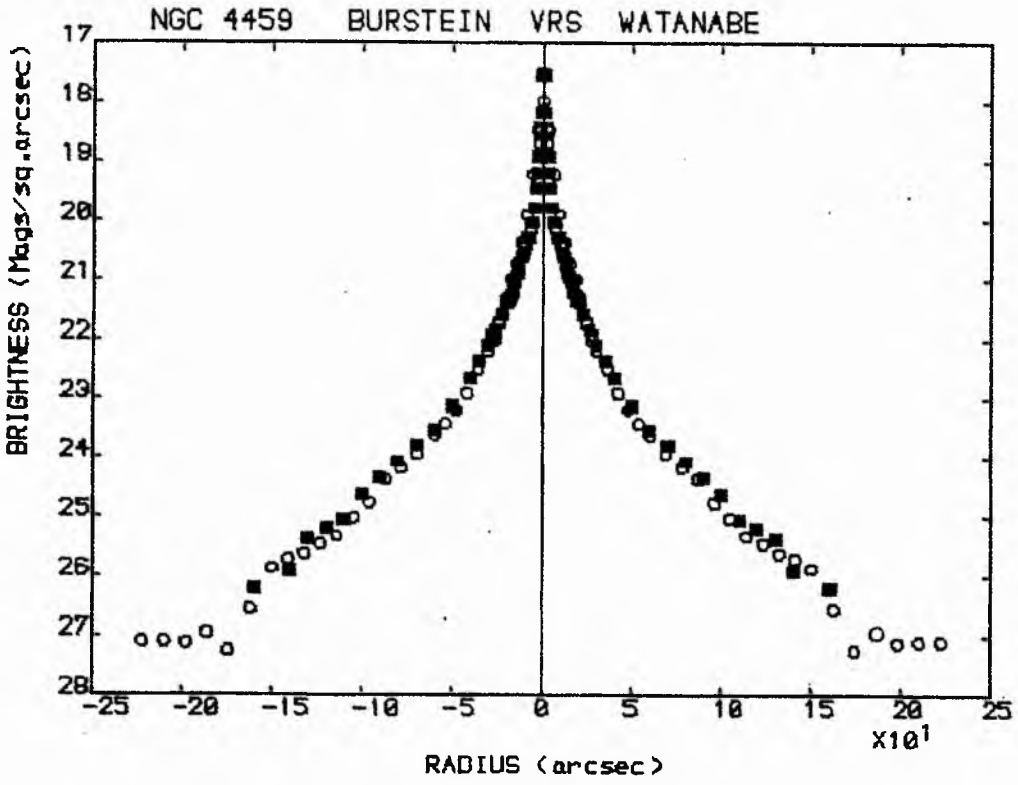
NGC 4459 BURSTEIN VRS WATANABE
BRIGHTNESS (Mags/sq.arcsec)
17
18
19
20
21
22
23
24
25
26
27
28
-25 -20 -15 -10 -5 0 5 10 15 20 25
X10¹
RADIUS (arcsec)

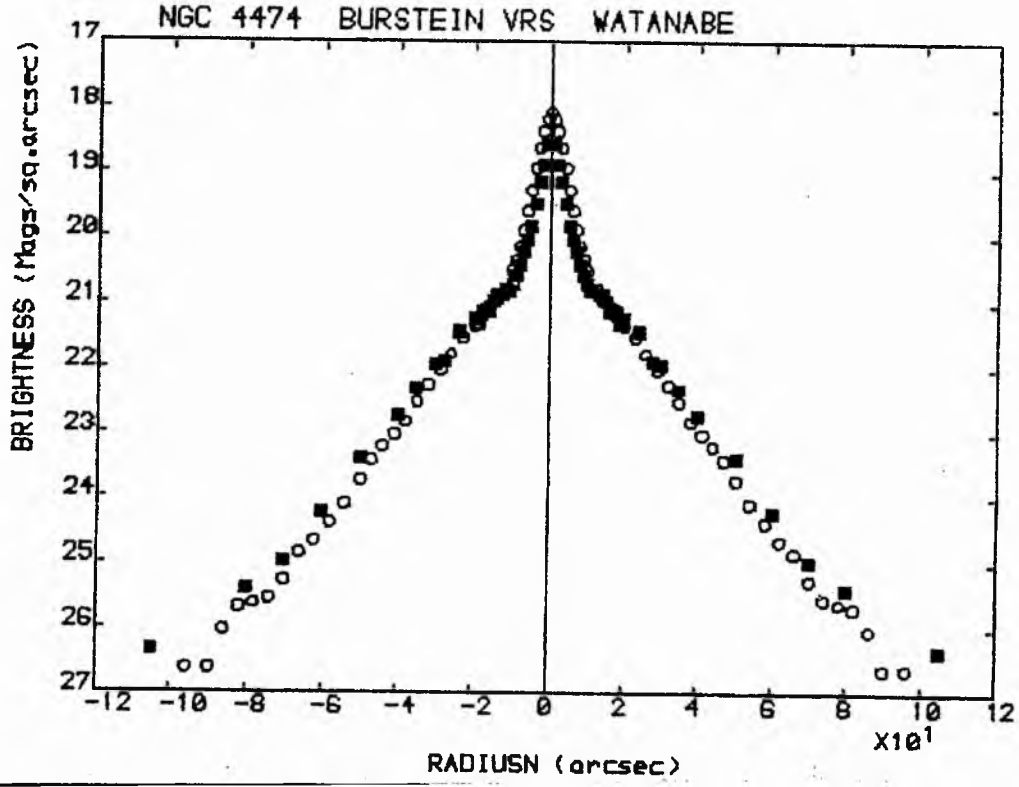
NGC 4474 BURSTEIN VRS WATANABE
BRIGHTNESS (Mags/sq.arcsec)
17
18
19
20
21
22
23
24
25
26
27
-12 -10 -8 -6 -4 -2 0 2 4 6 8 10 12
X10¹
RADIUSN (arcsec)

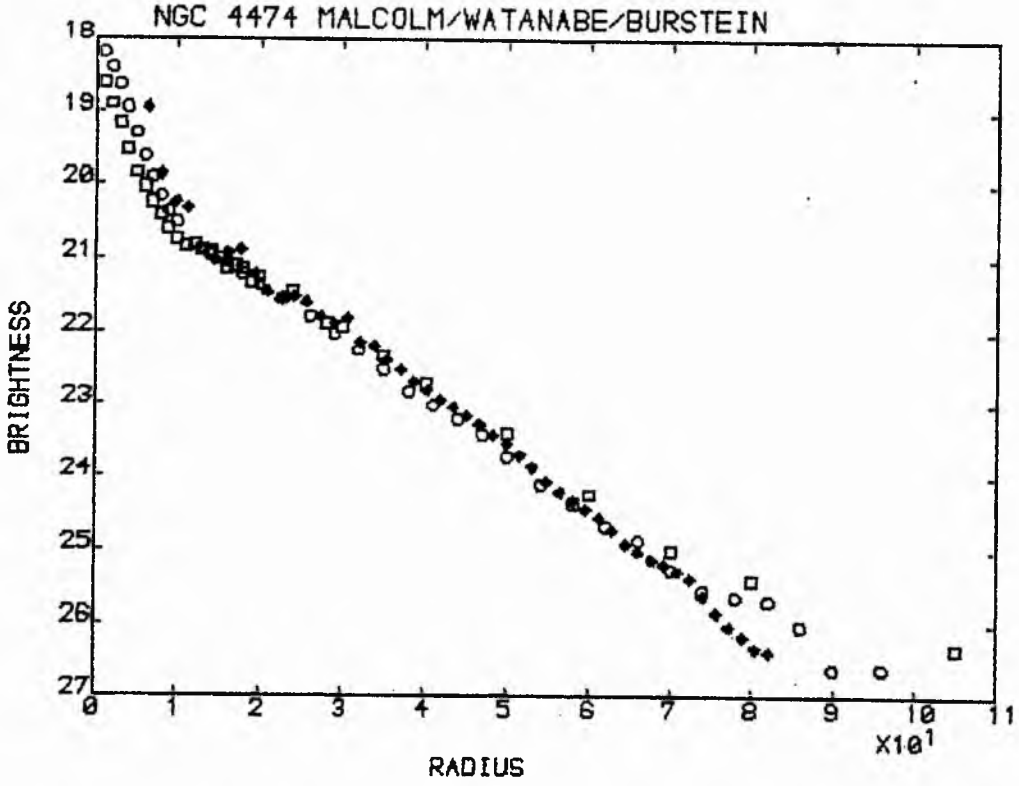
NGC 4474 MALCOLM/WATANABE/BURSTEIN
BRIGHTNESS
18
19
20
21
22
23
24
25
26
27
0
1
2
3
4
5
6
7
8
9
10
11
X10¹
RADIUS

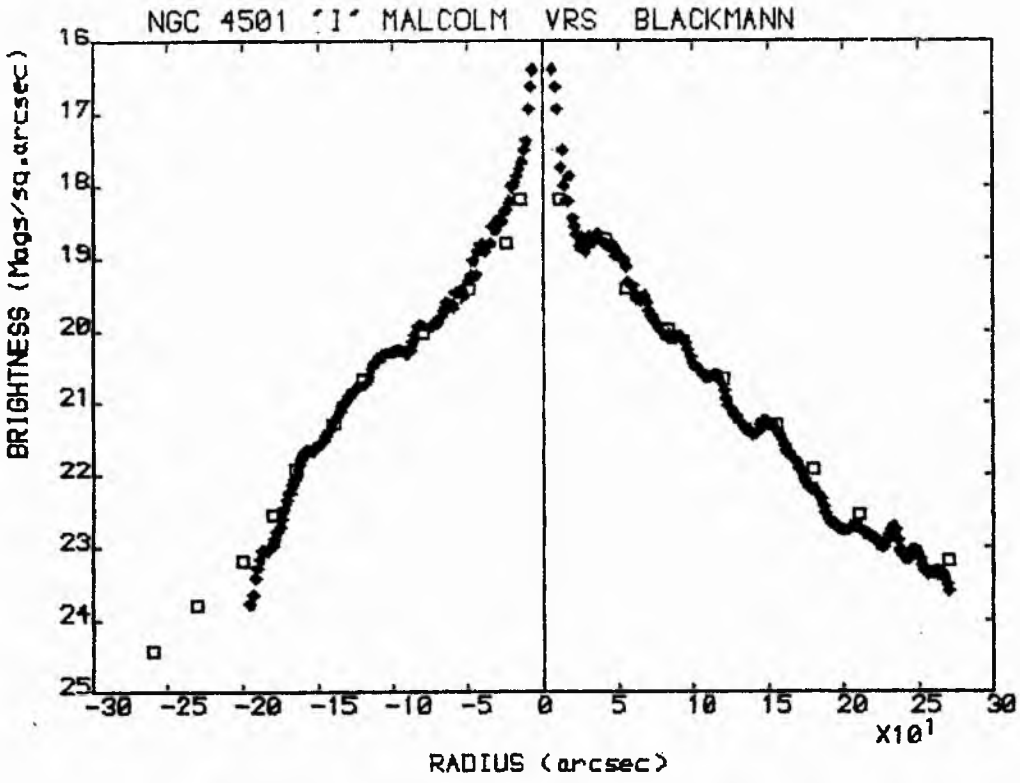
NGC 4501 'I' MALCOLM VRS BLACKMANN
BRIGHTNESS (Mags/sq.arcsec)
16
17
18
19
20
21
22
23
24
25
-30 -25 -20 -15 -10 -5 0 5 10 15 20 25 30
X10¹
RADIUS (arcsec)

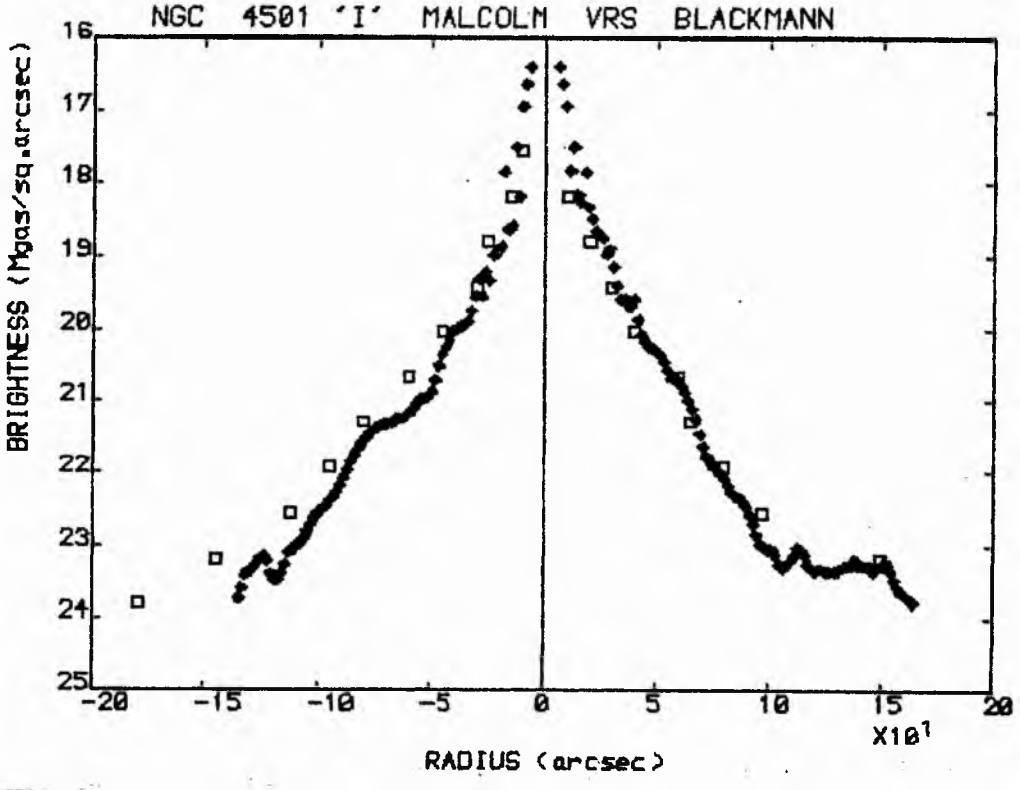
NGC 4501 'I' MALCOLM VRS BLACKMANN
BRIGHTNESS (Mags/sq.arcsec)
16
17
18
19
20
21
22
23
24
25
-20 -15 -10 -5 0 5 10 15 20
X10¹
RADIUS (arcsec)

NGC 4267 GJM vrs BSS

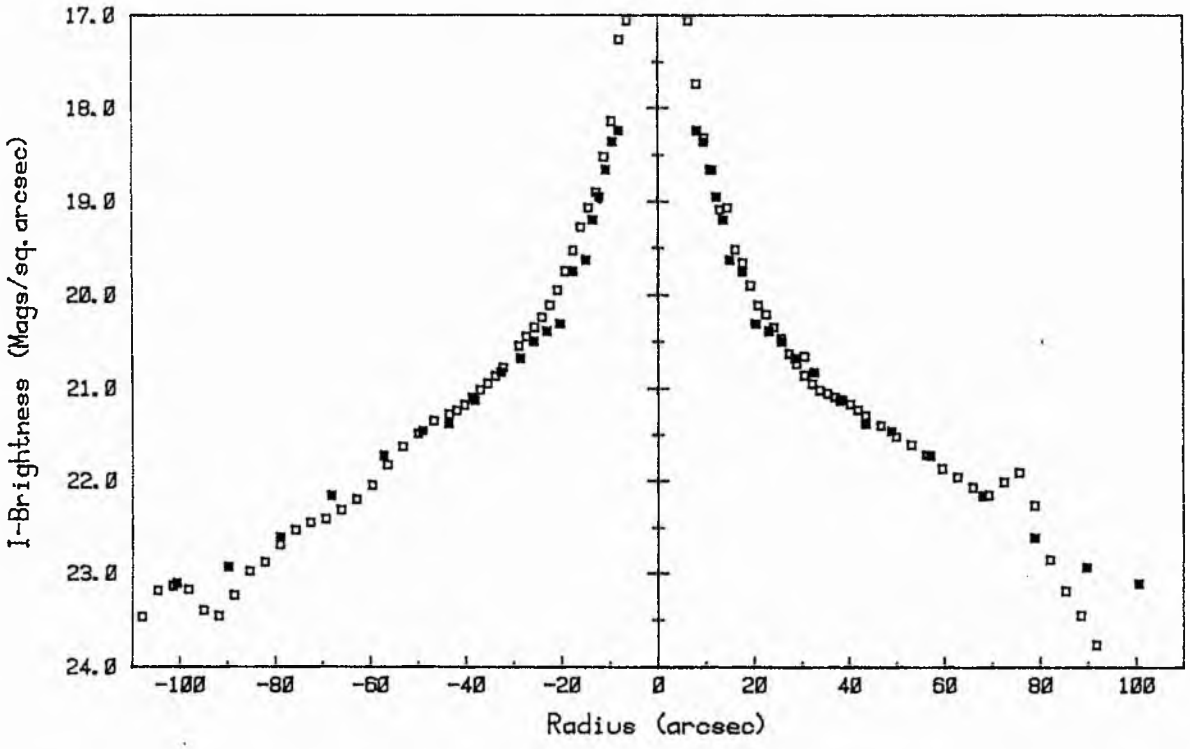

NGC 4419 GJM vrs BSS

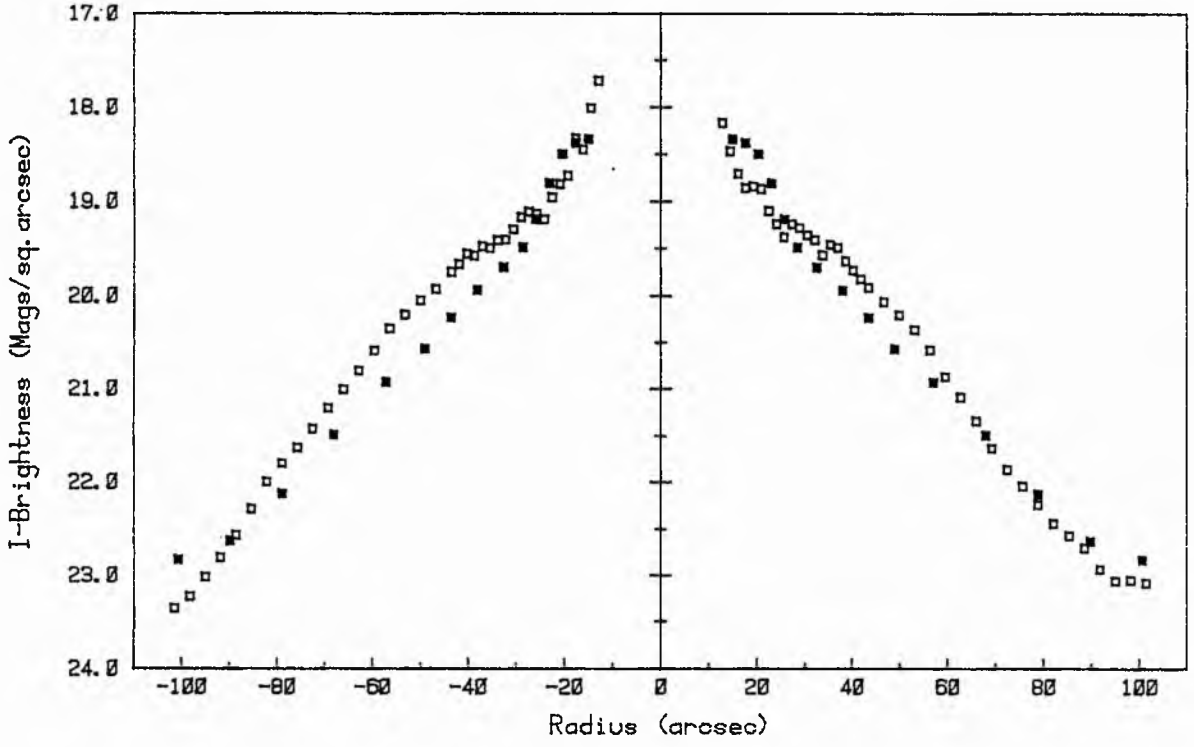

NGC 4425 GJM vrs BSS

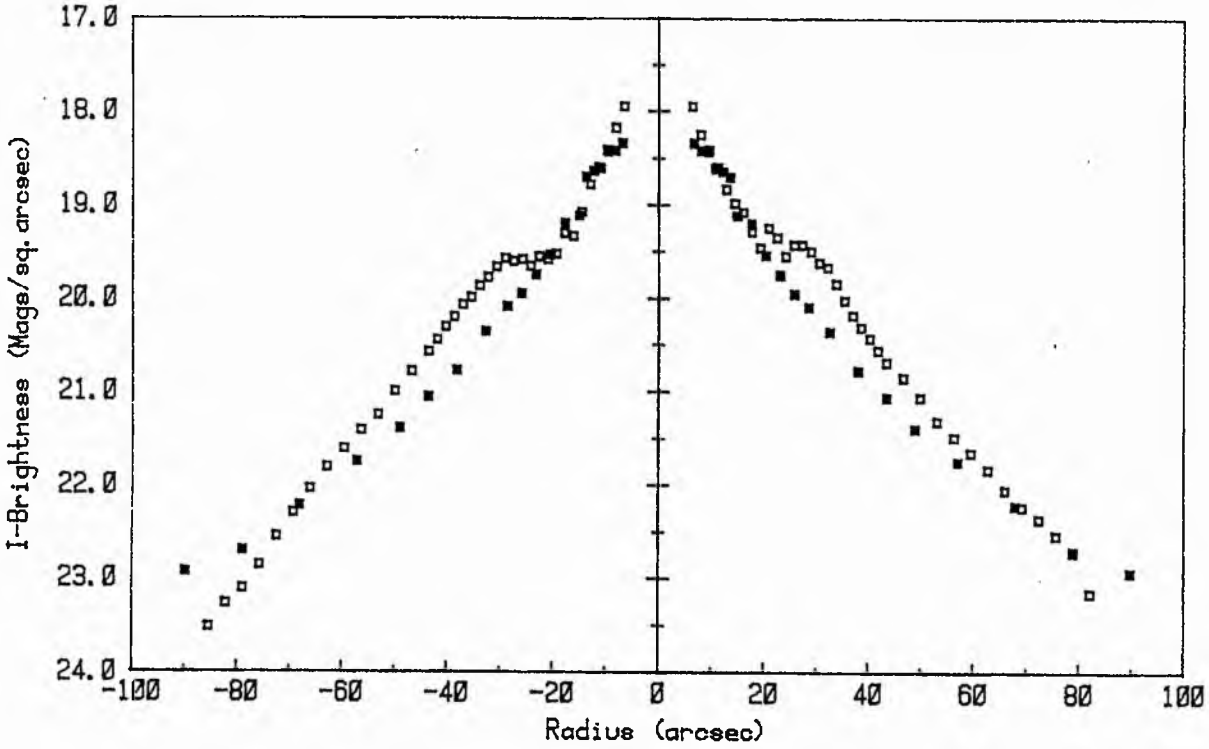

NGC 4429 GJM vrs BSS

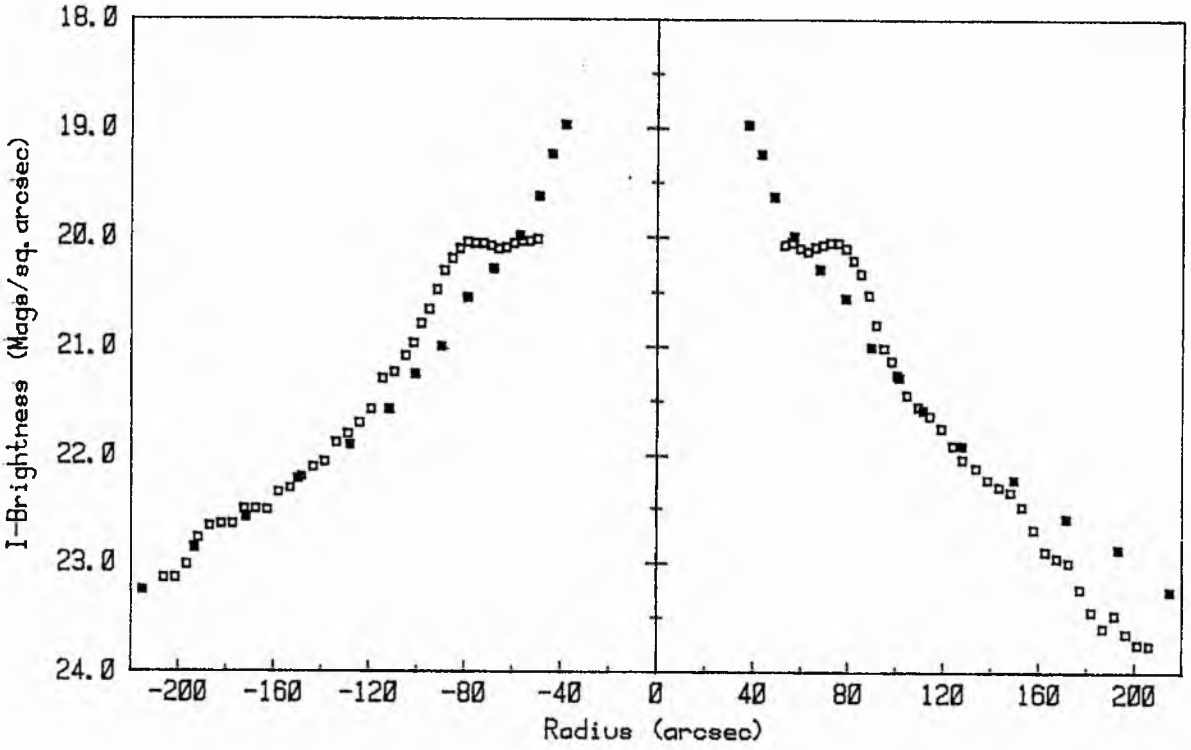

NGC 4435 GJM vrs BSS

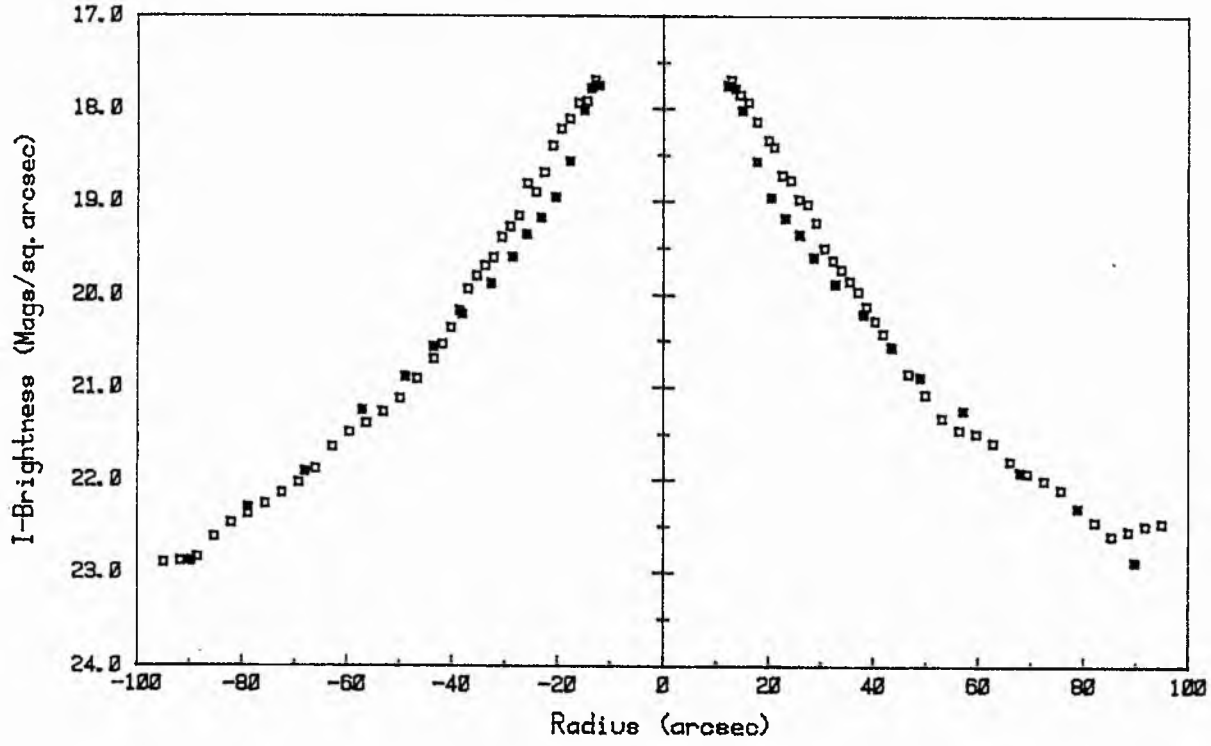

NGC 4459 GJM vrs BSS

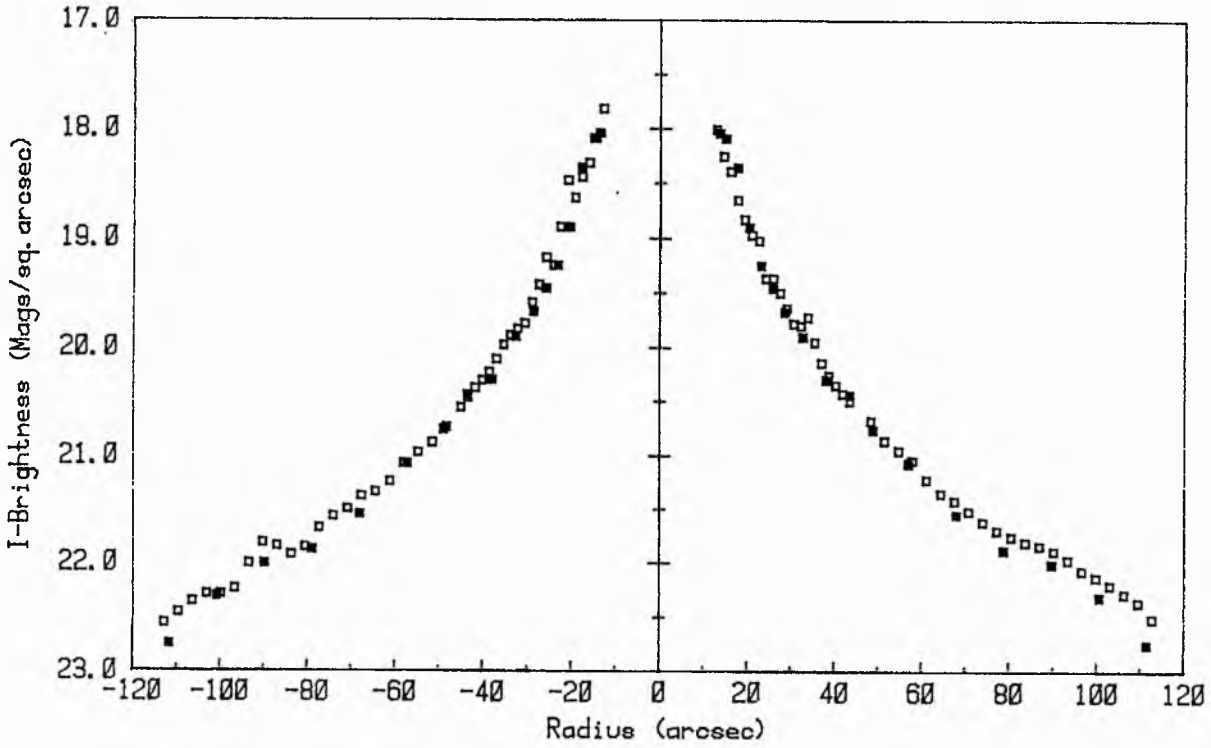

NGC 4474 GJM vrs BSS

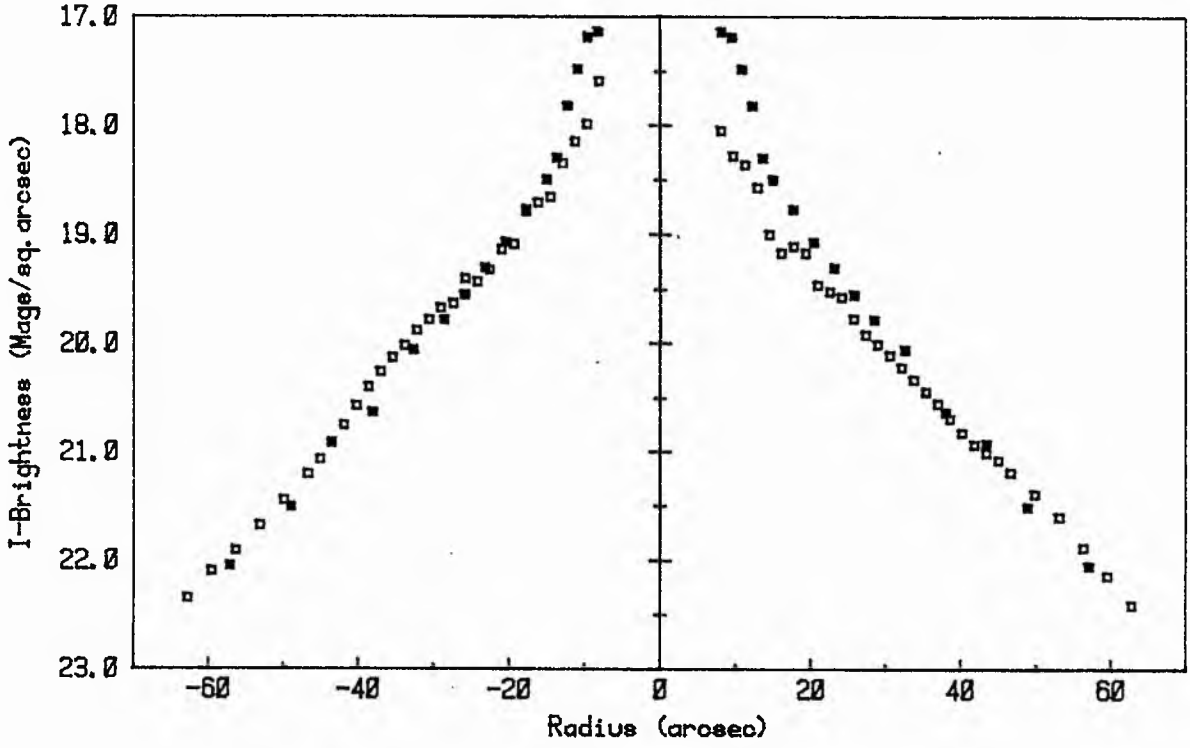

NGC 4461 GJM vrs BSS

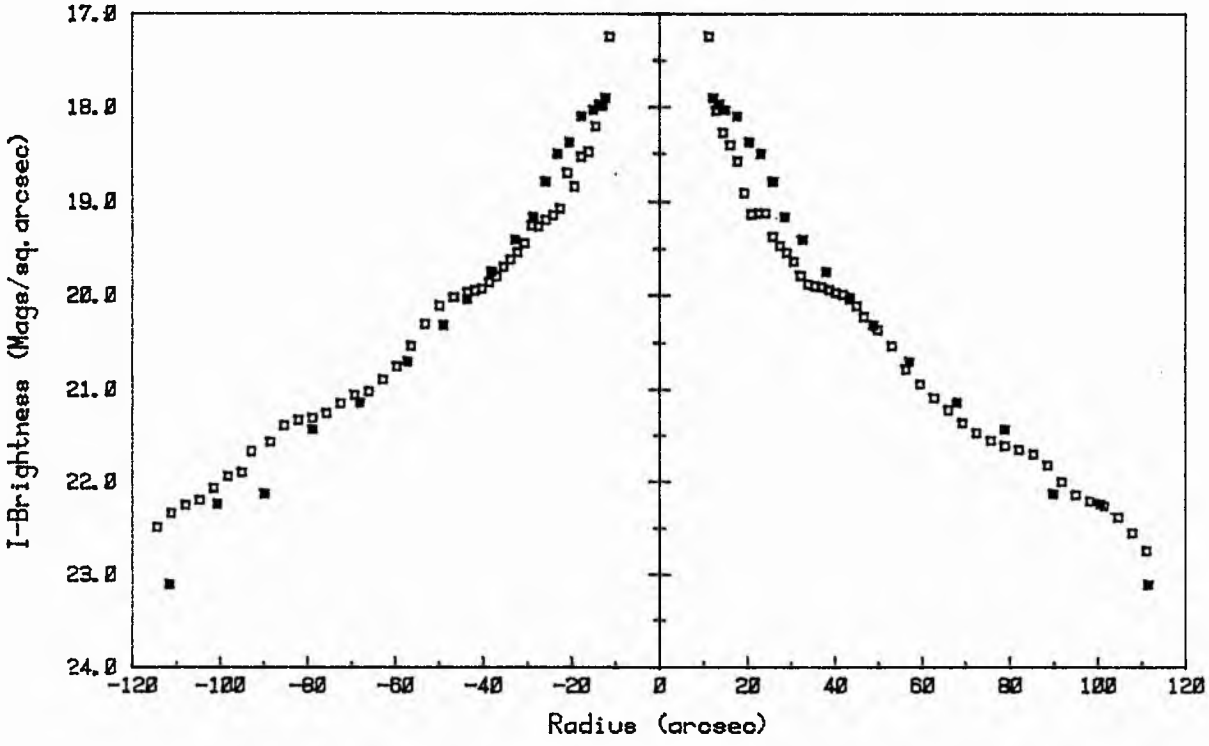

NGC 4477 GJM vrs BSS

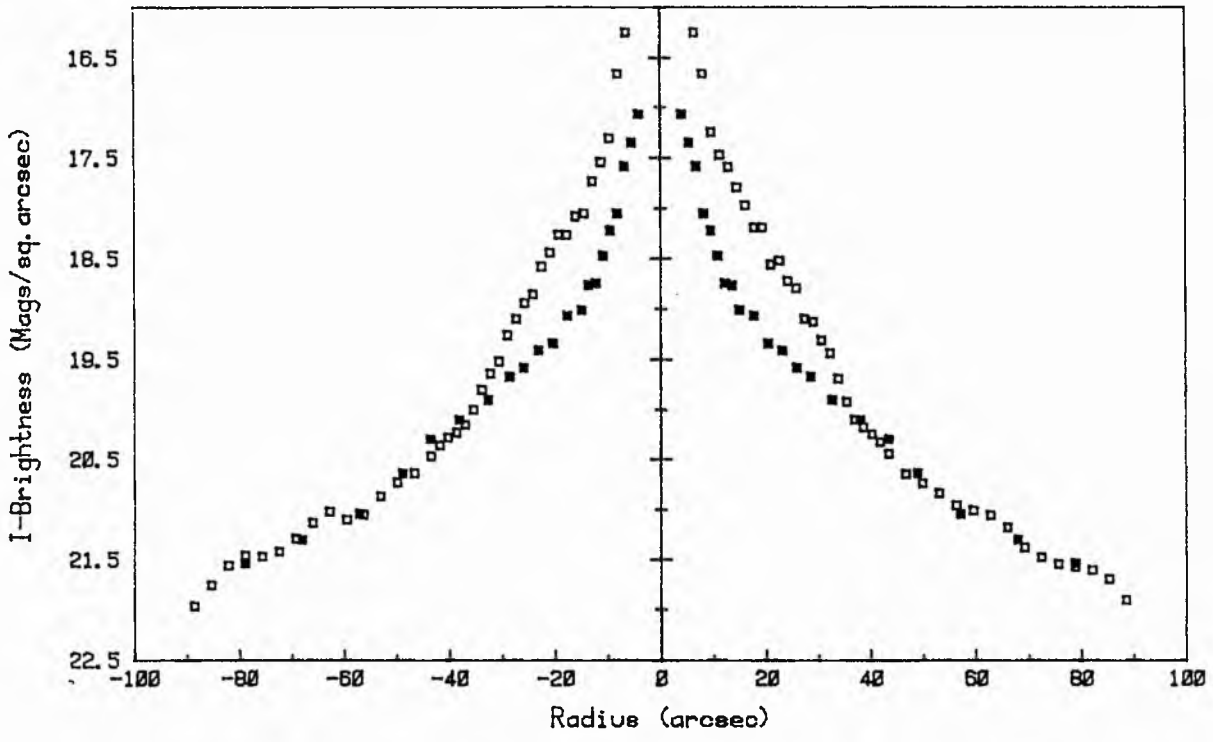

NGC 4477 WATANABE vrs BSS

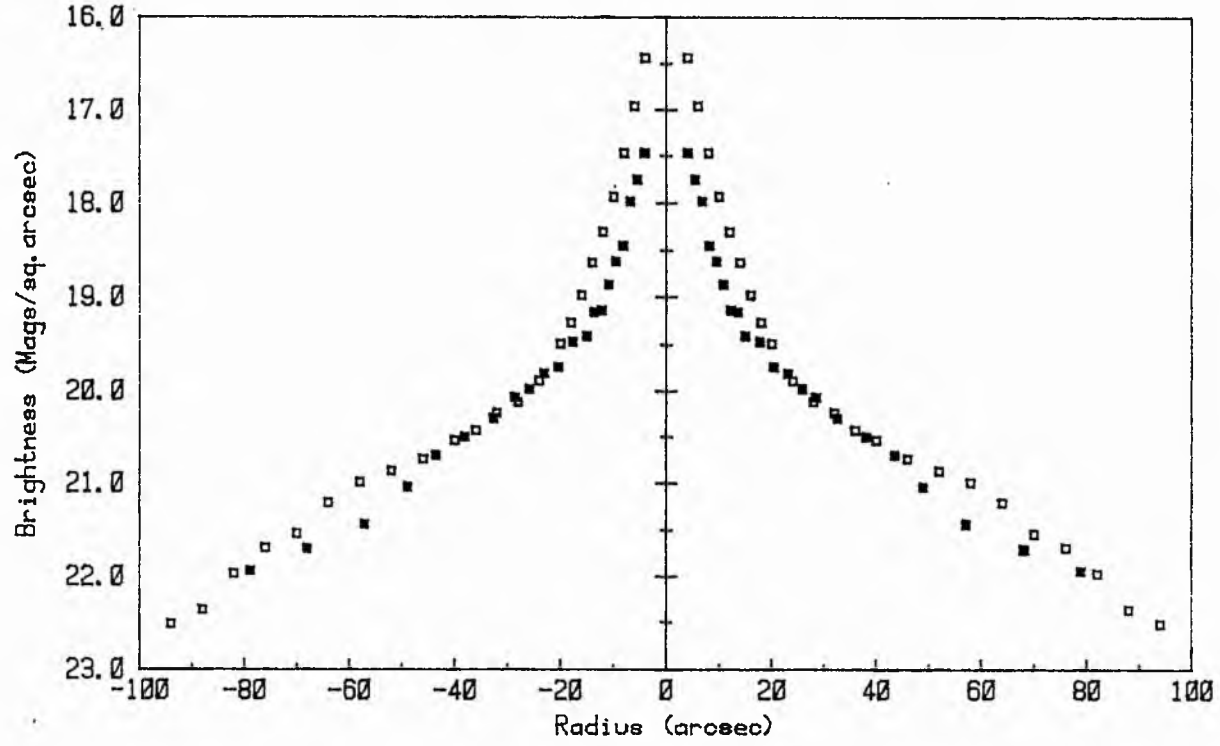

CHAPTER IV

A DESCRIPTIVE ANALYSIS OF EXTRACTED LUMINOSITY AND COLOUR PROFILES

Introductory Remarks

Detailed examination of extracted luminosity distributions provides a powerful tool for the morphological classification of galaxies since the various structural components (see e.g. Kormendy (1982) for an exhaustive review) may be distinguished as their brightness distributions have different functional forms. The luminosity profile of an elliptical galaxy, or the bulge component of a disk system usually follows an $R^{1/4}$ law (e.g. de Vaucouleurs (1959)), whereas the profiles of disk components (Freeman (1970)) generally follow an exponential distribution (with some exceptions, see e.g. Kormendy (1980)). Spiral arms, bars, lenses and rings may be identified by their distinctive two-dimensional appearance and by their characteristic signature of localized excess luminosity in the observed (composite) luminosity distribution.

The techniques and difficulties of the mathematical decomposition of the observed luminosity distribution will be discussed in more detail in Chapter VI, but the identification of the components is a rather more straightforward procedure and may be accomplished primarily by inspection of the extracted luminosity profiles and isophotal maps.

The method of extracting the luminosity profiles along the major and minor-axes of the programme galaxies has been described in Chapter II, and the reliability of the reduction procedures has been demonstrated in Chapter III, so a descriptive analysis of the data is now presented without further reference to these topics.

IV - 1 Luminosity Profiles and Morphological Classification

The extracted B, R and I major and minor-axes profiles are graphically displayed in Data Appendix 'A' and tabulated in Data Appendix 'I'; the B, R and I isophotal maps are presented in Data Appendix 'D'.

NGC 4267

This galaxy is classified by de Vaucouleurs et al. (1976) (hereafter in this chapter denoted as VVC) as SB(s) O^-:, classified by Sandage and Tammann (1981) (hereafter in this chapter denoted as ST) as SBO_1, and classification in the Revised DDO scheme (van den Bergh (1966) of SO b: is quoted by Giovanardi et al. (1983a) (hereafter in this chapter denoted by GHSK). Inspection of the B, R and I luminosity profiles reveals prominent bulge and disk components but little evidence for an additional luminosity component such as a bar. The isophotal maps support this conclusion as they appear relatively uncomplicated with no suggestion of a bar. The most appropriate classification in the RH (RDDO) schemes is considered to be SAO^- (SO b), with a type of -3.

NGC 4371

This system is classified by VVC as SB(r)0^+, by ST as $SBO_{2/3}(r)$, and by GHSK as SB a. This galaxy has a well-defined small bar approximately 10^o offset from the minor-axis; to emphasize the non-perpendicularity of the extracted luminosity axes they are labelled "Lens" and "Bar" axes instead of "major" and "minor"-axes respectively. The "Lens" axis is dominated by the bulge component and displays only a residual disk component; the "Bar" axis displays these features with the addition of obvious excess luminosity between approximately 20" and 40" from the galaxy centre which is identified as the contribution of the bar. In all the "Bar" profiles the Southern wing component appears more prominent than its Northern counterpart. Inspection of the isophotal maps confirms a lack of structure in the outer disk component and the published classifications are considered appropriate for this system. The adopted RH (RDDO) classification is thus SBO^+ (SBO a) with a type of -1.

NGC 4377

This small galaxy is classified by VVC as SAO^-, by ST as $SO_1(3)$, and by GHSK as SO a. This system displays both bulge and disk components in all extracted major-axis profiles, and an intrinsic excess luminosity between 20" and 30" from the galaxy centre is visible in both the B and R passbands. No features responsible for this excess luminosity have been identified from the uncomplicated isophotal maps or from inspection of the intensity frame (via an ARGS display) and the original plate material; the most likely explanation is a weak inner ring or vestigial disk structure. It is noticeable that the excess

luminosity appears more pronounced in the B profile than the R profile and is absent from the I profile; this point is discussed subsequently. All the minor-axis profiles show an excess luminosity at about 20" from the galaxy centre on the Western wing; this feature is an artifact caused by the removal of a star from the galaxy image and should consequently be ignored. The adopted RH (RDDO) classification of this system is SA(r?)O$^-$ (SO a), with a type of -3.

NGC 4419

This galaxy is classified by VVC as SB(s)a, sp, by ST as SB ab:, and by GHSK as AbIII:. Inspection of the isophotal maps and original plate material confirms that it is a disk system seen at significant inclination with a visual appearance very similar to NGC 4425; no evidence for a bar was detectable. The extracted major and minor-axis profiles display both disk and bulge components, although they are surprisingly difficult to disentangle in the R profile. The B and I major-axis profiles also show a slight excess luminosity between 30" and 50" from the galaxy centre which may be more pronounced in the blue; the most probable cause would seem to be either an inner ring or vestigial spiral structure, although a bar cannot be discounted. The general appearance of the system and similarity with NGC 4425 lead to the preferred RH(RDDO) classification of SA(rs)O(Ab); the type seems earlier than NGC 4429 and is therefore adopted as -2.

NGC 4425

This galaxy is classified by VVC as SBO:sp, by ST as SBO pec, and by GHSK as Ab. Examination of the isophotal maps

and extracted luminosity axes demonstrated a considerable morphological similarity with NGC 4419, although in this case the excess luminosity between 20" and 40" from the galaxy centre on the major-axis is most clearly distinguishable in the R and I passbands and is least visible in the B profile. Inspection of the original plate material supports the interpretation of the third component as vestigial disk structure (see also the V-band isophotal map presented by Watanabe (1983) p. 205), although a weak bar cannot be completely discounted. The similarity of this system with NGC 4419 suggests a preferred RH(RDDO) classification of SA(s?)O(Ab), with a type of -2.

NGC 4429

This galaxy is classified by VVC as $SA(r)O^+$, by ST as SO_3/Sa pec and by GHSK as SOa/Aa. Inspection of the extracted luminosity axes reveals well-defined bulge and disk components with considerable excess luminosity between 50" and 100" in all major-axis luminosity profiles. Examination of the isophotal maps excludes a bar component, and careful study of the original plate material and processed intensity frames revealed that the excess luminosity is due to a pair of tightly-wound low-contrast spiral arms. This identification has been subsequently confirmed by Watanabe (1983) (p. 206). The preferred RH(RDDO) classification is thus $SA(s)O^+$(Aa), with a type of -1.

NGC 4435

This sytem is classified by VVC as SB(s)O, by ST as SBO_1, and is not classified by GHSK. The image of NGC 4435 is in very close proximity to that of the peculiar system NGC 4438

(discussed in section I-V and subsequently), although the isophotes of NGC 4435 appear undisturbed at all passbands even at low surface brightnesses. In view of the drastic damage being done to the (apparently) larger NGC 4438, this lack of disturbance argues strongly for a projection proximity, and thus in favour of the ICM-interaction models for NGC 4438 described in section I-V. At very low surface brightnesses the outer isophotes of NGC 4435 overlap with the extended luminous "plume" to the South and East which is associated with NGC 4438. This plume is detected as excess luminosity in all passbands in the southern wing of the major-axis profiles. The south-eastern wings of all the minor-axis profiles have been extended to provide a cross-section of the plume; all the profiles show a luminosity maxima at about 170" from the centre of NGC 4435, although the maxima seems most pronounced in the B profile. At brighter light levels the luminosity profiles are dominated by the bulge component, with the disk component very weak and suggested by the "pyramidal" appearance of the luminosity profiles and inspection of the isophotal maps. The overall appearance of the system at brighter light levels is quite similar to NGC 4474 and 4477 with a weak bar aligned with the major-axis and no trace of structure in the outer (disk) regions. The preferred RH(RDDO) classification is SBO(SBO a), with a type of -2.

NGC 4438

This object is morphologically peculiar, appearing in Arp (1966) ("An Atlas on Interacting Galaxies"), and is classified by VVC as SA(s)/SOa Pec., by ST as Sb(tides), and

(rather non-commitally) as Irregular by GHSK. The system is characterized by two plumes of excess luminosity extending to the South-East and South-West of the galaxy, each with a definite "hooked" appearance. A prominent dust ridge is observed to the West of the galaxy nucleus. Luminosity axes were extracted along the main "plume" to the North-East (leaving the south-western wing of the major-axis relatively undisturbed), and along the bar axis (see below) which is aligned approximately 20^{o} from the perpendicular vector w.r.t. the major-axis. Inspection of the 'B' isophotal map and extracted luminosity axes clearly reveals a bar of relatively-high surface brightness and spiral arms aligned with the anomalous "plumes" of luminosity; these features are markedly less pronounced in the R-passband data and essentially absent in the I-passband data. The implication naturally arises that these features are indicative of a young blue stellar population in the inner regions of NGC 4438; this component might arise naturally via the mechanism of shock-induced star-formation if the galaxy is undergoing gas sweeping by ICM-interaction (e.g. Kotanyi and Ekers (1983)). In addition to the blue bar component the relatively undisturbed south-western wing of the major-axis shows both bulge and disk components. The bulge component appears most pronounced on the 'B' major-axis profile, which is also quite unusual. Morphological classification of this system is clearly very difficult; as the system is most plausibly modelled by the sweeping of gas and dust from a disk system, and the outer regions display no structure between the anomalous "plumes", the preferred classification adopted for this system is SB:/SBO pec. (for both RH and RDDO systems), with a type of Ø. Certainly this classification is

open to debate as the features of this most unusual system are not easily quantified by the standard classification schemes.

NGC 4459

This galaxy is classified as $SA(r)O^+$ by VVC, as SO_3 by ST, and as SOa: by GHSK. The isophotal maps obtained in this survey are generally smooth and devoid of structure in all three passbands; this impression is confirmed by examination of the extracted luminosity axes. The galaxy is clearly dominated by a bulge component (particularly in the I-passband) with only a very weak disk component. Sandage (1961) demonstrates that NGC 4459 has a small dust lane close to the nucleus, although this feature is not clearly revealed in the extracted luminosity profiles. Other than this feature, the overall appearance of this system is similar to NGC 4267, and the preferred RH(RDDO) classification is SAO^+(SOa), with a slightly later type of -2.

NGC 4461

This system is classified as $SB(s)O^+$ by VVC, as Sa by ST, and as SOat by GHSK. The galaxy has a visible appearance similar to NGC 4419 and NGC 4425 but is seen at a smaller inclination. The small elliptical system NGC 4458 appears close by to the North-West. Inspection of the extracted luminosity axes reveals stronge bulge and weak disk components, supplemented by a slight excess luminosity between 35" and 50" from the galaxy nucleus on the major-axis. This feature is most prominent in the R passband, being less so in I and only just discernible in B. Close inspection of the isophotal maps and original plate material, revealed very little evidence for a bar but suggested

possible low-contrast spiral structure in the disk; this impression was confirmed by inspection of the processed intensity frames (via an ARGS display) and is supported by the 'V' isophotal map of Watanabe (1983) (p. 210). The preferred RH(RDDO) classification of this galaxy is SA(s?)O^+(Aa), with a type of -1.

NGC 4474

This small galaxy is classified by VVC as SO pec.:, by ST as SO_1, and as SO:a by GHSK. Burstein (1978) considers that the galaxy appears more inclined at higher surface brightnesses, and that the bulge and disk contributions do not merge smoothly but come together sharply at a radius of about 10" from the galaxy centre on the major-axis. Inspection of the extracted luminosity axes reveals significant differences between the major and minor-axes: although the bulge and disk components are discernible in the minor-axes (although the bulge becomes increasingly dominant as the passband becomes redder), the components are much less readily disentangled on the major-axes which appear to have a less dominant bulge and a much brighter disk. It is apparent from the isophotal maps that these effects are primarily due to a distension of the isophotes at high surface brightnesses along the direction of the major-axis, with the distension diminishing with surface brightness. Some isophotal twisting is also visible in all three passbands. The most likely explanation for the observed features of the isophotal maps and luminosity profiles is the presence of a third luminosity component, such as a weak bar, aligned along the major-axis. The general features of the isophotal maps and the

original plate images are reminiscent of NGC 4477, which is consistently classified as a barred system (see below), which provides additional support for this hypothesis. Hence the preferred RH(RDDO) classification for this system is S(B)O: (S(B)O b:), with a type of -2.

NGC 4477

This large galaxy is classified as SB(s)O: by VVC, as SBO 1/2 by ST, and as S(B)O b by GHSK. The isophotal maps of the system are reminiscent of NGC 4474 seen at a smaller inclination at higher surface brightnesses. In addition to the bulge and disk components a third luminosity component is clearly visible in all the major and minor luminosity axes centred between 60" and 80", leading to the natural identification of a bar and probably an associated lens component (see e.g. Kormendy (1982) for a review of this association with particular reference to lenticular systems). The asymmetry of the extracted luminosity axes is quite marked and independently confirmed in each passband (e.g. the steep drop in luminosity between 80" and 100" on the south-eastern wing of the minor-axis). The adopted RH(RDDO) classification for this system is SBO(SBO b), with a type of -2.

NGC 4501 (M88)

This luminous system is classified as SA(rs)b by VVC, as S bc(s)II by ST, and as Sb* by GHSK. NGC 4501 is a normal "vigorous" spiral, with several well-developed spiral arms, in apparent proximity to the Virgo cluster core. In view of the drastic damage recently inflicted on NGC 4438, it seems likely

that this proximity is a projection effect with NGC 4501 being a foreground (or background) member of the Virgo cluster. This hypothesis receives some support from the observation that NGC 4501 has a radial velocity several hundred kilometres per second higher than most other probable members of the Virgo cluster core. Inspection of the isophotal maps and extracted luminosity axes confirms that this galaxy is dominated by a disk component and attendant spiral structure; considerable asymmetry is obvious in all extracted profiles, with the spiral arms having less importance as the passband becomes redder. The bulge component is well-determined and of increasing importance as the passband becomes redder. The standard classifications seem quite correct for this system, and the adopted RH(RDDO) classification is SA(rs)(Sb), with a type of 3.

NGC 4503

This galaxy is classified by VVC as SBO$^-$, by ST as Sa, and by GHSK as SO a/b. Inspection of the isophotal maps and extracted luminosity axes reveals well-determined bulge and disk components with no obvious third component. The isophotes appear smooth in all the passbands with a slight amount of twisting at the lowest extracted surface brightnesses. There is a region of excess luminosity between 60" and 90" from the galaxy centre on the south-western wing of the major-axis; this feature appears less prominent as the passband becomes redder and may represent possible vestigial structure in the disk. It would be interesting to obtain high-resolution ultra-violet images of this system to investigate this suggestion; until such data becomes available the adopted RH(RDDO) classification is SAO$^-$(SO a/b)

with a type of -3.

NGC 4531

This system has been rather neglected due to its low surface brightness, being simply classified as S by VVC and ST (Appendix A), and is not classified by GHSK. NGC 4531 was included in this work, however, because it fulfills the primary selection criterea: it is a disk system containing very little apparent structure, within 3^{o} of the Virgo cluster centre, and large enough to permit investigation by the standard techniques employed in this survey. Moreover, it is a particularly interesting system because it has a weak bulge in dramatic contrast to most lenticular systems. NGC 4531 has a much more luminous disk than the typical low surface brightness dwarf galaxy (e.g. NGC 4411 A or B), and has an appearance reminiscent of NGC 3913 which has a classification of SO/a derived by Romashin et al. (1983). It would seem reasonable, therefore, to consider NGC 4531 as an early-type system of low surface brightness. Inspection of the isophotal maps confirms that this galaxy has a well-determined disk but a very weak bulge component. This is particularly well-illustrated by comparison of the major-axis profiles with those of NGC 4425. For all passbands the disk surface brightness profiles are quite similar, but whereas the bulge component of NGC 4425 becomes increasingly obvious as the passband becomes redder, no bulge component becomes prominent in the case of NGC 4531. This is not to say that the bulge component is not present, as one should note that the profile is not plotted within 5" of the galaxy centre where the bulge contribution is strongest. The available radial

velocity data (e.g. Huchra et al. (1983)) is reasonably consistent with other low-velocity members of the Virgo cluster core, so unless the system can be demonstrated to be a foreground object the most appropriate RH(RDDO) classification would seem to be SO:pec (Abc:pec), with a type of -1. Alternative classification is feasible, but it seems quite possible that this is indeed a bulge-weak early-type disk system. It is unclear, however, whether this galaxy is part of the long-sought population of environmentally processed late-type spirals, or merely a disk system which has never developed a prominent bulge component.

NGC 4550

This galaxy is classified by VVC as SBO^{+}:sp, as $E7/SO_1$ by ST, and as SOa by GHSK. The galaxy is clearly a disk system seen at some inclination with a general appearance similar to NGC 4461. The galaxy is dominated by a bulge component with smooth isophotes in all passbands and no sign of a bar or structure in the disk itself. The galaxy has the small elliptical NGC 4551 as an apparently close companion with the outer isophotes of NGC 4550 exhibiting a slight twisting, but no evidence of significant tidal distortion is discernible for either system. The preferred RH(RDDO) classification for this system is SAO^{+}(Aa), with a type of -1.

NGC 4552 (M89)

This bright system is classified as EØ by VVC, as SO_1 by ST, and is not classified by GHSK. The galaxy has been shown by Malin (1979) to have anomalous features at extremely low surface brightnesses, including a jet and several luminous arcs.

In all passbands the inner regions of the galaxy are defined by smooth isophotes following an $R^{1/4}$ law, but there is clear evidence for excess luminosity at larger radii (as shown in Figure IV.1, where it is compared with the major-axis of NGC 4371 which has a pronounced disk component. The major-axis of NGC 4371 is labelled the "Lens" axis for reasons explained earlier in the text). This type of excess luminosity has been found in several Virgo ellipticals by Kormendy (1977b), and interpreted by him as probable evidence for tidal distension due to galaxy-galaxy interaction. An alternative hypothesis is suggested by the classification of ST, namely that these "ellipticals" may possess very weak disks. Inspection of the luminosity axes confirms that the contribution of this "second component" is dominated by the $R^{1/4}$ component. Kormendy's "correlation" of excess luminosity with a nearby companion (or companions) is certainly suggestive, but cannot be regarded as conclusive. In view of this uncertainty, the adopted RH(RDDO) classification is E0 pec/$S0^-$ (E0p/S0a), with a type of -4 as a compromise between the classifications.

Figure IV.1

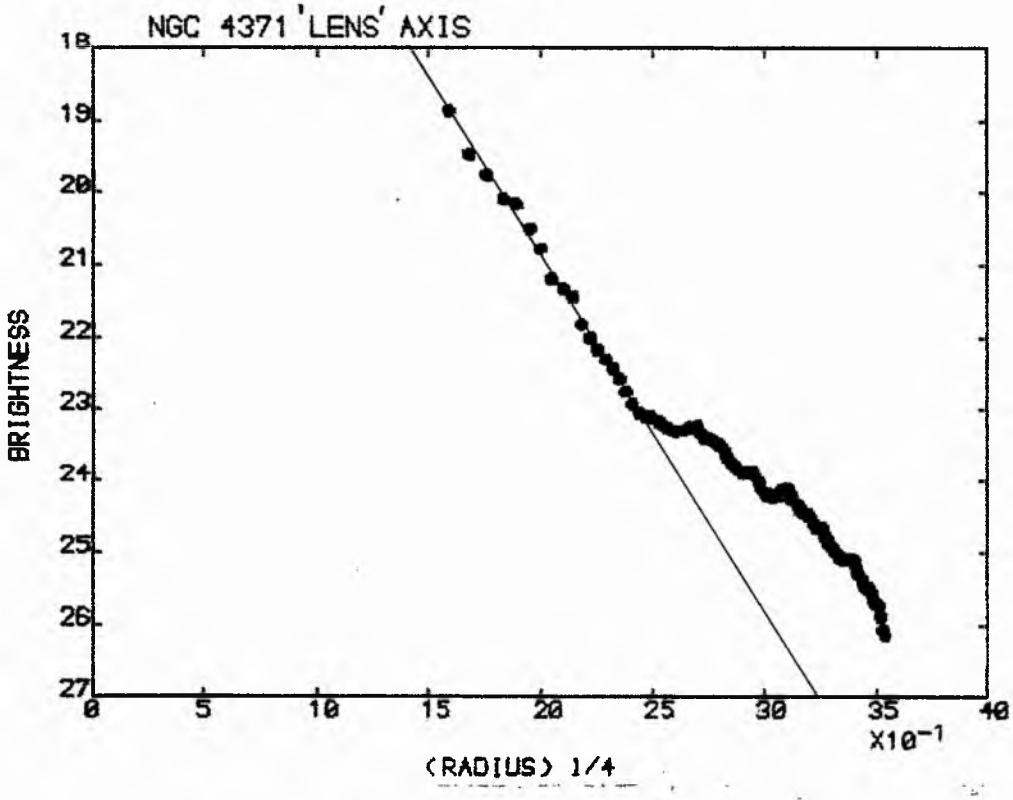
NGC 4371 'LENS' AXIS
BRIGHTNESS
18
19
20
21
22
23
24
25
26
27
0
5
10
15
20
25
30
35
40
X10⁻¹
(RADIUS) 1/4

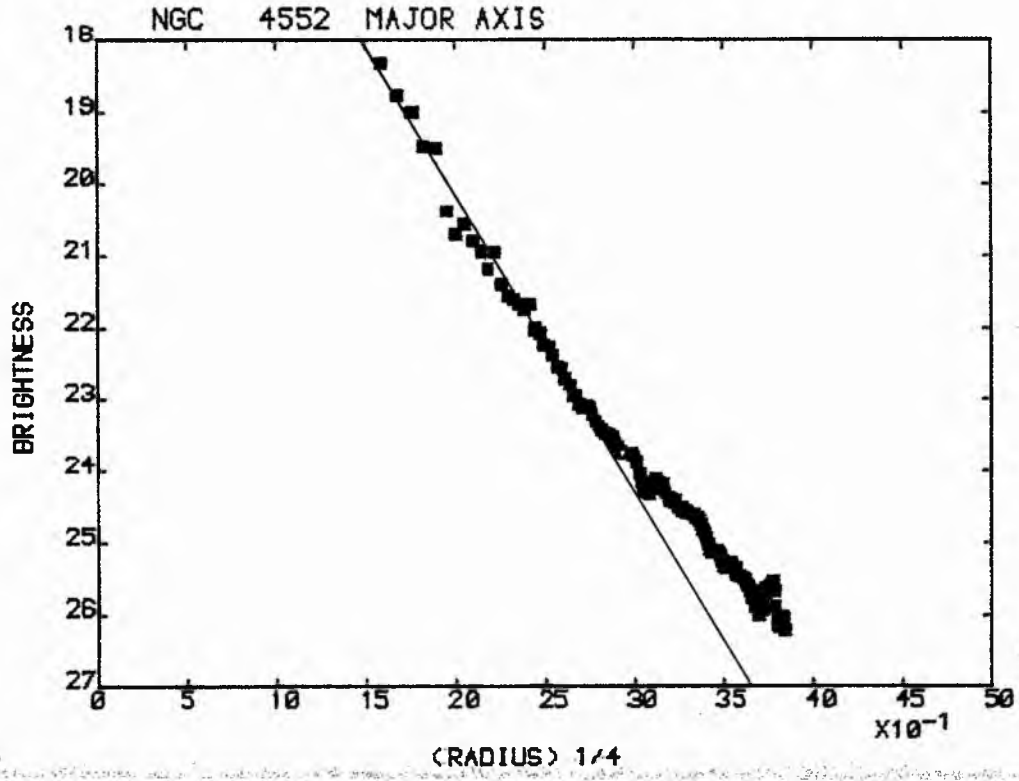
NGC 4552 MAJOR AXIS
BRIGHTNESS
18
19
20
21
22
23
24
25
26
27
0
5
10
15
20
25
30
35
40
45
50
X10⁻¹
(RADIUS) 1/4

IV - 2 Colour-Difference Profiles

The extracted major and minor-axis profiles were used to construct (B-R), (B-I) and (R-I) colour-difference profiles using the procedures described in Chapter II, Section 4.2; the colour-difference profiles are shown graphically in Data Appendix 'B' and tabulated in Data Appendix 'H'.

2.1 Systematic Uncertainties Affecting Colour-Difference Profiles

The interpretation of colour-difference profiles is considerably complicated by the inherent systematic errors of photographic photometry referred to in Chapter III (see also Boroson et al. (1983 a)). Two sources of systematic error are particularly important: the imperfect transformation from Photographic density to incident intensity which is almost invariably most serious at high surface brightnesses (e.g. Bingelli et al. (1984)), and errors in the adopted sky level in the intensity frame (e.g. due to contamination of the sky evaluation by the outer regions of the galaxy) which are most serious at low surface brightness. Both these sources of error typically manifest themselves in the form of systematic "bends" in the colour profile, at high and low surface brightnesses respectively.

Systematic errors at high surface brightnesses in the B and I-band data have been excluded by the comparison with previously published surface photometry performed in Chapter III; only the

R-band data has no direct verification. One can show, however, that such errors appear unlikely in the R-band by comparing some of (B-R) colour profiles. The bulges of NGC 4267, 4435, 4477 and 4552 have similar R-band surface brightnesses, but their (B-R) colour profiles within 20" of the galaxy centre have quite different gradients - ranging from nearly flat (NGC 4435) to a pronounced blueing towards the nucleus (NGC 4552). This effect is even more pronounced in the case of NGC 4501, where the major and minor-axes have similar 'R' surface brightnesses for the bulge, but quite different (B-R) colour gradients within 20" of the galaxy centre. Since the B-band photometry has been shown to be reliable at high surface brightnesses, if the R-band photometry were systematically in error then one might expect all galaxies with similar bulge surface brightness profiles to have (B-R) colour profiles of equivalent, or very similar, gradient at small radii. The observed disparity in the (B-R) colour profiles seems to exclude this possibility, and to provide circumstantial evidence that the R-band photometry is free from significant systematic error. Thus it seems reasonable to conclude that the colour-difference profiles are free from systematic errors at high surface brightnesses.

The method of calculating the sky intensity level and sky removal for each intensity frame has been described in detail in Chapter II (Sections 3.3 and 3.4), and considerable care was taken to ensure that this technique produced an accurate sky intensity level for each frame. It is clear from inspection of the colour-difference profiles that no characteristic "bends" (see e.g. Boroson et al. (1983 a) Fig. 5) are detectable at the

adopted termination threshold (either profile falls below 10% of the frame sky intensity). The absence of these "bends" is gratifying as it implies that the calculated frame sky intensities are accurate to a fraction of a percent, and the colour-difference profiles are free from systematic errors at low surface brightness.

Errors in the absolute intensity calibration of any frame (and associated luminosity profiles) are inevitable due to the paucity of available calibration photometry, but these errors will affect only the zero-points of the colour profiles and will not distort the profile shape. The problems of absolutely calibrating photographic surface photometry are notorious, and principally due to passband differences between photographic and photoelectric photometry, together with passband differences between different workers. Indeed, because zero-points are generally fairly arbitrary, profiles are often normalized to the nuclear magnitude, and accordingly the zero-points of the extracted colour profiles will not be discussed in this work.

2.2 Interpretation of Colour-Difference Profiles

Upon consideration of the arguments outlined in the previous sub-section, it seems reasonable to suppose that observed features of the colour-difference profiles are caused by intrinsic differences in the luminosity profiles, and one must consider what phenomena may be identified from the observations.

First of all, it should be borne in mind that since all tha surveyed cluster population are early-type systems (with the exception of NGC 4501), one would not expect significant colour gradients as a function of radius (from the galaxy centre) due to variations in the fractional contribution of young and old stellar components because early-type galaxies should be dominated by an evolved stellar population.

On the other hand, colour gradients as a function of radius caused by metallicity variations in the stellar population might well be detectable. The R-band "dip" observed in K and M-type giant stars (e.g. Whitford and Blanco (1979), Frogel and Whitford (1982)) is generally attributed to increased line-blanketing in stars of high metallicity, and might significantly affect the nuclear magnitudes of early-type systems (Boroson et al. (1983a)), in the sense of an inward blueing of (B-R) and corresponding reddening of (R-I).

Colour variations caused by non-stellar mechanisms must also be considered, even though the abundance of gas and dust should be low in early-type systems. The presence of dust (which might be expected to be centrally concentrated) should redden the observed colours, with (B-R) being three times more sensitive to this effect than (R-I) (Schild (1972)). Since H_α falls in the R-band, even weak H_α emission could significantly redden the (B-R) colours at small radii, and produce a corresponding blueing of the (R-I) colours.

2.3 Descriptive Analysis of the Extracted Colour Profiles

NGC 4267

The (B-R) and (B-I) major and minor-axis profiles show considerable similarity, with a gradual inward blueing and a slight blue "dip" at about 30 arcseconds radius (arcseconds are hereafter denoted in this chapter as ") suggested on close inspection of the data. The (R-I) profiles are generally flat, with a suggestion of the blue "dip" around 30" radius and a slight reddening on the minor-axis within 20" radius. The inward reddening on the minor-axis must be regarded as rather tentative as it is not supported by the major-axis data and the scatter of points is larger than usual. GHSK give the mass of hydrogen contained within NGC 4267 as $< 2.7 \times 10^8 M_\odot$, so the system is apparently gas-poor and the observed gradual inward blueing is certainly unexpected as it implies some residual star-forming activity in the inner regions of NGC 4267. This hypothesis receives some weak support from the blue "dip" at about 30" radius which might represent an inner ring of residual star-forming activity. It would be interesting to obtain some high-resolution ultra-violet images and spectra of the galaxy nucleus to investigate these suggestions.

NGC 4371

The innermost point of the colour profiles appears to be at variance with the rest of the data; inspection of the innermost points in the luminosity profiles suggests random errors in the R and I major-axes and the innermost point of the colour profiles is therefore discounted and is not considered in

the subsequent analysis.

The "lens" or major-axis profiles show a gradual inward reddening of the (B-I) and (R-I) colour profiles, and a corresponding gradual inward blueing of (B-R). These effects may imply a gradual inward increase of metallicity and dust in the inner regions of NGC 4371. The presence of dust is also suggested by the small reddening increases centred around 65" and 80" radius which are visible on all the colour profiles. The bar-axis profiles are generally flat in all passbands, with little suggestion of structure.

NGC 4377

The (B-R) and (B-I) major-axis colour profiles display a gradual inward reddening, with a pronounced blue "dip" between approximately 20" and 30" radius. The (R-I) major-axis profile is generally flat with a slight reddening around 20" from the galaxy centre. These features are coincident with the excess luminosity reported in section 4.1, and the suspected blue colour is confirmed. The observed features of the colour profiles suggest a gradual increase of dust towards the galaxy centre and a zone of residual star-formation (and possibly enhanced metallicity) about 20" - 30" from the galaxy centre.

The small number of data points and the artifact mentioned in section 4.1 precludes discussion of the minor-axis profiles except to note that the observed features are similar to the major-axis data.

NGC 4419

The (B-I) major-axis colour profile displays a progressive inward reddening within 60" radius of the galaxy centre; a faint outward reddening beyond this point may be a genuine colour gradient or due to imperfect sky subtraction. The (B-R) major-axis colour profile displays a progressive inward reddening within about 40" radius, is generally flat between 40" and 60" radius, and gradually reddens at radii greater than 60". Alternatively, one could consider the profile displays a gradual inward reddening within 30" radius and a blue "dip" between 30" and 70" radius. The latter explanation is perhaps supported by an apparent reddening of the (R-I) profile between approximately 30" and 65" which could imply a region of enhanced stellar metallicity. There is a pronounced blue "dip" in the (R-I) profile between approximately 10" and 30" radius which is partially due to dimming in the I-band (as (B-I) and (R-I) are blueing, but (B-R) is reddening), but may also indicate diffuse H_α emission near the galaxy nucleus; it is interesting to note that Stauffer (1983) reports weak H_α, N II and S II emission in the nucleus of NGC 4419 which may support this suggestion. The innermost point on the colour profiles appears slightly reddened on the (B-I) and (R-I) profiles and slightly blued on the (R-I)

profile, which may indicate an increase in dust and metallicity in the inner bulge of NGC 4419. The complex behaviour of the colour profiles is difficult to interpret uniquely, and it would be interesting to obtain spectra at various points along the major-axis to investigate the phenomena suggested by the colour profiles. The inclination of this system causes the minor-axis luminosity to fall off rapidly, resulting in too few data points on the colour profiles to merit discussion.

NGC 4425

The (B-I) major-axis profile shows a very slight reddening outward from about 40" radius, and a progressive inward reddening within 25" radius. A noticeable local peak of reddening is visible between about 30" and 35" radius; this feature is also visible on the (B-R) major-axis profile and seems to confirm the identification of disk structure mentioned in section 4.1. The (R-I) major-axis profile displays a gradual outward blueing beyond about 30" from the galaxy centre and a progressive inward blueing at radii within about 20". The inward reddening of the (B-R) profile within 30" of the galaxy centre seems more pronounced than the corresponding reddening of the (B-I) profile, and because the (R-I) profile is inwardly blueing it seems likely that there is an increase of dust and some $H\alpha$ emission towards the nucleus of NGC 4425. The slight outward reddening beyond 30" radius is more pronounced in (B-R) than (B-I), and when combined with the corresponding slight outward blueing of the (R-I) profile may suggest a slight outward decrease in metallicity. The inclination of NGC 4425 causes the minor-axis luminosity profiles to drop steeply, resulting in too

few points on the corresponding colour profiles to merit discussion.

NGC 4429

The (B-I) and (R-I) major and minor-axis profiles show the innermost data points to be considerably redder than the rest of the extracted colour profiles. Examination of the I-band luminosity axes confirms that the first three data points on both wings of the major and minor-axes are substantially brighter than those points at slightly larger radius. These points represent very high photographic densities, and it is suspected that these points are erroneously bright due to scanning saturation (see also section II-2); the innermost points of the (B-I) and (R-I) profiles are therefore discounted in the following discussion and all data points with I-magnitudes < 17 should be treated with caution.

The (B-I) major-axis profile is essentially flat with small blue "dips" centred around 40" and 80" radius from the galaxy centre. The (B-R) major-axis profile is generally flat with a blue "dip" extending from about 30" to 90" from the galaxy nucleus. The blueing seems to naturally correspond to the excess luminosity attributed to spiral structure in the disk (section 4.1), and to suggest a possible reddening due to dust at about 60" from the galaxy centre. This would correspond to an increase in dust just interior to the onset of the main spiral arm components detected in the luminosity profiles. The (R-I) profile shows a pronounced blueing inward of about 30" radius, a pronounced reddening between about 40" and 90", and is generally flat beyond 90"

radius. The reddening in (R-I) and corresponding blueing in (B-R) between 40" and 90" from the galaxy centre implies a metallicity increase in the spiral arms of NGC 4429. The inward blueing of (R-I) within about 30" radius may be due to H_α emission, an explanation which receives support from the slight inward reddening of the (B-R) profile in this region. Any H_α emission may be diffuse and confined to the inner spiral arms as Stauffer (1983) reports very little emission in the nucleus itself. GHSK confirm that this system is gas-poor, with a total hydrogen mass $< 3.2 \times 10^8 M_\odot$. The minor-axis colour profiles are similar to the major-axis data : the (B-I) profile is generally flat and the (B-R) profile displays a gradual outward reddening with a blue "dip" between 20" and 30" from the galaxy centre. The (R-I) profile displays a reddening increase between 20" and 30" radius and is probably indicative of a metallicity increase associated with the inner spiral arms. The small reddening increase detectable between 50" and 60" in the (R-I) and (B-I) profiles probably corresponds to a zone of slightly enhanced I-luminosity on the southern wing of the minor-axis luminosity profile.

NGC 4435

The (B-I) major-axis profile shows a gradual inward reddening with a small blue "dip" between 30" and 40" radius. The (B-R) major-axis profile is flat beyond about 45" from the galaxy centre, has a slight blue "dip" centred between 50" - 40" radius, and a slight inward reddening within 30" of the galaxy centre. The (R-I) major-axis profile displays a gradual inward

reddening within 30" radius and a well-defined increase in reddening between 35" and 45" from the galaxy nucleus. The observed features of the colour profiles at radii smaller than about 30" are consistent with a slight increase of dust, and possibly also metallicity. The well-defined features at 35" - 40" radius seem likely to be associated with the weak bar of NGC 4435, and to represent residual star-forming activity and a local metallicity increase. The minor-axis profiles of NGC 4435 are quite flat in all colours within 30" of the galaxy centre, implying that any dust is confined to the major-axis and is probably associated with the bar. At radii larger than 30" the (B-I) profile is flat, the (B-R) profile shows a gradual outward reddening, and the (R-I) profile a gradual outward blueing. These features would seem to be consistent with a progressive outward decrease in metallicity.

NGC 4438

Due to the gross asymmetry of the luminosity profiles presented in section 4.1 the major-axis colour profiles have not been "folded" for this system. The absence of data points, particularly between 140" and 180" radius on the north-eastern wing of the (B-I) and (R-I) profiles, is due to the I-surface-brightness being below 10% of the sky brightness adopted for the frame; the normal termination of the profile extraction was suppressed as the luminosity increased at larger radii and it was of interest to obtain data points along the anomalous "plume".

The extracted major-axis profiles display similar features in all

colours, although the scatter on the profiles is larger than usual because the folding process produces an extra smoothing. There is clear evidence of a strong inward reddening across the bar component, followed by a strong inward blueing within 15" of the galaxy centre. This implies that a considerable amount of dust is still associated with the bar and inner regions, and confirms the suspicion that the nucleus is anomalously blue (section 4.1). The north-eastern wing shows several features common to all colour passbands: a region between about 50" and 80" which is quite blue, a strong blue "dip" at around 90" radius, a slight reddening between 100" and 150", and a gradual outward blueing beyond about 150" radius from the galaxy centre. It seems natural to interpret these features as zones of enhanced star-formation with some patches of dust; inspection of the (B-R) profiles confirms that the "plume" is considerably bluer than inner regions of the minor (bar) axis as was first suggested by Markarian et al. (1965). The tendency for the "plume" to become progressively bluer at larger radii is particularly interesting, and may support the suggestion that the region of star-formation has been "blown downwind" along the "plume" (Kotanyi and Ekers (1983)). The minor (bar) axis profiles of NGC 4438 are generally flat in all colours with the innermost point slightly reddened, which may indicate an increase in dust in the innermost ends of the bar. NGC 4438 has been shown by Stauffer (1983) to have strong nuclear emission lines (H_α, N II and S II), and is reported by GHSK to have about $2.8 \times 10^8 M_\odot$ of hydrogen still contained in the system. In view of the unusual features confirmed in this work, it would be interesting to obtain high-quality spectra, and perhaps also Strömgren

CCD-photometry, to investigate this system further.

NGC 4459

The innermost point of the (B-R) and (R-I) profiles are at variance with the rest of the data, which implies that the R-profile is systematically too faint in the innermost regions; this suspicion is confirmed by inspection of the R-band luminosity profiles which show a slightly "pinched" appearance. The cause of this error is unknown, and presumably of random origin as profiles of equivalent surface brightness (e.g. NGC 4267, 4461) do not show this effect. The innermost point of the (B-R) and (R-I) profiles is therefore discounted and is not considered in the analysis.

The (B-I) major-axis profile shows a progressive inward blueing of essentially constant gradient reminiscent of that observed in NGC 4267, and which is equally unexpected. The minor-axis profile is very similar, and also shows the innermost point as slightly bluer than the general trend. The most obvious interpretation, as in the case of NGC 4267, is that there has been variation in the star-forming history of NGC 4267 as a function of radius. The (R-I) major-axis profile is generally flat beyond a radius of about 35", and displays a progressive inward blueing within this radius. The (B-R) major-axis profile shows an inward reddening within 35" of the galaxy centre, and is generally flat outwith this radius, with a very slight tendency towards an outward reddening. The (R-I) and (B-R) minor-axis profiles display similar features to those observed on the major-axis. The most likely explanation of these features would

seem to be provided by diffuse H_α emission within 35" radius; unfortunately, NGC 4459 was not observed by Stauffer (1983). The presence of residual gas near the nucleus may not be surprising in view of the inner dust lane reported by Sandage (1961).

NGC 4461

All the major and minor-axis colour profiles show inward reddening within a radius of about 20", which implies a central increase in dust. It is noticeable that the (B-R) gradient is less than the (B-I) gradient, and the (R-I) gradient is quite steep, which may imply an inward increase in metallicity as well. A blue "dip" between about 30" and 40" radius is discernible on all the major-axis colour profiles, but is particularly pronounced in (R-I). This would seem to confirm the identification of the excess disk luminosity with residual spiral structure (section 4.1), and may also suggest some H_α emission associated with these features. At radii larger than 50" the (B-I) major-axis profile is flat, the (B-R) profile shows a slight inward reddening, and the (R-I) profile shows an outward blueing; these features may indicate an outward metallicity decrease. The (B-R) and (B-I) minor-axis profiles show outward reddening beyond about 25" radius, whereas the (R-I) profile is flat; as NGC 4461 is seen at inclination if these gradients are genuine they may represent a weakening in the B-profile perpendicular to the disk.

NGC 4474

The (B-I) major-axis profile is generally flat beyond 30" radius from the galaxy centre, and shows a slight inward

reddening within this point. The (R-I) profile displays a gradual inward blueing, whereas the (B-R) profile shows a slight inward reddening within about 35" radius, is flat between 35" and 50" radius, and may show a slight outward reddening beyond 50" from the galaxy centre. The most plausible interpretation of these observations would seem to be a slight increase in dust within 30" radius associated with a region of diffuse H_α emission. Unfortunately no H_α data is available, as NGC 4474 was not observed by Stauffer (1983), and it would be interesting to obtain spectra of NGC 4474 to investigate this suggestion. An alternative explanation could be a central increase in dust coupled with an outward increase in metallicity, although this would seem less likely. The minor-axis colour profiles are essentially flat in all colours, which may imply that any gas and dust is associated with a weak bar aligned with the major-axis (section 4.1)

NGC 4477

The innermost points of the (B-R) and (R-I) major-axis profiles appear to be at variance with the rest of the data implying that the R-profile is systematically too faint; accordingly, the innermost point of these profiles is discounted and will not be discussed.

The (B-I) and (B-R) major-axis profiles show an inward reddening within about 30" radius, a generally flat section between about 30" and 60", a slight reddening between 60" and 70", and are generally flat beyond 70" radius from the galaxy centre. The (R-I) major-axis profile shows a progressive inward blueing

within 65" radius (with possibly a slight reddening within 25" radius), and a progressive outward blueing beyond 60" radius from the galaxy centre. These features are interpreted as indicating an increase of dust within 30" radius, which is probably associated with the bulge, and an increase of dust associated with the onset of the bar component at radii larger than 60" from the galaxy centre. In view of the lack of gas in the system (GHSK give the total hydrogen mass as $< 1.8 \times 10^8 M_\odot$), and the very weak H_α emission observed by Stauffer (1983), it seems preferable to attribute the (R-I) profile in terms of a slight metallicity increase inward of 30", and a local metallicity maxima around 65" radius. The bulge metallicity increase is supported by noting that the minor-axis (B-R) reddening gradient within 30" radius is less than the minor-axis (B-I) reddening gradient. The metallicity increase attributed to the bar component may also be supported by the behaviour of the minor-axis profiles between about 55" and 80" radius which can be identified with excess luminosity on the minor-axis which is probably associated with the bar component (section 4.1). In this range of radii the (B-I) profile is essentially flat, the (B-R) profile displays an outward blueing, and the (R-I) profile shows an outward reddening.

NGC 4501

All the major-axis colour profiles show a strong inward reddening which can be naturally attributed to the expected increase of dust in the inner regions of a spiral galaxy of this type. An increase in metallicity towards the centre of the galaxy may also be suggested by the observation that the

(B-R) inward reddening gradient is weaker than the (B-I) and (R-I) gradients. All the major-axis colour profiles show a number of blue "dips" between 40" and 110" radius which delineate several star-forming regions in the inner spiral arms. The (B-I) and (R-I) profiles show a pronounced blue "dip" between about 120" and 160" radius which can be attributed to a weakening in the I-band luminosity (the (B-R) profile is flat in this interval) as the colour profiles cross the two main spiral arms. The minor-axis colour profiles confirm the steep inward reddening within about 40" from the galaxy centre previously ascribed to an increase of dust. At larger radii the (B-I) minor-axis profile is generally flat, the (B-R) profile shows a slight inward reddening, and the (R-I) profile displays an inward blueing; these features may indicate a diffuse H_α emission weakening at larger radii. This explanation receives some support from the observations by Stauffer (1983) of the H_α and NII emission in the nuclear regions of NGC 4501. As GHSK report that NGC 4501 contains only $8.2 \times 10^8 M_\odot$ of hydrogen gas, rather less than might be expected for a galaxy of this type and luminosity, it would be interesting to obtain a high-resolution radio map of this galaxy to determine if there is an outward decrease in the hydrogen density which might be indicative of environmental gas depletion.

NGC 4503

The (B-R) and (B-I) major-axis colour profiles display a reddening within 20" which suggests an increase of dust in the inner bulge component. At radii between approximately 20" and 60" the (B-I) major-axis profile is essentially flat, whereas

the (B-R) profile displays a progressive inward blueing, and the (R-I) profile shows a progressive inward reddening; these features are also visible in the minor-axis profiles and suggest an inward metallicity increase in the stellar population. At radii beyond 60", all the major-axis profiles show evidence of a blueward "dip", with the (B-R) profile extending the furthest and suggesting the termination of the "dip" around 90" radius; this suggests that the blue "dip" may be naturally identified with the excess luminosity mentioned in section 4.1. The blue colour of this feature is confirmed, and the previous identification as vestigial star-forming activity in the disk seems the most plausible interpretation.

NGC 4531

All the major and minor-axis colour profiles show an inward reddening within about 20" radius which may be naturally attributed to an increase of dust in the central regions of NGC 4531. At radii larger than 20" the (B-I) profile displays a slight inward blueing, the (B-R) profile displays a more pronounced inward blueing, and the (R-I) profile exhibits a slight inward reddening. These features suggest some residual star-forming activity in the inner regions of this galaxy, probably associated with an inward increase in metallicity. This interpretation is generally supported by the behaviour of the minor-axis colour profiles beyond 30" radius: the (B-I) profile is generally flat, whereas the (B-R) profile is outwardly reddening and the (R-I) profile is outwardly blueing.

NGC 4550

At radii less than 30" the (B-I) major-axis profile is generally flat, whereas the (B-R) profile is inwardly reddening, and the (R-I) profile is inwardly blueing; this might imply a metallicity increase in the bulge population. Beyond 40" radius all the major-axis profiles are essentially flat, and evidence for some sort of population discontinuity is provided by the noticeable inward reddening of the (B-I) profile between 30" and 35" radius. Since the (B-I) profile is flat both inside and outside this transitional zone, it may be that the data beyond about 40" represents a younger disk population surrounding an older bulge population which may be of lower metallicity. Alternatively, the slightly redder bulge component and (B-R) and (R-I) colour gradients might indicate the presence of diffuse H_α emmission and an increase of dust in the inner regions of the system. It would be interesting to obtain high resolution spectra at various points along the major-axis to investigate these possibilities. The inclination of NGC 4550 causes the minor-axis luminosity profiles to drop steeply, resulting in too few points on the corresponding colour profiles to merit discussion.

NGC 4552

The innermost points of the (B-R) and (B-I) profiles are at variance with the rest of the data which implies that the R-profile is systematically too faint in a similar fashion to NGC 4459; the innermost points of these profiles are therefore discounted and are not considered in the analysis.

The (B-I) major-axis profile is generally quite flat, with a slight inward reddening within 30" of the galaxy centre. The (B-R) major-axis profile shows a gradual inward reddening with a small blue "dip" centred around 35" radius, and a small increase in reddening centred around 90" radius. The (R-I) major-axis profile is generally flat with an increase in reddening centred around 35" radius, and a slight blue "dip" at 90" radius. These features could represent regions of enhanced metallicity and H_α emission respectively. The (B-I) minor-axis profile displays a slightly more pronounced reddening within 20" radius than on the major-axis, and two distinctive blue "dips" centred around 30" and 35" radius. The (B-R) minor-axis profile also displays these two blue "dips" and a progressive inward blueing. The (R-I) minor-axis profile displays a distinct reddening centred around 30" radius and a blue "dip" at about 65" radius from the galaxy centre. These features would seem to indicate regions of residual star-forming activity with associated enhanced metallicity and a zone of H_α emission, and these regions may well correspond to the features identified on the major-axis. The detection of these features is certainly consistent with the complex evolutionary history suggested by the low-surface-brightness features discussed in section 4.1, and a thorough examination of the velocity-field of NGC 4552 might yield interesting information about the recent dynamical history of the system.

Concluding Remarks

The significance of the observed features of the luminosity and colour-difference profiles will be discussed more fully in Chapter VII, but it is worth noting at this juncture that although the definition of the class of lenticular galaxies (e.g. Sandage (1961)) would lead to an "a priori" expectation of relatively featureless systems, most of the galaxies examined in this survey have displayed interesting features in their extracted luminosity and colour-difference profiles. This finding is in good agreement with Burstein (1978), who notes that a surprisingly large fraction of his sample of lenticular galaxies, which was biassed towards simple (unbarred) systems, were peculiar in one way or another.

CHAPTER V

STANDARD PARAMETERS EXTRACTED FROM THE EQUIVALENT PROFILES

The definition of the equivalent luminosity profile and associated luminosity parameters has been detailed in Chapter II-4.4, and the extracted standard parameters are listed in Table V-i. Previous statistical studies of the properties of the equivalent profile and associated de Vaucouleurs parameters (e.g. de Vaucouleurs (1975, 1977 b)) have been largely concerned with the concentration indices and a similar procedure will be followed in this work.

The equivalent profiles of NGC 4435 and 4438 are shown in Chapter VI to be distorted at low light levels by the anomalous plumes of luminosity associated with NGC 4438. Accordingly, the luminosity parameters calculated for these galaxies are excluded from the forthcoming statistical analysis as they are considered unreliable.

V-1: Variation of Concentration Index with Morphological Type

The variation of the B-band concentration indices with morphological type is shown graphically as Figures V.1, V.2 and V.3; the mean trends reported by de Vaucouleurs (1974) for C_{21} and C_{32}, together with the mean relation for C_{31} derived from extensive photoelectric photometry (de Vaucouleurs (1977b)), are shown as solid lines in the appropriate graphs in the same

fashion as Davenhall (1984 a). The morphological types displayed are those adopted in Chapter IV.

De Vaucouleurs (1974, 1977 b) reports that the concentration indices have a large scatter about the mean trend at any given morphological type, although inclination effects may add considerably to the intrinsic (cosmic) scatter. In spite of the observed scatter de Vaucouleurs reports a significant inverse relationship between morphological type and concentration indices (i.e. smaller values at later stage). Inspection of Figures V.1, V.2 and V.3 confirms that although there is considerable scatter about the mean trends found by de Vaucouleurs, the same inverse relation is apparent. It is interesting to note that whereas NGC 4552 has high values for both C_{21} and C_{32}, NGC 4267 has a high inner concentration (C_{21}) but an outer concentration (C_{32}) lower than the mean trend. One may also note that about half the lenticular population (neglecting NGC 4267 and 4552) have C_{32} indices significantly above the mean trend, which implies that these galaxies have either an unusually strong bulge component, a weak disk component, or a combination of these trends.

It is desirable to evaluate more rigorously the relationship between concentration index and morphological type implied by inspection of Figures V.1, V.2 and V.3. A number of statistical tests of correlation are available, but only Non-Parametric techniques were considered appropriate for several reasons. Firstly, there seemed no valid 'a priori' reasons for regarding the parameter distribution of the lenticular population as either Normal or Symmetric. Secondly, the size of the sample (n) is

considerably below the level at which non-parametric tests approach normality, which is typically in the range n = 20 - 30.

The Olmstead-Tukey test (Olmstéad and Tukey (1947)) was not used because it places heavy emphasis on extreme variable values, and is clearly inappropriate if extreme values may be unrepresentative of the population as a whole. The Spearman (Rho) Test (Spearman (1905)) may be used to form a rank correlation coefficient for the data and the Kendall (Tau) Test (Kendall (1938)) may be used to form a statistic for evaluating the probability of association. The Kendall (Tau) Test is considerably more cumbersome to compute than the Spearman (Rho) Test when a considerable number of ties occur in one variable, which is the case in the morphological classification of this galaxy sample. Moreover, Daniel (1978 a) reports that the two tests have an identical asymptotic relative efficiency and rarely produce different conclusions in hypothesis-testing a sample population. Accordingly, the Spearman (Rho) Test was used for evaluating the correlation of morphological type and concentration indices and the results are summarized in Table V(ii).

The values of Spearman's Rho shown in Table V(ii) are sufficient to reject the null hypothesis (Ho) of independence at the 5% level of confidence, although the value for C_{31} is rather marginal and may be over 5% on some tables. If one considers that de Vaucouleurs' results are sufficient reason for assuming a hypothesis of inverse correlation, the null hypothesis may be rejected at the 2.5% level in all cases as the test becomes

one-tailed. Thus the statistical tests confirm the visual impression of Figures V.1, V.2 and V.3, and support an inverse correlation between morphological stage and concentration index as reported by de Vaucouleurs (1974 and 1977 b).

To investigate the variation of concentration index with colour as a function of morphological type the concentration index-ratios (in the sense: B/R, B/I and R/I) were formed for each galaxy. The calculated index-ratios are listed in Table V(iii) and plots of each index-ratio with morphological type are shown as Figures V.4 - V.12. Inspection of Figures V.4 - V.12 suggests that the index-ratios are essentially uncorrelated with morphological type. Statistical tests of the correlation of each index-ratio with morphological type (T) were performed and the results are listed in Table V(iv).

The values of Spearman's Rho shown in Table V(iv) are all insufficient to reject the null hypothesis of independence at any convincing level of significance, confirming the visual impression of Figures V.4 - V.12. The most positive statement that can be made is that the (R/I) concentration indices had lower correlation values in the opposite sign to the correlations of (B/R) and (B/I) concentration-index with morphological type. It should also be borne in mind that the galaxy sample has a limited range in morphological type and a much larger sample would be needed to form more definite conclusions.

V-2: Variation of Concentration Index with Colour

To investigate the variation of the concentration indices as a function of colour each of the indices was paired with the corresponding index in both of the other colours and non-parametric correlation tests were performed on the data sets in the same fashion as previously described. The results are summarized in Table V(v).

The values of Spearman's Rho shown in Table V(v) are sufficient to reject the null hypothesis (Ho) of independence at very high levels of significance, and suggest a direct correlation between all the variable pairs. The variation of concentration index with colour is shown graphically as Figures V.13 - V.21 where the C_{21}, C_{32} and C_{31} indices of each passband have been plotted against the corresponding indices in both other colours. Inspection of these graphs confirms the good correlation suggested from statistical testing, and indicates that each variable-pair may be described by a linear relationship. Least-squares fits of the form $y = mx + c$ were performed on each data set, with the best-fitting relations shown as solid lines on Figures V.13 - V.21 and listed in Table V(vi). The line $y = x$ is also shown for reference as a broken line on each graph. A number of $C_{31}(I)$ data values, and several additional indices of NGC 4267, seemed quite distinct from the locus occupied by the rest of the sample in several graphs, and these points have been excluded from the corresponding least-squares analysis; such points are denoted as open squares in Figures V.14, V.15, V.17, V.20 and V.21.

The sample size and intrinsic scatter of the data values restricts the precision of the linear fits, and the discarding of 'aberrant' points must always be viewed with caution. Moreover, as several of the least-square fits shown in Table V(vi) include a value of unity within the bounds of the standard errors on the gradient, it is desirable to evaluate the apparent differences between the various (colour) samples of each concentration index. A non-parametric test was chosen for the same reasons previously described, and the Daniel (1978 c) formulation of the Wilcoxon matched-pairs signed-ranks test (Wilcoxon (1945 a)) was used to test the null hypothesis that the various samples of each concentration index have identical distributions. It is important to note that this test carries the assumption that the population of differences is symmetric, so the analysis of each pair of samples was supplemented by the application of the simplest non-parametric procedure, the Sign Test (e.g. Sprent (1981 a)), which makes no assumptions regarding symmetry. The results of these tests are shown in Table V(vii).

It is gratifying that inspection of Table V(vii) generally confirms the results obtained by the least-squares fitting procedure: solutions which are obviously distinct from the $y = x$ relation have statistically significant differences between the variable samples, and those fits which are less well-determined have correspondingly less-significant rejections of the null hypothesis. Consideration of the results of both the statistical and graphical analyses suggests that the most reasonable conclusions regarding the variation of concentration index with

colour are as follows.

The C_{21} index, which measures the degree of concentration of the inner regions of a galaxy, appears to be numerically larger in the sequence R-B-I, although the differences between B and I-band indices are generally marginal. The C_{32} index, which measures the degree of concentration in the outer regions of a galaxy, appears to be numerically largest in the I-band and essentially identical in the B and R-bands. The C_{31} index, which is effectively the product of the C_{21} and C_{32} indices and provides a measure of the overall concentration of a galaxy, appears to be numerically smallest in R and approximately equal in the B and I-bands if one excludes a number of galaxies with exceptionally high $C_{31}(I)$ indices from the analysis. This point is discussed in more detail in section V-4.

If the C_{21} index is considered to be primarily a measure of bulge concentration for this galaxy sample, then one can conclude that the bulges appear fairly similar in the B and I-passbands and slightly more diffuse in the R-band. In an analogous fashion, if the C_{32} index is considered to measure primarily the disk concentration, the disks of this galaxy sample appear similar in the B and R-bands but more diffuse in the I-band. These trends will be discussed further in Chapter VII, together with the results of Chapter IV and VI.

V-3: Comparison of the Calculated Total Magnitudes with Previous Results.

An additional check of the validity of the equivalent profiles is provided by the total magnitude which may be calculated from each profile using the method described in Chapter II-4.5. The total B-magnitudes (hereafter B_T) may be compared with the values tabulated by de Vaucouleurs et al. (1976) and Sandage and Tammann (1981). It should be appreciated that these published values are the averages of many independent determinations and should therefore be more accurate than the values contained in Table V-viii.

The comparison of the various data sets is shown graphically in Figures V.22, V.23 and V.24; least-squares fits of the form $y = mx + c$ are shown as solid lines in each figure, with a broken line representing $y = x$ also shown for reference. The least-squares fitting results are summarized in Table V(ix).

It is apparent from inspection of Figures V.22 - V.24 and Table V-ix that the agreement between the values obtained in this work and those previously published is highly satisfactory for such a small sample. Further statistical tests of correlation were considered unnecessary. The small differences between the data sets may be due to the use of the Blackmann sky-correction technique in this work and zero-point shifts due to differing B-passbands.

V-4: Notes on Individual Galaxies

It is quite apparent that the concentration indices calculated for NGC 4267 are sufficiently unusual to warrant their exclusion from many parts of the graphical analysis described in section V-2. The $C_{21}(B)$ and $C_{21}(R)$ indices of this system are the highest in the samples, indicating the highest degree of central concentration, but the $C_{21}(I)$ index is much smaller and is close to the sample median. A similar trend is evident for the outer (disk) regions, where the $C_{32}(B)$ index is one of the highest in the sample and significantly larger than the corresponding R and I-band indices. These results confirm the strong inward blue gradient reported in Chapter IV from analysis of the major and minor luminosity-axes, and supports the hypothesis of central star-formation within the last few billion years.

With the exception of the C_{21} values of NGC 4267, NGC 4552 has the highest concentration indices in the galaxy sample in all passbands. This result emphasises the weak nature of any disk component, and may well support the elliptical classification preferred by de Vaucouleurs et al. (1976).

As mentioned in section V-2, several galaxies (NGC 4459, 4474 and 4552) have $C_{31}(I)$ indices much higher than their B and R-band values. These galaxies show higher concentrations in both their I-band C_{21} and C_{32} indices than their corresponding B and R-band indices, and it appears that these galaxies have either very dominant I-band bulges, exceptionally weak I-band disks, or a

combination of both effects. This point will be discussed again in Chapter VII.

Table V(i): Extracted Concentration Indices

NGC	C_{21}(B)	C_{32}(B)	C_{32}(I)	C_{21}(R)	C_{32}(R)	C_{31}(R)	C_{21}(I)	C_{32}(I)	C_{31}(I)
4267	3.66	2.50	9.16	3.36	1.94	6.51	2.56	1.75	4.49
4371	2.69	2.28	6.15	2.63	2.25	5.92	2.91	2.50	7.26
4377	2.61	2.37	6.18	2.05	2.01	4.13	2.64	2.26	5.96
4419	2.37	1.80	4.28	1.97	1.83	3.61	1.98	1.66	3.28
4425	2.01	1.84	3.68	2.09	1.95	4.06	2.05	1.88	4.05
4429	2.35	1.84	4.32	2.33	1.88	4.37	2.76	2.05	5.66
4435	3.62	3.56	12.87	2.29	2.80	6.42	2.56	2.65	6.80
4438	2.66	2.30	6.12	2.60	2.69	6.99	2.42	3.17	7.66
4459	2.52	2.47	6.21	2.42	2.45	5.92	4.00	3.12	12.47
4461	2.74	2.44	6.69	2.29	2.39	5.47	2.76	2.77	7.62
4474	2.59	2.36	6.10	2.42	2.46	5.94	3.13	3.21	10.06
4477	2.86	2.28	6.51	2.56	2.09	5.37	3.08	2.28	7.04
4501	1.91	1.65	3.16	1.95	1.77	3.46	2.26	1.89	4.27
4503	2.51	2.10	5.27	2.38	2.16	5.15	2.59	2.21	5.72
4531	1.95	1.81	3.52	1.97	1.72	3.40	2.11	2.08	4.40
4550	1.97	1.99	3.93	1.76	2.13	3.75	1.82	1.91	3.48
4552	3.36	3.05	10.26	2.91	2.78	8.10	3.63	4.06	14.70

Table V(ii): Correlation of B-band Concentration Indices with Morphological Type.

	Rho	Sample Size	R %
C_{21} and T	-0.529	15	< 5%
C_{32} and T	-0.530	15	< 5%
C_{31} and T	-0.518	15	$\simeq$ 5%

R % = probability of erroneously rejecting the null hypothesis (Ho)

Table V[iii]: Index-Ratios Calculated for the Sample

NGC	$C_{21}[B]/C_{21}[R]$	$C_{21}[B]/C_{21}[I]$	$C_{21}[R]/C_{21}[I]$	$C_{32}[B]/C_{32}[R]$	$C_{32}[B]/C_{32}[I]$	$C_{32}[R]/C_{32}[I]$	$C_{31}[B]/C_{31}[R]$	$C_{31}[B]/C_{31}[I]$	$C_{31}[R]/C_{31}[I]$
4267	1.09	1.29	1.41	1.43	1.43	2.04	1.31	1.11	1.45
4371	1.03	1.01	1.04	0.92	0.91	0.85	0.90	0.90	0.82
4377	1.27	1.18	1.50	0.99	1.05	1.04	0.78	0.89	0.69
4419	1.20	0.98	1.19	1.20	1.08	1.30	0.99	1.10	1.10
4425	0.96	0.94	0.91	0.98	0.93	0.91	1.02	0.98	1.00
4429	1.01	0.98	0.99	0.85	0.90	0.76	0.84	0.92	0.77
4459	1.04	1.01	1.05	0.63	0.79	0.50	0.61	0.79	0.47
4461	1.20	1.02	1.22	0.99	0.88	0.88	0.83	0.86	0.72
4474	1.07	0.96	1.03	0.83	0.74	0.61	0.77	0.77	0.59
4477	1.12	0.92	1.21	0.93	1.00	0.92	0.83	0.92	0.76
4501	0.98	0.93	0.91	0.85	0.87	0.74	0.86	0.94	0.81
4503	1.05	0.97	1.02	0.97	0.95	0.92	0.92	0.98	0.90
4531	0.99	1.05	1.04	0.92	0.87	0.80	0.93	0.83	0.77
4550	1.12	0.93	1.05	1.08	1.04	1.13	0.97	1.12	1.08
4552	1.15	1.10	1.27	0.93	0.75	0.70	0.80	0.68	0.55

Table V[iv]: Correlation Index-Ratio with Morhpological Type

	Rho	Sample Size	R %
$C_{21}[B]/C_{21}[R]$ vrs T	-0.395	15	20%
$C_{21}[B]/C_{21}[I]$ vrs T	-0.257	15	> 20%
$C_{21}[R]/C_{21}[I]$ vrs T	+0.149	15	> 20%
$C_{32}[B]/C_{32}[R]$ vrs T	-0.335	15	> 20%
$C_{32}[B]/C_{32}[I]$ vrs T	-0.176	15	> 20%
$C_{32}[R]/C_{32}[I]$ vrs T	+0.132	15	> 20%
$C_{31}[B]/C_{31}[R]$ vrs T	-0.442	15	20%
$C_{31}[B]/C_{31}[I]$ vrs T	-0.178	15	> 20%
$C_{31}[R]/C_{31}[I]$ vrs T	+0.149	15	> 20%

R % = probability of erroneously rejecting the null hypothesis [Ho]

Table V[v]: Correlation of Concentration Indices of Differing Passbands

	Rho	Sample Size	R %
C_{21}[B] vrs C_{21}[R]	0.832	15	< 1%
C_{21}[B] vrs C_{21}[I]	0.610	15	< 2%
C_{21}[R] vrs C_{21}[I]	0.726	15	< 1%
C_{32}[B] vrs C_{32}[R]	0.739	15	< 1%
C_{32}[B] vrs C_{32}[I]	0.641	15	< 2%
C_{32}[R] vrs C_{32}[I]	0.843	15	< 1%
C_{31}[B] vrs C_{31}[R]	0.862	15	< 1%
C_{31}[B] vrs C_{31}[I]	0.736	15	< 1%
C_{31}[R] vrs C_{31}[I]	0.792	15	< 1%

R % = probability of erroneously rejecting the null hypothesis [Ho]

Table V[vi]: Least-Squares Fits of the Form y = mx + c

X	Y	Gradient (m)	Intercept (c)	Sample Size
C_{21}[B]	C_{21}[R]	0.76 [±0.09]	0.40 [±0.23]	15
C_{21}[B]	C_{21}[I]	1.15 [±0.29]	-0.14 [±0.72]	14
C_{21}[R]	C_{21}[I]	1.64 [±0.32]	-1.03 [±0.72]	14
C_{32}[B]	C_{32}[R]	0.68 [±0.12]	0.64 [±0.26]	15
C_{32}[B]	C_{32}[I]	1.59 [±0.20]	-1.02 [±0.44]	14
C_{32}[R]	C_{32}[I]	2.02 [±0.23]	-1.90 [±0.49]	15
C_{31}[B]	C_{31}[R]	0.61 [±0.07]	1.54 [±0.41]	15
C_{31}[B]	C_{31}[I]	1.03 [±0.18]	0.30 [±0.90]	11
C_{31}[R]	C_{31}[I]	1.53 [±0.25]	-1.43 [±1.12]	11

Table V(vii): Paired-Sample Tests

Variable	Samples	Sample Size	T-statistic	R %	S-statistic	S %
C_{21}	B and R	15	9.5	< 0.8%	3	1.8%
C_{21}	B and I	15	30	≤ 9.5%	3	1.8%
C_{21}	R and I	15	16	0.8%	2	0.4%
C_{32}	B and R	15	50.5	> 10.7%	7	50.0%
C_{32}	B and I	14	20	< 4.8%	4	9.0%
C_{32}	R and I	15	19	< 4.8%	3	1.8%
C_{31}	B and R	15	8	< 0.8%	1	< 0.1%
C_{31}	B and I	15	26.5	< 5.5%	4	5.9%
C_{31}	R and I	15	17	1 %	4	5.9%

R % is the probability of erroneously rejecting the null hypothesis [Ho calculated from the Wilcoxon matched-pairs signed-ranks test.

Ho: the median of the population of differences is zero.

S % is the probability of erroneously rejecting the null hypothesis [Ho calculated from the Sign test.

Table V(viii): Calculated Total Magnitudes

NGC	B_T	R_T	I_T
4267	11.97	10.41	10.43
4371	11.81	10.11	9.84
4377	12.73	11.37	10.99
4419	12.16	10.64	10.58
4425	12.87	11.32	11.21
4429	11.25	9.59	9.09
4459	11.55	9.81	9.30
4461	12.03	10.50	9.84
4474	12.49	11.70	10.61
4477	11.59	9.83	9.24
4501	10.56	9.11	8.55
4503	12.23	10.44	10.18
4531	12.61	11.13	10.80
4550	12.56	10.98	10.81
4552	10.87	9.22	8.87

Table V[ix]: Least-Squares Fits of the form y = mx ± c

X	Y	Gradient (m)	Intercept (c)	Sample Size
B_T[GJM]	B_T[de V]	1.06 (±0.04)	-0.88 (±0.53)	15
B_T[GJM]	B_T[S+T]	1.08 (±0.05)	-1.06 (±0.59)	15
B_T[de V]	B_T[S+T]	1.01 (±0.04)	-0.11 (±0.44)	15

Figure V.1

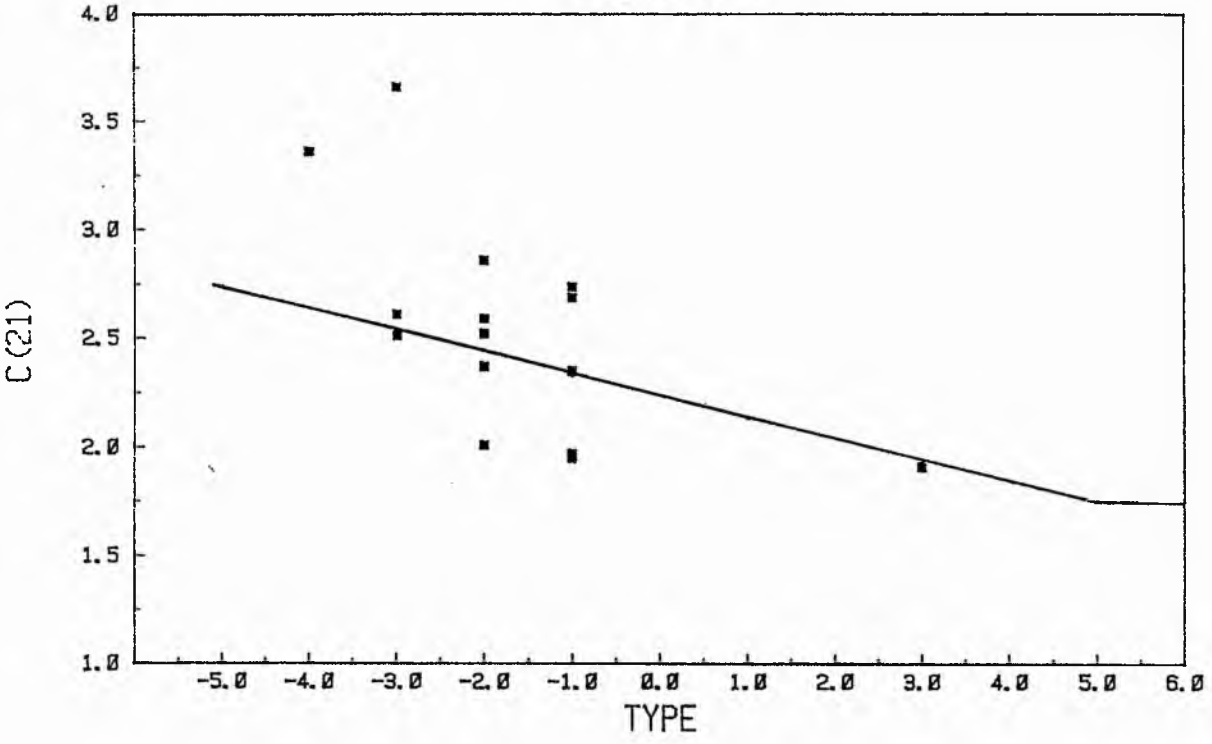

Figure V.2

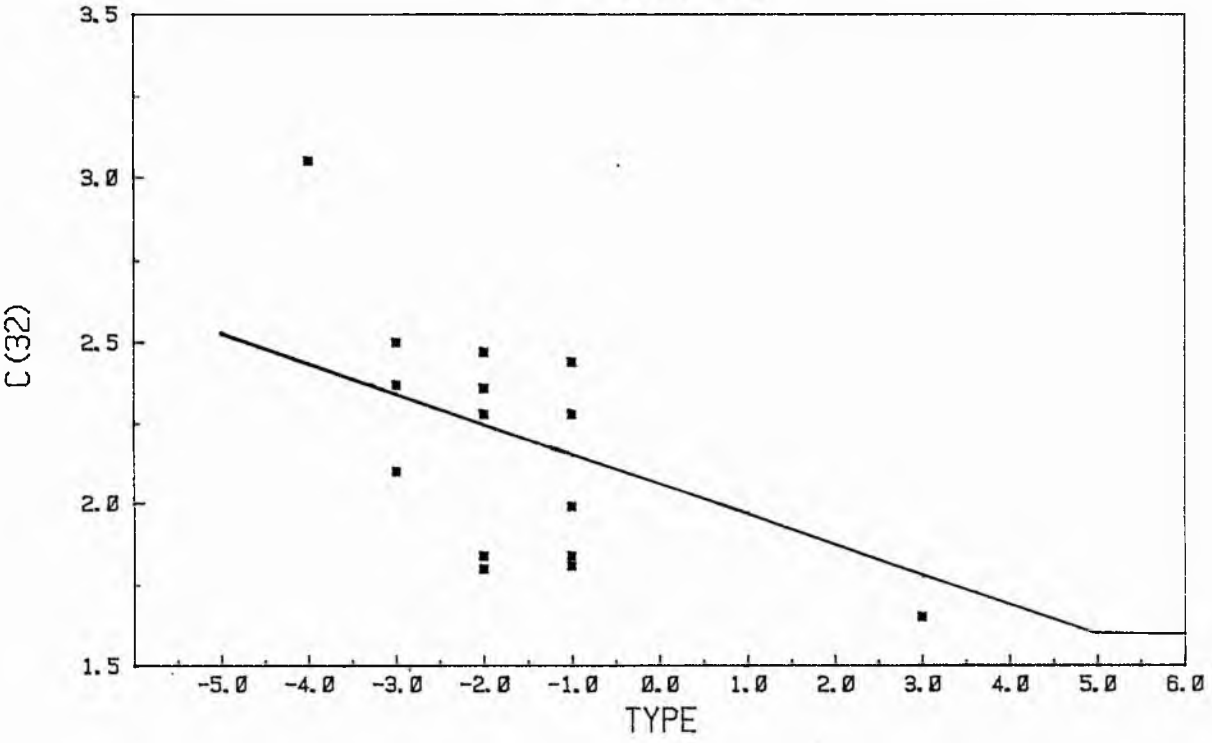

Figure V.3

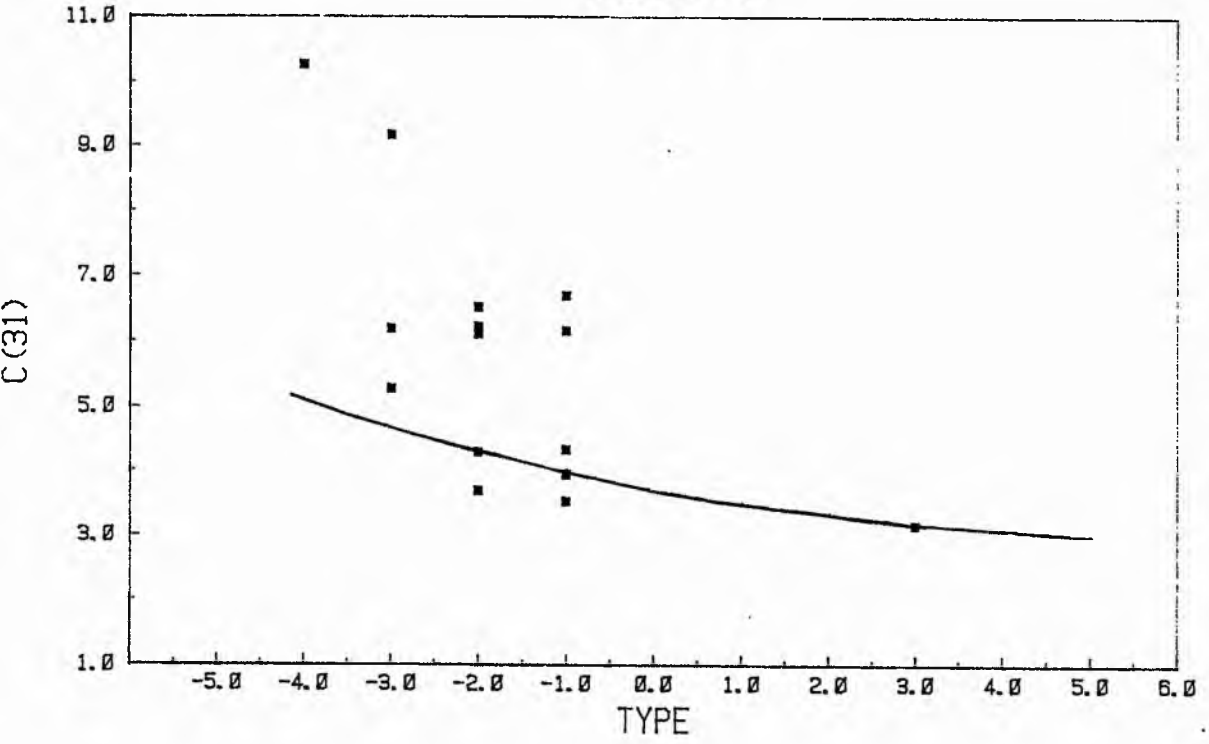

Figure V.4

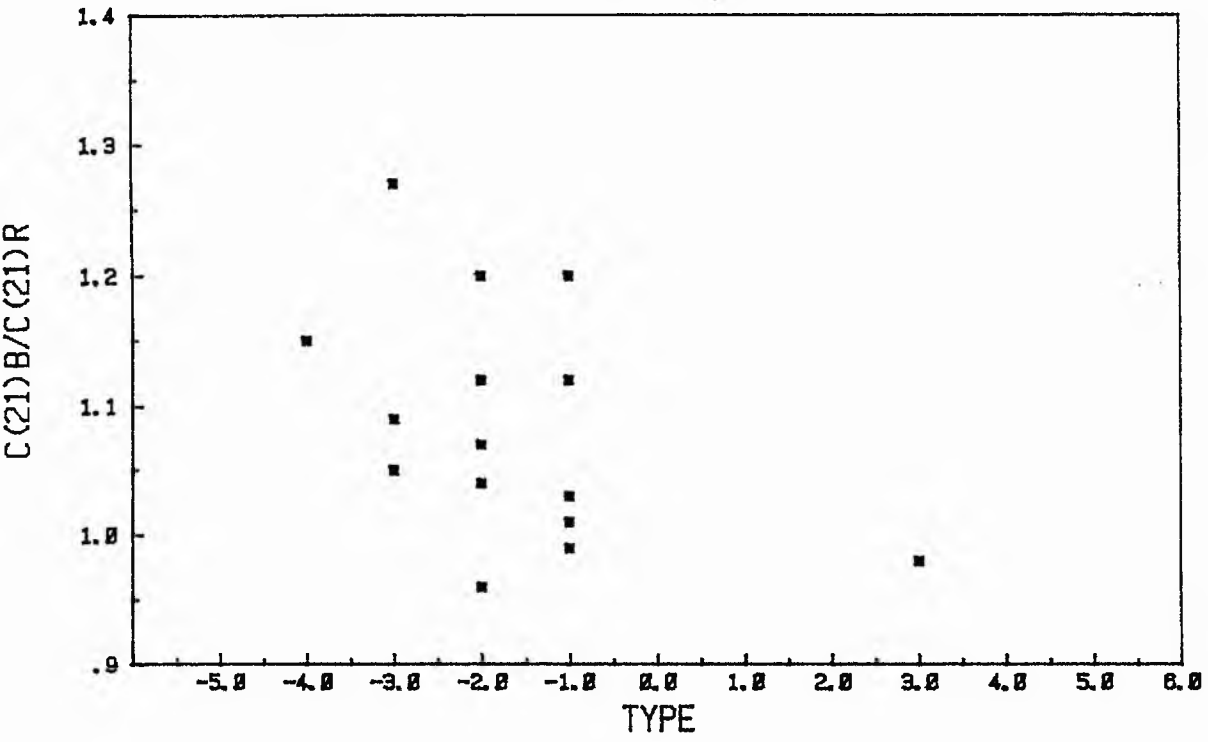

Figure V.5

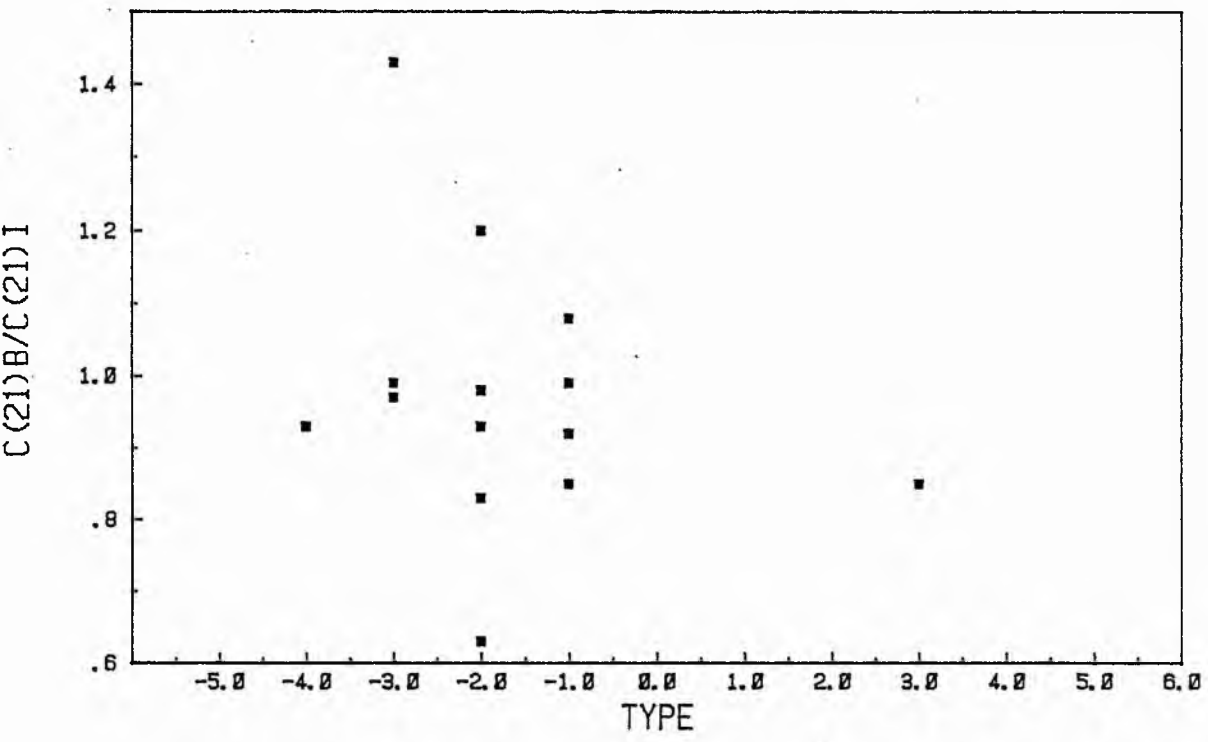

Figure V.6

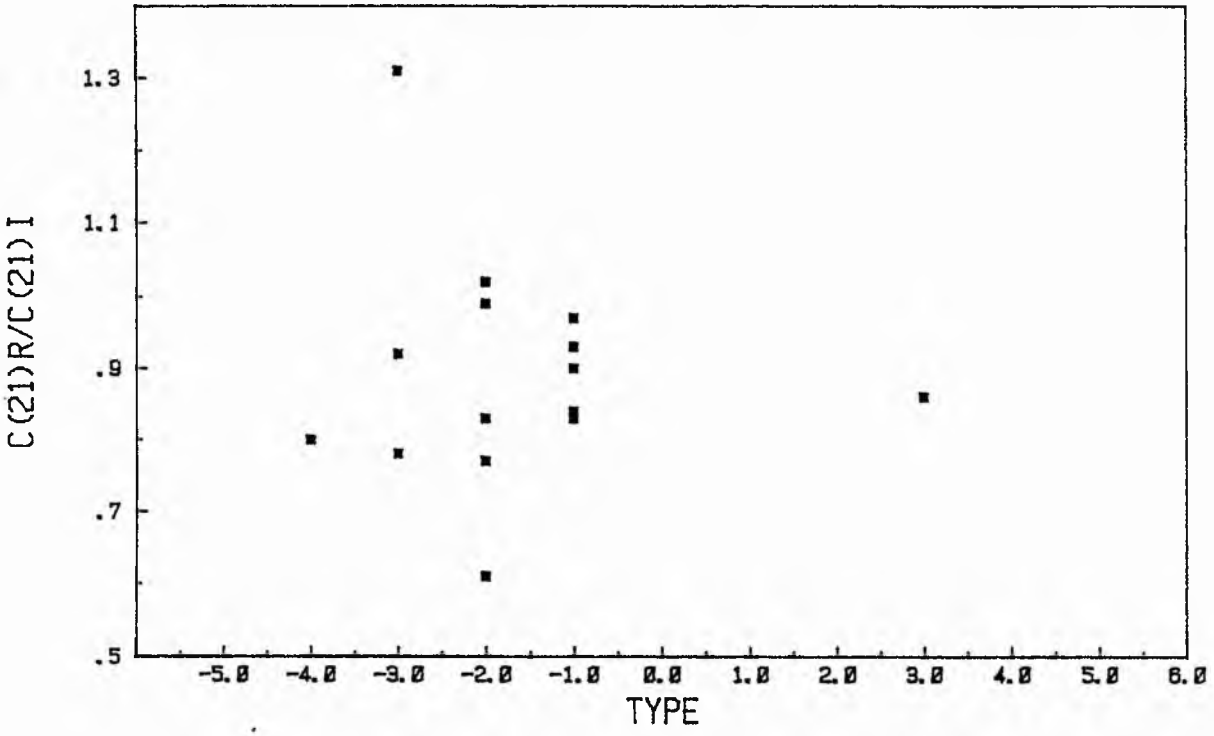

Figure V.7

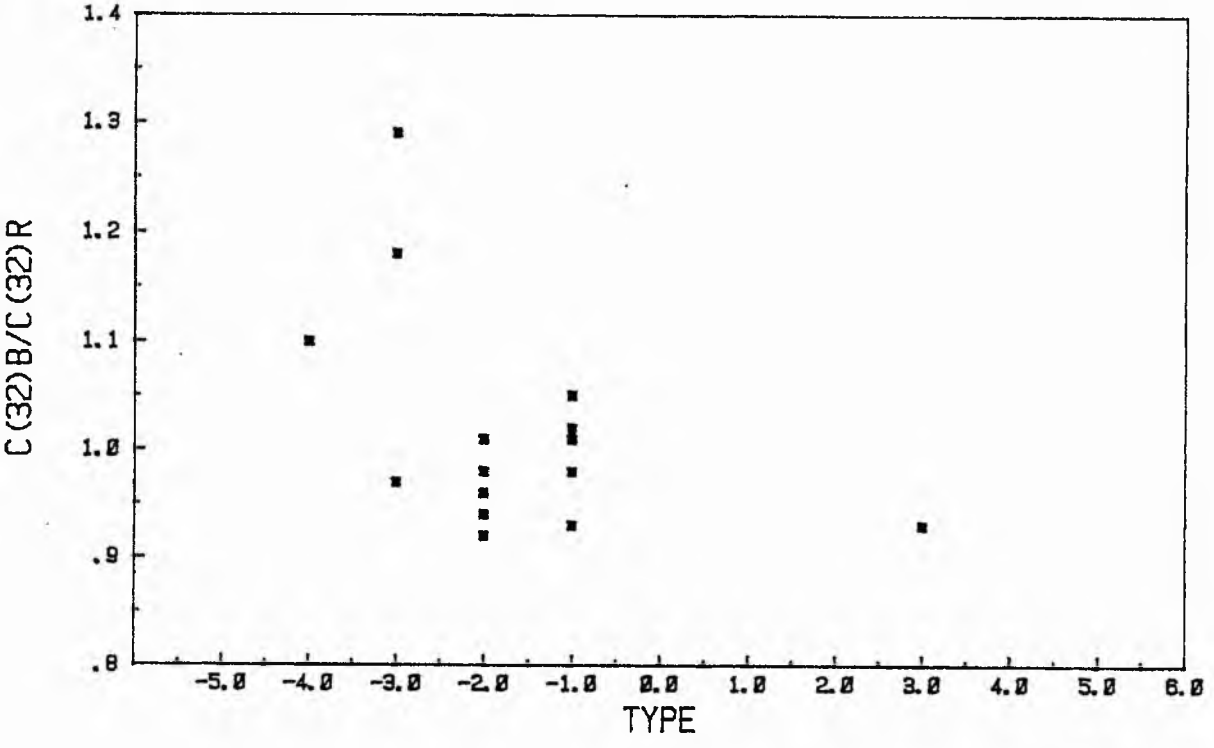

Figure V.8

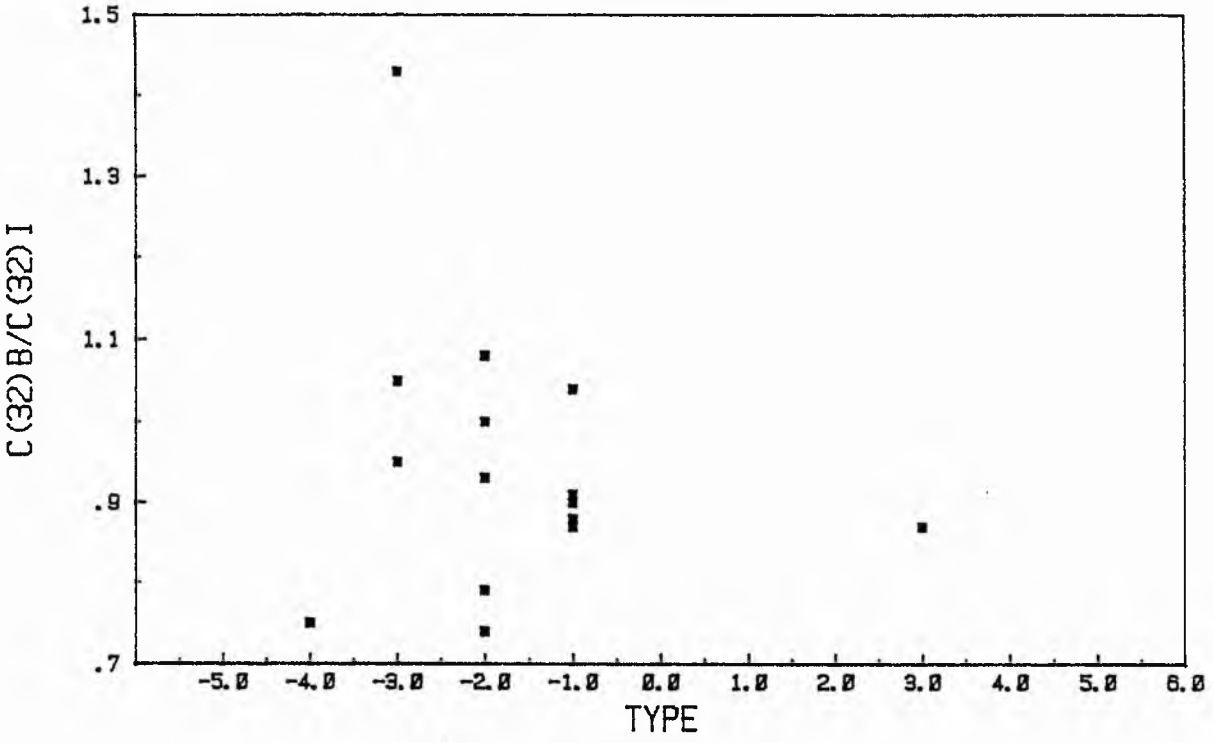

Figure V.9

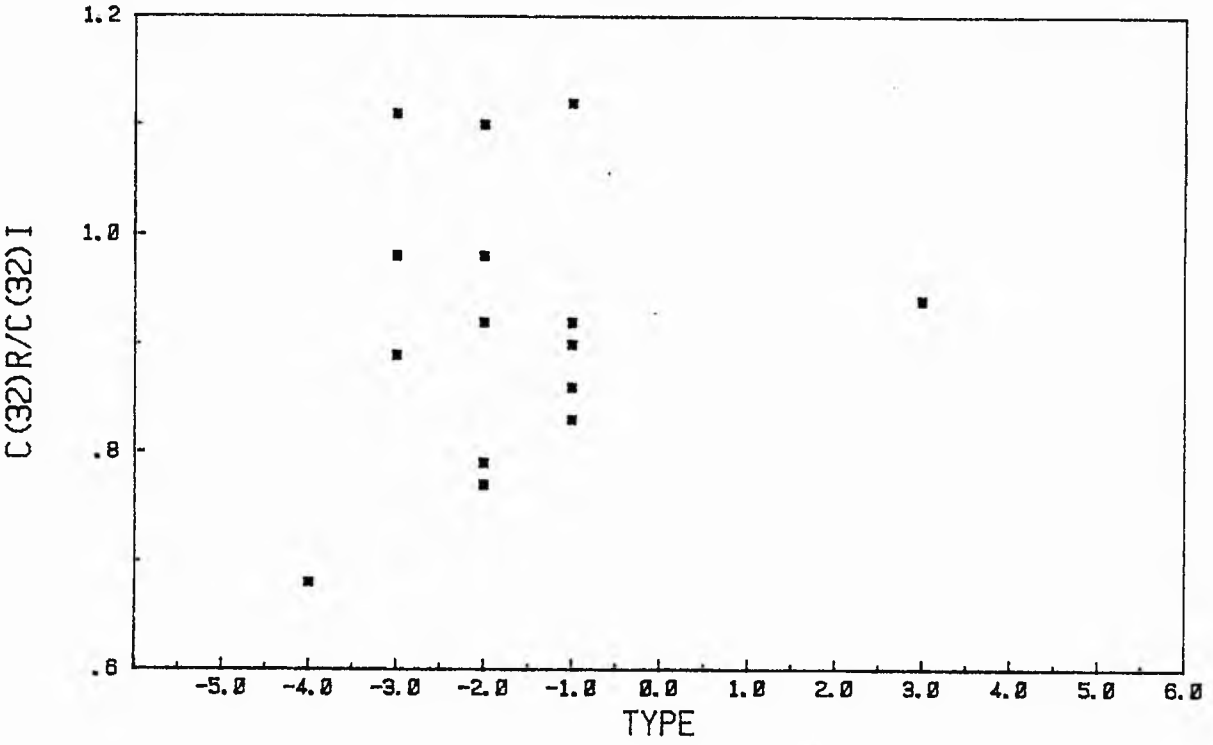

Figure V.10

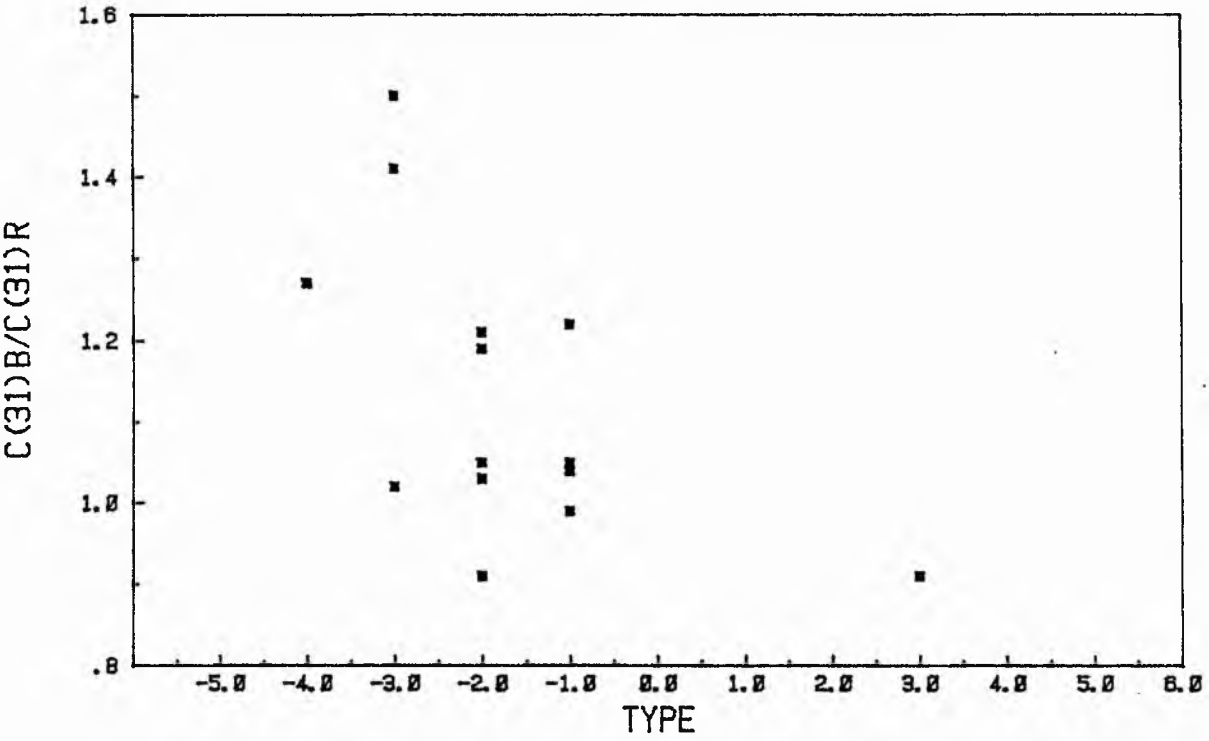

Figure V.11

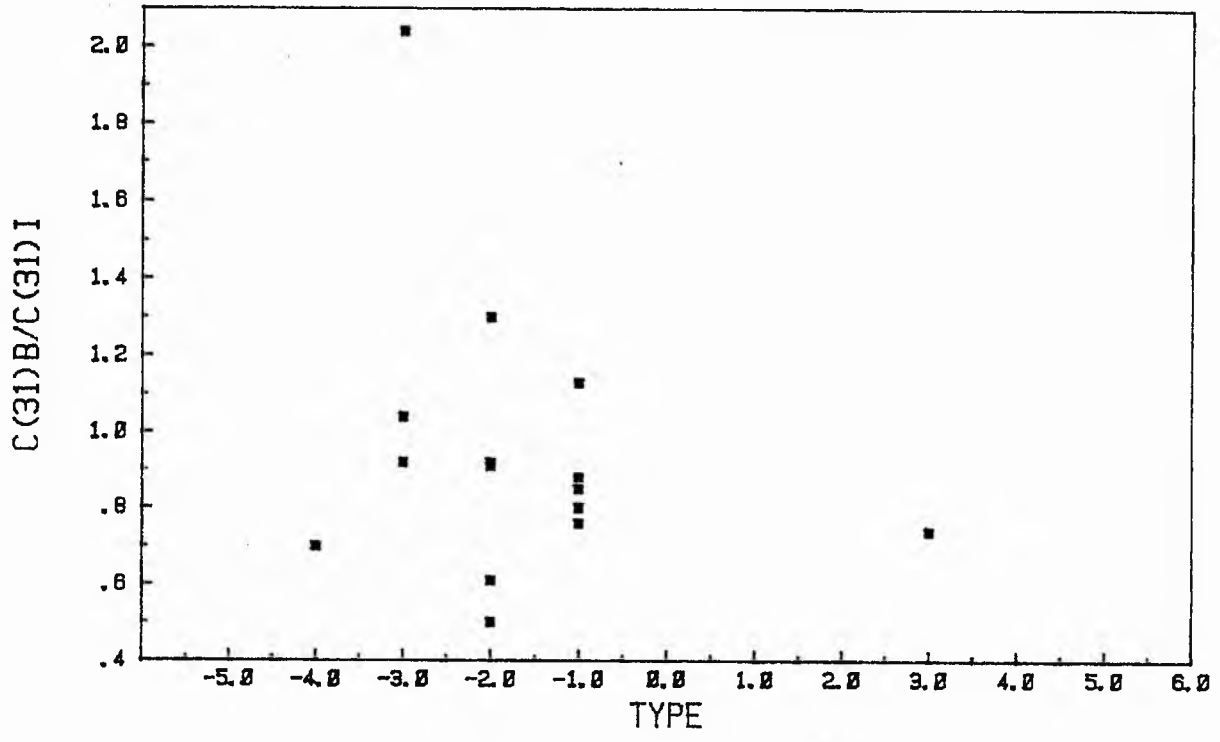

Figure V.12

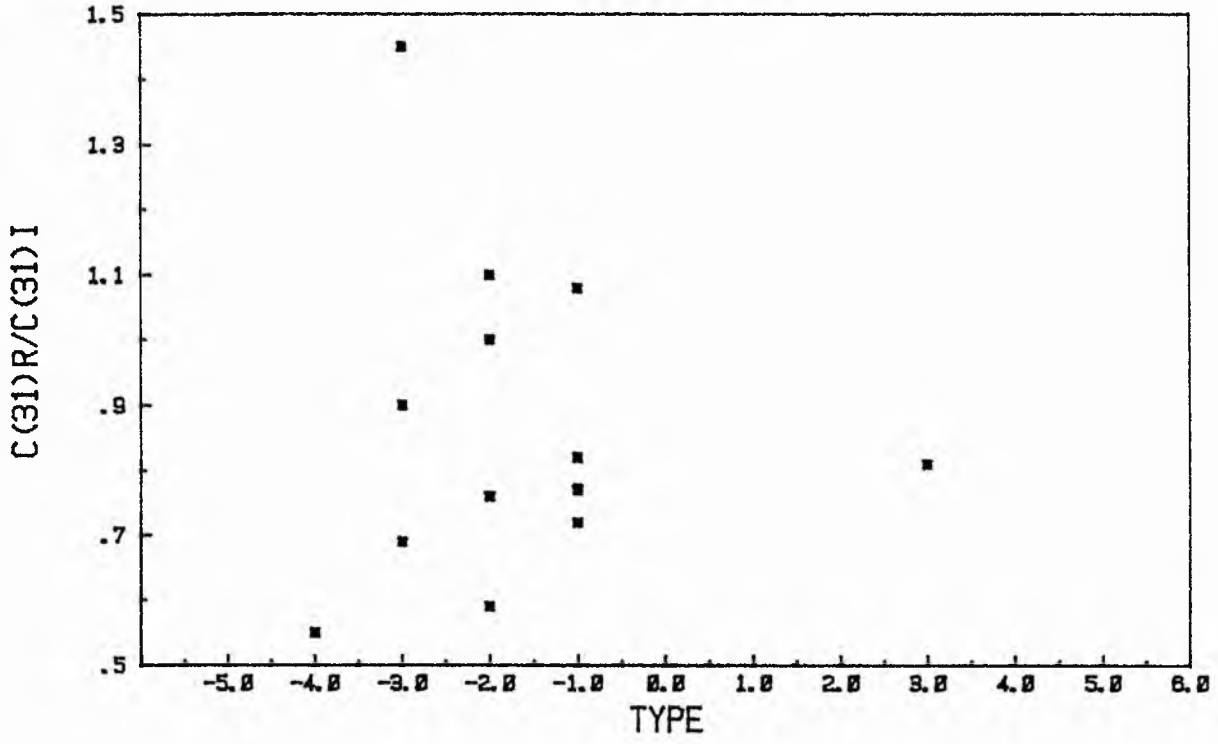

Figure V.13

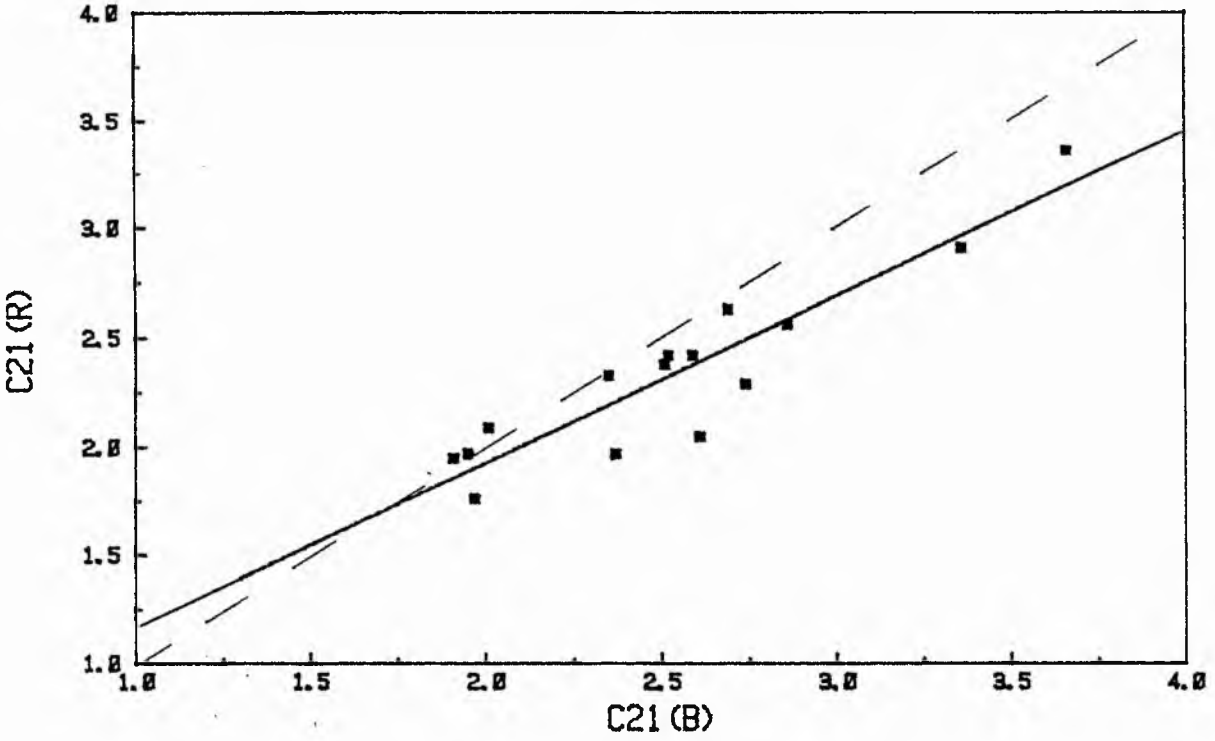

Figure V.14

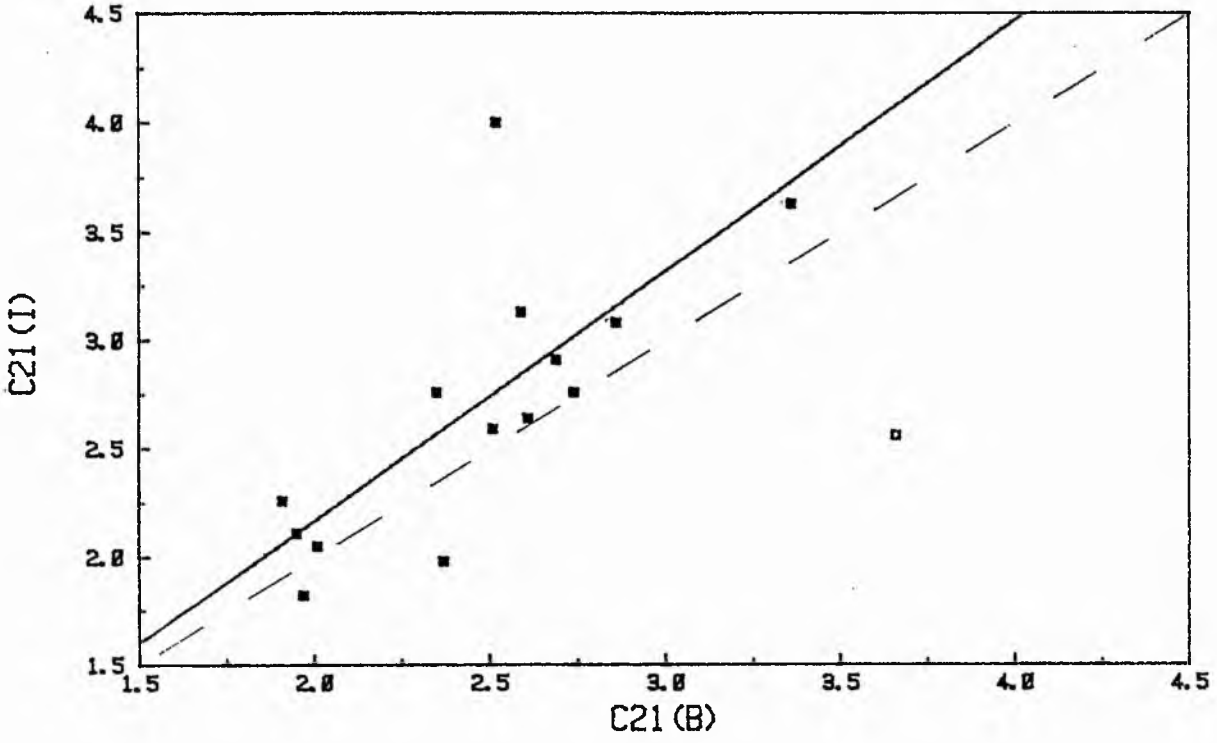

Figure V.15

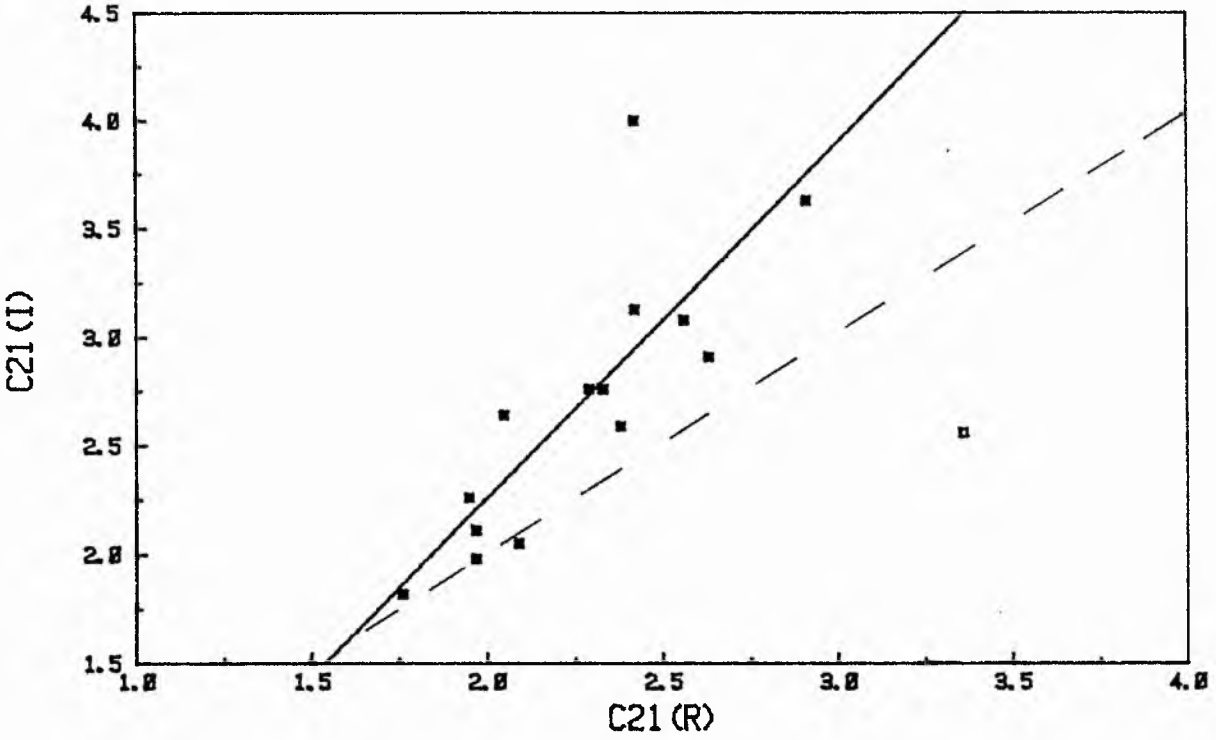

Figure V.16

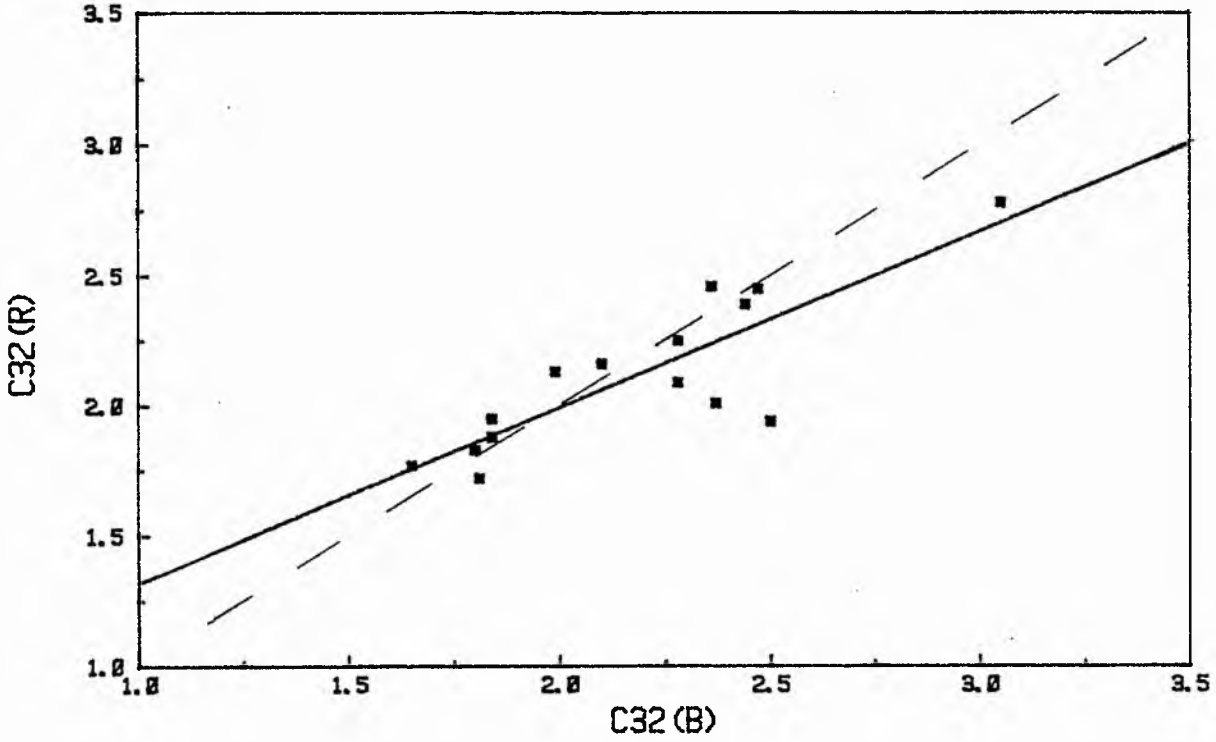

Figure V.17

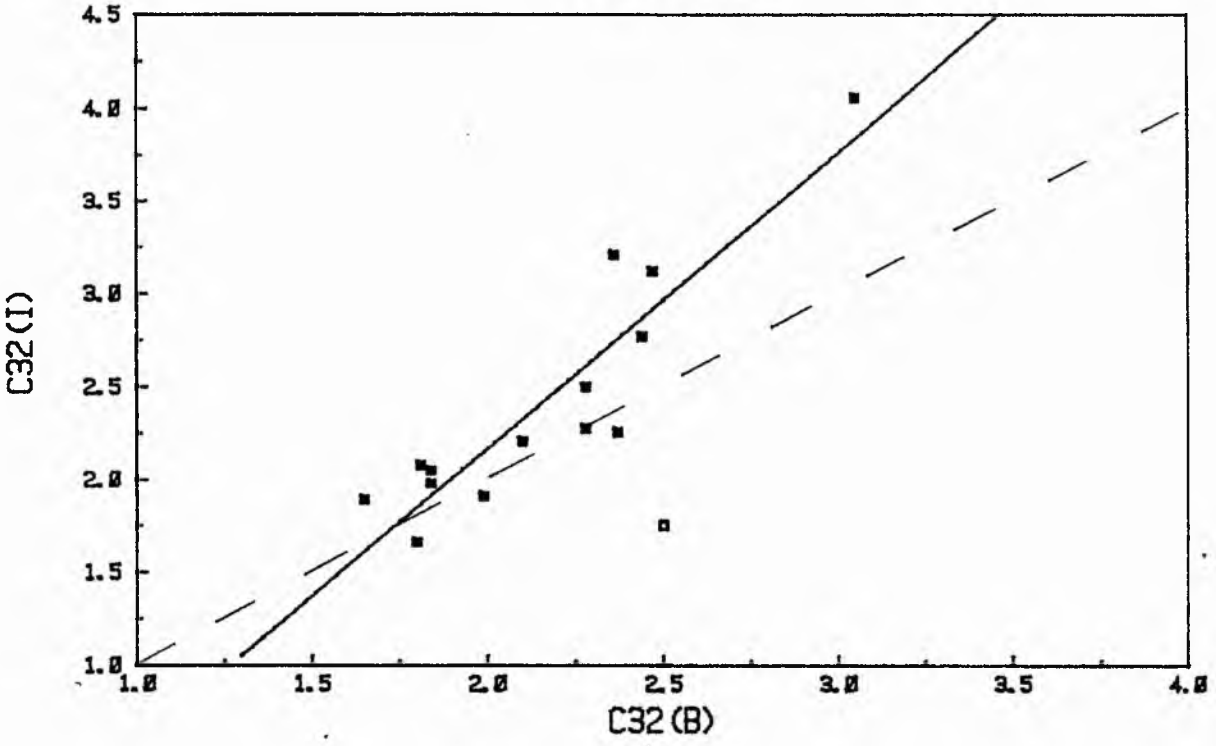

Figure V.18

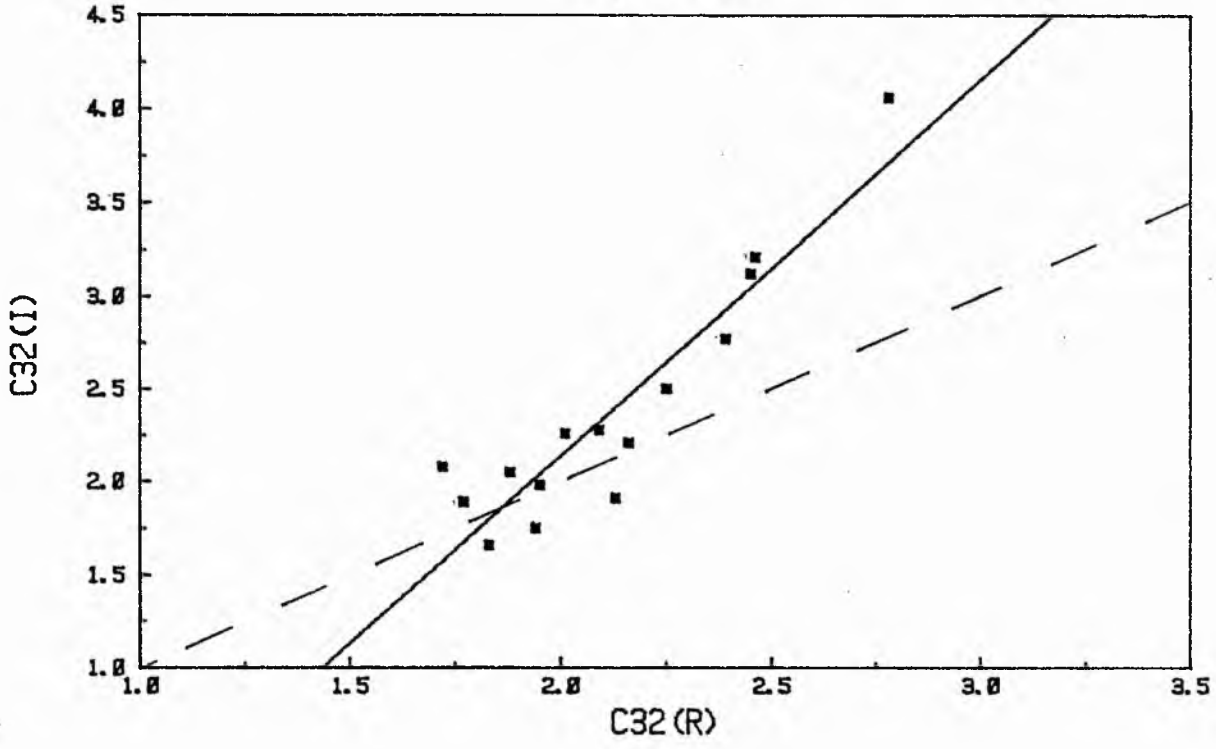

Figure V.19

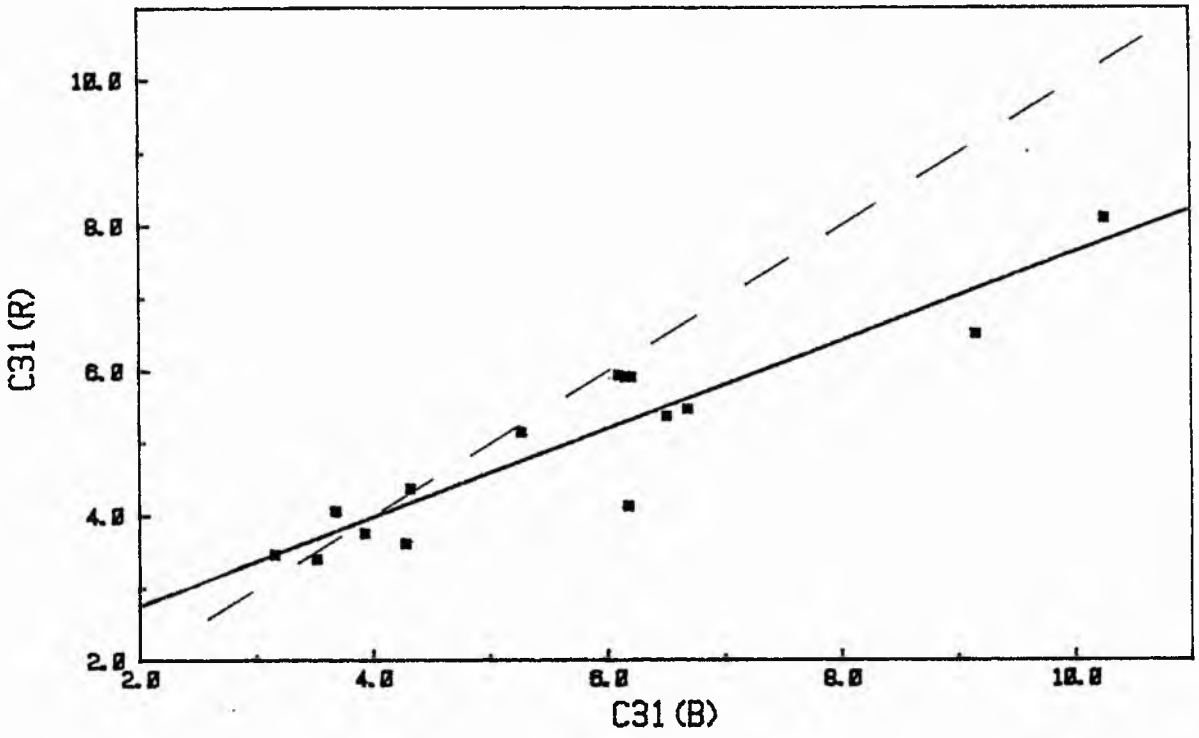

Figure V.20

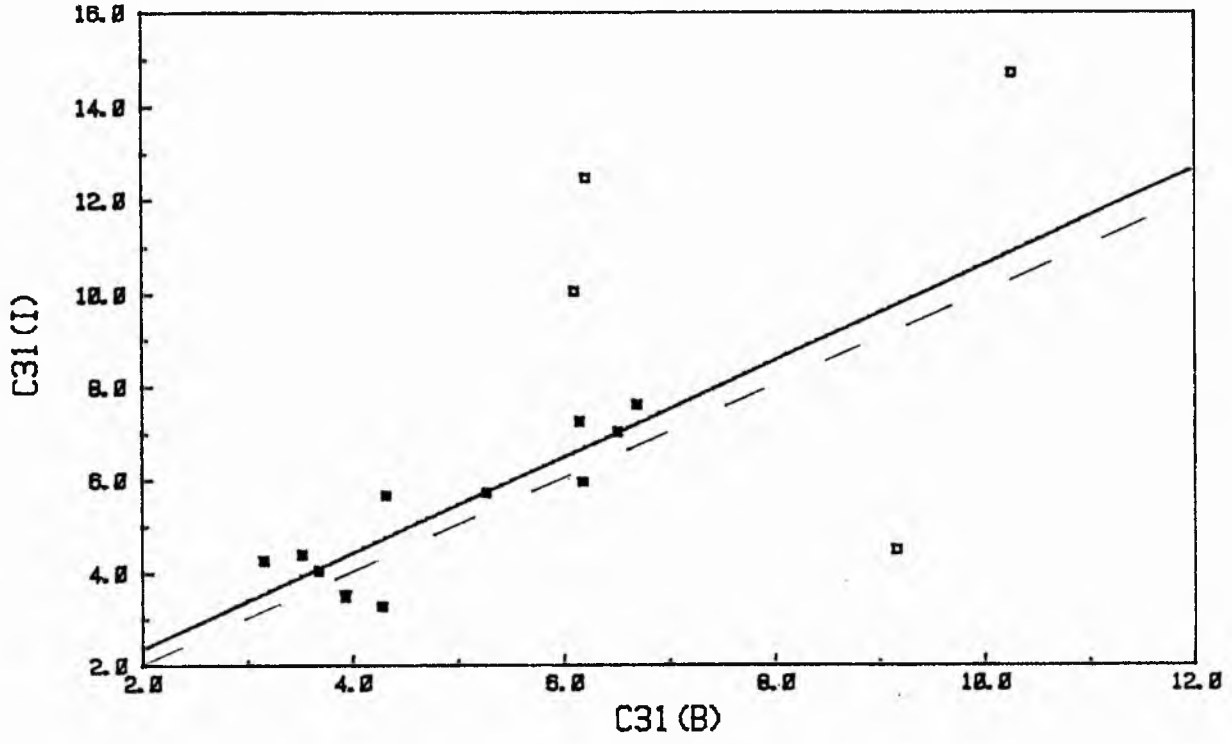

Figure V.21

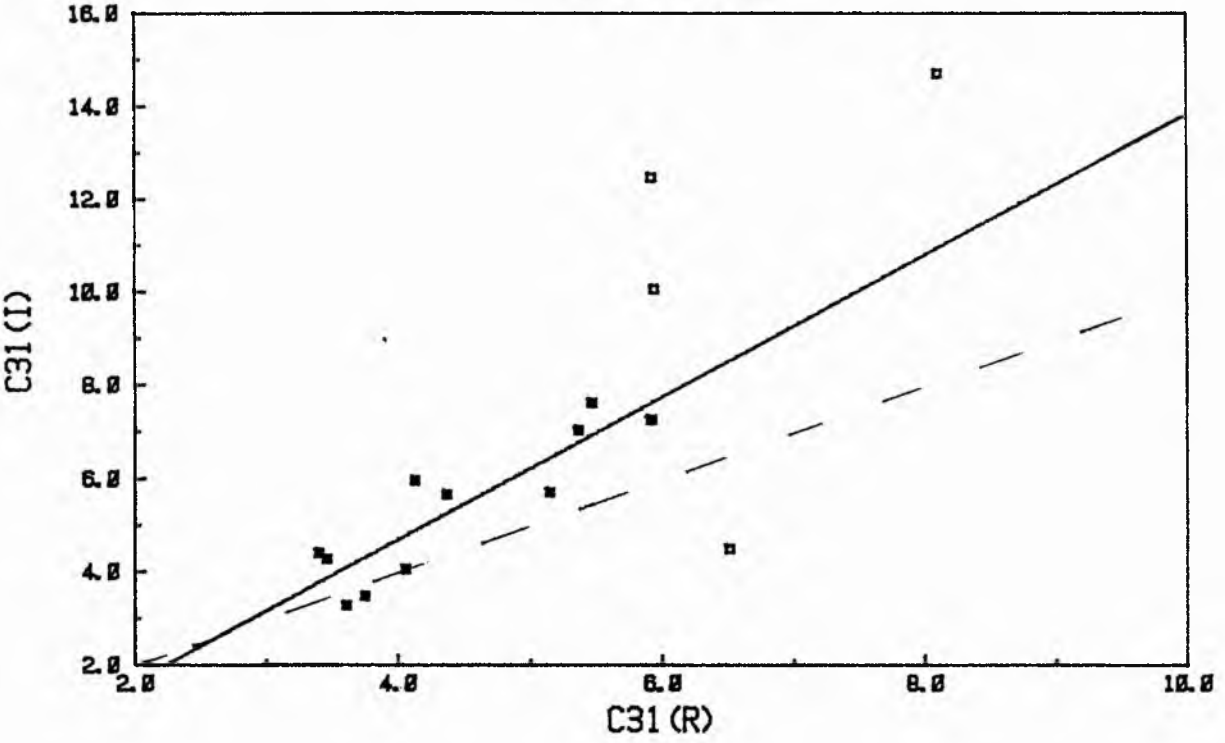

Figure V.22

B-total Magnitude Comparison

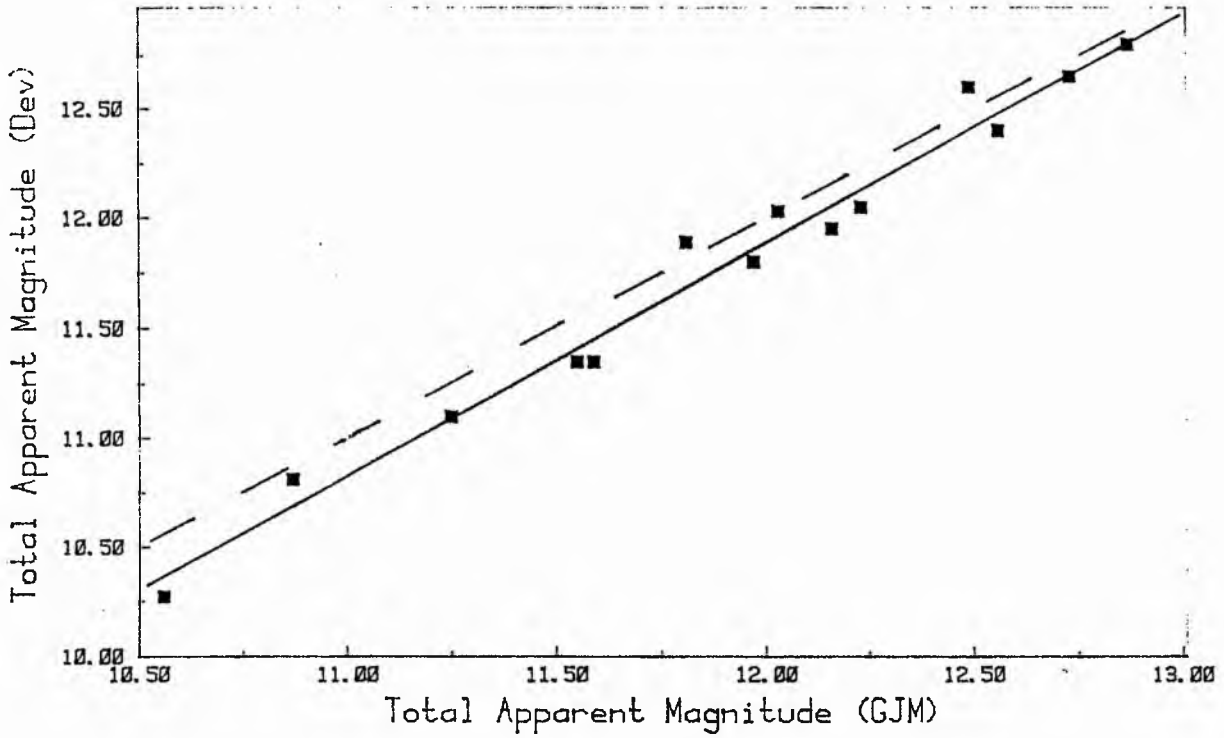

Figure V.23

B-total Magnitude Comparison

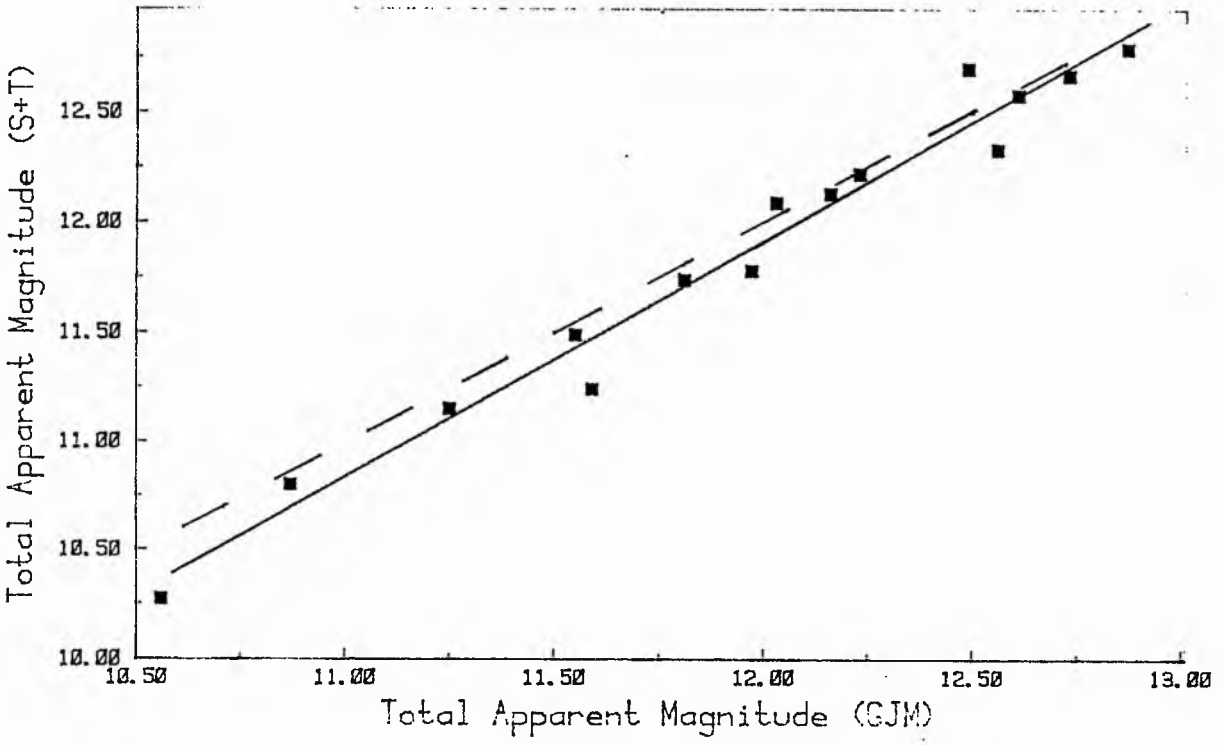

Figure V.24

B-total Magnitude Comparison

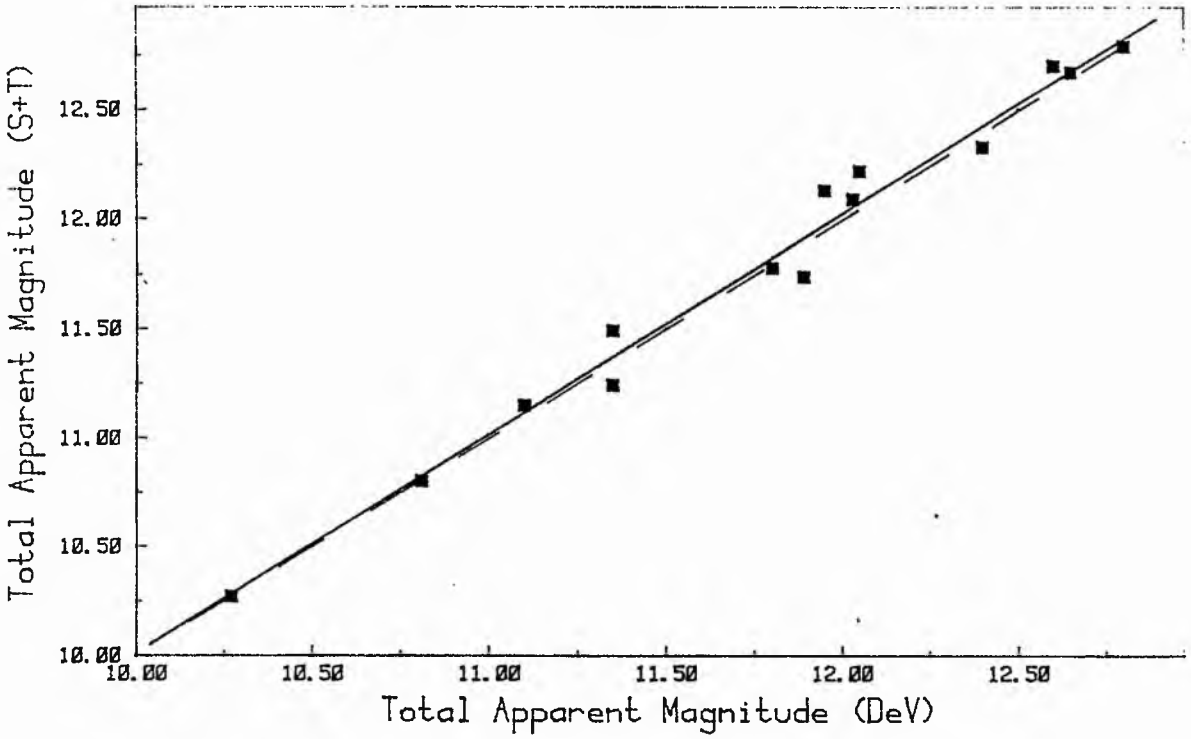

CHAPTER 6

ANALYSIS OF GALAXY LUMINOSITY COMPONENTS

VI-1 Decomposition Techniques and Inherent Problems

The importance of comparing the properties of the bulge and disk components of lenticular systems with those of spiral galaxies of later morphological type has been previously demonstrated in Chapter I. However, the observed luminosity distribution of a galaxy is the sum of all the intrinsic luminosity components, and the task of correctly disentangling the contributions of the luminosity components is complicated by several problems.

First of all, some functional form must be adopted to represent each luminosity component. The most commonly used fitting functions for the bulge and disk components are an $R^{1/4}$ law (de Vaucouleurs (1948)) and an exponential law (de Vaucouleurs (1959)), which are given as equations 6-(1) and (2) below.

$R^{1/4}$ law: $\log (I/I_o) = -3.33 ((R/R_o)^{1/4} - 1)$ 6 - (1)

Exponential law: $I(r) = I(o) \exp. (-\alpha r)$ 6 - (2)

Each function is described by two characteristic parameters: the $R^{1/4}$-law by a scale size R_o and the intensity I_o at R_o; the exponential law by the central intensity I(o) and a scale-length α^{-1}. Neither function has, at present, any 'a priori' basis from physical considerations, but both have been found

empirically to fit observational data.

The $R^{1/4}$-law is used because it gives a good fit to unperturbed ellipticals (e.g. Kormendy (1980)), and the exponential is chosen because it seems a good representation of the disks of many spiral and lenticular systems (e.g. Freeman (1970)). Clearly, it is of the utmost importance that the luminosity components of a galaxy can be accurately described by these fitting functions. Although these are observational differences between elliptical systems and the bulges of disk systems, these do not appear to be very significant (Kormendy (1982)). In addition, the choice of fitting function is not critical as the alternative distributions are very similar (Kormendy (1977 b), (1982)). The situation is more complicated in the case of the disk component, as there exists a considerable body of observational evidence (see e.g. Kormendy (1982) for a review) in favour of the frequent occurrence of non-exponential disks. Each galaxy must therefore be carefully examined to exclude non-exponential disk systems from analysis; inevitably discussions of disk parameters will be biassed by this procedure, but there appears no practical alternative.

With adopted functional forms for the bulge and disk components, the simplest procedure is then to compute independent best-fitting solutions to regions of the luminosity profile dominated by the bulge and disk components respectively. This procedure has, however, been shown to lead to systematic errors in the calculated characteristic parameters as either component

can contribute a significant fraction of light in regions thought to be dominated by the other component. Kormendy (1977 c) introduced techniques to circumvent this problem for luminosity axes extracted from a galaxy of low inclination. Techniques for use with edge-on systems have also been developed (e.g. Hamabe et al. (1979 a,b), (1980)), but they will not be described as they are not relevant to this work. Two of the techniques introduced by Kormendy are available in the PRFDECASP STARLINK routine used in the present work, and these may be termed 'Iterative' and 'Simultaneous Least-Squares' techniques following Kormendy's notation.

The Iterative technique requires the definition of two regions of the luminosity profile dominated by the bulge and disk respectively. An exponential law is fit by least-squares to the data within the disk-dominated fitting range. The best-fit exponential is then used to subtract the disk contribution in the bulge-dominated range and a least-squares fit of a de Vaucouleurs law is then made in the bulge-dominated range. The best-fit $R^{1/4}$-law is then used to subtract the bulge contribution in the disk-dominated range, and an exponential law fitted to this approximation to the disk profile. The process is then repeated until convergence is found, typically after approximately ten iterations (Davenhall (1984a)).

In the Simultaneous Least-Squares technique, the profile is regarded as the sum of a bulge and disk component (equation 6-(3)) and standard non-linear fitting procedures are used to

optimize the solution for the entire luminosity profile within selected limits.

$$I(R) = I(R_o)\ 10^{-3.33((R/R_o)^{1/4}-1)} + I(o)\ \exp.\ (-\alpha r) \quad 6 - (3)$$

The chief problem with the Iterative technique is that it is very sensitive to uncertainty in the intensity data values (due to e.g. small-scale structure or error-noise in the luminosity profile) and in such cases typically will fail to produce a convergent solution. In addition, a convergent solution may not be unique, as altering the fitting-ranges may produce some dispersion in the resultant characteristic parameters. This problem is more serious for the Least-Squares technique which, while much more likely to produce a convergent solution, generates values which are part of a wide range of bulge and disk parameters which can adequately reproduce the observed profile. The Least-Squares fitting technique is also particularly vulnerable in cases where one luminosity component dominates a large part of the profile; the solution typically minimizes this dominance by overestimating the contribution of the weaker component. For these reasons it is clear that solutions produced by the Iterative technique should be preferred wherever possible.

Two further points must be stressed. Firstly, when the fitting techniques cannot produce solutions which sum to the observed profile, one cannot unambiguously attribute the result either to the use of the wrong functional form for one of the luminosity

components or to the existence of a third luminosity component. Secondly, when one of the luminosity components is very dominant, even the iterative technique may produce non-unique solutions for the weaker luminosity components. The unavoidable difficulty in this case is that no region in the luminosity profile can be defined where the weaker component is sufficiently dominant.

1.1 Corrections to the Calculated Characteristic Parameters

The characteristic-intensity parameters may be converted to characteristic-brightness parameters via equation 6 - (4):

$$I_{\mu} = \mu_{SKY} - 2.5 \log I \qquad 6 - (4)$$

The disk central surface brightness (hereafter referred to as B(o), R(o) or I(o) when denoting a particular passband) must be corrected for galactic extinction (A) due to interstellar material in our galaxy; as this topic is rather controversial it will be discussed in more detail shortly. In addition, the disk central surface brightness must be corrected to a face-on value to compensate for the apparent luminosity increase due to the increase in path-length through the disk at higher inclinations. The traditional correction is:

$$I_{\mu}(o) = I_{\mu}(o) - 2.5 \log (\cos (i)) - A \qquad 6 - (5)$$

where cos(i) is given by the inverse of the disk ellipticity ratio (R). Since de Vaucouleurs et al. (1976) extensively

tabulate the ellipticities of bright galaxies, the correction to $I_\mu(o)$ may be more conveniently calculated from

$$I_\mu(o) = I_\mu(o) + 2.5 \log R - A \qquad 6 - (6)$$

The bulge characteristic surface brightness must be corrected for galactic absorption (A) only, and the bulge and disk scale-lengths must be corrected from the measurement scale to a physical size via the adopted distance to the object. As the distance to the Virgo cluster (and details of the distance-scale generally) is rather controversial, this topic will be discussed in more detail shortly. Two further corrections complicate the correction of the characterstic parameters of spiral systems: the effects of the young stellar population and dust content.

Since the young stellar population of a spiral disk is bluer and brighter than an old disk population of equal mass, a Mass:Luminosity (hereafter M/L) correction should be applied to ensure that the disk parameters of systems of differing morphological type can be properly compared. The M/L correction will be some function of galaxy colour, and should be most important for blue-passband investigations of disk parameters. Burstein (1979 a) suggested a colour correction based on the population models of Larson and Tinsely (1978) which was used by Boroson (1981). However, more recent work by Boroson et al. (1983 b) suggests that the actual M/L correction should be very much smaller than suggested by Burstein, and probably significantly smaller than the typical errors inherent in the

disk characteristic-brightness values produced by decomposition techniques.

The presence of dust in a galaxy of interest will produce: differing and unknown acounts of face-on internal absorption in the disk and bulge components; distortion of the inclination-correction procedure due to unknown internal absorption in the line-of-sight; and reddening of the observed galaxy colour and consequent biassing of the M/L correction. Boroson (1981) attempted to evaluate the significance of dust in spiral systems and concluded (from a simplified model) that for moderate inclinations B(o) was essentially unaffected, and $B(R_o)$ would be underestimated by about 0.3 magnitudes. As this is smaller than the typical errors inherent in the $B(R_o)$ values produced by decomposition techniques, the effects of dust can be neglected in the first approximation.

Since lenticular systems may be regarded as dominated by an old stellar population and essentially dust-free, neither of the corrections just discussed was applicable to the early-type systems studied in this survey.

1.2 The Total Luminosity of Bulge and Disk Components

The total luminosity of the bulge and disk components may be obtained by integrating the intensity distribution:

$$L_T = 2\pi \int_{\cdot}^{r} I(r) r dr \qquad 6 - (7)$$

The integration of the exponential law (6 - (2)) is relatively straightforward and yields:

$$L_T \text{ (disk)} = 6.283\ I(o)_c \alpha^{-2} \quad 6 - (8)$$

(c.f. Freeman (1970))

The integration of the $R^{1/4}$-law (6 - (1)) is rather more complex, and after considerable algebra one may obtain:

$$L_T \text{ (bulge)} = 22.67\ I_o R_o^2 \quad 6 - (9)$$

(c.f. King (1978))

Once the luminosities of the components are known, the Disk:Bulge luminosity ratio may be immediately formed. If one of the components is considered to be an unrealistic representation of the luminosity profile (e.g. if the disk is regarded as non-exponential), the Disk:Bulge ratio may be calculated from the known total magnitude of the galaxy and the total luminosity of the reliable component. This procedure will be discussed in more detail shortly.

VI-2 The Decomposition of Equivalent Profiles

The desirability of using Iterative decomposition techniques to disentangle the bulge and disk luminosity components from an observed luminosity profile was discussed in the previous section; in order to maximize the probability of obtaining a

observed luminosity profile was discussed in the previous section; in order to maximize the probability of obtaining a convergent solution, previous workers in the field have been forced to decompose very heavily smoothed major-axis profiles (e.g.: Burstein (1978), (1979 b)) or azimuthally-averaged profiles (e.g.: Boroson (1981), Boroson et al. (1983 b)). If the equivalent profile has been calculated for the galaxy of interest, then one already has a very heavily smoothed photometric profile which has been constructed from the entire information content of the image frame and which should be reliable to much fainter light-levels than the major-axis profile. The equivalent profile is thus an attractive alternative profile for decomposition, and this technique was first exploited by Davenhall (1984 a). It is important to realize that the relevant parameters are not equivalent to those obtained from analysis of major-axis profiles, but can be effectively "corrected" to the major-axis profile by the following procedure.

For elliptical isophotes the equivalent radius may be defined as:

$$r^* = (ab)^{1/2} \qquad 6 - (10)$$

where a and b are radii on the major and minor-axes.

The ellipticity of such isophotes may be defined as:

$$e^2 = 1 - b^2/a^2 \qquad 6 - (11)$$

Eliminating 'b' from 6 - (10) by means of 6 - (11) one may obtain:

$$a = r^{*}(1 - e^{2})^{-1/4} \qquad 6 - (12)$$

A more convenient form of equation 6 - (12) can be obtained by making the substitution R = a/b and eliminating 'e^{2}' by means of 6 - (10). One may then obtain:

$$a = r^{*}(R^{1/2}) \qquad 6 - (13)$$

As de Vaucouleurs et al. (1976) give extensive tabulation of R for nearly all bright galaxies, it is possible to "correct" characteristic scale-length parameters from their "equivalent" to major-axis dimensions. This procedure need only be applied to the calculated disk scale-length, as bulge components may be treated as spherical to a reasonable approximation (with circular isophotes), so the bulge scale-length requires no correction. The correction technique just described may only be used for galaxies that are well-approximated by elliptical isophotes of similar ellipticity at all disk brightness-levels.

The entire technique is analogous to that developed by Boroson (1981), and has the advantage (Adamson (1984)) that the effectiveness of the correction technique may be graphically evaluated for each galaxy. This may be readily accomplished by intercomparing the extracted major-axis profile and the

data sets were evaluated in Chapter III. The only difference is that no ordinate shifts are permissible in this case. Appendix 'F' shows the graphical comparison of the extracted major-axis and corrected equivalent profile for every galaxy in this survey in each passband. The major-axis profiles are shown as solid diamonds and the equivalent profiles as open squares.

2.1 The Validity of the Corrected Equivalent Profiles

Inspection of the graphs displayed in Appendix 'F' reveals that the corrected equivalent profiles are in excellent agreement with the majority of galaxy major-axis profiles; it must be borne in mind that local differences are inevitable due to the degree of smoothing inherent in the equivalent profile. Each galaxy will now be discussed individually.

NGC 4267: Agreement between the equivalent profile (hereafter denoted in this section as EQP) and the major-axis profile (hereafter denoted in this section as MAP) is satisfactory in all passbands, but especially so in the B-band.

NGC 4371: The asymmetry of the MAP is particularly marked for this galaxy, but the EQP appears to be a reasonable approximation to a smoothed and folded MAP in the B and I passbands. The R-band MAP appears to show regions of excess luminosity in the outer disk which are not shown in the R-band EQP. It is unclear whether the R-band disk is non-exponential or affected by some third luminosity component; as the features produce very little

excess luminosity in the corresponding regions of the EQP, they are presumably localized effects and the EQP probably gives a more realistic description of the outer disk of the system.

NGC 4377: Agreement between the EQP and MAP is satisfactory for the B and R-bands. At very low light-levels the I-band EQP appears artificially flat, probably due to an inadequate sky correction. Fitted I-band disk parameters are likely to be unrealistic.

NGC 4419: Agreement between the EQP and MAP is satisfactory for the R and I-passbands. The B-band MAP displays local structure not visible on the EQP, which may also cut off more sharply at faint light levels than the MAP. Fitted B-band disk solutions should therefore be viewed with caution.

NGC 4425: The MAP appears to cut off more sharply at faint light levels than the EQP in all passbands. Fitted solutions may be unrealistic for this system.

NGC 4429: Agreement between the EQP and MAP is satisfactory in all passbands. One may note that in all passbands the EQP shows less local distortion by spiral features than the MAP.

NGC 4435 and 4438: The anomalous plumes of luminosity extending from NGC 4438 result in gross disparity between the EQP and MAP in all passbands. Fitted disk parameters cannot be realistic and bulge parameters must be viewed with caution.

NGC 4459: Agreement between the EQP and MAP is satisfactory in the B and R-passbands, although the MAP has a slightly steeper gradient at low light levels. At faint light levels the I-band EQP appears rather flat, possibly due to an inadequate sky correction. Fitted I-band disk parameters should be viewed with caution.

NGC 4461: The MAP appears to cut off more sharply at faint light levels than the EQP in all passbands. Fitted disk solutions may be unrealistic for this system, and the bulge parameters should be viewed with caution.

NGC 4474: The MAP appears to cut off more sharply at faint light levels than the EQP in all passbands. Fitted disk solutions may be unrealistic for this system, and the bulge parameters should be viewed with caution.

NGC 4477: Agreement between the EQP and MAP is satisfactory in all passbands.

NGC 4501: The asymmetry of the MAP is particularly marked for this galaxy, but the EQP appears to be a reasonable approximation to a smoothed and folded MAP in all passbands.

NGC 4503: Agreement between the EQP and MAP is satisfactory in all passbands, but especially so in the B-band.

NGC 4531: Agreement between the EQP and MAP is satisfactory in all passbands, but the I-band MAP may cut of slightly more sharply than the EQP. Fitted I-band disk parameters should be viewed with some caution.

NGC 4550: Agreement between the EQP and MAP is satisfactory in all passbands.

NGC 4552: Agreement between the MAP and EQP is very good in all passbands, even at very faint light-levels.

From the above analysis it is apparent that the decomposition of equivalent profiles is a valid procedure for the majority of programme galaxies as there is a satisfactory level of agreement between the EQP and MAP in all passbands.

Although we have taken the conservative view that differences between the EQP and MAP at low light-levels renders the decomposed disk parameters unrealistic for these galaxies, it is important that this be confirmed by future photometry. The agreement at very low light-levels is best for the larger images (e.g. NGC 4552) which have more data points in the "pie-slice" major-axis extraction technique. This raises the possibility that the discrepancies between MAPs and EQPs at low light-levels are due to unreliability of the MAPs at very low light levels, and that the EQP more accurately represents the faint disk profile of these galaxies. This possibility will be discussed in more detail subsequently.

2.2 Decomposition Results

The STARLINK DECPRFASP routine was used to decompose the equivalent profiles listed in Appendix 'E' by both Iterative and Simultaneous-Least Square techniques. Following the recommendation of Davenhall (1984a), fits were performed in the (r, log I) plane to provide the most stable solutions. Those data points within an equivalent radius of 5" were generally excluded from bulge fitting-ranges for the same reasons discussed in Chapter II-4.1. The successful fits are shown graphically as Appendix 'G', where the bulge, disk and (bulge + disk) solutions are shown with each equivalent profile.

Inspection of the graphs shown in Appendix 'G' demonstrates the superiority of the Iterative technique, in that the (bulge + disk) luminosity profile produced by this method is typically a significantly better fit to the equivalent profile. The trend for the Simultaneous Least-Square technique to overestimate the weaker (disk) component is quite apparent. The "robustness" of the Simultaneous Least-Squares technique is also apparent, in that it very rarely fails to produce a convergent solution (unlike the Iterative technique), even when one of the calculated components is clearly unrealistic. Each galaxy will now be discussed individually, bearing in mind the remarks made in the previous section as to the similarity of the appropriate corrected equivalent profile and the extracted major-axis profile.

NGC 4267: Satisfactory Iterative and Simultaneous solutions were obtained in all passbands. The disk luminosity is probably overestimated in the R-band where the exponential approximation to the disk light is less convincing.

NGC 4371: Satisfactory Iterative and Simultaneous solutions were obtained in all passbands, although the B-band Iterative fit is clearly superior to the corresponding Simultaneous solution. Excess luminosity between the bulge and disk-dominated regions can be naturally identified with the bar component mentioned in Chapter IV.

NGC 4377: Iterative and Simultaneous solutions were obtained in all passbands, although the I-band fits are considered unrealistic and discarded from further analysis for reasons discussed in the previous section. Both B and R-band fits clearly show the presence of excess luminosity centred around $r^* = 20$ arcseconds. This may be due to a third component (see Chapter IV) but the disk parameters must be regarded with caution as the disk may be non-exponential.

NGC 4419: Iterative and Simultaneous solutions were obtained in the I-passband, and an Iterative and Simultaneous solution was obtained for the R and B-bands respectively. The B-band fit is not very successful and is discarded from further analysis for the reason discussed in the previous section. Both the R and I-band solutions seem reasonable, but the bulge luminosities may

be overestimated and the resultant parameters must be regarded with caution.

NGC 4425: No Iterative solutions could be obtained for this system, although Simultaneous fits were possible yn all passbands. The fitted solutions are all unsatisfactory and are discarded from future analysis.

NGC 4429: Iterative and Simultaneous solutions were obtained for the B and I-passbands, and a Simultaneous fit was possible in the R-band. The solutions appear satisfactory, although the superiority of the Iterative fits is quite clear. All the profiles show excess luminosity between the bulge and disk-dominated regions which may be naturally identified with the spiral-arm component mentioned in Chapter IV. It is interesting that this third component appears most prominent in the I-band; this point will be discussed in more detail in Chapter VII.

NGC 4435: Iterative and Simultaneous solutions were obtained in all passbands for this system. For reasons discussed in the previous section the disk solutions are regarded as unrealistic and discarded from subsequent analysis. The inner regions of the profiles appear well-dominated by the bulge component so the bulge solutions may be reasonable approximations, although they must be viewed with caution.

NGC 4438: Simultaneous solutions were obtained in all passbands for this system, and an Iterative fit was also possible for the

R-band profile. For reasons discussed in the previous section the disk solutions are regarded as unrealistic and discarded from the subsequent analysis. The inner regions of the profiles appear to be dominated by the bulge component, but are probably distorted by the bar component (particularly the B-band); because of this possibility the bulge solutions are also discarded from subsequent analysis.

NGC 4459: Satisfactory Iterative and Simultaneous solutions were obtained in all passbands for this system, although the solutions are made more difficult as the bulge is very dominant. Because of this dominance, and the reasons discussed in the previous section, the disk luminosity may be underestimated in all passbands and the solutions should be regarded with caution.

NGC 4461: Iterative and Simultaneous solutions were obtained for the B and I-passbands and a Simultaneous solution was also possible in the R-band. The disk solutions are regarded as unrealistic for the reasons discussed in the previous section and are discarded from future analysis. As the bulge appears to dominate the inner regions of all the observed profiles, the bulge solutions may be reasonable approximations although they must be regarded with caution.

NGC 4474: Iterative and Simultaneous solutions were obtained in all passbands for this system. For the reasons discussed in the previous section, the bulge solutions must be viewed with caution and the disk solutions are discarded from subsequent analysis.

NGC 4477: Satisfactory Iterative and Simultaneous solutions were obtained in all passbands, and the superiority of the Iterative fits is again obvious. Excess luminosity is apparent between the bulge and disk-dominated regions of the observed profile in all passbands; this may be naturally attributed to the contribution of the bar component discussed in Chapter IV.

NGC 4501: Simultaneous fits were obtained for each passband and an Iterative fit was also possible in the I-band. The fitting procedure was complicated by the strength of the spiral structure, which is apparent as a third luminosity component in all passbands. Despite this problem satisfactory fits were obtained in the B and I-passbands, although the R-band Simultaneous solution is clearly unsatisfactory and is therefore discarded from subsequent analysis.

NGC 4503: Satisfactory Iterative and Simultaneous solutions were obtained for the B and I-band profiles; an Iterative solution could not be obtained for the R-band profile and the best Simultaneous fit produced is clearly only an approximate solution.

NGC 4531: Iterative solutions could not be obtained in any passband for this system; Simultaneous solutions were possible for all three passbands, but the B and I-band solutions are clearly unsatisfactory. The R-band fit gives an approximate solution for the disk component but seriously overestimates the

bulge luminosity. Profile fitting is very difficult in this case because the bulge component is very weak and the disk may be non-exponential. The fitted solutions are regarded as unsatisfactory and are discarded from subsequent analysis. Although the R-band solution underestimates the disk luminosity, it may be regarded as a first approximation to the gross properties of the disk component, and provides an estimate of the maximum Bulge:Disk ratio of the system. This point will be discussed in more detail in Chapter VII.

NGC 4550: No Iterative solutions were obtained for this system, although Simultaneous fits were possible for all passbands. Profile decomposition is complicated in this case by the very dominant nature of the bulge component. The solutions clearly produce unrealistic bulge solutions in each passband and these are discarded from future analysis. The solutions probably overestimate the disk contribution, but may be regarded as reasonable approximations to the disk light; the resultant parameters should be viewed with appropriate caution.

NGC 4552: Iterative and Simultaneous fits were obtained in all passbands for this system. This galaxy illustrates the problem of fitting solutions when a well-determined profile is very-strongly dominated by the bulge component. In Chapter IV the departure from the $R^{1/4}$-law was shown to be noticeable at large radii and to suggest support for the Sandage and Tammann (1981) classification of this galaxy as an S0 system, as the excess luminosity may be interpreted as a <u>faint</u> disk.

Alternatively, the excess luminosity may be tidal in origin (Kormendy (1977 b)). The Iterative and Simultaneous techniques produce solutions of the B-band profile which interpret the profile in a sensible manner: as a very dominant bulge and a weak disk. In contrast, both the R and I-band solutions suggest an unrealistically strong disk which seems very unlikely in view of the morphological appearance of the system. The problem in this case is that at large radii a well-determined $R^{1/4}$-law is closely approximated by an exponential distribution, which can produce an erroneous convergent solution very rapidly. Fortunately such solutions can be identified as suspect fairly easily, and the R and I-band solutions are regarded as unrealistic and discarded from future analysis.

The characteristic parameters representing all the graphical solutions displayed in Appendix 'G' are listed in Tables VI - (i), (ii) and (iii). Those parameters which are adjudged to be unrealistic for the reasons already discussed are denoted by a double-colon suffix, and those regarded as uncertain are denoted by a single-colon suffix. The bulge scale-length units are arcseconds, the disk inverse scale-length in $(\text{arcseconds})^{-1}$, and the characteristic intensities are in units of the frame sky brightness.

2.3 Characteristic Parameters of Galaxy Components

The characteristic-length parameters (R_o and α_c^{-1}) must be converted to a physical size via the adopted distance to each

object. Unfortunately, as mentioned previously, the distance to the Virgo cluster (and the details of the distance-scale in general) is the subject of considerable controversy (see e.g. de Vaucouleurs (1982) for a review). The author prefers to adopt the so-called "short" distance scale $xH_o = 95(\pm 10)kms^{-1}\ Mpc^{-1}$), with an associated distance to the Virgo cluster 'core' of 12 Mpc, as it appears to have more self-consistent internal checks than the "long" distance-scale ($H_o = 50\ kms^{-1}$).

The characteristic brightness parameters, as mentioned previously, must be corrected for galactic absorption due to interstellar material in our galaxy. The amount of absorption at high galactic latitudes (including Virgo) is also the subject of considerable controversy (see e.g. de Vaucouleurs (1982) for a review). Two distinct views are promulgated: either the total absorption at the galactic poles is an approximately uniform 0.2(B) magnitudes, or it is essentially zero.

De Vaucouleurs et al. (1976) give an empirical formula for deriving the absorption along a line-of-sight defined by its galactic latitude (b^{II}):

$$A_B = 0.2 \text{ cosec } |b^{II}| \qquad 6 - (14)$$

which yields $A_B = 0.2$ at $|b^{II} = 90^o$.

An alternative method is given by Burstein and Heiles (1978), in which the absorption in a given direction is determined from the

observed gas:dust ratio and neutral-hydrogen column-density in that direction. This method produces very-small values of total absorption at the galactic poles.

Observational evidence in favour of both methods has been presented, and it does not seem in doubt that the amount of absorption can vary along lines of constant galactic latitude. Accordingly, it was considered preferable to use the method of Burstein and Heiles which relates the extinction to observed parameters, rather than more arbitrary interpolation formulae.

It should be noted that the adoption of the Burstein and Heiles absorption technique is not completely consistent with the de Vaucouleurs "short" distance-scale, which prefers the 0.2 cosec $|b^{II}|$-method. However, the absorption techniques produce object-distances differing by only 12%, which is insignificant in comparison with the errors in the distances to individual galaxies, which are estimated to be typically 20-40% (de Vaucouleurs (1982)).

The B and V-band extinction values were calculated for each programme galaxy using the data and method of Burstein and Heiles (1978) and a computer routine kindly made available by Davenhall (1984 b).

The data of Allen (1979) was used to evaluate the normalized absorption equations:

$$A_R = 0.70A_V \qquad 6 - (15)$$

$$A_I = 0.46A_V \qquad 6 - (16)$$

The absorption in the R and I-bands was then calculated from the results already obtained using equations 6 - (15) and 6 - (16). The results are shown in Table VI-(iv); the errors shown represent the standard deviation about the mean absorption of the sample. The values for NGC 4531 were produced from the average of the extinction values of the four nearest systems (NGC 4477, 4501, 4550 and 4552).

With the adoption of a distance-scale and the calculation of the absorption values shown in Table VI-(iv), corrected characteristic parameters may be calculated from equations 6 - (4), (6), and (13); values of the frame sky brightnesses and disk correction quantities are shown in Table VI-(v). Tables VI-(vi), (vii) and (viii) show the characteristic parameters for each galaxy which give the best solution; unrealistic solutions have been discarded, and those solutions which are regarded as uncertain are denoted by a single-colon suffix.

2.4 Luminosities of Galaxy Components

The characteristic parameters shown in Tables VI-(vi), (vii) and

(viii) may be used to calculate the ratio of the total luminosities of the bulge and disk components in a straightforward manner for those galaxies with good solutions for both components via equations 6 - (8) and (9).

If one component is deemed an unrealistic approximation to the intrinsic luminosity distribution of the galaxy, then in the absence of a significant third luminosity component, the Disk:Bulge luminosity ratio may be calculated by the following procedure. First of all, the total apparent magnitude of the well-determined component may be calculated from:

$$M_T = \mu_{SKY} - 2.5 \log (L_T) \qquad 6 - (17)$$

where L_T is determined from either 6 - (8) or 6 - (9).

The Disk:Bulge luminosity ratio may then be calculated from either:

$$(D/B) + 1 = 10^{((M_T(bulge) - M_T(galaxy)/2.5))} \qquad 6 - (18)$$

or:

$$(B/D) + 1 = 10^{((M_T(disk) - M_T(galaxy)/2.5))} \qquad 6 - (19)$$

where M_T (galaxy) is the absorption-corrected face-on total apparent magnitude of the galaxy. B-band M_T(galaxy) values are tabulated for all the programme galaxies by de Vaucouleurs et al. (1976), and Disk:Bulge ratios could be calculated for those systems with one uncertain luminosity component. In order to allow the same procedure to be used for the R and I-band data,

appropriate M_T(galaxy) values had to be calculated for each galaxy as no suitable data is available in the literature. To calculate these M_T(galaxy) values, the total apparent magnitudes calculated from the equivalent profiles by the method described in Chapter II were corrected for absorption using the values listed in Table VI-(iv), and extinction-corrected total-magnitude colours calculated for each galaxy. The B-band total apparent magnitudes were then corrected to face-on values by means of the procedure recommended by de Vaucouleurs et al. (1976), and corresponding M_T(galaxy) values calculated from the extinction-corrected (B-R) and (B-I) total-magnitude colours. This procedure is clearly not rigorous as it assumes that the correction-procedure recommended by de Vaucouleurs et al. (1976) is identical in all three passbands; however the procedure has no attractive alternative and is probably a reasonable approximation, considering the uncertainties involved (e.g. the absolute calibration of frame sky-intensities). The extinction-corrected total-magnitude colours and M_T (galaxy) values are shown in Table VI-(ix).

The procedure just described could not be used for NGC 4435 and 4438, as their total magnitudes and colours are distorted by the anomalous plumes of luminosity associated with NGC 4438; the B-band M_T (galaxy) values given by de Vaucouleurs et al. (1976) are listed in Table VI-(ix) for these galaxies.

All the Disk:Bulge luminosity ratios calculated from the characteristic parameters listed in Tables VI-(vi), (vii) and (viii) by the methods just described are listed in Table VI-(x)

with appropriate notes. Those values calculated from only one well-determined luminosity component are denoted by a single-colon suffix.

VI-3: Bulge and Disk Luminosity Components

Before considering the results produced in this work by the methods described in the previous section, it is desirable to evaluate the quality of the parameters listed in Tables VI-(vi), (vii) and (viii). The characteristic-brightness parameters are generally not very accurately determined even by modern iterative techniques, with typical uncertainties of $\pm$ 1 magnitude (Boroson (1981)). Comparison of the characteristic-brightness parameters obtained by different authors is therefore not considered very fruitful. The most stable parameter determined is the disk scale-length, and previous studies (e.g. Boroson et al. (1983 b), Davenhall (1984 a)) have concentrated on intercomparing these parameters, although the dearth of available data has severely restricted the extent of possible comparisons.

Three galaxies with well-determined disk solutions produced in this work have also been studied by Boroson et al. (1983 b): NGC 4267, 4419 and 4429. Comparison of the parameters of NGC 4477 is rendered invalid because of the serious discrepancy between the I-band bulge profiles previously discussed in Chapter III. For these three galaxies the values of Boroson et al. (1983 b) have been corrected to the same distance-scale adopted in this work (d(Virgo) = 12 M_{pc}), and the resulting comparison is shown in Table VI-(xi). Inspection of

Table VI-(xi) reveals that the results are very similar; this level of agreement (~10%) is regarded as very encouraging as Boroson et al.(1983 b) consider their agreement with the work of Burstein (1979 b) and Schweizer (1976) satisfactory at the 15-20% level. This result confirms that the accuracy of the results produced by the decomposition procedures described in the previous section is equivalent to that obtained by previous independent workers.

3.1 Results Produced in this Work

This work provides the first multi-colour decomposition data that has been reduced in a homogeneous fashion using complementary plate material and uniform data reduction and analysis techniques. Table VI-(xii) lists a comparison of the scale-length parameters for those galaxies which have solutions in more than one passband. Uncertain values are denoted by a single-colon suffix in the usual fashion.

The scatter in the values of the bulge scale-length (R_0) is quite evident, even for well-determined solutions, and reflects the typical uncertainty in bulge parameters produced even by modern techniques. One may note that there are no gross discrepancies between the results, and even the uncertain solutions agree within a factor of two, or within a few hundred parsecs for the smallest values. Inspection of Table VI-(xii) reveals that several galaxies (NGC 4371, 4429 and 4459) have B-band scale-lengths larger than their R and I-band values, and in order to decide whether there are significant differences between the

samples, the Daniel (1978 c) formulation of the Wilcoxon matched-pairs signed-ranks test (Wilcoxon (1945 a)) was used to test the null hypothesis that the various samples of bulge scale-length have identical distributions. The analyses of each pair of samples was supplemented by the application of a Sign test (which makes no assumptions regarding population symmetry) and the results are shown in Table VI-(xiii). The data values of NGC 4501 have been excluded from the analysis because this system is morphologically distinct from the rest of the sample ($T < 0$), and its solutions may have been influenced by a third luminosity component.

The most reasonable conclusion that can be drawn from the data is that the bulges of the lenticular systems studied in this sample are of similar size at B, R and I wavelengths. This result supports the view that the lenticular bulges are completely dominated by an old (red) stellar component. However, the inherent uncertainties in the R_o values and the small sample size must make such a conclusion tentative until confirmed by independent analysis of a larger sample.

The scatter in the values of the disk scale-length ($\propto \frac{-1}{c}$) shown in Table VI-(xii) is generally smaller than for the bulge scale-length values, as might be anticipated since this is the most stable parameter produced in the solutions. The parameters of NGC 4501 are excluded from the present discussion and analysis for the reasons previously mentioned. Inspection of Table VI-(xii) reveals no significant disparities in the results, and even the uncertain solutions agree to within 50%. Several

galaxies (NGC 4371, 4429 and 4477) appear to have I-band scale-lengths larger than the B and R-band values; to investigate whether there are significant differences between the samples statistical tests were carried out in an exactly analogous fashion to the bulge scale-length investigation, and the results are shown in Table VI-(xiv).

Inspection of Table VI-(xiv) reveals that there is no statistically significant difference between the B and R-band samples, and rather marginal evidence that the I-band scale-lengths are larger than the corresponding B and R-band values. In view of the inherent uncertainties in some of the scale-length values and the small sample sizes, the most reasonable conclusion would seem to be that there is no clear evidence for significant differences between the B, R and I-band samples of disk scale-length obtained in this work; clearly it is important to confirm this result by independent analysis of a larger galaxy sample, and such an extension is discussed in the next section.

The Disk:Bulge luminosity ratios, calculated by the procedures described in the previous section and listed in Table VI-(x), show a surprisingly small scatter in the results for each galaxy, with only the R-band values for NGC 4461 and 4474 being significantly different from the corresponding B and I-band values. This level of agreement, even for uncertain solutions, confirms the similarity of the bulge and disk components of lenticular galaxies at B, R and I-passbands. Two systems, NGC 4371 and 4429, which both have well-determined Iterative

solutions and showed variations in both bulge and disk scale-lengths, demonstrate corresponding variations in (D/B) ratio, in the sense that the bulge becomes less dominant at redder wavelengths. As both these systems have detectable third luminosity components (a bar and vestigial spiral structure respectively) this may be interpreted as evidence that these components are red; this point will be discussed in more detail in Chapter VII.

3.2 Construction of Homogeneous Data Sets

The statistical merit of the data produced in this work can be greatly improved by incorporation with the results of other authors who have used modern profile decomposition techniques to form a much larger data set. To form a homogeneous data set, all the data must utilize the same galactic absorption-correction and be converted to a uniform distance-scale. Davenhall (1984 a) constructed such an aggregate of the B-band work of Burstein (1979 b), Boroson (1981), Hamabe (1982) and his own results. The results produced in the current survey may be added to this data collection without further reduction, and the entire compilation is listed in Table VI-(xv). Those values which are deemed uncertain by the source have been denoted by a colon suffix in the usual manner, together with an explanatary note in certain cases. Galaxies with more than one source of characteristic parameters have had the solutions averaged, but uncertain solutions have not been used in the construction of average values. It is encouraging to note that there are no gross inconsistencies between the parameters produced by all five

independent authors, despite the differences in decomposition technique and selection effects inherent in each data subset.

It must be emphasized that the formation of a properly homogeneous data set is essential if the subsequent analysis is to have any statistical validity. The actual values of the absorption scheme and distance-scale which are adopted are irrelevant if they applied consistently to the entire sample. For the reasons detailed in section VI-I (M/L) disk-corrections have not been applied to any of the spiral systems in the data set. Full details of the conversion of the results of Burstein (1979 b), Boroson (1981) and Hamabe (1982) to form a homogeneous data set are given in Davenhall (1984 a), Appendix IV.

Apart from the results presented in this work, decomposition techniques have been applied to I-band photometry only by Boroson et al. (1983 b), who present disk parameters for 62 galaxies in the Virgo cluster. These results need only be converted to the distance-scale adopted in this work (d(Virgo) = 12 Mpc), as the effects of galactic absorption in the I-band are negligible (for the Virgo cluster) with respect to the likely errors in the disk central surface-brightness parameters.

The modified results of Boroson et al. (1983 b) have been combined with the results obtained in this work, and the compilation is listed in Table VI-(xvi). Boroson et al. (1983 b) exclude from their analysis solutions which they consider may have been influenced by the presence of a bar, and these galaxies have also been excluded from the compilation, together with all

systems which did not have morphological types given by de Vaucouleurs et al. (1976). NGC 4501 has also been excluded from the compilation as the solution may be influenced by a third luminosity component. Galaxies with more than one source of characteristic parameters have had the solutions averaged, but uncertain solutions have not been included in the calculation of average values.

3.3 Statistical Analysis of the Data Sets

Excluding uncertain solutions, the B-band data set listed in Table VI-(xv) contains characteristic parameters for 15 lenticular and 17 spiral bulges. Figures VI.1 and VI.2 show plots of B_o and R_o against morphological type, and Figure VI.3 shows the variation of B_o with $\log(R_o)$. Inspection of these graphs reveals no obvious trend for the bulges of lenticular systems to be larger than those of spiral systems, as reported by Dressler (1980), or for the characteristic-brightness to have any dependence on morphological type. In contrast, the well-known correlation between B_o and $\log R_o$ (Kormendy (1980)) is quite apparent in Figure VI.3. To quantify these visual impressions more precisely, Spearman (Rho) tests were performed to test the correlation of the variables. Due to the large amount of data, non-parametric tables could not be used to evaluate the probability of correlation, and the usual large-sample normal approximation ($Z = \sqrt{n}\,\rho$) has been used. The results of the correlation tests are shown in Table VI-(xvii).

The statistical analysis confirms the visual impression that R_o

and B_o are not correlated with morphological type, but confirms that R_o and B_o are related in some fashion at a very high level of significance. The appearance of Figure VI.3 suggested a relation of the form:

$$B_o = m \log (R_o) + c$$

and a least-squares fit to the data gave the result:

$$B_o = 3.65\ (\pm\ 0.32) \log (R_o) + 21.65\ (\pm\ 0.16)$$

where the uncertainties are standard errors. This relation is shown as a solid line in Figures VI.3 and VI.4. Kormendy (1982) found a similar relation for elliptical systems, of the form:

$$B_o = 3.28 \log (R_o) + 19.45$$

and he suggested that the bulges of disk systems were systematically more diffuse than ellipticals, in that they had fainter characteristic brightness and larger scale-lengths. Kormendy's relation is plotted as a broken line in Figure VI.3, and it is immediately apparent that the bulges of disk systems are indeed systematically more diffuse as all the points lie above the mean-line for elliptical galaxies.

Figure VI.4 shows the positions of lenticular and spiral bulges in the B_o - log (R_o) plane; lenticular bulges are represented by solid squares and spiral bulges by open squares. The populations appear to occupy the same locus, confirming the similarity of spiral and lenticular bulge components.

Excluding uncertain solutions, the B-band data set contains characteristic parameters for 18 spiral and 20 lenticular disks. In a pioneering study, Freeman (1970) found the central surface-brightness of the disks of 28 galaxies to be

approximately constant, with a mean value of 21.65 (B) magnitudes per square arcsecond and a standard deviation of only 0.3 magnitudes. Freeman used a 0.2 cosec |b| absorption-correction, which implies that his mean result would be about 0.15 magnitudes fainter on the system adopted in this work. For the 38 disks in the B-band data set the mean central surface brightness was 21.84, with a standard deviation of 1.04 magnitudes, in close agreement with the mean value found by Freeman. However, the standard deviation is over three times that of Freeman's sample, and this implies a much large "cosmic" scatter in the central surface brightnesses of disk systems. This result is in agreement with more modern investigations of disk systems (e.g. Boroson (1981), Kormendy (1982), Boroson et al. (1983 b)), and suggests that the formation of disk galaxies does not involve a small range in initial dynamical properties as proposed by Freeman (1970).

Figures VI.5 and VI.6 show plots of central surface brightness ($B(o)_c$) and scale-length (α^{-1}) against morphological type. Inspection of these graphs reveals no obvious trend in the variation of central surface brightness with type, but a noticeable trend for the disk scale-length to increase at later morphological type. To investigate these visual impressions more precisely, Spearman (Rho) tests were performed to evaluate the correlation of the data. Due to the sample size, non-parametric tables could not be used to evaluate the probability of correlation and the usual large-sample approximation to normality was used. The results of the correlation tests are shown in Table VI-(xviii).

Examination of Table VI-(xviii) reveals that the only reasonable conclusion that can be drawn regarding the disk central surface-brightness is that it is uncorrelated with morphological type. This result is in disagreement with Fraser (1977) who reported a dependence of $B(o)_c$ with morphological type of the form:

$$B(o)_c = 22.14 - 0.21\ T$$

This relation is shown as a broken line in Figure VI.5. Fraser's use of a 0.2 cosec |b| absorption-correction would produce a change in intercept of only about +0.15 magnitudes, and his relation cannot be reconciled with the present data. The discrepancy between Fraser's relation and the data set compiled in this work is probably due to his use of simple linear fits rather than modern decomposition techniques (Davenhall (1984 a)).

In contrast, the correlation of disk scale-length and morphological type seems highly likely as the null hypothesis of variable independence can be rejected at the 2% level significance. If one considers the appearance of Figure VI.6 sufficient evidence to consider only a direct relationship (i.e. larger values of α^{-1} at later type), then the null hypothesis can be rejected at the 1% level of significance (as the test becomes one-tailed).

There have been suggestions (Boroson (1981) and Hamabe (1982)) that $B(o)_c$ and disk scale-length may be correlated in a fashion

reminiscent of the B_o - log R_o relation, in the sense that larger scale-lengths have fainter central surface-brightnesses. Figure VI.7 shows the variation of central surface-brightness ($B(o)_c$) with disk scale-length (α^{-1}), and inspection of this graph seems to confirm the suggested trend. To evaluate this apparent trend more precisely, a Spearman (Rho) test was performed to evaluate the correlation between the variables, and the result is shown in Table VI-(xix). Due to the large amount of data the usual large-sample normal approximation was used, but no tie-correction procedure was necessary.

It is apparent from inspection of Table VI-(xix) that one can reject the null hypothesis of independence at a very high level of significance (0.2%). If it is considered that the appearance of Figure VI.7 is sufficient reason to consider only a direct relationship (i.e. larger scale-lengths at fainter $B(o)_c$ values) then the null hypothesis can be rejected at the 0.1% level of significance (as the test becomes one-tailed).

Figure VI.8 shows the positions of spiral and lenticular disks in the $B(o)_c$ - α^{-1} plane, with lenticulars denoted by solid squares and spirals by open squares; although the segregation is not complete, it is clear that the populations occupy different loci. The lenticular systems appear to have fainter central surface brightnesses at a given scale-length than the corresponding spiral galaxies, confirming the suggestions of Boroson (1981) and Davenhall (1984 a).

It is interesting that two of the spirals (NGC 2681 and 2855)

which lie in the lenticular locus have the transitional morphological type of zero, and two of the lenticular galaxies (NGC 4281 and 4526) which lie in the spiral locus have a prominent dust-lane and residual spiral features respectively (Burstein (1978)).

To quantify the apparent differences between spiral and lenticular disks in the $B(o)_c - \alpha^{-1}$ plane, the Mann-Whitney (Mann and Whitney (1947) extension of the Wilcoxon Rank Sum Test (Wilcoxon (1945 b)) was used to test the null hypothesis that the spiral and lenticular samples were drawn from the same population. The Daniel (1978 b) formulation of the Mann-Whitney U-test was selected as ranking had already been performed for the correlation tests. The results of the analysis are shown in Table VI-(xx).

Inspection of Table VI-(xx) reveals that the null hypothesis cannot be rejected at a convincing level for the $B(o)_c$ sample, but can be rejected at a 1% level of significance for the α^{-1} samples. If the appearance of Figure VI.8 is considered sufficient reason to consider only the possibility that the scale-lengths of lenticular galaxies are smaller than those of spiral systems, then the null hypothesis can be rejected at the 0.5% level (as the test becomes one-tailed). Thus the statistical analysis confirms the visual impression that the spiral and lenticular samples are significantly segregated in the $B(o)_c - \alpha^{-1}$ plane.

In order to ascertain whether the segregation of lenticular and

spiral disks in the $B(o)_c - \alpha^{-1}$ plane also implies differences in the absolute magnitudes of the disk components, a plot of $B(o)_c$ against $\log(\alpha^{-1})$ may be constructed (following Hamabe (1982)), and such a graph is shown as Figure VI.9.

Freeman (1970) introduced the distance-independent relation for the total absolute magnitude of the disk:

$$M_{disk} = B(o)_c - 5 \log \alpha + 38.56$$

This relation was used to calculate lines of constant disk luminosity, and several significant values are shown as broken lines in Figure VI.9. It is immediately apparent that the apparent segregation of spiral and lenticular disks implies a corresponding segregation in absolute magnitude; most lenticular disks are fainter than $M_d = -18^m.5$, whereas most spiral disks are brighter than this value. No disks are brighter than $M_d = -21^m$, in agreement with Burstein (1979 b) and Hamabe (1982); this may represent the upper limit of disk luminosity.

Inspection of Figure VI.8 reveals that relations of the form:

$$B(o)_c = m \alpha^{-1} + c$$

may describe the spiral and lenticular data values; least-square fits were performed on the data sets and the results are listed in Table VI-(xxi). The best-fit relations for spiral and lenticular disks in the $B(o)_c - \alpha^{-1}$ plane are shown in Figure VI.10 as solid and broken lines respectively. While the lenticular disks seem quite well-described by the relation:

$$B(o)_c = 1.05 \alpha^{-1} + 19.88$$

the spiral disks display considerably more scatter about their

best-fit relation. A larger data sample is needed to investigate relations of this form more thoroughly.

The B-band data set listed in Table VI-(xv) contains Disk:Bulge luminosity solutions for 31 galaxies with well-determined solutions for bulge and disk characteristic parameters and little evidence for any third luminosity component. The Disk:Bulge luminosity ratio is not particularly sensitive to uncertainties in the fitted solutions produced by modern decomposition techniques, so average (D/B) ratios were formed for the four systems which had more than one data source during the construction of the data set. A further 20 systems listed in Table VI-(xv) have (D/B) ratios which are uncertain because they have a solution for only one luminosity component, or have solutions with evidence of a significant third component. Three galaxies (NGC 4150, 4552 and 4594) are excluded from the analysis due to uncertainty in the morphological classification or solutions which are considered by the data-source as very uncertain.

The variation of log (D/B) ratio with morphological type is shown as Figure VI.11; the 31 well-determined values are shown as solid squares and the 20 less-certain solutions are denoted by open squares. The uncertain values appear to occupy essentially the same locus as the well-determined solutions, confirming the view that the (D/B) ratio is not particularly sensitive to uncertainties in the fitted solutions produced by decomposition techniques if clearly-unrealistic values are discarded. It is immediately apparent from inspection of Figure VI.11 that

early-type galaxies ($T \leq 0$) have much smaller (D/B) values than spiral systems ($T > 1$), and there appears to be a trend of increasing disk dominance with morphological type for the spiral systems. To evaluate the apparent variation of log (D/B) ratio with morphological type, Spearman (Rho) correlation tests were performed on both the well-determined sample ($n = 31$) and the full sample including the less-certain values ($n = 51$). Due to the large amount of data, the usual large-sample normal approximation was used, and the results are listed in Table VI-(xxii).

Inspection of Table VI-(xxii) reveals that the null hypothesis of independence can be rejected at a very high level of significance (0.2%), and one can conclude that the log (D/B) ratio shows a clear dependence on morphological type. If the appearance of Figure VI.11 is considered sufficient reason to consider only a direct relationship (i.e.: larger (D/B) values at later type), then the null hypothesis may be rejected at the 0.1% level of significance (as the test becomes one-tailed). This result confirms the conclusions of Burstein (1979 b), Boroson (1981), Hamabe (1982) and Davenhall (1984).

To evaluate more precisely the apparent differences between lenticular and spiral log (D/B) values, the Mann-Whitney extension of the Wilcoxon Rank Sum test was used to test the null hypothesis that the spiral and lenticular samples were drawn from the same population. The Daniel (1978 b) formulation of the Mann-Whitney U-test was selected as ranking had already been performed for the correlation tests. The results of the analysis

are shown in Table VI-(xxiii); for the extended data-set (n = 51) the large-sample approximation recommended by Daniel (1978 b) was adopted as the population size was too large for the use of non-parametric tables.

Inspection of Table VI-(xxiii) confirms that the null hypothesis can be rejected at a very high level of significance (0.2%) for both data sets. If the appearence of Figure VI.11 is considered sufficient reason to consider only the possibility that the lenticular log (D/B) values are smaller than the spiral values, then the null hypothesis can be rejected at the 0.1% level of significance (as the test becomes one-tailed). Thus the statistical analysis demonstrates that the log (D/B) values of lenticular galaxies are smaller than those of spiral systems in the B-band data set.

One may note that the statistical investigation of the B-band data set has strengthened the conclusions of Davenhall's (1984 a) analysis of a similar data set; weak correlations are statistically weaker, and strong correlations have been confirmed at similar or higher levels of significance. This is most encouraging, as it implies that the statistical merit of the B-band data set has been improved by the addition of the data produced in this work.

The I-band data set listed in Table VI-(xvi) contains characteristic parameters for the disks of 15 lenticular and 32 spiral galaxies in the Virgo cluster. Figures VI.12 and VI.13 show plots of disk central surface-brightness ($I(o)_c$) and

scale-length (α_c^{-1}) against morphological type, and Figure VI.14 shows the variation of $I(o)_c$ with α^{-1}. No obvious variation of either $I(o)_c$ or α^{-1} with morphological type is evident, but there does appear to be a trend for larger scale-lengths to have fainter central surface-brightnesses. In order to quantify these visual impressions more precisely, Spearman (Rho) tests were performed to evaluate the correlation between the variables. Due to the large amount of data non-parametric tables could not be used, and the usual large-sample normal approximation was adopted. The results of the statistical analysis are shown in Table VI-(xxiv).

Inspection of Table VI-(xxiv) reveals that the only reasonable conclusion that can be drawn regarding disk central surface-brightness and scale-length is that they are essentially uncorrelated with morphological type. In contrast, the null hypothesis of variable independence can be rejected at the 3.5% level of significance for the variation of $I(o)_c$ with α_c^{-1}. If the appearance of Figure VI.14 is considered sufficient reason to consider only a direct relationship (i.e.: disks with large scale-lengths have fainter central surface-brightnesses), then the null hypothesis can be rejected at the 2% level of significance (as the test becomes one-tailed). Although this correlation is not quite so convincingly established as the corresponding B-band relationship, it does seem very likely that there is a direct relation between $I(o)_c$ and α_c^{-1}.

Figure VI.15 shows the positions of lenticular and spiral disks in the $I(o)_c - \alpha^{-1}$ plane; no obvious segregation of the populations can be seen. Such a segregation might not be evident due to the unequal size of the populations, and it is noticeable that the majority of the largest disks (with the faintest central surface-brightnesses) are drawn from the lenticular sample. In order to evaluate possible differences between spiral and lenticular disks in the $I(o)_c - \alpha^{-1}$ plane, the Mann-Whitney extension of the Wilcoxon Rank Sum test was used to test the null hypothesis that the spiral and lenticular samples were drawn from the same population. The Daniel (1978 b) formulation of the Mann-Whitney U-test was used as ranking had already been performed for the correlation tests. Due to the large sample size non-parametric tables could not be used, and the usual large-sample normal approximation was adopted. The results of the analysis are shown in Table VI-(xxv).

Inspection of Table VI-(xxv) reveals that the null hypothesis cannot be rejected for either variable at any convincing level of significance, and the most reasonable conclusion that can be drawn is that there is no significant segregation of spiral and lenticular disks in the $I(o)_c - \alpha_c^{-1}$ plane, confirming the result of Boroson et al. (1983 b).

This conclusion is in marked contrast to the corresponding B-band result, where lenticular disks were found to be significantly smaller than their spiral counterparts at any given central surface-brightness. It is obviously pertinent to consider if the B-band disk scale-lengths of either spiral or lenticular systems

are significantly different from the corresponding I-band values. Figure VI.16 shows the variation of lenticular disk scale-length with morphological type; the 20 B-band data points are represented by solid squares, and the 15 I-band data points are displayed as open squares slightly offset in the interests of clarity. No significant segregation of the samples is obvious. Figure VI.17 shows the variation of spiral disk scale-length with morphological type; the 18 B-band data points are represented by solid squares, and the 32 I-band data points are shown as open squares. It is noticeable that the B-band spiral scale-lengths appear systematically larger than the majority of I-band spiral scale-lengths at each morphological stage ($0 \leq T \leq 6$). To quantify these visual impressions more precisely, the Mann-Whitney extension of the Wilcoxon Rank Sum test was used to test the null hypothesis that the spiral or lenticular B-band and I-band data samples of disk scale-length were drawn from the same population. The Daniel (1978 b) formulation of the Mann-Whitney U-test was used to test the lenticular data samples, whereas the Sprent (1981) formulation was preferred to test the larger spiral data samples for computational convenience. Due to the large amount of data, the usual large-sample normal approximation was adopted for both population tests; the lenticular test could also be evaluated from non-parametric tables. The results of the statistical analysis are shown in Table VI-(xxvi).

Inspection of Table VI-(xxvi) reveals that the null hypothesis cannot be rejected for the lenticular samples at any reasonable level of significance, and the analysis confirms the visual impression that lenticular disks have similar scale-length

distributions in both B and I-passbands. In contrast, the null hypothesis can be rejected at a very high level of significance (0.2%) for the spiral samples, and confirms the visual impression that there is a significant difference between the spiral samples of B and I-band disk scale-lengths. If the appearance of Figure VI.17 is sufficient inducement to consider only the possibility that the B-band spiral scale-lengths are generally larger than the I-band scale-lengths, then the null hypothesis may be rejected at the 0.1% level of significance (as the test becomes one-tailed).

Thus the statistical analysis reveals that the disparate conclusions reached as to the segregation of spiral and lenticular samples in the $B(o)_c - \alpha_c^{-1}$ and $I(o)_c - \alpha_c^{-1}$ planes is due to a variation in the properties of spiral disks only. The implications of this conclusion will be discussed in the next sub-section.

3.4 Conclusions

The statistical analysis presented in the last section indicated that neither the characteristic brightness nor the scale-length of the bulge components of disk galaxies correlate with morphological type. Thus there are no significant differences in size or luminosity between the bulges of spiral and lenticular systems in the sample investigated in this work. This result is in contradiction with the results of Dressler (1980), who concluded that the bulges of lenticulars are "systematically much larger" than the bulges of spiral systems. Dressler's analysis

is based on a much larger data sample, but uses a visual estimation technique which is clearly less than ideal, and may be invalid. As all the data studied in this work has been drawn from sources which have used modern decomposition techniques on high-quality photometric data, the analysis would seem to be much more securely established, and the subsequent conclusion of greater weight than Dressler's result.

The well-known correlation between log R_o and B_o (Kormendy (1980)) has been confirmed in the analysis presented in this work, and the bulges of disk systems are clearly more diffuse than elliptical galaxies, in agreement with Kormendy (1982). The similarity of the bulge components of spiral and lenticular systems is demonstrated by the lack of apparent segregation in the B_o - log R_o plane. The observed correlation beween these variables is probably due to parameter-coupling resulting from the similarity of the observed bulge profiles to one-parameter power laws (see e.g. Kormendy (1982) for a detailed discussion).

The statistical analysis presented in the last section suggested that while the disk central surface brightness was uncorrelated with morphological type, the disk scale-length was directly related to morphological type. In addition, the spiral and lenticular populations seem significantly segregated in the $B(o)_c - \alpha^{-1}$ plane, with spiral systems larger at any given $B(o)_c$. This form of segregation in the $B(o)_c - \alpha^{-1}$ plane has been shown to imply an equivalent segregation in absolute disk luminosity, with the disks of lenticular systems being typically about 1.5 - 2 magnitudes fainter than the disks of spiral systems.

Dressler (1980) points out that if the disks of lenticular systems were faded by this amount, his result of systematically larger lenticular bulges would be produced by selection-effects in his magnitude-limited sample. Kent (1981) further suggests that the selection-effects accompanying such a disk-fading could produce the systematic variation of morphology, bulge-luminosity and Disk:Bulge ratio found by Dressler (1980). In fact, the observed luminosity functions produced by this effect alone require only the production of some elliptical systems by collisional merging in regions of high local density to produce the observed cluster luminosity functions (White (1982)).

To recapitulate, the bulge components of spiral and lenticular systems seem very similar, but the disks of lenticular galaxies are significantly fainter than those of spiral galaxies. These results provide a natural explanation for the dramatic increase in Disk:Bulge luminosity ratio at later morphological type found in this work and several previous investigations.

In contrast, the analysis of the I-band data set demonstrates that there are no significant differences between the disks of spiral and lenticular systems. In fact, there do not appear to be significant differences between the disks of lenticular galaxies at B and I-wavelengths, whereas the B-band scale-lengths of spiral disks appear significantly larger than the I-band disk population. The inference which can be immediately drawn is that spiral disks are brighter in the bluer passband because of widespread recent star-formation, as this is the major morphological classification criterion.

As explained in Chapter I.4, the main argument against the production of lenticular galaxies by the environmental modification of spiral systems has been the reported differences in bulge size and luminosity between lenticular and spiral galaxies. This objection must be seriously, and perhaps fatally, weakened by the analysis presented in this work, as the bulge and 'old' disk components of spiral and lenticular systems are essentially indistinguishable.

The similarity of the 'old' disk components of spiral and lenticular galaxies virtually excludes the 'birth-defect' scenarios for the production of lenticular systems (see Chapter I.3), as any environmental interaction should affect the outer regions of a proto-galaxy most severely, and the removal of gas in the early history of a star-forming spiral would reduce the total luminosity of the disk component in subsequent epochs. The lack of difference between the bulge components of spiral and lenticular systems also renders the various 'intrinsic' gas-removal mechanisms which have efficiencies dependent upon bulge size (or Bulge:Disk ratio) rather improbable.

The most straightforward interpretation of the observations would seem to be that spiral galaxies have undergone vigorous star-formation in the relatively recent past (i.e. the last few billion years) while the lenticular systems have not. Larson et al. (1980) have produced models of gas-poor disks which show that the natural aging of disk stars produces a fade of 1.5 - 2 magnitudes over this timescale, in excellent agreement

with the results obtained in this work, and in strong support of the production of presently-observed lenticular and spiral galaxies from the same original population of disk systems. This result cannot be interpreted as direct evidence for environmental modification by external effects; the disks of lenticular galaxies might simply have exhausted all the available gaseous "fuel" for star-formation. It may very well be that the actual cause of gas removal is irrelevant; whether galaxy-galaxy encounters, galaxy-ICM interactions, or internal gas-depletion mechanisms remove the gas from a spiral disk, its eventual fate may be the fading of the disk with age and the attendant dynamical dissolution of spiral structure to form a lenticular galaxy.

Caveat

While the results of the statistical analysis presented in the previous sub-section seem well-established and consistent with some theoretical predictions, several reservations must be borne in mind when considering the conviction of the conclusions drawn.

Firstly, none of the samples used to construct the B and I-band data sets was complete, and all contained some selection effects. Even the sample produced in the current work, which attempted to be complete within 3^{o} of the centre of the Virgo cluster, was inevitably biassed towards those systems which produced reasonable solutions from modern decomposition techniques. The sample of Burstein (1979 a,b) was biassed towards lenticulars

with reasonably strong disk components, while the sample of Boroson (1981) was biassed towards spirals with prominent bulge components.

Secondly, although all the characteristic parameters forming the B and I-band data sets have been produced by modern decomposition techniques, the details of the adopted procedure differ between the various authors. It is possible that inconsistencies in the decomposition technique could introduce systematic errors in the characteristic parameters produced by the various authors. Certainly such effects must be fairly subtle, if they exist at all, as there is no obvious disagreement between the parameters produced by the various authors.

Thirdly, the I-band sample is drawn entirely from the Virgo cluster, whereas the B-band sample is drawn from the Virgo cluster and several nearby groups of lower local density; thus the comparison of disk scale-lengths could be influenced by differences in local galaxian density between the samples.

Fourthly, the results of Boroson et al. (1983 b) may be criticized on the grounds that they consider the calculated characteristic parameters of the bulge components of their iterative decompositions too uncertain for statistical analysis and subsequent publication. If the bulge solutions are erroneous they will introduce systematic errors into the disk solutions by the very nature of the iterative decomposition technique. In practice, however, the effect on the disk parameters will be small unless the bulge solution is quite unrealistic; the level

of agreement between the results of the current work and those of Boroson et al. (1983 b) for the three systems in common suggests that any errors due to this effect are probably negligible.

Lastly, the analysis of the correlation of the various characteristic parameters with morphological type may be criticized (e.g. Davenhall (1984 a)) on the grounds that the morphological type is measured on an ordinal scale, as it is an arbitrary digitization of a taxonomic system as opposed to a classification based on a scale of physical measurement. Non-parametric statistical tests are particularly suited to this contingency as they require only an ordinal scale of measurement and generally require no 'a prior' assumptions about the variable distribution.

Table VI-(i)

B-Band Results

	Iterative Solutions				Simultaneous Solutions			
NGC	log I_o	R_o	log I(o)	α	I_o	R_o	I(o)	α
4267	2.24	2.121	0.398	0.033	234.34	1.884	2.740	0.034
4371	0.65	14.168	-0.076	0.026	6.16	11.407	1.657	0.028
4377	1.85	2.569	0.081:	0.056:	70.95	2.534	1.802:	0.060:
4419	-	-	-	-	9.67::	8.715::	0.740::	0.032::
4425	-	-	-	-	0.96::	21.081::	1.120::	0.042::
4429	0.20	30.820	0.174	0.028	1.92	26.222	2.187	0.024
4435	1.21:	8.653:	-0.469::	0.008::	17.54:	8.254:	0.471::	0.009::
4438	-	-	-	-	0.76::	42.796::	1.001::	0.013::
4459	0.44	23.259	-0.757:	0.011:	4.38:	16.103	0.811:	0.017:
4461	0.84:	10.597:	-0.985::	0.009::	8.14:	9.482:	0.450::	0.020::
4474	0.91:	7.596:	-0.411::	0.024::	10.31:	6.605:	0.850::	0.030::
4477	0.90	11.801	0.140	0.026	10.56	9.802	2.070	0.027
4501	-	-	-	-	2.54:	17.119:	5.287:	0.027:
4503	0.69	11.554	-0.410	0.025	6.09	9.887	1.057	0.030
4531	-	-	-	-	0.03::	342.147::	0.916::	0.027::
4550	-	-	-	-	3.99::	13.953::	0.664:	0.038:
4552	0.83	17.587	-0.412	0.009	9.59	14.308	0.751	0.012

Table VI-(ii)

R-Band Results

	Iterative Solutions				Simultaneous Solutions			
NGC	log I_o	R_o	log I(o)	α	I_o	R_o	I(o)	α
4267	0.98	6.086	0.513	0.042	15.34	4.779	3.509	0.043
4371	0.97	8.478	-0.184	0.025	17.35	6.340	0.826	0.025
4377	1.99:	2.003:	0.007:	0.067:	111.16	1.896	1.243	0.067
4419	1.78:	3.100:	0.662	0.076	-	-	-	-
4425	-	-	-	-	1.17::	16.418::	0.298::	0.033::
4429	-	-	-	-	4.25:	14.764:	2.511:	0.027:
4435	0.65:	13.986:	-0.866::	0.012::	5.32:	12.551:	0.526::	0.019::
4438	0.41::	21.040::	-0.067::	0.008::	6.19::	12.720::	0.644::	0.015::
4459	0.72	14.650	-0.568:	0.016:	5.76	13.734	0.556:	0.018:
4461	-	-	-	-	2.38:	16.478:	0.123::	0.012::
4474	0.62:	9.006:	-0.928::	0.022::	5.59:	7.617:	0.329::	0.028::
4477	0.76	11.859	-0.140	0.025	7.67	10.073	1.031	0.025
4501	-	-	-	-	0.18::	168.728::	0.809::	0.019::
4503	-	-	-	-	1.83:	19.233:	0.346:	0.024:
4531	-	-	-	-	0.04::	114.54::	0.861:*	0.035:*
4550	-	-	-	-	84.47::	3.361::	0.150:	0.024:
4552	0.93:	12.631:	-0.335::	0.013::	9.58:	11.834:	0.633::	0.014::

* These parameters are used to establish a lower limit for the (D/B) ratio only; they are considered too uncertain for further analysis.

Table VI-(iii)

I-Band Results

	Iterative Solutions				Simultaneous Solutions			
NGC	log I_o	R_o	log I(o)	α	I_o	R_o	I(o)	α
4267	1.66	2.274	-0.084	0.034	45.76	2.235	0.957	0.035
4371	0.59	9.822	-0.764	0.016	5.70	7.766	0.256	0.018
4377	1.02::	4.021::	-1.604::	0.010::	20.47::	2.917::	0.080::	0.023::
4419	2.54:	1.038:	0.624	0.081	218.92:	1.241:	3.972	0.080
4425	-	-	-	-	0.17::	43.788::	0.231::	0.036::
4429	1.07	7.043	-0.519	0.015	137.59	2.197	0.355	0.015
4435	0.45:	13.185:	-1.468::	0.007::	4.44:	10.104:	0.332::	0.022::
4438	-	-	-	-	1.05::	23.957::	0.299::	0.014::
4459	0.32	18.449	-1.000:	0.010:	2.15	17.811	0.207:	0.012:
4461	0.34:	12.588:	-0.991::	0.014::	2.77:	11.049:	0.203::	0.017::
4474	0.17:	11.963:	-1.397::	0.008::	1.78:	10.731:	0.114::	0.015::
4477	0.60	11.880	-0.703	0.015	3.49	12.440	0.326	0.017
4501	0.13:	26.990:	-0.767:	0.013:	2.42:	17.165:	0.393:	0.014:
4503	0.44	10.799	-0.822	0.023	5.35	7.166	0.406	0.028
4531	-	-	-	-	0.02::	232.546::	0.161::	0.019::
4550	-	-	-	-	0.90::	22.098::	0.416:	0.046:
4551	1.43::	6.389::	-0.526::	0.012::	60.53::	4.477::	0.351::	0.013::

Table VI-(iv)

Calculated Absorption Values (in magnitudes)

NGC	A_B	A_V	A_R	A_I
4267	0.084	0.065	0.046	0.030
4371	0.014	0.011	0.008	0.005
4377	0.032	0.025	0.018	0.012
4419	0.033	0.025	0.018	0.012
4425	0.111	0.086	0.060	0.040
4429	0.014	0.010	0.007	0.005
4435	0.084	0.065	0.046	0.030
4438	0.084	0.064	0.045	0.029
4459	0.072	0.055	0.039	0.025
4461	0.071	0.055	0.039	0.025
4474	0.072	0.055	0.039	0.025
4477	0.072	0.055	0.039	0.025
4501	0.071	0.054	0.038	0.025
4503	0.014	0.011	0.008	0.005
4531	0.09	0.07	0.05	0.03
4550	0.111	0.085	0.060	0.039
4552	0.111	0.086	0.060	0.040
Errors	0.034	0.045	0.030	0.020

Table VI-[v]

NGC	Frame Sky Brightness (magnitudes/sq. arcsec) B	R	I	Inclination Correction (2.5 log R)	Major-Axis Correction ($R^{1/2}$)
4267	22.82	20.53	19.68	0.075	1.035
4371	22.84	20.53	19.68	0.500	1.259
4377	22.88	20.53	19.68	0.200	1.096
4419	22.85	20.53	19.68	1.075	1.641
4425	22.80	20.53	19.68	1.100	1.660
4429	22.91	20.64	19.89	0.825	1.462
4435	22.85	20.51	19.54	0.450	1.230
4438	22.85	20.51	19.54	0.950	1.549
4459	23.04	20.57	19.80	0.325	1.161
4461	22.83	20.52	19.43	0.950	1.549
4474	22.81	20.53	19.68	0.700	1.380
4477	22.95	20.58	19.55	0.125	1.059
4501	22.83	20.58	19.70	0.625	1.334
4503	22.93	20.53	19.68	0.750	1.413
4531	22.85	20.53	19.68	0.400	1.202
4550	22.86	20.53	19.68	1.275	1.799
4552	22.93	20.38	19.87	0.000	1.000

Table VI-(vi)

B-Band Characteristic Parameters

NGC	$B(R_o)$	R_o(kpc)	$B(o)_c$	α_c^{-1}(kpc)	Technique
4267	17.13	0.12	21.81	1.83	I
4371	21.20	0.82	23.52	2.81	I
4377	18.22	0.15	22.84:	1.14:	I
4419	-	-	-	-	
4425	-	-	-	-	
4429	22.40	1.79	23.29	3.04	I
4435	19.74:	0.50:	-	-	I
4438	-	-	-	-	
4459	21.86	1.35	25.18:	6.14:	I
4461	20.66:	0.62:	-	-	I
4474	20.45:	0.44:	-	-	I
4477	20.62	0.69	22.65	2.37	I
4501	21.75:	1.00:	21.58:	2.88:	S
4503	21.20	0.67	24.70	3.29	I
4531	-	-	-	-	
4550	-	-	24.47:	2.76:	S
4552	20.74	1.02	23.84	6.47	I

Table VI-(vii)

R-Band Characteristic Parameters

NGC	$R(R_0)$	R_0(kpc)	$R(c)_c$	α_c^{-1}(kpc)	Technique
4267	18.03	0.35	19.28	1.43	I
4371	18.10	0.49	21.48	2.93	I
4377	15.54:	0.12:	20.69	0.95	I
4419	16.06:	0.18:	19.93	1.27	I
4425	-	-	-	-	
4429	19.06:	0.86:	20.46:	3.15:	S
4435	18.84:	0.81:	-	-	I
4438	-	-	-	-	
4459	18.73	0.85	22.28:	4.22:	I
4461	19.54:	0.96:	-	-	S
4474	18.94:	0.52:	-	-	I
4477	18.59	0.69	20.97	2.47	I
4501	-	-	-	-	
4503	19.87:	1.12:	22.42:	3.43:	S
4531	-	-	21.04:*	2.00:*	S
4550	-	-	23.80:	4.36:	S
4552	-	-	-	-	

* Parameters are used only to provide a lower limit on the Disk:Bulge ratio.

Table VI-(viii)

I-band Characteristic Parameters

NGC	$I(R_o)$	R_o(kpc)	$I(o)_c$	α_c^{-1}(kpc)	Technique
4267	15.50	0.13	19.95	1.77	I
4371	18.20	0.57	22.10	4.58	I
4377	-	-	-	-	
4419	13.32:	0.06:	19.18	1.18	I
4425	-	-	-	-	
4429	17.21	0.41	22.02	5.67	I
4435	18.38:	0.77:	-	-	I
4438	-	-	-	-	
4459	18.97	1.07	22.60:	6.76:	I
4461	18.55:	0.73:	-	-	I
4474	19.23:	0.70:	-	-	I
4477	18.03	0.69	21.40	4.11	I
4501	19.35:	1.52:	22.22:	5.97:	I
4503	18.58	0.63	22.49	3.58	I
4531	-	-	-	-	
4550	-	-	21.87	2.28	S
4552	-	-	-	-	

Table VI-(ix)

The Calculation of Extinction-Corrected Total Apparent Magnitudes

	Extinction - Corrected Total-Magnitude Colours			M_T (galaxy)		
NGC	(B - R)	(B - I)	(R - I)	B	R	I
4267	1.82	1.96	0.14	11.86	10.08	9.95
4371	1.96	2.39	0.43	11.95	10.00	9.57
4377	1.62	2.16	0.54	12.52	10.91	10.38
4419	1.78	2.00	0.22	11.96	10.20	9.98
4425	1.81	2.08	0.27	12.57	10.81	10.56
4429	1.94	2.47	0.53	11.02	9.09	8.56
4435	-	-	-	11.54	-	-
4438	-	-	-	10.51	-	-
4459	2.01	2.65	0.64	11.41	9.43	8.81
4461	1.81	2.56	0.75	11.70	9.92	9.19
4474	1.68	2.30	0.62	12.29	10.64	10.04
4477	1.91	2.70	0.78	11.48	9.60	8.83
4501	1.74	2.31	0.57	10.27	8.56	8.01
4503	2.05	2.47	0.42	12.14	10.10	9.68
4531	1.74	2.23	0.49	12.42	10.72	10.25
4550	1.84	2.17	0.33	12.13	10.34	10.03
4552	1.97	2.41	0.44	10.75	8.83	8.41

Table VI-(x)

NGC	B-band log(D/B)	Remark	R-band log(D/B)	Remark	I-band log(D/B)	Remark
4267	-0.09	1	0.16	1	-0.08	1
4371	-0.42	1	-0.36	1	-0.31	1
4377	-0.57:	3	-0.59:	3	-	-
4419	-	-	-	-	-0.32:	3
4425	-	-	-	-	-	-
4429	-0.46	1	0.03:	2	-0.20	1
4435	-0.90:	4	-	-	-	-
4438	-	-	-	-	-	-
4459	-0.57:	3	-0.59:	3	-0.41	3
4461	-0.30:	4	-0.83:	4	-0.27:	4
4474	-0.38:	4	-0.86	4	-0.34:	4
4477	-0.30	1	-0.40	1	-0.36	1
4501	0.43:	2	-	-	-0.10:	2
4503	-0.58	1	-0.61:	2	-0.61	1
4531	-	-	0.1 :	6	-	-
4550	-0.71:	4	-0.77:	4	-0.67:	4
4552	-0.20	5	-	-	-	-

1 Both components determined by an Iterative Technique.

2 Both components determined by a Simultaneous Technique.

3 Both components determined by an Iterative Technique, one component uncertain.

4 Only one component determined, approximate value.

5 Morphological classification uncertain, 'disk' component could be tidal distorsion of bulge.

6 Lower limit only; produced from a very approximate solution.

Table VI-(xi)

Comparison of I-band Disk Scale-Length (kpc)

NGC	This Work	Boroson et al. (1983 b)	Difference	Average
4267	1.77	1.57	13%	1.67
4419	1.18	1.25	6%	1.22
4429	5.67	6.16	8%	5.92

Table VI-(xii)

Variation of Scale-Length parameters (kpc) with Passband

NGC	R_0 (B)	R_0 (R)	R_0 (I)	α_c^{-1} (B)	α_c^{-1} (R)	α_c^{-1} (I)
4267	0.12	0.35	0.13	1.83	1.43	1.77
4371	0.62	0.49	0.57	2.81	2.93	4.58
4377	0.15	0.12:	-	1.14:	0.95:	-
4419	-	0.18:	0.06:	-	1.27	1.18
4429	1.79	0.86:	0.41	3.04	3.15:	5.87
4435	0.50:	0.81:	0.77:	-	-	-
4459	1.35	0.85	1.07	6.14:	4.22:	6.76:
4461	0.62:	0.86:	0.73:	-	-	-
4474	0.44:	0.52:	0.70:	-	-	-
4477	0.89	0.69	0.69	2.37	2.47	4.11
4501	1.00:	-	1.52:	2.88:	-	5.97:
4503	0.67	1.12:	0.63	3.29	3.43:	3.58
4550	-	-	-	2.76:	-	2.28:

Table VI-(xiii)

Paired-Sample Tests

Variable	Samples	Sample Size	T-statistic	R%	S-statistic	S%
R_D	B and R	9	22	> 12.9%	4	50%
R_D	B and I	8	15	> 10.9%	4	63.7%
R_D	R and I	9	11.5	> 12.9%	3	25.4%

Table VI-(xiv)

Paired-Sample Tests

Variable	Samples	Sample Size	T-statistic	R%	S-statistic	S%
α_c^{-1}	B and R	7	10	> 10.9%	3	50%
α_c^{-1}	B and I	7	4	7.8%	2	22.7%
α_c^{-1}	R and I	7	1	1.6%	1	6.2%

R% is the probability of erroneously rejecting the null hypothesis [H_0], calculated from the Wilcoxon matched-pairs signed-ranks test.

H_0: the median of the population of differences in zero.

S% is the probability of erroneously rejecting the null hypothesis [H_0], calculated from the sign test.

Table VI-(xv)

B-band Composite Data Set

Lenticular Sample

NGC	Morphological Type	B_o	R_o (kpc)	$B(o)_c$	α^{-1} (kpc)	log(D/B)	Source	Note
3115	-3	-	-	21.05	0.78	-0.52	3	
3384	-3	18.62	0.36	22.15	1.89	-0.22	1,4	
4150	-2	15.41:	0.02:	20.49	0.33	-	1	*1
4203	-3	19.06	0.16	20.97	1.10	0.30	1	
4267	-3	17.13	0.12	21.81	1.83	-0.09	5	
4270	-2	22.71	1.45	21.58	1.71	0.00	1	
4281	-1	19.93	0.64	21.15	2.68	0.20	1	
4350	-2	22.06	0.95	20.70	0.86	-0.01	1,4	
4371	-1	21.20	0.82	23.52	2.81	-0.42	5	
4377	-3	18.75	0.18	20.86	0.79	-0.24	1,5	
4429	-1	22.40	1.79	23.29	3.04	-0.46:	5	
4435	-2	19.74:	0.50:	-	-	-0.90:	5	
4459	-2	22.08	1.67	22.30	1.99	-0.63	1,5	*3
4461	-1	20.66:	0.62:	-	-	-0.30:	5	
4474	-2	20.46:	0.44:	-	-	-0.38:	5	
4477	-2	20.62	0.69	22.65	2.37	-0.30	5	
4503	-3	21.20	0.67	24.70	3.29	-0.58	5	
4526	-2	22.62	2.61	22.31	3.78	-0.15	1	
4550	-1	-	-	24.47:	2.76:	-0.77:	5	
4552	-4	20.74:	1.02:	23.84:	6.47:	-0.20:	5	*2,3
4570	-2	19.19	0.23	20.99	1.36	0.26	1	
4576	-2	21.90	0.87	22.14	1.69	-0.05	1	
4710	-1	-	-	20.61	0.99	0.08	3	
4762	-2	-	-	22.97	2.40	-0.59	3	
5866	-1	-	-	19.53	0.70	-0.68	3	

Table VI-(xv) (continued)

B-band Composite Data Set

Spiral Sample

NGC	Morphological Type	B_o	R_o (kpc)	$B(o)^c$	α^{-1} (kpc)	log(D/B)	Source	Note
488	3	20.27	0.43	21.44	3.04	0.68	2	
628	5	23.30	0.85	21.77	2.87	1.10	2	
1058	5	–	–	–	–	1.00:	2	
2268	4	21.14	0.50	21.29	2.75	0.85	2	
2336	4	19.12	0.22	22.12	6.77	1.22	2	
2344	5	23.29	0.84	22.15	1.31	0.55	2	
2655	0	21.91	1.85	22.84	4.85	-0.09	2	
2681	0	19.64	0.30	21.47	1.59	0.16	2	
2775	2	22.52	1.28	22.28	1.99	-0.09	2	
2841	3	20.35	0.48	21.51	2.75	0.50	2	
2856	0	22.60	0.84	22.91	2.70	-0.08	2	
2967	5	17.37	0.03	20.46	1.40	1.40	2	
3147	4	20.95	0.93	20.96	3.37	0.55	2	
3277	2	–	–	–	–	-0.18:	2	
3338	5	–	–	21.00:	2.58:	–	4	
3351	3	16.92	0.09	21.32	2.22	0.46	4	
3367	5	–	–	18.14:	1.61:	–	4	
3368	2	–	–	22.39:	3.70:	0.11:	2,4	*4
3389	5	–	–	19.63:	1.28:	–	4	
3623	1	–	–	20.07:	1.50:	–	4	
3627	3	22.42	1.61	21.00	2.09	0.16	4	
3642	4	–	–	–	–	0.80:	2	
3898	2	21.12	0.86	23.37	3.91	-0.14	2	
4244	6	–	–	22.43	1.81	1.52	3	
4501	3	21.75:	1.00:	21.58:	2.88:	0.43:	5	
4594	1	–	–	21.18:	2.35:	-0.57:	3	*5
4725	2	–	–	–	–	0.64:	2	
4736	2	–	–	–	–	0.55:	2	
4941	2	–	–	–	–	1.10:	2	
5194	4	–	–	–	–	2.00:	2	
6340	0	22.82	2.22	21.93	2.99	0.06	2	
7217	2	–	–	–	–	0.41:	2	
7331	4	21.44	1.41	22.79	4.76	-0.04	2	

Source: 1 : Burstein [1979 b]
2 : Boroson [1981]
3 : Hamabe [1982]
4 : Devenhall [1984]
5 : This work

Note: *1 - Bulge parameters uncertain, Burstein [1978] gives no D/B estimate.
*2 - Morphological classification uncertain.
*3 - Morphological classification from Chapter IV
*4 - Disk parameters from Devenhall [1984], D/B estimate from Boroson [1981].
*5 - Disk may be contaminated by Bulge Light.

Table VI-[xvi]

I-Band Composite Data Set

Lenticular Sample

GALAXY	Morphological Type	$I(o)_c$	α^{-1} [kpc]	Source	Note
IC 3260	-2	20.58	0.83	1	
NGC 4259	-2	18.57	1.81	1	
NGC 4267	-3	19.49	1.67	1,2	
NGC 4371	-1	22.10	4.58	2	
NGC 4419	-2	18.86	1.22	1,2	*1
NGC 4429	-1	21.80	5.92	1,2	
NGC 4435	-2	18.45	1.20	1	
NGC 4442	-2	19.64	1.93	1	
NGC 4451	-2	19.99	0.71	1	
NGC 4459	-2	19.12	2.11	1	*1
NGC 4461	-1	19.21	1.54	1	
NGC 4474	-2	18.62	0.87	1	
NGC 4503	-3	22.48	3.58	2	
NGC 4694	-2	20.24	1.93	1	
NGC 4754	-3	20.76	3.26	1	

Source: 1 : Boroson et al [1983 b]

2 : This work.

*1 - morphological classification from Chapter IV.

Table VI-(xvi) (continued)

I-Band Composite Data Set

Spiral Sample

GALAXY	Morphological Type	$I(o)_c$	α^{-1} (kpc)	Source
IC 3267	6	20.15	1.01	1
IC 3322 a	6	20.88	1.75	1
IC 3322	6	21.03	1.49	1
IC 3392	3	19.18	1.11	1
NGC 4189	6	19.61	1.92	1
NGC 4192	2	18.99	1.84	1
NGC 4193	5	19.01	0.96	1
NGC 4206	4	20.77	2.11	1
NGC 4212	4	18.62	1.37	1
NGC 4254	5	18.03	1.71	1
NGC 4298	5	18.87	1.47	1
NGC 4304	3	20.36	1.37	1
NGC 4307	3	19.70	1.51	1
NGC 4312	2	19.61	1.68	1
NGC 4321	4	19.35	3.95	1
NGC 4343	3	19.83	1.12	1
NGC 4380	3	19.99	2.04	1
NGC 4383	1	19.56	1.01	1
NGC 4384	1	19.18	2.15	1
NGC 4390	4	20.01	1.05	1
NGC 4396	7	20.58	1.51	1
NGC 4405	0	18.57	0.80	1
NGC 4411 b	8	20.56	1.67	1
NGC 4413	3	19.23	1.01	1
NGC 4424	1	21.03	2.85	1
NGC 4445	2	19.94	1.17	1
NGC 4450	2	19.67	2.95	1
NGC 4469	0	18.81	1.47	1
NGC 4579	3	18.88	2.93	1
NGC 4606	1	19.85	1.77	1
NGC 4607	3	20.42	1.47	1
NGC 4746	3	19.29	0.93	1

Table VI-(xvii)

Correlation Tests

Variables	Spearman's Rho	Z	R%	R(T)%
R_o and Type	0.047	0.262	79%	84%
B_o and Type	0.194	1.080	28%	29%
B_o and R_o	0.850	4.733	< 0.1%	< 0.1%

Table VI - (xviii)

Correlation Tests

Variables	Spearman's Rho	Z	R%	R(T)%
$B(o)_c$ and Type	0.025	0.152	87%	94%
α^{-1} and Type	0.385	2.342	< 2%	< 2%

Table VI-(xix)

Correlation Test

Variables	Spearman's Rho	Z	R%
B(o)c and α^{-1}	0.628	3.820	< 0.2%

R% is the probability of erroneously rejecting the null hypothesis (H_o).

H_o : the variables are independant.

R(T)% is the probability of erroneously rejecting H_o after the tie-correction procedure suggested by Daniel (1978 a) has been applied.

Table VI-(xx)

Two-Sample Tests

Lenticular Sample Seize (n_1)	Spiral Sample Size (n_2)	Variable	U-statistic	R%
20	18	$B(o)_c$	196.5	> 20%
20	18	α^{-1}	270	< 1%

R% is the probability of erroneously rejecting the null hypothesis (H_o)

H_o : the samples are drawn from the same population.

Table VI-(xxi)

Least-Square Fits: $B(o)_c = m\alpha_c^{-1} + c$

	M	C
Lenticular Disks	1.05 (± 0.17)	19.88 (± 0.34)
Spiral Disks	0.24 (± 0.12)	21.20 (± 0.40)

Uncertainties shown are standard errors.

Table VI-(xxii)

Correlation Tests

Variables	Sample Size	Spearman's Rho	Z	R%	R(T)%
log (D/B) and Type	31	0.710	3.889	< 0.1%	< 0.1%
log (D/B) and Type	51	0.756	5.346	< 0.1%	< 0.1%

R% is the probability of erroneously rejecting the null hypothesis (H_o)

H_o : the variables are independant.

R(T)% is the probability of erroneously rejecting H_o after the tie-correction procedure suggested by Daniel (1978 a) has been applied.

Table VI-(xxiii)

Two-Sample Tests

Lenticular Sample Size	Sprial Sample Size	Variable	U-statistic	Z	R%
17	14	log (D/B)	40	-	< 0.2%
28	23	log (D/B)	58	4.998	< 0.2%

R% is the probability of erroneously rejecting H_o.

H_o : the samples are drawn from the same population.

Table VI-(xxiv)

Correlation Tests

Variables	Spearman's Rho	Z	R%	R(T)%
$I(o)_c$ and Type	0.068	0.461	64.5%	68.4%
α^{-1} and Type	-0.117	-0.793	42.8%	38.9%
$I(o)_c$ and α^{-1}	0.310	2.102	3.6%	3.6%

R% is the chance of erroneously rejecting the null hypothesis (H_o)

H_o : the variables are independant.

R(T)% is the chance of erroneously rejecting H_o after the tie-correction procedure suggested by Daniel (1978 b) has been applied.

Table VI-[xxv]

Two-Sample Tests

Lenticular Sample Size	Spiral Sample Size	Variable	U-statistic	Z	R%
15	32	$I[o]_c$	253	0.297	76.6%
15	32	α_c^{-1}	284	1.004	31.5%

Table VI-[xxvi]

Two-Sample Tests

B-band Sample Size	I-band Sample Size	Variable	U-statistic	R% (tables)	Z	R%
20	15	Lenticular scale-length	165	> 20%	0.500	61.7%
18	32	Spiral scale-length	100	-	-3.789	< 0.2%

R% is the probability of erroneously rejecting the null hypothesis [H_o]

H_o : the samples are drawn from the same population.

Figure VI.1

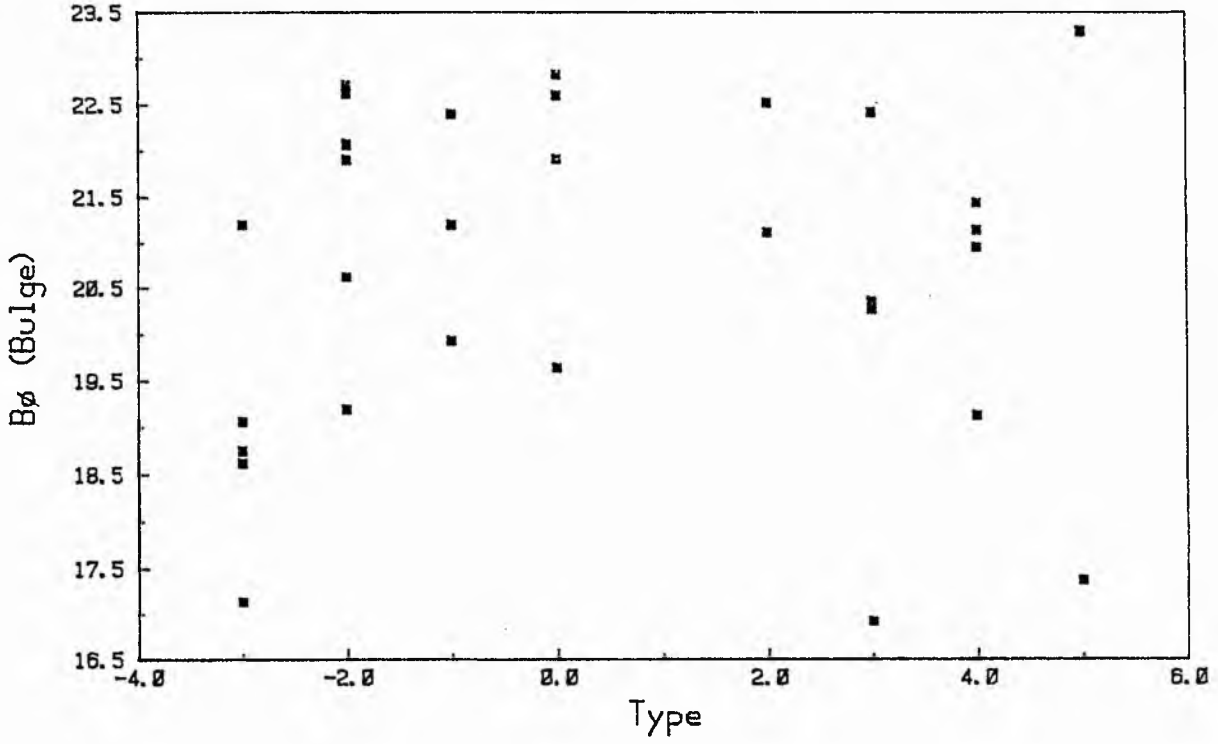

Figure VI.2

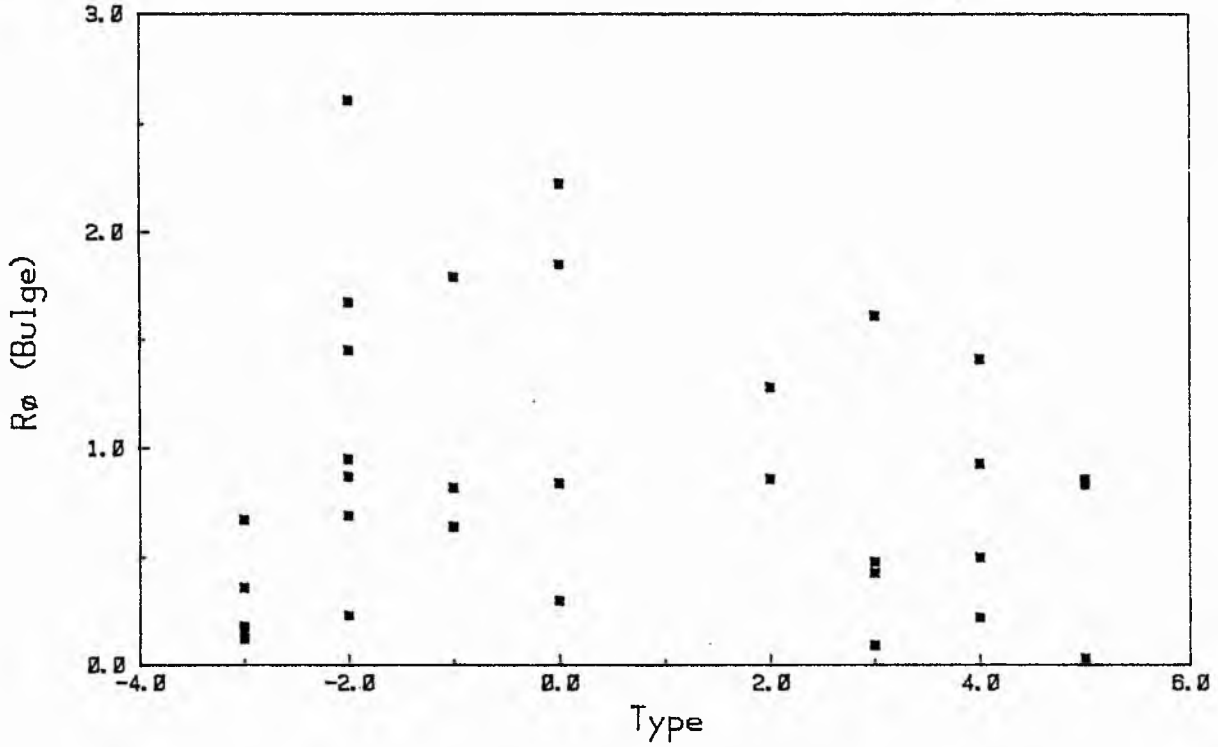

Figure VI.3

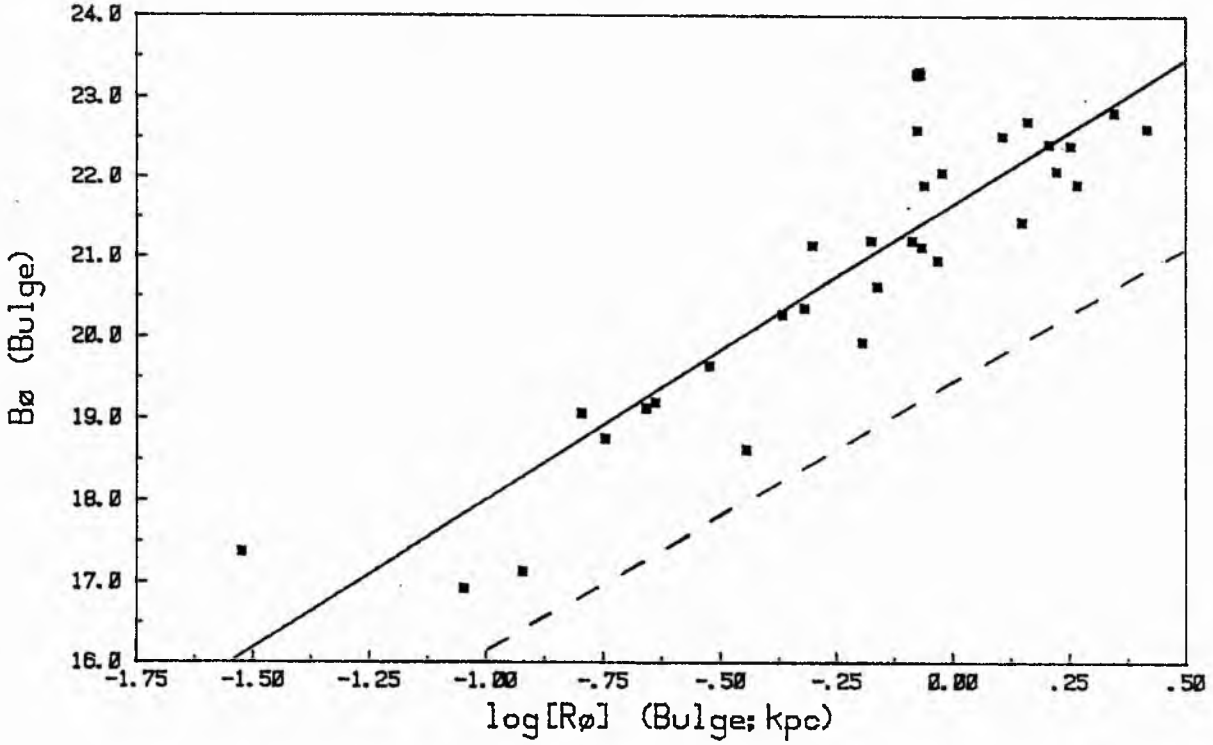

Figure VI.4

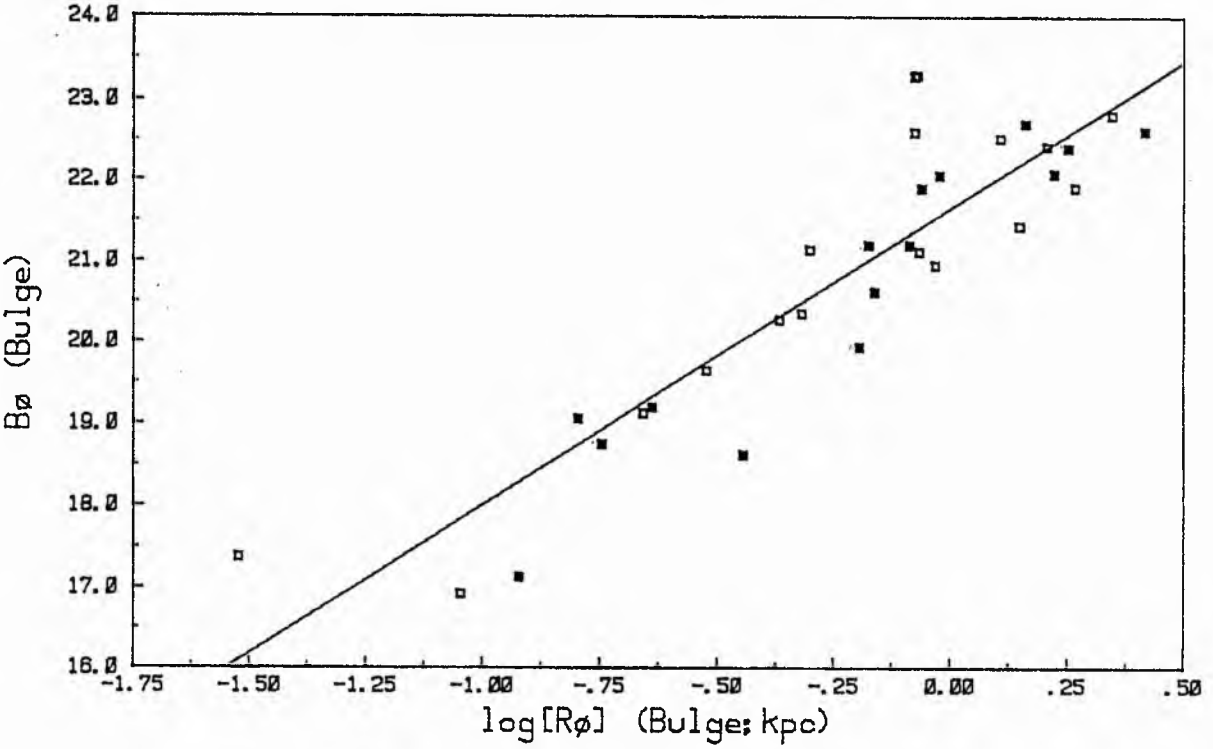

Figure VI.5

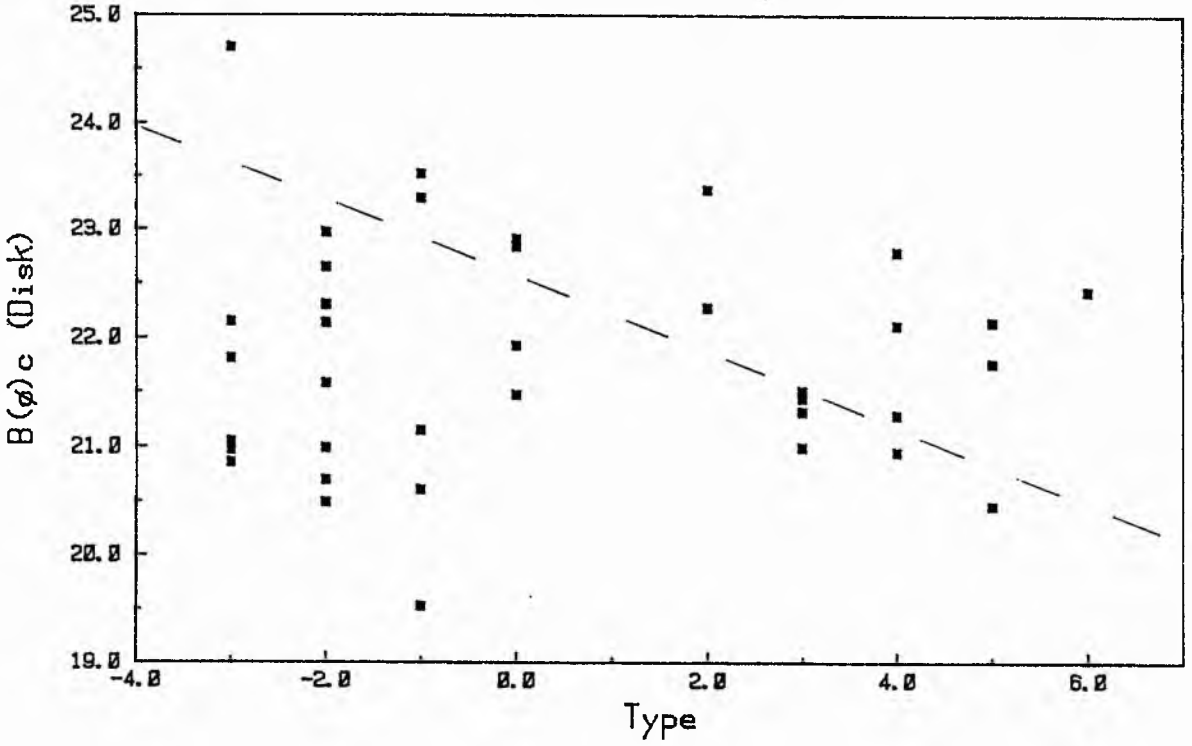

Figure VI.6

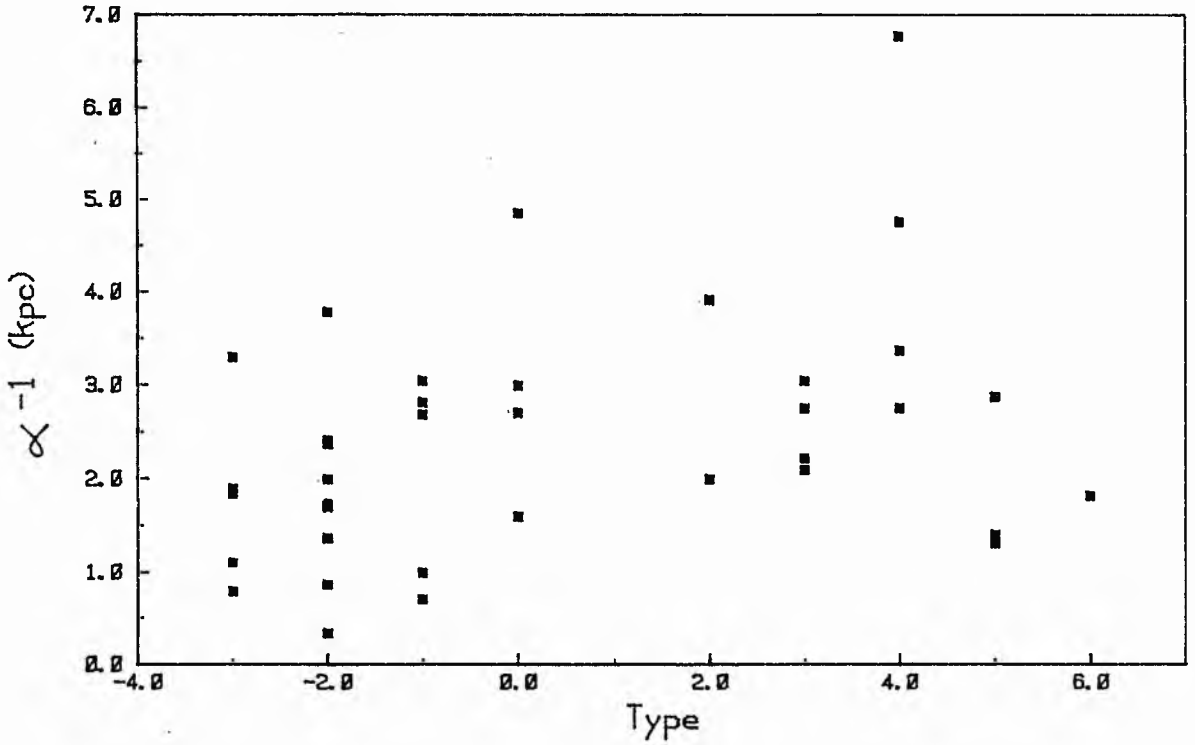

Figure VI.7

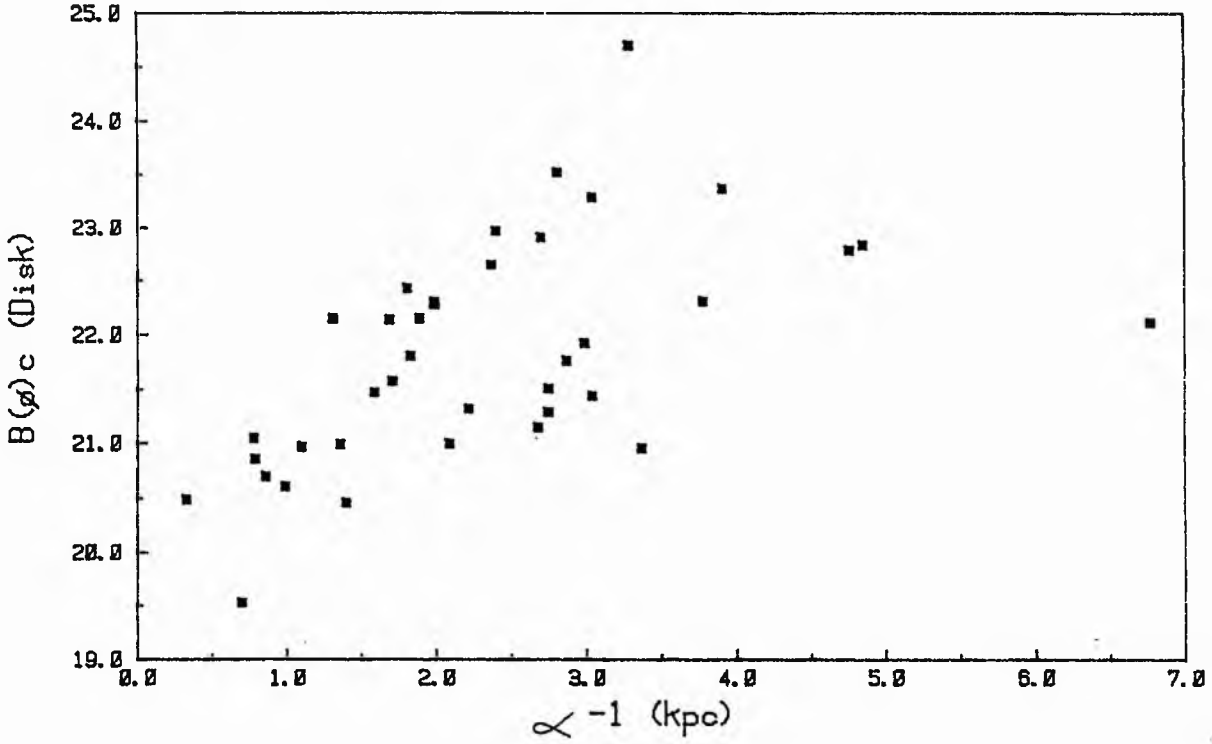

Figure VI.8

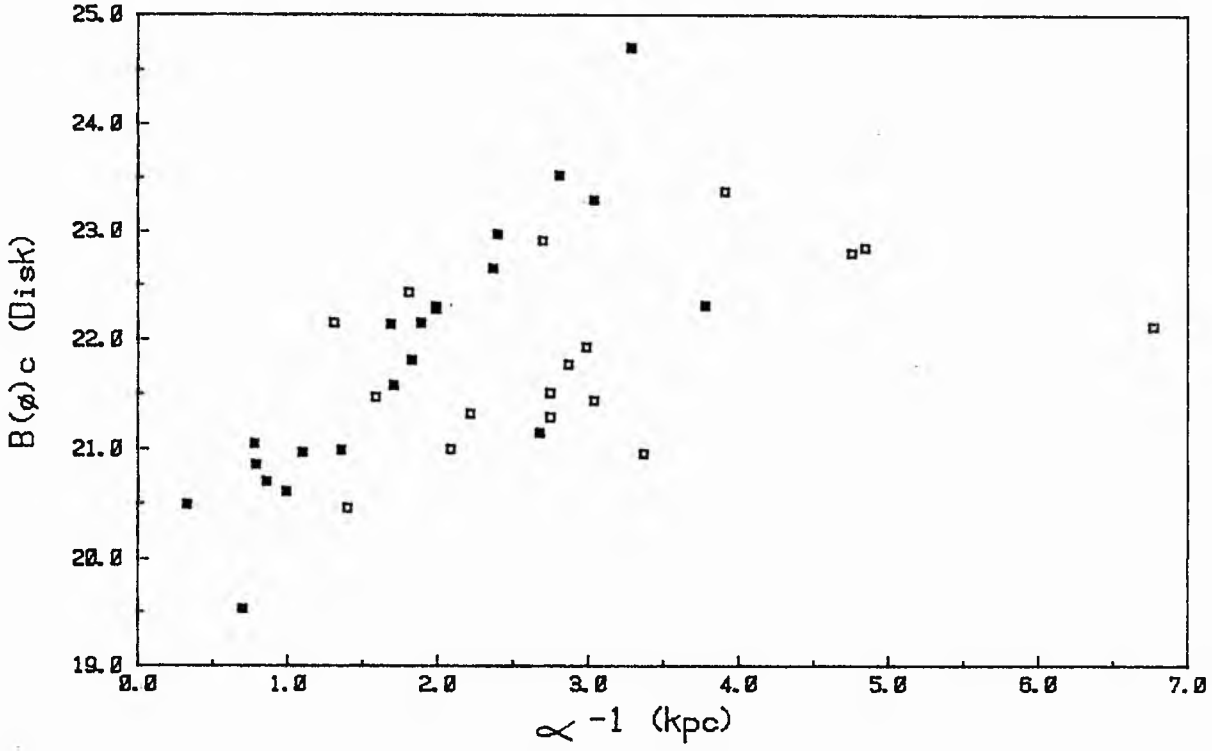

Figure VI.9

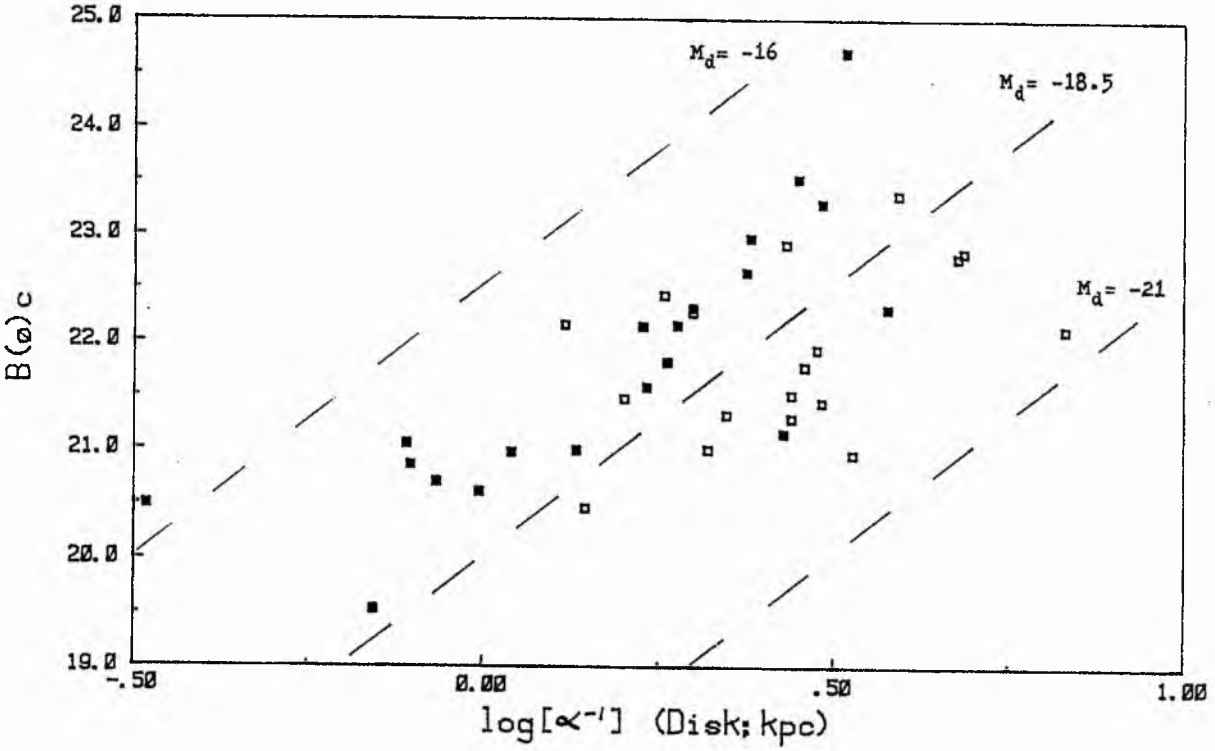

Figure VI.10

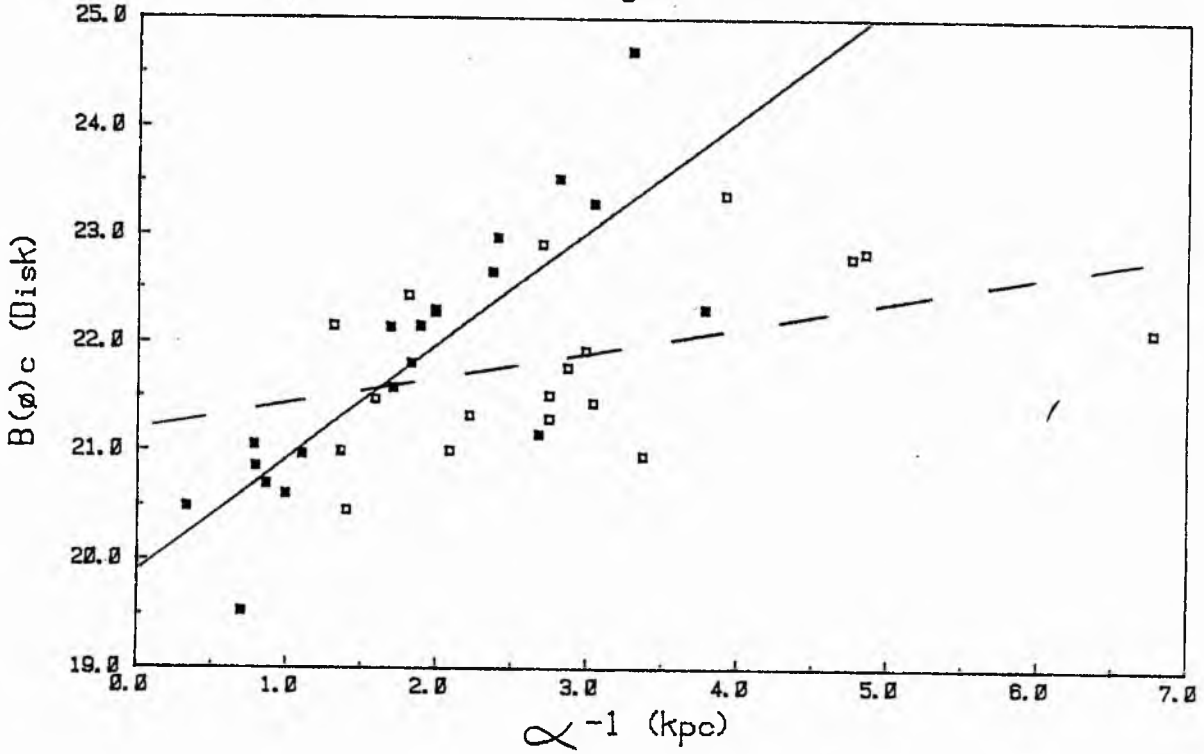

Figure VI.11

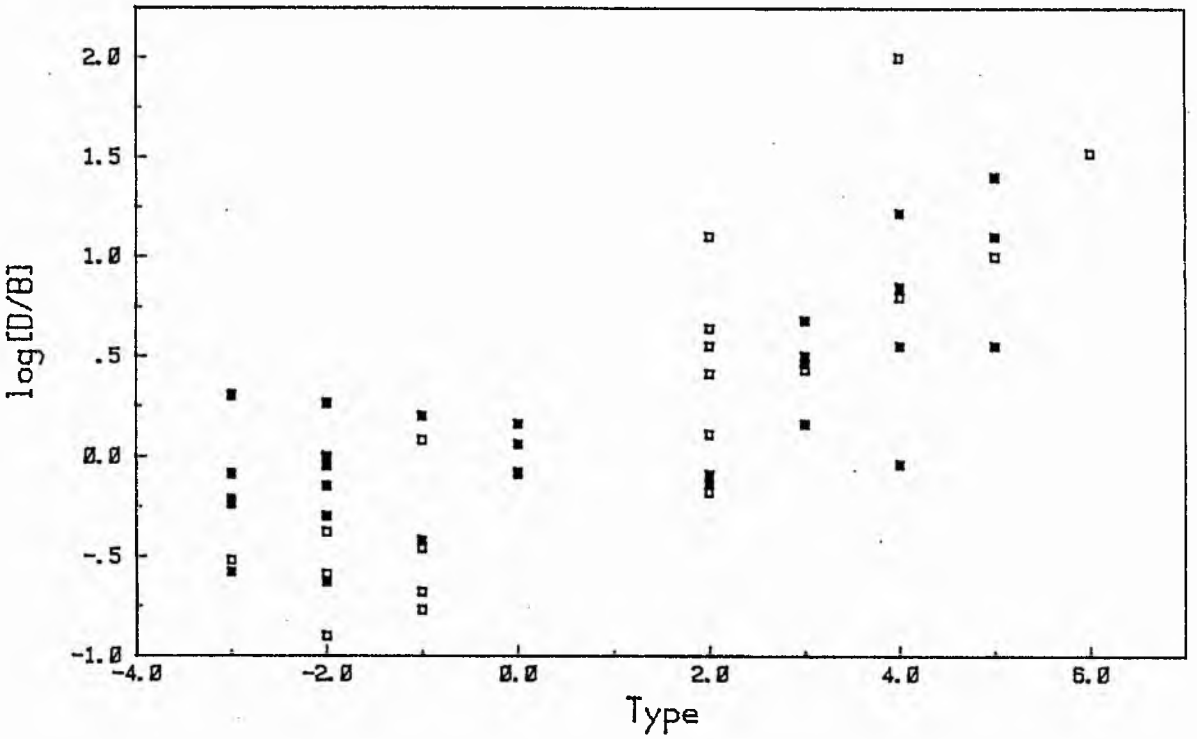

Figure VI.12

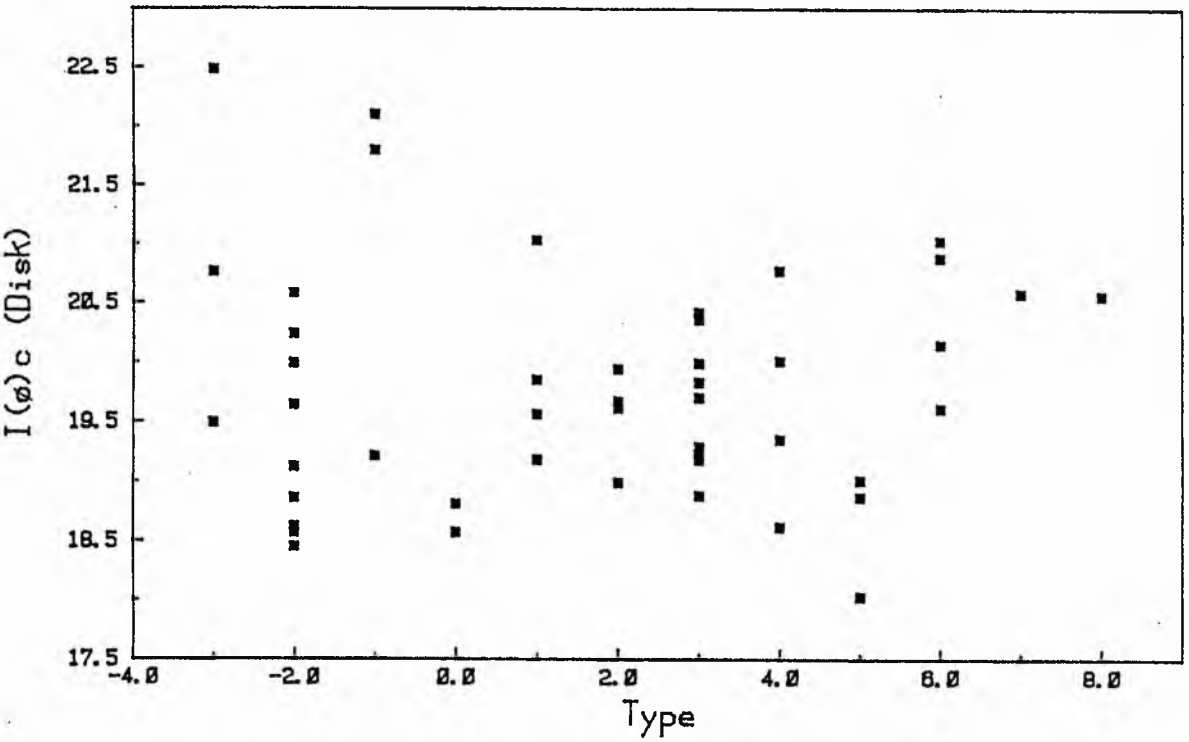

Figure VI.13

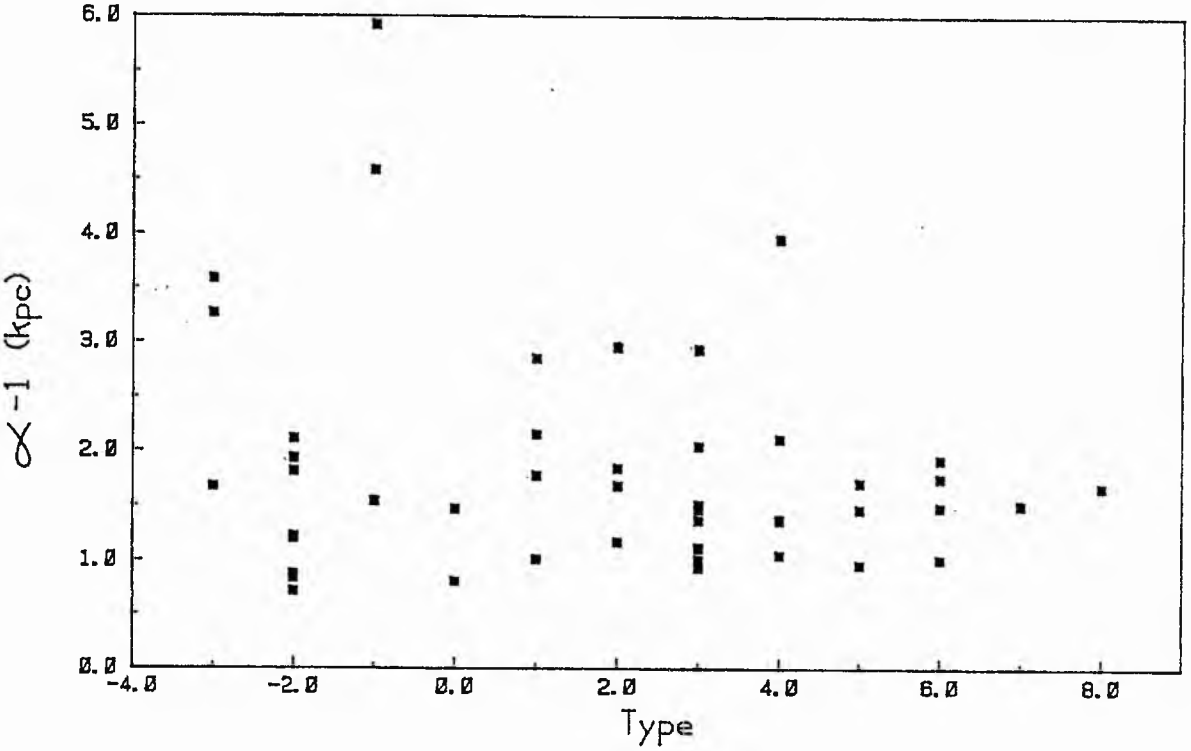

Figure VI.14

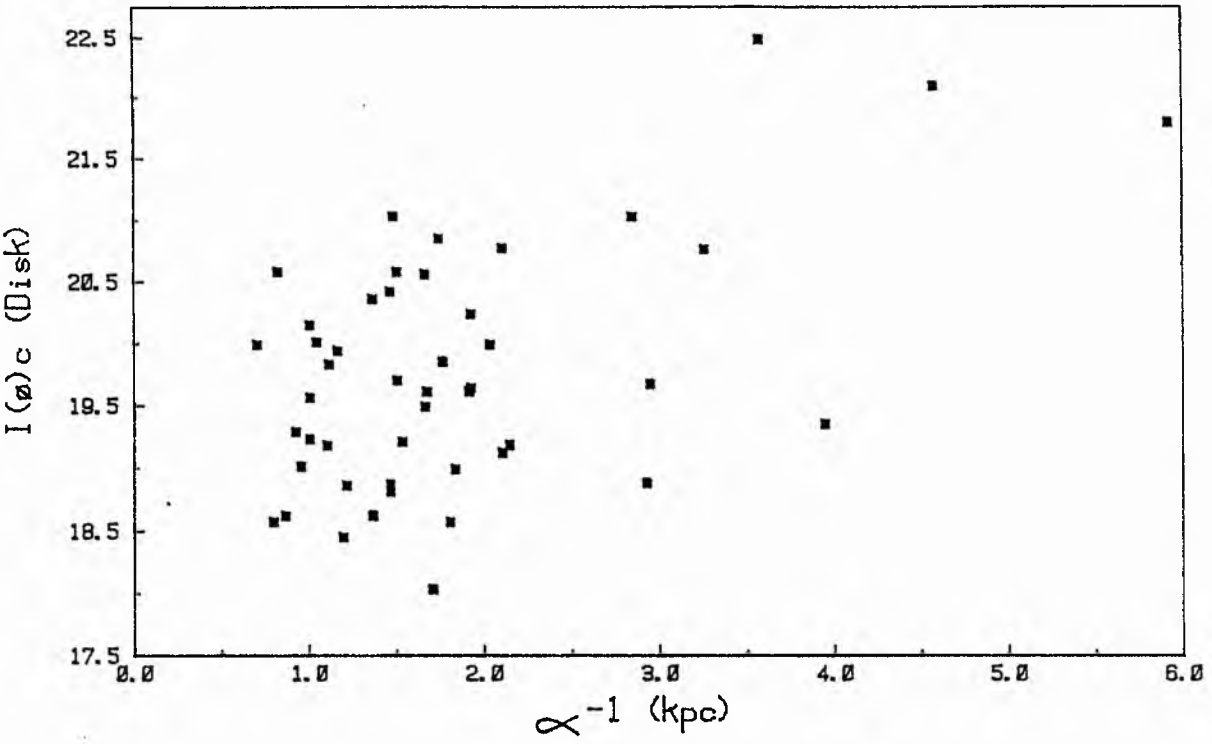

Figure VI.15

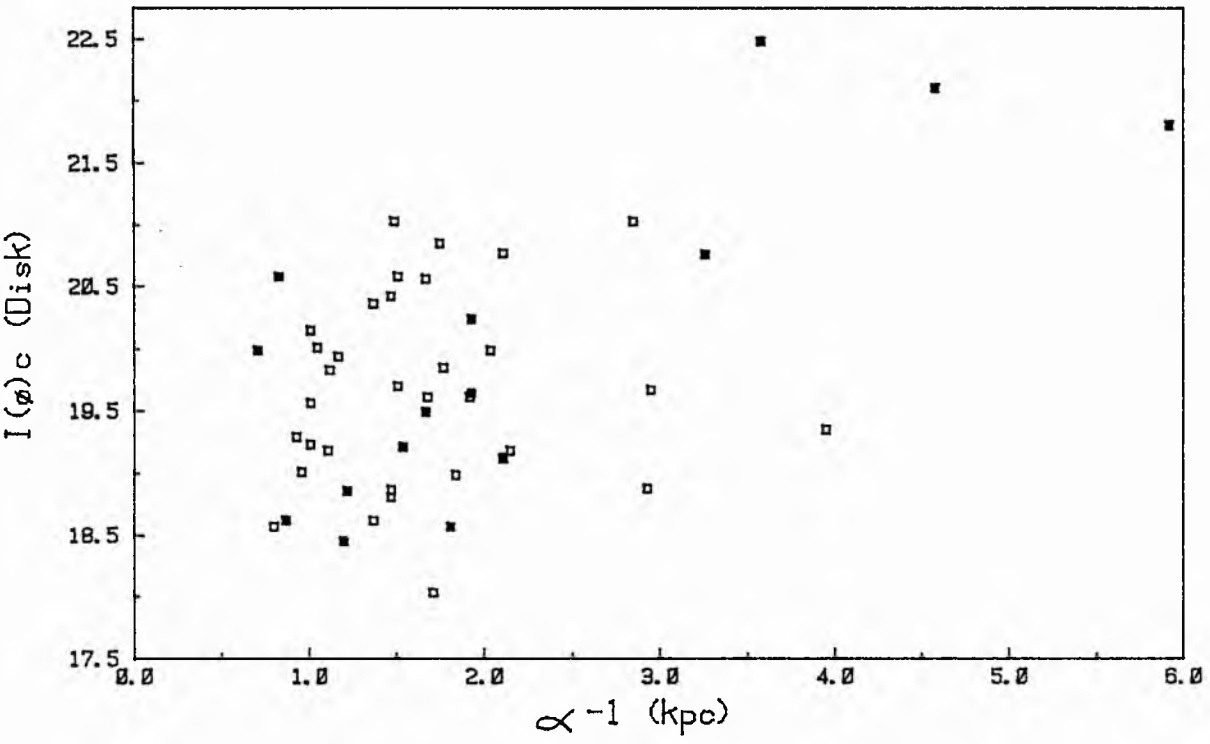

Figure VI.16

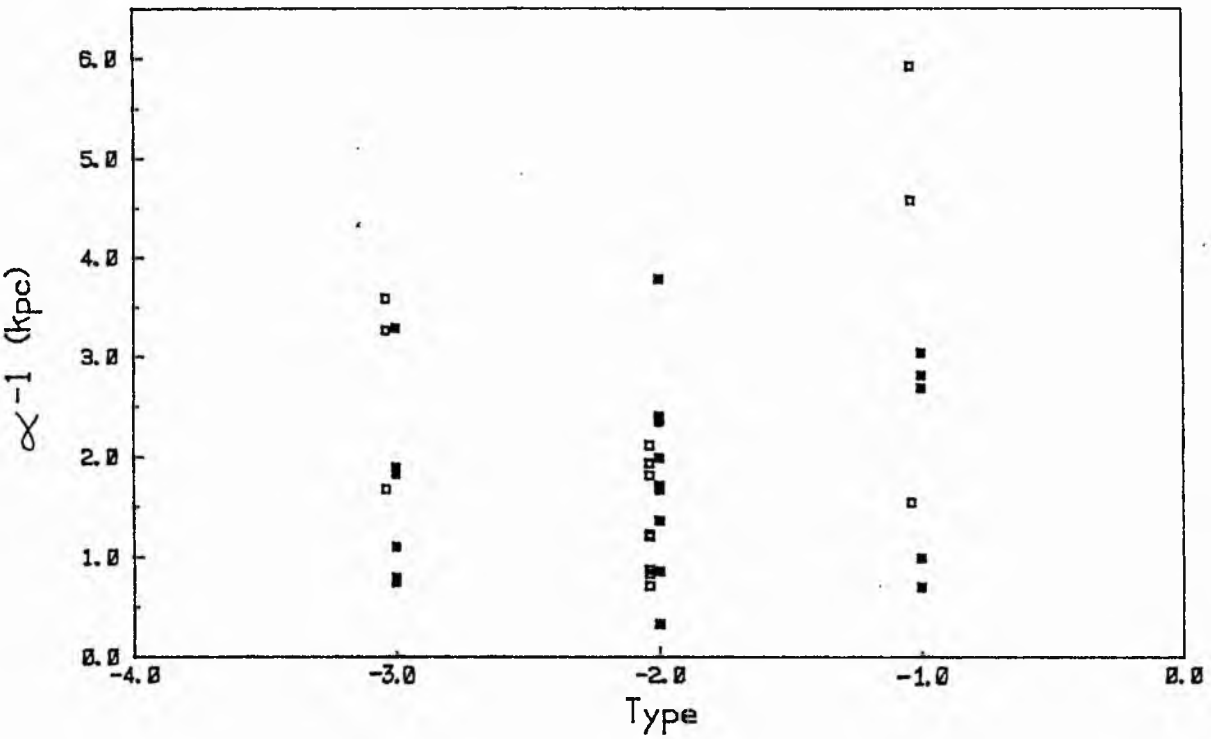

Figure VI.17

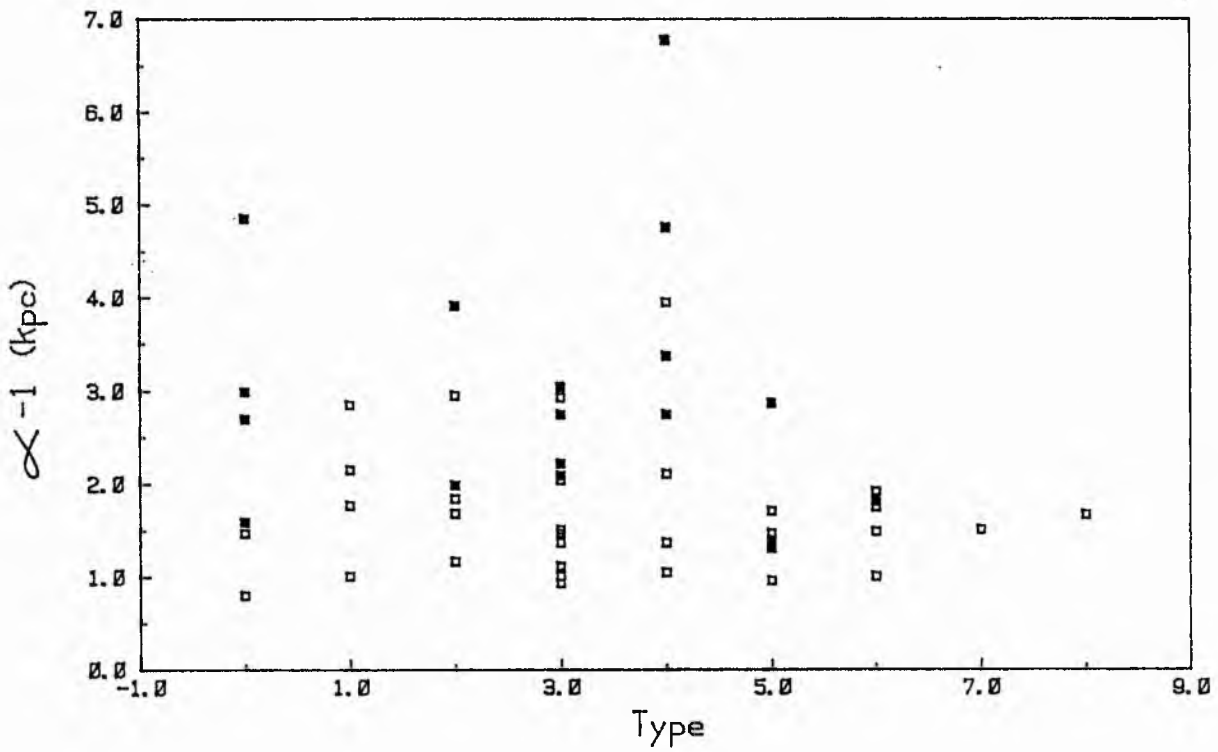

CHAPTER VII: Conclusions and Future Work

This chapter will review the results produced in this survey of the lenticular systems in the Virgo cluster core, and discuss the implications these observations have for theories of the formation and evolution of disk galaxies.

VII-1: Implications of the Results Produced in this Thesis.

In Chapter IV the B, R and I-band luminosity profiles of the programme galaxies were examined in detail, together with the colour-difference profiles produced from this data. The majority of the luminosity profiles presented show evidence for some structure in the disk component, a result in good agreement with Burstein (1978) who reported that a surprisingly large fraction of his sample of lenticular galaxies (which was biassed towards simple (unbarred) systems) displayed unexpected disk features.

The colour-difference profiles generally show distinct colour gradients in the inner regions of the programme galaxies, which may be indicative of an inward metallicity gradient in the bulge component. In many cases the bulge component also appears reddened with respect to the disk, which is most easily attributable to the effects of dust (e.g. NGC 4501) but could signify differences between the bulge and disk stellar populations. The populations could differ in age, metallicity or in the IMF of star-formation. The majority of the observed colour gradients are most noticeable in the (B-R) and (R-I)

profiles, and as the R-band photometry presented in this work cannot yet be verified by comparison with independent data, these results must be regarded with appropriate reservation.

Nevertheless, several galaxies show significant (B-I) colour gradients which are much larger than might be anticipated for lenticular systems supposedly dominated by an old (red) stellar component. These gradients are almost certainly genuine since both the B and I-band data has been verified by comparison with independent photometry. It is interesting that the two galaxies with the most pronounced (B-I) gradients, NGC 4267 and 4459, have similar morphology, with virtually featureless bulge and disk components. The unusual inward blue gradients may indicate recent episodes of star-formation in the inner regions of these systems, possibly triggered by environmental interactions (e.g. shock-induced star-formation via ICM-interaction with residual bulge gas).

The analysis of the luminosity and colour-difference profiles presented in Chapter IV suggests that nearly all the lenticular galaxies studied had disk structure or unusual features of some sort. Excluding two objects with uncertain morphological classification (NGC 4531 and 4552), the peculiar object NGC 4438, and the spiral system NGC 4501, thirteen lenticular systems were examined in this survey. Six galaxies: NGC 4377, 4419, 4425, 4429 (smooth spiral arms), 4461 and 4503 appear to have some vestigial disk structure associated with features in the colour-difference profiles, and two galaxies: NGC 4267 and 4459 have the unusual inward blue colour gradients already described,

which cannot be associated with structure in the luminosity profiles. Of the remaining five systems, four galaxies: NGC 4371, 4435, 4474 and 4477 have bar components, and only NGC 4550 appears to be a "normal" lenticular with a relatively uncomplicated structure. (However, the colour-difference profiles of NGC 4550 do show evidence for a population or content discontinuity between the bulge and disk components). Since it is essentially a universal belief that the dominant constituent of lenticular galaxies is an old (red) stellar component, the conclusion that many lenticular disks displayed more prominent structure in previous aeons seems almost inescapable. The alternate hypotheses, such as stochastic star-formation (in an otherwise featureless disk) driven by a variety of mechanisms or a substantial modification of the parameters of star-formation, seem much less attractive. Several pieces of circumstantial evidence may be advanced to support the idea that some lenticular disks had pronounced structure in previous epochs, and appeared similar to presently-observed spiral systems.

Firstly, of the six systems with vestigial disk structure detected in this survey, two show spiral-like distortions (NGC 4425 and 4461), and one displays unequivocal spiral structure (NGC 4429). Burstein (1978) reports a comparable detection frequency, with five out of sixteen "normal" lenticulars studied showing spiral-type distortions of the disk luminosity structure. (Note that one galaxy, NGC 4429, is detected by both investigations).

Secondly, the two systems with the most prominent vestigial spiral structure: NGC 4429 (this work) and NGC 4526 (Burstein (1978)), have spiral structure which is most pronounced at wavelengths redder than the B-band. This is in contrast to the typical structure observed in spiral galaxies, and implies that the spiral population in these lenticular galaxies is significantly evolved. The observation of the smooth red spiral arms of NGC 4429 and the tightly-wound spiral arms of NGC 4526 strongly suggests that some lenticular systems must have looked like spiral galaxies at some time in their history.

Thirdly, it is noticeable that all the barred lenticular systems observed in this survey have very little evidence for disk structure other than the bar, although several of the systems show interesting features in their colour-difference profiles. Theoretical models of galaxies demonstrate that bars can form easily during galaxy formation (e.g. Ostriker and Peebles (1973)) and are dynamically very robust structures; bars are also invoked as the driving force behind the evolution of numerous classes of disk structure (see e.g. Kormendy (1982) for a comprehensive review). Once a disk becomes gas-poor (for whatever reason) the bar will cease to drive the formation of structure (such as rings or spiral arms) due to a lack of gaseous "fuel", but will remain the dominant dynamical entity in the disk. Clearly, if the bar is as efficient at driving the evolution of secular disk structure as various proponents claim, it seems quite plausible that it should have a similar capability for destruction once star-forming activity dies out. The bar itself should prove dynamically very durable, and might be

expected to survive the destruction of lesser structure in the disk. (One may note that the bar of NGC 4371 becomes increasingly significant at redder wavelengths (Chapter VI), indicating considerable age). In this way the observed morphology of barred lenticular systems may be produced by the dynamical dissolution of structure in a barred spiral galaxy once star-formation has ceased.

In Chapter V and VI the structure of the programme galaxies was investigated from analysis of the equivalent luminosity profiles produced in this work. The results produced in Chapter V reveal considerable scatter in the concentration indices calulated and no significant correlation of the index (colour) ratios with morphological type. Comparison of the calculated C_{21} concentration indices by both graphical and statistical analysis indicates that the bulges of lenticular systems are similarly concentrated at B and I-band wavelengths, but were slightly more diffuse in the R-band. This observation could support the hypothesis of an R-band 'dip' caused by metallicity effects in the bulge, which was discussed in Chapter IV. The similarity of lenticular bulges at B, R and I wavelengths is confirmed by the statistical analysis of the decomposed bulge parameters presented in Chapter VI-3.1 and these results support the view that lenticular bulges are completely dominated by an old (red) stellar component. Comparison of the calculated C_{32} concentration indices by both graphical and statistical analysis suggests that the disks of lenticular systems are very similar at B and R wavelengths, but may be slightly more diffuse in the I-band. The last result is rather marginal and may be due to

sky contamination at very low light levels in some of the equivalent profiles (see Chapter VI-2). This result needs to be confirmed by independent analysis of a larger galaxy sample, but might be caused by inner disk structure (and excess luminosity) at wavelengths bluer than the I-band. This could be interpreted as structure which is younger than the underlying I-band 'old' disk, and more detailed observations might lead to estimates of the time interval between the original disk formation and the subsequent formation of structure in the disk.

It is clear that the results produced in Chapters IV, V, VI-2 and VI-3.2 are consistent with the conclusions reached from the statistical analysis of the homogeneous data sets discussed in Chapter VI-3.3; namely, that at least some lenticular and spiral systems originated from a common population of disk galaxies.

The resurrection of this hypothesis from the disfavour in which it has languished for the past few years may be the fundamental contribution of this thesis. It is of paramount importance that this conclusion be verified by further work, and this topic is addressed in the next section.

The hypothesis of a common origin of disk galaxies has been discussed in some detail in Chapter VI-3.4, and since it has now been shown to be harmonious with the balance of the results produced in this work it can now be developed further.

It is widely accepted that the observed variation in disk parameters, particularly $B(o)_c$ and $I(o)_c$, implies a considerable

diversity of initial dynamical conditions during the time of formation. Furthermore, if disk systems share a common origin (i.e. no fundamental initial differences between currently-observed spiral and lenticular galaxies), then the simplest explanation of the observed morphological segregation is that the internal gas-removal mechanisms produced lenticular galaxies, as no external agency need be invoked. These concepts suggest that either disk systems formed at a variety of redshifts or with heterogeneous local environments. In the former case, presently-observed lenticulars are identified as the now-aged early generations of disk systems, while spiral galaxies are their more youthful counterparts. In the latter case, the formation environment of a galaxy might profoundly influence the initial-mass-function and rate of star-formation in the disk component without producing significant effects on the size of the bulge or disk components. Some disks might then evolve much more rapidly than others, producing the observed differences between lenticular and spiral galaxies.

Alternatively, external interactions at later epochs in the evolution of disk systems could randomly affect the disks of some galaxies to remove the gas content and curtail star-formation; the lenticular population is then produced by the subsequent ageing of the 'victim' galaxies. Clearly the environmental mechanisms are now constrained (by the results of Chapter VI) to leave the bulge and 'old' disk components of the 'victim' unperturbed. This limitation is probably fatal for the more severe dynamical interactions discussed in Chapter I, but leaves numerous other viable candidates, such as galaxy-ICM

interactions. If clusters without a significant ICM can be shown to have a population of lenticular systems essentially indistinguishable from those in clusters with an ICM, then these mechanisms may also be embarrassed. In this eventuality, which seems quite feasible, the majority of 'external' modification processes would seem unlikely candidates in the search for the dominant agent responsible for the production of the lenticular systems currently observed.

Many questions remain to be answered before a coherent theory of galaxy formation and evolution may be isolated from its competitors; at this stage in the investigation it is not possible to prefer either of the two most attractive alternatives: the formation of disk galaxies at a variety of epochs or with a miscellany of formation conditions. One might flourish Occam's Razor (a dangerous weapon which has been said to make a virtue out of ignorance) and prefer the former alternative, which requires the simplest assumptions, but such an argument is regarded as too presumptive by the author. The most conclusive statements that can be made at this juncture are that the primary objections to the production of lenticular galaxies from spiral progenitors appear to have been discredited, together with several intrinsic-formation theories, and the hypothesis of the common origin of disk systems is strongly supported by the results and analysis presented in this survey.

VII-2: Future Work

In this section useful extensions of the work produced in this survey will be discussed, together with the important observational predictions of the hypothesis that lenticular and spiral galaxies shared a common origin.

First of all, the results obtained in this survey could be improved by the acquisition of multi-aperture photometry of all the programme galaxies. As mentioned in Chapter II, the dearth of published multi-aperture photometry is a crucial hindrance to all investigations utilizing the technique of photographic surface photometry, and a comprehensive programme of observations is really needed for all galaxies listed by de Vaucouleurs et al. (1976). This would be a substantial undertaking for any observatory and should ideally be a goal adopted by one of the U.K. national facilities. The acquisition of appropriate data for NGC 4267, 4371, 4377, 4419, 4425, 4474, 4503, 4531 and 4550 would allow the calculation of individual R and I-band sky values for those intensity frames for which average sky background values had to be adopted in this work. This would substantially reduce uncertainty in the absolute calibration of the corresponding luminosity and colour-difference profiles which is inherent in the results presented for these systems.

Secondly, the acquisition of independent R-band photometry for some of the programme galaxies would allow the verification of the R-band data presented in this work. This could be achieved by the analysis of a more modern R-band UKSTU plate of the Virgo

cluster 'core', or the acquisition of R-band major-axis profiles using scanning-CCD techniques (e.g. Boroson et al. (1983 a)). The latter technique could obviate the need for multi-aperture calibration photometry and would produce useful data with much greater facility than conventional photographic techniques.

Thirdly, the work presented in this survey must be extended to encompass a larger number of galaxies, allowing the production of larger homogeneous data sets and more powerful statistical investigation of the results suggested by this work. The spiral galaxy B-band data is predominantly drawn from one source (Boroson (1981)), and independent work would be particularly valuable in lessening the statistical dependence on this source, which could be affected by unknown systematic errors. Scanning-CCD techniques would seem a particularly powerful tool for this kind of investigation. The most important target for such investigations would be the acquisition of I-band bulge parameters for a large sample of spiral systems (e.g. the Virgo cluster sample of Boroson et al. (1983 b)). The data should be able to investigate the expected similarlity of lenticular and spiral bulges in the I-band. The subsequent calculation of I-band Disk:Bulge luminosity ratios for spiral galaxies will prove an important test of the hypothesis developed in this work. The results presented in this thesis suggest that the B-band spiral disks are brighter than those of lenticular systems, but no such segregation is apparent at I-band wavelengths. If the bulges of spiral and lenticular systems are essentially indistinguishable then spiral I-band Disk:Bulge ratios should be similar to lenticular Disk:Bulge ratios (i.e. less than their

B-band values). It is significant that this trend is clearly visible in the results obtained for the only spiral galaxy studied in this work (NGC 4501). Clearly a result based on only one system must be confirmed by further investigation, particularly since the analysis of this system is complicated by a third luminosity component, but it is encouraging that the result obtained for this system is consistent with the expected trend.

Lastly, this survey has revealed unusual features in the luminosity and colour-difference profiles of many of the programme galaxies, and these systems should be the subject of further intensive study. The following discussion will both supplement and recapitulate some of the recommendations already made in Chapters IV and VI.

(1) The unusual disk structure observed in NGC 4377, 4419, 4425, 4429, 4461 and 4503 should be investigated by generating colour-difference maps of the galaxy images. Experiments with photographic data have indicated that data of higher precision is needed to generate meaningful maps, but CCD-techniques could yield valuable information about vestigial structure in the disks of lenticular galaxies, and might be particularly effective in clarifying the spiral-type distortions frequently observed in lenticular systems.

(2) Those systems with unsatisfactory or unrealistic decomposed solutions of the equivalent profiles (see Chapter VI-2)

should be re-investigated to provided additional data on the lenticular population in the Virgo cluster 'core'. Once again, the scanning-CCD technique is likely to be the most powerful investigative tool available. It is particularly important to ascertain if the apparent low light-level discrepancies (see Chapter VI-2) between some I-band equivalent and major-axis profiles are real, or whether the suspect equivalent profiles accurately represent the faint-light distribution of each galaxy.

(3) The unusual blue gradients of NGC 4267 and 4459 should be investigated further, particularly with spectroscopic techniques, to confirm the hypothesis that recent episodes of star-formation may have taken place. Theoretical investigations following the approach of Bothun (1982) might usefully explore the suggestion that the observed gradients may be the signature of recent environmental interactions.

(4) The peculiar galaxy NGC 4438 appears to be a clear example of the ongoing environmental modification of a galaxy by ICM-interaction. Further work should investigate the suggestion that there has been a recent episode of vigorous star-formation in the inner regions of this galaxy, and should also consider what future course the evolution of NGC 4438 will follow (i.e. if there are no future interactions, what will the system look like in 10^9 years ?).

(5) Further efforts should be made to determine the morphological status of NGC 4531 and 4552. If the former is an early-type system, then it is a member of the long-sought disk-dominated lenticular galaxy population, as a lower-limit of the R-band log(Disk/Bulge) ratio has been estimated as 0.1 (Chapter VI-2.4). If the latter is a lenticular system, then the classification of several other Virgo ellipticals may be similarly questioned. Indeed, the misclassification of elliptical and lenticular systems (particularly S0/a galaxies) may be quite widespread. On the other hand, if NGC 4552 is a tidally-distorted elliptical system, the exponential distribution of the excess luminosity at large radii may place useful constraints on models of tidal interactions.

Author's Note: February, 1986

During the latter stages of the typing of this thesis, the paper of Kent (1985) became available for the author's inspection. The results presented by Kent (1985) are considered important enough to warrant discussion, even at this late stage in the presentation of this thesis.

Kent (1985) presents profile decompositions for galaxies of all morphological types, utilizing some of the R-band CCD-photometry previously published in Kent (1984). As admitted by Kent (1984), the photometric system employed is non-standard, and the transformation to the Johnson system is not well-defined. Kent (1984) adopted selection criteria which obviated any possible comparison with the photometry produced in this work, as he avoided the Virgo cluster completely. Comparison of the data with previously published work confirms that the photometry of Kent (1984) is free from major systematic error and is of comparable accuracy to the profiles presented in this work.

Kent (1985) reports the usual correlation of Bulge:Total luminosity-ratio with morphological type, and a large variation in the central surface brightnesses of disks, but finds a systematic variation in bulge characteristic-brightness with morphological type, and no apparent segregation of spiral and lenticular disks in the $r(o) - \log(\alpha^{-1})$ plane. The variation of bulge luminosity is considered responsible for the observed trend of the Bulge:Total luminosity-ratio, and these intrinsic structural differences of the bulge component are argued to

mitigate strongly against the formation of lenticular systems from spiral galaxies via gas depletion. Clearly, it is important to comment on the conclusion of Kent (1985), since it is contrary to the arguments presented in this work.

First of all, it is not surprising that there is considerable disparity in the conclusions reached with regard to bulge parameters, since the bulge scale-lengths produced by Kent are in very poor agreement with the systems in common with Boroson (1981) and Burstein (1979), being systematically much larger. Kent also reports a 20% discrepancy (in the opposite sense) with the result of Kormendy (1977) for a pure $R^{1/4}$ fit to NGC 524. Kent used a simultaneous least-squares technique to decompose his luminosity profiles, and notes that the discrepancies are substantially reduced if an iterative technique is employed. Even so, the results for NGC 488 cannot be reconciled with Boroson's (1981) value. The superiority of iterative fitting-techniques has been demonstrated in Chapter VI, and it is unfortunate that Kent did not make greater use of this technique. The systematic variation of bulge properties reported by Kent (1985) follows the trend of increasing disk dominance at later morphological type, and the suspicion is raised that these results could be produced by the parameter-coupling inherent in the simultaneous technique.

Kent (1985) does, however, provide a large sample of data which is homogeneous in acquisition, reduction and analysis procedures, and it seems quite possible that the reported differences between lenticular and spiral bulges are valid on an ordinal scale. To examine this conclusion the Daniel (1978) formulation of the

Kruskal-Wallis test was used to evaluate Kent's conclusion, based on a graphical presentation, that the bulges of late-type spirals have lower surface brightnesses than those of earlier type. The identical morphological binning and inclusion criteria used by Kent were adopted. The result is shown in Table A-(i). Inspection of Table A-(i) confirms that the null hypothesis of equal sample medians can be rejected at a high level of significance (0.5%). The Dunn (1964) extension of the Kruskal-Wallis test demonstrates that the lenticular and early-type spiral samples are not significantly different, but that the late-type spiral bulge sample is significantly fainter than both samples at the 2.5% level of significance (at least). However, as Kent admits, the results for all the bulge-dominated lenticulars have been excluded from the analysis. Whilst the exclusion of the disk components of such solutions from further analysis is laudible, the exclusion of the bulge parameters from the statistical analysis is much more questionable. Since the luminosity profiles of these galaxies are completely dominated by the bulge, uncertainties in the disk solution should have a very marginal effect on the bulge solutions. This can be demonstrated from Kent's data where the simultaneous bulge solution he presents for NGC 524 has a scale-length within 2% of the value he calculates via a pure $R^{1/4}$-fit (with no disk) for comparison with the result of Kormendy (1977).

Accordingly, the bulge solutions Kent excludes from analysis were added to the appropriate samples, and the Kruskal-Wallis test repeated on the larger data set. The result is shown in Table A-(ii). Inspection of Table A-(ii) shows the effect this has for hypothesis-testing: the null hypothesis can still be

rejected at quite a high level of significance (2.5%), with the Dunn extension producing the same result as before, but the population distributions of the SO/SOa and Sa/Sb samples now display nearly perfect statistical identity. This can be convincingly demonstrated from the result of a Mann-Whitney two-sample test shown in Table A-(iii). Since Kent (1985) does not claim to observe any morphological segregation of bulge scale-length, there can be no statistically significant difference in the bulge luminosity of the SO/SOa and Sa/Sb samples.

Comparison of the disk scale-length values produced by Kent reveals good agreement for the three systems in common with Boroson (1981), with differences of about 10%. This level of agreement implies that Kent's conclusions regarding the disk characteristic parameters (no significant morphological dependence on either central surface brightness or disk scale-length) should be much more securely established. However, due to the dominant selection effect in his sample (all galaxies of high intrinsic luminosity), the dispersion of disk luminosity in the r(o) - log α^{-1} plane is small. Consequently, one could not expect to see any segregation in disk luminosity between the spiral and lenticular systems in Kent's sample.

These arguments must seriously weaken Kent's conclusion that the properties of lenticular systems are inconsistent with their production from spiral systems via gas depletion.

Despite the reservations that have been expressed in this note with regard to the decomposition technique used and the

statistical significance of his conclusions, the results proferred by Kent (1985) are certainly interesting, and deserve extension to a larger data sample to continue the investigation. The idea that the bulges of late-type spirals are intrinsically different to those of disk systems of earlier morphological type could be related to the dearth of disk-dominated lenticular systems; for example, early-type disk systems may be significantly older than late-type spirals, which could be identified as those systems which had the opportunity to continue disk formation until far more recent epochs. As Kent himself notes, the case against the formation of lenticular galaxies from early-type spiral progenitors is rather weak, and his observations are thus reconcilable with the conclusions reached in this work.

Table A-[i]: Kruskal-Wallis Test for Three Samples

Sample	N_1	Sample	N_2	Sample	N_3	H	R%
SO/SOa	8	Sa/Sb	17	Sbc +	13	11.97	<0.5%

Table A-[ii]: Kruskal-Wallis Test for Three Samples

Sample	N_1	Sample	N_2	Sample	N_3	H	R%
SO/SOa	16	Sa/Sb	20	Sbc +	13	8.8	<2.5%

R% is the probability of erroneously rejecting the null hypothesis.

H_o: the population distributions have the same median.

Table A[iii]: Mann-Whitney Two-Sample Test

Samples	N1	N2	Variable	U-statistic	R%
SO/SOa and Sa/Sb	16	20	μ_o	163	>10%

R%, H_o have the same meaning as above.

Perfect statistical equality of the samples would correspond to U = 160.

References:

Boroson, T. (1981) Ap. J. Suppl. 46, 177

Burstein, D. (1979) Ap. J. 234, 435

Daniel, W. (1978) "Applied Nonparametric Statistics" [Houghton-Mifflin Co.] p. 200

Dunn, O. (1964) Technometrics 6, 241

Kent, S. (1984) Ap. J. Suppl. 56, 105

Kent, S. (1985) Ap. J. Suppl. 59, 115

Kormendy, J. (1977) Ap. J. 218, 333

Kruskal, W., and Wallis, W. (1952) Ann. Amer. Statist. Assoc. 47, 583

REFERENCES

Aarseth, S., and Fall, S. (1980) Ap. J. 236, 43

Aarseth, S., Gott, J., Turner, E. (1979) Ap. J. 228, 664

Adamson, A. (1984) [st. Andrews Univ.] private comm.

van Albada, T., and van Gorkum, J. (1977) Ap. J. 216, 194

Allen, C. (1979) "Allen's Astrophysical Quantities" 3 rd Ed.
[London Univ.] p. 264

Appleton, P. (1983) Mon. Not. R. Astron. Soc. 203, 533

Arp, H. (1966) Ap. J. Suppl. 14, 1

Austin, T., Godwin, J., and Peach, J. (1975)
Mon. Not. R. Astron. Soc. 171, 135

Austin, T., and Peach, J. (1974) Mon. Not. R. Astron. Soc.
168, 591

Bahcall, N., and Soneira, R. (1982) Ap. J. 262, 419

Baker, A. (1925) Proc. Roy. Soc. Edin. 45, 166

Barbon, R., Benacchio, L., and Capaccioli, M. (1978)
Astron. Astophys. 65, 165

Bechtold, J., Forman, W., Giaconni, R., Jones, C., Schwarz, J.,
Tucker, W., and van Speybroeck L. (1983) Ap. J. 265, 26

Beers, T., and Geller, M. (1983) Ap. J. 274, 491

Benedict, G. (1971) Ph.D. thesis N.Western Univ.

Bennachio, L. (1975) Ph.D. thesis Padua Univ.

van den Bergh, S. (1966) Ap. J. 206, 883

van den Bergh, S. (1977) Vistas in Ast. 21, 77

Bingelli, B., Sandage, A., and Tarenghi, M. (1984) A.J. 89, 64

Blackmann, C. (1979) "Phometry, Kinematics and Dynamics of
Galaxies" Ed. Evans [Univ. of Texas at Austin] p. 135

Blackmann, C. (1982) [R.O.E.] private comm.

Blackmann, C. (1983) Mon. Not. R. Astron. Soc. 202, 379

Bond, J., and Szalay, R. (1983) Ap. J. 274, 443

Boroson, T. (1981) Ap. J. Suppl. 46, 177

Boroson, T., Thomson, I., and Shectman, S. (1983 a) A.J. 88, 1707

Boroson, T., Strom, K., Strom, S. (1983 b) Ap. J. 274, 39

Bothun, G. (1982) Ap. J. Suppl. 50, 39

Bothum, G., Schommer, R., and Sullivan, W. (1982) A.J. 87, 731

Bottinelli, L., and Gouguenheim, L. (1974)
Astron. Astrophys. 36, 401

Bregmann, J. (1978) Ap. J. 224, 768

Bucknell, M., Godwin, J., and Peach, J. (1979)
Mon. Not. R. Astron. Soc. 188, 579

Burbidge, E., and Burbidge, G. (1969) "Galaxies and the Universe"
Ed. Sandage, Sandage and Kristian [Chicago Univ. Press] p. 81

Burkhead, M., and Kalowinski, J. (1974) A.J. 79, 835

Burstein, D. (1978) Ph.D. thesis Univ. of California at Santa Cruz

Burstein, D. (1979 a) Ap. J. Suppl. 41, 435

Burstein, D. (1979 b) Ap. J. 234, 435

Burstin, D., and Heiles, C. (1978) Ap. J. 225, 40

Canizares, C., Clark, G., Markent, T., Berg, C., Smedeira, D.,
Bardas, H., Schoffer, H., and Kalata, K. (1979) Ap. J. 234, L33

Capaccioli, M., and de Vaucouleurs, G. (1983) Ap. J. Suppl. 52, 465

Charmaraux, P., Balkowski, C., and Gerard, E. (1980)
Astron. Astrophs. 83, 38

Carr, B. (1975) Ap. J. 201, 1

Carr, B. (1977) Astron. Astrophs. 56, 377

Carr, B., and Rees, M. (1984 a) Mon. Not. R. Astron. Soc. 206, 315

Carr, B., and Rees, M. (1984 b) Mon. Not. R. Astron. Soc. 206, 801

Carter, D., Allen, D., and Malin, D. (1982) Nature 295, 126

Carter, D. and Dixon, K. (1978) A.J. 83, 574

Carter, D. and Godwin, J. (1979) Mon. Not. R. Astron. Soc. 187, 711

Chincarini, G., Giovanelli, R., and Haynes, M. (1979) A.J. 84, 1500

Chincarini, G., Giovanelli, R., and Haynes, M. (1983 a) Ap.J. 269, 13

Chincarini, G., Giovanelli, R., Haynes, M. and Fontanelli, P.
(1983 b) Ap. J. 2671, 511

Chincarini, G., and de Souza, R. (1985) Eso Preprint No. 383

Cousins, A. (1980) S.A.A.O Circ. 1, No. 5

Cowie, L., and McKee, C. (1977) Ap. J. 211, 135

Cowie, L., and Songaila, A. (1977) Nature 266, 501

Curry, M. (1982) [R.G.O] private comm.

Daniel, W. (1978 a) "Applied Non-Parametric Statistics"
[Hougton-Mifflin] p. 314

Daniel, W. (1978 b) "Applied Non-Parametric Statistics" p. 82

Daniel, W. (1978 c) "Applied Non-Parametric Statistics" p. 135

Davenhall, A. (1983) [R.O.E] private comm.

Davenhall, A. (1984 a) Ph.D. thesis St. Andrews Univ.

Davenhall, A. (1984 b) [R.O.E] private comm.

Davies, E. (1981) [R.G.O] private comm.

Davis, M., and Geller, M. (1976) Ap. J. 208, 13

Davis, M., Huchra,1 J., Latham, D., and Tonry, J. (1982)
Ap. J. 253, 423

Davis, R. and Lewis, B. (1973) Mon. Not. R. Astron. Soc. 165, 231

Dawe, J. and Metcalfe, N. (1981) U.K.S.T.U Int. Report SSO/02/81

Dixon, K. (1981) "Proceedings of the Second Measuring Machine
Workshop" [R.O.E.] p. 133

Doroshkevich, A., Kotak, E., Novikov, I., Polyudov, A., Shandarin, S. and Sigov, Yu. (1980) Mon. Not. R. Astron. Soc. 192, 321

Dressler, A. (1978) Ap. J. 223, 765

Dressler, A. (1980) Ap. J. 236, 351

Dressler, A. (1984) Ann. Rev. of Astron. Astrophys. 22, 185

Dressler, A., and Sandage, A. (1983) Ap. J. 265, 664

Efstathiou, G., Fall, S., and Hogan, C. (1979) Mon. Not. R. Astron. Soc. 189, 203

Elmegreen, B., and Lada, C. (1977) Ap. J. 271, 752

Faber, S. (1973) Ap. J. 179, 423

Faber, S. (1977) "The Evolution of Galaxies and Stellar Populations" Ed. Tinsley and Larson [New Haven] p. 157

Faber, S., and Gallagher, J. (1976) Ap. J. 204, 365

Faber, S., and Gallagher, J. (1979) Ann. Rev. of Astron. Astrophys. 17, 135

Faber, S., and Jackson, R. (1976) Ap. J. 204, 668

Fabian, A., Hu, E., Cowie, L., and Grindlay, J. (1981) Ap.J. 248, 47

Fabian, A., Schwarz, J., and Forman, W. (1980) Mon. Not. R. Astron. Soc. 192, 135

Farouki, R., Shapiro, S. (1980) Ap. J. 241, 928

Feitzinger, J., Nicolov, A., Schmidt-Kaler, T., and Tennigkeit, J. (1983) Astron. Astrophys. 126, 352

Fong, R., Godwin, J., and Spencer, S. (1981) "Proceedings of the Secand Measuring Machine Workkshop" [R.O.E.] p. 123

Forman, W., and Jones, C. (1982) Ann. Rev. of Astron. Astrophys. 20, 547

Forman, W., Shwarz, J., Jones, C., Liller, W., and Fabian, A. (1979) ap. J. Lett. 234, L27

Fraser, C. (1977) Astron. Astrophys. Suppl. 29, 161

Freeman, K. (1970) Ap. J. 160, 811

Freese, K., Price, R., and Schramm, D. (1983) Ap. J. 275, 405

Frenk, C., White, S., and Davis, M. (1983) Ap. J. 271, 417

Frogel, J., and Whitford, A. (1982) Ap. J. Lett. 252, L7

Gallagher, J., and Ostriker, J. (1972) A.J. 77, 288

Gilmore, G., and Hewett, P. (1983) Nature 306, 669

Giovanardi, C., Helou, G., Salpeter, E., and Krumm, N. (1983 a)
Ap. J. 267, 35

Giovanardi, C., Krumm, N., and Salpeter, E. (1983 b) A.J. 88, 1719

Giovanelli, R., Chincarini, G., and Haynes, M. (1981) Ap. J. 247, 383

Giovanelli, R., and Haynes, M. (1983) A.J. 88, 881

Giovanelli, R., and Haynes, M. (1985) Ap. J. 292, 404

Giovanelli, R., Haynes, M. and Chinarini, G. (1982) Ap. J. 262, 442

Gisler, G. (1978) Mon. Not. R. Astron. Soc. 183, 633

Godwin, J. (1976) Report of the Dept. Astrophysics, Oxford Univ. No.1

Godwin, J. and Peach, J. (1977) Mon. Not. R. Astron. Soc 181, 323

Godwin, J. and Peach, J. (1982) Mon. Not. R. Astron. Soc. 200, 733

Gorbatskij, V. (1982) Astrofizica 18, 143

Gott, J. (1977) Ann. Rev. of Astorn. Astrophys. 15, 235

Gott, J., Gunn, J., Shramm, D. and Tinsley, B. (1974) Ap. J. 194, 543

Griersmith, D., Hyland, A., and Jones, T. (1982) A.J. 87, 1106

Gunn, J. and Gott, J. (1972) Ap. J. 176, 1

Hanabe, M. (1982) P.A.S. Jap. 34, 423

Hanabe, M., (1983) Private comm.

Hanabe, M., Kodaira, K., Okamura, S., and Takase, B.
(1979 a) P.A.S. Jap. 31, 431

Hanabe, M., Kodaira, K., Okamura, S., and Takase, B. (1977 b) "Photometry, Kinematics and Dynamics of Galaxies" [Univ. of Texas at Austin] p. 109

Hanabe, M., Kodaira, K., Okamura, S., and Takase, B. (1980) P.A.S. Jap. 32, 197

Hanes, D., Harris, E., Madore, B. (1976) Mon. Not. R. Astron. Soc. 77, 653

Harris, W. (1981) Ap. J. 251, 497

Haynes, M., Giovanelli, R., and Chincarini, G. (1984) Ann. Rev. of Astron. Astrophys. 22, 445

Head, C., Uomoto, A., and Green, J. (1976) P.A.S.P. 88, 656

Henry, J., Branduardi, G., Briel, U., Fabricant, D., Feigelson, E., Murray, S., Soltan, A., and Tanabaum, H. (1979) Ap. J. Lett. 234, L15

Hodge, P. and Michie, R. (1969) A.J. 74, 587

Hoessel, J. (1980) Ap. J. 241, 493

Holmberg, E. (1958) Medd. Lund. Astron. Obs. Series II, No. 136

van Houten, C. (1961) Bull. Ast. Inst. Netherlands 16, 1

Hubble, E. (1936) "The Realm of the Nebulae" [New Haven: Yale Univ. Press]

Huchra, J., Davis, M., Latham, D., and Tonry, J. (1983) Ap. J. Suppl. 52, 89

Huchtmeir, W., Tammann, G. and Wendker, H. (1976) Astron. Astrophys. 46, 381

Jones, B., Palmer, P., and Wyse, R. (1981) Mon. Not. R. Astron. Soc. 197, 967

Jones, C., and Forman, W. (1982) Ann. Rev. of Astorn. Astrophys. 20, 547

Jones, C., Mandel, E., Schwarz, J., Forman, W., Murray, S., and Harriden, F. (1979) Ap. J. Lett. 234, L21

Jones, W., Obitts, D., Gallet, R. and de Vaucouleurs, G. (1967) Publ. Dept. Astron. Univ. Texas Series II No. 1, p. 8

Kashlinsky, A. (1982) Mon. Not. R. Astron. Soc. 200, 585

Keenan, D. (1981) Astron. Astrophys. 95, 340

Kendall, M. (1938) Biometrika 30, 81

Kennicutt, R. (1983) A.J. 88, 483

Kennicutt, R., Bothun, G., and Schommer, R. (1984) A.J. 89, 1279

Kent, S. (1981) Ap. J. 245, 801

Kilkenny, D., and Malcolm, G. (1984) Mon. Not. R. Astron. Soc. 209, 169

King, I. (1962) Ap. J. 67, 471

King, I. (1966) Ap. J. 71, 64

King, I. (1978) Ap. J. 222, 1

Kormendy, J. (1977 a) Ap. J. 214, 359

Kormendy, J. (1977 b) Ap. J. 218, 333

Kormendy, J. (1977 c) Ap. J. 217, 406

Kormendy, J. (1980) "ESO Workshop on Two-Dimensional Photometry" [E.S.O.] Ed. Crane and Kjar p. 191

Kormendy, J. (1982) "Morphology and Dynamics of Galaxies" [Geneva Obs.] Ed. Martinet and Mayor p. 115

Kotanyi, C., and Ekers, R. (1983) Astron. Astrophys. 122, 267

Kotani, C., van Gorkum, J., and Ekers, R. (1983) Ap. J. Lett. 273, L7

Krumm, N., and Salpeter, E. (1979 a) Ap. J. 227, 776

Krumm, N. and Salpeter, E. (1979 b) Ap. J. 228, 64

Lacy, J., Townes, C., and Hollenbach, D. (1982) Ap. J. 262, 120

Larson, R., and Tinsley, B. (1978) Aop. J. 219, 46

Larson, R., Tinsley, B., and Caldwell, N. (1980) Ap. J. 237, 692

Leir, A., and van den Bergh, S. (1977) Ap. J. Suppl. 34, 381

Liller, M. (1960) Ap. J. 132, 306

Liller, M. (1966) Ap. J. 146, 28

Longmore, A., Hawarden, T., Cannon, R., Allen, D. and Nebold, U. (1979) Mon. Not. R. Astron. Soc. 188, 285

Lynden-Bell, D. (1969) Nature 223, 690

Malin, D. (1979) Nature 227, 279

Malin, D. (1981) A.A.S. Photo-Bull. 27, 4

Malin, D., and Carter, D. (1980) Nature 285, 643

Mann, H., and Whitney, D. (1947) Ann. Math. Stat. 18, 50

Markarian, B., Organesion, E., and Arakelian, A. (1965) Astrofizica 1, 38

Mathews, W., and Baker, J. (1971) Ap. J. 170, 241

Mellot, A. (1983) Ap. J. 264, 59

Merritt, D. (1983) Ap. J. 264, 24

Meszaros, P (1975) Astron. Astrophys. 38, 5

Miller, R. (1984) ESO Preprint No. 343

Miller, R., and Smith B. (1980) Ap. J. 235, 793

Morgan, W., and Osterbrock, D. (1969) A.J. 74, 515

Muzzio, J., Martinez, R. and Rabolli, M. (1984) Ap. J. 285, 7

Nulsen, P. (1982) Mon. Not. R. Astron. Soc. 198, 1007

Oemler, A. (1974) Ap. J. 194, 1

Okamura, S. (1977) Ann. Tokyo. Astron. Obs. 16, No. 3, p. 111 and p. 122

Okamura, S., Davenhall, A.C., and MacGillivray, H. (1982) "Proceedings of the Second Measuring Machine Workshop" [R.O.E] p. 95

Olive, K., Schramm, D., Steigman, G., Turner, M., and Yang, J. (1981) Ap. J. 246, 557

Olmstead, P. and Tukey, J. (1947) Ann. Math. Statis. 18, 495

Ostriker, J. and Cowie, L. (1981) Ap. J. 243, L127

Ostriker, J. and Peebles, P. (1973) Ap. J. 186, 467

Pacheco, J. de Freitas, de Souza, R. and Arakaki, L. (1983) A.J. 88, 1435

Peebles, P. (1970) A.J. 75, 13

Peebles, P. (1974) Astron. Astrophys. 32, 197

Peebles, P. (1981) Ap. J. 248, 885

Penny, A. (1982) Private Comm.

Peterson, B., Strom, S., and Strom, K. (1979) A.J. 84, 735

Press, W. and Davis, M. (1982) Ap. J. 259, 449

Redman, R. (1936) Mon. Not. R. Astron. Soc. 96, 588

Redman, R. and Shirley, E. (1937) Mon. Not. R. Astron. Soc. 97, 416

Rephaeli, Y. and Salpeter, E. (1980) Ap. J. 240, 20

Richstone, D. (1975) Ap. J. 200, 535

Richstone, D. (1976) Ap. J. 204, 642

Roberts, M. (1971) "Galaxies and the Universe" Ed. Sandage, Sandage and Kristian [Chigcago Univ. Press] p. 309

Romashin, W. Strom, K. and Strom, S. (1983) Ap. J. Suppl. 53, 105

Rood, H., Page, T., Kinter, E., and Kind, I. (1972) Ap. J. 175, 627

Roos, N. (1981) Astron. Astrophys. 95, 349

Rubin, V., Ford, W. and Thonnard, N. (1978) Ap. J. Lett. 225, L107

Sadler, E. and Sharp, N. (1984) Ap. J. 287, 80

Sandage, A. (1961) "Hubble Atlas of Galaxies" [Carnegie Inst. of Washington]

Sandage, A., Freeman, K. and Stokes, N. (1970) Ap. J. 160, 831

Sandage A. and Tammam, G. (1981) "Revised Shapely-Ames Catalogue" [Carnegie Inst. of Washington]

Sandage, A. and Visvanathan, N. (1977) Ap. J. 216, 214

Sandage, A. and Visvanathan, N. (1978) Ap. J. 225, 742

Sargent, W. Young, P., Boksenberg, A., Shortridge, K., Lynds, C. and Hartwick, F. (1978) Ap. J. 221, 731

Schechter, P. 1976) Ap. J. 203, 297

Shild, R. (1972) A.J. 82, 337

Schneider, D., Gunn, J. and Hoessel, J. (1983) Ap. J. 268, 476

Schommer, R., Sullivan, W., and Bothun, G. (1981) A.J. 86, 943

Schraum, D. and Steigman, G. (1981) Ap. I. 243, 1

Schweizer, F. (1976) Ap. J. Suppl. 31, 313

Schweizer, F. (1982) Ap. J. 252, 455

Shapiro, P., Struck-Marcell, C. and Mellot, A. (1983) Ap. J. 275, 413

Shostak, G., Hummel, E., Shaver, P., van der Hulst, J., van der Kruit, P. (1982) Astron. Astrophys. 115, 293

Silk, J. (1977 a) Ap. J. 211, 638

Silk, J. (1977 b) Ap. J. 214, 152

Silk, J. (1977 c) Ap. J. 214, 725

Silk, J. (1978) Ap. J. 220, 390

Silk, J. and Wilson, M. (1981) Ap. J. Lett. 244, L37

Spearman, C. (1905) Am. J. Psychol. 15, 72

Spitzer, L. and Baade, W. (1951) Ap. J. 113, 413

Sprent, P. (1981 b) "Quick Statistics - an Introduction to non-Parametric methods" [Penguin] p. 138

Stauffer, J. (1983) Ap. J. 264, 14

Stewart, G., Fabian, A., Jones, c. and Forman, W. (1984) Ap.J. 285, 1

Stobie, R. (1982) [R.O.E] Private Comm.

Strom. K. and Strom. S. (1978 a) A.J. 83, 73

Strom, K. and Strom, S. (1978 c) A.J. 83, 1293

Strom, K. and Strom, S. (1979 e) "Structure and Properties of Nearby Galaxies" Ed. Barkhaijsen and Wielebinski [Dordrecht: Reidel] p. 69

Strom, S. and Strom, K. (1978 b) A.J. 83, 782

Strom, S. and Strom, K. (1979 d) Ap. J. Lett. 225, L93

Sullivan, W,., Bothun, G., Bates, B. and Schommer, R. (1981) A.J. 86, 919

Sullivan, W. and Johnson, P. (1978) Ap. J. 225, 751

Takeda, H., Nulsen, P. and Fabian, A. (1984) Mon. Not. R. Astron. Soc. 208, 261

Thompson, L., Gregory, S. (1980) Ap. J. 242, 1

Tonry, J. and Davis, M. (1981) Ap. J. 246, 680

Toomre, A. and Toomre, J. (1972) Ap. J. 178, 623

Tremaine, S. (1976) Ap. J. 203, 72

Tsikoudi, V. (1977) Publ. Dept. Astron. Univ. Texas No. 10, p. 1

de Vaucouleurs, G. (1948) Ann d'Ap 11, 247

de Vaucouleurs, G. (1959) Handbuch d. Phys. 53, 311

de Vaucouleurs, G. (1960) Ap. J. 131, 574

de Vaucouleurs, G. (1961) Ap. J. Suppl. 6, 213

de Vaucouleurs, G. (1962) IAU Symp. 15, 3

de Vaucouleurs, G. (1968) Applied Optics 7, 1513

de Vaucouleurs, G. (1974) IAU Symp. 58, 1

de Vaucouleurs, G. (1976) Occ. Rep. R.O.E. No. 2, p. 16

de Vaucouleurs, G. (1977 a) "Evolution of Galaxies and Stellar Populations" Ed. Tinsley and Laison [New Haven] p. 43

de Vaukouleurs, G. (1977 b) Ap. J. Suppl. 33, 211

de Vaucouleurs, G. (1982) Observatory 102, 178

de Vaucouleurs, G., and Capaccioli, M. (1983) Ap. J. Suppl. 40, 699

de Vaucouleurs, G., de Vaucouleurs, A., and Corwin, H. (1976)
"Second Reference Catalogue of Bright Galaxies"
[Univ. of Texas]

de Vaucouleurs, G., and Page, T. (1962) Ap. J. 136, 107

Visvanathan, N., and Sandage, A. (1977) Ap. J. 216, 214

Watanabe, M. (1983) Ann. Tokyo Ast. Obs. Second Series 19, No. 2

Weinberg, S. (1979) Phys. Rev. Lett. 42, 407

White, S. (1976 a) Mon. Not. R. Astron. Soc. 174, 19

White, S. (1976 b) Mon. Not. R. Astron. Soc. 177, 717

White, S. (1977) Mon. Not. R. Astron. Soc. 179, 33

White, S. (1978) Mon. Not. R. Astron. Soc. 184, 185

White, S. (1982) "Morphology and Dynamics of Galaxies"
Ed Martinet and Mayor [Geneva Obs.] p. 289

White, S., Frenk, C., and Davis, M. (1983) Ap. J. Lett. 274, L1

White, S., and Rees, M. (1978) Mon. Not. R. Aston. Soc. 183, 341

White, S., and Silk, J. (1980) Ap. J. 241, 864

Whitford, A. and Blanco, V. (1979) Bull. Am. Astron. Soc. 11, 675

Wilcoxon, F. (1945 a) Biometrics 1, 80

Wilcoxon, F. (1945 b) Biometrics 8, 33

Yoshizawa, M., and Wakamatsu, K. (1975) Astron. Astrophys. 44, 363

Zasov, A. (1975) Soviet Astron. 18, 426

Zel'dovich, Ya. (1970) Astron. Astrophys. 5, 84

Zel'dovich, Ya., Einasto, J., and Shandarin, S. (1982)
Nature 300, 407

A Three-Colour Photometric Survey of Virgo 'Core' Lenticular Galaxies

by Gordon J. Malcolm

VOLUME TWO: DATA APPENDICES

TABLE OF CONTENTS

APPENDIX 'A'

B, R and I-Band Luminosity Profiles

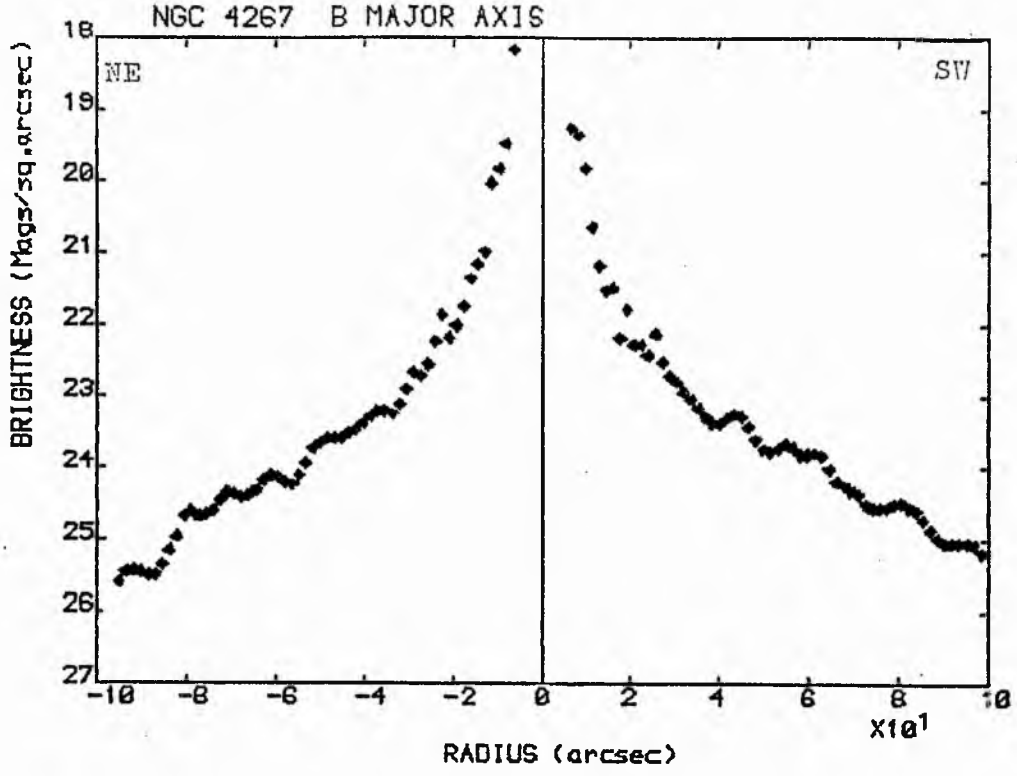
NGC 4267 B MAJOR AXIS
NE
SW
BRIGHTNESS (Mags/sq.arcsec)
18
19
20
21
22
23
24
25
26
27
-10
-8
-6
-4
-2
0
2
4
6
8
10
X10¹
RADIUS (arcsec)

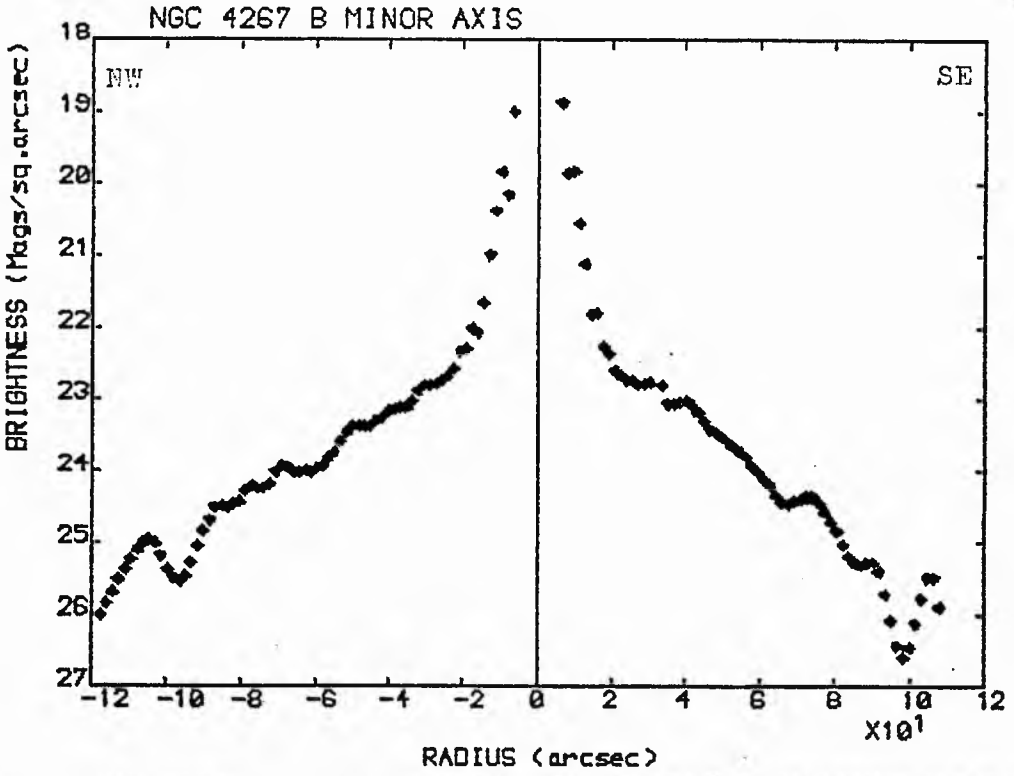
NGC 4267 B MINOR AXIS
NW
SE
BRIGHTNESS (Mags/sq.arcsec)
18
19
20
21
22
23
24
25
26
27
-12
-10
-8
-6
-4
-2
0
2
4
6
8
10
12
X10¹
RADIUS (arcsec)

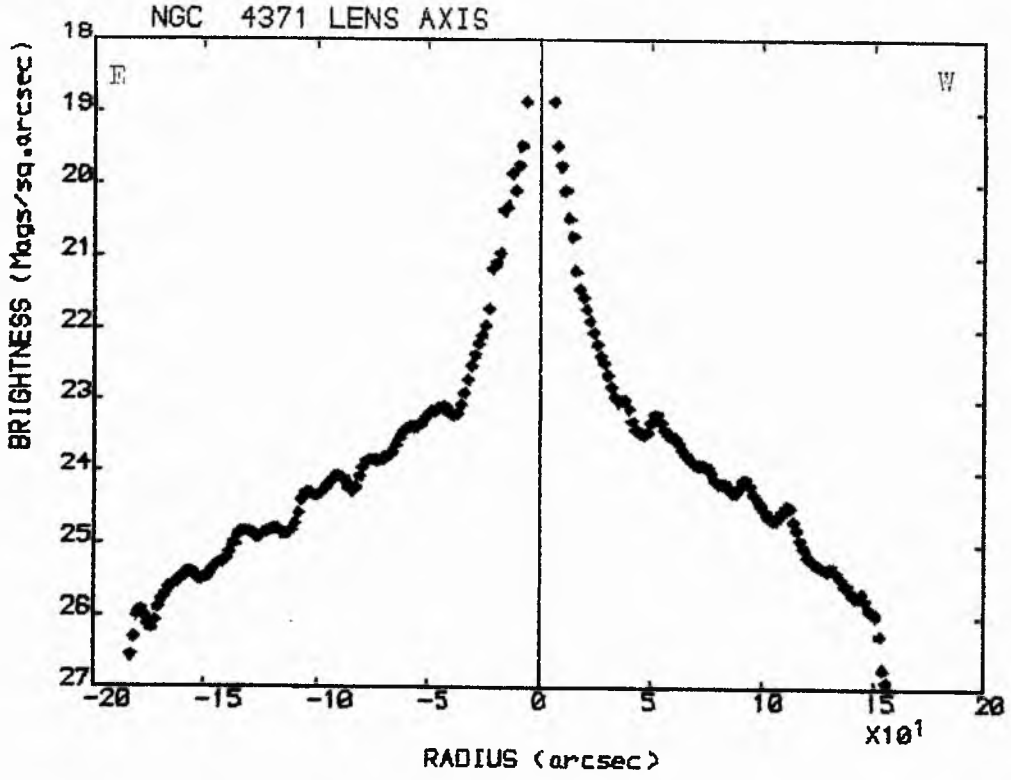
NGC 4371 LENS AXIS
E
W
BRIGHTNESS (Mags/sq.arcsec)
18
19
20
21
22
23
24
25
26
27
-20
-15
-10
-5
0
5
10
15
20
X10¹
RADIUS (arcsec)

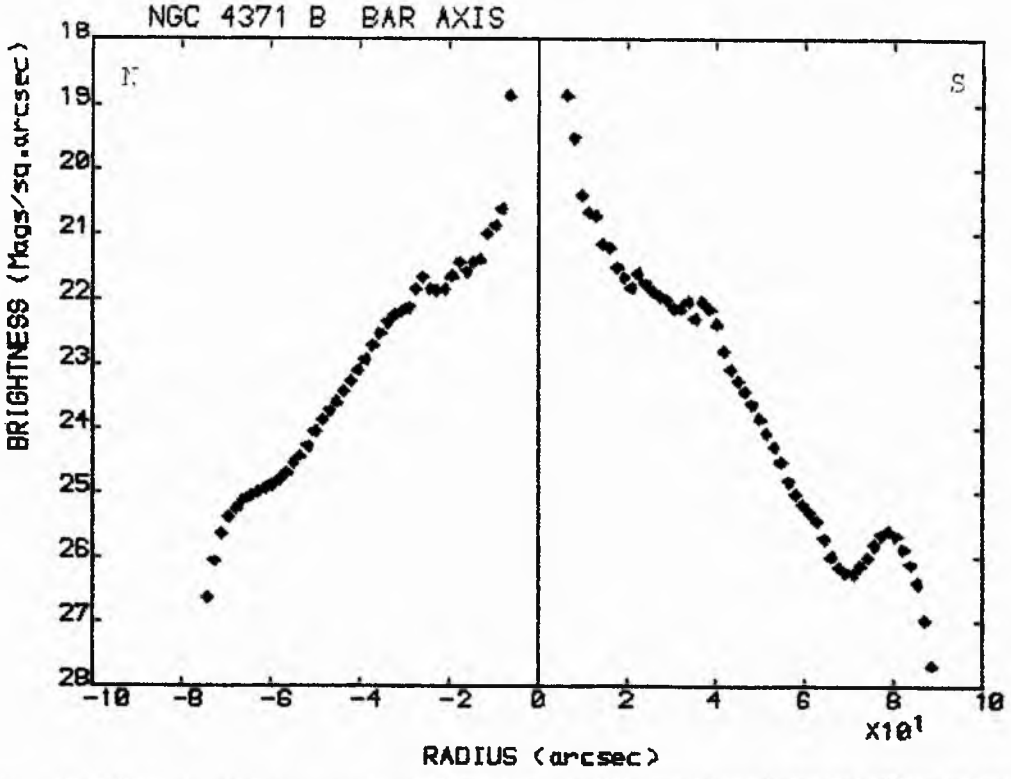
NGC 4371 B BAR AXIS
N
S
BRIGHTNESS (Mags/sq.arcsec)
18
19
20
21
22
23
24
25
26
27
28
-10
-8
-6
-4
-2
0
2
4
6
8
10
X10¹
RADIUS (arcsec)

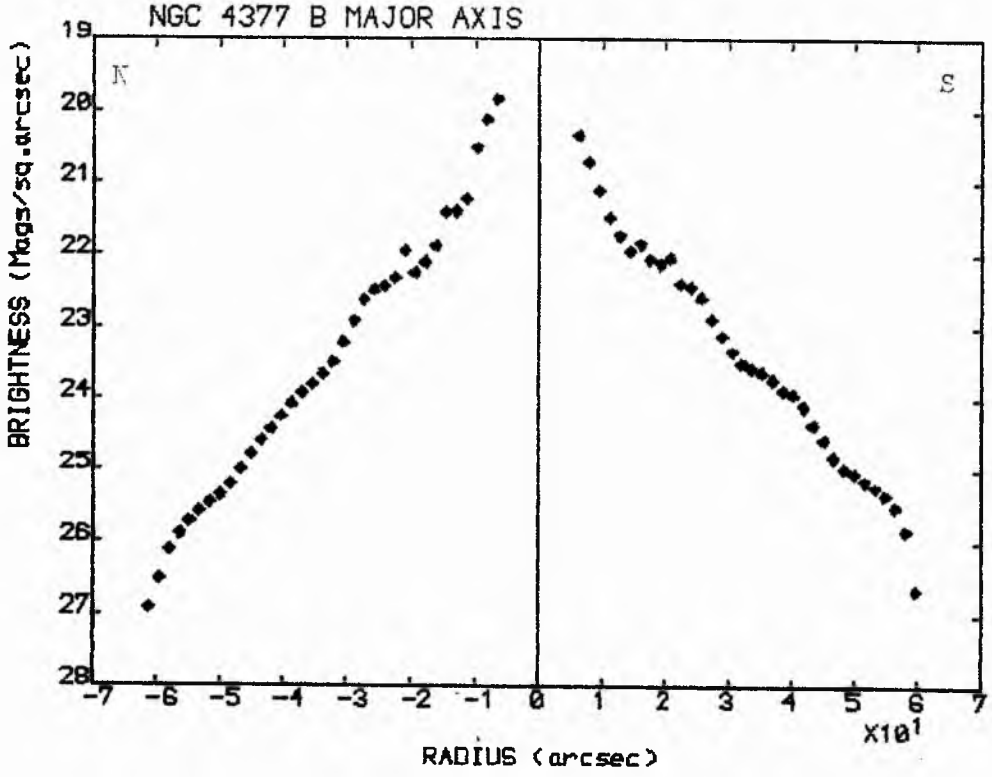
NGC 4377 B MAJOR AXIS
N
S
BRIGHTNESS (Mags/sq.arcsec)
19
20
21
22
23
24
25
26
27
28
-7 -6 -5 -4 -3 -2 -1 0 1 2 3 4 5 6 7
X10¹
RADIUS (arcsec)

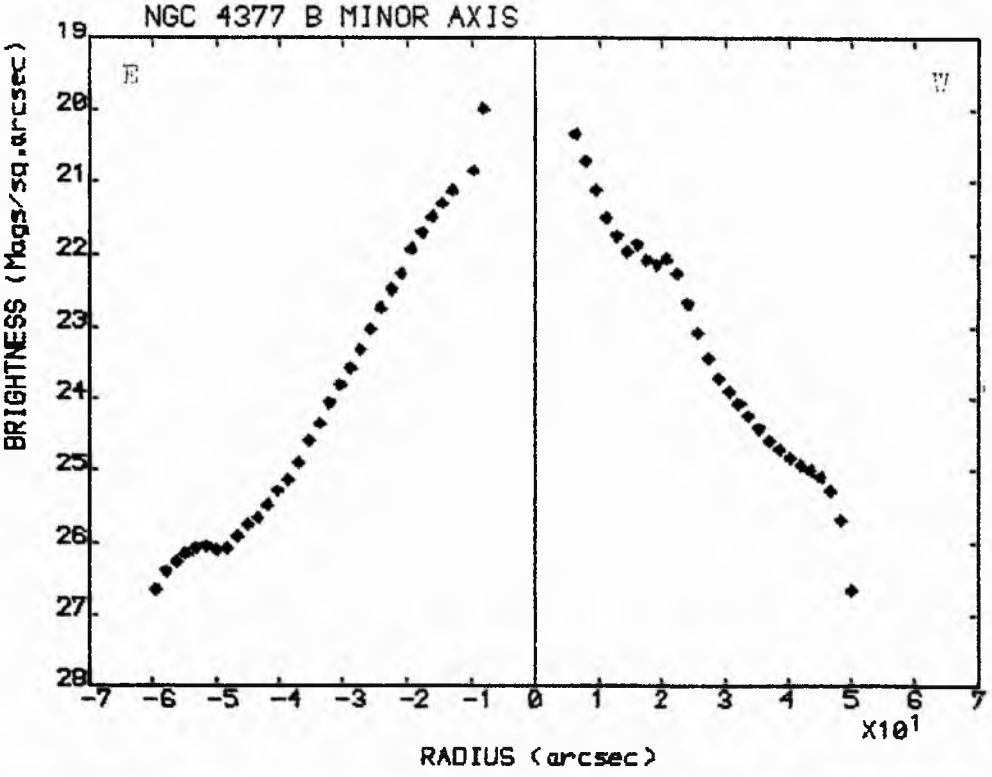
NGC 4377 B MINOR AXIS
E
W
BRIGHTNESS (Mags/sq.arcsec)
19
20
21
22
23
24
25
26
27
28
-7 -6 -5 -4 -3 -2 -1 0 1 2 3 4 5 6 7
X10¹
RADIUS (arcsec)

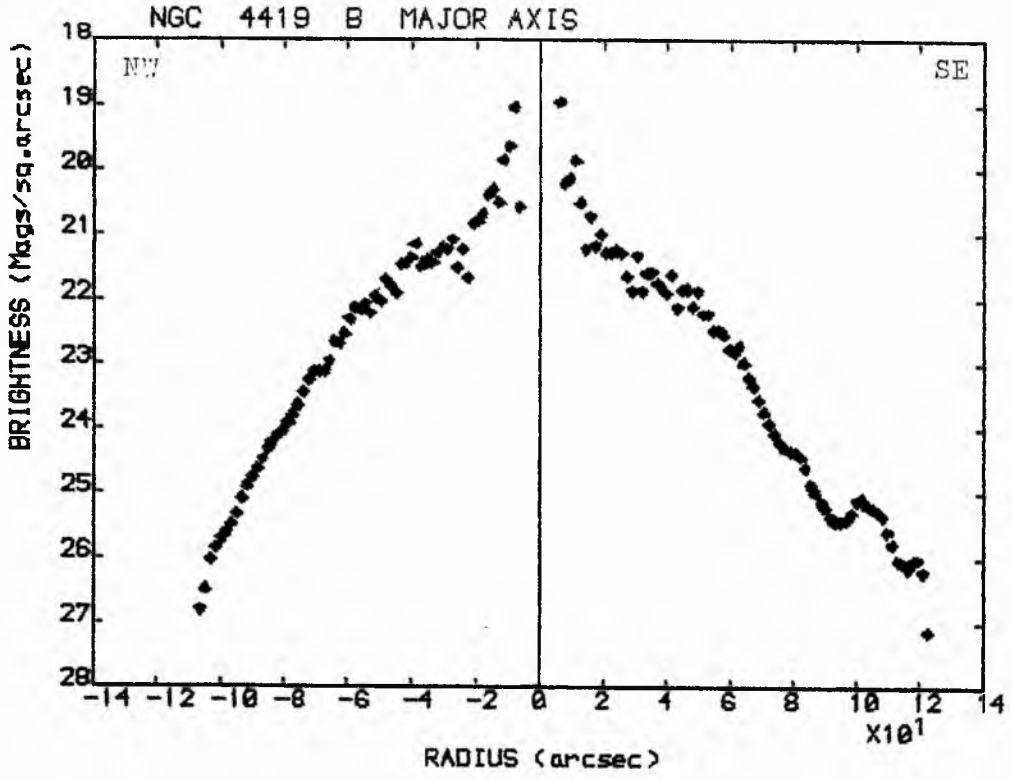
NGC 4419 B MAJOR AXIS
NW
SE
BRIGHTNESS (Mags/sq.arcsec)
18
19
20
21
22
23
24
25
26
27
28
-14 -12 -10 -8 -6 -4 -2 0 2 4 6 8 10 12 14
X10¹
RADIUS (arcsec)

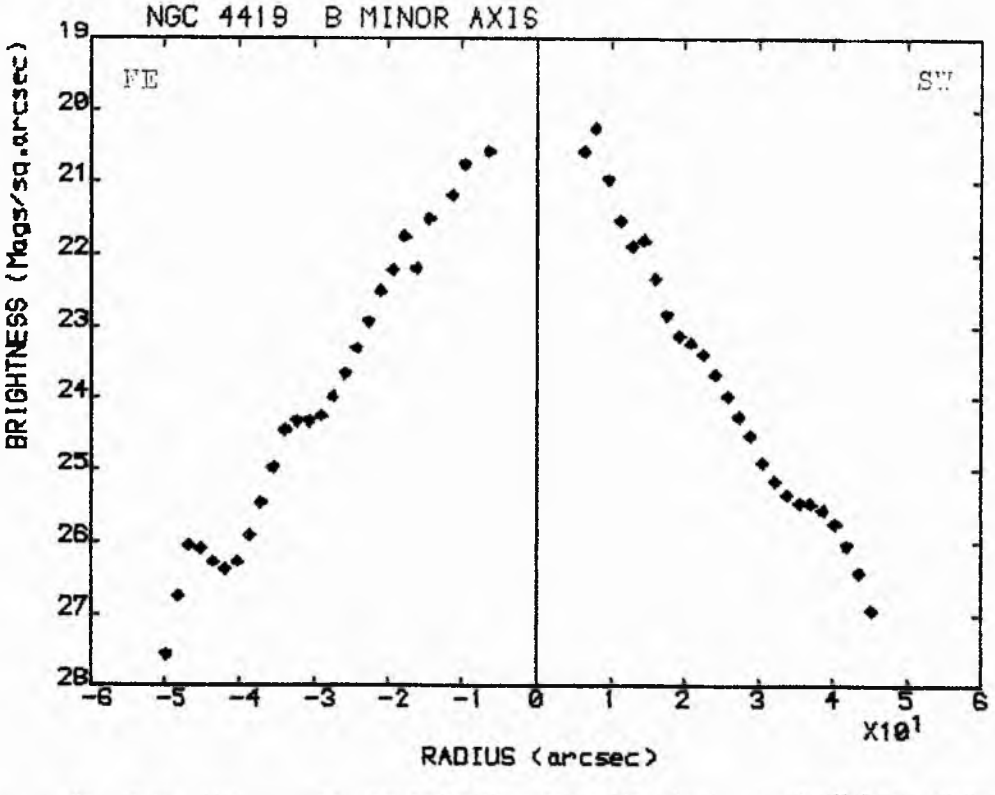
NGC 4419 B MINOR AXIS
NE
SW
BRIGHTNESS (Mags/sq.arcsec)
19
20
21
22
23
24
25
26
27
28
-6 -5 -4 -3 -2 -1 0 1 2 3 4 5 6
X10¹
RADIUS (arcsec)

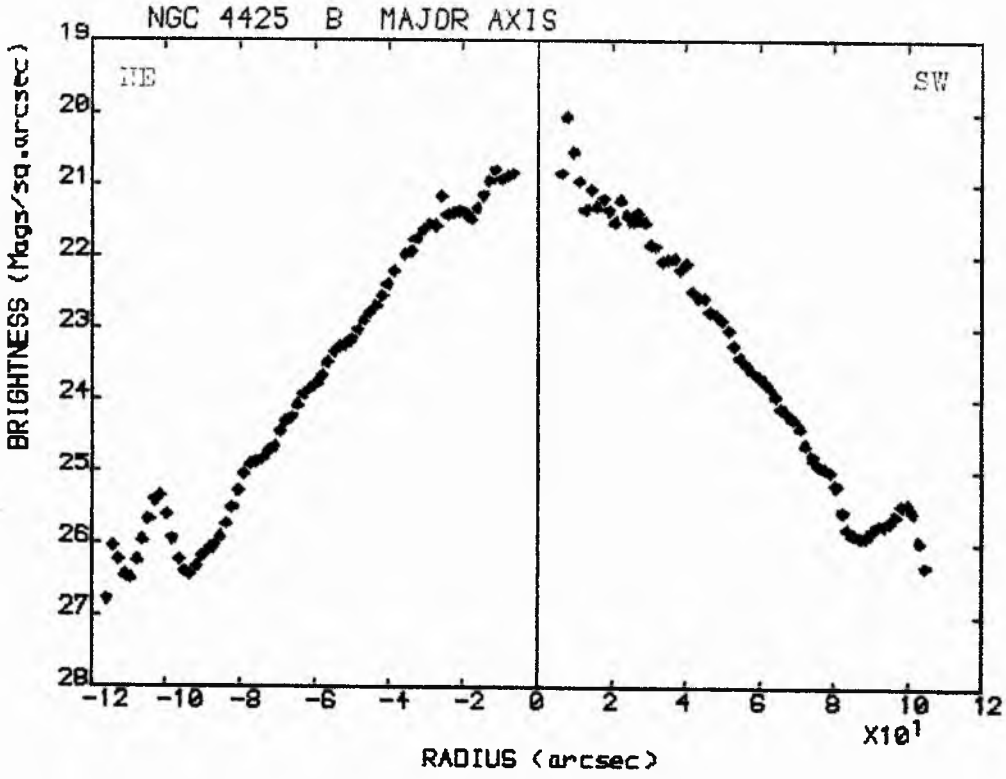
NGC 4425 B MAJOR AXIS
NE
SW
BRIGHTNESS (Mags/sq.arcsec)
19
20
21
22
23
24
25
26
27
28
-12 -10 -8 -6 -4 -2 0 2 4 6 8 10 12
X10¹
RADIUS (arcsec)

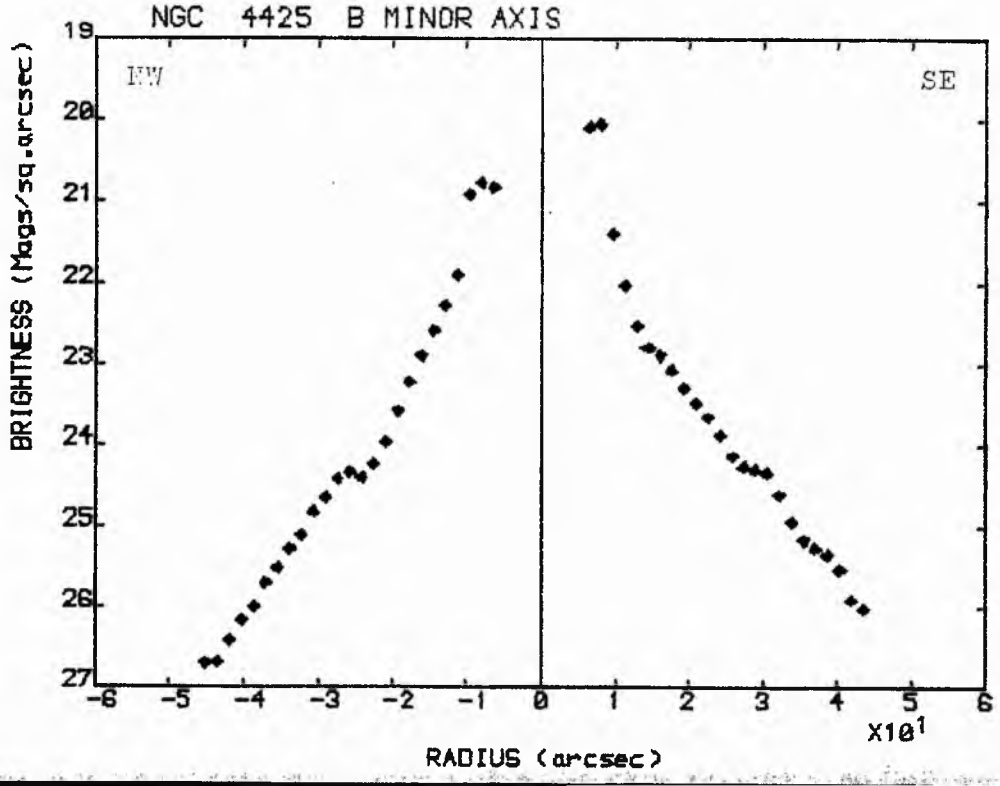
NGC 4425 B MINOR AXIS
NW
SE
BRIGHTNESS (Mags/sq.arcsec)
19
20
21
22
23
24
25
26
27
-6 -5 -4 -3 -2 -1 0 1 2 3 4 5 6
X10¹
RADIUS (arcsec)

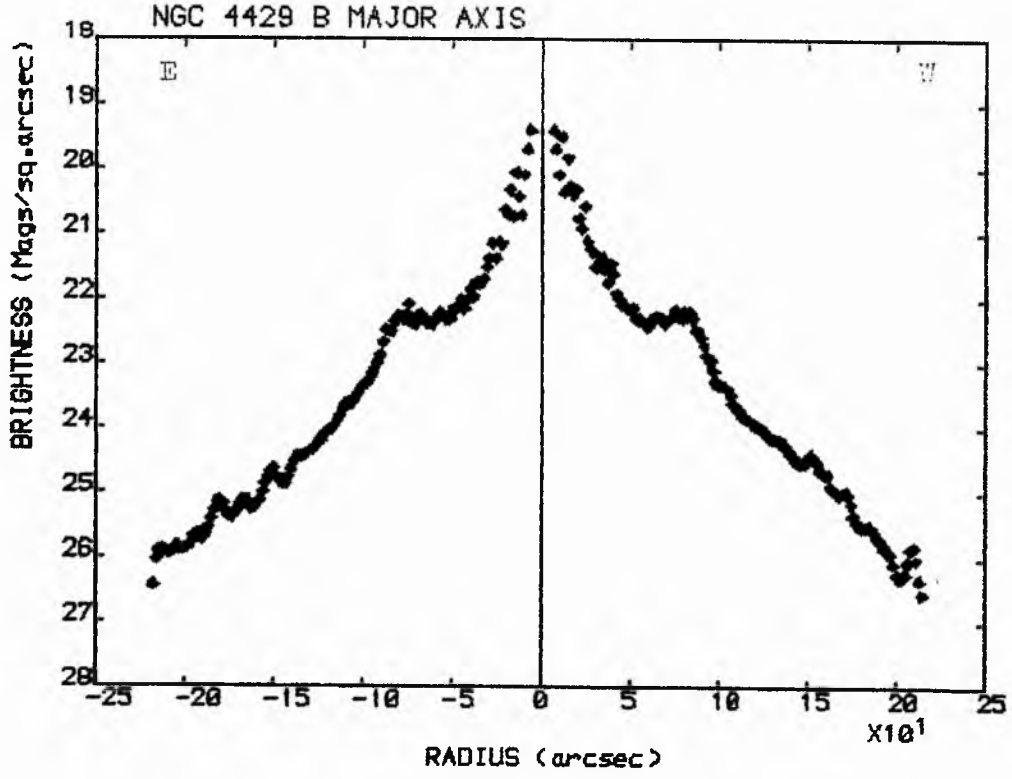
NGC 4429 B MAJOR AXIS
E
W
BRIGHTNESS (Mags/sq.arcsec)
18
19
20
21
22
23
24
25
26
27
28
-25 -20 -15 -10 -5 0 5 10 15 20 25
X10¹
RADIUS (arcsec)

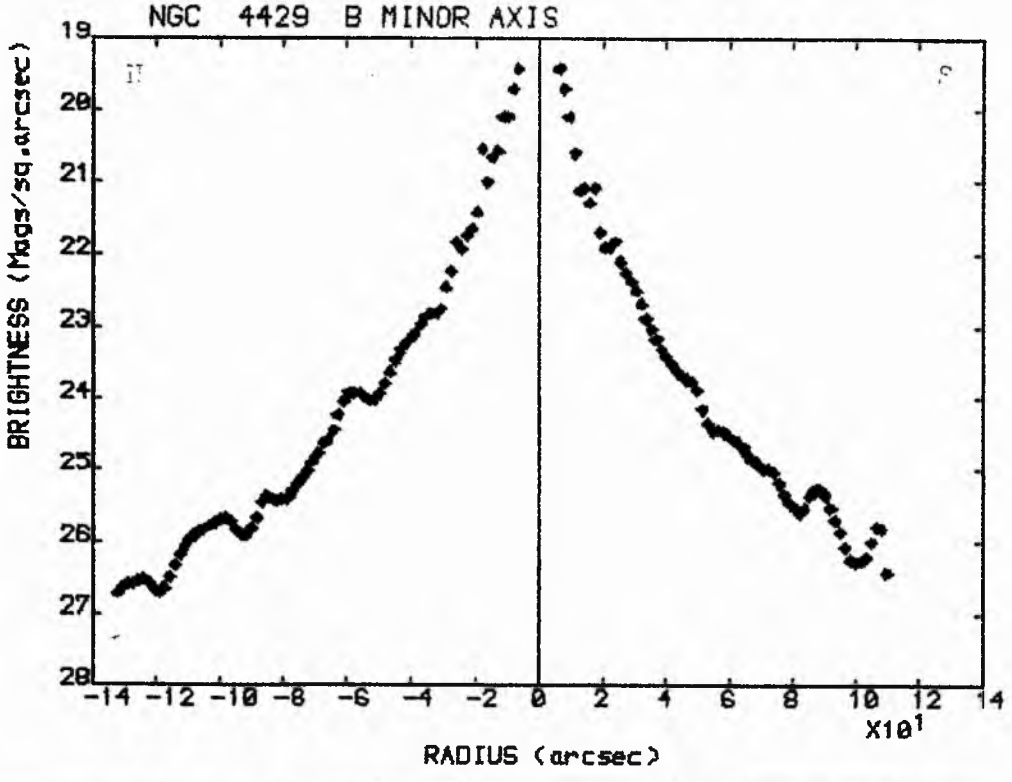
NGC 4429 B MINOR AXIS
N
S
BRIGHTNESS (Mags/sq.arcsec)
19
20
21
22
23
24
25
26
27
28
-14 -12 -10 -8 -6 -4 -2 0 2 4 6 8 10 12 14
X10¹
RADIUS (arcsec)

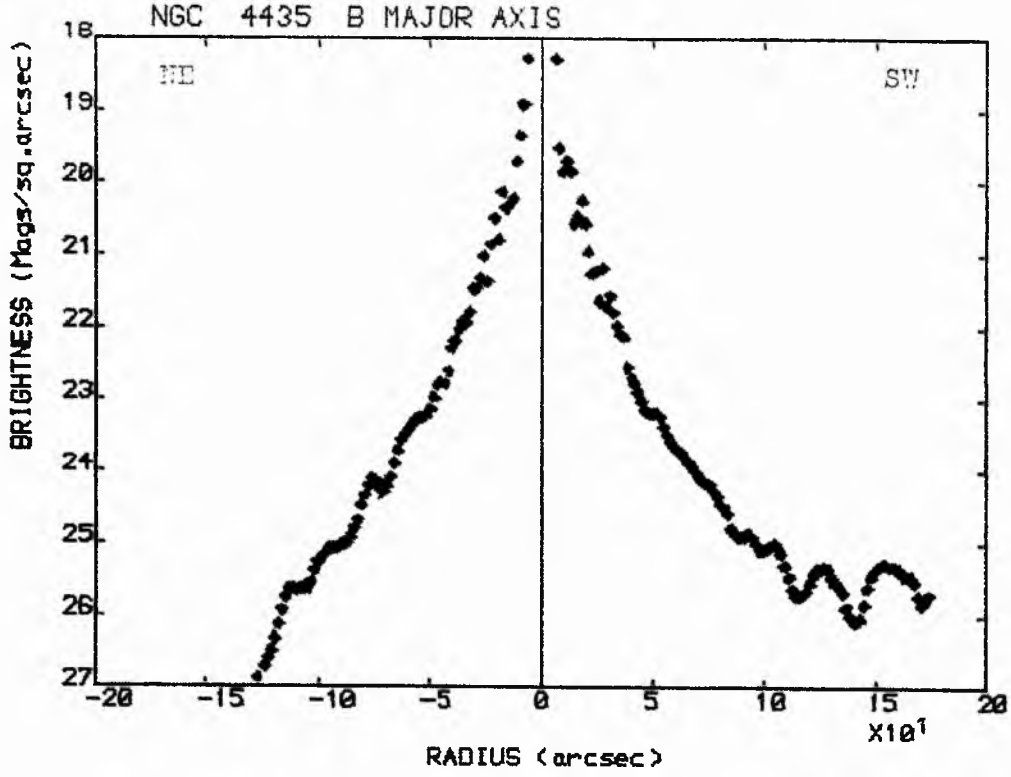
NGC 4435 B MAJOR AXIS
NE
SW
BRIGHTNESS (Mags/sq.arcsec)
18
19
20
21
22
23
24
25
26
27
-20
-15
-10
-5
0
5
10
15
20
X10¹
RADIUS (arcsec)

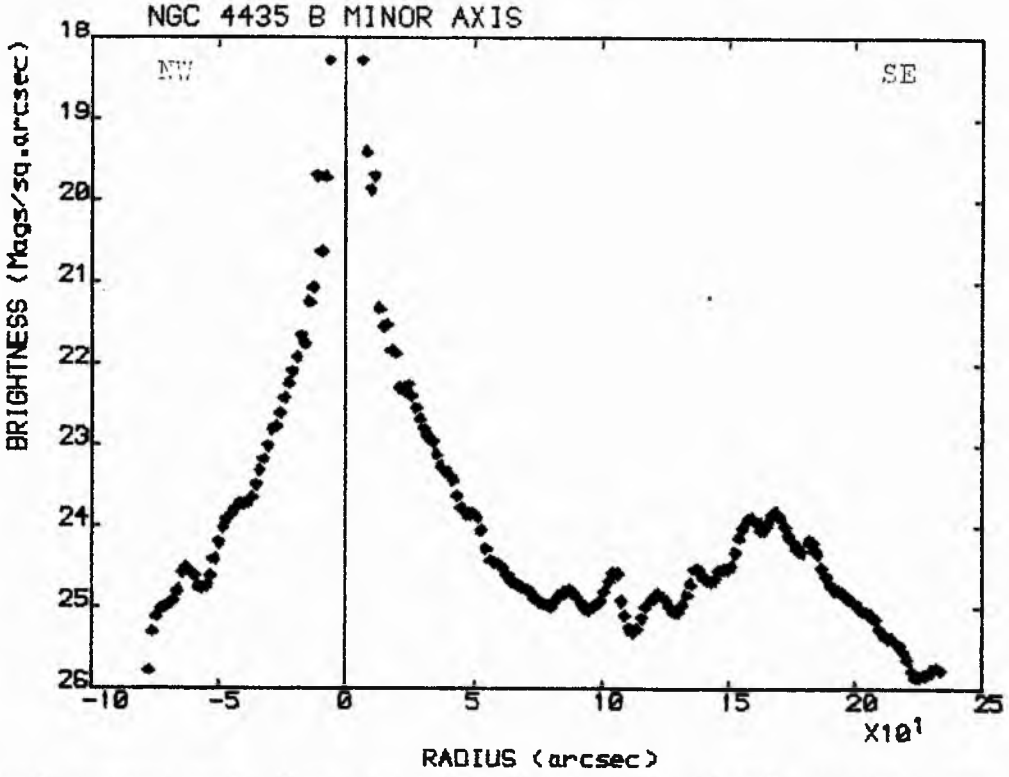
NGC 4435 B MINOR AXIS
NW
SE
BRIGHTNESS (Mags/sq.arcsec)
18
19
20
21
22
23
24
25
26
-10
-5
0
5
10
15
20
25
X10¹
RADIUS (arcsec)

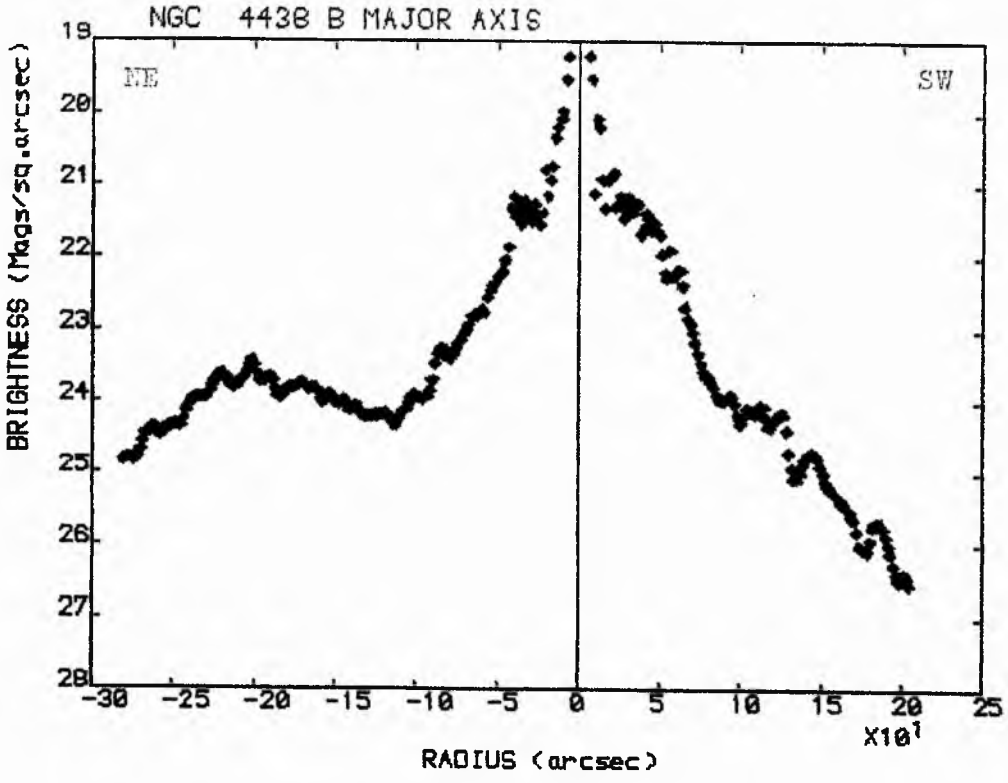
NGC 4438 B MAJOR AXIS
NE
SW
BRIGHTNESS (Mags/sq.arcsec)
19
20
21
22
23
24
25
26
27
28
-30 -25 -20 -15 -10 -5 0 5 10 15 20 25
X10¹
RADIUS (arcsec)

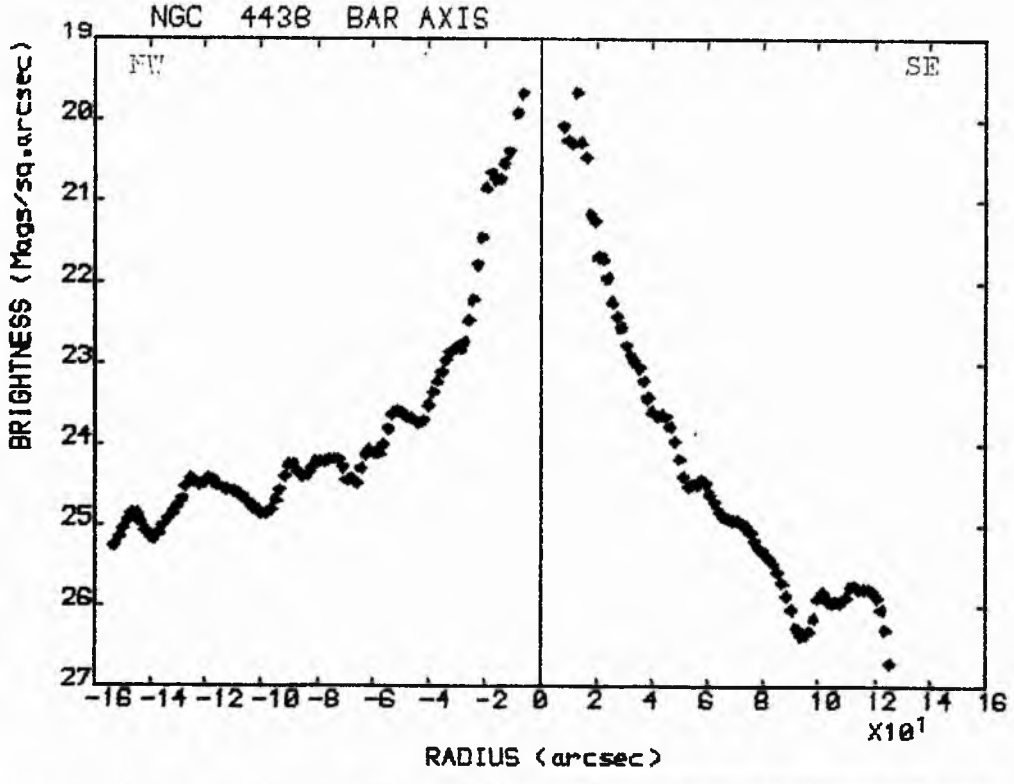
NGC 4438 BAR AXIS
NW
SE
BRIGHTNESS (Mags/sq.arcsec)
19
20
21
22
23
24
25
26
27
-16 -14 -12 -10 -8 -6 -4 -2 0 2 4 6 8 10 12 14 16
X10¹
RADIUS (arcsec)

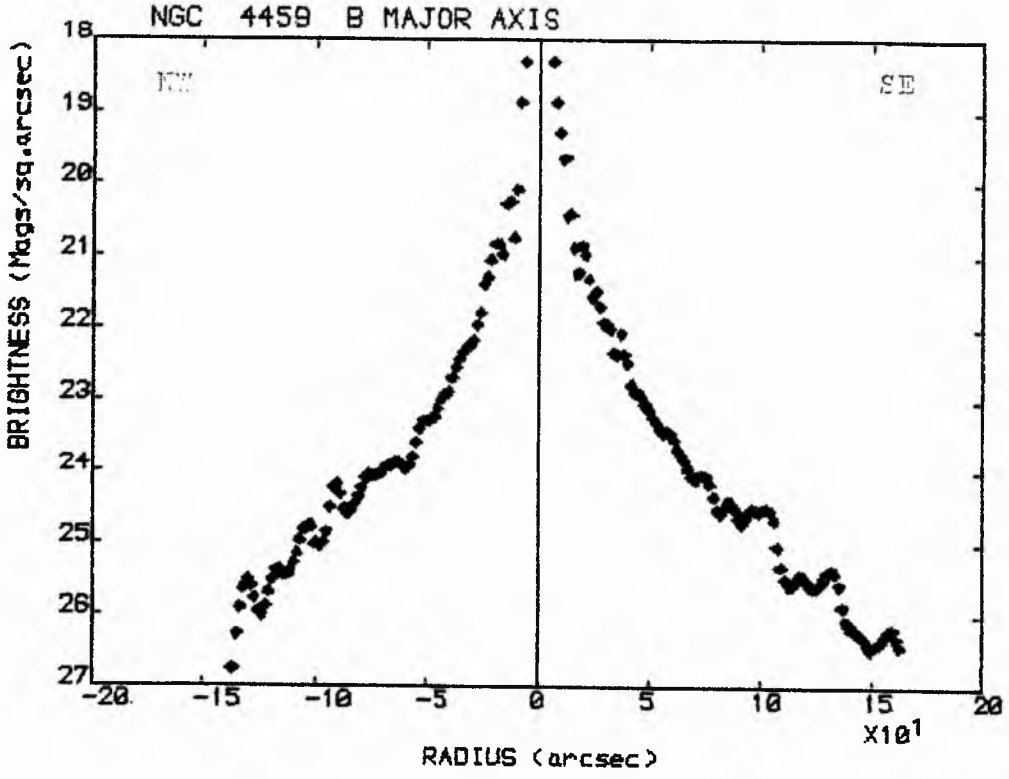
NGC 4459 B MAJOR AXIS
NW
SE
BRIGHTNESS (Mags/sq.arcsec)
18
19
20
21
22
23
24
25
26
27
-20
-15
-10
-5
0
5
10
15
20
X10¹
RADIUS (arcsec)

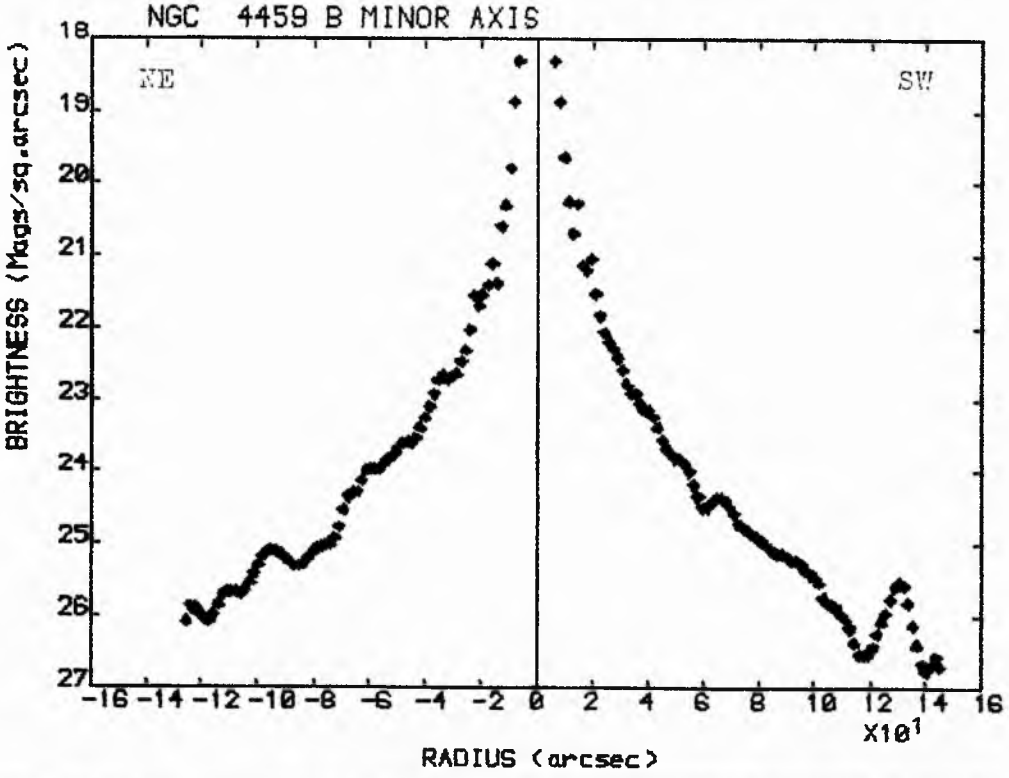
NGC 4459 B MINOR AXIS
NE
SW
BRIGHTNESS (Mags/sq.arcsec)
18
19
20
21
22
23
24
25
26
27
-16 -14 -12 -10 -8 -6 -4 -2 0 2 4 6 8 10 12 14 16
X10¹
RADIUS (arcsec)

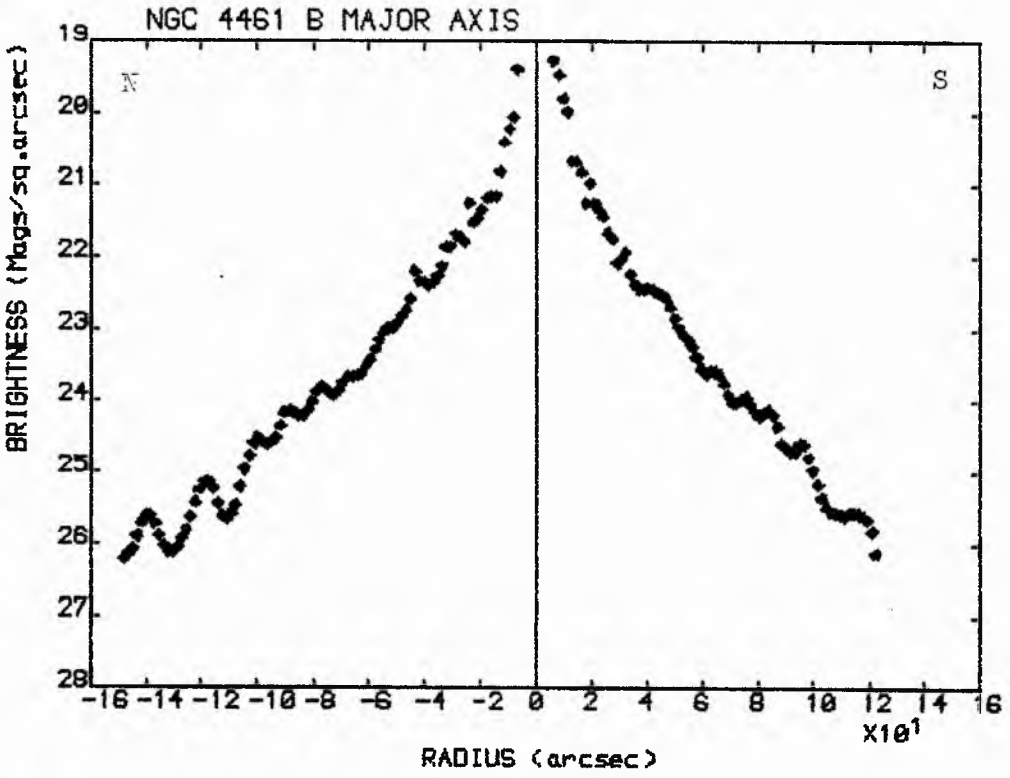
NGC 4461 B MAJOR AXIS
N
S
BRIGHTNESS (Mags/sq.arcsec)
19
20
21
22
23
24
25
26
27
28
-16 -14 -12 -10 -8 -6 -4 -2 0 2 4 6 8 10 12 14 16
X10¹
RADIUS (arcsec)

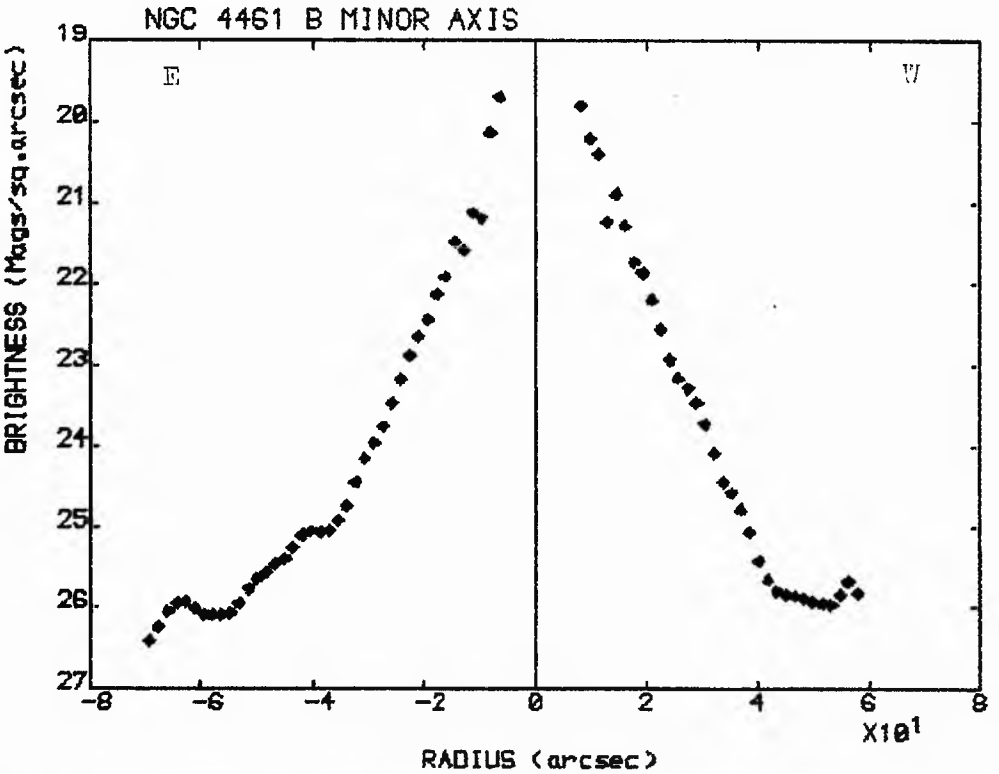
NGC 4461 B MINOR AXIS
E
W
BRIGHTNESS (Mags/sq.arcsec)
19
20
21
22
23
24
25
26
27
-8 -6 -4 -2 0 2 4 6 8
X10¹
RADIUS (arcsec)

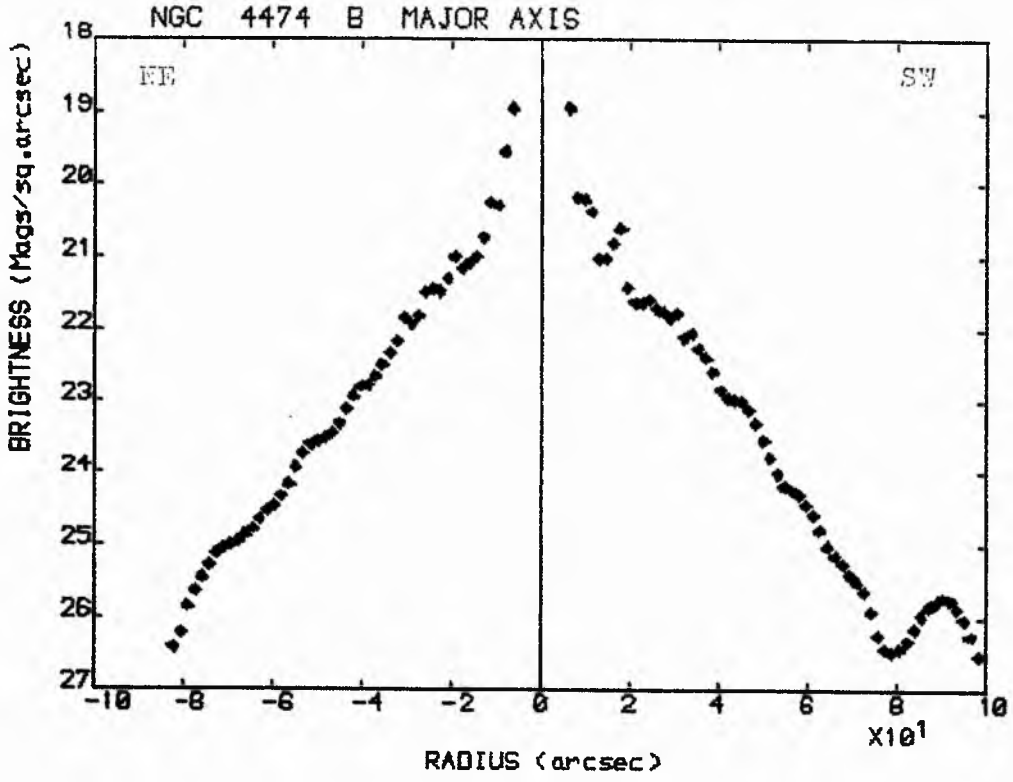
NGC 4474 B MAJOR AXIS
NE
SW
BRIGHTNESS (Mags/sq.arcsec)
18
19
20
21
22
23
24
25
26
27
-10
-8
-6
-4
-2
0
2
4
6
8
10
X10¹
RADIUS (arcsec)

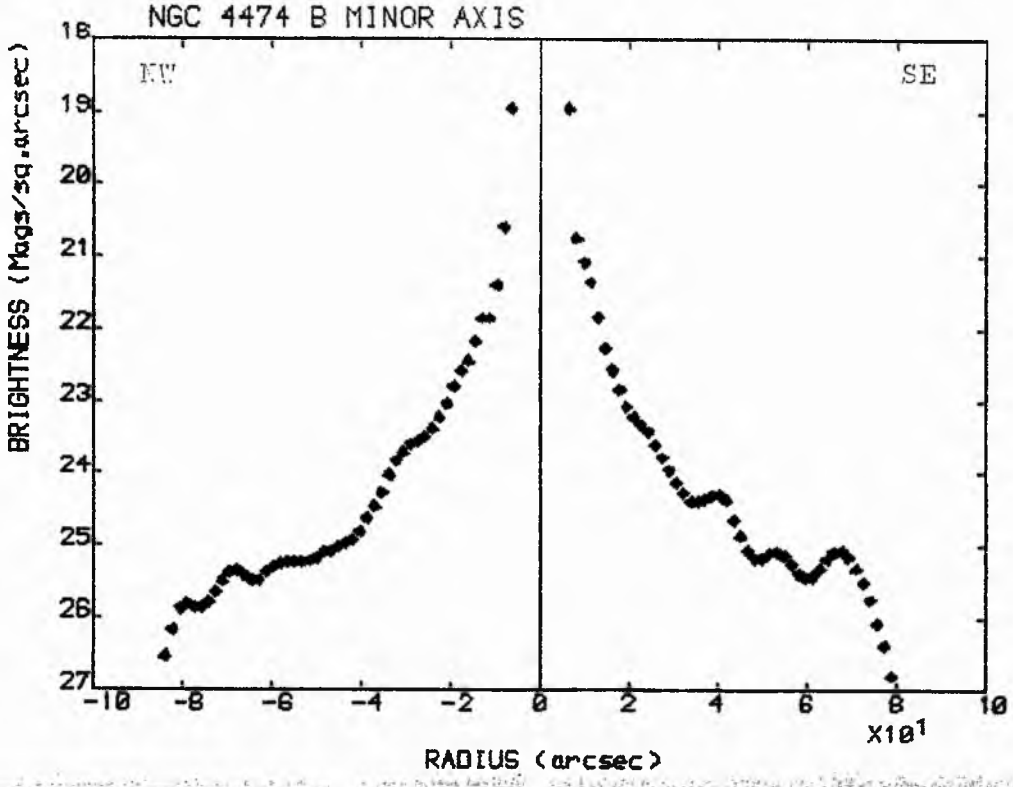
NGC 4474 B MINOR AXIS
NW
SE
BRIGHTNESS (Mags/sq.arcsec)
18
19
20
21
22
23
24
25
26
27
-10
-8
-6
-4
-2
0
2
4
6
8
10
X10¹
RADIUS (arcsec)

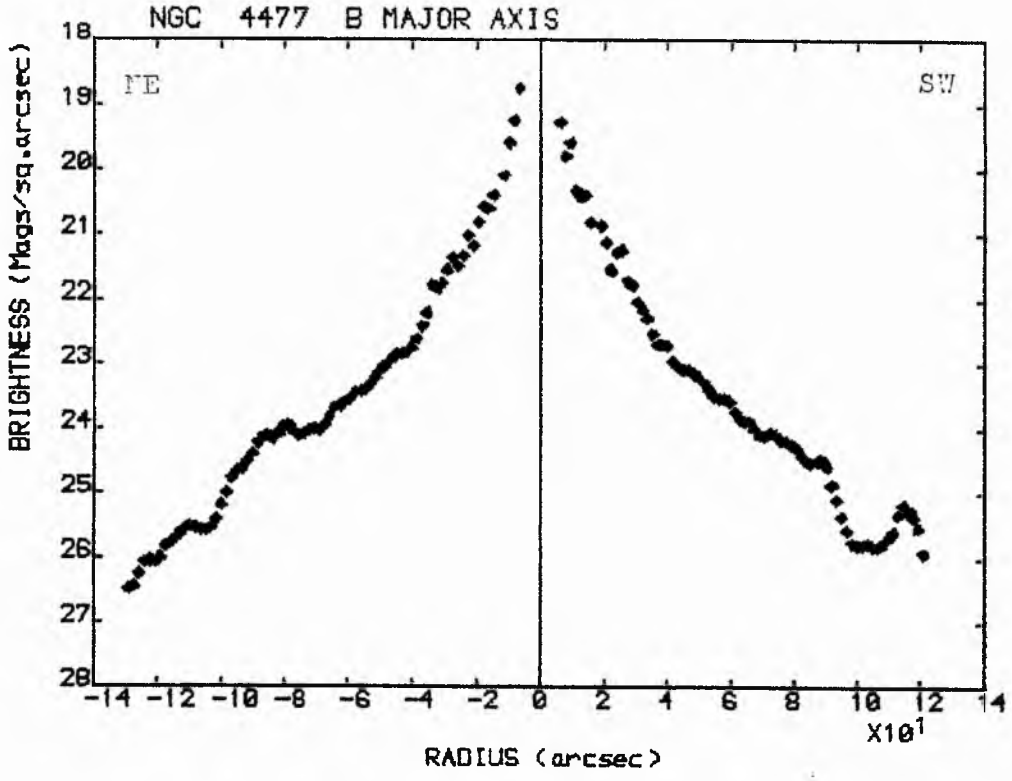
NGC 4477 B MAJOR AXIS
NE
SW
BRIGHTNESS (Mags/sq.arcsec)
18
19
20
21
22
23
24
25
26
27
28
-14 -12 -10 -8 -6 -4 -2 0 2 4 6 8 10 12 14
X10¹
RADIUS (arcsec)

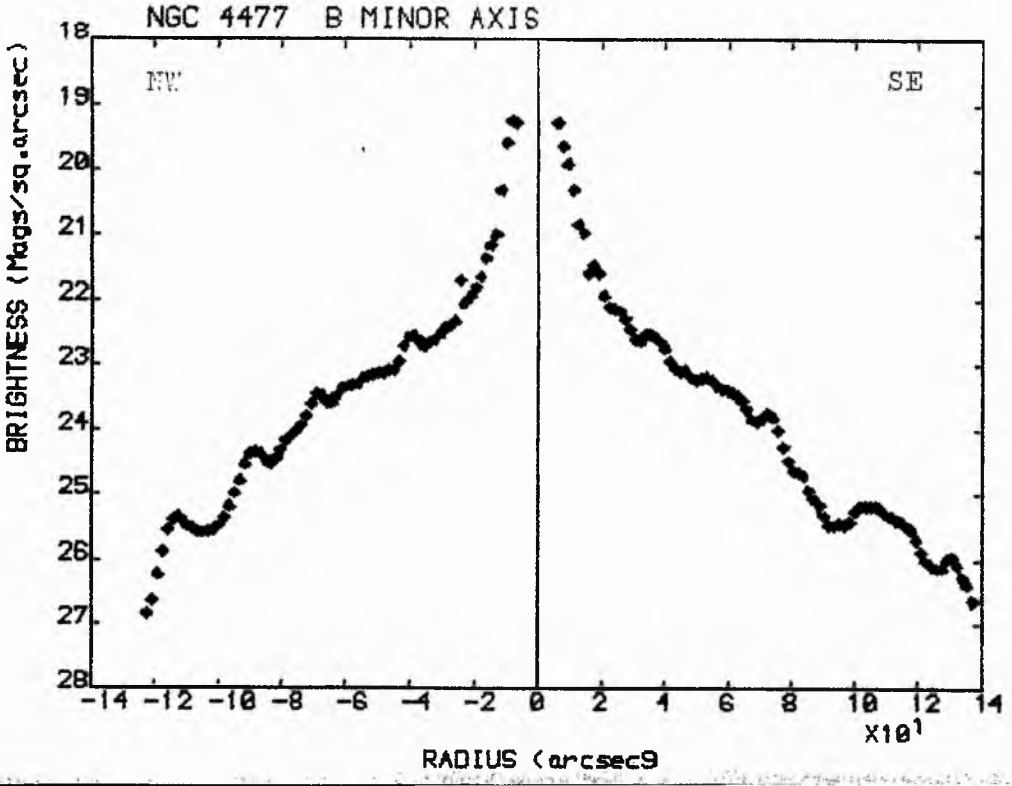
NGC 4477 B MINOR AXIS
NW
SE
BRIGHTNESS (Mags/sq.arcsec)
18
19
20
21
22
23
24
25
26
27
28
-14 -12 -10 -8 -6 -4 -2 0 2 4 6 8 10 12 14
X10¹
RADIUS (arcsec9

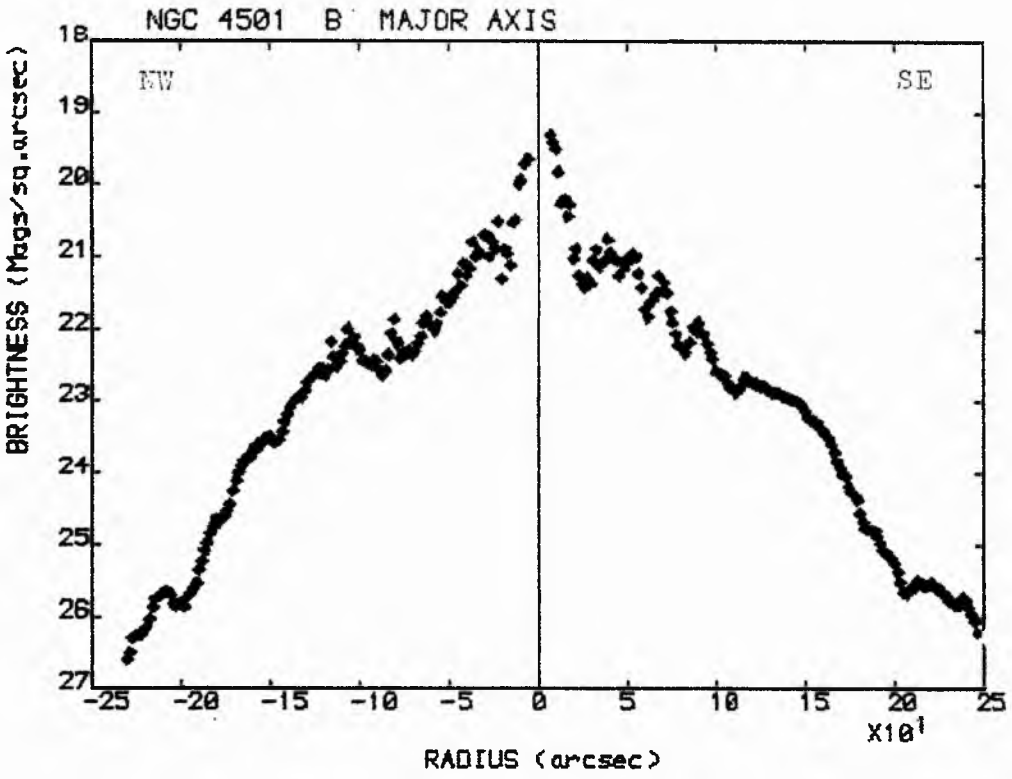
NGC 4501 B MAJOR AXIS
NW
SE
BRIGHTNESS (Mags/sq.arcsec)
18
19
20
21
22
23
24
25
26
27
-25 -20 -15 -10 -5 0 5 10 15 20 25
X10¹
RADIUS (arcsec)

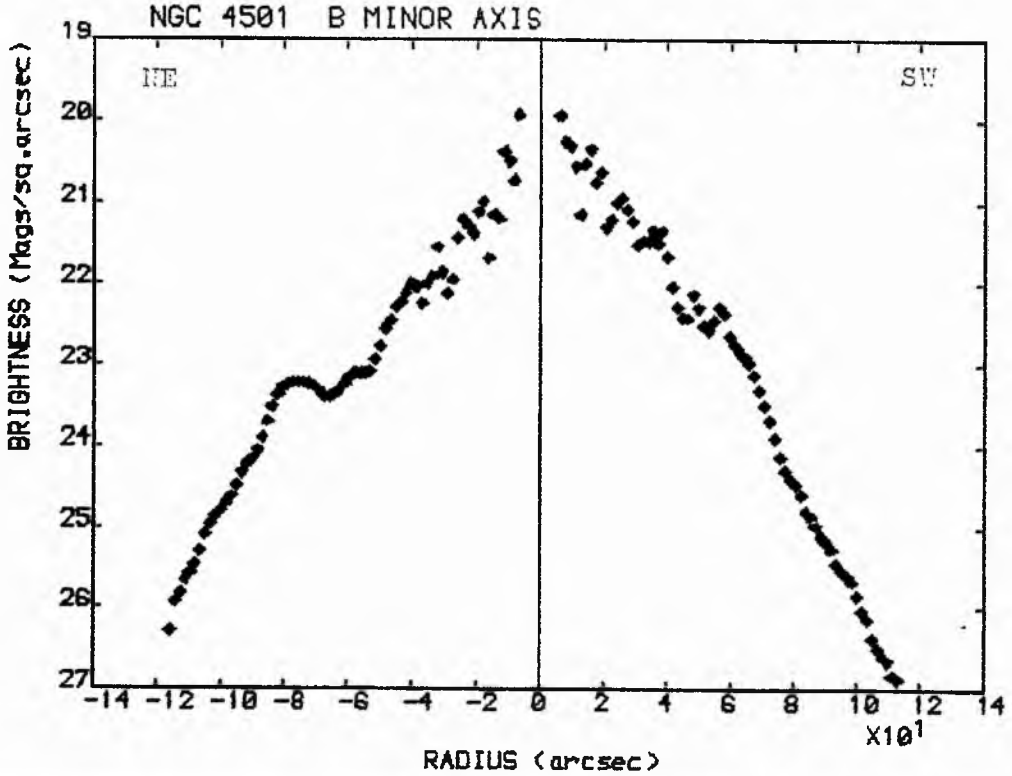
NGC 4501 B MINOR AXIS
NE
SW
BRIGHTNESS (Mags/sq.arcsec)
19
20
21
22
23
24
25
26
27
-14 -12 -10 -8 -6 -4 -2 0 2 4 6 8 10 12 14
X10¹
RADIUS (arcsec)

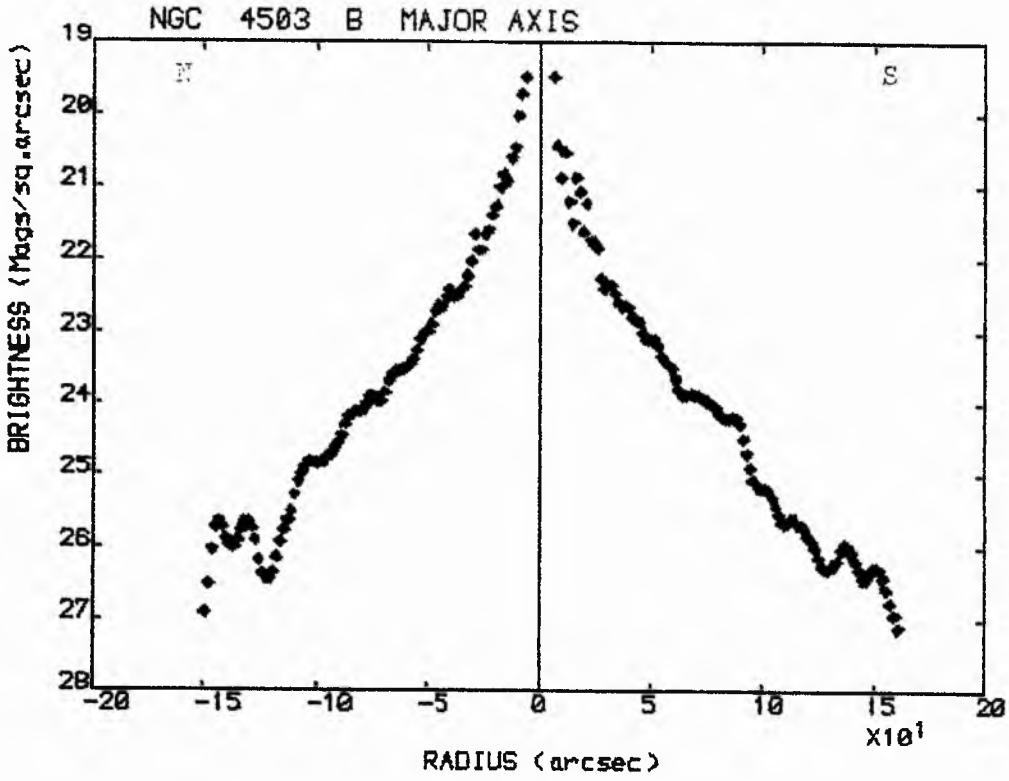
NGC 4503 B MAJOR AXIS
N
S
BRIGHTNESS (Mags/sq.arcsec)
19
20
21
22
23
24
25
26
27
28
-20
-15
-10
-5
0
5
10
15
20
X10¹
RADIUS (arcsec)

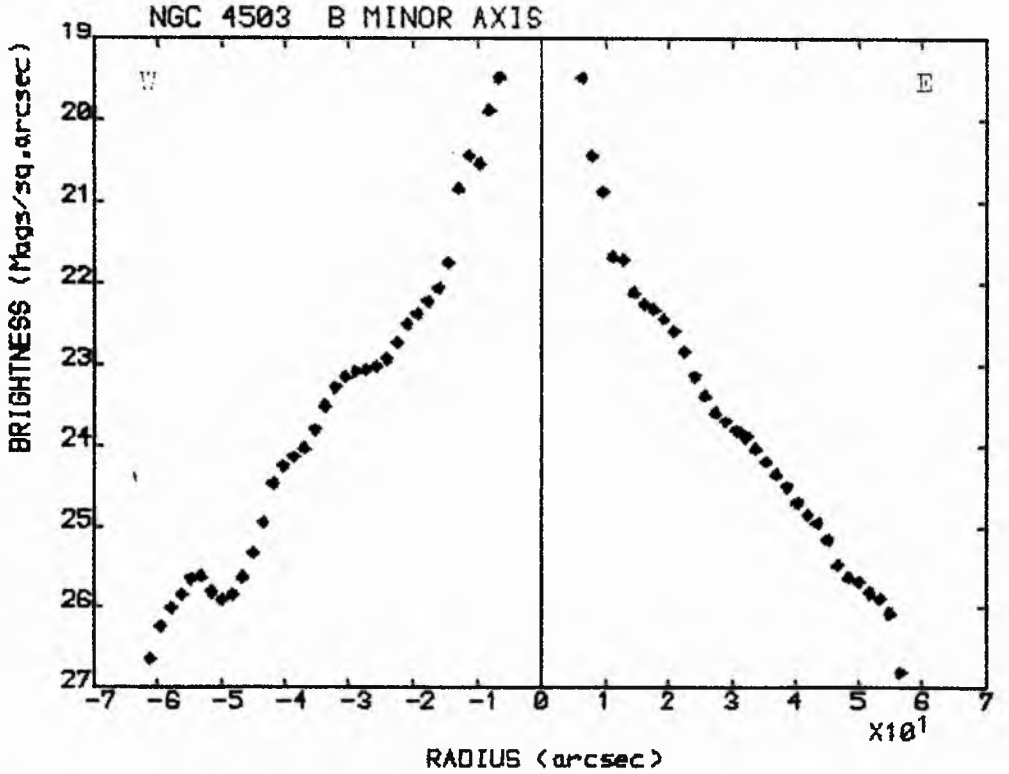
NGC 4503 B MINOR AXIS
W
E
BRIGHTNESS (Mags/sq.arcsec)
19
20
21
22
23
24
25
26
27
-7
-6
-5
-4
-3
-2
-1
0
1
2
3
4
5
6
7
X10¹
RADIUS (arcsec)

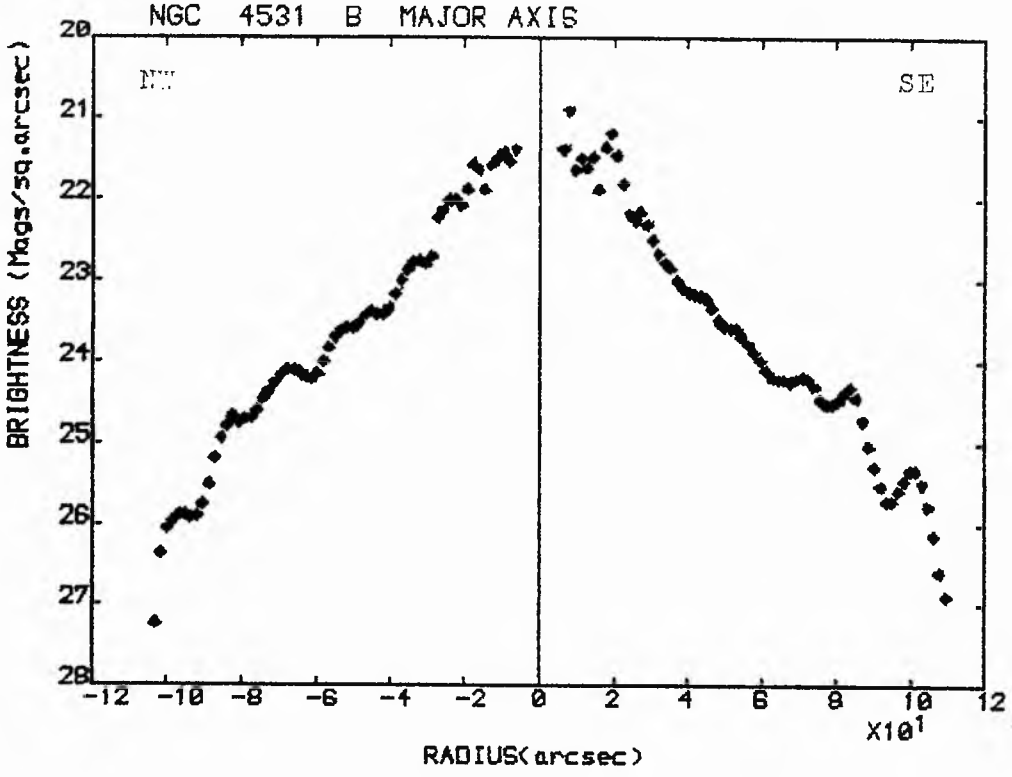
NGC 4531 B MAJOR AXIS
NW
SE
BRIGHTNESS (Mags/sq.arcsec)
20
21
22
23
24
25
26
27
28
-12 -10 -8 -6 -4 -2 0 2 4 6 8 10 12
X10¹
RADIUS(arcsec)

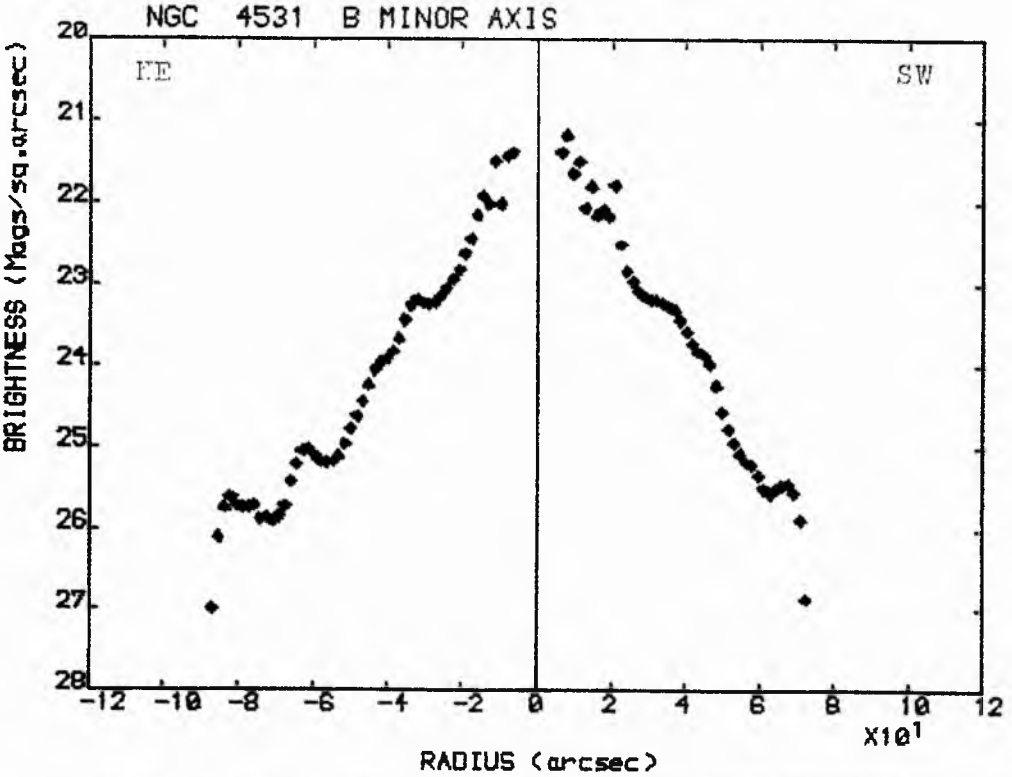
NGC 4531 B MINOR AXIS
NE
SW
BRIGHTNESS (Mags/sq.arcsec)
20
21
22
23
24
25
26
27
28
-12 -10 -8 -6 -4 -2 0 2 4 6 8 10 12
X10¹
RADIUS (arcsec)

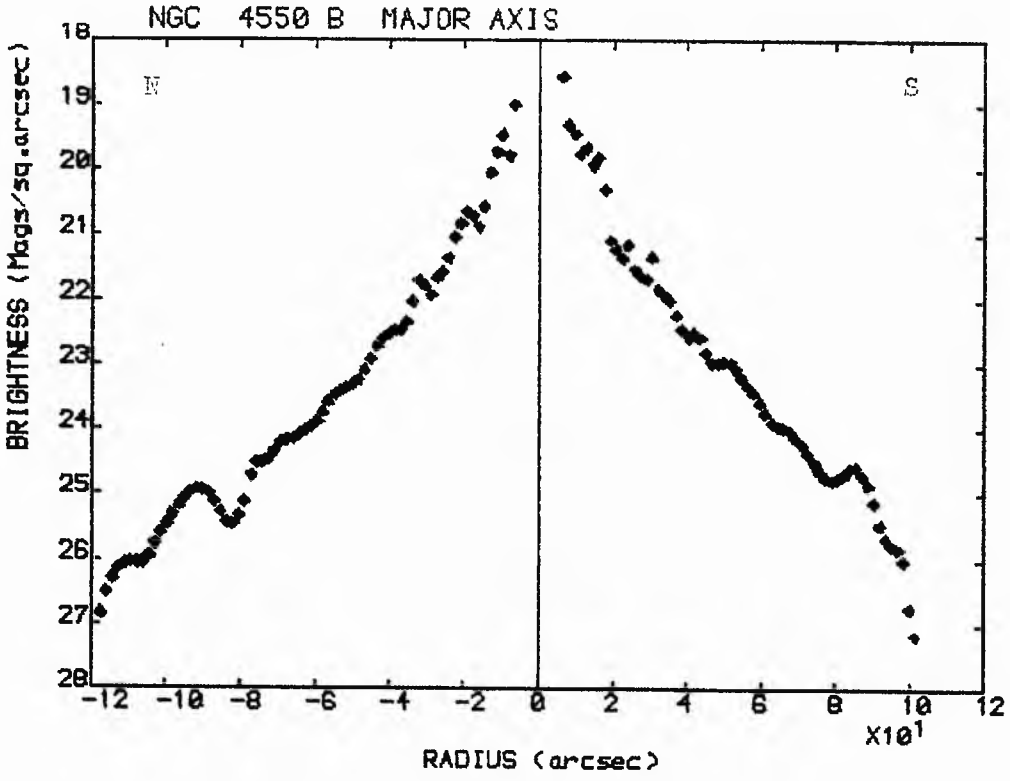
NGC 4550 B MAJOR AXIS
N
S
BRIGHTNESS (Mags/sq.arcsec)
18
19
20
21
22
23
24
25
26
27
28
-12
-10
-8
-6
-4
-2
0
2
4
6
8
10
12
X10¹
RADIUS (arcsec)

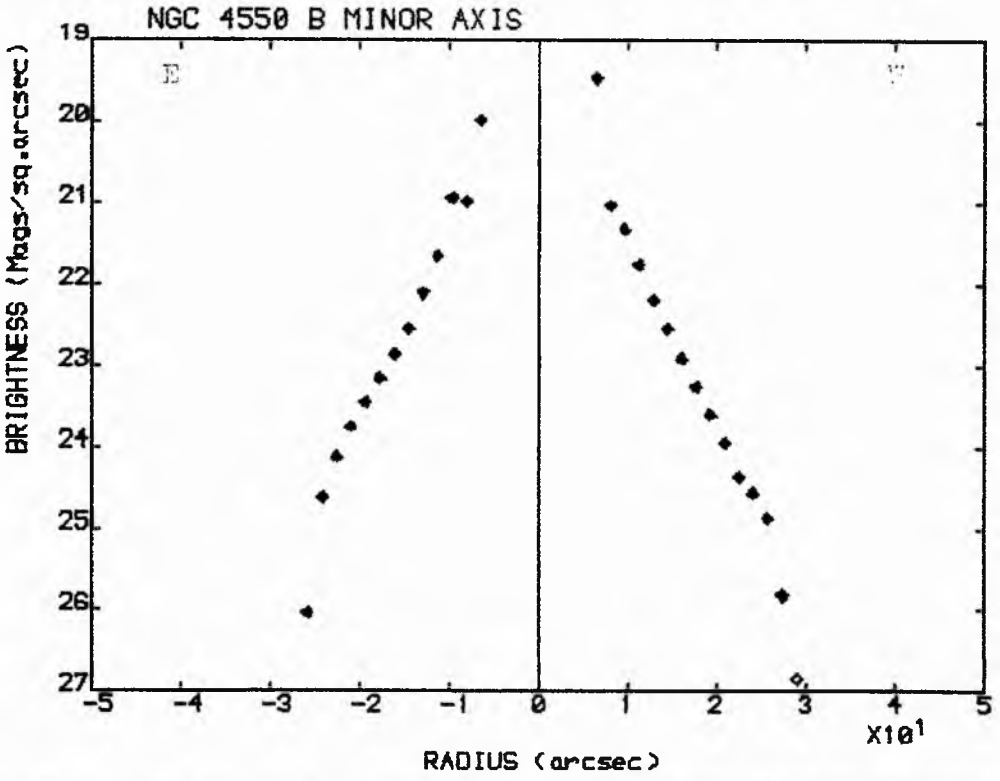
NGC 4550 B MINOR AXIS
E
W
BRIGHTNESS (Mags/sq.arcsec)
19
20
21
22
23
24
25
26
27
-5
-4
-3
-2
-1
0
1
2
3
4
5
X10¹
RADIUS (arcsec)

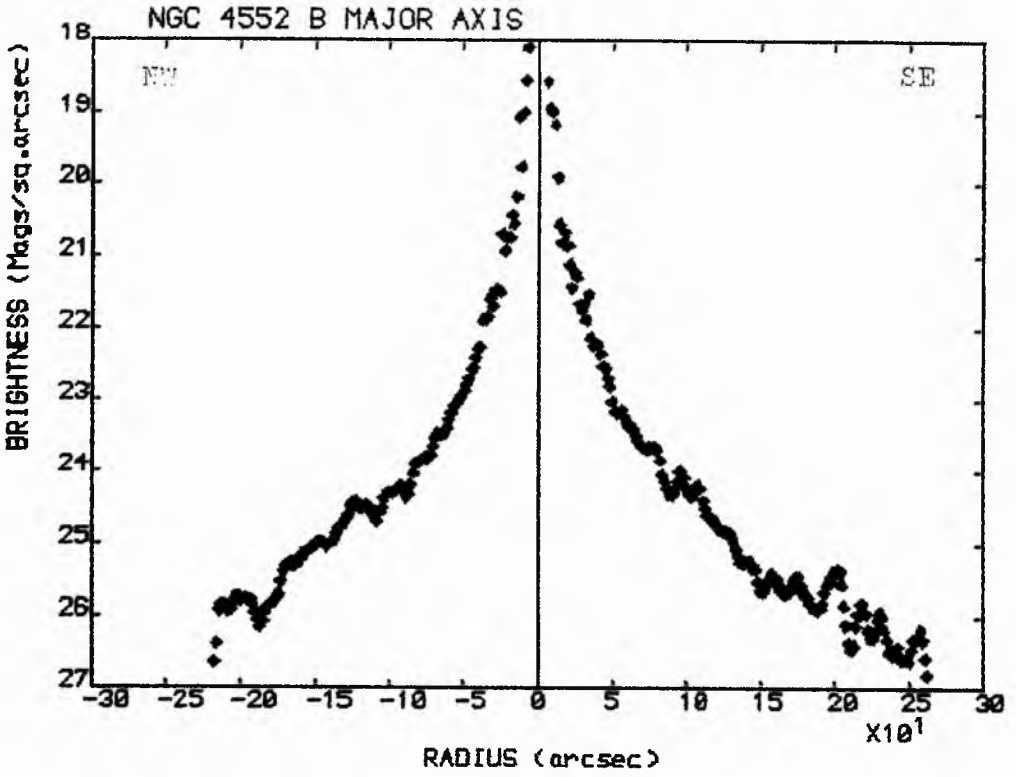
NGC 4552 B MAJOR AXIS
NW
SE
BRIGHTNESS (Mags/sq.arcsec)
18
19
20
21
22
23
24
25
26
27
-30 -25 -20 -15 -10 -5 0 5 10 15 20 25 30
X10¹
RADIUS (arcsec)

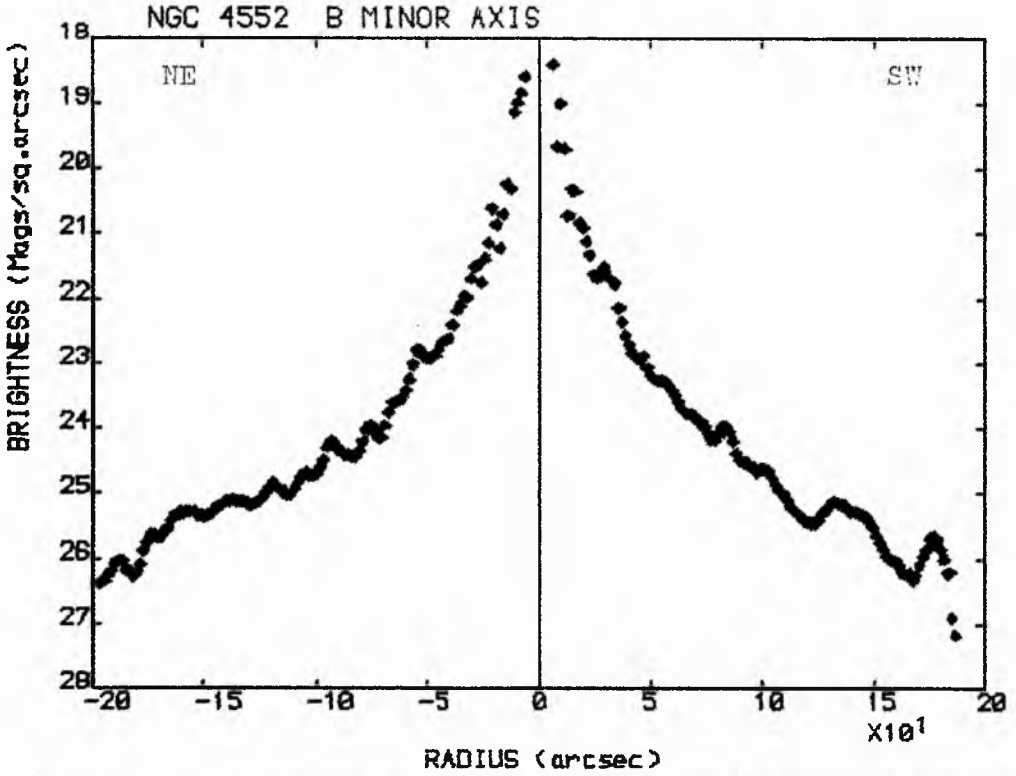
NGC 4552 B MINOR AXIS
NE
SW
BRIGHTNESS (Mags/sq.arcsec)
18
19
20
21
22
23
24
25
26
27
28
-20 -15 -10 -5 0 5 10 15 20
X10¹
RADIUS (arcsec)

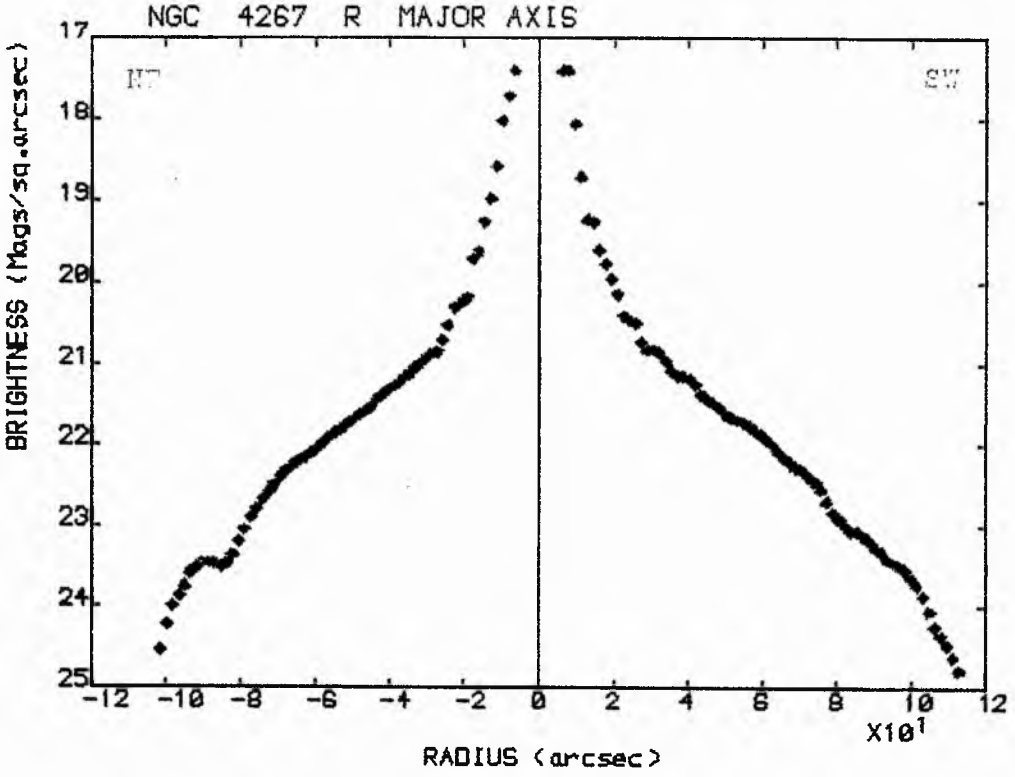
NGC 4267 R MAJOR AXIS
NE
SW
BRIGHTNESS (Mags/sq.arcsec)
17
18
19
20
21
22
23
24
25
-12 -10 -8 -6 -4 -2 0 2 4 6 8 10 12
X10¹
RADIUS (arcsec)

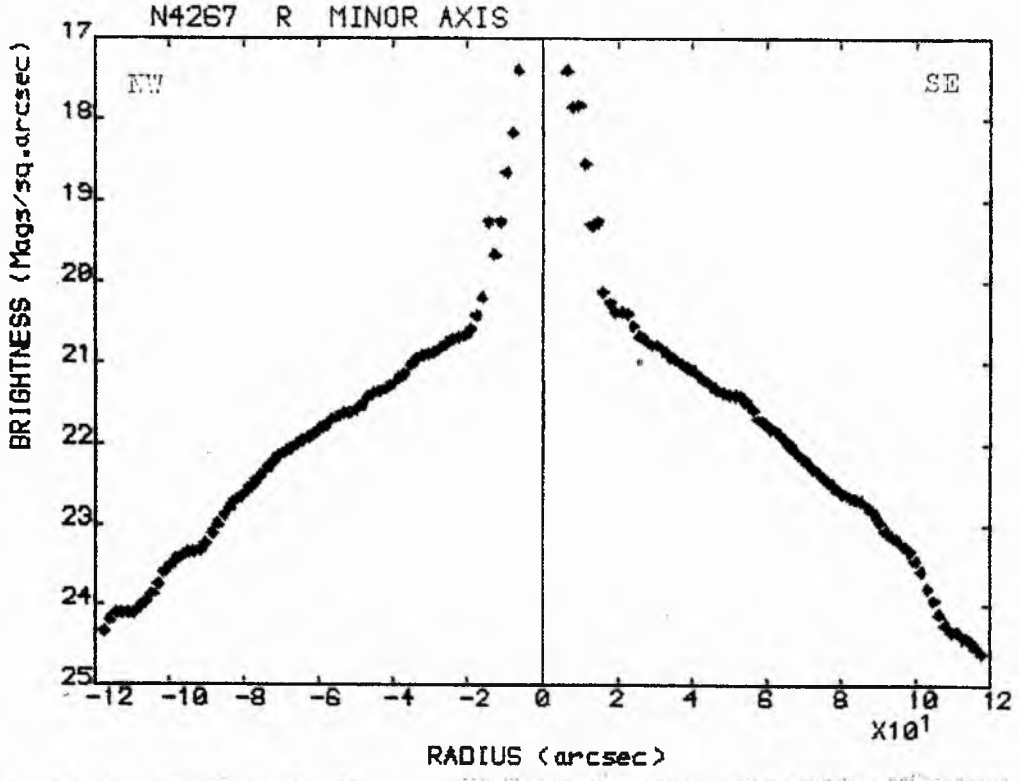
N4267 R MINOR AXIS
NW
SE
BRIGHTNESS (Mags/sq.arcsec)
17
18
19
20
21
22
23
24
25
-12 -10 -8 -6 -4 -2 0 2 4 6 8 10 12
X10¹
RADIUS (arcsec)

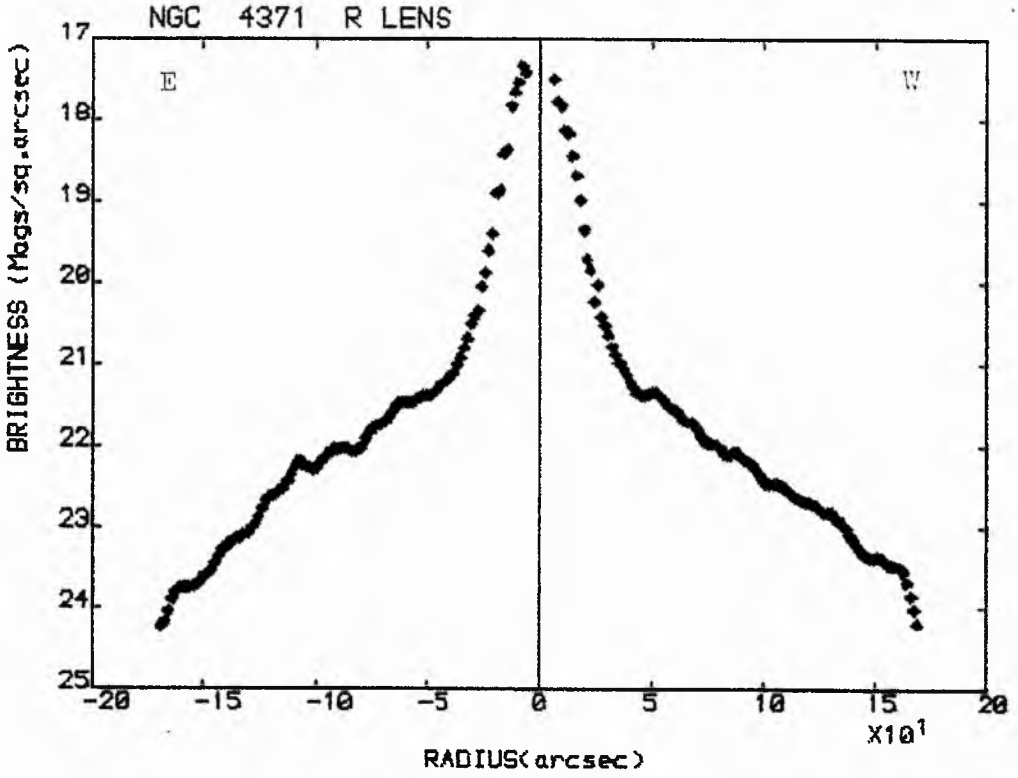
NGC 4371 R LENS
E
W
BRIGHTNESS (Mags/sq.arcsec)
17
18
19
20
21
22
23
24
25
-20
-15
-10
-5
0
5
10
15
20
X10¹
RADIUS(arcsec)

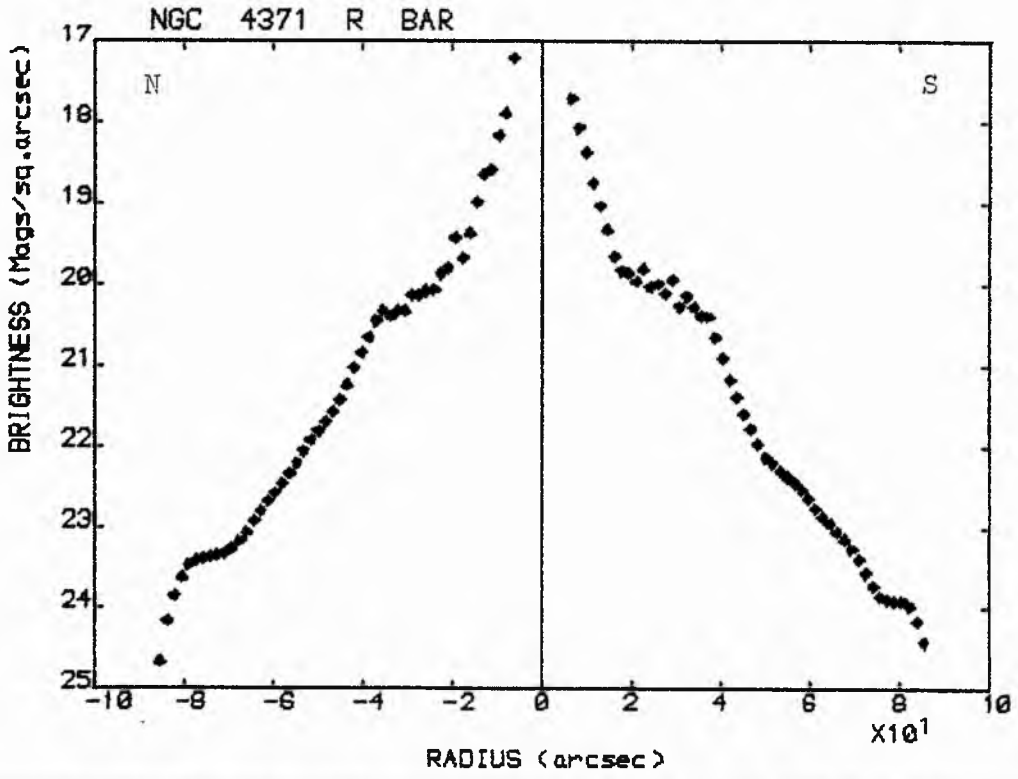
NGC 4371 R BAR
N
S
BRIGHTNESS (Mags/sq.arcsec)
17
18
19
20
21
22
23
24
25
-10
-8
-6
-4
-2
0
2
4
6
8
10
X10¹
RADIUS (arcsec)

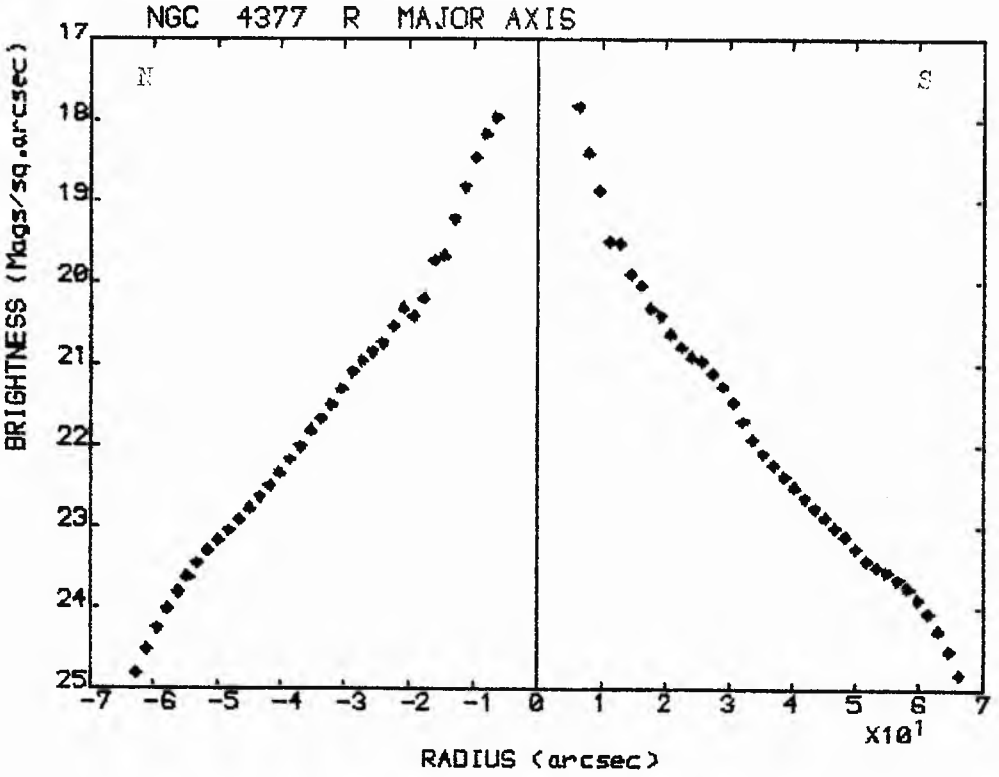
NGC 4377 R MAJOR AXIS
N
S
BRIGHTNESS (Mags/sq.arcsec)
17
18
19
20
21
22
23
24
25
-7 -6 -5 -4 -3 -2 -1 0 1 2 3 4 5 6 7
X10¹
RADIUS (arcsec)

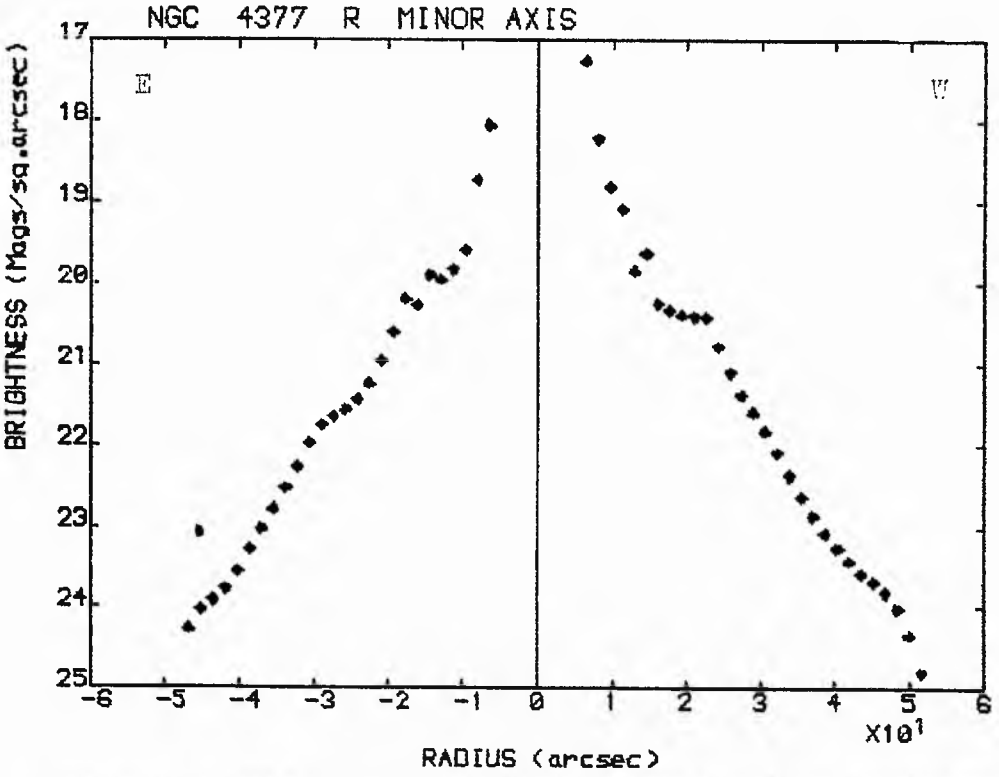
NGC 4377 R MINOR AXIS
E
W
BRIGHTNESS (Mags/sq.arcsec)
17
18
19
20
21
22
23
24
25
-6 -5 -4 -3 -2 -1 0 1 2 3 4 5 6
X10¹
RADIUS (arcsec)

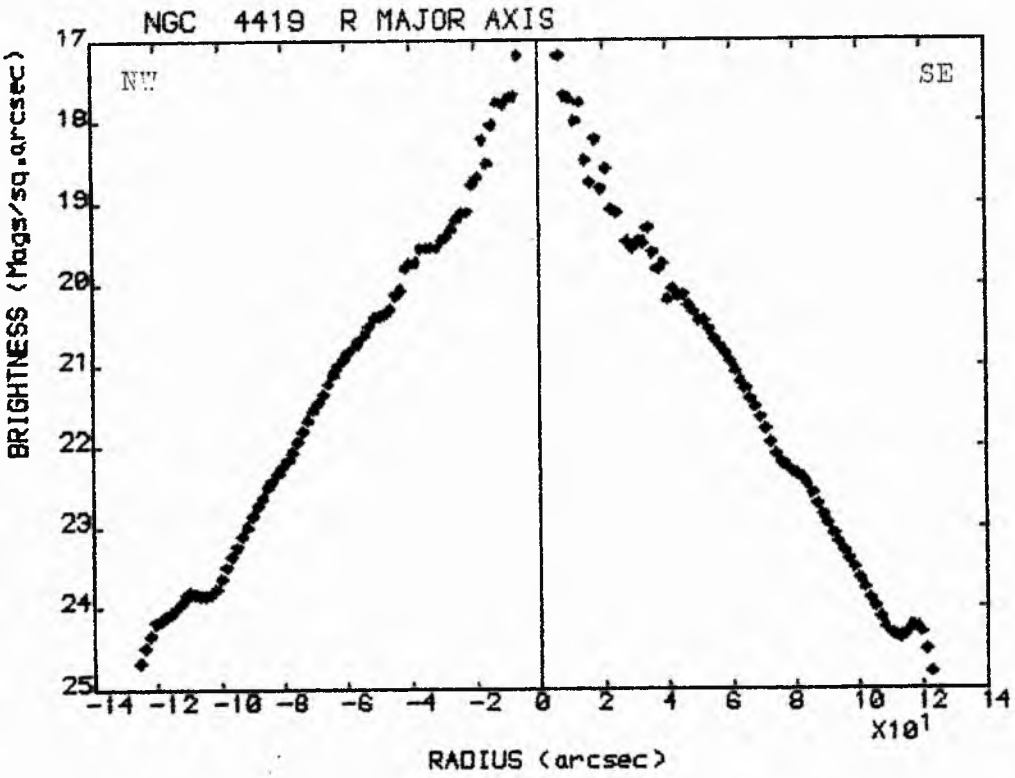
NGC 4419 R MAJOR AXIS
NW
SE
BRIGHTNESS (Mags/sq.arcsec)
17
18
19
20
21
22
23
24
25
-14 -12 -10 -8 -6 -4 -2 0 2 4 6 8 10 12 14
X10¹
RADIUS (arcsec)

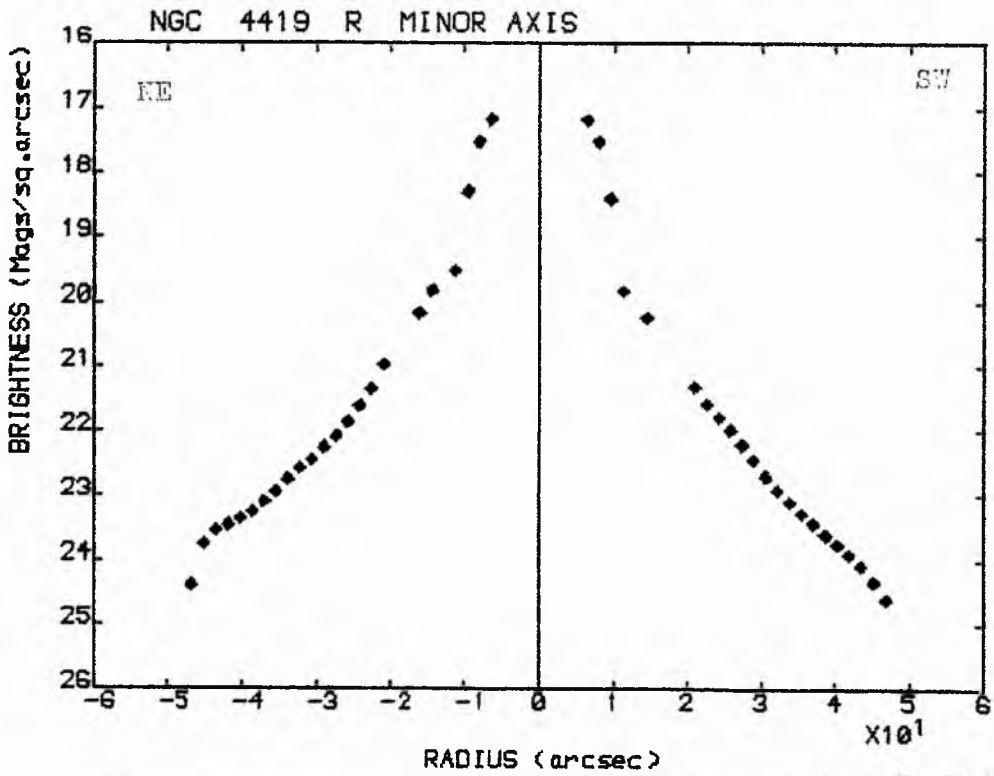
NGC 4419 R MINOR AXIS
NE
SW
BRIGHTNESS (Mags/sq.arcsec)
16
17
18
19
20
21
22
23
24
25
26
-6 -5 -4 -3 -2 -1 0 1 2 3 4 5 6
X10¹
RADIUS (arcsec)

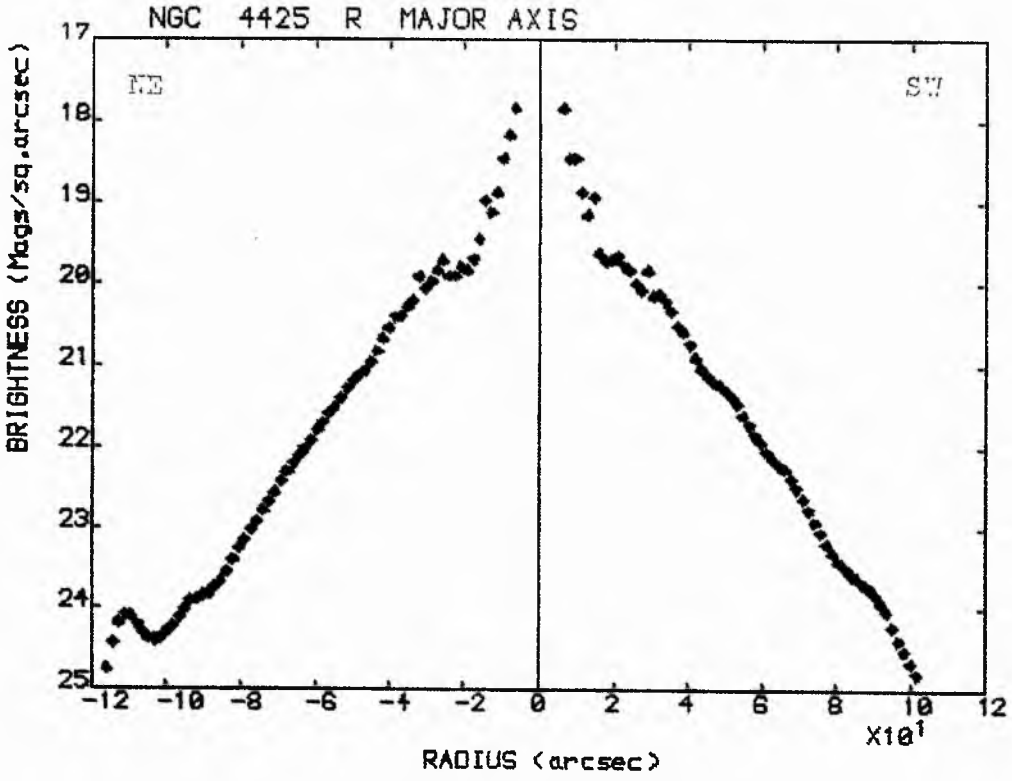
NGC 4425 R MAJOR AXIS
NE
SW
BRIGHTNESS (Mags/sq.arcsec)
17
18
19
20
21
22
23
24
25
-12 -10 -8 -6 -4 -2 0 2 4 6 8 10 12
X10¹
RADIUS (arcsec)

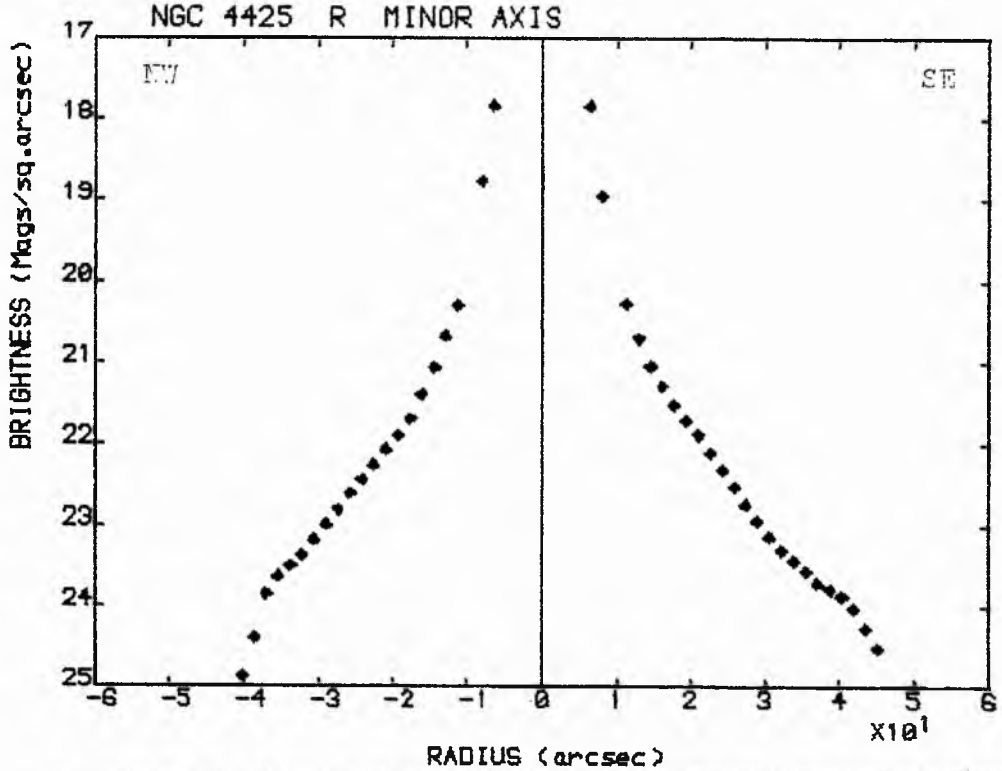
NGC 4425 R MINOR AXIS
NW
SE
BRIGHTNESS (Mags/sq.arcsec)
17
18
19
20
21
22
23
24
25
-6 -5 -4 -3 -2 -1 0 1 2 3 4 5 6
X10¹
RADIUS (arcsec)

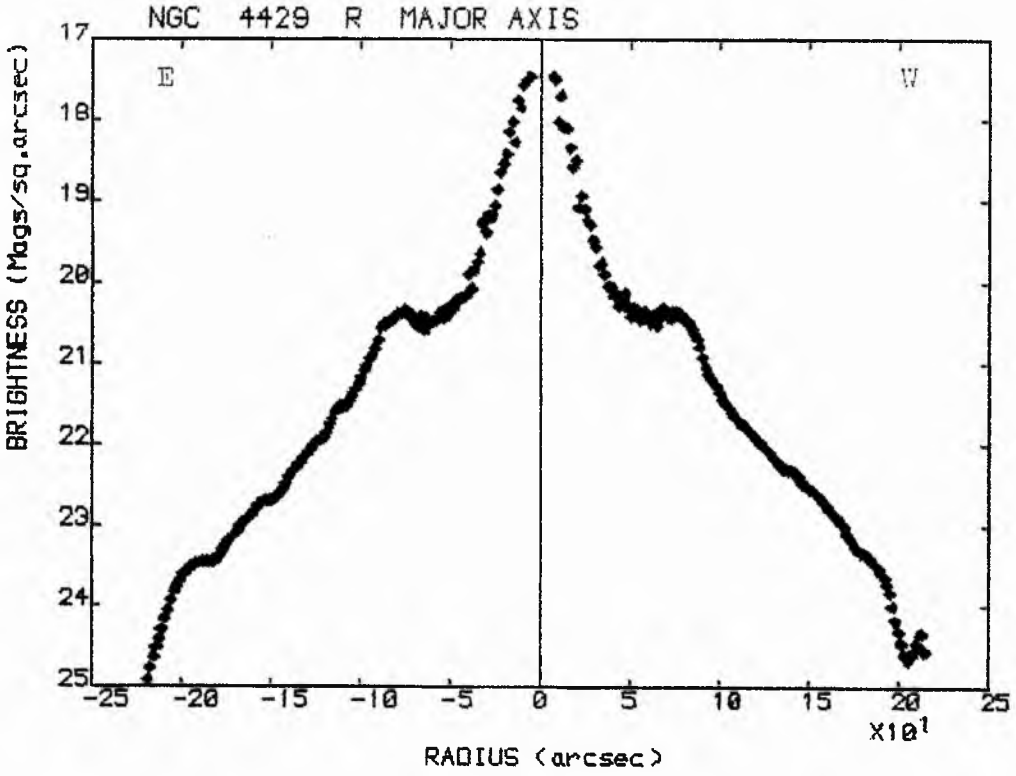
NGC 4429 R MAJOR AXIS
E
W
BRIGHTNESS (Mags/sq.arcsec)
17
18
19
20
21
22
23
24
25
-25 -20 -15 -10 -5 0 5 10 15 20 25
X10¹
RADIUS (arcsec)

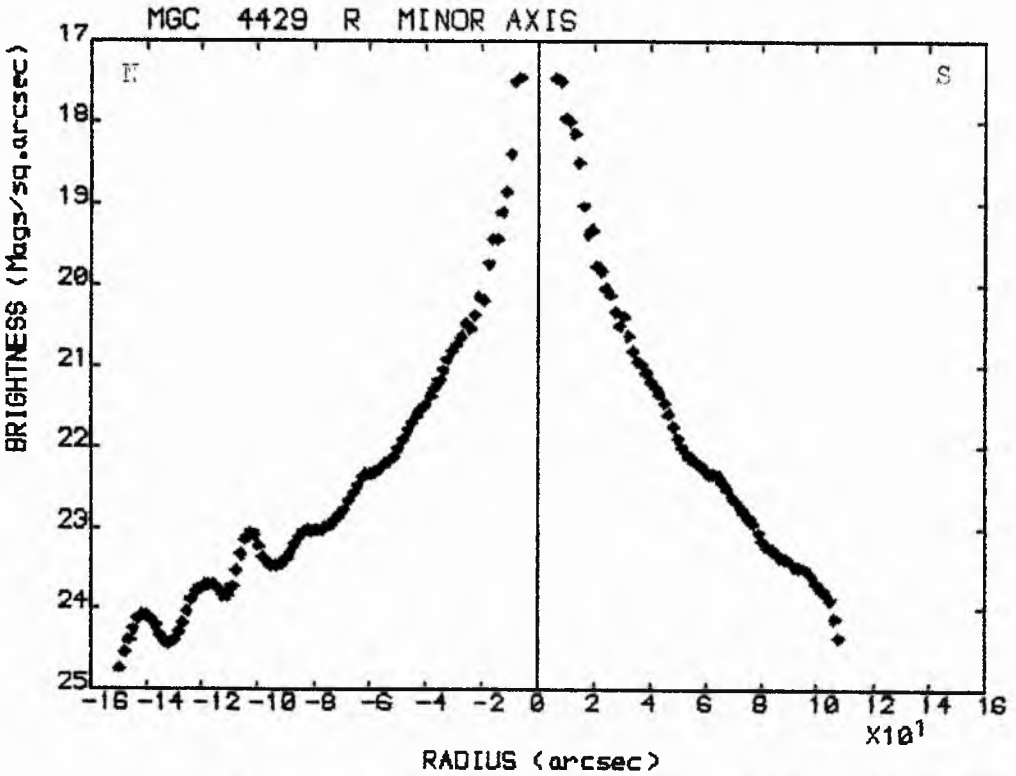
MGC 4429 R MINOR AXIS
N
S
BRIGHTNESS (Mags/sq.arcsec)
17
18
19
20
21
22
23
24
25
-16 -14 -12 -10 -8 -6 -4 -2 0 2 4 6 8 10 12 14 16
X10¹
RADIUS (arcsec)

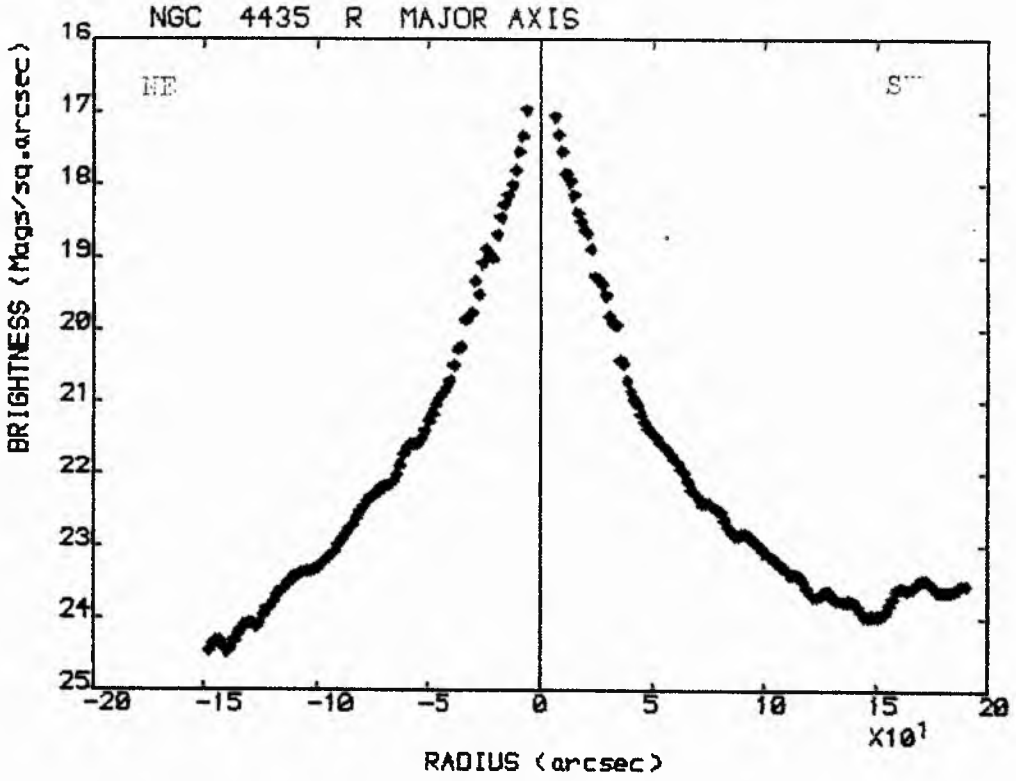
NGC 4435 R MAJOR AXIS
NE
S
BRIGHTNESS (Mags/sq.arcsec)
16
17
18
19
20
21
22
23
24
25
-20
-15
-10
-5
0
5
10
15
20
X10¹
RADIUS (arcsec)

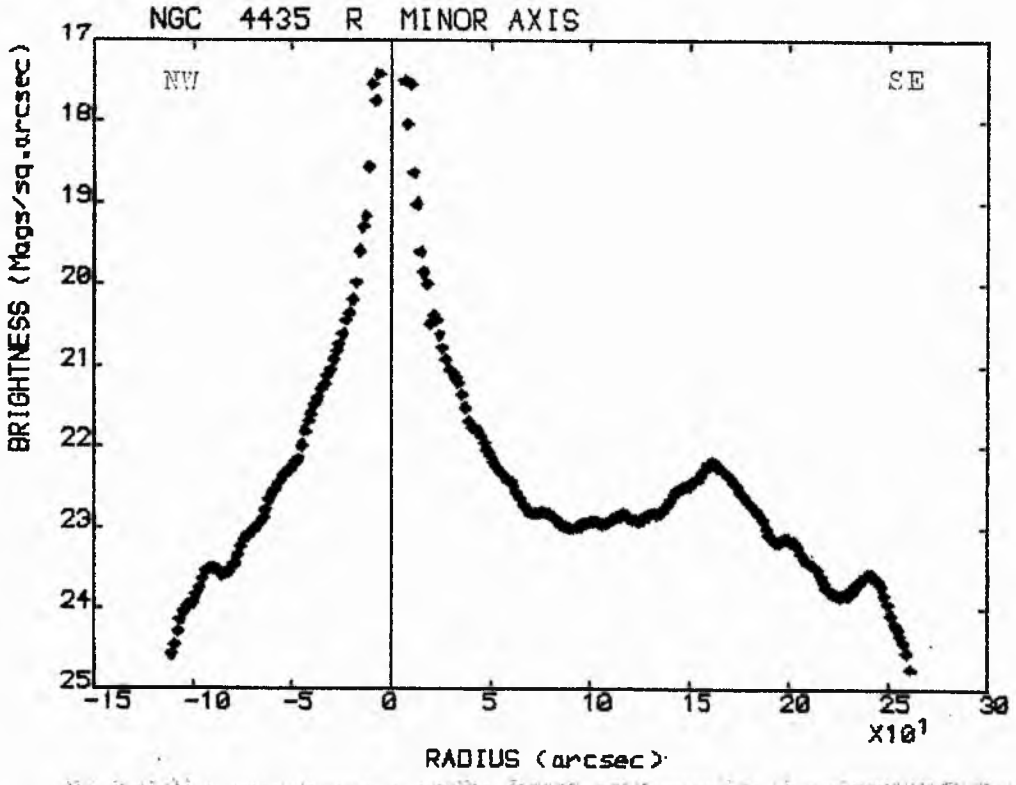
NGC 4435 R MINOR AXIS
NW
SE
BRIGHTNESS (Mags/sq.arcsec)
17
18
19
20
21
22
23
24
25
-15
-10
-5
0
5
10
15
20
25
30
X10¹
RADIUS (arcsec)

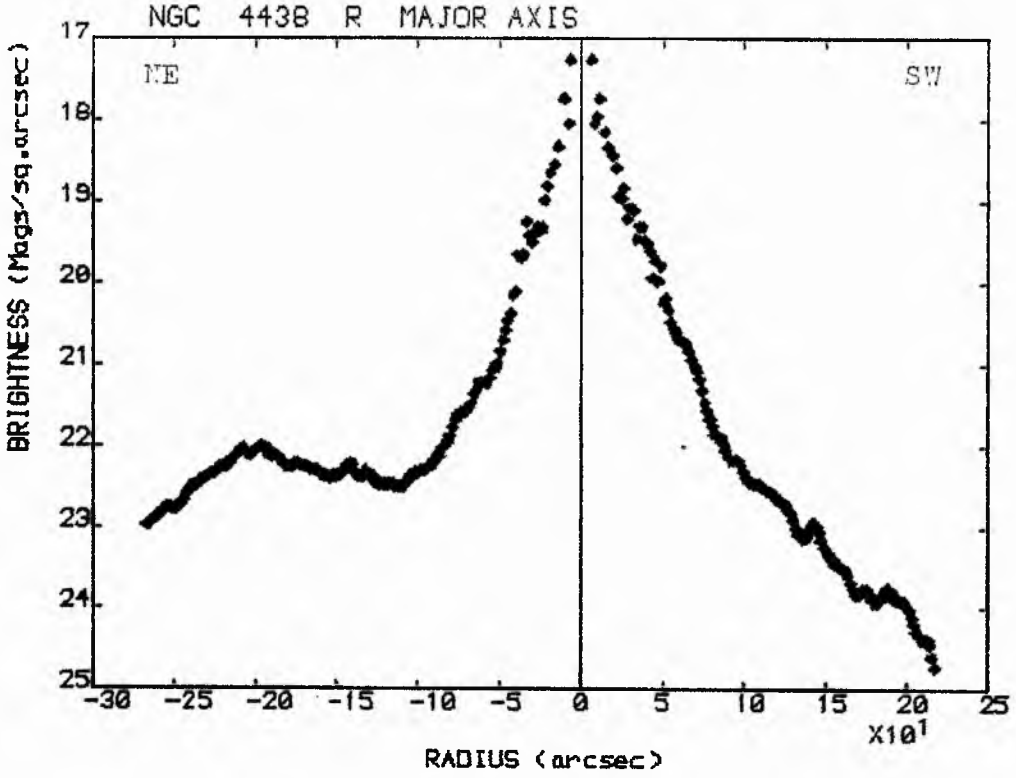
NGC 4438 R MAJOR AXIS
NE
SW
BRIGHTNESS (Mags/sq.arcsec)
17
18
19
20
21
22
23
24
25
-30 -25 -20 -15 -10 -5 0 5 10 15 20 25
X10¹
RADIUS (arcsec)

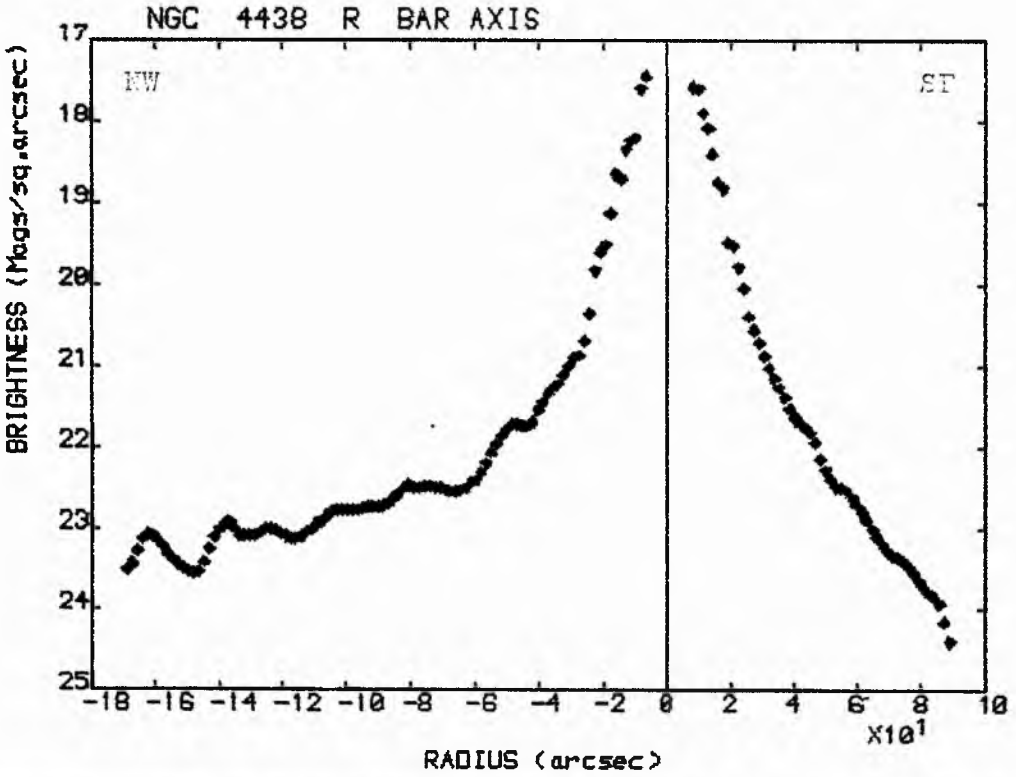
NGC 4438 R BAR AXIS
NW
SE
BRIGHTNESS (Mags/sq.arcsec)
17
18
19
20
21
22
23
24
25
-18 -16 -14 -12 -10 -8 -6 -4 -2 0 2 4 6 8 10
X10¹
RADIUS (arcsec)

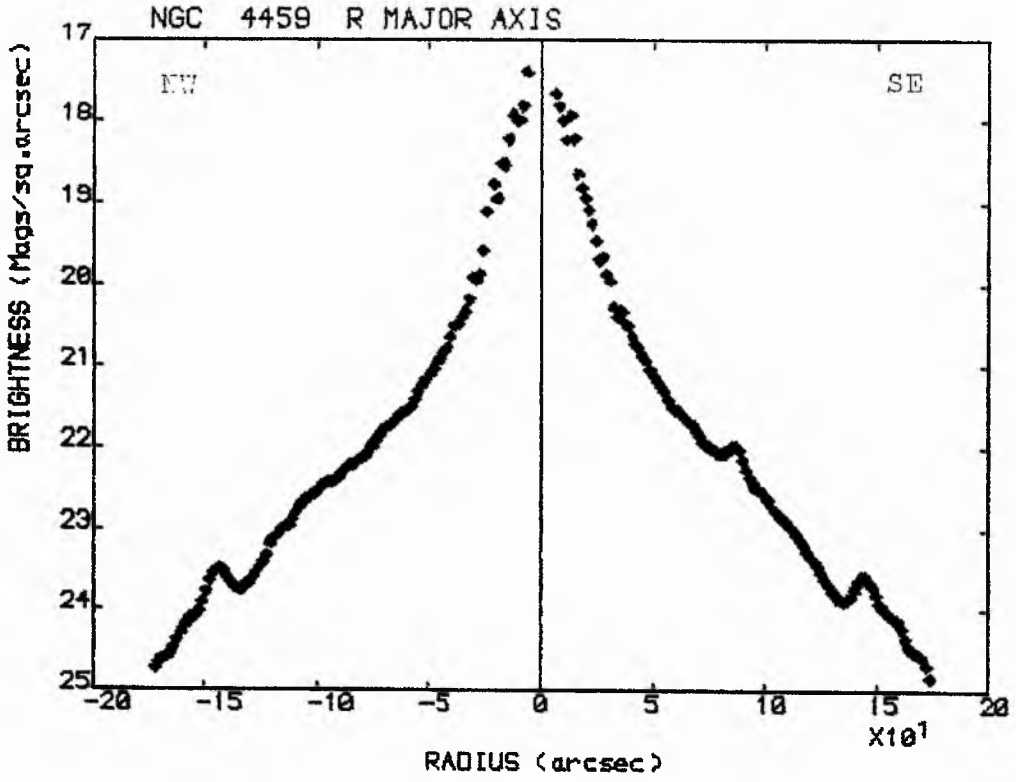
NGC 4459 R MAJOR AXIS
NW
SE
BRIGHTNESS (Mags/sq.arcsec)
17
18
19
20
21
22
23
24
25
-20
-15
-10
-5
0
5
10
15
20
X10¹
RADIUS (arcsec)

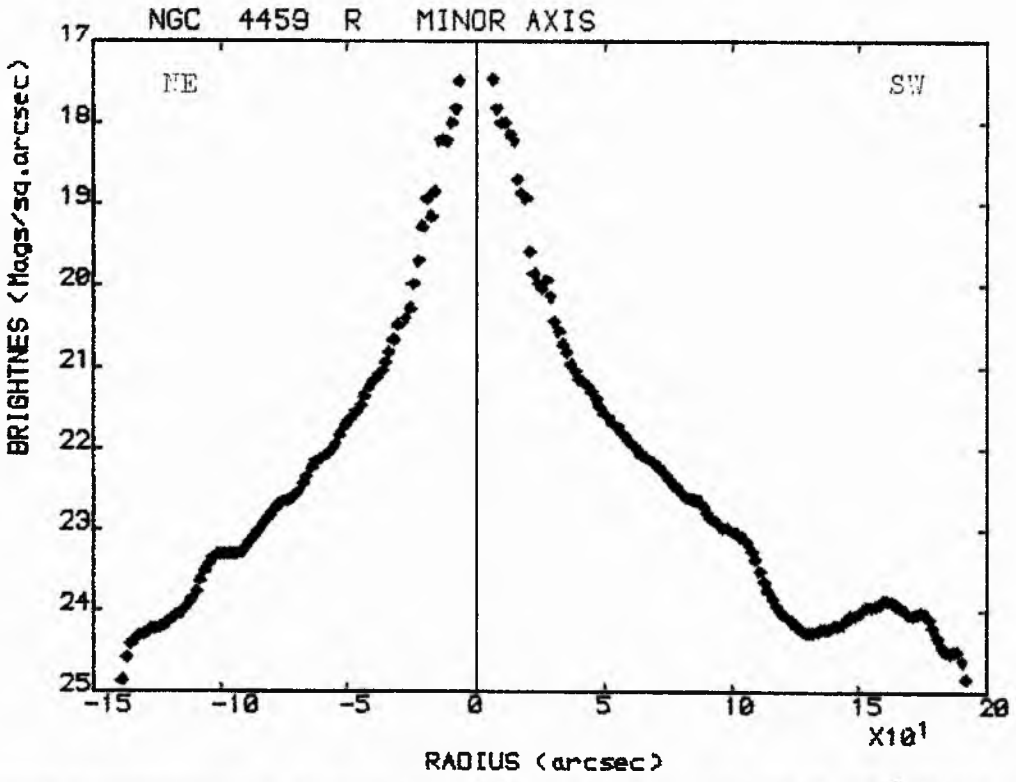
NGC 4459 R MINOR AXIS
NE
SW
BRIGHTNES (Mags/sq.arcsec)
17
18
19
20
21
22
23
24
25
-15
-10
-5
0
5
10
15
20
X10¹
RADIUS (arcsec)

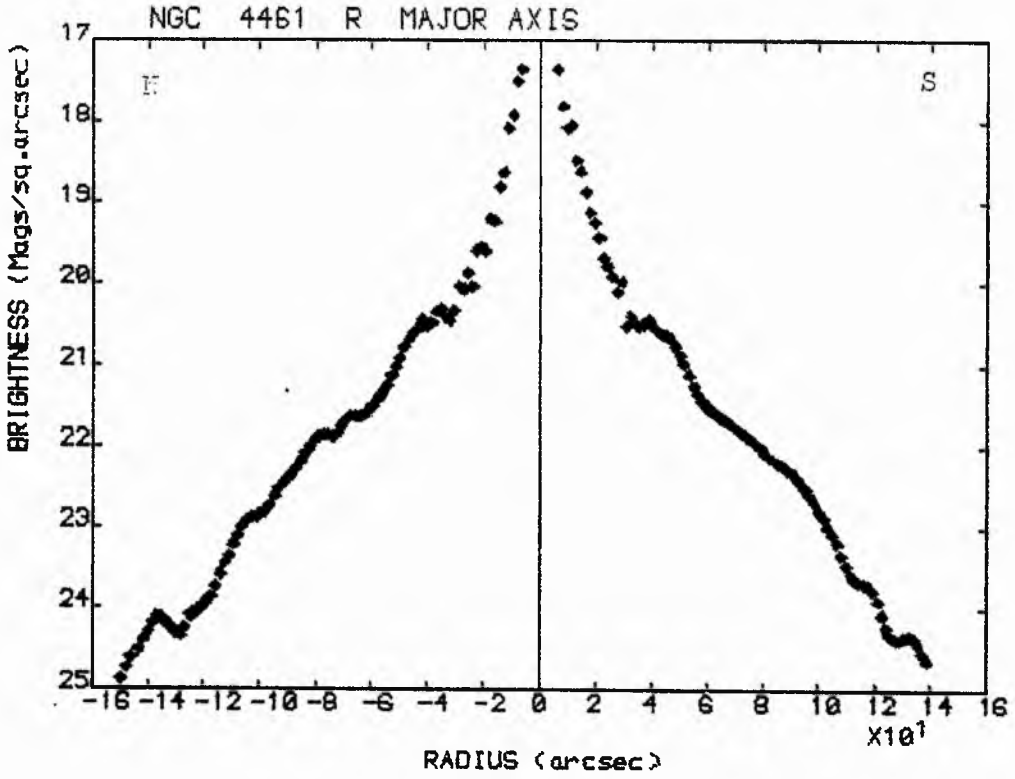
NGC 4461 R MAJOR AXIS
N
S
BRIGHTNESS (Mags/sq.arcsec)
17
18
19
20
21
22
23
24
25
-16 -14 -12 -10 -8 -6 -4 -2 0 2 4 6 8 10 12 14 16
X10¹
RADIUS (arcsec)

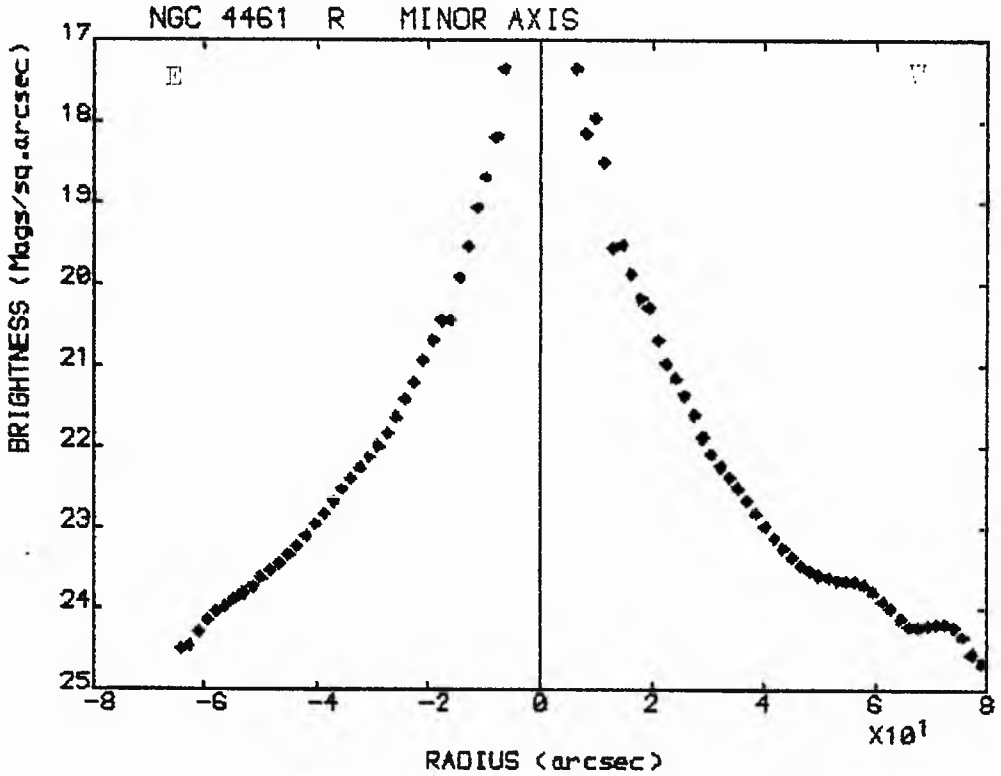
NGC 4461 R MINOR AXIS
E
W
BRIGHTNESS (Mags/sq.arcsec)
17
18
19
20
21
22
23
24
25
-8 -6 -4 -2 0 2 4 6 8
X10¹
RADIUS (arcsec)

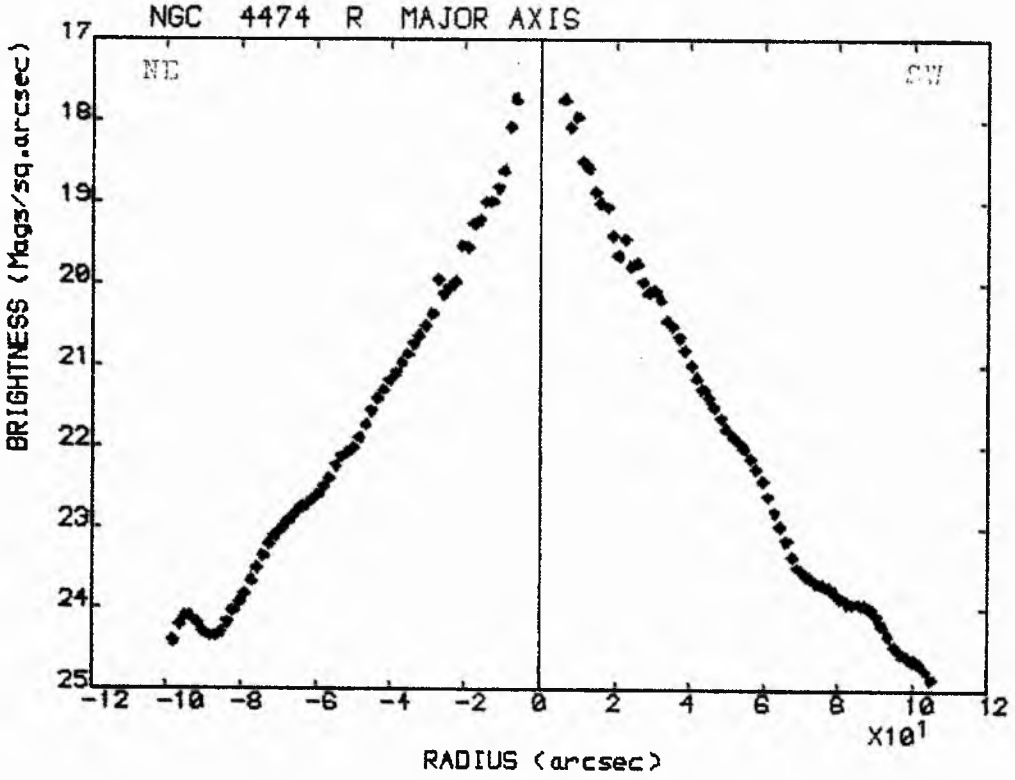
NGC 4474 R MAJOR AXIS
NE
SW
BRIGHTNESS (Mags/sq.arcsec)
17
18
19
20
21
22
23
24
25
-12 -10 -8 -6 -4 -2 0 2 4 6 8 10 12
X10¹
RADIUS (arcsec)

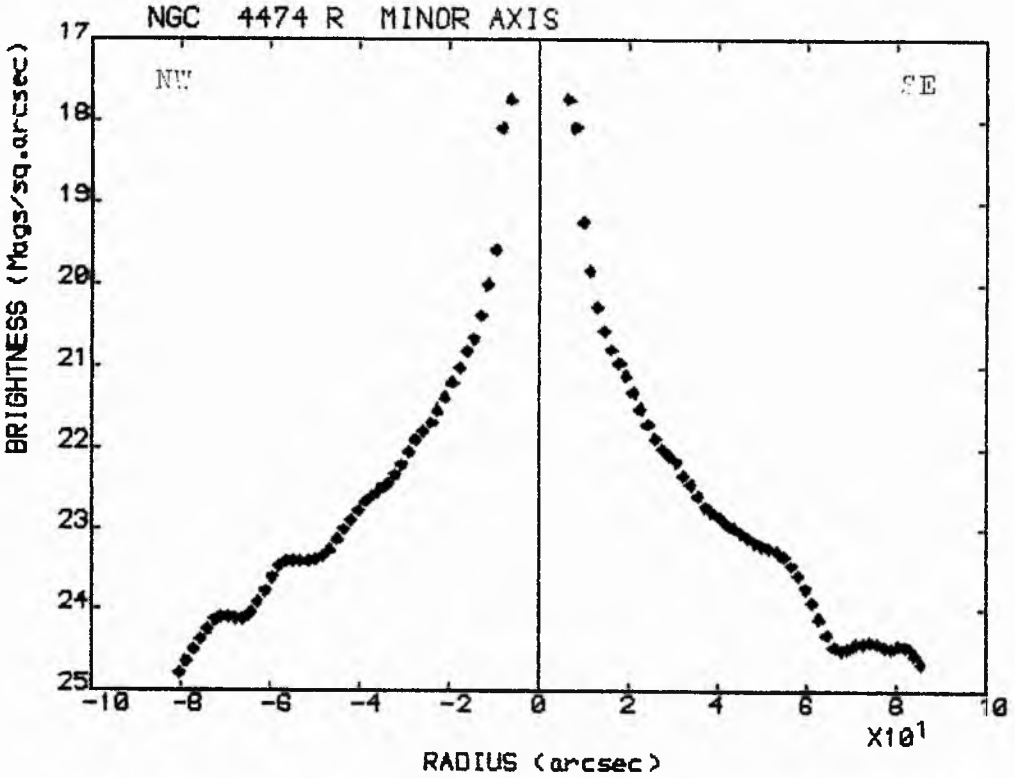
NGC 4474 R MINOR AXIS
NW
SE
BRIGHTNESS (Mags/sq.arcsec)
17
18
19
20
21
22
23
24
25
-10 -8 -6 -4 -2 0 2 4 6 8 10
X10¹
RADIUS (arcsec)

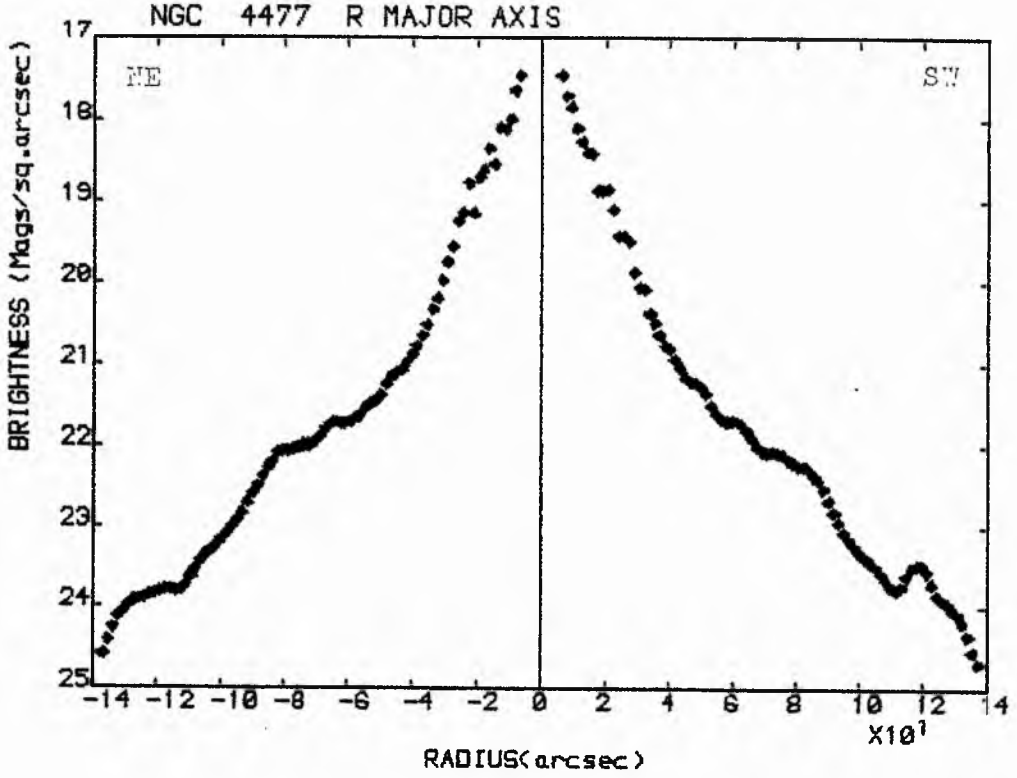
NGC 4477 R MAJOR AXIS
NE
SW
BRIGHTNESS (Mags/sq.arcsec)
17
18
19
20
21
22
23
24
25
-14 -12 -10 -8 -6 -4 -2 0 2 4 6 8 10 12 14
X10¹
RADIUS(arcsec)

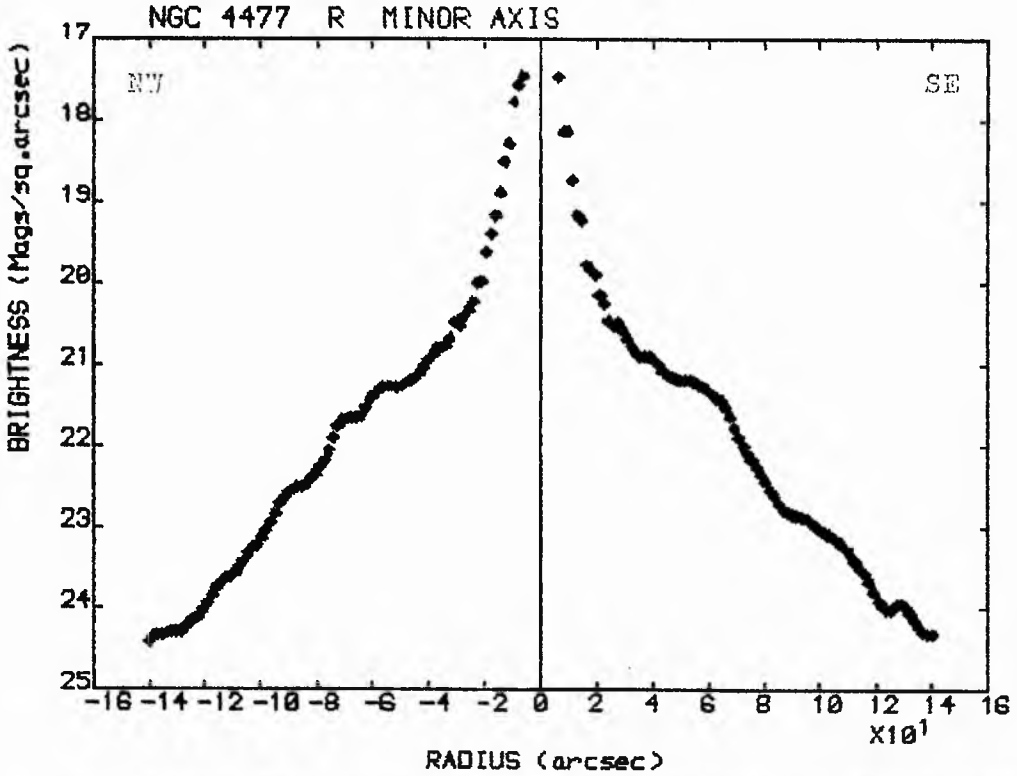
NGC 4477 R MINOR AXIS
NW
SE
BRIGHTNESS (Mags/sq.arcsec)
17
18
19
20
21
22
23
24
25
-16 -14 -12 -10 -8 -6 -4 -2 0 2 4 6 8 10 12 14 16
X10¹
RADIUS (arcsec)

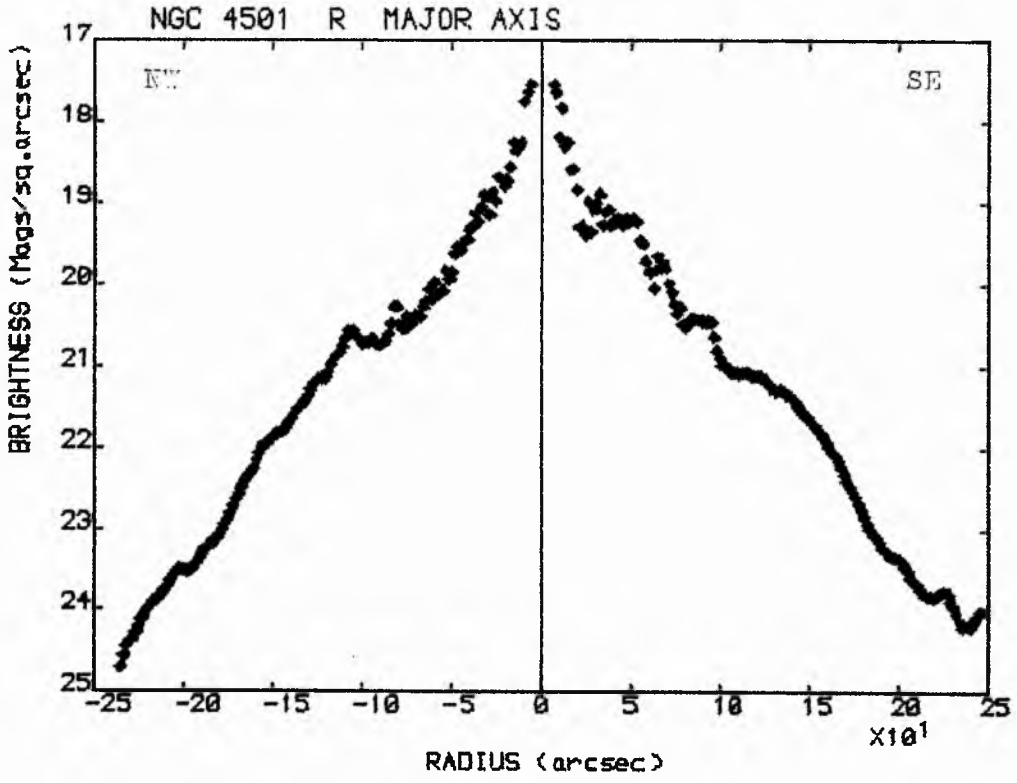
NGC 4501 R MAJOR AXIS
NW
SE
BRIGHTNESS (Mags/sq.arcsec)
17
18
19
20
21
22
23
24
25
-25 -20 -15 -10 -5 0 5 10 15 20 25
X10¹
RADIUS (arcsec)

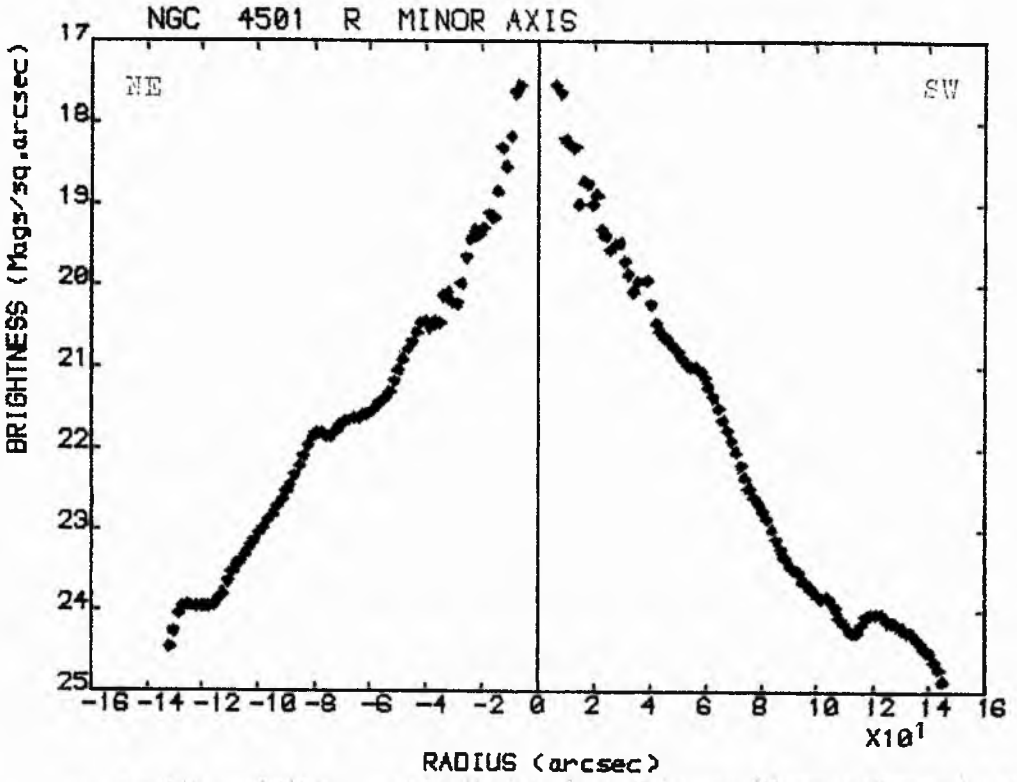
NGC 4501 R MINOR AXIS
NE
SW
BRIGHTNESS (Mags/sq.arcsec)
17
18
19
20
21
22
23
24
25
-16 -14 -12 -10 -8 -6 -4 -2 0 2 4 6 8 10 12 14 16
X10¹
RADIUS (arcsec)

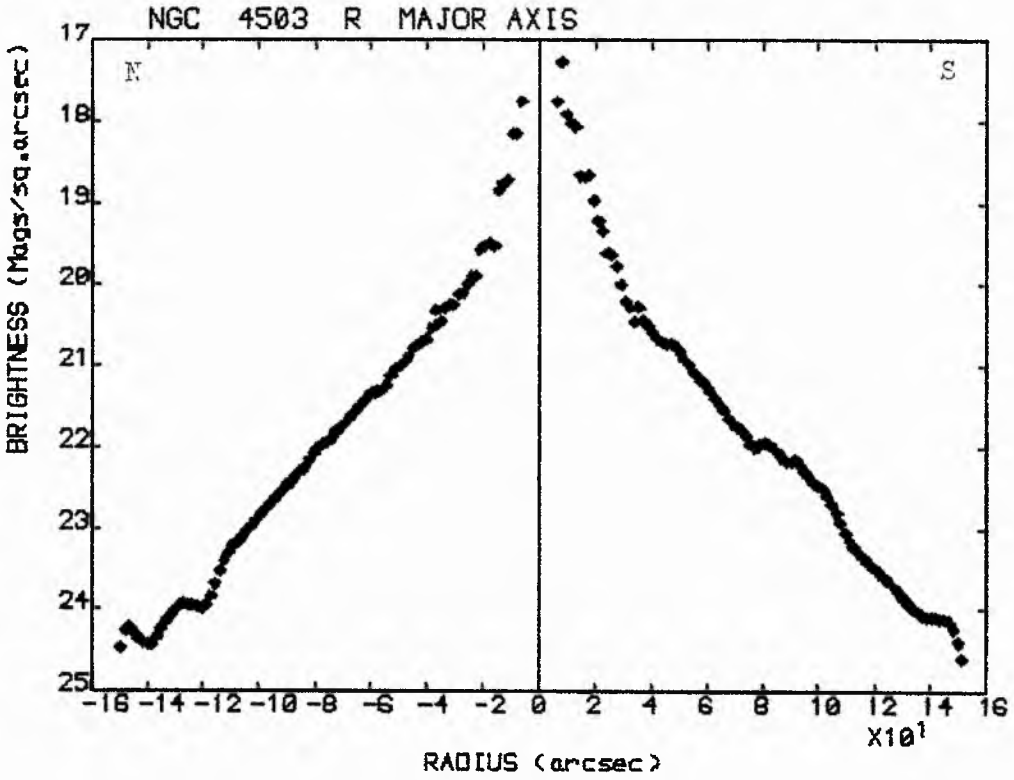
NGC 4503 R MAJOR AXIS
N
S
BRIGHTNESS (Mags/sq.arcsec)
17
18
19
20
21
22
23
24
25
-16 -14 -12 -10 -8 -6 -4 -2 0 2 4 6 8 10 12 14 16
X10¹
RADIUS (arcsec)

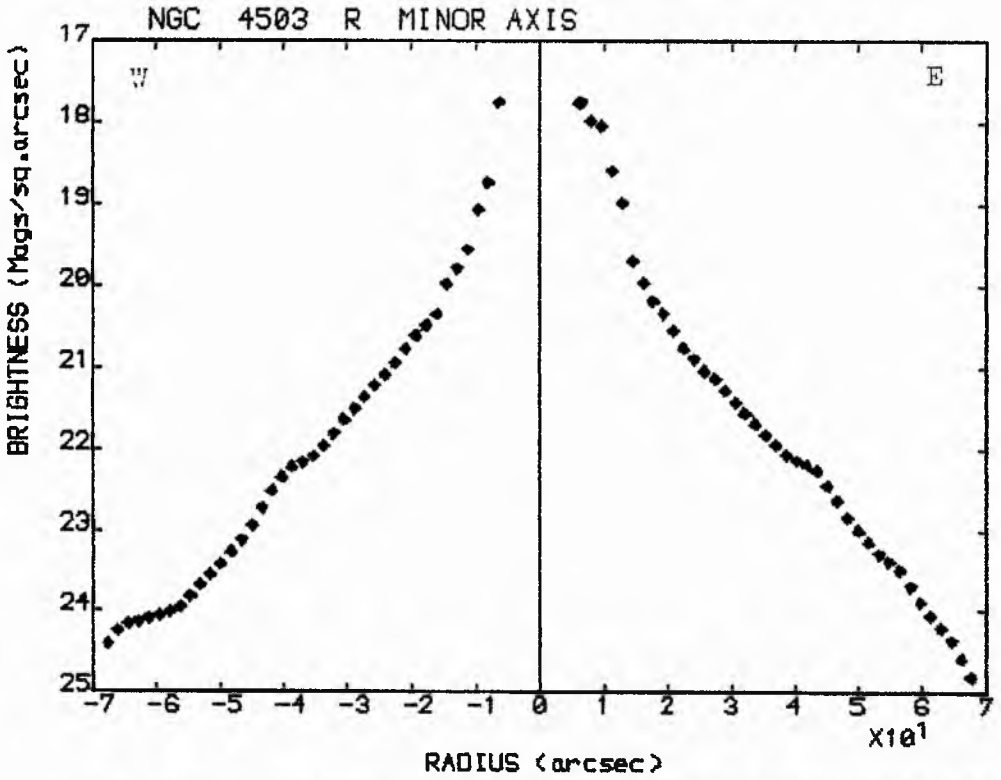
NGC 4503 R MINOR AXIS
W
E
BRIGHTNESS (Mags/sq.arcsec)
17
18
19
20
21
22
23
24
25
-7 -6 -5 -4 -3 -2 -1 0 1 2 3 4 5 6 7
X10¹
RADIUS (arcsec)

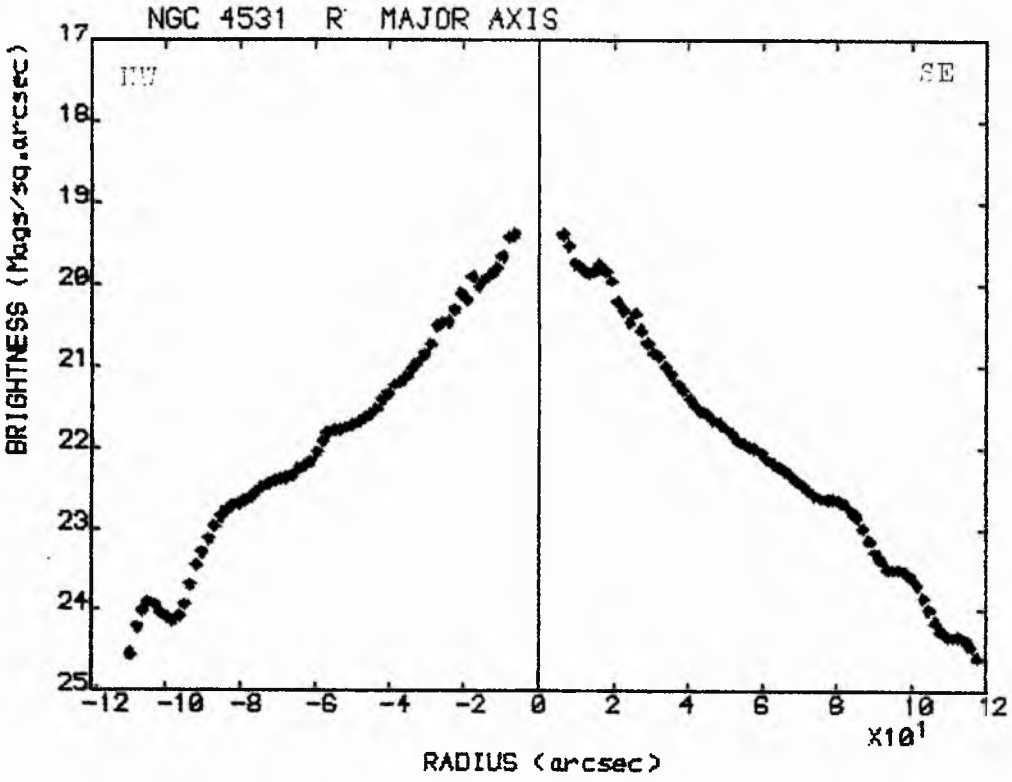
NGC 4531 R MAJOR AXIS
NW
SE
BRIGHTNESS (Mags/sq.arcsec)
17
18
19
20
21
22
23
24
25
-12 -10 -8 -6 -4 -2 0 2 4 6 8 10 12
X10¹
RADIUS (arcsec)

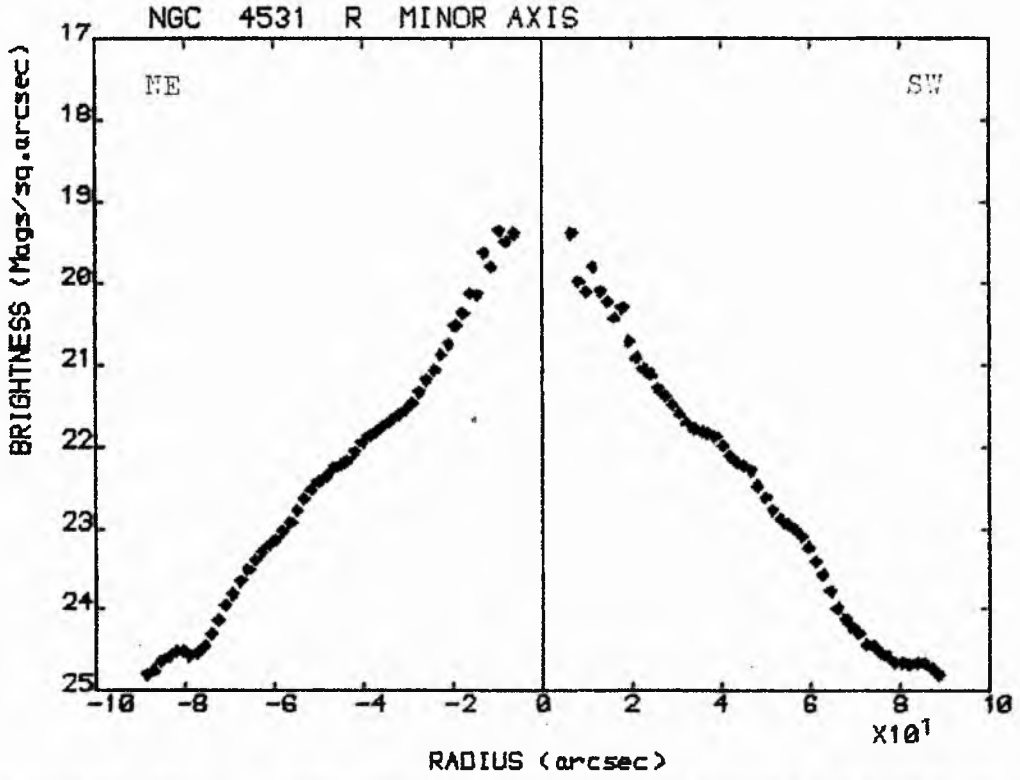
NGC 4531 R MINOR AXIS
NE
SW
BRIGHTNESS (Mags/sq.arcsec)
17
18
19
20
21
22
23
24
25
-10 -8 -6 -4 -2 0 2 4 6 8 10
X10¹
RADIUS (arcsec)

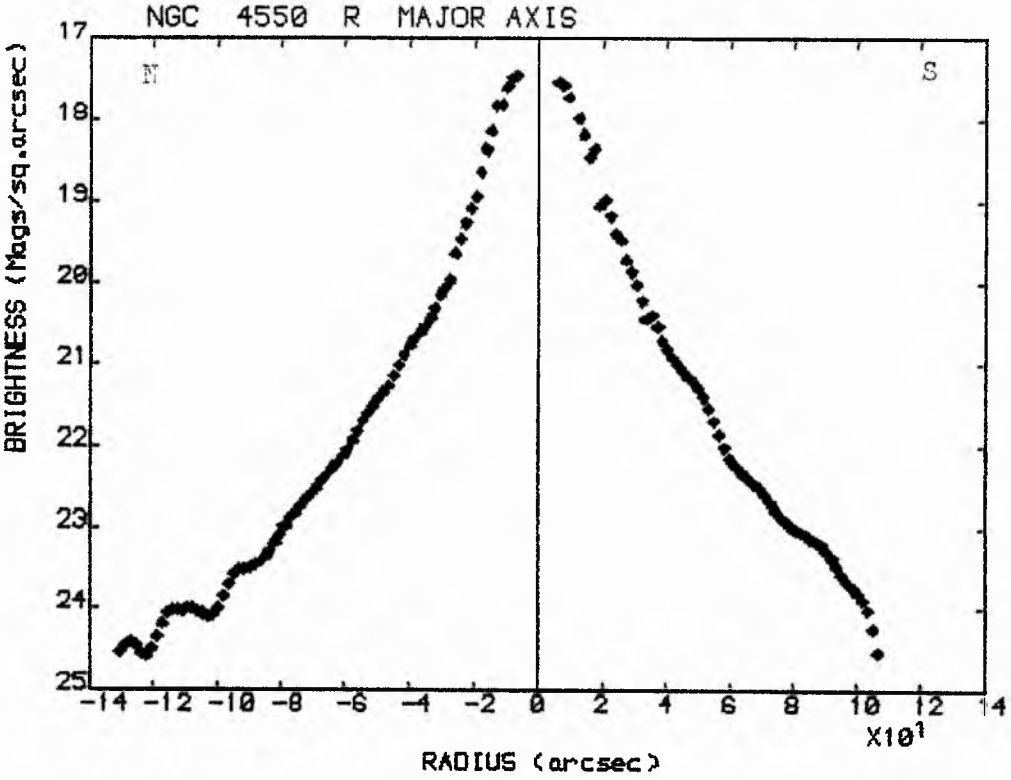
NGC 4550 R MAJOR AXIS
N
S
BRIGHTNESS (Mags/sq.arcsec)
17
18
19
20
21
22
23
24
25
-14 -12 -10 -8 -6 -4 -2 0 2 4 6 8 10 12 14
X10¹
RADIUS (arcsec)

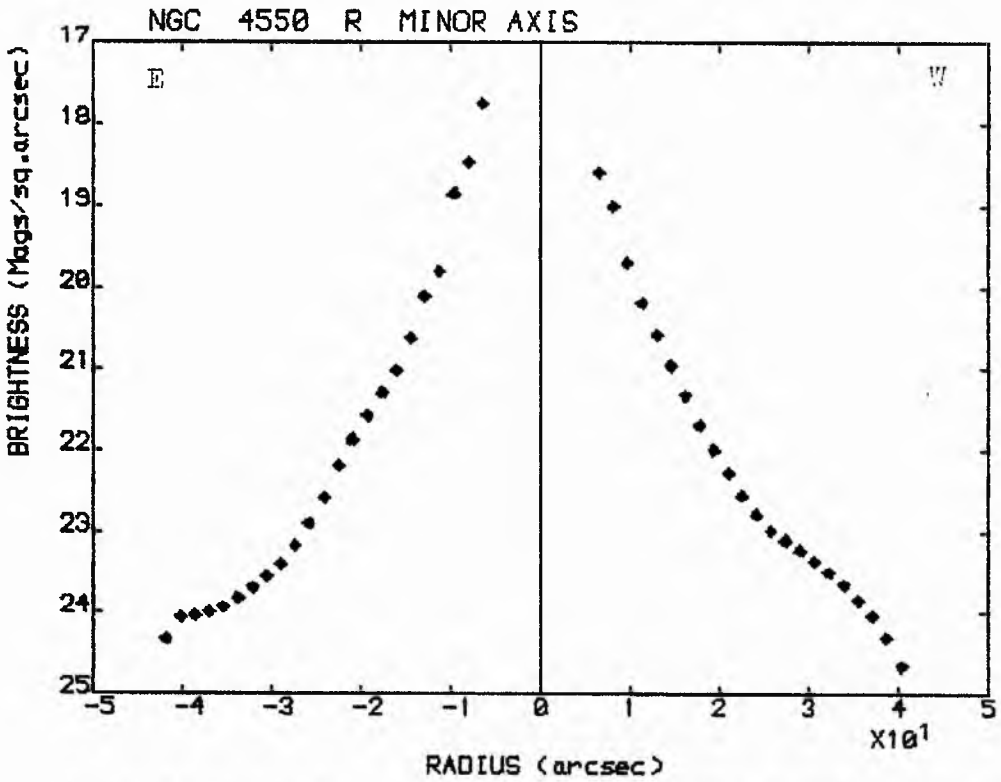
NGC 4550 R MINOR AXIS
E
W
BRIGHTNESS (Mags/sq.arcsec)
17
18
19
20
21
22
23
24
25
-5 -4 -3 -2 -1 0 1 2 3 4 5
X10¹
RADIUS (arcsec)

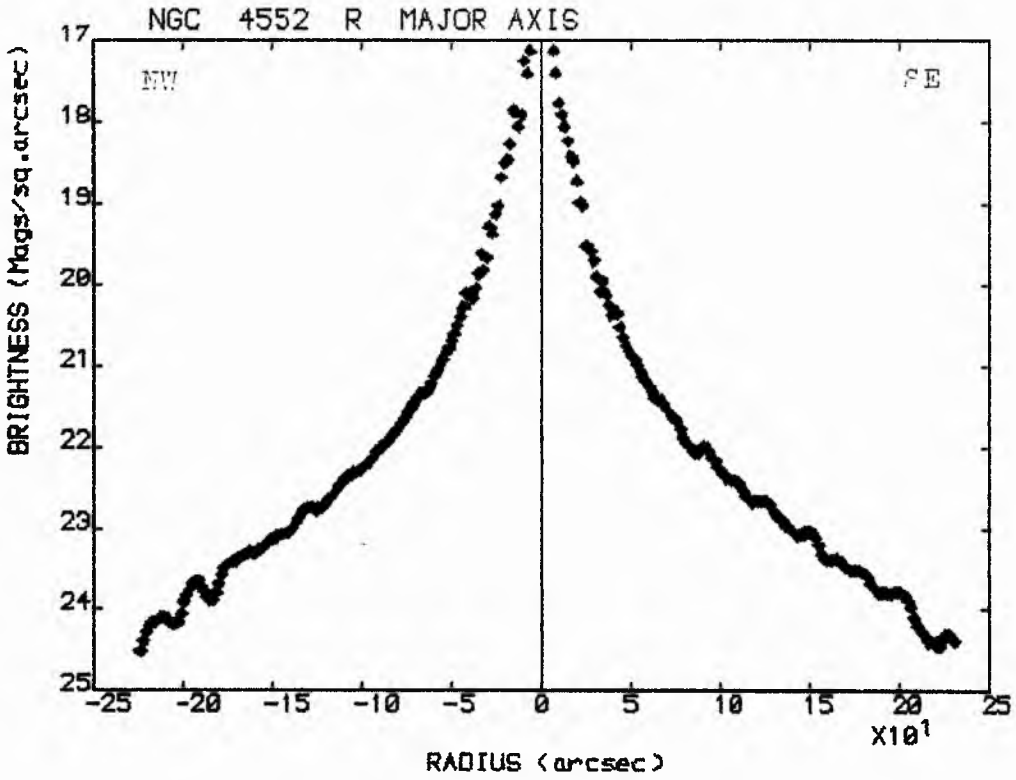
NGC 4552 R MAJOR AXIS
NW
SE
BRIGHTNESS (Mags/sq.arcsec)
17
18
19
20
21
22
23
24
25
-25
-20
-15
-10
-5
0
5
10
15
20
25
X10¹
RADIUS (arcsec)

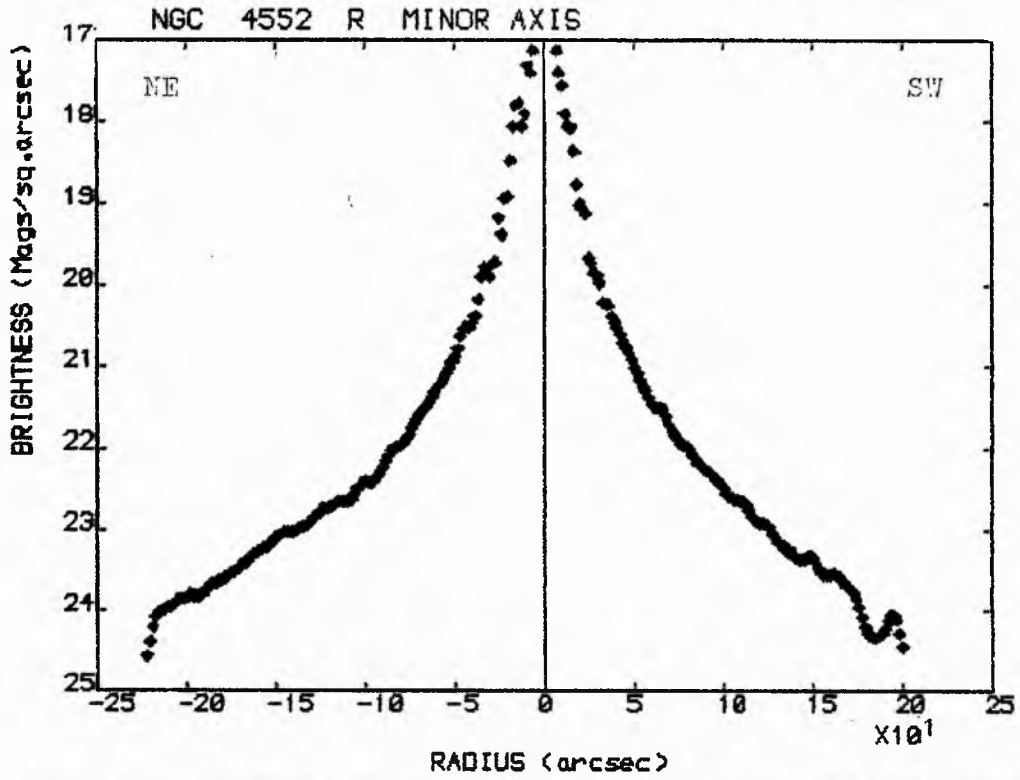
NGC 4552 R MINOR AXIS
NE
SW
BRIGHTNESS (Mags/sq.arcsec)
17
18
19
20
21
22
23
24
25
-25
-20
-15
-10
-5
0
5
10
15
20
25
X10¹
RADIUS (arcsec)

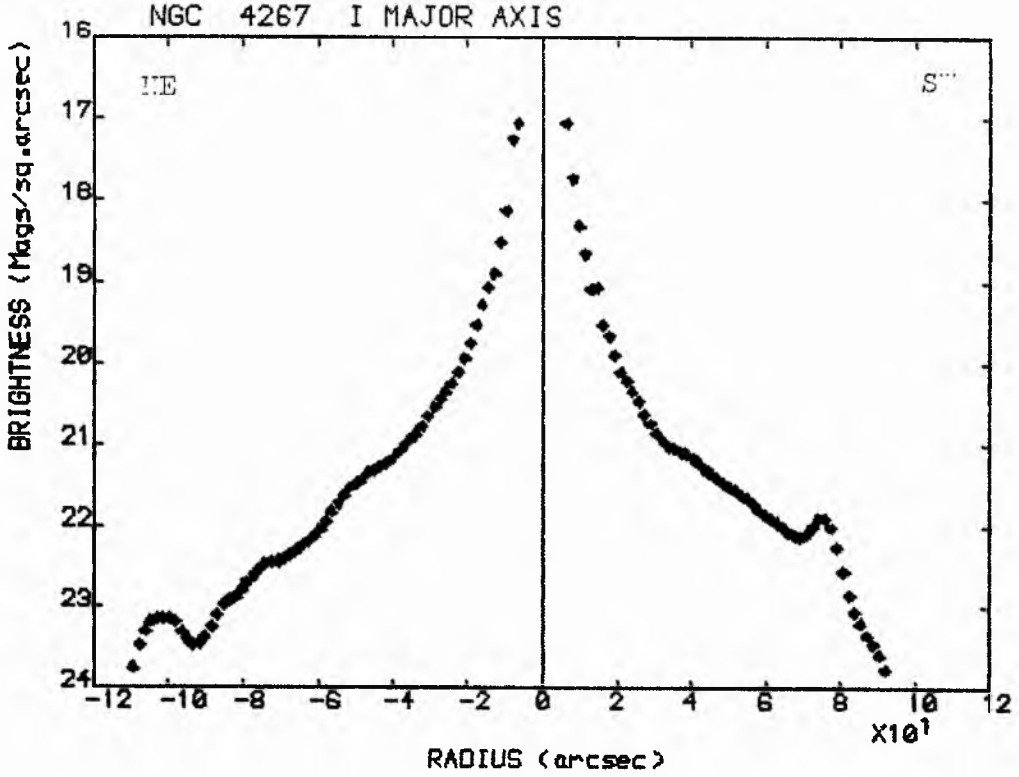
NGC 4267 I MAJOR AXIS
NE
SW
BRIGHTNESS (Mags/sq.arcsec)
16
17
18
19
20
21
22
23
24
-12 -10 -8 -6 -4 -2 0 2 4 6 8 10 12
X10¹
RADIUS (arcsec)

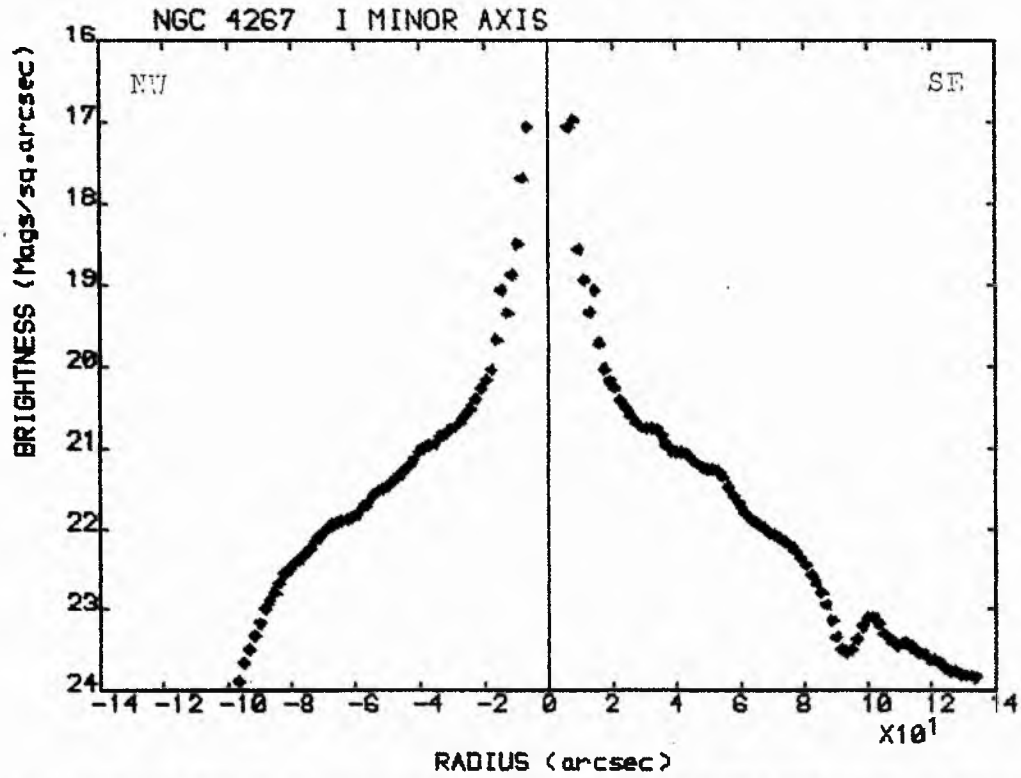
NGC 4267 I MINOR AXIS
NW
SE
BRIGHTNESS (Mags/sq.arcsec)
16
17
18
19
20
21
22
23
24
-14 -12 -10 -8 -6 -4 -2 0 2 4 6 8 10 12 14
X10¹
RADIUS (arcsec)

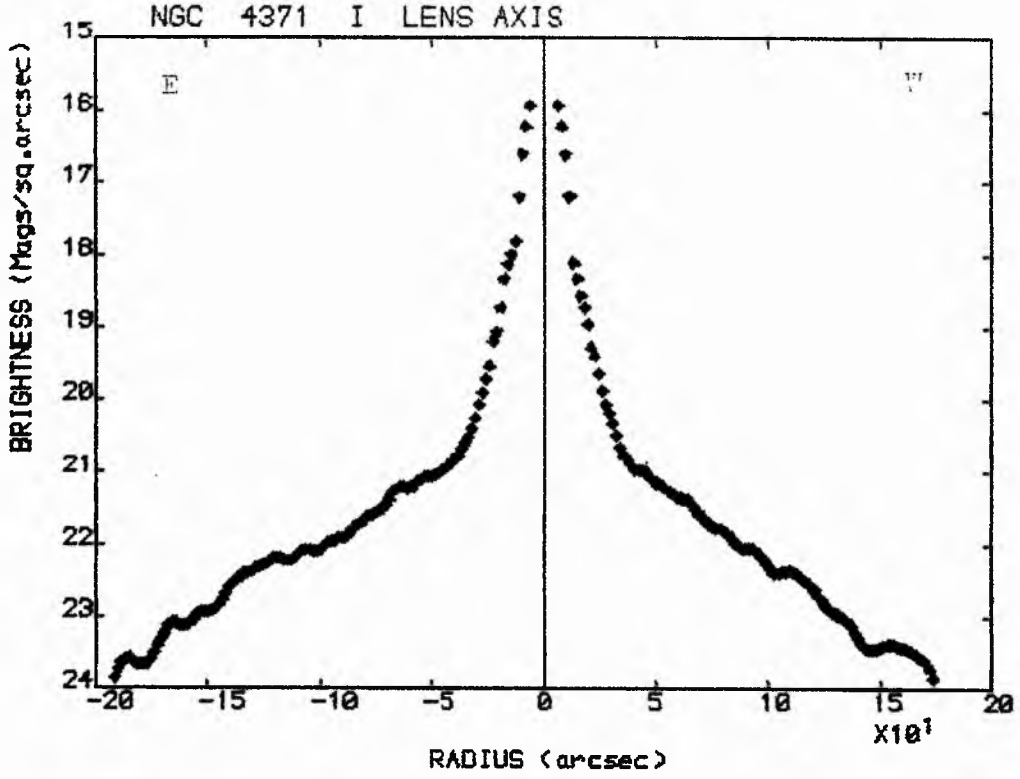
NGC 4371 I LENS AXIS
E
W
BRIGHTNESS (Mags/sq.arcsec)
15
16
17
18
19
20
21
22
23
24
-20
-15
-10
-5
0
5
10
15
20
X10¹
RADIUS (arcsec)

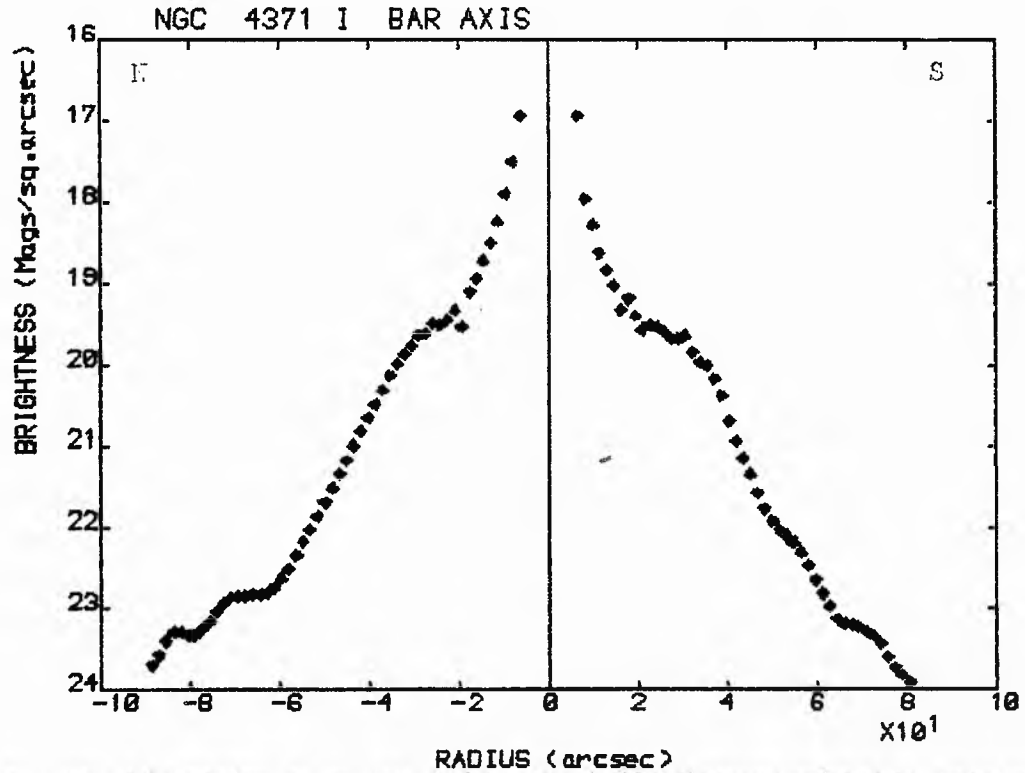
NGC 4371 I BAR AXIS
N
S
BRIGHTNESS (Mags/sq.arcsec)
16
17
18
19
20
21
22
23
24
-10
-8
-6
-4
-2
0
2
4
6
8
10
X10¹
RADIUS (arcsec)

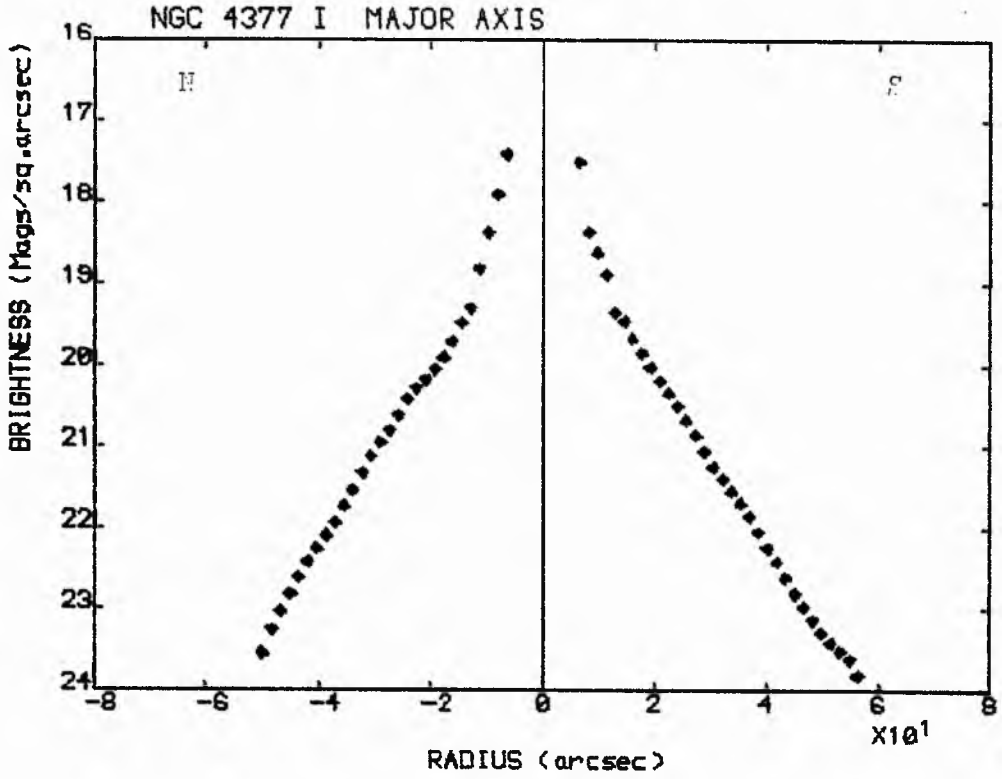
NGC 4377 I MAJOR AXIS
N
S
BRIGHTNESS (Mags/sq.arcsec)
16
17
18
19
20
21
22
23
24
-8
-6
-4
-2
0
2
4
6
8
X10¹
RADIUS (arcsec)

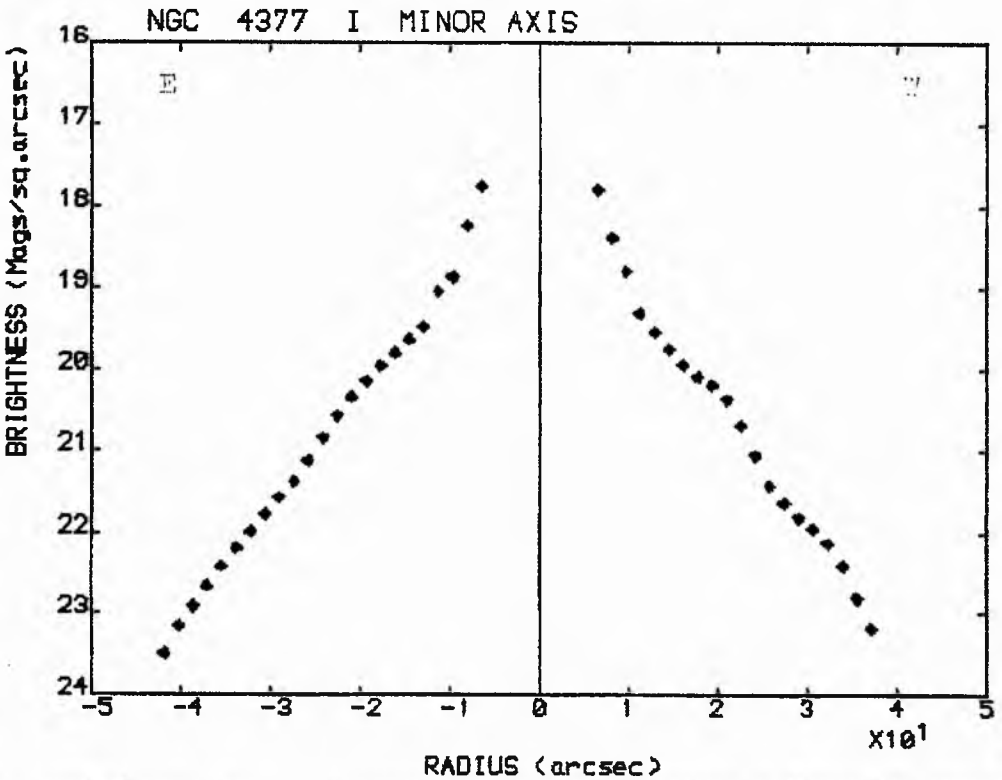
NGC 4377 I MINOR AXIS
E
W
BRIGHTNESS (Mags/sq.arcsec)
16
17
18
19
20
21
22
23
24
-5
-4
-3
-2
-1
0
1
2
3
4
5
X10¹
RADIUS (arcsec)

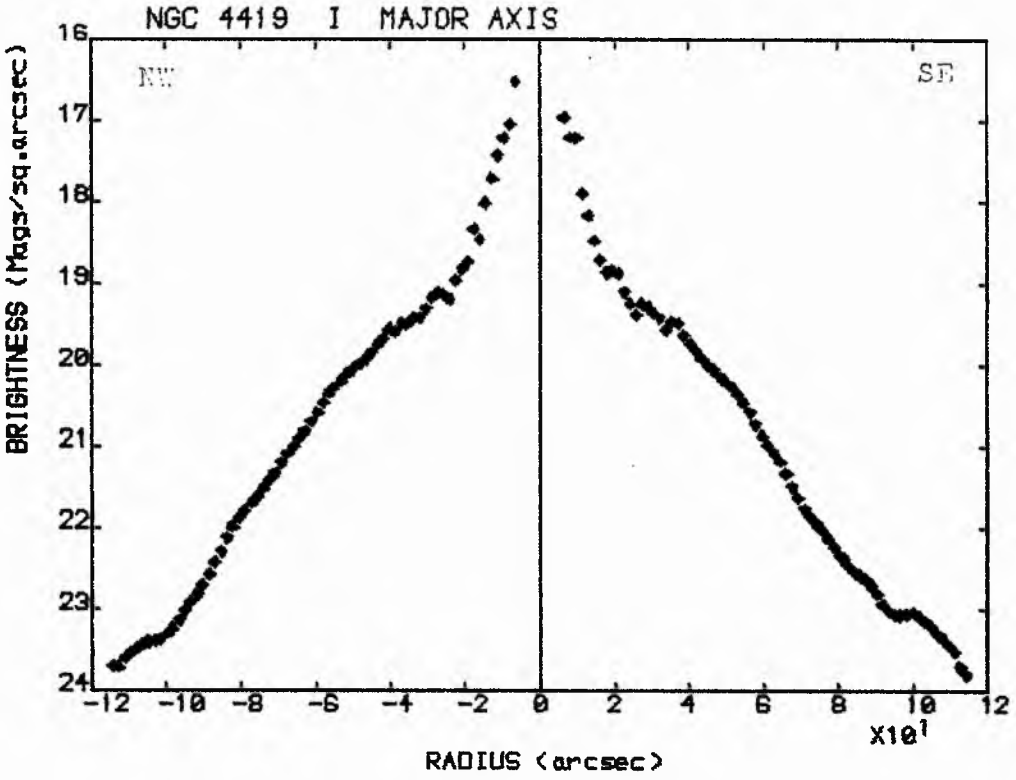
NGC 4419 I MAJOR AXIS
NW
SE
BRIGHTNESS (Mags/sq.arcsec)
16
17
18
19
20
21
22
23
24
-12 -10 -8 -6 -4 -2 0 2 4 6 8 10 12
X10¹
RADIUS (arcsec)

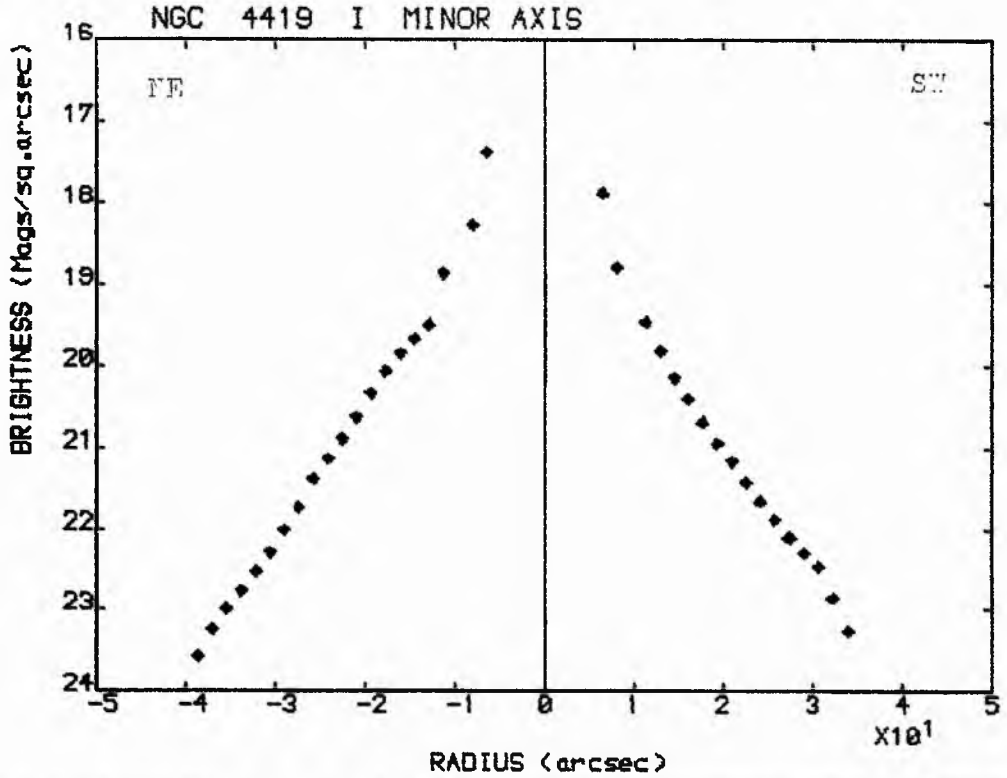
NGC 4419 I MINOR AXIS
NE
SW
BRIGHTNESS (Mags/sq.arcsec)
16
17
18
19
20
21
22
23
24
-5 -4 -3 -2 -1 0 1 2 3 4 5
X10¹
RADIUS (arcsec)

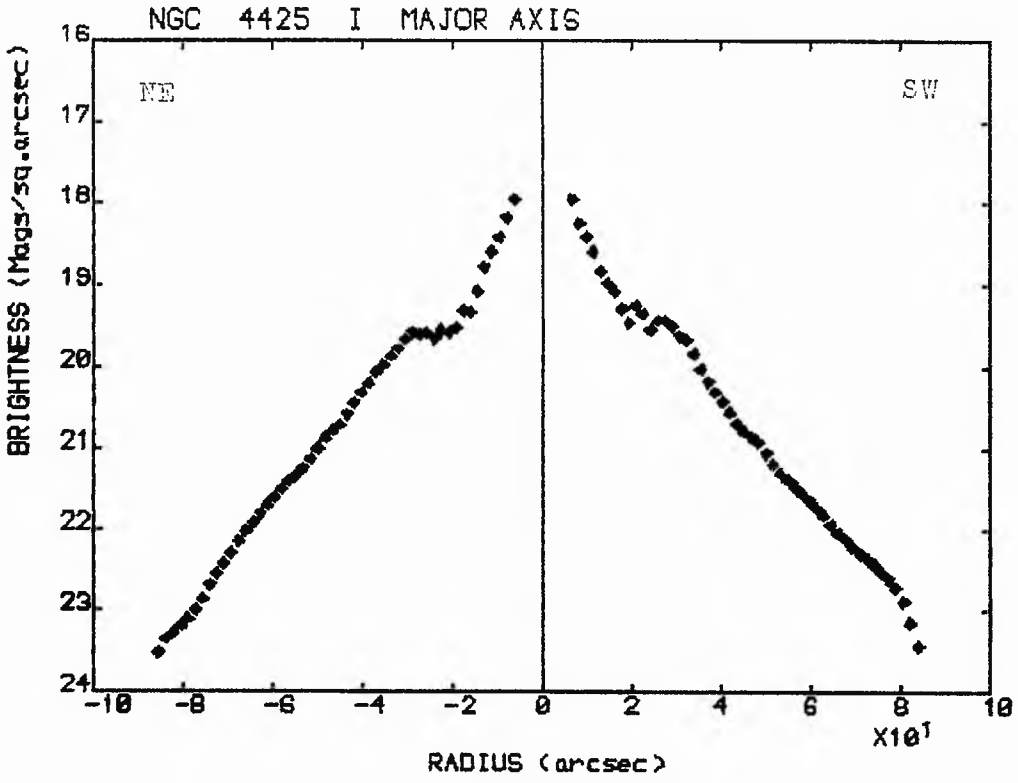
NGC 4425 I MAJOR AXIS
NE
SW
BRIGHTNESS (Mags/sq.arcsec)
16
17
18
19
20
21
22
23
24
-10
-8
-6
-4
-2
0
2
4
6
8
10
X10¹
RADIUS (arcsec)

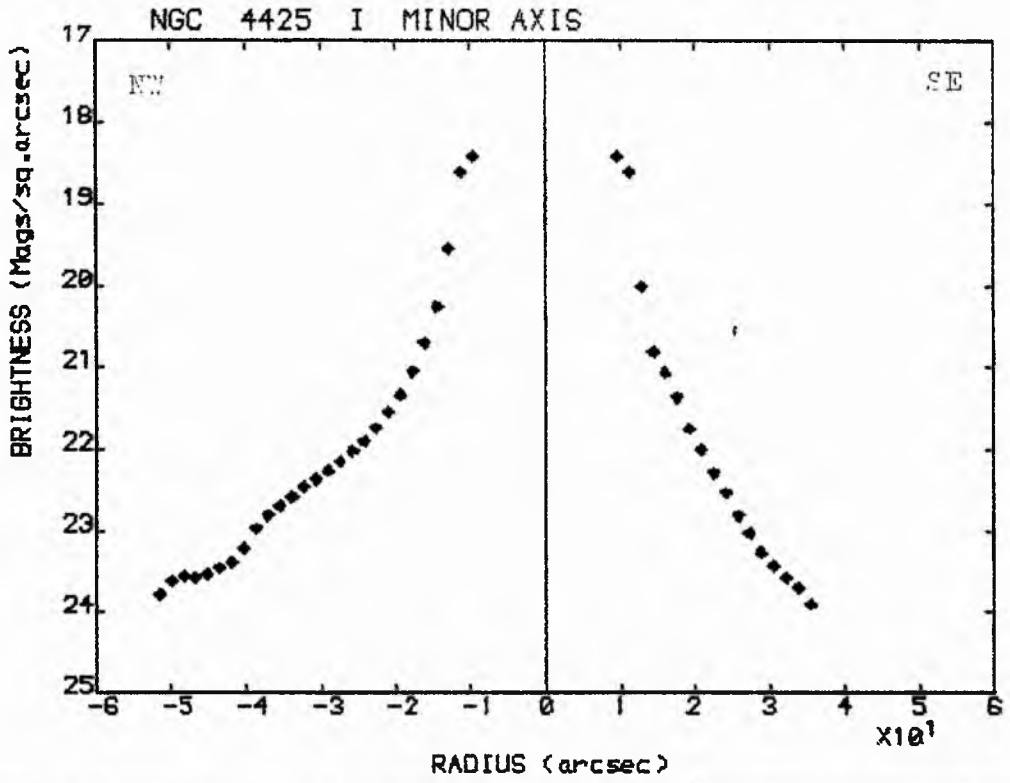
NGC 4425 I MINOR AXIS
NW
SE
BRIGHTNESS (Mags/sq.arcsec)
17
18
19
20
21
22
23
24
25
-6
-5
-4
-3
-2
-1
0
1
2
3
4
5
6
X10¹
RADIUS (arcsec)

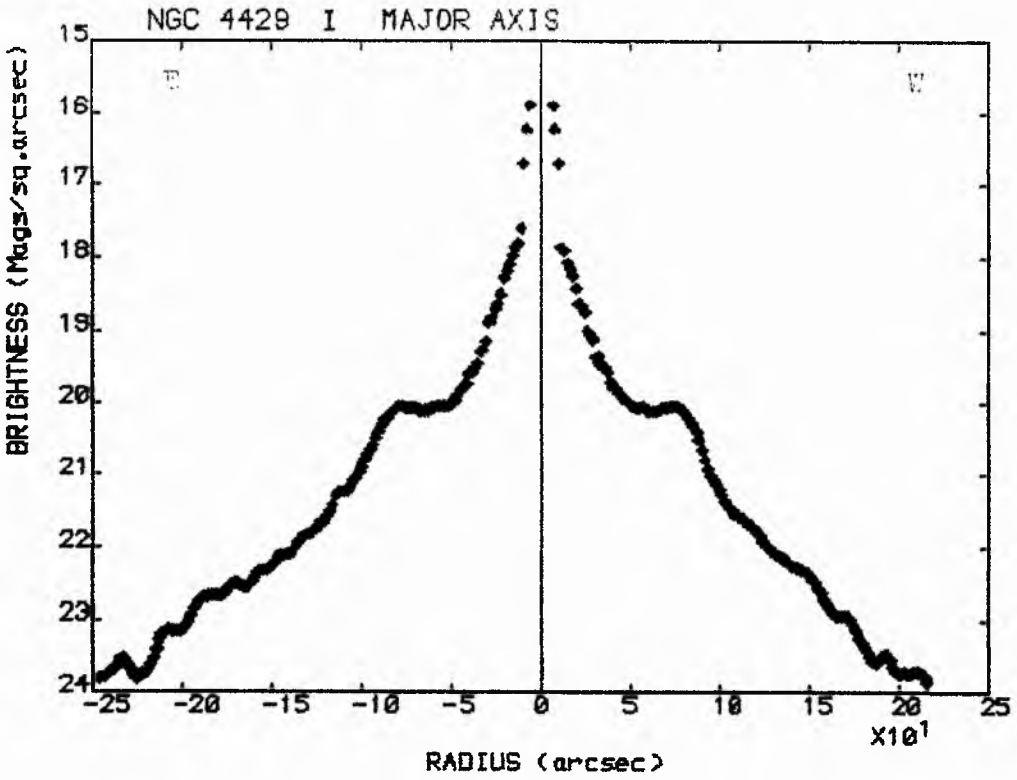
NGC 4429 I MAJOR AXIS
E
W
BRIGHTNESS (Mags/sq.arcsec)
15
16
17
18
19
20
21
22
23
24
-25 -20 -15 -10 -5 0 5 10 15 20 25
X10¹
RADIUS (arcsec)

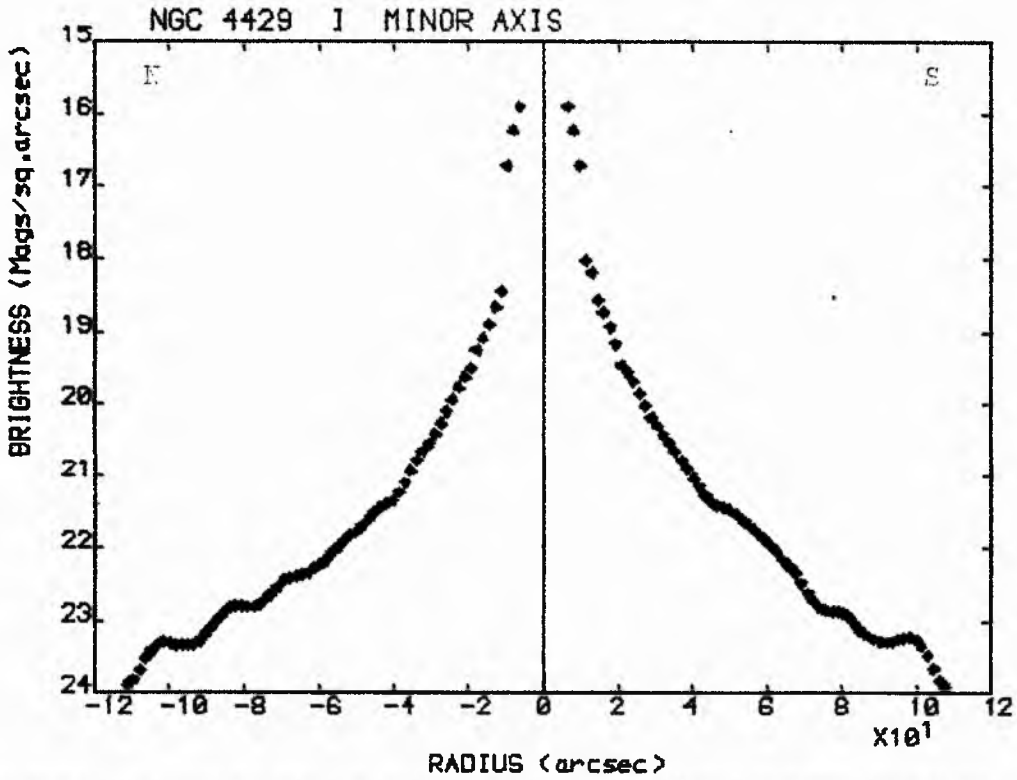
NGC 4429 I MINOR AXIS
N
S
BRIGHTNESS (Mags/sq.arcsec)
15
16
17
18
19
20
21
22
23
24
-12 -10 -8 -6 -4 -2 0 2 4 6 8 10 12
X10¹
RADIUS (arcsec)

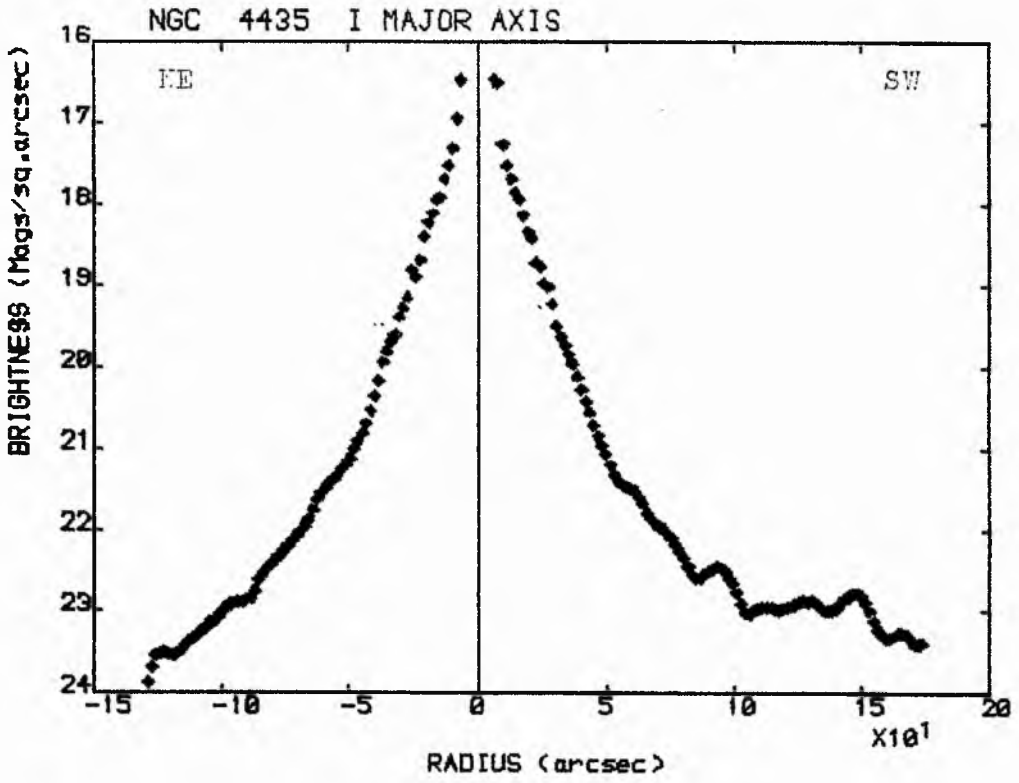
NGC 4435 I MAJOR AXIS
NE
SW
BRIGHTNESS (Mags/sq.arcsec)
16
17
18
19
20
21
22
23
24
-15
-10
-5
0
5
10
15
20
X10¹
RADIUS (arcsec)

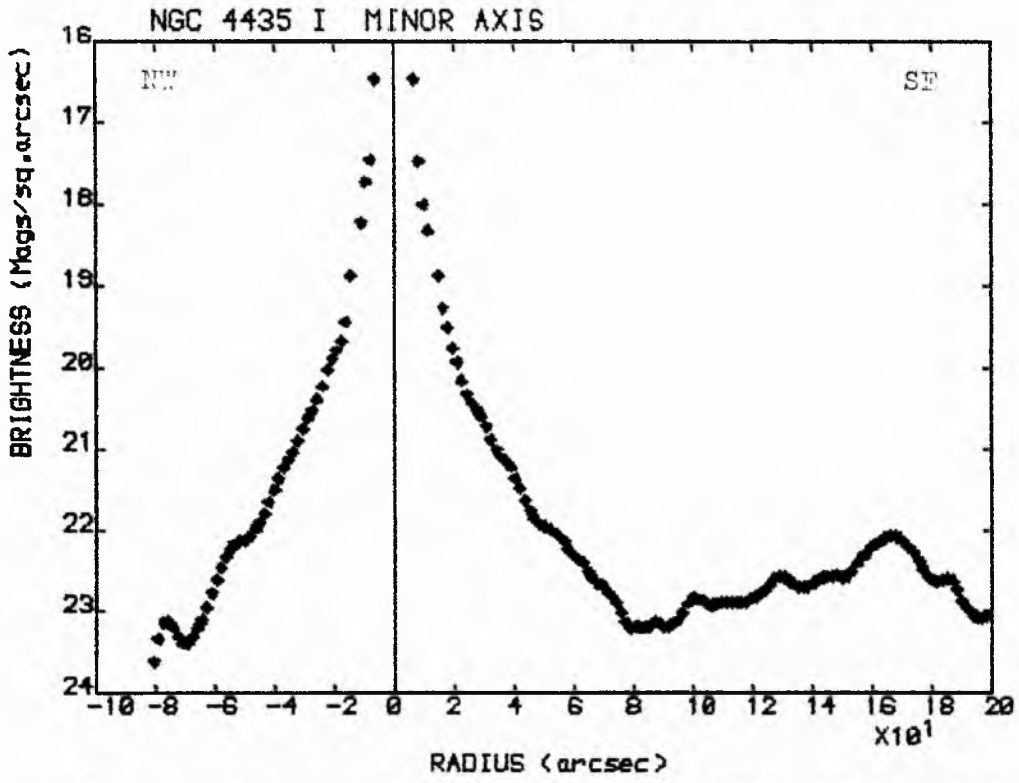
NGC 4435 I MINOR AXIS
NW
SE
BRIGHTNESS (Mags/sq.arcsec)
16
17
18
19
20
21
22
23
24
-10
-8
-6
-4
-2
0
2
4
6
8
10
12
14
16
18
20
X10¹
RADIUS (arcsec)

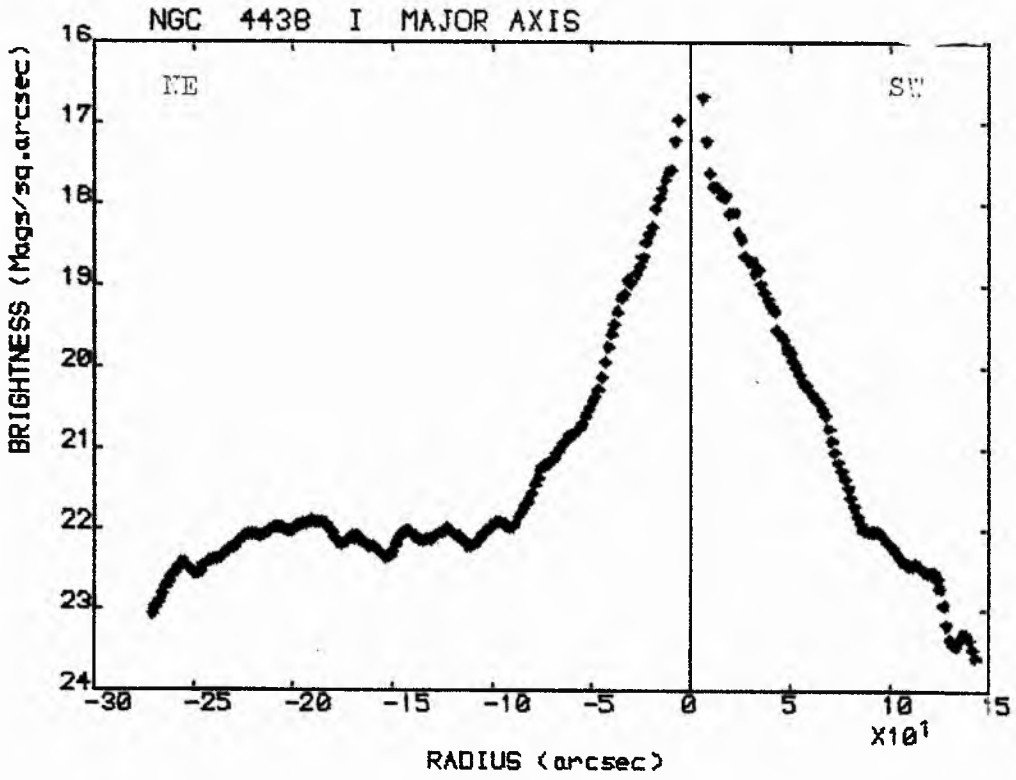
NGC 4438 I MAJOR AXIS
NE
SW
BRIGHTNESS (Mags/sq.arcsec)
16
17
18
19
20
21
22
23
24
-30
-25
-20
-15
-10
-5
0
5
10
15
X10¹
RADIUS (arcsec)

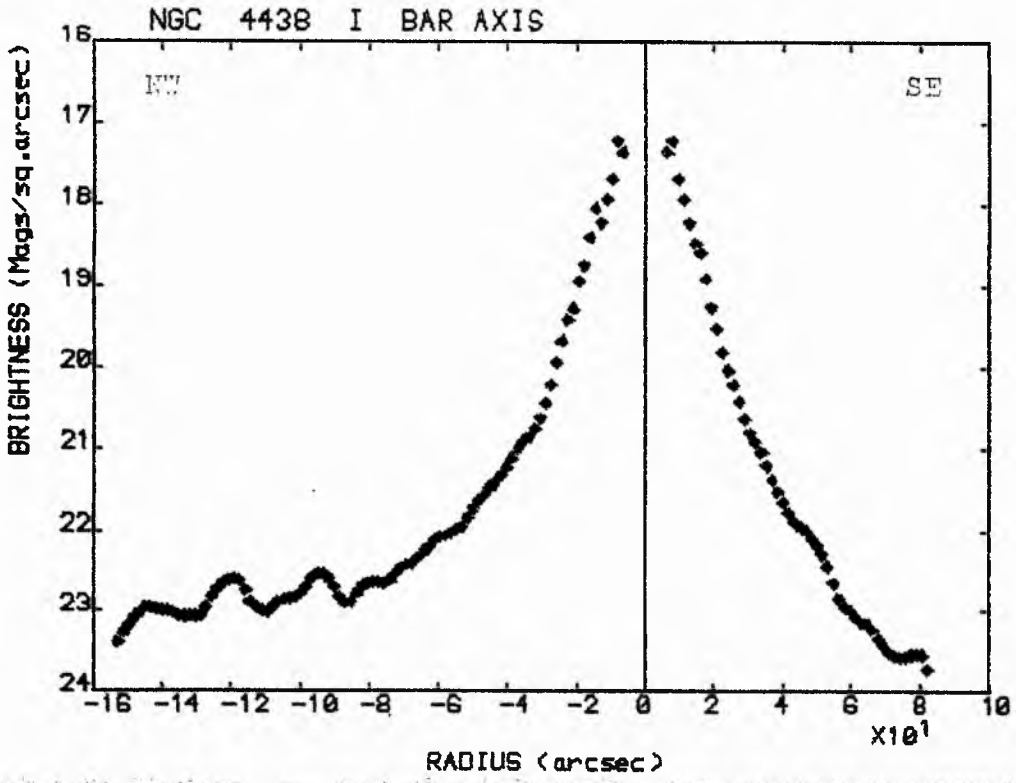
NGC 4438 I BAR AXIS
NW
SE
BRIGHTNESS (Mags/sq.arcsec)
16
17
18
19
20
21
22
23
24
-16
-14
-12
-10
-8
-6
-4
-2
0
2
4
6
8
10
X10¹
RADIUS (arcsec)

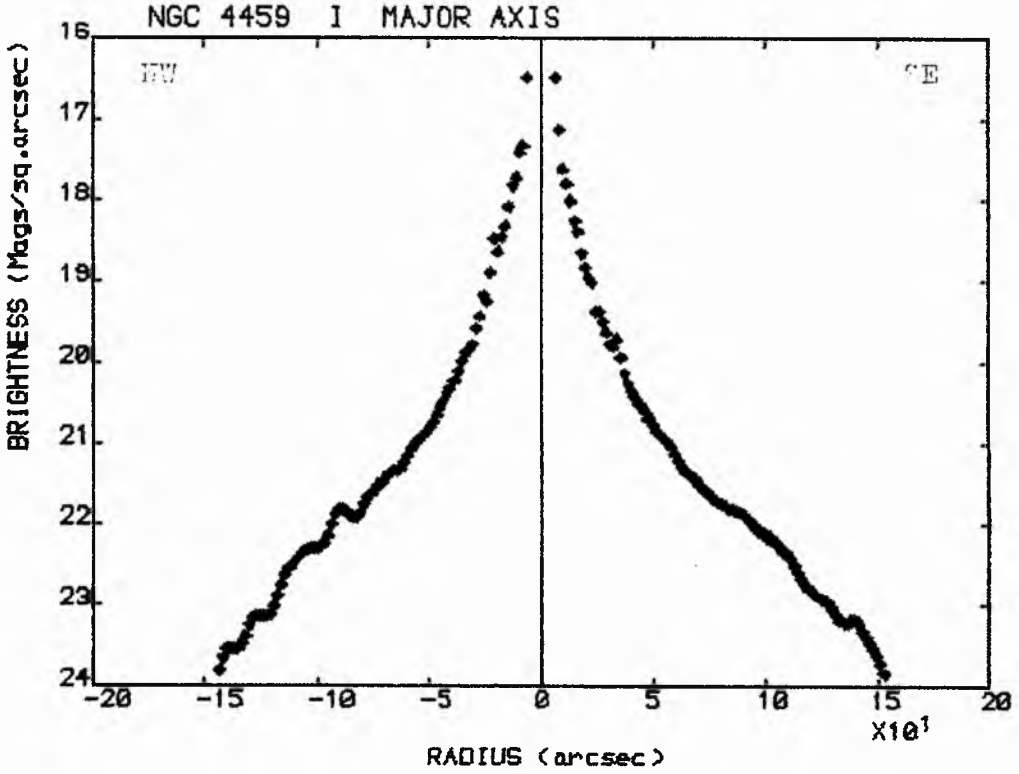
NGC 4459 I MAJOR AXIS
NW
SE
BRIGHTNESS (Mags/sq.arcsec)
16
17
18
19
20
21
22
23
24
-20
-15
-10
-5
0
5
10
15
20
X10¹
RADIUS (arcsec)

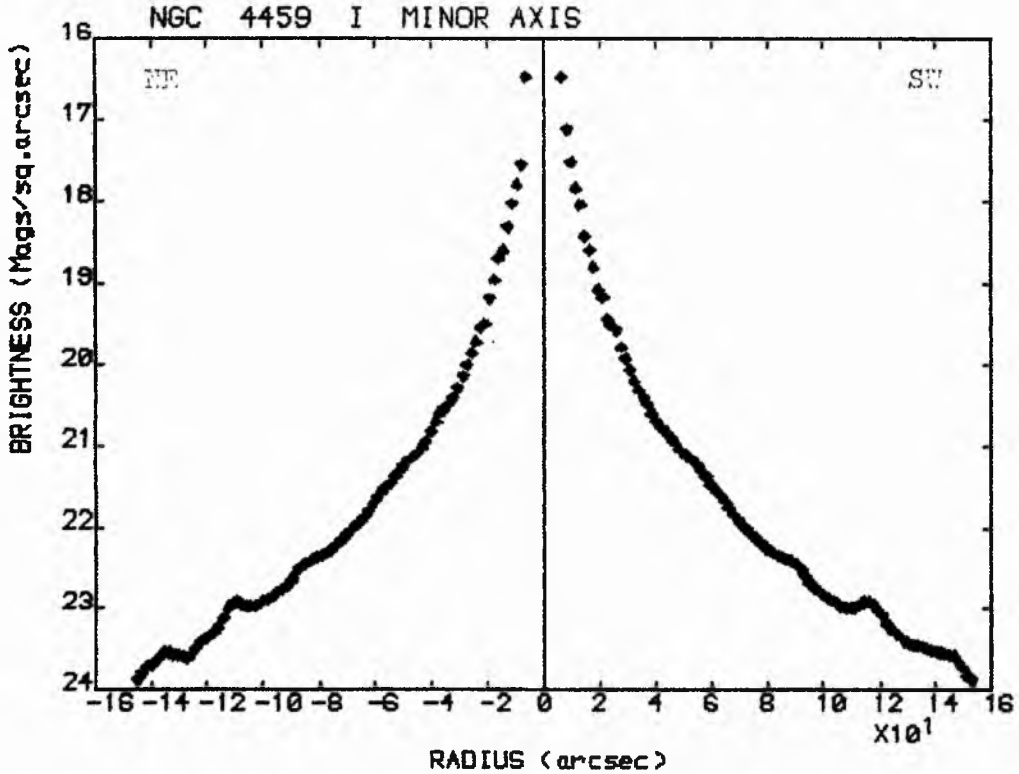
NGC 4459 I MINOR AXIS
NE
SW
BRIGHTNESS (Mags/sq.arcsec)
16
17
18
19
20
21
22
23
24
-16
-14
-12
-10
-8
-6
-4
-2
0
2
4
6
8
10
12
14
16
X10¹
RADIUS (arcsec)

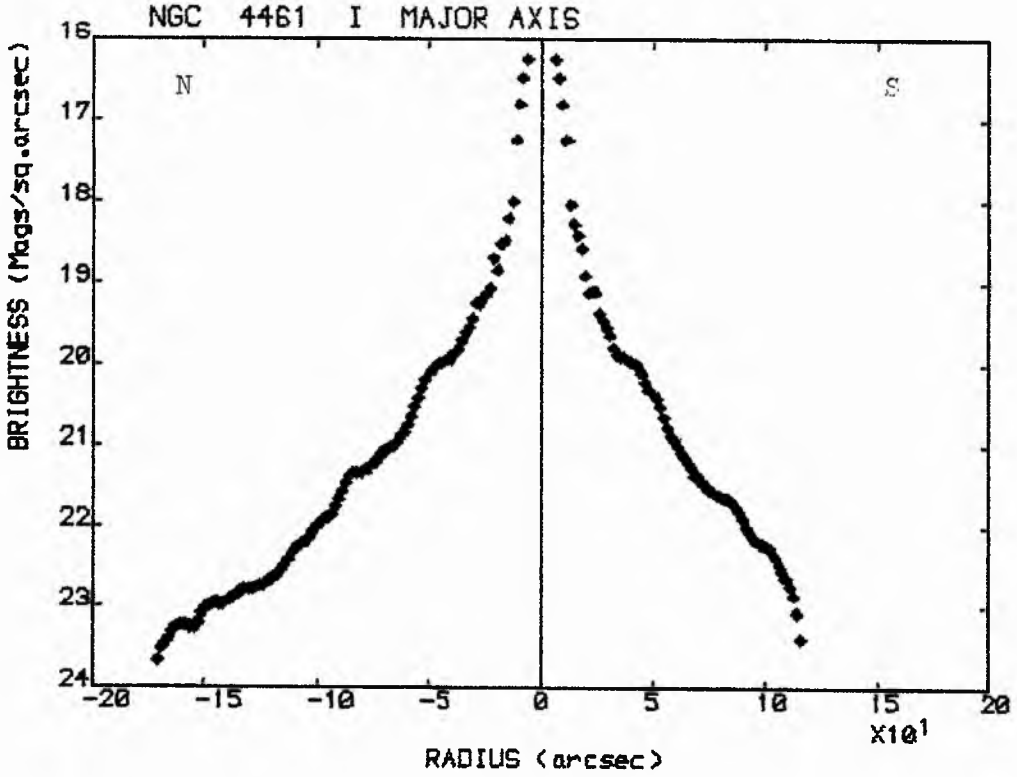
NGC 4461 I MAJOR AXIS
N
S
BRIGHTNESS (Mags/sq.arcsec)
16
17
18
19
20
21
22
23
24
-20
-15
-10
-5
0
5
10
15
20
X10¹
RADIUS (arcsec)

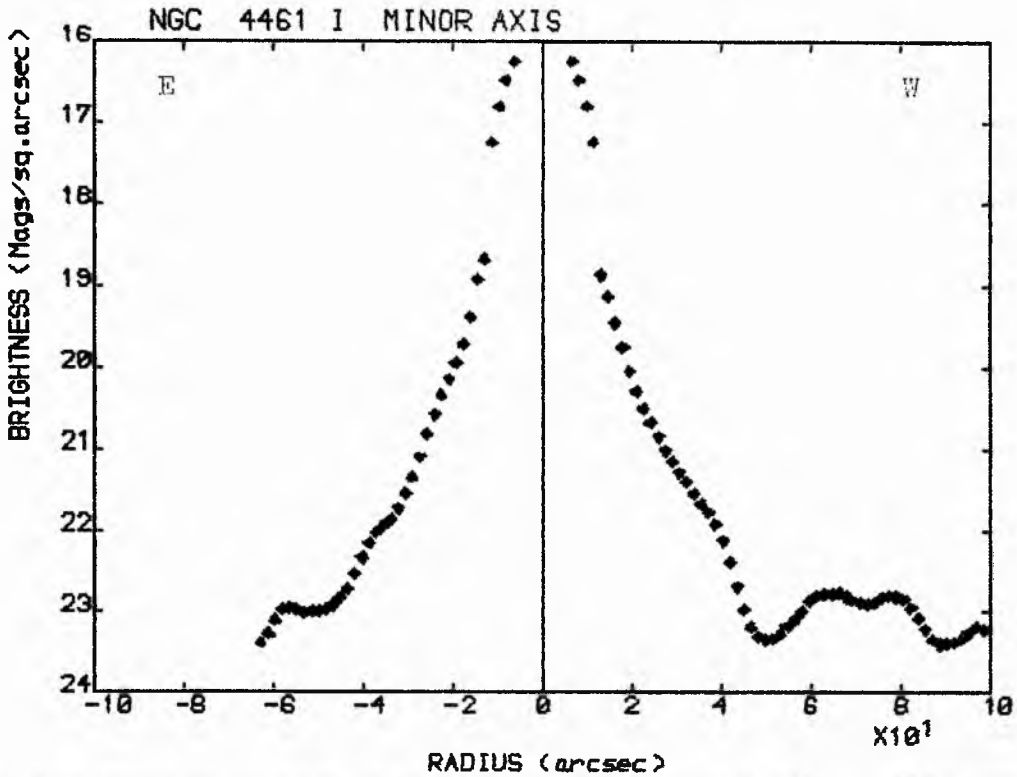
NGC 4461 I MINOR AXIS
E
W
BRIGHTNESS (Mags/sq.arcsec)
16
17
18
19
20
21
22
23
24
-10
-8
-6
-4
-2
0
2
4
6
8
10
X10¹
RADIUS (arcsec)

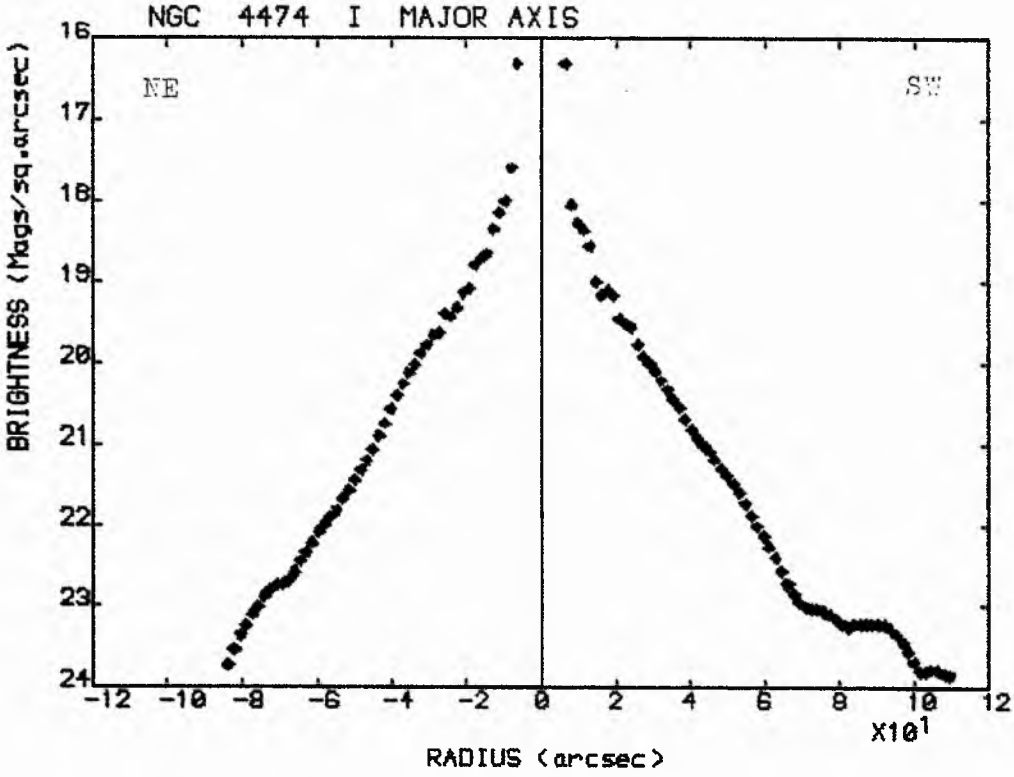
NGC 4474 I MAJOR AXIS
NE
SW
BRIGHTNESS (Mags/sq.arcsec)
16
17
18
19
20
21
22
23
24
-12 -10 -8 -6 -4 -2 0 2 4 6 8 10 12
X10¹
RADIUS (arcsec)

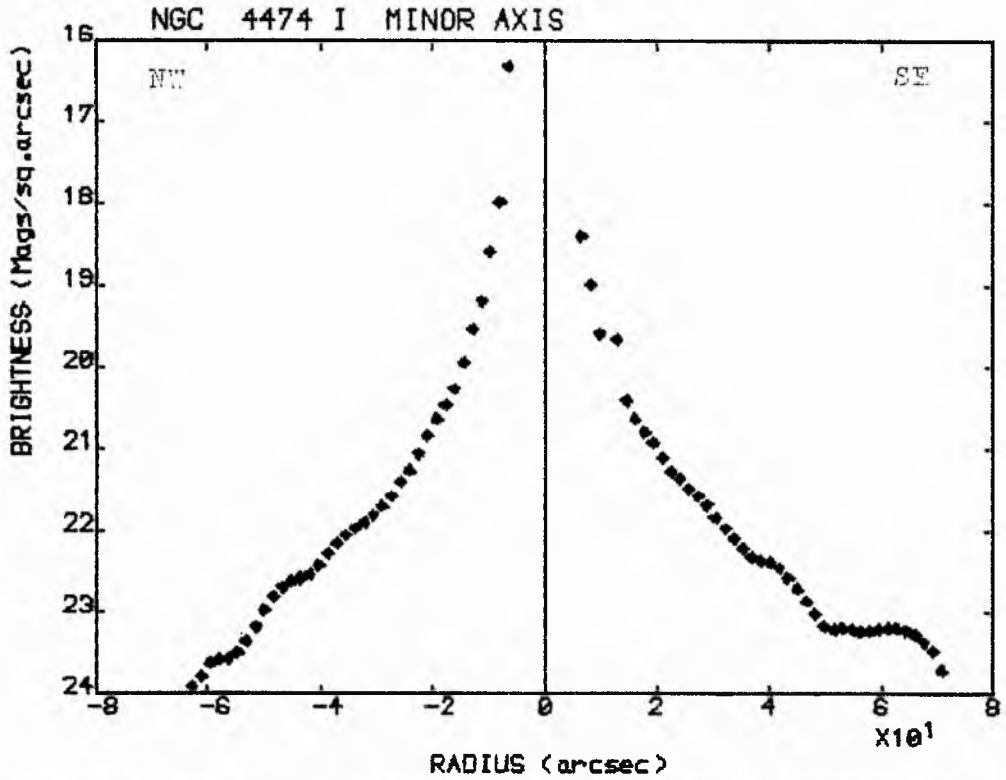
NGC 4474 I MINOR AXIS
NW
SE
BRIGHTNESS (Mags/sq.arcsec)
16
17
18
19
20
21
22
23
24
-8 -6 -4 -2 0 2 4 6 8
X10¹
RADIUS (arcsec)

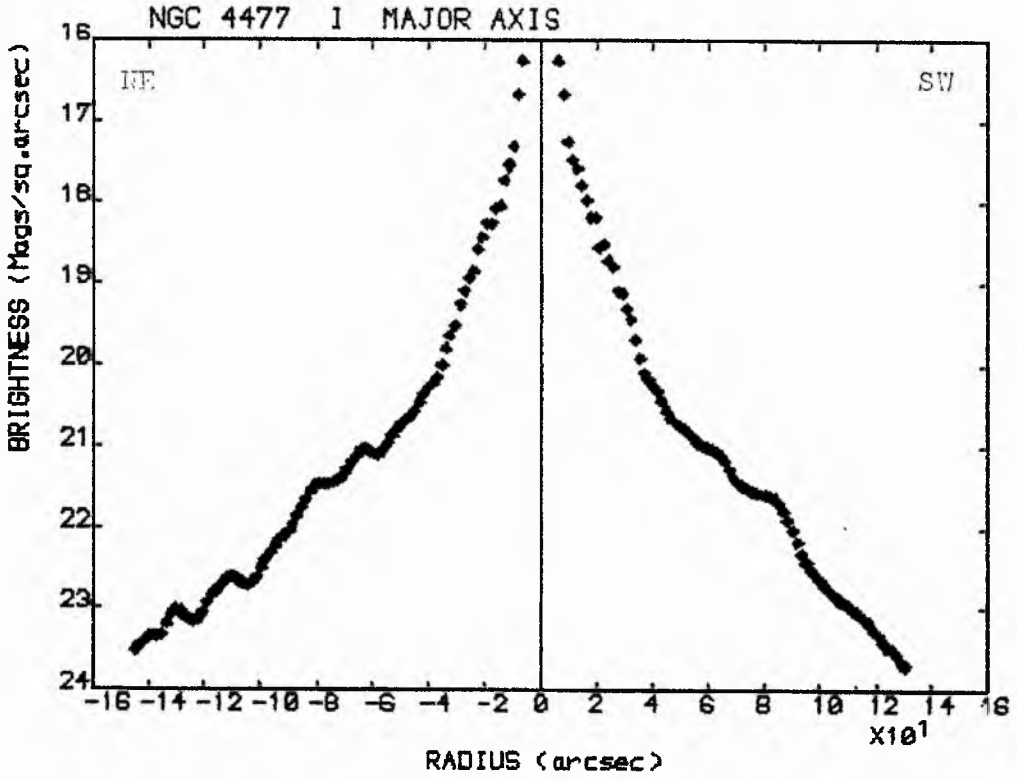
NGC 4477 I MAJOR AXIS
NE
SW
BRIGHTNESS (Mags/sq.arcsec)
16
17
18
19
20
21
22
23
24
-16 -14 -12 -10 -8 -6 -4 -2 0 2 4 6 8 10 12 14 16
X10¹
RADIUS (arcsec)

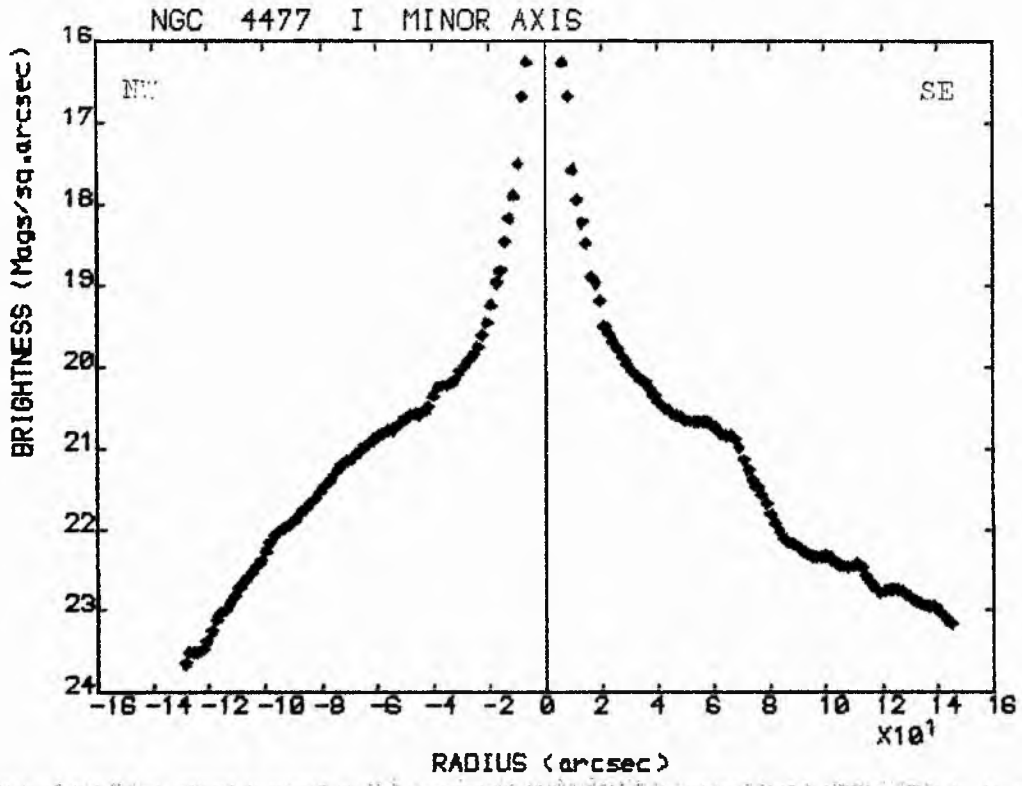
NGC 4477 I MINOR AXIS
NW
SE
BRIGHTNESS (Mags/sq.arcsec)
16
17
18
19
20
21
22
23
24
-16 -14 -12 -10 -8 -6 -4 -2 0 2 4 6 8 10 12 14 16
X10¹
RADIUS (arcsec)

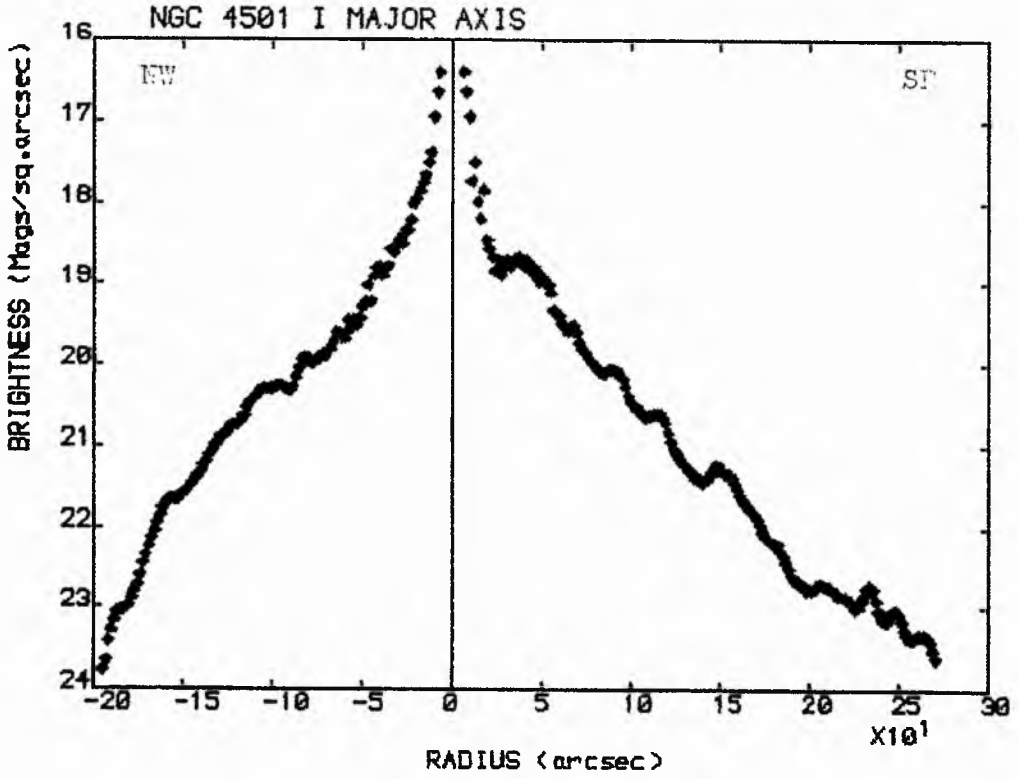
NGC 4501 I MAJOR AXIS
NW
SE
BRIGHTNESS (Mags/sq.arcsec)
16
17
18
19
20
21
22
23
24
-20
-15
-10
-5
0
5
10
15
20
25
30
X10¹
RADIUS (arcsec)

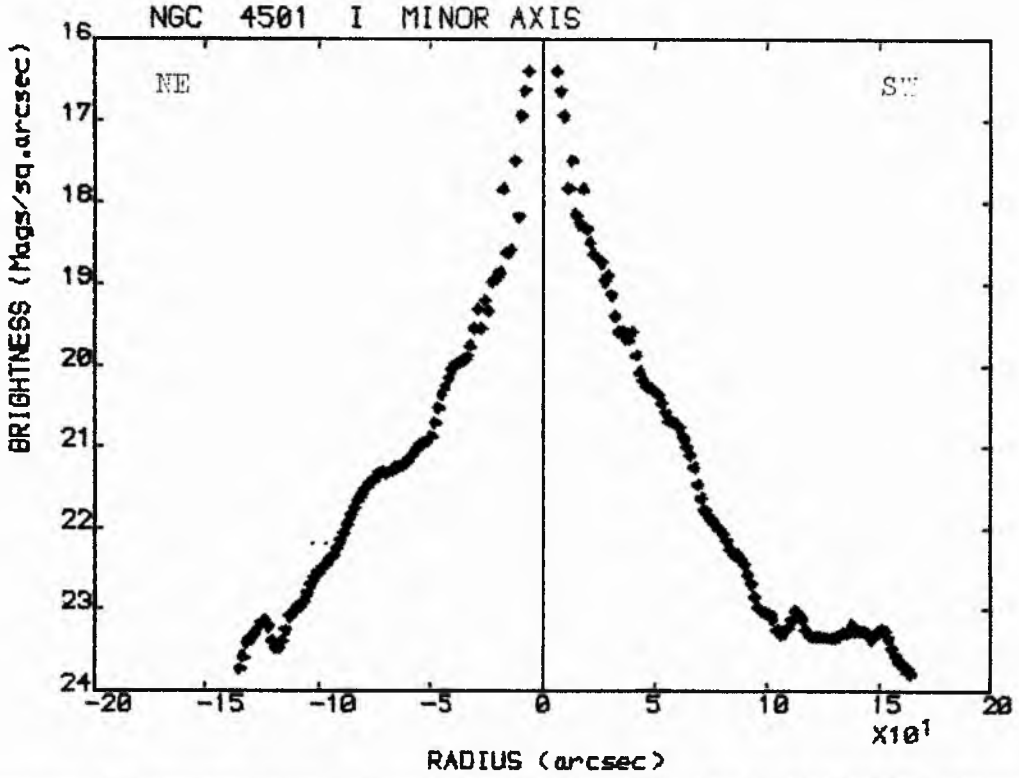
NGC 4501 I MINOR AXIS
NE
SW
BRIGHTNESS (Mags/sq.arcsec)
16
17
18
19
20
21
22
23
24
-20
-15
-10
-5
0
5
10
15
20
X10¹
RADIUS (arcsec)

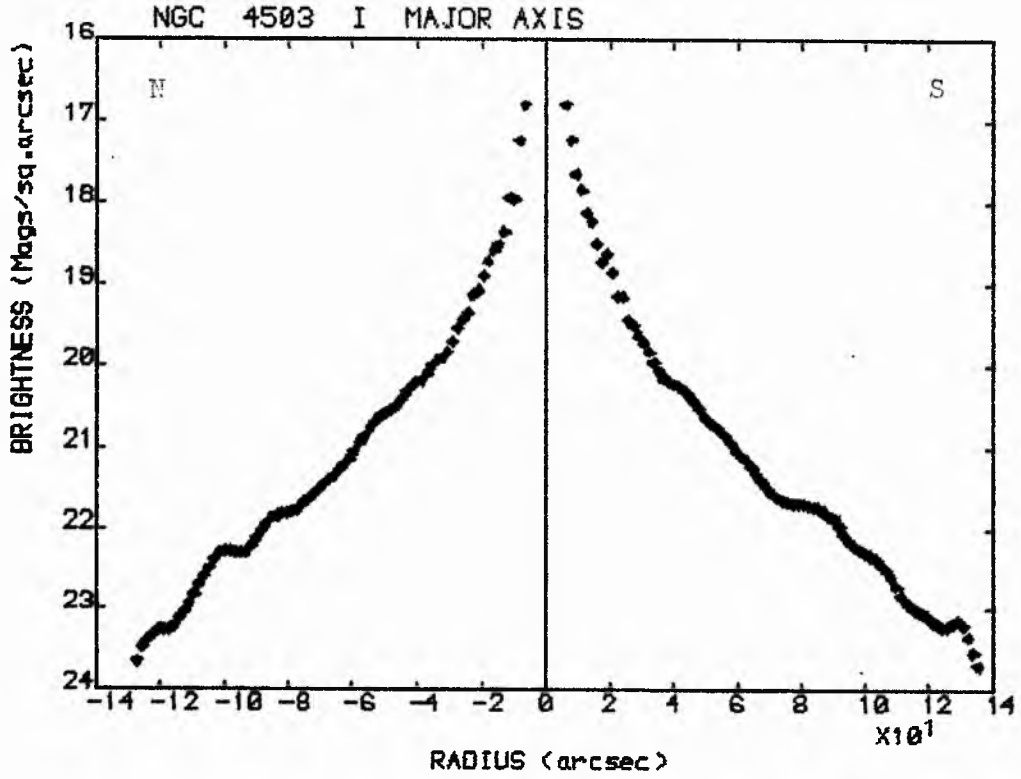
NGC 4503 I MAJOR AXIS
N
S
BRIGHTNESS (Mags/sq.arcsec)
16
17
18
19
20
21
22
23
24
-14 -12 -10 -8 -6 -4 -2 0 2 4 6 8 10 12 14
X10¹
RADIUS (arcsec)

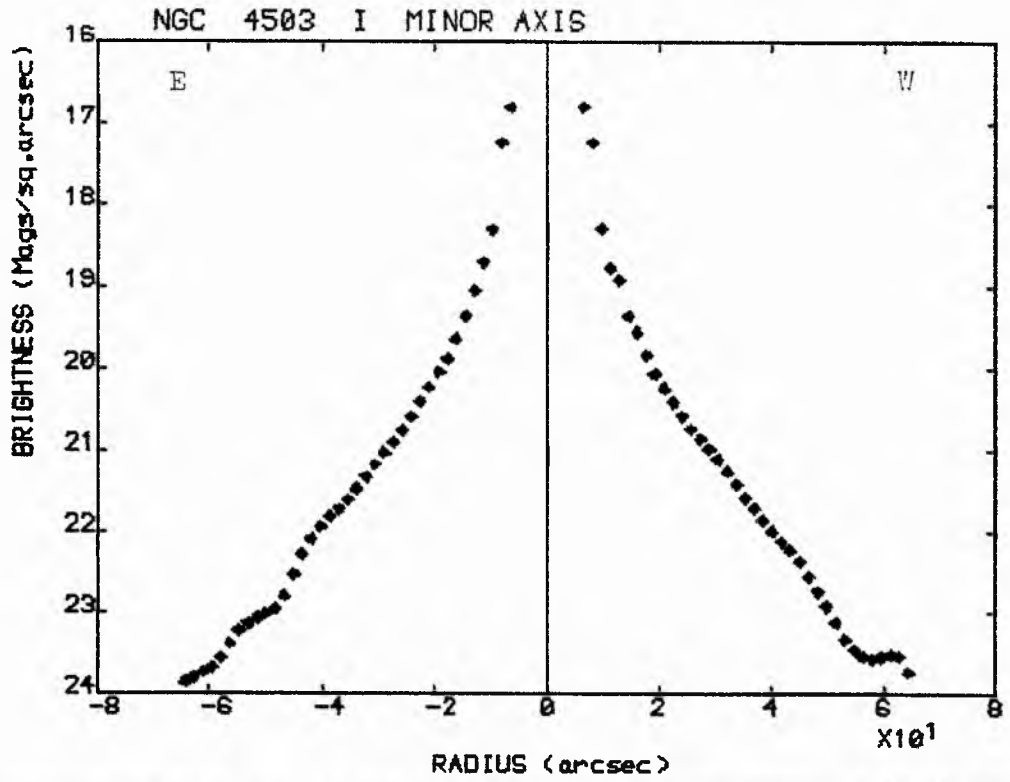
NGC 4503 I MINOR AXIS
E
W
BRIGHTNESS (Mags/sq.arcsec)
16
17
18
19
20
21
22
23
24
-8 -6 -4 -2 0 2 4 6 8
X10¹
RADIUS (arcsec)

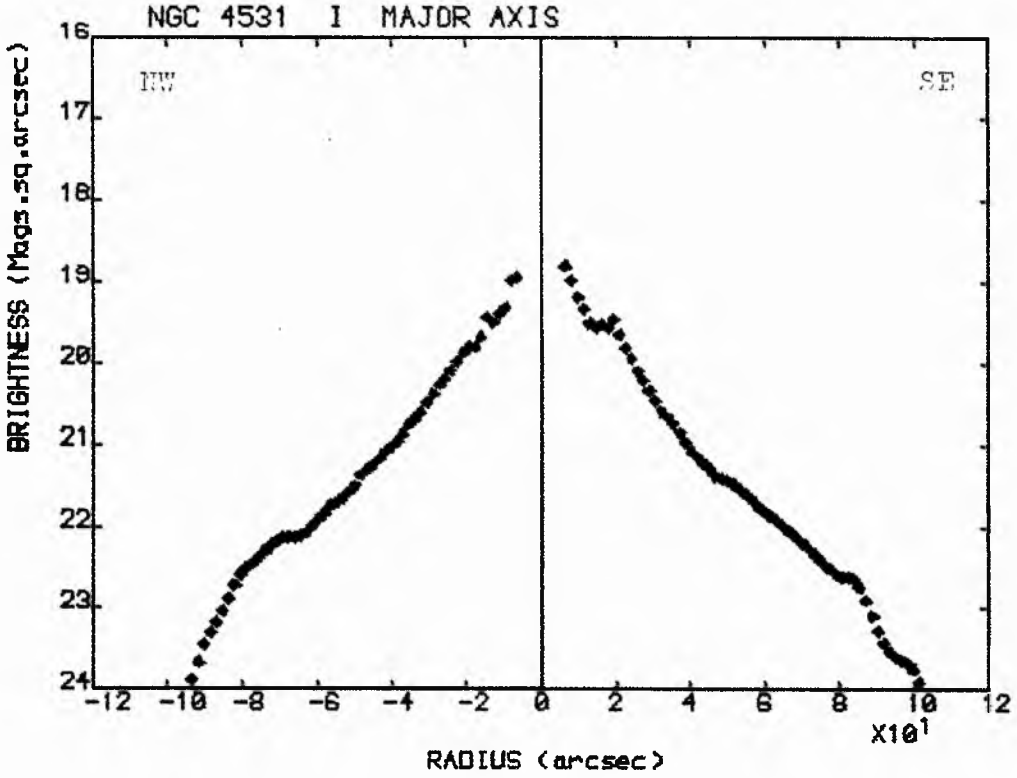
NGC 4531 I MAJOR AXIS
NW
SE
BRIGHTNESS (Mags.sq.arcsec)
16
17
18
19
20
21
22
23
24
-12 -10 -8 -6 -4 -2 0 2 4 6 8 10 12
X10¹
RADIUS (arcsec)

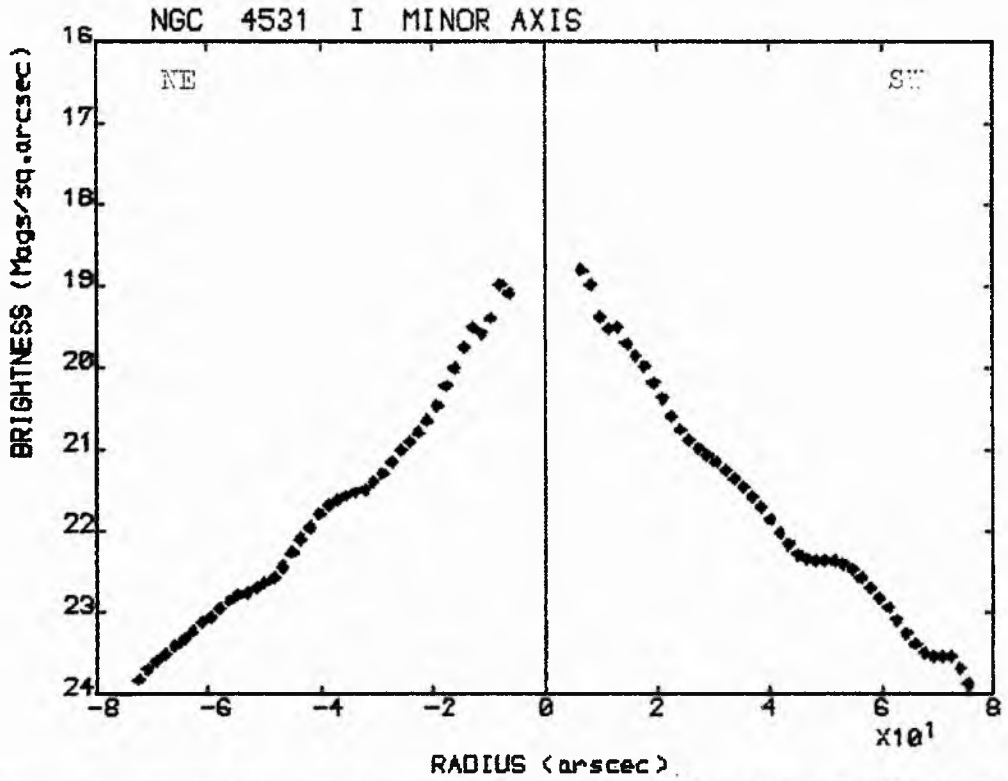
NGC 4531 I MINOR AXIS
NE
SW
BRIGHTNESS (Mags/sq.arcsec)
16
17
18
19
20
21
22
23
24
-8 -6 -4 -2 0 2 4 6 8
X10¹
RADIUS (arcsec)

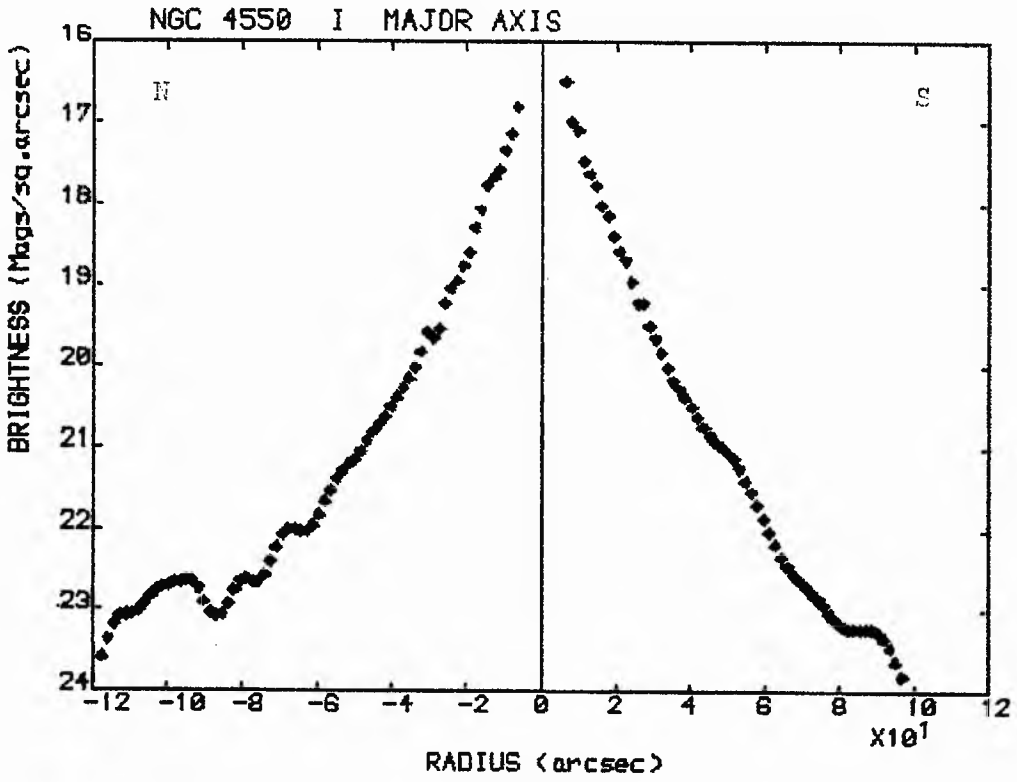
NGC 4550 I MAJOR AXIS
N
S
BRIGHTNESS (Mags/sq.arcsec)
16
17
18
19
20
21
22
23
24
-12 -10 -8 -6 -4 -2 0 2 4 6 8 10 12
X10¹
RADIUS (arcsec)

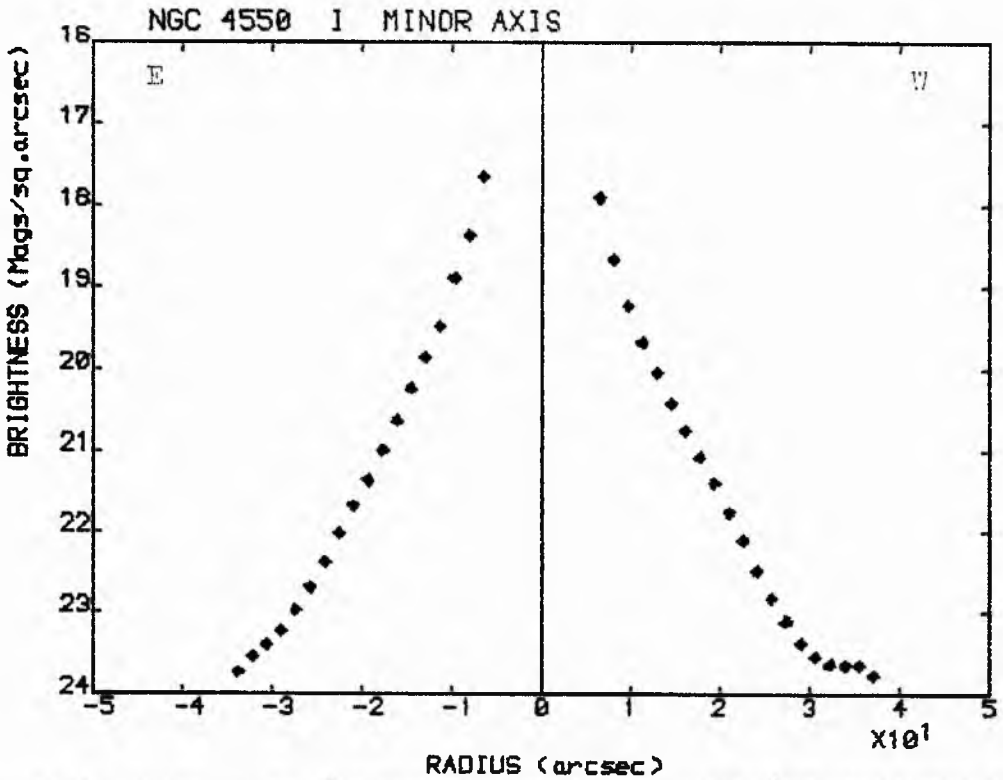
NGC 4550 I MINOR AXIS
E
W
BRIGHTNESS (Mags/sq.arcsec)
16
17
18
19
20
21
22
23
24
-5 -4 -3 -2 -1 0 1 2 3 4 5
X10¹
RADIUS (arcsec)

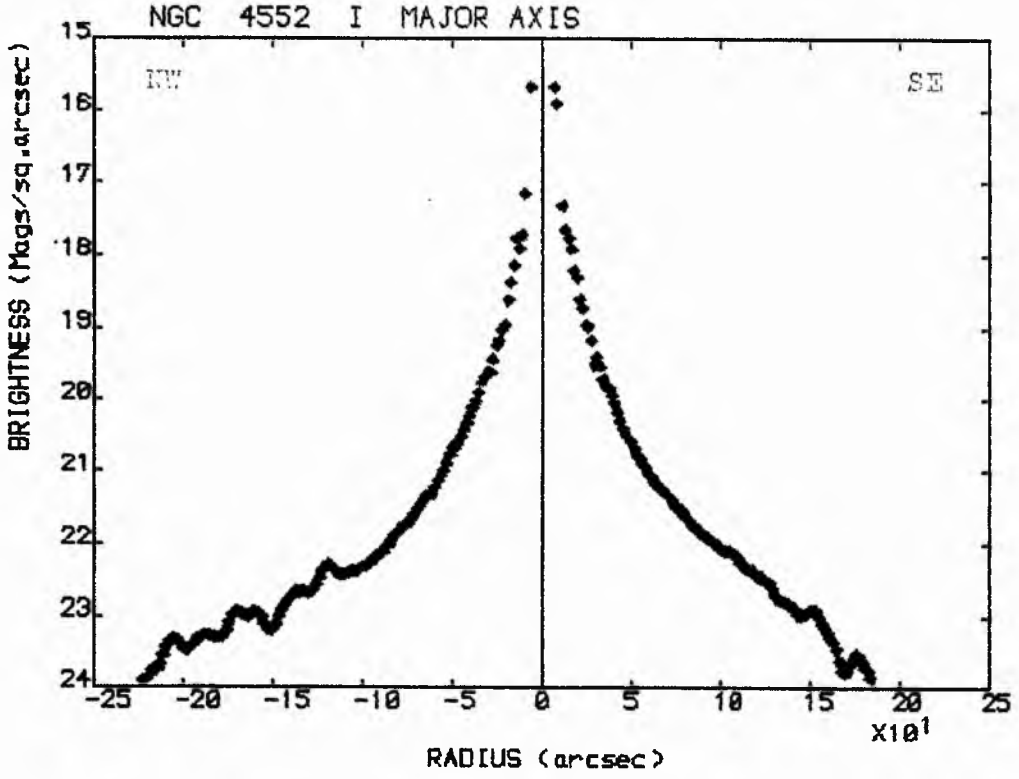
NGC 4552 I MAJOR AXIS
NW
SE
BRIGHTNESS (Mags/sq.arcsec)
15
16
17
18
19
20
21
22
23
24
-25
-20
-15
-10
-5
0
5
10
15
20
25
X10¹
RADIUS (arcsec)

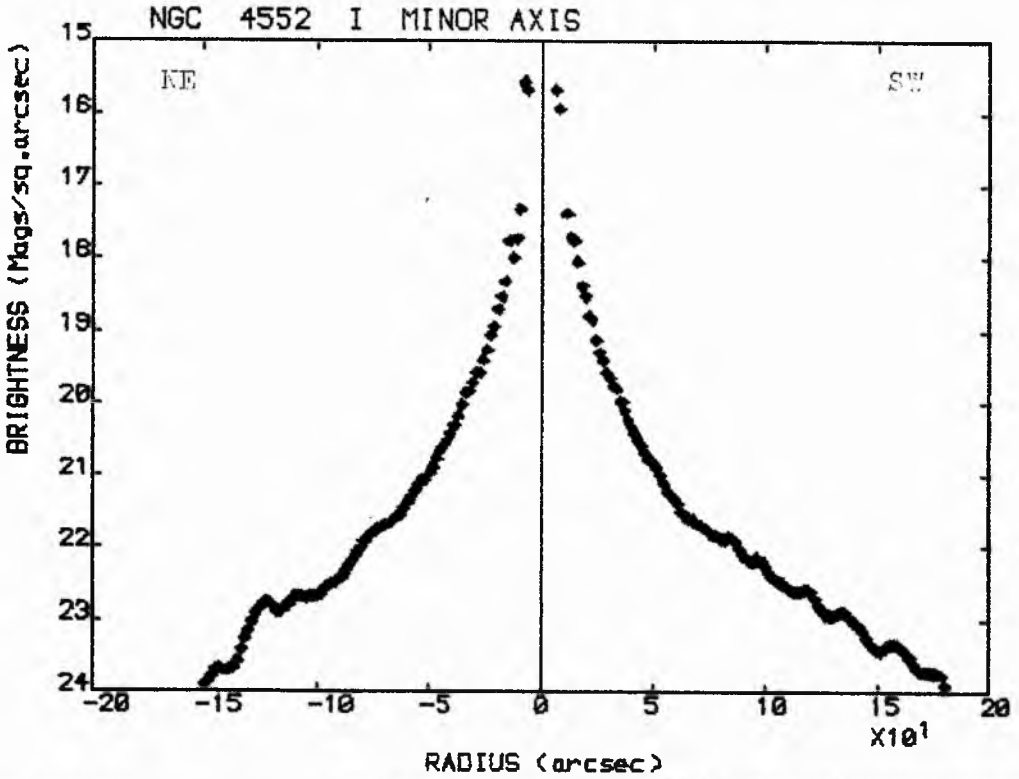
NGC 4552 I MINOR AXIS
NE
SW
BRIGHTNESS (Mags/sq.arcsec)
15
16
17
18
19
20
21
22
23
24
-20
-15
-10
-5
0
5
10
15
20
X10¹
RADIUS (arcsec)

APPENDIX 'B'

(B - R), (B - I) and (R - I) Colour-Difference Profiles

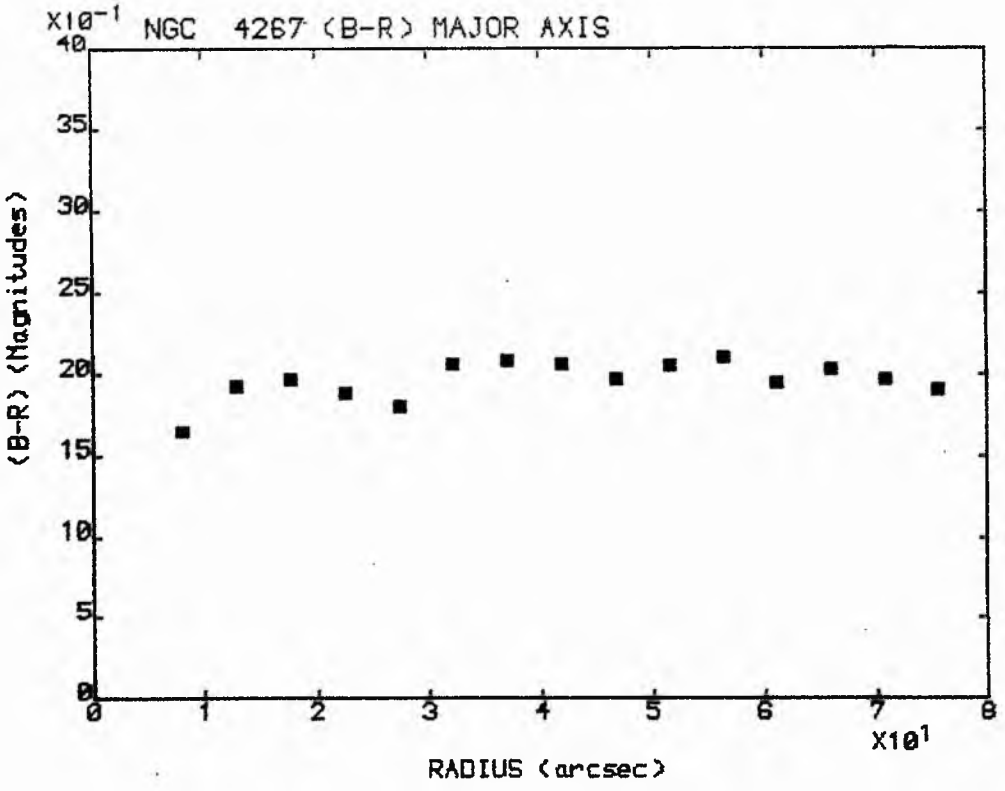
X10⁻¹
NGC 4267 (B-R) MAJOR AXIS
(B-R) (Magnitudes)
40
35
30
25
20
15
10
5
0
0 1 2 3 4 5 6 7 8
X10¹
RADIUS (arcsec)

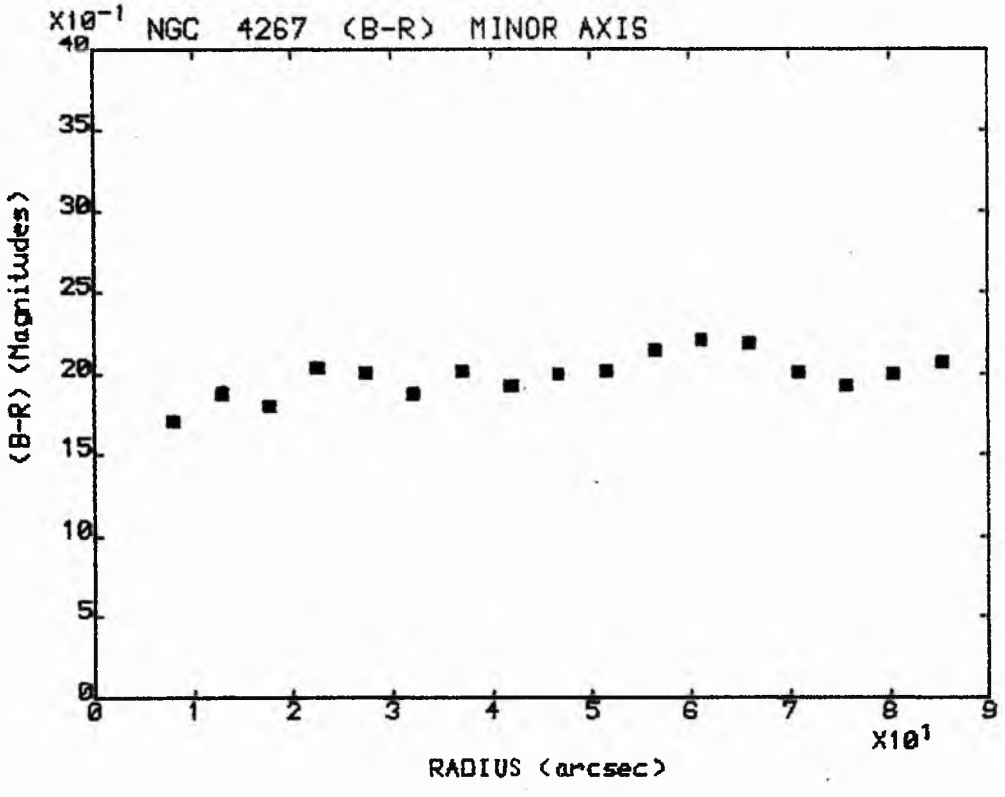
X10⁻¹
NGC 4267 (B-R) MINOR AXIS
(B-R) (Magnitudes)
40
35
30
25
20
15
10
5
0
0 1 2 3 4 5 6 7 8 9
X10¹
RADIUS (arcsec)

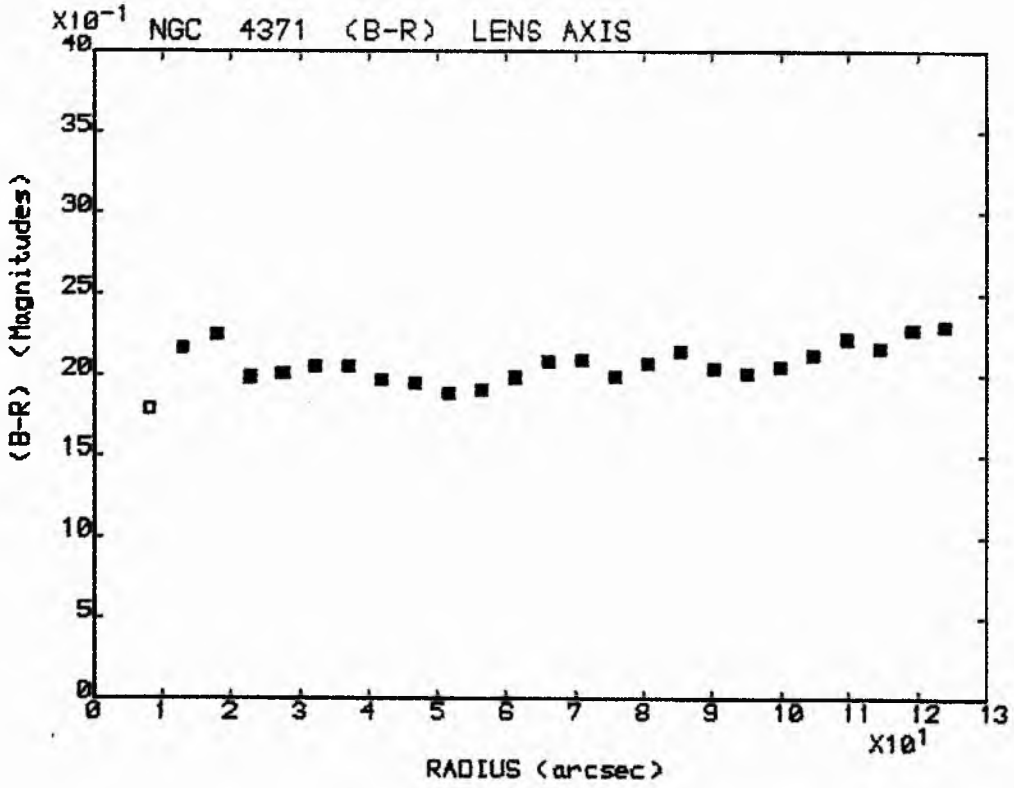
X10⁻¹
NGC 4371 (B-R) LENS AXIS
(B-R) (Magnitudes)
RADIUS (arcsec)
X10¹

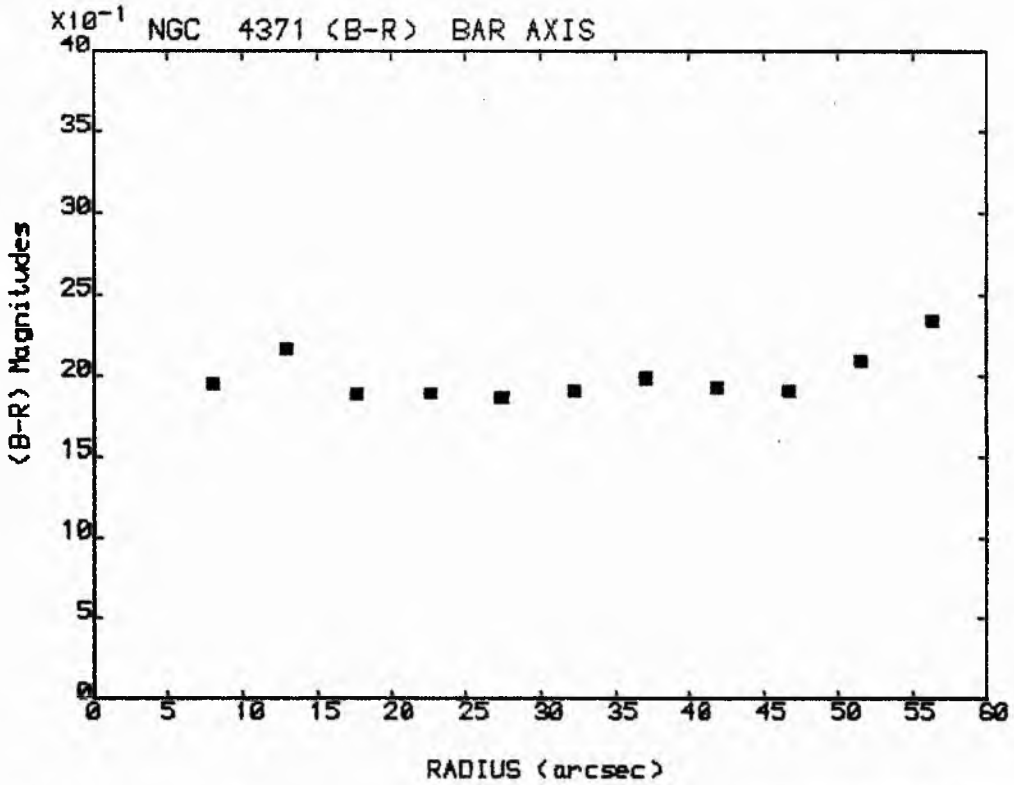
X10⁻¹
NGC 4371 (B-R) BAR AXIS
(B-R) Magnitudes
RADIUS (arcsec)

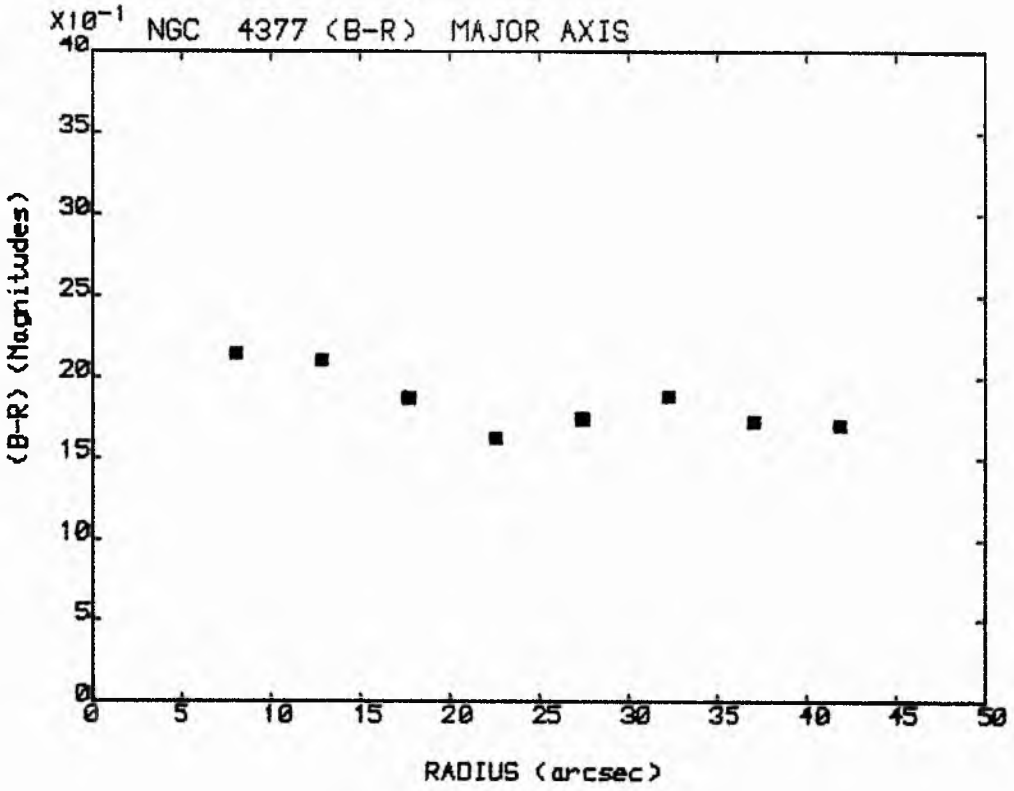
X10⁻¹
NGC 4377 (B-R) MAJOR AXIS
(B-R) (Magnitudes)
RADIUS (arcsec)
40
35
30
25
20
15
10
5
0
0
5
10
15
20
25
30
35
40
45
50

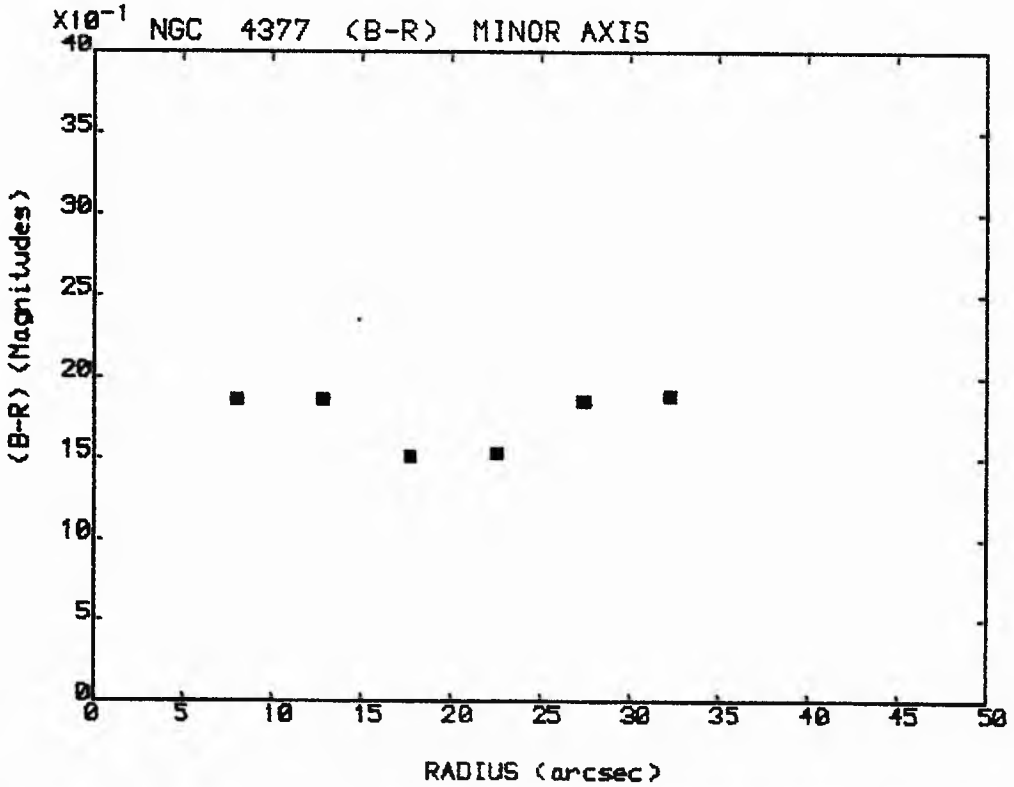
X10⁻¹
NGC 4377 (B-R) MINOR AXIS
(B-R) (Magnitudes)
RADIUS (arcsec)
40
35
30
25
20
15
10
5
0
0
5
10
15
20
25
30
35
40
45
50

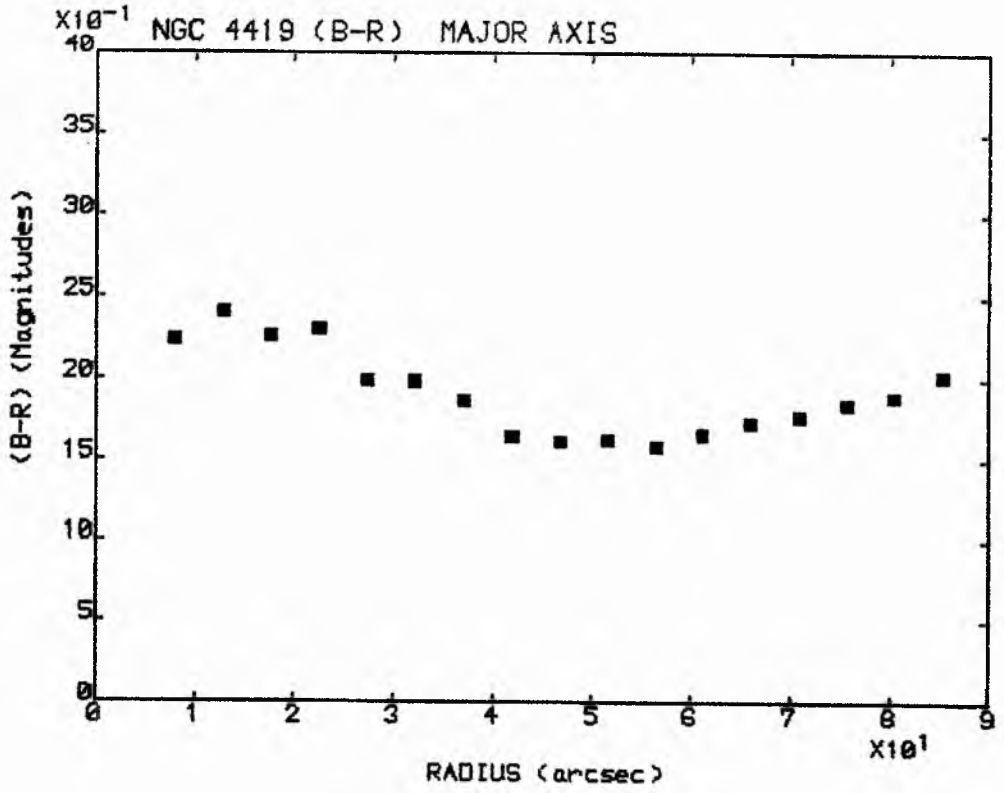
X10⁻¹
NGC 4419 (B-R) MAJOR AXIS
(B-R) (Magnitudes)
RADIUS (arcsec)
X10¹

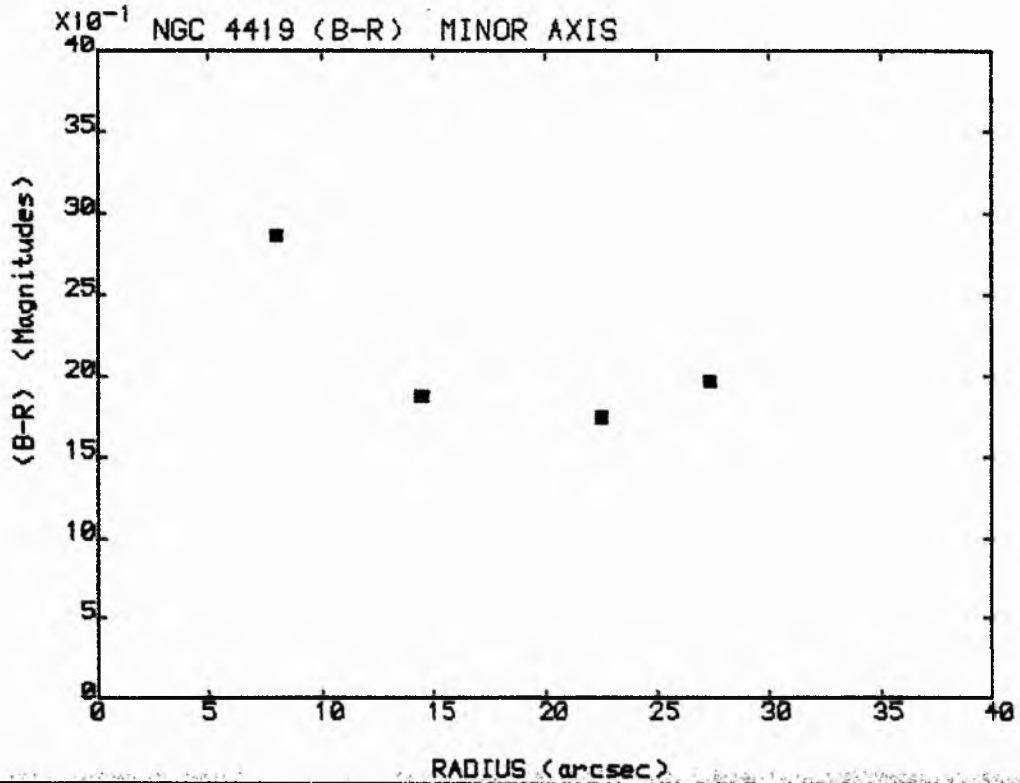
X10⁻¹
NGC 4419 (B-R) MINOR AXIS
(B-R) (Magnitudes)
RADIUS (arcsec)

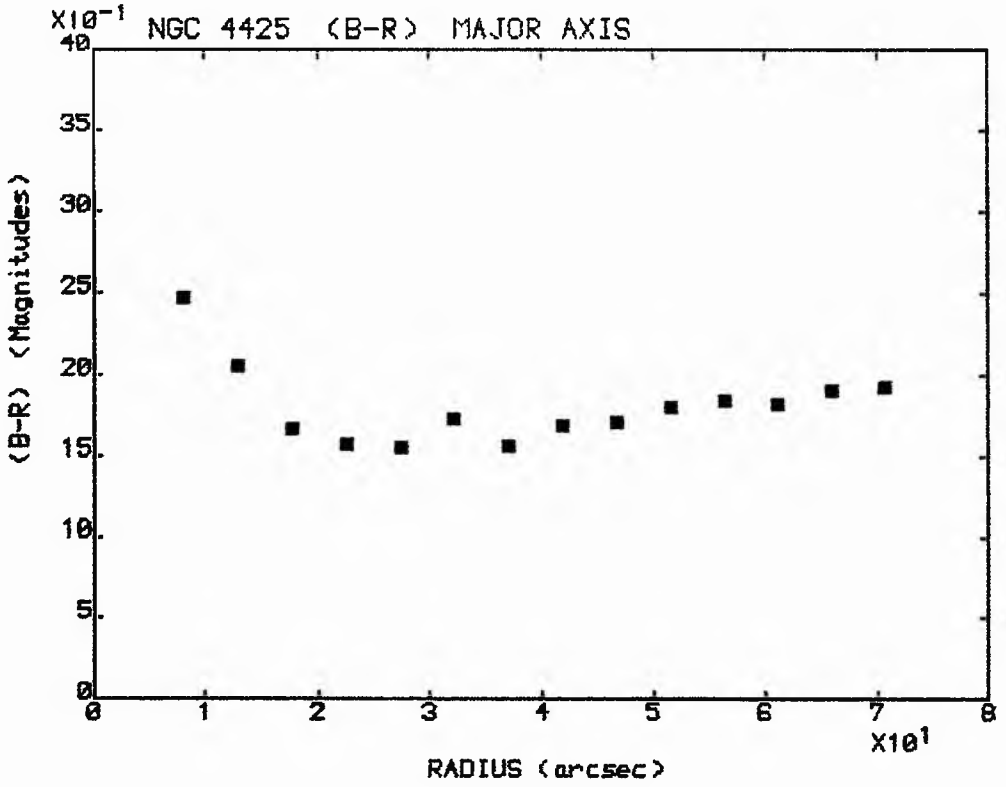
X10⁻¹
NGC 4425 (B-R) MAJOR AXIS
(B-R) (Magnitudes)
40
35
30
25
20
15
10
5
0
0
1
2
3
4
5
6
7
8
X10¹
RADIUS (arcsec)

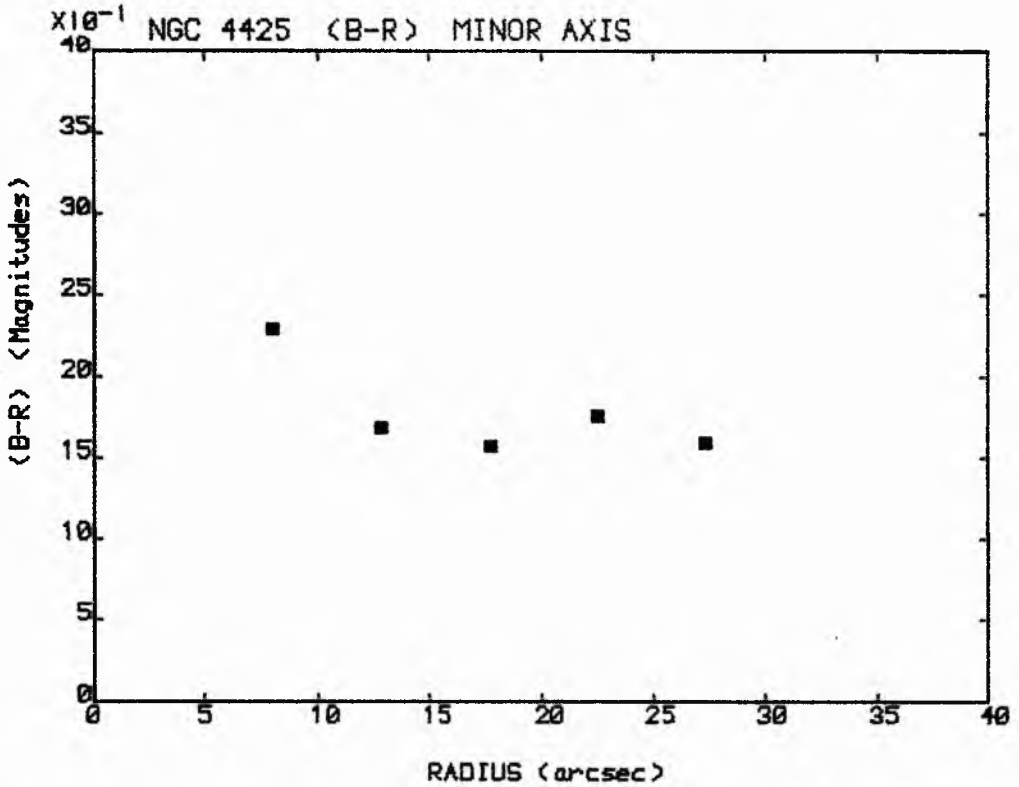
X10⁻¹
NGC 4425 (B-R) MINOR AXIS
(B-R) (Magnitudes)
40
35
30
25
20
15
10
5
0
0
5
10
15
20
25
30
35
40
RADIUS (arcsec)

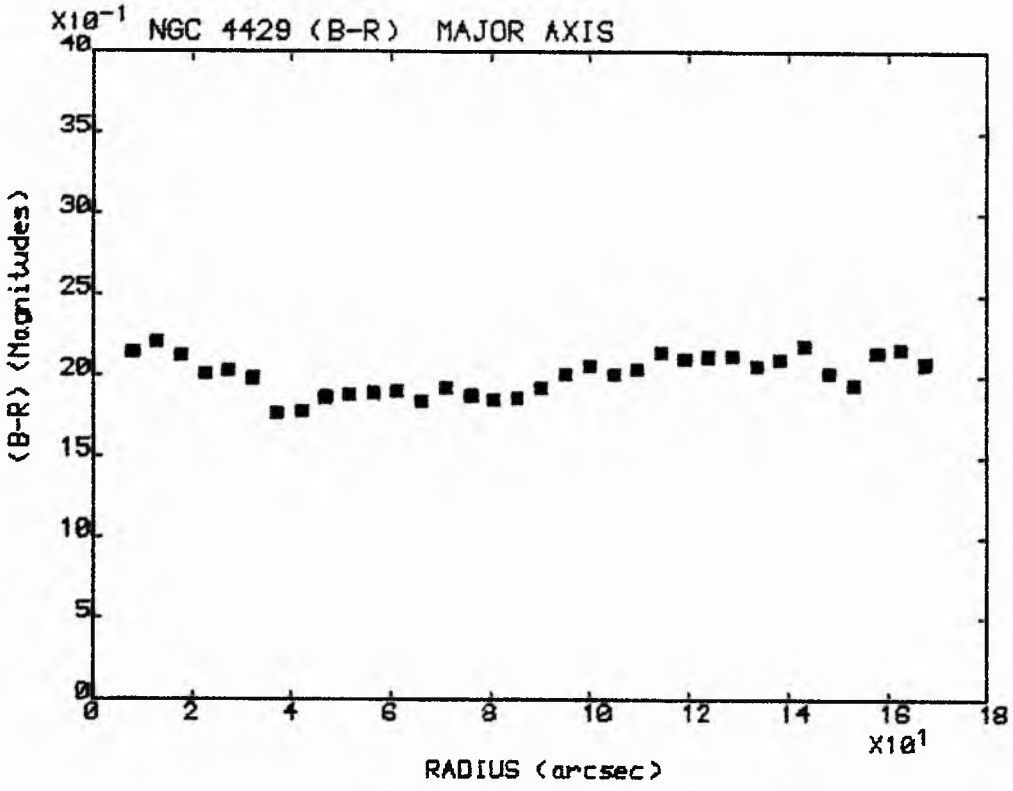
X10⁻¹
NGC 4429 (B-R) MAJOR AXIS
(B-R) (Magnitudes)
40
35
30
25
20
15
10
5
0
0
2
4
6
8
10
12
14
16
18
X10¹
RADIUS (arcsec)

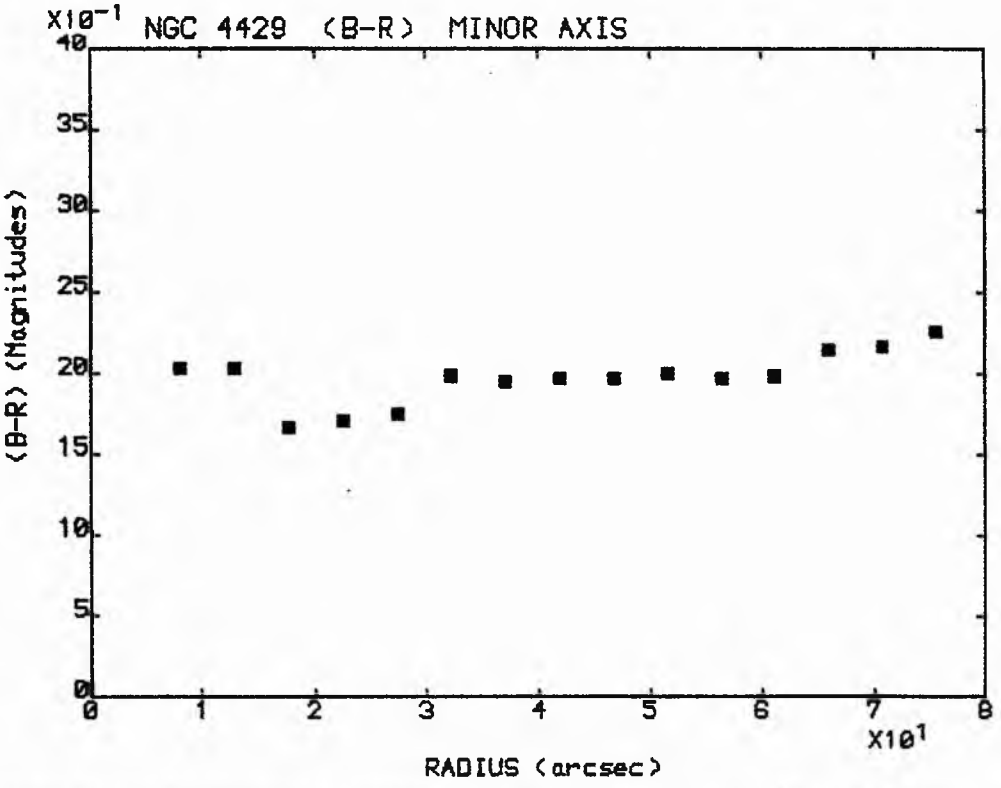
X10⁻¹
NGC 4429 (B-R) MINOR AXIS
(B-R) (Magnitudes)
40
35
30
25
20
15
10
5
0
0
1
2
3
4
5
6
7
8
X10¹
RADIUS (arcsec)

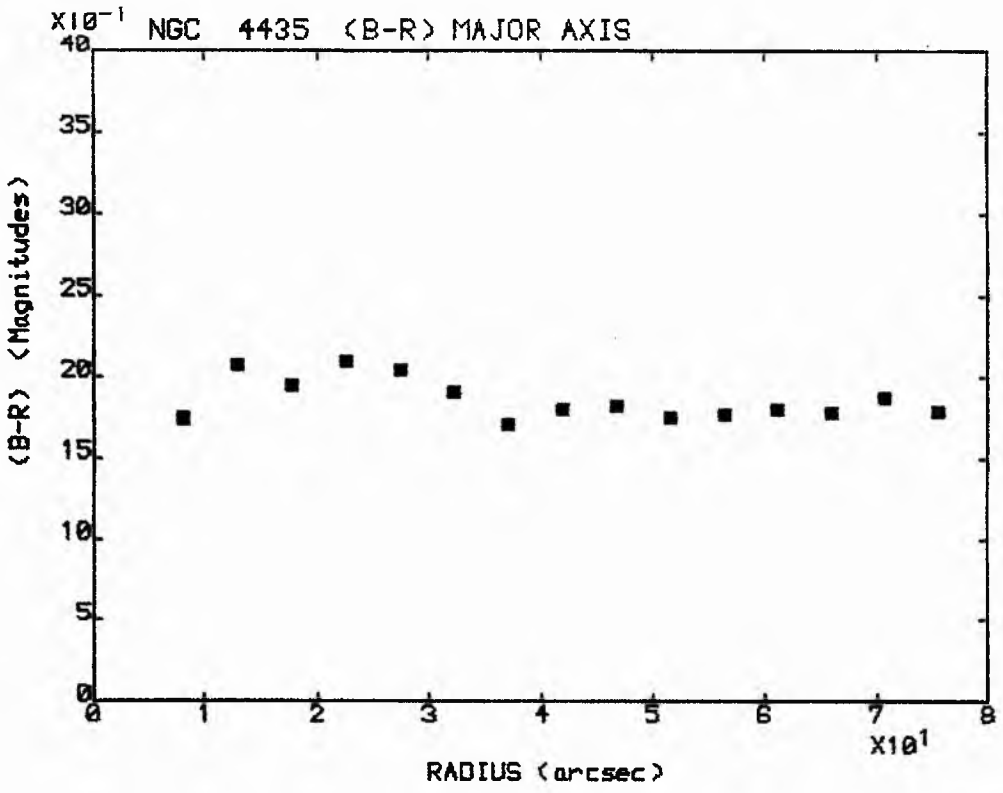
X10⁻¹
NGC 4435 (B-R) MAJOR AXIS
(B-R) (Magnitudes)
40
35
30
25
20
15
10
5
0
0
1
2
3
4
5
6
7
8
X10¹
RADIUS (arcsec)

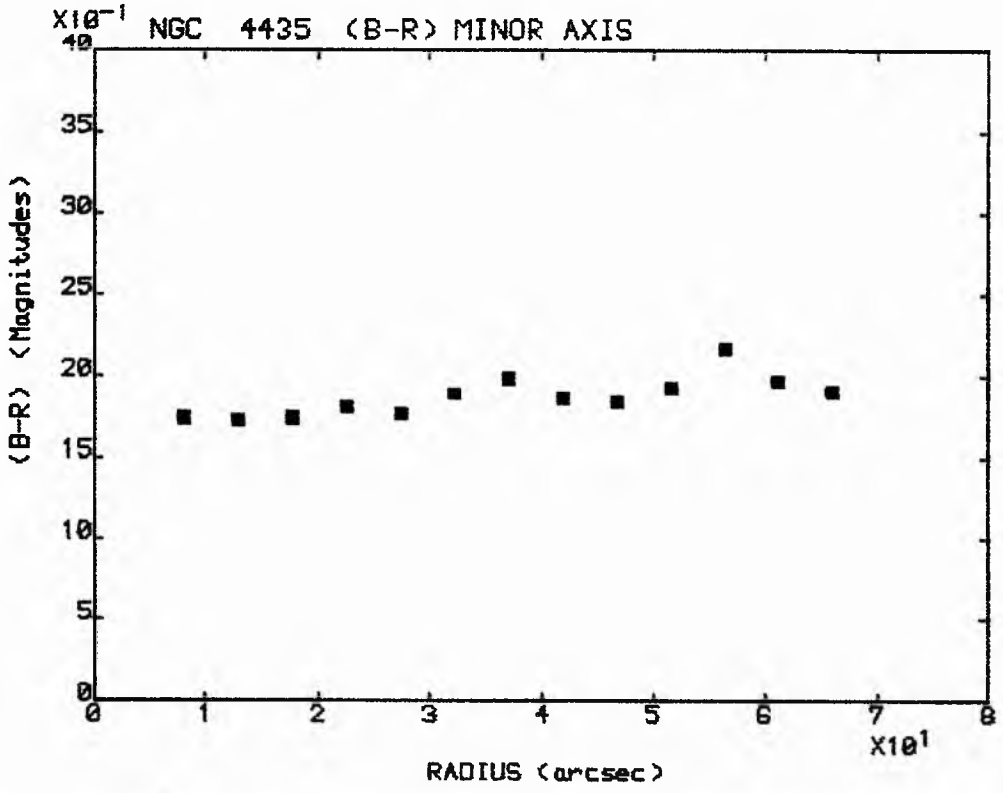
X10⁻¹
NGC 4435 (B-R) MINOR AXIS
(B-R) (Magnitudes)
40
35
30
25
20
15
10
5
0
0
1
2
3
4
5
6
7
8
X10¹
RADIUS (arcsec)

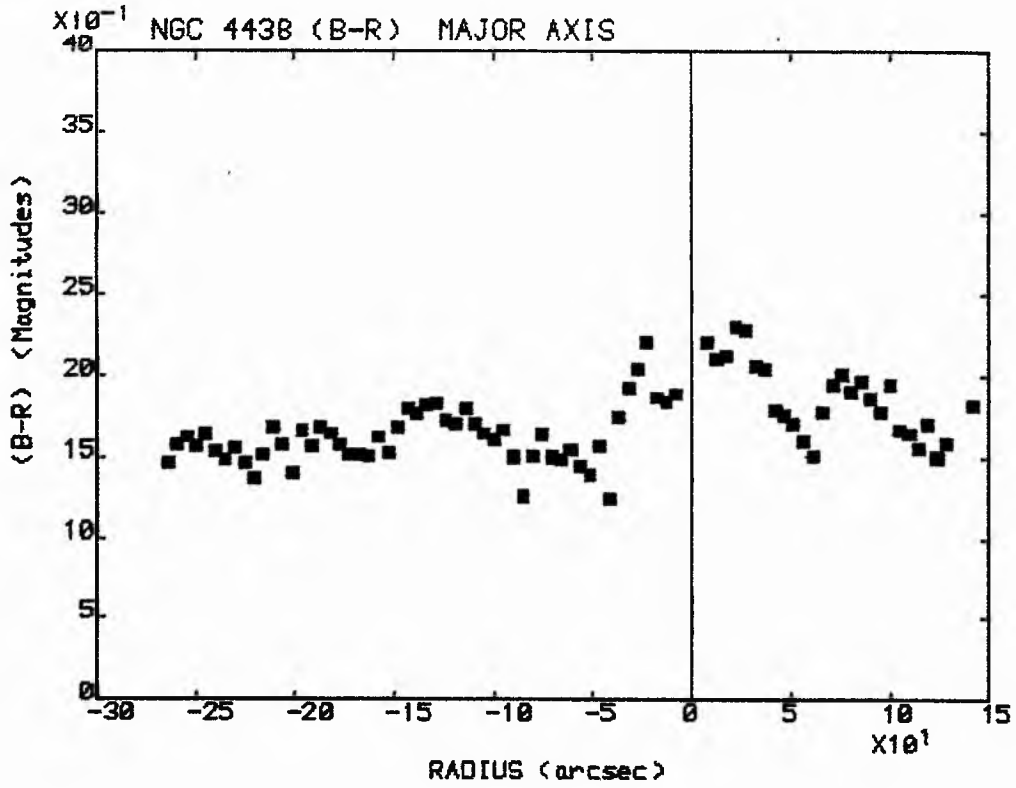
X10⁻¹
NGC 4438 (B-R) MAJOR AXIS
(B-R) (Magnitudes)
40
35
30
25
20
15
10
5
0
-30
-25
-20
-15
-10
-5
0
5
10
15
X10¹
RADIUS (arcsec)

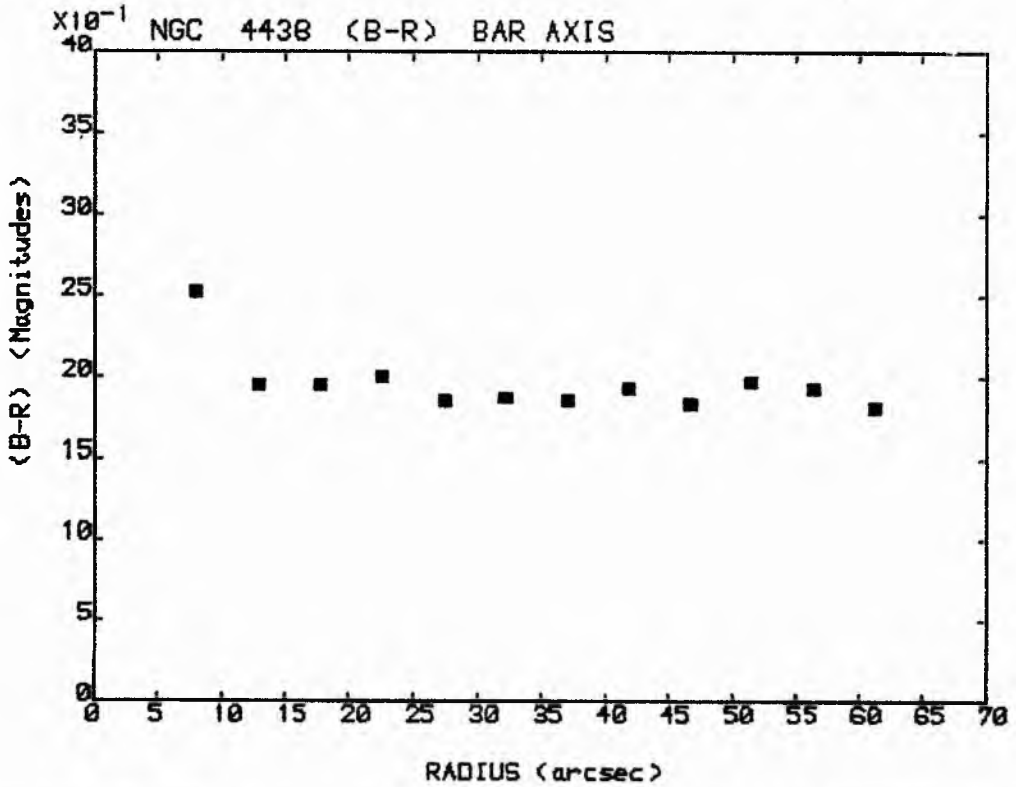
X10⁻¹
NGC 4438 (B-R) BAR AXIS
(B-R) (Magnitudes)
40
35
30
25
20
15
10
5
0
0
5
10
15
20
25
30
35
40
45
50
55
60
65
70
RADIUS (arcsec)

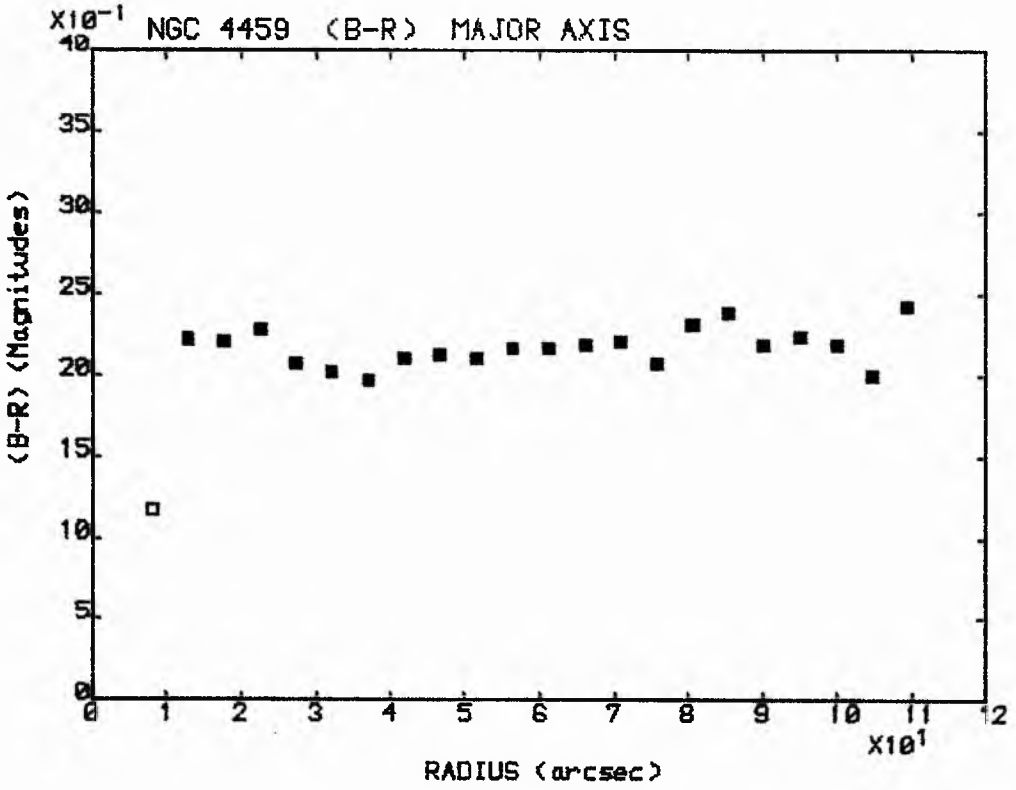
X10⁻¹
NGC 4459 (B-R) MAJOR AXIS
(B-R) (Magnitudes)
RADIUS (arcsec)
X10¹

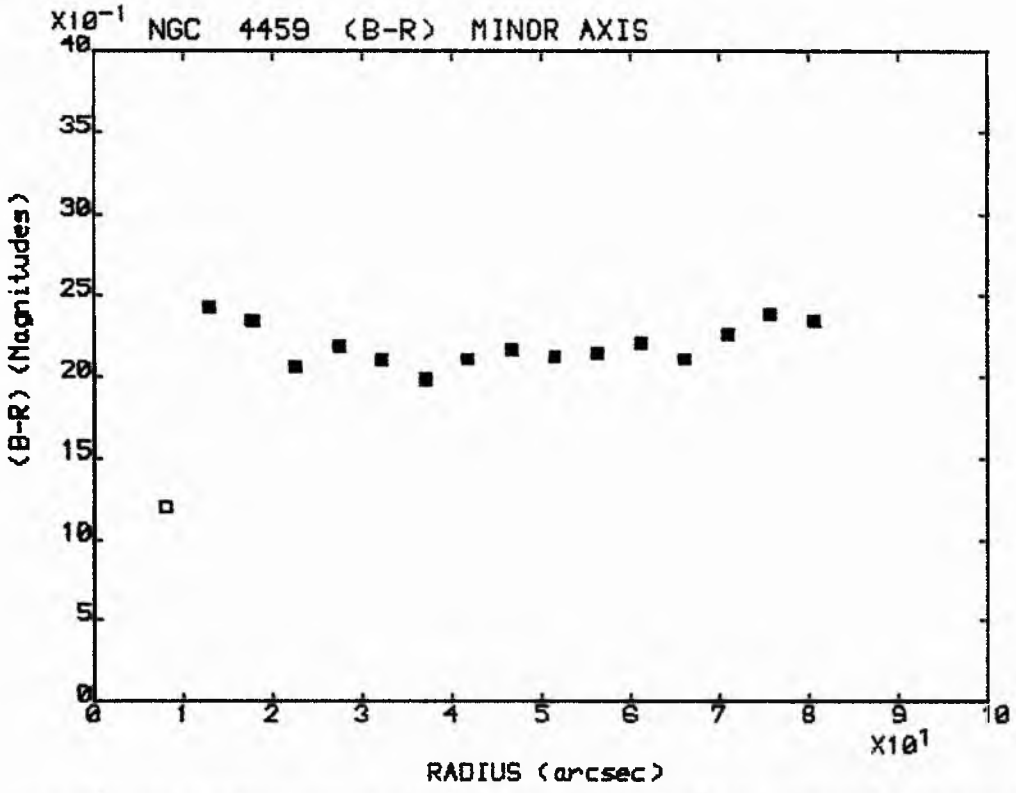
X10⁻¹
NGC 4459 (B-R) MINOR AXIS
(B-R) (Magnitudes)
RADIUS (arcsec)
X10¹

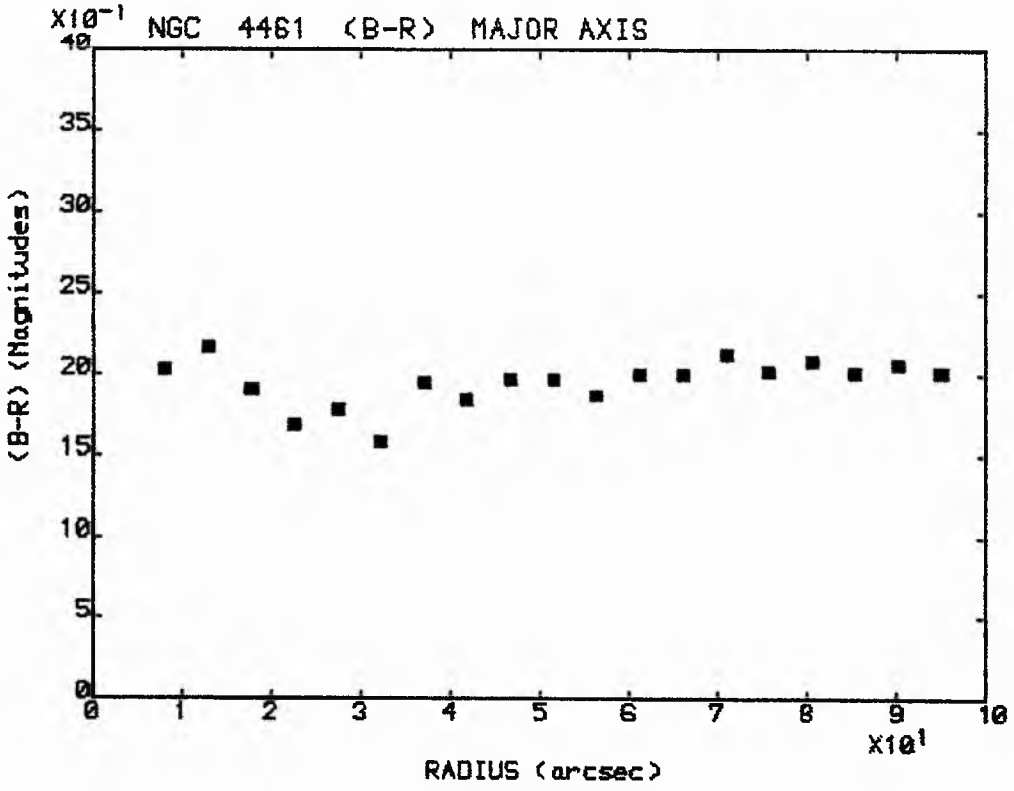
X10⁻¹
NGC 4461 (B-R) MAJOR AXIS
(B-R) (Magnitudes)
40
35
30
25
20
15
10
5
0
0 1 2 3 4 5 6 7 8 9 10
X10¹
RADIUS (arcsec)

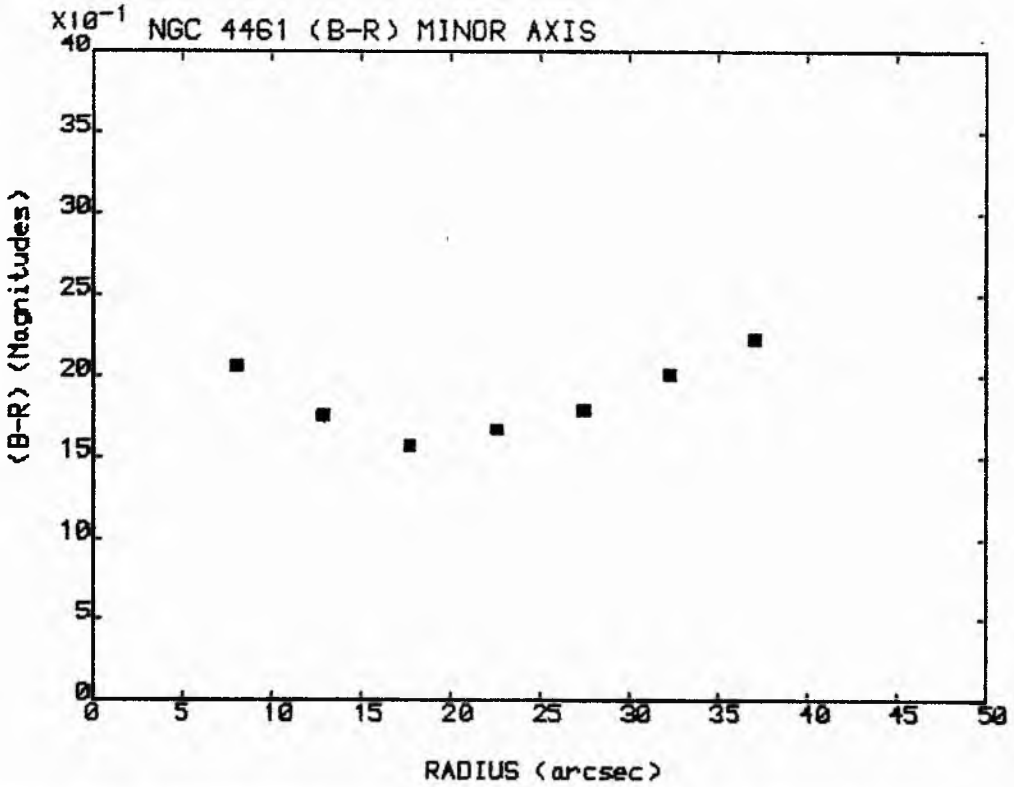
X10⁻¹
NGC 4461 (B-R) MINOR AXIS
(B-R) (Magnitudes)
40
35
30
25
20
15
10
5
0
0 5 10 15 20 25 30 35 40 45 50
RADIUS (arcsec)

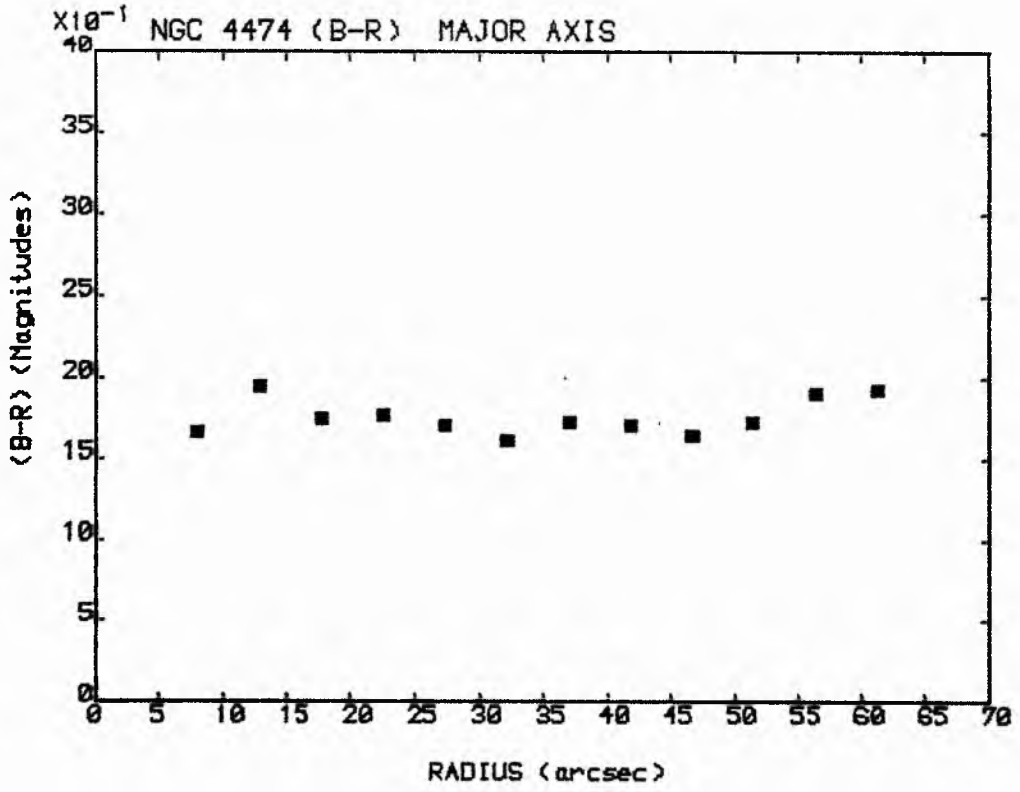
X10⁻¹
NGC 4474 (B-R) MAJOR AXIS
(B-R) (Magnitudes)
RADIUS (arcsec)
0
5
10
15
20
25
30
35
40
45
50
55
60
65
70

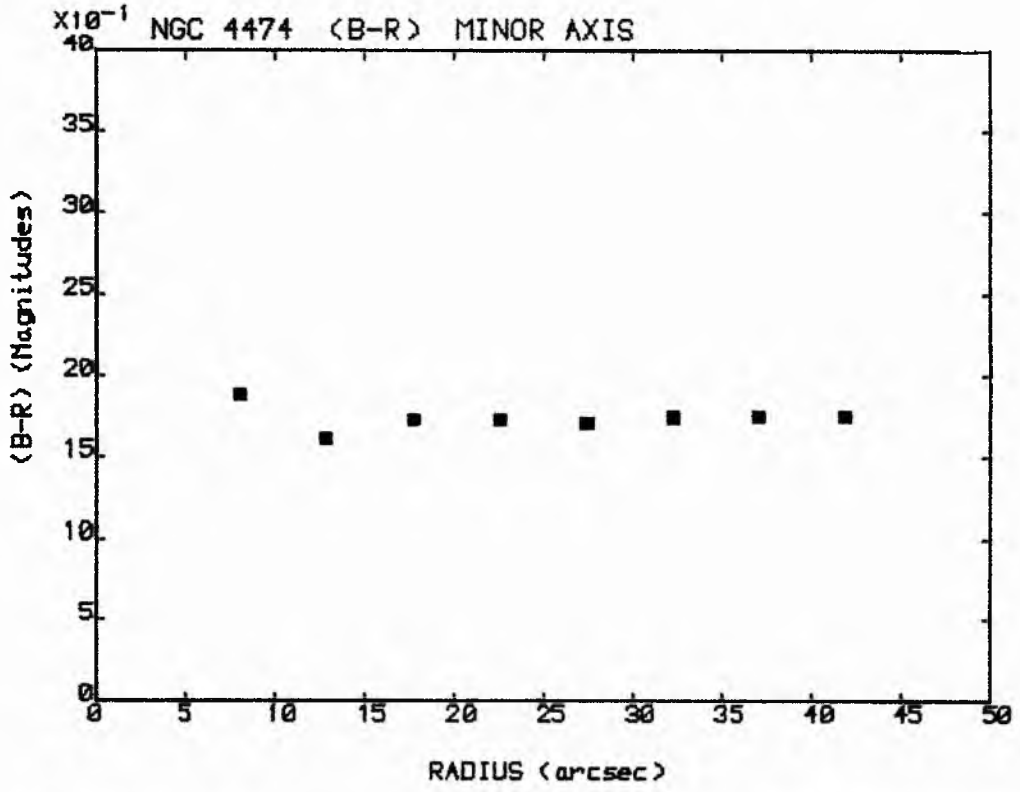
X10⁻¹
NGC 4474 (B-R) MINOR AXIS
(B-R) (Magnitudes)
RADIUS (arcsec)
0
5
10
15
20
25
30
35
40
45
50

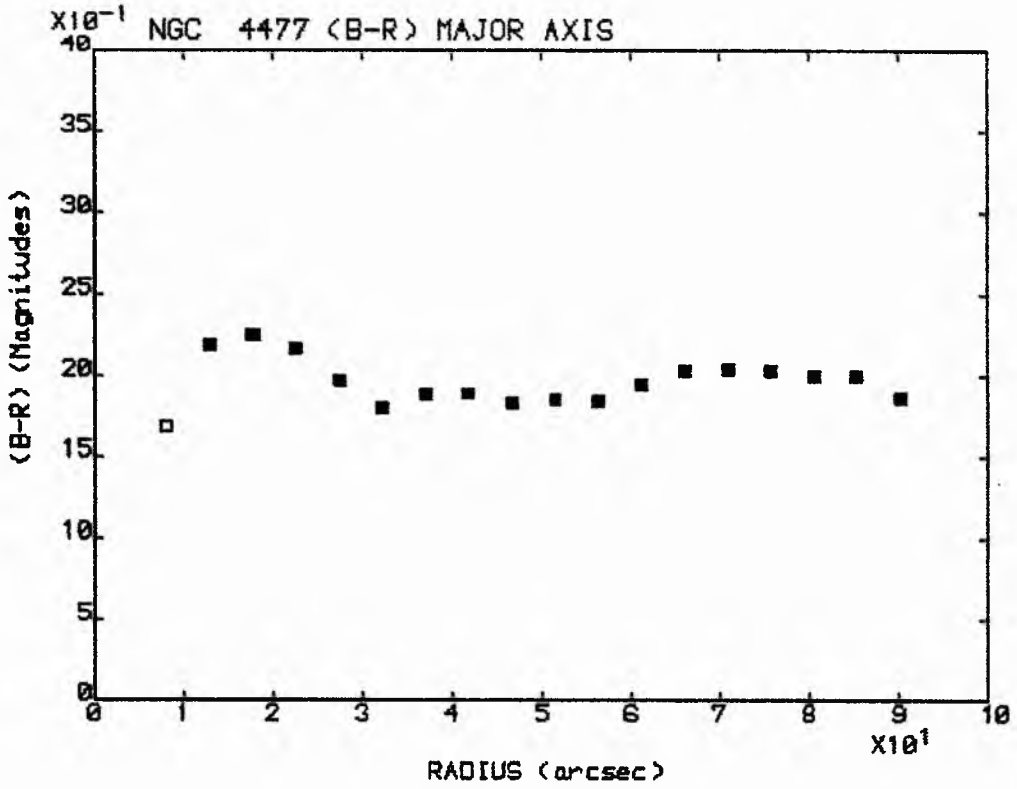
X10⁻¹
NGC 4477 (B-R) MAJOR AXIS
(B-R) (Magnitudes)
40
35
30
25
20
15
10
5
0
0 1 2 3 4 5 6 7 8 9 10
X10¹
RADIUS (arcsec)

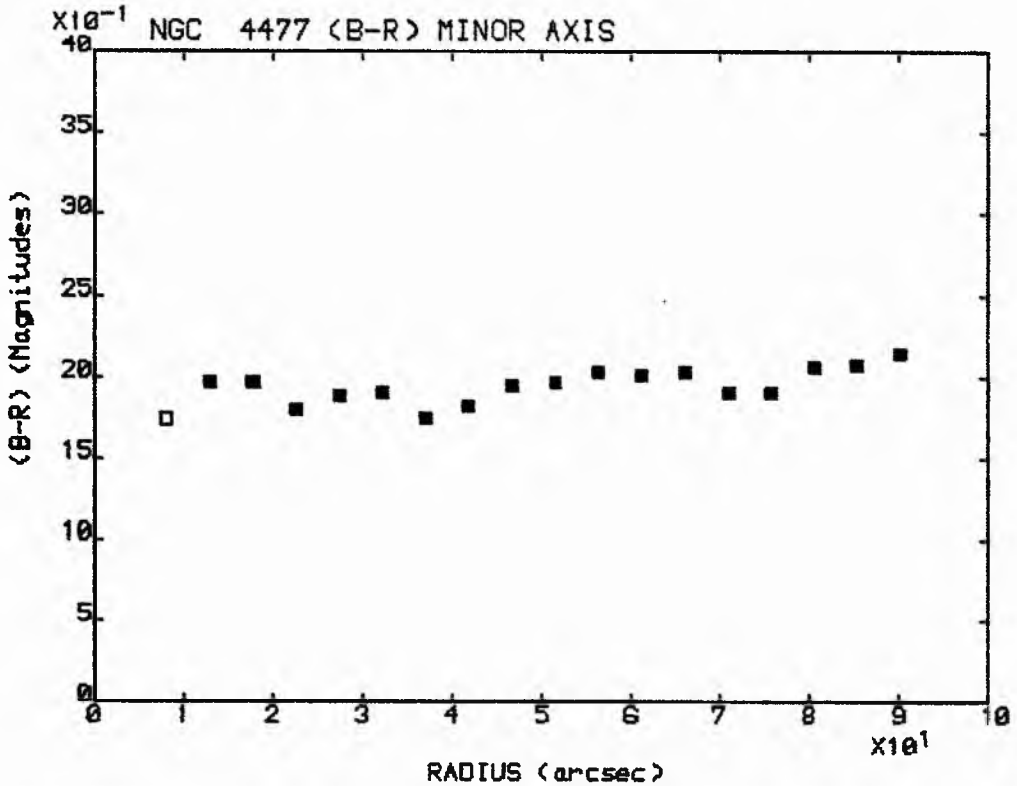
X10⁻¹
NGC 4477 (B-R) MINOR AXIS
(B-R) (Magnitudes)
40
35
30
25
20
15
10
5
0
0 1 2 3 4 5 6 7 8 9 10
X10¹
RADIUS (arcsec)

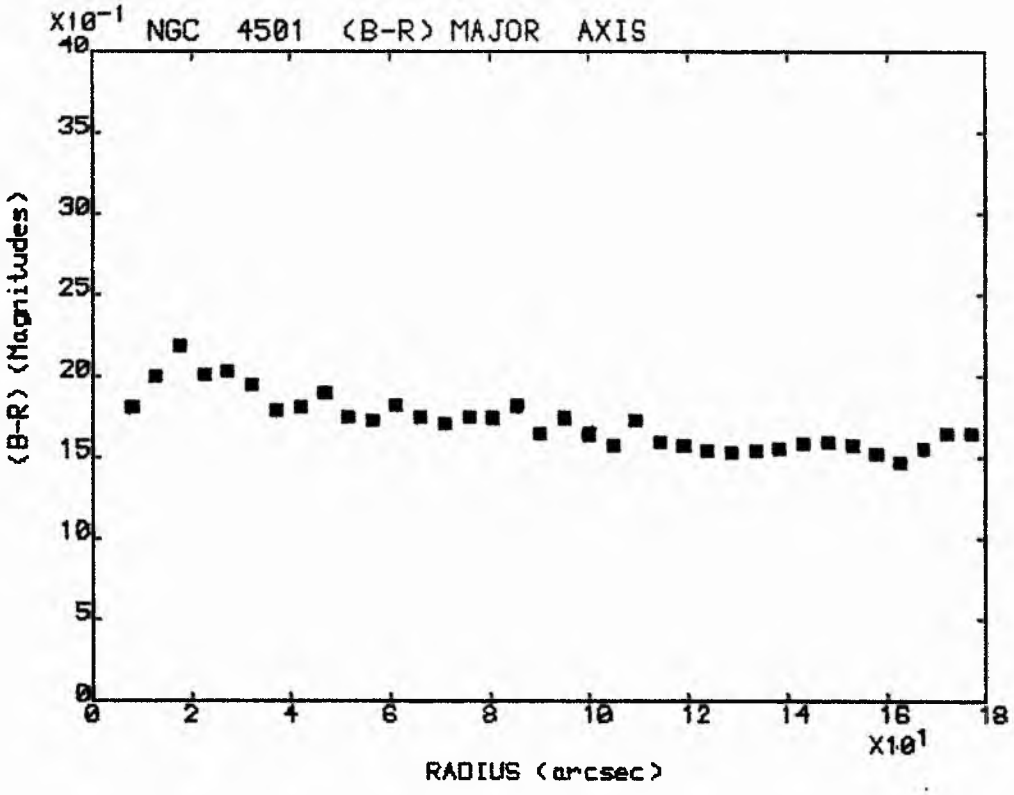
X10⁻¹
NGC 4501 (B-R) MAJOR AXIS
(B-R) (Magnitudes)
40
35
30
25
20
15
10
5
0
0
2
4
6
8
10
12
14
16
18
X10¹
RADIUS (arcsec)

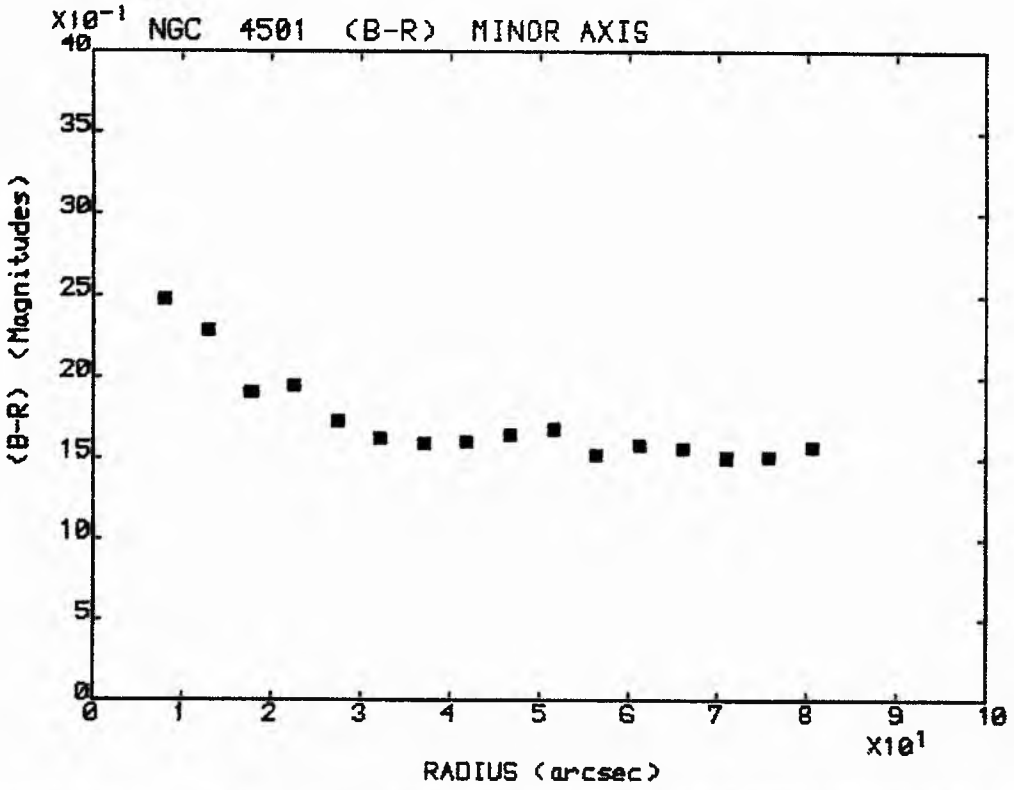
X10⁻¹
NGC 4501 (B-R) MINOR AXIS
(B-R) (Magnitudes)
40
35
30
25
20
15
10
5
0
0
1
2
3
4
5
6
7
8
9
10
X10¹
RADIUS (arcsec)

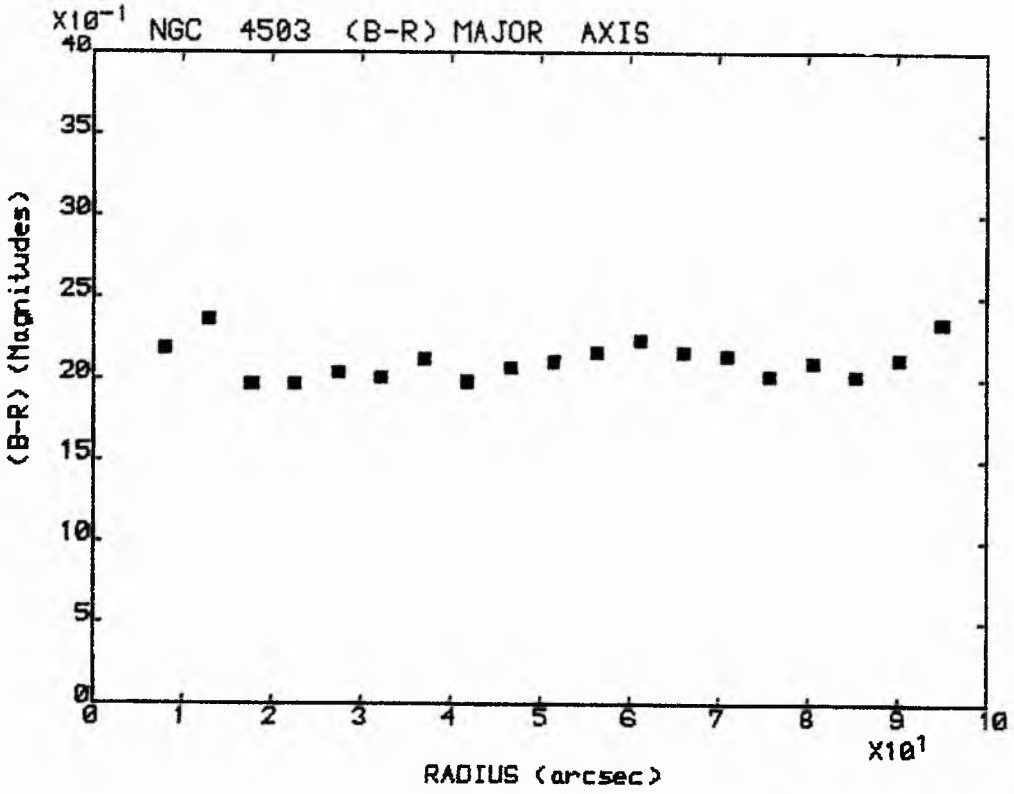
X10⁻¹
NGC 4503 (B-R) MAJOR AXIS
(B-R) (Magnitudes)
40
35
30
25
20
15
10
5
0
0 1 2 3 4 5 6 7 8 9 10
X10¹
RADIUS (arcsec)

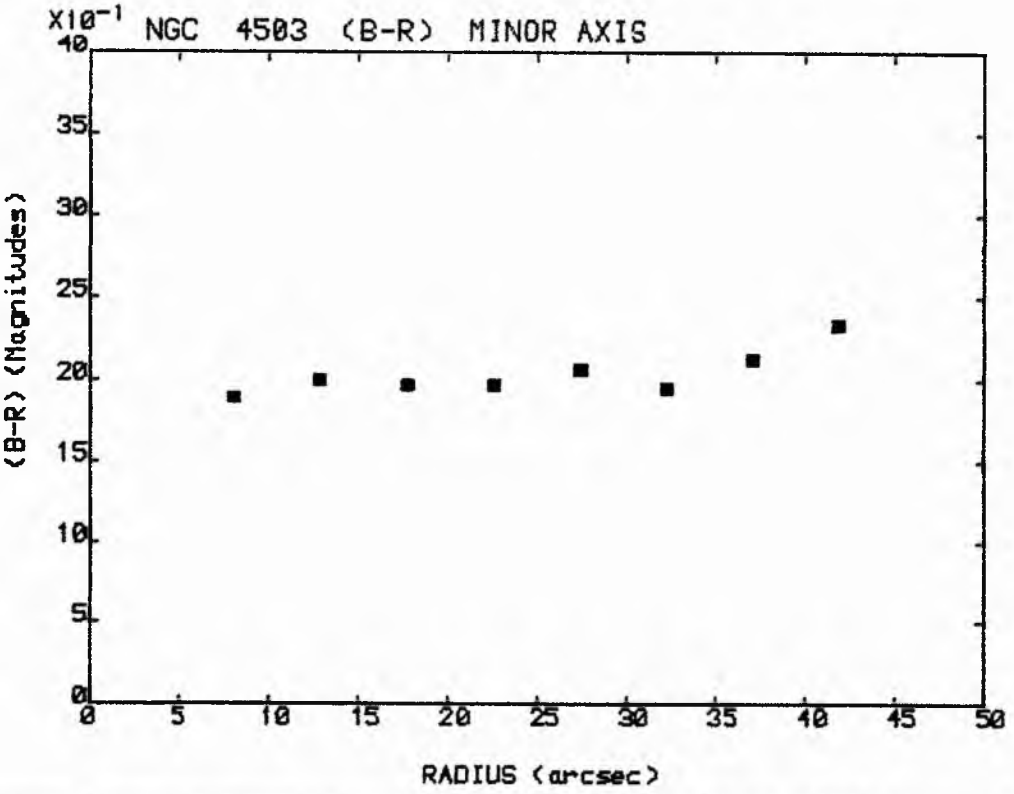
X10⁻¹
NGC 4503 (B-R) MINOR AXIS
(B-R) (Magnitudes)
40
35
30
25
20
15
10
5
0
0 5 10 15 20 25 30 35 40 45 50
RADIUS (arcsec)

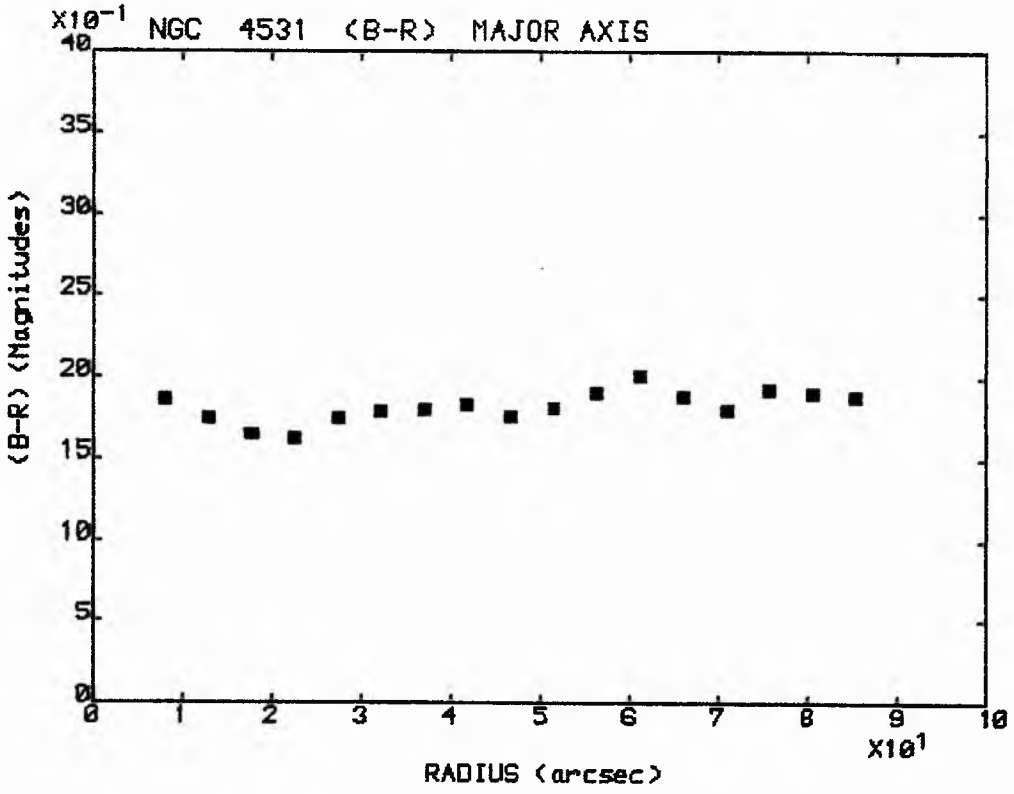
X10⁻¹
NGC 4531 (B-R) MAJOR AXIS
(B-R) (Magnitudes)
40
35
30
25
20
15
10
5
0
0 1 2 3 4 5 6 7 8 9 10
X10¹
RADIUS (arcsec)

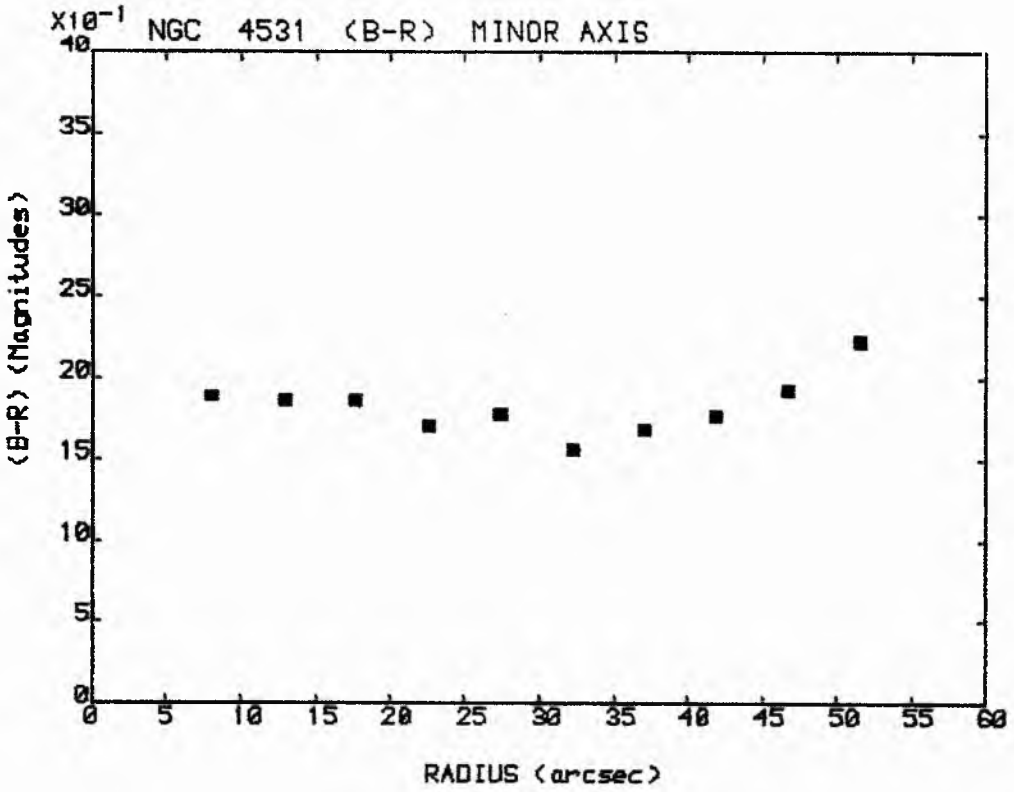
X10⁻¹
NGC 4531 (B-R) MINOR AXIS
(B-R) (Magnitudes)
40
35
30
25
20
15
10
5
0
0 5 10 15 20 25 30 35 40 45 50 55 60
RADIUS (arcsec)

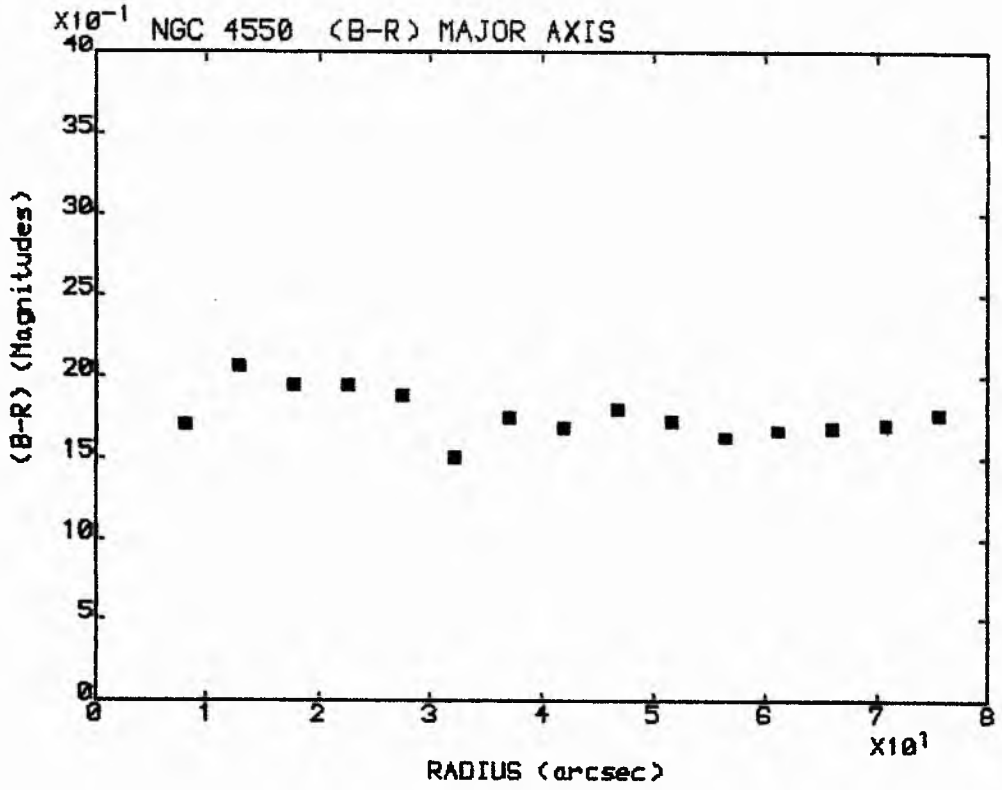
X10⁻¹
NGC 4550 (B-R) MAJOR AXIS
(B-R) (Magnitudes)
0
5
10
15
20
25
30
35
40
0
1
2
3
4
5
6
7
8
X10¹
RADIUS (arcsec)

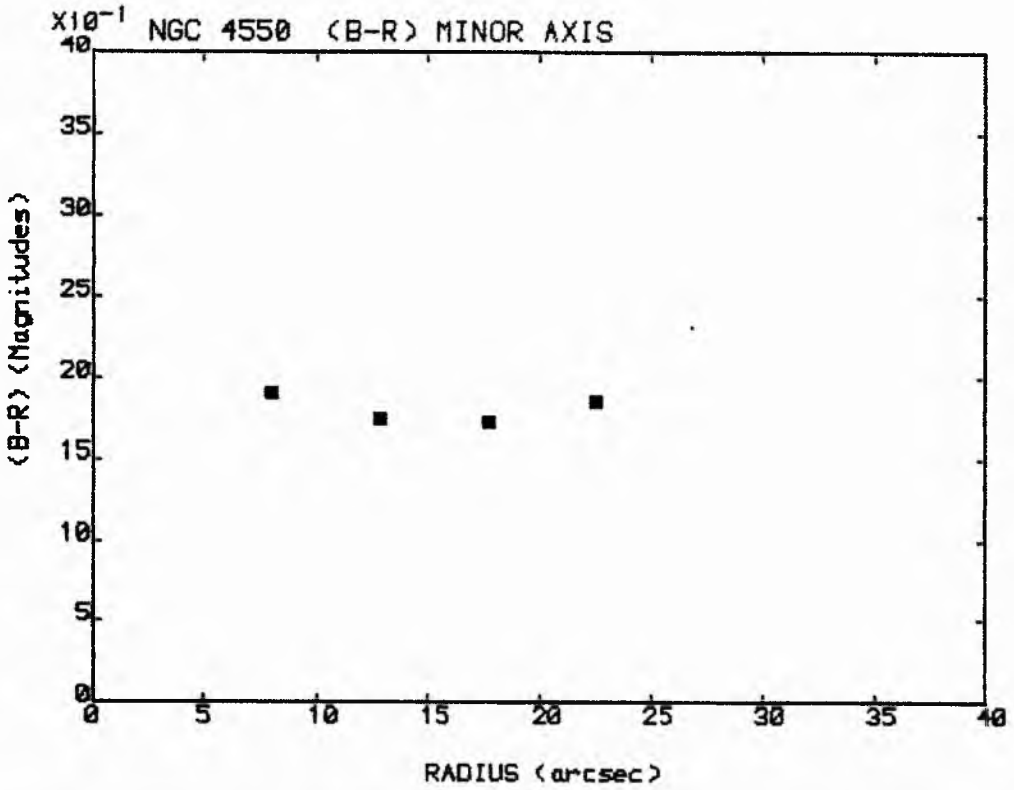
X10⁻¹
NGC 4550 (B-R) MINOR AXIS
(B-R) (Magnitudes)
0
5
10
15
20
25
30
35
40
0
5
10
15
20
25
30
35
40
RADIUS (arcsec)

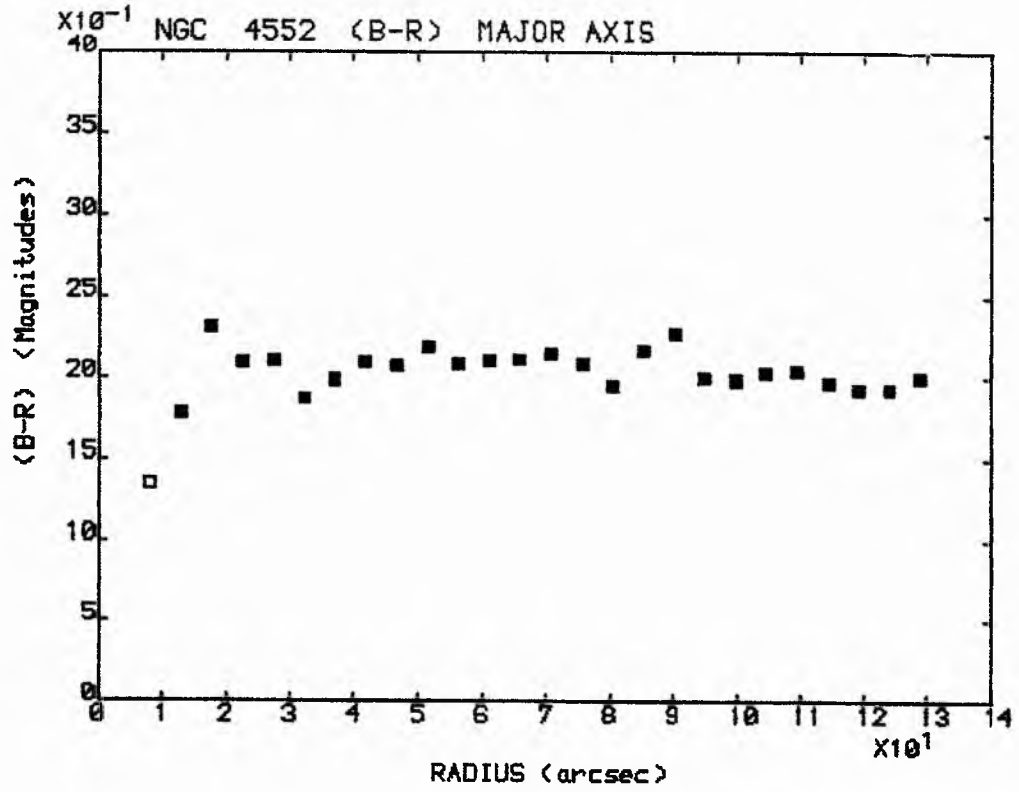
X10⁻¹
NGC 4552 (B-R) MAJOR AXIS
(B-R) (Magnitudes)
RADIUS (arcsec)
X10¹

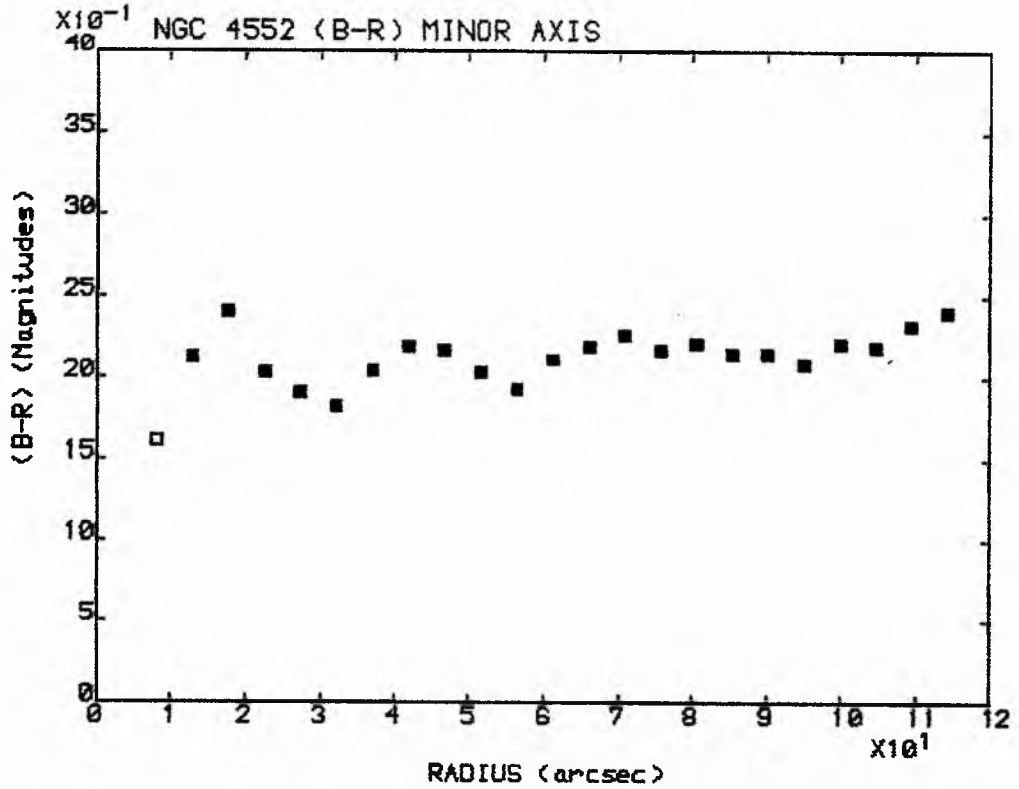
X10⁻¹
NGC 4552 (B-R) MINOR AXIS
(B-R) (Magnitudes)
RADIUS (arcsec)
X10¹

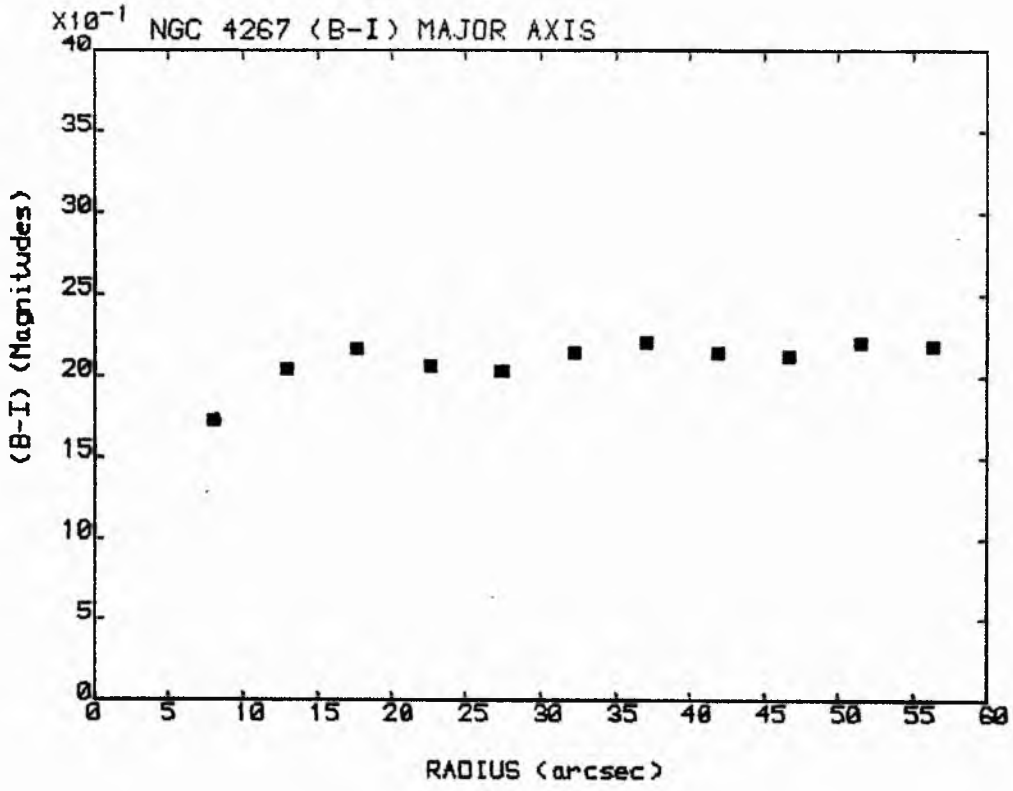
X10⁻¹
NGC 4267 (B-I) MAJOR AXIS
(B-I) (Magnitudes)
40
35
30
25
20
15
10
5
0
0 5 10 15 20 25 30 35 40 45 50 55 60
RADIUS (arcsec)

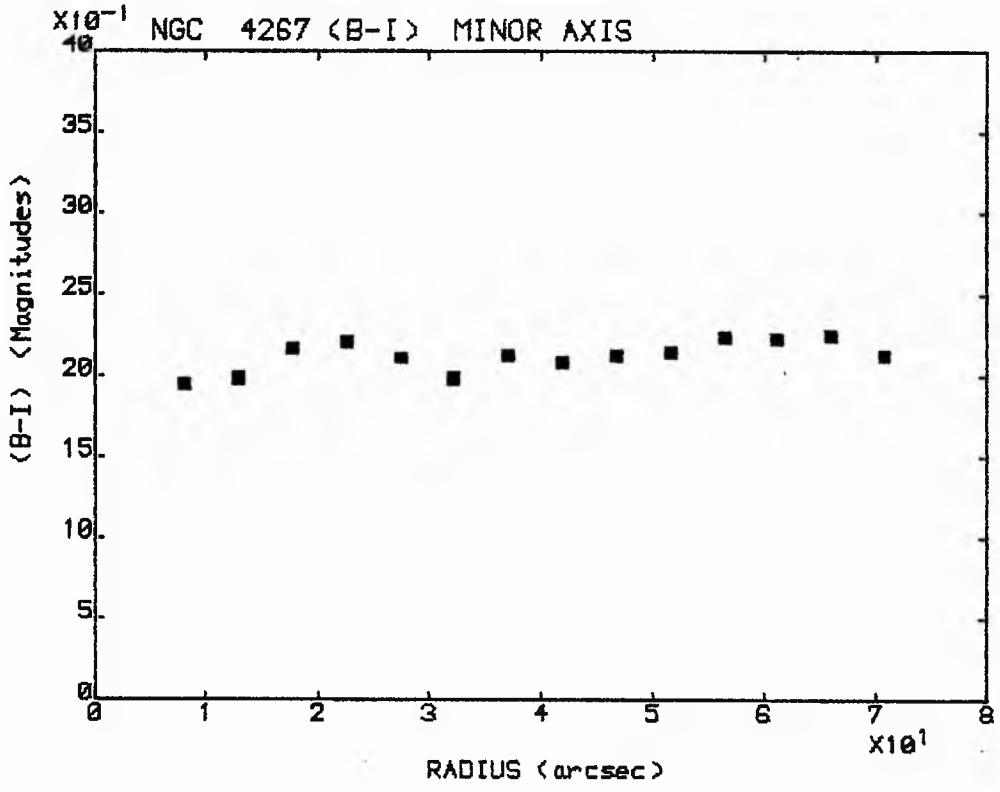
X10⁻¹
NGC 4267 (B-I) MINOR AXIS
(B-I) (Magnitudes)
40
35
30
25
20
15
10
5
0
0 1 2 3 4 5 6 7 8
X10¹
RADIUS (arcsec)

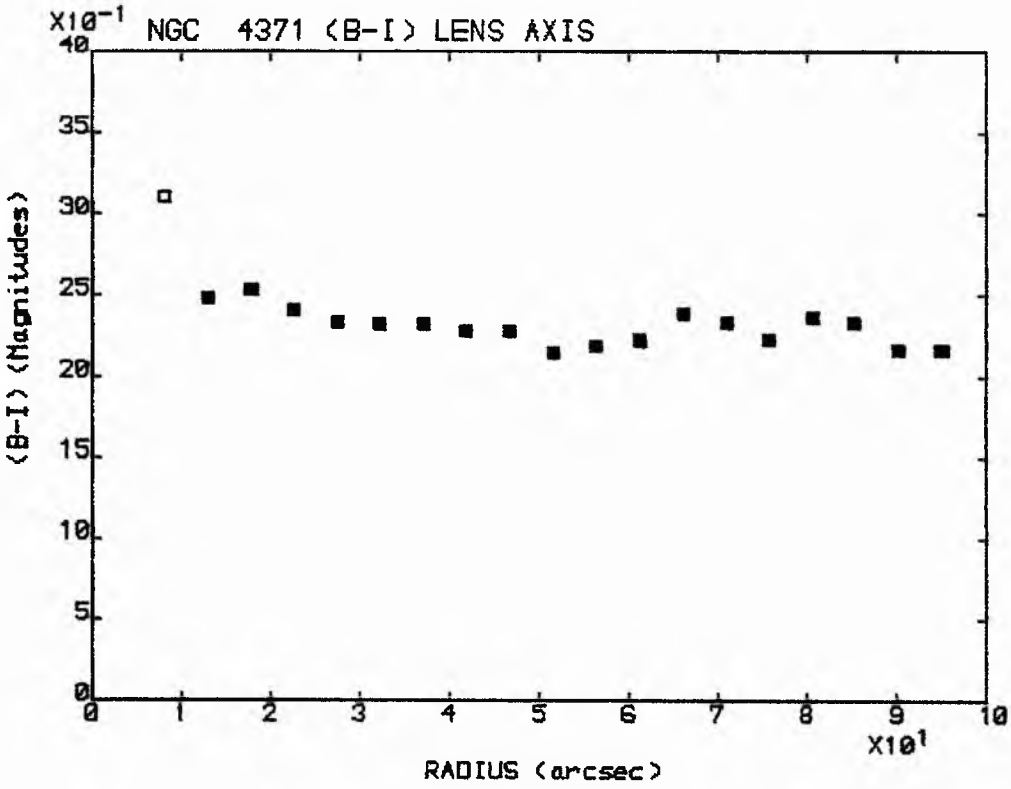
X10⁻¹ NGC 4371 (B-I) LENS AXIS
(B-I) (Magnitudes)
40
35
30
25
20
15
10
5
0
0 1 2 3 4 5 6 7 8 9 10
X10¹
RADIUS (arcsec)

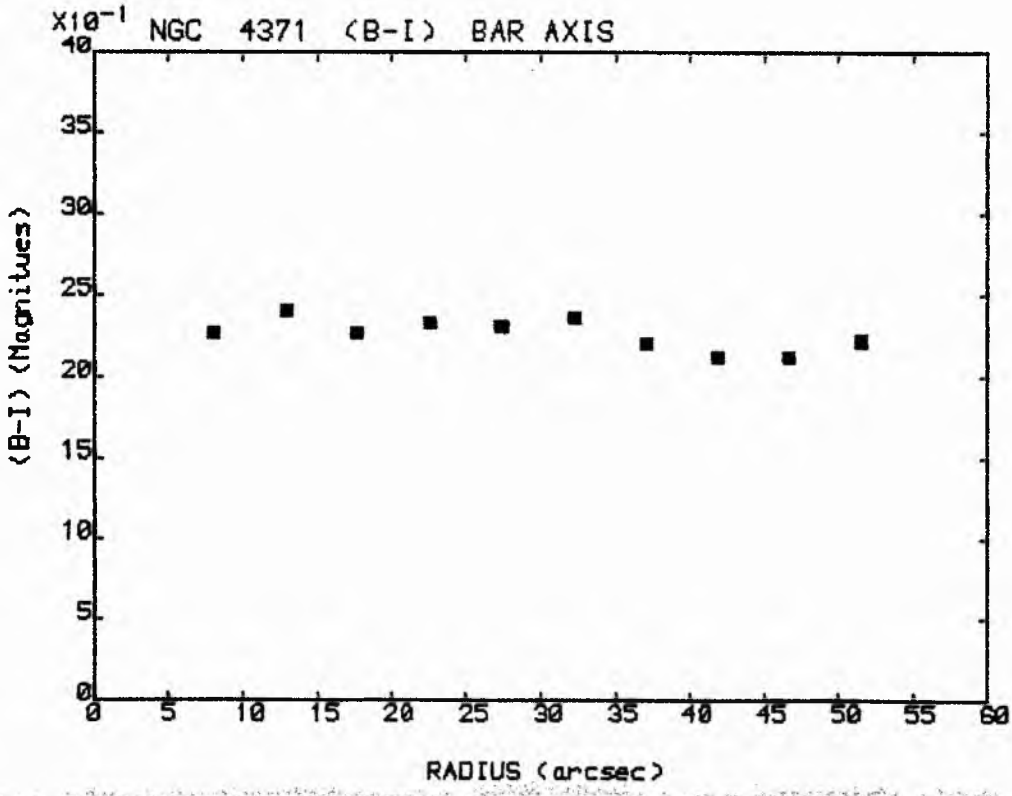
X10⁻¹ NGC 4371 (B-I) BAR AXIS
(B-I) (Magnitues)
40
35
30
25
20
15
10
5
0
0 5 10 15 20 25 30 35 40 45 50 55 60
RADIUS (arcsec)

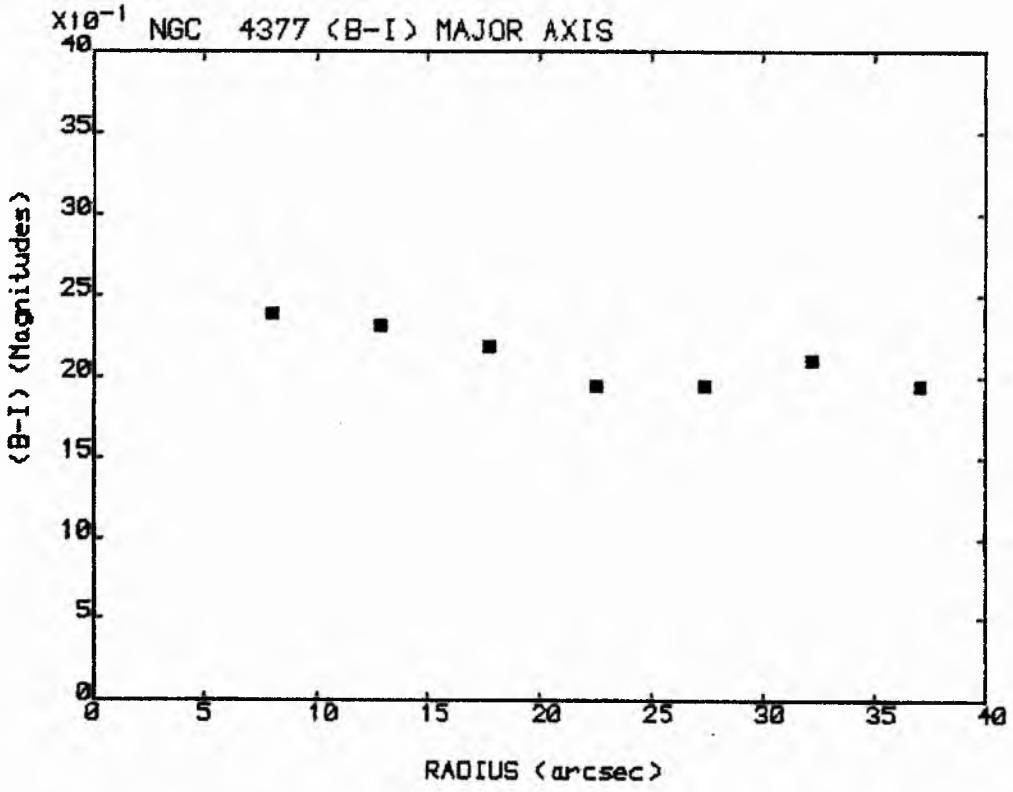
X10⁻¹
NGC 4377 (B-I) MAJOR AXIS
(B-I) (Magnitudes)
RADIUS (arcsec)
0
5
10
15
20
25
30
35
40

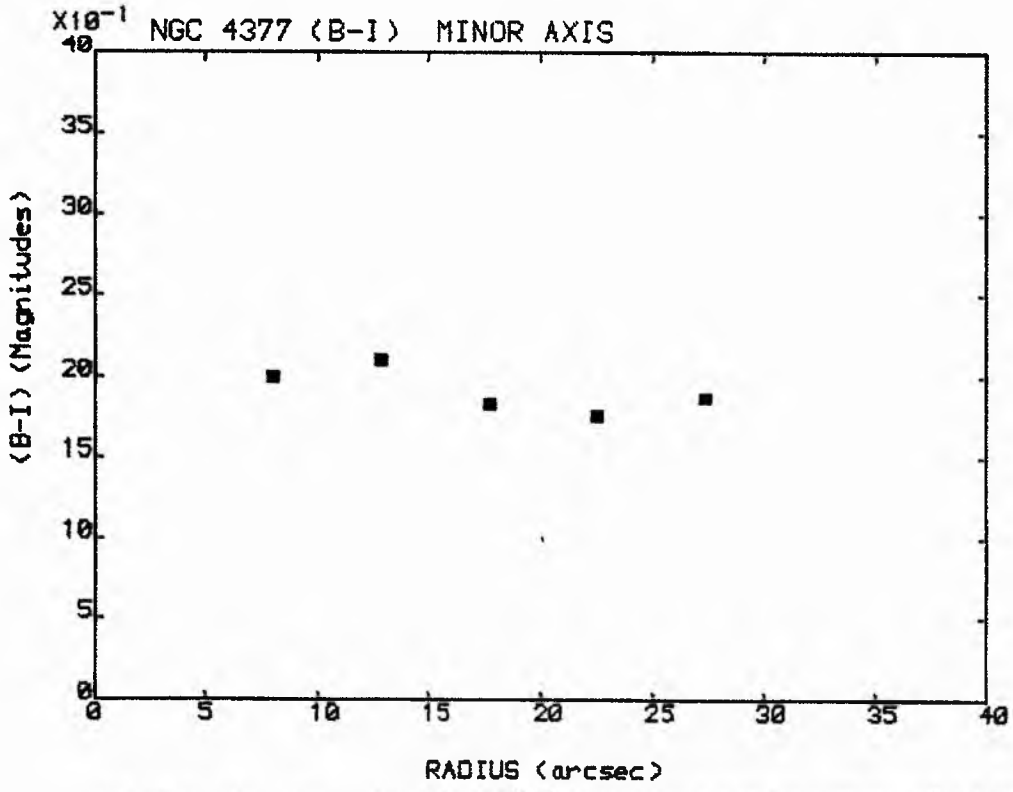
X10⁻¹
NGC 4377 (B-I) MINOR AXIS
(B-I) (Magnitudes)
RADIUS (arcsec)
0
5
10
15
20
25
30
35
40

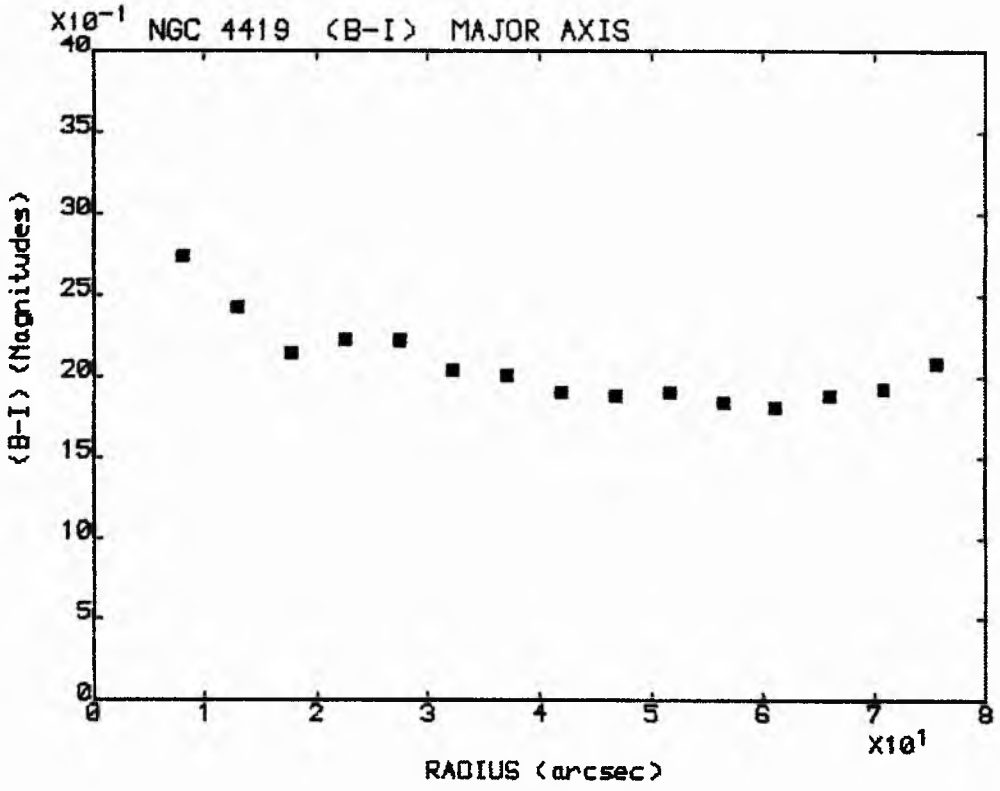
X10⁻¹ NGC 4419 (B-I) MAJOR AXIS
(B-I) (Magnitudes)
RADIUS (arcsec)
X10¹

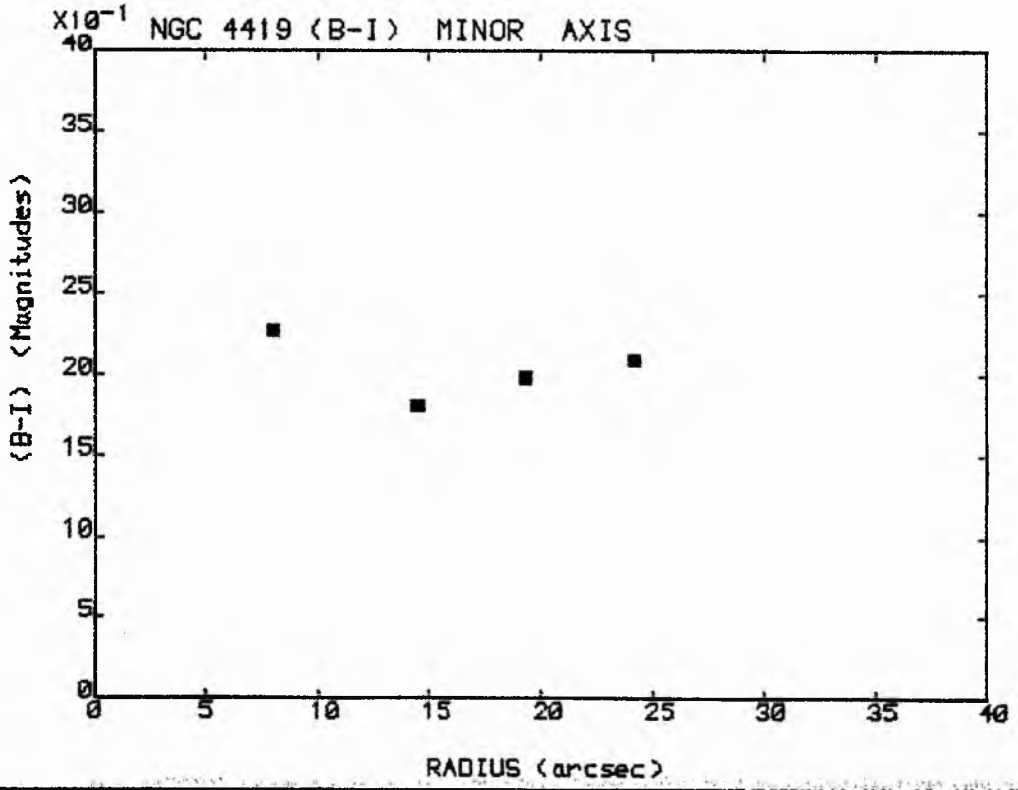
X10⁻¹ NGC 4419 (B-I) MINOR AXIS
(B-I) (Magnitudes)
RADIUS (arcsec)

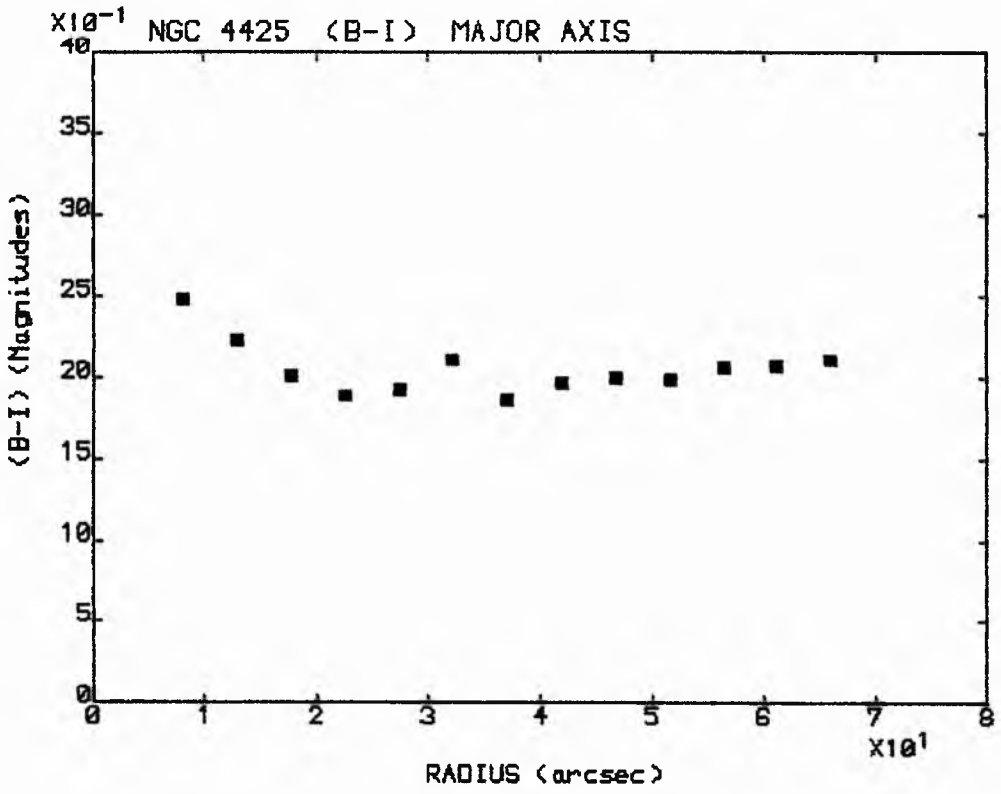
X10⁻¹
NGC 4425 (B-I) MAJOR AXIS
40
35
30
25
20
15
10
5
0
(B-I) (Magnitudes)
0
1
2
3
4
5
6
7
8
X10¹
RADIUS (arcsec)

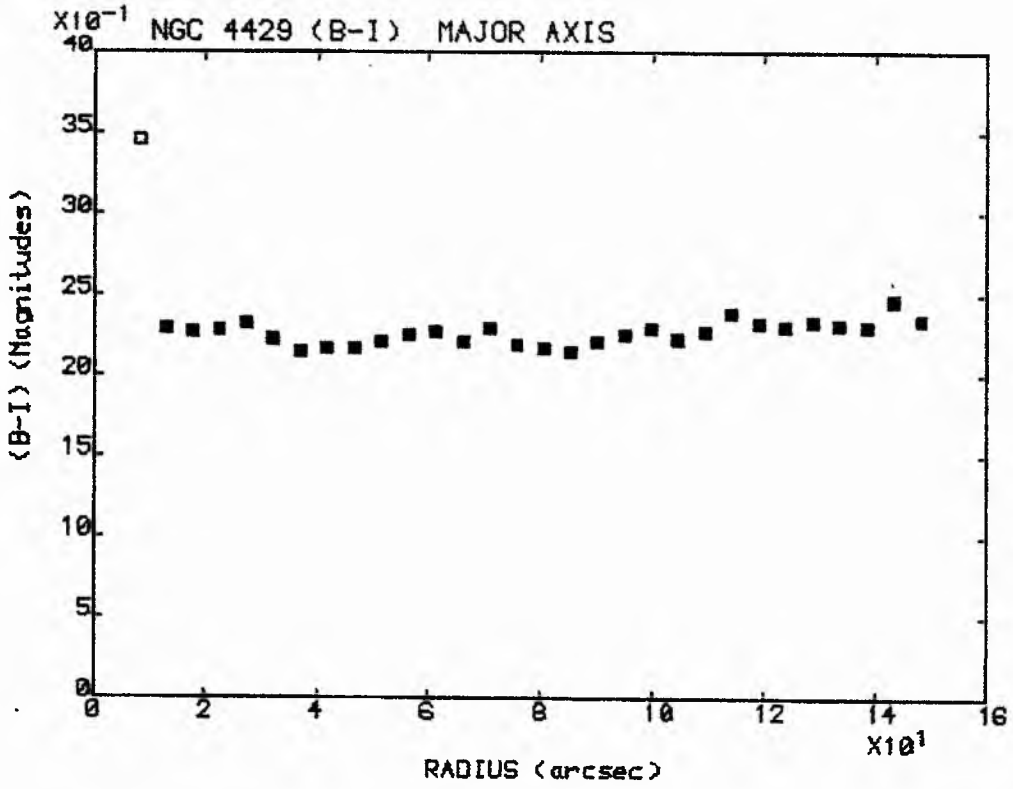
X10⁻¹
NGC 4429 (B-I) MAJOR AXIS
(B-I) (Magnitudes)
40
35
30
25
20
15
10
5
0
0
2
4
6
8
10
12
14
16
X10¹
RADIUS (arcsec)

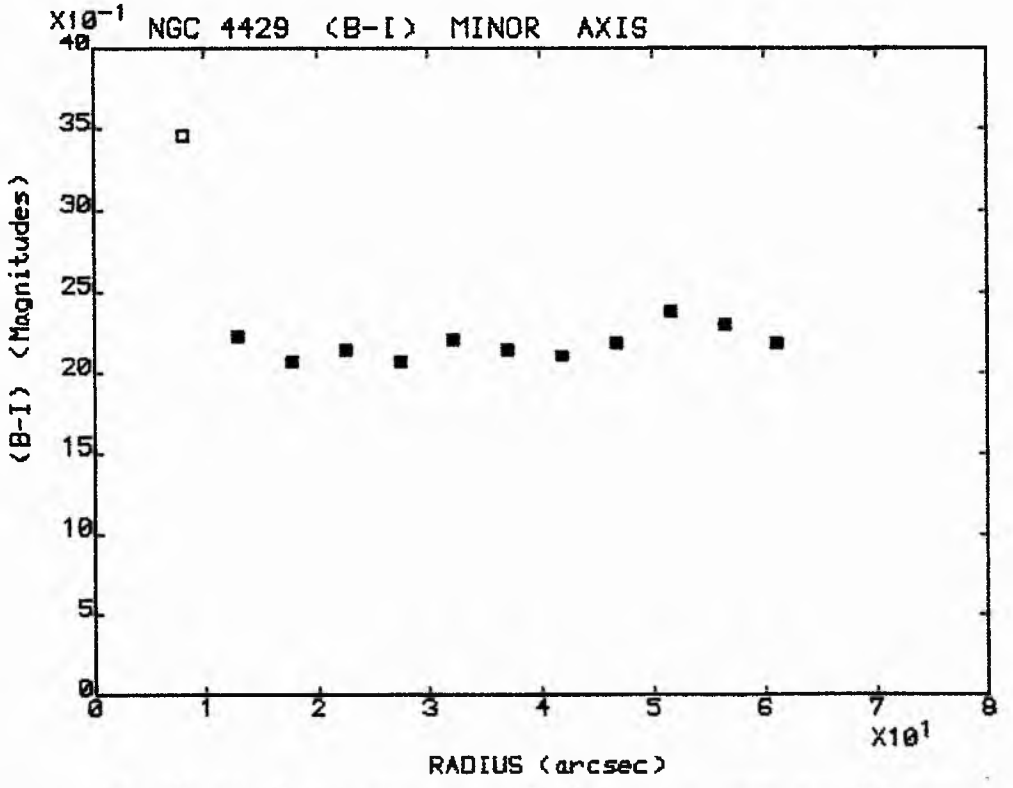
X10⁻¹
NGC 4429 (B-I) MINOR AXIS
(B-I) (Magnitudes)
40
35
30
25
20
15
10
5
0
0
1
2
3
4
5
6
7
8
X10¹
RADIUS (arcsec)

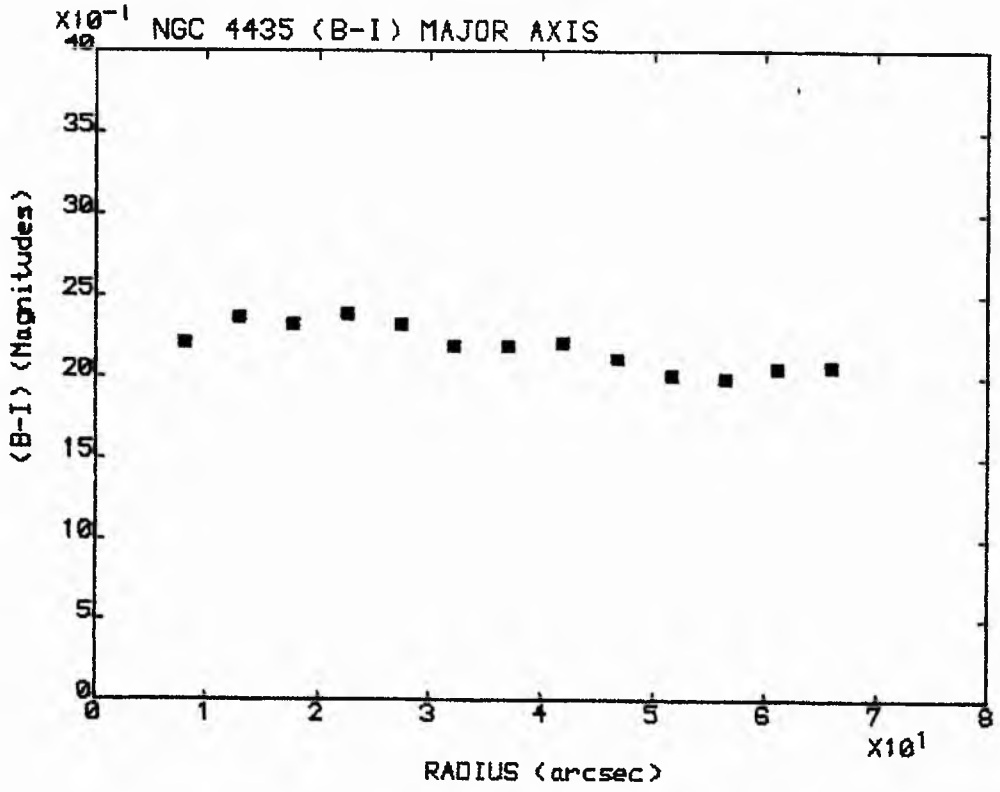
X10⁻¹
NGC 4435 (B-I) MAJOR AXIS
40
35
30
25
20
15
10
5
0
(B-I) (Magnitudes)
0
1
2
3
4
5
6
7
8
X10¹
RADIUS (arcsec)

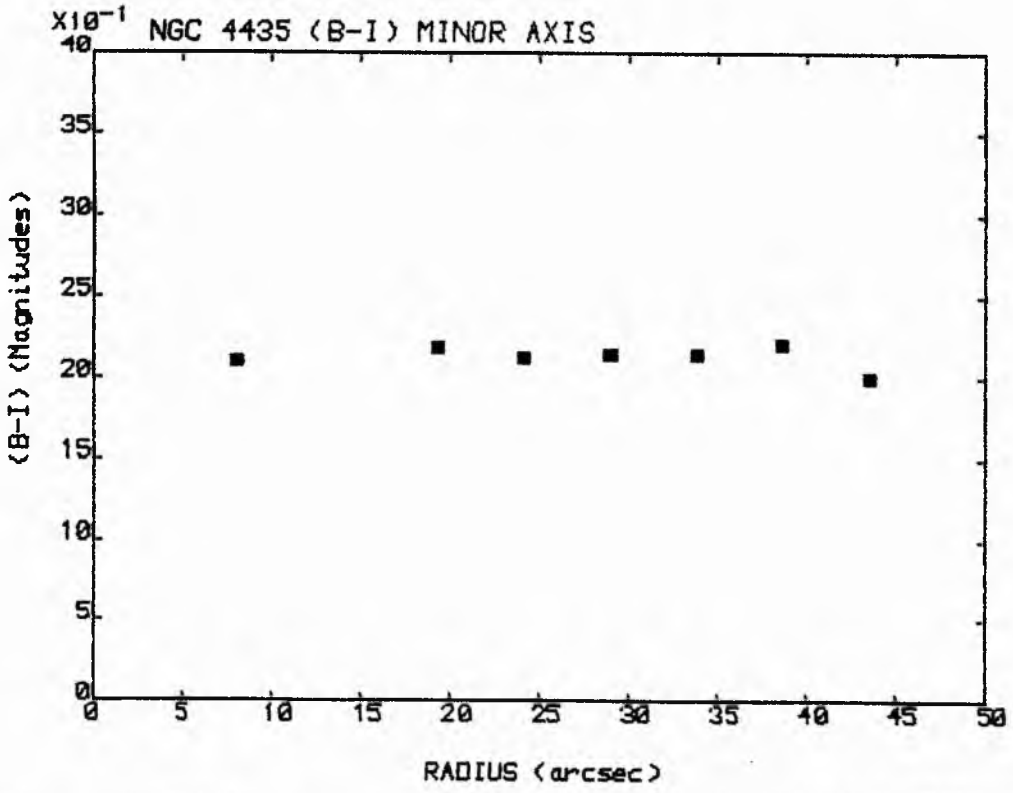
X10⁻¹
NGC 4435 (B-I) MINOR AXIS
40
35
30
25
20
15
10
5
0
(B-I) (Magnitudes)
0
5
10
15
20
25
30
35
40
45
50
RADIUS (arcsec)

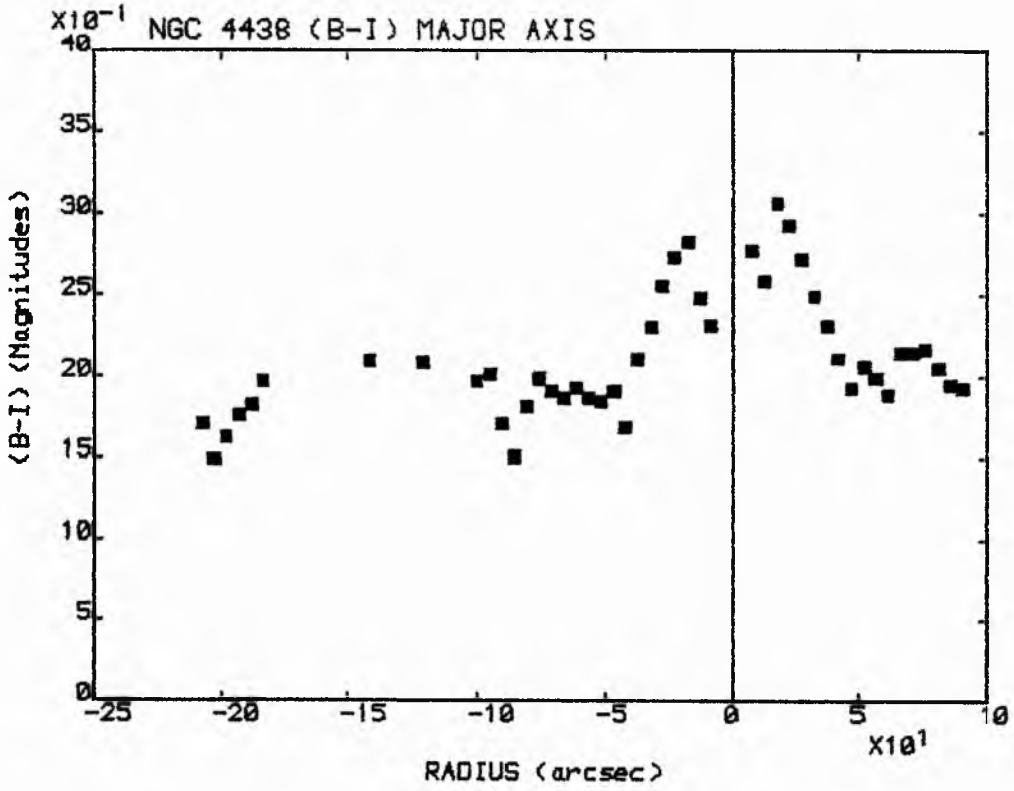
X10⁻¹
NGC 4438 (B-I) MAJOR AXIS
(B-I) (Magnitudes)
40
35
30
25
20
15
10
5
0
-25
-20
-15
-10
-5
0
5
10
X10¹
RADIUS (arcsec)

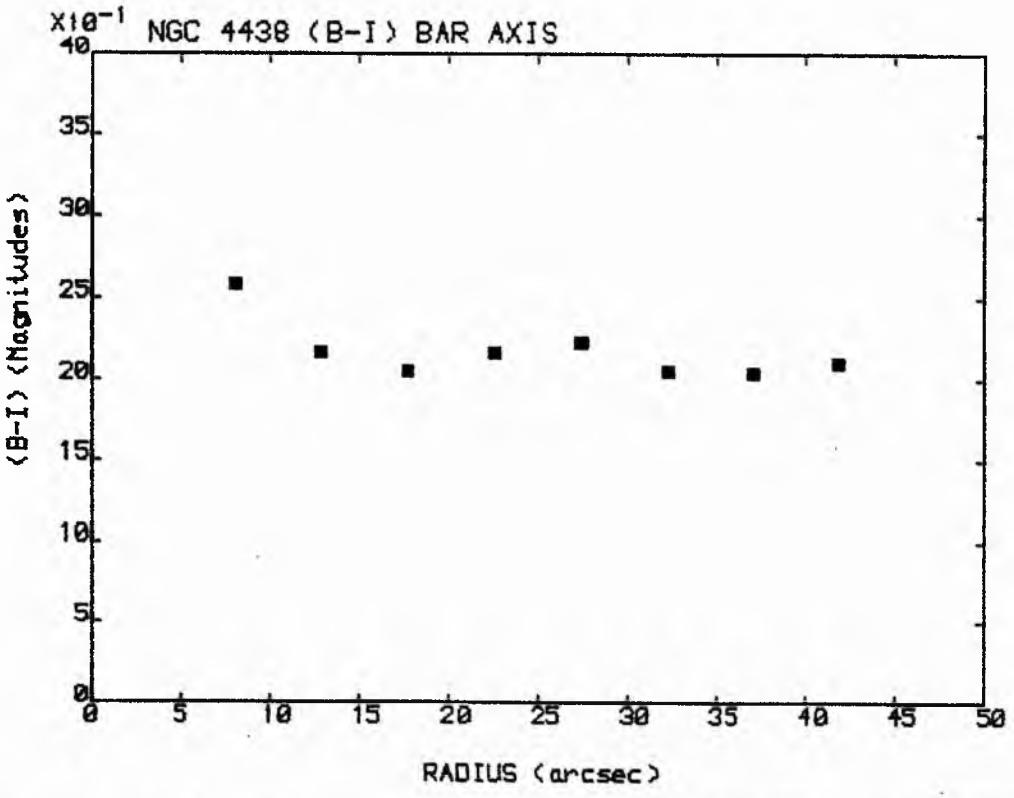
X10⁻¹
NGC 4438 (B-I) BAR AXIS
(B-I) (Magnitudes)
40
35
30
25
20
15
10
5
0
0
5
10
15
20
25
30
35
40
45
50
RADIUS (arcsec)

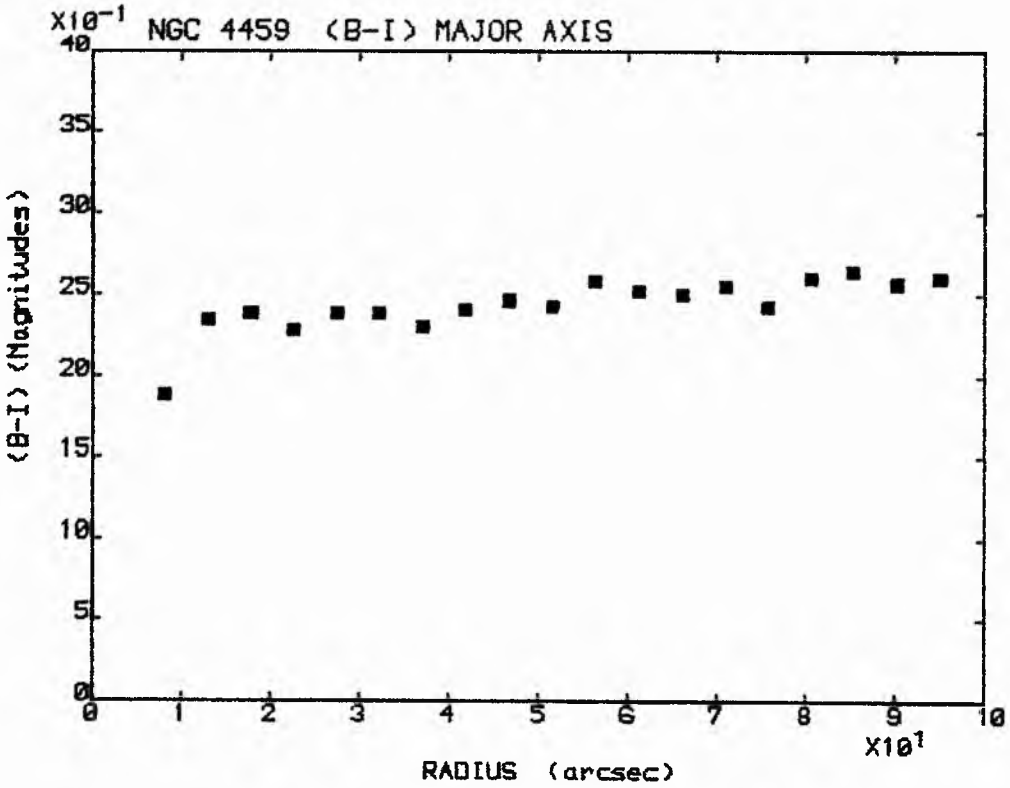
X10⁻¹
NGC 4459 (B-I) MAJOR AXIS
40
35
30
25
20
15
10
5
0
(B-I) (Magnitudes)
0 1 2 3 4 5 6 7 8 9 10
X10¹
RADIUS (arcsec)

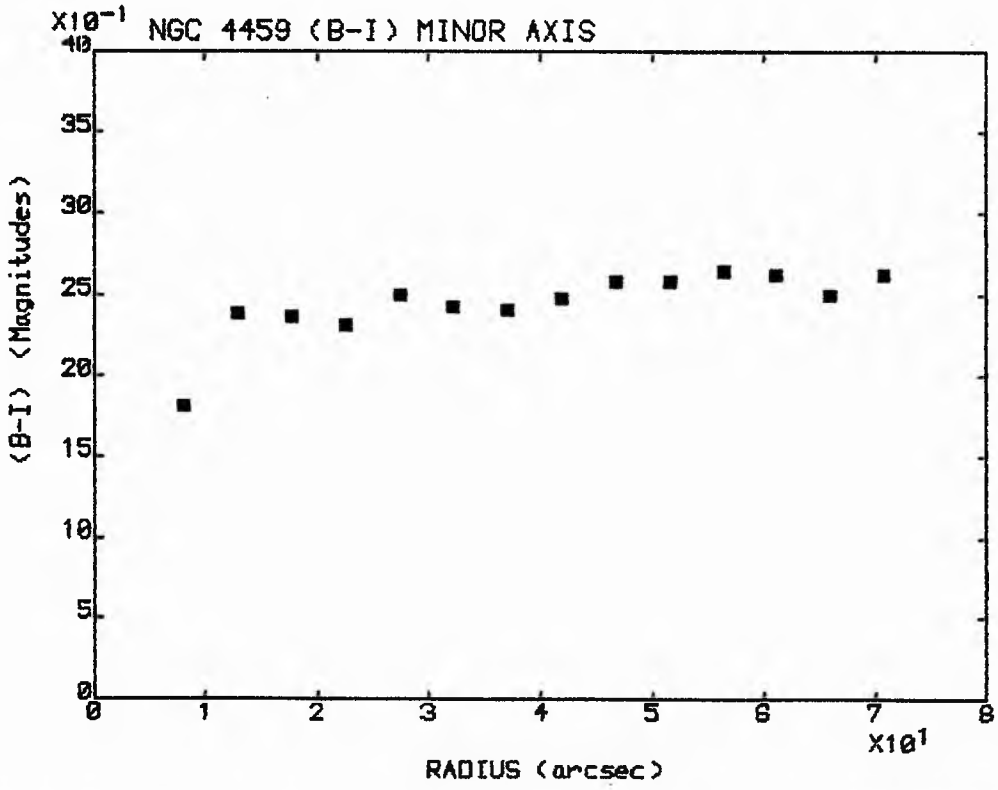
X10⁻¹
NGC 4459 (B-I) MINOR AXIS
40
35
30
25
20
15
10
5
0
(B-I) (Magnitudes)
0 1 2 3 4 5 6 7 8
X10¹
RADIUS (arcsec)

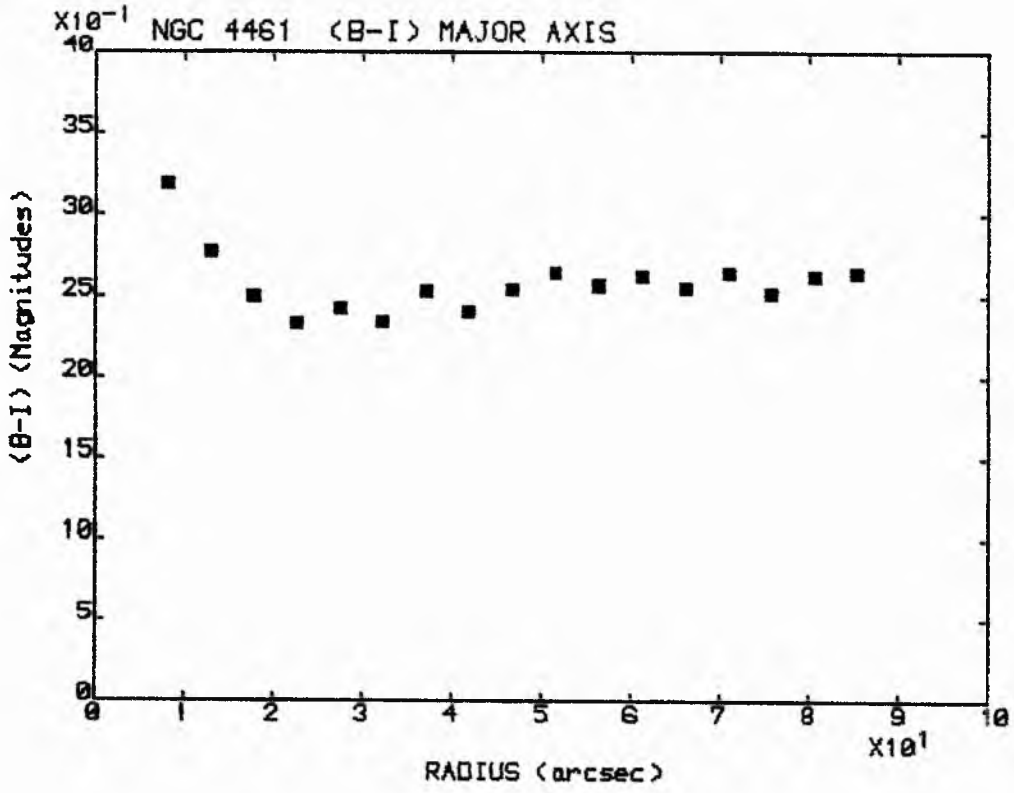
X10⁻¹
NGC 4461 (B-I) MAJOR AXIS
(B-I) (Magnitudes)
40
35
30
25
20
15
10
5
0
0 1 2 3 4 5 6 7 8 9 10
X10¹
RADIUS (arcsec)

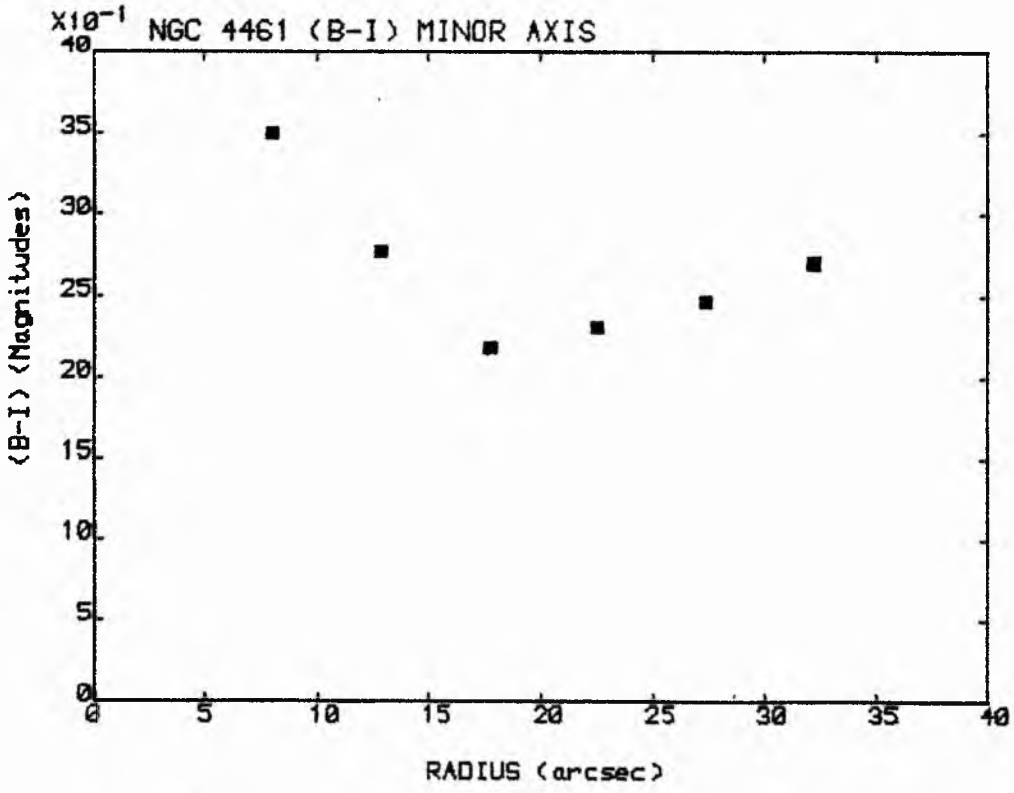
X10⁻¹
NGC 4461 (B-I) MINOR AXIS
(B-I) (Magnitudes)
40
35
30
25
20
15
10
5
0
0 5 10 15 20 25 30 35 40
RADIUS (arcsec)

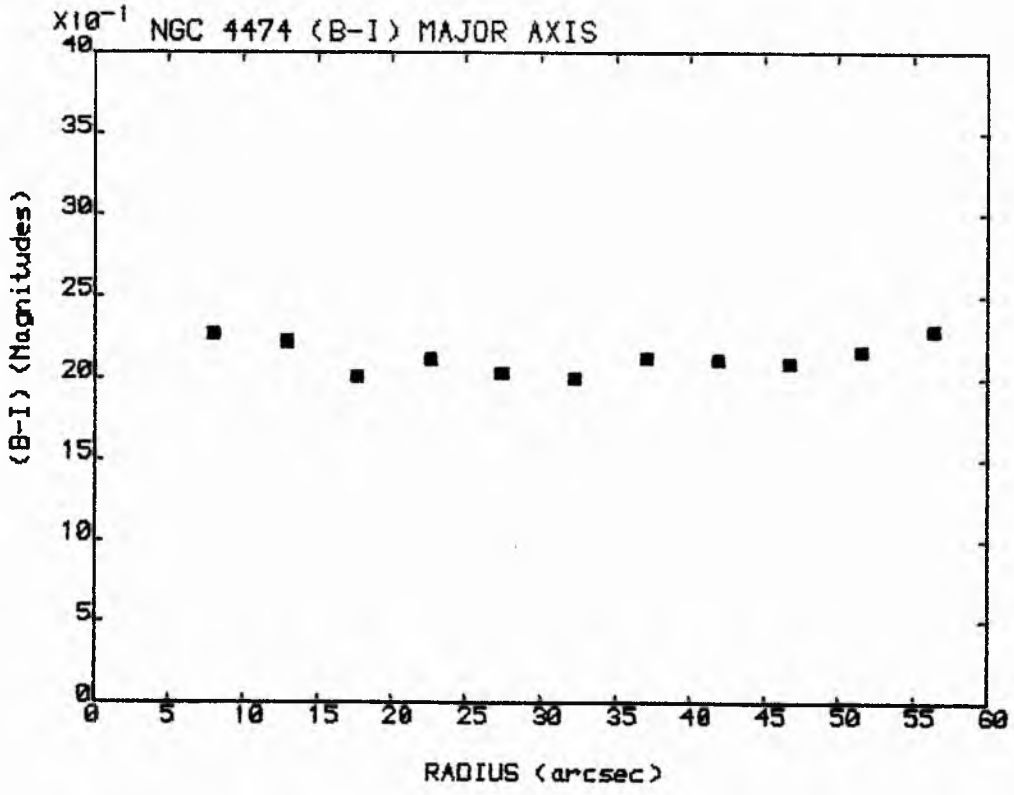
X10⁻¹
NGC 4474 (B-I) MAJOR AXIS
(B-I) (Magnitudes)
RADIUS (arcsec)
0
5
10
15
20
25
30
35
40
45
50
55
60

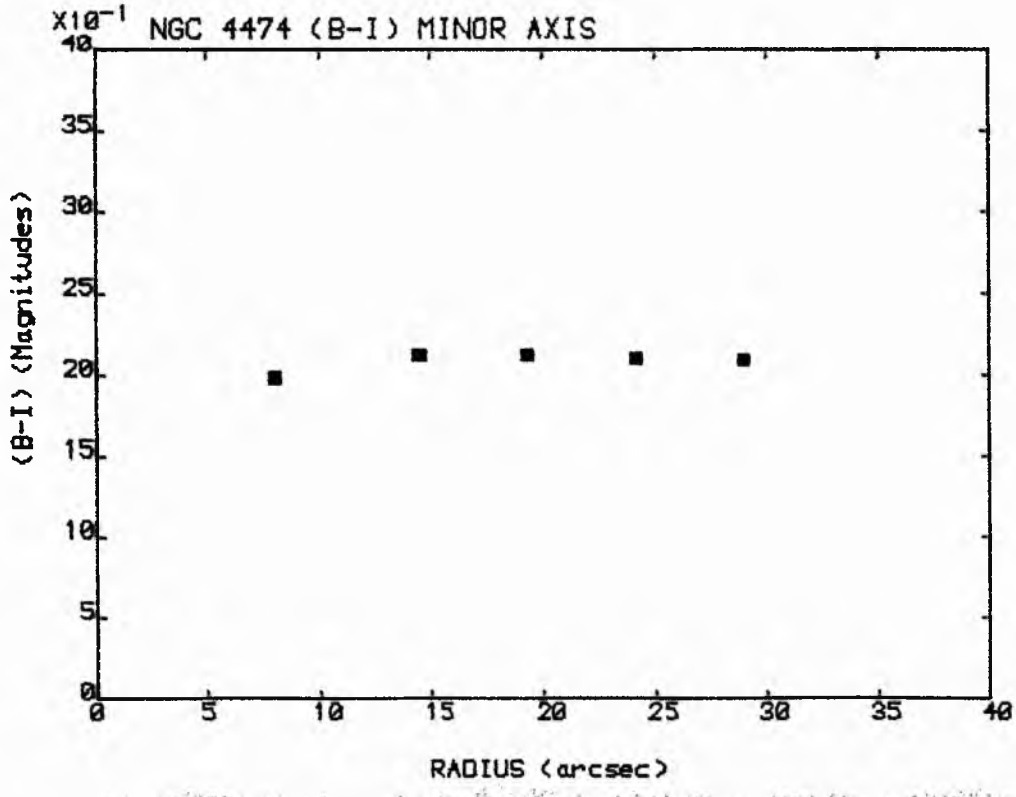
X10⁻¹
NGC 4474 (B-I) MINOR AXIS
(B-I) (Magnitudes)
RADIUS (arcsec)
0
5
10
15
20
25
30
35
40

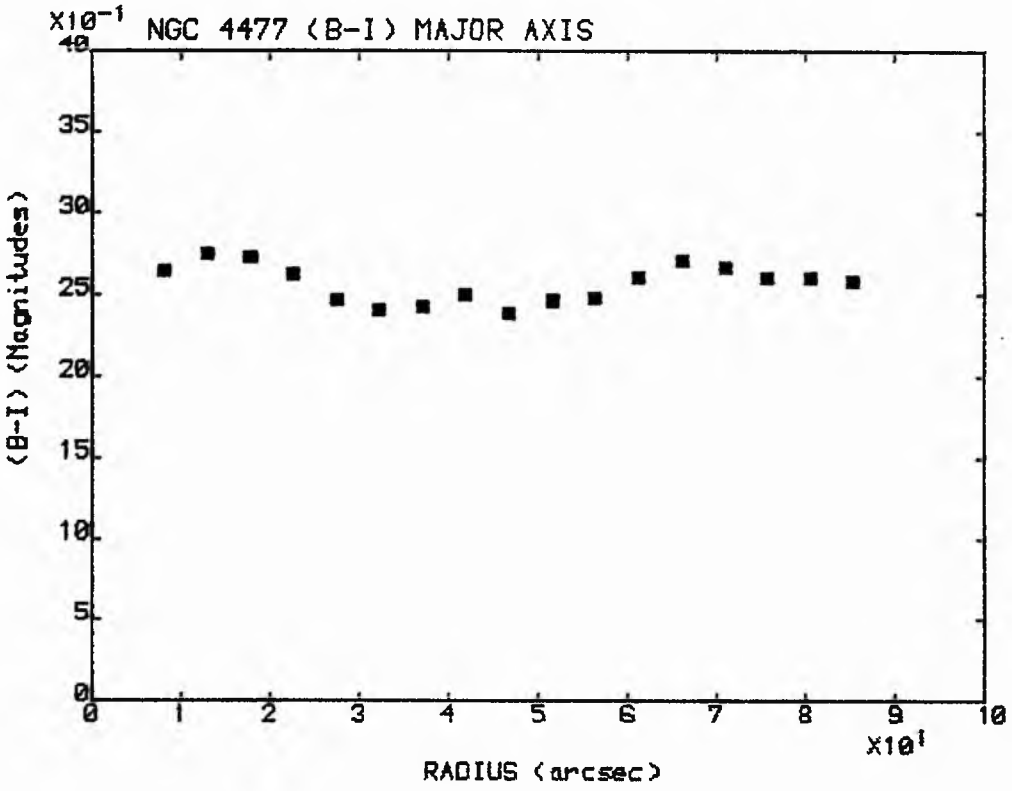
X10⁻¹
NGC 4477 (B-I) MAJOR AXIS
(B-I) (Magnitudes)
40
35
30
25
20
15
10
5
0
0 1 2 3 4 5 6 7 8 9 10
X10¹
RADIUS (arcsec)

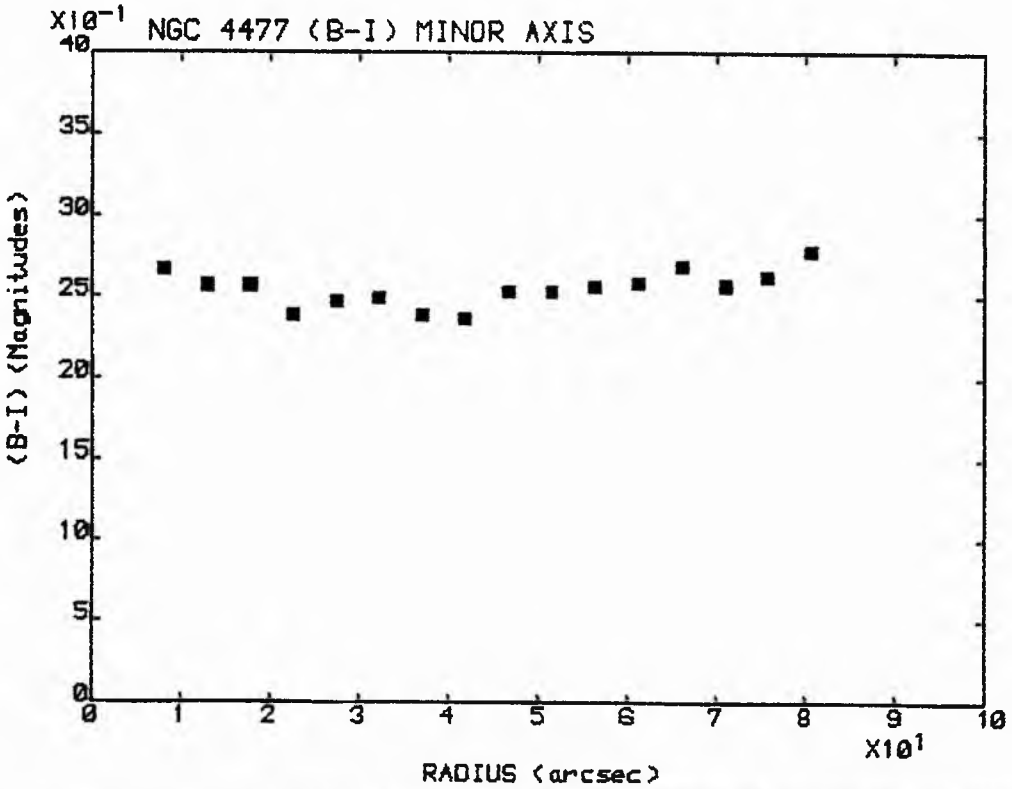
X10⁻¹
NGC 4477 (B-I) MINOR AXIS
(B-I) (Magnitudes)
40
35
30
25
20
15
10
5
0
0 1 2 3 4 5 6 7 8 9 10
X10¹
RADIUS (arcsec)

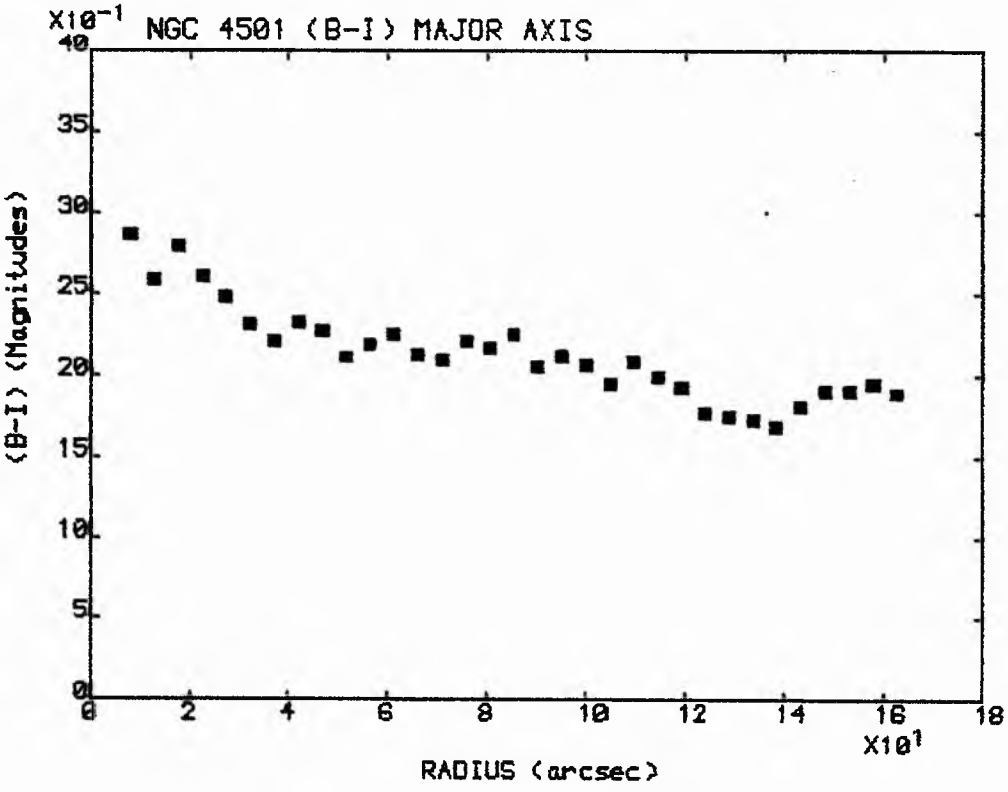
X10⁻¹
NGC 4501 (B-I) MAJOR AXIS
(B-I) (Magnitudes)
40
35
30
25
20
15
10
5
0
0
2
4
6
8
10
12
14
16
18
X10¹
RADIUS (arcsec)

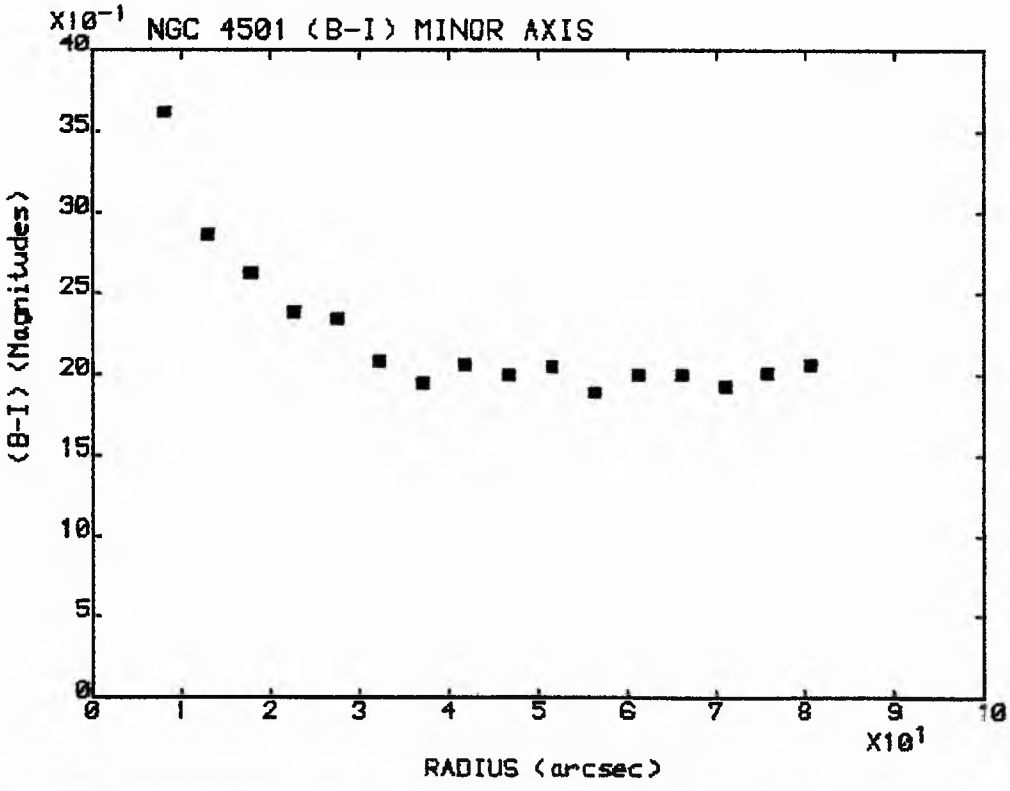
X10⁻¹
NGC 4501 (B-I) MINOR AXIS
(B-I) (Magnitudes)
40
35
30
25
20
15
10
5
0
0
1
2
3
4
5
6
7
8
9
10
X10¹
RADIUS (arcsec)

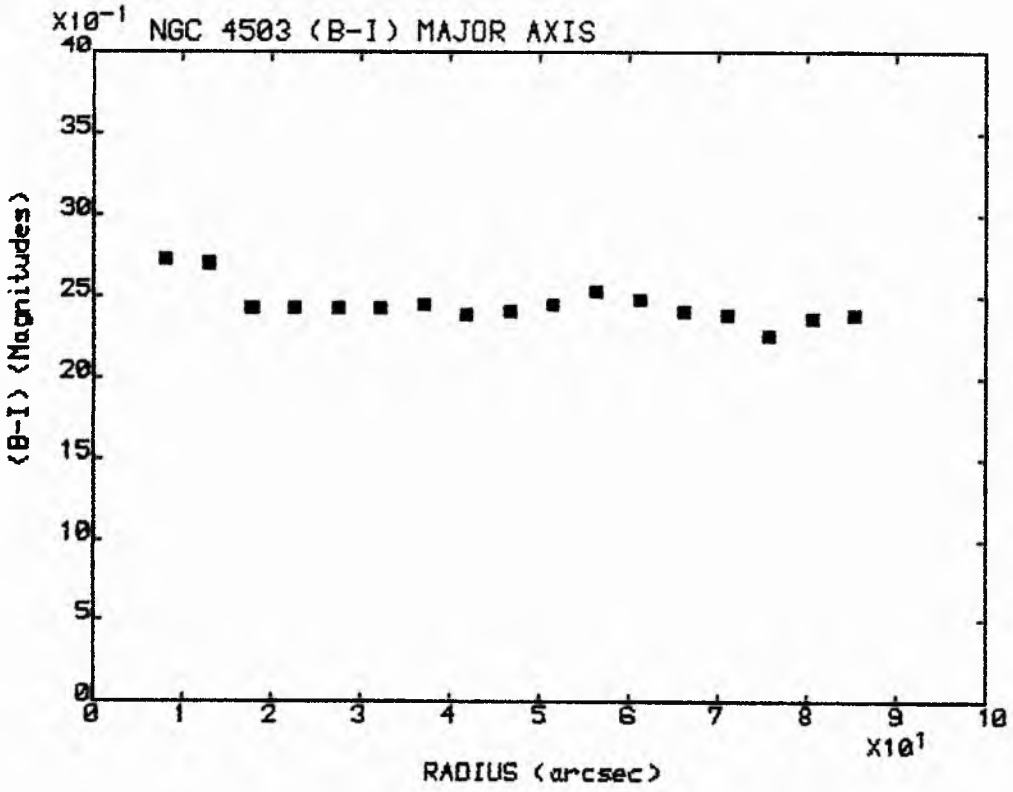
X10⁻¹
NGC 4503 (B-I) MAJOR AXIS
(B-I) (Magnitudes)
40
35
30
25
20
15
10
5
0
0
1
2
3
4
5
6
7
8
9
10
X10¹
RADIUS (arcsec)

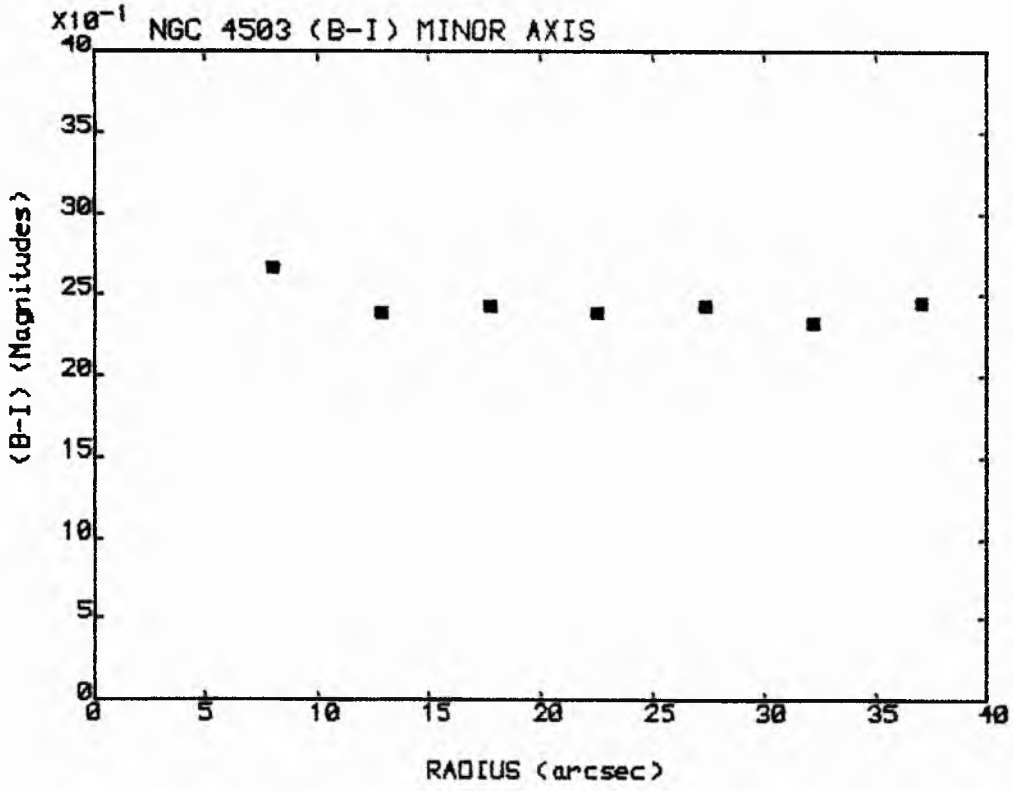
X10⁻¹
NGC 4503 (B-I) MINOR AXIS
(B-I) (Magnitudes)
40
35
30
25
20
15
10
5
0
0
5
10
15
20
25
30
35
40
RADIUS (arcsec)

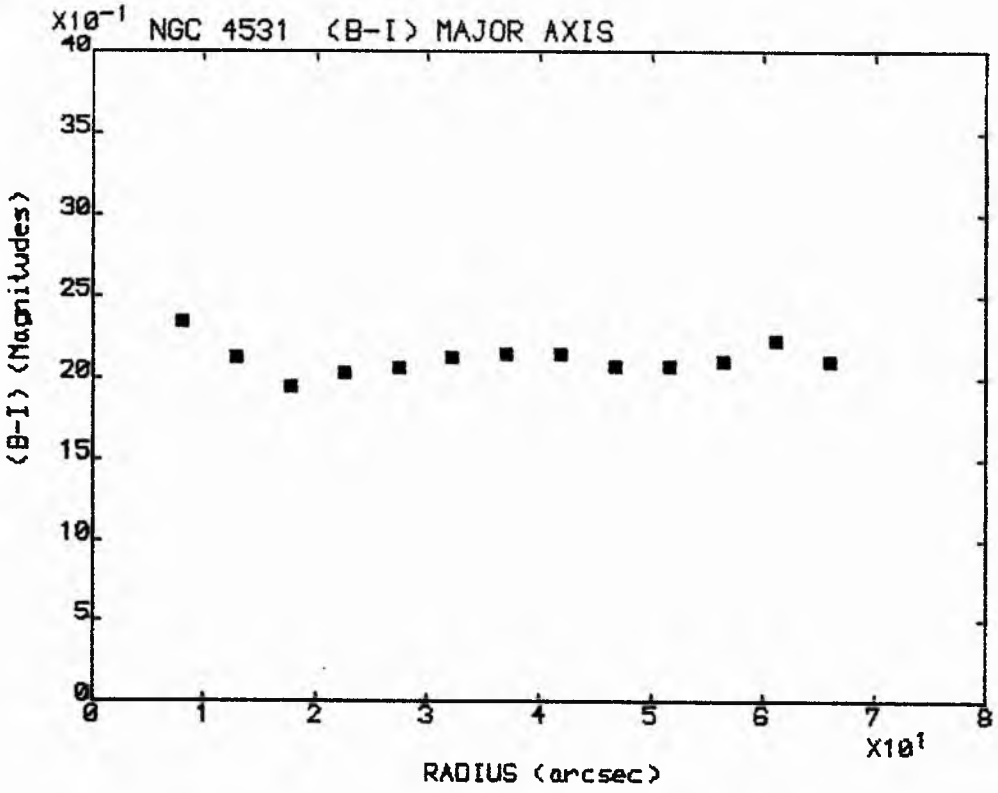
X10⁻¹ NGC 4531 (B-I) MAJOR AXIS
(B-I) (Magnitudes)
40
35
30
25
20
15
10
5
0
0 1 2 3 4 5 6 7 8
X10¹
RADIUS (arcsec)

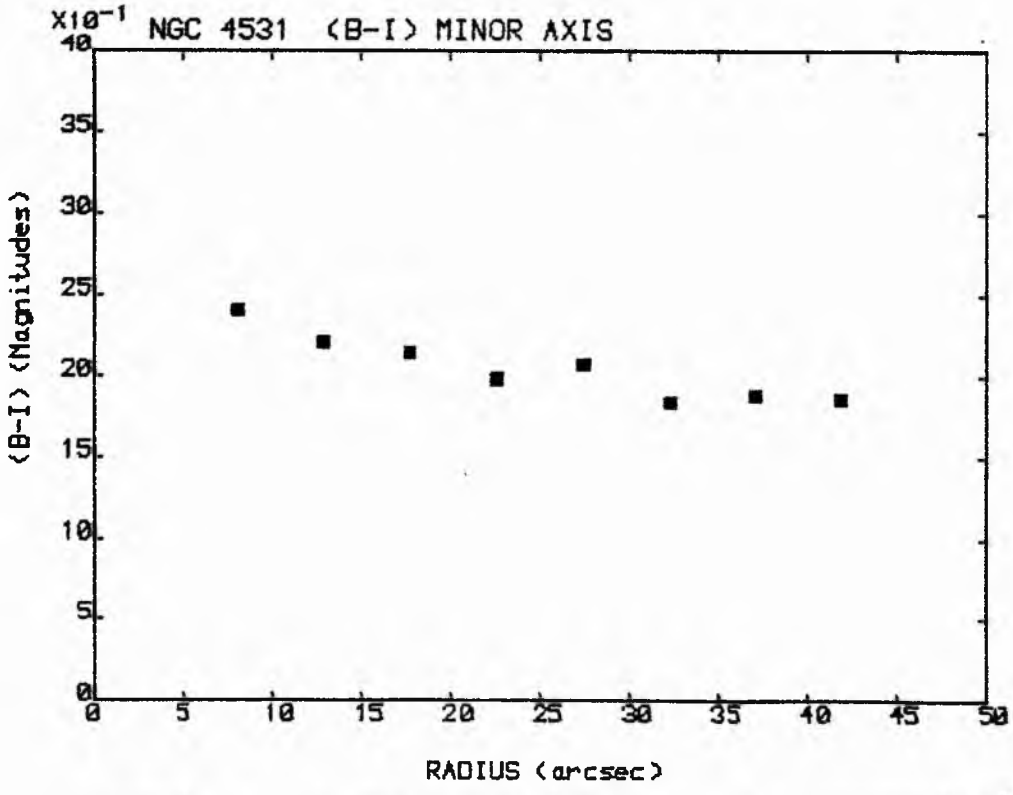
X10⁻¹ NGC 4531 (B-I) MINOR AXIS
(B-I) (Magnitudes)
40
35
30
25
20
15
10
5
0
0 5 10 15 20 25 30 35 40 45 50
RADIUS (arcsec)

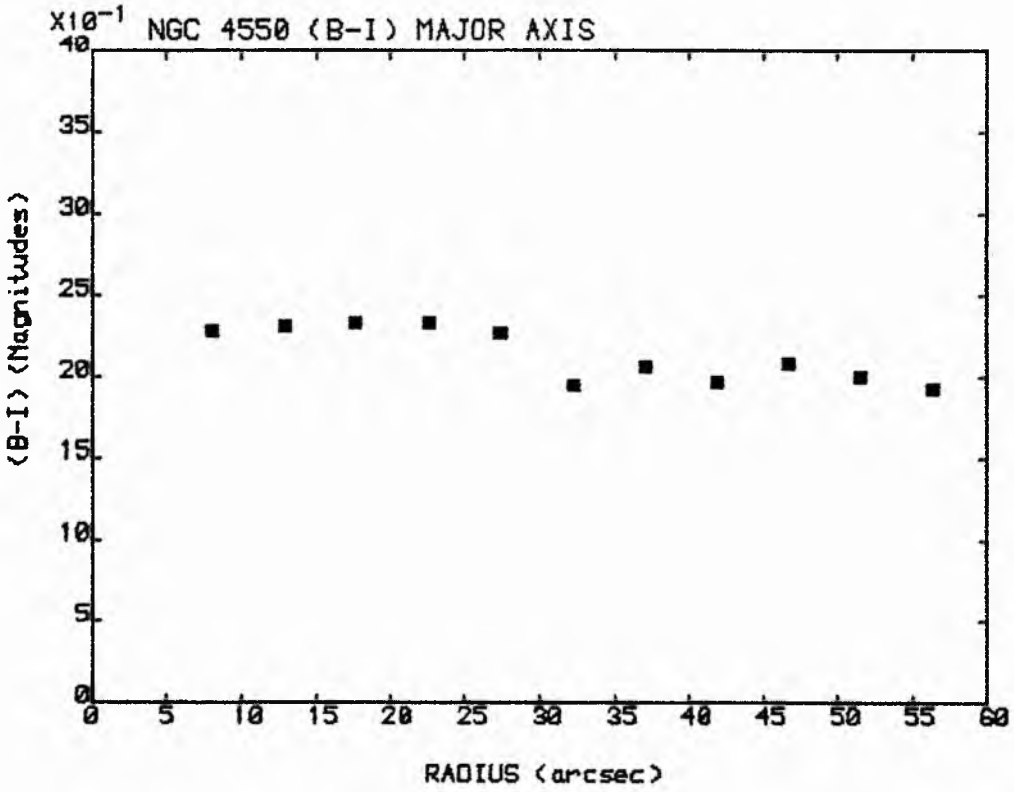
X10⁻¹
NGC 4550 (B-I) MAJOR AXIS
(B-I) (Magnitudes)
RADIUS (arcsec)
0
5
10
15
20
25
30
35
40
45
50
55
60

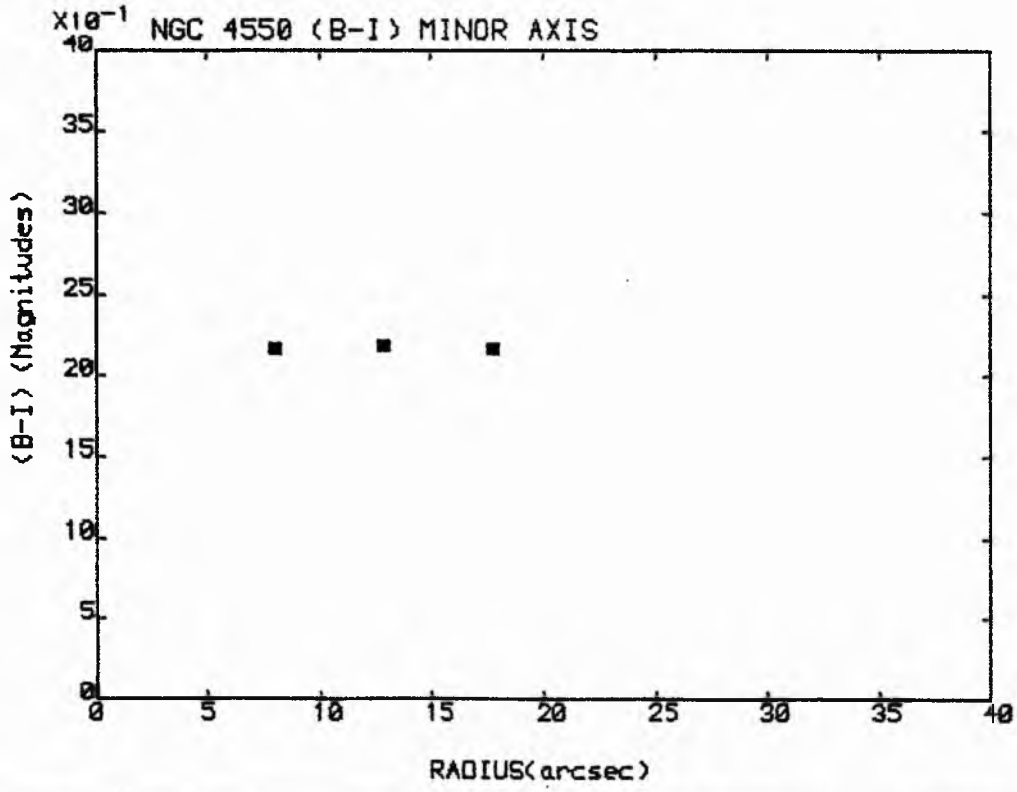
X10⁻¹
NGC 4550 (B-I) MINOR AXIS
(B-I) (Magnitudes)
RADIUS(arcsec)
0
5
10
15
20
25
30
35
40

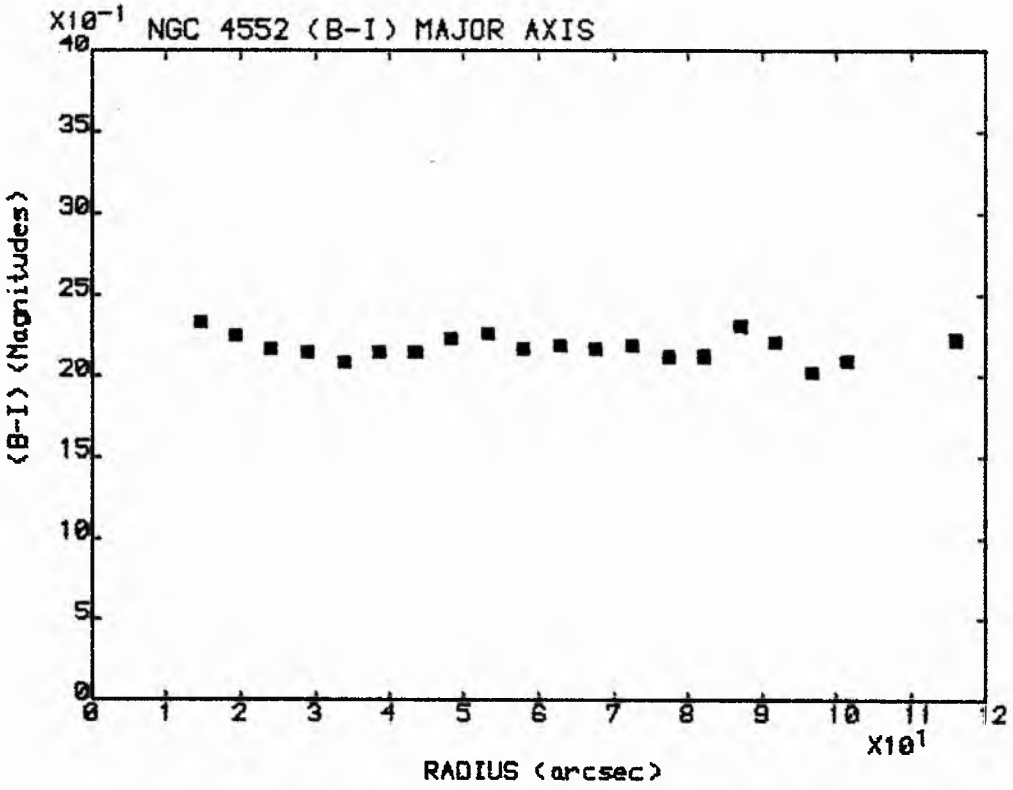
X10⁻¹
NGC 4552 (B-I) MAJOR AXIS
(B-I) (Magnitudes)
40
35
30
25
20
15
10
5
0
0 1 2 3 4 5 6 7 8 9 10 11 12
X10¹
RADIUS (arcsec)

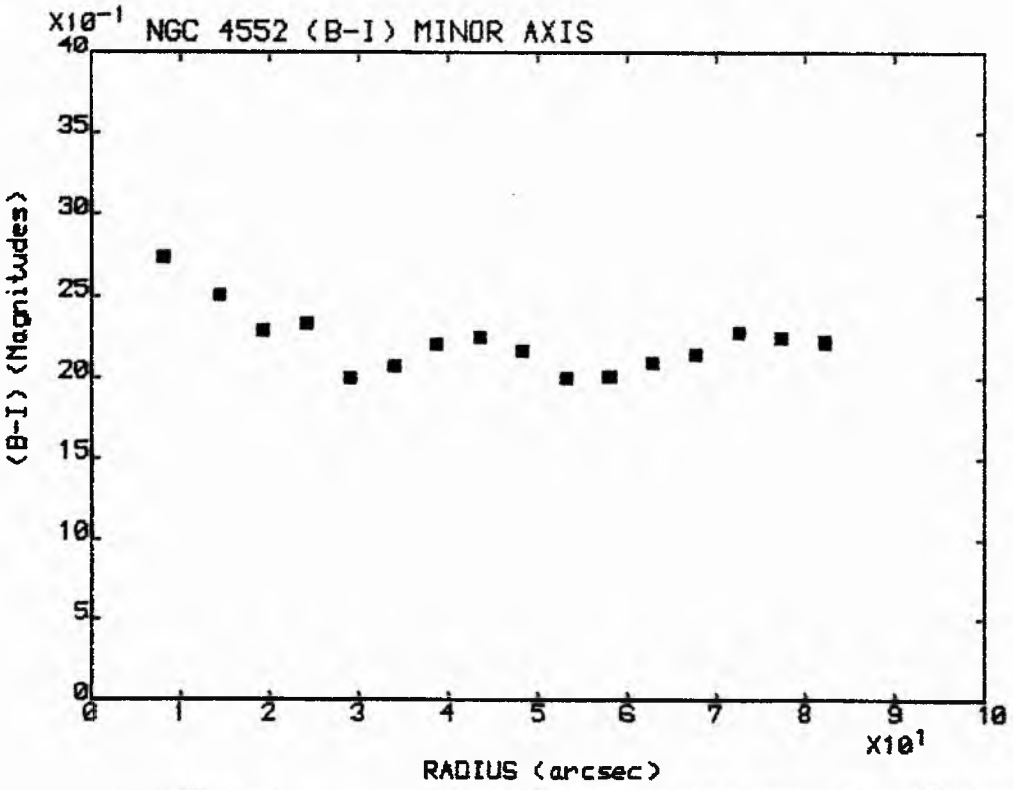
X10⁻¹
NGC 4552 (B-I) MINOR AXIS
(B-I) (Magnitudes)
40
35
30
25
20
15
10
5
0
0 1 2 3 4 5 6 7 8 9 10
X10¹
RADIUS (arcsec)

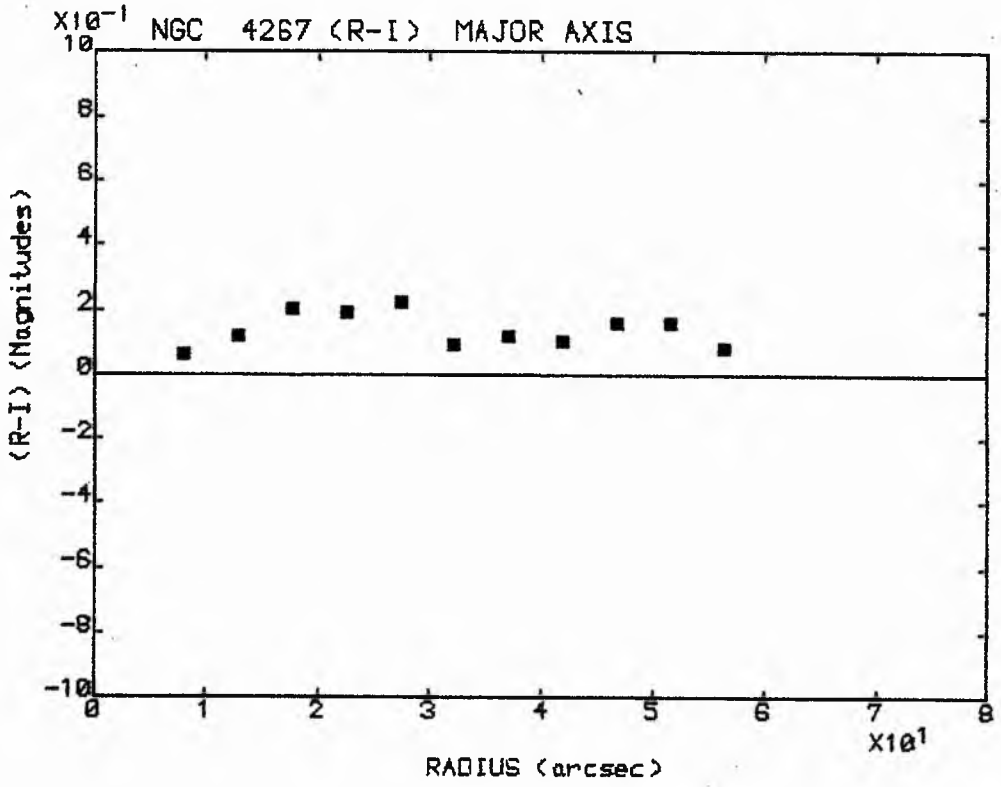
X10⁻¹
NGC 4267 (R-I) MAJOR AXIS
(R-I) (Magnitudes)
RADIUS (arcsec)
X10¹

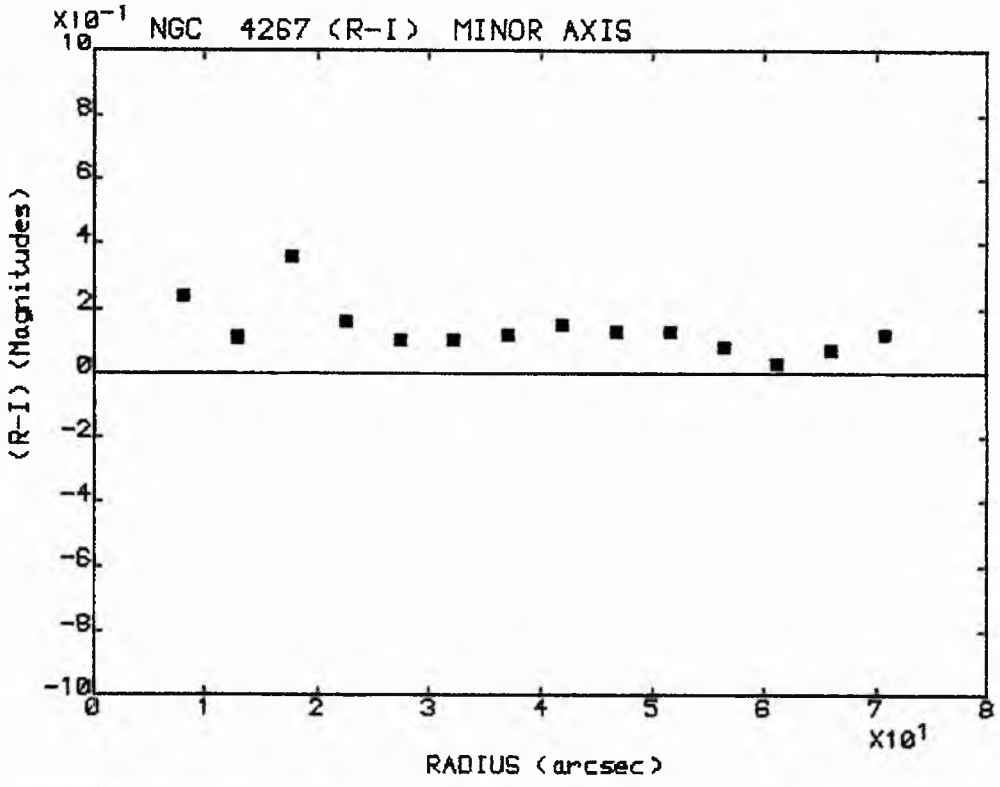
X10⁻¹
NGC 4267 (R-I) MINOR AXIS
(R-I) (Magnitudes)
RADIUS (arcsec)
X10¹

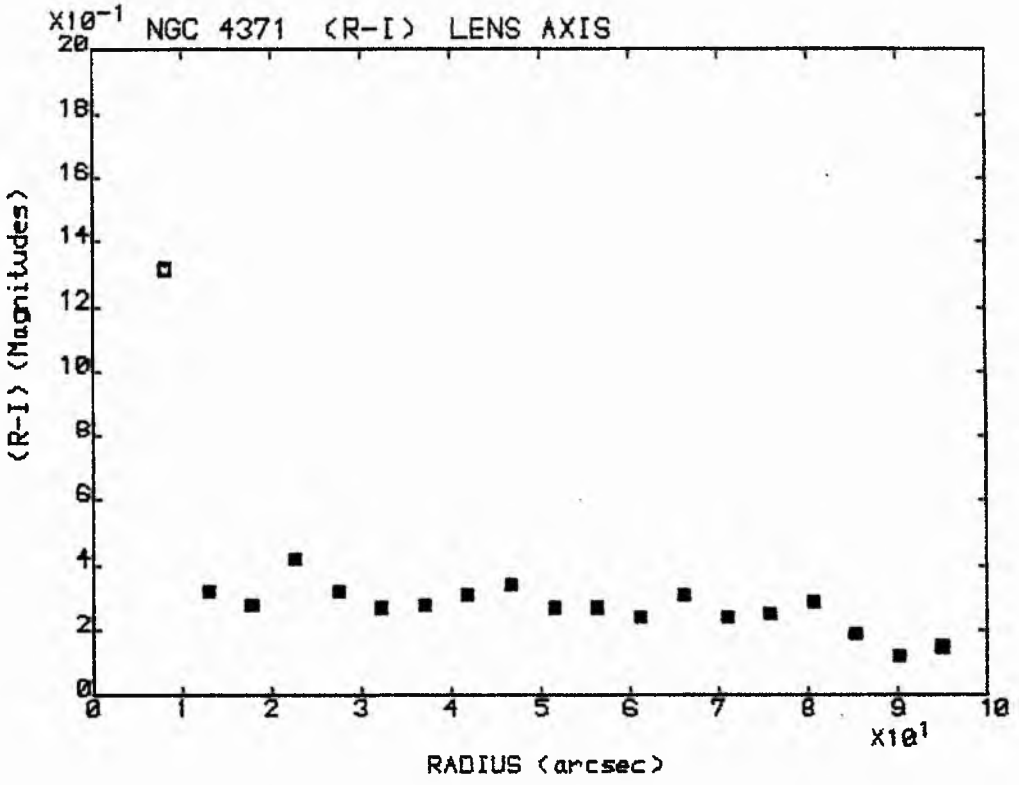
X10⁻¹
NGC 4371 (R-I) LENS AXIS
(R-I) (Magnitudes)
RADIUS (arcsec)
X10¹

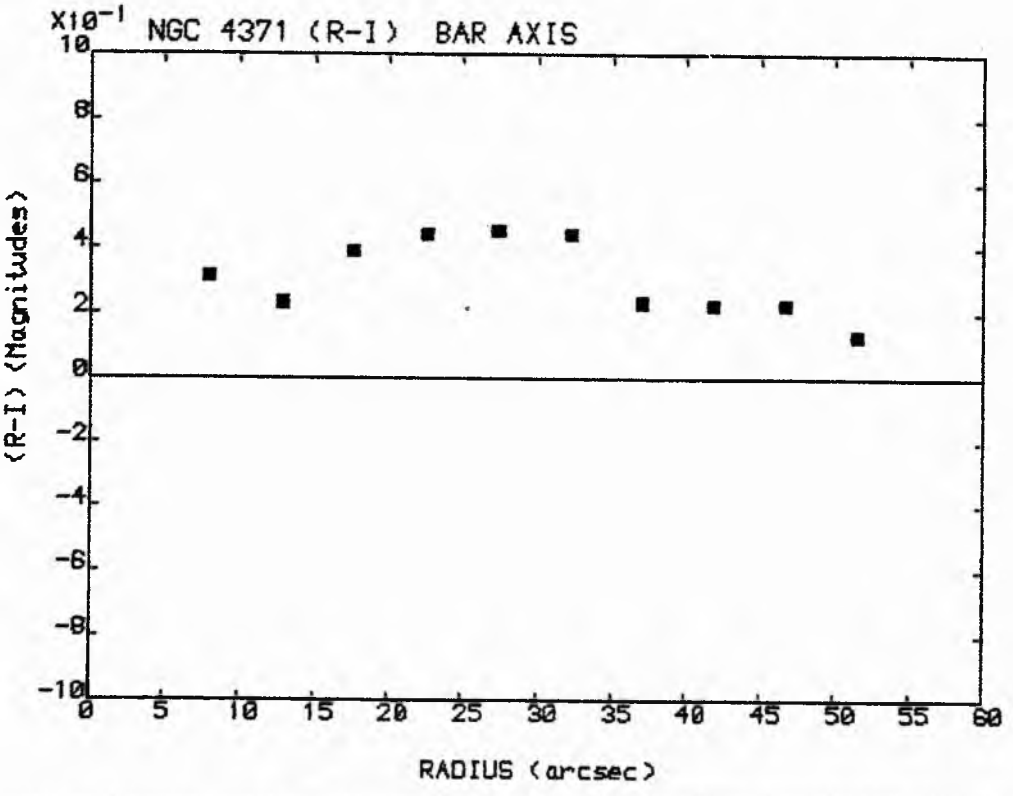
X10⁻¹
NGC 4371 (R-I) BAR AXIS
(R-I) (Magnitudes)
RADIUS (arcsec)

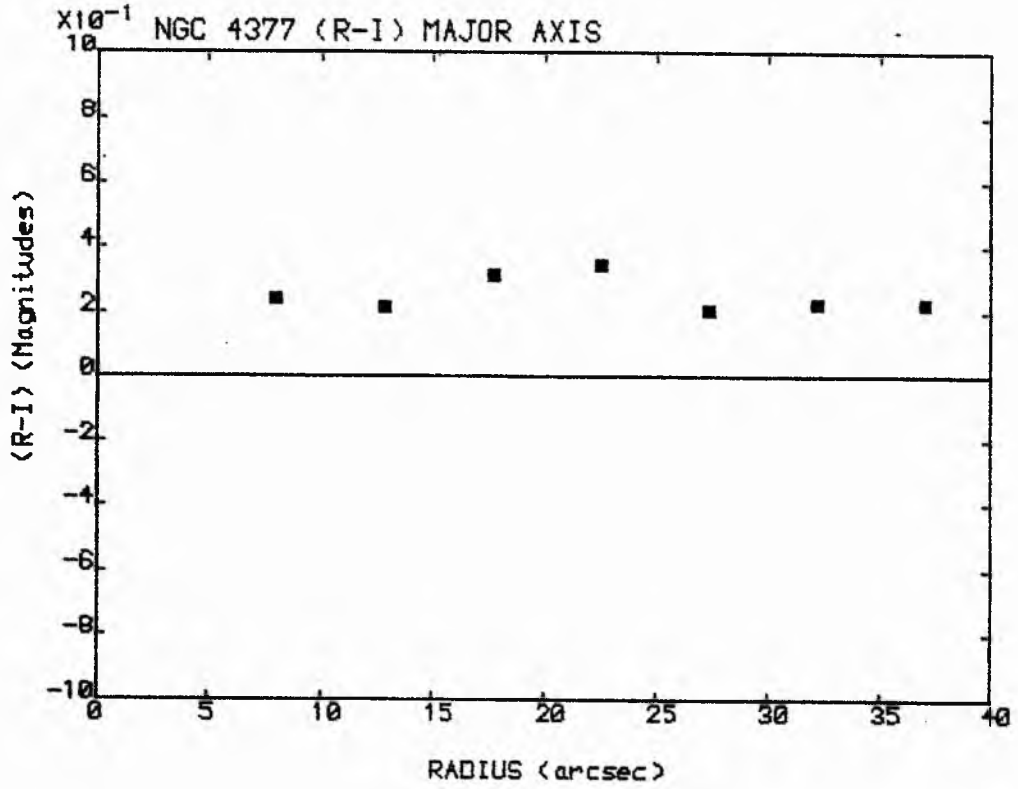
X10⁻¹
NGC 4377 (R-I) MAJOR AXIS
(R-I) (Magnitudes)
RADIUS (arcsec)
10
8
6
4
2
0
-2
-4
-6
-8
-10
0
5
10
15
20
25
30
35
40

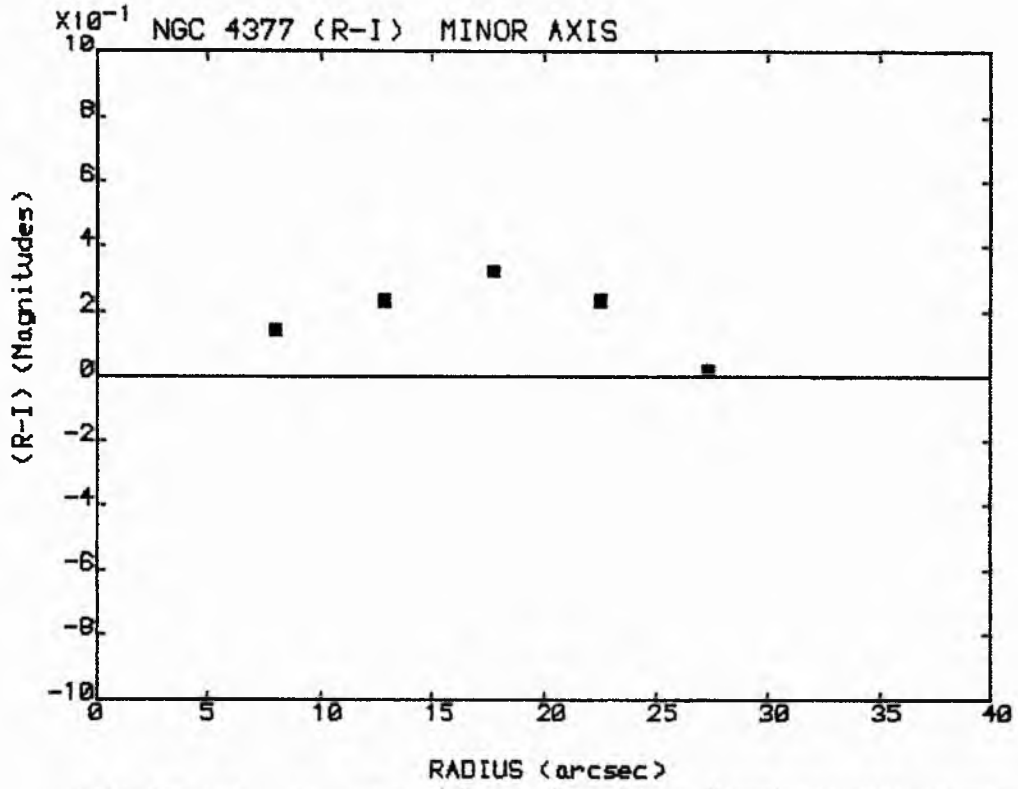
X10⁻¹
NGC 4377 (R-I) MINOR AXIS
(R-I) (Magnitudes)
RADIUS (arcsec)
10
8
6
4
2
0
-2
-4
-6
-8
-10
0
5
10
15
20
25
30
35
40

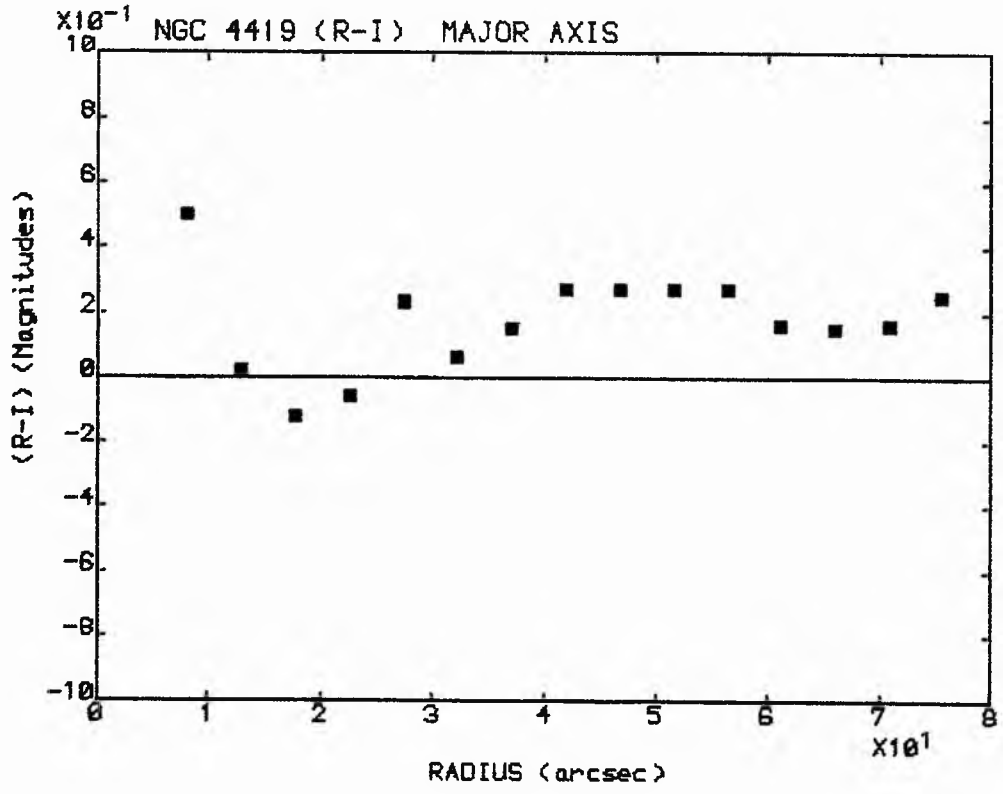
X10⁻¹
NGC 4419 (R-I) MAJOR AXIS
10
8
6
4
2
0
-2
-4
-6
-8
-10
(R-I) (Magnitudes)
0
1
2
3
4
5
6
7
8
X10¹
RADIUS (arcsec)

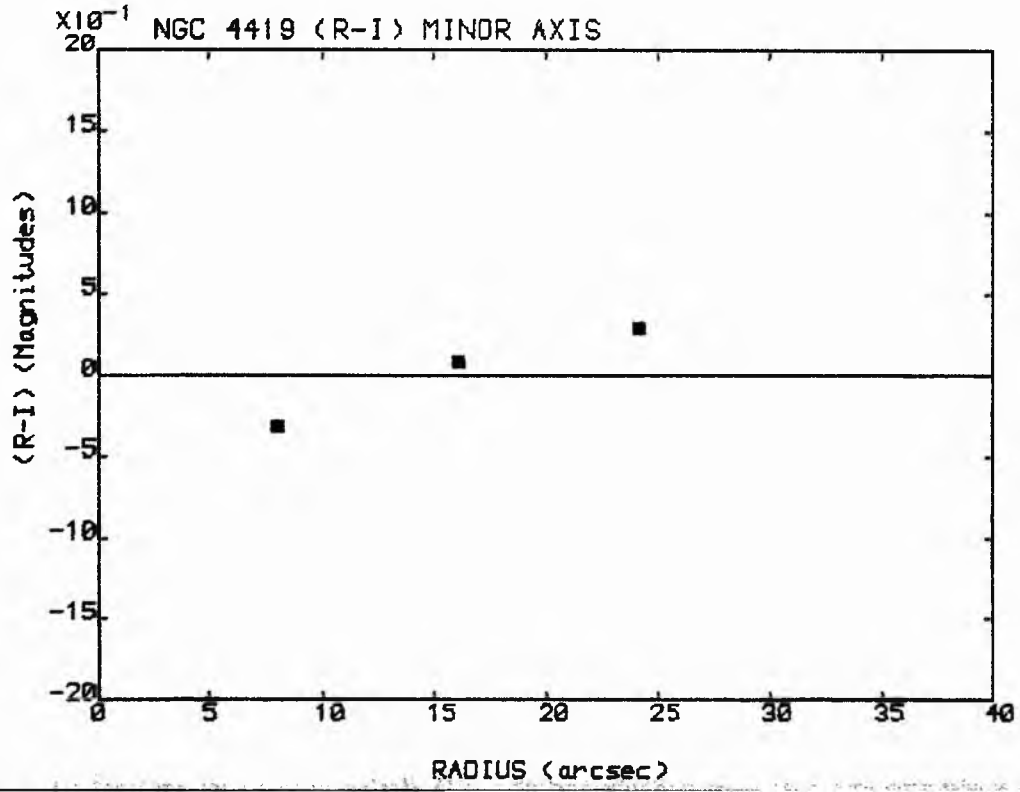
X10⁻¹
NGC 4419 (R-I) MINOR AXIS
20
15
10
5
0
-5
-10
-15
-20
(R-I) (Magnitudes)
0
5
10
15
20
25
30
35
40
RADIUS (arcsec)

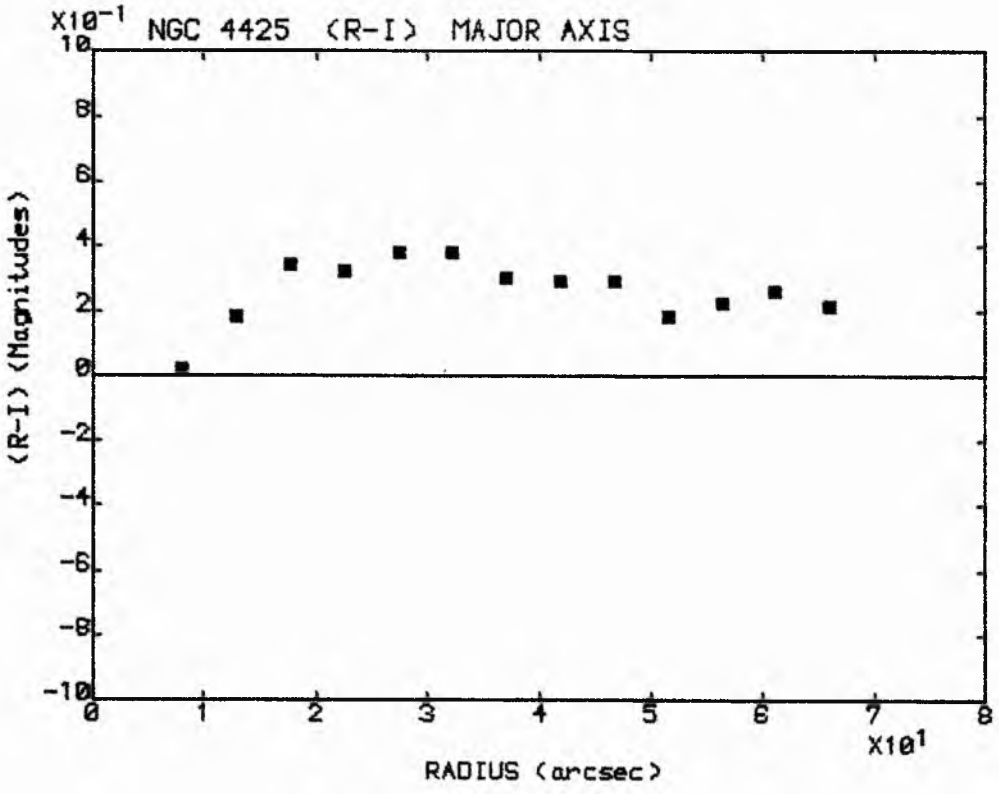
X10⁻¹
NGC 4425 (R-I) MAJOR AXIS
10
8
6
4
2
0
-2
-4
-6
-8
-10
(R-I) (Magnitudes)
0
1
2
3
4
5
6
7
8
X10¹
RADIUS (arcsec)

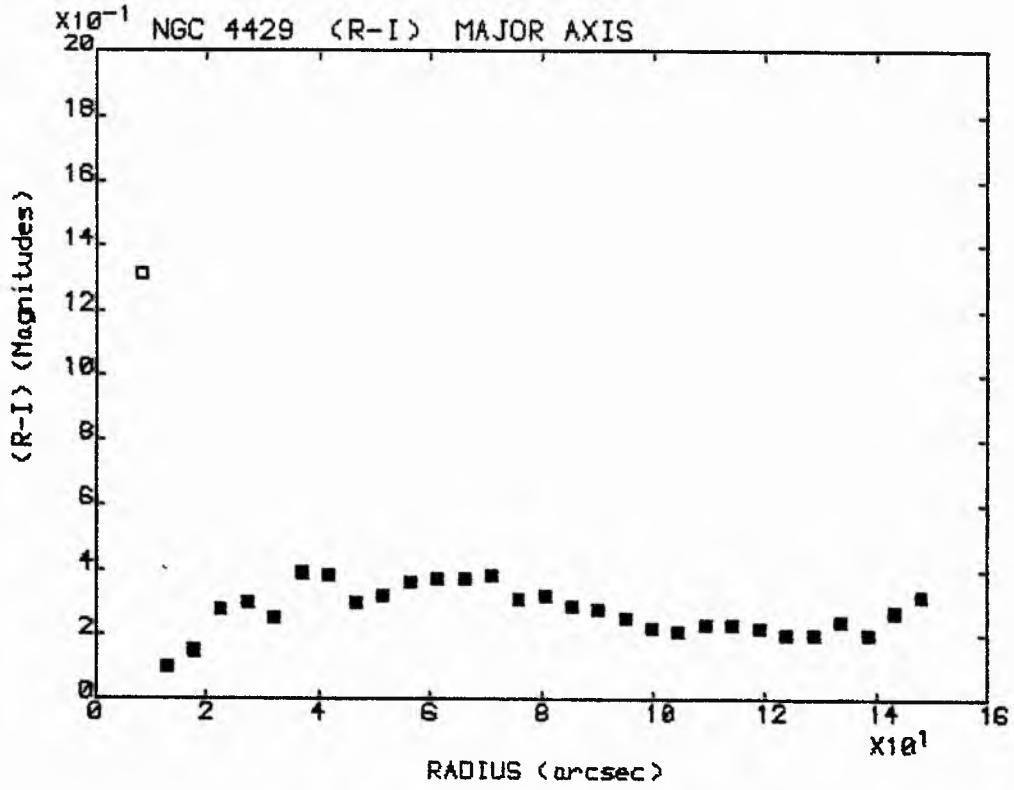
X10⁻¹
NGC 4429 (R-I) MAJOR AXIS
(R-I) (Magnitudes)
RADIUS (arcsec)
X10¹

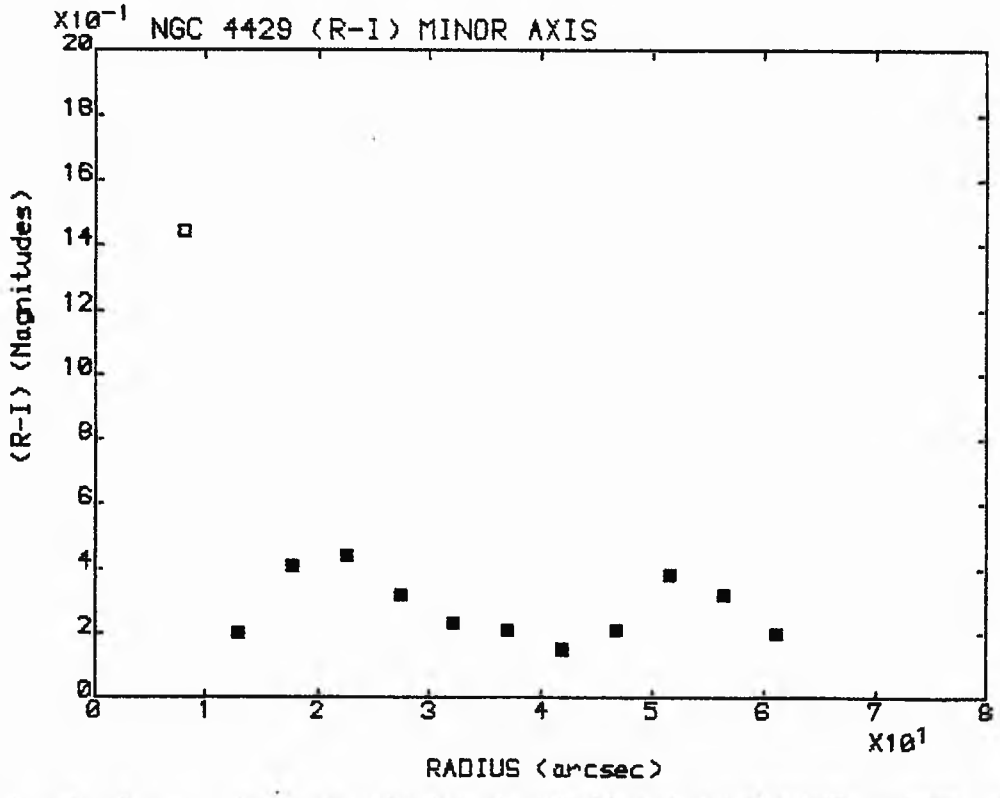
X10⁻¹
NGC 4429 (R-I) MINOR AXIS
(R-I) (Magnitudes)
RADIUS (arcsec)
X10¹

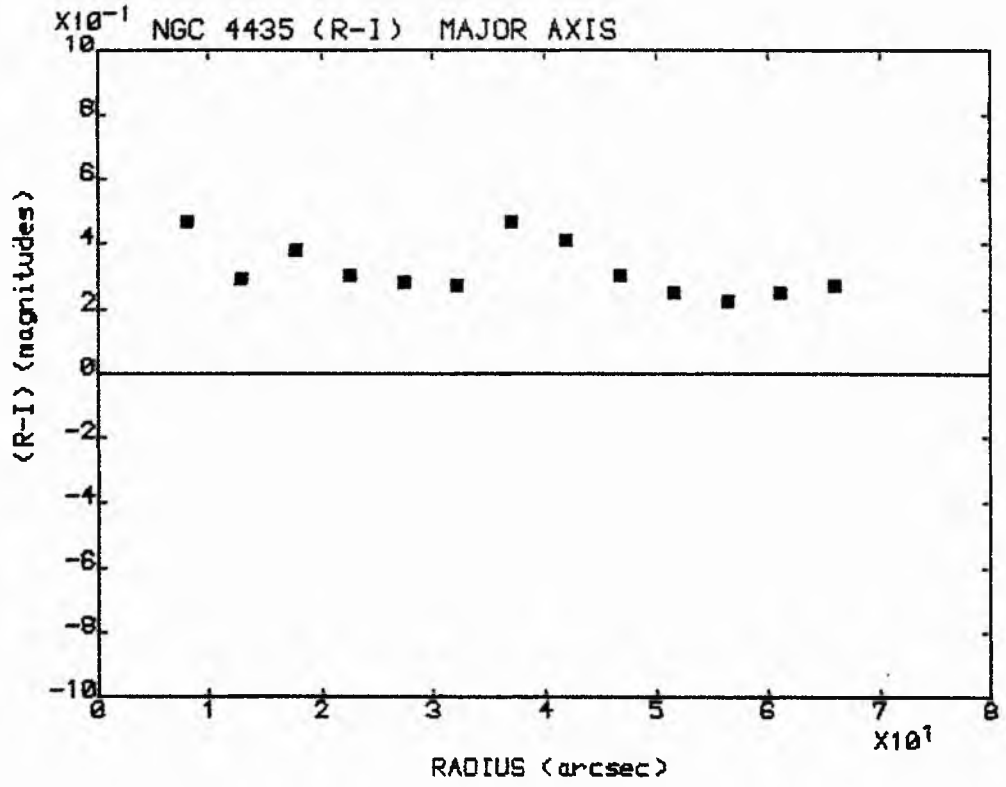
X10⁻¹
NGC 4435 (R-I) MAJOR AXIS
(R-I) (magnitudes)
10
8
6
4
2
0
-2
-4
-6
-8
-10
0
1
2
3
4
5
6
7
8
X10¹
RADIUS (arcsec)

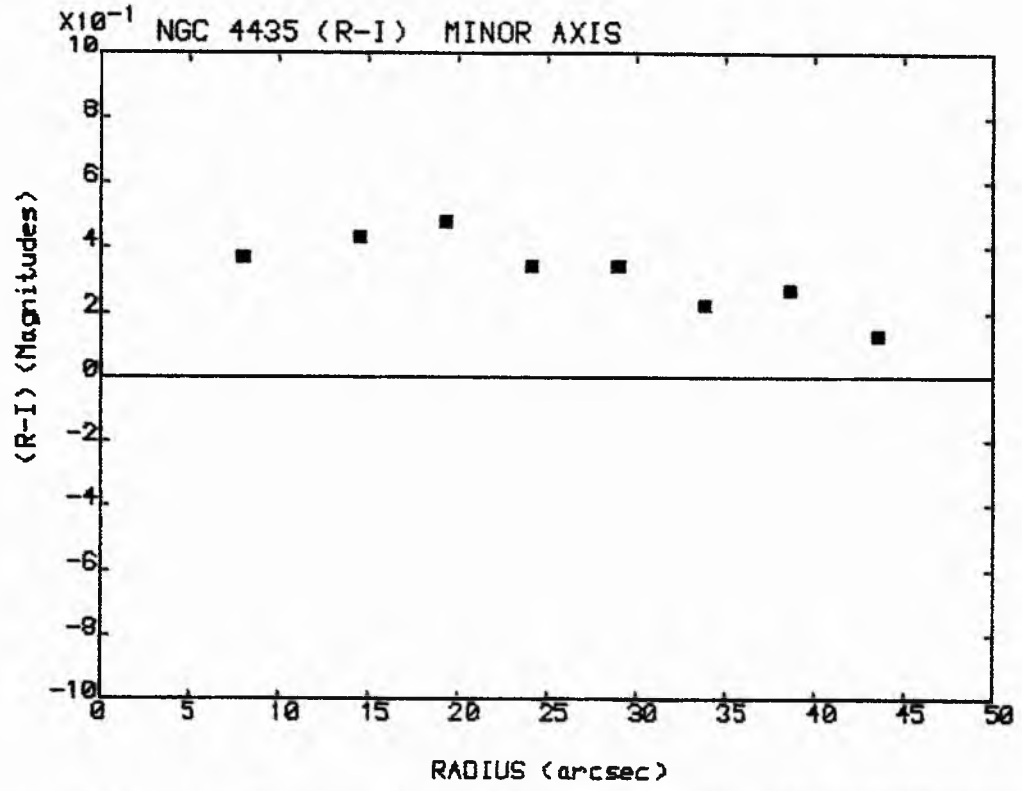
X10⁻¹
NGC 4435 (R-I) MINOR AXIS
(R-I) (Magnitudes)
10
8
6
4
2
0
-2
-4
-6
-8
-10
0
5
10
15
20
25
30
35
40
45
50
RADIUS (arcsec)

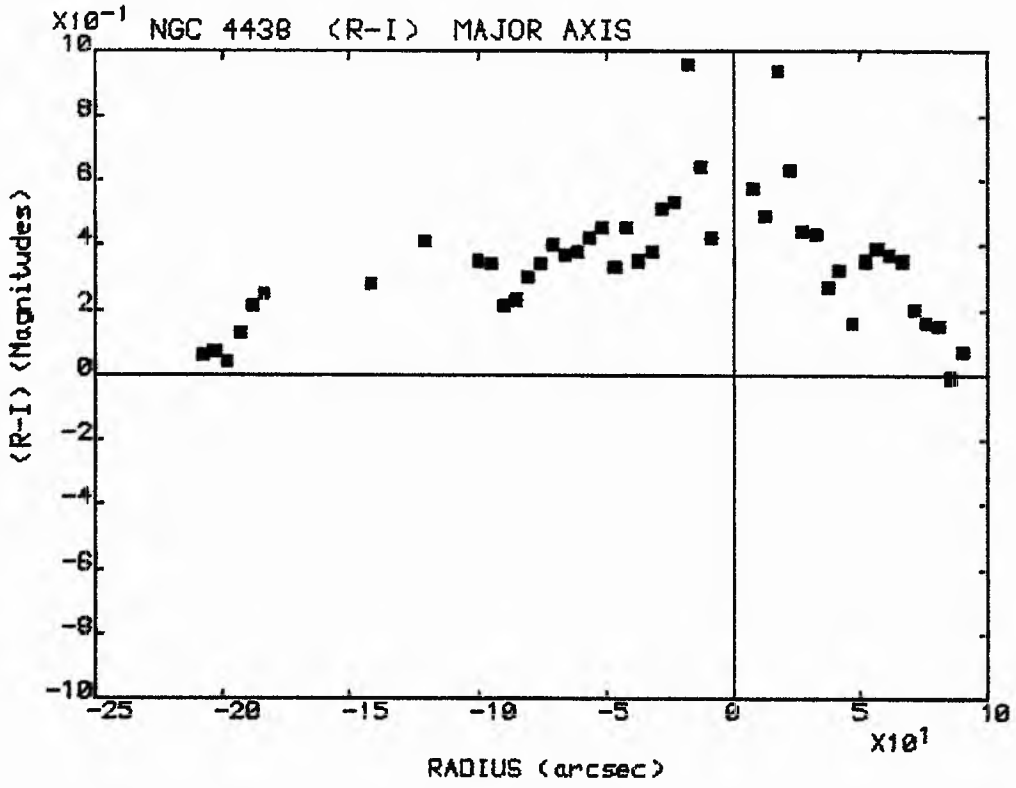
X10⁻¹
NGC 4438 (R-I) MAJOR AXIS
(R-I) (Magnitudes)
RADIUS (arcsec)
X10¹

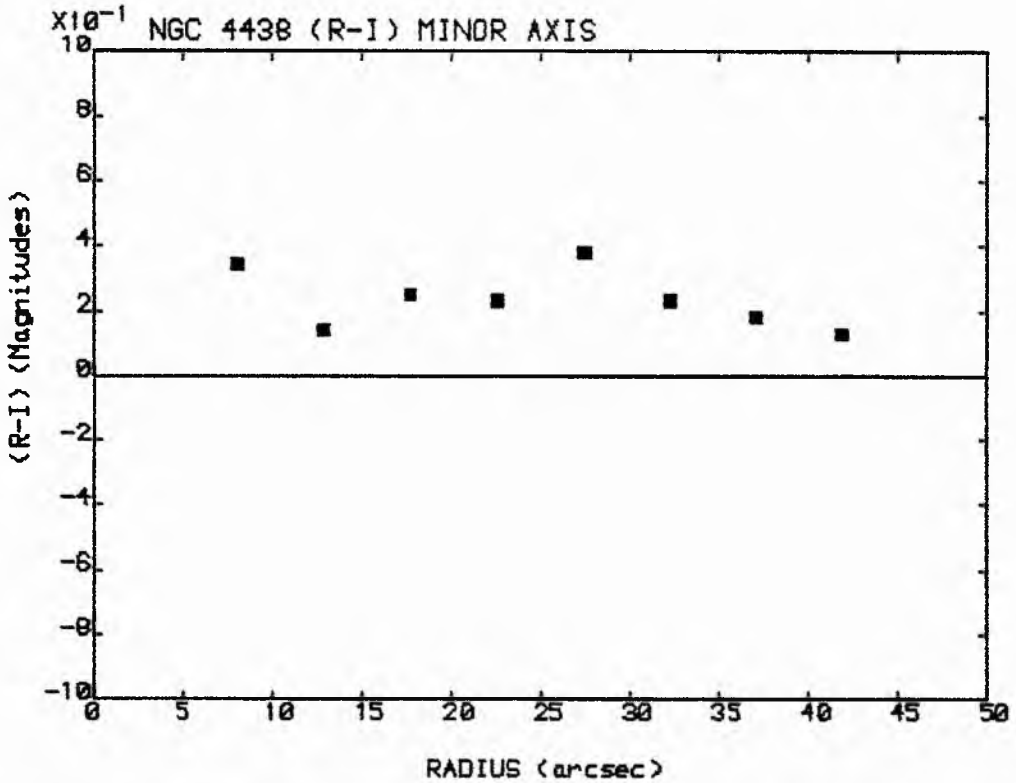
X10⁻¹
NGC 4438 (R-I) MINOR AXIS
(R-I) (Magnitudes)
RADIUS (arcsec)

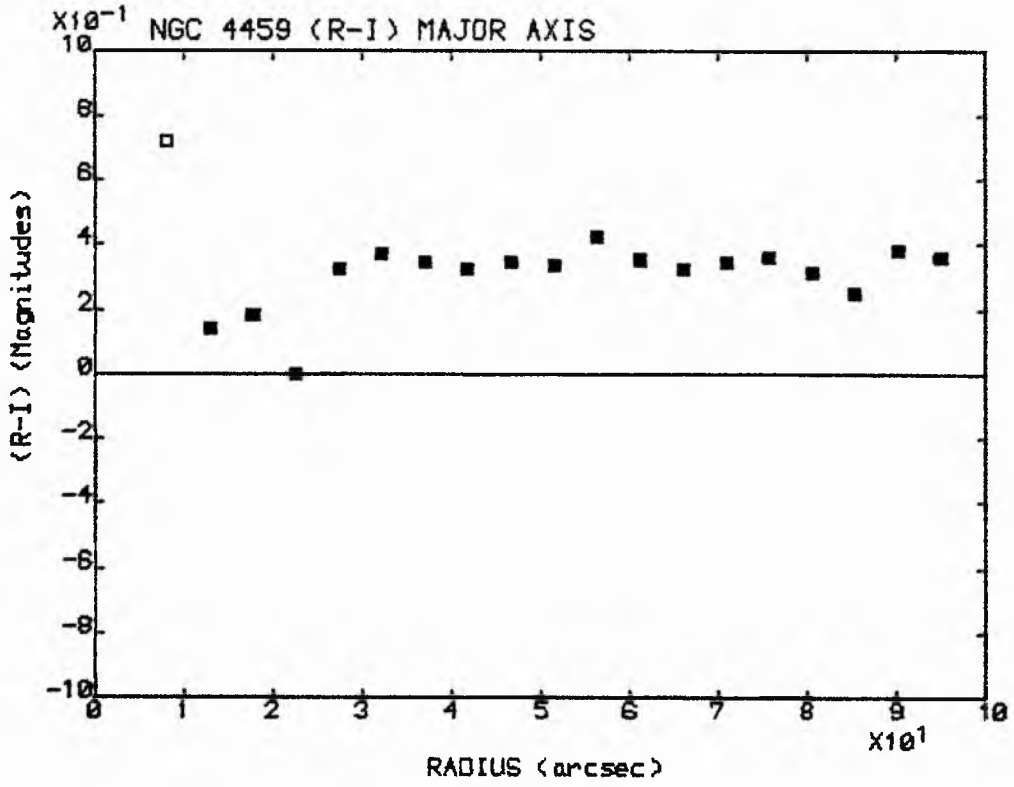
X10⁻¹
NGC 4459 (R-I) MAJOR AXIS
(R-I) (Magnitudes)
10
8
6
4
2
0
-2
-4
-6
-8
-10
0 1 2 3 4 5 6 7 8 9 10
X10¹
RADIUS (arcsec)

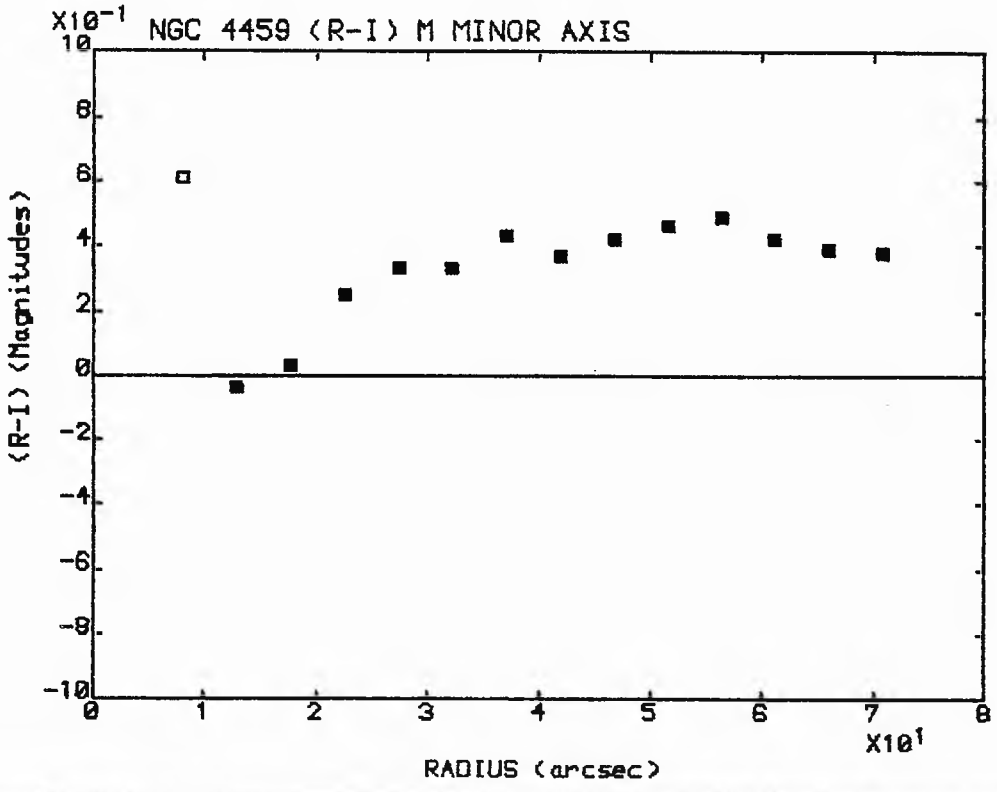
X10⁻¹
NGC 4459 (R-I) M MINOR AXIS
(R-I) (Magnitudes)
10
8
6
4
2
0
-2
-4
-6
-8
-10
0 1 2 3 4 5 6 7 8
X10¹
RADIUS (arcsec)

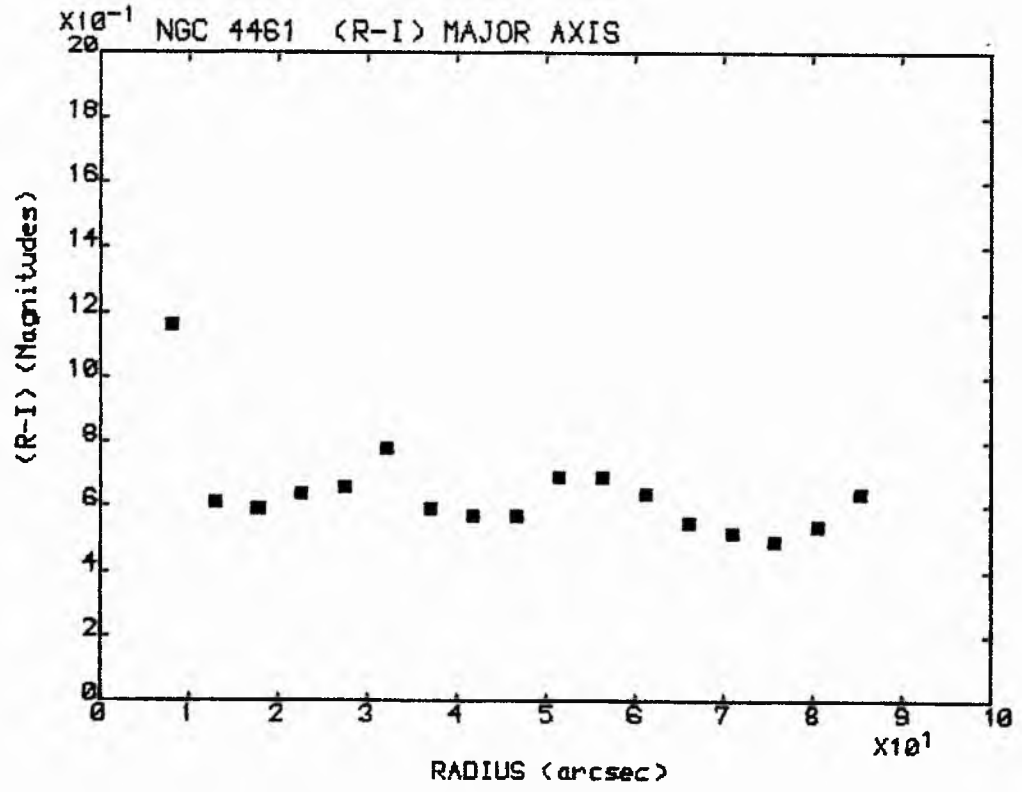
X10⁻¹ NGC 4461 (R-I) MAJOR AXIS
(R-I) (Magnitudes)
RADIUS (arcsec)
X10¹

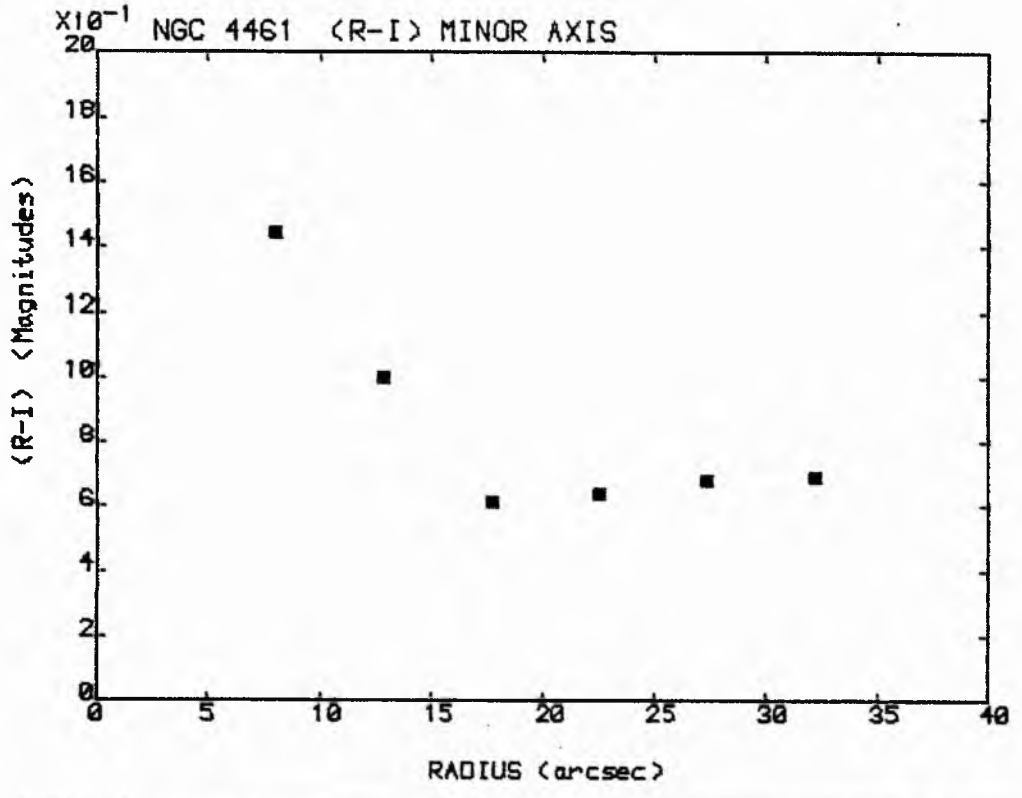
X10⁻¹ NGC 4461 (R-I) MINOR AXIS
(R-I) (Magnitudes)
RADIUS (arcsec)

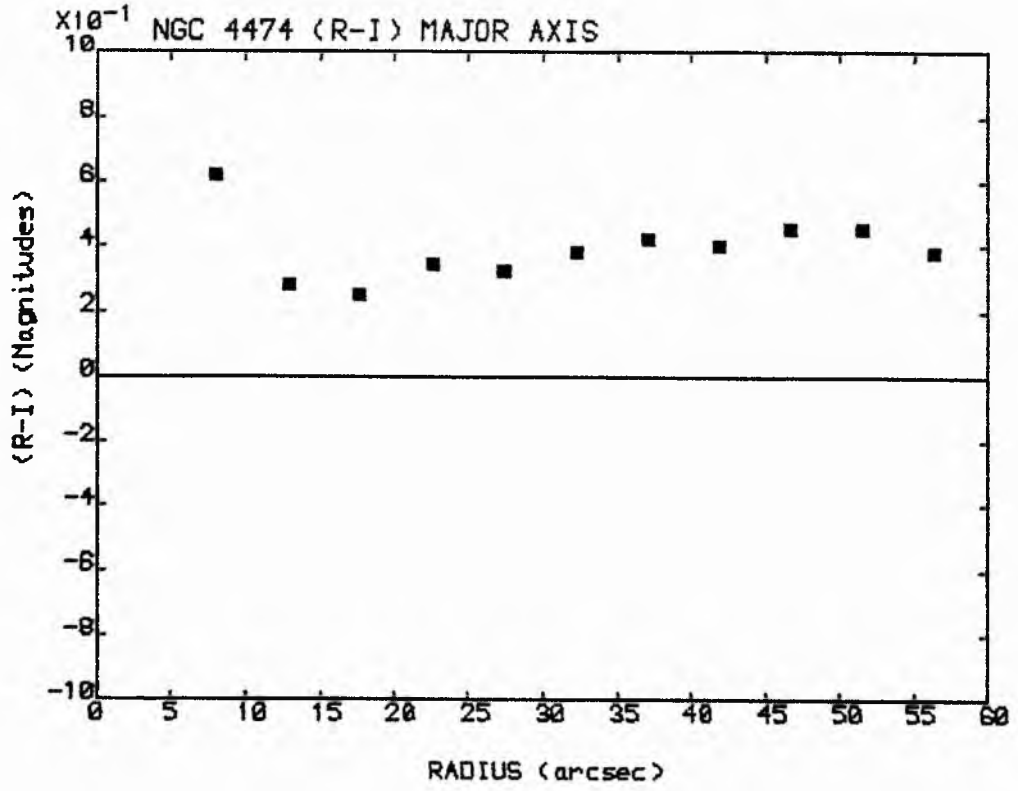
X10⁻¹
NGC 4474 (R-I) MAJOR AXIS
(R-I) (Magnitudes)
10
8
6
4
2
0
-2
-4
-6
-8
-10
0
5
10
15
20
25
30
35
40
45
50
55
60
RADIUS (arcsec)

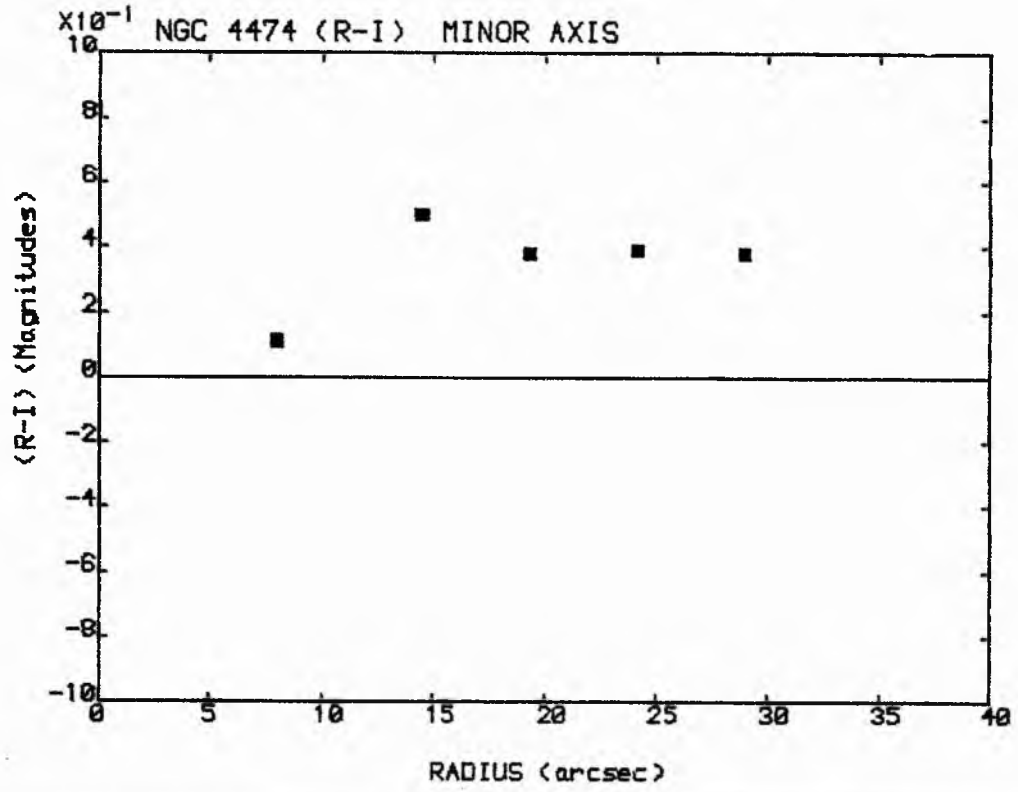
X10⁻¹
NGC 4474 (R-I) MINOR AXIS
(R-I) (Magnitudes)
10
8
6
4
2
0
-2
-4
-6
-8
-10
0
5
10
15
20
25
30
35
40
RADIUS (arcsec)

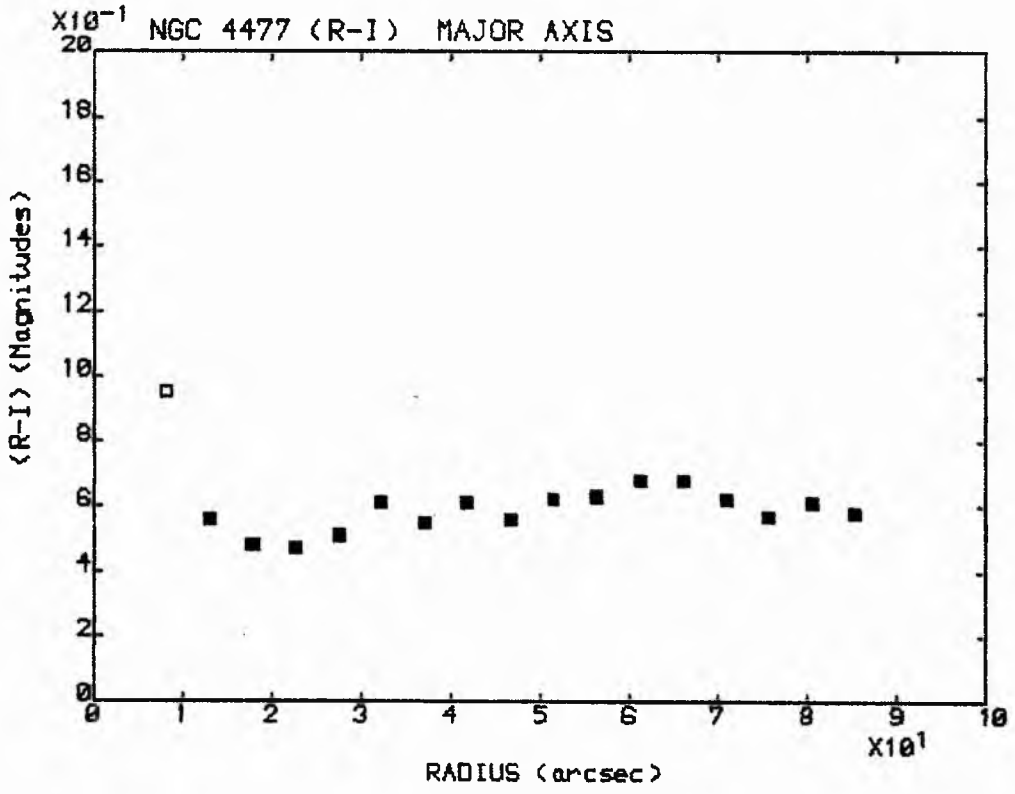
X10⁻¹
NGC 4477 (R-I) MAJOR AXIS
(R-I) (Magnitudes)
RADIUS (arcsec)
X10¹

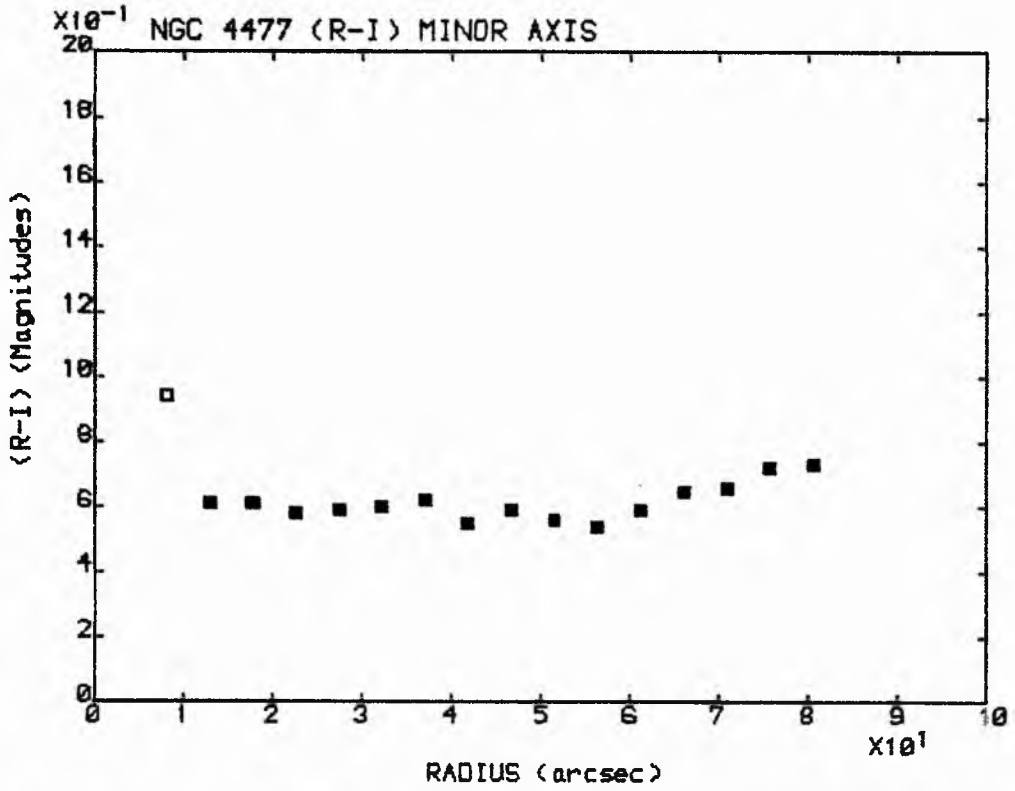
X10⁻¹
NGC 4477 (R-I) MINOR AXIS
(R-I) (Magnitudes)
RADIUS (arcsec)
X10¹

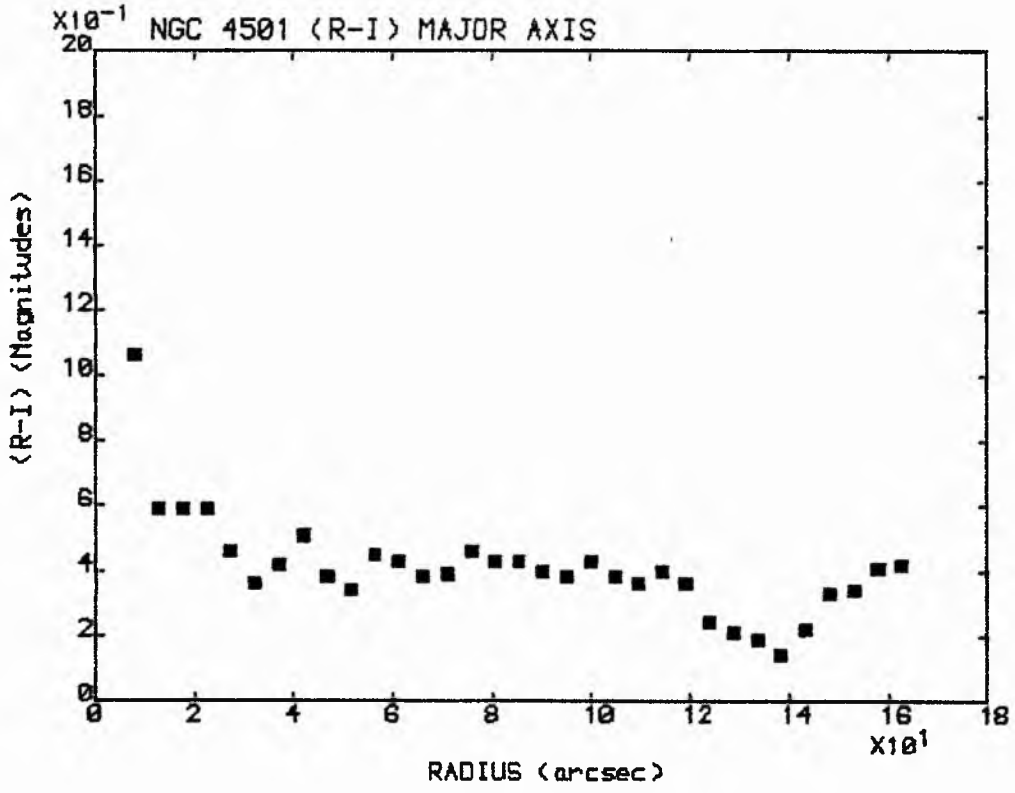
X10⁻¹
NGC 4501 (R-I) MAJOR AXIS
(R-I) (Magnitudes)
RADIUS (arcsec)
X10¹

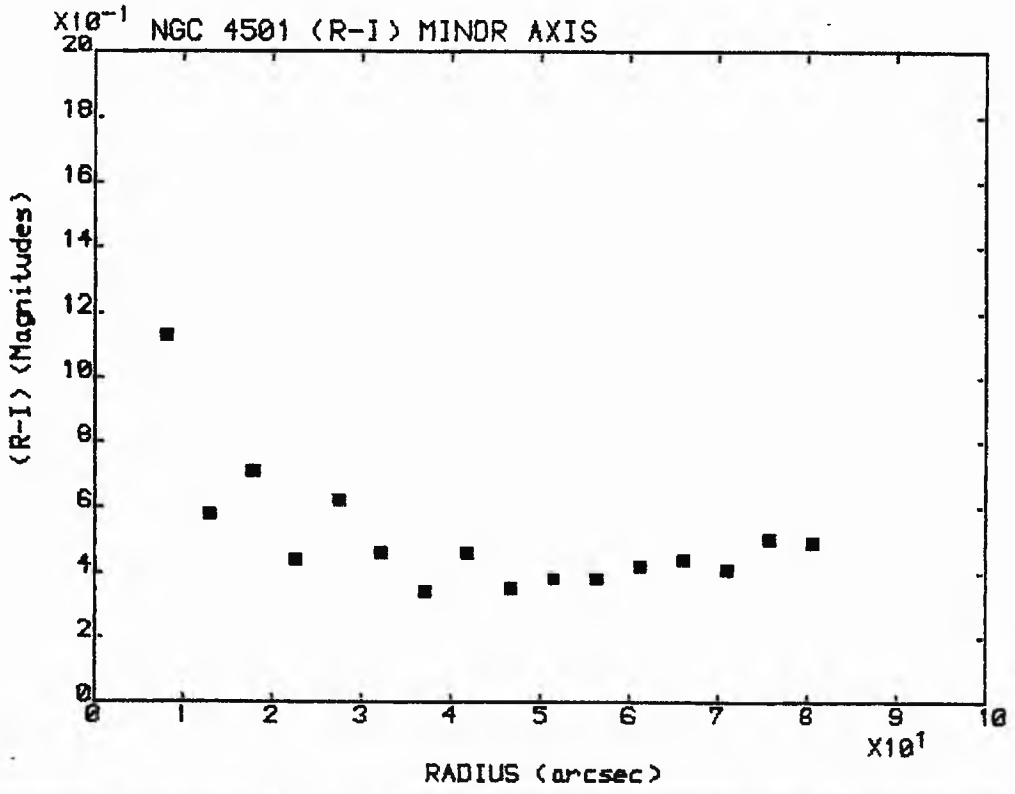
X10⁻¹
NGC 4501 (R-I) MINOR AXIS
(R-I) (Magnitudes)
RADIUS (arcsec)
X10¹

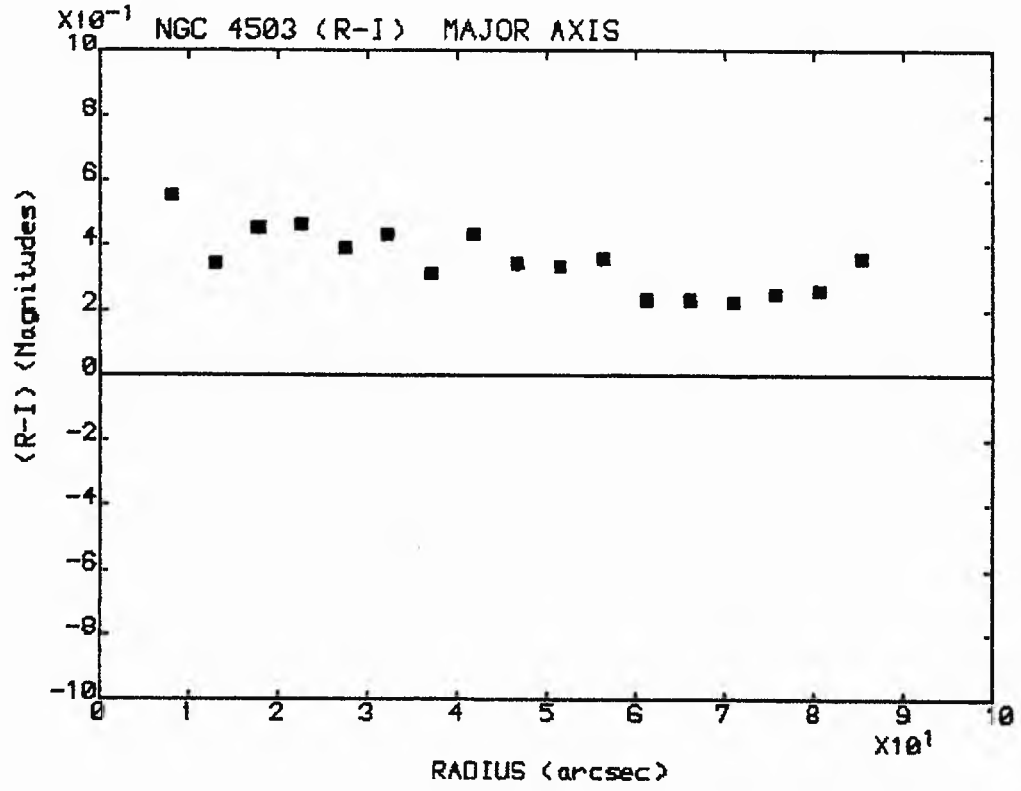
X10⁻¹ NGC 4503 (R-I) MAJOR AXIS
(R-I) (Magnitudes)
RADIUS (arcsec)
X10¹

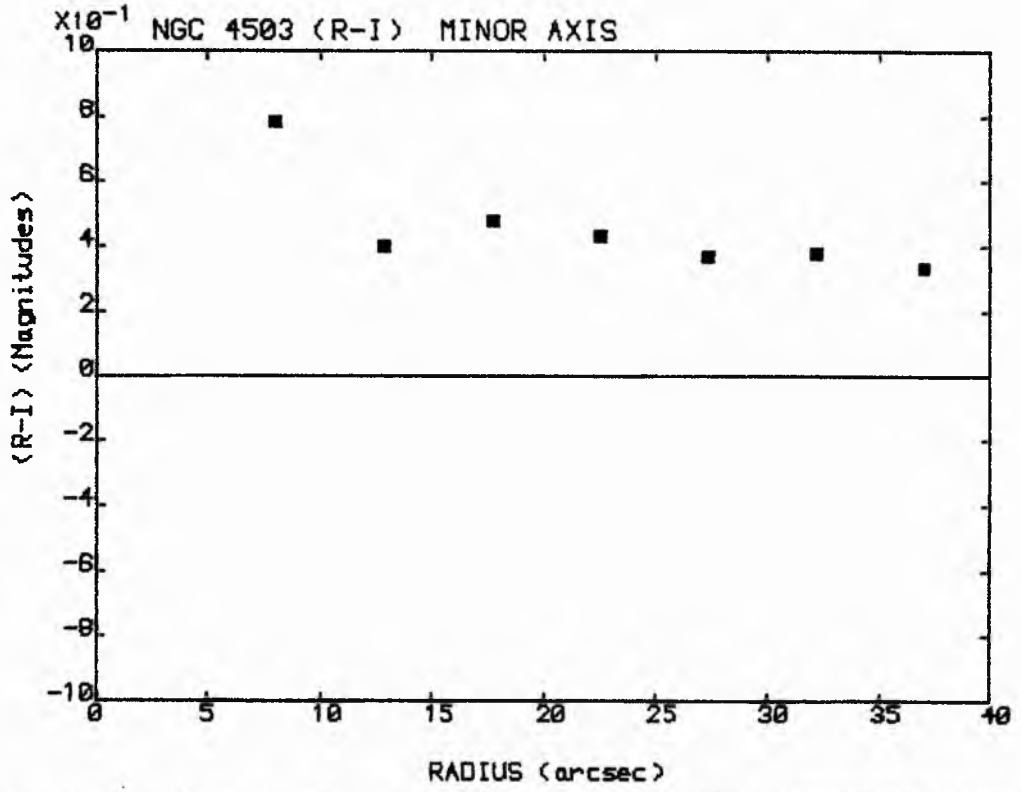
X10⁻¹ NGC 4503 (R-I) MINOR AXIS
(R-I) (Magnitudes)
RADIUS (arcsec)

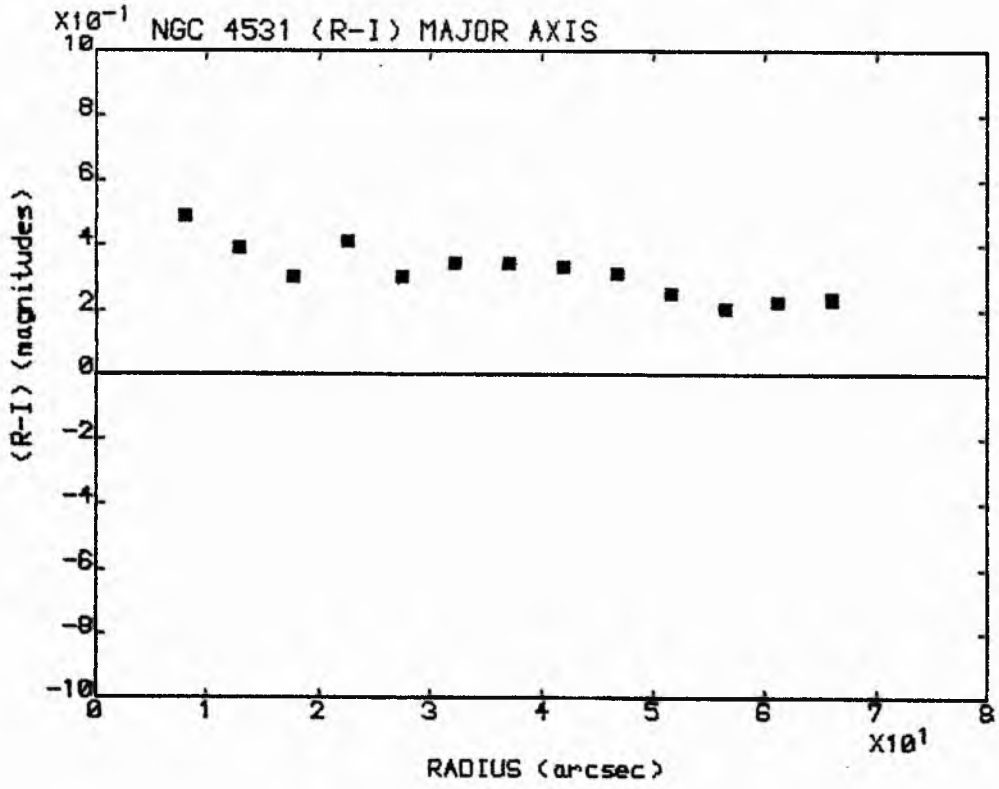
X10⁻¹
NGC 4531 (R-I) MAJOR AXIS
10
8
6
4
2
0
-2
-4
-6
-8
-10
(R-I) (magnitudes)
0
1
2
3
4
5
6
7
8
X10¹
RADIUS (arcsec)

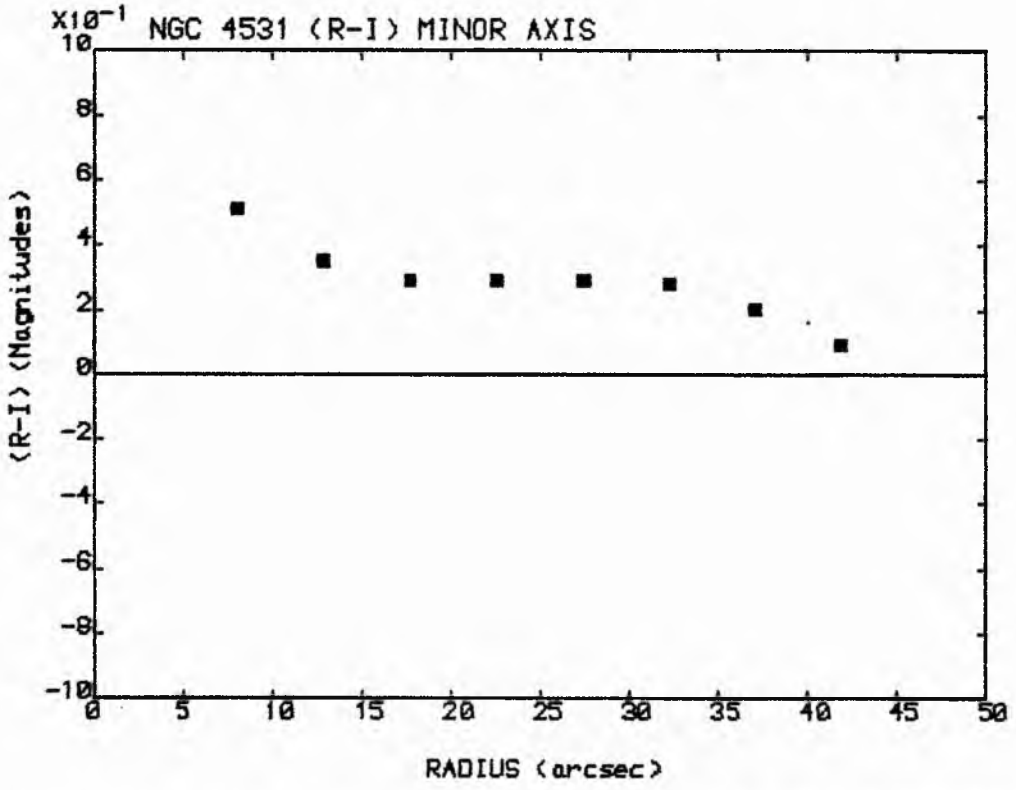
X10⁻¹
NGC 4531 (R-I) MINOR AXIS
10
8
6
4
2
0
-2
-4
-6
-8
-10
(R-I) (Magnitudes)
0
5
10
15
20
25
30
35
40
45
50
RADIUS (arcsec)

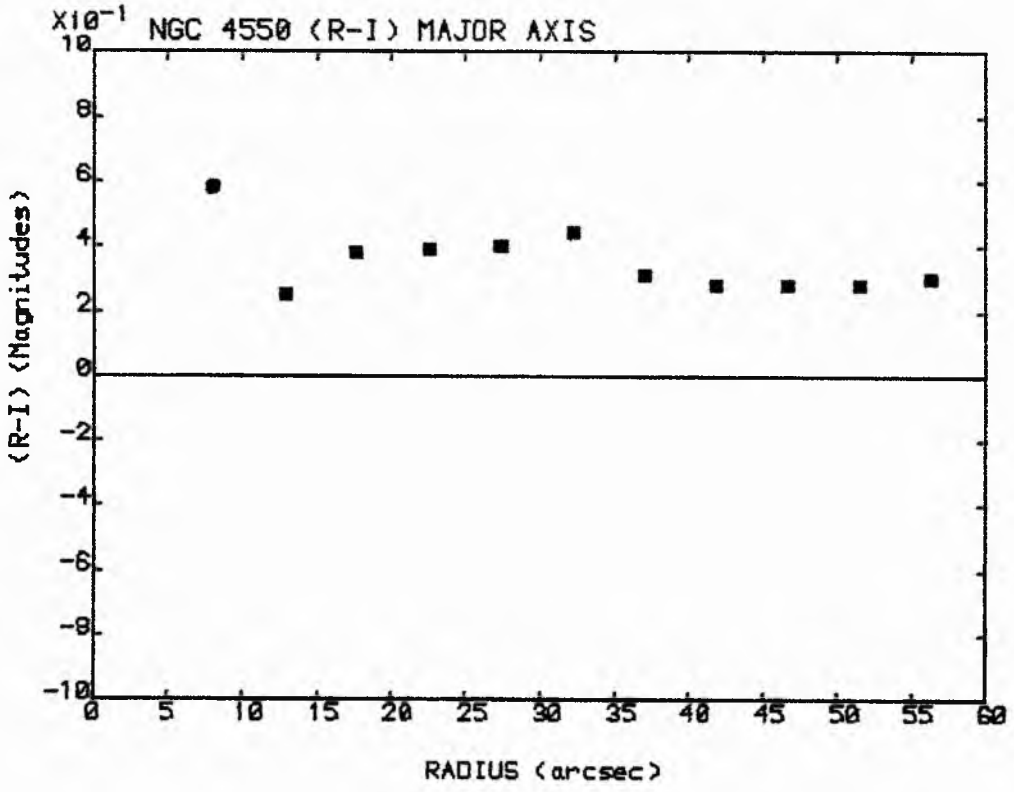
X10⁻¹
NGC 4550 (R-I) MAJOR AXIS
(R-I) (Magnitudes)
10
8
6
4
2
0
-2
-4
-6
-8
-10
0
5
10
15
20
25
30
35
40
45
50
55
60
RADIUS (arcsec)

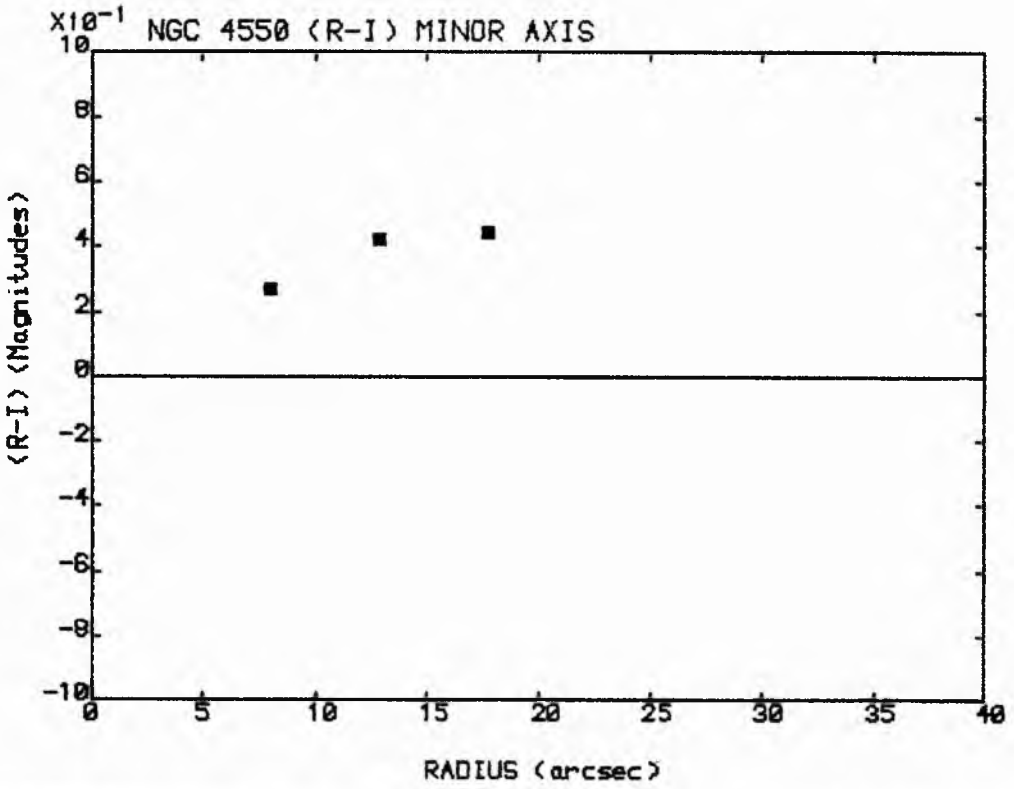
X10⁻¹
NGC 4550 (R-I) MINOR AXIS
(R-I) (Magnitudes)
10
8
6
4
2
0
-2
-4
-6
-8
-10
0
5
10
15
20
25
30
35
40
RADIUS (arcsec)

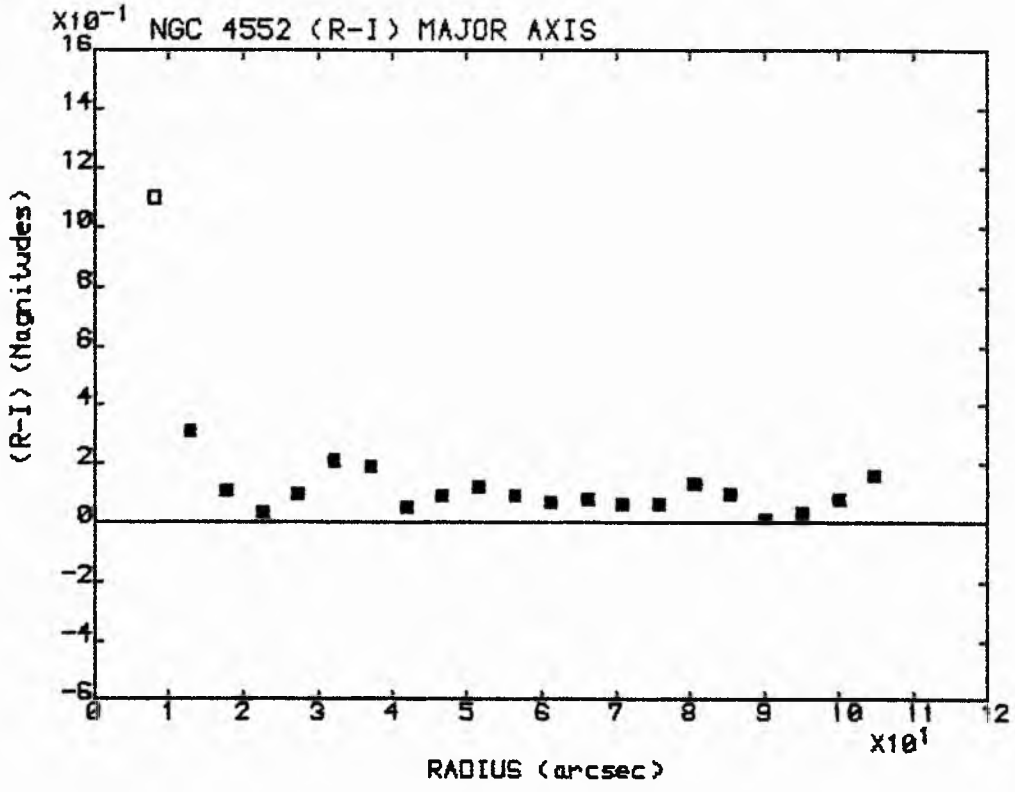
X10⁻¹
NGC 4552 (R-I) MAJOR AXIS
(R-I) (Magnitudes)
16
14
12
10
8
6
4
2
0
-2
-4
-6
0 1 2 3 4 5 6 7 8 9 10 11 12
X10¹
RADIUS (arcsec)

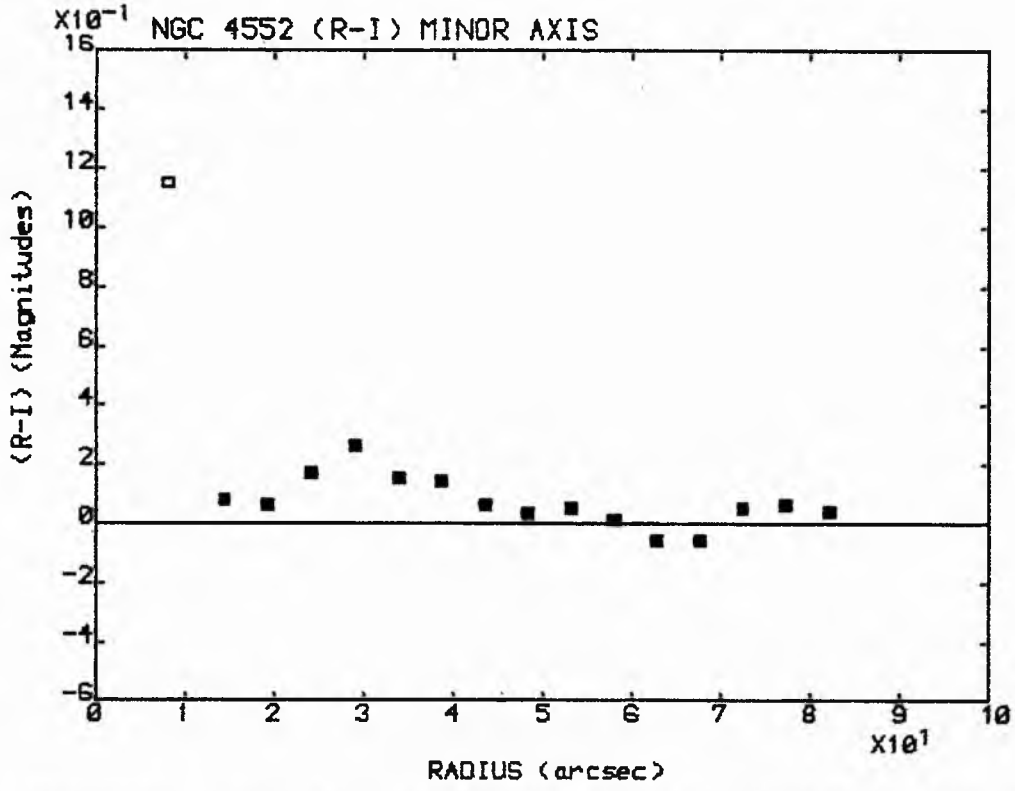
X10⁻¹
NGC 4552 (R-I) MINOR AXIS
(R-I) (Magnitudes)
16
14
12
10
8
6
4
2
0
-2
-4
-6
0 1 2 3 4 5 6 7 8 9 10
X10¹
RADIUS (arcsec)

APPENDIX 'C'

Graphical Evaluation of B and I-Band Data

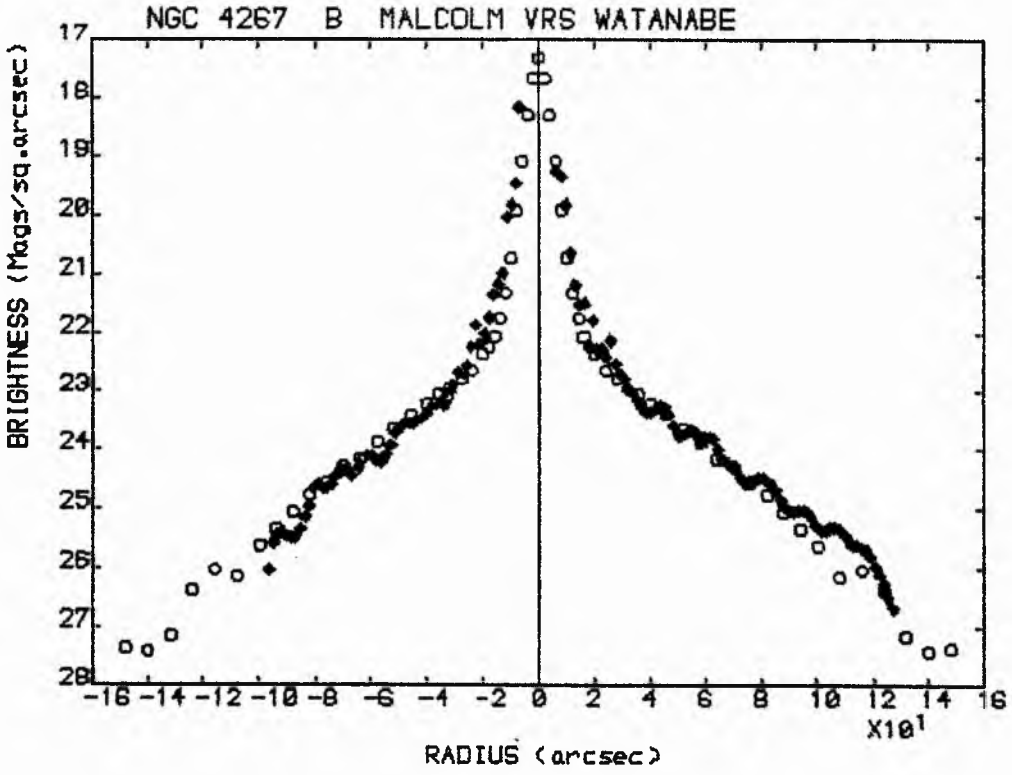
NGC 4267 B MALCOLM VRS WATANABE
BRIGHTNESS (Mags/sq.arcsec)
17
18
19
20
21
22
23
24
25
26
27
28
-16 -14 -12 -10 -8 -6 -4 -2 0 2 4 6 8 10 12 14 16
X10¹
RADIUS (arcsec)

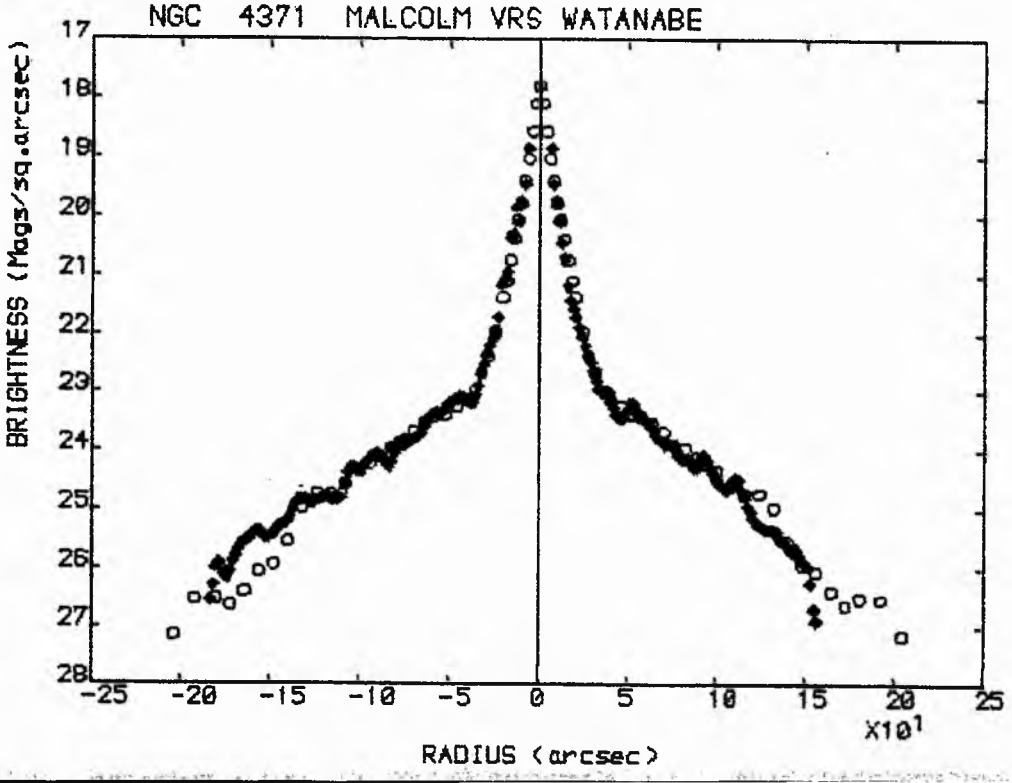
NGC 4371 MALCOLM VRS WATANABE
BRIGHTNESS (Mags/sq.arcsec)
17
18
19
20
21
22
23
24
25
26
27
28
-25 -20 -15 -10 -5 0 5 10 15 20 25
X10¹
RADIUS (arcsec)

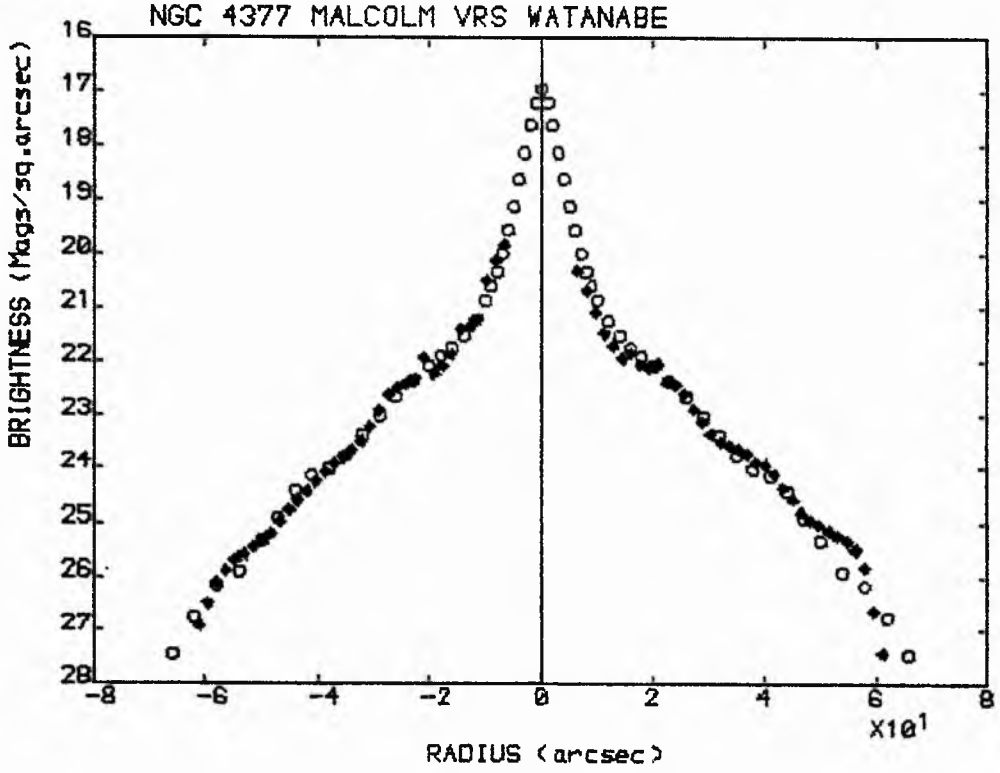
NGC 4377 MALCOLM VRS WATANABE
BRIGHTNESS (Mags/sq.arcsec)
16
17
18
19
20
21
22
23
24
25
26
27
28
-8
-6
-4
-2
0
2
4
6
8
X10¹
RADIUS (arcsec)

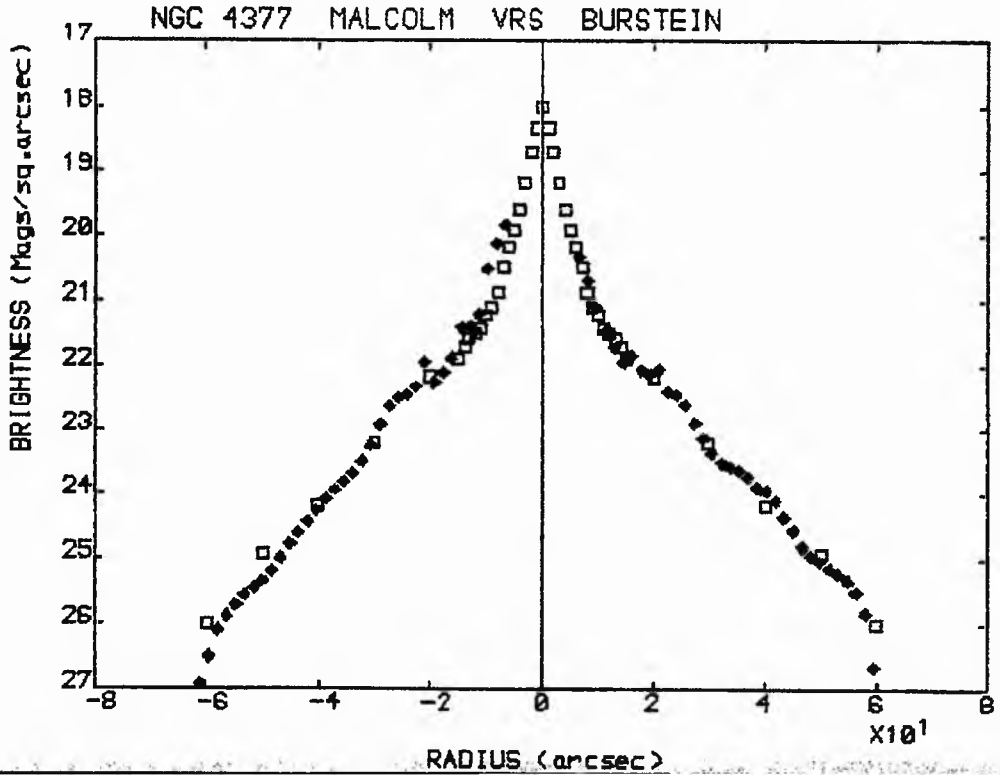
NGC 4377 MALCOLM VRS BURSTEIN
BRIGHTNESS (Mags/sq.arcsec)
17
18
19
20
21
22
23
24
25
26
27
-8
-6
-4
-2
0
2
4
6
8
X10¹
RADIUS (arcsec)

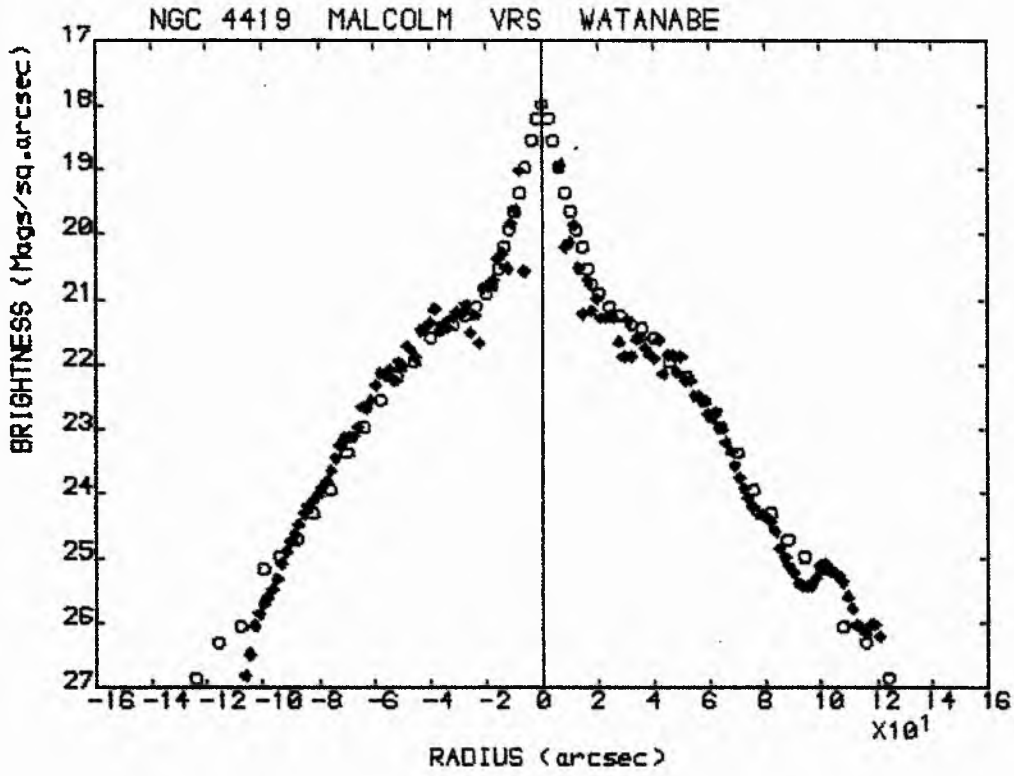
NGC 4419 MALCOLM VRS WATANABE
BRIGHTNESS (Mags/sq.arcsec)
17
18
19
20
21
22
23
24
25
26
27
-16 -14 -12 -10 -8 -6 -4 -2 0 2 4 6 8 10 12 14 16
X10¹
RADIUS (arcsec)

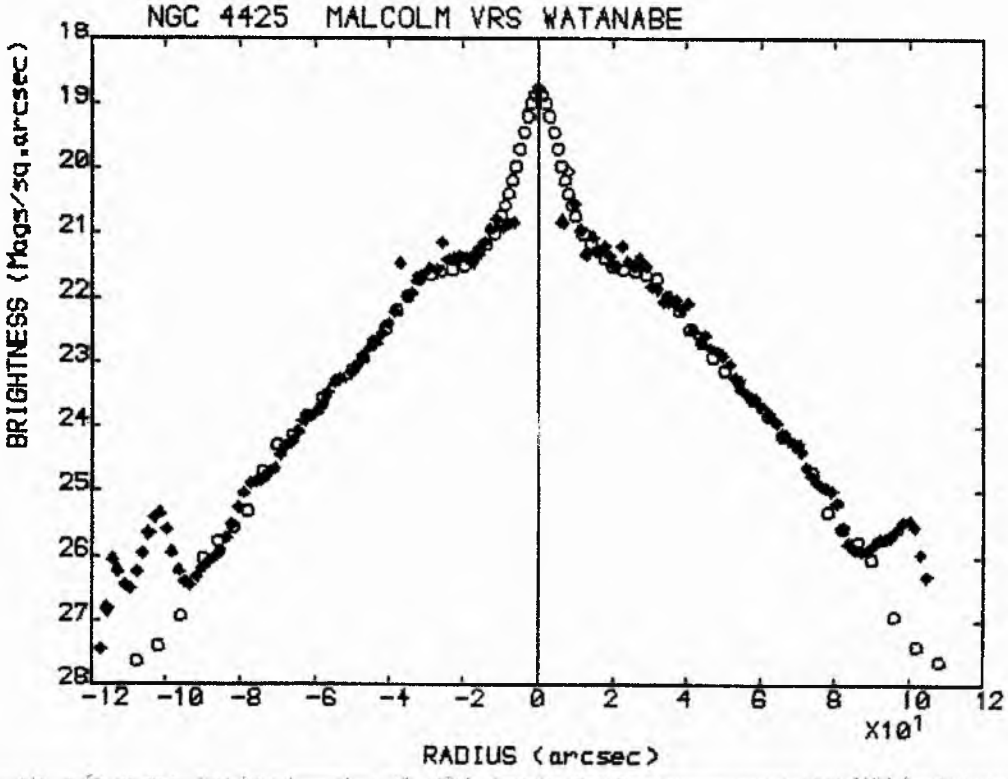
NGC 4425 MALCOLM VRS WATANABE
BRIGHTNESS (Mags/sq.arcsec)
18
19
20
21
22
23
24
25
26
27
28
-12 -10 -8 -6 -4 -2 0 2 4 6 8 10 12
X10¹
RADIUS (arcsec)

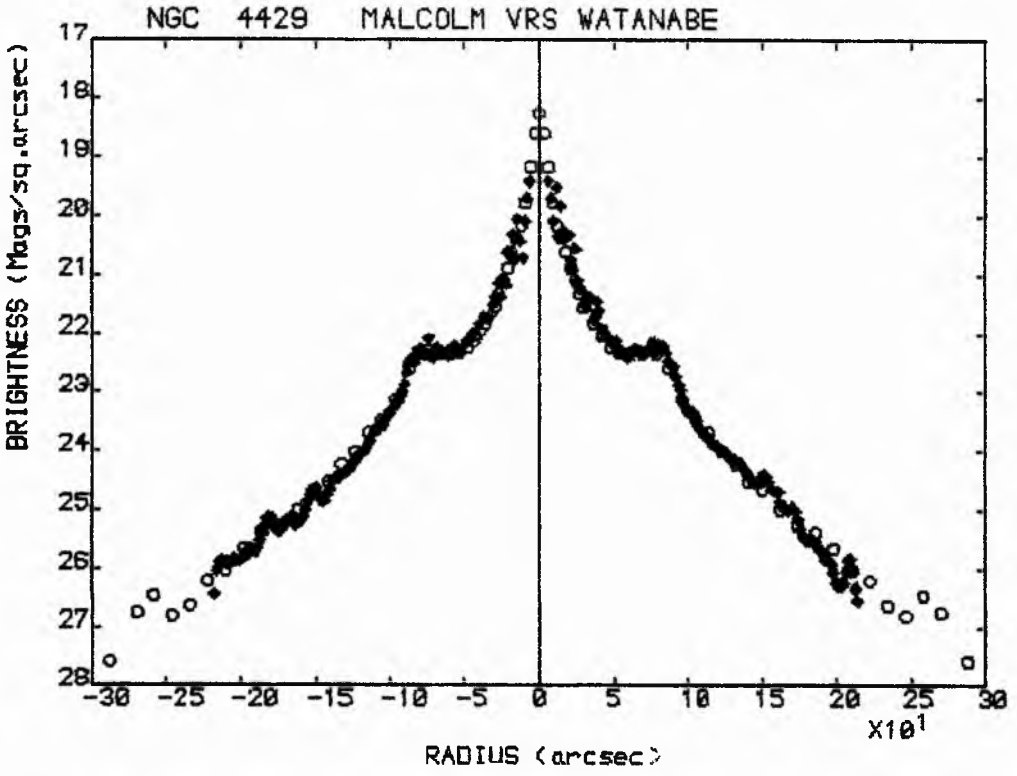
NGC 4429 MALCOLM VRS WATANABE
BRIGHTNESS (Mags/sq.arcsec)
17
18
19
20
21
22
23
24
25
26
27
28
-30 -25 -20 -15 -10 -5 0 5 10 15 20 25 30
X10¹
RADIUS (arcsec)

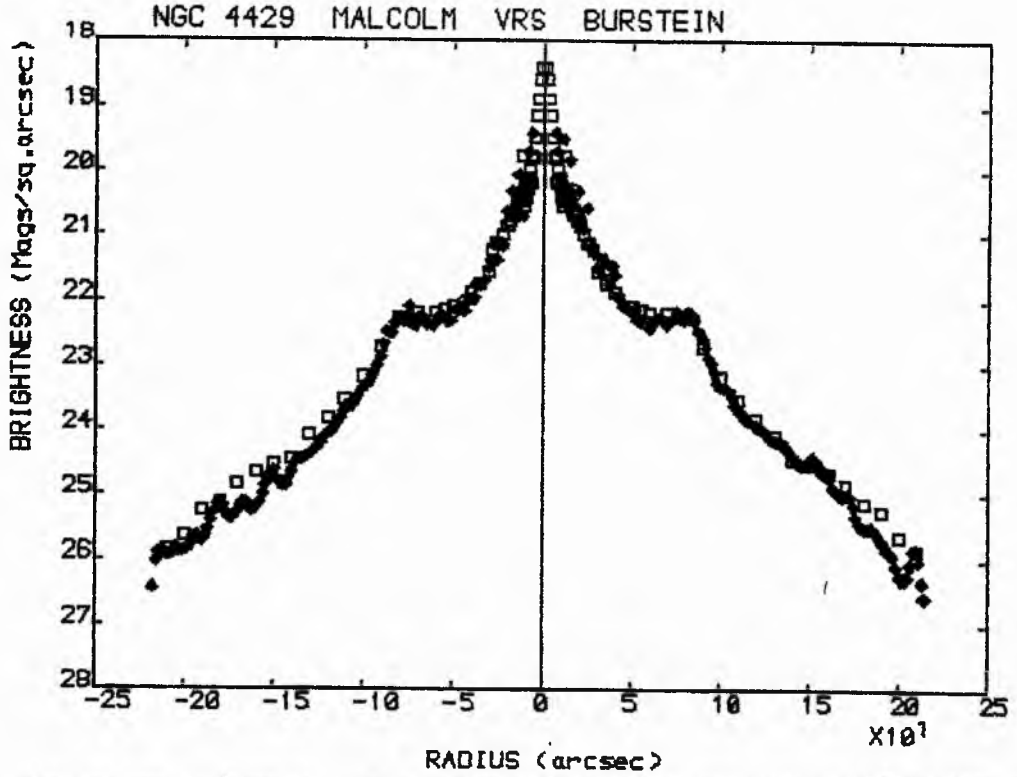
NGC 4429 MALCOLM VRS BURSTEIN
BRIGHTNESS (Mags/sq.arcsec)
18
19
20
21
22
23
24
25
26
27
28
-25 -20 -15 -10 -5 0 5 10 15 20 25
X10¹
RADIUS (arcsec)

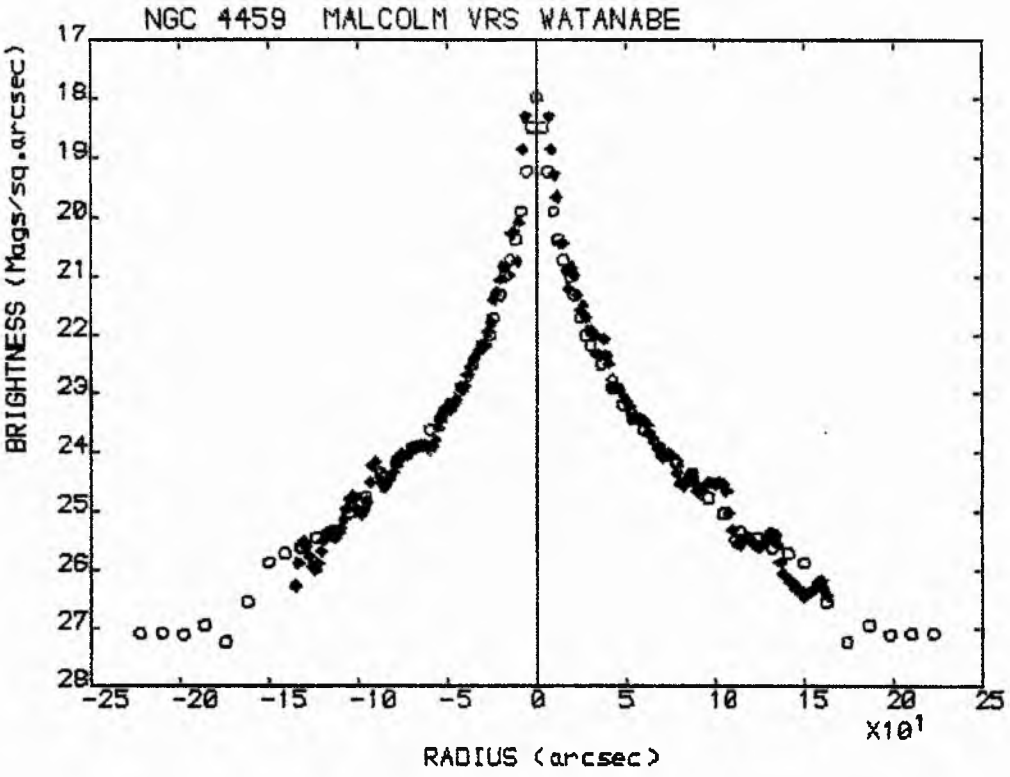
NGC 4459 MALCOLM VRS WATANABE
BRIGHTNESS (Mags/sq.arcsec)
17
18
19
20
21
22
23
24
25
26
27
28
-25 -20 -15 -10 -5 0 5 10 15 20 25
X10¹
RADIUS (arcsec)

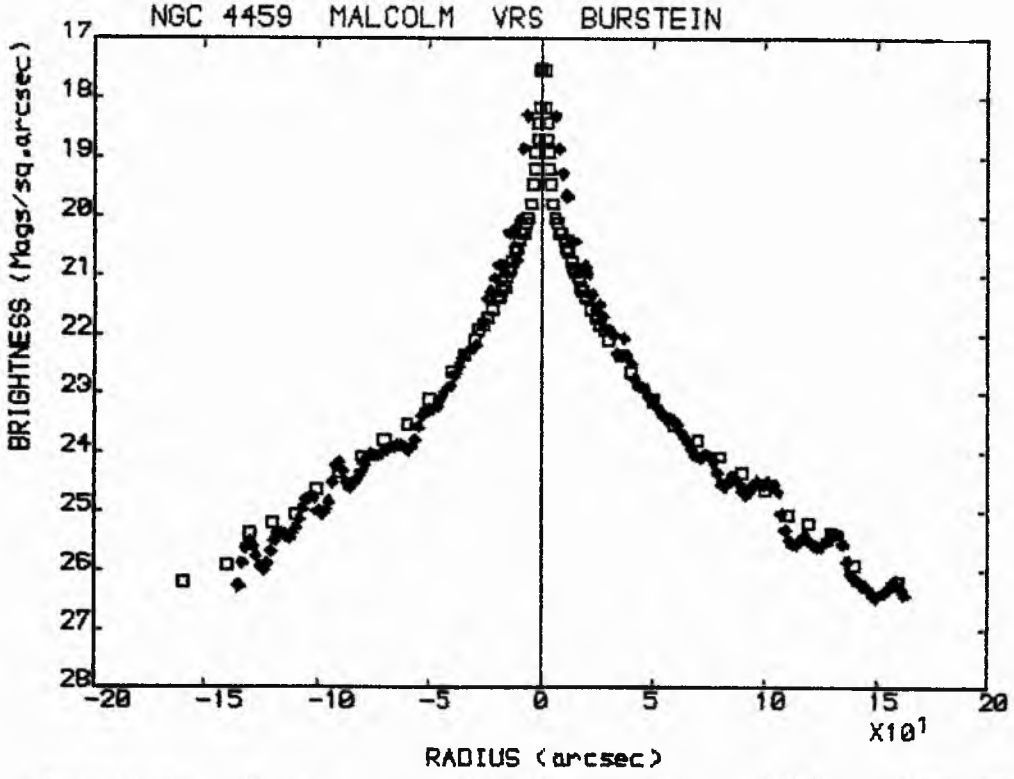
NGC 4459 MALCOLM VRS BURSTEIN
BRIGHTNESS (Mags/sq.arcsec)
17
18
19
20
21
22
23
24
25
26
27
28
-20 -15 -10 -5 0 5 10 15 20
X10¹
RADIUS (arcsec)

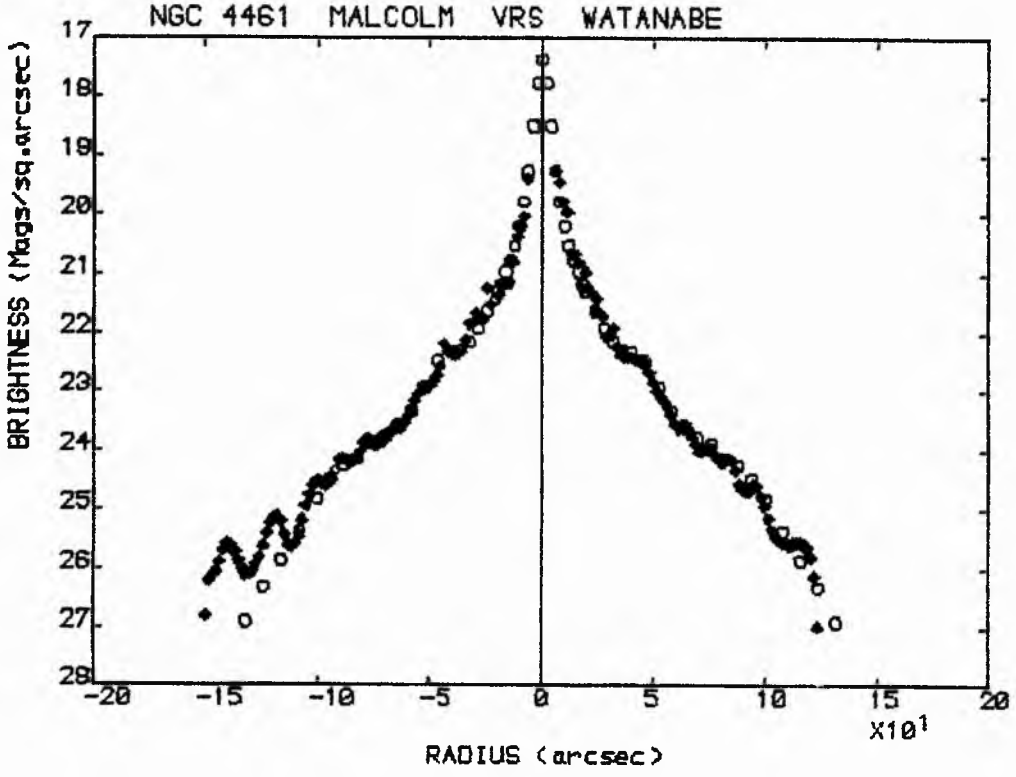
NGC 4461 MALCOLM VRS WATANABE
BRIGHTNESS (Mags/sq.arcsec)
17
18
19
20
21
22
23
24
25
26
27
28
-20
-15
-10
-5
0
5
10
15
20
X10¹
RADIUS (arcsec)

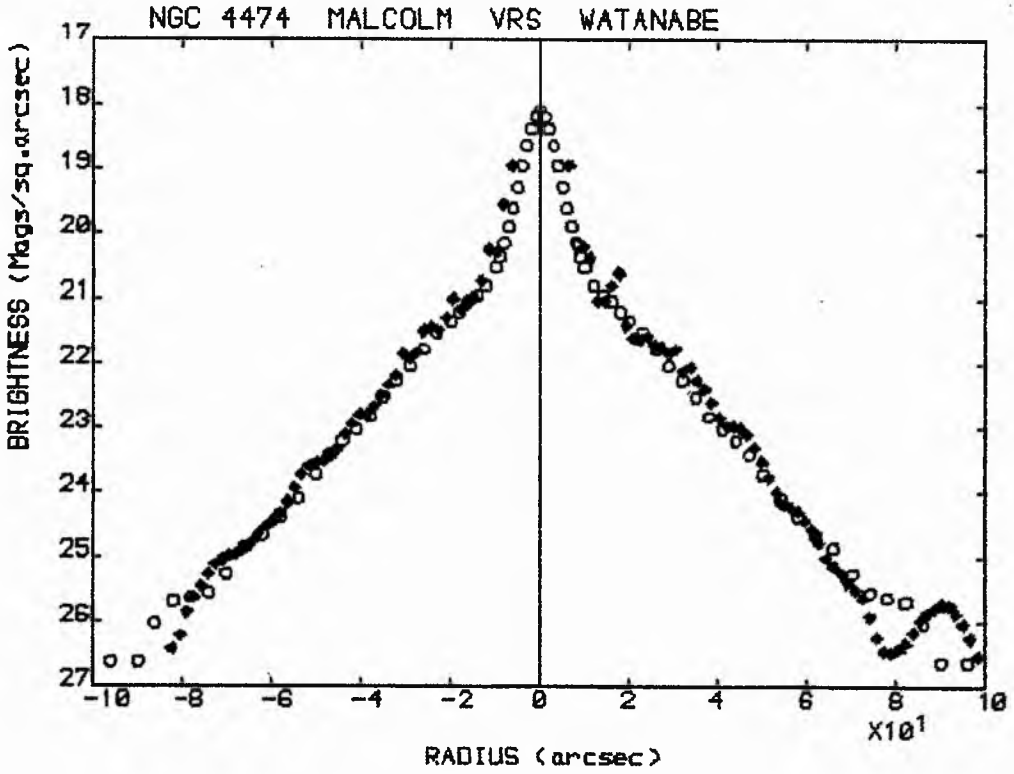
NGC 4474 MALCOLM VRS WATANABE
BRIGHTNESS (Mags/sq.arcsec)
17
18
19
20
21
22
23
24
25
26
27
-10 -8 -6 -4 -2 0 2 4 6 8 10
X10¹
RADIUS (arcsec)

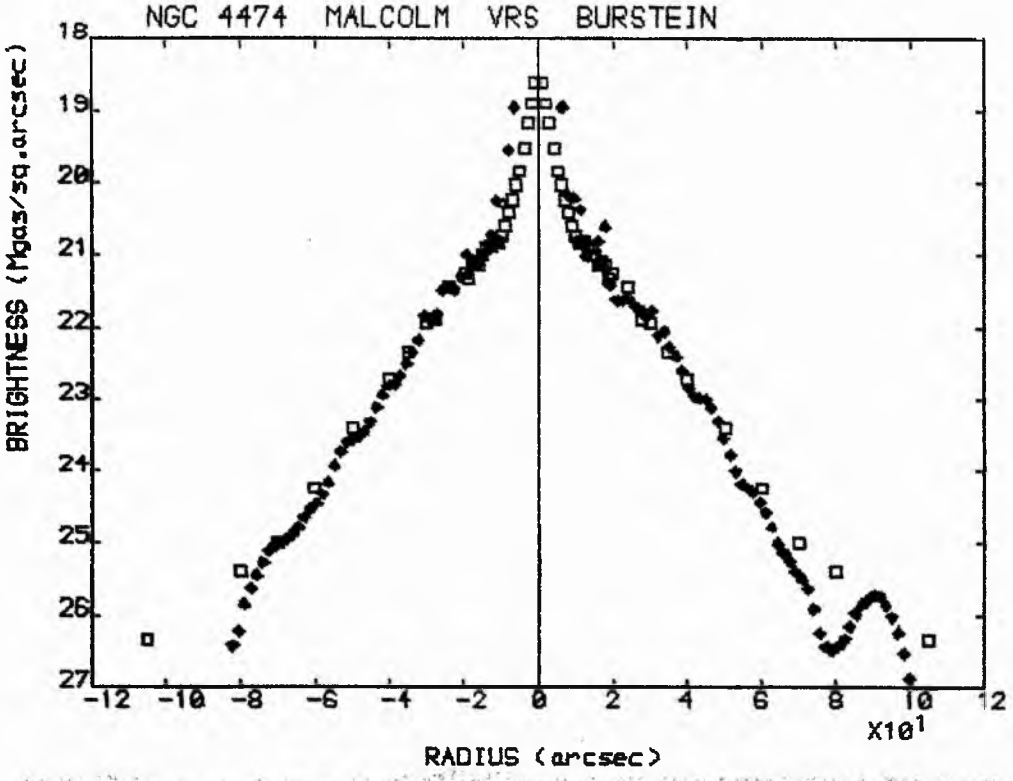
NGC 4474 MALCOLM VRS BURSTEIN
BRIGHTNESS (Mags/sq.arcsec)
18
19
20
21
22
23
24
25
26
27
-12 -10 -8 -6 -4 -2 0 2 4 6 8 10 12
X10¹
RADIUS (arcsec)

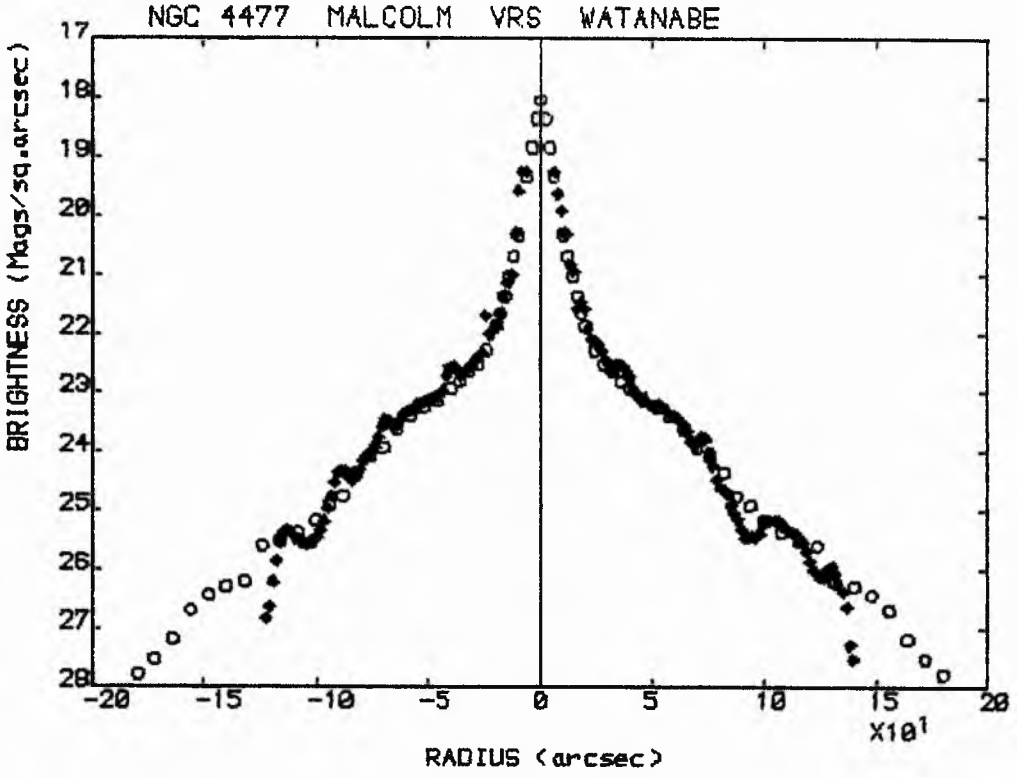
NGC 4477 MALCOLM VRS WATANABE
BRIGHTNESS (Mags/sq.arcsec)
17
18
19
20
21
22
23
24
25
26
27
28
-20
-15
-10
-5
0
5
10
15
20
X10¹
RADIUS (arcsec)

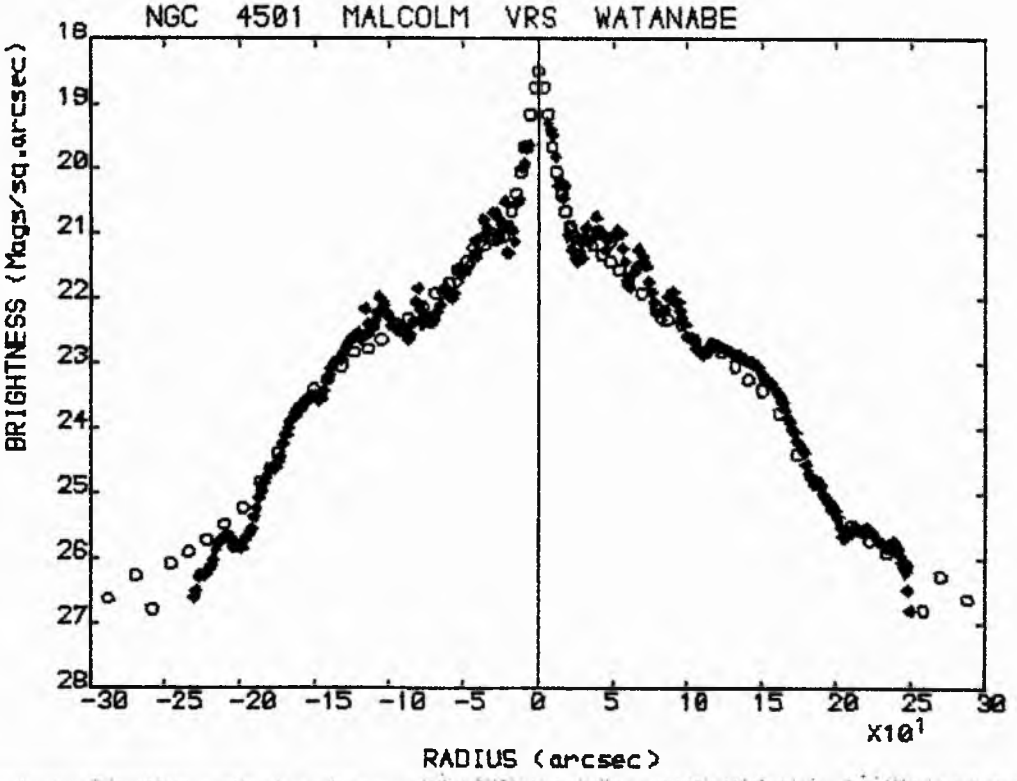
NGC 4501 MALCOLM VRS WATANABE
BRIGHTNESS (Mags/sq.arcsec)
18
19
20
21
22
23
24
25
26
27
28
-30
-25
-20
-15
-10
-5
0
5
10
15
20
25
30
X10¹
RADIUS (arcsec)

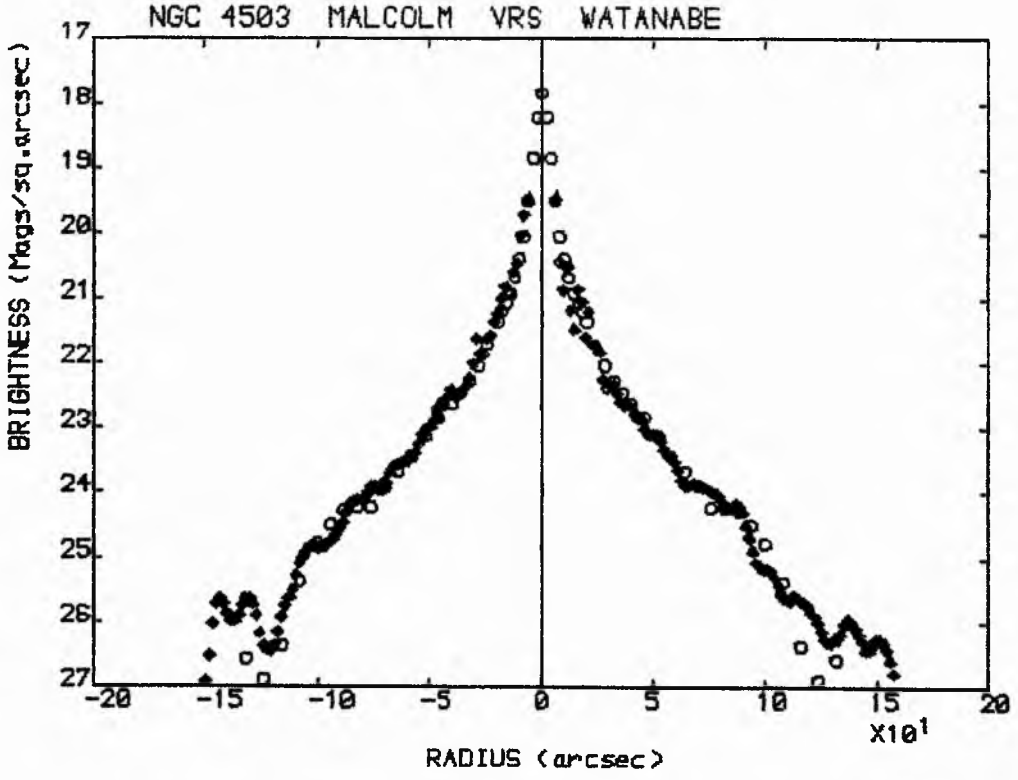
NGC 4503 MALCOLM VRS WATANABE
BRIGHTNESS (Mags/sq.arcsec)
17
18
19
20
21
22
23
24
25
26
27
-20
-15
-10
-5
0
5
10
15
20
X10¹
RADIUS (arcsec)

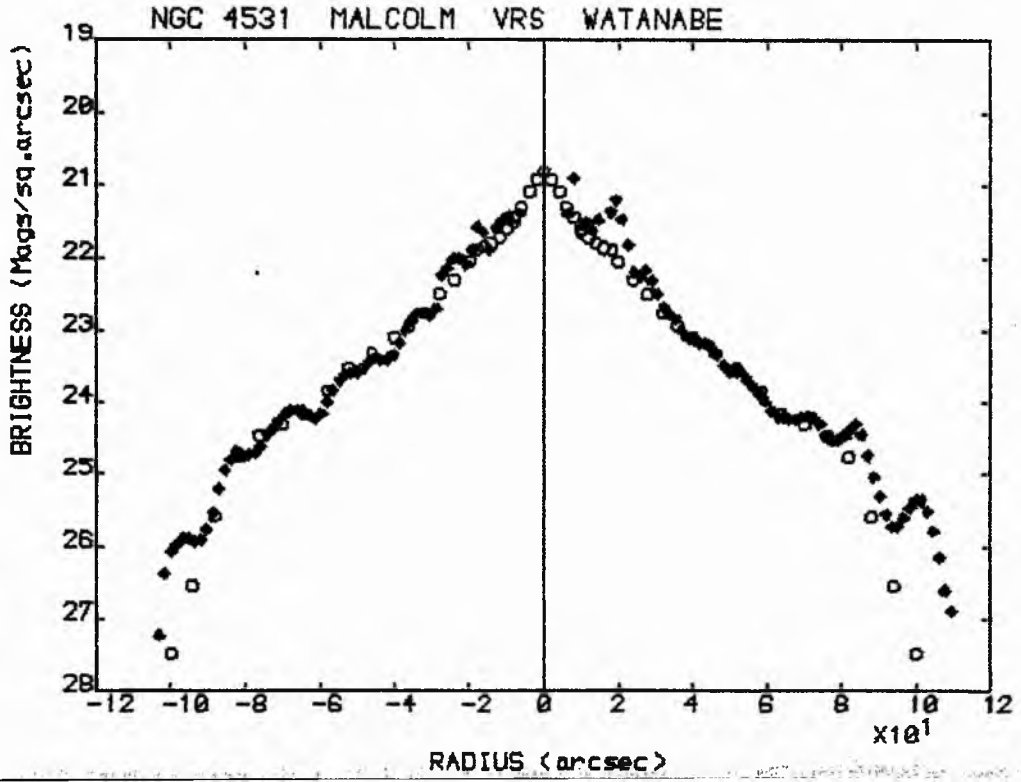
NGC 4531 MALCOLM VRS WATANABE
BRIGHTNESS (Mags/sq.arcsec)
19
20
21
22
23
24
25
26
27
28
-12
-10
-8
-6
-4
-2
0
2
4
6
8
10
12
X10¹
RADIUS (arcsec)

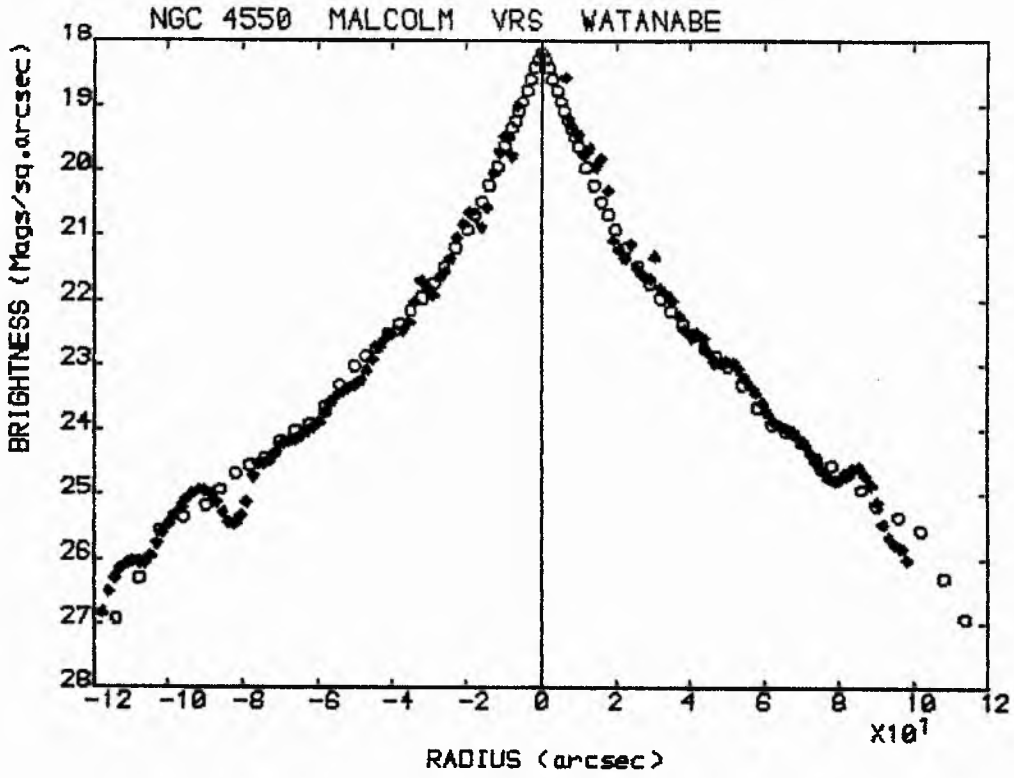
NGC 4550 MALCOLM VRS WATANABE
BRIGHTNESS (Mags/sq.arcsec)
18
19
20
21
22
23
24
25
26
27
28
-12 -10 -8 -6 -4 -2 0 2 4 6 8 10 12
X10¹
RADIUS (arcsec)

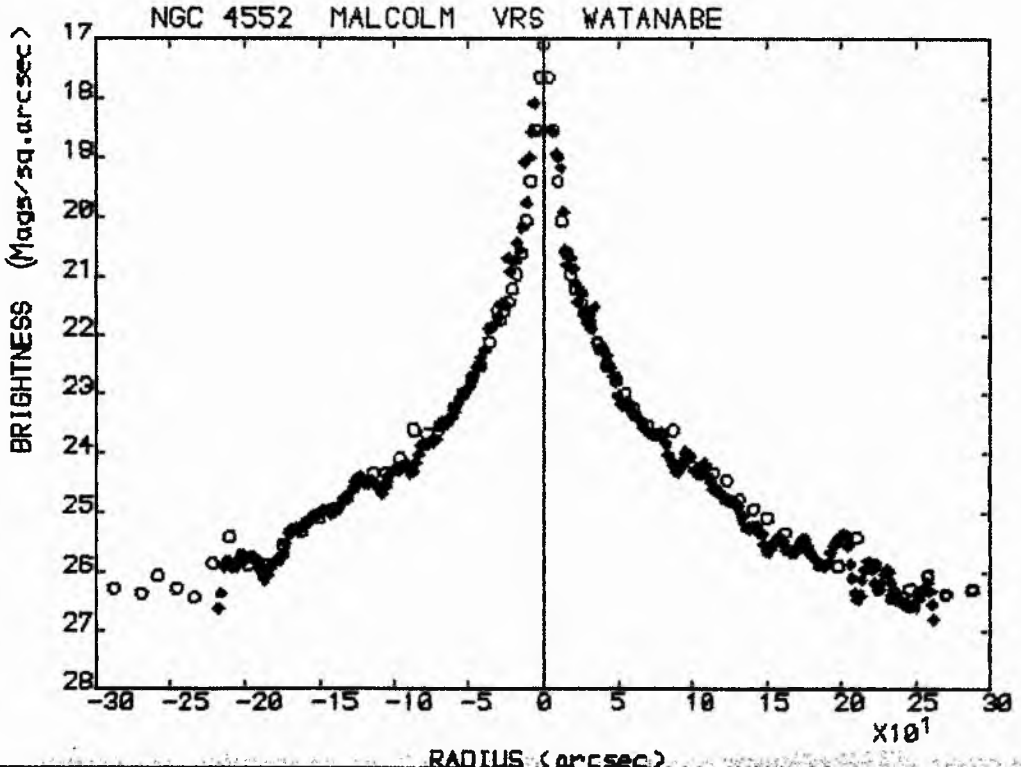
NGC 4552 MALCOLM VRS WATANABE
BRIGHTNESS (Mags/sq.arcsec)
17
18
19
20
21
22
23
24
25
26
27
28
-30 -25 -20 -15 -10 -5 0 5 10 15 20 25 30
X10¹
RADIUS (arcsec)

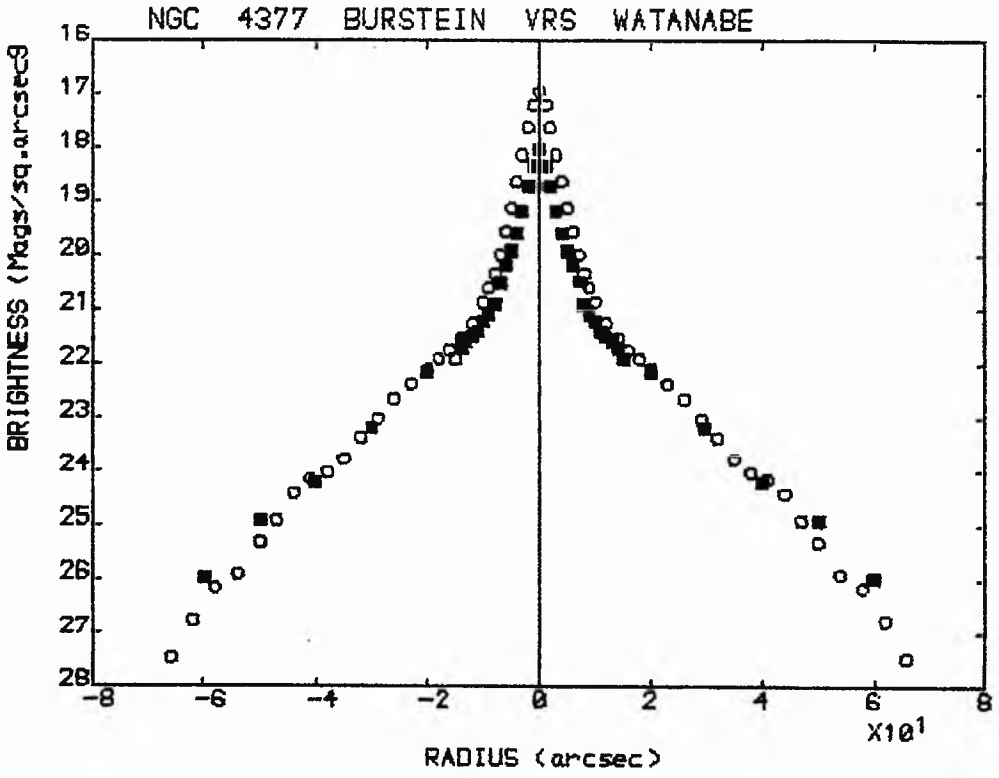
NGC 4377 BURSTEIN VRS WATANABE
BRIGHTNESS (Mags/sq.arcsec)
16
17
18
19
20
21
22
23
24
25
26
27
28
-8
-6
-4
-2
0
2
4
6
8
X10¹
RADIUS (arcsec)

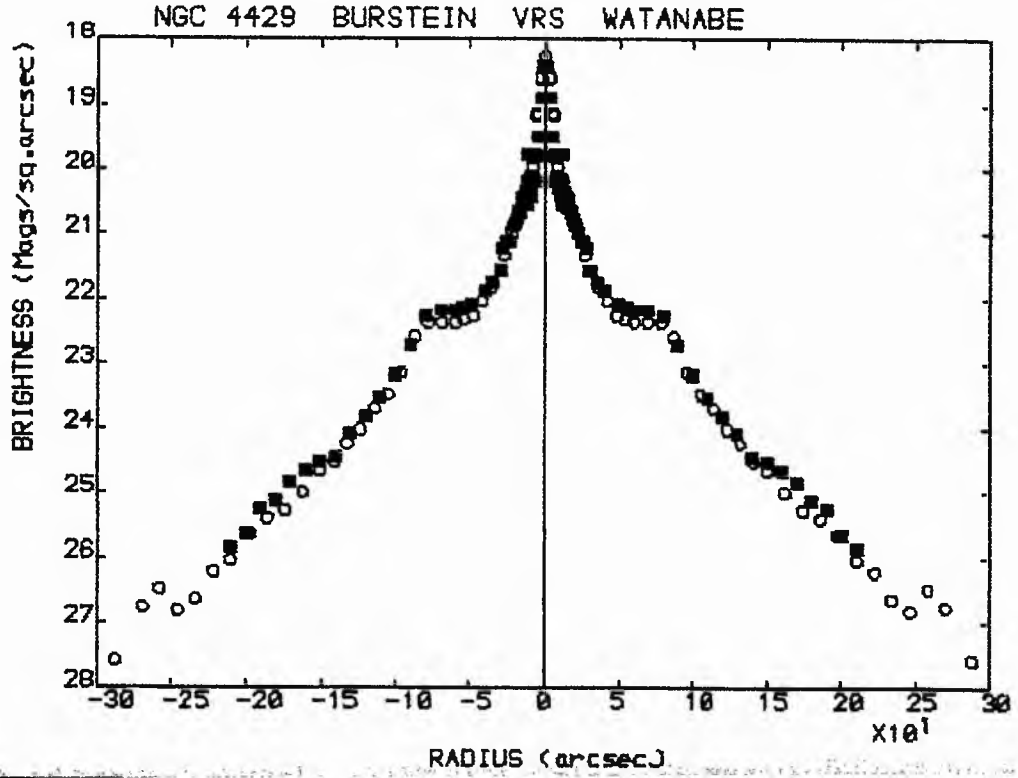
NGC 4429 BURSTEIN VRS WATANABE
BRIGHTNESS (Mags/sq.arcsec)
18
19
20
21
22
23
24
25
26
27
28
-30
-25
-20
-15
-10
-5
0
5
10
15
20
25
30
X10¹
RADIUS (arcsec)

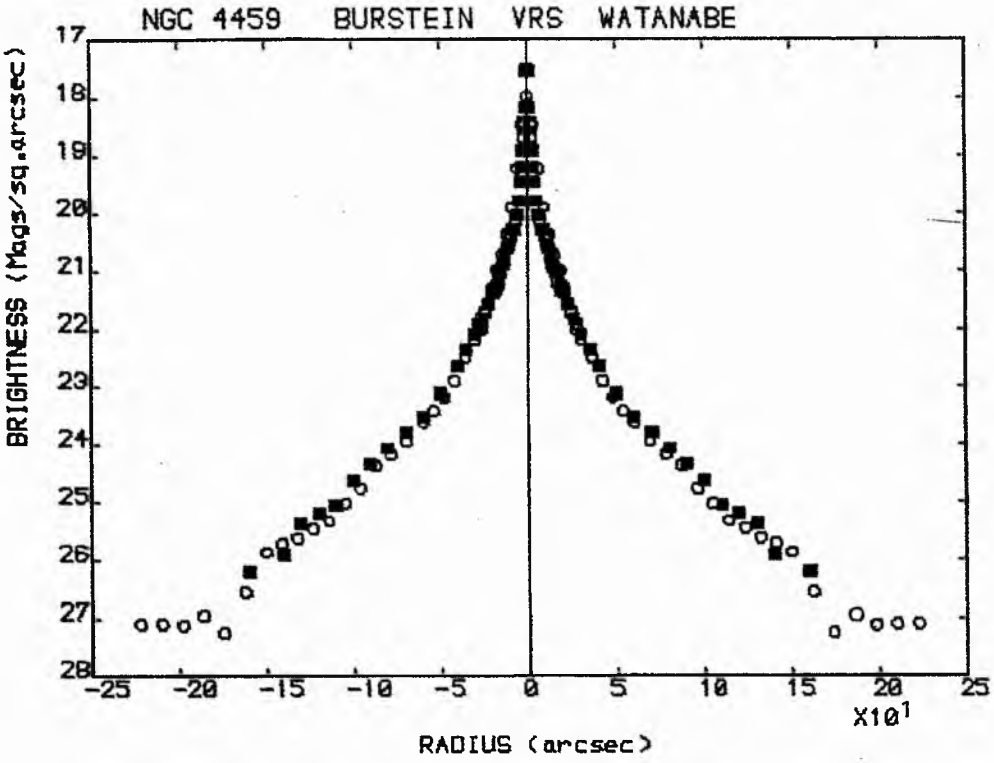
NGC 4459 BURSTEIN VRS WATANABE
BRIGHTNESS (Mags/sq.arcsec)
17
18
19
20
21
22
23
24
25
26
27
28
-25 -20 -15 -10 -5 0 5 10 15 20 25
X10¹
RADIUS (arcsec)

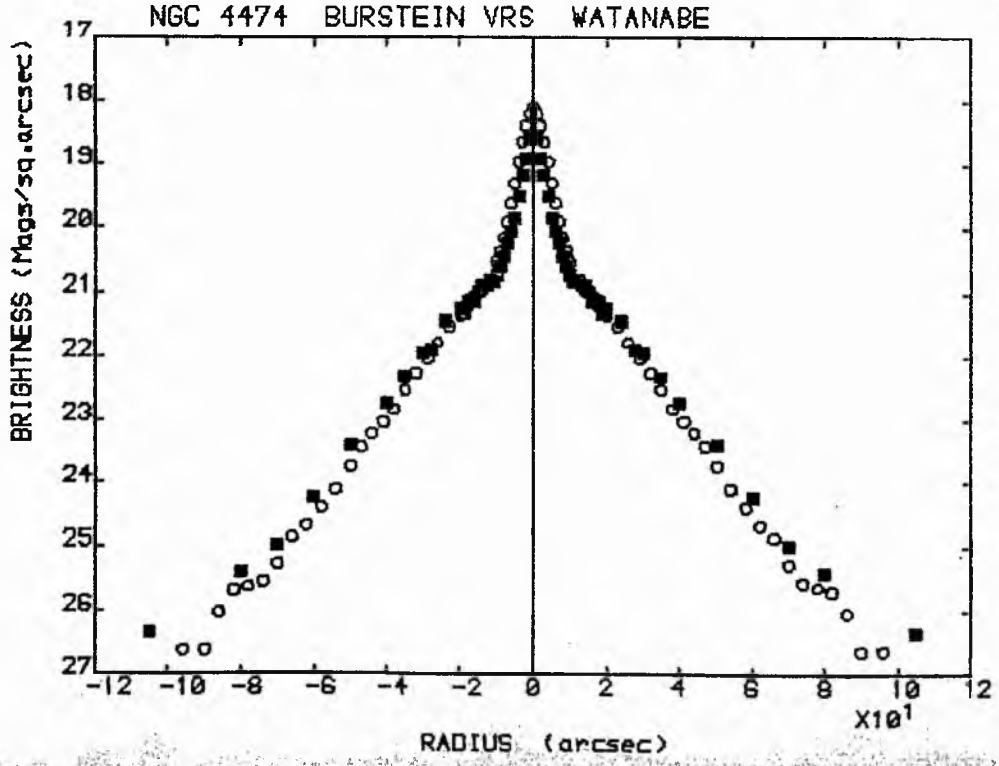
NGC 4474 BURSTEIN VRS WATANABE
BRIGHTNESS (Mags/sq.arcsec)
17
18
19
20
21
22
23
24
25
26
27
-12 -10 -8 -6 -4 -2 0 2 4 6 8 10 12
X10¹
RADIUS (arcsec)

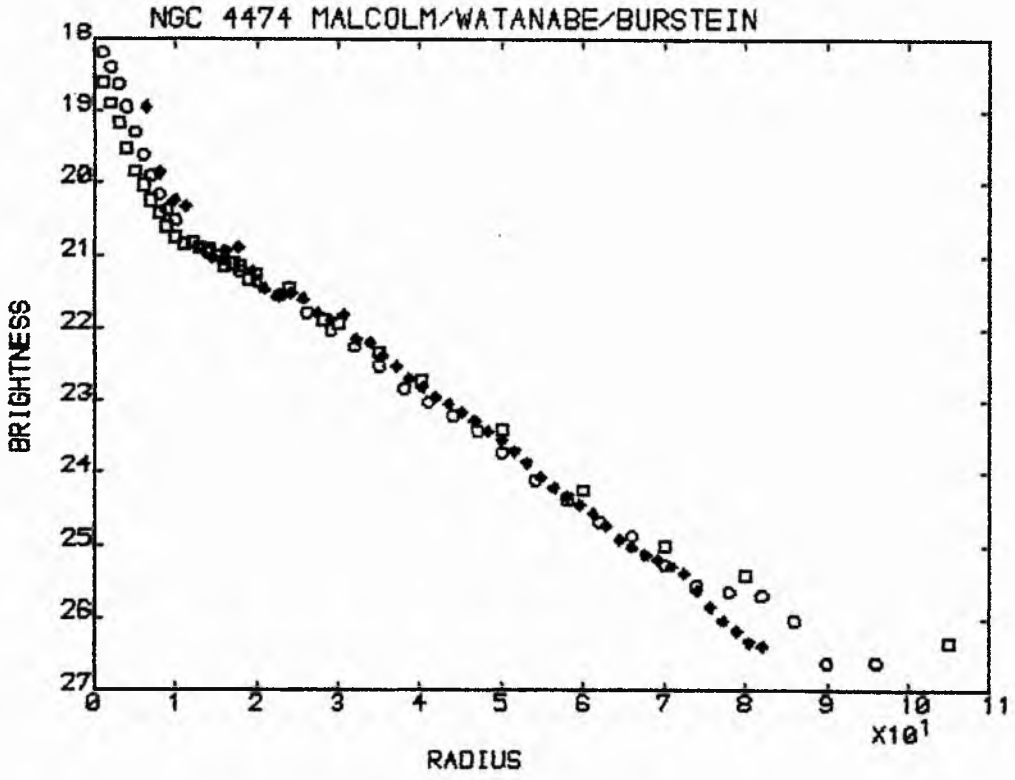
NGC 4474 MALCOLM/WATANABE/BURSTEIN
BRIGHTNESS
18
19
20
21
22
23
24
25
26
27
0
1
2
3
4
5
6
7
8
9
10
11
X10¹
RADIUS

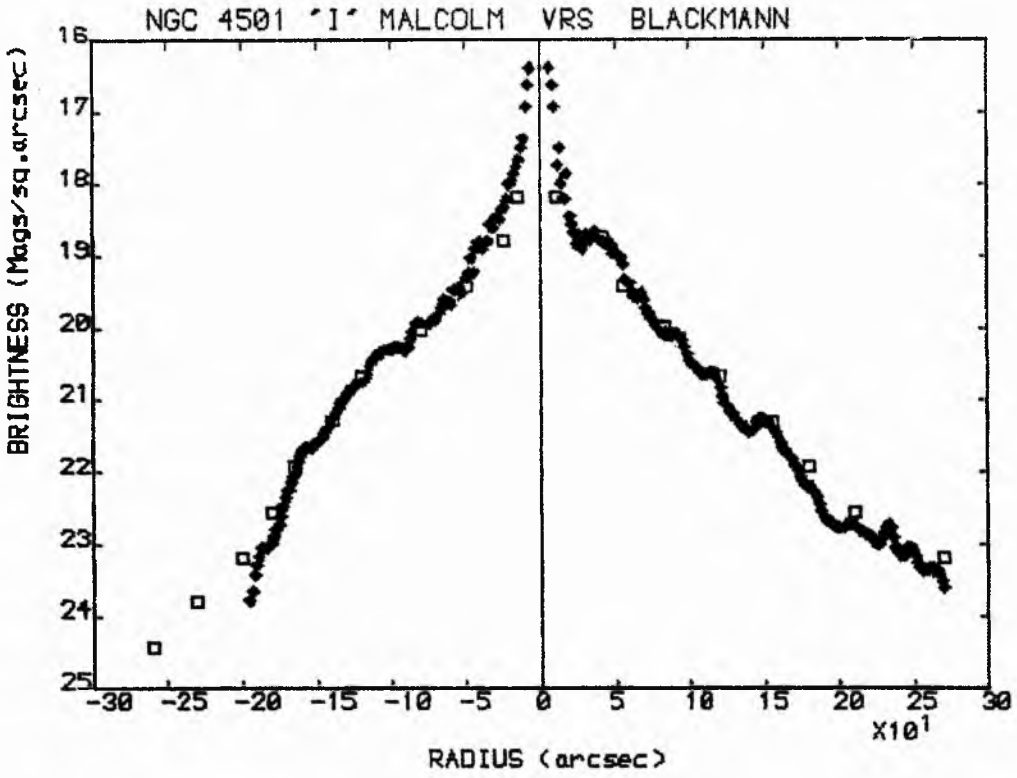
NGC 4501 'I' MALCOLM VRS BLACKMANN
BRIGHTNESS (Mags/sq.arcsec)
16
17
18
19
20
21
22
23
24
25
-30 -25 -20 -15 -10 -5 0 5 10 15 20 25 30
X10¹
RADIUS (arcsec)

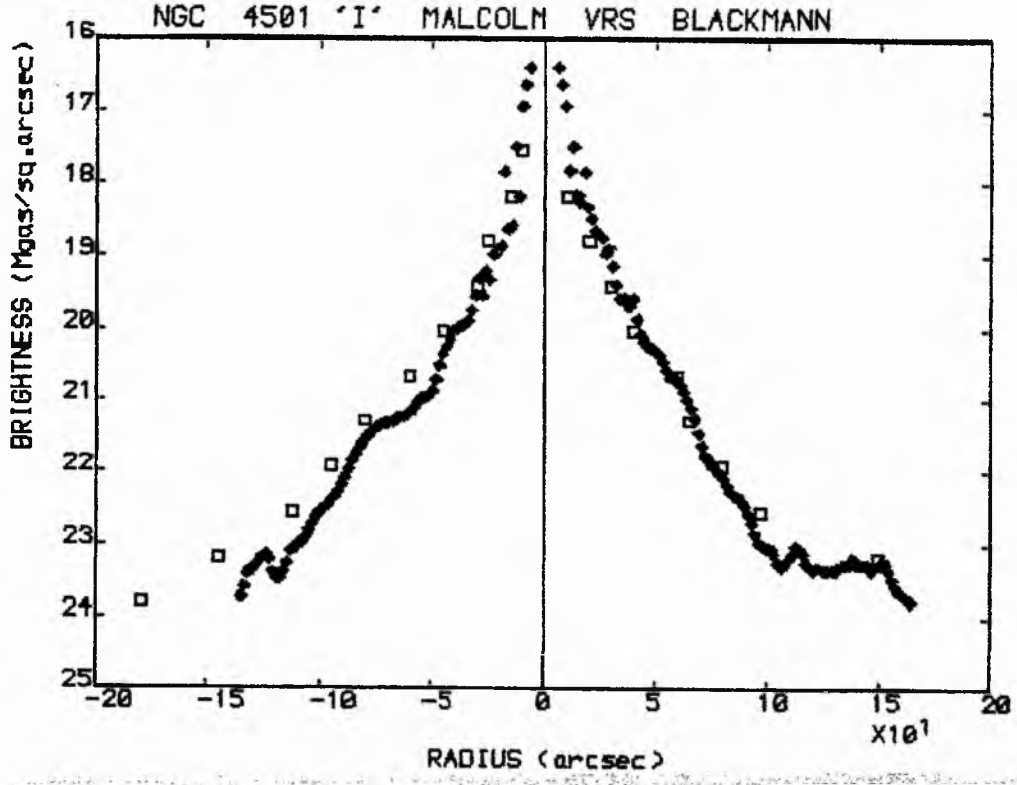
NGC 4501 'I' MALCOLM VRS BLACKMANN
BRIGHTNESS (Mags/sq.arcsec)
16
17
18
19
20
21
22
23
24
25
-20 -15 -10 -5 0 5 10 15 20
X10¹
RADIUS (arcsec)

NGC 4267 CJM vrs BSS

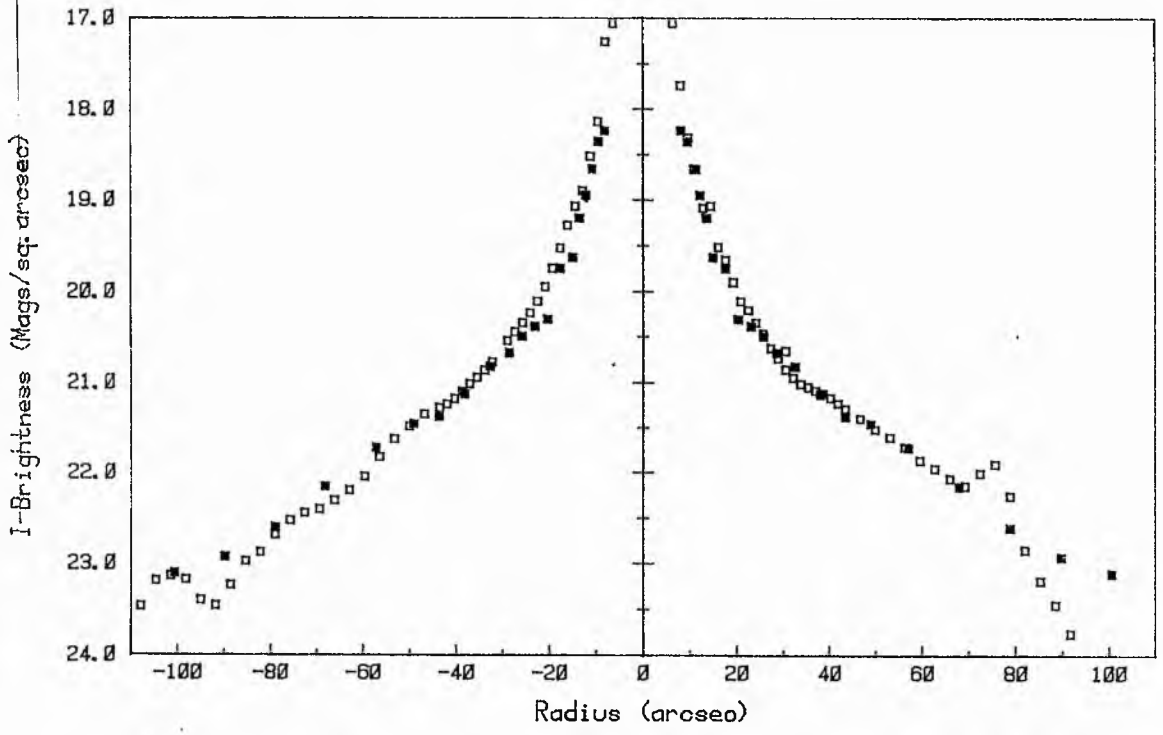

NGC 4419 CJM vrs BSS

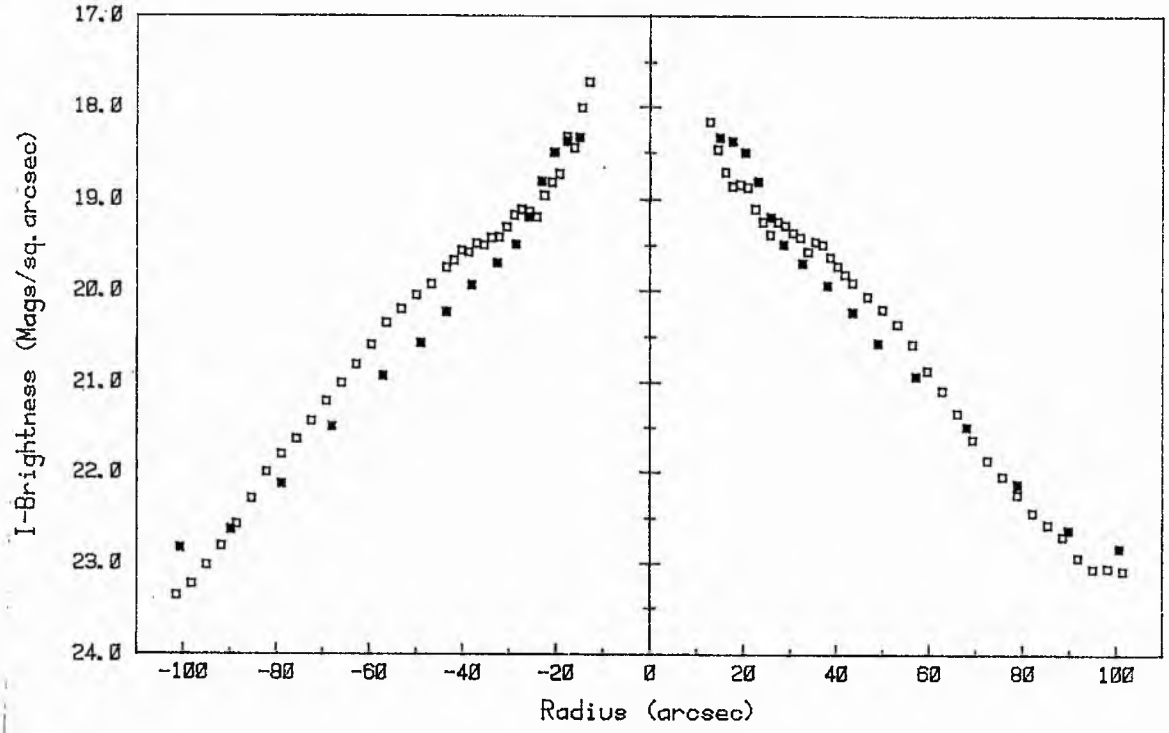

NGC 4425 GJM vrs BSS

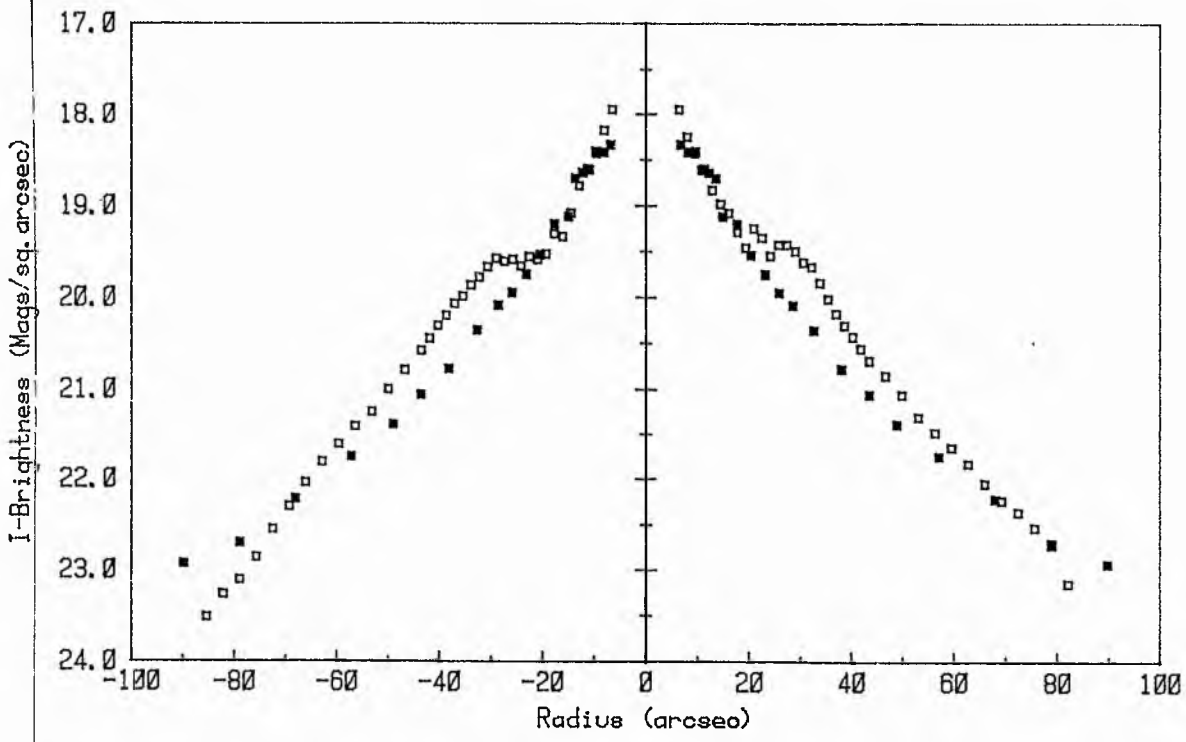

NGC 4429 GJM vrs BSS

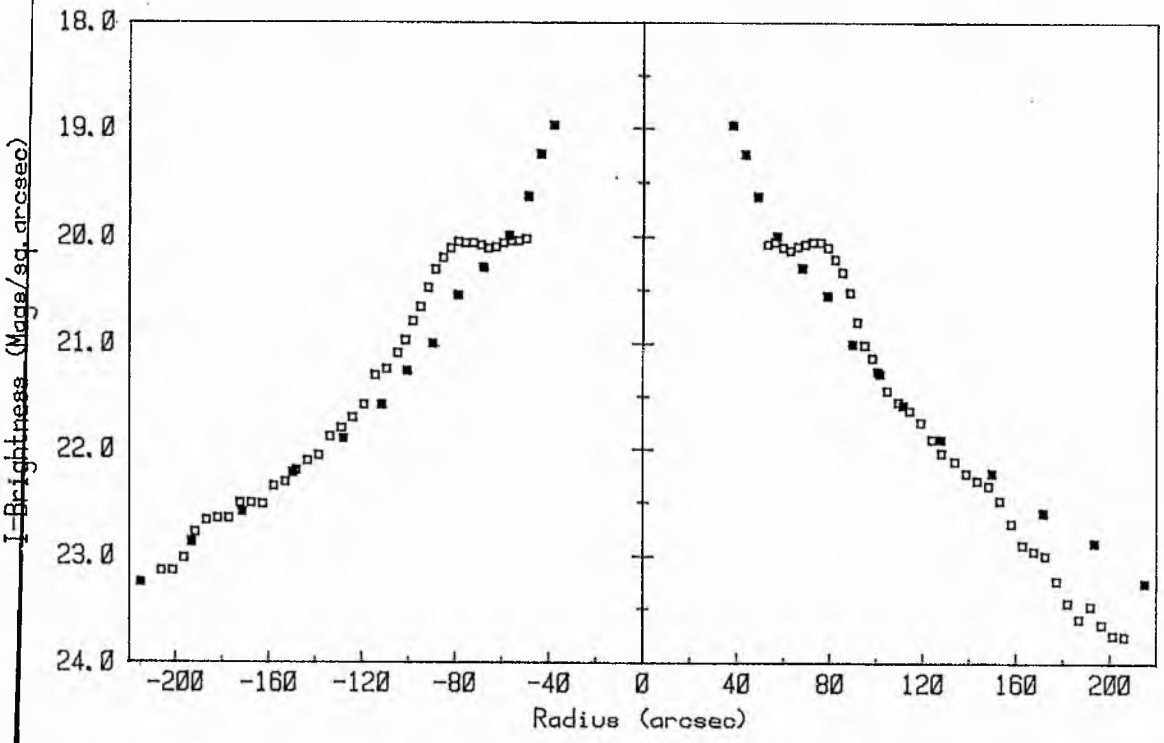

NGC 4435 GJM vrs BSS

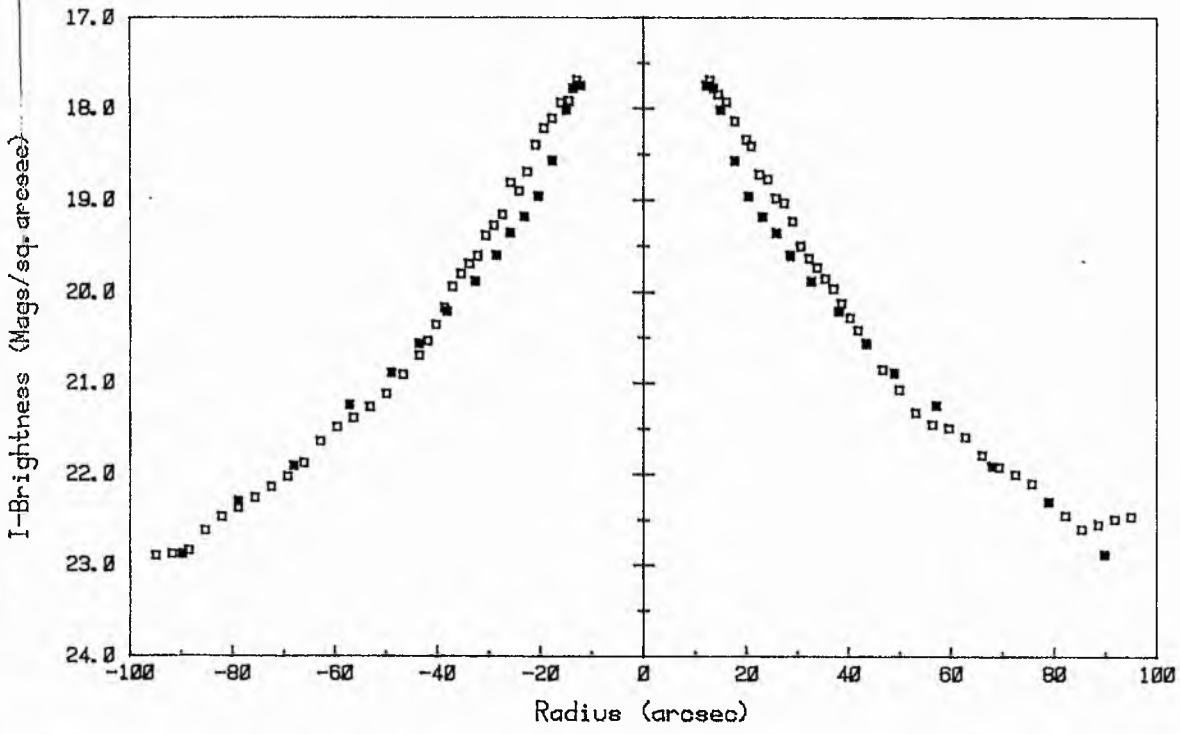

NGC 4459 GJM vrs BSS

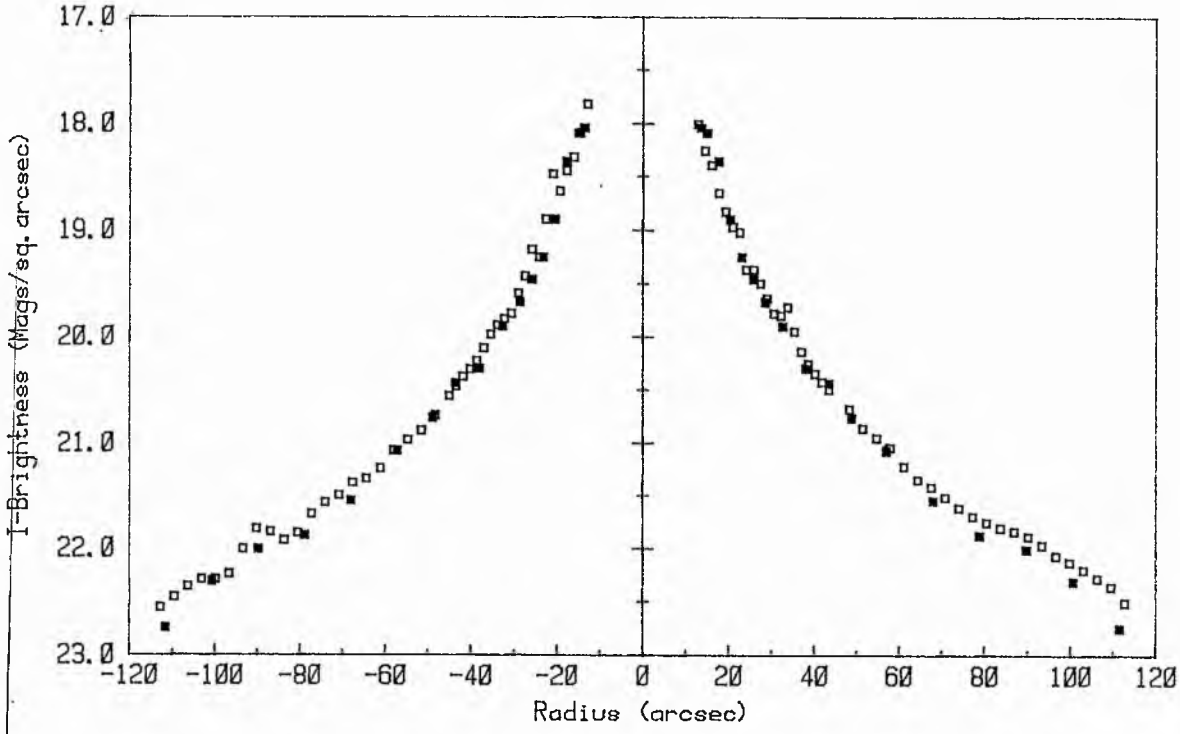

NGC 4474 GJM vrs BSS

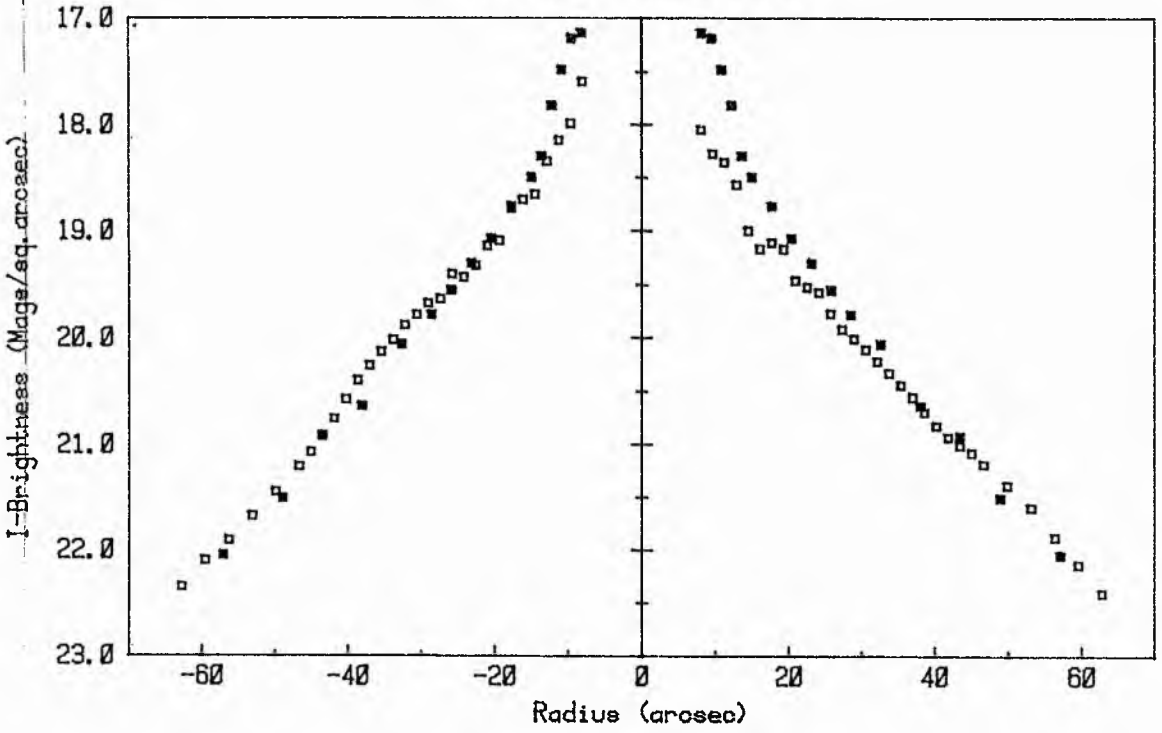

NGC 4461 GJM vrs BSS

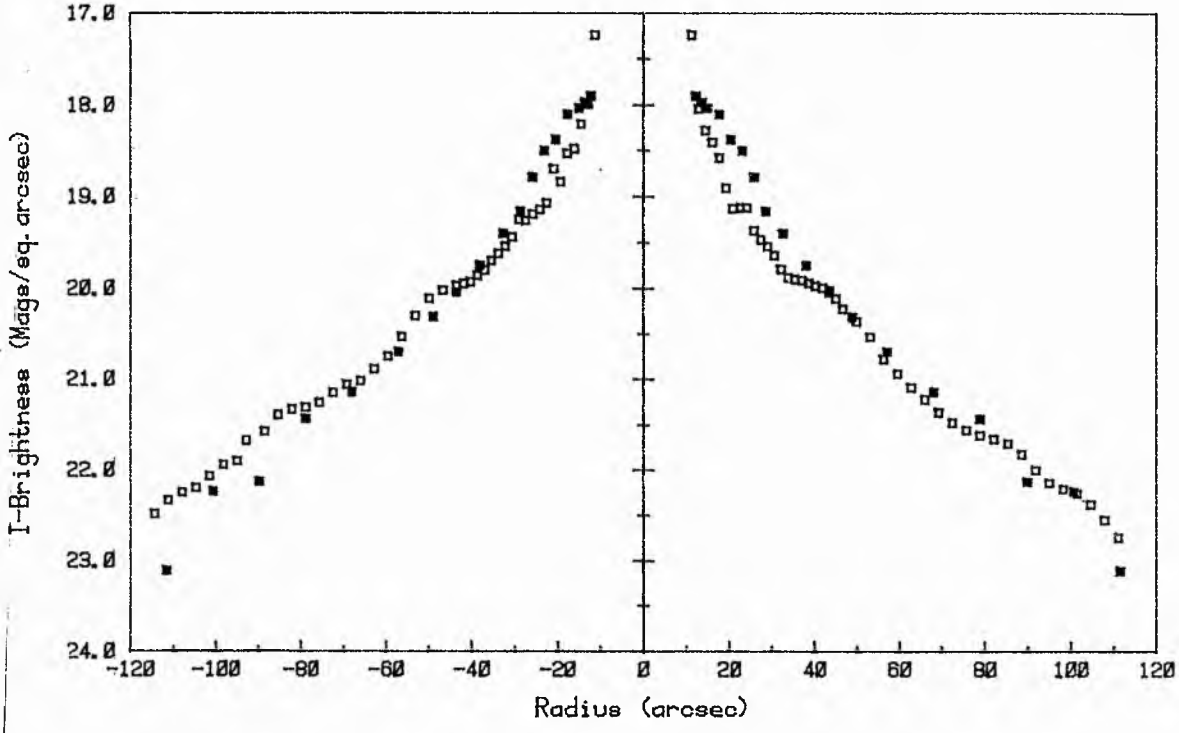

NGC 4477 GJM vrs BSS

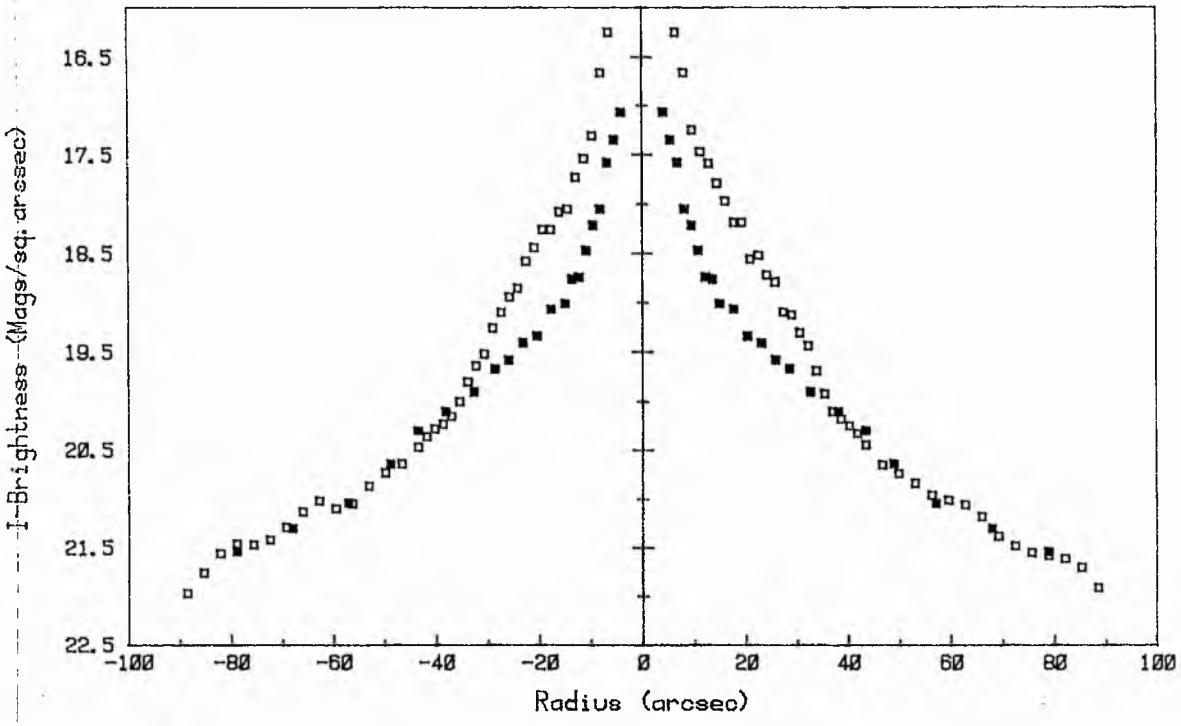

NGC 4477 WATANABE vrs BSS

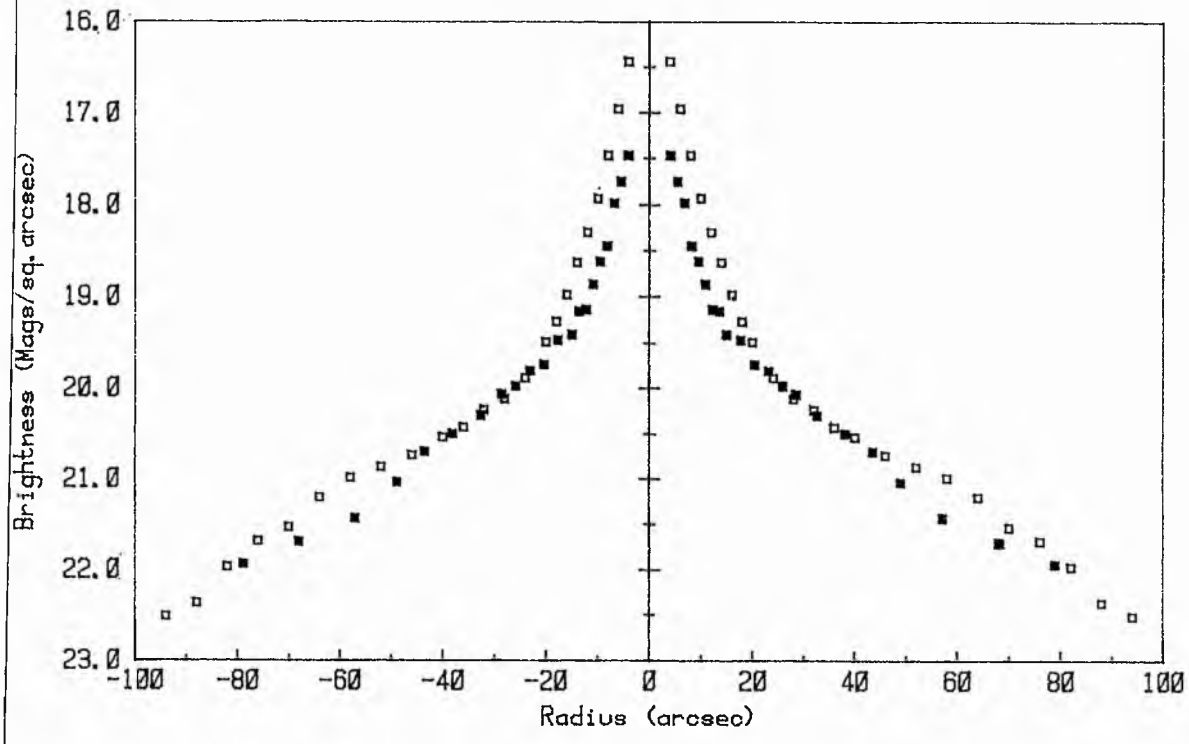

ORDINATE SHIFTS W.R.T. PREVIOUS PHOTOMETRY

B-BAND			I-BAND		
GALAXY	SHIFT	SOURCE	GALAXY	SHIFT	SOURCE
4267	+ 0.95	WATANABE	4267	+ 0.8	BSS
4371	+ 1.0	"	4419	+ 0.9	"
4377	+ 0.8	"	4425	+ 0.9	"
4419	+ 0.9	"	4429	+ 0.8	"
4425	+ 0.9	"	4435	+ 0.3	"
4429	+ 1.2	"	4459	+ 0.6	"
4459	+ 1.2	"	4461	+ 0.4	"
4461	+ 0.90	"	4474	- 0.3	"
4474	+ 1.0	"	4477	+ 0.4	"
4477	+ 1.2	"	4501	0.0	BLACKMANN
4501	+ 1.0	"			
4503	+ 1.1	"			
4531	+ 1.1	"			
4550	+ 1.0	"			
4552	+ 1.1	"			
4377	+ 0.2	BURSTEIN			
4429	- 0.3	"			
4459	+ 0.3	"			
4474	0.0	"			

APPENDIX 'D'

B, R and I-Band Isophotal Maps

1 pixel = 1.61 arcseconds

NGC 4267 'B'

THRESHOLD = 25.00 INCREMENT = 1.00 SKY LEVEL = 22.82

X10** 2 ALL VALUES IN MAGNITUDES / SQUARE ARCSECOND.

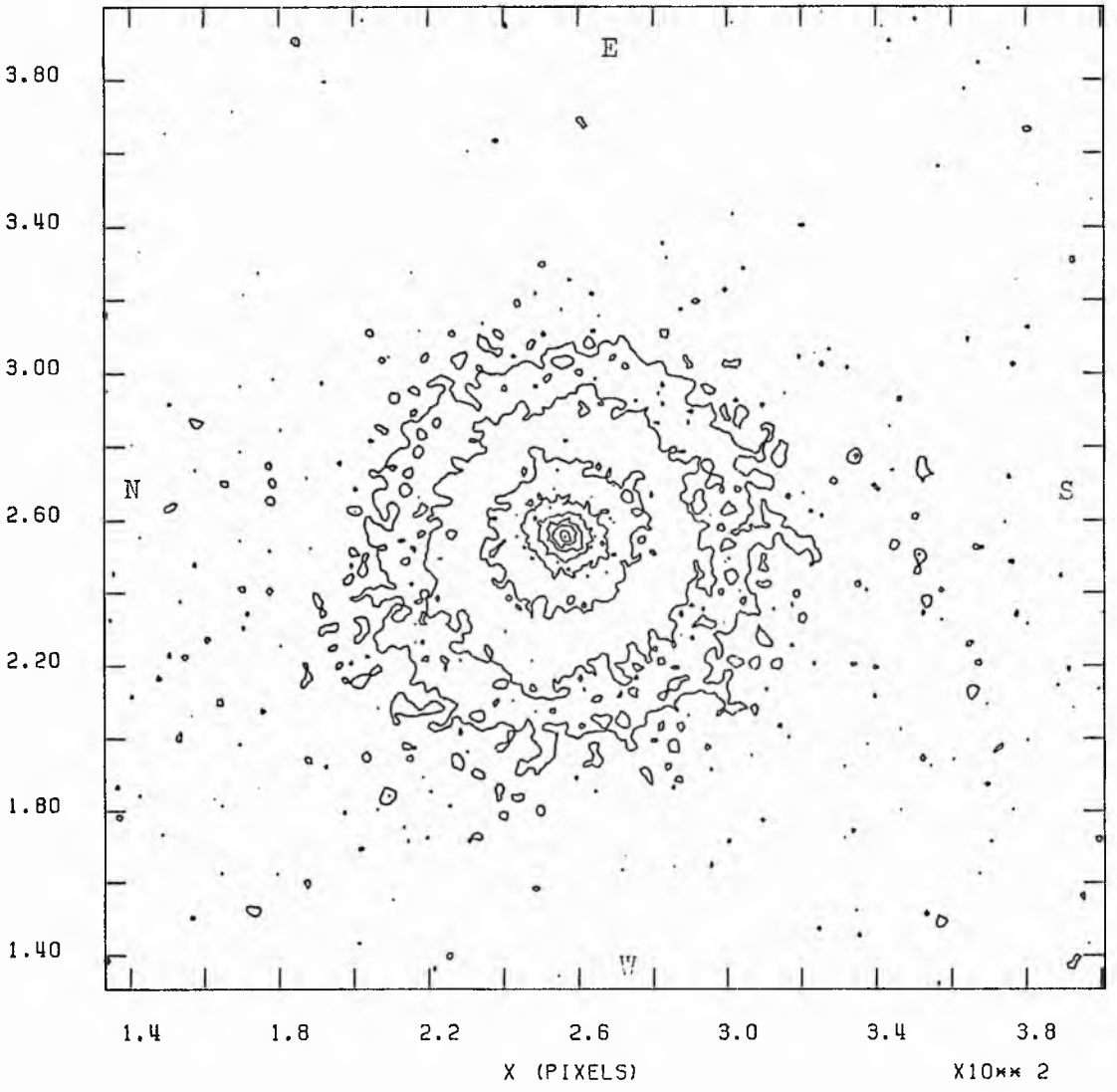

NGC 4371 'B' ISOPHOTAL MAP

THRESHOLD = 25.00 INCREMENT = 1.00 SKY LEVEL = 22.84

X10** 2 ALL VALUES IN MAGNITUDES / SQUARE ARCSECOND.

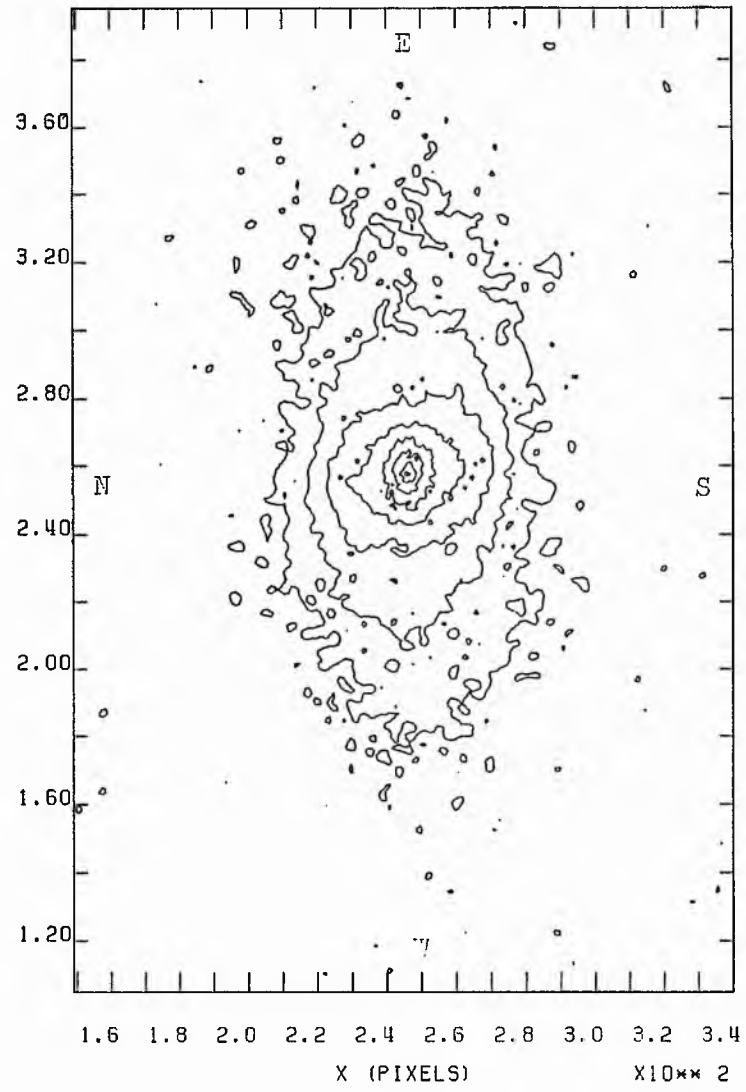

NGC 4377 'B' ISOPHOTAL MAP

THRESHOLD = 25.00 INCREMENT = 1.00 SKY LEVEL = 22.88

X10** 2 ALL VALUES IN MAGNITUDES / SQUARE ARCSECOND.

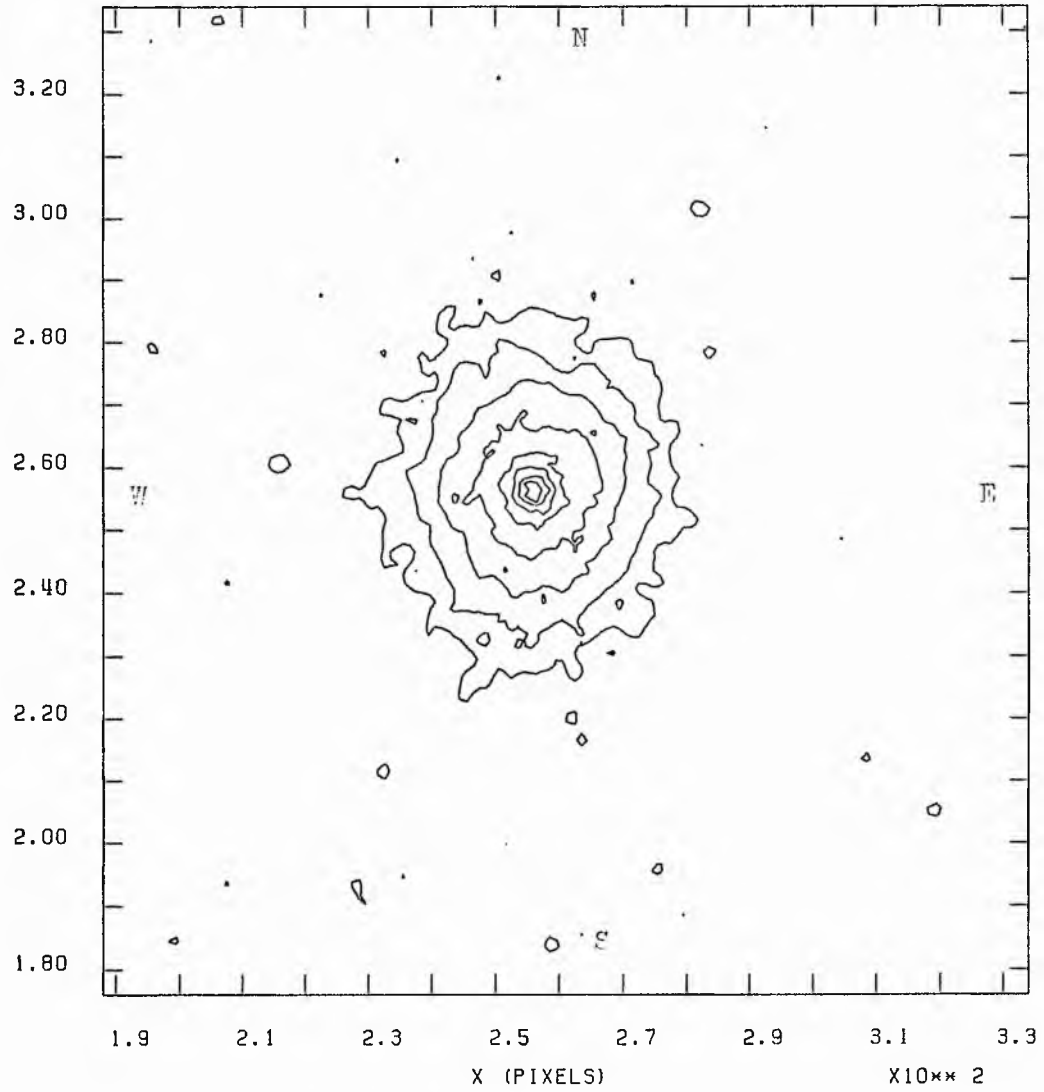

NGC 4419 'B' ISOPHOTAL MAP

THRESHOLD = 25.00 INCREMENT = 1.00 SKY LEVEL = 22.85

ALL VALUES IN MAGNITUDES / SQUARE ARCSECOND.

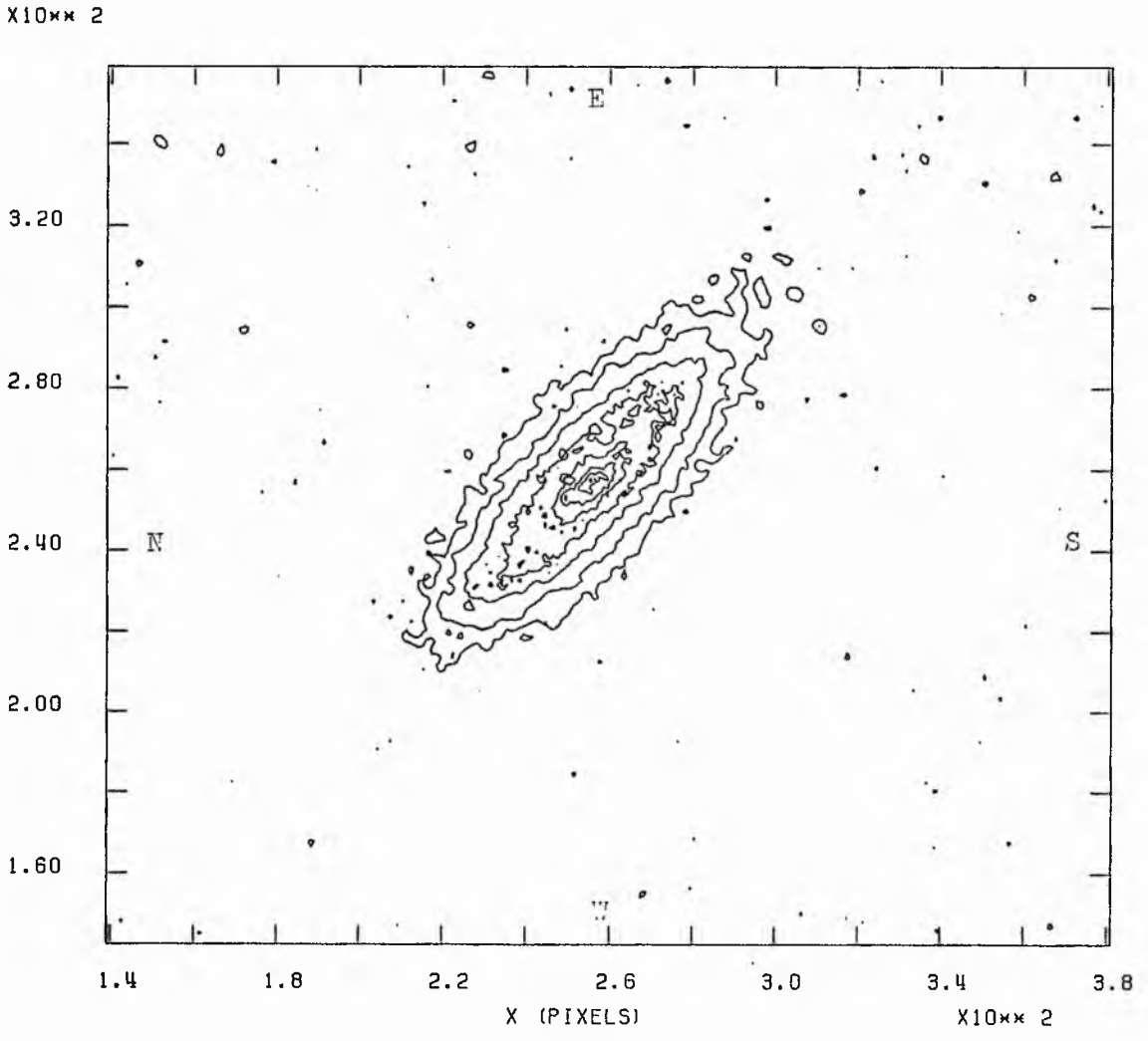

NGC 4425 'B' ISOPHOTAL MAP

THRESHOLD = 25.00 INCREMENT = 1.00 SKY LEVEL = 22.80

X10** 2 . ALL VALUES IN MAGNITUDES / SQUARE ARCSECOND.

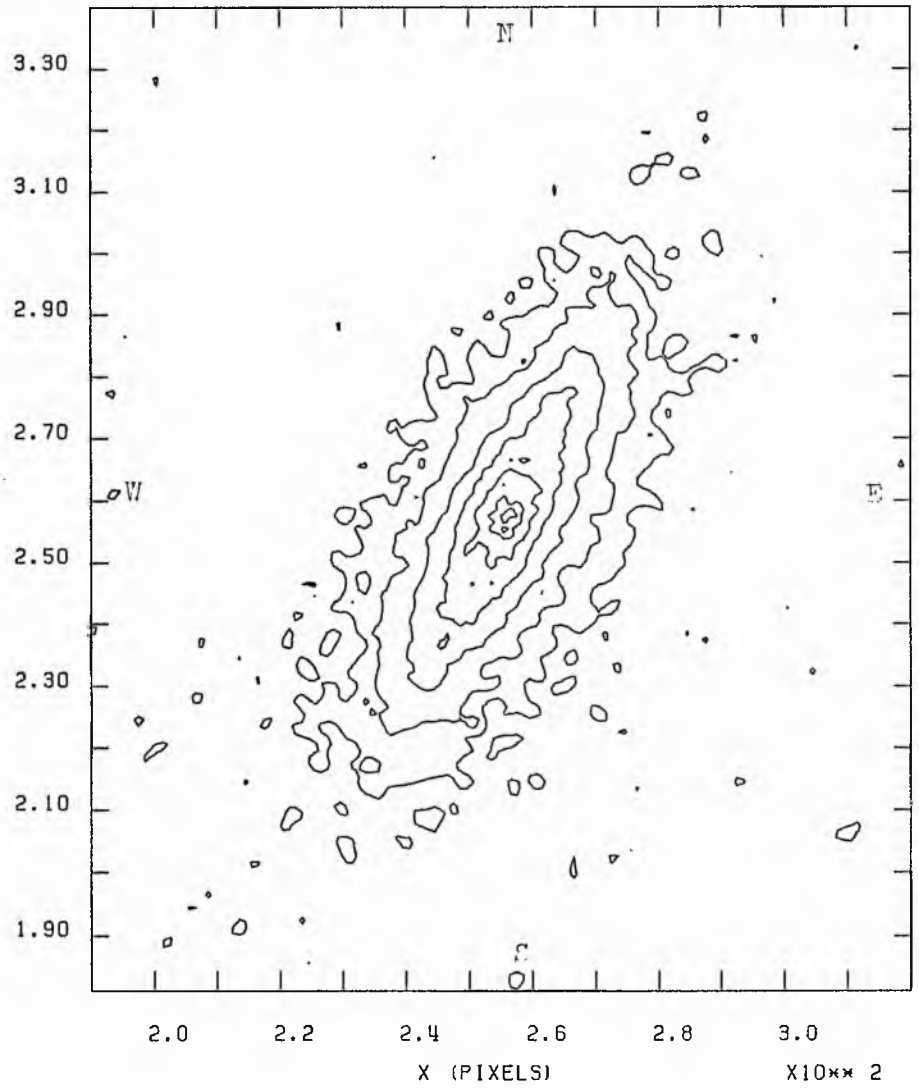

NGC 4429 'B' ISOPHOTAL MAP

THRESHOLD = 25.00 INCREMENT = 1.00 SKY LEVEL = 22.91

X10** 2 ALL VALUES IN MAGNITUDES / SQUARE ARCSECOND.

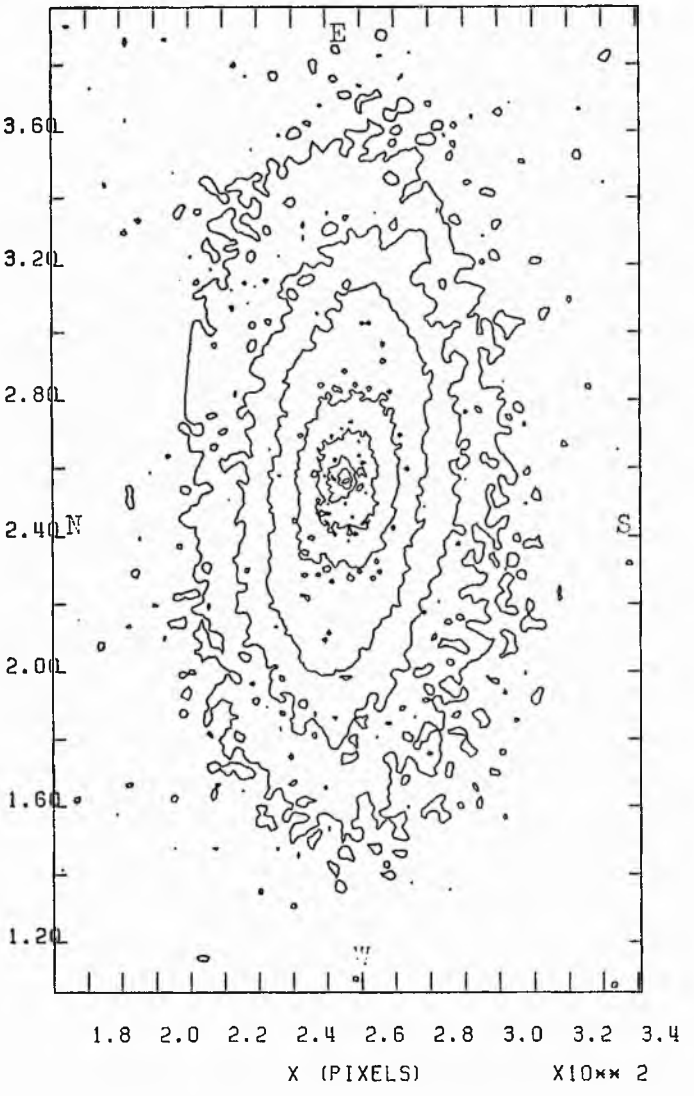

NGC 4435 / 4438

THRESHOLD = 25.00 INCREMENT = 1.00 SKY LEVEL = 22.85

X10** 2 ALL VALUES IN MAGNITUDES / SQUARE ARCSECOND.

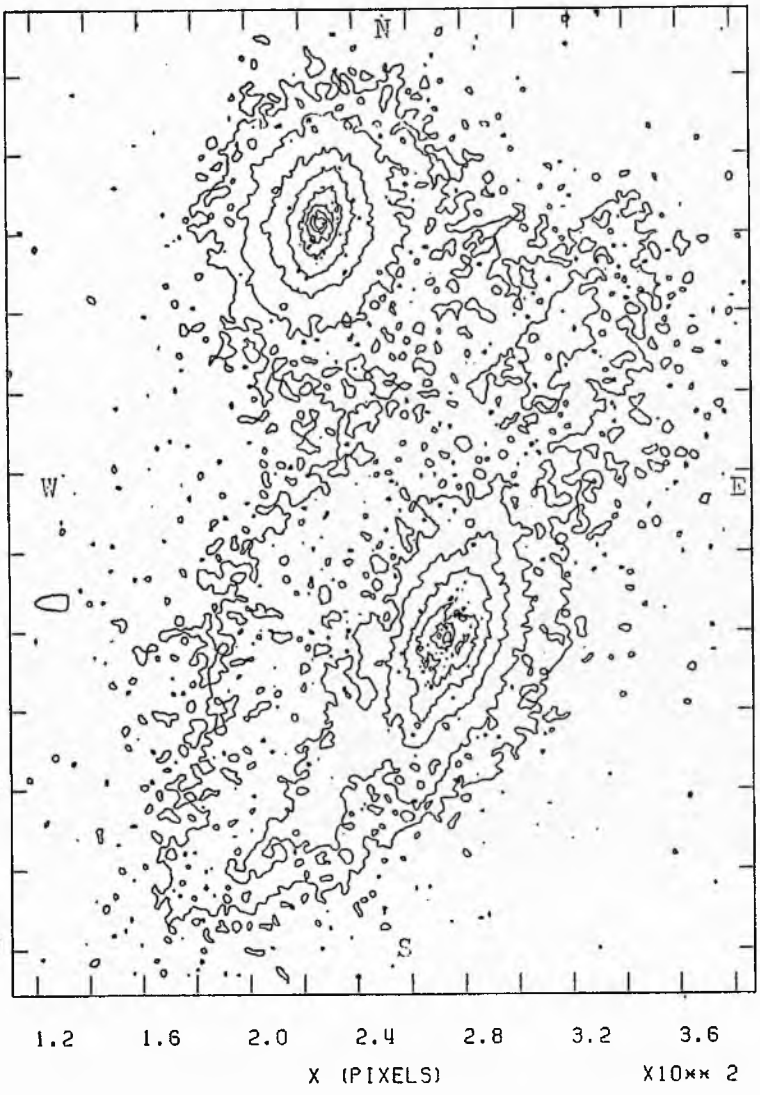

NGC 4458 / 4461

THRESHØLD = 25.00 INCREMENT = 1.00 SKY LEVEL = 22.83

X10** 2 ALL VALUES IN MAGNITUDES / SQUARE ARCSECOND.

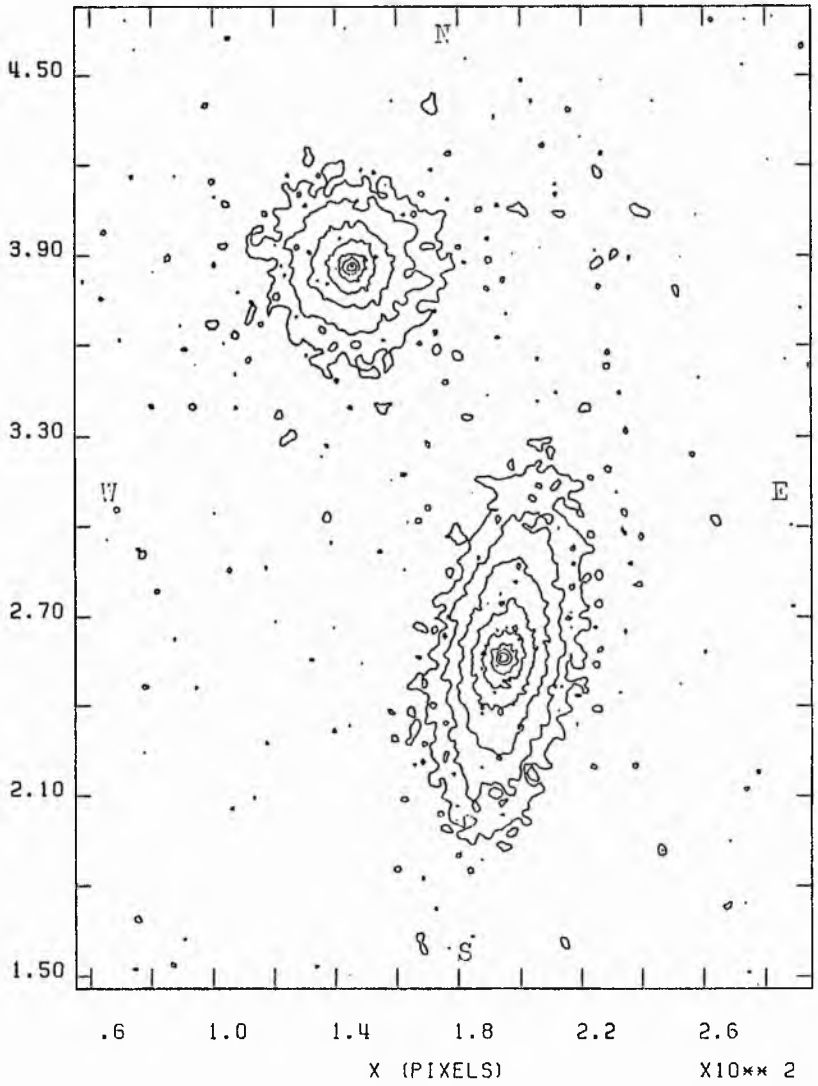

NGC 4459 'B' ISOPHOTAL MAP

THRESHOLD = 25.00 INCREMENT = 1.00 SKY LEVEL = 23.04

ALL VALUES IN MAGNITUDES / SQUARE ARCSECOND.

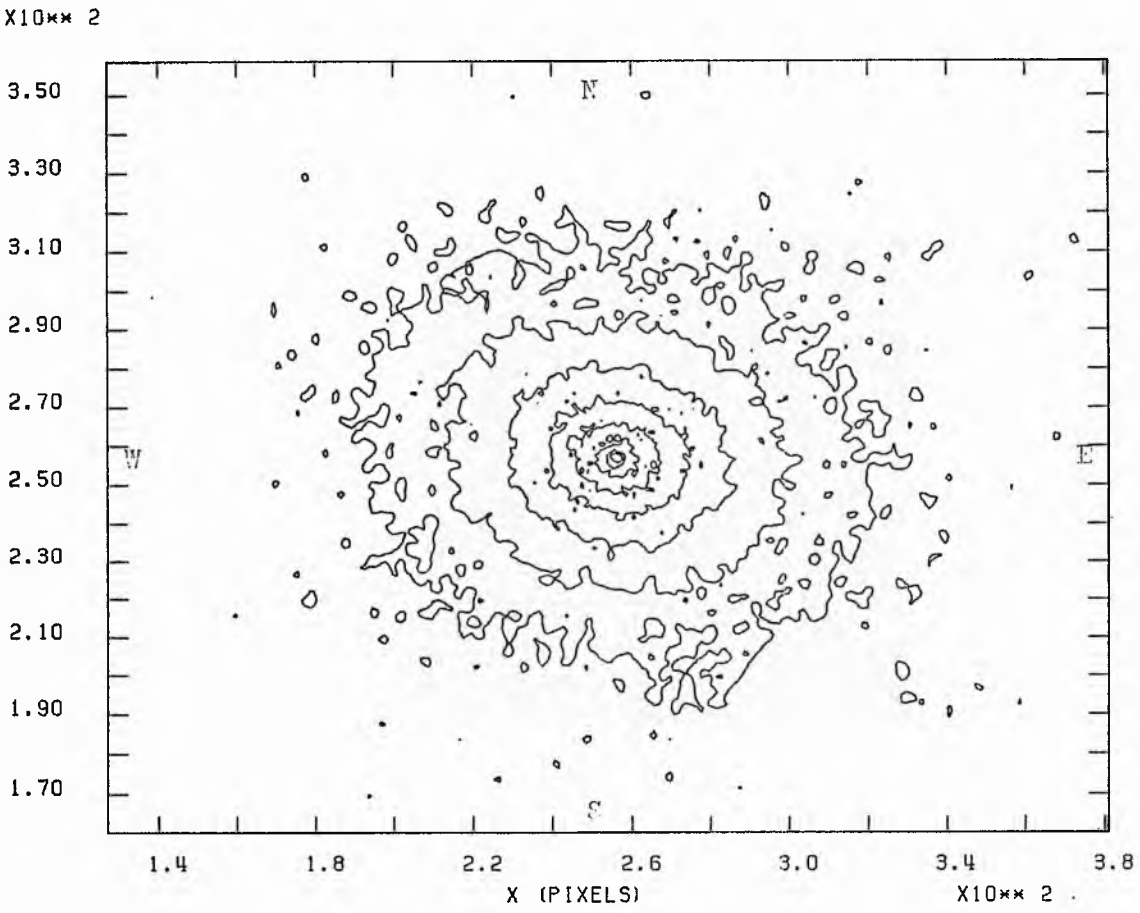

NGC 4474 'B' ISOPHOTAL MAP

THRESHOLD = 25.00 INCREMENT = 1.00 SKY LEVEL = 22.81

ALL VALUES IN MAGNITUDES / SQUARE ARCSECOND.

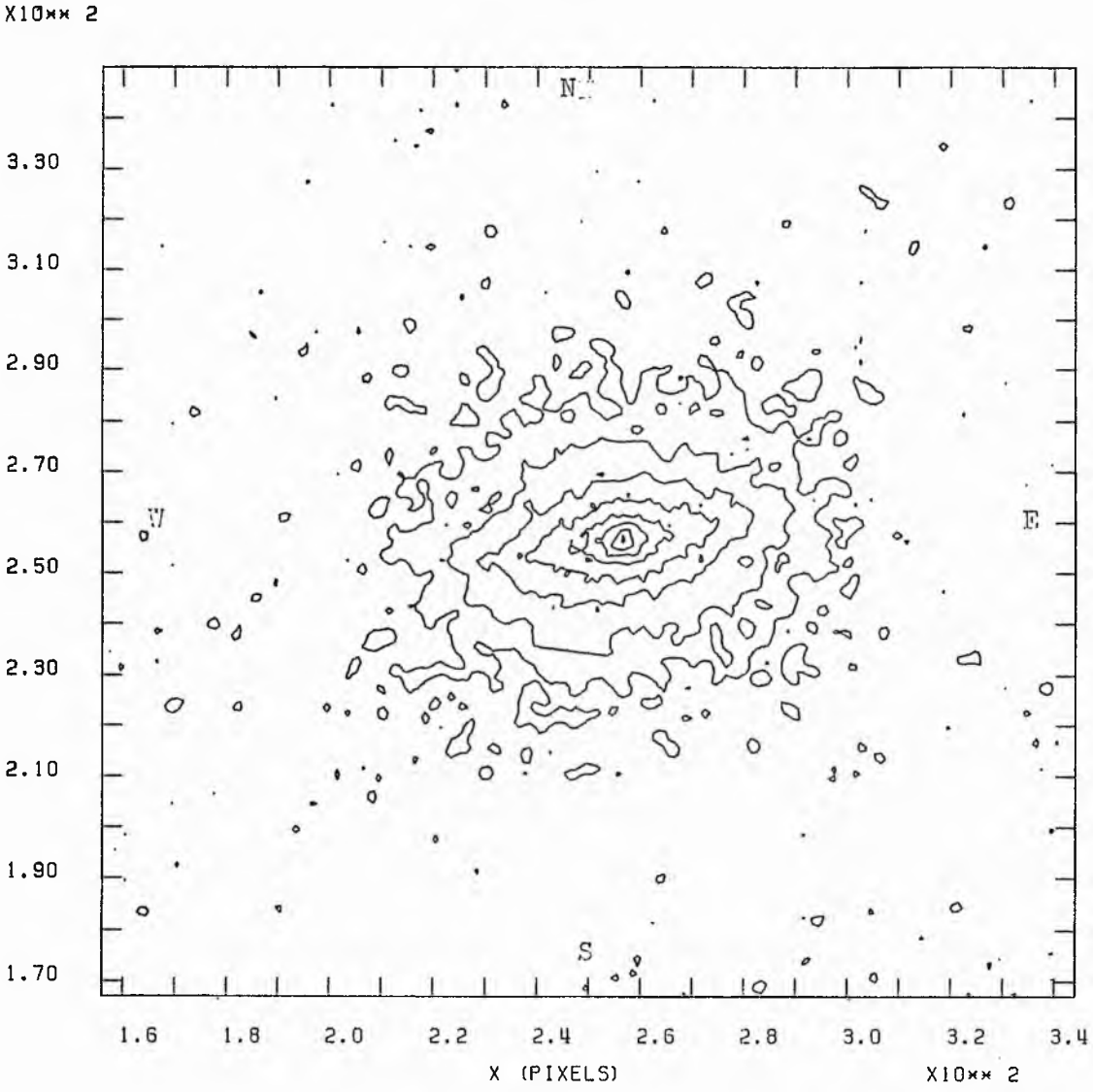

NGC 4477 'B' ISOPHOTAL MAP

THRESHOLD = 25.00 INCREMENT = 1.00 SKY LEVEL = 22.95

ALL VALUES IN MAGNITUDES / SQUARE ARCSECOND.

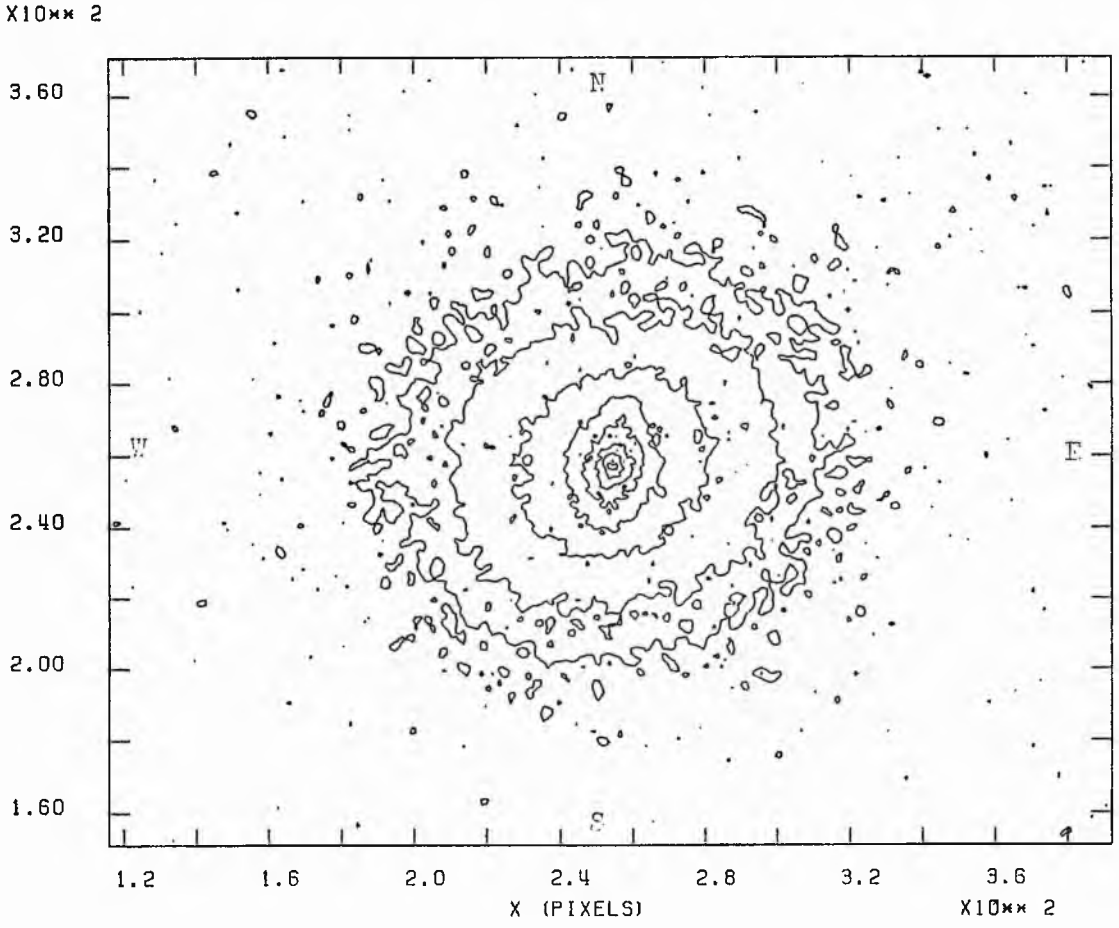

NGC 4501 'B' ISOPHOTAL MAP

THRESHOLD = 25.00 INCREMENT = 1.00 SKY LEVEL = 22.83

X10** 2 ALL VALUES IN MAGNITUDES / SQUARE ARCSECOND.

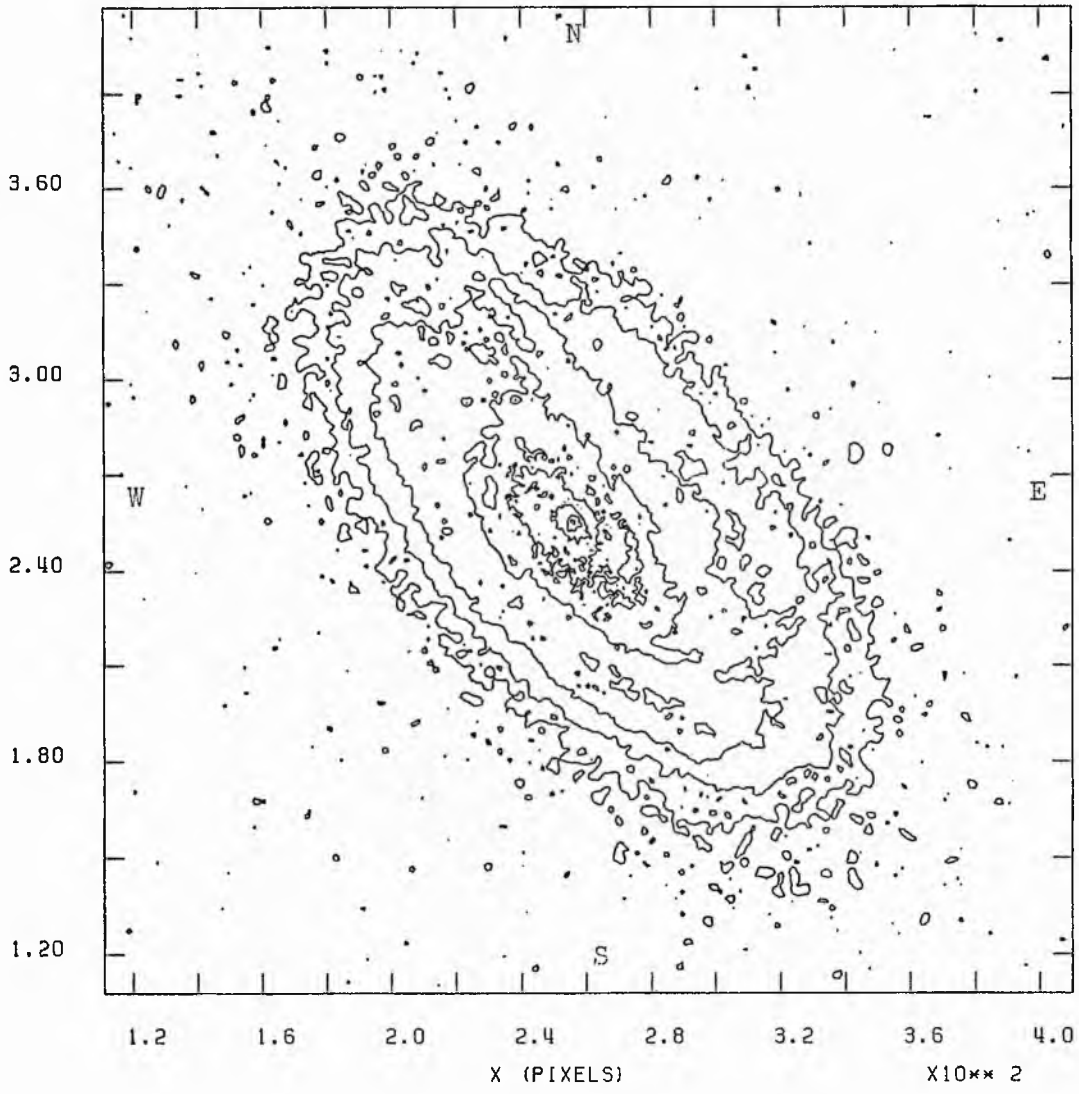

NGC 4503 'B' ISOPHOTAL MAP

THRESHOLD = 25.00 INCREMENT = 1.00 SKY LEVEL = 22.93

ALL VALUES IN MAGNITUDES / SQUARE ARCSECOND.

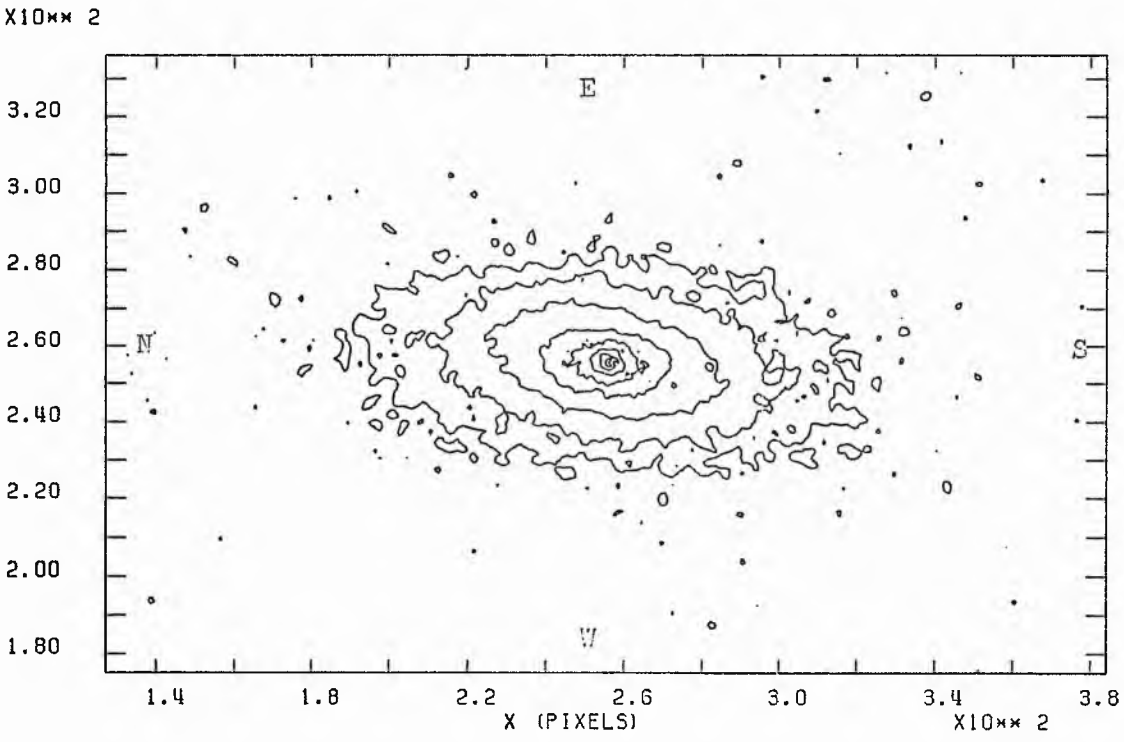

NGC 4531 'B' ISOPHOTAL MAP

THRESHOLD = 25.00 INCREMENT = 1.00 SKY LEVEL = 22.85

ALL VALUES IN MAGNITUDES / SQUARE ARCSECOND.

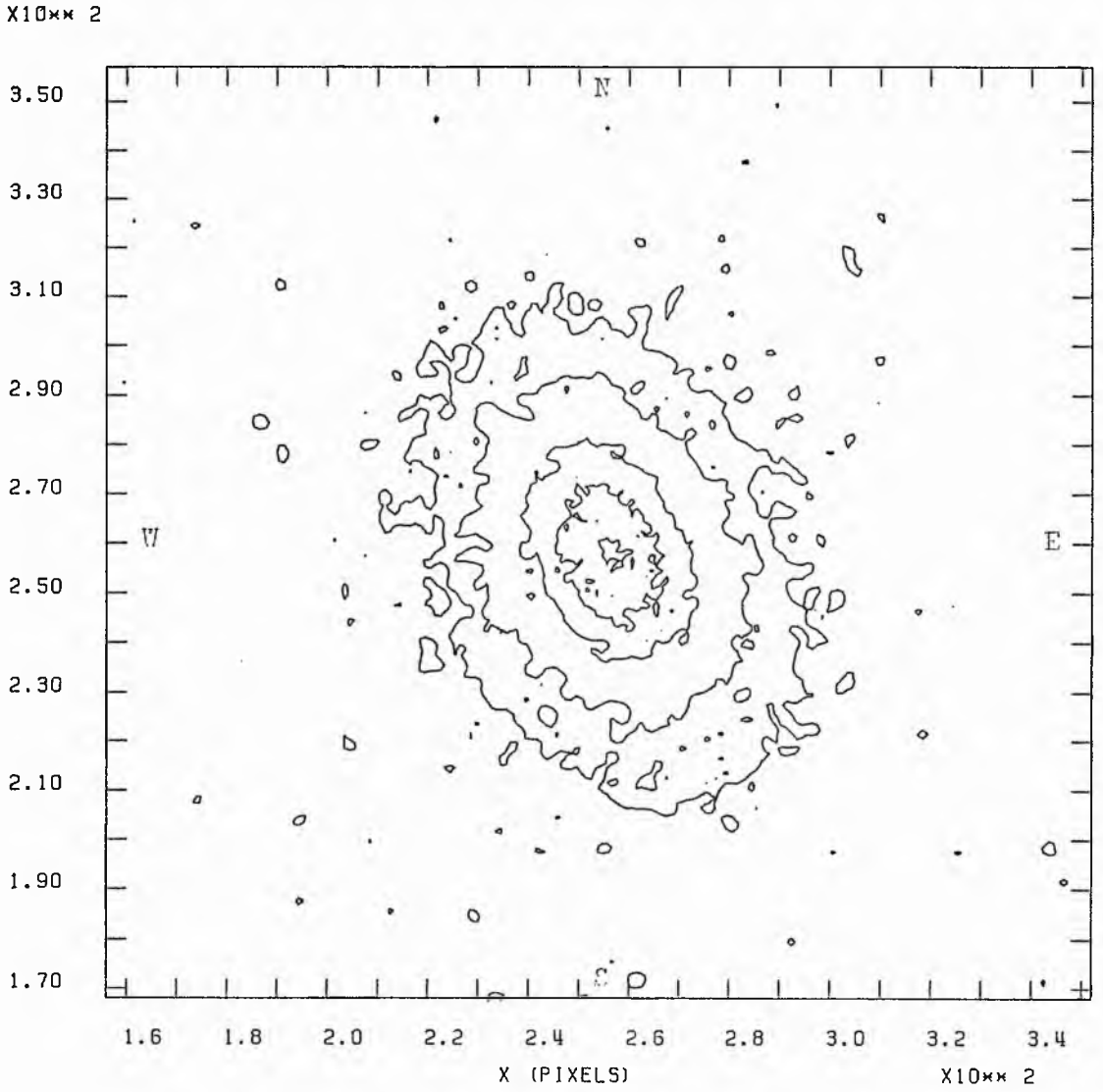

NGC 4550/4[illegible] 'B'

THRESHOLD = 25.00 INCREMENT = 1.00 SKY LEVEL = 22.86

X10** 2 ALL VALUES IN MAGNITUDES / SQUARE ARCSECOND.

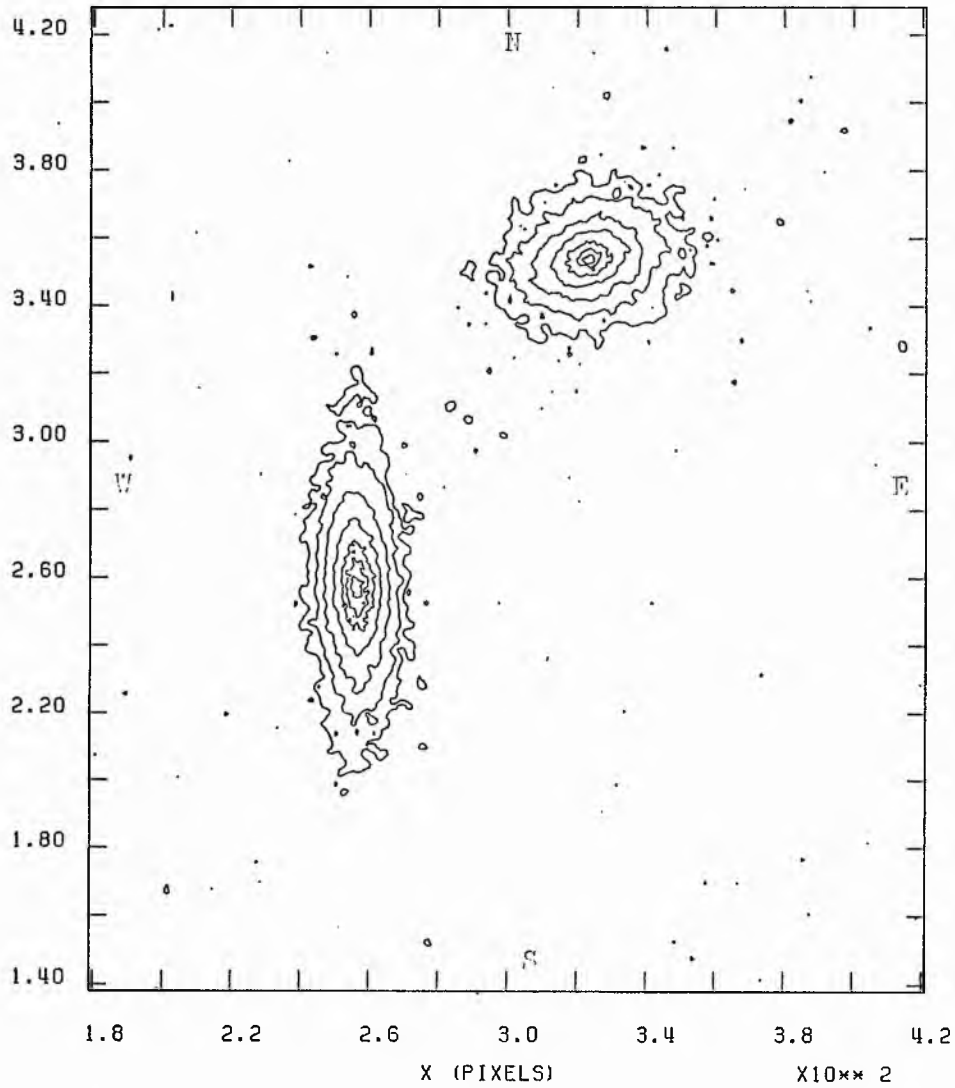

NGC 4552 'B' ISOPHOTAL MAP

THRESHOLD = 25.00 INCREMENT = 1.00 SKY LEVEL = 22.93

ALL VALUES IN MAGNITUDES / SQUARE ARCSECOND.

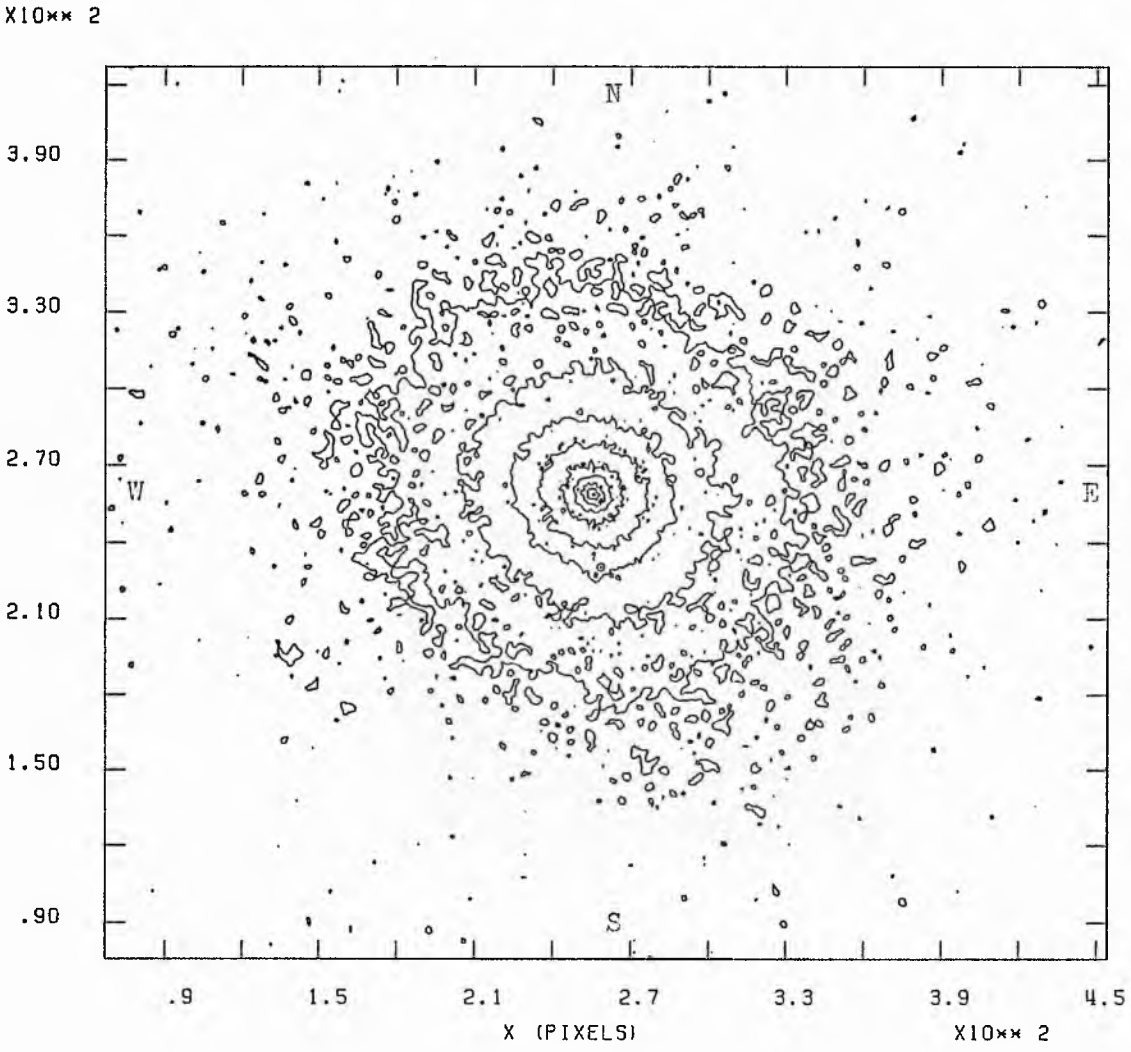

NGC 4267 R (J)

THRESHOLD = 24.00 INCREMENT = 1.00 SKY LEVEL = 20.53

ALL VALUES IN MAGNITUDES / SQUARE ARCSECOND.

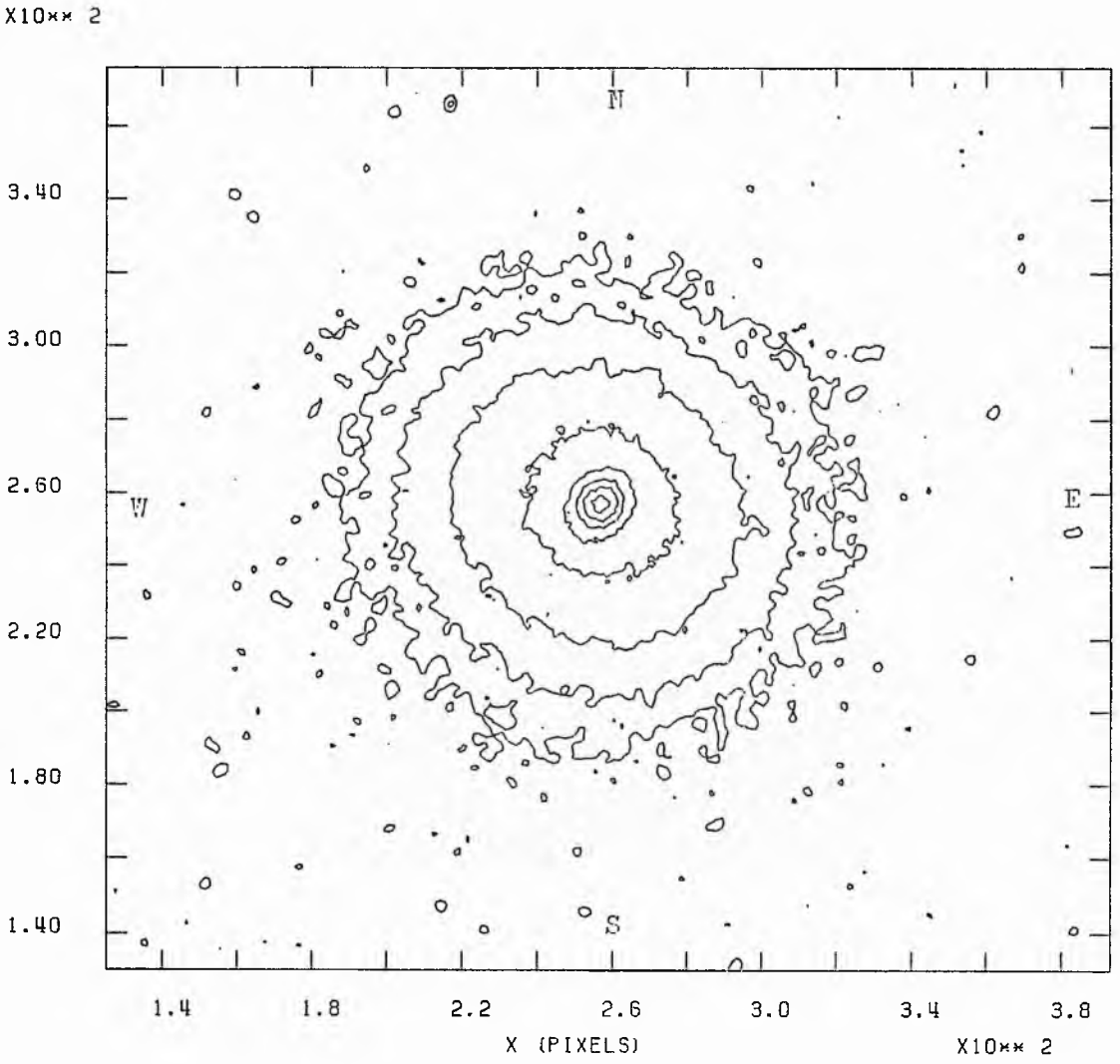

NGC 4371 R (J)

THRESHOLD = 24.00 INCREMENT = 1.00 SKY LEVEL = 20.53

X10** 2 ALL VALUES IN MAGNITUDES / SQUARE ARCSECOND.

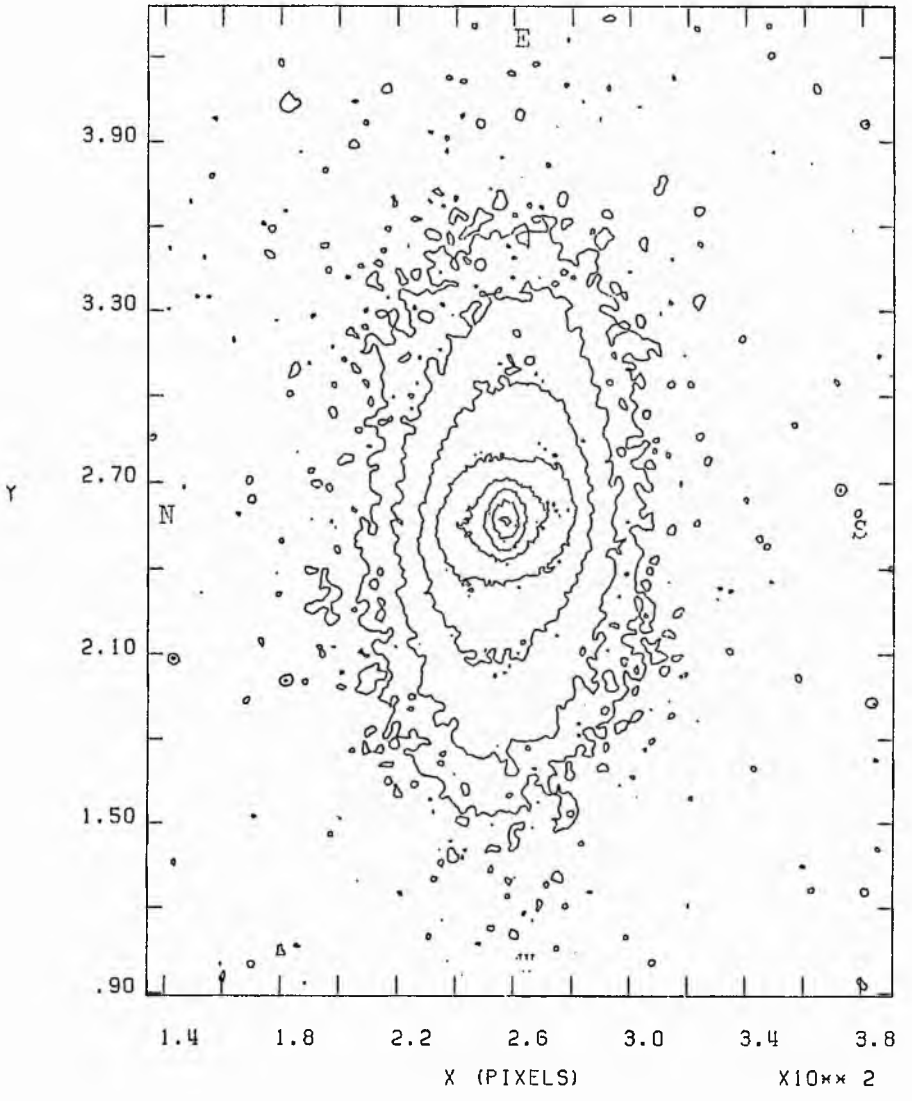

NGC 4377 R (J)

THRESHOLD = 24.00 INCREMENT = 1.00 SKY LEVEL = 20.53

X10** 2 ALL VALUES IN MAGNITUDES / SQUARE ARCSECOND.

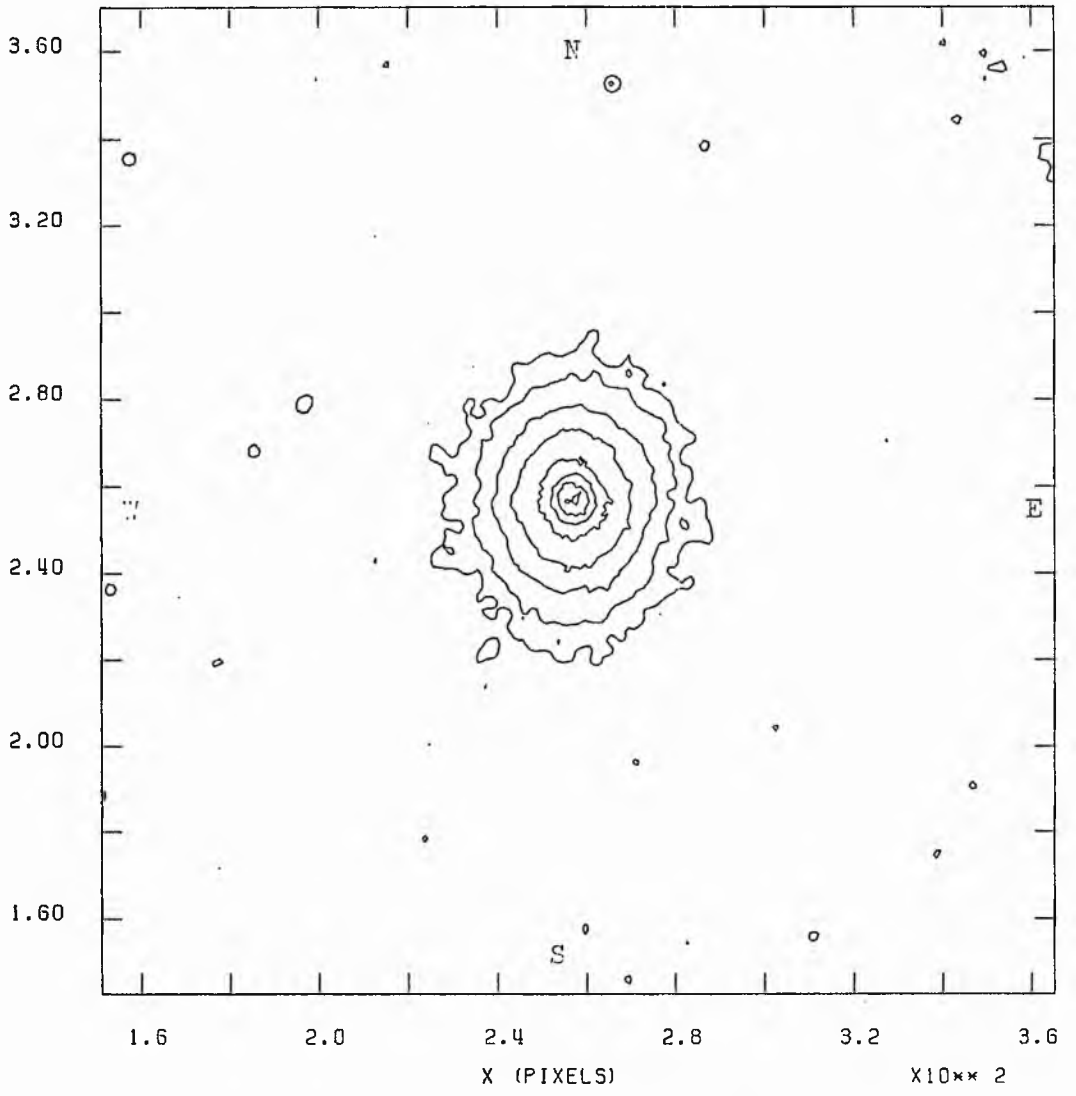

NGC 4419 R (J)

THRESHOLD = 24.00 INCREMENT = 1.00 SKY LEVEL = 20.53

X10** 2 ALL VALUES IN MAGNITUDES / SQUARE ARCSECOND.

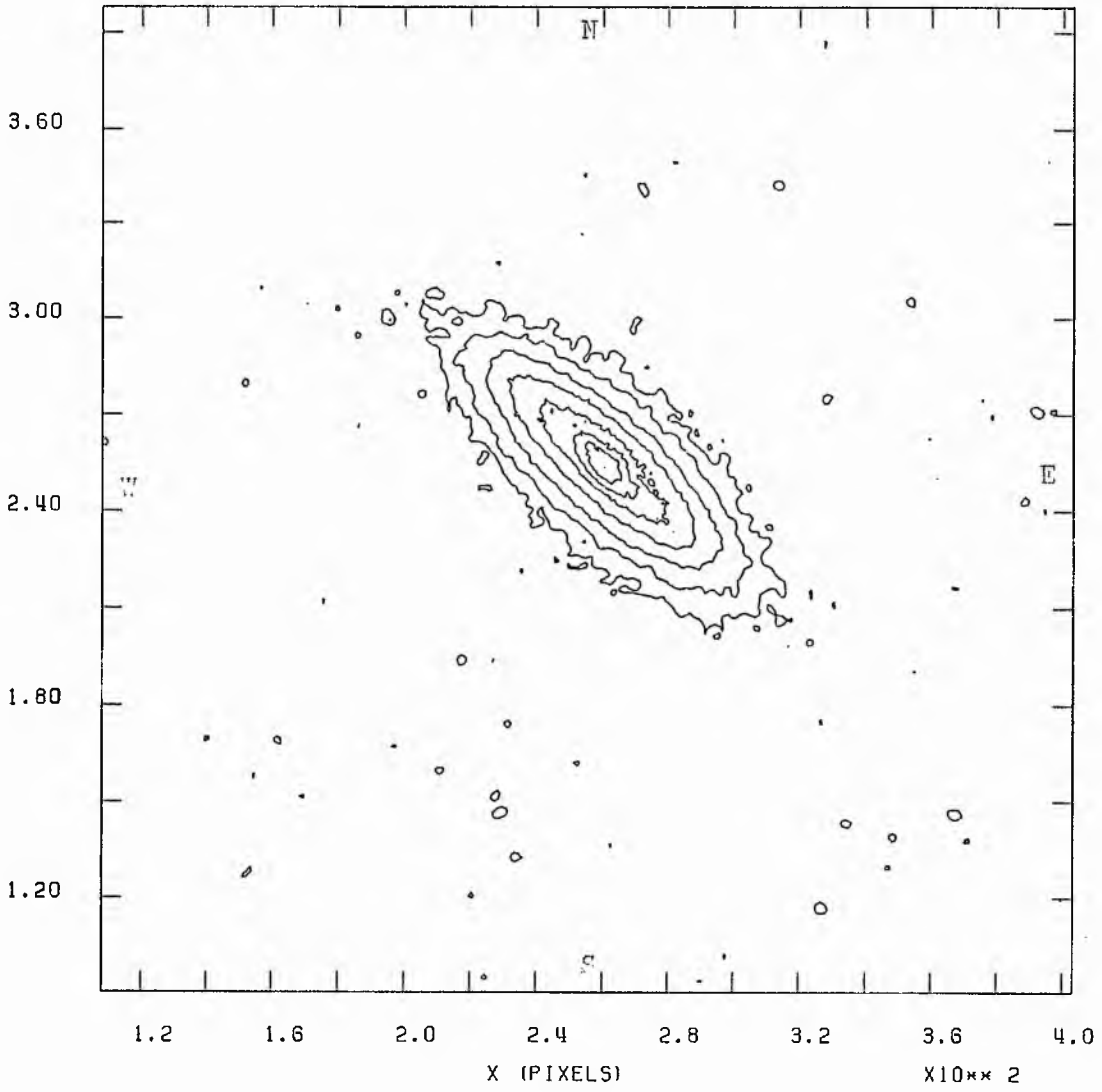

NGC 4425 R (J)

THRESHOLD = 24.00 INCREMENT = 1.00 SKY LEVEL = 20.53

ALL VALUES IN MAGNITUDES / SQUARE ARCSECOND.

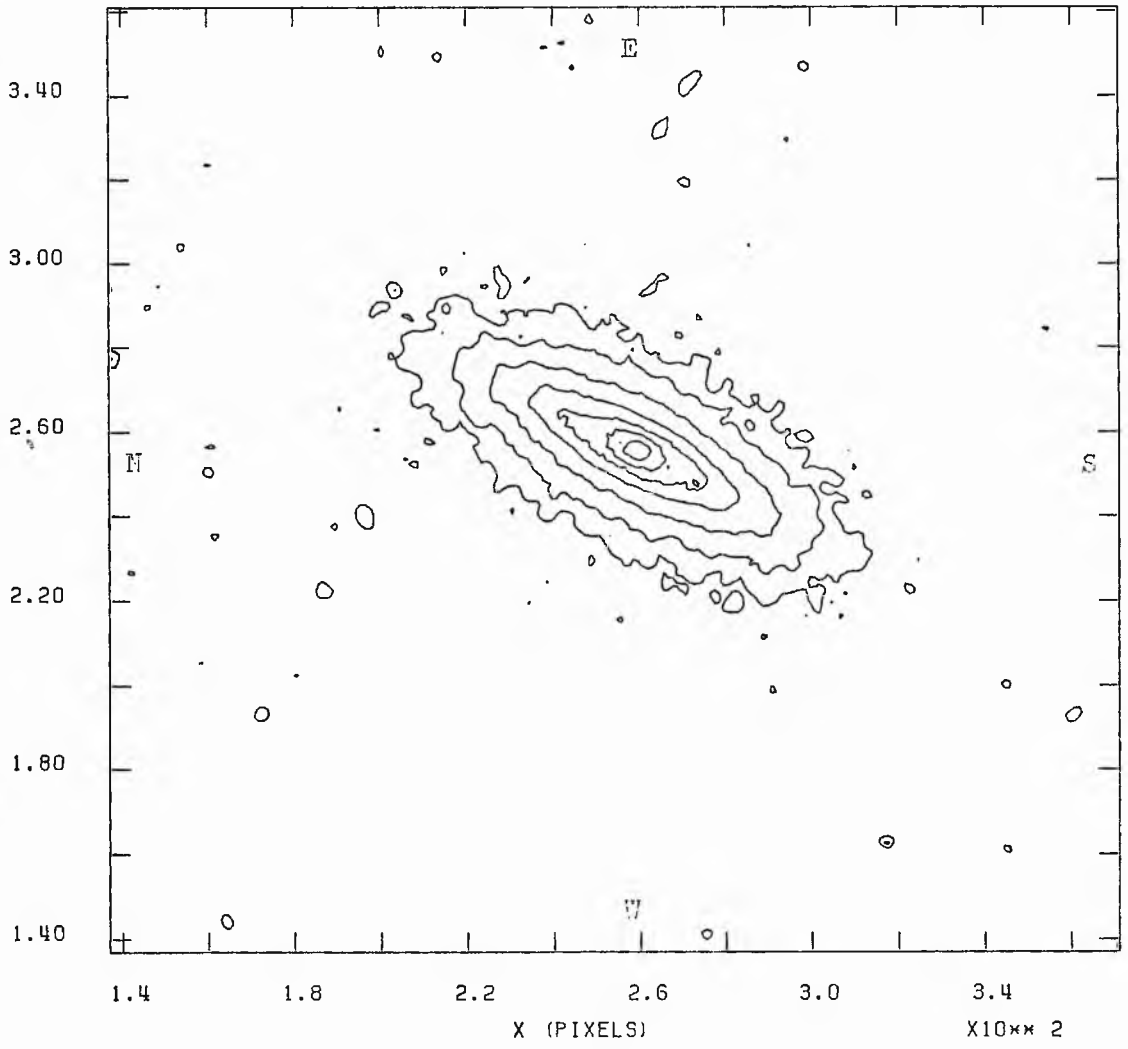

NGC 4429 R (J)

THRESHOLD = 24.00 INCREMENT = 1.00 SKY LEVEL = 20.64

X10** 2 ALL VALUES IN MAGNITUDES / SQUARE ARCSECOND.

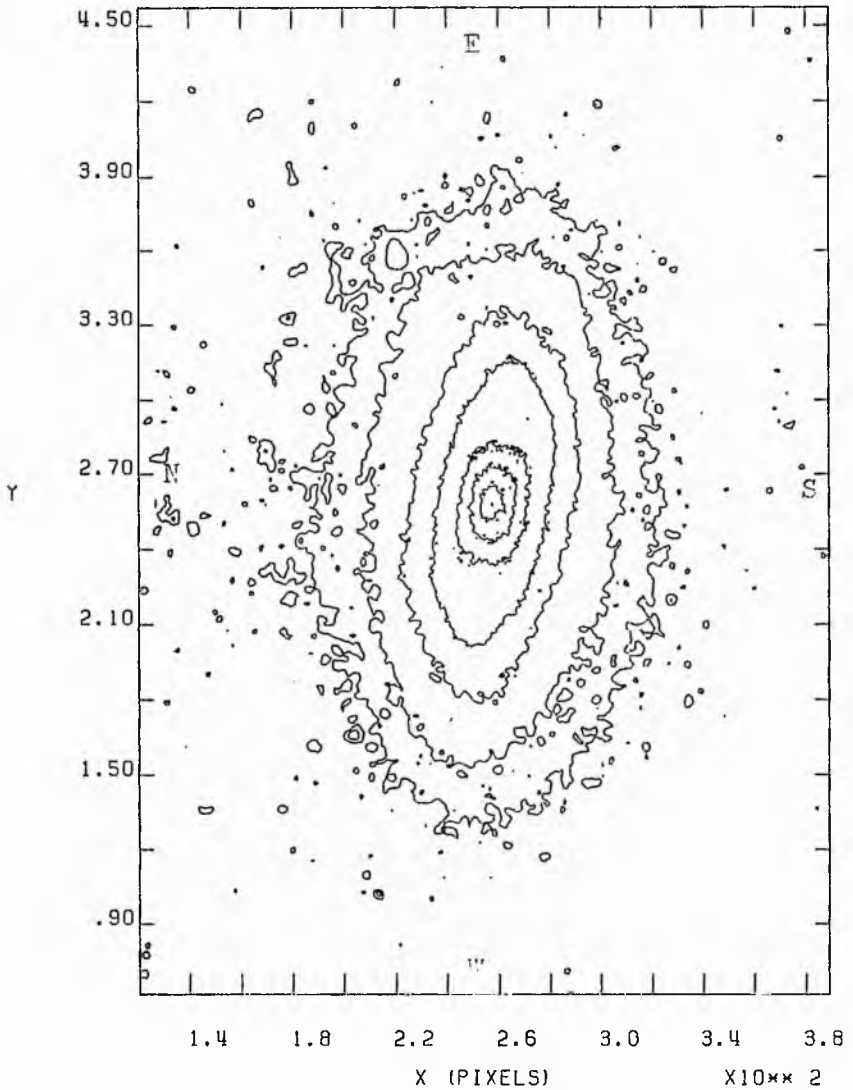

NGC 4435 + 4438 R (J)

THRESHOLD = 24.00 INCREMENT = 1.00 SKY LEVEL = 20.51

ALL VALUES IN MAGNITUDES / SQUARE ARCSECOND.

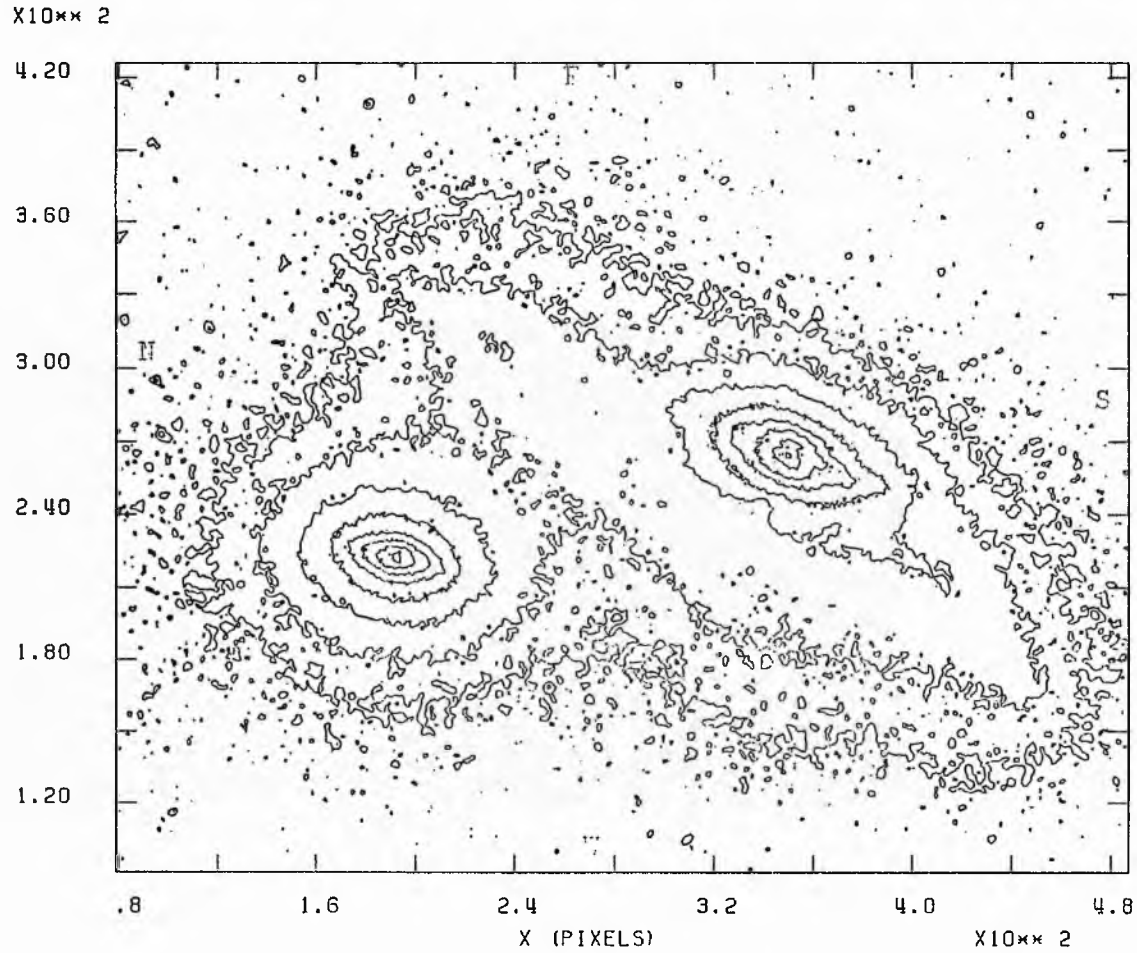

NGC 4459 R (J)

THRESHOLD = 24.00 INCREMENT = 1.00 SKY LEVEL = 20.57

X10** 2 ALL VALUES IN MAGNITUDES / SQUARE ARCSECOND.

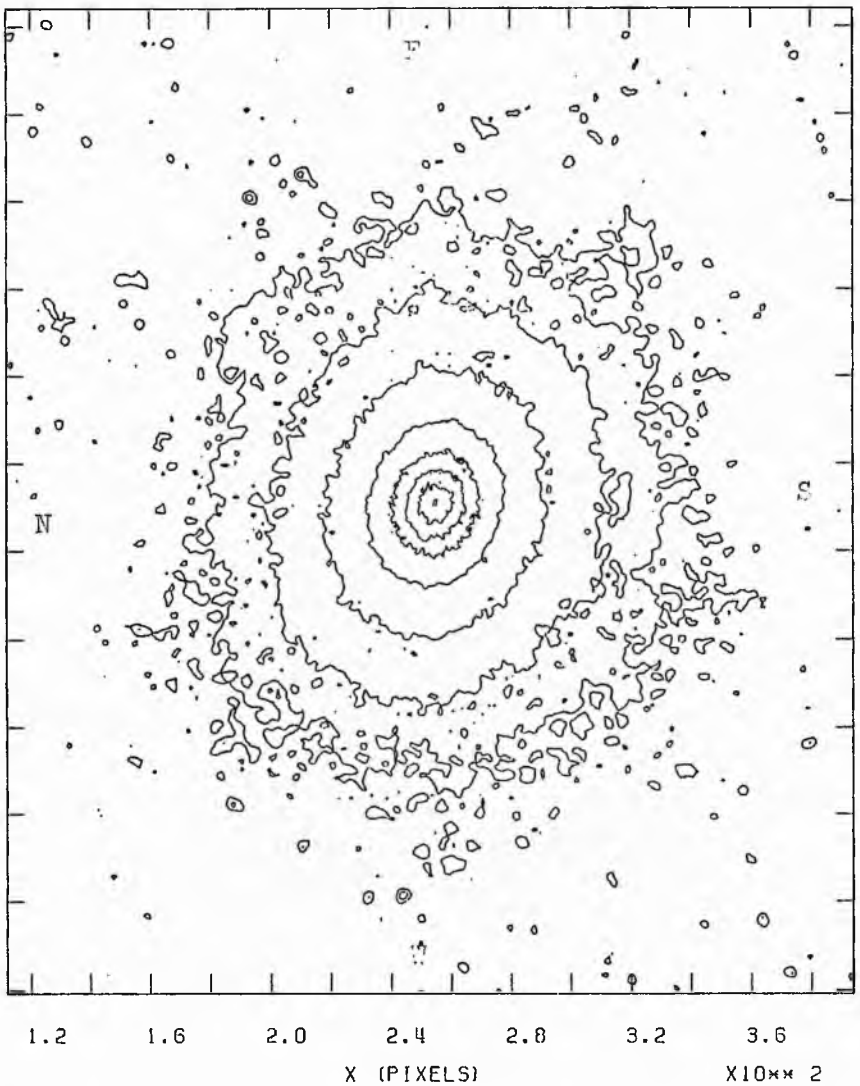

NGC 4461 + 4458 R (J)

THRESHOLD = 24.00 INCREMENT = 1.00 SKY LEVEL = 20.52

ALL VALUES IN MAGNITUDES / SQUARE ARCSECOND.

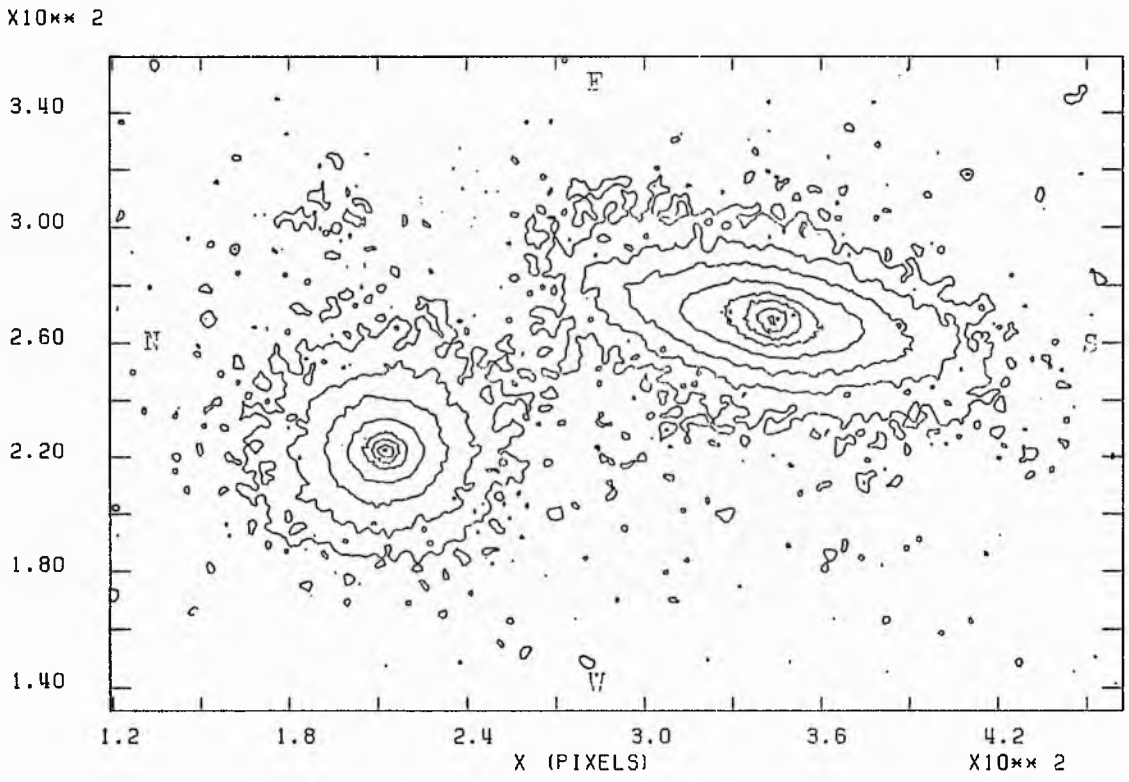

NGC 4474 R (J)

THRESHOLD = 24.00 INCREMENT = 1.00 SKY LEVEL = 20.53

X10** 2 ALL VALUES IN MAGNITUDES / SQUARE ARCSECOND.

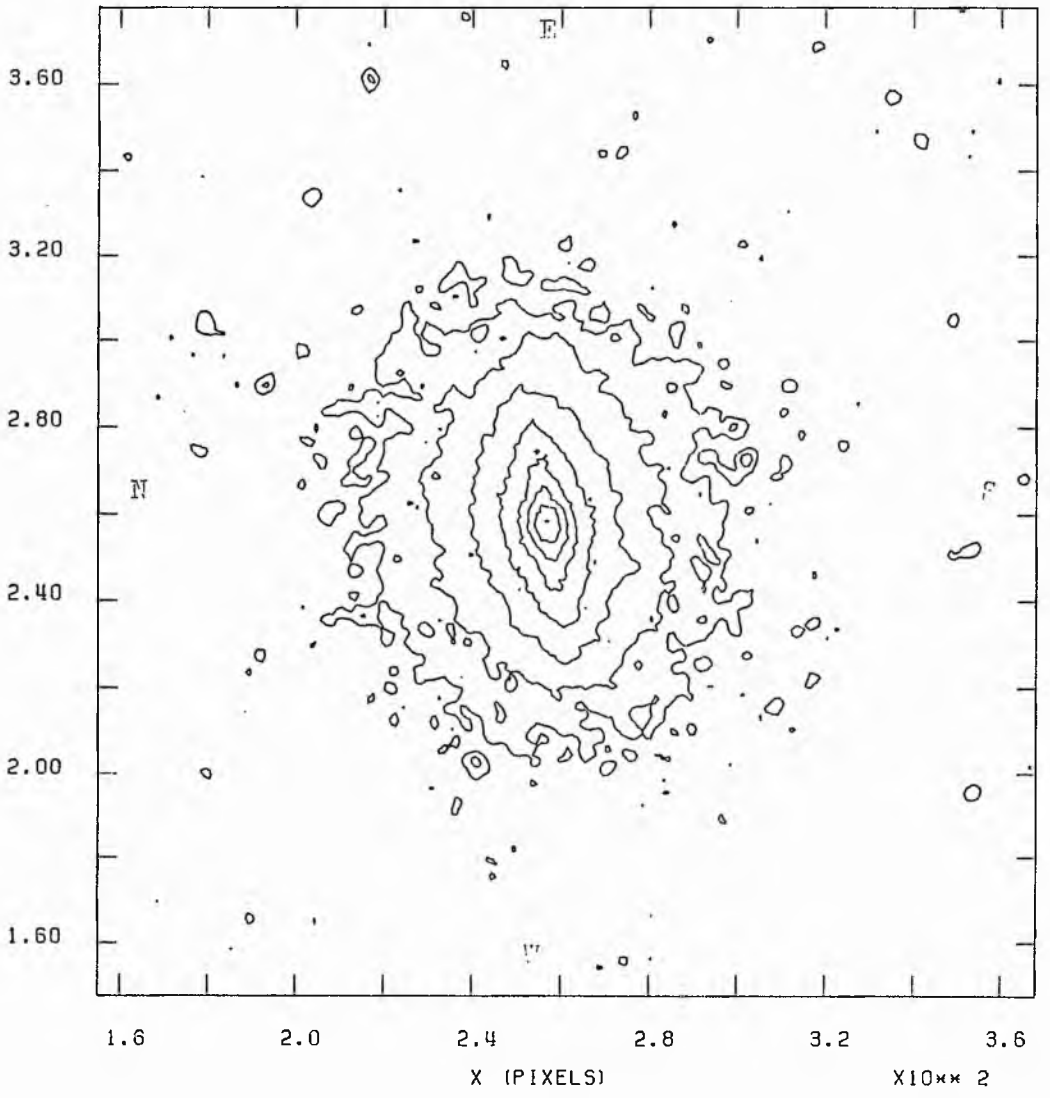

NGC 4477 R (J)

THRESHOLD = 24.00 INCREMENT = 1.00 SKY LEVEL = 20.53

X10** 2 ALL VALUES IN MAGNITUDES / SQUARE ARCSECOND.

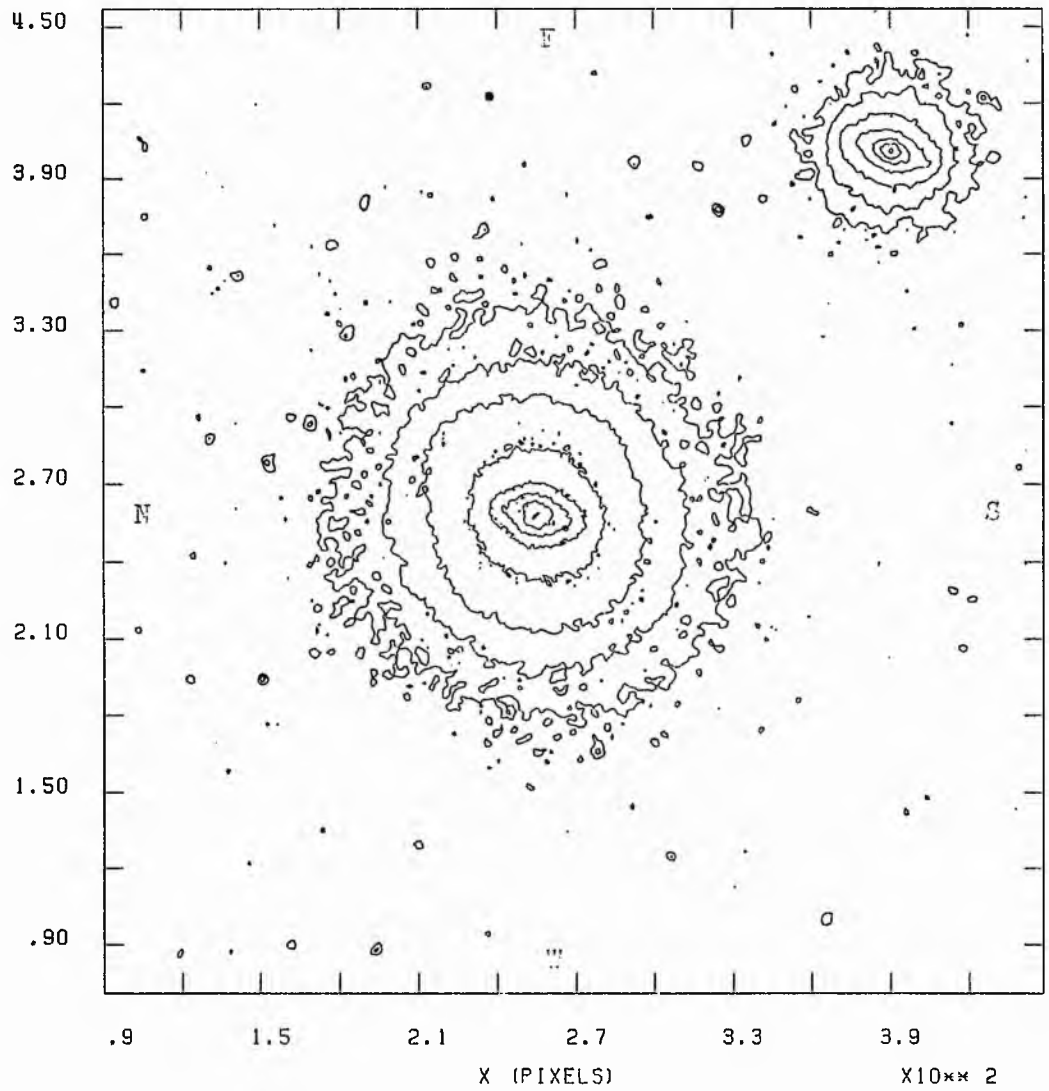

NGC 4501 R (J)

THRESHOLD = 24.00 INCREMENT = 1.00 SKY LEVEL = 20.58

X10** 2 ALL VALUES IN MAGNITUDES / SQUARE ARCSECOND.

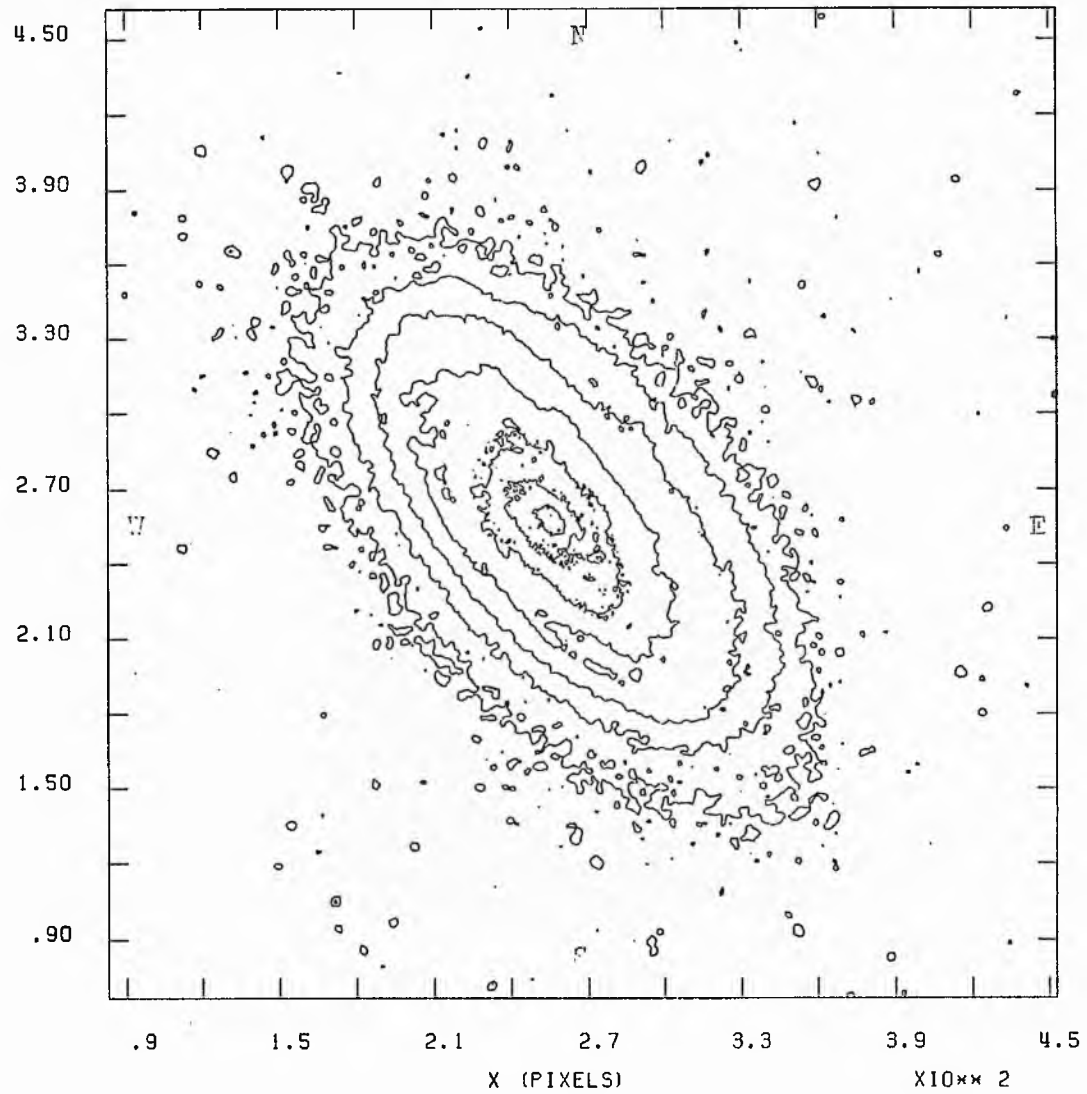

NGC 4503 R (J)

THRESHOLD = 24.00 INCREMENT = 1.00 SKY LEVEL = 20.53

ALL VALUES IN MAGNITUDES / SQUARE ARCSECOND.

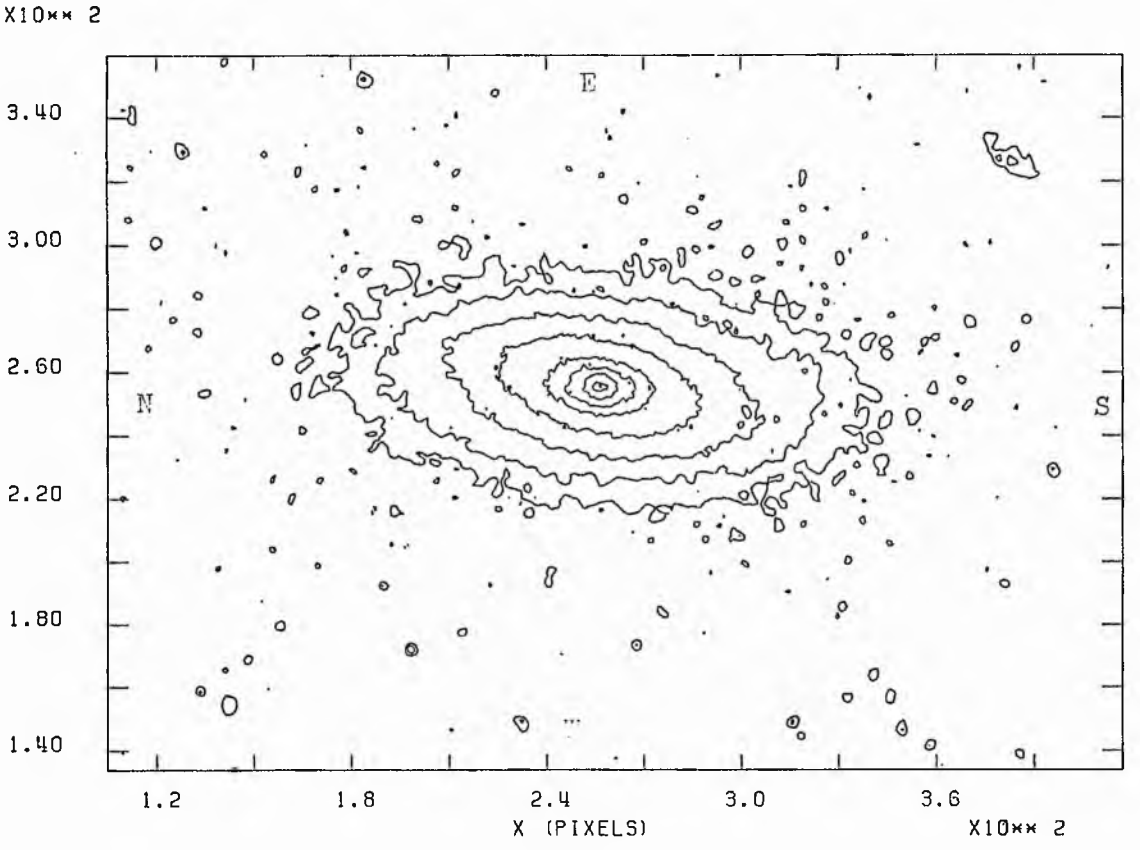

NGC 4531 R (J)

THRESHOLD = 24.00 INCREMENT = 1.00 SKY LEVEL = 20.53

X10** 2 ALL VALUES IN MAGNITUDES / SQUARE ARCSECOND.

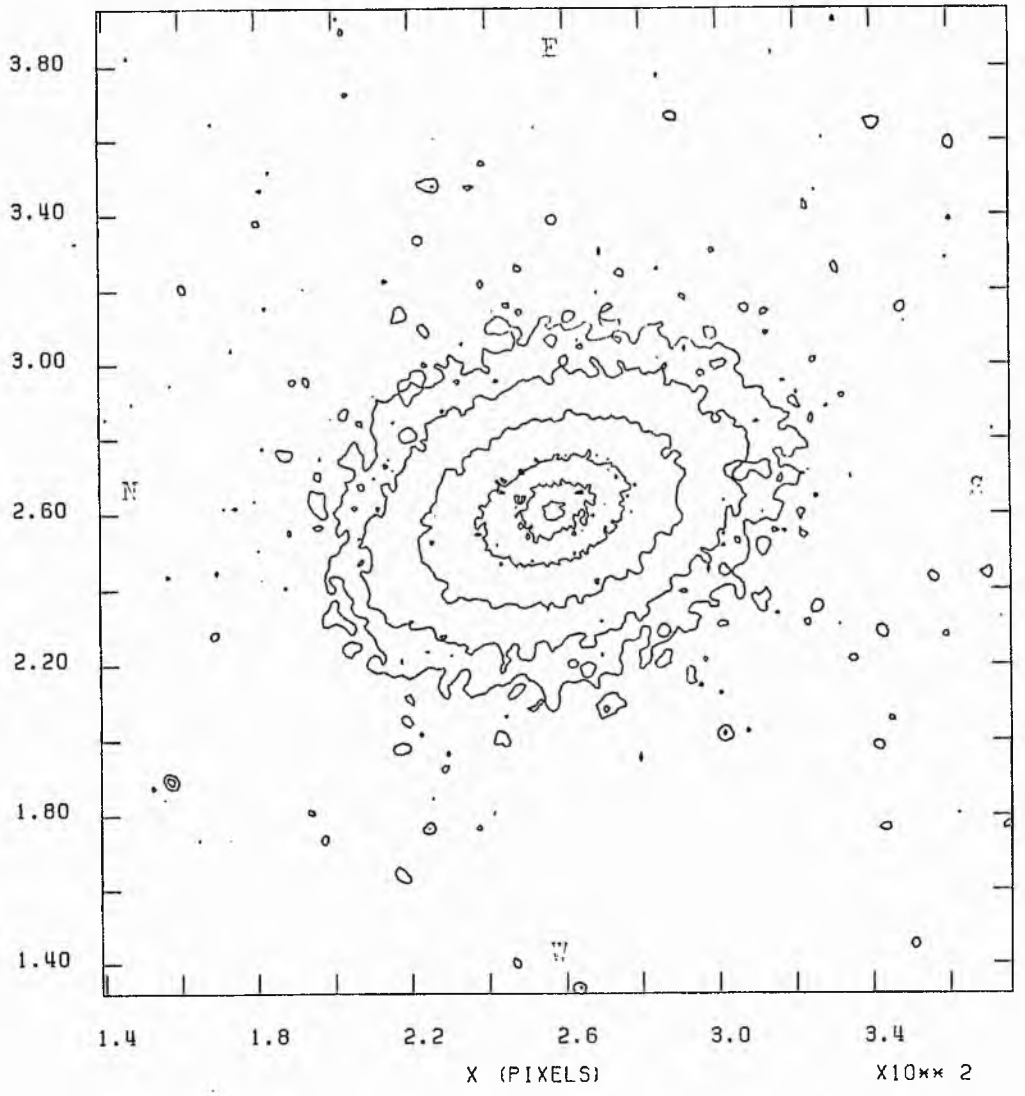

NGC 4550 R (J)

THRESHOLD = 24.00 INCREMENT = 1.00 SKY LEVEL = 20.53

ALL VALUES IN MAGNITUDES / SQUARE ARCSECOND.

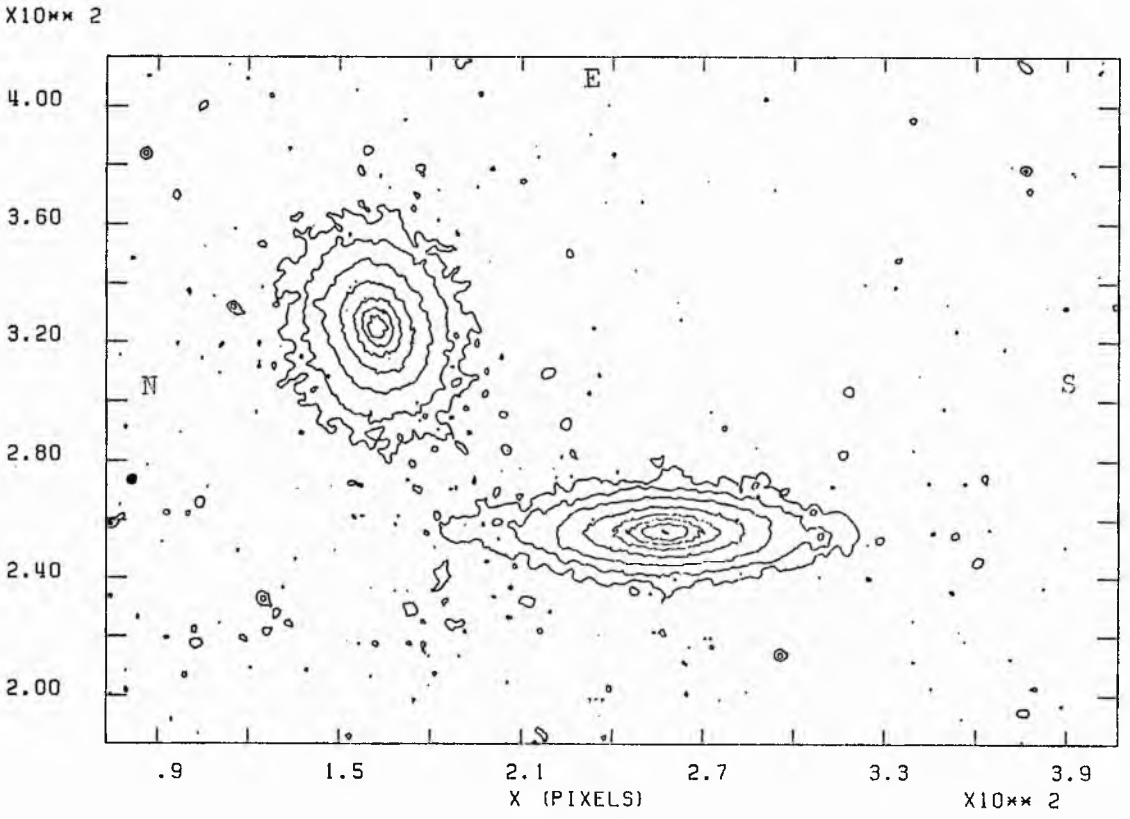

NGC 4552 R (J)

THRESHOLD = 24.00 INCREMENT = 1.00 SKY LEVEL = 20.38

ALL VALUES IN MAGNITUDES / SQUARE ARCSECOND.

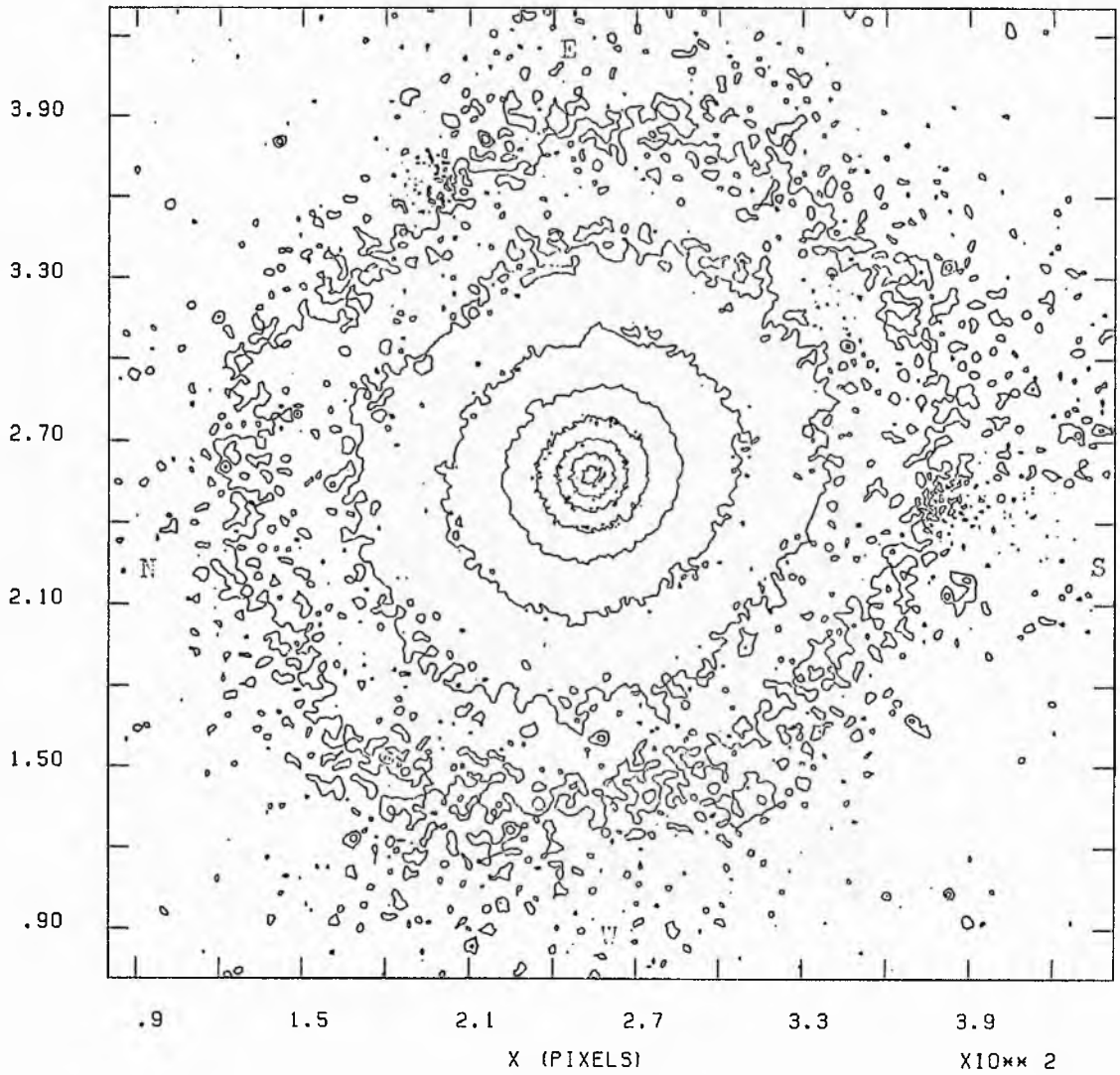

NGC 4267 I (J)

THRESHOLD = 23.50 INCREMENT = 1.00 SKY LEVEL = 19.68

ALL VALUES IN MAGNITUDES / SQUARE ARCSECOND.

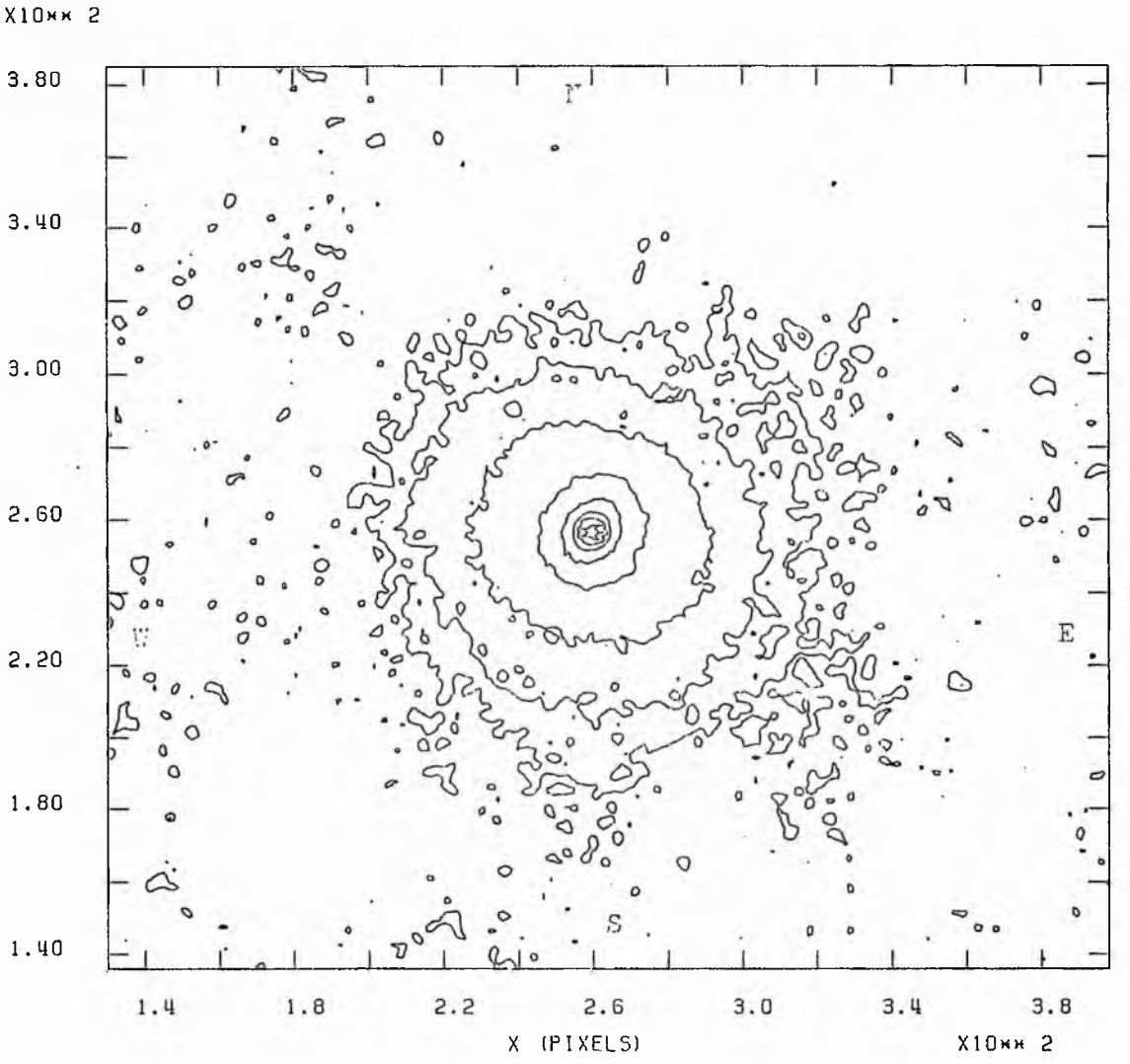

NGC 4371 I (J)

THRESHOLD = 23.50 INCREMENT = 1.00 SKY LEVEL = 19.68

ALL VALUES IN MAGNITUDES / SQUARE ARCSECOND.

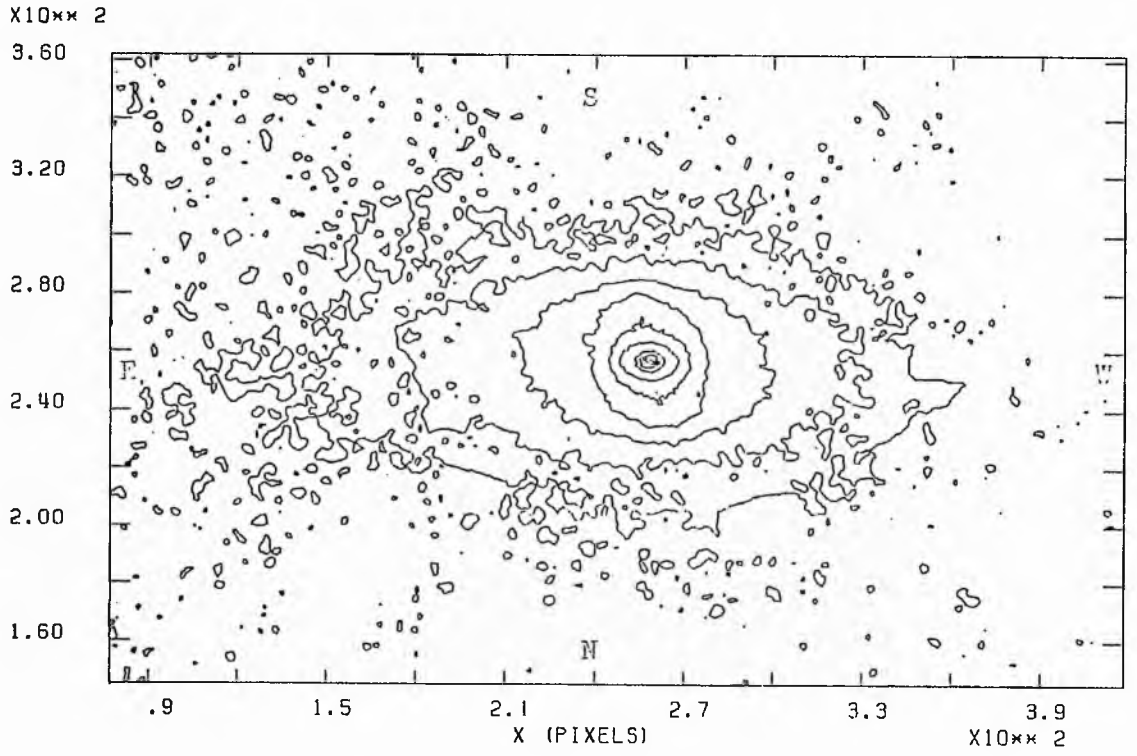

NGC 4377 I (J)

THRESHOLD = 23.50 INCREMENT = 1.00 SKY LEVEL = 19.68

ALL VALUES IN MAGNITUDES / SQUARE ARCSECOND.

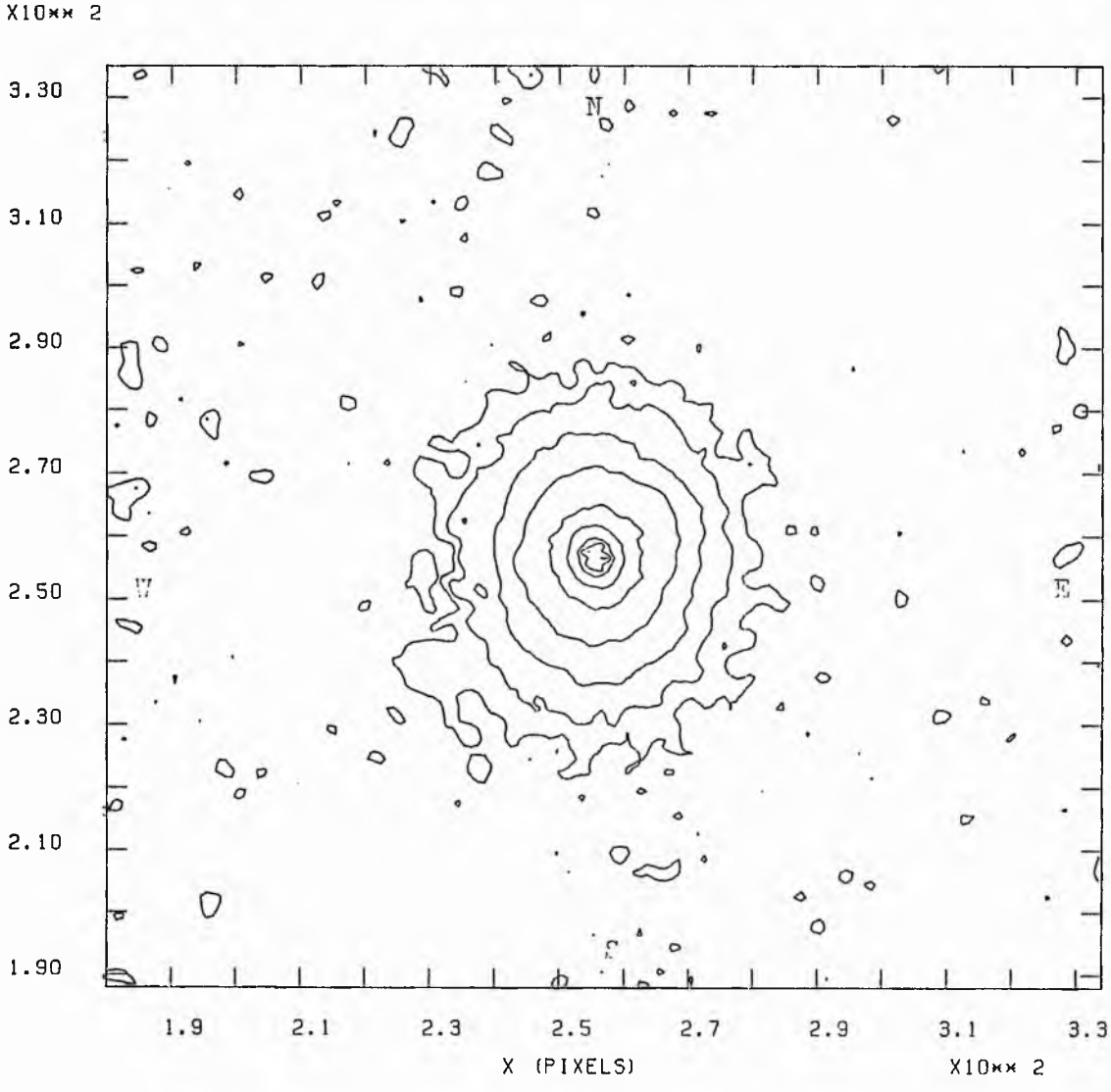

NGC 4419 I (J)

THRESHOLD = 23.50 INCREMENT = 1.00 SKY LEVEL = 19.68

X10** 2 ALL VALUES IN MAGNITUDES / SQUARE ARCSECOND.

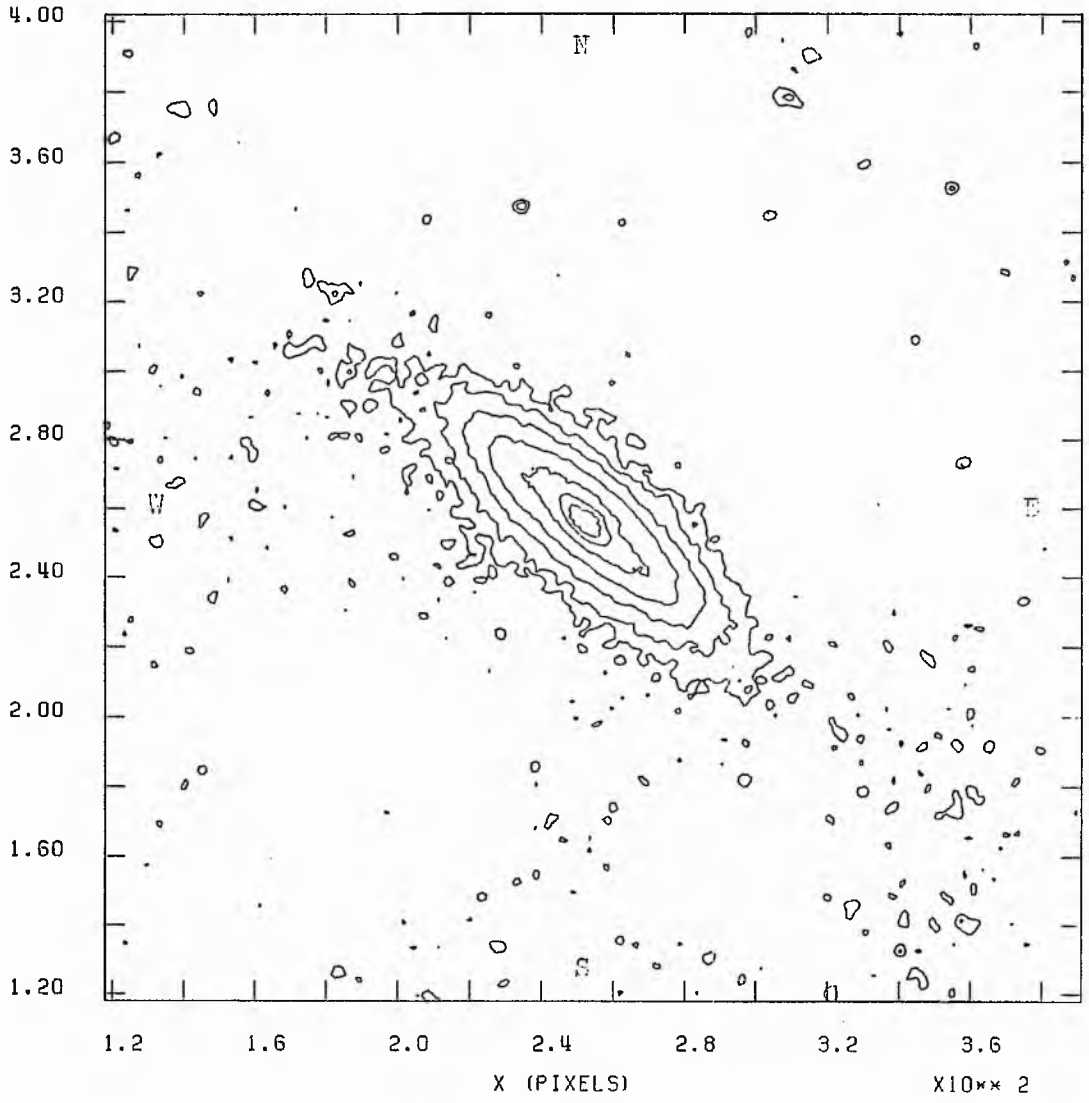

NGC 4425 I (J)

THRESHOLD = 23.50 INCREMENT = 1.00 SKY LEVEL = 19.68

X10** 2 ALL VALUES IN MAGNITUDES / SQUARE ARCSECOND.

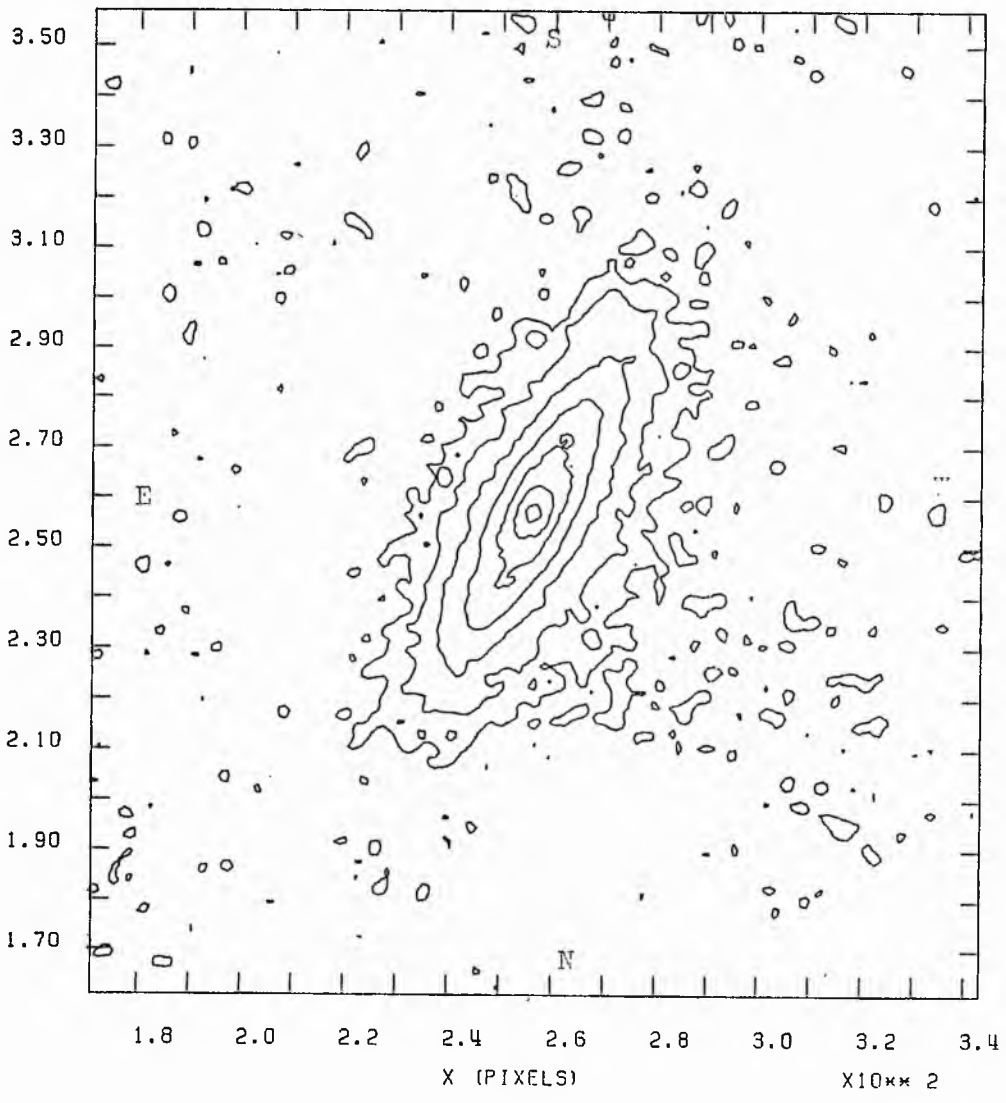

NGC 4429 I (J)

THRESHOLD = 23.50 INCREMENT = 1.00 SKY LEVEL = 19.89

ALL VALUES IN MAGNITUDES / SQUARE ARCSECOND.

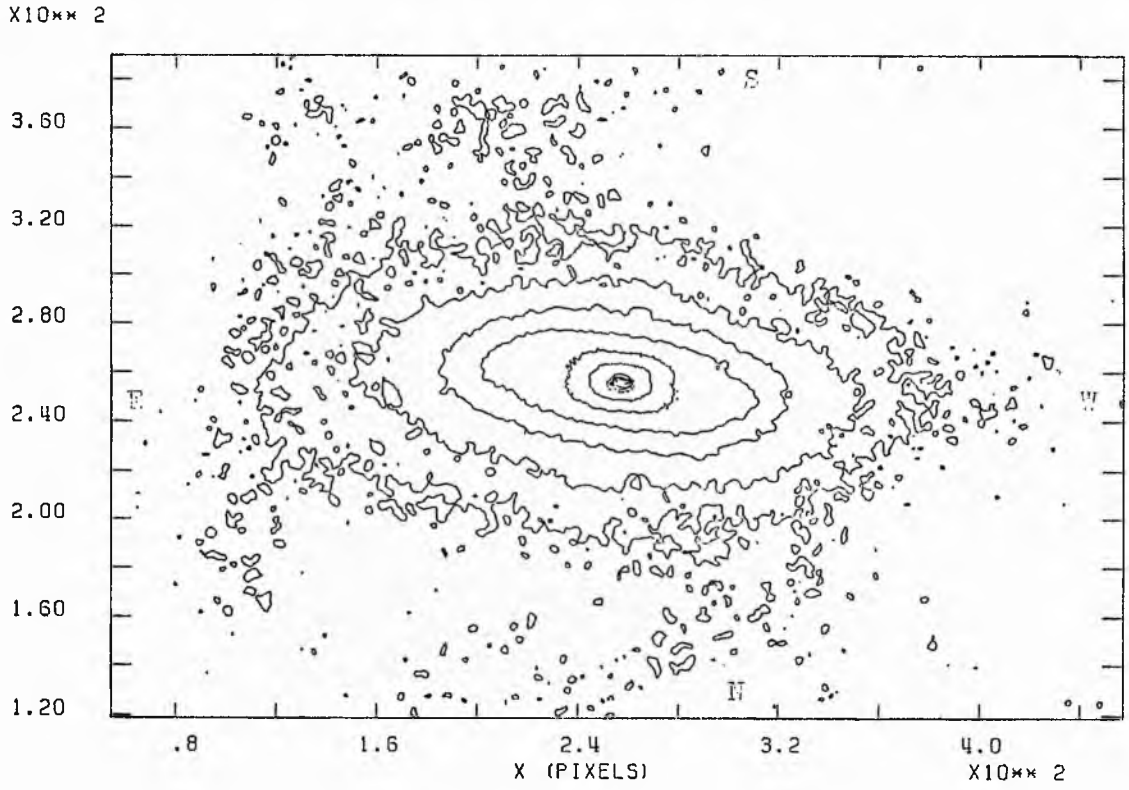

NGC 4435 + 4438 I (J)

THRESHOLD = 23.50 INCREMENT = 1.00 SKY LEVEL = 19.54

X10** 2 ALL VALUES IN MAGNITUDES / SQUARE ARCSECOND.

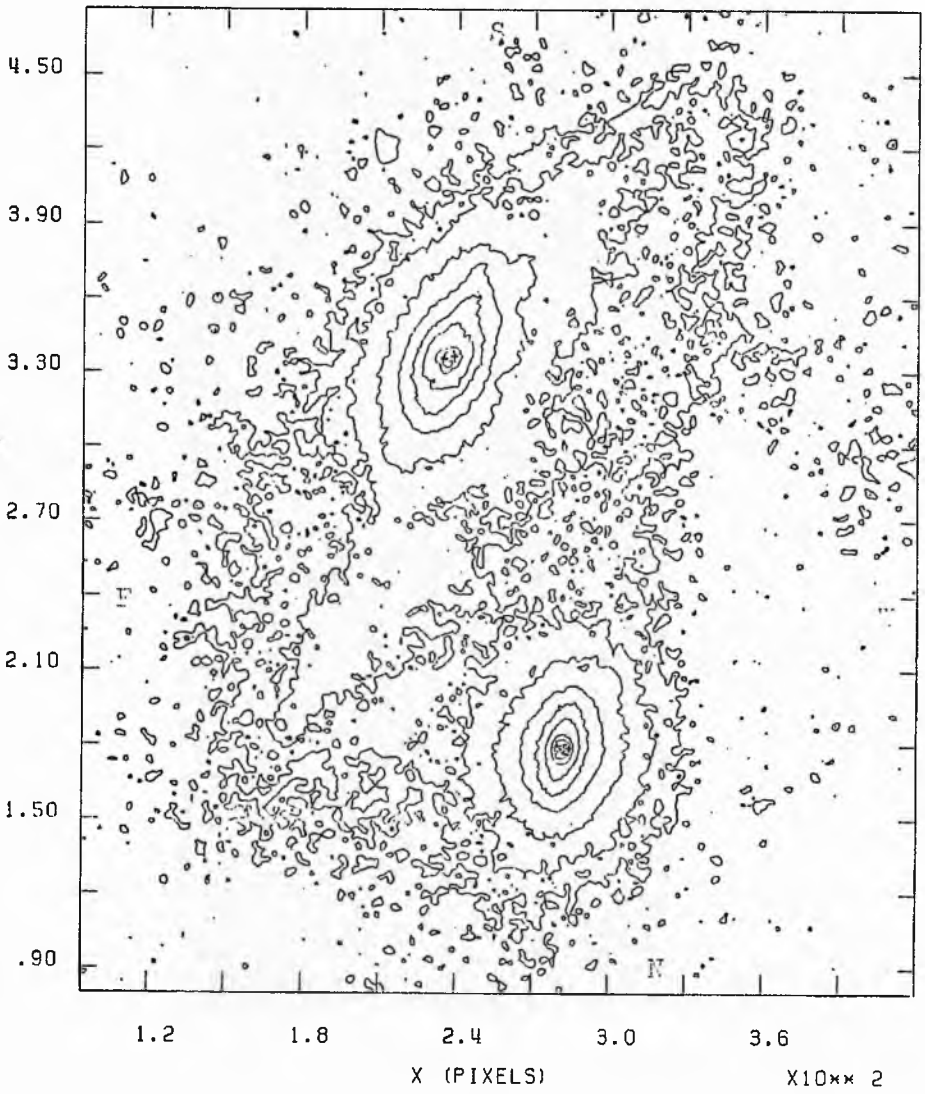

NGC 4459 I (J)

THRESHOLD = 23.50 INCREMENT = 1.00 SKY LEVEL = 19.80

ALL VALUES IN MAGNITUDES / SQUARE ARCSECOND.

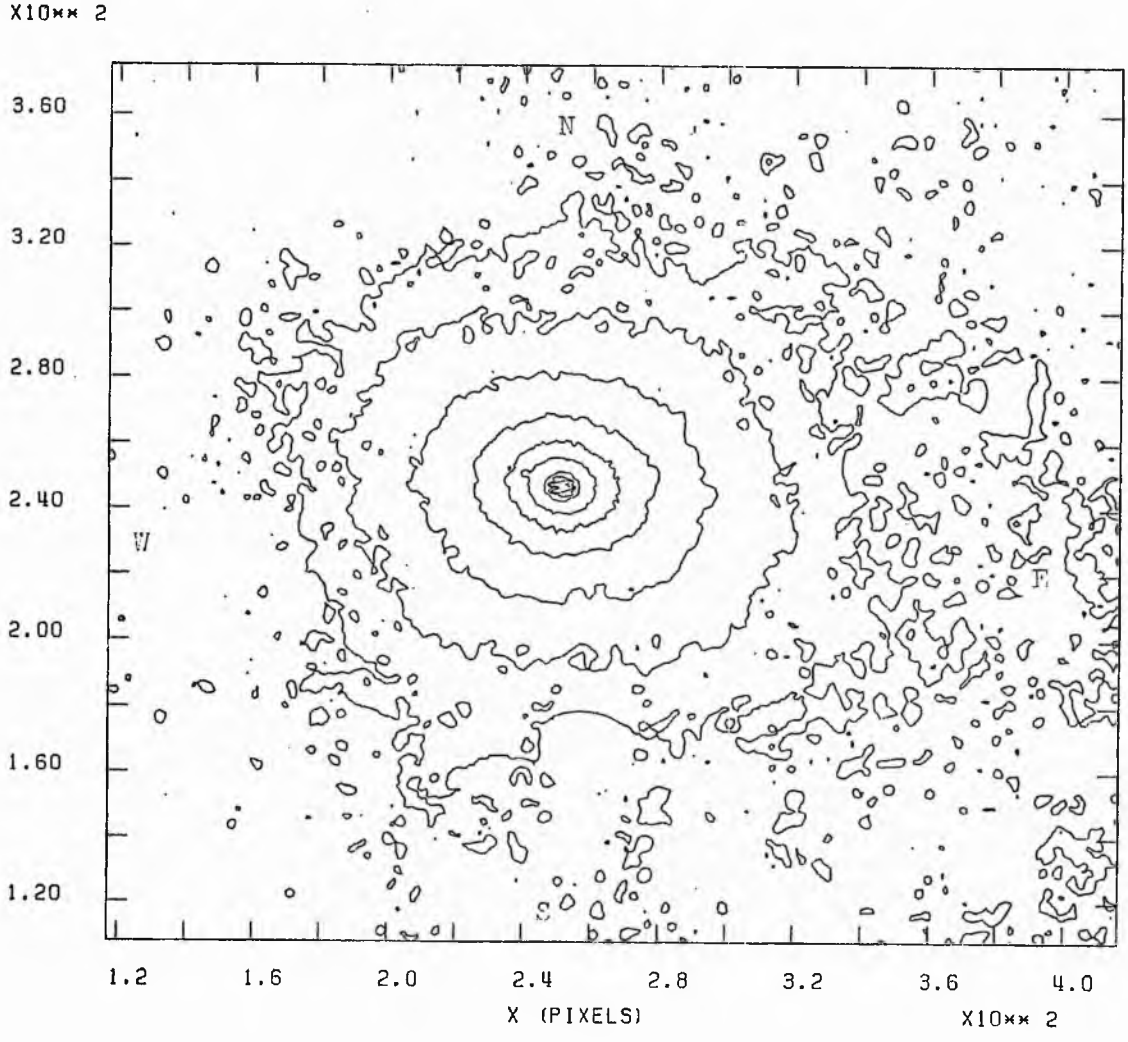

NGC 4461 + 4458 I (J)

THRESHOLD = 23.50 INCREMENT = 1.00 SKY LEVEL = 19.43

X10** 2 ALL VALUES IN MAGNITUDES / SQUARE ARCSECOND.

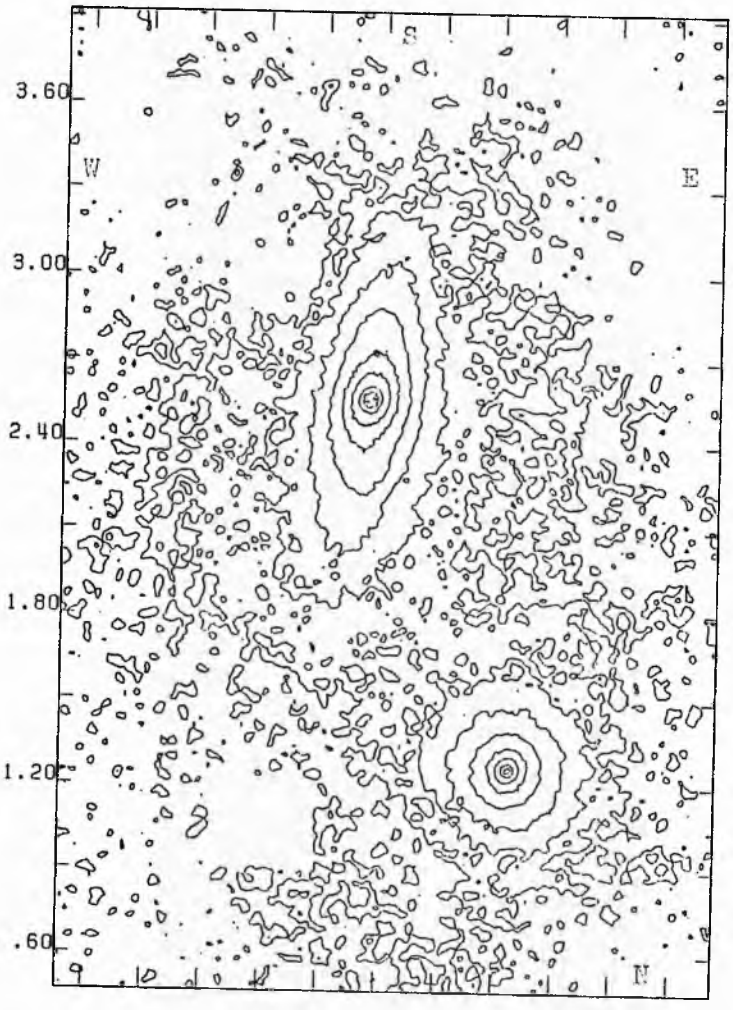

NGC 4474 I (J)

THRESHOLD = 23.50 INCREMENT = 1.00 SKY LEVEL = 19.68

ALL VALUES IN MAGNITUDES / SQUARE ARCSECOND.

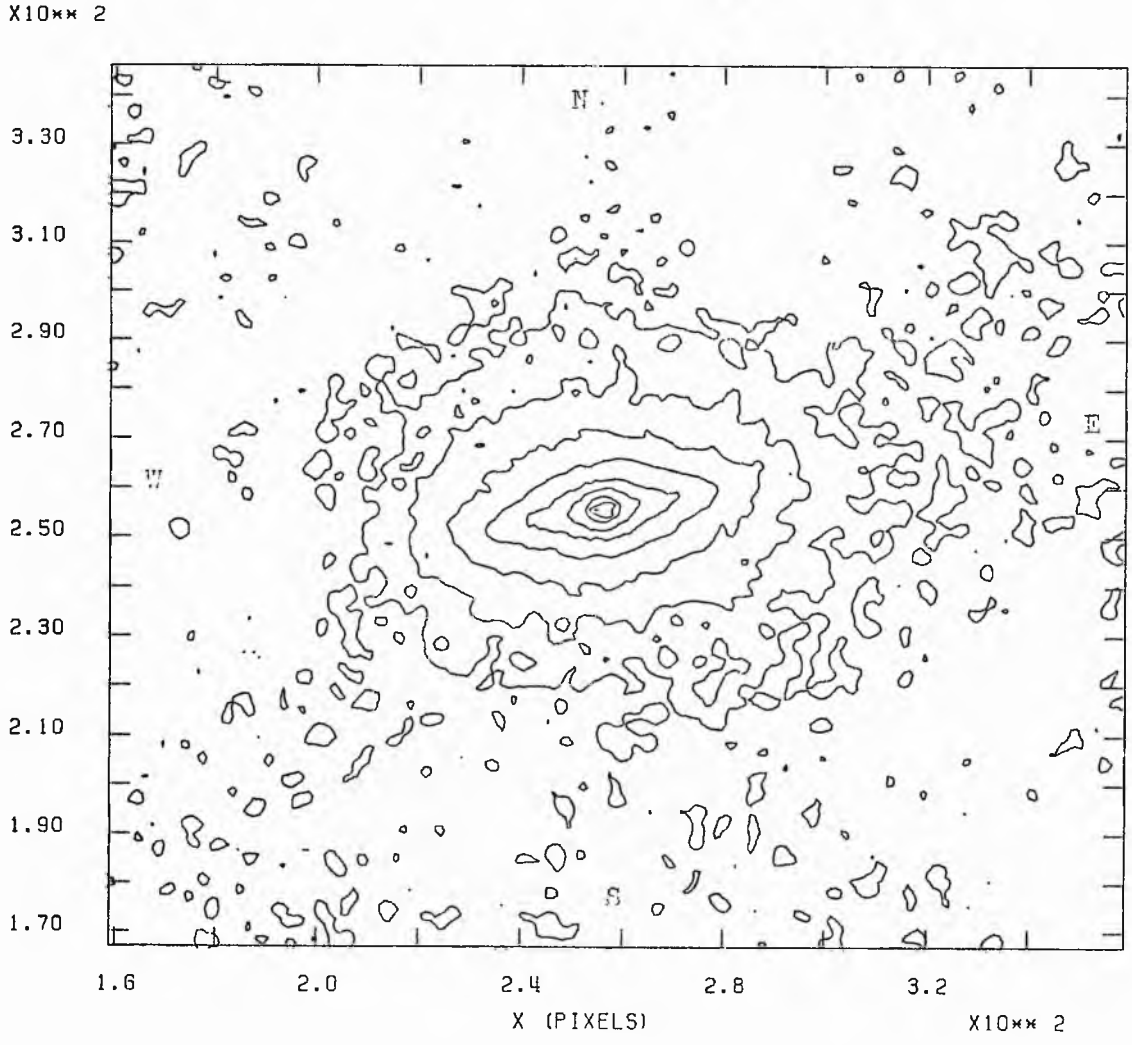

NGC 4477 I (J)

THRESHOLD = 23.50 INCREMENT = 1.00 SKY LEVEL = 19.55

X10** 2 ALL VALUES IN MAGNITUDES / SQUARE ARCSECOND.

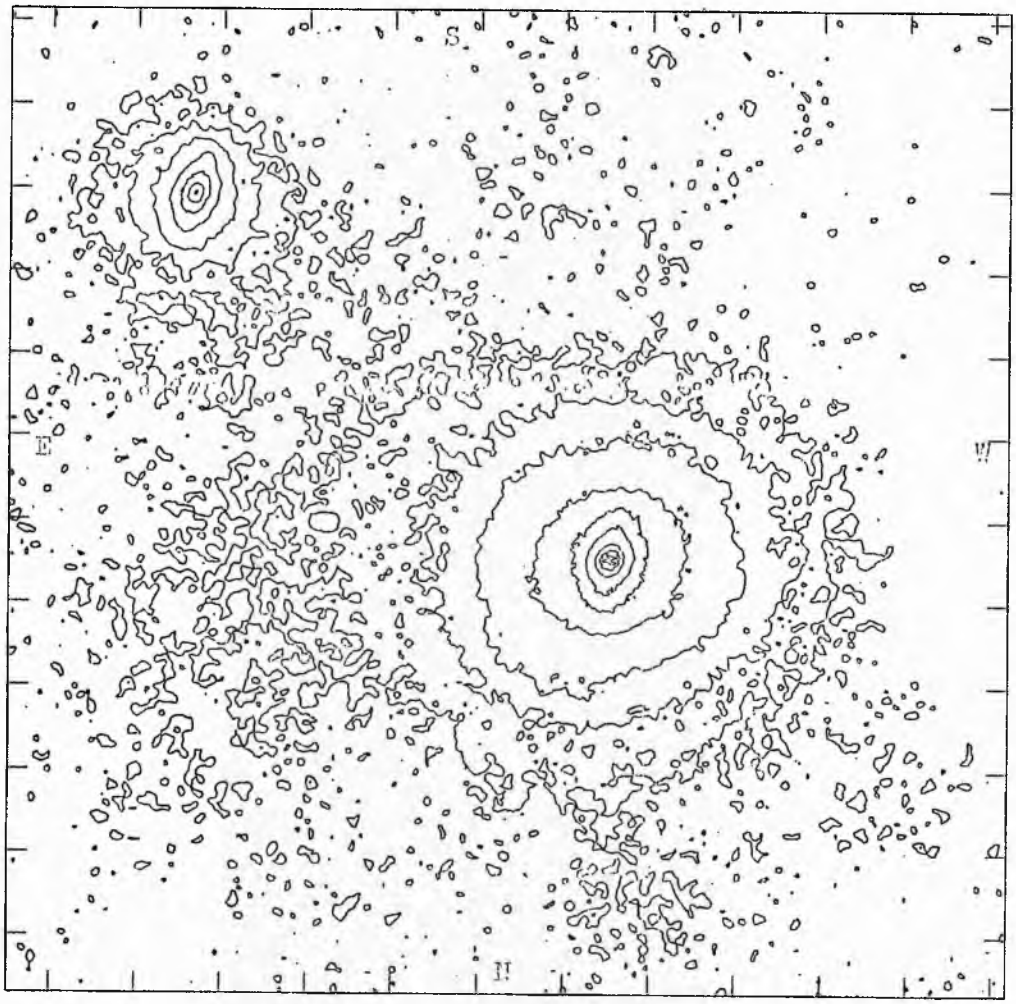

NGC 4501 I (J)

THRESHOLD = 23.50 INCREMENT = 1.00 SKY LEVEL = 19.70

X10** 2 ALL VALUES IN MAGNITUDES / SQUARE ARCSECOND.

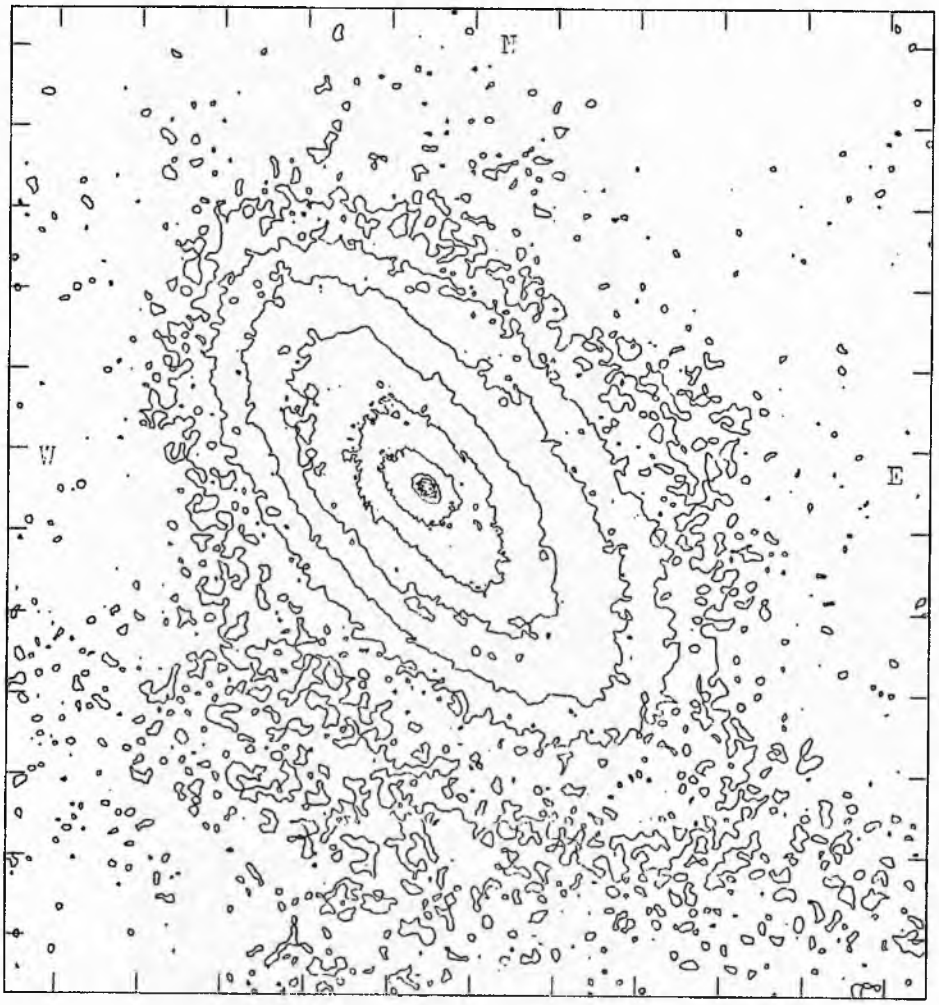

NGC 4503 I (J)

THRESHOLD = 23.50 INCREMENT = 1.00 SKY LEVEL = 19.68

X10** 2 ALL VALUES IN MAGNITUDES / SQUARE ARCSECOND.

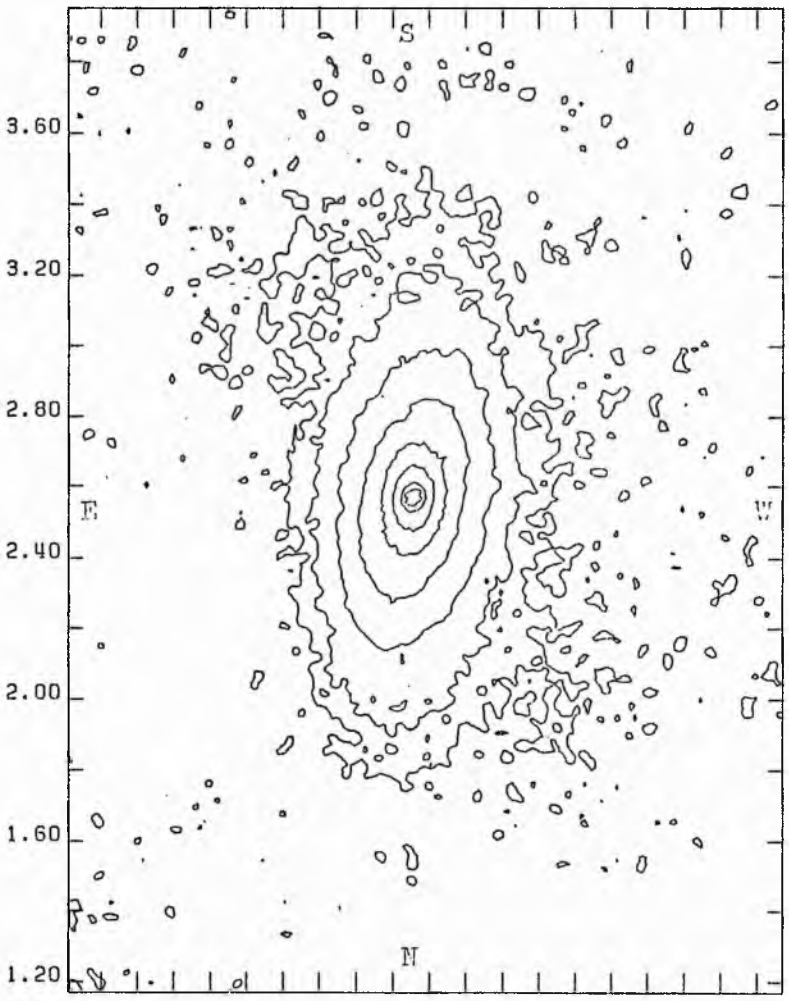

NGC 4531 I (J)

THRESHOLD = 23.50 INCREMENT = 1.00 SKY LEVEL = 19.68

X10** 2 ALL VALUES IN MAGNITUDES / SQUARE ARCSECOND.

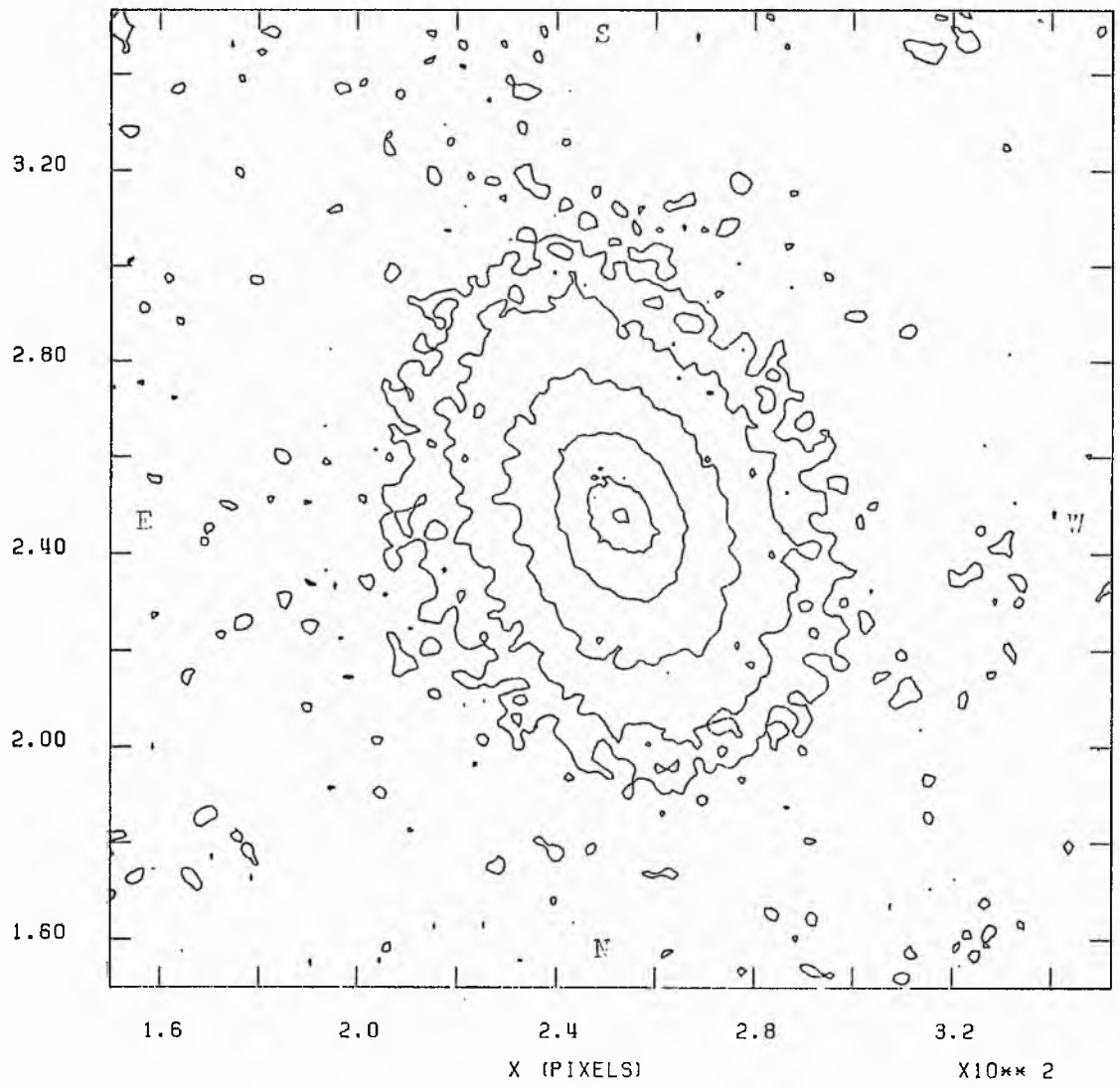

NGC 4550 I (J)

THRESHOLD = 23.50 INCREMENT = 1.00 SKY LEVEL = 19.68

X10** 2 ALL VALUES IN MAGNITUDES / SQUARE ARCSECOND.

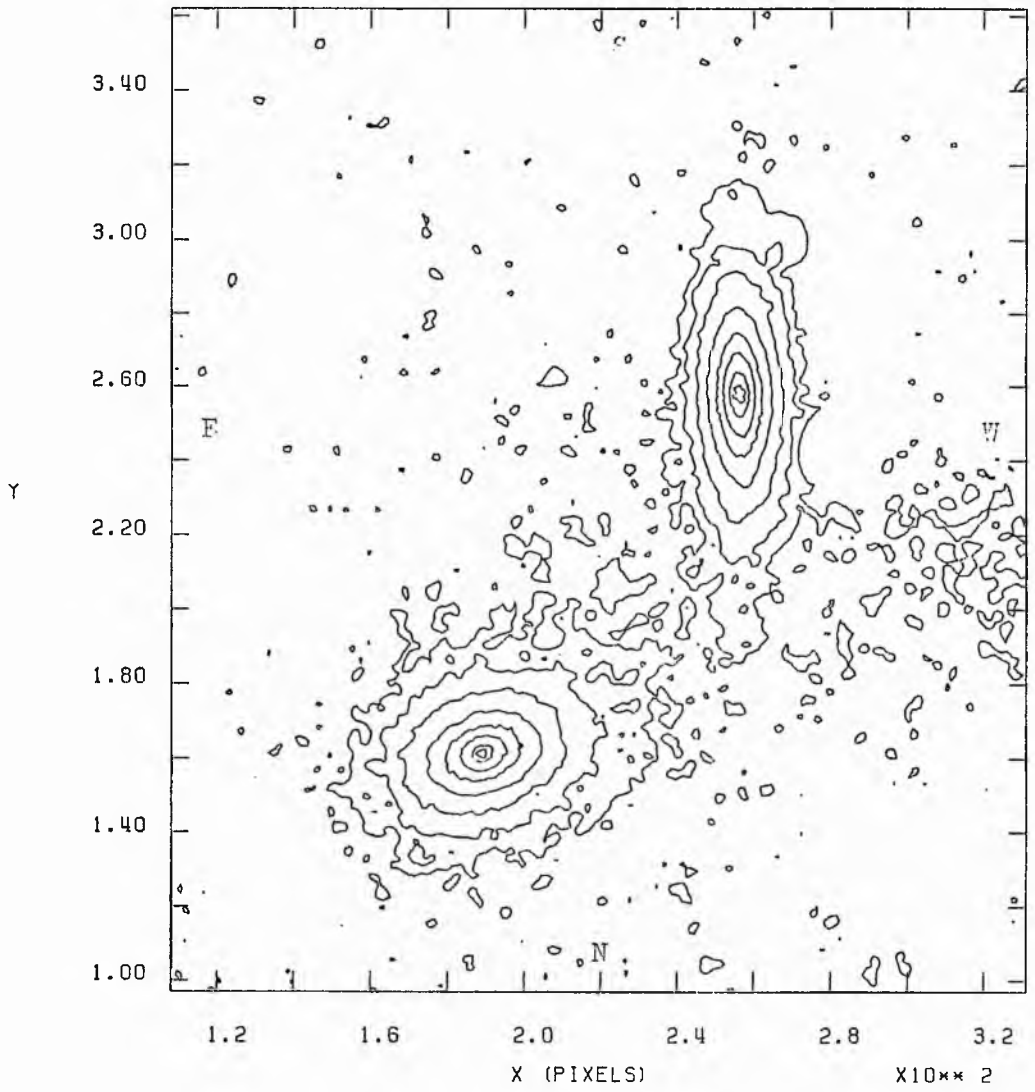

NGC 4552 I (J)

THRESHOLD = 23.50 INCREMENT = 1.00 SKY LEVEL = 19.87

X10** 2 ALL VALUES IN MAGNITUDES / SQUARE ARCSECOND.

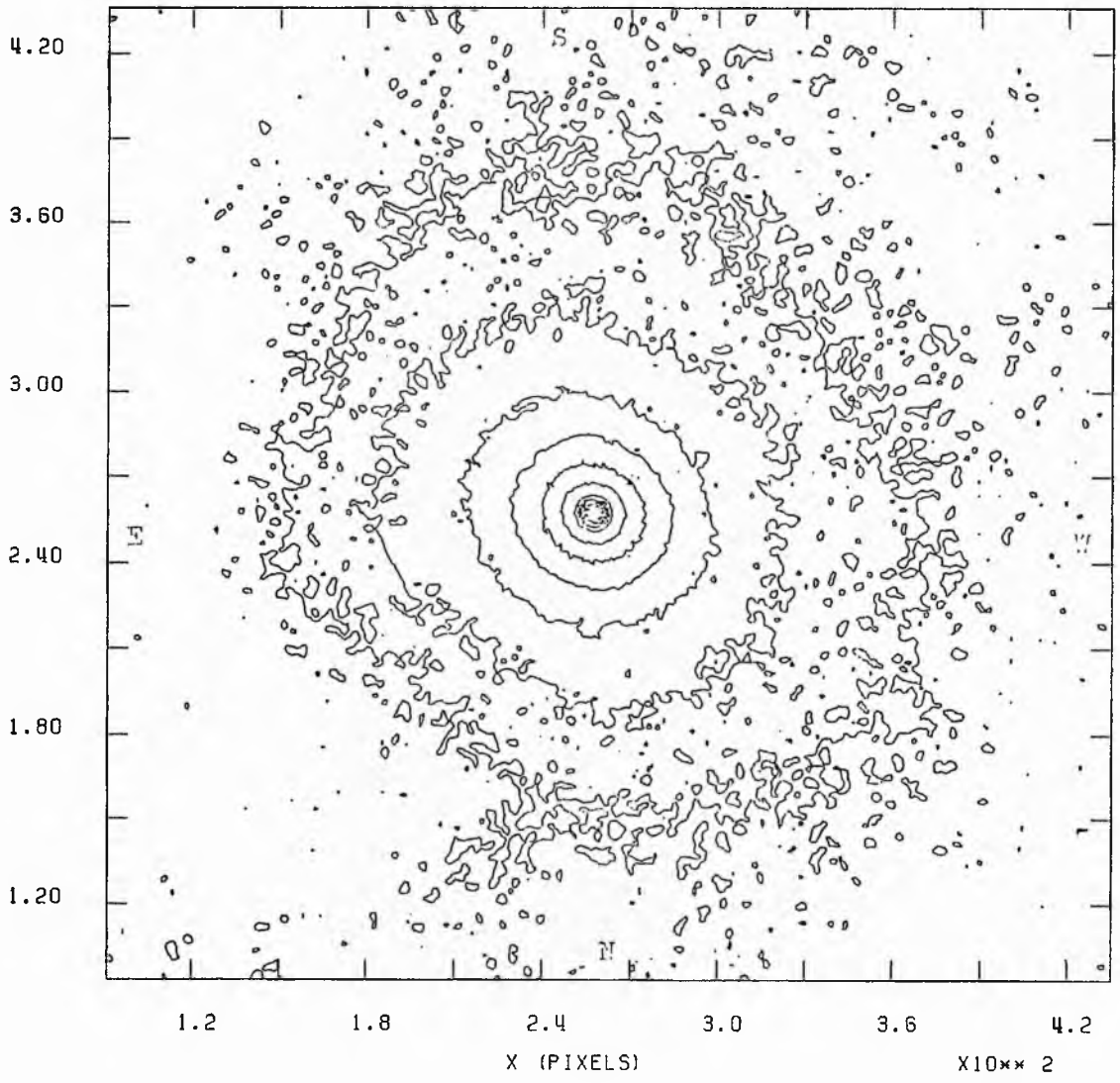

APPENDIX 'E'

B, R and I-Band Integration Tables

Integration table for NGC 4267 B

Log I	A	P	Sum P	K	R*	Rho	Log J	Mu
2.300	0.001		0.000	0.000	0.9	0.045	2.061	17.07
		0.117						
2.100	0.001		0.117	0.020	1.3	0.064	1.861	17.57
		0.244						
2.000	0.004		0.362	0.061	2.0	0.101	1.761	17.82
		0.129						
1.900	0.005		0.491	0.083	2.4	0.120	1.661	18.07
		0.360						
1.800	0.010		0.851	0.144	3.4	0.170	1.561	18.32
		0.122						
1.700	0.012		0.973	0.165	3.7	0.187	1.461	18.57
		0.195						
1.600	0.017		1.168	0.197	4.4	0.217	1.361	18.82
		0.180						
1.500	0.022		1.348	0.228	5.0	0.248	1.261	19.07
		0.143						
1.400	0.027		1.491	0.252	5.5	0.276	1.161	19.32
		0.114						
1.300	0.032		1.605	0.271	6.0	0.301	1.061	19.57
		0.116						
1.200	0.038		1.721	0.291	6.6	0.330	0.961	19.82
		0.123						
1.100	0.047		1.844	0.312	7.3	0.366	0.861	20.07
		0.106						
1.000	0.056		1.950	0.330	8.0	0.401	0.761	20.32
		0.155						
0.900	0.074		2.105	0.356	9.2	0.458	0.661	20.57
		0.092						
0.800	0.087		2.198	0.372	10.0	0.497	0.561	20.82
		0.110						
0.700	0.106		2.308	0.390	11.0	0.550	0.461	21.07
		0.094						
0.600	0.127		2.402	0.406	12.1	0.602	0.361	21.32
		0.126						
0.500	0.162		2.528	0.427	13.6	0.680	0.261	21.57
		0.149						
0.400	0.215		2.677	0.453	15.7	0.783	0.161	21.82
		0.140						
0.300	0.277		2.817	0.476	17.8	0.889	0.061	22.07
		0.231						
0.200	0.406		3.048	0.515	21.6	1.076	-0.039	22.32
		0.138						
0.100	0.503		3.187	0.539	24.0	1.198	-0.139	22.57
		0.229						
0.000	0.706		3.415	0.577	28.4	1.419	-0.239	22.82
		0.303						
-0.100	1.044		3.719	0.629	34.6	1.726	-0.339	23.07
		0.354						
-0.200	1.541		4.073	0.689	42.0	2.096	-0.439	23.32
		0.309						
-0.300	2.087		4.382	0.741	48.9	2.440	-0.539	23.57
		0.314						
-0.400	2.784		4.696	0.794	56.5	2.818	-0.639	23.82
		0.266						
-0.500	3.529		4.961	0.839	63.6	3.173	-0.739	24.07
		0.208						
-0.600	4.261		5.169	0.874	69.9	3.486	-0.839	24.32
		0.183						
-0.700	5.073		5.352	0.905	76.2	3.804	-0.939	24.57

Integration table for NGC 4267 B Continued.

Log I	A	P	Sum P	K	R*	Rho	Log J	Mu
-0.800	5.964		5.512	0.932	82.7	4.124	-1.039	24.82
		0.160						
-0.900	6.863		5.637	0.954	88.7	4.424	-1.139	25.07
		0.128						
-1.000	7.732		5.738	0.970	94.1	4.696	-1.239	25.32
		0.098						
-1.100	8.484		5.805	0.982	98.6	4.919	-1.339	25.57
		0.067						
-1.200	9.228		5.858	0.991	102.8	5.130	-1.439	25.82
		0.053						
-1.300	9.885		5.895	0.997	106.4	5.310	-1.539	26.07
		0.037						
-1.400	10.001		5.901	0.998	107.1	5.341	-1.639	26.32
		0.005						
-1.500	10.204		5.908	0.999	108.1	5.395	-1.739	26.57
		0.007						
		0.006	5.914	1.000				

Sky Constant = 22.82

Integration table for NGC 4371 B

Log I	A	P	Sum P	K	R*	Rho	Log J	Mu
2.000	0.001		0.000	0.000	0.9	0.038	1.683	17.84
		0.129						
1.900	0.002		0.129	0.018	1.6	0.066	1.583	18.09
		0.257						
1.800	0.006		0.386	0.054	2.6	0.108	1.483	18.34
		0.122						
1.700	0.008		0.509	0.071	3.0	0.127	1.383	18.59
		0.097						
1.600	0.010		0.606	0.085	3.4	0.143	1.283	18.84
		0.206						
1.500	0.016		0.812	0.113	4.3	0.179	1.183	19.09
		0.245						
1.400	0.025		1.057	0.148	5.3	0.223	1.083	19.34
		0.260						
1.300	0.036		1.317	0.184	6.4	0.270	0.983	19.59
		0.155						
1.200	0.045		1.472	0.206	7.2	0.301	0.883	19.84
		0.225						
1.100	0.061		1.697	0.237	8.3	0.350	0.783	20.09
		0.212						
1.000	0.079		1.909	0.267	9.5	0.401	0.683	20.34
		0.207						
0.900	0.102		2.116	0.296	10.8	0.455	0.583	20.59
		0.231						
0.800	0.135		2.347	0.328	12.4	0.523	0.483	20.84
		0.224						
0.700	0.174		2.572	0.359	14.1	0.595	0.383	21.09
		0.256						
0.600	0.231		2.828	0.395	16.3	0.685	0.283	21.34
		0.265						
0.500	0.306		3.093	0.432	18.7	0.787	0.183	21.59
		0.292						
0.400	0.409		3.385	0.473	21.6	0.910	0.083	21.84
		0.236						
0.300	0.513		3.621	0.506	24.3	1.020	-0.017	22.09
		0.301						
0.200	0.681		3.921	0.548	27.9	1.175	-0.117	22.34
		0.247						
0.100	0.855		4.168	0.582	31.3	1.316	-0.217	22.59
		0.247						
0.000	1.073		4.415	0.617	35.1	1.475	-0.317	22.84
		0.235						
-0.100	1.336		4.651	0.650	39.1	1.645	-0.417	23.09
		0.276						
-0.200	1.723		4.926	0.688	44.4	1.868	-0.517	23.34
		0.267						
-0.300	2.194		5.193	0.725	50.1	2.109	-0.617	23.59
		0.225						
-0.400	2.695		5.418	0.757	55.6	2.337	-0.717	23.84
		0.198						
-0.500	3.248		5.616	0.784	61.0	2.566	-0.817	24.09
		0.222						
-0.600	4.030		5.838	0.815	68.0	2.858	-0.917	24.34
		0.212						
-0.700	4.971		6.050	0.845	75.5	3.174	-1.017	24.59
		0.183						
-0.800	5.991		6.233	0.871	82.9	3.484	-1.117	24.84
		0.164						
-0.900	7.141		6.396	0.893	90.5	3.804	-1.217	25.09

Integration table for NGC 4371 B Continued.

Log I	A	P	Sum P	K	R*	Rho	Log J	Mu
-1.000	8.533		6.553	0.915	98.9	4.158	-1.317	25.34
		0.157						
-1.100	10.043		6.689	0.934	107.3	4.511	-1.417	25.59
		0.135						
-1.200	11.718		6.808	0.951	115.9	4.873	-1.517	25.84
		0.119						
-1.300	13.366		6.901	0.964	123.8	5.204	-1.617	26.09
		0.093						
-1.400	15.194		6.984	0.975	132.0	5.549	-1.717	26.34
		0.082						
-1.500	16.644		7.035	0.983	138.1	5.808	-1.817	26.59
		0.052						
-1.600	17.718		7.066	0.987	142.5	5.992	-1.917	26.84
		0.030						
-1.700	18.732		7.089	0.990	146.5	6.161	-2.017	27.09
		0.023						
-1.800	19.824		7.108	0.993	150.7	6.338	-2.117	27.34
		0.020						
-1.900	20.573		7.119	0.994	153.5	6.457	-2.217	27.59
		0.011						
-2.000	21.616		7.131	0.996	157.4	6.618	-2.317	27.84
		0.012						
		0.029						
			7.160	1.000				

Sky Constant = 22.84

Integration table for NGC 4377 B

Log I	A	P	Sum P	K	R*	Rho	Log J	Mu
2.200	0.001		0.000	0.000	0.9	0.109	1.398	17.38
		0.307						
2.100	0.003		0.307	0.097	1.8	0.219	1.298	17.63
		0.081						
2.000	0.004		0.389	0.123	2.0	0.245	1.198	17.88
		0.259						
1.900	0.006		0.648	0.205	2.7	0.328	1.098	18.13
		0.051						
1.800	0.007		0.699	0.221	2.9	0.346	0.998	18.38
		0.082						
1.700	0.009		0.781	0.247	3.1	0.379	0.898	18.63
		0.130						
1.600	0.012		0.910	0.288	3.6	0.438	0.798	18.88
		0.077						
1.500	0.014		0.987	0.313	4.0	0.477	0.698	19.13
		0.082						
1.400	0.017		1.069	0.339	4.4	0.525	0.598	19.38
		0.065						
1.300	0.019		1.134	0.359	4.7	0.568	0.498	19.63
		0.142						
1.200	0.027		1.276	0.404	5.6	0.674	0.398	19.88
		0.041						
1.100	0.030		1.317	0.417	5.9	0.709	0.298	20.13
		0.073						
1.000	0.037		1.390	0.440	6.5	0.781	0.198	20.38
		0.103						
0.900	0.048		1.494	0.473	7.4	0.896	0.098	20.63
		0.087						
0.800	0.061		1.581	0.501	8.3	1.003	-0.002	20.88
		0.106						
0.700	0.079		1.687	0.534	9.5	1.147	-0.102	21.13
		0.130						
0.600	0.108		1.817	0.575	11.1	1.340	-0.202	21.38
		0.108						
0.500	0.138		1.925	0.610	12.6	1.516	-0.302	21.63
		0.186						
0.400	0.204		2.111	0.668	15.3	1.840	-0.402	21.88
		0.110						
0.300	0.253		2.222	0.703	17.0	2.050	-0.502	22.13
		0.121						
0.200	0.321		2.343	0.742	19.2	2.308	-0.602	22.38
		0.125						
0.100	0.409		2.468	0.781	21.6	2.605	-0.702	22.63
		0.090						
0.000	0.488		2.558	0.810	23.6	2.847	-0.802	22.89
		0.074						
-0.100	0.570		2.631	0.833	25.6	3.077	-0.902	23.13
		0.058						
-0.200	0.632		2.689	0.852	27.3	3.289	-1.002	23.38
		0.058						
-0.300	0.734		2.747	0.870	29.4	3.538	-1.102	23.63
		0.055						
-0.400	0.876		2.802	0.887	31.7	3.813	-1.202	23.88
		0.046						
-0.500	1.005		2.848	0.902	33.9	4.085	-1.302	24.13
		0.039						
-0.600	1.143		2.887	0.914	36.2	4.356	-1.402	24.38
		0.034						
-0.700	1.295		2.922	0.925	38.5	4.637	-1.502	24.63

Integration table for NGC 4377 B Continued.

Log I	A	P	Sum P	K	R*	Rho	Log J	Mu
		0.030						
-0.800	1.465		2.952	0.935	41.0	4.932	-1.602	24.88
		0.033						
-0.900	1.698		2.985	0.945	44.1	5.310	-1.702	25.13
		0.031						
-1.000	1.973		3.016	0.955	47.5	5.724	-1.802	25.38
		0.029						
-1.100	2.291		3.045	0.964	51.2	6.167	-1.902	25.63
		0.031						
-1.200	2.733		3.076	0.974	56.0	6.736	-2.002	25.88
		0.022						
-1.300	3.118		3.098	0.981	59.8	7.196	-2.102	26.13
		0.025						
-1.400	3.669		3.123	0.989	64.8	7.805	-2.202	26.38
		0.007						
-1.500	3.863		3.130	0.991	66.5	8.009	-2.302	26.63
		0.009						
-1.600	4.174		3.138	0.994	69.2	8.325	-2.402	26.88
		0.008						
-1.700	4.530		3.146	0.996	72.0	8.673	-2.502	27.13
		0.004						
-1.800	4.739		3.150	0.997	73.7	8.870	-2.602	27.38
		0.002						
-1.900	4.904		3.153	0.998	75.0	9.024	-2.702	27.63
		0.006						
			3.158	1.000				

Sky Constant = 22.88

Integration table for NGC 4419 B

Log I	A	P	Sum P	K	R*	Rho	Log J	Mu
2.000	0.001		0.000	0.000	0.9	0.053	1.426	17.85
		0.162						
1.700	0.003		0.162	0.031	1.8	0.107	1.126	18.60
		0.227						
1.600	0.008		0.389	0.075	3.0	0.177	1.026	18.85
		0.283						
1.500	0.016		0.673	0.130	4.3	0.250	0.926	19.10
		0.225						
1.400	0.024		0.898	0.173	5.2	0.306	0.826	19.35
		0.130						
1.300	0.030		1.028	0.198	5.8	0.341	0.726	19.60
		0.219						
1.200	0.042		1.247	0.240	6.9	0.406	0.626	19.85
		0.195						
1.100	0.056		1.442	0.278	8.0	0.468	0.526	20.10
		0.130						
1.000	0.067		1.572	0.303	8.8	0.514	0.426	20.35
		0.155						
0.900	0 084		1.727	0.333	9.8	0.577	0.326	20.60
		0.195						
0.800	0.112		1.923	0.371	11.3	0.664	0.226	20.85
		0.220						
0.700	0.151		2.143	0.413	13.1	0.771	0.126	21.10
		0.383						
0.600	0.236		2.526	0.487	16.4	0.964	0.026	21.35
		0.258						
0.500	0.308		2.783	0.536	18.8	1.102	-0.074	21.60
		0.346						
0.400	0.430		3.127	0.603	22.2	1.302	-0.174	21.85
		0.367						
0.300	0.593		3.496	0.674	26.1	1.529	-0.274	22.10
		0.293						
0.200	0.756		3.789	0.730	29.4	1.727	-0.374	22.35
		0.140						
0.100	0.855		3.930	0.757	31.3	1.836	-0.474	22.60
		0.137						
0.000	0.976		4.066	0.784	33.4	1.962	-0.574	22.85
		0.132						
-0.100	1.123		4.198	0.809	35.9	2.104	-0.674	23.10
		0.105						
-0.200	1.271		4.304	0.829	38.2	2.239	-0.774	23.35
		0.083						
-0.300	1.418		4.387	0.846	40.3	2.365	-0.874	23.60
		0.071						
-0.400	1.577		4.458	0.859	42.5	2.493	-0.974	23.85
		0.071						
-0.500	1.777		4.530	0.873	45.1	2.646	-1.074	24.10
		0.062						
-0.600	1.994		4.591	0.885	47.8	2.804	-1.174	24.35
		0.058						
-0.700	2.250		4.649	0.896	50.8	2.979	-1.274	24.60
		0.055						
-0.800	2.558		4.704	0.907	54.1	3.176	-1.374	24.85
		0.047						
-0.900	2.891		4.751	0.916	57.6	3.376	-1.474	25.10
		0.065						
-1.000	3.467		4.816	0.928	63.0	3.697	-1.574	25.35
		0.075						
-1.100	4.307		4.892	0.943	70.2	4.120	-1.674	25.60

Integration table for NGC 4419 B Continued.

Log I	A	P	Sum P	K	R*	Rho	Log J	Mu
		0.062						
-1.200	5.174		4.954	0.955	77.0	4.516	-1.774	25.85
		0.081						
-1.300	6.600		5.034	0.970	87.0	5.101	-1.874	26.10
		0.039						
-1.400	7.459		5.073	0.978	92.5	5.423	-1.974	26.35
		0.034						
-1.500	8.423		5.107	0.984	98.2	5.762	-2.074	26.60
		0.037						
-1.600	9.729		5.144	0.992	105.6	6.193	-2 174	26.85
		0.017						
-1.700	10.467		5.161	0.995	109.5	6.424	-2 274	27.10
		0.006						
-1.800	10.807		5.167	0.996	111.3	6.527	-2.374	27.35
		0.008						
-1.900	11.373		5.175	0.997	114.2	6.696	-2.474	27.60
		0.005						
-2.000	11.812		5.180	0.998	116.3	6.824	-2.574	27.85
		0.008						
			5.188	1.000				

Sky Constant = 22.85

Integration table for NGC 4425 B

Log I	A	P	Sum P	K	R*	Rho	Log J	Mu
1.600	0.001		0.000	0.000	1.3	0.082	1.174	18.80
		0.077						
1.500	0.004		0.077	0.030	2.0	0.129	1.074	19.05
		0.020						
1.400	0.004		0.098	0.038	2.2	0.142	0.974	19.30
		0.065						
1.300	0.007		0.163	0.063	2.9	0.183	0.874	19.55
		0.077						
1.200	0.012		0.240	0.093	3.6	0.231	0.774	19.80
		0.072						
1.100	0.017		0.312	0.121	4.4	0.278	0.674	20.05
		0.114						
1.000	0.027		0.426	0.166	5.5	0.352	0.574	20.30
		0.110						
0.900	0.039		0.536	0.208	6.7	0.425	0.474	20.55
		0.149						
0.800	0.060		0.685	0.266	8.3	0.527	0.374	20.80
		0.126						
0.700	0.082		0.811	0.315	9.7	0.618	0.274	21.05
		0.162						
0.600	0.118		0.973	0.378	11.6	0.741	0.174	21.30
		0.160						
0.500	0.163		1.133	0.440	13.7	0.870	0.074	21.55
		0.196						
0.400	0.232		1.327	0.517	16.3	1.038	-0.026	21.80
		0.107						
0.300	0.280		1.435	0.558	17.9	1.140	-0.126	22.05
		0.117						
0.200	0.345		1.554	0.604	19.9	1.267	-0.226	22.30
		0.115						
0.100	0.426		1.669	0.649	22.1	1.407	-0.326	22.55
		0.093						
0.000	0.508		1.761	0.685	24.1	1.537	-0.426	22.80
		0.074						
-0.100	0.591		1.836	0.714	26.0	1.657	-0.526	23.05
		0.081						
-0.200	0.705		1.917	0.745	28.4	1.810	-0.626	23.30
		0.076						
-0.300	0.840		1.993	0.775	31.0	1.975	-0.726	23.55
		0.066						
-0.400	0.988		2.060	0.801	33.6	2.142	-0.826	23.80
		0.061						
-0.500	1.157		2.120	0.824	36.4	2.318	-0.926	24.05
		0.054						
-0.600	1.346		2.174	0.845	39.3	2.501	-1.026	24.30
		0.053						
-0.700	1.581		2.227	0.866	42.6	2.710	-1.126	24.55
		0.053						
-0.800	1.878		2.280	0.886	46.4	2.954	-1.226	24.80
		0.061						
-0.900	2.310		2.341	0.910	51.5	3.276	-1.326	25.05
		0.065						
-1.000	2.883		2.406	0.935	57.5	3.660	-1.426	25.30
		0.047						
-1.100	3.412		2.454	0.954	62.5	3.981	-1.526	25.55
		0.036						
-1.200	3.910		2.489	0.968	66.9	4.262	-1.626	25.80
		0.027						
-1.300	4.381		2.516	0.978	70.9	4.511	-1.726	26.05

Integration table for NGC 4425 B Continued.

Log I	A	P	Sum P	K	R*	Rho	Log J	Mu
-1.400	4.734		2.532	0.984	73.7	4.690	-1.826	26.30
		0.016						
-1.500	5.092		2.544	0.989	76.4	4.864	-1.926	26.55
		0.013						
-1.600	5.385		2.553	0.992	78.6	5.002	-2.026	26.80
		0.008						
-1.700	5.695		2.560	0.995	80.8	5.144	-2.126	27.05
		0.007						
-1.800	5.886		2.563	0.996	82.1	5.229	-2.226	27.30
		0.003						
-1.900	6.170		2.567	0.998	84.1	5.354	-2.326	27.55
		0.004						
-2.000	6.296		2.569	0.998	84.9	5.408	-2.426	27.80
		0.001						
		0.004						
			2.573	1.000				

Sky Constant = 22.80

Integration table for NGC 4429 B

Log I	A	P	Sum P	K	R*	Rho	Log J	Mu
2.100	0.001		0.000	0.000	0.9	0.026	1.772	17.66
		0.222						
1.900	0.003		0.222	0.017	1.8	0.052	1.572	18.16
		0.205						
1.800	0.006		0.427	0.033	2.6	0.074	1.472	18.41
		0.082						
1.700	0.007		0.509	0.039	2.9	0.082	1.372	18.66
		0.259						
1.600	0.013		0.768	0.060	3.9	0.110	1 272	18.91
		0.103						
1.500	0.016		0.871	0.068	4.3	0.122	1.172	19.16
		0.266						
1.400	0.025		1.137	0.088	5.4	0.154	1.072	19.41
		0.227						
1.300	0.035		1.365	0.106	6.4	0.182	0.972	19.66
		0.335						
1.200	0.054		1.700	0.132	7.9	0.225	0.872	19.91
		0.441						
1.100	0.085		2.141	0.166	9.9	0.283	0.772	20.16
		0.578						
1.000	0.136		2.719	0.211	12.5	0.358	0.672	20.41
		0.524						
0.900	0.195		3.243	0.252	14.9	0.428	0.572	20.66
		0.509						
0.800	0.266		3.751	0.291	17.5	0.500	0.472	20.91
		0.506						
0.700	0.355		4.257	0.330	20.2	0.578	0.372	21.16
		0.444						
0.600	0.454		4.701	0.365	22.8	0.654	0.272	21.41
		0.626						
0.500	0.629		5.327	0.413	26.9	0.769	0.172	21.66
		0.587						
0.400	0.836		5.914	0.459	31.0	0.887	0.072	21.91
		0.773						
0.300	1.179		6.687	0.519	36.8	1.053	-0.028	22.16
		1.106						
0.200	1.797		7.793	0.605	45.4	1.300	-0.128	22.41
		0.677						
0.100	2.273		8.470	0.657	51.0	1.462	-0.228	22.66
		0.476						
0.000	2.695		8.947	0.694	55.6	1.592	-0.328	22.91
		0.387						
-0.100	3.126		9.333	0.724	59.9	1.715	-0.428	23.16
		0.346						
-0.200	3.611		9.679	0.751	64.3	1.843	-0.528	23.41
		0.319						
-0.300	4.175		9.998	0.776	69.2	1.982	-0.628	23.66
		0.358						
-0.400	4.971		10.356	0.803	75.5	2.162	-0.728	23.91
		0.371						
-0.500	6.009		10.727	0.832	83.0	2.377	-0.828	24.16
		0.342						
-0.600	7.213		11.068	0.859	90.9	2.605	-0.928	24.41
		0.305						
-0.700	8.566		11.373	0.882	99.1	2.838	-1.028	24.66
		0.298						
-0.800	10.232		11.671	0.906	108.3	3.102	-1.128	24.91
		0.276						
-0.900	12.174		11.948	0.927	118.1	3.384	-1.228	25.16

Integration table for NGC 4429 B Continued.

Log I	A	P	Sum P	K	R*	Rho	Log J	Mu
		0.228						
-1.000	14.192		12.176	0.945	127.5	3.654	-1.328	25.41
		0.209						
-1.100	16.525		12.385	0.961	137.6	3.942	-1.428	25.66
		0.157						
-1.200	18.729		12.542	0.973	146.5	4.197	-1.528	25.91
		0.114						
-1.300	20.743		12.656	0.982	154.2	4.417	-1.628	26.16
		0.078						
-1.400	22.480		12.734	0.988	160.5	4.598	-1.728	26.41
		0.050						
-1.500	23.893		12.784	0.992	165.5	4.741	-1.828	26.66
		0.042						
-1.600	25.361		12.826	0.995	170.5	4.884	-1.928	26.91
		0.027						
-1.700	26.549		12.853	0.997	174.4	4.997	-2.028	27.16
		0.015						
-1.800	27.369		12.868	0.998	177.1	5.074	-2.128	27.41
		0.010						
-1.900	28.081		12.878	0.999	179.4	5.139	-2.228	27.66
		0.004						
-2.000	28.430		12.882	0.999	180.5	5.171	-2.328	27.91
		0.008						
			12.887	1.000				

Sky Constant = 22.91

Integration table for NGC 4435 B

Log I	A	P	Sum P	K	R*	Rho	Log J	Mu
2.200	0.001		0.000	0.000	0.9	0.030	2.088	17.35
2.100	0.003	0.307	0.307	0.027	1.8	0.060	1.988	17.60
2.000	0.008	0.570	0.877	0.077	3.0	0.099	1.888	17.85
1.900	0.011	0.259	1.136	0.100	3.5	0.116	1.788	18.10
1.800	0.016	0.360	1.496	0.132	4.3	0.140	1.688	18.35
1.700	0.019	0.163	1.659	0.146	4.6	0.152	1.588	18.60
1.600	0.022	0.162	1.821	0.160	5.1	0.166	1.488	18.85
1.500	0.030	0.283	2.104	0.185	5.9	0.194	1.388	19.10
1.400	0.041	0.307	2.411	0.212	6.9	0.226	1.288	19.35
1.300	0.053	0.276	2.687	0.237	7.8	0.257	1.188	19.60
1.200	0.067	0.245	2.932	0.258	8.8	0.288	1.088	19.85
1.100	0.084	0.236	3.168	0.279	9.8	0.322	0.988	20.10
1.000	0.110	0.293	3.461	0.305	11.2	0.369	0.888	20.35
0.900	0.139	0.265	3.726	0.328	12.6	0.415	0.788	20.60
0.800	0.177	0.272	3.998	0.352	14.3	0.469	0.688	20.85
0.700	0.219	0.237	4.235	0.373	15.8	0.521	0.588	21.10
0.600	0.281	0.279	4.514	0.397	17.9	0.590	0.488	21.35
0.500	0.350	0.245	4.758	0.419	20.0	0.658	0.388	21.60
0.400	0.456	0.303	5.061	0.445	22.9	0.752	0.288	21.85
0.300	0.541	0.190	5.251	0.462	24.9	0.819	0.188	22.10
0.200	0.673	0.236	5.487	0.483	27.8	0.913	0.088	22.35
0.100	0.826	0.218	5.706	0.502	30.8	1.012	-0.012	22.60
0.000	1.014	0.212	5.918	0.521	34.1	1.121	-0.112	22.85
-0.100	1.241	0.204	6.122	0.539	37.7	1.240	-0.212	23.10
-0.200	1.530	0.205	6.327	0.557	41.9	1.377	-0.312	23.35
-0.300	1.917	0.220	6.547	0.576	46.9	1.542	-0.412	23.60
-0.400	2.366	0.202	6.748	0.594	52.1	1.712	-0.512	23.85
-0.500	3.053	0.245	6.994	0.616	59.1	1.945	-0.612	24.10
-0.600	4.088	0.294	7.287	0.641	68.4	2.251	-0.712	24.35
-0.700	6.722	0.594	7.881	0.694	87.8	2.886	-0.812	24.60

Integration table for NGC 4435 B Continued.

Log I	A	P	Sum P	K	R*	Rho	Log J	Mu
-0.800	11.348	0.828	8.709	0.767	114.0	3.750	-0.912	24.85
-0.900	17.285	0.844	9.553	0.841	140.7	4.629	-1.012	25.10
-1.000	23.024	0.648	10.201	0.898	162.4	5.342	-1.112	25.35
-1.100	27.799	0.428	10.630	0.936	178.5	5.870	-1.212	25.60
-1.200	32.084	0.305	10.935	0.962	191.7	6.306	-1.312	25.85
-1.300	35.227	0.178	11.113	0.978	200.9	6.608	-1.412	26.10
-1.400	37.301	0.093	11.206	0.986	206.7	6.799	-1.512	26.35
-1.500	39.056	0.063	11.269	0.992	211.6	6.958	-1.612	26.60
-1.600	40.429	0.039	11.308	0.995	215.2	7.079	-1.712	26.85
-1.700	41.319	0.020	11.328	0.997	217.6	7.156	-1.812	27.10
-1.800	42.202	0.016	11.344	0.998	219.9	7.232	-1.912	27.35
-1.900	42.396	0.003	11.347	0.999	220.4	7.249	-2.012	27.60
-2.000	43.157	0.009	11.355	0.999	222.4	7.314	-2.112	27.85
		0.006	11.361	1.000				

Sky Constant = 22.85

Integration table for NGC 4438 B

Log I	A	P	Sum P	K	R*	Rho	Log J	Mu
1.700	0.002		0.000	0.000	1.6	0.030	1.899	18.60
		0.194						
1.600	0.006		0.194	0.015	2.7	0.053	1.799	18.85
		0.077						
1.500	0.009		0.272	0.021	3.1	0.061	1.699	19.10
		0.143						
1.400	0.014		0.415	0.032	4.0	0.076	1.599	19.35
		0.097						
1.300	0.018		0.512	0.040	4.5	0.088	1.499	19.60
		0.271						
1.200	0.033		0.783	0.060	6.2	0.119	1.399	19.85
		0.430						
1.100	0.063		1.214	0.094	8.5	0.164	1.299	20.10
		0.456						
1.000	0.104		1.670	0.129	10.9	0.210	1.199	20.35
		0.498						
0.900	0.159		2.168	0.167	13.5	0.261	1.099	20.60
		0.539						
0.800	0.235		2.707	0.209	16.4	0.316	0.999	20.85
		0.473						
0.700	0.319		3.180	0.245	19.1	0.369	0.899	21.10
		0.541						
0.600	0.439		3.722	0.287	22.4	0.433	0.799	21.35
		0.469						
0.500	0.570		4.190	0.323	25.6	0.493	0.699	21.60
		0.466						
0.400	0.735		4.656	0.359	29.0	0.560	0.599	21.85
		0.239						
0.300	0.840		4.895	0.378	31.0	0.599	0.499	22.10
		0.314						
0.200	1.016		5.209	0.402	34.1	0.658	0.399	22.35
		0.313						
0.100	1.235		5.521	0.426	37.6	0.726	0.299	22.60
		0.288						
0.000	1.491		5.810	0.448	41.3	0.797	0.199	22.85
		0.298						
-0.100	1.823		6.108	0.471	45.7	0.882	0.099	23.10
		0.379						
-0.200	2.354		6.486	0.500	51.9	1.002	-0.001	23.35
		0.435						
-0.300	3.123		6.921	0.534	59.8	1.154	-0.101	23.60
		0.566						
-0.400	4.382		7.487	0.578	70.9	1.367	-0.201	23.85
		0.696						
-0.500	6.329		8.183	0.631	85.2	1.643	-0.301	24.10
		0.817						
-0.600	9.210		9.000	0.694	102.7	1.981	-0.401	24.35
		0.806						
-0.700	12.789		9.807	0.757	121.1	2.335	-0.501	24.60
		0.725						
-0.800	16.838		10.532	0.813	138.9	2.679	-0.601	24.85
		0.677						
-0.900	21.599		11.209	0.865	157.3	3.034	-0.701	25.10
		0.549						
-1.000	26.459		11.758	0.907	174.1	3.358	-0.801	25.35
		0.393						
-1.100	30.838		12.150	0.937	188.0	3.626	-0.901	25.60
		0.298						
-1.200	35.017		12.448	0.960	200.3	3.864	-1.001	25.85

Integration table for NGC 4438 B Continued.

Log I	A	P	Sum P	K	R*	Rho	Log J	Mu
-1.300	38.604		12.651	0.976	210.3	4.057	-1.101	26.10
		0.203						
-1.400	41.307		12.773	0.985	217.6	4.196	-1.201	26.35
		0.122						
-1.500	43.440		12.849	0.991	223.1	4.303	-1.301	26.60
		0.076						
-1.600	45.163		12.898	0.995	227.5	4.388	-1.401	26.85
		0.049						
-1.700	46.354		12.925	0.997	230.5	4.445	-1.501	27.10
		0.027						
-1.800	47.304		12.942	0.998	232.8	4.491	-1.601	27.35
		0.017						
-1.900	47.830		12.949	0.999	234.1	4.515	-1.701	27.60
		0.007						
-2.000	48.346		12.955	0.999	235.4	4.540	-1.801	27.85
		0.006						
		0.007	12.962	1.000				

Sky Constant = 22.85

Integration table for NGC 4459 B

Log I	A	P	Sum P	K	R*	Rho	Log J	Mu
2.300	0.001		0.000	0.000	1.3	0.047	1.948	17.29
		0.129						
2.200	0.002		0.129	0.012	1.6	0.057	1.848	17.54
		0.102						
2.100	0.003		0.232	0.022	1.8	0.066	1.748	17.79
		0.163						
2.000	0.004		0.394	0.037	2.2	0.081	1.648	18.04
		0.194						
1.900	0.006		0.588	0.055	2.7	0.099	1.548	18.29
		0.154						
1.800	0.009		0.742	0.070	3.1	0.114	1.448	18.54
		0.041						
1.700	0.009		0.783	0.073	3.3	0.119	1.348	18.79
		0.065						
1.600	0.011		0.848	0.079	3.5	0.128	1.248	19.04
		0.257						
1.500	0.018		1.106	0.103	4.5	0.165	1.148	19.29
		0.286						
1.400	0.028		1.392	0.130	5.7	0.206	1.048	19.54
		0.309						
1.300	0.042		1.700	0.159	6.9	0.252	0.948	19.79
		0.413						
1.200	0.065		2.113	0.198	8.6	0.313	0.848	20.04
		0.553						
1.100	0 104		2.667	0.250	10.9	0.396	0.748	20.29
		0.366						
1.000	0.136		3.033	0.284	12.5	0.454	0.648	20.54
		0.375						
0.900	0.178		3.408	0.319	14.3	0.519	0.548	20.79
		0.360						
0.800	0.228		3.768	0.353	16.2	0.588	0.448	21.04
		0.367						
0.700	0.293		4.135	0.387	18.3	0.666	0.348	21.29
		0.314						
0.600	0.363		4.447	0.417	20.4	0.741	0.248	21.54
		0.376						
0.500	0.469		4.825	0.452	23.2	0.842	0.148	21.79
		0.356						
0.400	0.594		5.181	0.485	26.1	0.948	0.048	22.04
		0.331						
0.300	0.741		5.513	0.516	29.1	1.059	-0.052	22.29
		0.337						
0.200	0.929		5.849	0.548	32.6	1.186	-0.152	22.54
		0.334						
0.100	1.164		6.183	0.579	36.5	1.327	-0.252	22.79
		0.379						
0.000	1.500		6.563	0.614	41.5	1.507	-0.352	23.04
		0.315						
-0.100	1.851		6.878	0.644	46.1	1.674	-0.452	23.29
		0.332						
-0.200	2.317		7.210	0.675	51.5	1.873	-0.552	23.54
		0.329						
-0.300	2.898		7.539	0.706	57.6	2.094	-0.652	23.79
		0.312						
-0.400	3.593		7.851	0.735	64.2	2.332	-0.752	24.04
		0.306						
-0.500	4.450		8.158	0.764	71.4	2.595	-0.852	24.29
		0.282						
-0.600	5.446		8.440	0.790	79.0	2.871	-0.952	24.54

Integration table for NGC 4459 B Continued.

Log I	A	P	Sum P	K	R*	Rho	Log J	Mu
		0.286						
-0.700	6.717		8.726	0.817	87.7	3.188	-1.052	24.79
		0.274						
-0.800	8.246		9.000	0.843	97.2	3.533	-1.152	25.04
		0.294						
-0.900	10.311		9.294	0.870	108.7	3.950	-1.252	25.29
		0.309						
-1.000	13.048		9.603	0.899	122.3	4.444	-1.352	25.54
		0.278						
-1.100	16.148		9.881	0.925	136.0	4.944	-1.452	25.79
		0.227						
-1.200	19.328		10.108	0.946	148.8	5.408	-1.552	26.04
		0.196						
-1.300	22.793		10.304	0.965	161.6	5.873	-1.652	26.29
		0.104						
-1.400	25.102		10.408	0.974	169.6	6.164	-1.752	26.54
		0.080						
-1.500	27.329		10.487	0.982	177.0	6.431	-1.852	26.79
		0.050						
-1.600	29.075		10.537	0.986	182.5	6.634	-1.952	27.04
		0.037						
-1.700	30.736		10.574	0.990	187.7	6.820	-2.052	27.29
		0.022						
-1.800	31.978		10.596	0.992	191.4	6.957	-2.152	27.54
		0.023						
-1.900	33.598		10.619	0.994	196.2	7.131	-2 252	27.79
		0.017						
-2.000	35.078		10.636	0.996	200.5	7.286	-2.352	28.04
		0.046						
			10.682	1.000				

Sky Constant = 23.04

Integration table for NGC 4461 B

Log I	A	P	Sum P	K	R*	Rho	Log J	Mu
2.200	0.001		0.000	0.000	0.9	0.056	1.666	17.33
		0.307						
2.100	0.003		0.307	0.053	1.8	0.112	1.566	17.58
		0.081						
2.000	0.004		0.387	0.067	2.0	0.125	1.466	17.83
		0.194						
1.900	0.006		0.583	0.101	2.6	0.158	1.366	18.08
		0.103						
1.800	0.007		0.686	0.119	2.9	0.176	1.266	18.33
		0.122						
1.700	0.009		0.808	0.140	3.3	0.201	1.166	18.58
		0.162						
1.600	0.013		0.970	0.168	3.9	0.237	1.066	18.83
		0.103						
1.500	0.016		1.073	0.186	4.3	0.262	0.966	19.08
		0.184						
1.400	0.022		1.257	0.218	5.1	0.311	0.866	19.33
		0.146						
1.300	0.029		1.403	0.243	5.7	0.353	0.766	19.58
		0.194						
1.200	0.040		1.597	0.277	6.7	0.414	0.666	19.83
		0.143						
1.100	0.050		1.740	0.302	7.5	0.464	0.566	20.08
		0.204						
1.000	0.068		1.944	0.337	8.8	0.541	0.466	20.33
		0.213						
0.900	0.092		2.157	0.374	10.2	0.629	0.366	20.58
		0.211						
0.800	0.121		2.368	0.410	11.8	0.723	0.266	20.83
		0.216						
0.700	0.159		2.584	0.448	13.5	0.830	0.166	21.08
		0.191						
0.600	0.202		2.775	0.481	15.2	0.934	0.066	21.33
		0.167						
0.500	0.249		2.943	0.510	16.9	1.037	-0.034	21.58
		0.227						
0.400	0.329		3.170	0.549	19.4	1.192	-0.134	21.83
		0.174						
0.300	0.406		3.344	0.579	21.6	1.324	-0.234	22.09
		0.154						
0.200	0.492		3.497	0.606	23.7	1.457	-0.334	22.33
		0.231						
0.100	0.654		3.728	0.646	27.4	1.681	-0.434	22.58
		0.193						
0.000	0.825		3.921	0.679	30.7	1.888	-0.534	22.83
		0.175						
-0.100	1.020		4.096	0.710	34.2	2.099	-0.634	23.08
		0.128						
-0.200	1.199		4.224	0.732	37.1	2.276	-0.734	23.33
		0.134						
-0.300	1.436		4.358	0.755	40.6	2.491	-0.834	23.58
		0.106						
-0.400	1.672		4.464	0.774	43.8	2.688	-0.934	23.83
		0.110						
-0.500	1.979		4.574	0.793	47.6	2.924	-1.034	24.08
		0.098						
-0.600	2.326		4.672	0.810	51.6	3.170	-1.134	24.33
		0.087						
-0.700	2.713		4.759	0.825	55.8	3.424	-1.234	24.58

Integration table for NGC 4461 B Continued.

Log I	A	P	Sum P	K	R*	Rho	Log J	Mu
		0.097						
-0.800	3.252		4.856	0.842	61.0	3.748	-1.334	24.83
		0.092						
-0.900	3.901		4.948	0.857	66.9	4.105	-1.434	25.08
		0.140						
-1.000	5.139		5.088	0.882	76.7	4.712	-1.534	25.33
		0.158						
-1.100	6.903		5.246	0.909	88.9	5.461	-1.634	25.58
		0.141						
-1.200	8.885		5.387	0.934	100.9	6.196	-1.734	25.83
		0.117						
-1.300	10.951		5.504	0.954	112.0	6.879	-1.834	26.08
		0.083						
-1.400	12.798		5.587	0.968	121.1	7.436	-1.934	26.33
		0.060						
-1.500	14.471		5.647	0.979	128.8	7.907	-2.034	26.58
		0.035						
-1.600	15.707		5.682	0.985	134.2	8.238	-2.134	26.83
		0.022						
-1.700	16.667		5.704	0.988	138.2	8.486	-2.234	27.08
		0.015						
-1.800	17.513		5.719	0.991	141.7	8.699	-2.334	27.33
		0.013						
-1.900	18.408		5.732	0.993	145.2	8.918	-2.434	27.58
		0.012						
-2.000	19.476		5.744	0.995	149.4	9.173	-2.534	27.83
		0.027						
			5.770	1.000				

Sky Constant = 22.83

Integration table for NGC 4474 B

Log I	A	P	Sum P	K	R*	Rho	Log J	Mu
1.900	0.001		0.000	0.000	1.3	0.080	1.506	18.06
		0.103						
1.800	0.003		0.103	0.020	1.8	0.113	1.406	18.31
		0.122						
1.700	0.005		0.225	0.042	2.4	0.149	1.306	18.56
		0.206						
1.500	0.010		0.431	0.119	3.4	0.211	1.106	19.06
		0.143						
1.400	0.015		0.575	0.158	4.2	0.258	1.006	19.31
		0.146						
1.300	0.022		0.721	0.199	5.0	0.309	0.906	19.56
		0.052						
1.200	0.025		0.772	0.213	5.3	0.328	0.806	19.81
		0.133						
1.100	0.034		0.906	0.250	6.2	0.386	0.706	20.06
		0.114						
1.000	0.044		1.020	0.281	7.1	0.440	0.606	20.31
		0.058						
0.900	0.050		1.078	0.297	7.6	0.471	0.506	20.56
		0.128						
0.800	0.068		1.206	0.333	8.9	0.549	0.406	20.81
		0.147						
0.700	0.094		1.353	0.373	10.4	0.645	0.306	21.06
		0.133						
0.600	0.124		1.486	0.410	11.9	0.739	0.206	21.31
		0.172						
0.500	0.172		1.658	0.457	14.1	0.871	0.106	21.56
		0.147						
0.400	0.224		1.806	0.498	16.0	0.993	0.006	21.81
		0.120						
0.300	0.278		1.926	0.531	17.8	1.105	-0.094	22.06
		0.119						
0.200	0.344		2.045	0.564	19.8	1.230	-0.194	22.31
		0.115						
0.100	0.425		2.159	0.595	22.1	1.367	-0.294	22.56
		0.104						
0.000	0.517		2.264	0.624	24.3	1.508	-0.394	22.81
		0.123						
-0.100	0.654		2.386	0.658	27.4	1.696	-0.494	23.06
		0.107						
-0.200	0.804		2.493	0.688	30.3	1.881	-0.594	23.31
		0.113						
-0.300	1.003		2.606	0.719	33.9	2.101	-0.694	23.56
		0.096						
-0.400	1.217		2.702	0.745	37.3	2.314	-0.794	23.81
		0.083						
-0.500	1.450		2.785	0.768	40.8	2.526	-0.894	24.06
		0.079						
-0.600	1.727		2.864	0.790	44.5	2.757	-0.994	24.31
		0.091						
-0.700	2.129		2.955	0.815	49.4	3.061	-1.094	24.56
		0.099						
-0.800	2.680		3.053	0.842	55.4	3.435	-1.194	24.81
		0.103						
-0.900	3.405		3.156	0.870	62.5	3.871	-1.294	25.06
		0.109						
-1.000	4.371		3.265	0.900	70.8	4.386	-1.394	25.31
		0.085						
-1.100	5.320		3.351	0.924	78.1	4.839	-1.494	25.56

Integration table for NGC 4474 B Continued.

Log I	A	P	Sum P	K	R*	Rho	Log J	Mu
		0.075						
-1.200	6.379		3.426	0.945	85.5	5.299	-1.594	25.81
		0.060						
-1.300	7.438		3.486	0.961	92.3	5.722	-1.694	26.06
		0.045						
-1.400	8.434		3.531	0.974	98.3	6.093	-1.794	26.31
		0.038						
-1.500	9.509		3.569	0.984	104.4	6.469	-1.894	26.56
		0.014						
-1.600	9.998		3.583	0.988	107.0	6.633	-1.994	26.81
		0.014						
-1.700	10.622		3.597	0.992	110.3	6.837	-2.094	27.06
		0.007						
-1.800	11.012		3.604	0.994	112.3	6.962	-2.194	27.31
		0.008						
-1.900	11.546		3.612	0.996	115.0	7.129	-2.294	27.56
		0.005						
-2.000	11.958		3.616	0.997	117.1	7.255	-2.394	27.81
		0.010						
			3.627	1.000				

Sky Constant = 22.81

Integration table for NGC 4477 B

Log I	A	P	Sum P	K	R*	Rho	Log J	Mu
2.100	0.001		0.000	0.000	0.9	0.035	1.785	17.70
		0.244						
2.000	0.003		0.244	0.025	1.8	0.070	1.685	17.95
		0.259						
1.900	0.006		0.503	0.052	2.6	0.099	1.585	18.20
		0.205						
1.800	0.009		0.708	0.073	3.1	0.121	1.485	18.45
		0.245						
1.700	0.013		0.953	0.098	3.9	0.148	1.385	18.70
		0.259						
1.600	0.019		1.212	0.125	4.6	0.178	1.285	18.95
		0.180						
1.500	0.024		1.393	0.144	5.2	0.201	1.185	19.20
		0.327						
1.400	0.035		1.720	0.177	6.4	0.244	1.085	19.45
		0.325						
1.300	0.050		2.045	0.211	7.5	0.290	0.985	19.70
		0.245						
1.200	0.063		2.290	0.236	8.5	0.327	0.885	19.95
		0.277						
1.100	0.083		2.567	0.265	9.7	0.374	0.785	20.20
		0.212						
1.000	0.102		2.778	0.286	10.8	0.414	0.685	20.45
		0.323						
0.900	0.138		3.102	0.320	12.6	0.482	0.585	20.70
		0.313						
0.800	0.182		3.415	0.352	14.4	0.554	0.485	20.95
		0.298						
0.700	0.234		3.713	0.383	16.4	0.629	0.385	21.20
		0.292						
0.600	0.299		4.005	0.413	18.5	0.711	0.285	21.45
		0.345						
0.500	0.396		4.350	0.448	21.3	0.818	0.185	21.70
		0.262						
0.400	0.488		4.611	0.475	23.6	0.908	0.085	21.95
		0.279						
0.300	0.612		4.891	0.504	26.5	1.017	-0.015	22.20
		0.259						
0.200	0.757		5.150	0.531	29.4	1.131	-0.115	22.45
		0.431						
0.100	1.060		5.582	0.576	34.9	1.339	-0.215	22.70
		0.426						
0.000	1.437		6.007	0.619	40.6	1.559	-0.315	22.95
		0.602						
-0.100	2.108		6.609	0.682	49.2	1.888	-0.415	23.20
		0.550						
-0.200	2.880		7.160	0.738	57.5	2.207	-0.515	23.45
		0.378						
-0.300	3.549		7.538	0.777	63.8	2.449	-0.615	23.70
		0.320						
-0.400	4.261		7.858	0.810	69.9	2.684	-0.715	23.95
		0.283						
-0.500	5.054		8.141	0.839	76.1	2.923	-0.815	24.20
		0.222						
-0.600	5.838		8.364	0.862	81.8	3.141	-0.915	24.45
		0.212						
-0.700	6.779		8.576	0.884	88.1	3.385	-1.015	24.70
		0.193						
-0.800	7.855		8.769	0.904	94.9	3.644	-1.115	24.95

Integration table for NGC 4477 B Continued.

Log I	A	P	Sum P	K	R*	Rho	Log J	Mu
-0.900	9.285		8.972	0.925	103.1	3.962	-1.215	25.20
		0.203						
-1.000	10.910		9.155	0.944	111.8	4.294	-1.315	25.45
		0.184						
-1.100	12.718		9.318	0.961	120.7	4.637	-1.415	25.70
		0.162						
-1.200	14.422		9.439	0.973	128.6	4.937	-1.515	25.95
		0.121						
-1.300	15.960		9.526	0.982	135.2	5.194	-1.615	26.20
		0.087						
-1.400	17.077		9.576	0.987	139.9	5.373	-1.715	26.45
		0.050						
-1.500	18.194		9.616	0.992	144.4	5.546	-1.815	26.70
		0.040						
-1.600	19.326		9.648	0.995	148.8	5.716	-1.915	26.95
		0.032						
-1.700	20.160		9.667	0.997	152.0	5.838	-2.015	27.20
		0.019						
-1.800	20.809		9.679	0.998	154.4	5.931	-2.115	27.45
		0.012						
-1.900	21.237		9.685	0.999	156.0	5.991	-2.215	27.70
		0.006						
-2.000	21.696		9.690	0.999	157.7	6.056	-2.315	27.95
		0.005						
		0.008						
			9.698	1.000				

Sky Constant = 22.95

Integration table for NGC 4501 B

Log I	A	P	Sum P	K	R*	Rho	Log J	Mu
2.000	0.001	0.129	0.000	0.000	0.9	0.018	1.653	17.83
1.900	0.002	0.154	0.129	0.006	1.6	0.031	1.553	18.08
1.800	0.004	0.041	0.284	0.013	2.2	0.044	1.453	18.33
1.700	0.005	0.195	0.324	0.014	2.4	0.048	1.353	18.58
1.600	0.009	0.180	0.519	0.023	3.3	0.065	1.253	18.83
1.500	0.014	0.123	0.699	0.031	4.1	0.081	1.153	19.08
1.400	0.019	0.211	0.822	0.036	4.6	0.092	1.053	19.33
1.300	0.028	0.271	1.033	0.046	5.7	0.112	0.953	19.58
1.200	0.043	0.369	1.304	0.058	7.0	0.139	0.853	19.83
1.100	0.069	0.562	1.673	0.074	8.9	0.176	0.753	20.08
1.000	0.119	0.880	2.235	0.099	11.7	0.231	0.653	20.33
0.900	0.217	1.315	3.115	0.138	15.8	0.312	0.553	20.58
0.800	0.402	1.657	4.430	0.196	21.5	0.425	0.453	20.83
0.700	0.694	1.686	6.087	0.270	28.2	0.559	0.353	21.08
0.600	1.069	1.640	7.773	0.345	35.0	0.693	0.253	21.33
0.500	1.529	1.321	9.414	0.417	41.9	0.829	0.153	21.58
0.400	1.994	1.014	10.735	0.476	47.8	0.947	0.053	21.83
0.300	2.444	1.815	11.749	0.521	52.9	1.048	-0.047	22.08
0.200	3.458	1.913	13.564	0.601	62.9	1.247	-0.147	22.33
0.100	4.804	1.587	15.477	0.686	74.2	1.470	-0.247	22.58
0.000	6.209	1.287	17.064	0.757	84.3	1.671	-0.347	22.83
-0.100	7.644	0.878	18.352	0.814	93.6	1.854	-0.447	23.08
-0.200	8.876	0.647	19.230	0.853	100.9	1.998	-0.547	23.33
-0.300	10.020	0.477	19.877	0.881	107.2	2.123	-0.647	23.58
-0.400	11.081	0.341	20.355	0.903	112.7	2.232	-0.747	23.83
-0.500	12.036	0.262	20.696	0.918	117.4	2.326	-0.847	24.08
-0.600	12.959	0.222	20.957	0.929	121.9	2.414	-0.947	24.33
-0.700	13.943	0.214	21.179	0.939	126.4	2.504	-1.047	24.58
-0.800	15.137	0.223	21.393	0.949	131.7	2.609	-1.147	24.83
-0.900	16.708		21.616	0.958	138.4	2.741	-1.247	25.08

Integration table for NGC 4501 B Continued.

Log I	A	P	Sum P	K	R*	Rho	Log J	Mu
-1.000	18.425	0.194	21.810	0.967	145.3	2.878	-1.347	25.33
-1.100	20.572	0.193	22.003	0.976	153.5	3.041	-1.447	25.58
-1.200	23.084	0.179	22.182	0.984	162.6	3.222	-1.547	25.83
-1.300	25.325	0.127	22.309	0.989	170.4	3.374	-1.647	26.08
-1.400	27.249	0.087	22.395	0.993	176.7	3.500	-1.747	26.33
-1.500	28.686	0.051	22.447	0.995	181.3	3.591	-1.847	26.58
-1.600	29.896	0.034	22.481	0.997	185.1	3.666	-1.947	26.83
-1.700	31.090	0.027	22.508	0.998	188.8	3.739	-2.047	27.08
-1.800	31.743	0.012	22.520	0.999	190.7	3.778	-2.147	27.33
-1.900	32.594	0.012	22.532	0.999	193.3	3.828	-2.247	27.58
-2.000	33.178	0.007	22.538	0.999	195.0	3.862	-2.347	27.83
		0.014	22.552	1.000				

Sky Constant = 22.83

Integration table for NGC 4503 B

Log I	A	P	Sum P	K	R*	Rho	Log J	Mu
2.000	0.002		0.000	0.000	1.6	0.078	1.672	17.93
1.900	0.004	0.129	0.129	0.025	2.0	0.100	1.572	18.18
1.800	0.005	0.103	0.232	0.046	2.4	0.119	1.472	18.43
1.700	0.008	0.163	0.395	0.078	3.0	0.149	1.372	18.68
1.600	0.009	0.065	0.460	0.090	3.3	0.162	1.272	18.93
1.500	0.011	0.051	0.512	0.100	3.5	0.174	1.172	19.18
1.400	0.014	0.102	0.614	0.121	4.1	0.200	1.072	19.43
1.300	0.023	0.195	0.809	0.159	5.1	0.253	0.972	19.68
1.200	0.034	0.194	1.002	0.197	6.2	0.307	0.872	19.93
1.100	0.039	0.072	1.074	0.211	6.7	0.329	0.772	20.18
1.000	0.054	0.171	1.245	0.244	7.9	0.388	0.672	20.43
0.900	0.079	0.226	1.471	0.289	9.5	0.470	0.572	20.68
0.800	0.097	0.123	1.595	0.313	10.5	0.519	0.472	20.93
0.700	0.133	0.208	1.803	0.354	12.4	0.610	0.372	21.18
0.600	0.187	0.243	2.046	0.402	14.7	0.723	0.272	21.43
0.500	0.243	0.198	2.244	0.441	16.7	0.823	0.172	21.68
0.400	0.309	0.186	2.430	0.477	18.8	0.927	0.072	21.93
0.300	0.381	0.162	2.593	0.509	20.9	1.030	-0.028	22.18
0.200	0.536	0.279	2.871	0.564	24.8	1.222	-0.128	22.43
0.100	0.715	0.254	3.126	0.614	28.6	1.411	-0.228	22.68
0.000	0.885	0.192	3.318	0.651	31.8	1.570	-0.328	22.93
-0.100	1.082	0.177	3.494	0.686	35.2	1.736	-0.428	23.18
-0.200	1.356	0.195	3.689	0.724	39.4	1.944	-0.528	23.43
-0.300	1.671	0.178	3.868	0.759	43.8	2.158	-0.628	23.68
-0.400	1.996	0.146	4.014	0.788	47.8	2.358	-0.728	23.93
-0.500	2.398	0.144	4.158	0.816	52.4	2.585	-0.828	24.18
-0.600	2.828	0.122	4.280	0.840	56.9	2.807	-0.928	24.43
-0.700	3.321	0.111	4.391	0.862	61.7	3.042	-1.028	24.68
-0.800	3.803	0.086	4.477	0.879	66.0	3.255	-1.128	24.93
-0.900	4.494	0.098	4.575	0.898	71.8	3.539	-1.228	25.18

Integration table for NGC 4503 B Continued.

Log I	A	P	Sum P	K	R*	Rho	Log J	Mu
-1.000	5.338	0.095	4.670	0.917	78.2	3.856	-1.328	25.43
-1.100	6.449	0.100	4.770	0.936	86.0	4.239	-1.428	25.68
-1.200	7.628	0.084	4.854	0.953	93.5	4.610	-1.528	25.93
-1.300	9.126	0.085	4.939	0.970	102.3	5.042	-1.628	26.18
-1.400	10.151	0.046	4.985	0.979	107.9	5.318	-1.728	26.43
-1.500	10.927	0.028	5.013	0.984	111.9	5.517	-1.828	26.68
-1.600	11.709	0.022	5.035	0.988	115.8	5.711	-1.928	26.93
-1.700	12.317	0.014	5.049	0.991	118.8	5.858	-2.028	27.18
-1.800	12.949	0.011	5.060	0.993	121.8	6.006	-2.128	27.43
-1.900	13.920	0.014	5.074	0.996	126.3	6.227	-2.228	27.68
-2.000	14.272	0.004	5.078	0.997	127.9	6.306	-2.328	27.93
		0.016	5.094	1.000				

Sky Constant = 22.93

Integration table for NGC 4531 B

Log I	A	P	Sum P	K	R*	Rho	Log J	Mu
0.900	0.001		0.000	0.000	0.9	0.028	1.027	20.60
		0.046						
0.800	0.007		0.046	0.013	2.9	0.087	0.927	20.85
		0.118						
0.700	0.028		0.165	0.047	5.7	0.172	0.827	21.10
		0.136						
0.600	0.058		0.301	0.086	8.2	0.248	0.727	21.35
		0.221						
0.500	0.120		0.522	0.150	11.7	0.357	0.627	21.60
		0.252						
0.400	0.209		0.774	0.222	15.5	0.470	0.527	21.85
		0.278						
0.300	0.332		1.051	0.302	19.5	0.593	0.427	22.10
		0.107						
0.200	0.392		1.159	0.332	21.2	0.644	0.327	22.35
		0.172						
0.100	0.513		1.331	0.382	24.3	0.737	0.227	22.60
		0.155						
0.000	0.650		1.485	0.426	27.3	0.829	0.127	22.85
		0.200						
-0.100	0.874		1.686	0.484	31.6	0.961	0.027	23.10
		0.212						
-0.200	1.171		1.898	0.545	36.6	1.113	-0.073	23.35
		0.190						
-0.300	1.507		2.088	0.599	41.6	1.262	-0.173	23.60
		0.158						
-0.400	1.858		2.246	0.645	46.1	1.401	-0.273	23.85
		0.152						
-0.500	2.283		2.398	0.688	51.1	1.553	-0.373	24.10
		0.152						
-0.600	2.820		2.550	0.732	56.8	1.726	-0.473	24.35
		0.123						
-0.700	3.365		2.673	0.767	62.1	1.886	-0.573	24.60
		0.097						
-0.800	3.906		2.770	0.795	66.9	2.032	-0.673	24.85
		0.106						
-0.900	4.653		2.876	0.825	73.0	2.218	-0.773	25.10
		0.107						
-1.000	5.599		2.983	0.856	80.1	2.433	-0.873	25.35
		0.118						
-1.100	6.914		3.101	0.890	89.0	2.703	-0.973	25.60
		0.111						
-1.200	8.466		3.211	0.922	98.5	2.991	-1.073	25.85
		0.073						
-1.300	9.758		3.284	0.943	105.7	3.211	-1.173	26.10
		0.076						
-1.400	11.441		3.360	0.964	114.5	3.477	-1.273	26.35
		0.039						
-1.500	12.537		3.399	0.975	119.9	3.640	-1.373	26.60
		0.028						
-1.600	13.517		3.427	0.983	124.5	3.780	-1.473	26.85
		0.030						
-1.700	14.831		3.457	0.992	130.4	3.959	-1.573	27.10
		0.009						
-1.800	15.315		3.465	0.994	132.5	4.023	-1.673	27.35
		0.008						
-1.900	15.896		3.474	0.997	135.0	4.099	-1.773	27.60
		0.004						
-2.000	16.235		3.477	0.998	136.4	4.142	-1.873	27.85

Integration table for NGC 4531 B Continued.

Log I	A	P	Sum P	K	R*	Rho	Log J	Mu
		0.007						
			3.485	1.000				

Sky Constant = 22.85

Integration table for NGC 4550 B

Log I	A	P	Sum P	K	R*	Rho	Log J	Mu
1.900	0.001		0.000	0.000	0.9	0.084	1.071	18.11
		0.051						
1.800	0.001		0.051	0.014	1.3	0.119	0.971	18.36
		0.204						
1.700	0.005		0.255	0.070	2.4	0.223	0.871	18.61
		0.130						
1.600	0.008		0.385	0.106	3.0	0.280	0.771	18.86
		0.232						
1.500	0.014		0.617	0.169	4.1	0.378	0.671	19.11
		0.143						
1.400	0.019		0.760	0.209	4.7	0.439	0.571	19.36
		0.195						
1.300	0.028		0.955	0.262	5.7	0.528	0.471	19.61
		0.206						
1.200	0.040		1.161	0.319	6.7	0.626	0.371	19.86
		0.287						
1.100	0.060		1.448	0.398	8.3	0.770	0.271	20.11
		0.122						
1.000	0.071		1.570	0.431	9.0	0.836	0.171	20.36
		0.149						
0.900	0.087		1.717	0.472	10.0	0.929	0.071	20.61
		0.144						
0.800	0.107		1.863	0.512	11.1	1.031	-0.029	20.86
		0.155						
0.700	0.135		2.018	0.554	12.4	1.155	-0.129	21.11
		0.149						
0.600	0.168		2.167	0.595	13.9	1.289	-0.229	21.36
		0.172						
0.500	0.216		2.340	0.642	15.7	1.463	-0.329	21.61
		0.125						
0.400	0.260		2.464	0.677	17.3	1.605	-0.429	21.86
		0.115						
0.300	0.311		2.580	0.708	18.9	1.756	-0.529	22.11
		0.094						
0.200	0.364		2.674	0.734	20.4	1.898	-0.629	22.36
		0.126						
0.100	0.453		2.800	0.769	22.8	2.117	-0.729	22.61
		0.091						
0.000	0.533		2.891	0.794	24.7	2.298	-0.829	22.86
		0.085						
-0.100	0.628		2.976	0.817	26.8	2.493	-0.929	23.11
		0.083						
-0.200	0.744		3.059	0.840	29.2	2.714	-1.029	23.36
		0.060						
-0.300	0.851		3.119	0.856	31.2	2.902	-1.129	23.61
		0.054						
-0.400	0.970		3.173	0.871	33.3	3.099	-1.229	23.86
		0.050						
-0.500	1.111		3.223	0.885	35.7	3.316	-1.329	24.11
		0.045						
-0.600	1.270		3.268	0.897	38.1	3.546	-1.429	24.36
		0.032						
-0.700	1.413		3.300	0.906	40.2	3.740	-1.529	24.61
		0.041						
-0.800	1.640		3.341	0.917	43.4	4.030	-1.629	24.86
		0.044						
-0.900	1.951		3.385	0.930	47.3	4.395	-1.729	25.11
		0.039						
-1.000	2.296		3.424	0.940	51.3	4.767	-1.829	25.36

Integration table for NGC 4550 B Continued.

Log I	A	P	Sum P	K	R*	Rho	Log J	Mu
		0.041						
-1.100	2.749		3.465	0.951	56.1	5.217	-1.929	25.61
		0.042						
-1.200	3.340		3.507	0.963	61.9	5.750	-2.029	25.86
		0.043						
-1.300	4.101		3.550	0.975	68.5	6.372	-2.129	26.11
		0.031						
-1.400	4.796		3.581	0.983	74.1	6.890	-2.229	26.36
		0.019						
-1.500	5.329		3.600	0.989	78.1	7.264	-2.329	26.61
		0.011						
-1.600	5.723		3.611	0.992	81.0	7.527	-2.429	26.86
		0.011						
-1.700	6.220		3.623	0.995	84.4	7.847	-2.529	27.11
		0.007						
-1.800	6.589		3.629	0.997	86.9	8.077	-2.629	27.36
		0.004						
-1.900	6.889		3.634	0.998	88.9	8.258	-2.729	27.61
		0.002						
-2.000	7.094		3.636	0.998	90.2	8.380	-2.829	27.86
		0.006						
			3.642	1.000				

Sky Constant = 22.86

Integration table for NGC 4552 R ELL

Log J	A	P	Sum P	K	R*	Rho	Log J	Mu
2.500	0.001	0.186	0.000	0.000	0.7	0.026	2.214	16.68
2.300	0.001	0.316	0.186	0.010	1.3	0.036	2.014	17.18
2.200	0.004	0.307	0.702	0.038	2.2	0.063	1.914	17.43
2.100	0.006	0.407	1.009	0.055	2.7	0.077	1.814	17.68
2.000	0.010	0.323	1.417	0.077	3.4	0.096	1.714	17.93
1.900	0.014	0.411	1.740	0.095	4.0	0.112	1.614	18.18
1.800	0.019	0.530	2.151	0.117	4.7	0.134	1.514	18.43
1.700	0.027	0.357	2.681	0.146	5.7	0.163	1.414	18.68
1.600	0.037	0.412	3.038	0.166	6.5	0.184	1.314	18.93
1.500	0.048	0.470	3.450	0.188	7.4	0.210	1.214	19.18
1.400	0.065	0.390	3.920	0.214	8.6	0.244	1.114	19.43
1.300	0.088	0.465	4.310	0.235	9.7	0.274	1.014	19.68
1.200	0.100	0.377	4.774	0.260	11.1	0.315	0.914	19.93
1.100	0.135	0.399	5.154	0.281	12.4	0.351	0.814	20.18
1.000	0.170	0.420	5.553	0.303	14.0	0.395	0.714	20.43
0.900	0.217	0.473	5.973	0.326	15.8	0.446	0.614	20.68
0.800	0.280	0.457	6.446	0.352	18.0	0.510	0.514	20.93
0.700	0.364	0.532	6.903	0.377	20.4	0.578	0.414	21.18
0.600	0.469	0.626	7.434	0.406	23.5	0.665	0.314	21.43
0.500	0.597	0.661	8.060	0.440	27.4	0.776	0.214	21.68
0.400	0.890	0.387	8.720	0.476	31.9	0.903	0.114	21.93
0.300	1.062	0.455	9.107	0.497	34.9	0.986	0.014	22.18
0.200	1.316	0.428	9.562	0.522	38.8	1.098	-0.086	22.43
0.100	1.618	0.409	9.991	0.545	43.1	1.218	-0.186	22.68
0.000	1.979	0.459	10.399	0.567	47.6	1.347	-0.286	22.93
-0.100	2.491	0.463	10.859	0.592	53.4	1.511	-0.386	23.18
-0.200	3.141	0.486	11.321	0.618	60.0	1.697	-0.486	23.43
-0.300	3.999	0.475	11.807	0.644	67.7	1.915	-0.586	23.68
-0.400	5.056	0.512	12.283	0.670	76.1	2.153	-0.686	23.93
-0.500	6.490		12.795	0.698	86.2	2.439	-0.786	24.18

Integration table for NGC 4552 R ELL Continued.

Log J	A	P	Sum P	K	R*	Rho	Log J	Mu
-0.600	8.348	0.527	13.322	0.727	97.8	2.764	-0.886	24.43
-0.700	11.170	0.636	13.958	0.761	113.1	3.200	-0.986	24.68
-0.800	15.029	0.691	14.649	0.799	131.2	3.711	-1.086	24.93
-0.900	19.947	0.699	15.348	0.837	151.2	4.276	-1.186	25.18
-1.000	25.655	0.645	15.993	0.872	171.5	4.849	-1.286	25.43
-1.100	31.296	0.506	16.499	0.900	187.4	5.306	-1.386	25.68
-1.200	36.760	0.389	16.888	0.921	205.2	5.804	-1.486	25.93
-1.300	41.601	0.274	17.162	0.936	218.3	6.175	-1.586	26.18
-1.400	45.501	0.179	17.341	0.946	228.5	6.464	-1.686	26.43
-1.500	48.383	0.100	17.441	0.951	235.5	6.659	-1.786	26.68
-1.600	50.719	0.066	17.507	0.955	241.1	6.818	-1.886	26.93
-1.700	52.470	0.039	17.547	0.957	245.2	6.935	-1.986	27.18
-1.800	54.299	0.031	17.578	0.959	249.3	7.050	-2.086	27.43
-1.900	55.486	0.018	17.596	0.960	252.2	7.131	-2.186	27.68
-2.000	56.960	0.017	17.613	0.961	255.5	7.226	-2.286	27.93
		0.718	18.331	1.000				

Sky Constant = 22.93

Integration table for NGC 4267 R (J)

Log I	A	P	Sum P	K	R*	Rho	Log J	Mu
1.500	0.004		0.000	0.000	2.2	0.073	1.670	16.78
		0.184						
1.400	0.011		0.184	0.048	3.5	0.116	1.570	17.03
		0.162						
1.300	0.018		0.347	0.090	4.5	0.149	1.470	17.28
		0.181						
1.200	0.028		0.527	0.137	5.7	0.187	1.370	17.53
		0.113						
1.100	0.036		0.640	0.167	6.4	0.211	1.270	17.78
		0.130						
1.000	0.048		0.770	0.200	7.4	0.243	1.170	18.03
		0.110						
0.900	0.060		0.880	0.229	8.3	0.272	1.070	18.28
		0.067						
0.800	0.069		0.947	0.246	8.9	0.293	0.970	18.53
		0.078						
0.700	0.083		1.025	0.267	9.7	0.321	0.870	18.78
		0.058						
0.600	0.096		1.083	0.282	10.5	0.345	0.770	19.03
		0.075						
0.500	0.117		1.158	0.301	11.6	0.380	0.670	19.28
		0.055						
0.400	0.136		1.213	0.316	12.5	0.411	0.570	19.53
		0.070						
0.300	0.167		1.283	0.334	13.8	0.455	0.470	19.78
		0.079						
0.200	0.211		1.362	0.354	15.6	0.512	0.370	20.03
		0.090						
0.100	0.275		1.452	0.378	17.7	0.583	0.270	20.28
		0.130						
0.000	0.390		1.582	0.412	21.1	0.695	0.170	20.53
		0.175						
-0.100	0.585		1.757	0.457	25.9	0.852	0.070	20.78
		0.248						
-0.200	0.934		2.006	0.522	32.7	1.076	-0.030	21.03
		0.267						
-0.300	1.405		2.273	0.591	40.1	1.320	-0.130	21.28
		0.247						
-0.400	1.955		2.520	0.656	47.3	1.557	-0.230	21.53
		0.255						
-0.500	2.669		2.775	0.722	55.3	1.819	-0.330	21.78
		0.215						
-0.600	3.427		2.990	0.778	62.7	2.061	-0.430	22.03
		0.164						
-0.700	4.154		3.153	0.820	69.0	2.269	-0.530	22.28
		0.145						
-0.800	4.963		3.298	0.858	75.4	2.480	-0.630	22.53
		0.096						
-0.900	5.636		3.394	0.883	80.4	2.643	-0.730	22.78
		0.084						
-1.000	6.377		3.478	0.905	85.5	2.811	-0.830	23.03
		0.075						
-1.100	7.215		3.553	0.924	90.9	2.990	-0.930	23.28
		0.061						
-1.200	8.069		3.614	0.940	96.2	3.162	-1.030	23.53
		0.053						
-1.300	9.010		3.667	0.954	101.6	3.342	-1.130	23.78
		0.048						
-1.400	10.076		3.715	0.966	107.5	3.534	-1.230	24.03

Integration table for NGC 4267 R (J) Continued.

Log I	A	P	Sum P	K	R*	Rho	Log J	Mu
		0.036						
-1.500	11.074		3.751	0.976	112.7	3.705	-1.330	24.28
		0.034						
-1.600	12.256		3.784	0.984	118.5	3.897	-1.430	24.53
		0.019						
-1.700	13.100		3.803	0.989	122.5	4.029	-1.530	24.78
		0.017						
-1.800	14.028		3.820	0.994	126.8	4.170	-1.630	25.03
		0.010						
-1.900	14.726		3.830	0.996	129.9	4.272	-1.730	25.28
		0.004						
-2.000	15.065		3.834	0.997	131.4	4.321	-1.830	25.53
		0.010						
			3.844	1.000				

Sky Constant = 20.53

Integration table for NGC 4371 R (J)

Log I	A	P	Sum P	K	R*	Rho	Log J	Mu
1.500	0.002		0.000	0.000	1.6	0.056	1.461	16.78
		0.061						
1.400	0.004		0.061	0.012	2.2	0.080	1.361	17.03
		0.227						
1.300	0.014		0.289	0.056	4.1	0.145	1.261	17.28
		0.271						
1.200	0.030		0.560	0.108	5.8	0.208	1.161	17.53
		0.277						
1.100	0.049		0.837	0.161	7.5	0.268	1.061	17.78
		0.187						
1.000	0.066		1.024	0.197	8.7	0.310	0.961	18.03
		0.175						
0.900	0.085		1.199	0.231	9.7	0.353	0.861	18.28
		0.144						
0.800	0.105		1.343	0.258	11.0	0.393	0.761	18.53
		0.167						
0.700	0.135		1.510	0.291	12.4	0.445	0.661	18.78
		0.152						
0.600	0.169		1.662	0.320	13.9	0.497	0.561	19.03
		0.100						
0.500	0.197		1.763	0.339	15.0	0.537	0.461	19.28
		0.164						
0.400	0.255		1.926	0.371	17.1	0.611	0.361	19.53
		0.136						
0.300	0.315		2.063	0.397	19.0	0.680	0.261	19.78
		0.190						
0.200	0.421		2.253	0.434	22.0	0.786	0.161	20.03
		0.221						
0.100	0.577		2.474	0.476	25.7	0.920	0.061	20.28
		0.199						
0.000	0.753		2.673	0.514	29.4	1.051	-0.039	20.53
		0.180						
-0.100	0.953		2.853	0.549	33.0	1.182	-0.139	20.78
		0.196						
-0.200	1.229		3.049	0.587	37.5	1.342	-0.239	21.03
		0.201						
-0.300	1.584		3.250	0.625	42.6	1.524	-0.339	21.28
		0.231						
-0.400	2.077		3.481	0.670	49.0	1.754	-0.439	21.53
		0.185						
-0.500	2.614		3.665	0.705	54.7	1.958	-0.539	21.78
		0.180						
-0.600	3.247		3.845	0.740	61.0	2.182	-0.639	22.03
		0.196						
-0.700	4.116		4.041	0.778	68.7	2.457	-0.739	22.28
		0.165						
-0.800	5.039		4.206	0.809	76.0	2.719	-0.839	22.53
		0.141						
-0.900	6.032		4.347	0.837	83.1	2.975	-0.939	22.78
		0.107						
-1.000	6.981		4.454	0.857	89.4	3.200	-1.039	23.03
		0.103						
-1.100	8.130		4.557	0.877	96.5	3.453	-1.139	23.28
		0.083						
-1.200	9.296		4.641	0.893	103.2	3.693	-1.239	23.53
		0.075						
-1.300	10.627		4.716	0.908	110.4	3.948	-1.339	23.78
		0.073						
-1.400	12.248		4.789	0.922	118.5	4.239	-1.439	24.03

Integration table for NGC 4371 R (J) Continued.

Log I	A	P	Sum P	K	R*	Rho	Log J	Mu
		0.074						
-1.500	14.315		4.863	0.936	128.1	4.582	-1.539	24.28
		0.070						
-1.600	16.767		4.932	0.949	138.6	4.959	-1.639	24.53
		0.063						
-1.700	19.558		4.995	0.961	149.7	5.356	-1.739	24.78
		0.046						
-1.800	22.109		5.041	0.970	157.2	5.695	-1.839	25.03
		0.036						
-1.900	24.618		5.076	0.977	168.0	6.009	-1.939	25.28
		0.022						
-2.000	26.562		5.098	0.981	174.5	6.242	-2.039	25.53
		0.098						
			5.196	1.000				

Sky Constant = 20.53

Integration table for NGC 4377 R (J)

Log I	A	P	Sum P	K	R*	Rho	Log J	Mu
1.400	0.004		0.000	0.000	2.2	0.193	1.095	17.03
		0.146						
1.300	0.011		0.146	0.096	3.5	0.306	0.995	17.28
		0.052						
1.200	0.014		0.198	0.129	4.0	0.344	0.895	17.53
		0.133						
1.100	0.023		0.331	0.216	5.1	0.447	0.795	17.78
		0.073						
1.000	0.030		0.404	0.264	5.8	0.506	0.695	18.03
		0.058						
0.900	0.036		0.463	0.302	6.4	0.558	0.595	18.28
		0.057						
0.800	0.044		0.519	0.339	7.1	0.617	0.495	18.53
		0.053						
0.700	0.053		0.572	0.374	7.8	0.679	0.395	18.78
		0.055						
0.600	0.066		0.627	0.410	8.7	0.753	0.295	19.03
		0.041						
0.500	0.077		0.669	0.437	9.4	0.817	0.195	19.28
		0.049						
0.400	0.094		0.718	0.469	10.4	0.904	0.095	19.53
		0.050						
0.300	0.117		0.768	0.502	11.6	1.005	-0.005	19.78
		0.071						
0.200	0.156		0.839	0.548	13.4	1.163	-0.105	20.03
		0.087						
0.100	0.218		0.926	0.605	15.8	1.373	-0.205	20.28
		0.077						
0.000	0.286		1.003	0.655	18.1	1.572	-0.305	20.53
		0.075						
-0.100	0.369		1.078	0.704	20.6	1.787	-0.405	20.78
		0.067						
-0.200	0.463		1.145	0.748	23.0	2.001	-0.505	21.03
		0.053						
-0.300	0.557		1.198	0.782	25.3	2.196	-0.605	21.28
		0.046						
-0.400	0.660		1.244	0.813	27.5	2.389	-0.705	21.53
		0.035						
-0.500	0.756		1.279	0.835	29.4	2.558	-0.805	21.78
		0.032						
-0.600	0.868		1.310	0.856	31.5	2.740	-0.905	22.03
		0.034						
-0.700	1.020		1.345	0.878	34.2	2.971	-1.005	22.28
		0.027						
-0.800	1.172		1.372	0.896	36.6	3.184	-1.105	22.53
		0.019						
-0.900	1.307		1.391	0.908	38.7	3.362	-1.205	22.78
		0.016						
-1.000	1.447		1.407	0.919	40.7	3.538	-1.305	23.03
		0.013						
-1.100	1.590		1.420	0.927	42.7	3.709	-1.405	23.28
		0.012						
-1.200	1.759		1.432	0.935	44.9	3.901	-1.505	23.53
		0.012						
-1.300	1.973		1.444	0.943	47.5	4.132	-1.605	23.78
		0.012						
-1.400	2.237		1.456	0.951	50.6	4.399	-1.705	24.03
		0.012						
-1.500	2.567		1.467	0.958	54.2	4.713	-1.805	24.28

Integration table for NGC 4377 R (J) Continued.

Log I	A	P	Sum P	K	R*	Rho	Log J	Mu
		0.012						
-1.600	2.989		1.479	0.966	58.5	5.085	-1.905	24.53
		0.018						
-1.700	3.776		1.497	0.978	65.8	5.715	-2.005	24.78
		0.009						
-1.800	4.273		1.506	0.984	70.0	6.080	-2.105	25.03
		0.005						
-1.900	4.633		1.511	0.987	72.9	6.331	-2.205	25.28
		0.004						
-2.000	4.968		1.515	0.989	75.4	6.556	-2.305	25.53
		0.016						
			1.531	1.000				

Sky Constant = 20.53

Integratio table for NGC 4419 R (J)

Log I	A	P	Sum P	K	R*	Rho	Log J	Mu
1.400	0.001		0.000	0.000	0.9	0.060	0.935	17.03
		0.179						
1.300	0.009		0.179	0.056	3.1	0.207	0.835	17.28
		0.207						
1.200	0.020		0.385	0.121	4.8	0.316	0.735	17.53
		0.236						
1.100	0.037		0.621	0.194	6.5	0.427	0.635	17.78
		0.228						
1.000	0.057		0.849	0.266	8.1	0.531	0.535	18.03
		0.155						
0.900	0.074		1.004	0.314	9.2	0.606	0.435	18.28
		0.118						
0.800	0.091		1.123	0.351	10.2	0.670	0.335	18.53
		0.147						
0.700	0.117		1.269	0.397	11.6	0.760	0.235	18.78
		0.156						
0.600	0.151		1.425	0.446	13.2	0.866	0.135	19.03
		0.121						
0.500	0.185		1.546	0.484	14.6	0.958	0.035	19.28
		0.164						
0.400	0.243		1.710	0.535	16.7	1.097	-0.065	19.53
		0.177						
0.300	0.322		1.887	0.590	17.2	1.261	-0.165	19.78
		0.196						
0.200	0.431		2.083	0.652	22.2	1.461	-0.265	20.03
		0.165						
0.100	0.547		2.248	0.703	25.0	1.646	-0.365	20.28
		0.151						
0.000	0.681		2.399	0.751	27.9	1.835	-0.465	20.53
		0.116						
-0.100	0.810		2.515	0.787	30.5	2.003	-0.565	20.78
		0.103						
-0.200	0.955		2.619	0.819	33.1	2.174	-0.665	21.03
		0.083						
-0.300	1.102		2.701	0.845	35.5	2.335	-0.765	21.28
		0.070						
-0.400	1.257		2.771	0.867	38.0	2.494	-0.865	21.53
		0.061						
-0.500	1.420		2.832	0.886	40.5	2.659	-0.965	21.78
		0.051						
-0.600	1.608		2.883	0.902	42.9	2.821	-1.065	22.03
		0.048						
-0.700	1.820		2.931	0.917	45.7	3.001	-1.165	22.28
		0.041						
-0.800	2.048		2.972	0.930	48.4	3.184	-1.265	22.53
		0.032						
-0.900	2.276		3.004	0.940	51.1	3.356	-1.365	22.78
		0.028						
-1.000	2.519		3.032	0.949	53.7	3.531	-1.465	23.03
		0.025						
-1.100	2.796		3.057	0.956	56.6	3.720	-1.565	23.28
		0.023						
-1.200	3.112		3.079	0.963	59.7	3.924	-1.665	23.53
		0.023						
-1.300	3.515		3.102	0.971	63.5	4.170	-1.765	23.78
		0.020						
-1.400	3.951		3.122	0.977	67.3	4.422	-1.865	24.03
		0.022						
-1.500	4.572		3.144	0.984	72.4	4.757	-1.965	24.28

Integration table for NGC 4419 R (J) Continued.

Log I	A	P	Sum P	K	R*	Rho	Log J	Mu
		0.019						
-1.600	5.236		3.163	0.990	77.5	5.090	-2.065	24.53
		0.013						
-1.700	5.794		3.175	0.993	81.5	5.355	-2.165	24.78
		0.006						
-1.800	6.118		3.181	0.995	83.7	5.502	-2.265	25.03
		0.004						
-1.900	6.384		3.185	0.996	85.5	5.620	-2.365	25.28
		0.011						
			3.196	1.000				

Sky Constant = 20.53

Integration table for NGC 4425 R (J)

Log I	A	P	Sum P	K	R*	Rho	Log J	Mu
1.300	0.003		0.000	0.000	1.8	0.116	1.099	17.28
		0.052						
1.200	0.006		0.052	0.031	2.6	0.164	0.999	17.53
		0.072						
1.100	0.011		0.123	0.074	3.5	0.225	0.899	17.78
		0.065						
1.000	0.017		0.189	0.114	4.4	0.279	0.799	18.03
		0.071						
0.900	0.025		0.260	0.156	5.3	0.339	0.699	18.28
		0.087						
0.800	0.037		0.347	0.209	6.5	0.415	0.599	18.53
		0.061						
0.700	0.048		0.408	0.246	7.4	0.472	0.499	18.78
		0.065						
0.600	0.062		0.473	0.285	8.4	0.539	0.399	19.03
		0.072						
0.500	0.082		0.545	0.328	9.7	0.621	0.299	19.28
		0.078						
0.400	0.110		0.623	0.375	11.2	0.717	0.199	19.53
		0.104						
0.300	0.156		0.727	0.438	13.4	0.854	0.099	19.78
		0.105						
0.200	0.214		0.832	0.501	15.7	1.002	-0.001	20.03
		0.069						
0.100	0.262		0.900	0.542	17.3	1.109	-0.101	20.28
		0.068						
0.000	0.322		0.968	0.583	19.2	1.229	-0.201	20.53
		0.067						
-0.100	0.397		1.035	0.623	21.3	1.364	-0.301	20.78
		0.057						
-0.200	0.477		1.092	0.657	23.4	1.494	-0.401	21.03
		0.063						
-0.300	0.588		1.155	0.695	26.0	1.660	-0.501	21.28
		0.053						
-0.400	0.707		1.208	0.727	28.5	1.820	-0.601	21.53
		0.048						
-0.500	0.842		1.256	0.757	31.1	1.986	-0.701	21.78
		0.045						
-0.600	1.002		1.302	0.784	33.9	2.167	-0.801	22.03
		0.041						
-0.700	1.186		1.343	0.809	36.9	2.357	-0.901	22.28
		0.039						
-0.800	1.402		1.382	0.832	40.1	2.563	-1.001	22.53
		0.029						
-0.900	1.606		1.411	0.850	42.9	2.743	-1.101	22.78
		0.028						
-1.000	1.851		1.439	0.866	46.1	2.945	-1.201	23.03
		0.021						
-1.100	2.080		1.459	0.879	48.8	3.122	-1.301	23.28
		0.020						
-1.200	2.367		1.480	0.891	52.1	3.330	-1.401	23.53
		0.022						
-1.300	2.748		1.501	0.904	56.1	3.588	-1.501	23.78
		0.018						
-1.400	3.158		1.520	0.915	60.2	3.846	-1.601	24.03
		0.026						
-1.500	3.876		1.545	0.930	66.6	4.262	-1.701	24.28
		0.026						
-1.600	4.780		1.571	0.946	74.0	4.732	-1.801	24.53

Integration table for NGC 4425 R (J) Continued.

Log I	A	P	Sum P	K	R*	Rho	Log J	Mu
		0.028						
-1.700	6.016		1.599	0.963	83.0	5.309	-1.901	24.78
		0.011						
-1.800	6.653		1.610	0.970	87.3	5.583	-2.001	25.03
		0.015						
-1.900	7.694		1.625	0.978	93.9	6.004	-2.101	25.28
		0.007						
-2.000	8.284		1.632	0.982	97.4	6.230	-2.201	25.53
		0.029						
			1.661	1.000				

Sky Constant = 20.53

Integration table for NGC 4429 R (J)

Log I	A	P	Sum P	K	R*	Rho	Log J	Mu
1.500	0.001		0.000	0.000	0.9	0.024	1.362	16.89
		0.082						
1.400	0.004		0.082	0.009	2.0	0.055	1.262	17.14
		0.227						
1.300	0.014		0.309	0.032	4.0	0.106	1.162	17.39
		0.245						
1.200	0.027		0.555	0.058	5.6	0.150	1.062	17.64
		0.410						
1.100	0.056		0.965	0.101	8.0	0.215	0.962	17.89
		0.407						
1.000	0.072		1.372	0.144	10.3	0.276	0.862	18.14
		0.498						
0.700	0.148		1.870	0.196	13.0	0.349	0.762	18.39
		0.349						
0.800	0.197		2.219	0.233	15.0	0.403	0.662	18.64
		0.400						
0.700	0.268		2.619	0.274	17.5	0.470	0.562	18.89
		0.337						
0.600	0.342		2.957	0.310	19.8	0.531	0.462	19.14
		0.314						
0.500	0.430		3.271	0.343	22.2	0.596	0.362	19.39
		0.284						
0.400	0.531		3.555	0.372	24.7	0.662	0.262	19.64
		0.361						
0.300	0.691		3.916	0.410	28.1	0.755	0.162	19.89
		0.449						
0.200	0.942		4.365	0.457	32.8	0.881	0.062	20.14
		0.712						
0.100	1.442		5.076	0.532	40.7	1.091	-0.038	20.39
		0.704						
0.000	2.065		5.780	0.606	48.6	1.305	-0.138	20.64
		0.423						
-0.100	2.537		6.203	0.650	53.9	1.446	-0.238	20.89
		0.318						
-0.200	2.982		6.521	0.683	58.5	1.568	-0.338	21.14
		0.304						
-0.300	3.520		6.825	0.715	63.5	1.704	-0.438	21.39
		0.280						
-0.400	4.143		7.105	0.744	68.9	1.848	-0.538	21.64
		0.303						
-0.500	4.991		7.408	0.776	75.6	2.029	-0.638	21.89
		0.334						
-0.600	6.167		7.742	0.811	84.1	2.255	-0.738	22.14
		0.302						
-0.700	7.507		8.044	0.843	92.8	2.488	-0.838	22.39
		0.272						
-0.800	9.026		8.316	0.871	101.7	2.728	-0.938	22.64
		0.249						
-0.900	10.777		8.565	0.897	111.1	2.981	-1.038	22.89
		0.210						
-1.000	12.637		8.775	0.919	120.3	3.228	-1.138	23.14
		0.157						
-1.100	14.391		8.932	0.936	128.4	3.445	-1.238	23.39
		0.142						
-1.200	16.381		9.074	0.951	137.0	3.676	-1.338	23.64
		0.123						
-1.300	18.558		9.197	0.964	145.8	3.912	-1.438	23.89
		0.094						
-1.400	20.644		9.291	0.973	153.8	4.126	-1.538	24.14

Integration table for NGC 4429 R (J) Continued.

Log I	A	P	Sum P	K	R*	Rho	Log J	Mu
-1.500	22.775		9.367	0.981	161.5	4.334	-1.638	24.39
		0.076						
-1.600	25.150		9.434	0.988	169.8	4.554	-1.738	24.64
		0.067						
-1.700	27.216		9.481	0.993	176.6	4.738	-1.838	24.89
		0.047						
-1.800	28.707		9.508	0.996	181.4	4.866	-1.938	25.14
		0.027						
-1.900	29.894		9.525	0.998	185.1	4.965	-2.038	25.39
		0.017						
-2.000	30.473		9.531	0.999	186.9	5.013	-2.138	25.64
		0.007						
		0.014	9.545	1.000				

Sky Constant = 20.64

Integration table for NGC 4435 R (J)

Log I	A	P	Sum P	K	R*	Rho	Log J	Mu
1.500	0.001		0.000	0.000	0.9	0.042	1.284	16.76
		0.225						
1.400	0.009		0.225	0.043	3.1	0.147	1.184	17.01
		0.292						
1.300	0.022		0.517	0.100	5.0	0.232	1.084	17.26
		0.297						
1.200	0.038		0.814	0.157	6.6	0.308	0.984	17.51
		0.226						
1.100	0.054		1.040	0.201	7.9	0.367	0.884	17.76
		0.252						
1.000	0.076		1.292	0.250	9.4	0.436	0.784	18.01
		0.239						
0.900	0.103		1.532	0.296	10.9	0.507	0.684	18.26
		0.185						
0.800	0.129		1.717	0.331	12.2	0.567	0.584	18.51
		0.200						
0.700	0.164		1.917	0.370	13.7	0.640	0.484	18.76
		0.165						
0.600	0.201		2.082	0.402	15.2	0.708	0.384	19.01
		0.147						
0.500	0.242		2.229	0.430	16.7	0.777	0.284	19.26
		0.129						
0.400	0.288		2.358	0.455	18.2	0.846	0.184	19.51
		0.127						
0.300	0.344		2.484	0.480	19.9	0.925	0.084	19.76
		0.125						
0.200	0.414		2.610	0.504	21.8	1.015	-0.016	20.01
		0.133						
0.100	0.508		2.743	0.530	24.1	1.124	-0.116	20.26
		0.137						
0.000	0.627		2.880	0.556	26.8	1.251	-0.216	20.51
		0.144						
-0.100	0.790		3.024	0.584	30.1	1.402	-0.316	20.76
		0.135						
-0.200	0.978		3.159	0.610	33.5	1.561	-0.416	21.01
		0.151						
-0.300	1.244		3.309	0.639	37.8	1.760	-0.516	21.26
		0.127						
-0.400	1.528		3.437	0.664	41.8	1.950	-0.616	21.51
		0.149						
-0.500	1.944		3.585	0.692	47.2	2.200	-0.716	21.76
		0.134						
-0.600	2.415		3.719	0.718	52.6	2.452	-0.816	22.01
		0.150						
-0.700	3.000		3.869	0.747	59.4	2.769	-0.916	22.26
		0.148						
-0.800	3.909		4.017	0.776	66.9	3.120	-1.016	22.51
		0.148						
-0.900	4.952		4.166	0.804	75.3	3.511	-1.116	22.76
		0.166						
-1.000	6.423		4.332	0.836	85.8	3.999	-1.216	23.01
		0.157						
-1.100	8.173		4.489	0.867	96.8	4.511	-1.316	23.26
		0.155						
-1.200	10.351		4.644	0.897	108.9	5.077	-1.416	23.51
		0.141						
-1.300	12.849		4.785	0.924	121.3	5.656	-1.516	23.76
		0.113						
-1.400	15.366		4.898	0.946	132.7	6.185	-1.616	24.01

Integration table for NGC 4435 R (J) Continued.

Log I	A	P	Sum P	K	R*	Rho	Log J	Mu
		0.086						
-1.500	17.770		4.984	0.962	142.7	6.652	-1.716	24.26
		0.062						
-1.600	19.959		5.046	0.974	151.2	7.049	-1.816	24.51
		0.048						
-1.700	22.068		5.094	0.984	159.0	7.413	-1.916	24.76
		0.027						
-1.800	23.567		5.121	0.989	164.3	7.660	-2.016	25.01
		0.018						
-1.900	24.856		5.139	0.992	168.8	7.867	-2.116	25.26
		0.013						
-2.000	25.980		5.152	0.995	172.5	8.043	-2.216	25.51
		0.028						
			5.179	1.000				

Sky Constant = 20.51

Integration table for NGC 4438 R (J)

Log I	A	P	Sum P	K	R*	Rho	Log J	Mu
1.400	0.004		0.000	0.000	2.2	0.054	1.641	17.01
		0.162						
1.300	0.012		0.162	0.020	3.6	0.088	1.541	17.26
		0.142						
1.200	0.019		0.304	0.038	4.7	0.115	1.441	17.51
		0.236						
1.100	0.036		0.540	0.068	6.4	0.156	1.341	17.76
		0.375						
1.000	0.069		0.915	0.115	8.9	0.216	1.241	18.01
		0.433						
0.900	0.118		1.348	0.169	11.6	0.282	1.141	18.26
		0.349						
0.800	0.167		1.698	0.213	13.8	0.336	1.041	18.51
		0.310						
0.700	0.221		2.008	0.252	15.9	0.387	0.941	18.76
		0.314						
0.600	0.291		2.322	0.291	18.3	0.444	0.841	19.01
		0.263						
0.500	0.365		2.585	0.324	20.4	0.497	0.741	19.26
		0.239						
0.400	0.449		2.824	0.354	22.7	0.551	0.641	19.51
		0.210						
0.300	0.542		3.034	0.381	24.9	0.606	0.541	19.76
		0.199						
0.200	0.653		3.233	0.406	27.4	0.665	0.441	20.01
		0.176						
0.100	0.777		3.409	0.428	29.8	0.725	0.341	20.26
		0.160						
0.000	0.919		3.570	0.448	32.5	0.789	0.241	20.51
		0.156						
-0.100	1.093		3.725	0.467	35.4	0.860	0.141	20.76
		0.180						
-0.200	1.346		3.906	0.490	39.3	0.954	0.041	21.01
		0.193						
-0.300	1.687		4.099	0.514	44.0	1.069	-0.059	21.26
		0.164						
-0.400	2.053		4.263	0.535	48.5	1.179	-0.159	21.51
		0.176						
-0.500	2.546		4.439	0.557	54.0	1.313	-0.259	21.76
		0.244						
-0.600	3.405		4.683	0.587	62.5	1.518	-0.359	22.01
		0.352						
-0.700	4.969		5.036	0.632	75.5	1.834	-0.459	22.26
		0.549						
-0.800	8.035		5.584	0.701	96.0	2.332	-0.559	22.51
		0.618						
-0.900	12.381		6.202	0.778	119.1	2.895	-0.659	22.76
		0.438						
-1.000	16.257		6.640	0.833	136.5	3.317	-0.759	23.01
		0.359						
-1.100	20.259		6.999	0.878	152.4	3.703	-0.859	23.26
		0.300						
-1.200	24.466		7.299	0.916	167.4	4.069	-0.959	23.51
		0.218						
-1.300	28.323		7.517	0.943	180.2	4.378	-1.059	23.76
		0.151						
-1.400	31.678		7.668	0.962	190.5	4.630	-1.159	24.01
		0.104						
-1.500	34.577		7.772	0.975	199.1	4.837	-1.259	24.26

Integration table for NGC 4438 R (J) Continued.

Log I	A	P	Sum P	K	R*	Rho	Log J	Mu
		0.074						
-1.600	37.186		7.846	0.984	206.4	5.017	-1.359	24.51
		0.047						
-1.700	39.261		7.893	0.990	212.1	5.155	-1.459	24.76
		0.029						
-1.800	40.880		7.922	0.994	216.4	5.260	-1.559	25.01
		0.020						
-1.900	42.273		7.941	0.996	220.1	5.349	-1.659	25.26
		0.010						
-2.000	43.194		7.952	0.997	222.5	5.407	-1.759	25.51
		0.020						
			7.972	1.000				

Sky Constant = 20.51

Integration table for NGC 4459 R (J)

log I	A	P	Sum P	K	R*	Rho	Log J	Mu
1.400	0.004		0.000	0.000	2.2	0.069	1.383	17.07
		0.211						
1.300	0.014		0.211	0.030	4.0	0.123	1.283	17.32
		0.271						
1.200	0.029		0.482	0.068	5.7	0.179	1.183	17.57
		0.369						
1.100	0.055		0.851	0.119	7.9	0.247	1.083	17.82
		0.415						
1.000	0.092		1.267	0.178	10.2	0.319	0.983	18.07
		0.298						
0.900	0.125		1.564	0.219	12.0	0.372	0.883	18.32
		0.313						
0.800	0.169		1.878	0.263	13.9	0.433	0.783	18.57
		0.257						
0.700	0.214		2.135	0.299	15.7	0.488	0.683	18.82
		0.237						
0.600	0.267		2.372	0.333	17.5	0.544	0.583	19.07
		0.219						
0.500	0.328		2.590	0.363	19.4	0.604	0.483	19.32
		0.162						
0.400	0.385		2.752	0.386	21.0	0.654	0.383	19.57
		0.214						
0.300	0.480		2.967	0.416	23.5	0.730	0.283	19.82
		0.207						
0.200	0.596		3.173	0.445	26.1	0.813	0.183	20.07
		0.214						
0.100	0.746		3.387	0.475	29.2	0.911	0.083	20.32
		0.214						
0.000	0.936		3.601	0.505	32.7	1.020	-0.017	20.57
		0.264						
-0.100	1.230		3.865	0.542	37.5	1.169	-0.117	20.82
		0.198						
-0.200	1.508		4.064	0.570	41.6	1.294	-0.217	21.07
		0.231						
-0.300	1.916		4.295	0.602	46.9	1.459	-0.317	21.32
		0.246						
-0.400	2.464		4.541	0.637	53.1	1.655	-0.417	21.57
		0.264						
-0.500	3.204		4.805	0.674	60.6	1.886	-0.517	21.82
		0.251						
-0.600	4.088		5.056	0.709	68.4	2.131	-0.617	22.07
		0.262						
-0.700	5.250		5.318	0.746	77.6	2.415	-0.717	22.32
		0.223						
-0.800	6.495		5.541	0.777	86.3	2.686	-0.817	22.57
		0.190						
-0.900	7.831		5.731	0.804	94.7	2.949	-0.917	22.82
		0.185						
-1.000	9.466		5.915	0.830	104.1	3.243	-1.017	23.07
		0.180						
-1.100	11.470		6.095	0.855	114.6	3.570	-1.117	23.32
		0.150						
-1.200	13.570		6.245	0.876	124.7	3.883	-1.217	23.57
		0.140						
-1.300	16.045		6.385	0.896	135.6	4.222	-1.317	23.82
		0.143						
-1.400	19.233		6.528	0.916	148.5	4.622	-1.417	24.07
		0.118						
-1.500	22.536		6.646	0.932	160.7	5.004	-1.517	24.32

Integration table for NGC 4459 R (J) Continued.

Log I	A	P	Sum P	K	R*	Rho	Log J	Mu
		0.116						
-1.600	26.630		6.762	0.949	174.7	5.439	-1.617	24.57
		0.094						
-1.700	30.805		6.857	0.962	187.9	5.850	-1.717	24.82
		0.071						
-1.800	34.745		6.927	0.972	199.5	6.213	-1.817	25.07
		0.042						
-1.900	37.733		6.970	0.978	207.9	6.474	-1.917	25.32
		0.035						
-2.000	40.842		7.005	0.983	216.3	6.736	-2.017	25.57
		0.124						
			7.129	1.000				

Sky Constant = 20.57

Integration table for NGC 4461 R (J)

Log I	A	P	Sum P	K	R*	Rho	Log J	Mu
1.400	0.006		0.000	0.000	2.7	0.124	1.335	17.02
		0.146						
1.300	0.013		0.146	0.041	3.9	0.175	1.235	17.27
		0.181						
1.200	0.023		0.327	0.092	5.1	0.233	1.135	17.52
		0.113						
1.100	0.031		0.440	0.124	6.0	0.270	1.035	17.77
		0.155						
1.000	0.045		0.594	0.168	7.2	0.325	0.935	18.02
		0.142						
0.900	0.061		0.737	0.208	8.3	0.378	0.835	18.27
		0.185						
0.800	0.087		0.922	0.260	10.0	0.452	0.735	18.52
		0.131						
0.700	0.110		1.052	0.297	11.2	0.508	0.635	18.77
		0.133						
0.600	0.139		1.185	0.335	12.6	0.573	0.535	19.02
		0.136						
0.500	0.177		1.322	0.373	14.3	0.647	0.435	19.27
		0.088						
0.400	0.208		1.410	0.398	15.5	0.701	0.335	19.52
		0.102						
0.300	0.254		1.512	0.427	17.1	0.774	0.235	19.77
		0.108						
0.200	0.314		1.621	0.458	19.0	0.861	0.135	20.02
		0.106						
0.100	0.389		1.726	0.488	21.1	0.957	0.035	20.27
		0.138						
0.000	0.510		1.864	0.527	24.2	1.097	-0.065	20.52
		0.165						
-0.100	0.694		2.029	0.573	28.2	1.280	-0.165	20.77
		0.114						
-0.200	0.854		2.142	0.605	31.3	1.419	-0.265	21.02
		0.106						
-0.300	1.041		2.248	0.635	34.5	1.567	-0.365	21.27
		0.097						
-0.400	1.257		2.346	0.663	38.0	1.722	-0.465	21.52
		0.107						
-0.500	1.557		2.453	0.693	42.2	1.916	-0.565	21.77
		0.086						
-0.600	1.861		2.539	0.717	46.2	2.095	-0.665	22.02
		0.070						
-0.700	2.173		2.609	0.737	49.9	2.264	-0.765	22.27
		0.069						
-0.800	2.560		2.678	0.757	54.2	2.457	-0.865	22.52
		0.053						
-0.900	2.933		2.732	0.772	58.0	2.630	-0.965	22.77
		0.045						
-1.000	3.330		2.776	0.784	61.8	2.803	-1.065	23.02
		0.052						
-1.100	3.912		2.829	0.799	67.0	3.038	-1.165	23.27
		0.049						
-1.200	4.574		2.877	0.813	72.6	3.292	-1.265	23.52
		0.063						
-1.300	5.706		2.940	0.831	80.9	3.668	-1.365	23.77
		0.104						
-1.400	8.013		3.044	0.860	95.8	4.347	-1.465	24.02
		0.130						
-1.500	11.659		3.174	0.897	115.6	5.244	-1.565	24.27

Integration table for NGC 4461 R (J) Continued.

Log I	A	P	Sum P	K	R*	Rho	Log J	Mu
		0.120						
-1.600	15.872		3.294	0.931	134.9	6.118	-1.665	24.52
		0.090						
-1.700	19.860		3.383	0.956	150.9	6.844	-1.765	24.77
		0.049						
-1.800	22.583		3.432	0.970	160.9	7.298	-1.865	25.02
		0.033						
-1.900	24.939		3.466	0.979	169.0	7.669	-1.965	25.27
		0.021						
-2.000	26.842		3.487	0.985	175.4	7.957	-2.065	25.52
		0.052						
			3.539	1.000				

Sky Constant = 20.52

Integration table for NGC 4474 R (J)

Log I	A	P	Sum P	K	R*	Rho	Log J	Mu
1.400	0.001		0.000	0.000	0.9	0.054	1.319	17.03
		0.114						
1.300	0.006		0.114	0.053	2.6	0.152	1.219	17.28
		0.077						
1.200	0.010		0.191	0.089	3.4	0.202	1.119	17.53
		0.113						
1.100	0.018		0.304	0.142	4.5	0.270	1.019	17.78
		0.106						
1.000	0.027		0.410	0.191	5.6	0.332	0.919	18.03
		0.078						
0.900	0.036		0.487	0.227	6.4	0.381	0.819	18.28
		0.087						
0.800	0.048		0.575	0.268	7.4	0.441	0.719	18.53
		0.057						
0.700	0.058		0.632	0.295	8.2	0.485	0.619	18.78
		0.088						
0.600	0.078		0.719	0.335	7.4	0.560	0.519	19.03
		0.070						
0.500	0.097		0.789	0.368	10.6	0.626	0.419	19.28
		0.068						
0.400	0.121		0.857	0.399	11.8	0.699	0.319	19.53
		0.063						
0.300	0.149		0.920	0.429	13.1	0.776	0.219	19.78
		0.068						
0.200	0.187		0.988	0.461	14.7	0.869	0.119	20.03
		0.071						
0.100	0.237		1.059	0.494	16.5	0.978	0.019	20.28
		0.070						
0.000	0.299		1.129	0.526	18.5	1.098	-0.081	20.53
		0.069						
-0.100	0.376		1.198	0.559	20.8	1.232	-0.181	20.78
		0.079						
-0.200	0.487		1.277	0.595	23.6	1.401	-0.281	21.03
		0.064						
-0.300	0.599		1.341	0.625	26.2	1.554	-0.381	21.28
		0.067						
-0.400	0.748		1.407	0.656	29.3	1.736	-0.481	21.53
		0.061						
-0.500	0.919		1.468	0.685	32.4	1.924	-0.581	21.78
		0.062						
-0.600	1.136		1.530	0.713	36.1	2.140	-0.681	22.03
		0.059						
-0.700	1.395		1.588	0.741	40.0	2.372	-0.781	22.28
		0.060						
-0.800	1.729		1.648	0.768	44.5	2.640	-0.881	22.53
		0.049						
-0.900	2.070		1.697	0.791	48.7	2.889	-0.981	22.78
		0.043						
-1.000	2.450		1.740	0.811	53.0	3.143	-1.081	23.03
		0.048						
-1.100	2.982		1.787	0.833	58.5	3.467	-1.181	23.28
		0.041						
-1.200	3.557		1.828	0.852	63.8	3.786	-1.281	23.53
		0.040						
-1.300	4.259		1.868	0.871	69.9	4.144	-1.381	23.78
		0.040						
-1.400	5.151		1.908	0.890	76.8	4.557	-1.481	24.03
		0.039						
-1.500	6.230		1.947	0.908	84.5	5.012	-1.581	24.28

Integration table for NGC 4474 R (J) Continued.

Log I	A	P	Sum P	K	R*	Rho	Log J	Mu
		0.036						
-1.600	7.507		1.983	0.924	92.7	5.501	-1.681	24.53
		0.033						
-1.700	8.978		2.016	0.940	101.4	6.016	-1.781	24.78
		0.026						
-1.800	10.425		2.042	0.952	109.3	6.483	-1.881	25.03
		0.017						
-1.900	11.574		2.059	0.960	115.3	6.837	-1.981	25.28
		0.016						
-2.000	13.044		2.075	0.967	122.3	7.251	-2.081	25.53
		0.070						
			2.145	1.000				

Sky Constant = 20.53

Integration table for NGC 4477 R (J)

Log I	A	P	Sum P	K	R*	Rho	Log J	Mu
1.400	0.002		0.000	0.000	1.6	0.050	1.439	17.03
		0.325						
1.300	0.017		0.325	0.053	4.4	0.139	1.339	17.28
		0.194						
1.200	0.027		0.519	0.085	5.6	0.179	1.239	17.53
		0.246						
1.100	0.045		0.765	0.126	7.2	0.229	1.139	17.78
		0.261						
1.000	0.068		1.025	0.169	8.8	0.282	1.039	18.03
		0.272						
0.900	0.098		1.297	0.213	10.6	0.339	0.939	18.28
		0.185						
0.800	0.124		1.482	0.244	11.9	0.381	0.839	18.53
		0.282						
0.700	0.174		1.764	0.290	14.1	0.451	0.739	18.78
		0.162						
0.600	0.210		1.926	0.317	15.5	0.496	0.639	19.03
		0.201						
0.500	0.266		2.127	0.350	17.5	0.558	0.539	19.28
		0.139						
0.400	0.315		2.266	0.373	19.0	0.608	0.439	19.53
		0.169						
0.300	0.390		2.435	0.400	21.1	0.676	0.339	19.78
		0.165						
0.200	0.482		2.600	0.428	23.5	0.752	0.239	20.03
		0.168						
0.100	0.601		2.768	0.455	26.2	0.839	0.139	20.28
		0.185						
0.000	0.764		2.953	0.486	29.6	0.946	0.039	20.53
		0.250						
-0.100	1.043		3.203	0.527	34.6	1.105	-0.061	20.78
		0.335						
-0.200	1.513		3.538	0.582	41.6	1.331	-0.161	21.03
		0.392						
-0.300	2.206		3.930	0.646	50.3	1.607	-0.261	21.28
		0.385						
-0.400	3.061		4.314	0.710	59.2	1.894	-0.361	21.53
		0.263						
-0.500	3.796		4.577	0.753	66.0	2.109	-0.461	21.78
		0.208						
-0.600	4.530		4.785	0.787	72.1	2.304	-0.561	22.03
		0.206						
-0.700	5.442		4.991	0.821	79.0	2.525	-0.661	22.28
		0.153						
-0.800	6.297		5.144	0.846	84.9	2.716	-0.761	22.53
		0.117						
-0.900	7.121		5.261	0.865	90.3	2.888	-0.861	22.78
		0.104						
-1.000	8.043		5.365	0.883	96.0	3.070	-0.961	23.03
		0.110						
-1.100	9.272		5.475	0.901	103.1	3.296	-1.061	23.28
		0.108						
-1.200	10.786		5.583	0.918	111.2	3.555	-1.161	23.53
		0.095						
-1.300	12.460		5.678	0.934	119.5	3.820	-1.261	23.78
		0.090						
-1.400	14.464		5.768	0.949	128.7	4.116	-1.361	24.03
		0.074						
-1.500	16.546		5.842	0.961	137.7	4.403	-1.461	24.28

Integration table for NGC 4477 R (J) Continued.

Log I	A	P	Sum P	K	R*	Rho	Log J	Mu
-1.600	18.728		5.904	0.971	146.5	4.684	-1.561	24.53
		0.062						
-1.700	20.625		5.947	0.978	153.7	4.915	-1.661	24.78
		0.043						
-1.800	22.801		5.986	0.985	161.6	5.168	-1.761	25.03
		0.039						
-1.900	24.274		6.007	0.988	166.8	5.333	-1.861	25.28
		0.021						
-2.000	25.866		6.025	0.991	172.2	5.505	-1.961	25.53
		0.018						
		0.054						
			6.079	1.000				

Sky Constant = 20.53

Integration table for NGC 4501 R (J)

Log I	A	P	Sum P	K	R*	Rho	Log J	Mu
1.400	0.001		0.000	0.000	1.3	0.028	1.223	17.08
		0.244						
1.300	0.012		0.244	0.017	3.7	0.080	1.123	17.33
		0.181						
1.200	0.022		0.424	0.030	5.1	0.108	1.023	17.58
		0.338						
1.100	0.046		0.763	0.054	7.3	0.156	0.923	17.83
		0.326						
1.000	0.075		1.089	0.077	9.3	0.198	0.823	18.08
		0.369						
0.900	0.116		1.457	0.103	11.5	0.247	0.723	18.33
		0.545						
0.800	0.193		2.002	0.141	14.9	0.318	0.623	18.58
		0.718						
0.700	0.319		2.720	0.192	19.1	0.409	0.523	18.83
		0.927						
0.600	0.526		3.647	0.258	24.5	0.525	0.423	19.08
		1.025						
0.500	0.813		4.672	0.330	30.5	0.653	0.323	19.33
		0.884						
0.400	1.124		5.556	0.393	35.9	0.768	-0.223	19.58
		0.692						
0.300	1.431		6.248	0.442	40.5	0.867	0.123	19.83
		0.687						
0.200	1.815		6.935	0.490	45.6	0.976	0.023	20.08
		0.595						
0.100	2.233		7.530	0.532	50.6	1.083	-0.077	20.33
		0.839						
0.000	2.976		8.368	0.591	58.4	1.250	-0.177	20.58
		0.882						
-0.100	3.959		9.251	0.654	67.4	1.442	-0.277	20.83
		1.024						
-0.200	5.395		10.274	0.726	78.6	1.683	-0.377	21.08
		0.742						
-0.300	6.706		11.016	0.779	87.7	1.876	-0.477	21.33
		0.546						
-0.400	7.920		11.562	0.817	95.3	2.039	-0.577	21.58
		0.408						
-0.500	9.061		11.970	0.846	101.9	2.181	-0.677	21.83
		0.351						
-0.600	10.299		12.321	0.871	108.6	2.325	-0.777	22.08
		0.265						
-0.700	11.474		12.586	0.890	114.7	2.454	-0.877	22.33
		0.206						
-0.800	12.627		12.792	0.904	120.3	2.574	-0.977	22.58
		0.154						
-0.900	13.710		12.946	0.915	125.3	2.683	-1.077	22.83
		0.139						
-1.000	14.943		13.085	0.925	130.9	2.801	-1.177	23.08
		0.132						
-1.100	16.409		13.217	0.934	137.1	2.935	-1.277	23.33
		0.124						
-1.200	18.143		13.340	0.943	144.2	3.086	-1.377	23.58
		0.129						
-1.300	20.417		13.469	0.952	153.0	3.274	-1.477	23.83
		0.120						
-1.400	23.087		13.589	0.960	162.7	3.481	-1.577	24.08
		0.120						
-1.500	26.444		13.709	0.969	174.1	3.726	-1.677	24.33

Integration table for NGC 4501 R (J) Continued.

Log I	A	P	Sum P	K	R*	Rho	Log J	Mu
		0.106						
-1.600	30.172		13.815	0.976	185.9	3.980	-1.777	24.58
		0.097						
-1.700	34.478		13.912	0.983	198.8	4.254	-1.877	24.83
		0.066						
-1.800	38.183		13.978	0.988	209.2	4.477	-1.977	25.08
		0.036						
-1.900	40.749		14.015	0.991	216.1	4.625	-2.077	25.33
		0.032						
-2.000	43.581		14.047	0.993	223.5	4.783	-2.177	25.58
		0.102						
			14.148	1.000				

Sky Constant = 20.58

Integration table for NGC 4503 R (J)

Log I	A	P	Sum P	K	R*	Rho	Log J	Mu
1.500	0.001		0.000	0.000	0.9	0.044	1.347	16.78
		0.143						
1.400	0.006		0.143	0.037	2.6	0.123	1.247	17.03
		0.195						
1.300	0.014		0.338	0.088	4.1	0.195	1.147	17.28
		0.155						
1.200	0.023		0.493	0.128	5.1	0.246	1.047	17.53
		0.123						
1.100	0.032		0.616	0.160	6.0	0.289	0.947	17.78
		0.163						
1.000	0.046		0.779	0.202	7.3	0.348	0.847	18.03
		0.181						
0.900	0.066		0.960	0.249	8.7	0.417	0.747	18.28
		0.113						
0.800	0.082		1.073	0.278	9.7	0.465	0.647	18.53
		0.159						
0.700	0.110		1.232	0.319	11.2	0.538	0.547	18.78
		0.152						
0.600	0.144		1.385	0.359	12.9	0.616	0.447	19.03
		0.136						
0.500	0.182		1.521	0.394	14.5	0.692	0.347	19.28
		0.117						
0.400	0.224		1.638	0.424	16.0	0.766	0.247	19.53
		0.110						
0.300	0.273		1.748	0.453	17.7	0.846	0.147	19.78
		0.114						
0.200	0.336		1.862	0.482	19.6	0.940	0.047	20.03
		0.161						
0.100	0.449		2.023	0.524	22.7	1.086	-0.053	20.28
		0.192						
0.000	0.619		2.215	0.574	26.6	1.276	-0.153	20.53
		0.161						
-0.100	0.799		2.376	0.616	30.3	1.449	-0.253	20.78
		0.175						
-0.200	1.044		2.551	0.661	34.6	1.656	-0.353	21.03
		0.142						
-0.300	1.295		2.693	0.698	38.5	1.845	-0.453	21.28
		0.128						
-0.400	1.580		2.821	0.731	42.5	2.037	-0.553	21.53
		0.125						
-0.500	1.931		2.946	0.763	47.0	2.252	-0.653	21.78
		0.116						
-0.600	2.342		3.063	0.793	51.8	2.480	-0.753	22.03
		0.109						
-0.700	2.824		3.172	0.822	56.9	2.724	-0.853	22.28
		0.102						
-0.800	3.393		3.273	0.848	62.4	2.986	-0.953	22.53
		0.072						
-0.900	3.899		3.345	0.867	66.8	3.201	-1.053	22.78
		0.060						
-1.000	4.433		3.406	0.882	71.3	3.413	-1.153	23.03
		0.050						
-1.100	4.988		3.455	0.895	75.6	3.620	-1.253	23.28
		0.046						
-1.200	5.633		3.501	0.907	80.3	3.847	-1.353	23.53
		0.044						
-1.300	6.407		3.545	0.918	85.7	4.103	-1.453	23.78
		0.045						
-1.400	7.417		3.591	0.930	92.2	4.415	-1.553	24.03

Integration table for NGC 4503 R (J) Continued.

Log I	A	P	Sum P	K	R*	Rho	Log J	Mu
		0.055						
-1.500	8.956		3.646	0.944	101.3	4.851	-1.653	24.28
		0.055						
-1.600	10.898		3.701	0.959	111.8	5.351	-1.753	24.53
		0.048						
-1.700	13.044		3.749	0.971	122.3	5.854	-1.853	24.78
		0.030						
-1.800	14.711		3.779	0.979	129.8	6.217	-1.953	25.03
		0.022						
-1.900	16.264		3.801	0.985	136.5	6.537	-2.053	25.28
		0.013						
-2.000	17.391		3.814	0.988	141.2	6.760	-2.153	25.53
		0.046						
			3.860	1.000				

Sky Constant = 20.53

Integration table for NGC 4531 R (J)

Log I	A	P	Sum P	K	R*	Rho	Log J	Mu
0.800	0.001		0.000	0.000	1.3	0.039	1.148	18.53
		0.033						
0.700	0.007		0.033	0.016	2.7	0.088	1.048	18.78
		0.039						
0.600	0.016		0.072	0.035	4.3	0.131	0.948	19.03
		0.036						
0.500	0.026		0.108	0 053	5.5	0.167	0.848	19.28
		0.094						
0.400	0.057		0.202	0.099	8.2	0.252	0.748	19.53
		0.058						
0.300	0.085		0.260	0.128	9.9	0.303	0.648	19.78
		0.128						
0.200	0.156		0.388	0.190	13.4	0.410	0.548	20.03
		0.159						
0.100	0.268		0.547	0.268	17.5	0.537	0.448	20.28
		0.104						
0.000	0.361		0.651	0.317	20.3	0.623	0.348	20.53
		0.097						
-0.100	0.469		0.748	0.367	23.2	0.710	0.248	20.78
		0.104						
-0.200	0.614		0.852	0 418	26.5	0.813	0.148	21.03
		0.117						
-0.300	0.821		0.969	0.475	30.7	0.940	0.048	21.28
		0.107						
-0.400	1.059		1.076	0.527	34.8	1.068	-0.052	21.53
		0.151						
-0.500	1.482		1.227	0.601	41.2	1.263	-0.152	21.78
		0.135						
-0.600	1.956		1.362	0.667	47.3	1.451	-0.252	22.03
		0.104						
-0.700	2.419		1.466	0.718	52.7	1.614	-0.352	22.28
		0.099						
-0.800	2.972		1.565	0.767	58.4	1.789	-0.452	22.53
		0.084						
-0.900	3.560		1.648	0.808	63.9	1.958	-0.552	22.78
		0.065						
-1.000	4.132		1.713	0.840	68.8	2.109	-0.652	23.03
		0.049						
-1.100	4.679		1.762	0.864	73.2	2.244	-0.752	23.28
		0.041						
-1.200	5.254		1.803	0.884	77.6	2.378	-0.852	23.53
		0.039						
-1.300	5.935		1.842	0.903	82.5	2.528	-0.952	23.78
		0.037						
-1.400	6.757		1.879	0.921	88.0	2.697	-1.052	24.03
		0.037						
-1.500	7.786		1.915	0.939	94.5	2.895	-1.152	24.28
		0.034						
-1.600	8.998		1.950	0.956	101.5	3.112	-1.252	24.53
		0.029						
-1.700	10.298		1.979	0.970	108.6	3.330	-1.352	24.78
		0.022						
-1.800	11.533		2.001	0.981	115.0	3.524	-1.452	25.03
		0.010						
-1.900	12.249		2.011	0.986	118.5	3.631	-1.552	25.28
		0.007						
-2.000	12.895		2.019	0.989	121.6	3.726	-1.652	25.53
		0.022						
			2.040	1.000				

Sky Constant = 20.53

Integration table for NGC 4550 R (J)

Log I	A	P	Sum P	K	R*	Rho	Log J	Mu
1.400	0.002		0.000	0.000	1.6	0.137	0.787	17.03
		0.097						
1.300	0.006		0.097	0.043	2.7	0.238	0.687	17.28
		0.219						
1.200	0.019		0.317	0.138	4.6	0.404	0.587	17.53
		0.226						
1.100	0.035		0.542	0.237	6.3	0.549	0.487	17.78
		0.195						
1.000	0.052		0.738	0.322	7.7	0.673	0.387	18.03
		0.123						
0.900	0.066		0.861	0.376	8.7	0.756	0.287	18.28
		0.123						
0.800	0.083		0.984	0.429	9.7	0.850	0.187	18.53
		0.086						
0.700	0.098		1.070	0.467	10.6	0.924	0.087	18.78
		0.088						
0.600	0.118		1.157	0.505	11.6	1.012	-0.013	19.03
		0.088						
0.500	0.142		1.245	0.543	12.8	1.112	-0.113	19.28
		0.063						
0.400	0.164		1.308	0.571	13.7	1.197	-0.213	19.53
		0.062						
0.300	0.192		1.370	0.598	14.8	1.293	-0.313	19.78
		0.075						
0.200	0.234		1.445	0.630	16.4	1.427	-0.413	20.03
		0.068						
0.100	0.281		1.513	0.660	18.0	1.565	-0.513	20.28
		0.064						
0.000	0.337		1.576	0.688	19.7	1.715	-0.613	20.53
		0.063						
-0.100	0.407		1.639	0.715	21.6	1.884	-0.713	20.78
		0.073						
-0.200	0.510		1.712	0.747	24.2	2.109	-0.813	21.03
		0.049						
-0.300	0.598		1.762	0.769	26.2	2.282	-0.913	21.28
		0.049						
-0.400	0.706		1.810	0.790	28.4	2.480	-1.013	21.53
		0.049						
-0.500	0.844		1.860	0.811	31.1	2.712	-1.113	21.78
		0.034						
-0.600	0.963		1.894	0.826	33.2	2.897	-1.213	22.03
		0.031						
-0.700	1.101		1.925	0.840	35.5	3.097	-1.313	22.28
		0.030						
-0.800	1.266		1.954	0.852	38.1	3.321	-1.413	22.53
		0.025						
-0.900	1.442		1.979	0.863	40.6	3.545	-1.513	22.78
		0.021						
-1.000	1.631		2.001	0.873	43.2	3.769	-1.613	23.03
		0.019						
-1.100	1.842		2.019	0.881	45.9	4.006	-1.713	23.28
		0.019						
-1.200	2.111		2.039	0.889	49.2	4.289	-1.813	23.53
		0.019						
-1.300	2.439		2.057	0.897	52.9	4.610	-1.913	23.78
		0.017						
-1.400	2.819		2.074	0.905	56.8	4.956	-2.013	24.03
		0.023						
-1.500	3.475		2.098	0.915	63.1	5.503	-2.113	24.28

Integration table for NGC 4550 R (J) Continued.

Log I	A	P	Sum P	K	R*	Rho	Log J	Mu
-1.600	4.833		2.136	0.932	74.4	6.489	-2.213	24.53
		0.039						
-1.700	6.230		2.168	0.946	84.5	7.367	-2.313	24.78
		0.031						
-1.800	7.625		2.193	0.957	93.5	8.151	-2.413	25.03
		0.025						
-1.900	8.863		2.210	0.964	100.8	8.788	-2.513	25.28
		0.018						
-2.000	9.898		2.222	0.969	106.5	9.286	-2.613	25.53
		0.012						
			2.234	0.974				
		0.070						
			2.292	1.000				

Sky Constant = 20.53

Integration table for NGC 4552 R

Log I	A	P	Sum P	K	R*	Rho	Log J	Mu
1.500	0.000		0.000	0.000	1.8	0.040	1.656	16.63
		0.327						
1.400	0.014		0.327	0.022	4.1	0.009	1.556	16.88
		0.365						
1.300	0.040		0.692	0.081	6.8	0.148	1.456	17.13
		0.361						
1.200	0.061		1.054	0.113	8.3	0.182	1.356	17.38
		0.461						
1.100	0.093		1.735	0.155	10.3	0.225	1.256	17.63
		0.318						
1.000	0.121		2.053	0.183	11.8	0.257	1.156	17.88
		0.382						
0.900	0.164		2.434	0.217	13.7	0.298	1.056	18.13
		0.313						
0.800	0.200		2.748	0.245	15.4	0.336	0.956	18.38
		0.309						
0.700	0.240		3.086	0.275	17.5	0.382	0.856	18.63
		0.279						
0.600	0.280		3.365	0.300	19.4	0.423	0.756	18.88
		0.281						
0.500	0.408		3.646	0.325	21.6	0.471	0.656	19.13
		0.305						
0.400	0.516		3.951	0.352	24.3	0.530	0.556	19.38
		0.288						
0.300	0.640		4.238	0.378	27.1	0.592	0.456	19.63
		0.325						
0.200	0.855		4.564	0.407	30.7	0.670	0.356	19.88
		0.292						
0.100	1.030		4.856	0.433	34.4	0.747	0.256	20.13
		0.305						
0.000	1.301		5.161	0.460	38.6	0.841	0.156	20.38
		0.292						
-0.100	1.626		5.453	0.486	43.2	0.941	0.056	20.63
		0.287						
-0.200	2.029		5.740	0.511	48.2	1.051	-0.044	20.88
		0.318						
-0.300	2.591		6.058	0.540	54.5	1.187	-0.144	21.13
		0.295						
-0.400	3.248		6.354	0.566	61.0	1.329	-0.244	21.38
		0.317						
-0.500	4.196		6.672	0.596	69.3	1.511	-0.344	21.63
		0.363						
-0.600	5.409		7.035	0.627	78.7	1.715	-0.444	21.88
		0.341						
-0.700	6.916		7.376	0.657	89.0	1.940	-0.544	22.13
		0.361						
-0.800	8.934		7.737	0.689	101.2	2.205	-0.644	22.38
		0.368						
-0.900	11.584		8.105	0.722	114.7	2.504	-0.744	22.63
		0.361						
-1.000	14.719		8.466	0.754	129.9	2.830	-0.844	22.88
		0.335						
-1.100	18.673		8.801	0.786	146.3	3.187	-0.944	23.13
		0.331						
-1.200	23.311		9.151	0.815	163.4	3.561	-1.044	23.38
		0.283						
-1.300	28.305		9.434	0.841	180.1	3.924	-1.144	23.63
		0.236						
-1.400	33.550		9.670	0.862	196.1	4.273	-1.244	23.88

Interation table for NGC 4552 R FLL Continued.

Log I	A	P	Sum P	K	R*	Rho	Log J	Mu
-1.500	37.479		9.880	0.880	212.5	4.631	-1.344	24.13
		0.210						
-1.600	41.553		10.054	0.896	228.5	4.978	-1.444	24.38
		0.174						
-1.700	50.577		10.167	0.906	240.7	5.246	-1.544	24.63
		0.113						
-1.800	55.447		10.254	0.914	252.1	5.493	-1.644	24.88
		0.087						
-1.900	59.103		10.306	0.918	260.2	5.671	-1.744	25.13
		0.052						
-2.000	61.600		10.335	0.921	265.9	5.793	-1.844	25.38
		0.029						
		0.869	11.204	1.000				

Sky Constant = 20.30

Integration table for NGC 4267 I (J)

Log I	A	P	Sum P	K	R*	Rho	Log J	Mu
1.200	0.019		0.000	0.000	4.6	0.135	1.702	16.68
		0.062						
1.100	0.023		0.062	0.035	5.1	0.150	1.602	16.93
		0.016						
1.000	0.025		0.078	0.044	5.3	0.154	1.502	17.18
		0.039						
0.900	0.029		0.117	0.066	5.7	0.167	1.402	17.43
		0.026						
0.800	0.032		0.142	0.081	6.1	0.178	1.302	17.68
		0.045						
0.700	0.040		0.187	0.107	6.8	0.198	1.202	17.93
		0.036						
0.600	0.048		0.223	0.127	7.4	0.217	1.102	18.18
		0.026						
0.500	0.056		0.249	0.142	8.0	0.232	1.002	18.43
		0.049						
0.400	0.073		0.298	0.170	9.1	0.266	0.902	18.68
		0.041						
0.300	0.091		0.338	0.193	10.2	0.297	0.802	18.93
		0.044						
0.200	0.115		0.382	0.218	11.5	0.335	0.702	19.18
		0.039						
0.100	0.143		0.421	0.240	12.8	0.372	0.602	19.43
		0.046						
0.000	0.183		0.467	0.266	14.5	0.422	0.502	19.68
		0.056						
-0.100	0.246		0.523	0.298	16.8	0.489	0.402	19.93
		0.059						
-0.200	0.329		0.582	0.332	19.4	0.565	0.302	20.18
		0.069						
-0.300	0.450		0.651	0.371	22.7	0.661	0.202	20.43
		0.097						
-0.400	0.665		0.747	0.426	27.6	0.804	0.102	20.68
		0.128						
-0.500	1.023		0.875	0.499	34.2	0.997	0.002	20.93
		0.128						
-0.600	1.475		1.003	0.572	41.1	1.197	-0.098	21.18
		0.128						
-0.700	2.044		1.132	0.645	48.4	1.409	-0.198	21.43
		0.111						
-0.800	2.666		1.243	0.708	55.3	1.609	-0.298	21.68
		0.092						
-0.900	3.315		1.335	0.761	61.6	1.794	-0.398	21.93
		0.083						
-1.000	4.049		1.418	0.808	68.1	1.983	-0.498	22.18
		0.067						
-1.100	4.795		1.485	0.846	74.1	2.158	-0.598	22.43
		0.045						
-1.200	5.422		1.530	0.872	78.8	2.295	-0.698	22.68
		0.039						
-1.300	6.112		1.569	0.894	83.7	2.436	-0.798	22.93
		0.038						
-1.400	6.953		1.607	0.916	89.3	2.599	-0.898	23.18
		0.044						
-1.500	8.190		1.651	0.941	96.9	2.820	-0.998	23.43
		0.030						
-1.600	9.263		1.681	0.958	103.0	2.999	-1.098	23.68
		0.026						
-1.700	10.436		1.708	0.973	109.4	3.184	-1.198	23.93

Integration table for NGC 4267 I (J) Continued.

Log I	A	P	Sum P	K	R*	Rho	Log J	Mu
		0.025						
-1.800	11.842		1.733	0.988	116.5	3.391	-1.298	24.18
		0.010						
-1.900	12.533		1.743	0.993	119.8	3.489	-1.398	24.43
		0.003						
-2.000	12.817		1.746	0.995	121.2	3.528	-1.498	24.68
		0.009						
			1.755	1.000				

Sky Constant = 19.68

Integration table for NGC 4371 I (J)

Log I	A	P	Sum P	K	R*	Rho	Log J	Mu
1.800	0.001		0.000	0.000	1.3	0.053	1.850	15.18
		0.122						
1.700	0.004		0.122	0.035	2.0	0.084	1.750	15.43
		0.162						
1.600	0.007		0.285	0.082	2.9	0.119	1.650	15.68
		0.052						
1.500	0.009		0.336	0.097	3.1	0.130	1.550	15.93
		0.061						
1.400	0.011		0.397	0.114	3.5	0.145	1.450	16.18
		0.049						
1.300	0.013		0.446	0.128	3.9	0.159	1.350	16.43
		0.065						
1.200	0.017		0.511	0.147	4.4	0.180	1.250	16.68
		0.051						
1.100	0.020		0.562	0.162	4.8	0.199	1.150	16.93
		0.033						
1.000	0.023		0.595	0.171	5.1	0.212	1.050	17.18
		0.084						
0.900	0.032		0.679	0.195	6.1	0.252	0.950	17.43
		0.139						
0.800	0.052		0.817	0.235	7.7	0.318	0.850	17.68
		0.127						
0.700	0.074		0.744	0.271	9.2	0.381	0.750	17.93
		0.101						
0.600	0.097		1.044	0.300	10.5	0.434	0.650	18.18
		0.113						
0.500	0.128		1.158	0.333	12.1	0.501	0.550	18.43
		0.096						
0.400	0.162		1.254	0.360	13.6	0.563	0.450	18.68
		0.086						
0.300	0.200		1.340	0.385	15.2	0.626	0.350	18.93
		0.103						
0.200	0.258		1.443	0.415	17.2	0.710	0.250	19.18
		0.101						
0.100	0.330		1.545	0.444	19.4	0.802	0.150	19.43
		0.132						
0.000	0.446		1.677	0.482	22.6	0.934	0.050	19.68
		0.124						
-0.100	0.584		1.800	0.518	25.9	1.068	-0.050	19.93
		0.113						
-0.200	0.743		1.913	0.550	29.2	1.204	-0.150	20.18
		0.116						
-0.300	0.948		2.030	0.583	33.0	1.361	-0.250	20.43
		0.101						
-0.400	1.173		2.131	0.613	36.7	1.513	-0.350	20.68
		0.108						
-0.500	1.475		2.238	0.643	41.1	1.697	-0.450	20.93
		0.127						
-0.600	1.924		2.366	0.680	47.0	1.938	-0.550	21.18
		0.111						
-0.700	2.415		2.476	0.712	52.6	2.171	-0.650	21.43
		0.093						
-0.800	2.932		2.569	0.739	58.0	2.393	-0.750	21.68
		0.103						
-0.900	3.655		2.672	0.768	64.7	2.671	-0.850	21.93
		0.099						
-1.000	4.533		2.771	0.797	72.1	2.975	-0.950	22.18
		0.110						
-1.100	5.760		2.881	0.828	81.2	3.353	-1.050	22.43

Integration table for NGC 4371 I (J) Continued.

Log I	A	P	Sum P	K	R*	Rho	Log J	Mu
		0.081						
-1.200	6.892		2.962	0.851	88.9	3.668	-1.150	22.68
		0.069						
-1.300	8.105		3.030	0.871	96.4	3.978	-1.250	22.93
		0.079						
-1.400	9.861		3.109	0.894	106.3	4.388	-1.350	23.18
		0.085						
-1.500	12.238		3.194	0.918	118.4	4.888	-1.450	23.43
		0.078						
-1.600	14.983		3.272	0.941	131.0	5.409	-1.550	23.68
		0.079						
-1.700	18.504		3.352	0.963	145.6	6.011	-1.650	23.93
		0.037						
-1.800	20.544		3.388	0.974	153.4	6.333	-1.750	24.18
		0.030						
-1.900	22.656		3.418	0.983	161.1	6.651	-1.850	24.43
		0.015						
-2.000	23.948		3.433	0.987	165.7	6.838	-1.950	24.68
		0.046						
			3.479	1.000				

Sky Constant = 19.68

Integration table for NGC 4377 I (J)

Log I	A	P	Sum P	K	R*	Rho	Log J	Mu
1.600	0.003		0.000	0.000	1.8	0.154	1.506	15.68
1.500	0.006	0.103	0.103	0.092	2.6	0.217	1.406	15.93
1.400	0.007	0.041	0.144	0.128	2.9	0.243	1.306	16.18
1.300	0.009	0.032	0.176	0.157	3.1	0.266	1.206	16.43
1.200	0.011	0.039	0.215	0.192	3.5	0.298	1.106	16.68
1.100	0.012	0.010	0.225	0.201	3.6	0.307	1.006	16.93
1.000	0.013	0.016	0.242	0.216	3.9	0.326	0.906	17.18
0.900	0.016	0.026	0.268	0.239	4.3	0.360	0.806	17.43
0.800	0.021	0.036	0.304	0.271	4.9	0.414	0.706	17.68
0.700	0.032	0.061	0.365	0.325	6.0	0.510	0.606	17.93
0.600	0.037	0.023	0.387	0.346	6.5	0.549	0.506	18.18
0.500	0.045	0.031	0.418	0.373	7.2	0.610	0.406	18.43
0.400	0.056	0.031	0.449	0.401	8.0	0.678	0.306	18.68
0.300	0.071	0.034	0.483	0.431	9.0	0.764	0.206	18.93
0.200	0.087	0.027	0.510	0.455	10.0	0.842	0.106	19.18
0.100	0.120	0.047	0.557	0.497	11.7	0.990	0.006	19.43
0.000	0.164	0.050	0.607	0.541	13.7	1.157	-0.094	19.68
-0.100	0.215	0.046	0.653	0.582	15.7	1.326	-0.194	19.93
-0.200	0.280	0.052	0.705	0.629	18.2	1.536	-0.294	20.18
-0.300	0.367	0.044	0.750	0.669	20.5	1.733	-0.394	20.43
-0.400	0.446	0.036	0.786	0.701	22.6	1.911	-0.494	20.68
-0.500	0.529	0.029	0.815	0.727	24.6	2.080	-0.594	20.93
-0.600	0.606	0.022	0.837	0.747	26.4	2.228	-0.694	21.18
-0.700	0.697	0.020	0.858	0.765	28.3	2.389	-0.794	21.43
-0.800	0.792	0.017	0.875	0.780	30.1	2.547	-0.894	21.68
-0.900	0.923	0.019	0.893	0.797	32.5	2.748	-0.994	21.93
-1.000	1.053	0.015	0.908	0.810	34.7	2.935	-1.094	22.18
-1.100	1.190	0.012	0.920	0.821	36.9	3.121	-1.194	22.43
-1.200	1.330	0.010	0.930	0.830	39.0	3.299	-1.294	22.68
-1.300	1.490	0.009	0.939	0.838	41.3	3.492	-1.394	22.93

Integration table for NGC 4377 I (J) Continued.

Log I	A	P	Sum P	K	R*	Rho	Log J	Mu
-1.400	1.691	0.009	0.948	0.846	44.0	3.720	-1.494	23.18
-1.500	1.982	0.010	0.959	0.855	47.7	4.028	-1.594	23.43
-1.600	2.470	0.014	0.972	0.867	53.2	4.496	-1.694	23.68
-1.700	3.021	0.012	0.985	0.878	58.8	4.972	-1.794	23.93
-1.800	4.209	0.021	1.006	0.897	69.4	5.869	-1.894	24.18
-1.900	5.919	0.024	1.030	0.919	82.4	6.960	-1.994	24.43
-2.000	6.352	0.005	1.035	0.923	85.3	7.210	-2.094	24.68
		0.086	1.121	1.000				

Sky Constant = 19.68

Integration table for NGC 4419 I (J)

log I	A	P	Sum P	K	R*	Rho	Log J	Mu
1.200	0.017		0.000	0.000	4.4	0.237	1.135	16.68
		0.031						
1.100	0.019		0.031	0.020	4.6	0.252	1.035	16.93
		0.065						
1.000	0.025		0.096	0.062	5.3	0.289	0.935	17.18
		0.065						
0.900	0.032		0.161	0.104	6.0	0.328	0.835	17.43
		0.067						
0.800	0.041		0.227	0.148	6.9	0.374	0.735	17.68
		0.053						
0.700	0.050		0.280	0.182	7.6	0.414	0.635	17.93
		0.075						
0.600	0.067		0.355	0.231	8.8	0.477	0.535	18.18
		0.044						
0.500	0.077		0.399	0.259	9.5	0.519	0.435	18.43
		0.053						
0.400	0.098		0.452	0.294	10.6	0.577	0.335	18.68
		0.078						
0.300	0.133		0.530	0.344	12.3	0.671	0.235	18.93
		0.081						
0.200	0.178		0.611	0.397	14.3	0.778	0.135	19.18
		0.118						
0.100	0.261		0.729	0.474	17.3	0.942	0.035	19.43
		0.115						
0.000	0.363		0.844	0.548	20.4	1.110	-0.065	19.68
		0.116						
-0.100	0.492		0.960	0.623	23.7	1.293	-0.165	19.93
		0.096						
-0.200	0.626		1.055	0.685	26.8	1.458	-0.265	20.18
		0.073						
-0.300	0.756		1.129	0.733	29.4	1.602	-0.365	20.43
		0.062						
-0.400	0.893		1.190	0.773	32.0	1.741	-0.465	20.68
		0.049						
-0.500	1.029		1.239	0.805	34.3	1.870	-0.565	20.93
		0.039						
-0.600	1.167		1.278	0.830	36.6	1.991	-0.665	21.18
		0.033						
-0.700	1.312		1.311	0.852	38.8	2.111	-0.765	21.43
		0.031						
-0.800	1.488		1.343	0.872	41.3	2.249	-0.865	21.68
		0.024						
-0.900	1.659		1.367	0.888	43.6	2.374	-0.965	21.93
		0.022						
-1.000	1.854		1.389	0.902	46.1	2.510	-1.065	22.18
		0.018						
-1.100	2.058		1.407	0.914	48.6	2.644	-1.165	22.43
		0.021						
-1.200	2.352		1.428	0.928	51.9	2.827	-1.265	22.68
		0.017						
-1.300	2.644		1.445	0.938	55.0	2.997	-1.365	22.93
		0.012						
-1.400	2.906		1.456	0.946	57.7	3.142	-1.465	23.18
		0.009						
-1.500	3.160		1.465	0.952	60.2	3.277	-1.565	23.43
		0.014						
-1.600	3.644		1.479	0.961	64.6	3.519	-1.665	23.68
		0.060						
			1.540	1.000				

Sky Constant = 19.68

Integration table for NGC 4425 I (J)

Log I	A	P	Sum P	K	R*	Rho	Log J	Mu
1.100	0.002		0.000	0.000	1.6	0.094	1.179	16.93
0.900	0.005	0.030	0.030	0.030	2.4	0.143	0.979	17.43
0.800	0.009	0.031	0.060	0.062	3.3	0.195	0.879	17.68
0.700	0.017	0.045	0.105	0.107	4.5	0.265	0.779	17.93
0.600	0.027	0.045	0.151	0.154	5.6	0.333	0.679	18.18
0.500	0.038	0.039	0.189	0.193	6.6	0.394	0.579	18.43
0.400	0.052	0.039	0.228	0.233	7.7	0.459	0.479	18.68
0.300	0.071	0.044	0.272	0.278	9.0	0.538	0.379	18.93
0.200	0.097	0.045	0.317	0.324	10.5	0.626	0.279	19.18
0.100	0.141	0.064	0.381	0.389	12.7	0.757	0.179	19.43
0.000	0.201	0.068	0.448	0.458	15.2	0.903	0.079	19.68
-0.100	0.258	0.051	0.500	0.510	17.2	1.023	-0.021	19.93
-0.200	0.314	0.040	0.540	0.551	19.0	1.129	-0.121	20.18
-0.300	0.383	0.039	0.578	0.590	20.9	1.246	-0.221	20.43
-0.400	0.463	0.036	0.614	0.627	23.0	1.370	-0.321	20.68
-0.500	0.557	0.034	0.648	0.661	25.3	1.504	-0.421	20.93
-0.600	0.654	0.027	0.676	0.689	27.4	1.629	-0.521	21.18
-0.700	0.766	0.025	0.701	0.715	29.6	1.762	-0.621	21.43
-0.800	0.915	0.027	0.727	0.742	32.4	1.927	-0.721	21.68
-0.900	1.082	0.024	0.751	0.766	35.2	2.095	-0.821	21.93
-1.000	1.268	0.021	0.772	0.788	38.1	2.268	-0.921	22.18
-1.100	1.483	0.019	0.791	0.807	41.2	2.453	-1.021	22.43
-1.200	1.722	0.017	0.808	0.825	44.4	2.643	-1.121	22.68
-1.300	2.007	0.016	0.825	0.841	48.0	2.854	-1.221	22.93
-1.400	2.285	0.012	0.837	0.854	51.2	3.044	-1.321	23.18
-1.500	2.722	0.016	0.853	0.870	55.9	3.323	-1.421	23.43
-1.600	3.313	0.017	0.870	0.887	61.6	3.666	-1.521	23.68
-1.700	3.930	0.014	0.883	0.901	67.1	3.993	-1.621	23.93
-1.800	4.812	0.016	0.899	0.917	74.3	4.418	-1.721	24.18
-1.900	5.751	0.013	0.913	0.931	81.2	4.830	-1.821	24.43

Integration table for NGC 4425 I (J) Continued.

Log I	A	P	Sum P	K	R*	Rho	Log J	Mu
-2.000	6.453	0.008	0.920	0.939	86.0	5.116	-1.921	24.68
		0.060	0.980	1.000				

Sky Constant = 19.68

Integration table for NGC 4429 I (J)

Log I	A	P	Sum P	K	R*	Rho	Log J	Mu
2.100	0.006		0.000	0.000	2.7	0.080	2.107	14.64
		0.081						
2.000	0.007		0.081	0.012	2.9	0.084	2.007	14.89
		0.259						
1.900	0.010		0.340	0.049	3.4	0.099	1.907	15.14
		0.103						
1.800	0.012		0.443	0.064	3.6	0.106	1.807	15.39
		0.204						
1.700	0.015		0.647	0.093	4.2	0.122	1.707	15.64
		0.032						
1.600	0.016		0.679	0.098	4.3	0.125	1.607	15.89
		0.103						
1.500	0.019		0.782	0.113	4.6	0.135	1.507	16.14
		0.061						
1.400	0.021		0.844	0.121	4.9	0.143	1.407	16.39
		0.081						
1.300	0.025		0.925	0.133	5.3	0.155	1.307	16.64
		0.026						
1.200	0.026		0.951	0.137	5.5	0.159	1.207	16.89
		0.072						
1.100	0.031		1.023	0.147	6.0	0.174	1.107	17.14
		0.065						
1.000	0.037		1.088	0.156	6.5	0.190	1.007	17.39
		0.129						
0.900	0.051		1.217	0.175	7.7	0.224	0.907	17.64
		0.236						
0.800	0.084		1.454	0.209	9.8	0.287	0.807	17.89
		0.310						
0.700	0.139		1.764	0.254	12.6	0.369	0.707	18.14
		0.237						
0.600	0.192		2.000	0.288	14.8	0.433	0.607	18.39
		0.237						
0.500	0.258		2.237	0.322	17.2	0.503	0.507	18.64
		0.235						
0.400	0.341		2.473	0.356	19.8	0.578	0.407	18.89
		0.203						
0.300	0.431		2.676	0.385	22.2	0.650	0.307	19.14
		0.230						
0.200	0.560		2.905	0.418	25.3	0.740	0.207	19.39
		0.251						
0.100	0.736		3.157	0.454	29.0	0.849	0.107	19.64
		0.289						
0.000	0.992		3.446	0.496	33.7	0.985	0.007	19.89
		0.601						
-0.100	1.662		4.047	0.582	43.6	1.275	-0.093	20.14
		0.345						
-0.200	2.147		4.392	0.632	49.6	1.449	-0.193	20.39
		0.235						
-0.300	2.561		4.627	0.665	54.2	1.583	-0.293	20.64
		0.185						
-0.400	2.973		4.812	0.692	58.4	1.706	-0.393	20.89
		0.175						
-0.500	3.464		4.987	0.717	63.0	1.841	-0.493	21.14
		0.169						
-0.600	4.059		5.156	0.741	68.2	1.993	-0.593	21.39
		0.167						
-0.700	4.799		5.323	0.765	74.2	2.167	-0.693	21.64
		0.179						
-0.800	5.797		5.501	0.791	81.5	2.382	-0.793	21.89

Integration table for NGC 4429 I (J) Continued.

Log I	A	P	Sum P	K	R*	Rho	Log J	Mu
-0.900	6.950		5.665	0.815	89.2	2.608	-0.893	22.14
		0.164						
-1.000	8.300		5.818	0.837	97.5	2.850	-0.993	22.39
		0.153						
-1.100	10.018		5.972	0.859	107.1	3.131	-1.093	22.64
		0.154						
-1.200	11.949		6.110	0.879	117.0	3.419	-1.193	22.89
		0.138						
-1.300	14.311		6.243	0.898	128.1	3.742	-1.293	23.14
		0.134						
-1.400	17.512		6.387	0.919	141.7	4.139	-1.393	23.39
		0.144						
-1.500	21.781		6.540	0.940	158.0	4.617	-1.493	23.64
		0.152						
-1.600	25.983		6.659	0.958	172.6	5.042	-1.593	23.89
		0.119						
-1.700	30.771		6.767	0.973	187.8	5.487	-1.693	24.14
		0.108						
-1.800	34.566		6.835	0.983	199.0	5.816	-1.793	24.39
		0.068						
-1.900	37.465		6.876	0.989	207.2	6.055	-1.893	24.64
		0.041						
-2.000	39.275		6.896	0.992	212.1	6.199	-1.993	24.89
		0.020						
		0.057	6.954	1.000				

Sky Constant = 19.89

Integration table for NGC 4435 I (J)

Log I	A	P	Sum P	K	R*	Rho	Log J	Mu
1.700	0.004		0.000	0.000	2.0	0.142	1.304	15.29
1.600	0.010	0.292	0.292	0.094	3.4	0.238	1.204	15.54
1.500	0.016	0.206	0.498	0.161	4.3	0.298	1.104	15.79
1.400	0.020	0.123	0.621	0.201	4.8	0.336	1.004	16.04
1.300	0.026	0.130	0.751	0.243	5.5	0.382	0.904	16.29
1.200	0.027	0.026	0.776	0.251	5.6	0.392	0.804	16.54
1.100	0.032	0.072	0.848	0.275	6.1	0.427	0.704	16.79
1.000	0.036	0.041	0.889	0.288	6.4	0.450	0.604	17.04
0.900	0.046	0.091	0.979	0.317	7.3	0.509	0.504	17.29
0.800	0.059	0.092	1.072	0.347	8.2	0.576	0.404	17.54
0.700	0.086	0.151	1.223	0.396	9.9	0.694	0.304	17.79
0.600	0.109	0.104	1.327	0.430	11.2	0.781	0.204	18.04
0.500	0.138	0.103	1.430	0.463	12.6	0.879	0.104	18.29
0.400	0.177	0.110	1.540	0.499	14.2	0.995	0.004	18.54
0.300	0.217	0.091	1.631	0.528	15.8	1.103	-0.096	18.79
0.200	0.264	0.084	1.715	0.555	17.4	1.217	-0.196	19.04
0.100	0.328	0.091	1.806	0.585	19.4	1.356	-0.296	19.29
0.000	0.400	0.081	1.888	0.611	21.4	1.498	-0.396	19.54
-0.100	0.493	0.083	1.971	0.638	23.8	1.663	-0.496	19.79
-0.200	0.609	0.082	2.053	0.665	26.4	1.847	-0.596	20.04
-0.300	0.742	0.076	2.129	0.689	29.2	2.040	-0.696	20.29
-0.400	0.896	0.069	2.198	0.712	32.0	2.242	-0.796	20.54
-0.500	1.092	0.070	2.268	0.734	35.4	2.474	-0.896	20.79
-0.600	1.347	0.072	2.340	0.758	39.3	2.748	-0.996	21.04
-0.700	1.662	0.071	2.411	0.781	43.6	3.053	-1.096	21.29
-0.800	2.086	0.076	2.487	0.805	48.9	3.420	-1.196	21.54
-0.900	2.525	0.062	2.550	0.826	53.8	3.763	-1.296	21.79
-1.000	3.023	0.056	2.606	0.844	58.9	4.117	-1.396	22.04
-1.100	3.731	0.064	2.670	0.864	65.4	4.574	-1.496	22.29
-1.200	4.765	0.074	2.743	0.888	73.9	5.169	-1.596	22.54

Integration table for NGC 4435 I (J) Continued.

Log I	A	P	Sum P	K	R*	Rho	Log J	Mu
-1.300	6.164	0.079	2.822	0.914	84.0	5.880	-1.696	22.79
-1.400	7.768	0.072	2.895	0.937	94.3	6.600	-1.796	23.04
-1.500	9.536	0.063	2.958	0.958	104.5	7.313	-1.896	23.29
-1.600	11.350	0.051	3.009	0.974	114.0	7.978	-1.996	23.54
-1.700	12.717	0.031	3.040	0.984	120.7	8.445	-2.096	23.79
-1.800	13.816	0.020	3.060	0.991	125.8	8.802	-2.196	24.04
-1.900	14.564	0.011	3.070	0.994	129.2	9.037	-2.296	24.29
-2.000	15.153	0.007	3.077	0.996	131.8	9.219	-2.396	24.54
		0.012	3.089	1.000				

Sky Constant = 19.54

Integration table for NGC 4438 I (J)

Log I	A	P	Sum P	K	R*	Rho	Log J	Mu
1.700	0.001		0.000	0.000	1.3	0.046	1.750	15.29
		0.162						
1.600	0.005		0.162	0.035	2.4	0.085	1.650	15.54
		0.129						
1.500	0.009		0.291	0.062	3.1	0.112	1.550	15.79
		0.041						
1.400	0.010		0.332	0.071	3.4	0.121	1.450	16.04
		0.097						
1.300	0.014		0.429	0.092	4.1	0.144	1.350	16.29
		0.052						
1.200	0.017		0.481	0.103	4.5	0.158	1.250	16.54
		0.082						
1.100	0.023		0.563	0.120	5.1	0.183	1.150	16.79
		0.024						
1.000	0.025		0.587	0.125	5.4	0.191	1.050	17.04
		0.071						
0.900	0.035		0.678	0.145	6.4	0.226	0.950	17.29
		0.164						
0.800	0.058		0.842	0.180	8.2	0.291	0.850	17.54
		0.265						
0.700	0.105		1.108	0.236	11.0	0.390	0.750	17.79
		0.220						
0.600	0.154		1.328	0.284	13.3	0.472	0.650	18.04
		0.209						
0.500	0.213		1.537	0.328	15.6	0.554	0.550	18.29
		0.190						
0.400	0.280		1.727	0.369	17.9	0.636	0.450	18.54
		0.151						
0.300	0.347		1.878	0.401	17.9	0.708	0.350	18.79
		0.165						
0.200	0.437		2.043	0.436	22.4	0.797	0.250	19.04
		0.120						
0.100	0.523		2.163	0.462	24.5	0.870	0.150	19.29
		0.116						
0.000	0.626		2.279	0.487	26.8	0.951	0.050	19.54
		0.125						
-0.100	0.765		2.404	0.513	29.6	1.051	-0.050	19.79
		0.102						
-0.200	0.908		2.506	0.535	32.3	1.146	-0.150	20.04
		0.089						
-0.300	1.066		2.595	0.554	35.0	1.241	-0.250	20.29
		0.093						
-0.400	1.274		2.689	0.574	38.2	1.357	-0.350	20.54
		0.086						
-0.500	1.514		2.774	0.592	41.7	1.479	-0.450	20.79
		0.096						
-0.600	1.854		2.871	0.613	46.1	1.637	-0.550	21.04
		0.090						
-0.700	2.251		2.960	0.632	50.8	1.804	-0.650	21.29
		0.086						
-0.800	2.733		3.047	0.650	56.0	1.987	-0.750	21.54
		0.115						
-0.900	3.543		3.162	0.675	63.7	2.263	-0.850	21.79
		0.185						
-1.000	5.178		3.347	0.714	77.0	2.736	-0.950	22.04
		0.270						
-1.100	8.183		3.616	0.772	96.8	3.439	-1.050	22.29
		0.266						
-1.200	11.913		3.882	0.829	116.8	4.149	-1.150	22.54

Integration table for NGC 4438 I (J) Continued.

Log I	A	P	Sum P	K	R*	Rho	Log J	Mu
		0.200						
-1.300	15.452		4.082	0.872	133.1	4.725	-1.250	22.79
		0.165						
-1.400	19.118		4.247	0.907	148.0	5.256	-1.350	23.04
		0.131						
-1.500	22.792		4.378	0.935	161.6	5.739	-1.450	23.29
		0.111						
-1.600	26.703		4.489	0.958	174.9	6.212	-1.550	23.54
		0.068						
-1.700	29.719		4.557	0.973	184.5	6.553	-1.650	23.79
		0.046						
-1.800	32.315		4.604	0.983	192.4	6.834	-1.750	24.04
		0.030						
-1.900	34.405		4.633	0.989	198.6	7.051	-1.850	24.29
		0.016						
-2.000	35.798		4.649	0.993	202.5	7.193	-1.950	24.54
		0.035						
			4.684	1.000				

Sky Constant = 19.54

Integration table for NGC 4457 I (J)

Log I	A	P	Sum P	K	R*	Rho	Log J	Mu
2.100	0.001		0.000	0.000	0.9	0.036	2.022	14.55
		0.244						
2.000	0.003		0.244	0.039	1.8	0.073	1.922	14.80
		0.518						
1.900	0.009		0.762	0.122	3.1	0.126	1.822	15.05
		0.103						
1.800	0.010		0.865	0.138	3.4	0.137	1.722	15.30
		0.122						
1.700	0.012		0.987	0.158	3.7	0.150	1.622	15.55
		0.227						
1.600	0.017		1.214	0.194	4.5	0.179	1.522	15.80
		0.077						
1.500	0.019		1.291	0.206	4.7	0.190	1.422	16.05
		0.061						
1.400	0.022		1.353	0.216	5.0	0.200	1.322	16.30
		0.081						
1.300	0.025		1.434	0.229	5.4	0.216	1.222	16.55
		0.052						
1.200	0.028		1.485	0.238	5.7	0.228	1.122	16.80
		0.051						
1.100	0.032		1.537	0.246	6.0	0.242	1.022	17.05
		0.073						
1.000	0.038		1.610	0.257	6.6	0.266	0.922	17.30
		0.142						
0.900	0.054		1.752	0.280	7.9	0.316	0.822	17.55
		0.164						
0.800	0.077		1.917	0.306	9.4	0.377	0.722	17.80
		0.220						
0.700	0.116		2.137	0.342	11.5	0.463	0.622	18.05
		0.175						
0.600	0.155		2.312	0.370	13.3	0.535	0.522	18.30
		0.175						
0.500	0.204		2.487	0.398	15.3	0.614	0.422	18.55
		0.160						
0.400	0.260		2.647	0.423	17.3	0.693	0.322	18.80
		0.145						
0.300	0.324		2.792	0.446	19.3	0.774	0.222	19.05
		0.154						
0.200	0.410		2.945	0.471	21.7	0.870	0.122	19.30
		0.150						
0.100	0.516		3.095	0.495	24.3	0.976	0.022	19.55
		0.149						
0.000	0.647		3.244	0.519	27.2	1.093	-0.078	19.80
		0.165						
-0.100	0.831		3.409	0.545	30.9	1.239	-0.178	20.05
		0.146						
-0.200	1.036		3.555	0.568	34.5	1.383	-0.278	20.30
		0.165						
-0.300	1.328		3.720	0.595	39.0	1.566	-0.378	20.55
		0.165						
-0.400	1.695		3.885	0.621	44.1	1.769	-0.478	20.80
		0.169						
-0.500	2.170		4.055	0.648	49.9	2.001	-0.578	21.05
		0.196						
-0.600	2.859		4.250	0.680	57.2	2.297	-0.678	21.30
		0.159						
-0.700	3.563		4.409	0.705	63.9	2.565	-0.778	21.55
		0.166						
-0.800	4.492		4.575	0.732	71.7	2.880	-0.878	21.80

Integration table for NGC 4459 I (J) Continued.

Log I	A	P	Sum P	K	R*	Rho	Log J	Mu
		0.171						
-0.900	5.695		4.746	0.759	80.8	3.243	-0.978	22.05
		0.160						
-1.000	7.114		4.906	0.784	90.3	3.624	-1.078	22.30
		0.137						
-1.100	8.642		5.043	0.806	99.5	3.994	-1.178	22.55
		0.140						
-1.200	10.606		5.183	0.829	110.2	4.425	-1.278	22.80
		0.139						
-1.300	13.060		5.322	0.851	122.3	4.910	-1.378	23.05
		0.143						
-1.400	16.244		5.466	0.874	136.4	5.476	-1.478	23.30
		0.173						
-1.500	21.081		5.638	0.902	155.4	6.238	-1.578	23.55
		0.179						
-1.600	27.398		5.818	0.930	177.2	7.112	-1.678	23.80
		0.118						
-1.700	32.649		5.936	0.949	193.4	7.764	-1.778	24.05
		0.106						
-1.800	38.570		6.042	0.966	210.2	8.438	-1.878	24.30
		0.065						
-1.900	43.165		6.107	0.976	222.4	8.927	-1.978	24.55
		0.032						
-2.000	46.010		6.139	0.982	229.6	9.216	-2.078	24.80
		0.115						
			6.254	1.000				

Sky Constant = 19.80

Integration table for NGC 4461 I (J)

Log I	A	P	Sum P	K	R*	Rho	Log J	Mu
1.600	0.003		0.000	0.000	1.8	0.079	1.747	15.43
		0.129						
1.500	0.006		0.129	0.049	2.7	0.118	1.647	15.68
		0.061						
1.400	0.009		0.190	0.073	3.1	0.137	1.547	15.93
		0.097						
1.300	0.013		0.288	0.110	3.9	0.167	1.447	16.18
		0.013						
1.200	0.014		0.301	0.115	4.0	0.172	1.347	16.43
		0.072						
1.100	0.019		0.372	0.143	4.6	0.201	1.247	16.68
		0.016						
1.000	0.020		0.389	0.149	4.8	0.209	1.147	16.93
		0.052						
0.900	0.026		0.440	0.169	5.5	0.237	1.047	17.18
		0.087						
0.800	0.038		0.528	0.203	6.6	0.287	0.947	17.43
		0.094						
0.700	0.055		0.622	0.239	7.9	0.344	0.847	17.68
		0.088						
0.600	0.074		0.709	0.272	9.2	0.401	0.747	17.93
		0.095						
0.500	0.101		0.804	0.309	10.8	0.467	0.647	18.18
		0.080						
0.400	0.129		0.884	0.339	12.2	0.528	0.547	18.43
		0.068						
0.300	0.159		0.952	0.366	13.5	0.587	0.447	18.68
		0.084						
0.200	0.206		1.036	0.398	15.4	0.668	0.347	18.93
		0.079						
0.100	0.262		1.115	0.428	17.3	0.752	0.247	19.18
		0.068						
0.000	0.322		1.184	0.454	19.2	0.835	0.147	19.43
		0.080						
-0.100	0.412		1.264	0.485	21.7	0.943	0.047	19.68
		0.085						
-0.200	0.531		1.349	0.518	24.7	1.072	-0.053	19.93
		0.106						
-0.300	0.718		1.455	0.558	28.7	1.246	-0.153	20.18
		0.079						
-0.400	0.893		1.534	0.589	32.0	1.389	-0.253	20.43
		0.063						
-0.500	1.070		1.597	0.613	35.0	1.521	-0.353	20.68
		0.063						
-0.600	1.292		1.660	0.637	38.5	1.671	-0.453	20.93
		0.059						
-0.700	1.555		1.719	0.660	42.2	1.833	-0.553	21.18
		0.063						
-0.800	1.906		1.782	0.684	46.7	2.029	-0.653	21.43
		0.052						
-0.900	2.270		1.834	0.704	51.0	2.215	-0.753	21.68
		0.050						
-1.000	2.711		1.883	0.723	55.7	2.420	-0.853	21.93
		0.048						
-1.100	3.244		1.931	0.741	61.0	2.647	-0.953	22.18
		0.057						
-1.200	4.047		1.988	0.763	68.1	2.957	-1.053	22.43
		0.069						
-1.300	5.267		2.057	0.790	77.7	3.373	-1.153	22.68

Integration table for NGC 4461 I (J) Continued

Log I	A	P	Sum P	K	R*	Rho	Log J	Mu
		0.090						
-1.400	7.259		2.147	0.824	91.2	3.960	-1.253	22.93
		0.103						
-1.500	10.156		2.251	0.864	107.9	4.684	-1.353	23.18
		0.077						
-1.600	12.865		2.327	0.893	121.4	5.272	-1.453	23.43
		0.080						
-1.700	16.401		2.407	0.924	137.1	5.953	-1.553	23.68
		0.044						
-1.800	18.850		2.451	0.941	147.0	6.382	-1.653	23.93
		0.038						
-1.900	21.553		2.489	0.956	157.2	6.824	-1.753	24.18
		0.026						
-2.000	23.817		2.515	0.965	165.2	7.174	-1.853	24.43
		0.090						
			2.605	1.000				

Sky Constant = 19.43

Integration table for NGC 4474 I (J)

Log I	A	P	Sum P	K	R*	Rho	Log J	Mu
1.700	0.001		0.000	0.000	0.9	0.051	1.838	15.43
		0.065						
1.600	0.002		0.065	0.038	1.6	0.088	1.738	15.68
		0.103						
1.500	0.005		0.168	0.099	2.4	0.135	1.638	15.93
		0.020						
1.400	0.006		0.188	0.111	2.6	0.144	1.538	16.18
		0.049						
1.300	0.008		0.237	0.140	3.0	0.169	1.438	16.43
		0.026						
1.200	0.009		0.263	0.155	3.3	0.183	1.338	16.68
		0.031						
1.100	0.012		0.294	0.173	3.6	0.203	1.238	16.93
		0.016						
1.000	0.013		0.310	0.183	3.9	0.216	1.138	17.18
		0.045						
0.900	0.018		0.355	0.209	4.5	0.254	1.038	17.43
		0.041						
0.800	0.024		0.396	0.234	5.2	0.292	0.938	17.68
		0.053						
0.700	0.033		0.449	0.265	6.2	0.345	0.838	17.93
		0.045						
0.600	0.043		0.495	0.292	7.0	0.394	0.738	18.18
		0.044						
0.500	0.056		0.539	0.318	8.0	0.446	0.638	18.43
		0.041						
0.400	0.070		0.579	0.342	9.0	0.501	0.538	18.68
		0.054						
0.300	0.094		0.633	0.373	10.4	0.580	0.438	18.93
		0.052						
0.200	0.123		0.685	0.404	11.9	0.663	0.338	19.18
		0.044						
0.100	0.154		0.729	0.430	13.3	0.742	0.238	19.43
		0.049						
0.000	0.197		0.778	0.458	15.0	0.841	0.138	19.68
		0.054						
-0.100	0.257		0.831	0.490	17.2	0.960	0.038	19.93
		0.043						
-0.200	0.317		0.874	0.515	19.0	1.066	-0.062	20.18
		0.048						
-0.300	0.402		0.922	0.544	21.5	1.201	-0.162	20.43
		0.043						
-0.400	0.497		0.965	0.569	23.9	1.335	-0.262	20.68
		0.037						
-0.500	0.600		1.002	0.591	26.2	1.467	-0.362	20.93
		0.040						
-0.600	0.741		1.042	0.614	29.1	1.631	-0.462	21.18
		0.040						
-0.700	0.919		1.082	0.638	32.5	1.816	-0.562	21.43
		0.040						
-0.800	1.143		1.122	0.662	36.2	2.025	-0.662	21.68
		0.031						
-0.900	1.362		1.153	0.680	39.5	2.211	-0.762	21.93
		0.030						
-1.000	1.624		1.183	0.697	43.1	2.414	-0.862	22.18
		0.033						
-1.100	1.991		1.216	0.717	47.8	2.673	-0.962	22.43
		0.028						
-1.200	2.389		1.244	0.734	52.3	2.928	-1.062	22.68

Integration table for NGC 4474 I (J) Continued.

Log I	A	P	Sum P	K	R*	Rho	Log J	Mu
-1.300	3.000		1.279	0.754	58.6	3.281	-1.162	22.93
		0.035						
-1.400	3.989		1.323	0.780	67.6	3.784	-1.262	23.18
		0.044						
-1.500	6.054		1.397	0.824	83.3	4.661	-1.362	23.43
		0.074						
-1.600	8.835		1.476	0.870	100.6	5.631	-1.462	23.68
		0.079						
-1.700	12.031		1.548	0.913	117.4	6.571	-1.562	23.93
		0.072						
-1.800	14.249		1.587	0.936	127.8	7.151	-1.662	24.18
		0.040						
-1.900	16.484		1.619	0.955	137.4	7.692	-1.762	24.43
		0.032						
-2.000	17.926		1.636	0.964	143.3	8.021	-1.862	24.68
		0.016						
		0.061						
			1.696	1.000				

Sky Constant = 19.68

Integration table for NGC 4477 I (J)

Log I	A	P	Sum P	K	R*	Rho	Log J	Mu
1.700	0.004		0.000	0.000	2.2	0.070	1.901	15.30
1.600	0.010	0.259	0.259	0.053	3.4	0.106	1.801	15.55
1.500	0.016	0.206	0.465	0.096	4.3	0.133	1.701	15.80
1.400	0.017	0.041	0.506	0.104	4.5	0.139	1.601	16.05
1.300	0.023	0.130	0.636	0.131	5.1	0.161	1.501	16.30
1.200	0.024	0.013	0.649	0.133	5.2	0.163	1.401	16.55
1.100	0.032	0.113	0.762	0.156	6.0	0.188	1.301	16.80
1.000	0.038	0.073	0.835	0.172	6.6	0.207	1.201	17.05
0.900	0.048	0.091	0.926	0.190	7.4	0.232	1.101	17.30
0.800	0.069	0.149	1.075	0.221	8.9	0.278	1.001	17.55
0.700	0.097	0.155	1.230	0.253	10.5	0.329	0.901	17.80
0.600	0.131	0.156	1.386	0.285	12.3	0.383	0.801	18.05
0.500	0.169	0.136	1.522	0.313	13.9	0.435	0.701	18.30
0.400	0.218	0.137	1.659	0.341	15.8	0.493	0.601	18.55
0.300	0.273	0.125	1.784	0.366	17.7	0.553	0.501	18.80
0.200	0.338	0.116	1.900	0.390	19.7	0.615	0.401	19.05
0.100	0.428	0.127	2.028	0.416	22.1	0.691	0.301	19.30
0.000	0.538	0.125	2.152	0.442	24.8	0.775	0.201	19.55
-0.100	0.691	0.137	2.289	0.470	28.1	0.879	0.101	19.80
-0.200	0.893	0.144	2.434	0.500	32.0	0.999	0.001	20.05
-0.300	1.263	0.209	2.643	0.543	38.0	1.188	-0.099	20.30
-0.400	1.727	0.208	2.851	0.586	44.5	1.389	-0.199	20.55
-0.500	2.609	0.315	3.166	0.650	54.7	1.707	-0.299	20.80
-0.600	3.383	0.220	3.386	0.695	62.3	1.944	-0.399	21.05
-0.700	4.074	0.156	3.542	0.727	68.3	2.134	-0.499	21.30
-0.800	4.920	0.151	3.693	0.758	75.1	2.345	-0.599	21.55
-0.900	5.739	0.117	3.810	0.782	81.1	2.533	-0.699	21.80
-1.000	6.602	0.097	3.907	0.802	87.0	2.716	-0.799	22.05
-1.100	7.716	0.100	4.007	0.823	94.0	2.937	-0.899	22.30
-1.200	9.030	0.094	4.101	0.842	101.7	3.177	-0.999	22.55

Integration table for NGC 4477 I (J) Continued.

Log I	A	P	Sum P	K	R*	Rho	Log J	Mu
-1.300	11.004	0.112	4.213	0.865	112.3	3.507	-1.099	22.80
-1.400	13.873	0.129	4.342	0.892	126.1	3.938	-1.199	23.05
-1.500	16.982	0.111	4.453	0.914	139.5	4.356	-1.299	23.30
-1.600	20.645	0.104	4.557	0.936	153.8	4.803	-1.399	23.55
-1.700	24.036	0.076	4.633	0.951	166.0	5.183	-1.499	23.80
-1.800	27.239	0.057	4.690	0.963	176.7	5.517	-1.599	24.05
-1.900	30.575	0.047	4.738	0.973	187.2	5.845	-1.699	24.30
-2.000	32.983	0.027	4.765	0.979	194.4	6.071	-1.799	24.55
		0.104	4.869	1.000				

Sky Constant = 19.55

Integration table for NGC 4501 I (J)

Log J	A	P	Sum P	K	R*	Rho	Log J	Mu
2.000	0.002		0.000	0.000	1.6	0.036	1.926	14.70
		0.323						
1.900	0.006		0.323	0.031	2.6	0.059	1.826	14.95
		0.154						
1.800	0.008		0.478	0.046	3.0	0.069	1.726	15.20
		0.204						
1.700	0.012		0.682	0.065	3.6	0.083	1.626	15.45
		0.097						
1.600	0.014		0.779	0.074	4.0	0.091	1.526	15.70
		0.077						
1.500	0.016		0.856	0.082	4.3	0.098	1.426	15.95
		0.082						
1.400	0.019		0.938	0.089	4.6	0.106	1.326	16.20
		0.081						
1.300	0.022		1.019	0.097	5.1	0.116	1.226	16.45
		0.065						
1.200	0.026		1.084	0.103	5.5	0.125	1.126	16.70
		0.072						
1.100	0.031		1.156	0.110	6.0	0.137	1.026	16.95
		0.073						
1.000	0.037		1.229	0.117	6.6	0.150	0.926	17.20
		0.136						
0.900	0.053		1.365	0.130	7.8	0.178	0.826	17.45
		0.206						
0.800	0.081		1.570	0.150	9.7	0.222	0.726	17.70
		0.286						
0.700	0.132		1.856	0.177	12.3	0.282	0.626	17.95
		0.373						
0.600	0.215		2.229	0.213	15.7	0.360	0.526	18.20
		0.440						
0.500	0.338		2.669	0.254	19.7	0.452	0.426	18.45
		0.691						
0.400	0.582		3.361	0.320	25.8	0.593	0.326	18.70
		0.743						
0.300	0.911		4.103	0.391	32.3	0.742	0.226	18.95
		0.490						
0.200	1.185		4.594	0.438	36.9	0.846	0.126	19.20
		0.519						
0.100	1.550		5.112	0.487	42.1	0.967	0.026	19.45
		0.482						
0.000	1.977		5.595	0.533	47.6	1.092	-0.074	19.70
		0.399						
-0.100	2.422		5.994	0.571	52.7	1.209	-0.174	19.95
		0.514						
-0.200	3.143		6.507	0.620	60.0	1.377	-0.274	20.20
		0.646						
-0.300	4.284		7.153	0.682	70.1	1.608	-0.374	20.45
		0.616						
-0.400	5.654		7.769	0.741	80.5	1.847	-0.474	20.70
		0.400						
-0.500	6.773		8.169	0.779	88.1	2.022	-0.574	20.95
		0.317						
-0.600	7.892		8.486	0.809	95.1	2.182	-0.674	21.20
		0.282						
-0.700	9.143		8.768	0.836	102.4	2.349	-0.774	21.45
		0.213						
-0.800	10.336		8.982	0.856	108.8	2.498	-0.874	21.70
		0.160						
-0.900	11.461		9.142	0.872	114.6	2.630	-0.974	21.95

Integration table for NGC 4501 I (J) Continued.

Log I	A	P	Sum P	K	R*	Rho	Log J	Mu
		0.143						
-1.000	12.725		9.285	0.885	120.8	2.771	-1.074	22.20
		0.130						
-1.100	14.179		9.415	0.898	127.5	2.925	-1.174	22.45
		0.128						
-1.200	15.969		9.543	0.910	135.3	3.104	-1.274	22.70
		0.151						
-1.300	18.641		9.694	0.924	146.2	3.354	-1.374	22.95
		0.154						
-1.400	22.062		9.848	0.939	159.0	3.649	-1.474	23.20
		0.174						
-1.500	26.935		10.022	0.956	175.7	4.032	-1.574	23.45
		0.139						
-1.600	31.835		10.161	0.969	191.0	4.383	-1.674	23.70
		0.120						
-1.700	37.175		10.281	0.980	206.4	4.737	-1.774	23.95
		0.064						
-1.800	40.755		10.345	0.986	216.1	4.959	-1.874	24.20
		0.052						
-1.900	44.379		10.397	0.991	225.5	5.175	-1.974	24.45
		0.024						
-2.000	46.528		10.421	0.994	230.9	5.299	-2.074	24.70
		0.067						
			10.488	1.000				

Sky Constant = 19.70

Integration table for NGC 4503 I (J)

Log I	A	P	Sum P	K	R*	Rho	Log J	Mu
1.600	0.001		0.000	0.000	0.9	0.048	1.543	15.68
		0.180						
1.500	0.006		0.180	0.070	2.6	0.135	1.443	15.93
		0.082						
1.400	0.009		0.262	0.102	3.1	0.166	1.343	16.18
		0.049						
1.300	0.011		0.311	0.121	3.5	0.185	1.243	16.43
		0.052						
1.200	0.014		0.362	0.141	4.0	0.208	1.143	16.68
		0.041						
1.100	0.017		0.403	0.157	4.4	0.229	1.043	16.93
		0.033						
1.000	0.019		0.436	0.170	4.7	0.248	0.943	17.18
		0.071						
0.900	0.027		0.507	0.198	5.6	0.295	0.843	17.43
		0.092						
0.800	0.040		0.600	0.234	6.8	0.358	0.743	17.68
		0.106						
0.700	0.059		0.706	0.275	8.2	0.433	0.643	17.93
		0.081						
0.600	0.077		0.787	0.307	9.4	0.494	0.543	18.18
		0.095						
0.500	0.104		0.882	0.344	10.9	0.573	0.443	18.43
		0.096						
0.400	0.138		0.978	0.382	12.6	0.660	0.343	18.68
		0.106						
0.300	0.185		1.084	0.423	14.5	0.764	0.243	18.93
		0.086						
0.200	0.233		1.170	0.456	16.3	0.859	0.143	19.18
		0.075						
0.100	0.286		1.245	0.486	18.1	0.951	0.043	19.43
		0.092						
0.000	0.367		1.337	0.522	20.5	1.078	-0.057	19.68
		0.118						
-0.100	0.499		1.456	0.568	23.9	1.257	-0.157	19.93
		0.107						
-0.200	0.650		1.563	0.610	27.3	1.434	-0.257	20.18
		0.102						
-0.300	0.831		1.665	0.650	30.9	1.622	-0.357	20.43
		0.100						
-0.400	1.053		1.766	0.689	34.7	1.826	-0.457	20.68
		0.087						
-0.500	1.298		1.853	0.723	38.6	2.027	-0.557	20.93
		0.077						
-0.600	1.568		1.930	0.753	42.4	2.228	-0.657	21.18
		0.073						
-0.700	1.893		2.003	0.781	46.6	2.448	-0.757	21.43
		0.066						
-0.800	2.260		2.068	0.807	50.9	2.675	-0.857	21.68
		0.068						
-0.900	2.736		2.136	0.833	56.0	2.943	-0.957	21.93
		0.059						
-1.000	3.260		2.195	0.856	61.1	3.213	-1.057	22.18
		0.050						
-1.100	3.815		2.245	0.876	66.1	3.476	-1.157	22.43
		0.044						
-1.200	4.429		2.289	0.893	71.2	3.745	-1.257	22.68
		0.040						
-1.300	5.134		2.329	0.908	76.7	4.032	-1.357	22.93

Integration table for NGC 4503 I (J) Continued.

Log I	A	P	Sum P	K	R*	Rho	Log J	Mu
		0.036						
-1.400	5.933		2.365	0.922	82.5	4.334	-1.457	23.18
		0.039						
-1.500	7.014		2.403	0.937	89.7	4.713	-1.557	23.43
		0.041						
-1.600	8.444		2.444	0.953	98.4	5.171	-1.657	23.68
		0.036						
-1.700	10.020		2.479	0.967	107.2	5.633	-1.757	23.93
		0.026						
-1.800	11.471		2.505	0.977	114.7	6.027	-1.857	24.18
		0.012						
-1.900	12.346		2.518	0.982	118.9	6.252	-1.957	24.43
		0.011						
-2.000	13.289		2.529	0.986	123.4	6.487	-2.057	24.68
		0.035						
			2.564	1.000				

Sky Constant = 19.68

Integration table for NGC 4531 I (J)

Log I	A	P	Sum P	K	R*	Rho	Log J	Mu
0.600	0.001		0.000	0.000	0.9	0.023	1.296	18.18
		0.008						
0.500	0.003		0.008	0.005	1.8	0.046	1.196	18.43
		0.020						
0.400	0.010		0.028	0.019	3.4	0.086	1.096	18.68
		0.039						
0.300	0.027		0.067	0.046	5.6	0.142	0.996	18.93
		0.037						
0.200	0.048		0.105	0.071	7.4	0.189	0.896	19.18
		0.064						
0.100	0.093		0.168	0.115	10.3	0.262	0.796	19.43
		0.071						
0.000	0.156		0.239	0.163	13.4	0.339	0.696	19.68
		0.100						
-0.100	0.268		0.339	0.231	17.5	0.444	0.596	19.93
		0.062						
-0.200	0.354		0.401	0.273	20.1	0.511	0.496	20.18
		0.061						
-0.300	0.461		0.462	0.314	23.0	0.583	0.396	20.43
		0.063						
-0.400	0.602		0.525	0.357	26.3	0.666	0.296	20.68
		0.068						
-0.500	0.792		0.593	0.404	30.1	0.764	0.196	20.93
		0.068						
-0.600	1.033		0.661	0.450	34.4	0.873	0.096	21.18
		0.076						
-0.700	1.371		0.737	0.502	39.6	1.006	-0.004	21.43
		0.079						
-0.800	1.815		0.817	0.556	45.6	1.157	-0.104	21.68
		0.053						
-0.900	2.190		0.870	0.593	50.1	1.271	-0.204	21.93
		0.050						
-1.000	2.634		0.920	0.627	54.9	1.394	-0.304	22.18
		0.048						
-1.100	3.164		0.968	0.659	60.2	1.528	-0.404	22.43
		0.039						
-1.200	3.708		1.007	0.685	65.2	1.654	-0.504	22.68
		0.028						
-1.300	4.211		1.035	0.705	69.5	1.762	-0.604	22.93
		0.028						
-1.400	4.823		1.063	0.724	74.3	1.886	-0.704	23.18
		0.045						
-1.500	6.087		1.108	0.754	83.5	2.119	-0.804	23.43
		0.057						
-1.600	8.085		1.164	0.793	96.3	2.442	-0.904	23.68
		0.049						
-1.700	10.250		1.213	0.826	108.4	2.749	-1.004	23.93
		0.038						
-1.800	12.361		1.251	0.852	119.0	3.019	-1.104	24.18
		0.036						
-1.900	14.918		1.287	0.877	130.7	3.317	-1.204	24.43
		0.024						
-2.000	17.080		1.312	0.893	137.9	3.549	-1.304	24.68
		0.157						
			1.469	1.000				

Sky Constant = 19.68

Integration table for NGC 4550 I (J)

Log I	A	P	Sum P	K	R*	Rho	Log J	Mu
1.400	0.003		0.000	0.000	1.8	0.177	0.859	16.18
		0.081						
1.300	0.006		0.081	0.059	2.7	0.266	0.759	16.43
		0.077						
1.200	0.011		0.159	0.114	3.5	0.343	0.659	16.68
		0.041						
1.100	0.014		0.200	0.144	4.0	0.386	0.559	16.93
		0.098						
1.000	0.022		0.297	0.214	5.1	0.493	0.459	17.18
		0.065						
0.900	0.030		0.362	0.261	5.8	0.567	0.359	17.43
		0.108						
0.800	0.045		0.470	0.339	7.2	0.698	0.259	17.68
		0.098						
0.700	0.062		0.568	0.409	8.4	0.822	0.159	17.93
		0.084						
0.600	0.081		0.652	0.470	9.6	0.938	0.059	18.18
		0.067						
0.500	0.100		0.719	0.518	10.7	1.041	-0.041	18.43
		0.051						
0.400	0.118		0.770	0.555	11.6	1.131	-0.141	18.68
		0.050						
0.300	0.140		0.821	0.592	12.7	1.234	-0.241	18.93
		0.049						
0.200	0.167		0.870	0.627	13.8	1.350	-0.341	19.18
		0.048						
0.100	0.201		0.918	0.662	15.2	1.480	-0.441	19.43
		0.047						
0.000	0.243		0.965	0.696	16.7	1.627	-0.541	19.68
		0.042						
-0.100	0.290		1.007	0.726	18.2	1.777	-0.641	19.93
		0.040						
-0.200	0.346		1.047	0.755	19.9	1.942	-0.741	20.18
		0.039						
-0.300	0.415		1.086	0.783	21.8	2.125	-0.841	20.43
		0.036						
-0.400	0.495		1.122	0.809	23.8	2.321	-0.941	20.68
		0.034						
-0.500	0.591		1.156	0.834	26.0	2.536	-1.041	20.93
		0.032						
-0.600	0.702		1.188	0.856	28.4	2.764	-1.141	21.18
		0.024						
-0.700	0.810		1.212	0.874	30.5	2.970	-1.241	21.43
		0.020						
-0.800	0.921		1.232	0.888	32.5	3.167	-1.341	21.68
		0.018						
-0.900	1.047		1.250	0.901	34.6	3.377	-1.441	21.93
		0.016						
-1.000	1.186		1.266	0.912	36.9	3.594	-1.541	22.18
		0.014						
-1.100	1.342		1.280	0.922	39.2	3.823	-1.641	22.43
		0.017						
-1.200	1.581		1.297	0.935	42.6	4.150	-1.741	22.68
		0.016						
-1.300	1.872		1.313	0.947	46.3	4.515	-1.841	22.93
		0.015						
-1.400	2.215		1.329	0.958	50.4	4.912	-1.941	23.18
		0.021						
-1.500	2.802		1.350	0.973	56.7	5.525	-2.041	23.43

Integration table for NGC 4550 I (J) Continued.

Log I	A	P	Sum P	K	R*	Rho	Log J	Mu
		0.014						
-1.600	3.281		1.363	0.983	61.3	5.978	-2.141	23.68
		0.010						
-1.700	3.721		1.373	0.990	65.3	6.366	-2.241	23.93
		0.004						
-1.800	3.967		1.378	0.993	67.4	6.574	-2.341	24.18
		0.003						
-1.900	4.167		1.380	0.995	69.1	6.737	-2.441	24.43
		0.003						
-2.000	4.419		1.383	0.997	71.2	6.938	-2.541	24.68
		0.004						
			1.387	1.000				

Sky Constant = 19.68

Integration table for NGC 4552 I

Log I	A	P	Sum P	K	R*	Rho	Log J	Mu
2.100	0.001		0.000	0.000	0.9	0.041	1.771	14.62
		0.407						
2.000	0.004		0.407	0.040	2.2	0.100	1.671	14.87
		0.970						
1.900	0.015		1.378	0.135	4.2	0.187	1.571	15.12
		0.771						
1.800	0.026		2.148	0.210	5.5	0.245	1.471	15.37
		0.531						
1.700	0.035		2.679	0.262	6.4	0.286	1.371	15.62
		0.097						
1.600	0.037		2.776	0.272	6.6	0.295	1.271	15.87
		0.258						
1.500	0.045		3.034	0.297	7.2	0.322	1.171	16.12
		0.123						
1.400	0.049		3.156	0.309	7.5	0.337	1.071	16.37
		0.146						
1.300	0.056		3.303	0.323	8.0	0.359	0.971	16.62
		0.103						
1.200	0.061		3.406	0.334	8.4	0.377	0.871	16.87
		0.103						
1.100	0.068		3.508	0.344	8.9	0.399	0.771	17.12
		0.155						
1.000	0.082		3.663	0.359	9.7	0.437	0.671	17.37
		0.129						
0.900	0.097		3.793	0.371	10.5	0.474	0.571	17.62
		0.236						
0.800	0.130		4.029	0.395	12.2	0.549	0.471	17.87
		0.241						
0.700	0.176		4.270	0.420	14.2	0.639	0.371	18.12
		0.224						
0.600	0.226		4.514	0.442	16.1	0.724	0.271	18.37
		0.216						
0.500	0.286		4.730	0.463	18.1	0.815	0.171	18.62
		0.217						
0.400	0.363		4.947	0.484	20.4	0.917	0.071	18.87
		0.226						
0.300	0.463		5.173	0.507	23.0	1.036	-0.029	19.12
		0.228						
0.200	0.591		5.401	0.529	26.0	1.171	-0.129	19.37
		0.227						
0.100	0.750		5.628	0.551	29.3	1.319	-0.229	19.62
		0.226						
0.000	0.950		5.854	0.573	33.0	1.485	-0.329	19.87
		0.198						
-0.100	1.171		6.052	0.593	36.6	1.649	-0.429	20.12
		0.198						
-0.200	1.449		6.251	0.612	40.8	1.834	-0.529	20.37
		0.193						
-0.300	1.770		6.444	0.631	45.3	2.038	-0.629	20.62
		0.190						
-0.400	2.213		6.634	0.650	50.4	2.266	-0.729	20.87
		0.189						
-0.500	2.742		6.823	0.668	56.1	2.523	-0.829	21.12
		0.202						
-0.600	3.454		7.025	0.688	62.9	2.831	-0.929	21.37
		0.196						
-0.700	4.325		7.221	0.707	70.4	3.168	-1.029	21.62
		0.217						
-0.800	5.539		7.438	0.728	79.7	3.585	-1.129	21.87

Integration table for NGC 4552 I ELL Continued.

Log I	A	P	Sum P	K	R*	Rho	Log J	Mu
		0.227						
-0.700	7.134		7.665	0.751	90.4	4.069	-1.229	22.12
		0.252						
-1.000	9.369		7.917	0.775	103.6	4.663	-1.329	22.37
		0.284						
-1.100	12.533		8.201	0.803	117.8	5.393	-1.429	22.62
		0.259						
-1.200	16.172		8.461	0.828	136.1	6.126	-1.529	22.87
		0.242						
-1.300	20.446		8.703	0.852	153.1	6.889	-1.629	23.12
		0.237						
-1.400	25.715		8.939	0.875	171.7	7.735	-1.729	23.37
		0.199						
-1.500	31.276		9.138	0.895	189.3	8.520	-1.829	23.62
		0.189						
-1.600	37.932		9.327	0.913	208.5	9.383	-1.929	23.87
		0.104						
-1.700	42.528		9.431	0.923	220.8	9.935	-2.029	24.12
		0.064						
-1.800	46.005		9.494	0.930	229.0	10.342	-2.129	24.37
		0.055						
-1.900	49.973		9.549	0.935	239.3	10.769	-2.229	24.62
		0.034						
-2.000	52.906		9.584	0.938	246.4	11.089	-2.329	24.87
		0.629						
			10.212	1.000				

Sky Constant = 19.87

APPENDIX 'F'

Comparison of Major Axis and 'Corrected' Equivalent Profiles

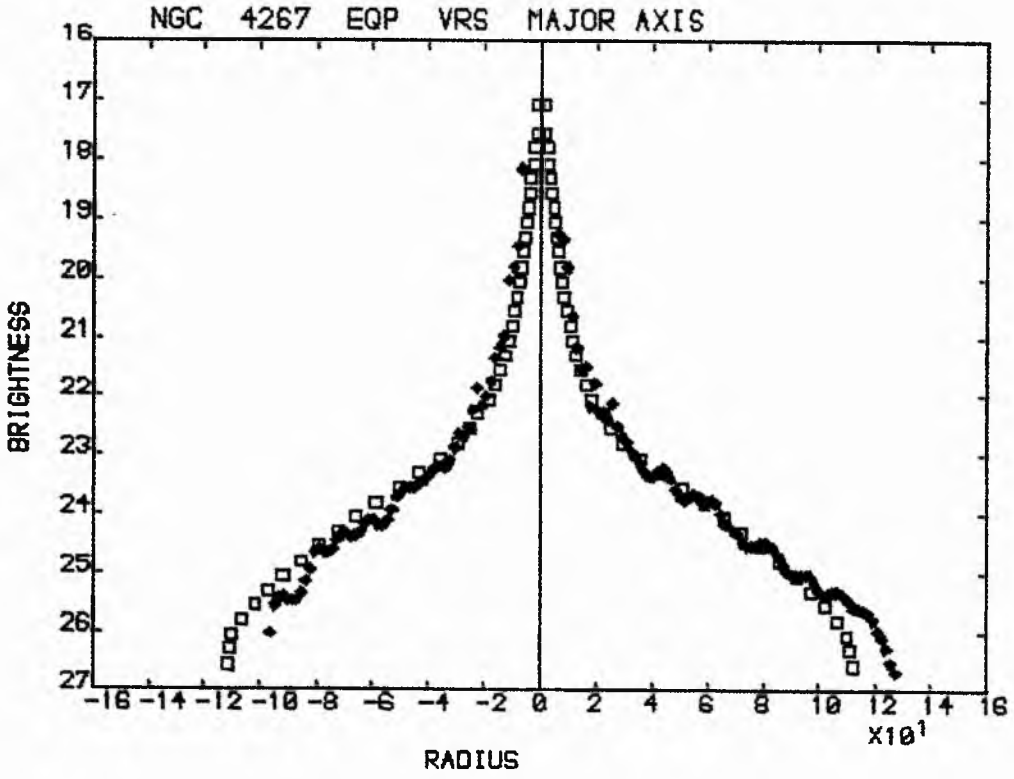
NGC 4267 EQP VRS MAJOR AXIS
BRIGHTNESS
16
17
18
19
20
21
22
23
24
25
26
27
-16 -14 -12 -10 -8 -6 -4 -2 0 2 4 6 8 10 12 14 16
X10¹
RADIUS

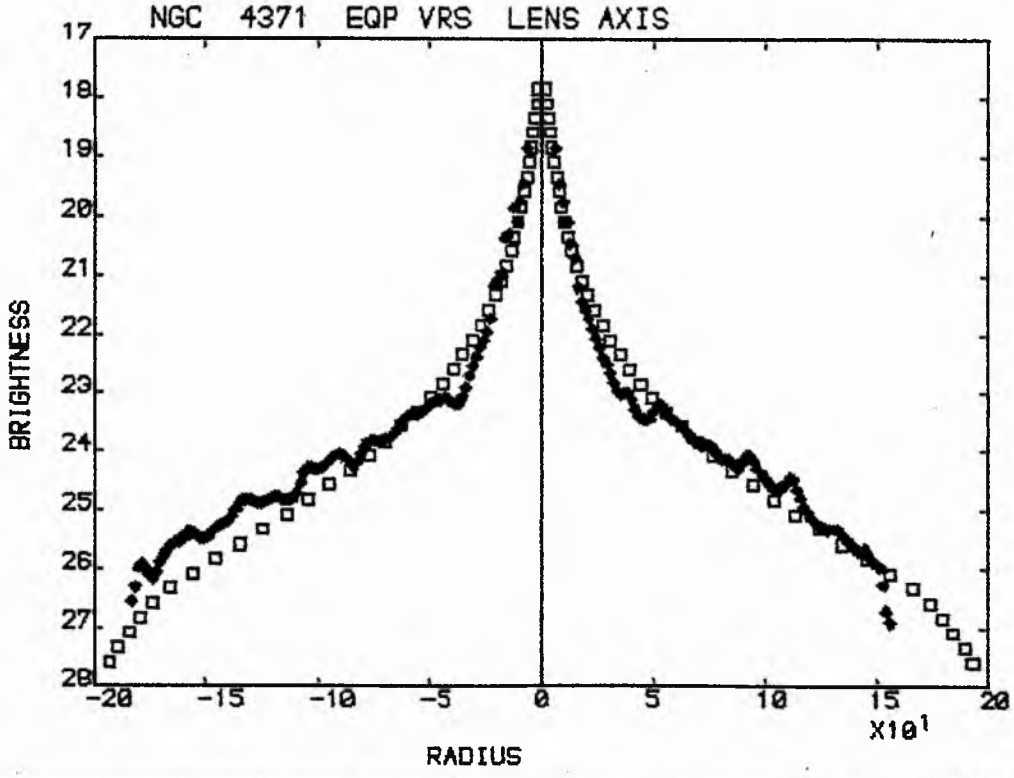
NGC 4371 EQP VRS LENS AXIS
BRIGHTNESS
17
18
19
20
21
22
23
24
25
26
27
28
-20 -15 -10 -5 0 5 10 15 20
X10¹
RADIUS

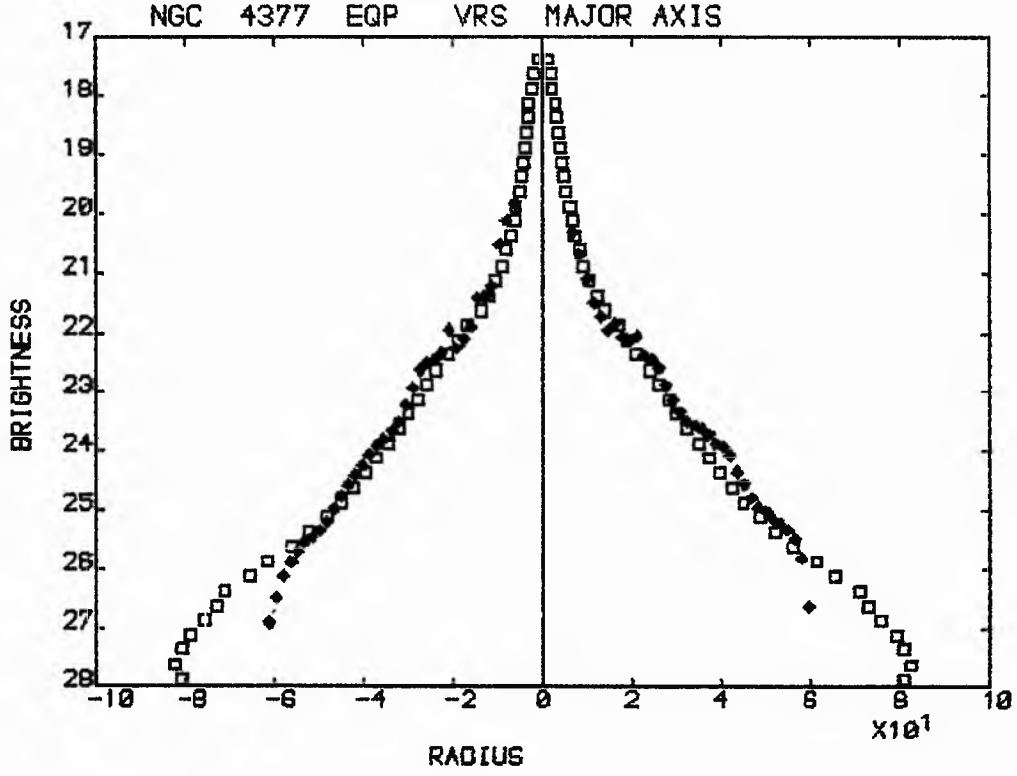
NGC 4377 EQP VRS MAJOR AXIS
BRIGHTNESS
17
18
19
20
21
22
23
24
25
26
27
28
-10
-8
-6
-4
-2
0
2
4
6
8
10
X10¹
RADIUS

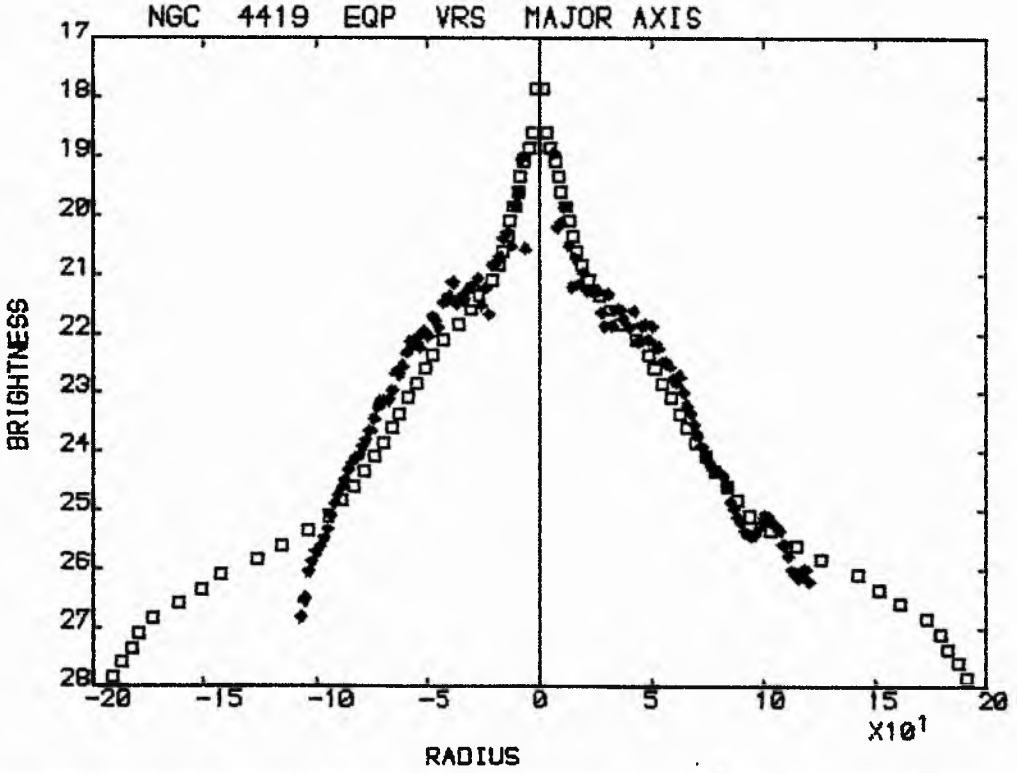
NGC 4419 EQP VRS MAJOR AXIS
BRIGHTNESS
17
18
19
20
21
22
23
24
25
26
27
28
-20
-15
-10
-5
0
5
10
15
20
X10¹
RADIUS

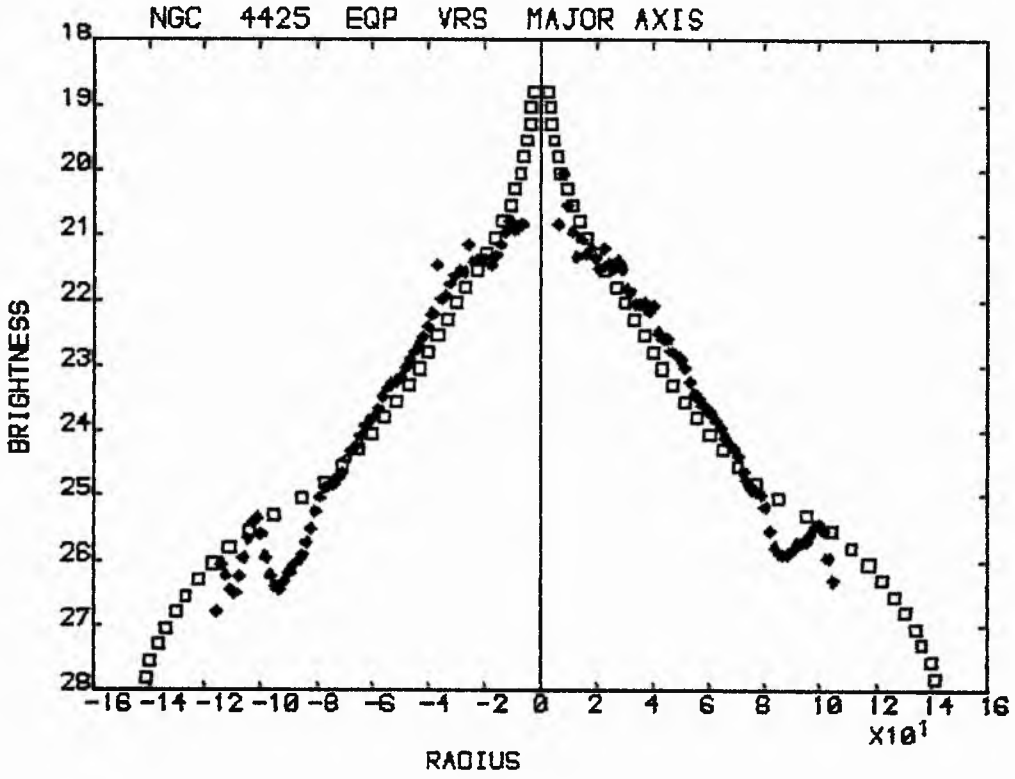
NGC 4425 EQP VRS MAJOR AXIS
BRIGHTNESS
18
19
20
21
22
23
24
25
26
27
28
-16 -14 -12 -10 -8 -6 -4 -2 0 2 4 6 8 10 12 14 16
X10¹
RADIUS

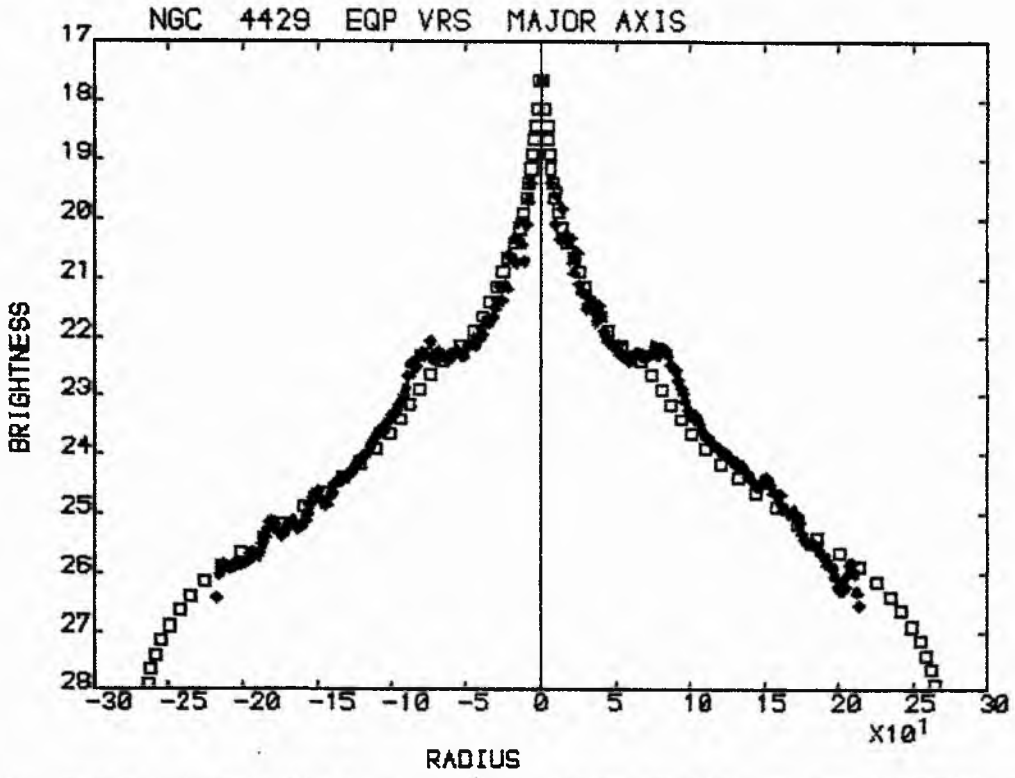
NGC 4429 EQP VRS MAJOR AXIS
BRIGHTNESS
17
18
19
20
21
22
23
24
25
26
27
28
-30 -25 -20 -15 -10 -5 0 5 10 15 20 25 30
X10¹
RADIUS

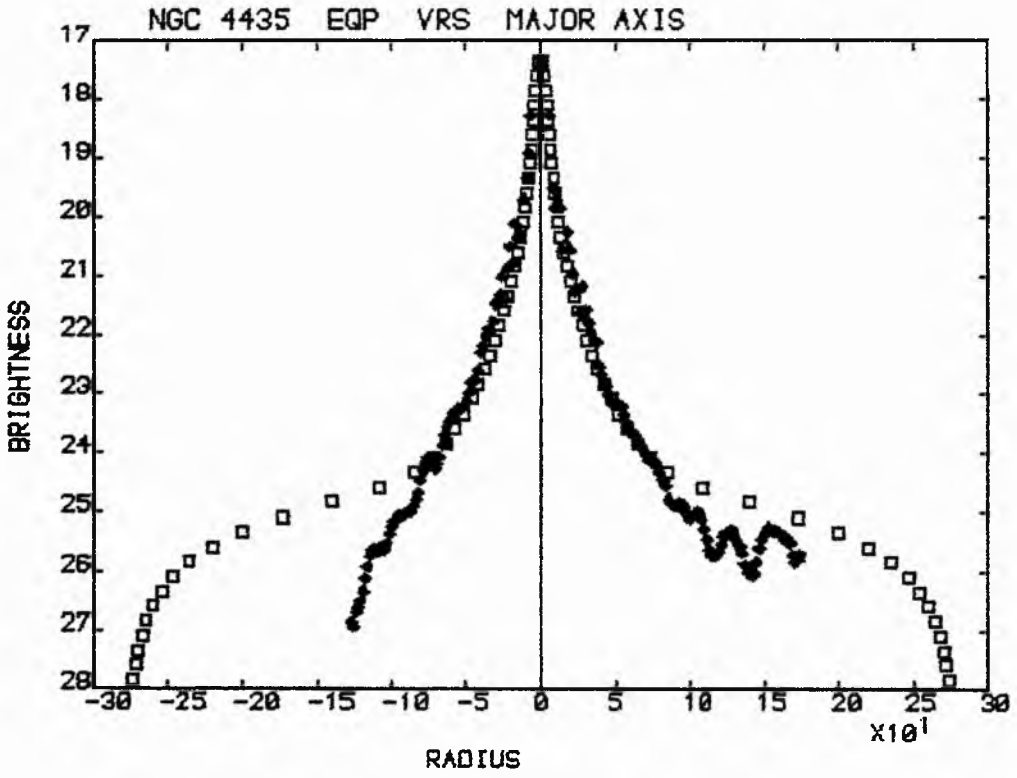
NGC 4435 EQP VRS MAJOR AXIS
BRIGHTNESS
17
18
19
20
21
22
23
24
25
26
27
28
-30 -25 -20 -15 -10 -5 0 5 10 15 20 25 30
X10¹
RADIUS

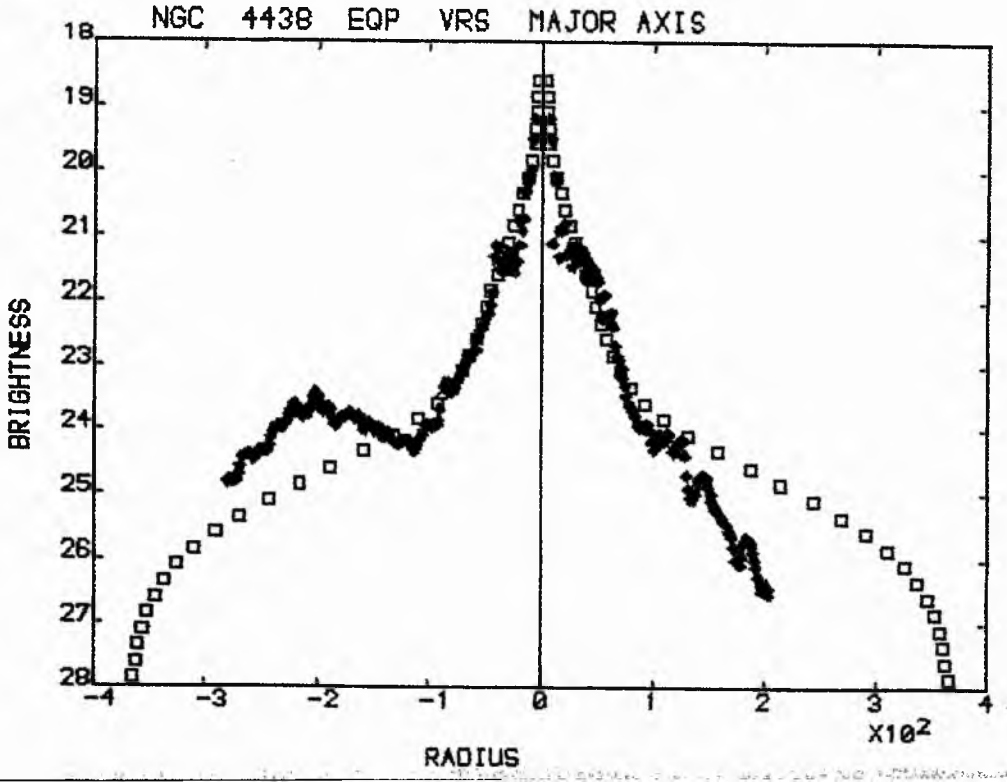
NGC 4438 EQP VRS MAJOR AXIS
BRIGHTNESS
18
19
20
21
22
23
24
25
26
27
28
-4 -3 -2 -1 0 1 2 3 4
X10²
RADIUS

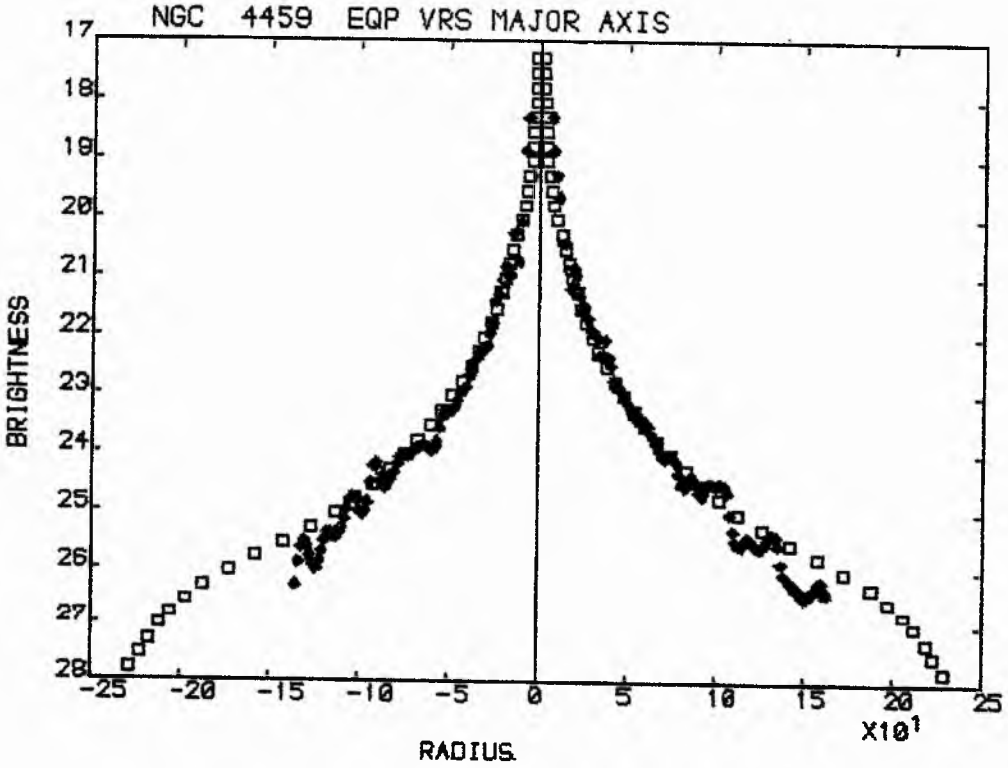
NGC 4459 EQP VRS MAJOR AXIS
BRIGHTNESS
17
18
19
20
21
22
23
24
25
26
27
28
-25
-20
-15
-10
-5
0
5
10
15
20
25
X10¹
RADIUS

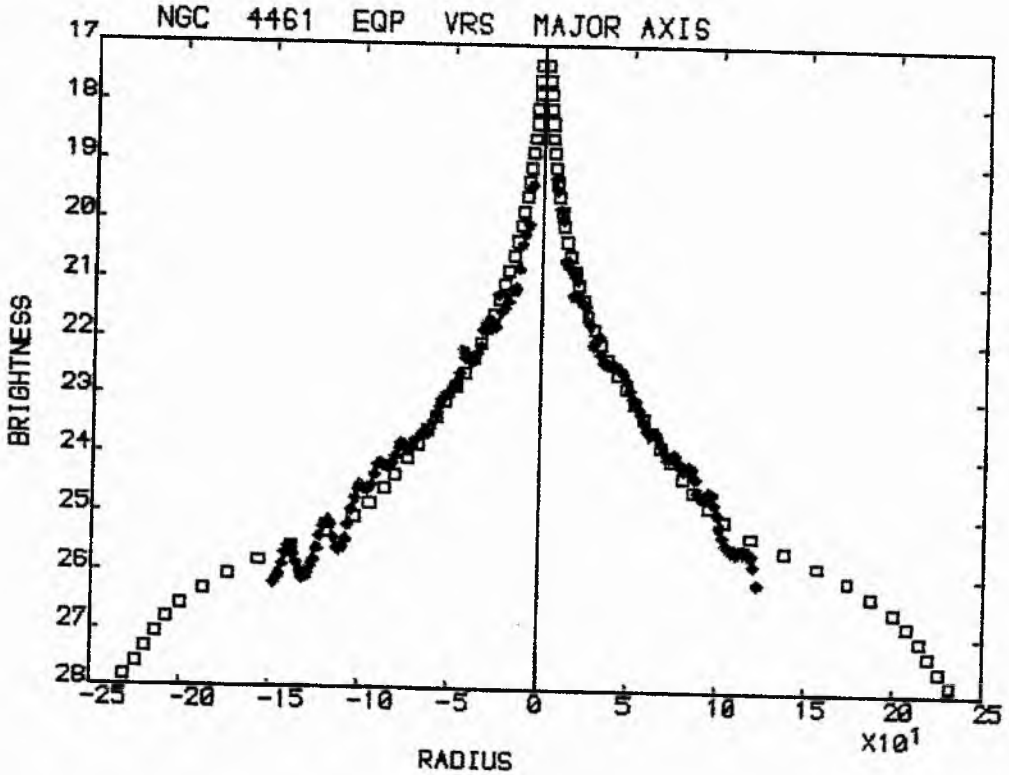
NGC 4461 EQP VRS MAJOR AXIS
BRIGHTNESS
17
18
19
20
21
22
23
24
25
26
27
28
-25
-20
-15
-10
-5
0
5
10
15
20
25
X10¹
RADIUS

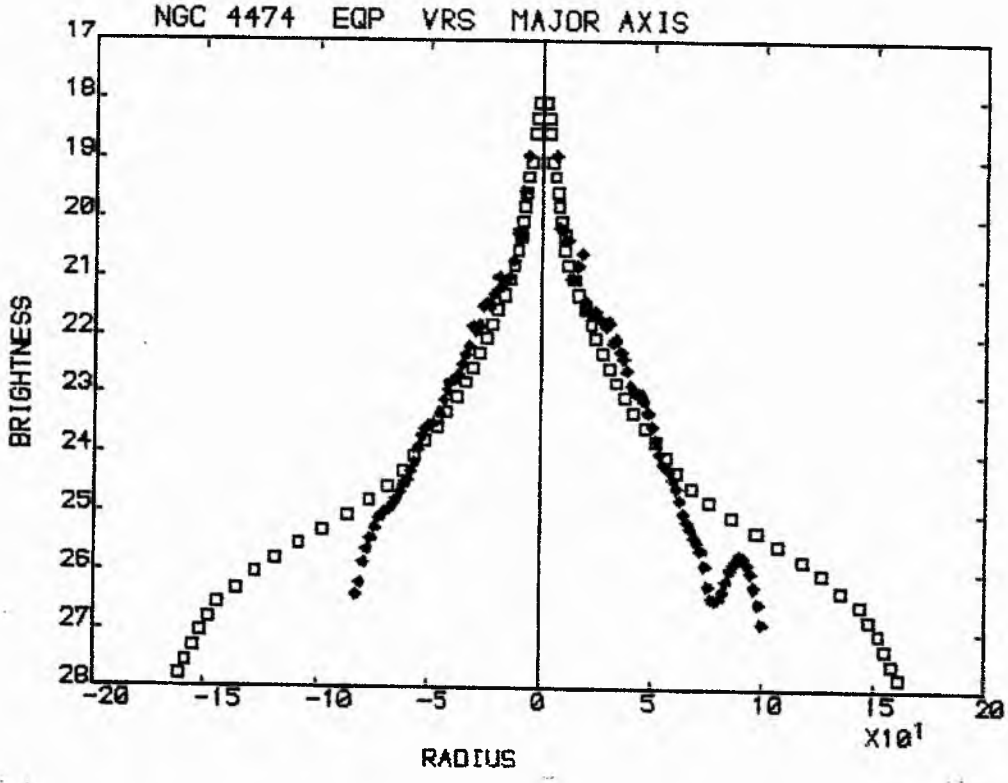
NGC 4474 EQP VRS MAJOR AXIS
BRIGHTNESS
17
18
19
20
21
22
23
24
25
26
27
28
-20
-15
-10
-5
0
5
10
15
20
X10¹
RADIUS

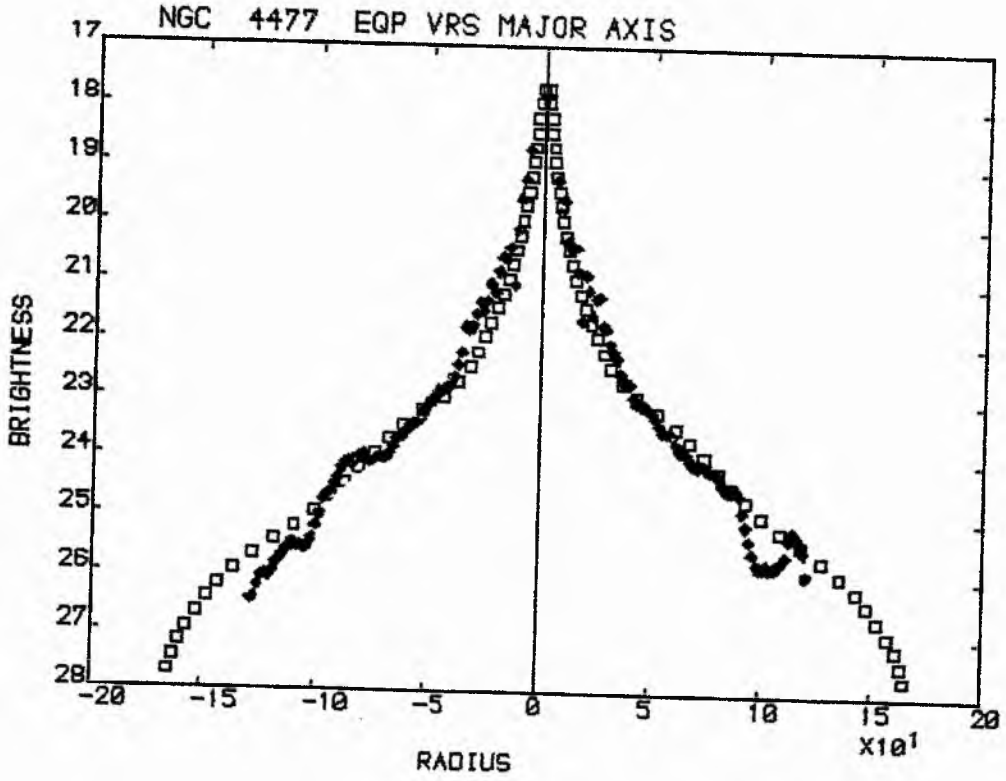
NGC 4477 EQP VRS MAJOR AXIS
BRIGHTNESS
17
18
19
20
21
22
23
24
25
26
27
28
-20
-15
-10
-5
0
5
10
15
20
X10¹
RADIUS

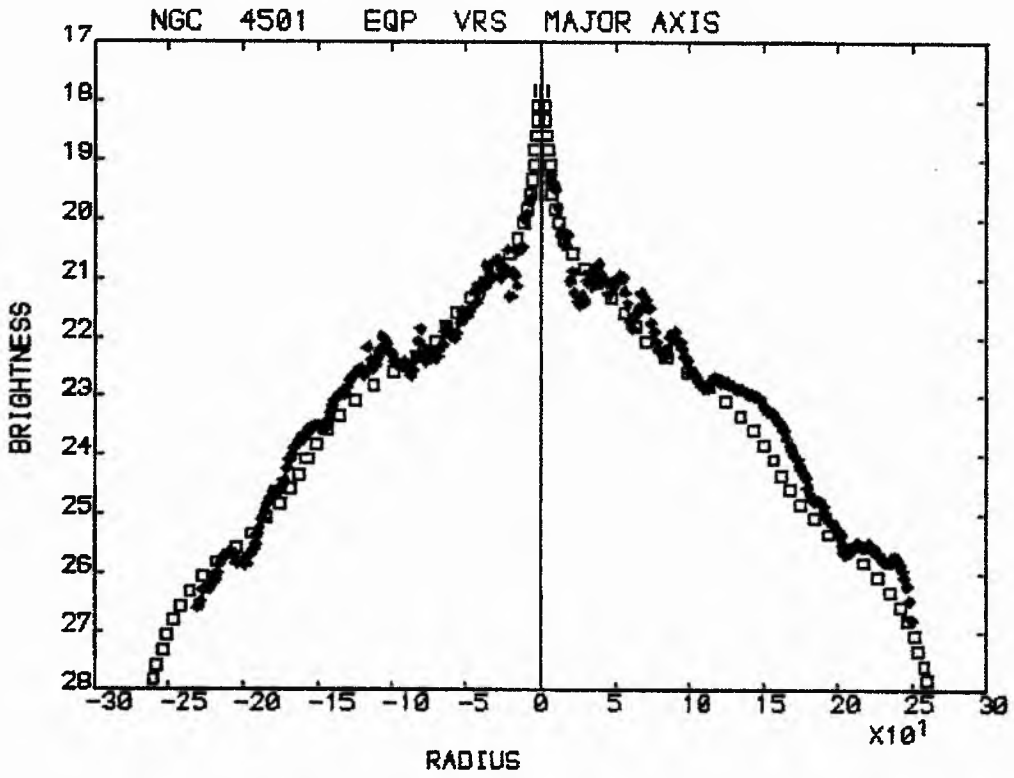
NGC 4501 EQP VRS MAJOR AXIS
BRIGHTNESS
17
18
19
20
21
22
23
24
25
26
27
28
-30 -25 -20 -15 -10 -5 0 5 10 15 20 25 30
X10¹
RADIUS

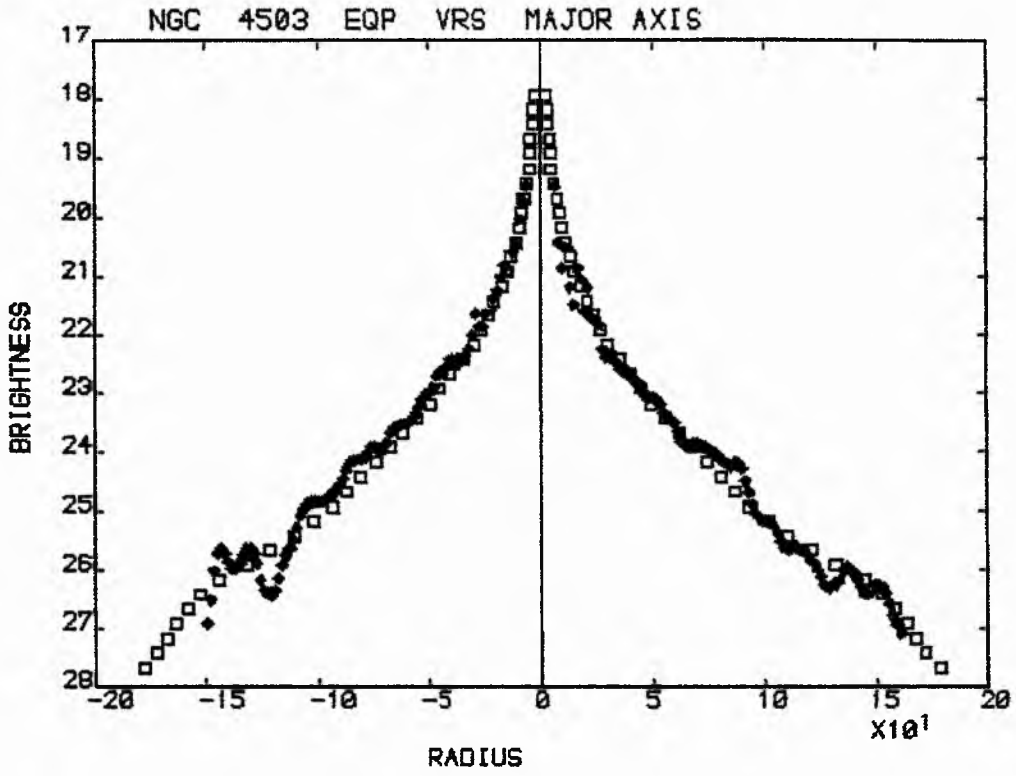
NGC 4503 EQP VRS MAJOR AXIS
BRIGHTNESS
17
18
19
20
21
22
23
24
25
26
27
28
-20
-15
-10
-5
0
5
10
15
20
X10¹
RADIUS

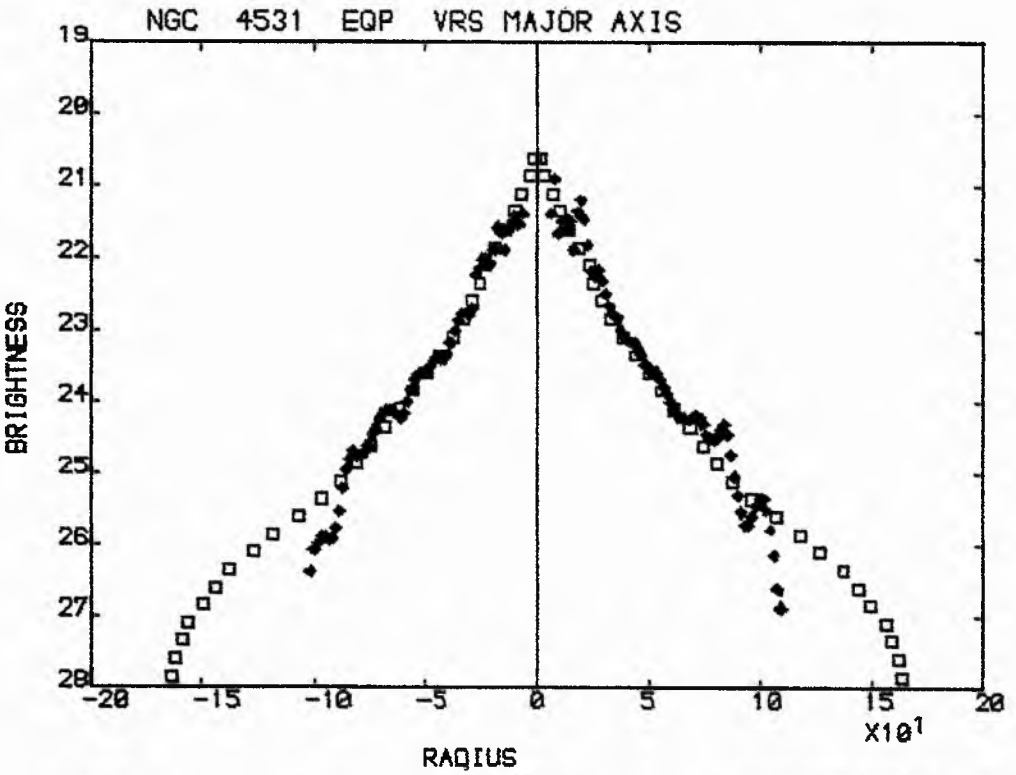
NGC 4531 EQP VRS MAJOR AXIS
BRIGHTNESS
19
20
21
22
23
24
25
26
27
28
-20
-15
-10
-5
0
5
10
15
20
X10¹
RADIUS

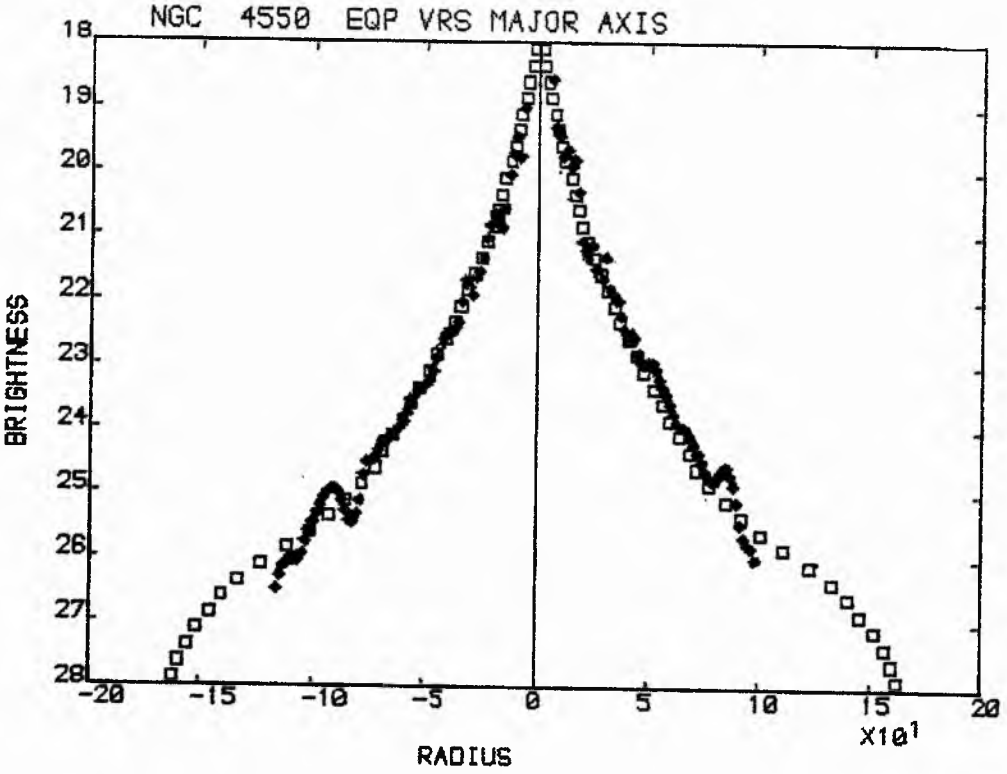
NGC 4550 EQP VRS MAJOR AXIS
BRIGHTNESS
18
19
20
21
22
23
24
25
26
27
28
-20
-15
-10
-5
0
5
10
15
20
X10¹
RADIUS

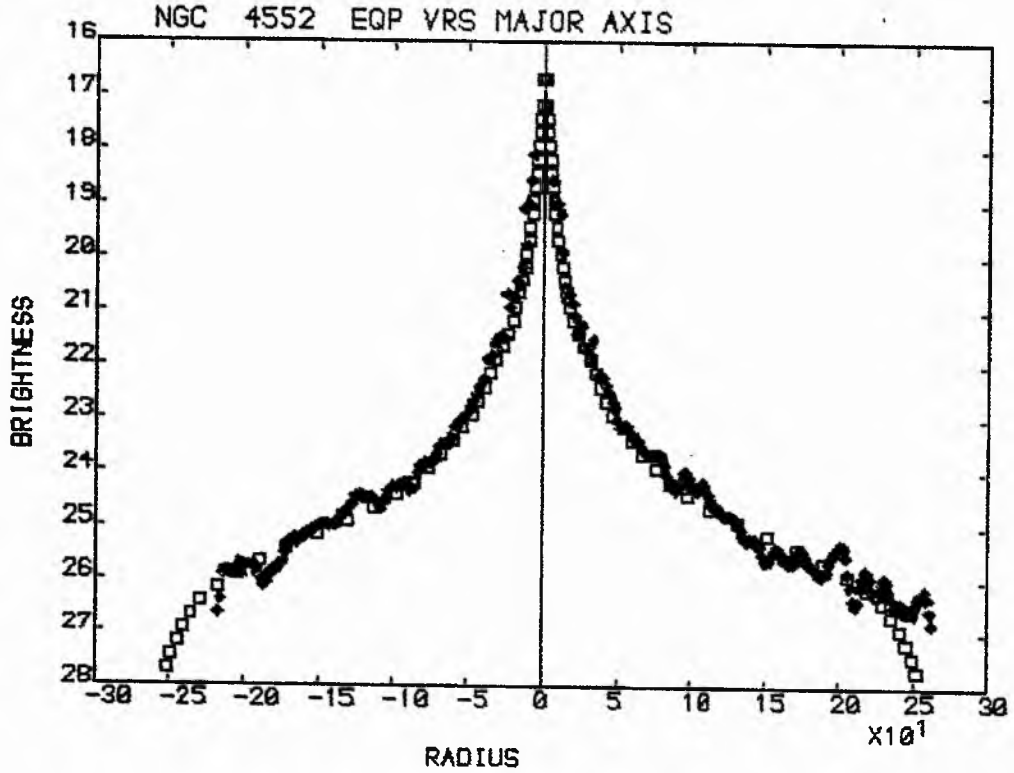
NGC 4552 EQP VRS MAJOR AXIS
BRIGHTNESS
16
17
18
19
20
21
22
23
24
25
26
27
28
-30
-25
-20
-15
-10
-5
0
5
10
15
20
25
30
X10¹
RADIUS

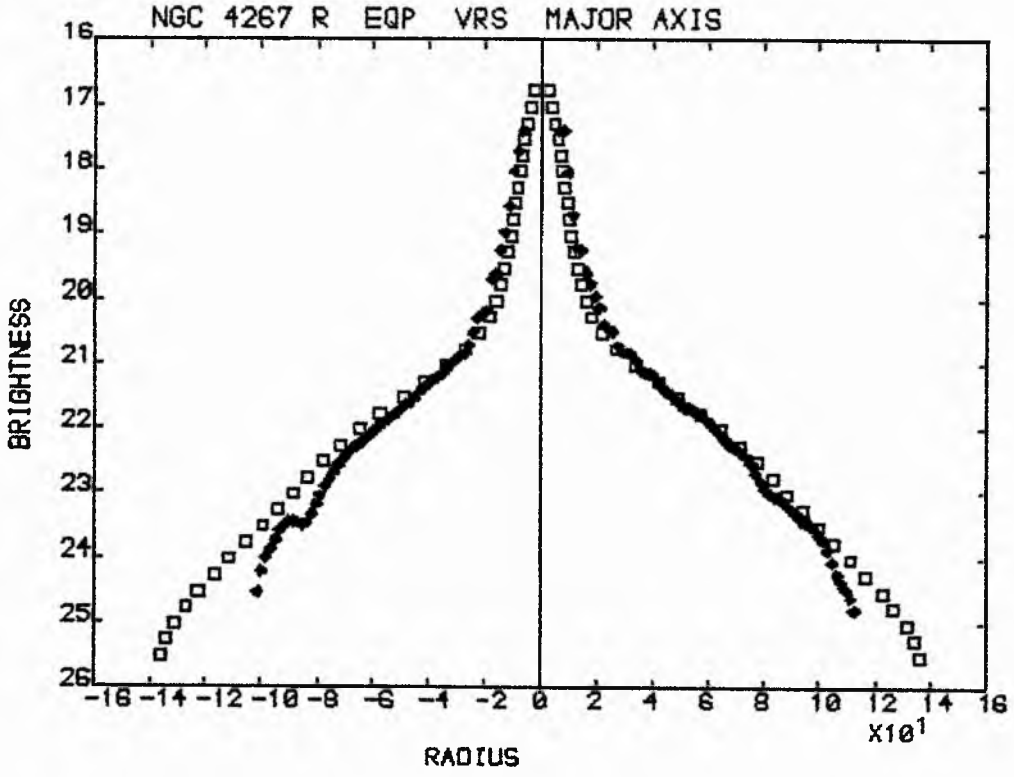
NGC 4267 R EQP VRS MAJOR AXIS
BRIGHTNESS
16
17
18
19
20
21
22
23
24
25
26
-16 -14 -12 -10 -8 -6 -4 -2 0 2 4 6 8 10 12 14 16
X10¹
RADIUS

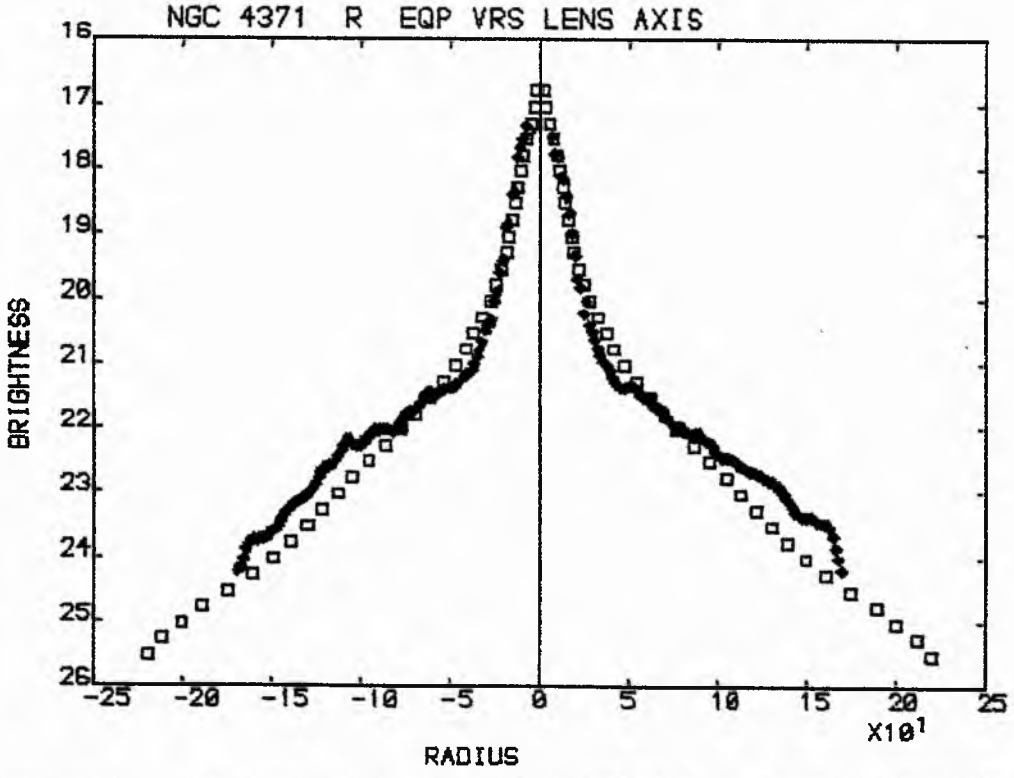
NGC 4371 R EQP VRS LENS AXIS
BRIGHTNESS
16
17
18
19
20
21
22
23
24
25
26
-25 -20 -15 -10 -5 0 5 10 15 20 25
X10¹
RADIUS

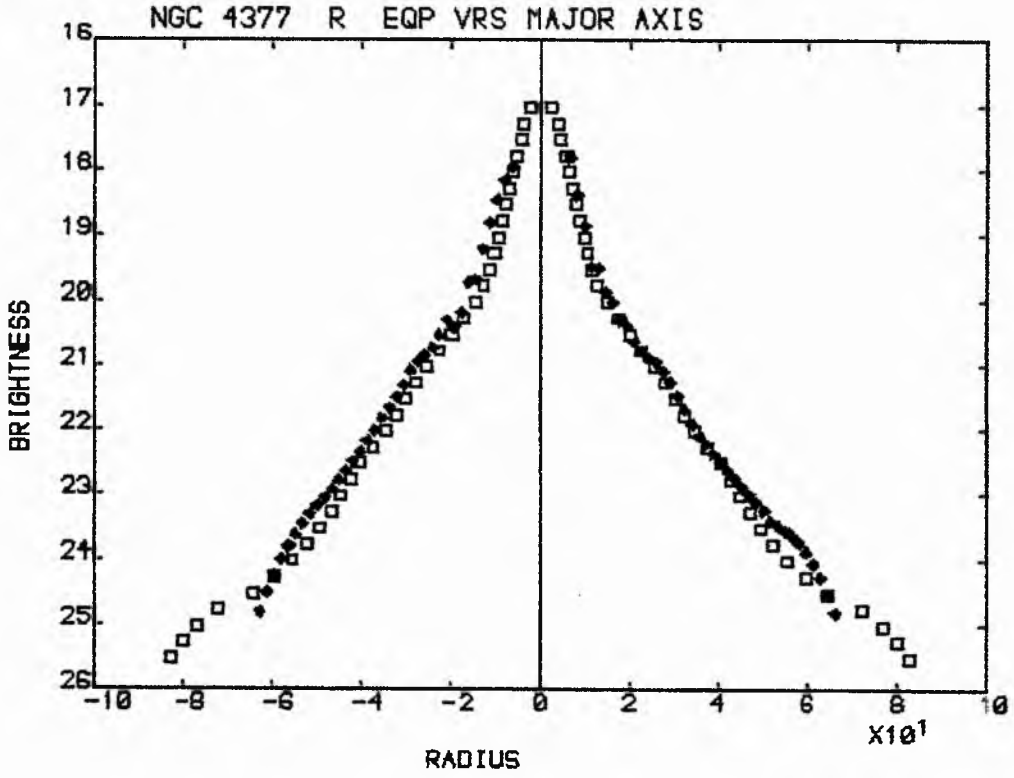
NGC 4377 R EQP VRS MAJOR AXIS
BRIGHTNESS
16
17
18
19
20
21
22
23
24
25
26
-10 -8 -6 -4 -2 0 2 4 6 8 10
X10¹
RADIUS

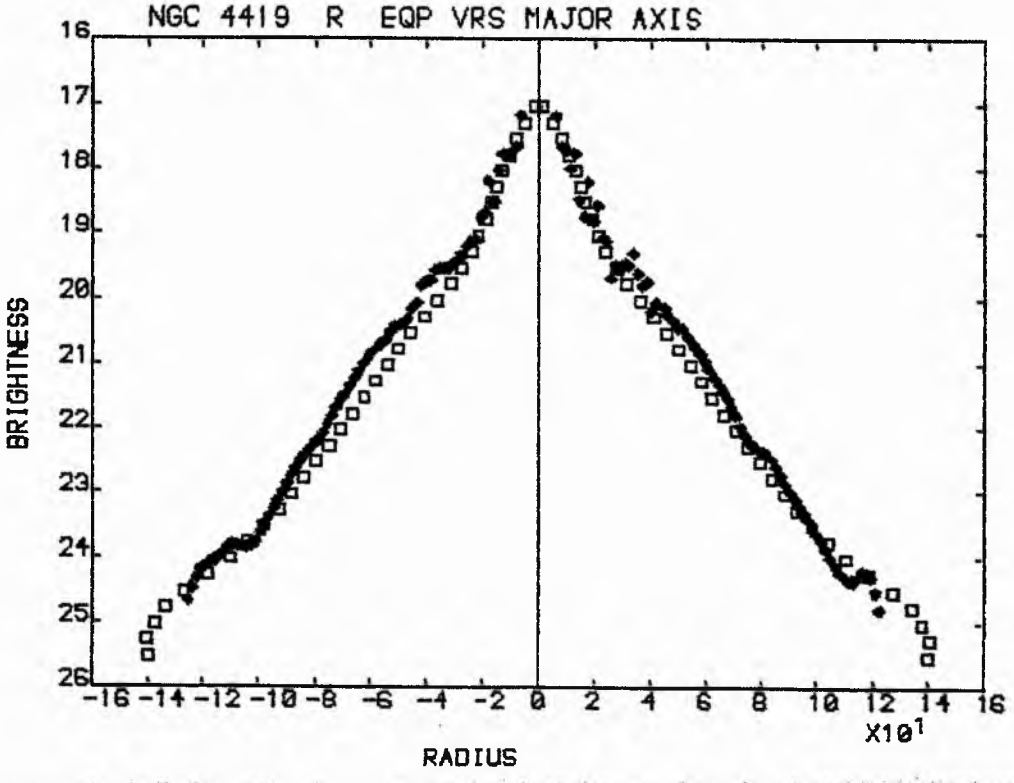
NGC 4419 R EQP VRS MAJOR AXIS
BRIGHTNESS
16
17
18
19
20
21
22
23
24
25
26
-16 -14 -12 -10 -8 -6 -4 -2 0 2 4 6 8 10 12 14 16
X10¹
RADIUS

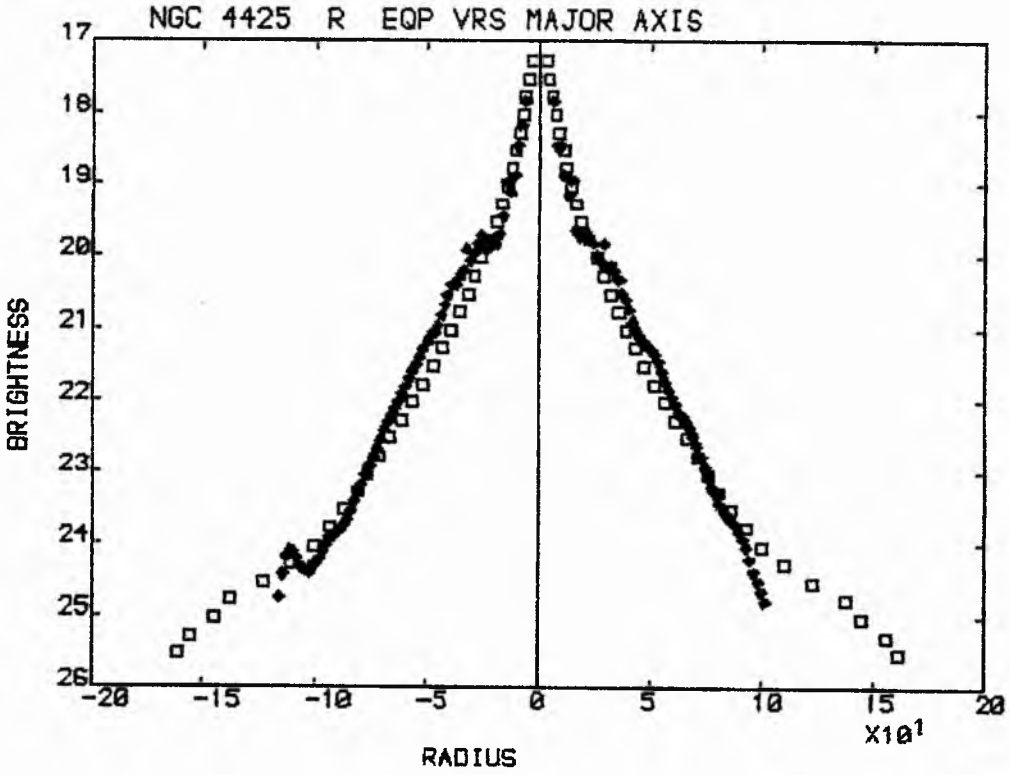
NGC 4425 R EQP VRS MAJOR AXIS
BRIGHTNESS
17
18
19
20
21
22
23
24
25
26
-20
-15
-10
-5
0
5
10
15
20
X10¹
RADIUS

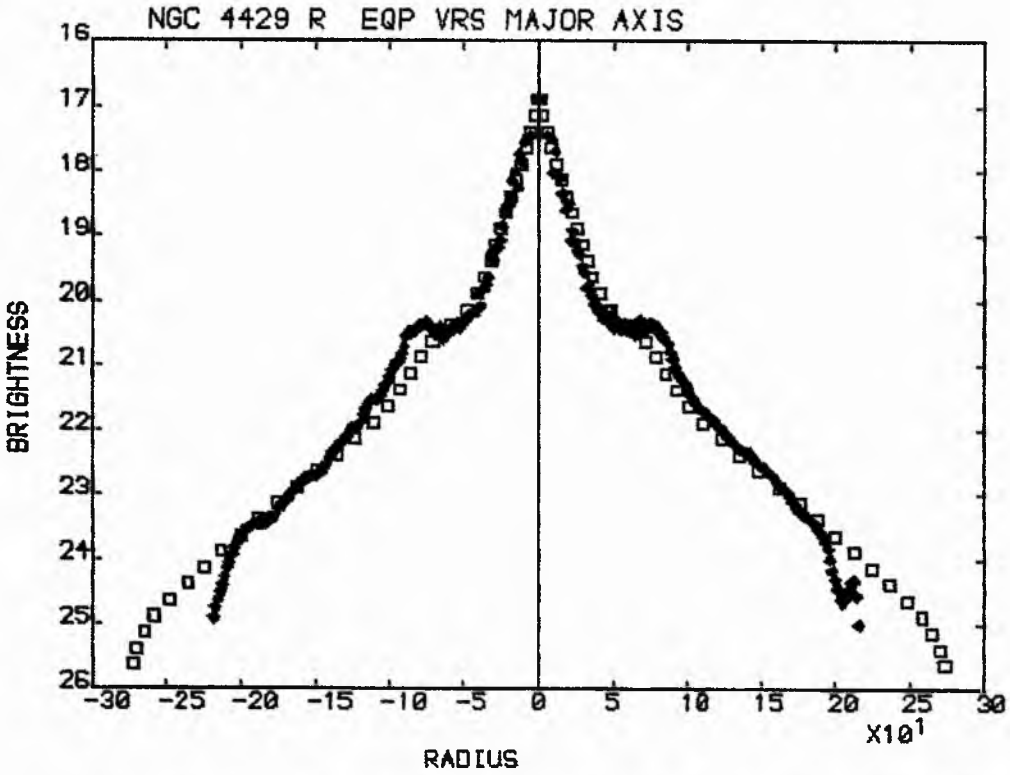
NGC 4429 R EQP VRS MAJOR AXIS
BRIGHTNESS
16
17
18
19
20
21
22
23
24
25
26
-30
-25
-20
-15
-10
-5
0
5
10
15
20
25
30
X10¹
RADIUS

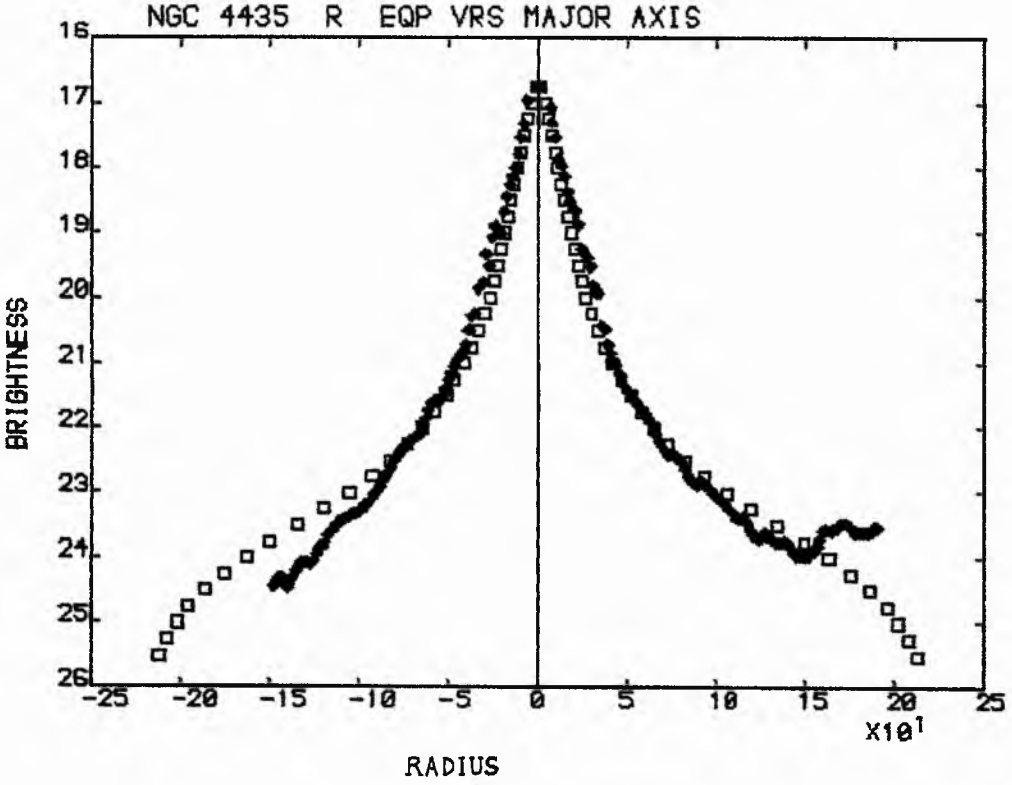
NGC 4435 R EQP VRS MAJOR AXIS
BRIGHTNESS
16
17
18
19
20
21
22
23
24
25
26
-25 -20 -15 -10 -5 0 5 10 15 20 25
X10¹
RADIUS

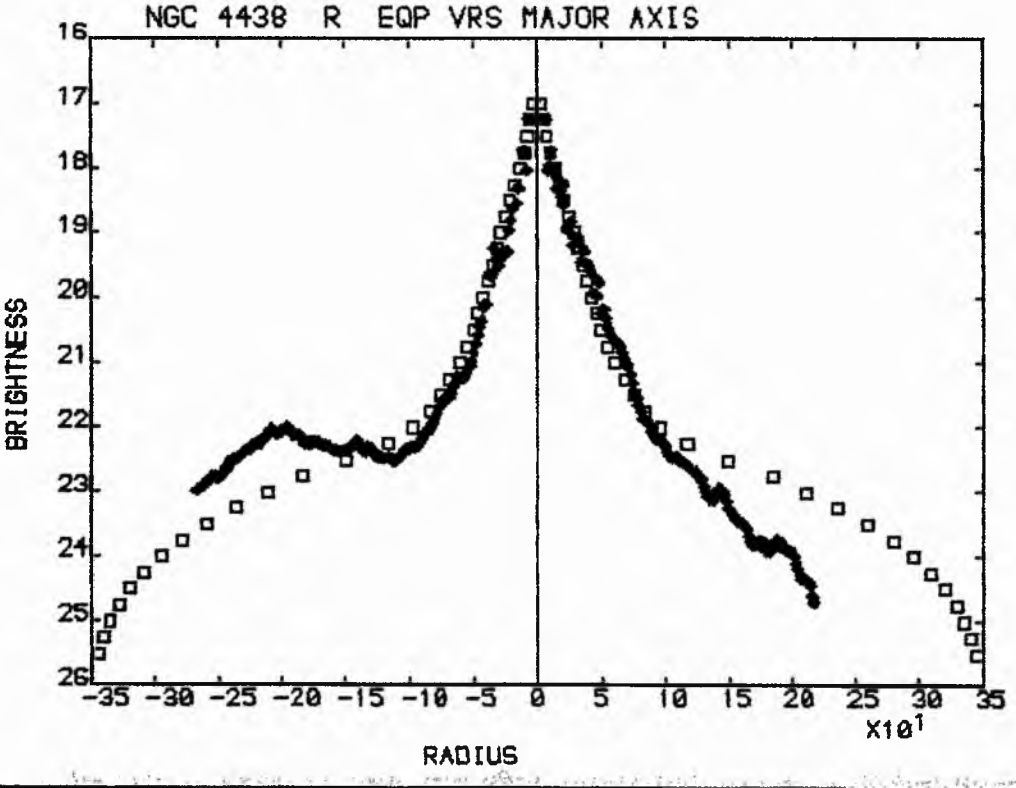
NGC 4438 R EQP VRS MAJOR AXIS
BRIGHTNESS
16
17
18
19
20
21
22
23
24
25
26
-35 -30 -25 -20 -15 -10 -5 0 5 10 15 20 25 30 35
X10¹
RADIUS

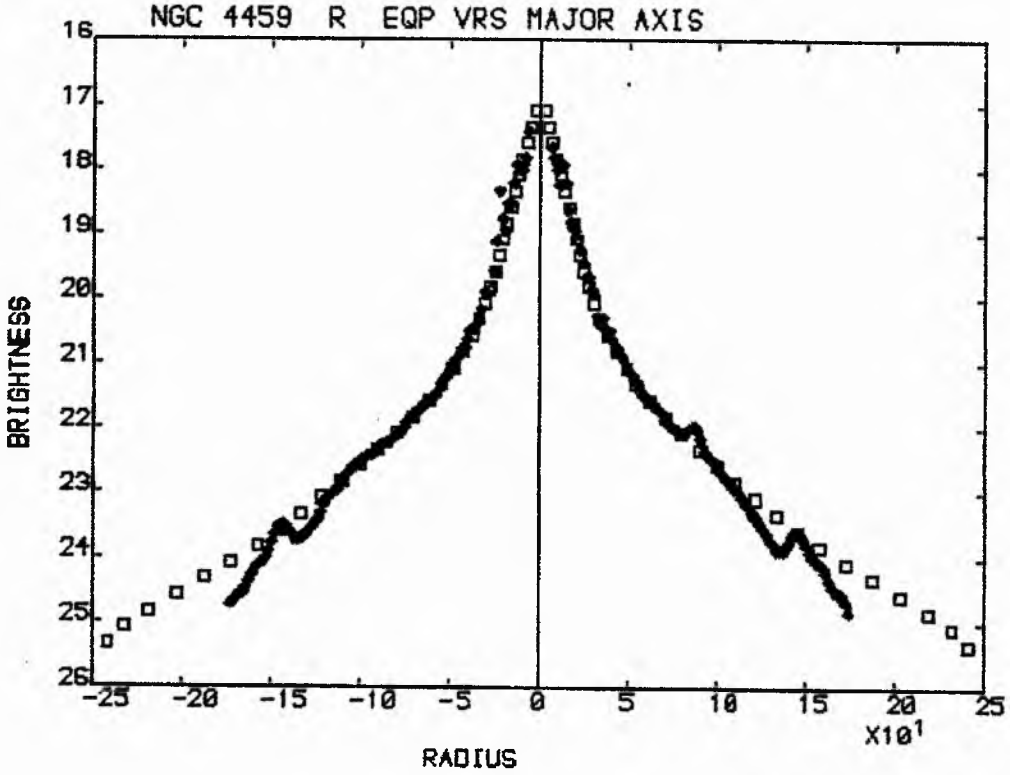
NGC 4459 R EQP VRS MAJOR AXIS
BRIGHTNESS
16
17
18
19
20
21
22
23
24
25
26
-25 -20 -15 -10 -5 0 5 10 15 20 25
X10¹
RADIUS

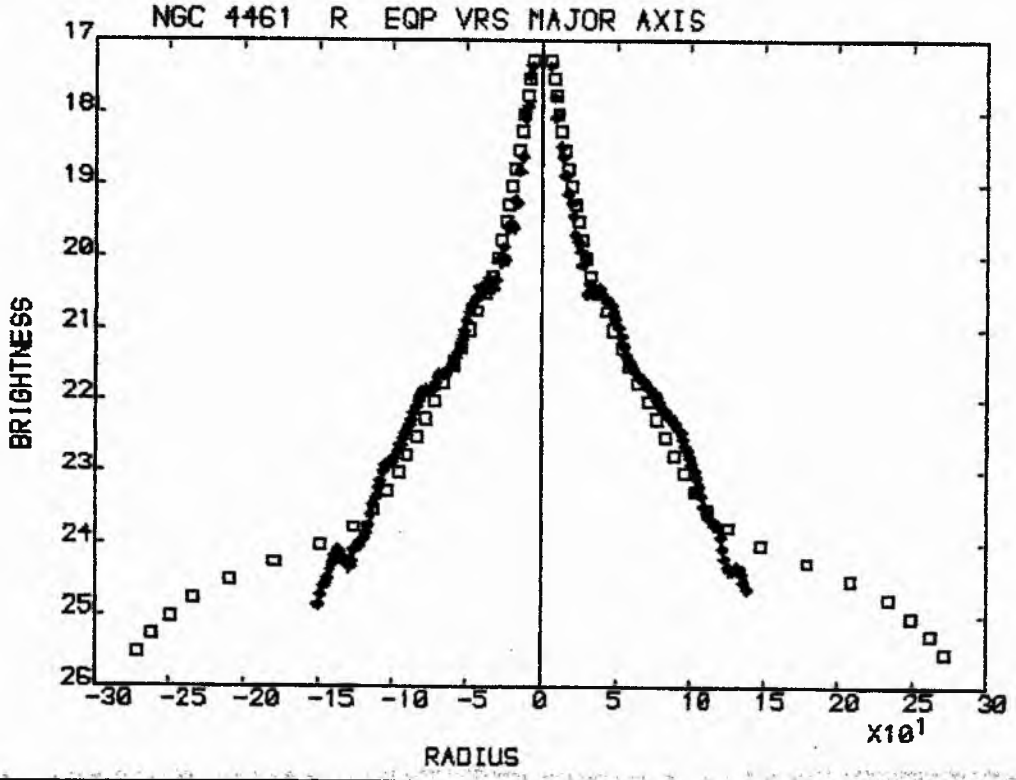
NGC 4461 R EQP VRS MAJOR AXIS
BRIGHTNESS
17
18
19
20
21
22
23
24
25
26
-30 -25 -20 -15 -10 -5 0 5 10 15 20 25 30
X10¹
RADIUS

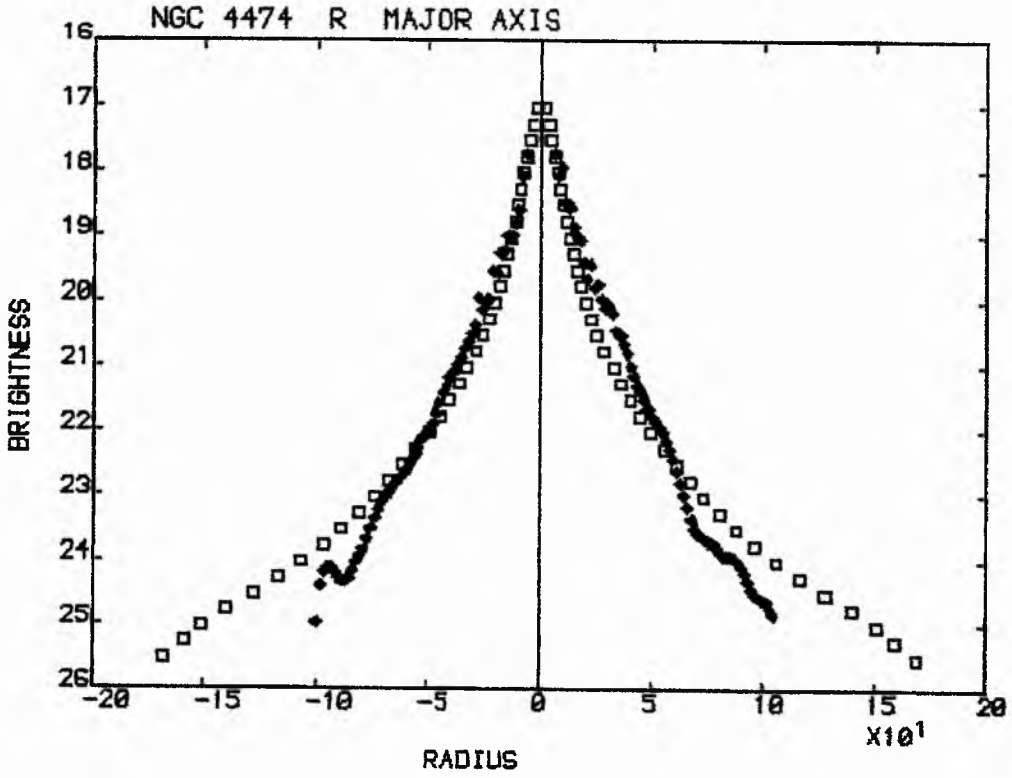
NGC 4474 R MAJOR AXIS
BRIGHTNESS
16
17
18
19
20
21
22
23
24
25
26
-20
-15
-10
-5
0
5
10
15
20
X10¹
RADIUS

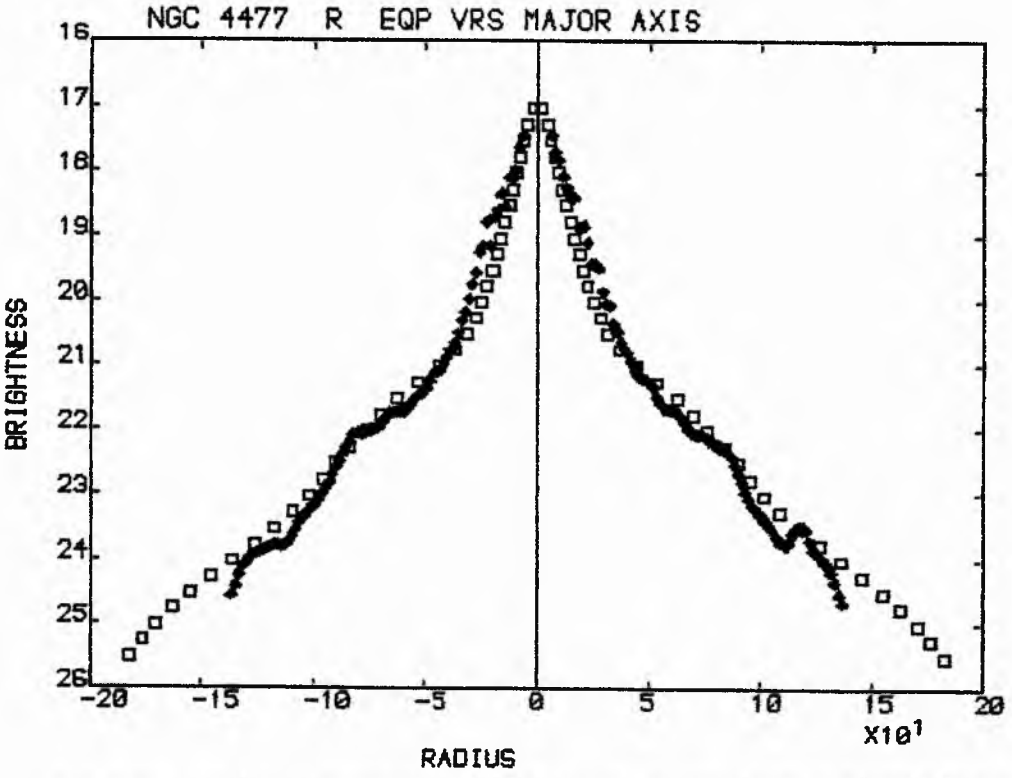
NGC 4477 R EQP VRS MAJOR AXIS
BRIGHTNESS
16
17
18
19
20
21
22
23
24
25
26
-20
-15
-10
-5
0
5
10
15
20
X10¹
RADIUS

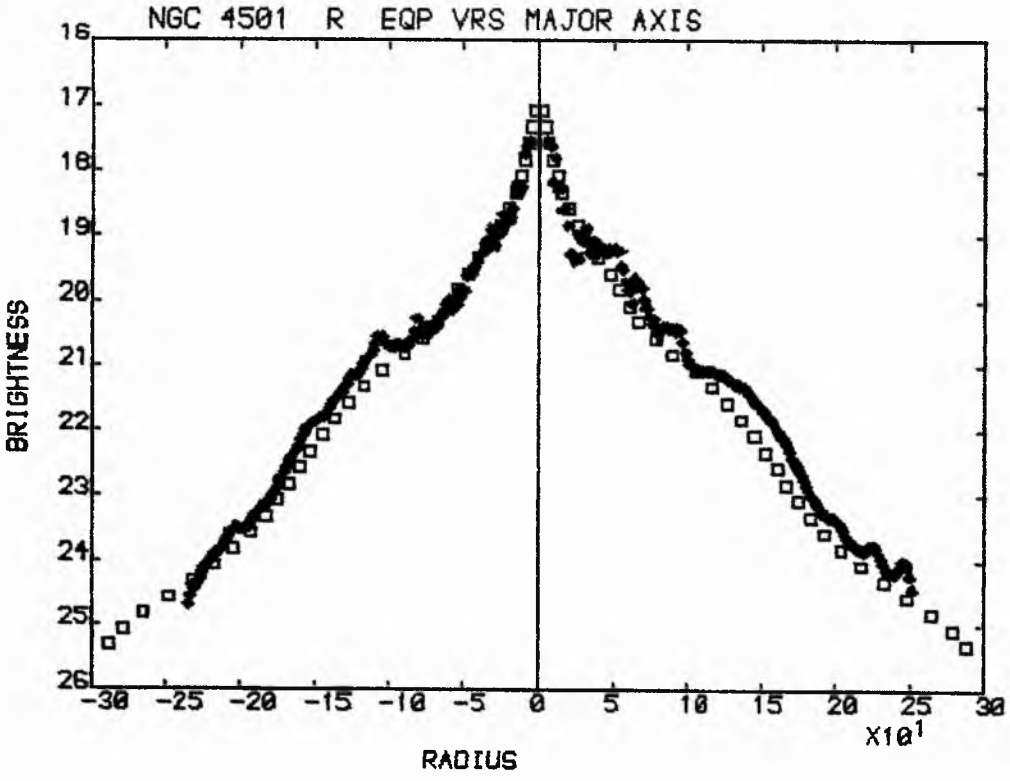
NGC 4501 R EQP VRS MAJOR AXIS
BRIGHTNESS
16
17
18
19
20
21
22
23
24
25
26
-30 -25 -20 -15 -10 -5 0 5 10 15 20 25 30
X10¹
RADIUS

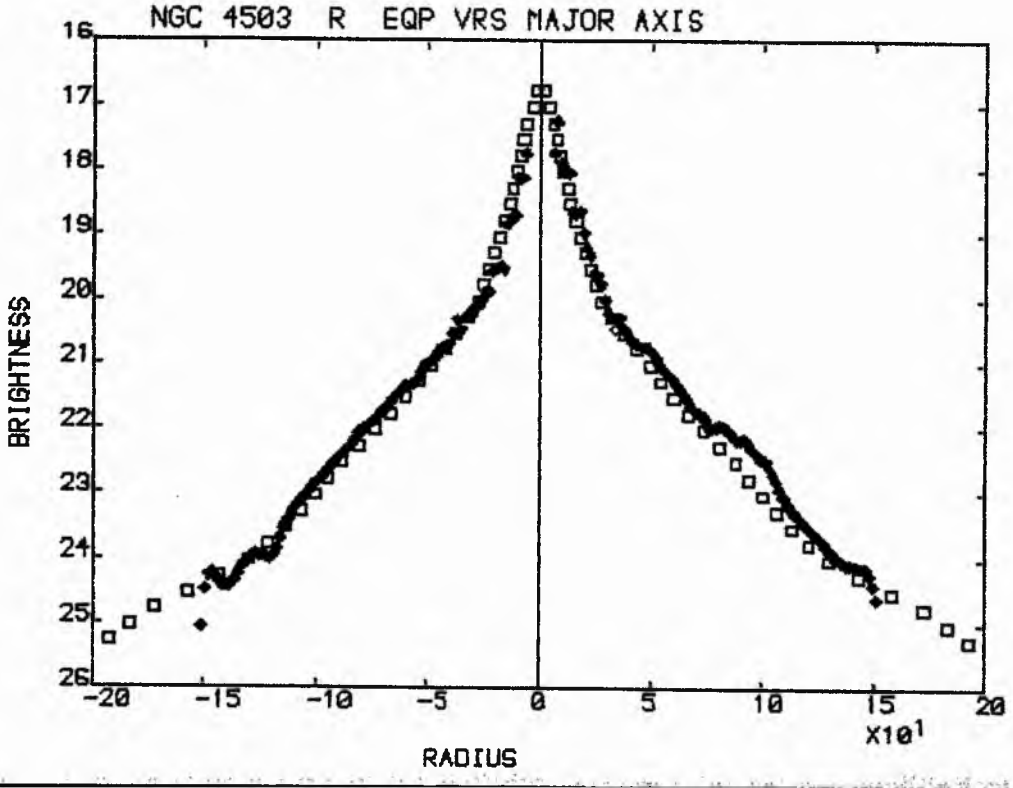
NGC 4503 R EQP VRS MAJOR AXIS
BRIGHTNESS
16
17
18
19
20
21
22
23
24
25
26
-20 -15 -10 -5 0 5 10 15 20
X10¹
RADIUS

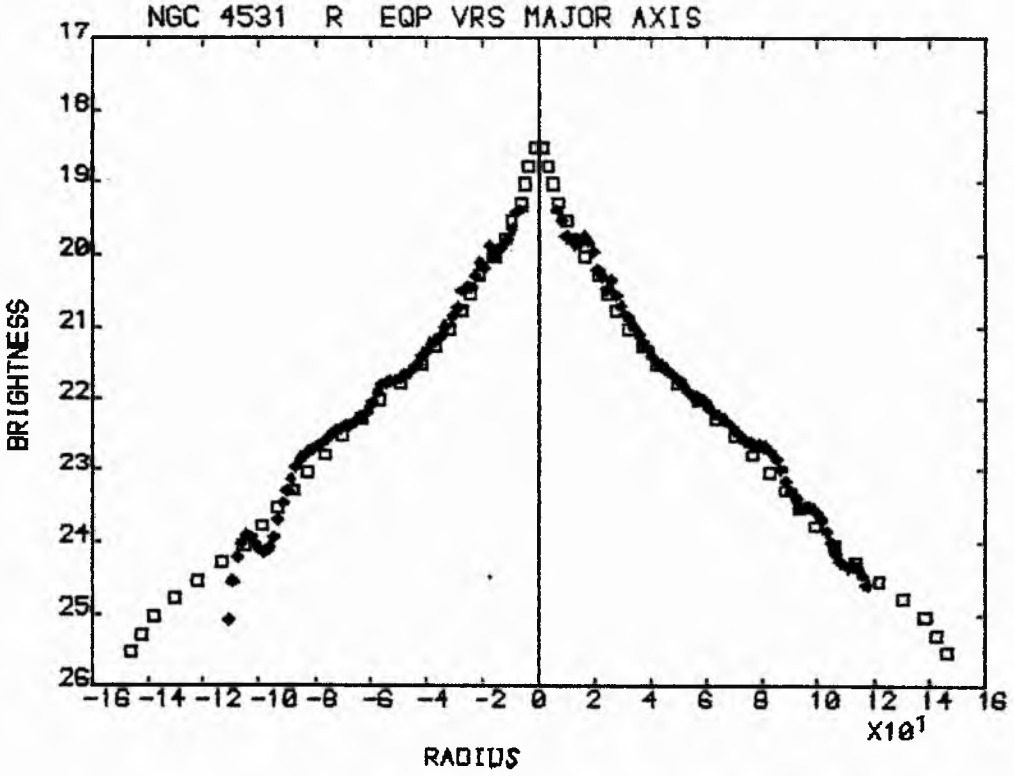
NGC 4531 R EQP VRS MAJOR AXIS
BRIGHTNESS
17
18
19
20
21
22
23
24
25
26
-16 -14 -12 -10 -8 -6 -4 -2 0 2 4 6 8 10 12 14 16
X10¹
RADIUS

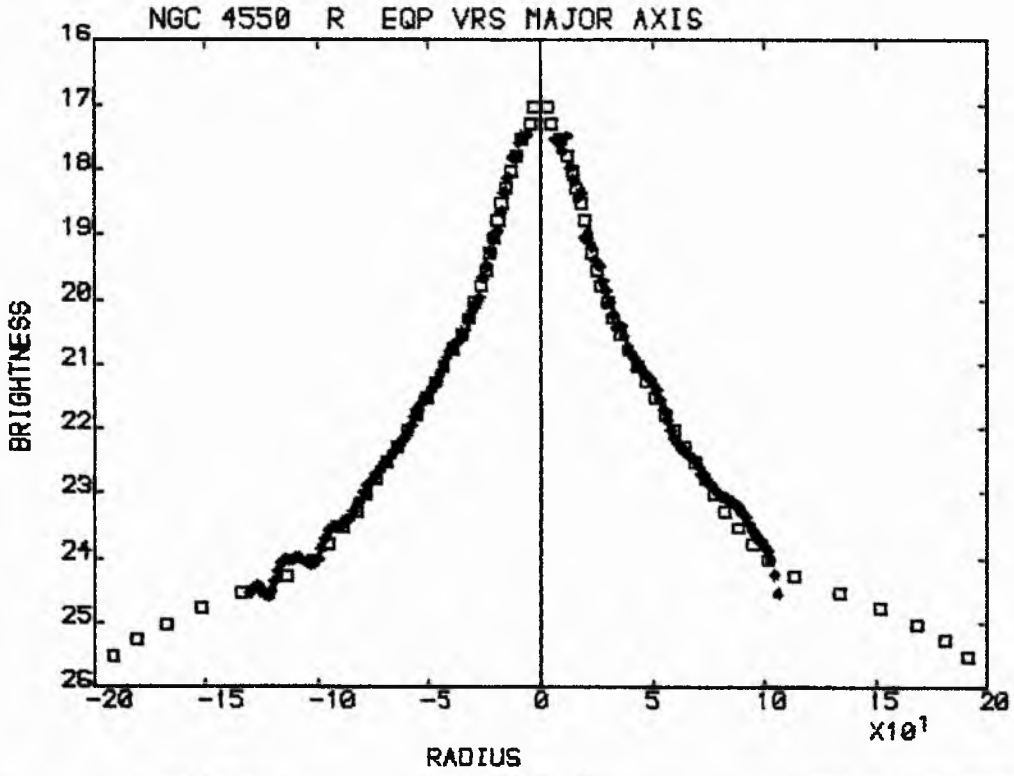
NGC 4550 R EQP VRS MAJOR AXIS
BRIGHTNESS
16
17
18
19
20
21
22
23
24
25
26
-20 -15 -10 -5 0 5 10 15 20
X10¹
RADIUS

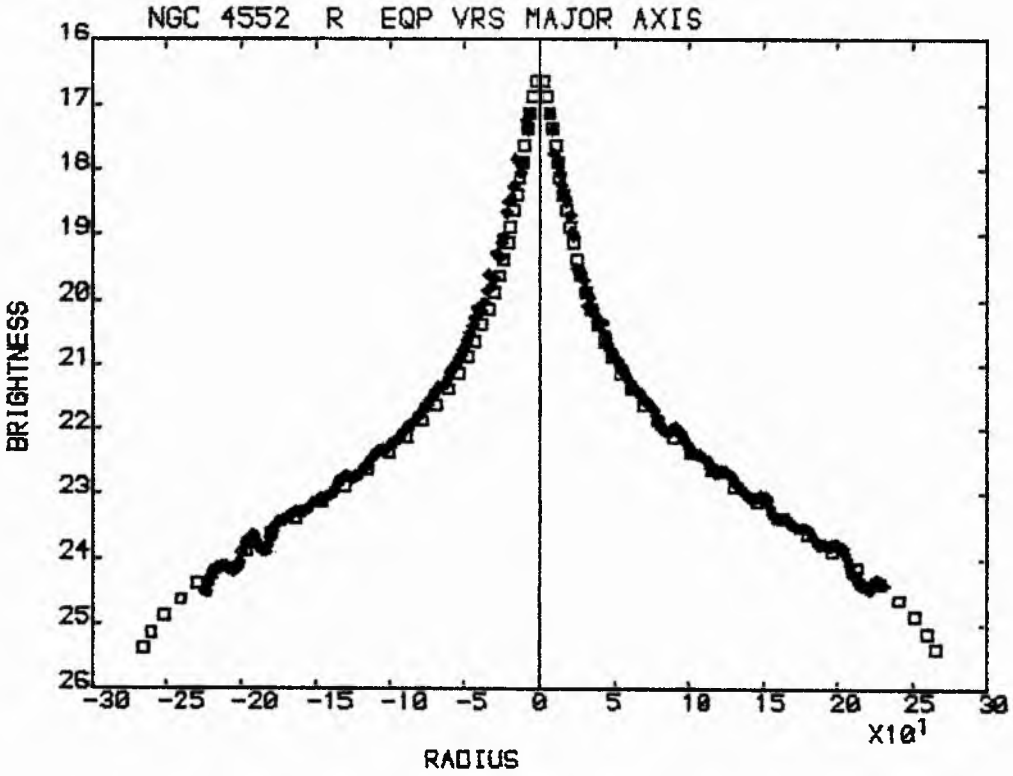
NGC 4552 R EQP VRS MAJOR AXIS
BRIGHTNESS
16
17
18
19
20
21
22
23
24
25
26
-30 -25 -20 -15 -10 -5 0 5 10 15 20 25 30
X10¹
RADIUS

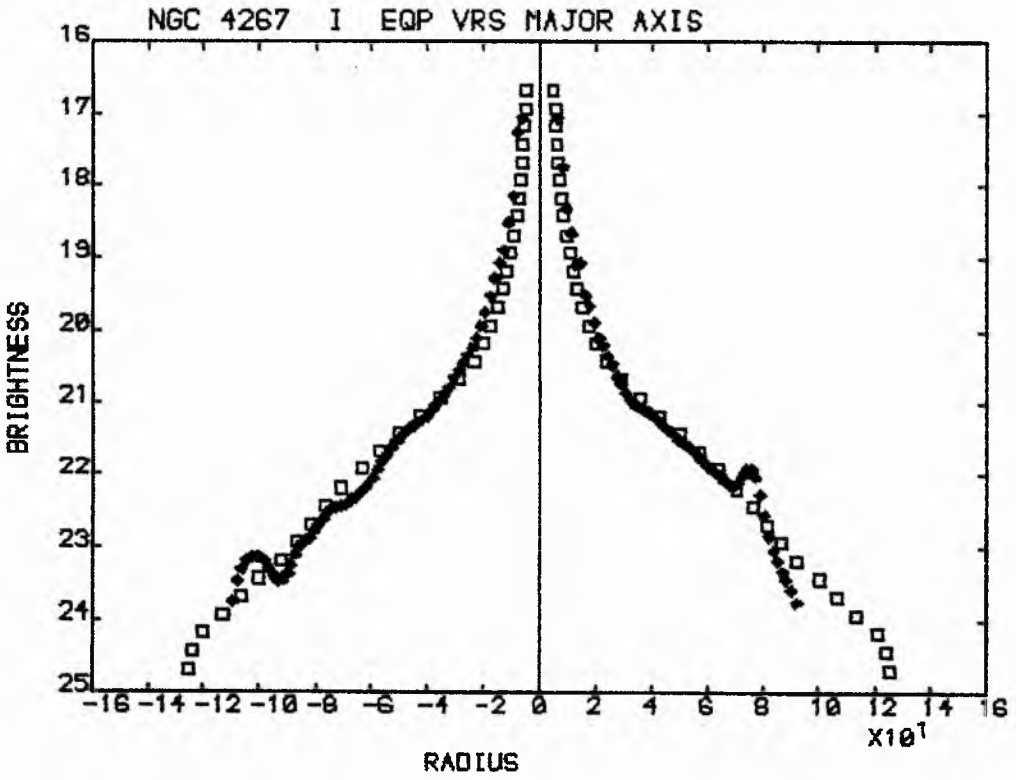
NGC 4267 I EQP VRS MAJOR AXIS
BRIGHTNESS
16
17
18
19
20
21
22
23
24
25
-16 -14 -12 -10 -8 -6 -4 -2 0 2 4 6 8 10 12 14 16
X10¹
RADIUS

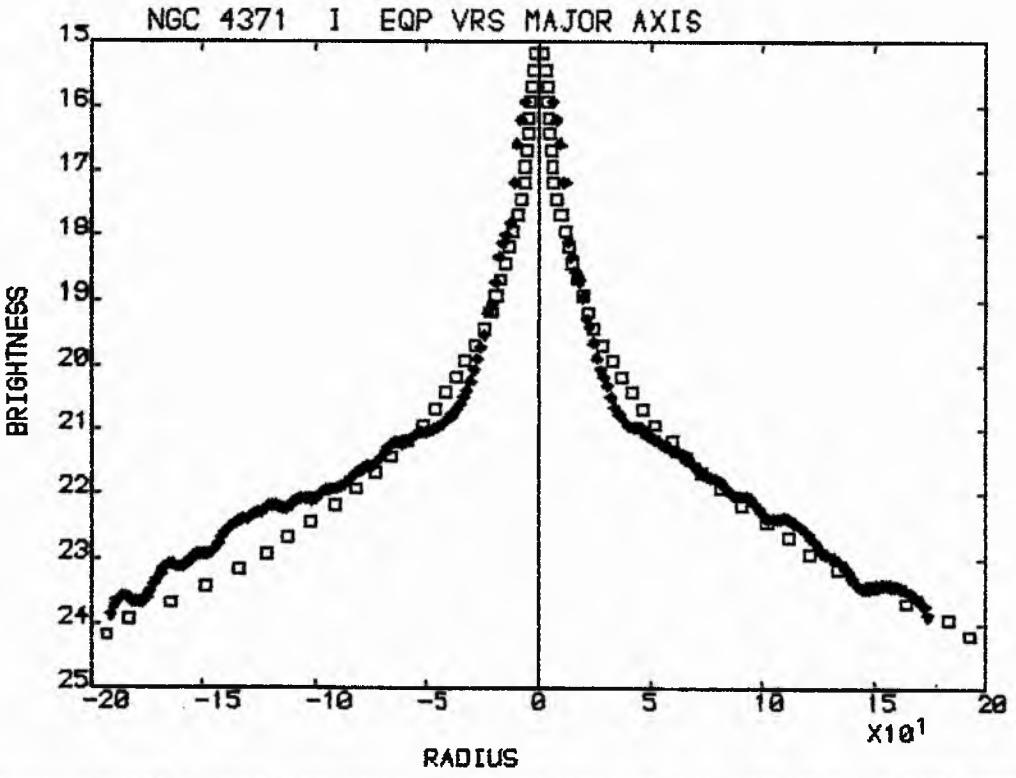
NGC 4371 I EQP VRS MAJOR AXIS
BRIGHTNESS
15
16
17
18
19
20
21
22
23
24
25
-20 -15 -10 -5 0 5 10 15 20
X10¹
RADIUS

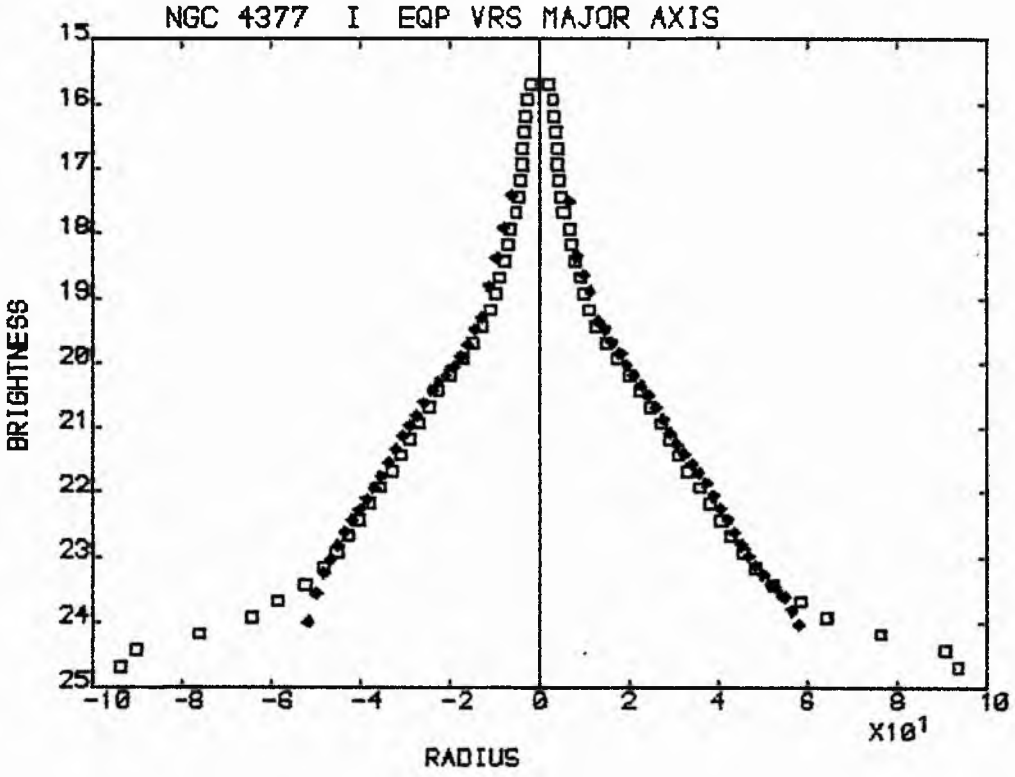
NGC 4377 I EQP VRS MAJOR AXIS
BRIGHTNESS
15
16
17
18
19
20
21
22
23
24
25
-10 -8 -6 -4 -2 0 2 4 6 8 10
X10¹
RADIUS

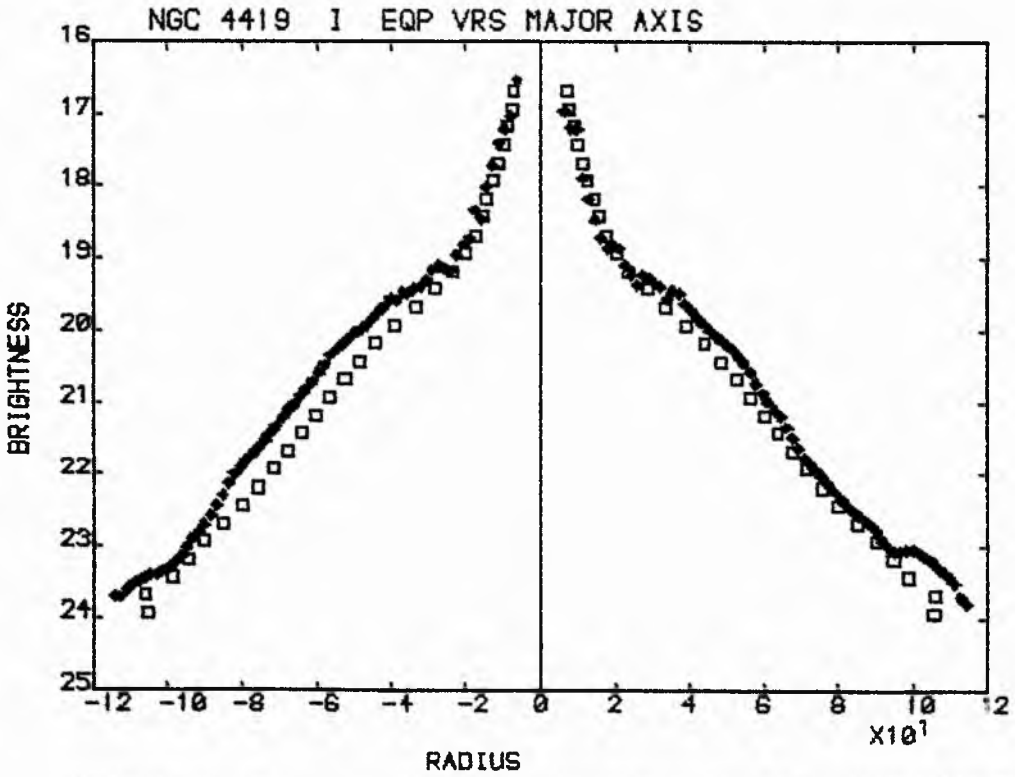
NGC 4419 I EQP VRS MAJOR AXIS
BRIGHTNESS
16
17
18
19
20
21
22
23
24
25
-12 -10 -8 -6 -4 -2 0 2 4 6 8 10 12
X10¹
RADIUS

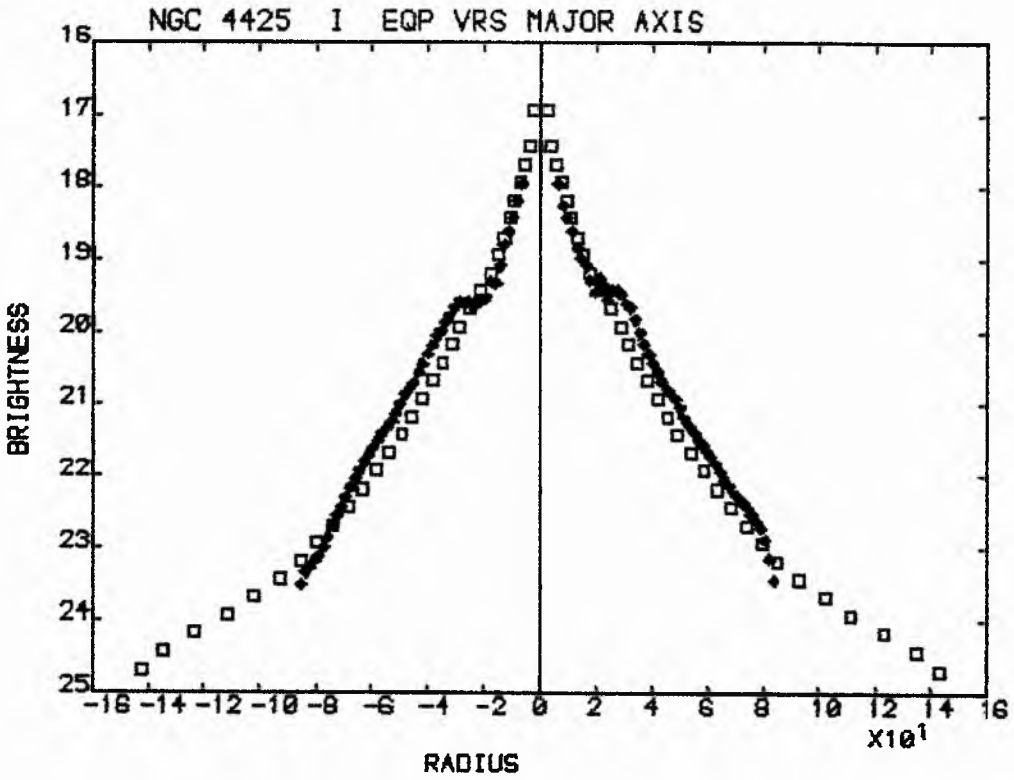
NGC 4425 I EQP VRS MAJOR AXIS
BRIGHTNESS
16
17
18
19
20
21
22
23
24
25
-16 -14 -12 -10 -8 -6 -4 -2 0 2 4 6 8 10 12 14 16
X10¹
RADIUS

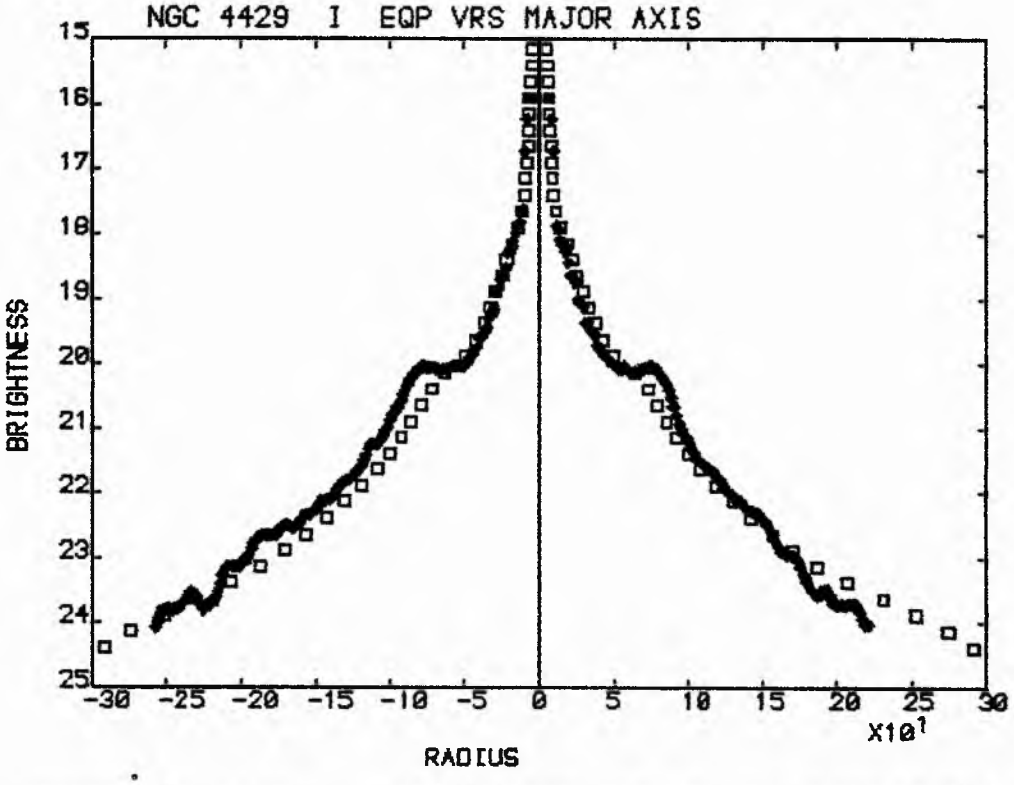
NGC 4429 I EQP VRS MAJOR AXIS
BRIGHTNESS
15
16
17
18
19
20
21
22
23
24
25
-30 -25 -20 -15 -10 -5 0 5 10 15 20 25 30
X10¹
RADIUS

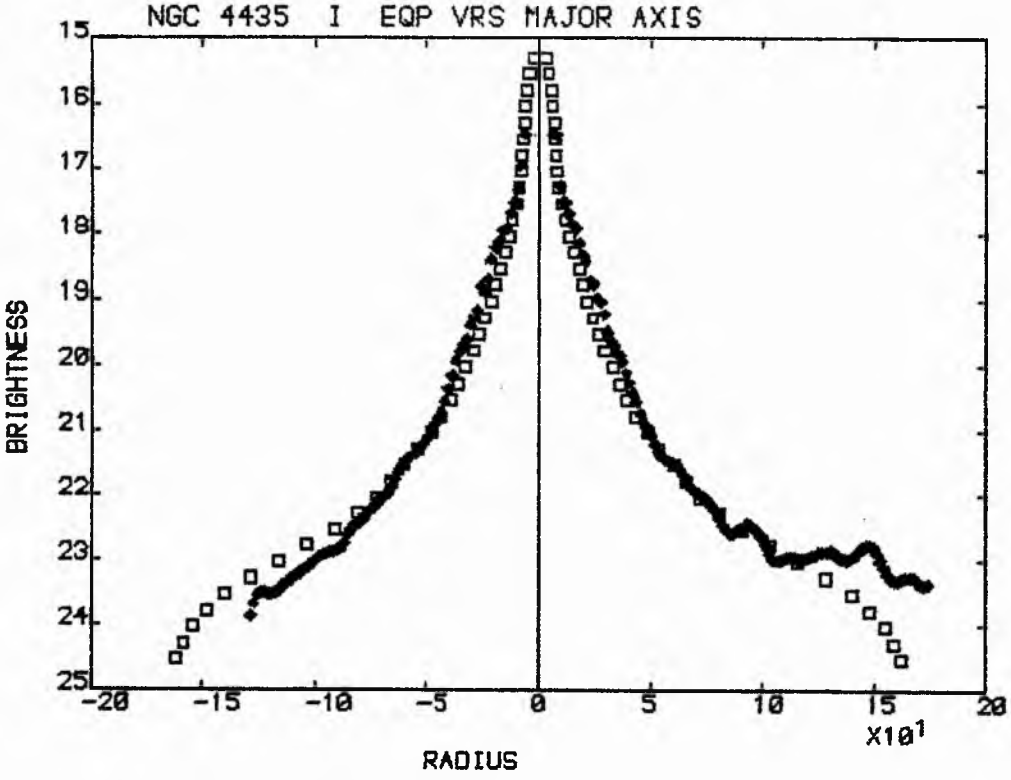
NGC 4435 I EQP VRS MAJOR AXIS
BRIGHTNESS
15
16
17
18
19
20
21
22
23
24
25
-20
-15
-10
-5
0
5
10
15
20
X10¹
RADIUS

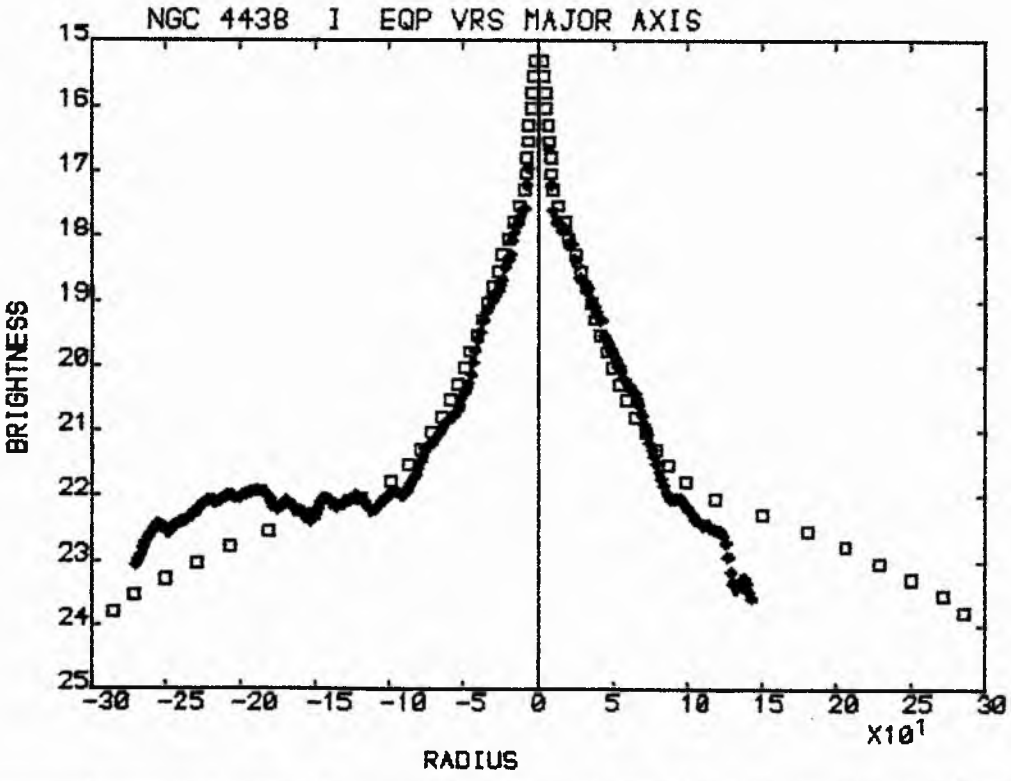
NGC 4438 I EQP VRS MAJOR AXIS
BRIGHTNESS
15
16
17
18
19
20
21
22
23
24
25
-30
-25
-20
-15
-10
-5
0
5
10
15
20
25
30
X10¹
RADIUS

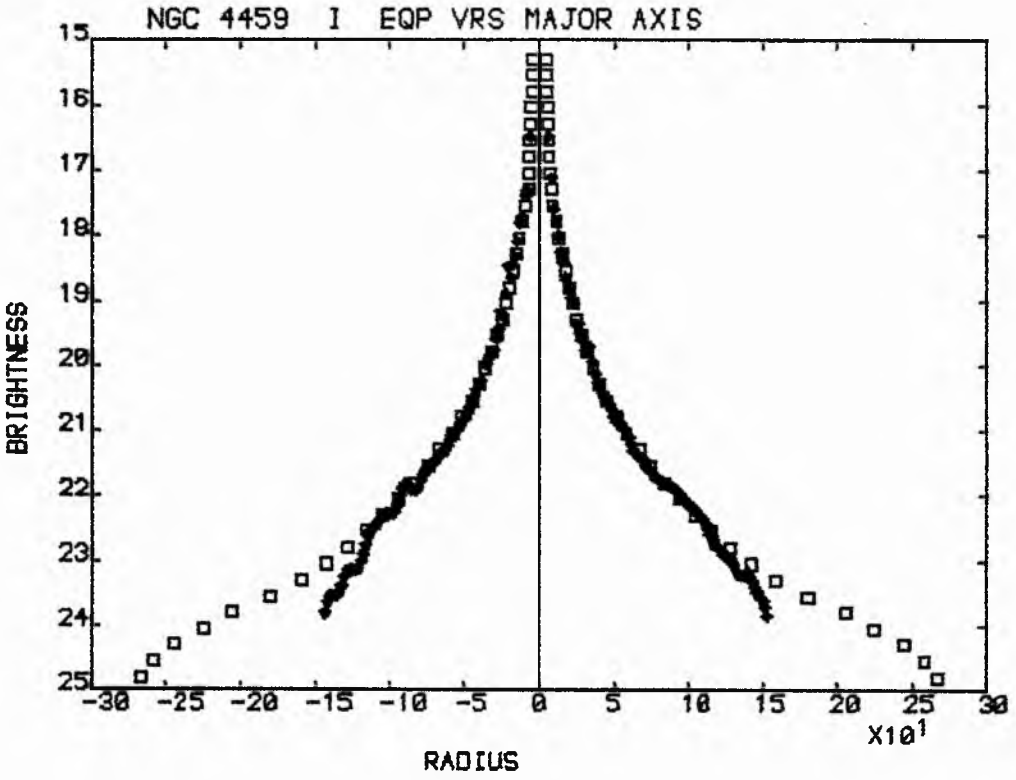
NGC 4459 I EQP VRS MAJOR AXIS
BRIGHTNESS
15
16
17
18
19
20
21
22
23
24
25
-30 -25 -20 -15 -10 -5 0 5 10 15 20 25 30
X10¹
RADIUS

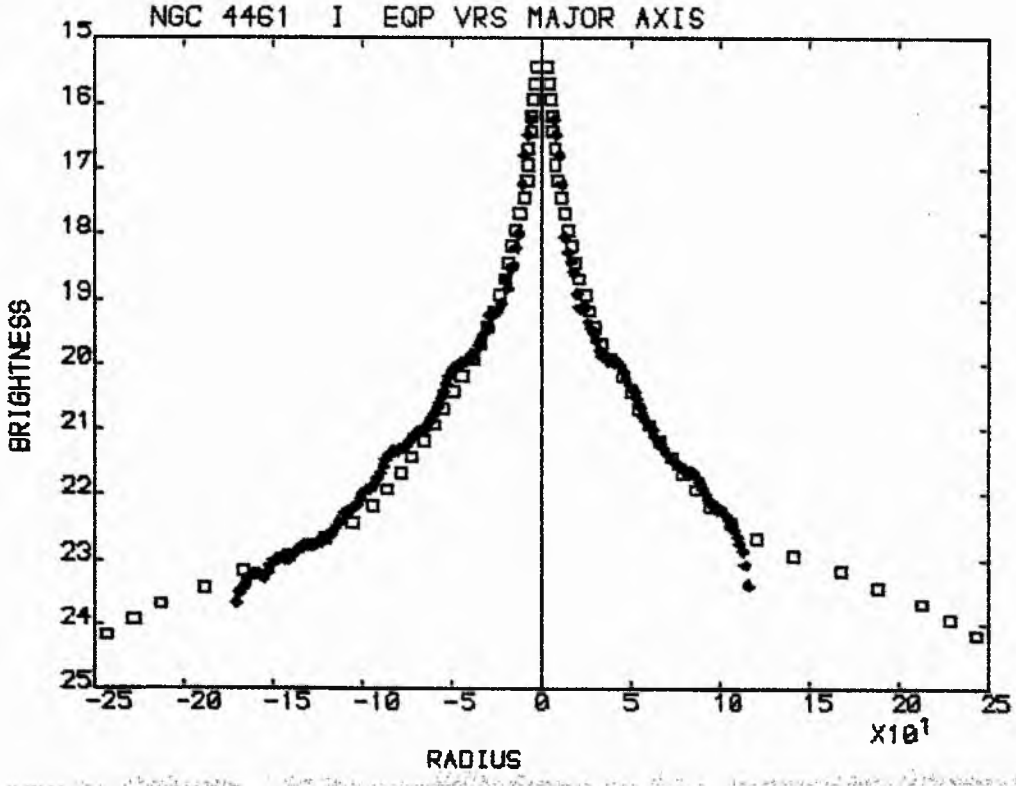
NGC 4461 I EQP VRS MAJOR AXIS
BRIGHTNESS
15
16
17
18
19
20
21
22
23
24
25
-25 -20 -15 -10 -5 0 5 10 15 20 25
X10¹
RADIUS

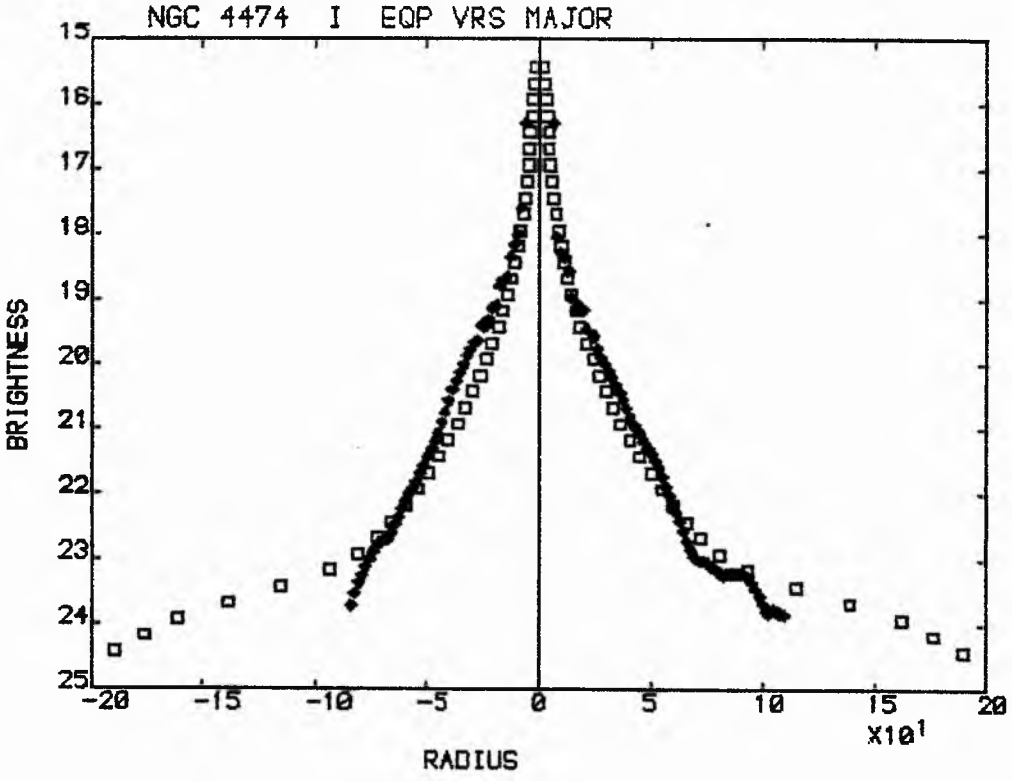
NGC 4474 I EQP VRS MAJOR
BRIGHTNESS
15
16
17
18
19
20
21
22
23
24
25
-20
-15
-10
-5
0
5
10
15
20
X10¹
RADIUS

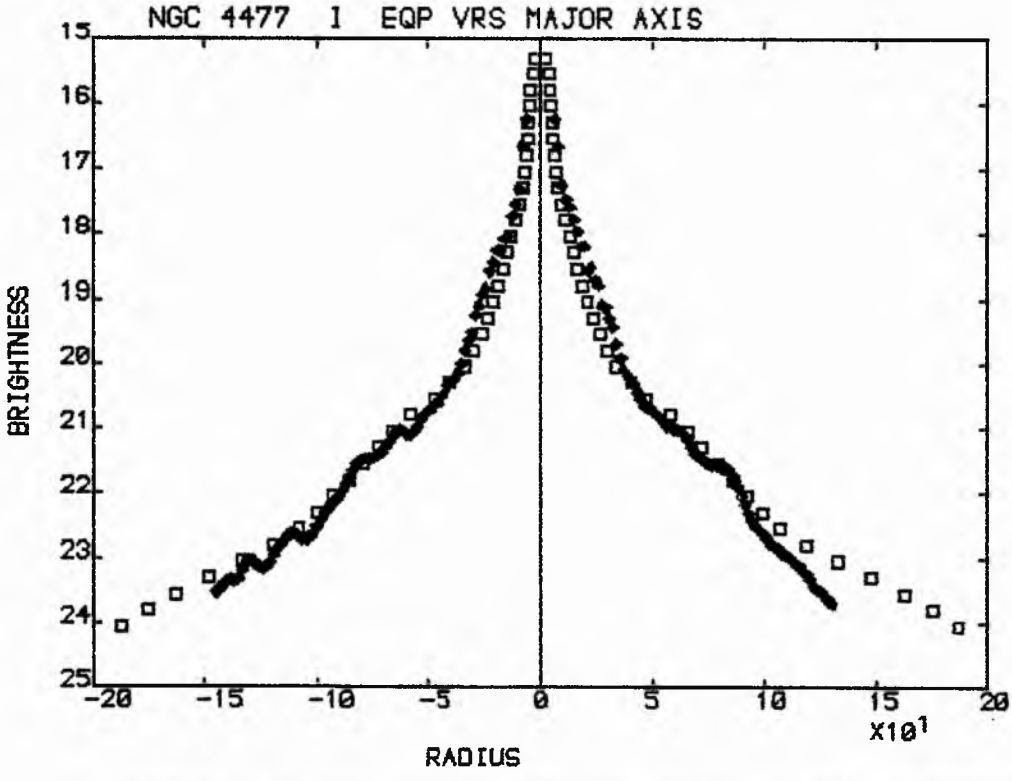
NGC 4477 I EQP VRS MAJOR AXIS
BRIGHTNESS
15
16
17
18
19
20
21
22
23
24
25
-20
-15
-10
-5
0
5
10
15
20
X10¹
RADIUS

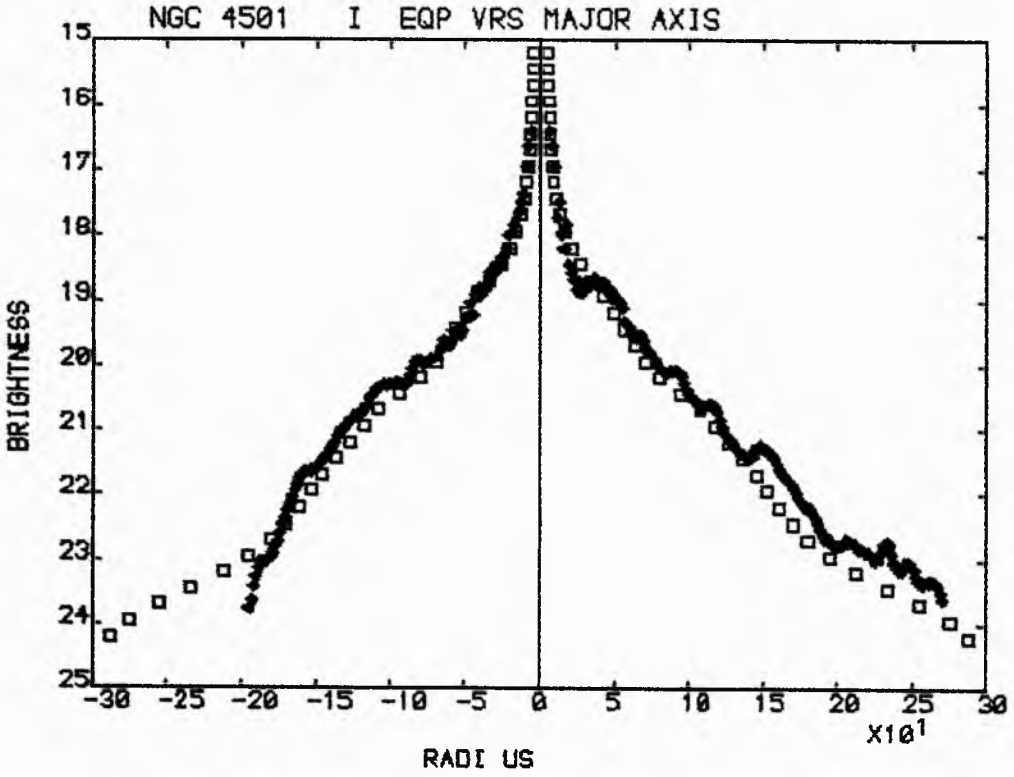
NGC 4501 I EQP VRS MAJOR AXIS
BRIGHTNESS
15
16
17
18
19
20
21
22
23
24
25
-30 -25 -20 -15 -10 -5 0 5 10 15 20 25 30
X10¹
RADI US

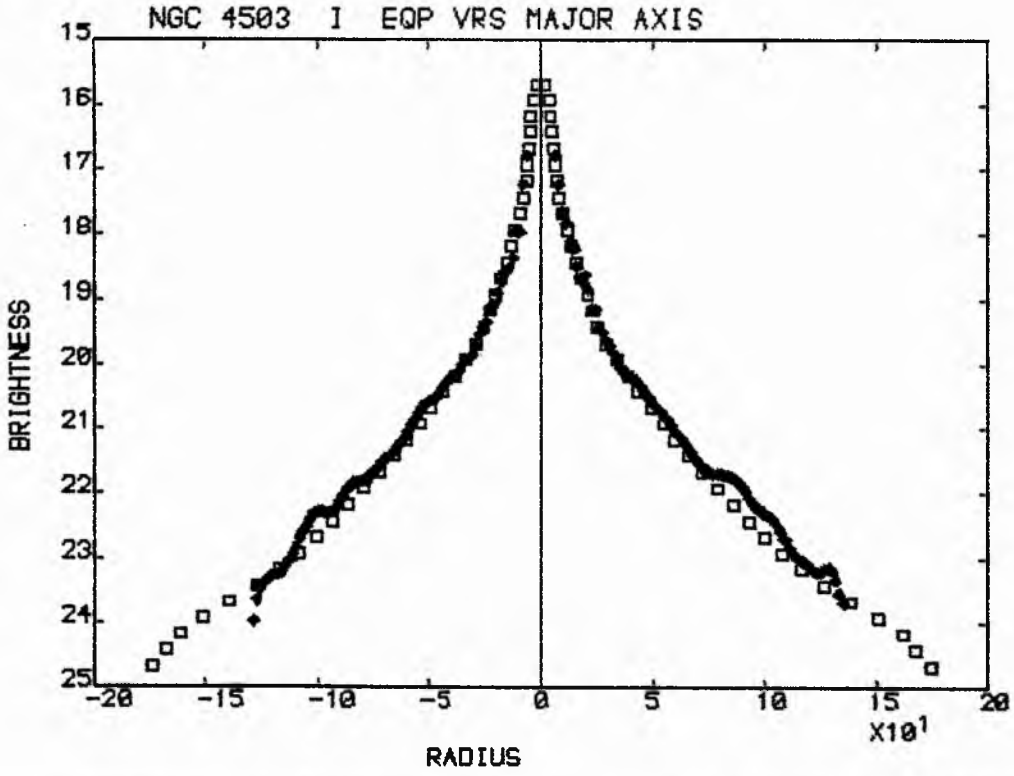
NGC 4503 I EQP VRS MAJOR AXIS
BRIGHTNESS
15
16
17
18
19
20
21
22
23
24
25
-20 -15 -10 -5 0 5 10 15 20
X10¹
RADIUS

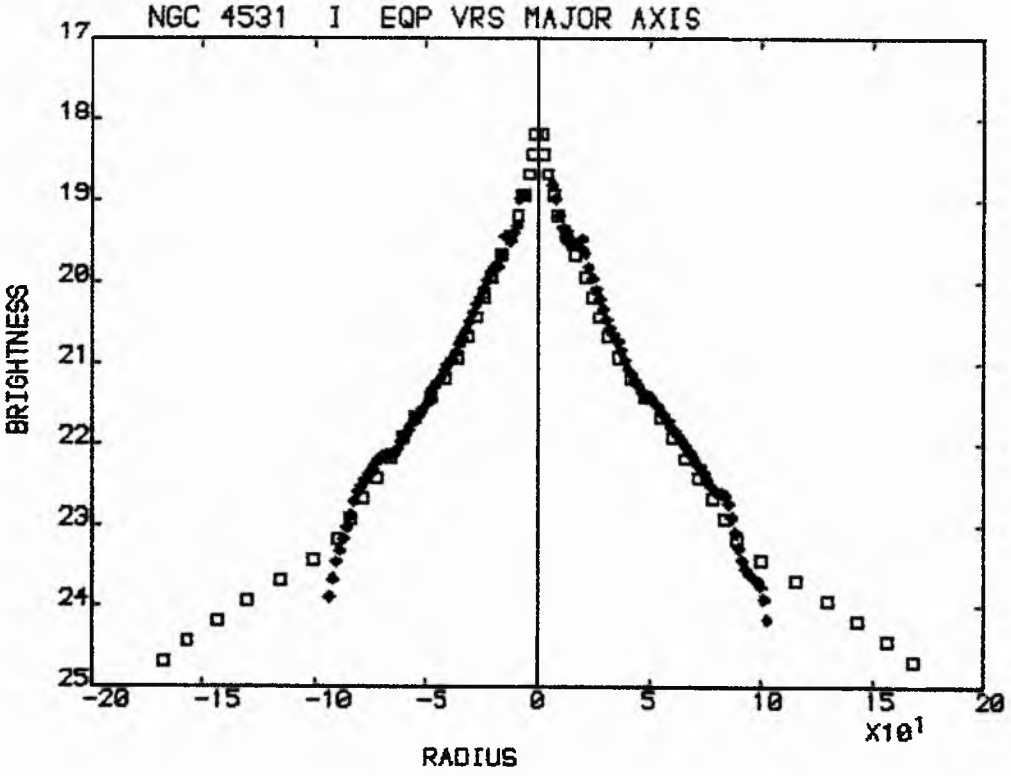
NGC 4531 I EQP VRS MAJOR AXIS
BRIGHTNESS
17
18
19
20
21
22
23
24
25
-20 -15 -10 -5 0 5 10 15 20
X10¹
RADIUS

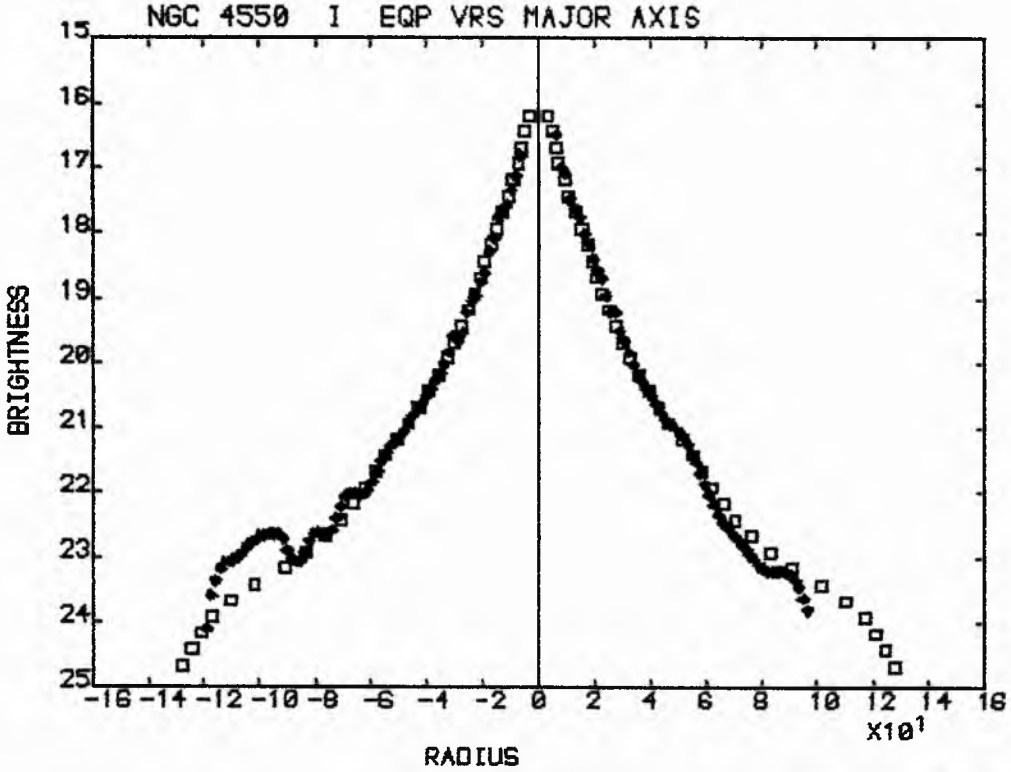
NGC 4550 I EQP VRS MAJOR AXIS
BRIGHTNESS
15
16
17
18
19
20
21
22
23
24
25
-16 -14 -12 -10 -8 -6 -4 -2 0 2 4 6 8 10 12 14 16
X10¹
RADIUS

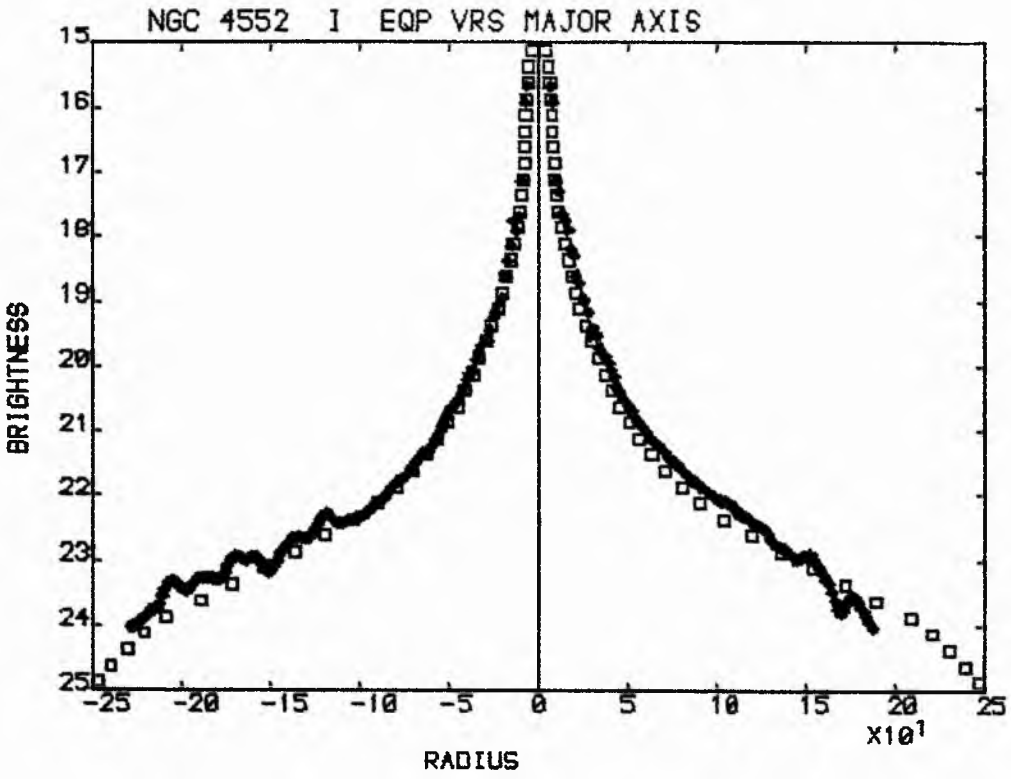
NGC 4552 I EQP VRS MAJOR AXIS
BRIGHTNESS
15
16
17
18
19
20
21
22
23
24
25
-25
-20
-15
-10
-5
0
5
10
15
20
25
X10¹
RADIUS

APPENDIX 'G'

Decomposition of B, R and I-Band Equivalent Profiles

NGC 4267 B

ITERATIVE FITTING.

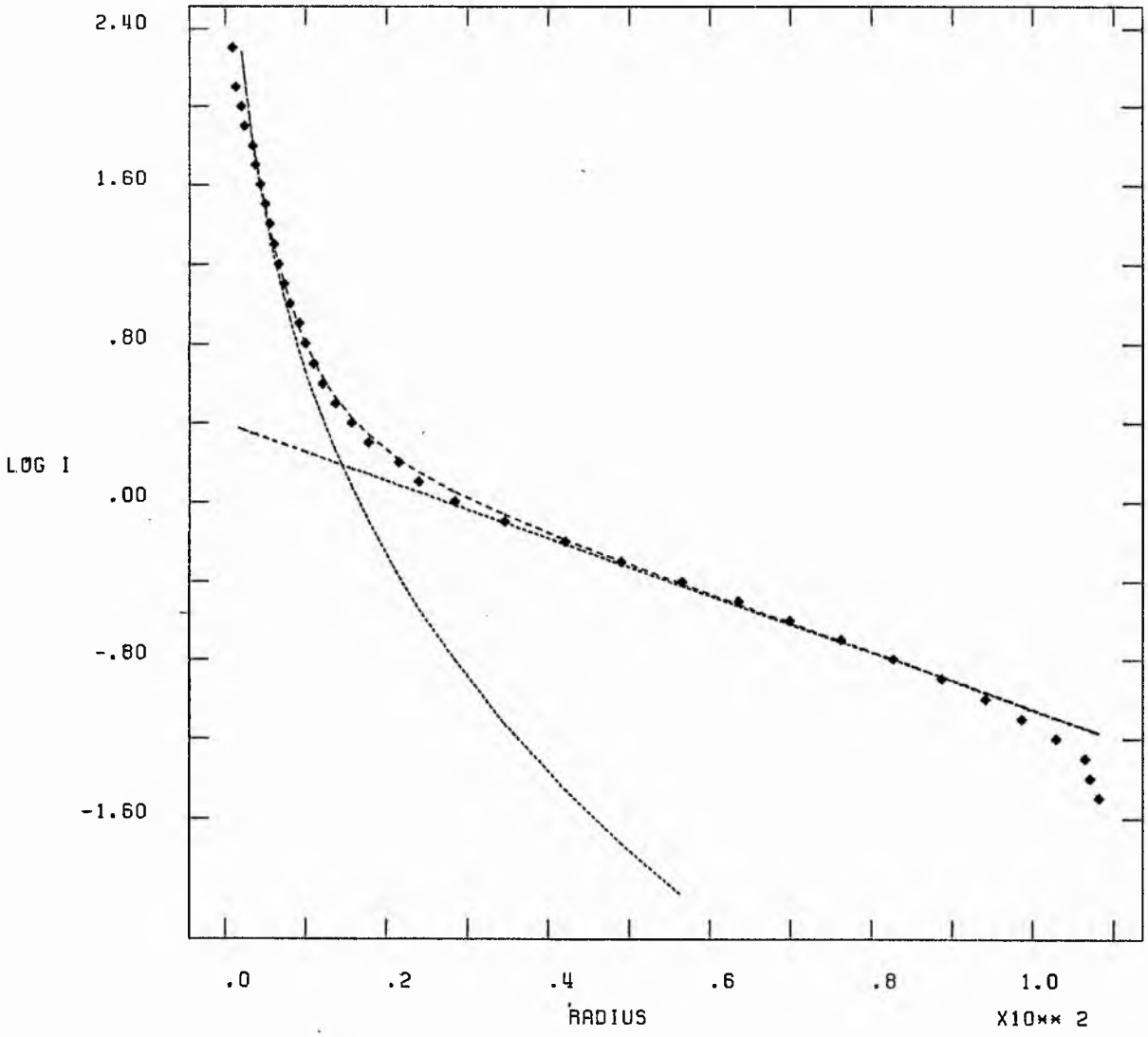

NGC 4267 B

SIMULTANEOUS LEAST SQUARES

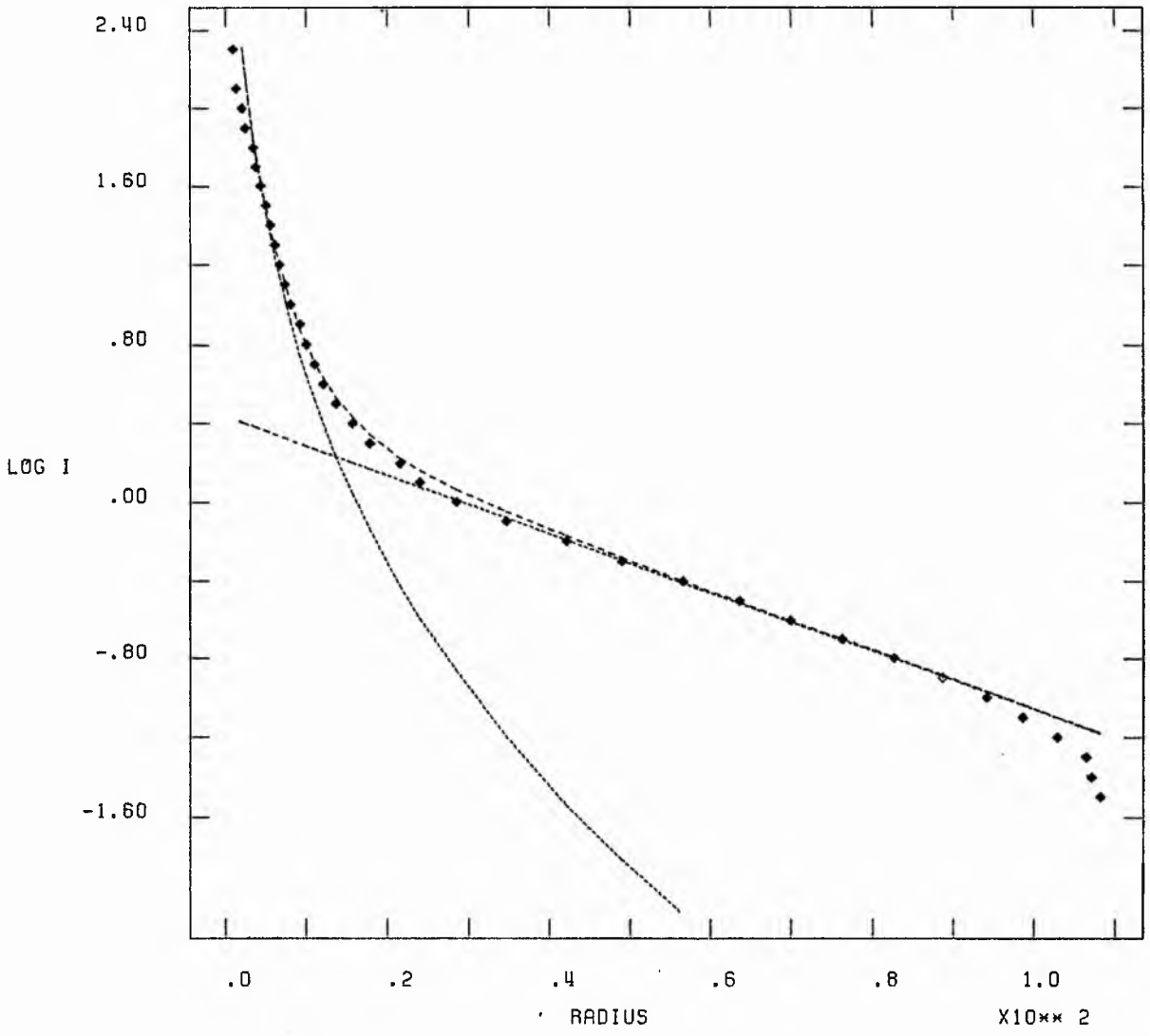

NGC 4371 B

ITERATIVE FITTING.

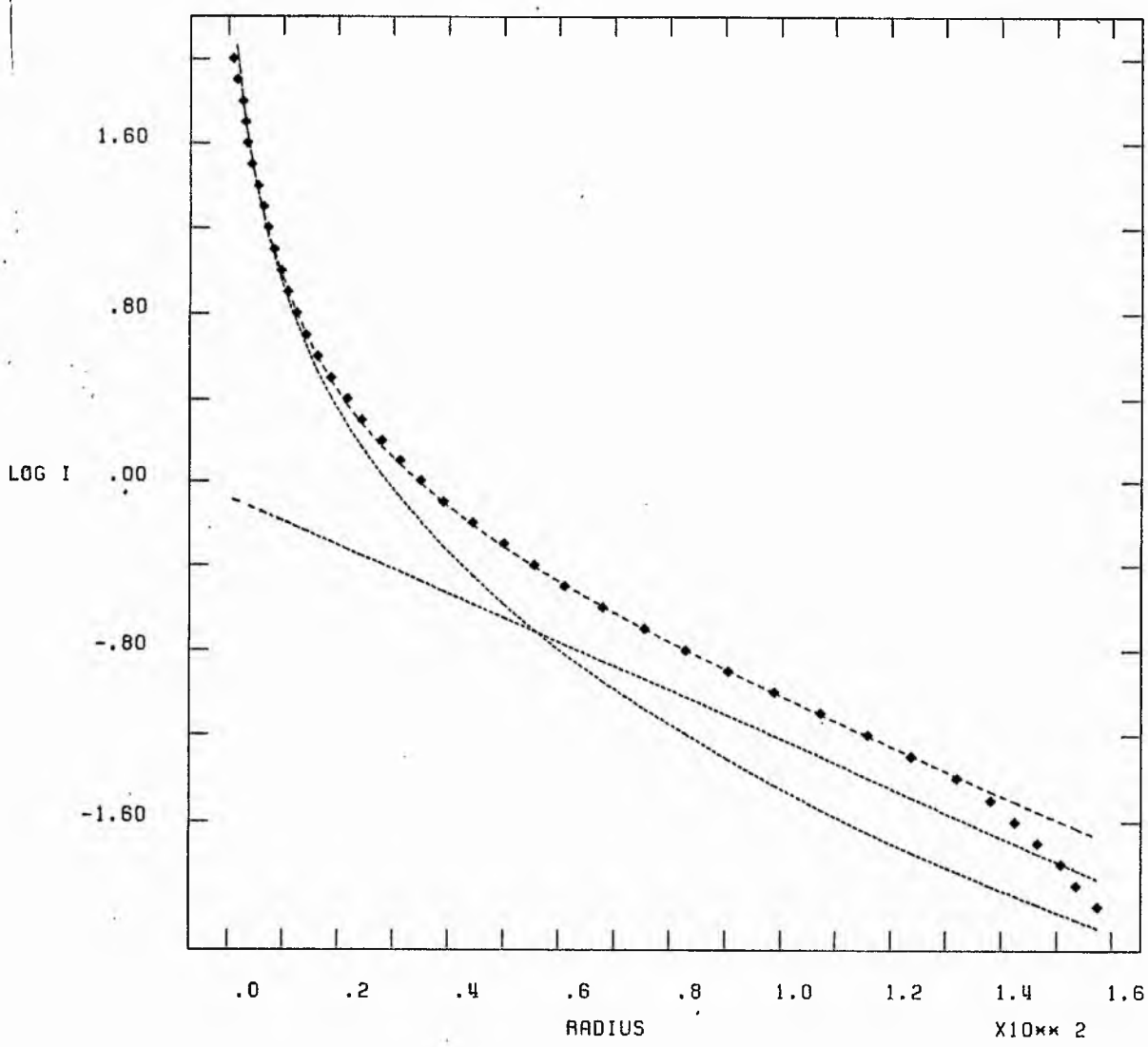

NGC 4371 B

SIMULTANEOUS LEAST SQUARES

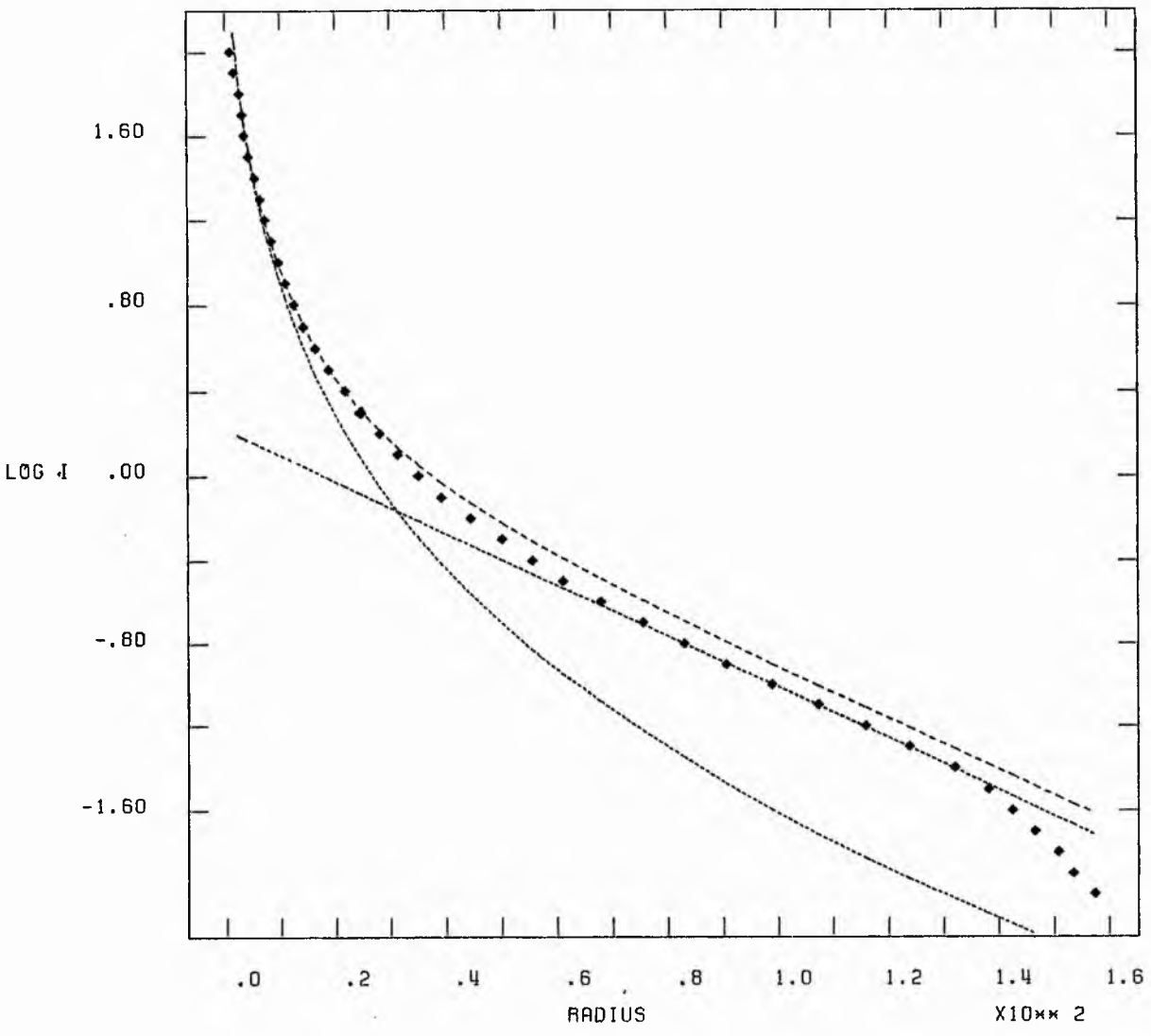

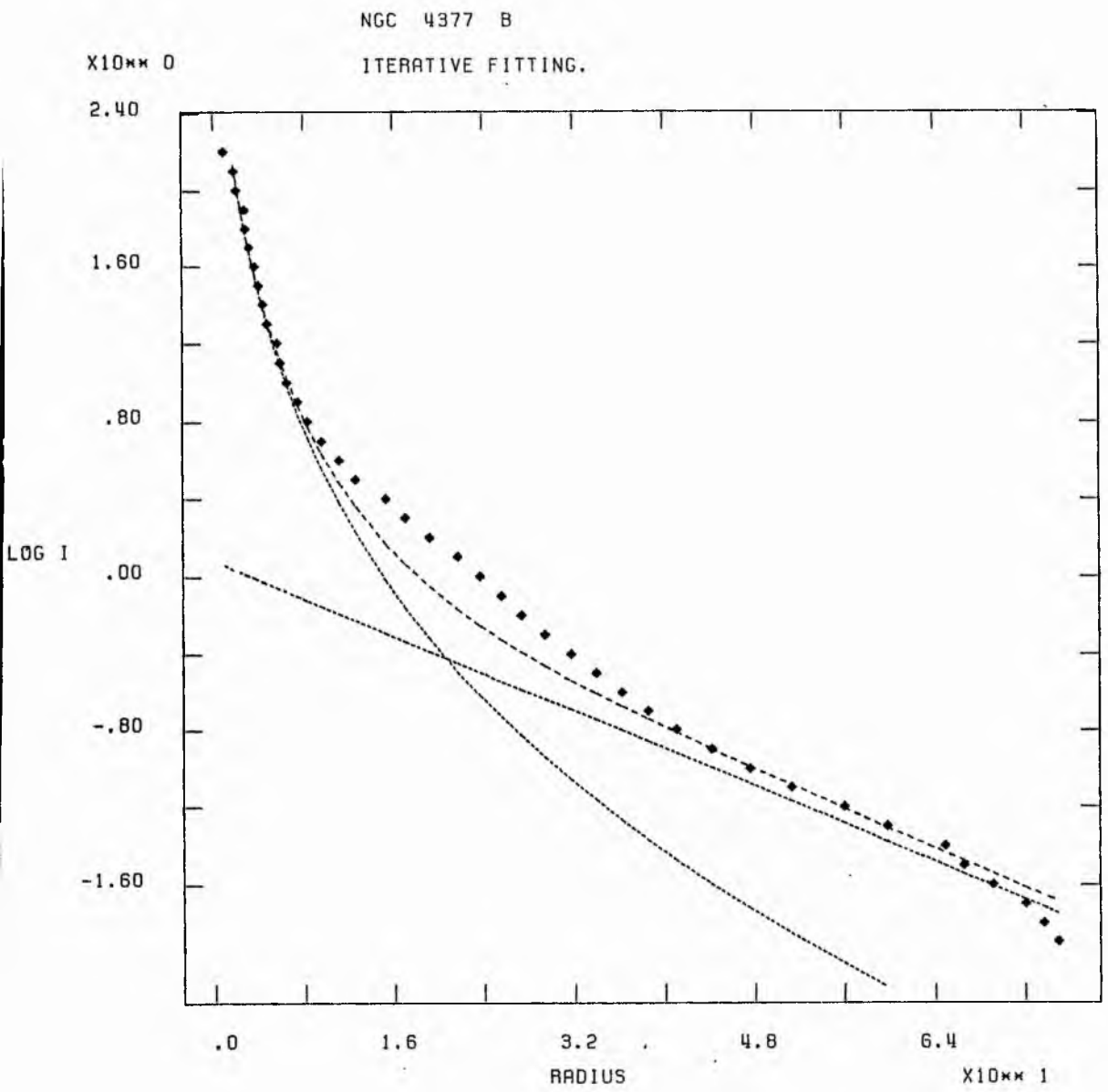
NGC 4377 B
ITERATIVE FITTING.
X10** 0
2.40
1.60
.80
LOG I
.00
-.80
-1.60
.0
1.6
3.2
4.8
6.4
RADIUS
X10** 1

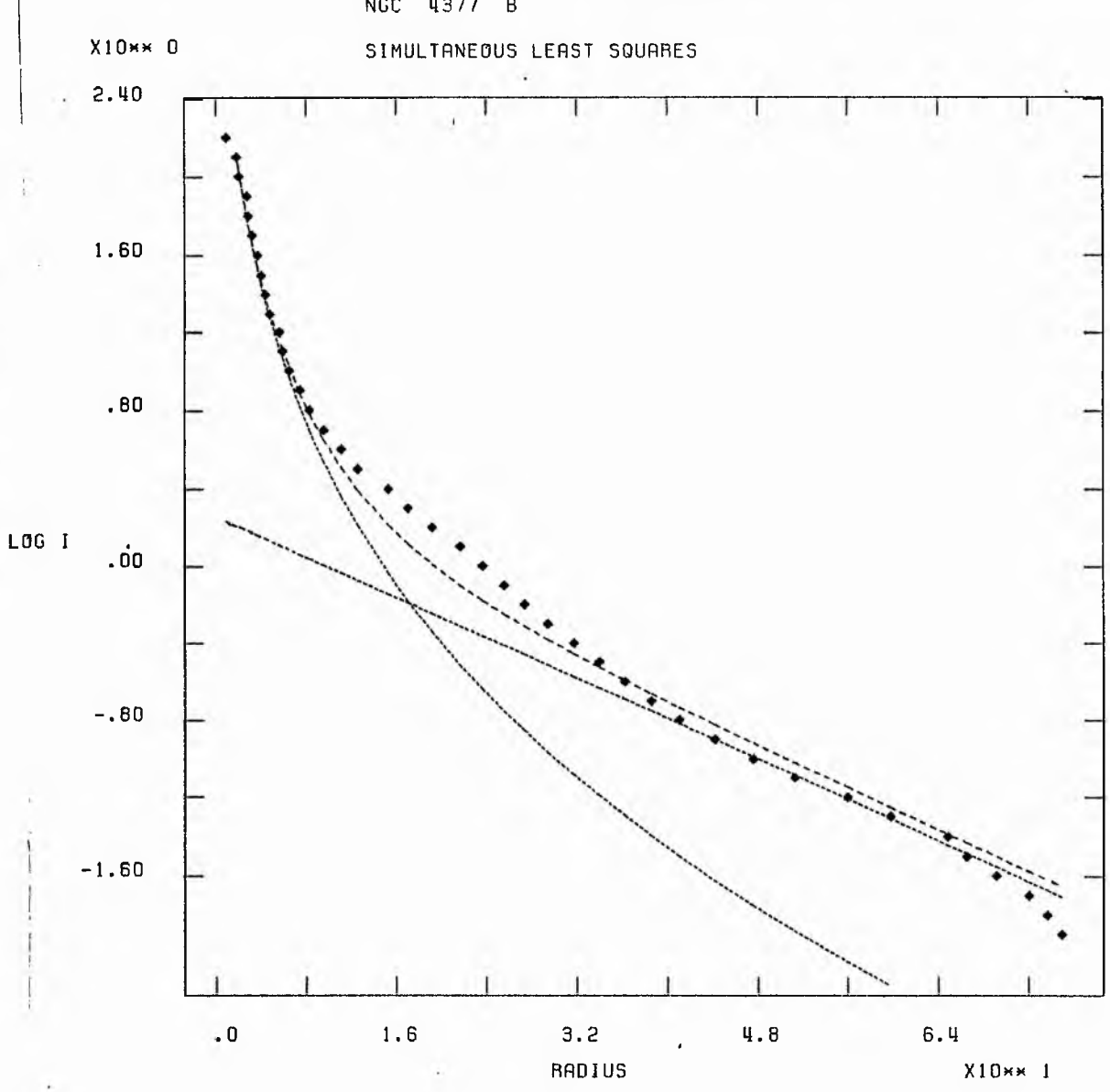
NGC 4377 B
SIMULTANEOUS LEAST SQUARES
X10** 0
2.40
1.60
.80
.00
-.80
-1.60
LOG I
.0
1.6
3.2
4.8
6.4
RADIUS
X10** 1

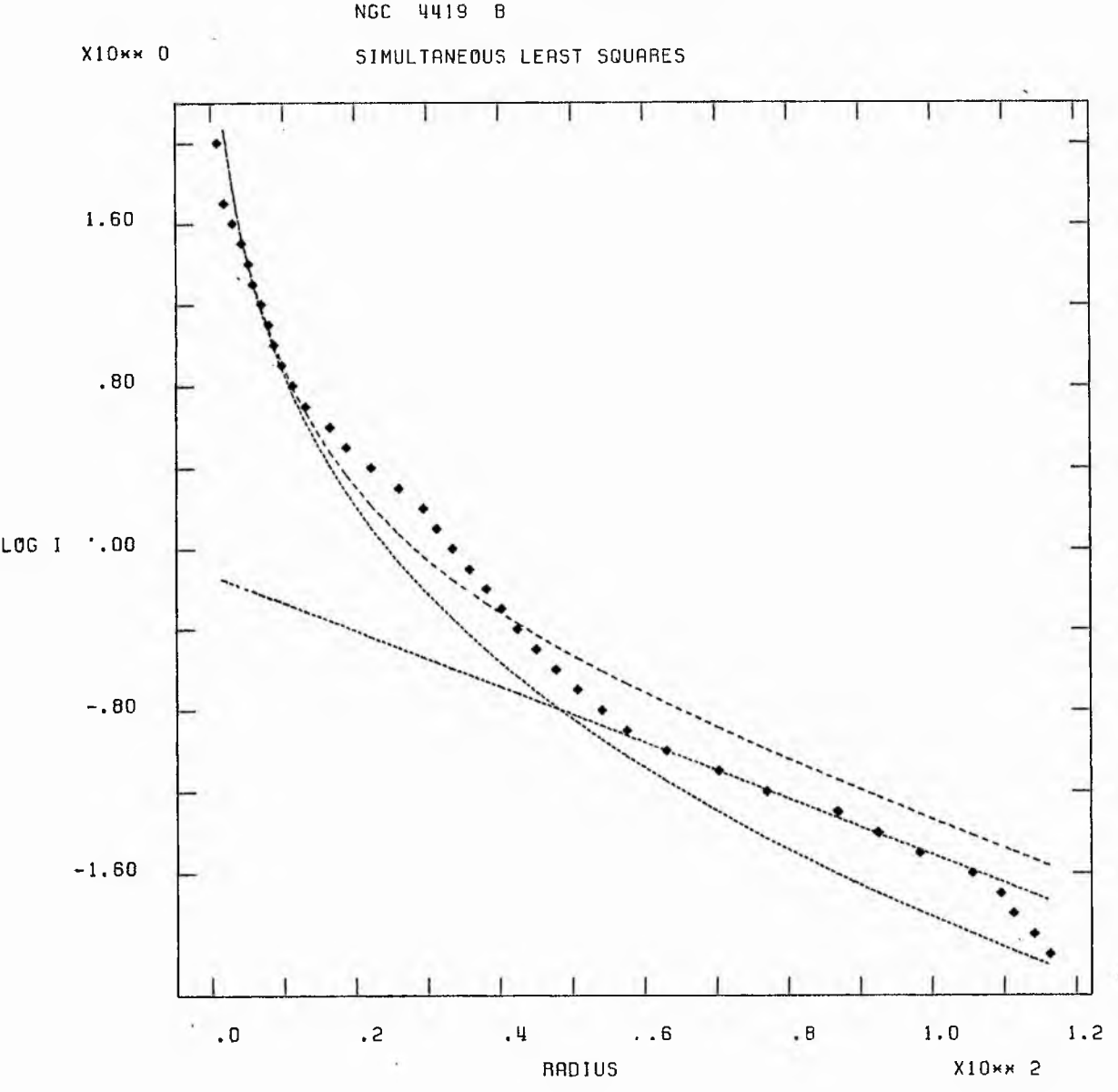
NGC 4419 B
SIMULTANEOUS LEAST SQUARES
X10** 0
1.60
.80
LOG I .00
-.80
-1.60
.0
.2
.4
..6
.8
1.0
1.2
RADIUS
X10** 2

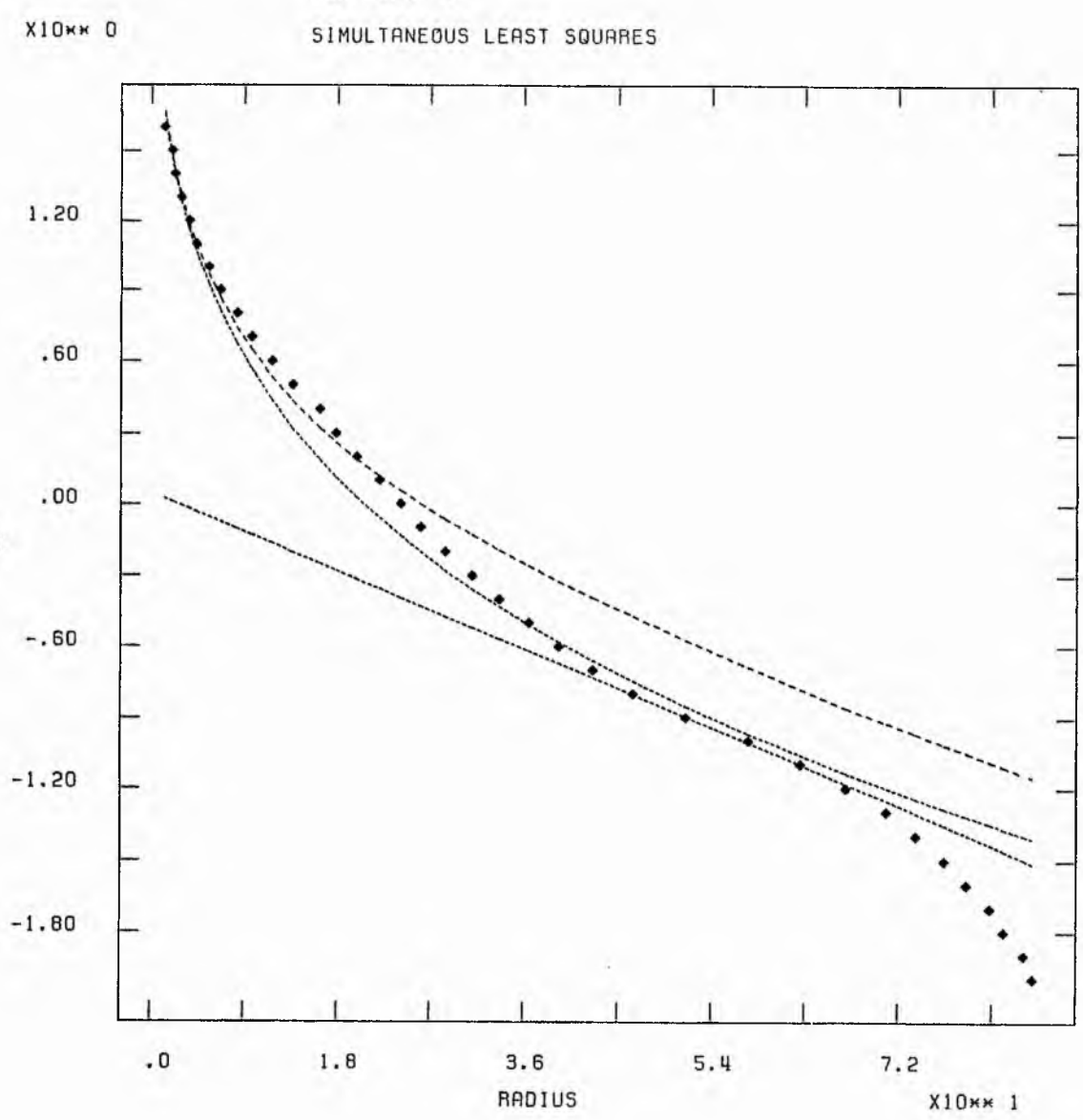
NGC 4425 B
SIMULTANEOUS LEAST SQUARES
X10** 0
1.20
.60
.00
LOG I
-.60
-1.20
-1.80
.0
1.8
3.6
5.4
7.2
RADIUS
X10** 1

NGC 4429 B

ITERATIVE FITTING.

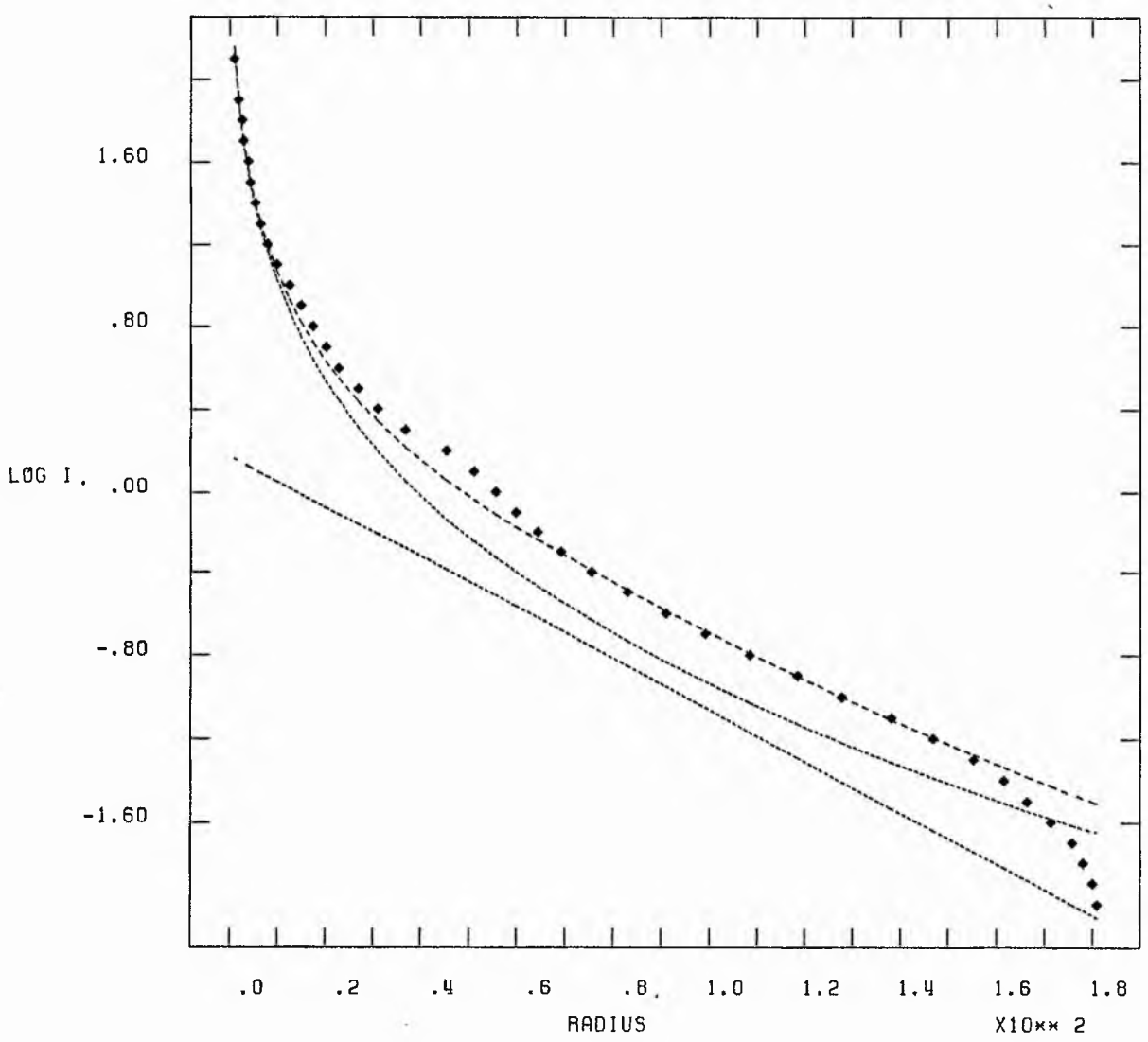

NGC 4429 B

SIMULTANEOUS LEAST SQUARES

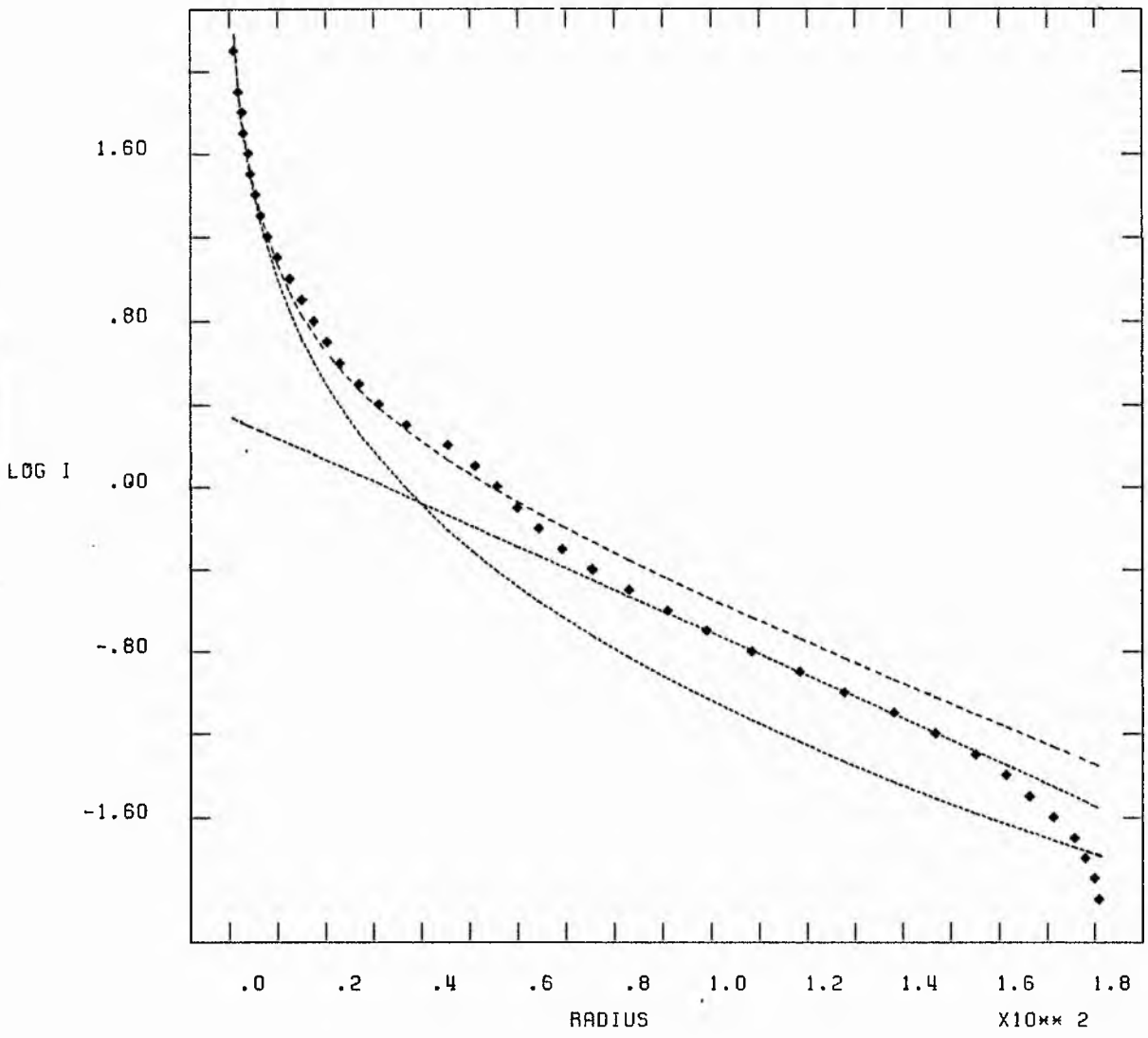

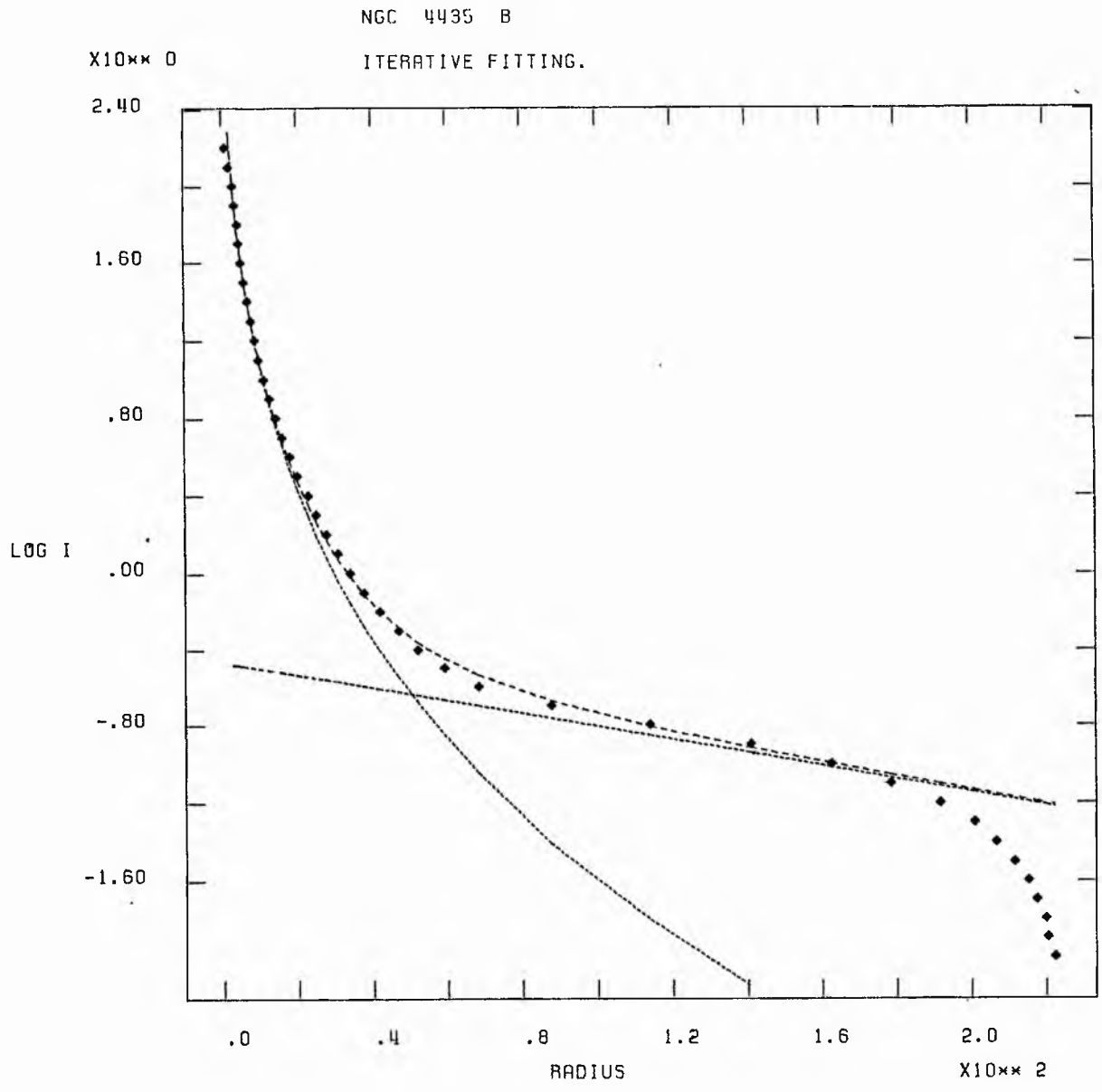
NGC 4435 B
ITERATIVE FITTING.
X10** 0
2.40
1.60
.80
.00
-.80
-1.60
LOG I
.0
.4
.8
1.2
1.6
2.0
RADIUS
X10** 2

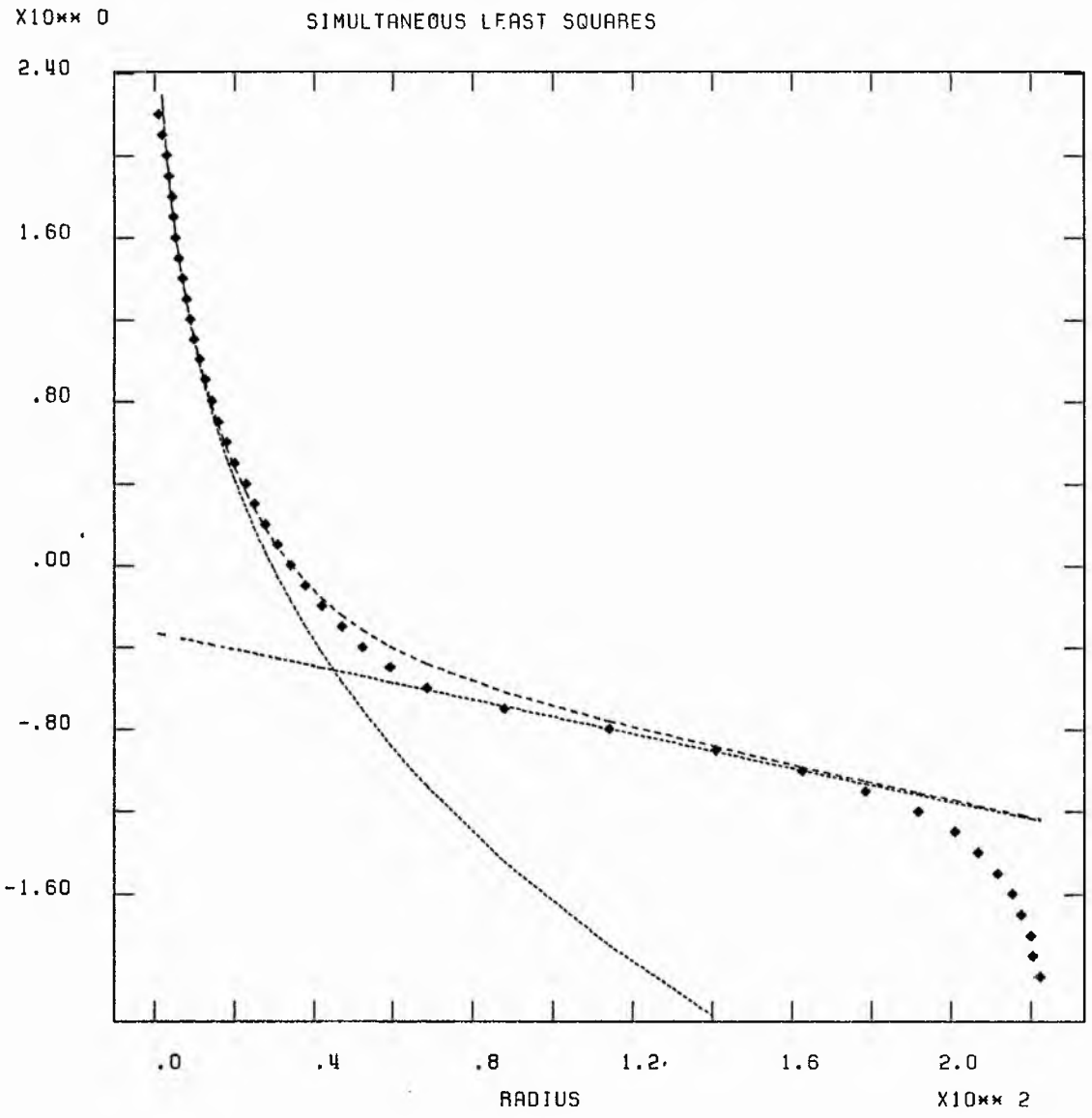
NGC 4435 B
SIMULTANEOUS LEAST SQUARES
X10** 0
2.40
1.60
.80
.00
-.80
-1.60
LOG I
.0
.4
.8
1.2
1.6
2.0
RADIUS
X10** 2

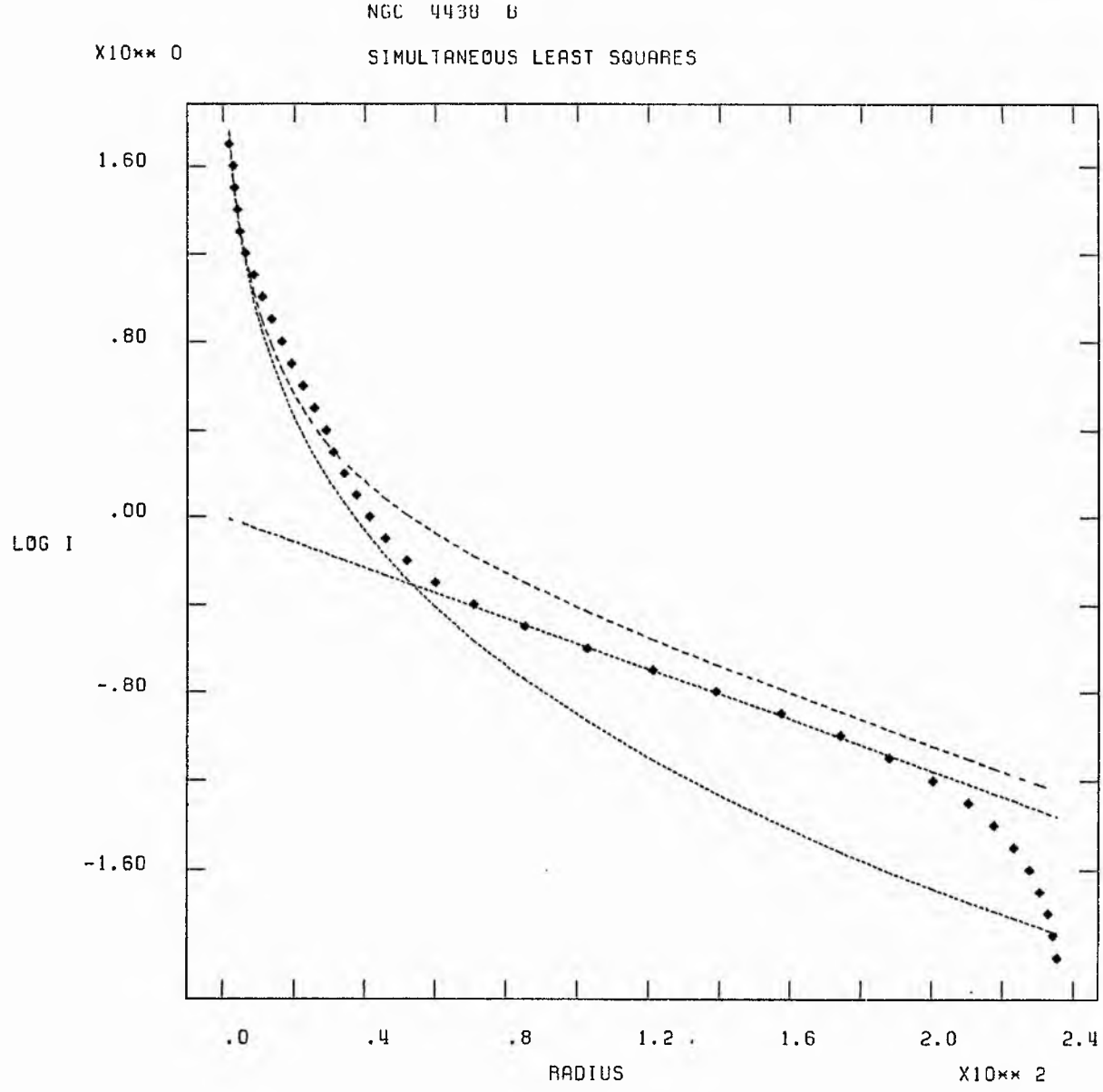
NGC 4438 B
X10** 0
SIMULTANEOUS LEAST SQUARES
1.60
.80
.00
-.80
-1.60
LOG I
.0
.4
.8
1.2
1.6
2.0
2.4
RADIUS
X10** 2

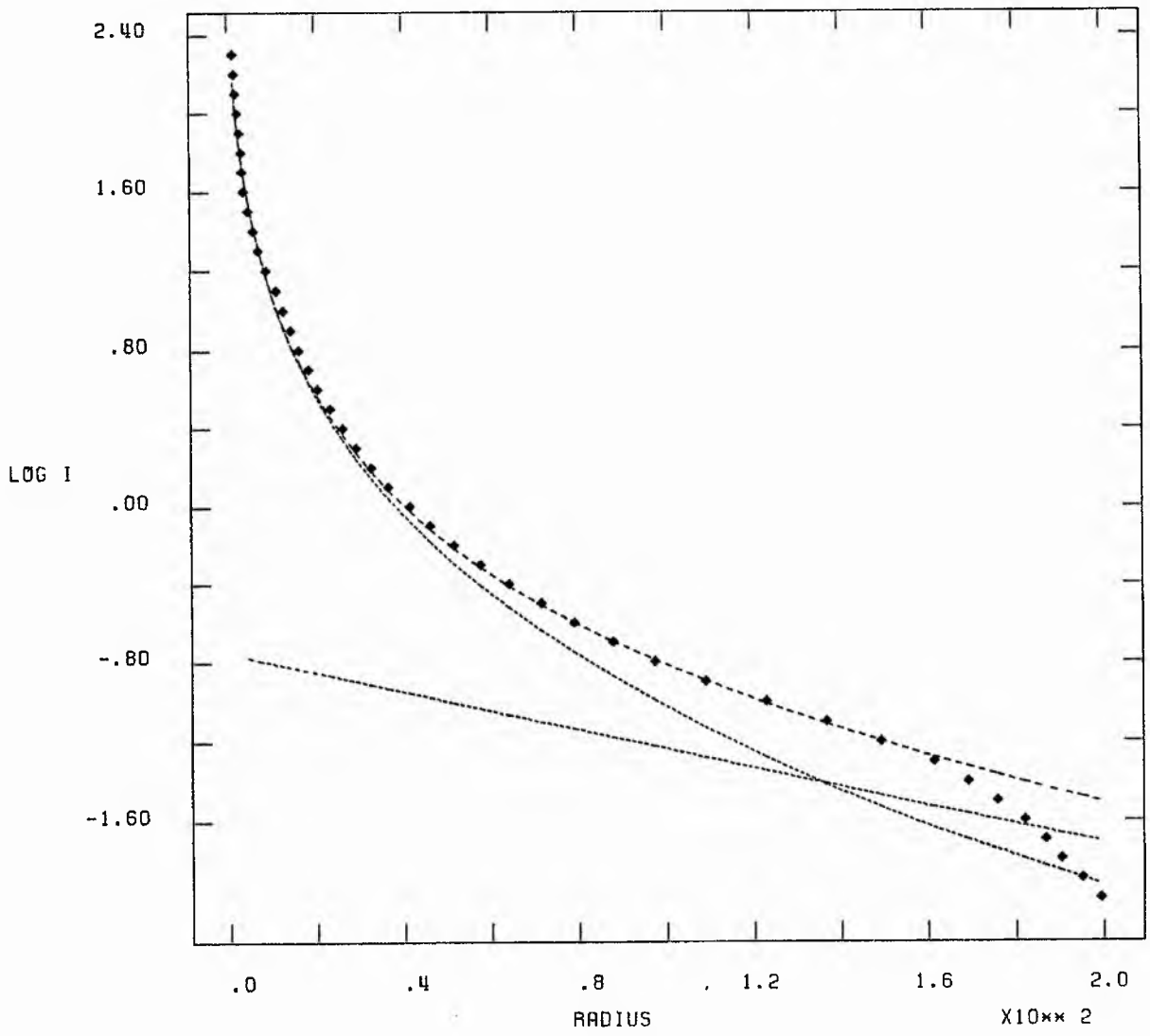
NGC 4459 8
ITERATIVE FITTING.
X10** 0
2.40
1.60
.80
.00
-.80
-1.60
LOG I
.0
.4
.8
1.2
1.6
2.0
RADIUS
X10** 2

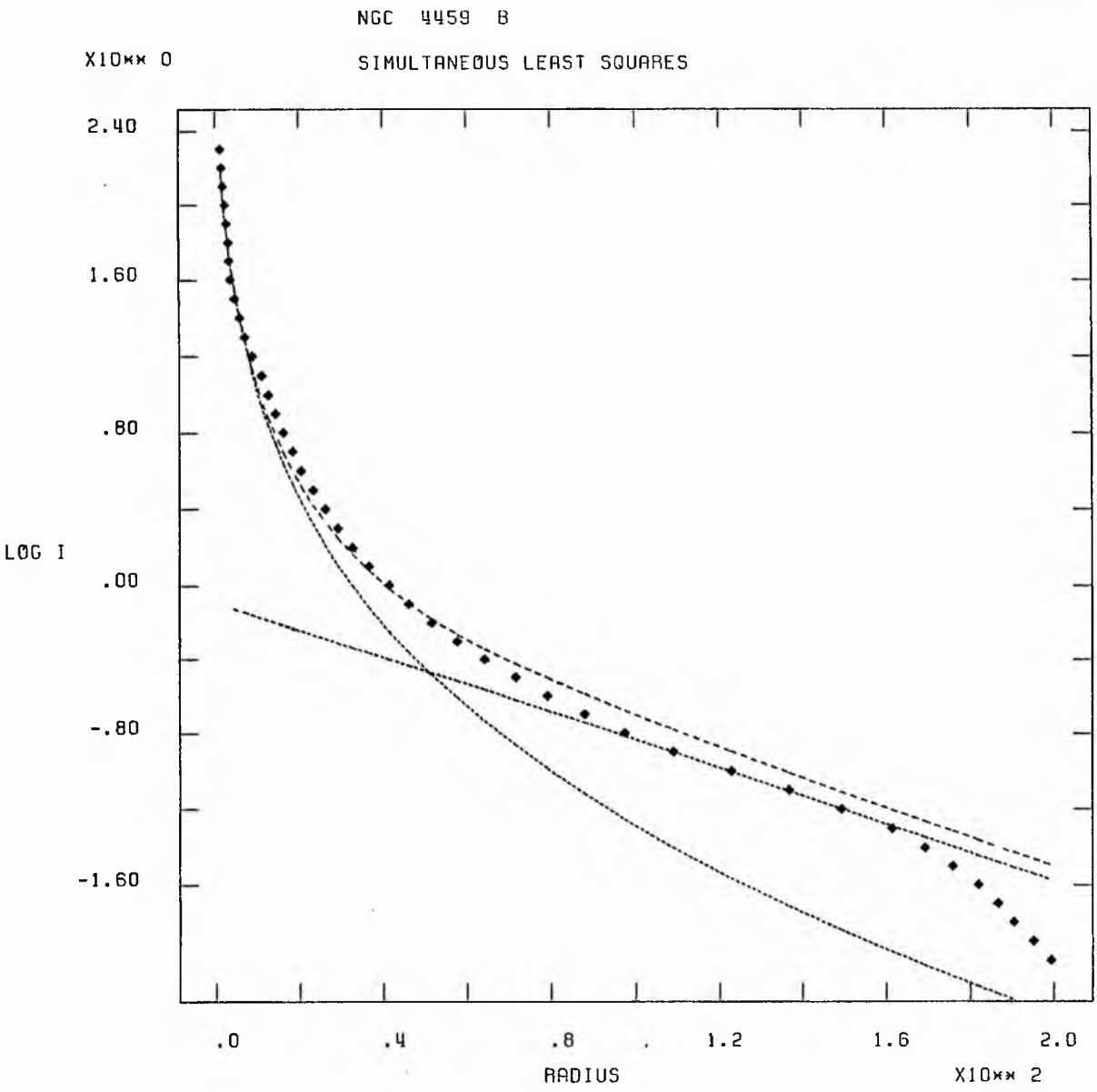
NGC 4459 B
SIMULTANEOUS LEAST SQUARES
X10** 0
2.40
1.60
.80
.00
-.80
-1.60
LOG I
.0
.4
.8
1.2
1.6
2.0
RADIUS
X10** 2

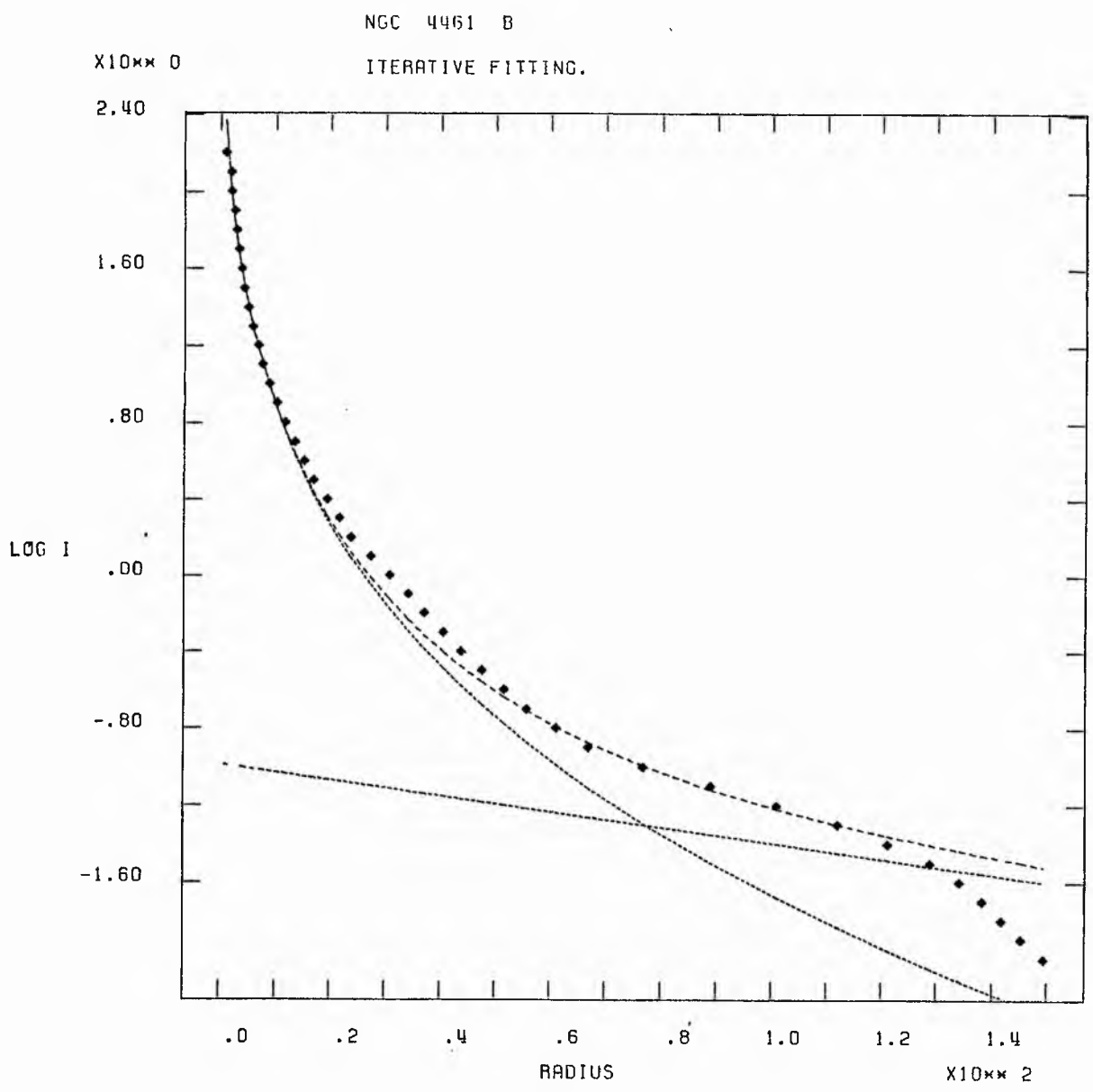
NGC 4461 B
ITERATIVE FITTING.
X10** 0
2.40
1.60
.80
.00
-.80
-1.60
LOG I
.0
.2
.4
.6
.8
1.0
1.2
1.4
RADIUS
X10** 2

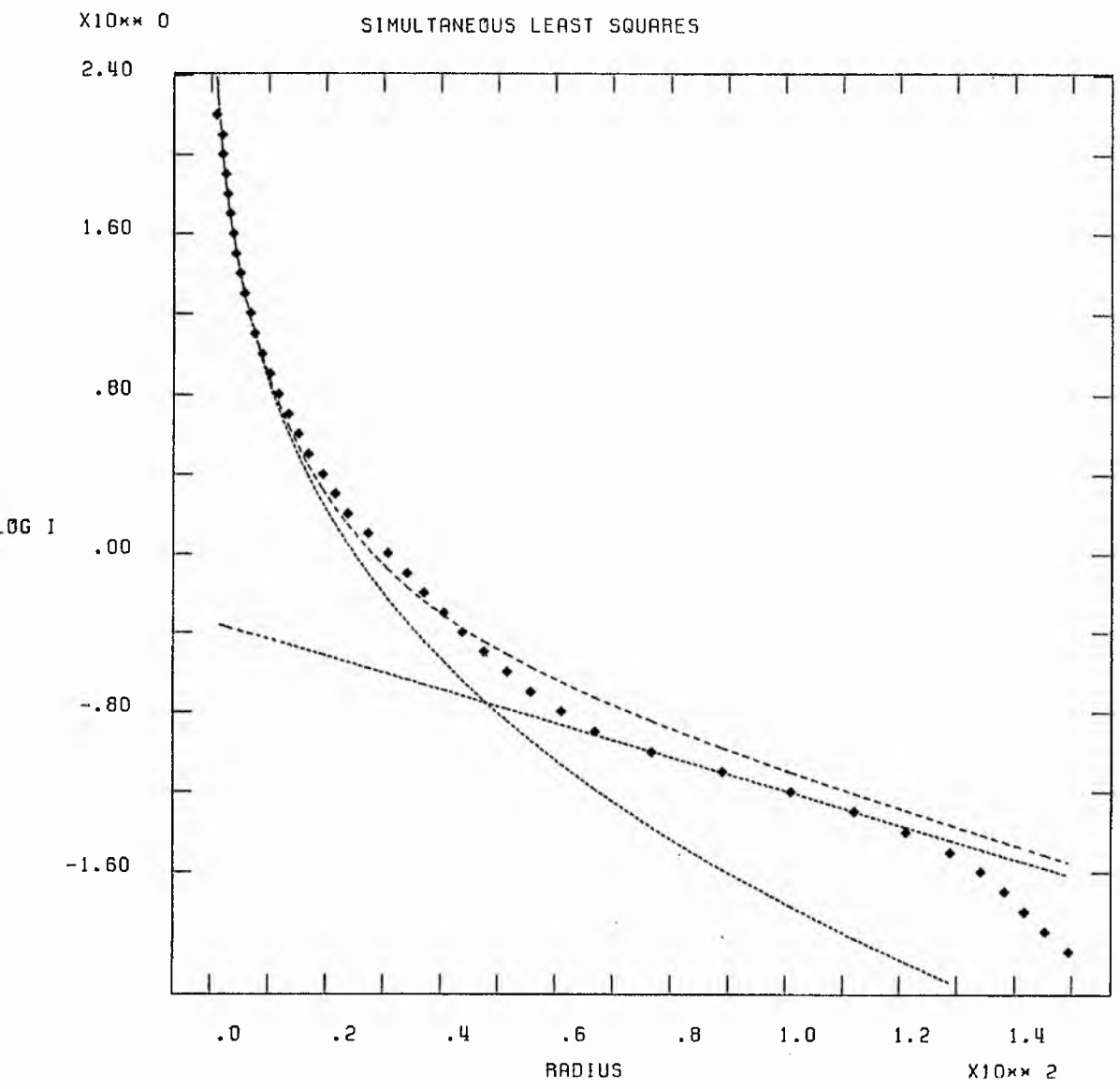
NGC 4461 B
SIMULTANEOUS LEAST SQUARES
X10×× 0
2.40
1.60
.80
.00
-.80
-1.60
LOG I
.0
.2
.4
.6
.8
1.0
1.2
1.4
RADIUS
X10×× 2

NGC 4474 B

X10** 0 ITERATIVE FITTING.

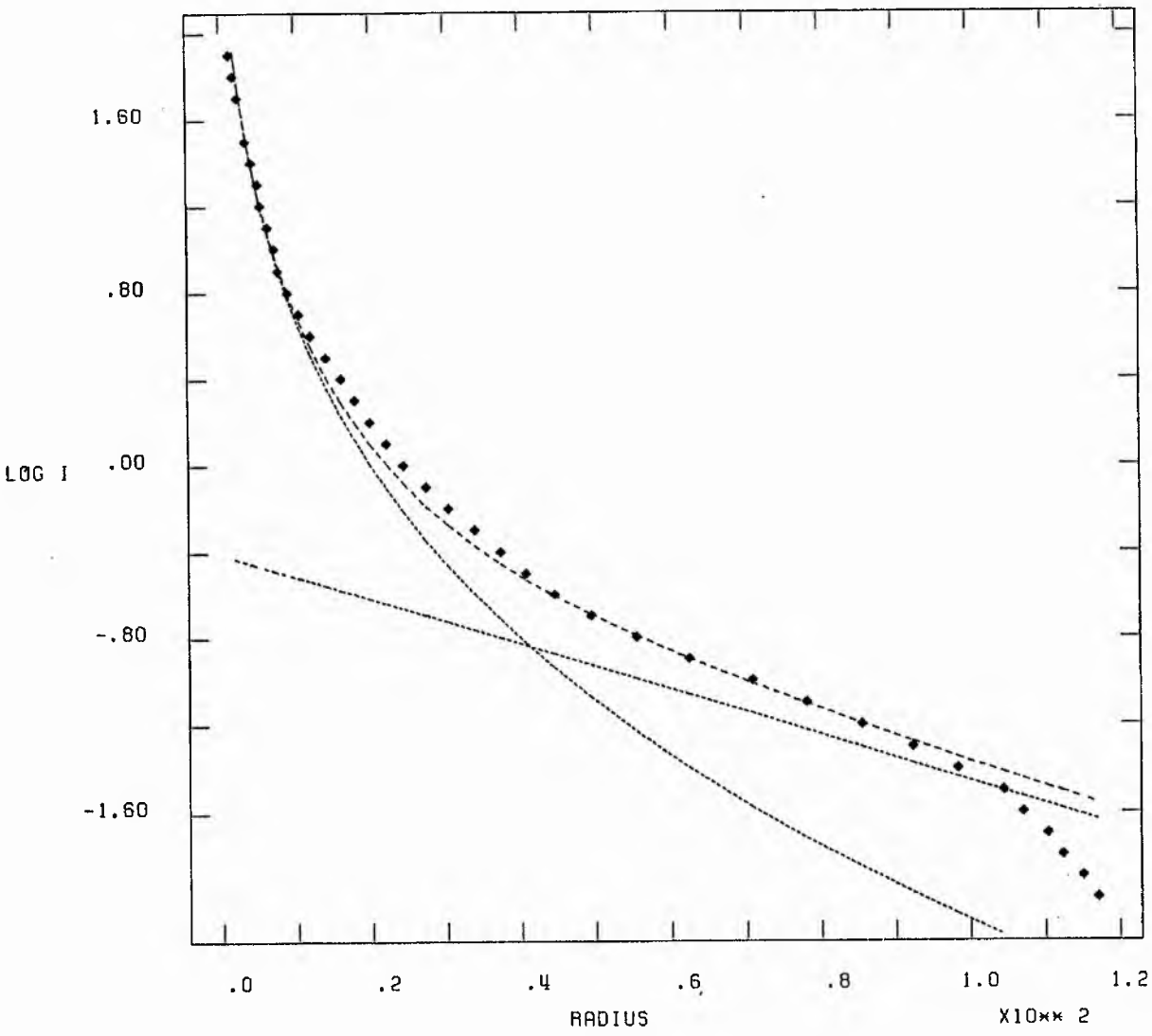

NGC 4474 B

X10** 0

SIMULTANEOUS LEAST SQUARES

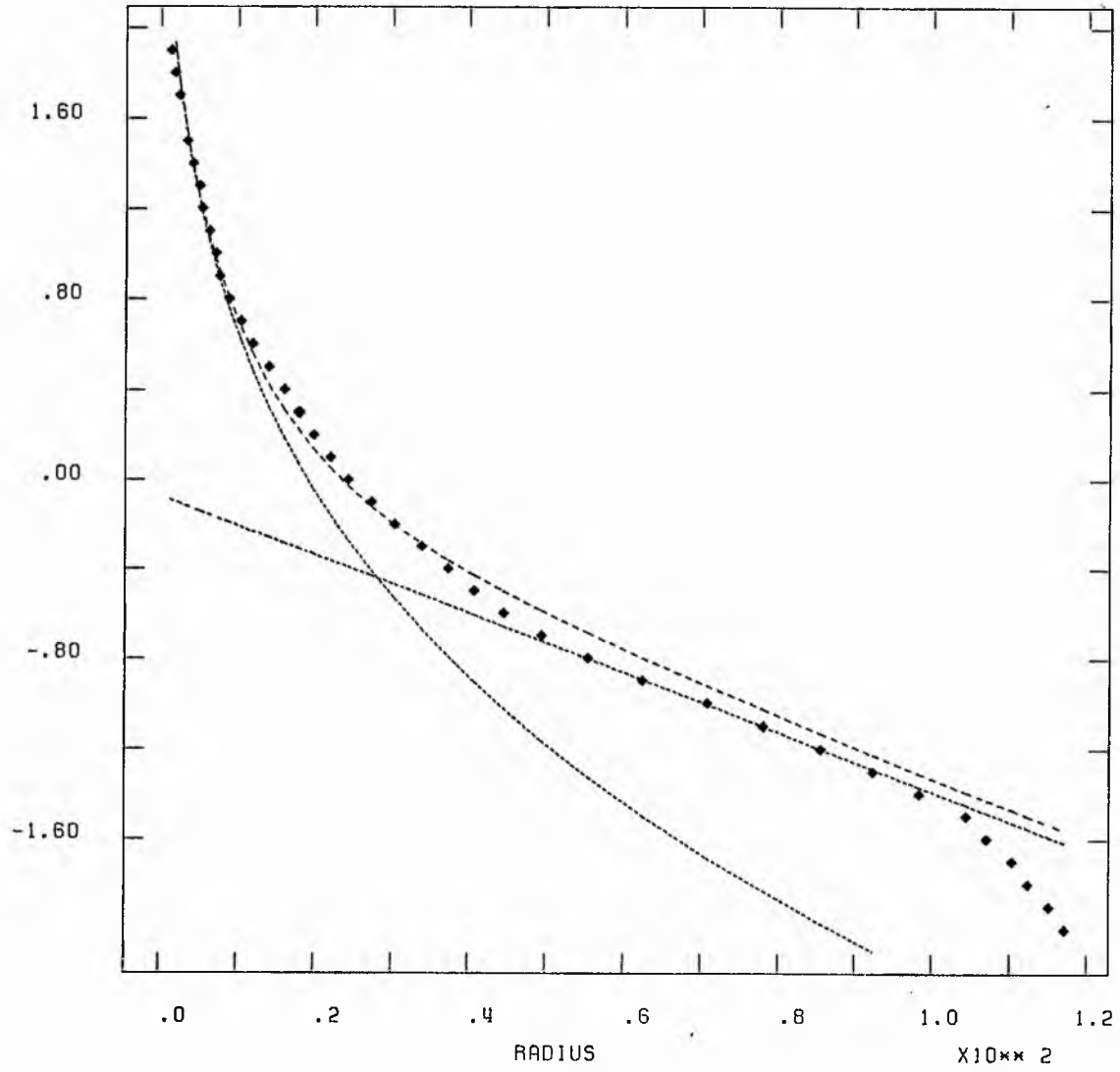

NGC 4477 B

X10** 0

ITERATIVE FITTING.

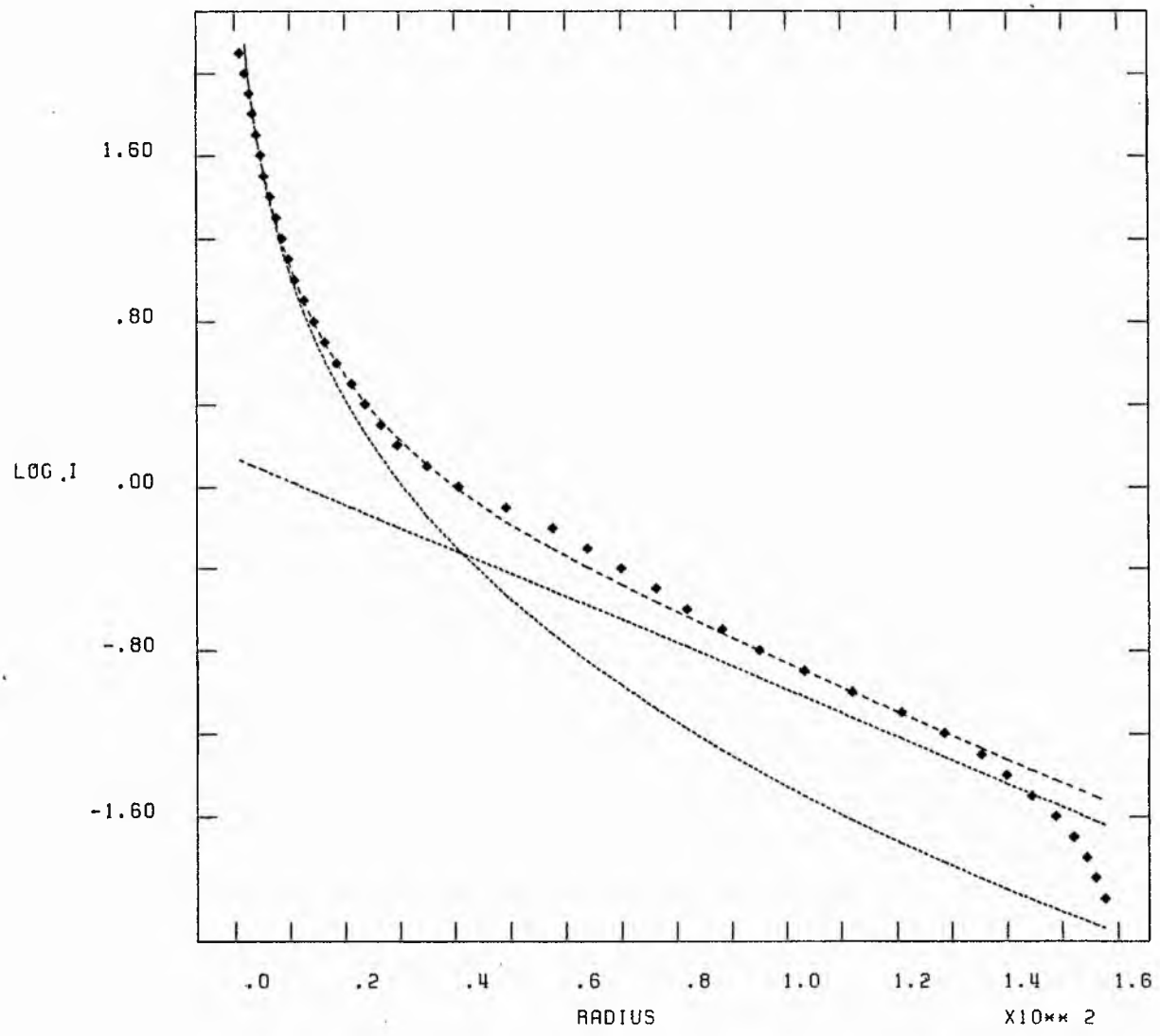

NGC 4477 B

SIMULTANEOUS LEAST SQUARES

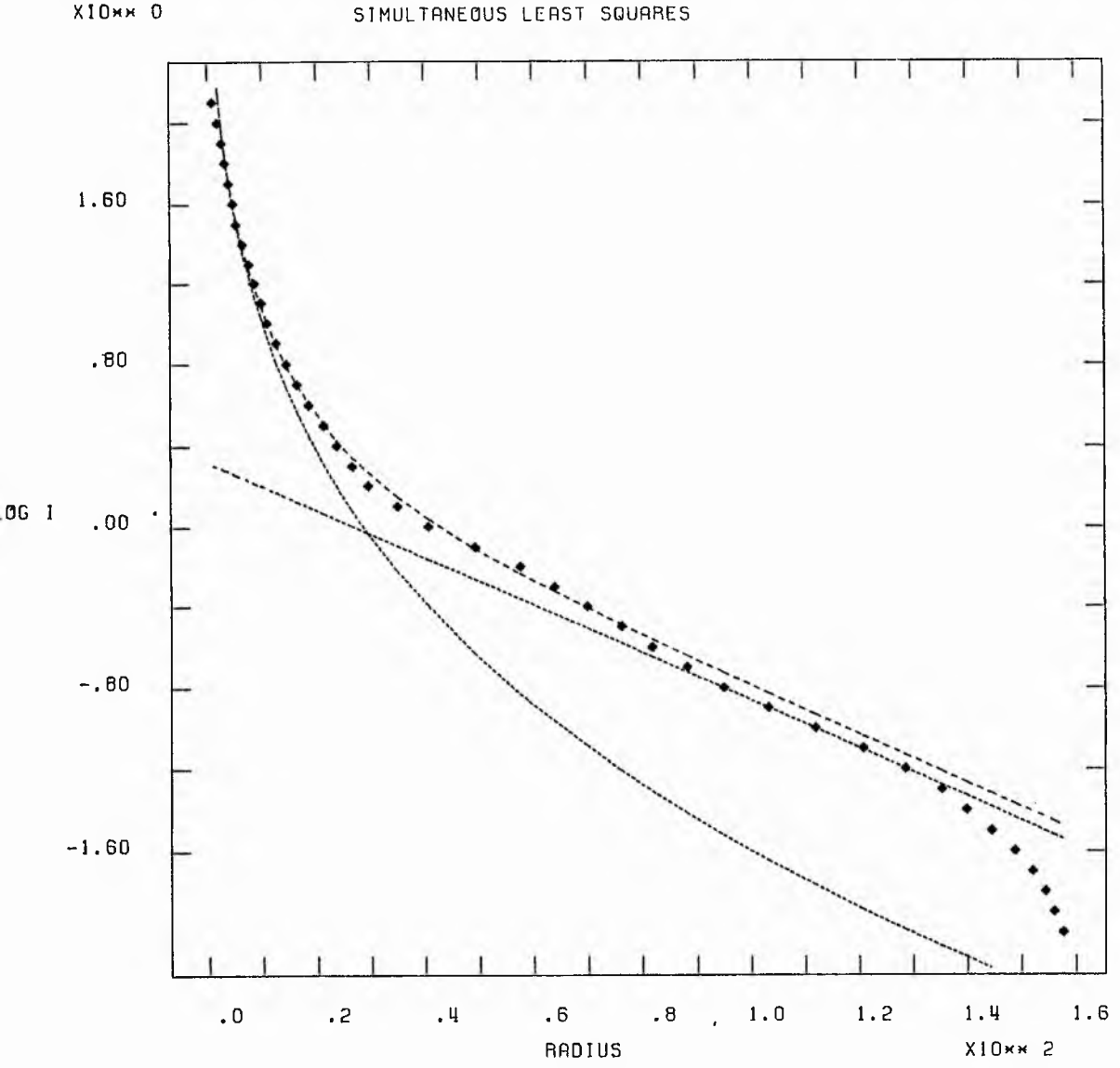

NGC 4501 B

SIMULTANEOUS LEAST SQUARES

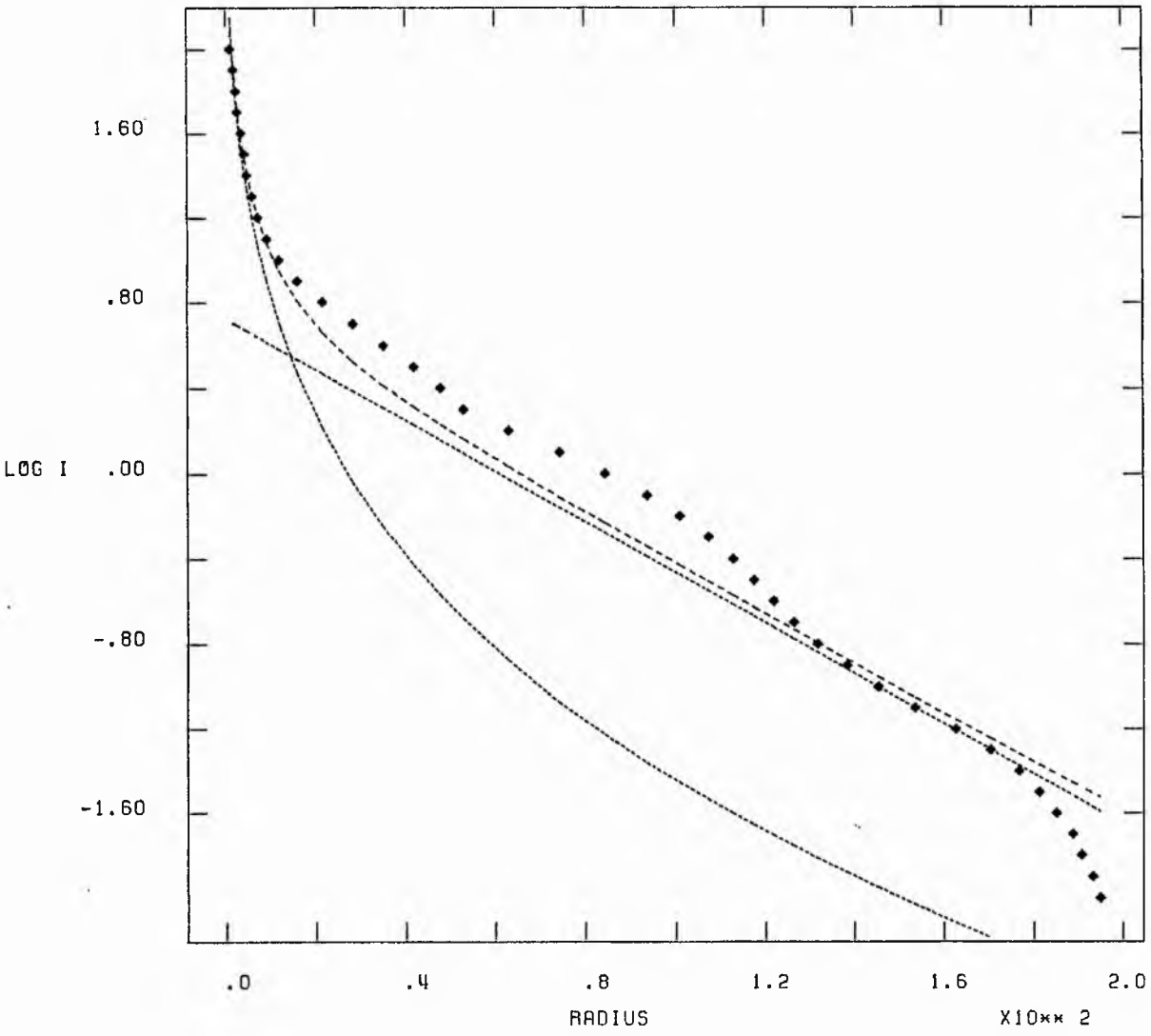

NGC 4503 B

ITERATIVE FITTING.

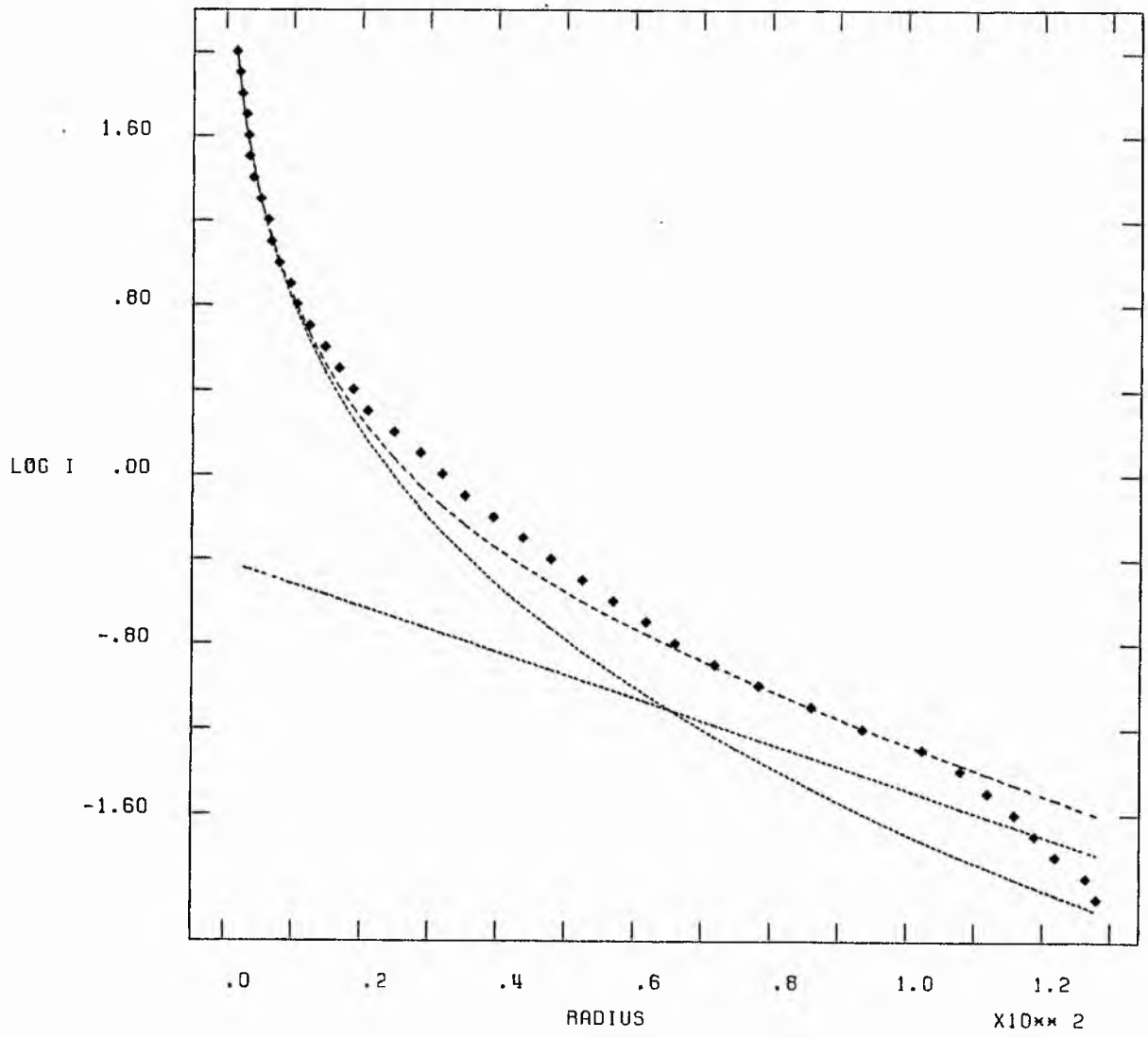

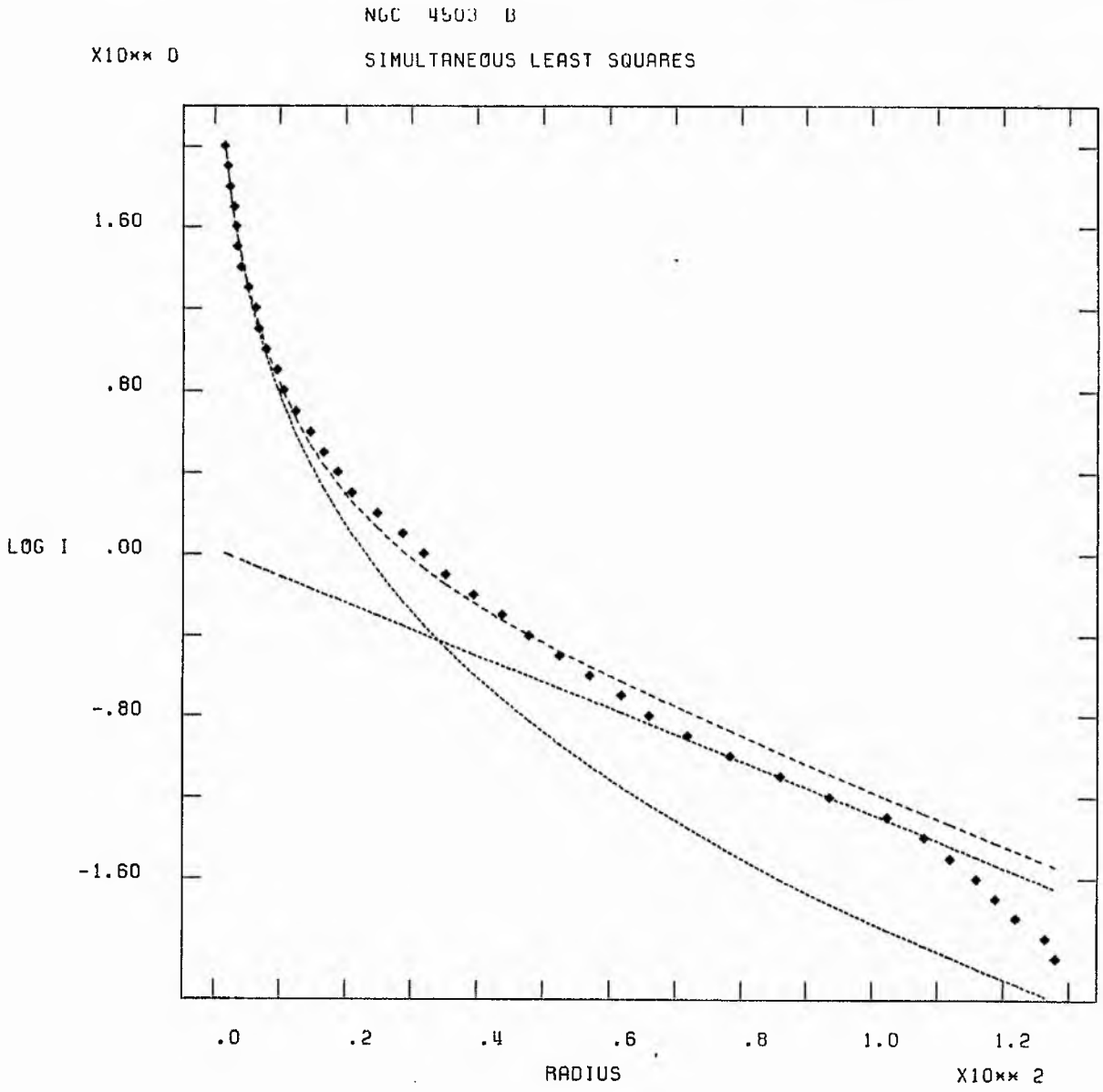
NGC 4503 B
X10** 0
SIMULTANEOUS LEAST SQUARES
1.60
.80
LOG I .00
-.80
-1.60
.0
.2
.4
.6
.8
1.0
1.2
RADIUS
X10** 2

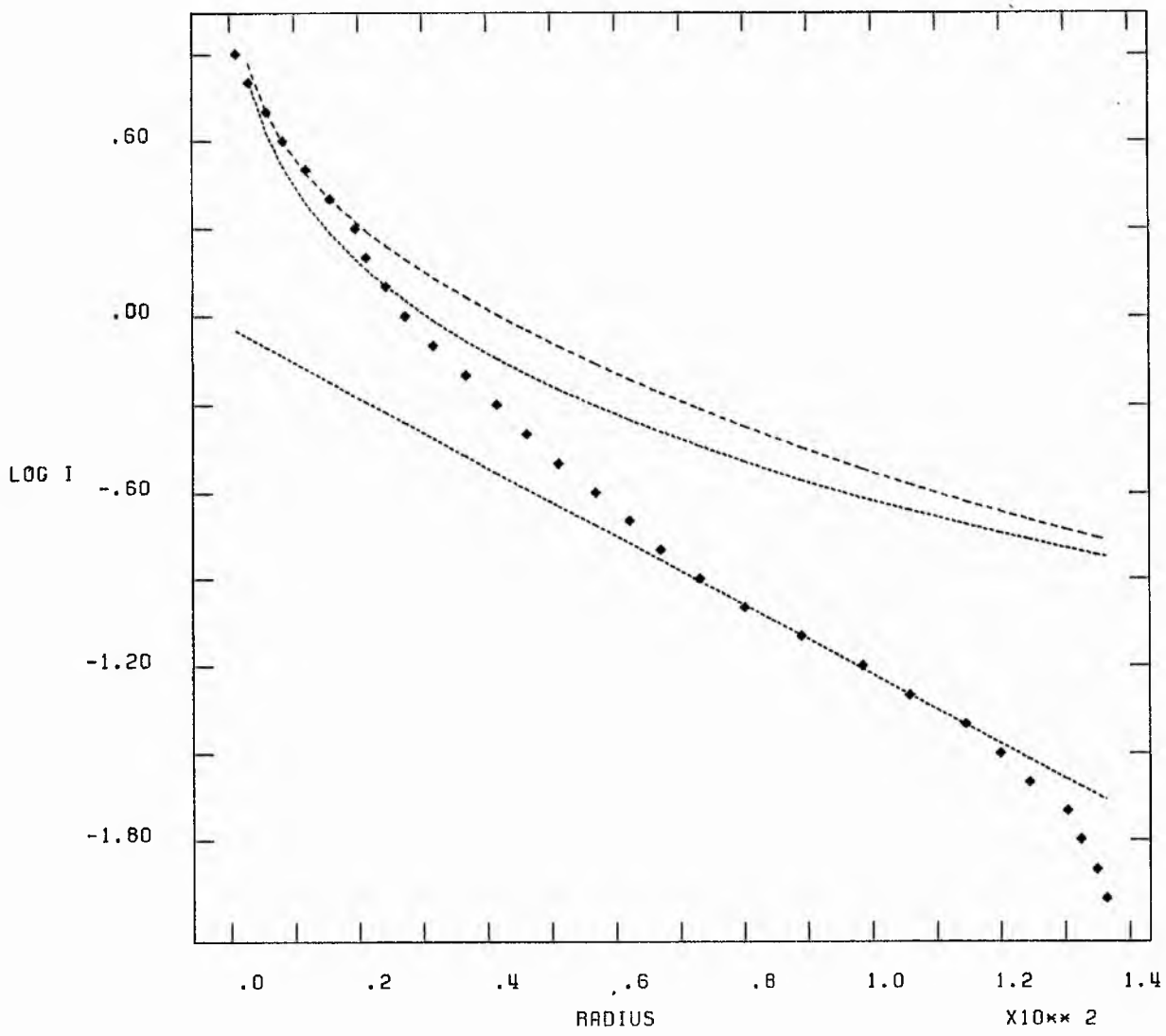
NGC 4531 B
SIMULTANEOUS LEAST SQUARES
X10** 0
.60
.00
LOG I
-.60
-1.20
-1.80
.0
.2
.4
.6
.8
1.0
1.2
1.4
RADIUS
X10** 2

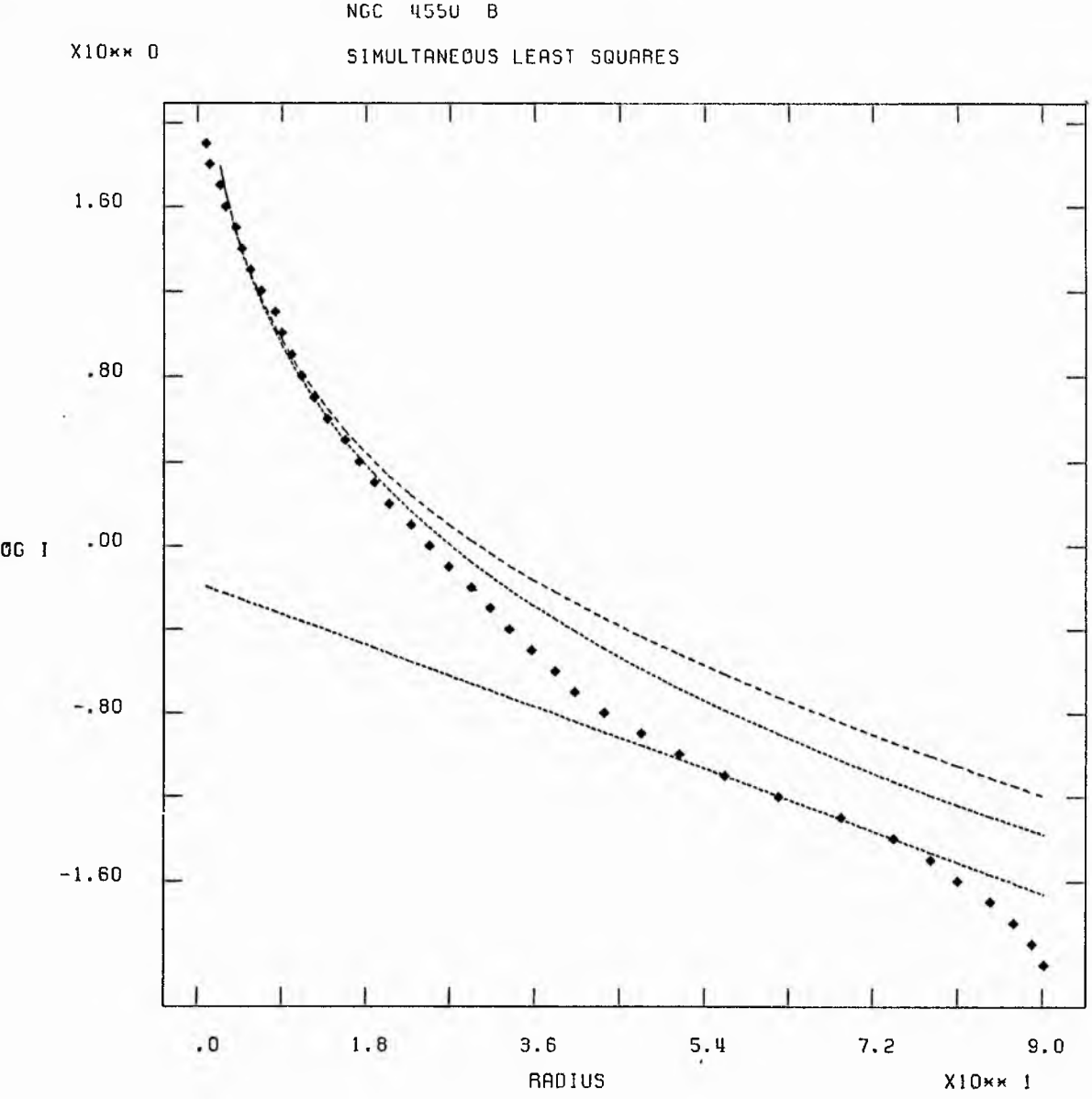
NGC 4550 B
SIMULTANEOUS LEAST SQUARES
X10** 0
1.60
.80
.00
-.80
-1.60
0G I
.0
1.8
3.6
5.4
7.2
9.0
RADIUS
X10** 1

NGC 4552 B

ITERATIVE FITTING.

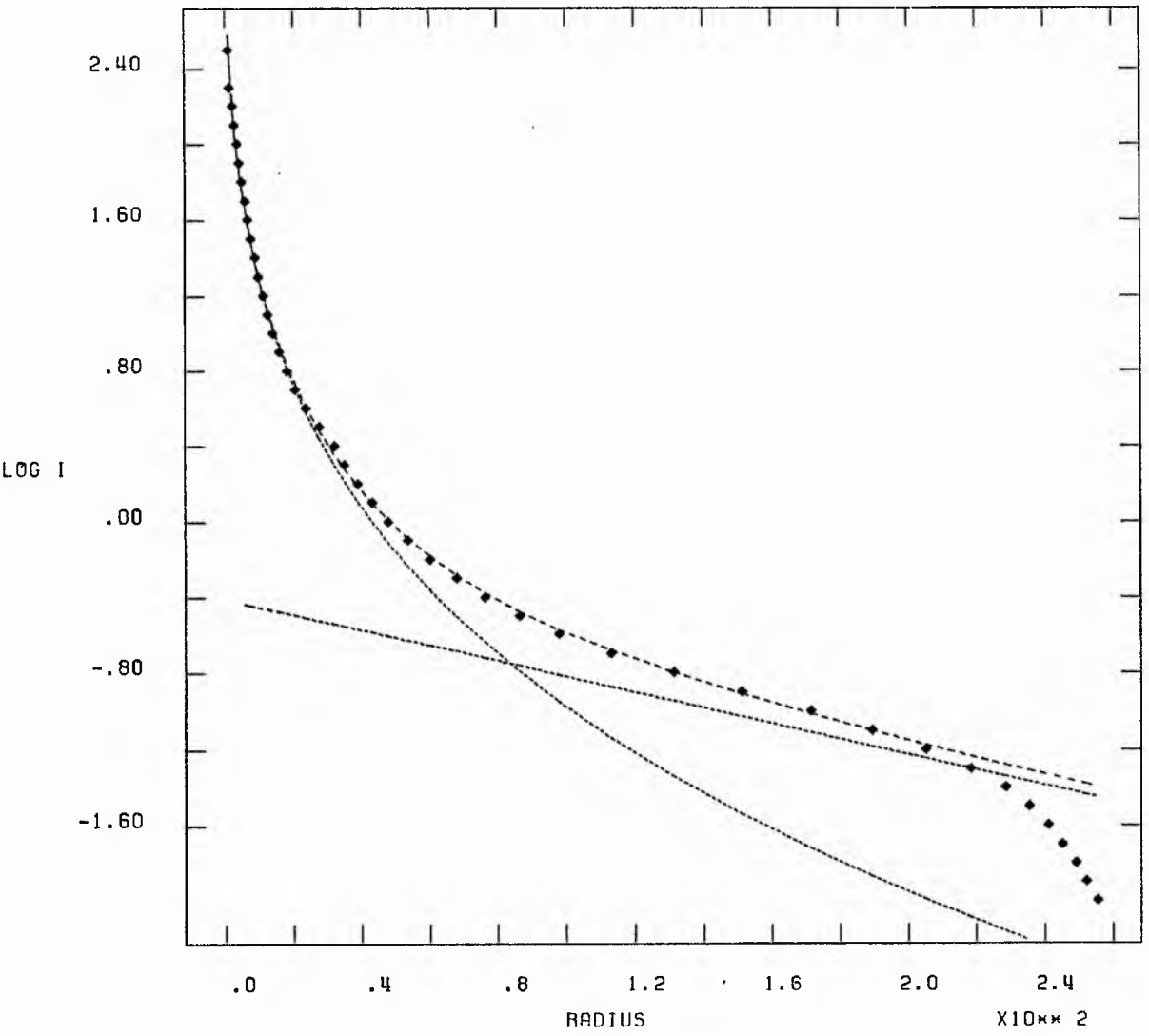

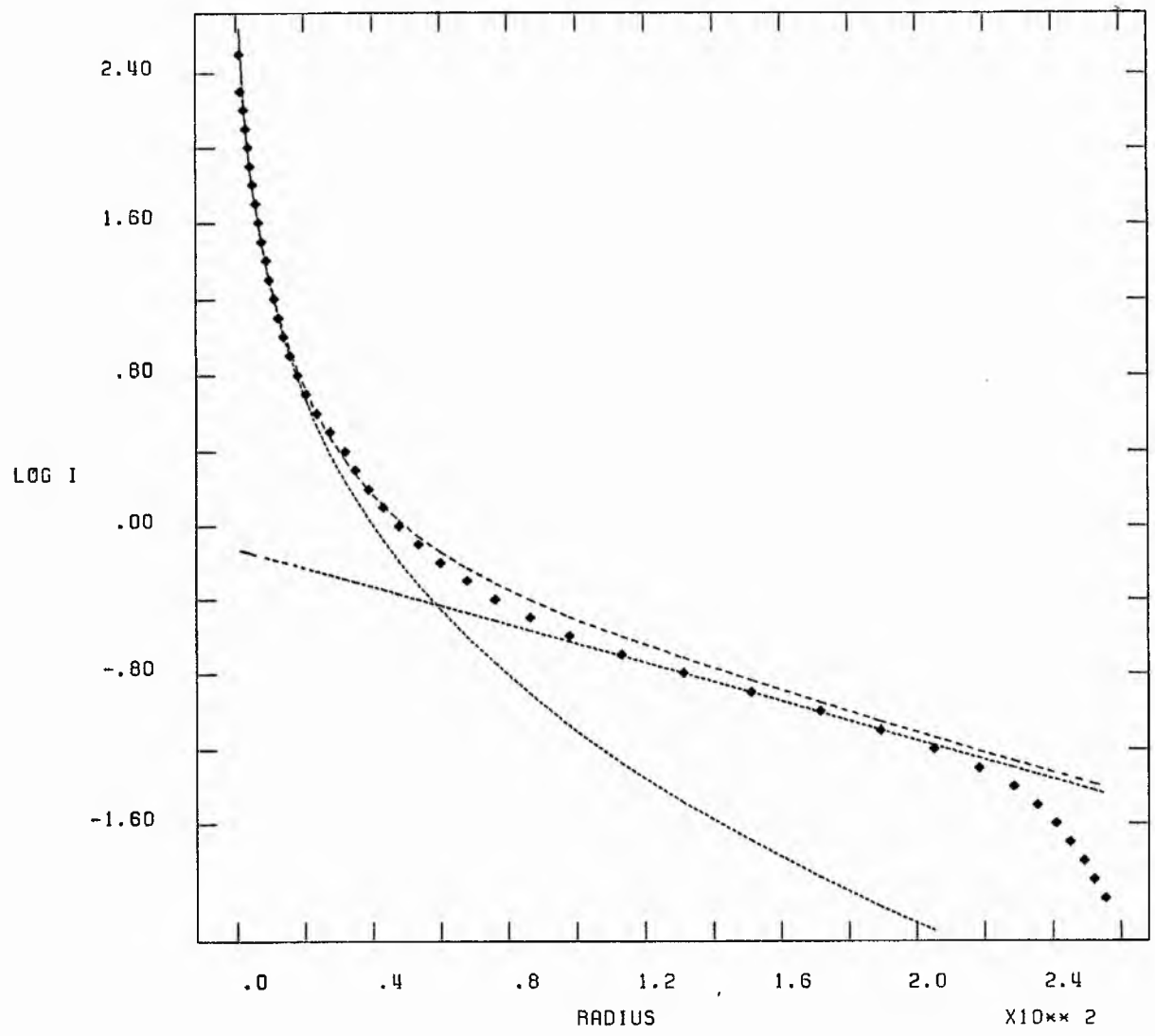
NGC 4552 B
SIMULTANEOUS LEAST SQUARES
X10** 0
2.40
1.60
.80
LOG I
.00
-.80
-1.60
.0
.4
.8
1.2
1.6
2.0
2.4
RADIUS
X10** 2

NGC 4267 R

ITERATIVE FITTING.

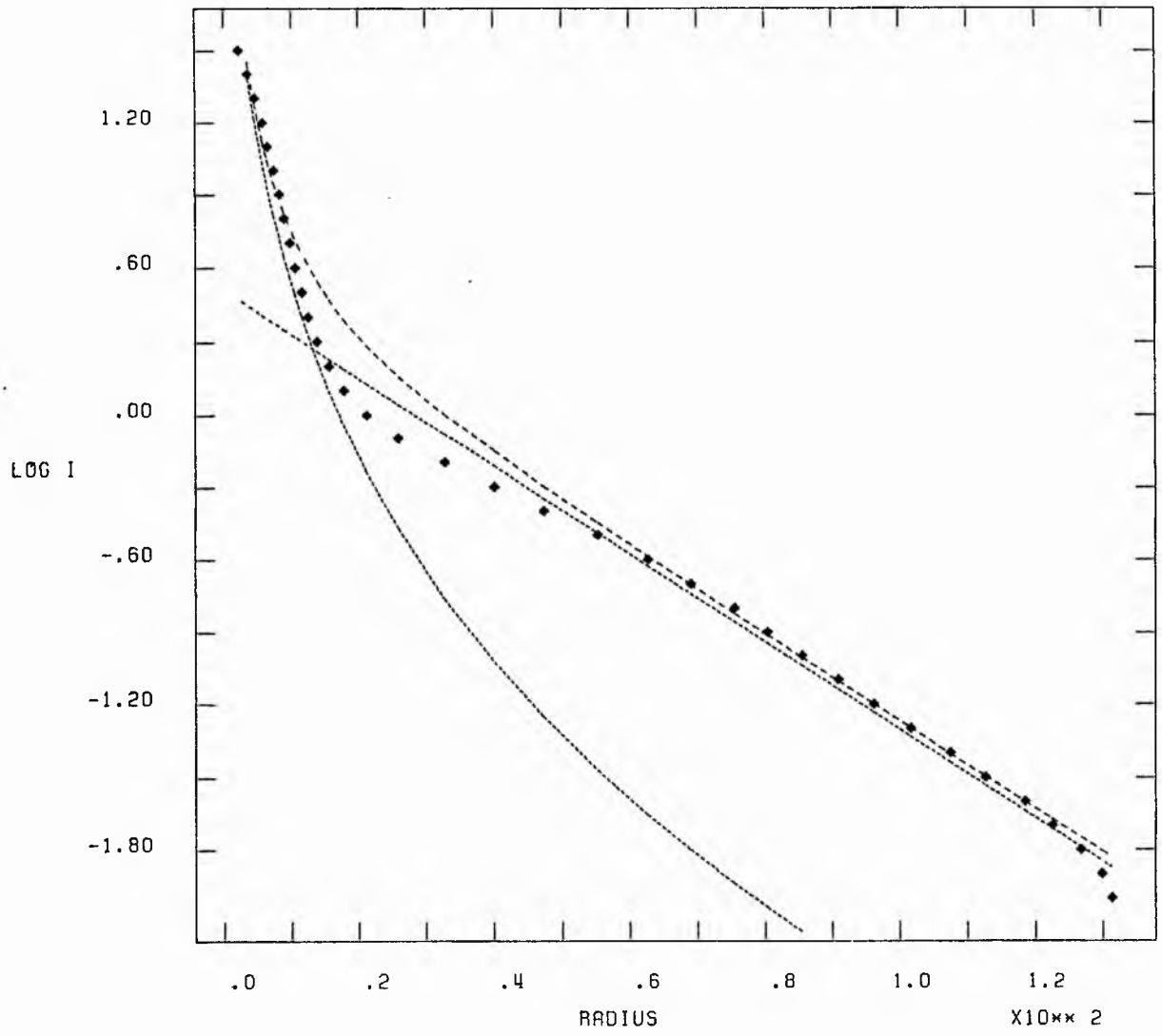

NGC 4267 R

SIMULTANEOUS LEAST SQUARES

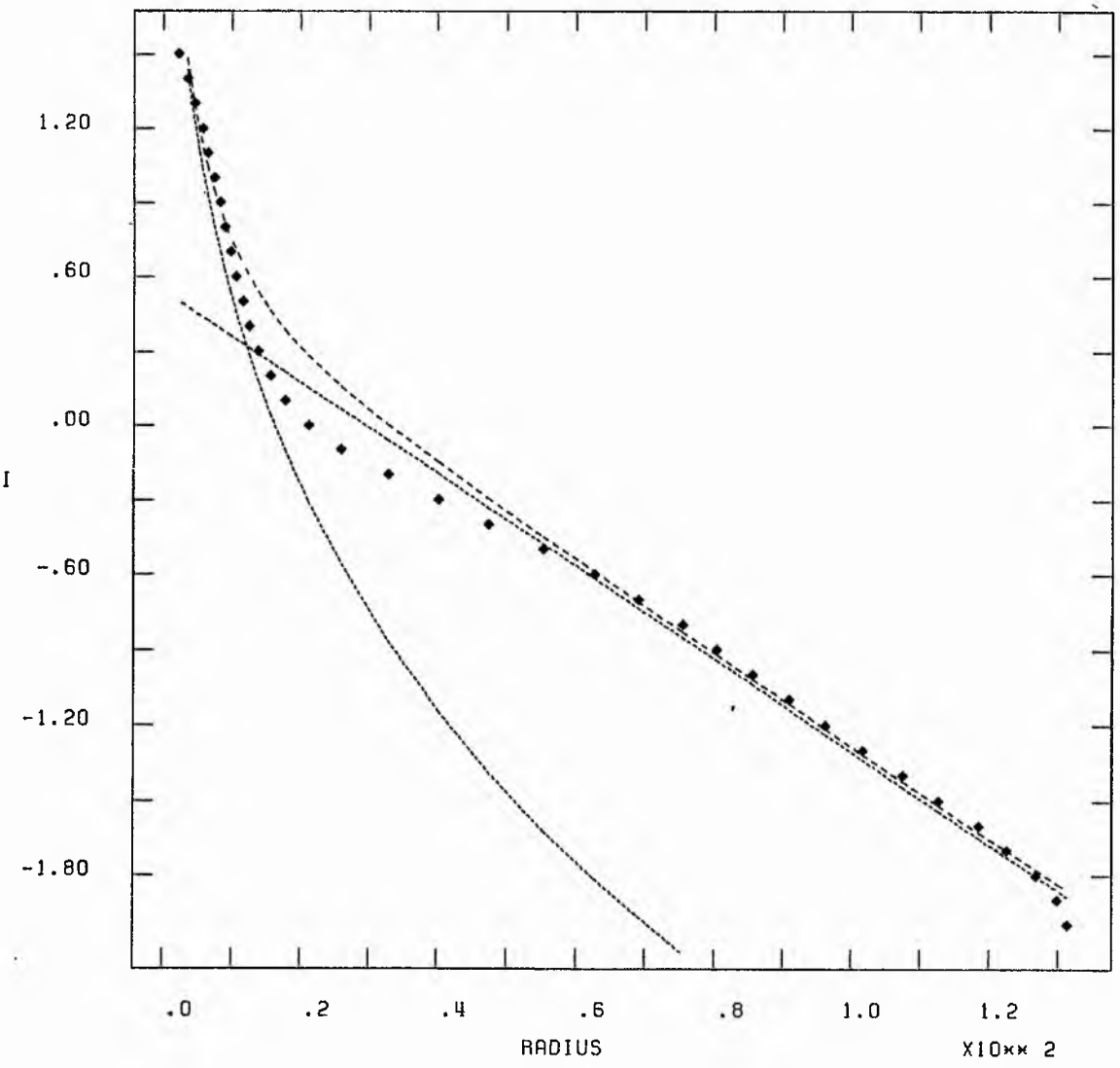

NGC 4371 R

ITERATIVE FITTING.

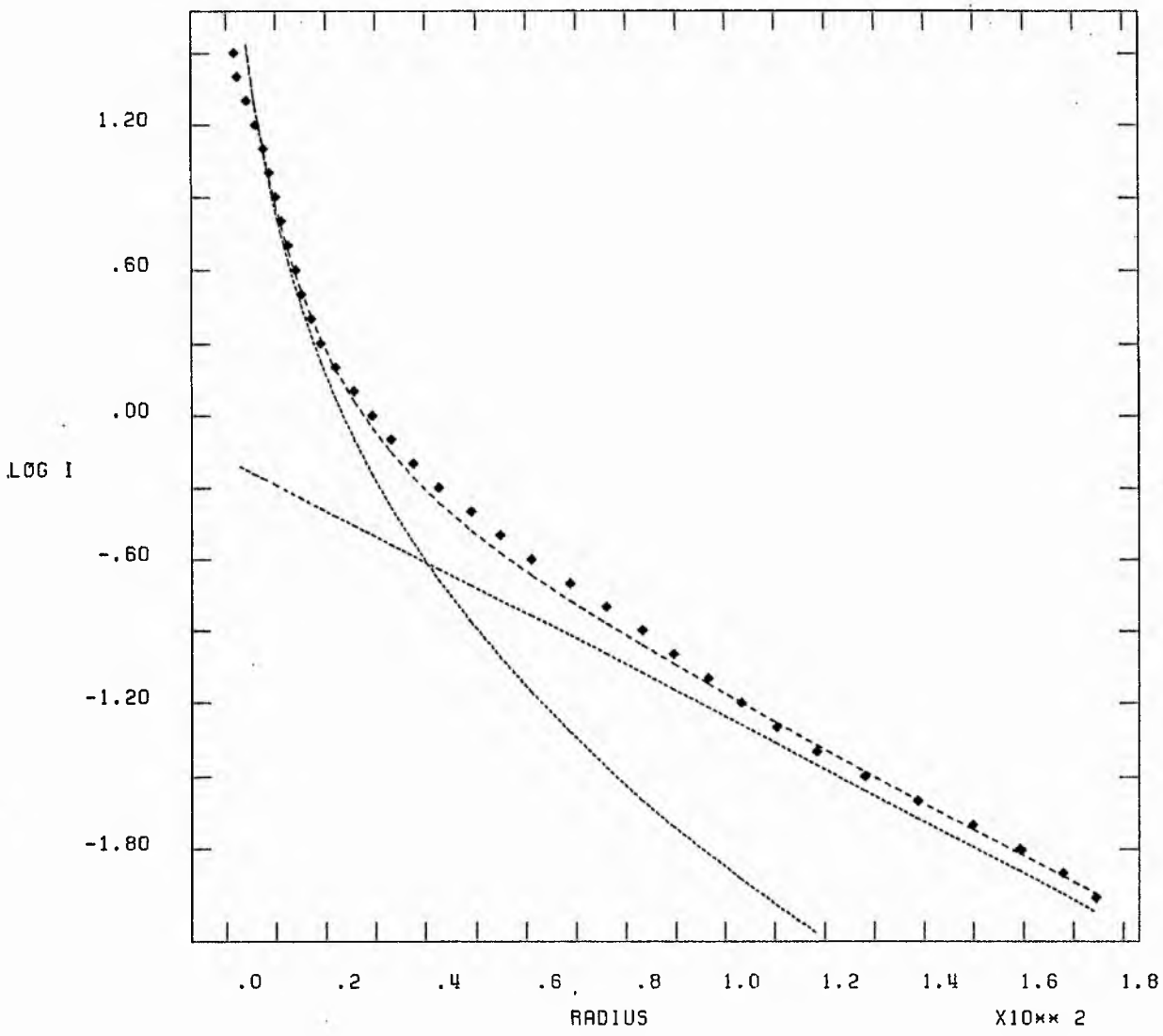

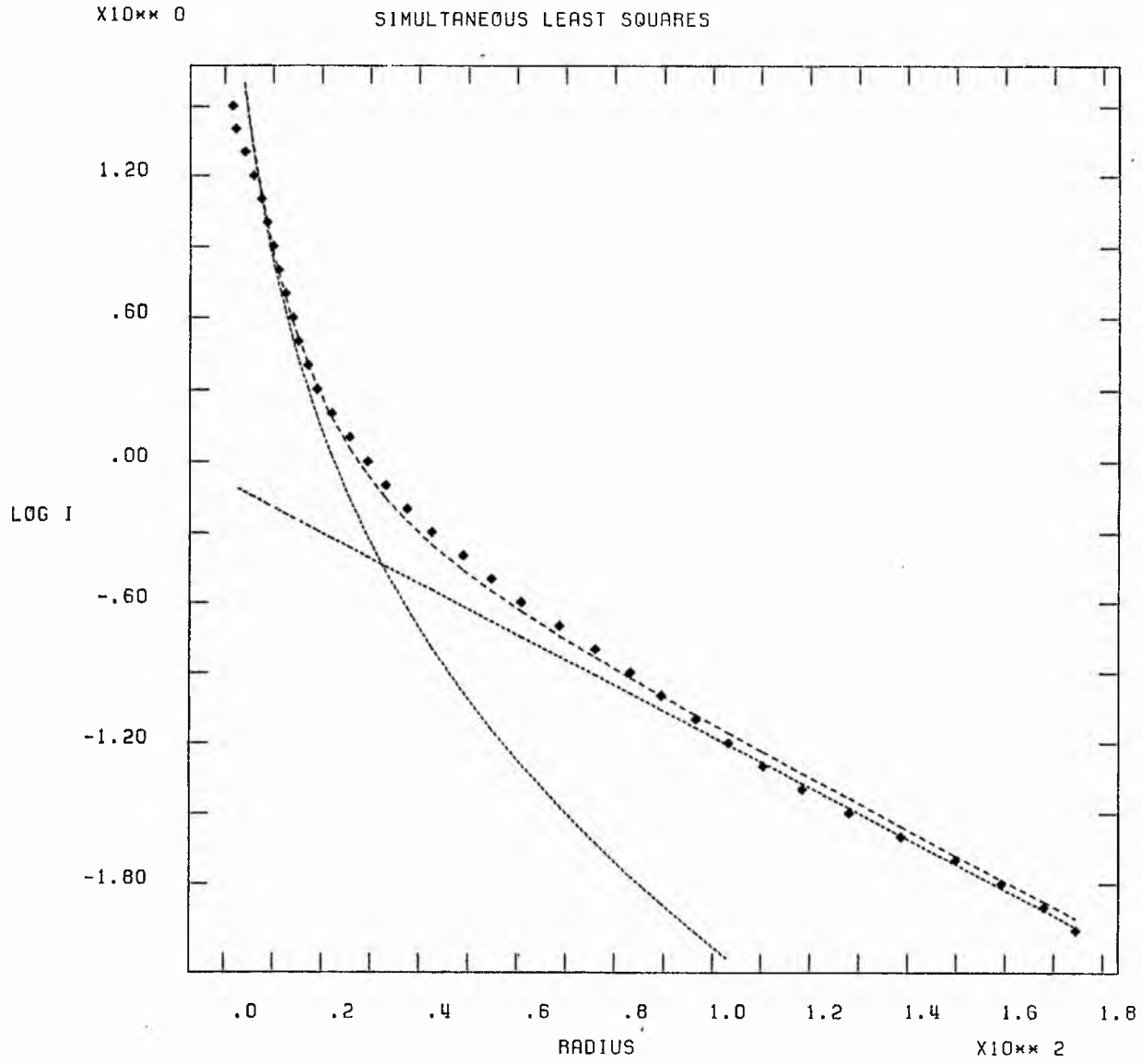
NGC 4371 R
SIMULTANEOUS LEAST SQUARES
X10** 0
1.20
.60
.00
LOG I
-.60
-1.20
-1.80
.0
.2
.4
.6
.8
1.0
1.2
1.4
1.6
1.8
RADIUS
X10** 2

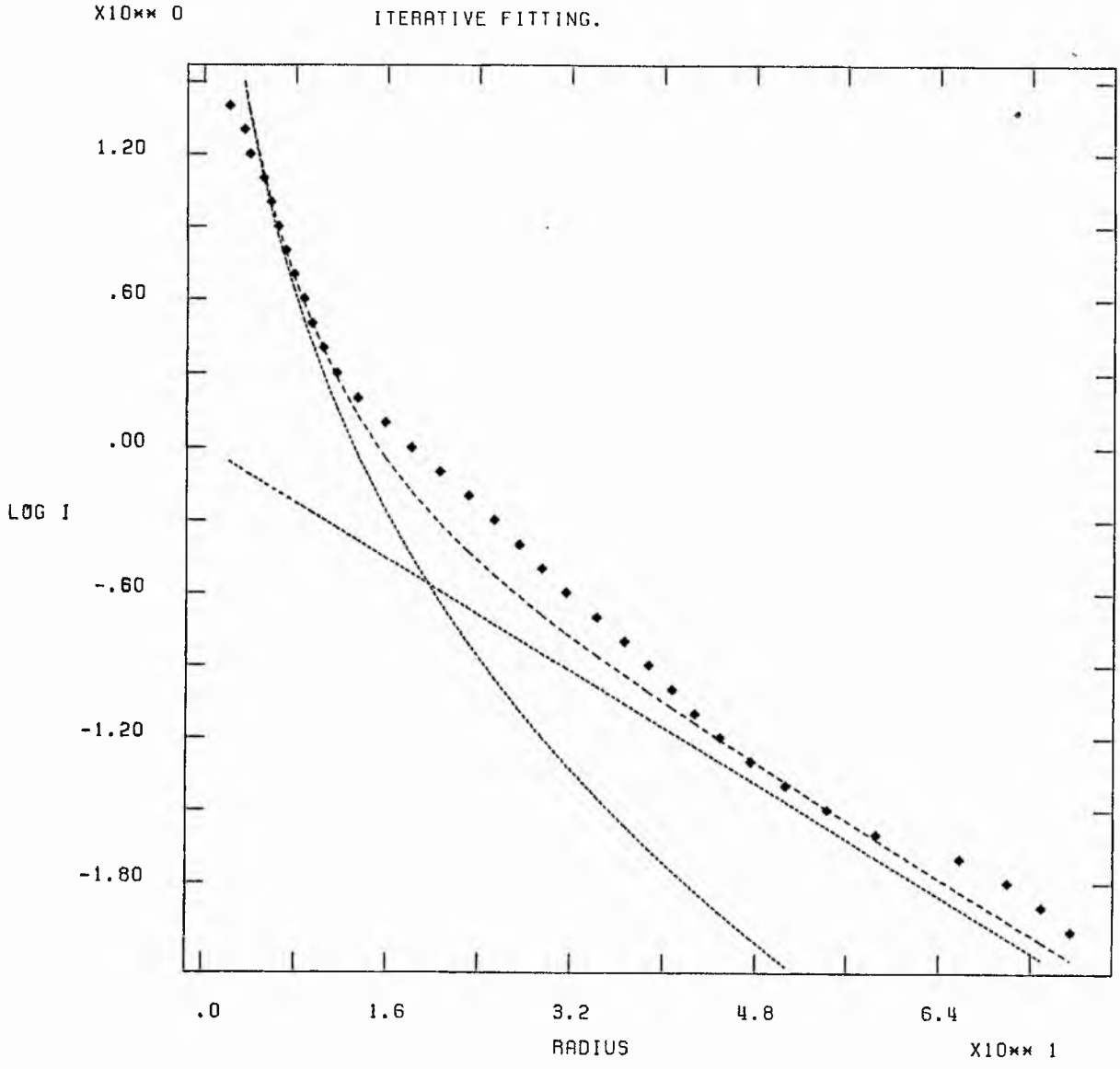
NGC 4377 R
ITERATIVE FITTING.
X10** 0
1.20
.60
.00
LOG I
-.60
-1.20
-1.80
.0
1.6
3.2
4.8
6.4
RADIUS
X10** 1

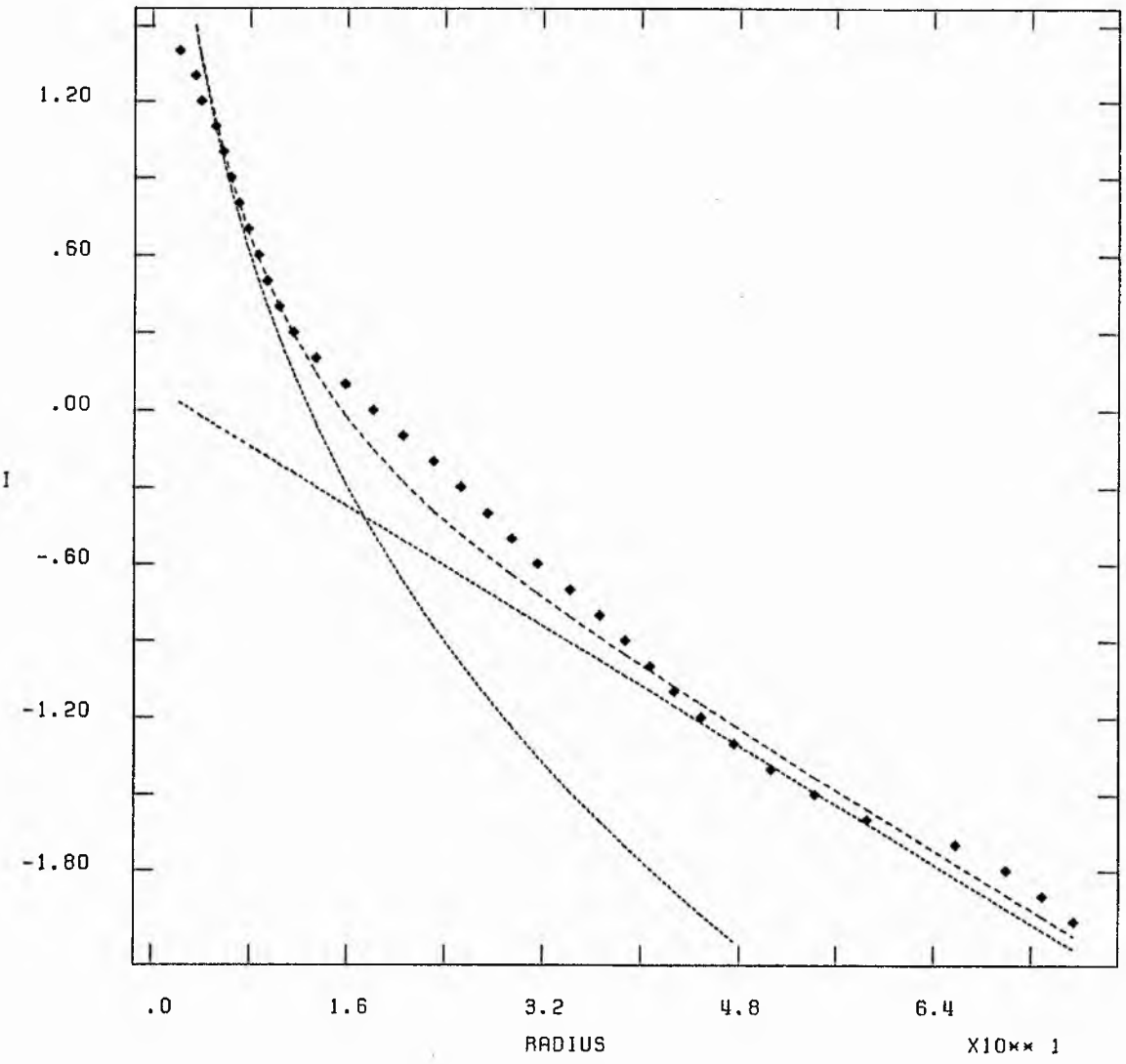
NGC 4377 R
SIMULTANEOUS LEAST SQUARES
X10** 0
1.20
.60
.00
LOG I
-.60
-1.20
-1.80
.0
1.6
3.2
4.8
6.4
RADIUS
X10** 1

NGC 4419 R

X10** 0

ITERATIVE FITTING.

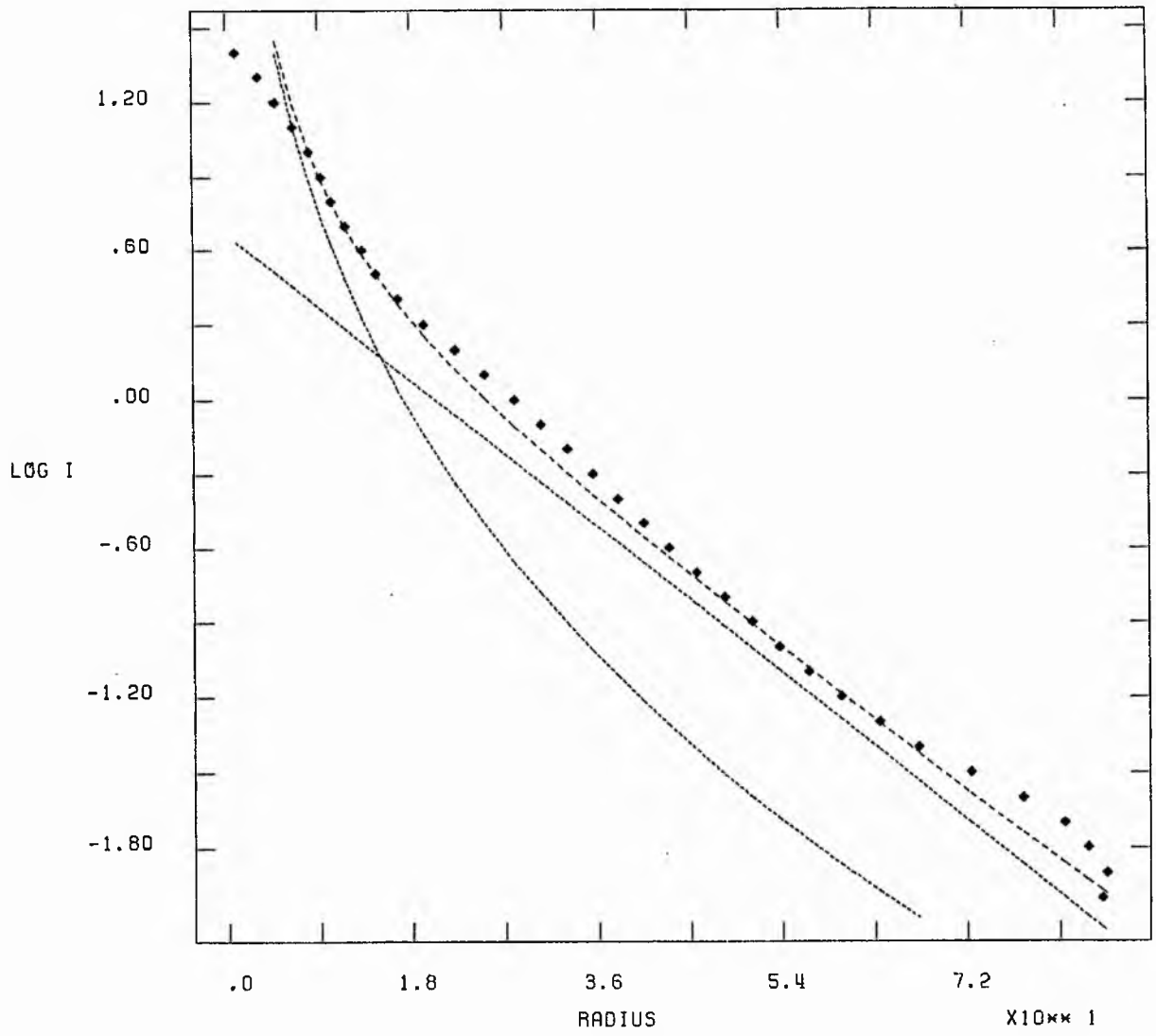

NGC 4425 R

SIMULTANEOUS LEAST SQUARES

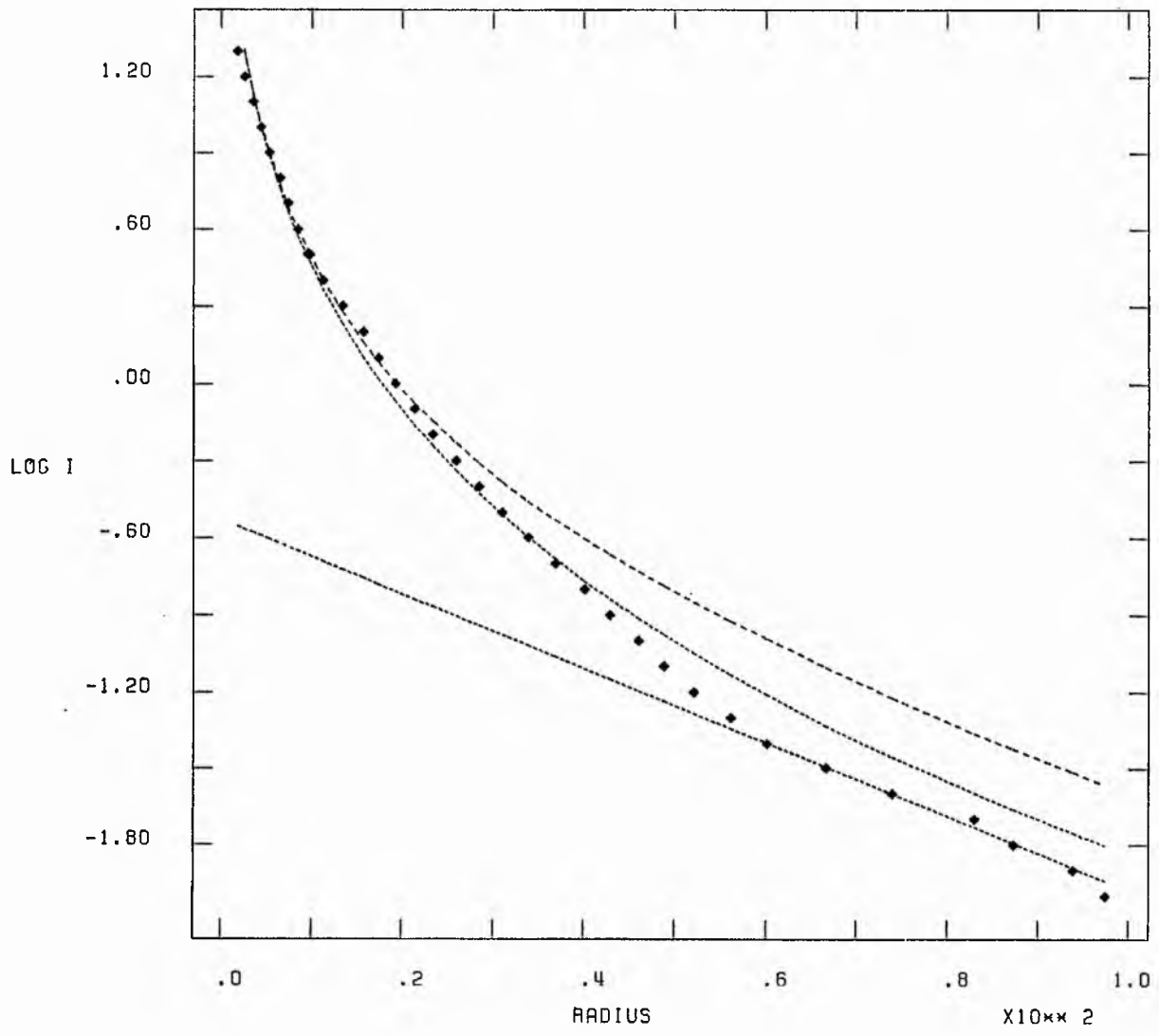

NGC 4429 R

SIMULTANEOUS LEAST SQUARES

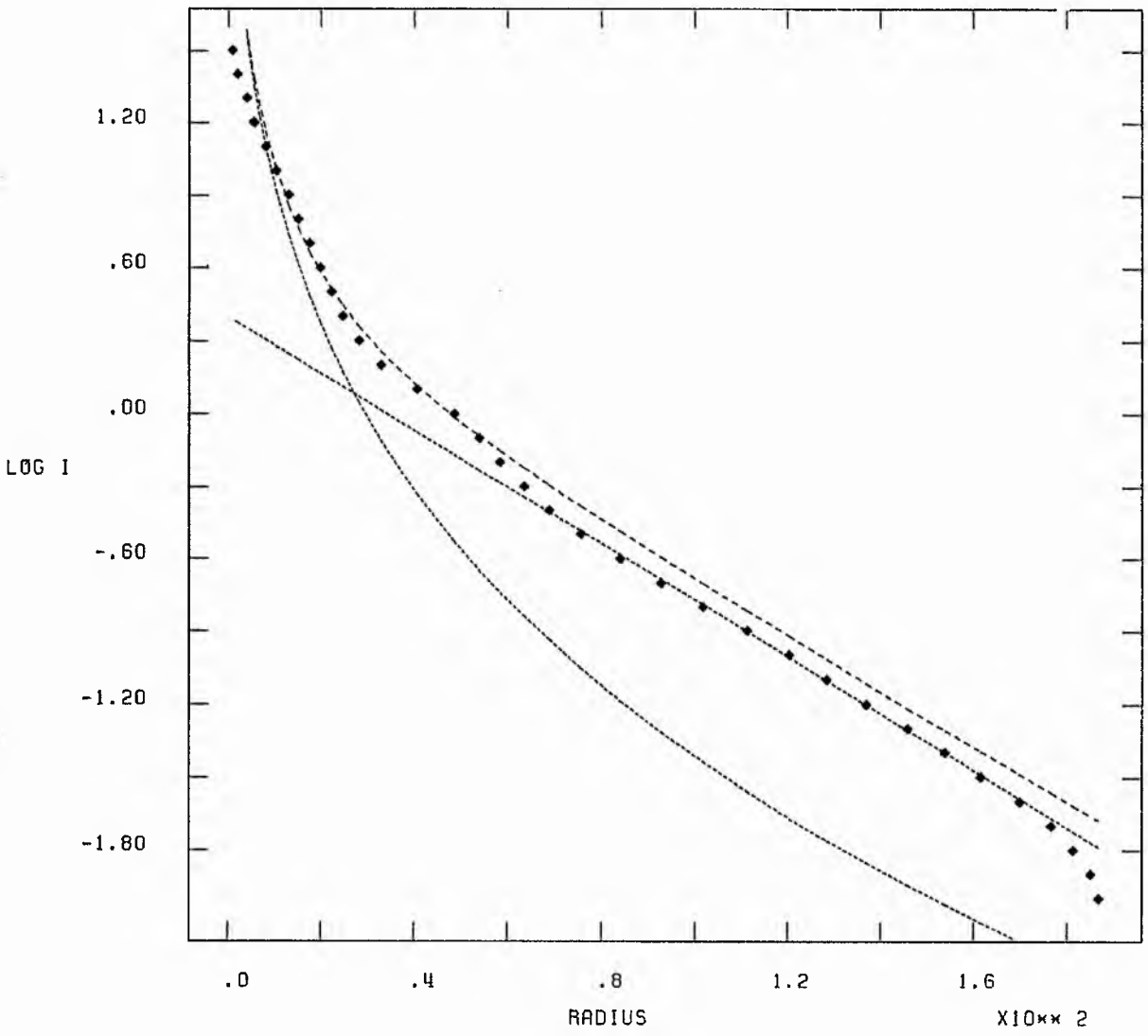

NGC 4435 B

ITERATIVE FITTING.

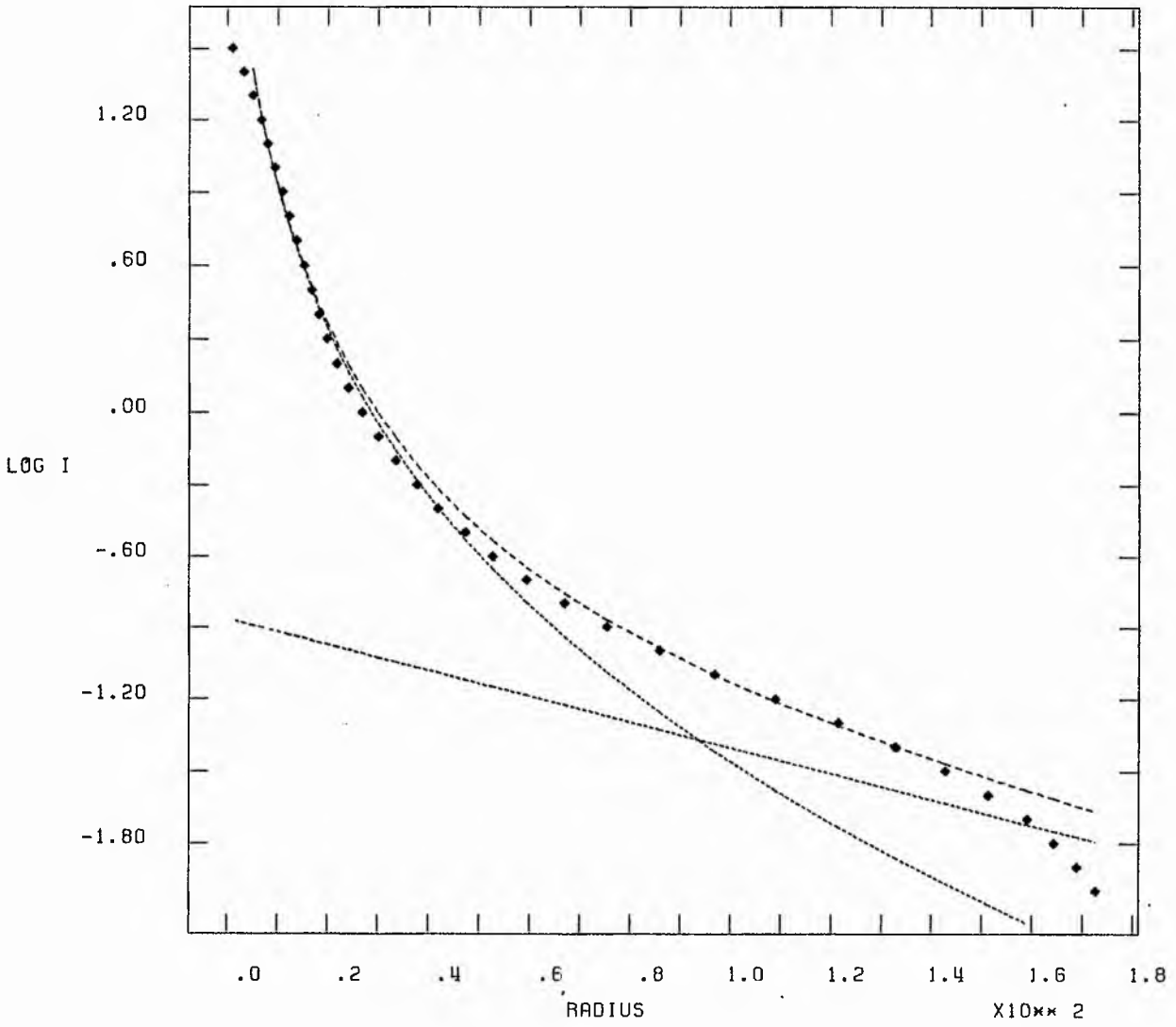

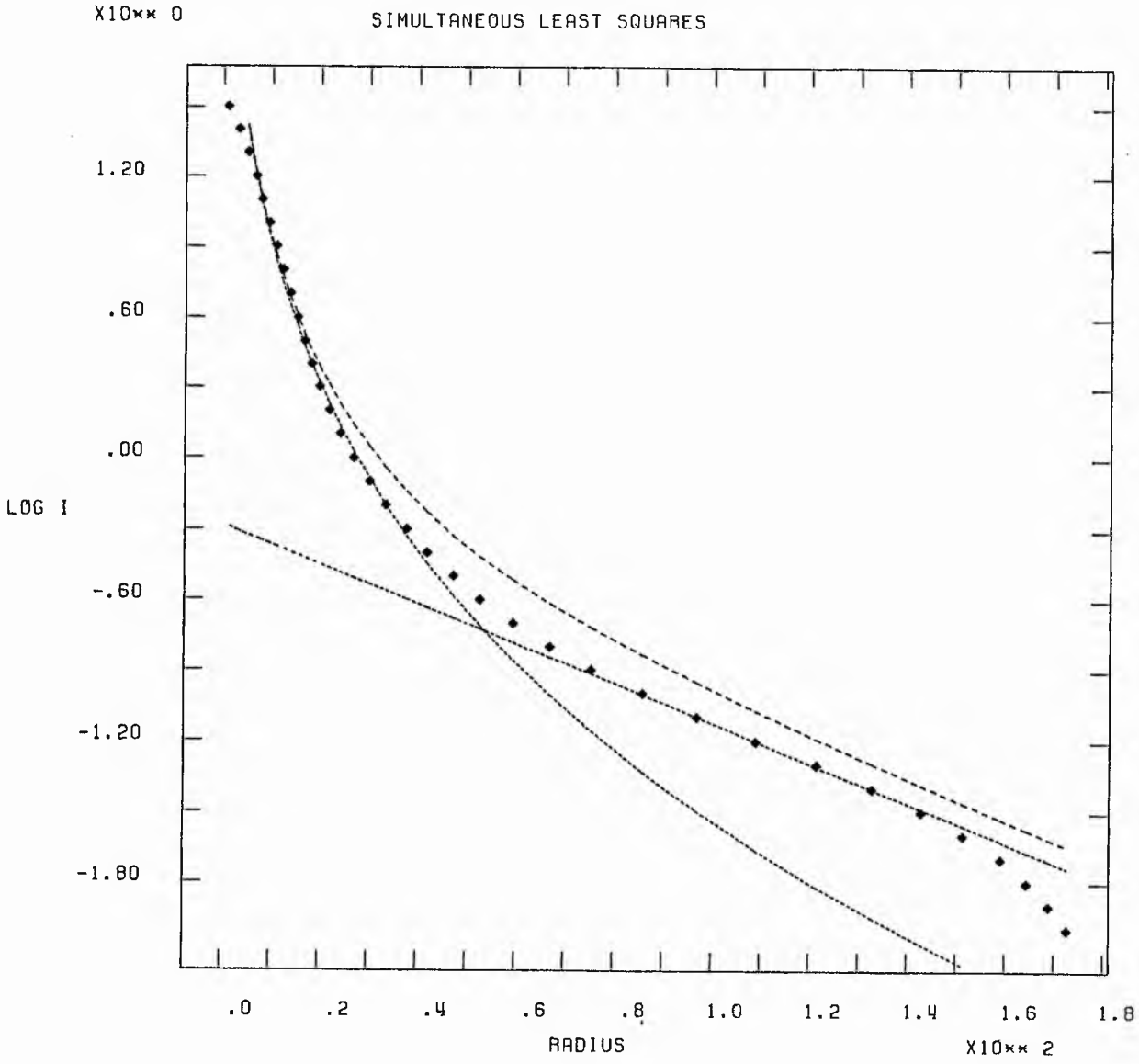
NGC 4435 R
SIMULTANEOUS LEAST SQUARES
X10** 0
1.20
.60
.00
LOG I
-.60
-1.20
-1.80
.0
.2
.4
.6
.8
1.0
1.2
1.4
1.6
1.8
RADIUS
X10** 2

NGC 4438 R

X10** 0

ITERATIVE FITTING.

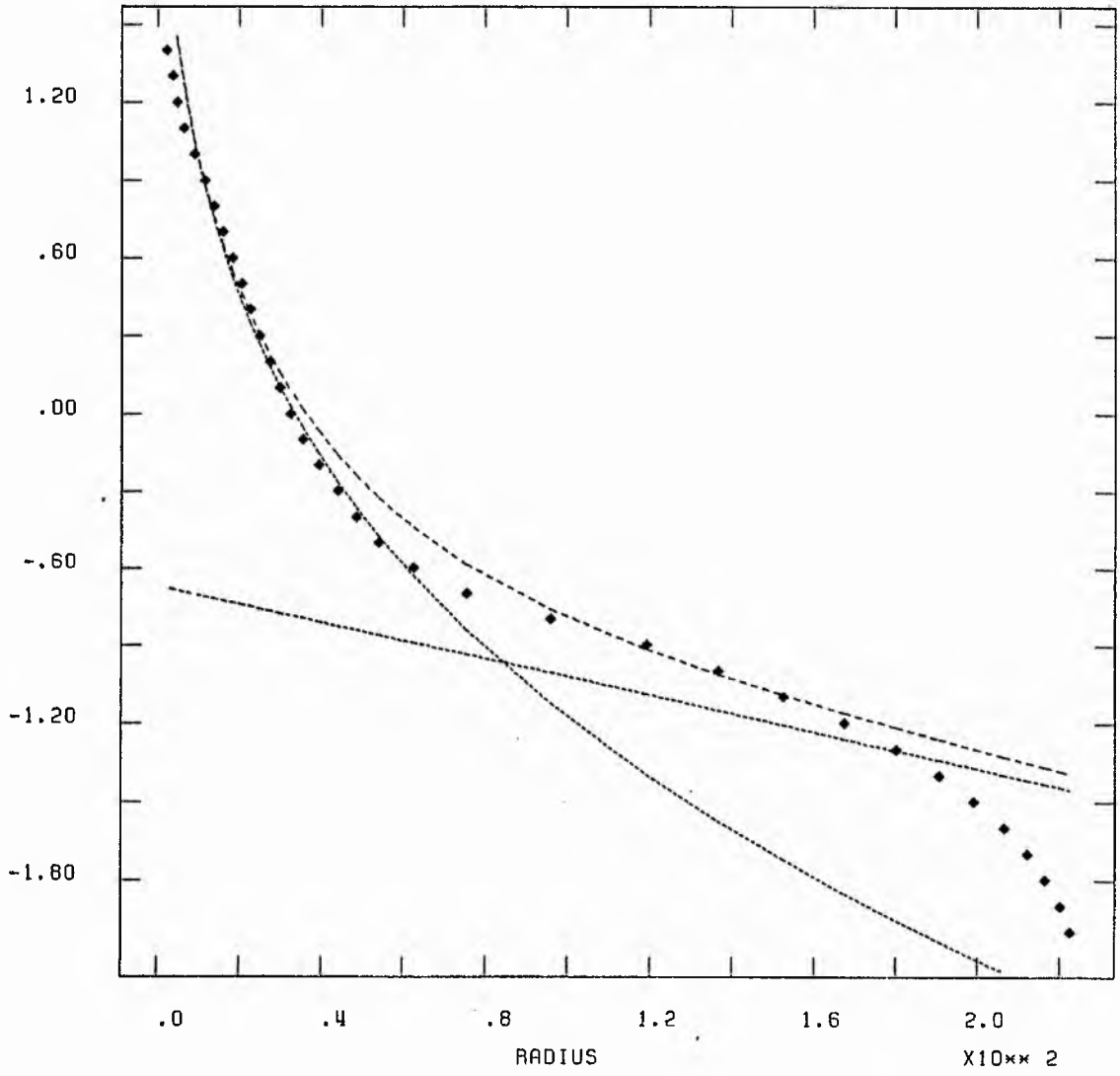

0G I

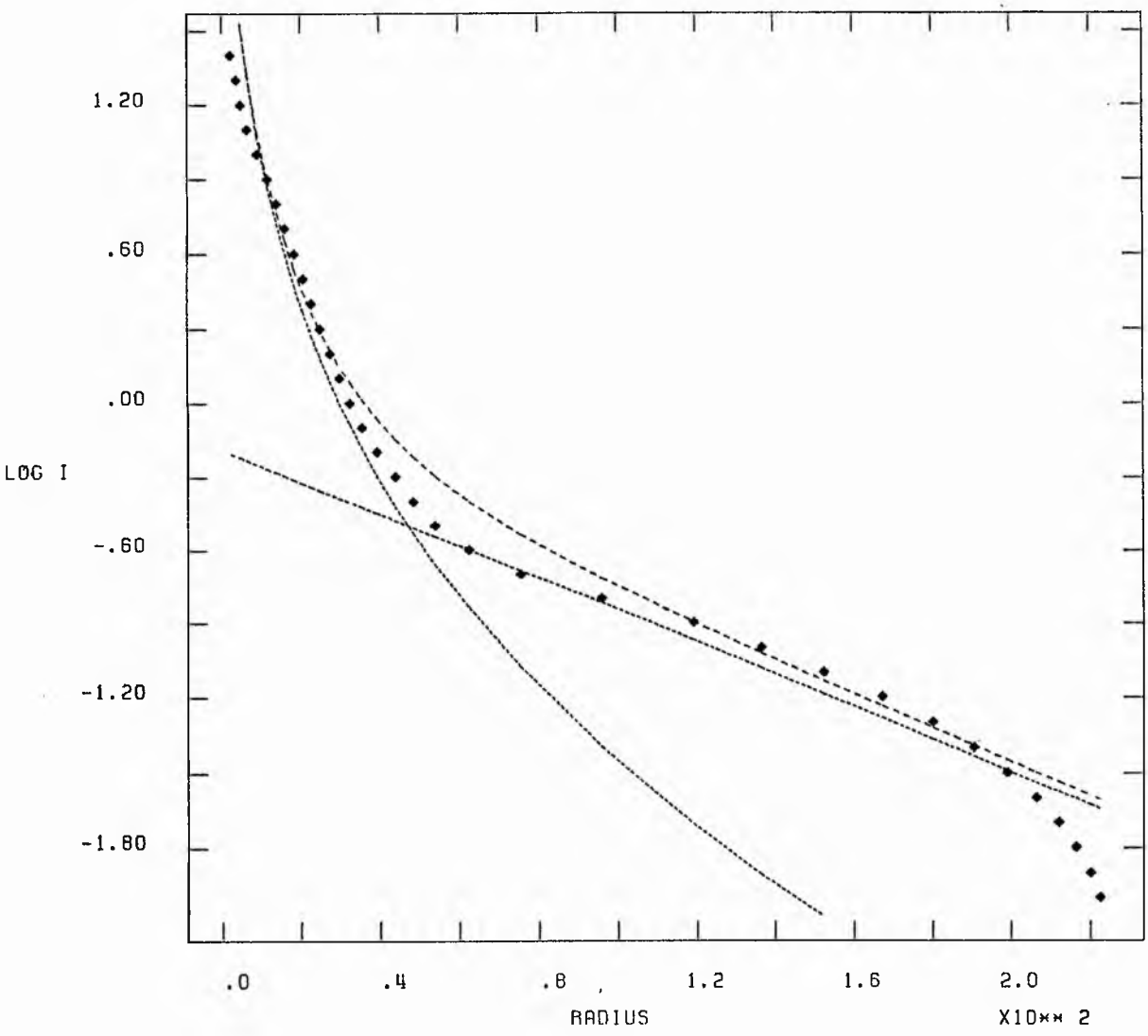
NGC 4438 R
SIMULTANEOUS LEAST SQUARES
X10** 0
1.20
.60
.00
LOG I
-.60
-1.20
-1.80
.0
.4
.8
1.2
1.6
2.0
RADIUS
X10** 2

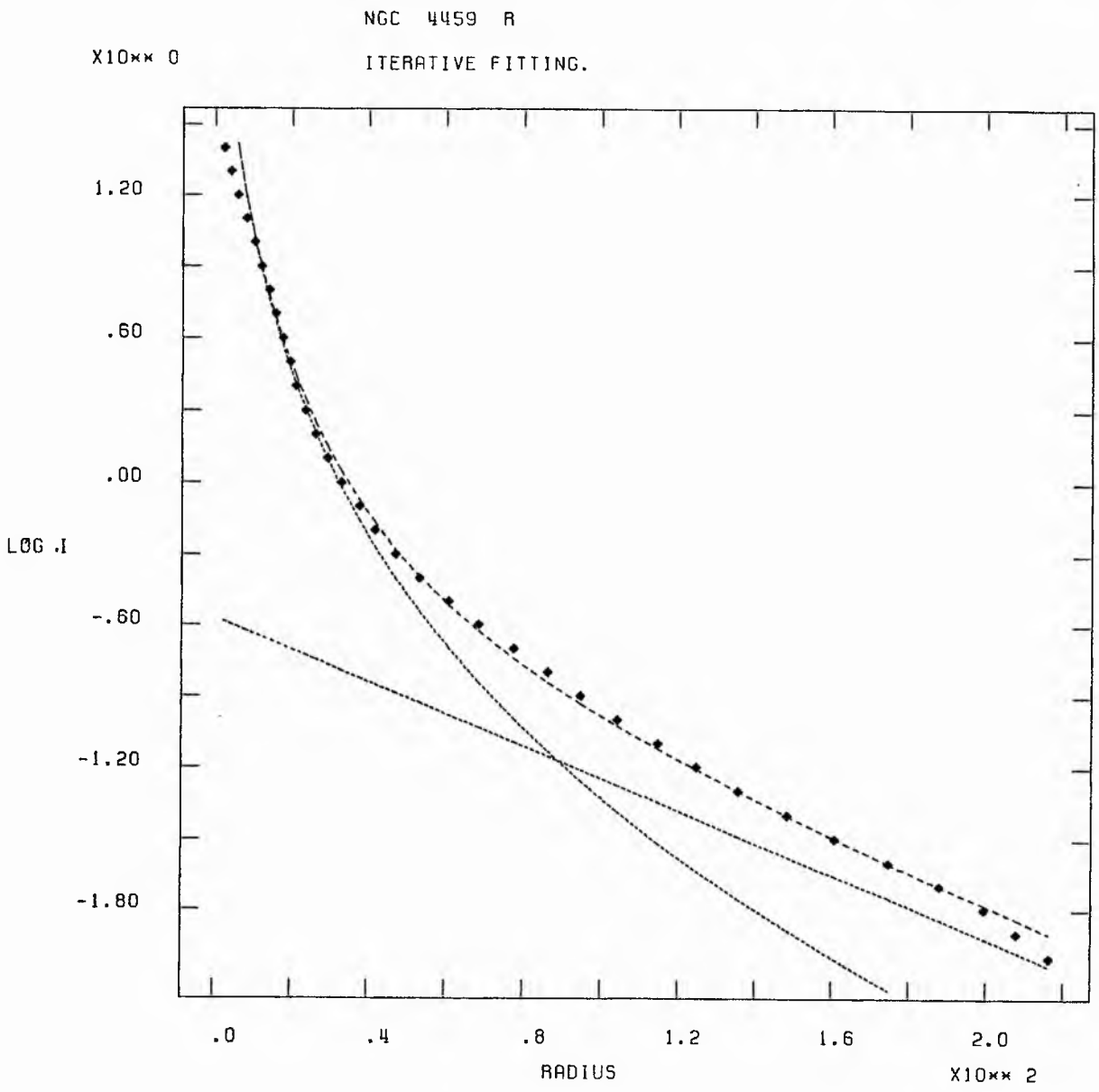
NGC 4459 R
ITERATIVE FITTING.
X10** 0
1.20
.60
.00
LOG .I
-.60
-1.20
-1.80
.0
.4
.8
1.2
1.6
2.0
RADIUS
X10** 2

NGC 4459 R

SIMULTANEOUS LEAST SQUARES

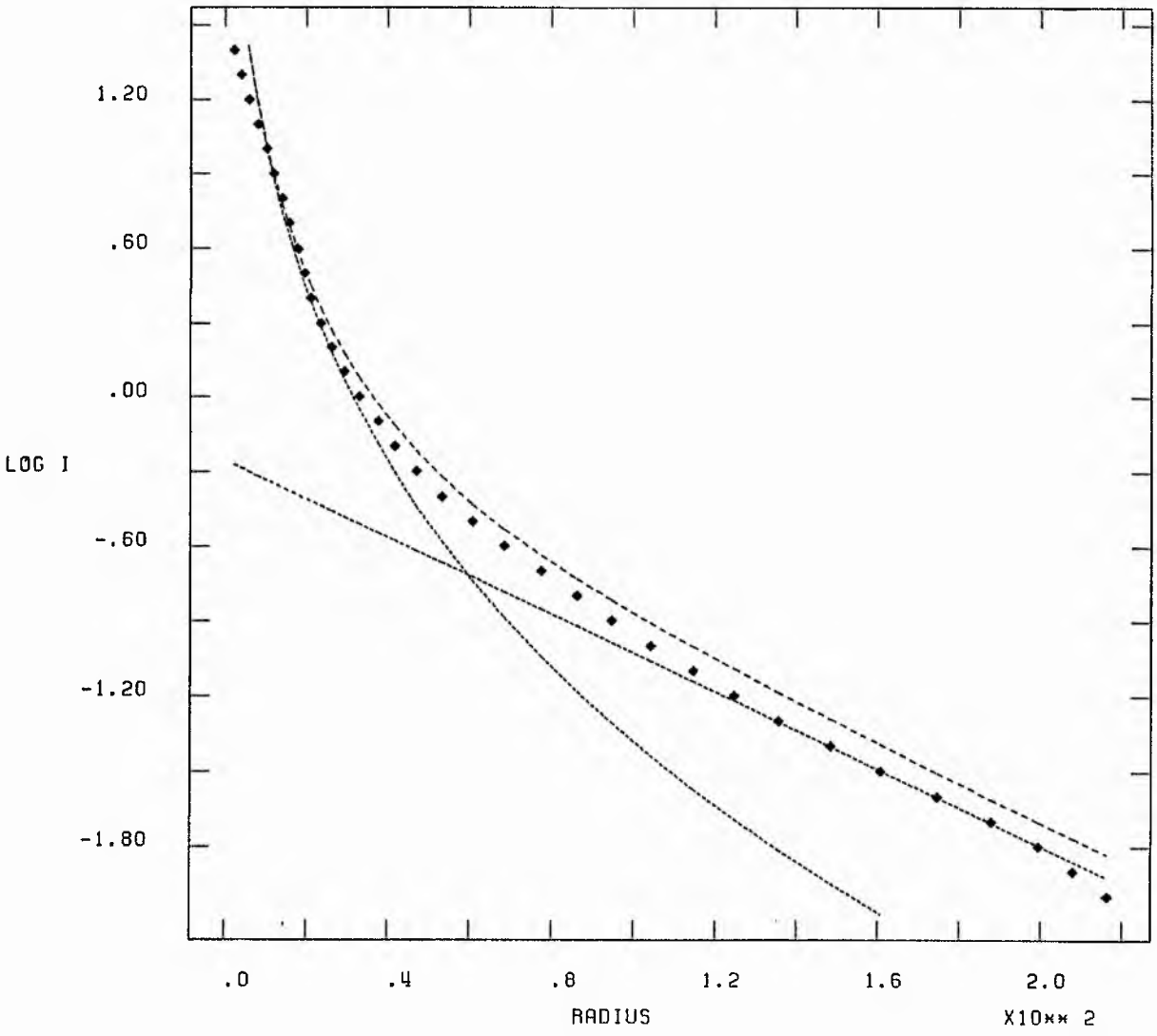

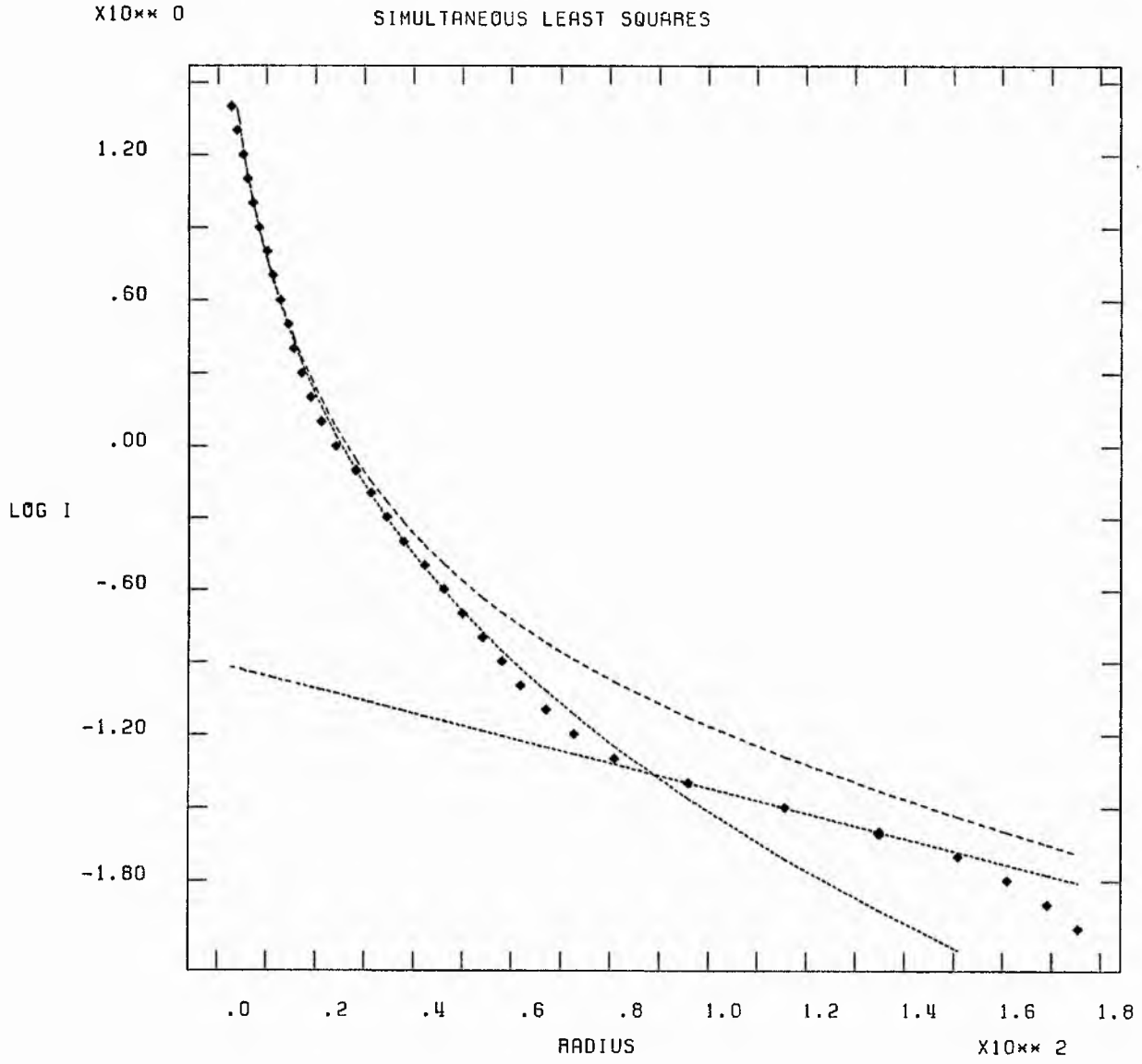
NGC 4461 R
SIMULTANEOUS LEAST SQUARES
X10** 0
1.20
.60
.00
-.60
-1.20
-1.80
LOG I
.0
.2
.4
.6
.8
1.0
1.2
1.4
1.6
1.8
RADIUS
X10** 2

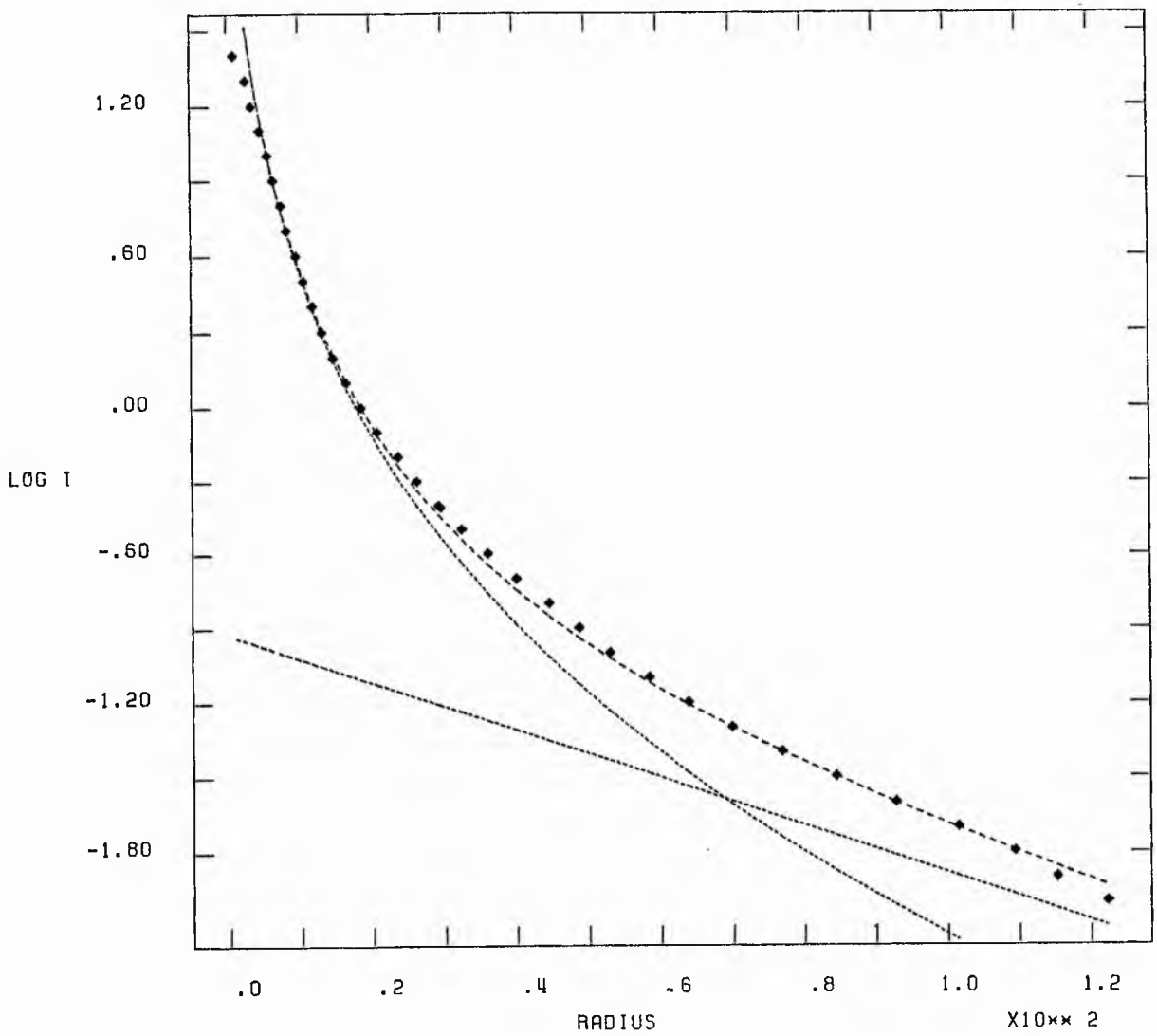
NGC 4474 R
X10** 0
ITERATIVE FITTING.
1.20
.60
.00
LOG I
-.60
-1.20
-1.80
.0
.2
.4
.6
.8
1.0
1.2
RADIUS
X10** 2

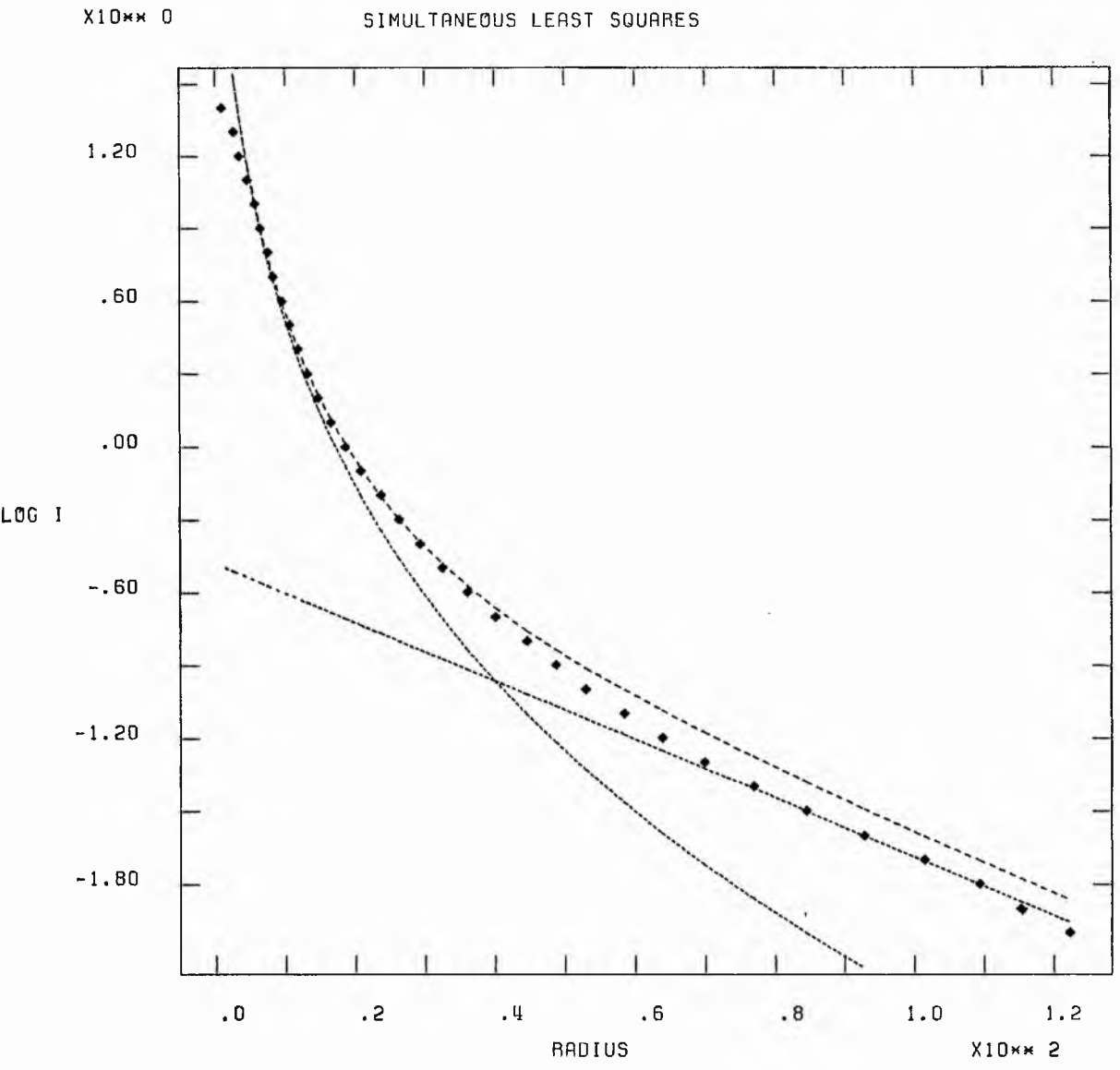
NGC 4474 R
SIMULTANEOUS LEAST SQUARES
X10** 0
1.20
.60
.00
LOG I
-.60
-1.20
-1.80
.0
.2
.4
.6
.8
1.0
1.2
RADIUS
X10** 2

NGC 4477 R

ITERATIVE FITTING.

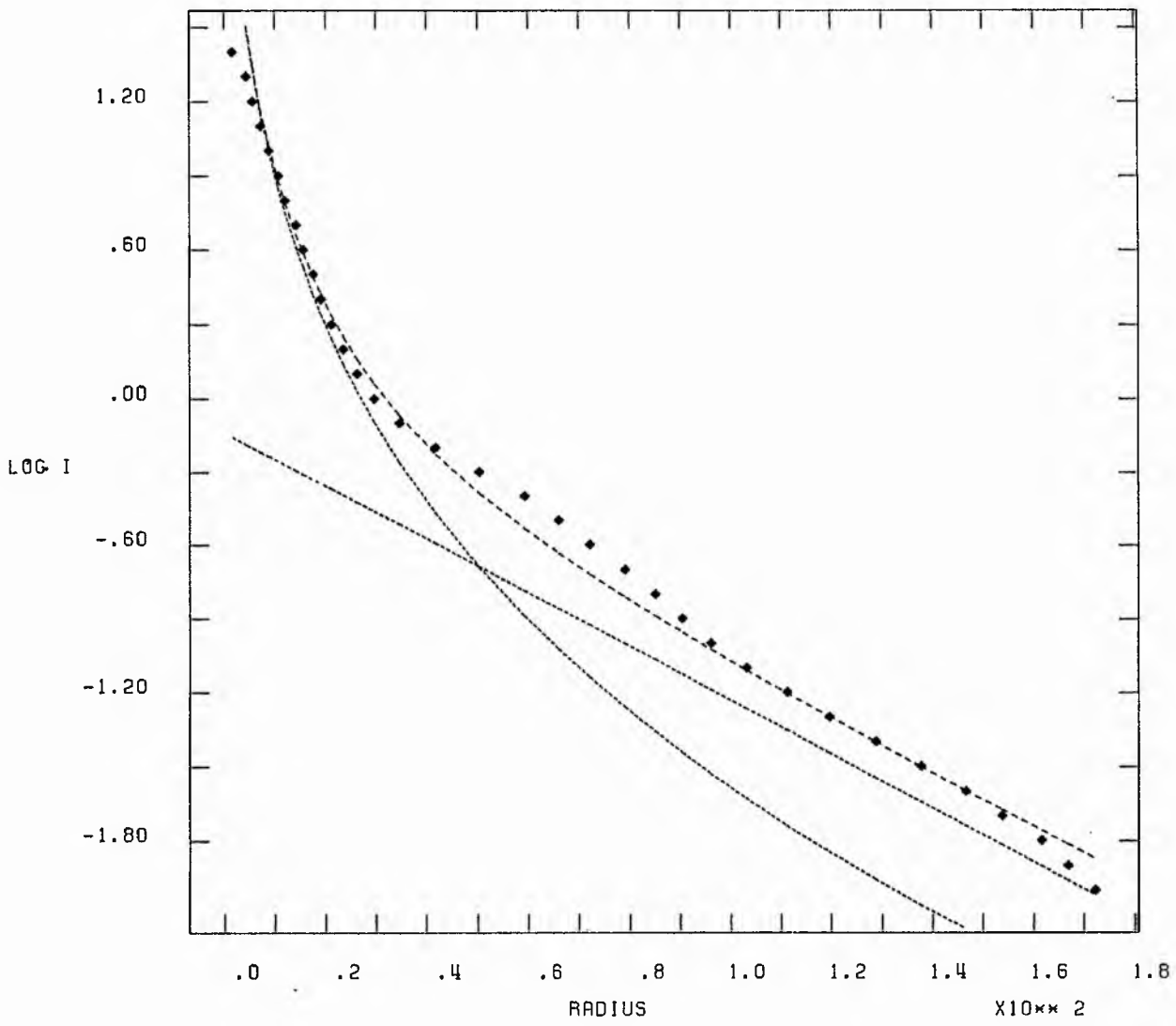

NGC 4477 R

X10** 0

SIMULTANEOUS LEAST SQUARES

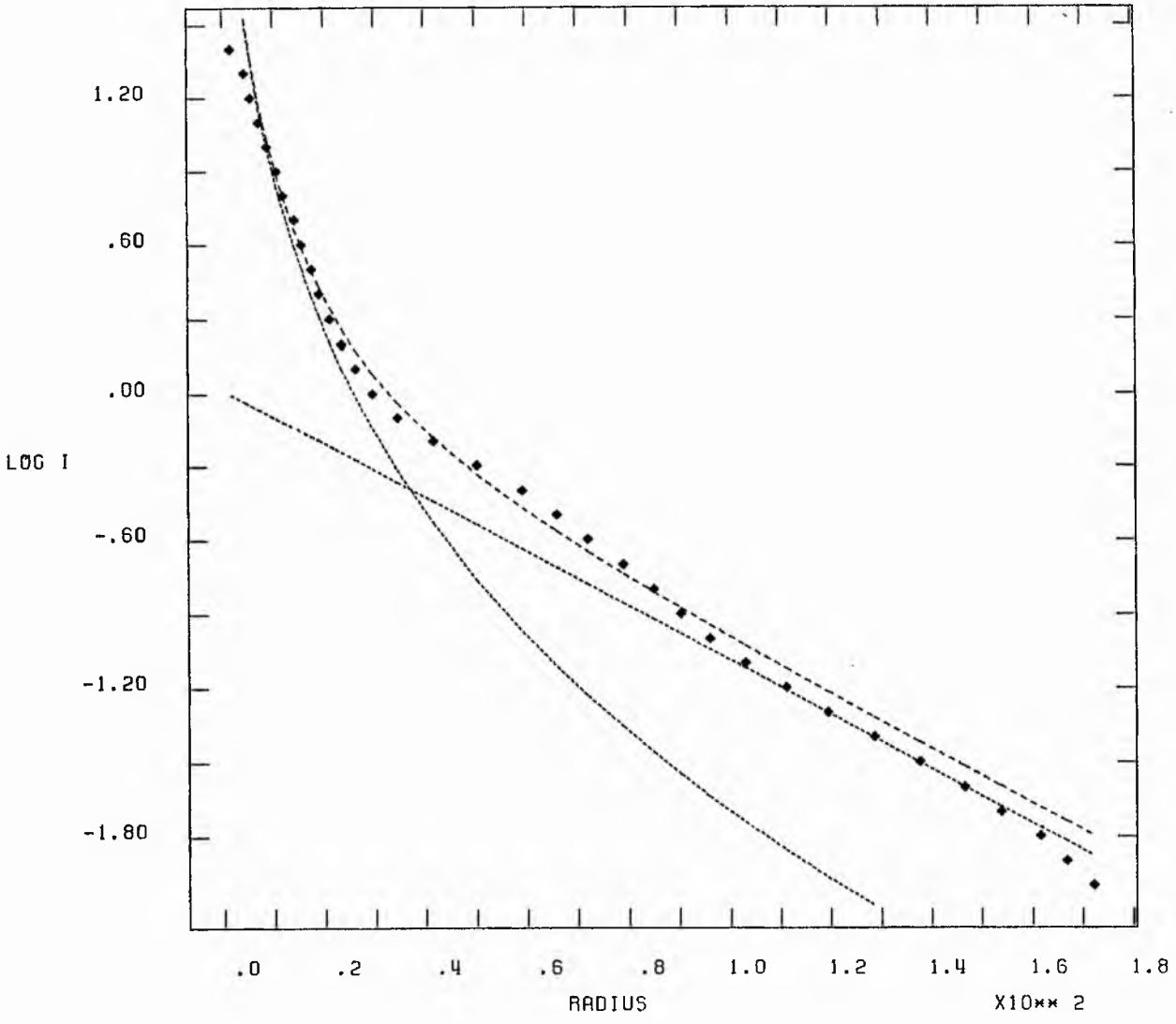

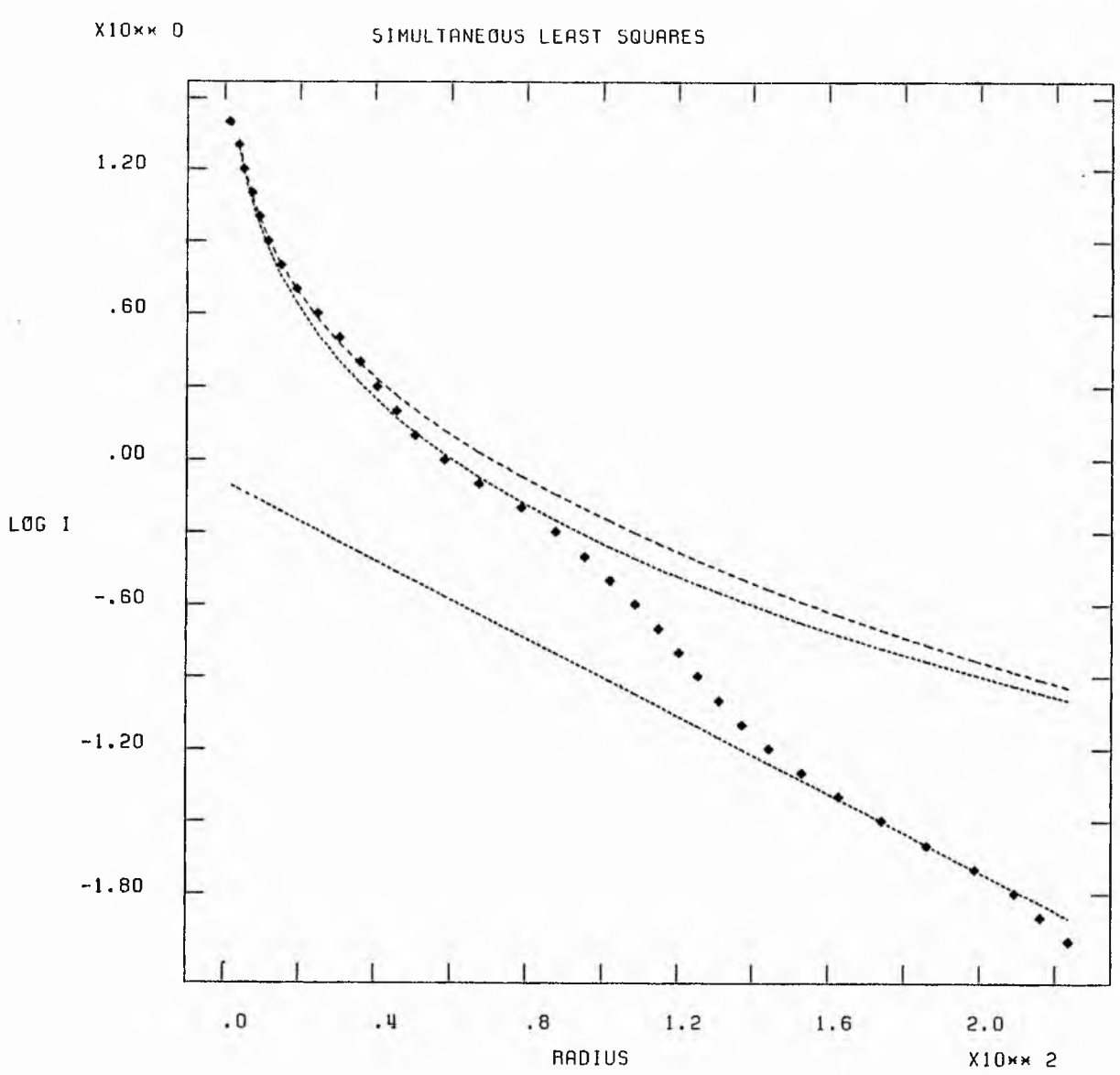
NGC 4501 R
SIMULTANEOUS LEAST SQUARES
X10** 0
1.20
.60
.00
LOG I
-.60
-1.20
-1.80
.0
.4
.8
1.2
1.6
2.0
RADIUS
X10** 2

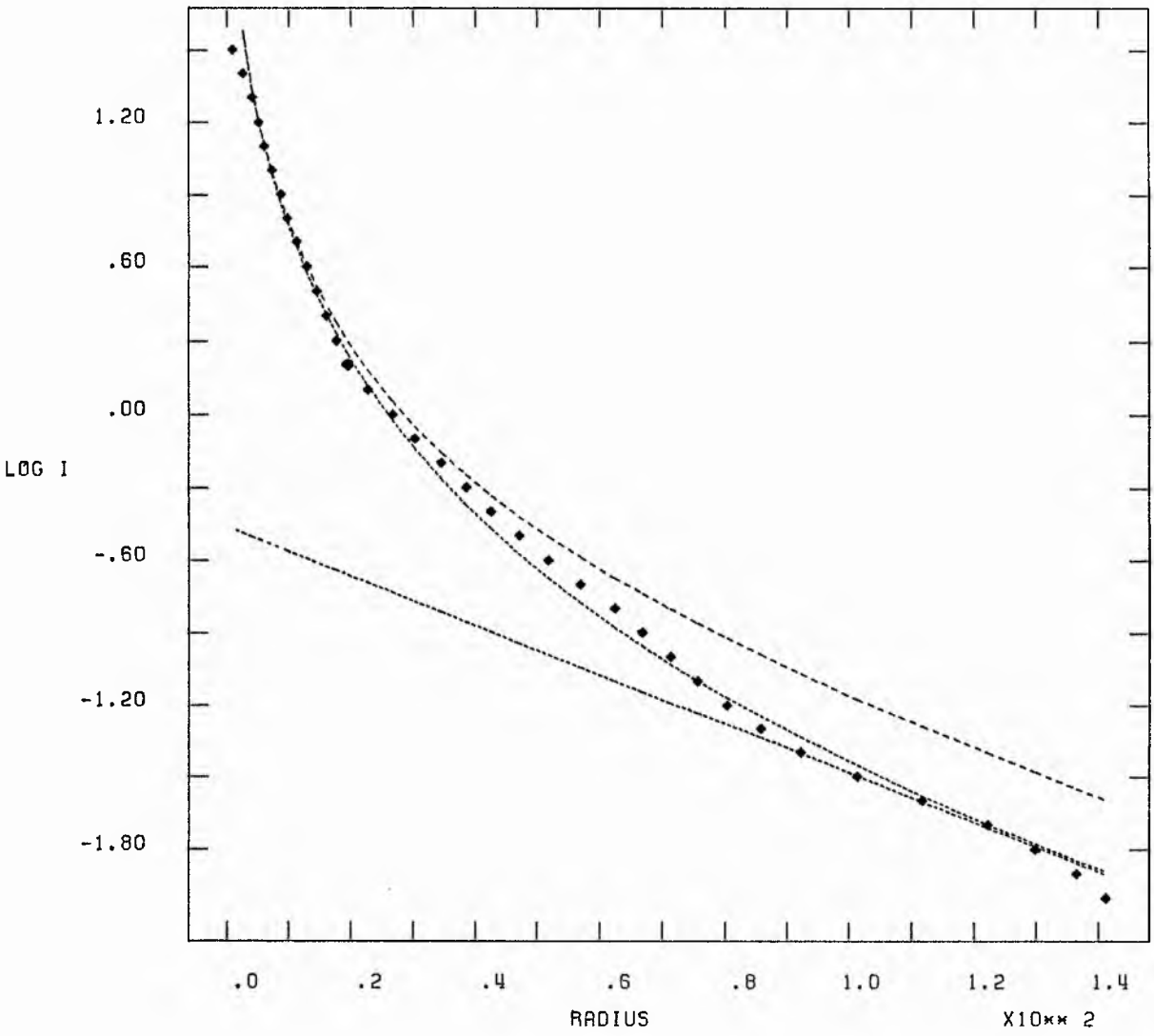
NGC 4503 R
SIMULTANEOUS LEAST SQUARES
X10** 0
1.20
.60
.00
LOG I
-.60
-1.20
-1.80
.0
.2
.4
.6
.8
1.0
1.2
1.4
RADIUS
X10** 2

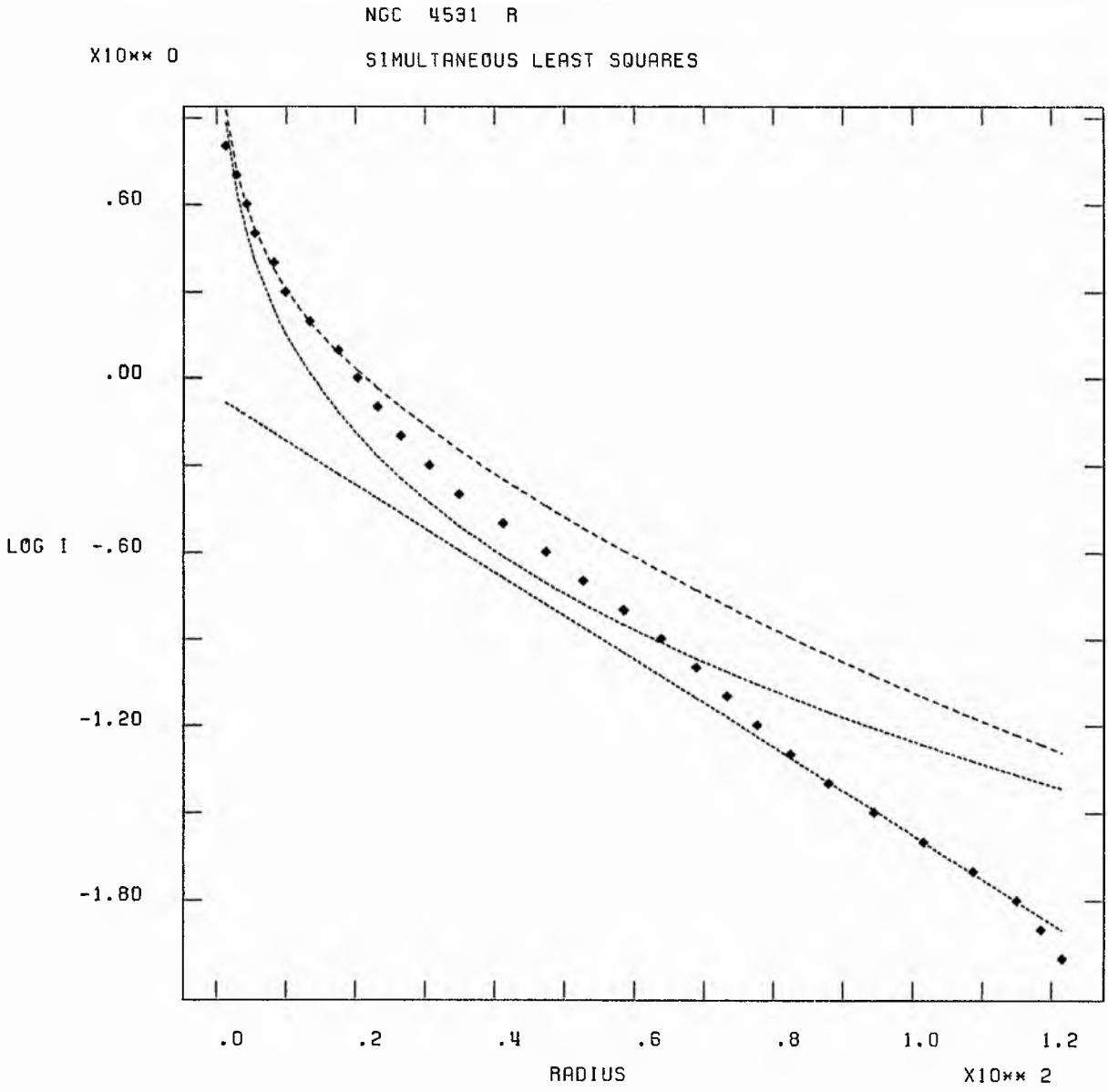
NGC 4531 R
X10** 0
SIMULTANEOUS LEAST SQUARES
.60
.00
LOG I -.60
-1.20
-1.80
.0
.2
.4
.6
.8
1.0
1.2
RADIUS
X10** 2

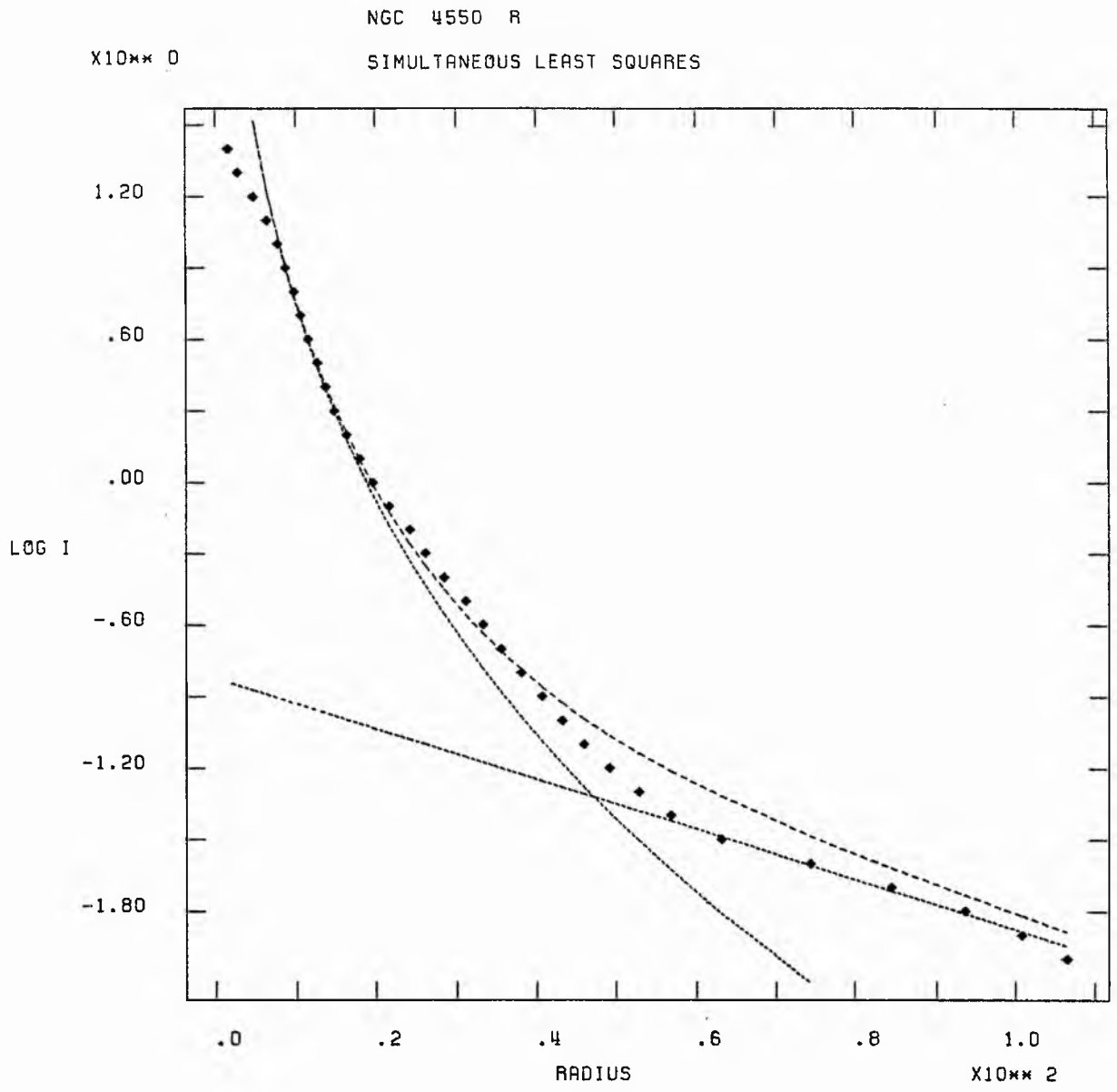
NGC 4550 R
SIMULTANEOUS LEAST SQUARES
X10** 0
1.20
.60
.00
LOG I
-.60
-1.20
-1.80
.0
.2
.4
.6
.8
1.0
RADIUS
X10** 2

NGC 4552 R

X10** 0

ITERATIVE FITTING.

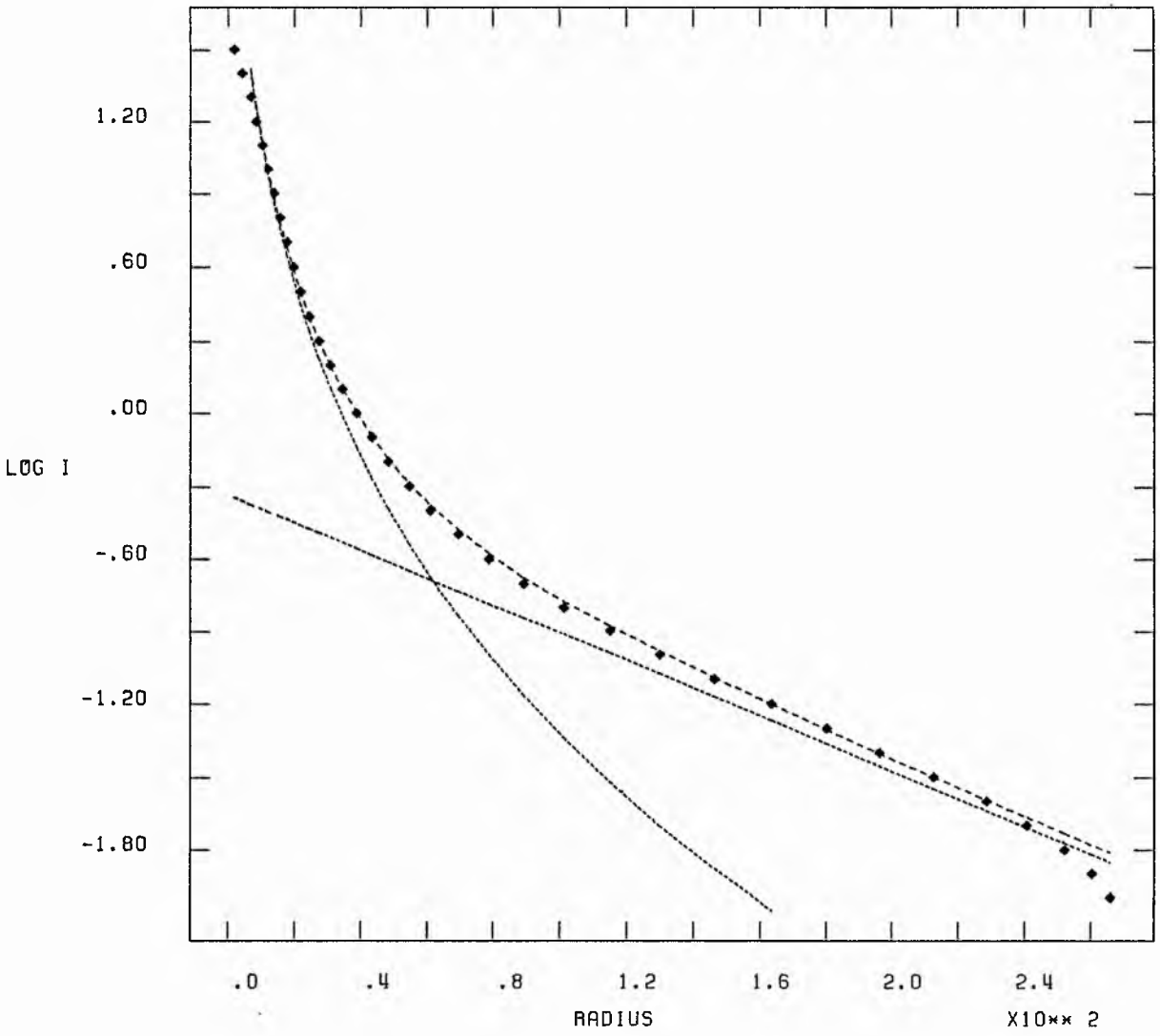

NGC 4552 R

SIMULTANEOUS LEAST SQUARES

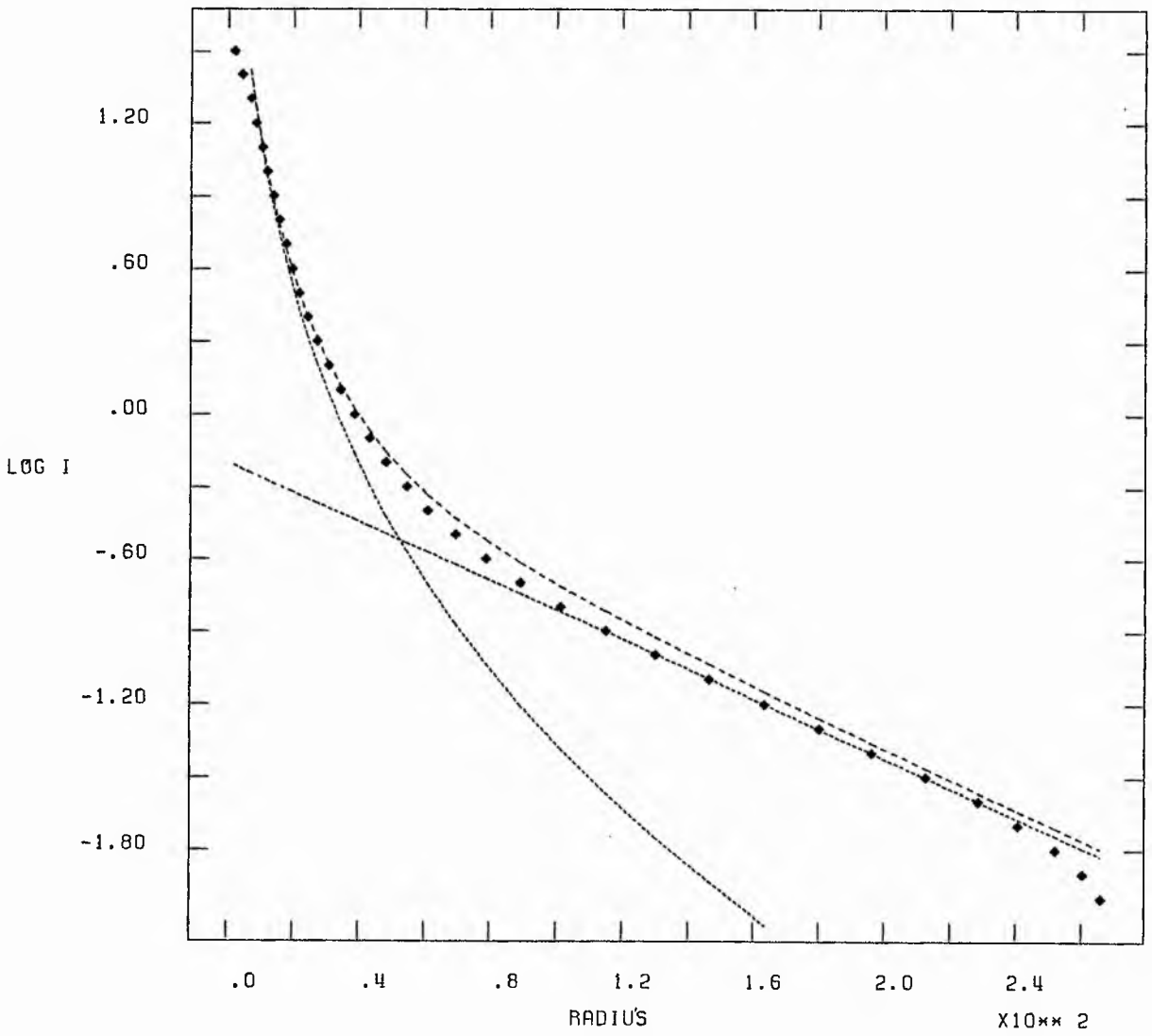

NGC 4267 I

ITERATIVE FITTING.

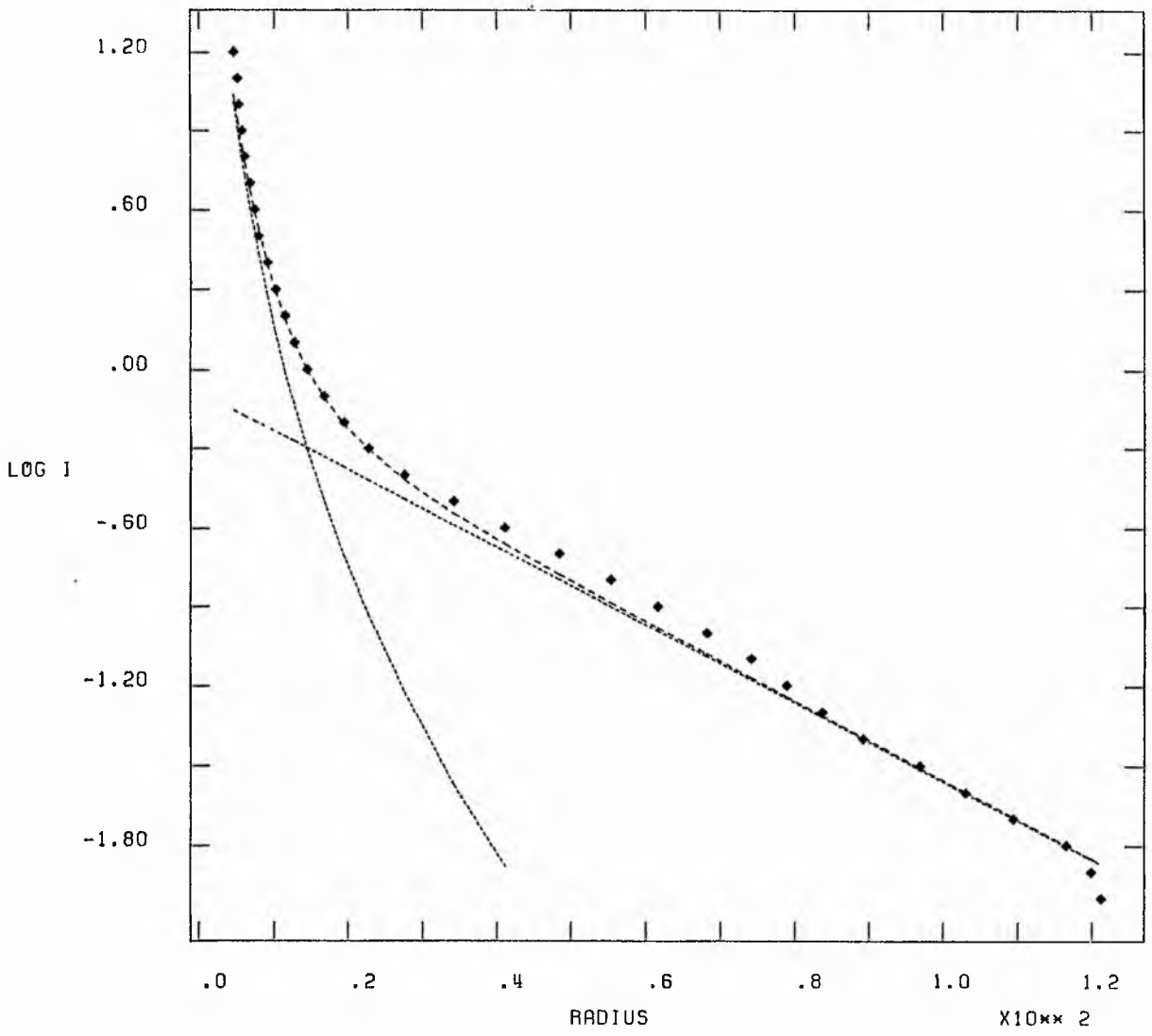

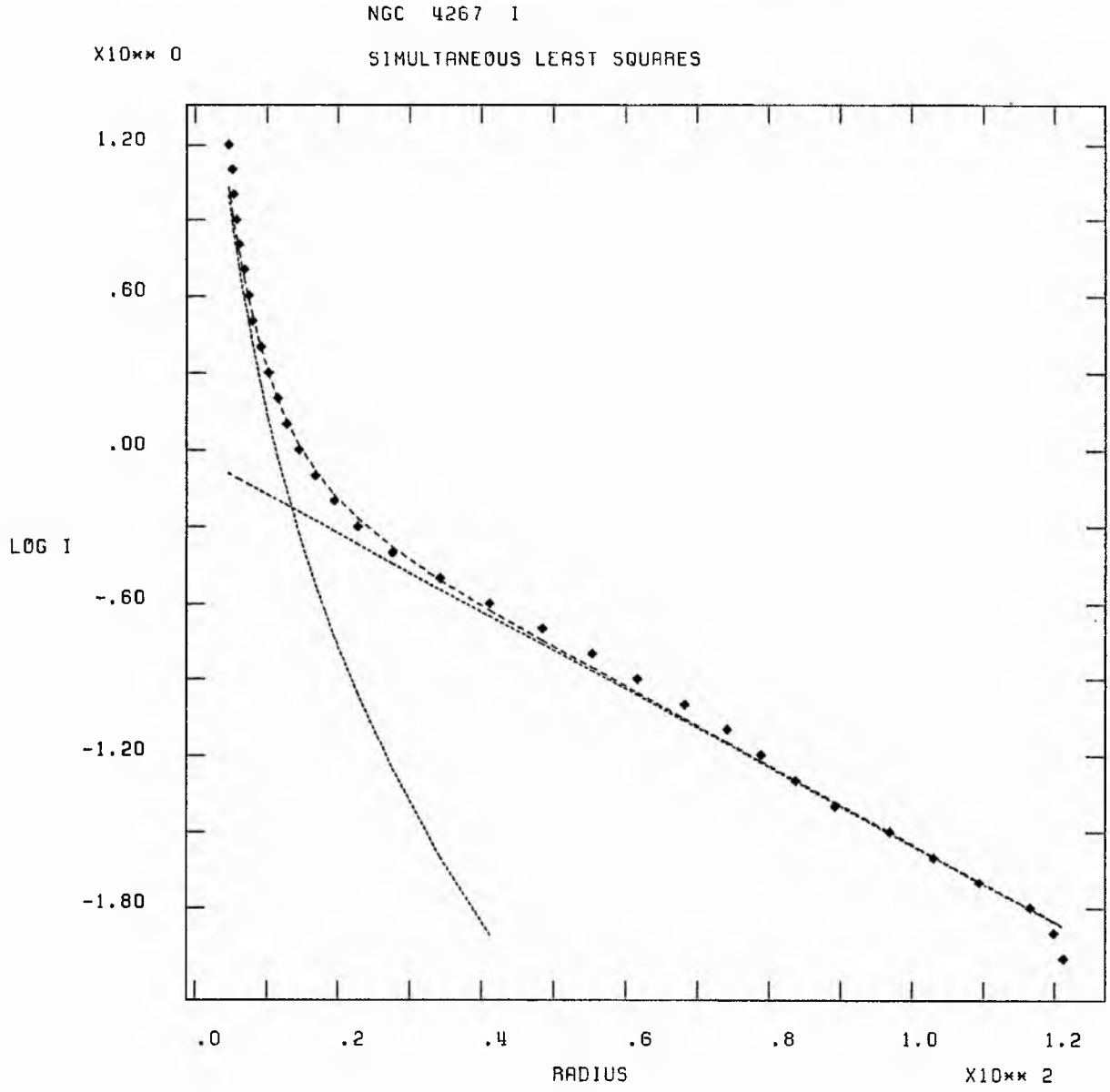
NGC 4267 I
SIMULTANEOUS LEAST SQUARES
X10** 0
1.20
.60
.00
LOG I
-.60
-1.20
-1.80
.0
.2
.4
.6
.8
1.0
1.2
RADIUS
X10** 2

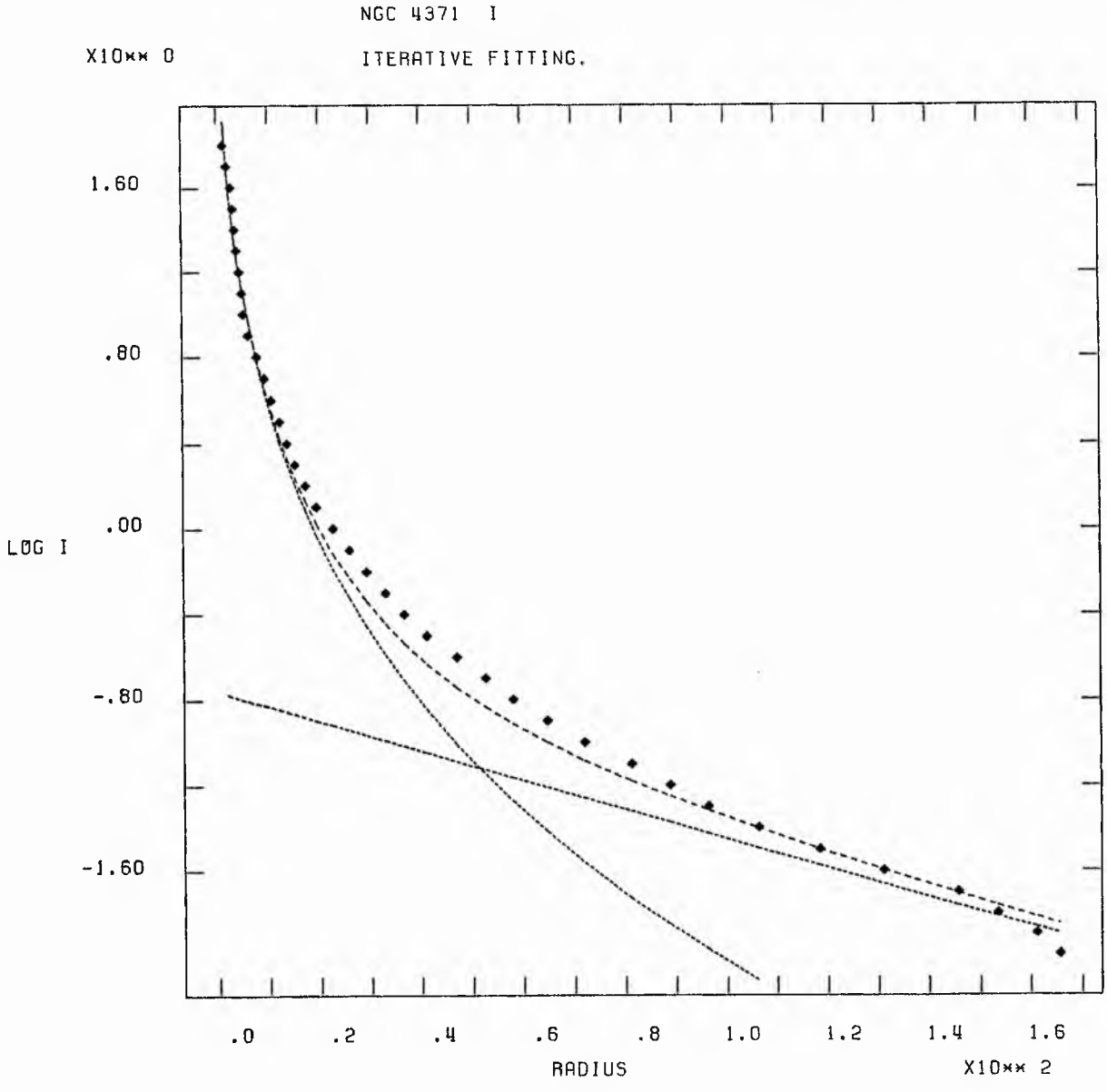
NGC 4371 I
ITERATIVE FITTING.
X10** 0
1.60
.80
.00
-.80
-1.60
LOG I
.0
.2
.4
.6
.8
1.0
1.2
1.4
1.6
RADIUS
X10** 2

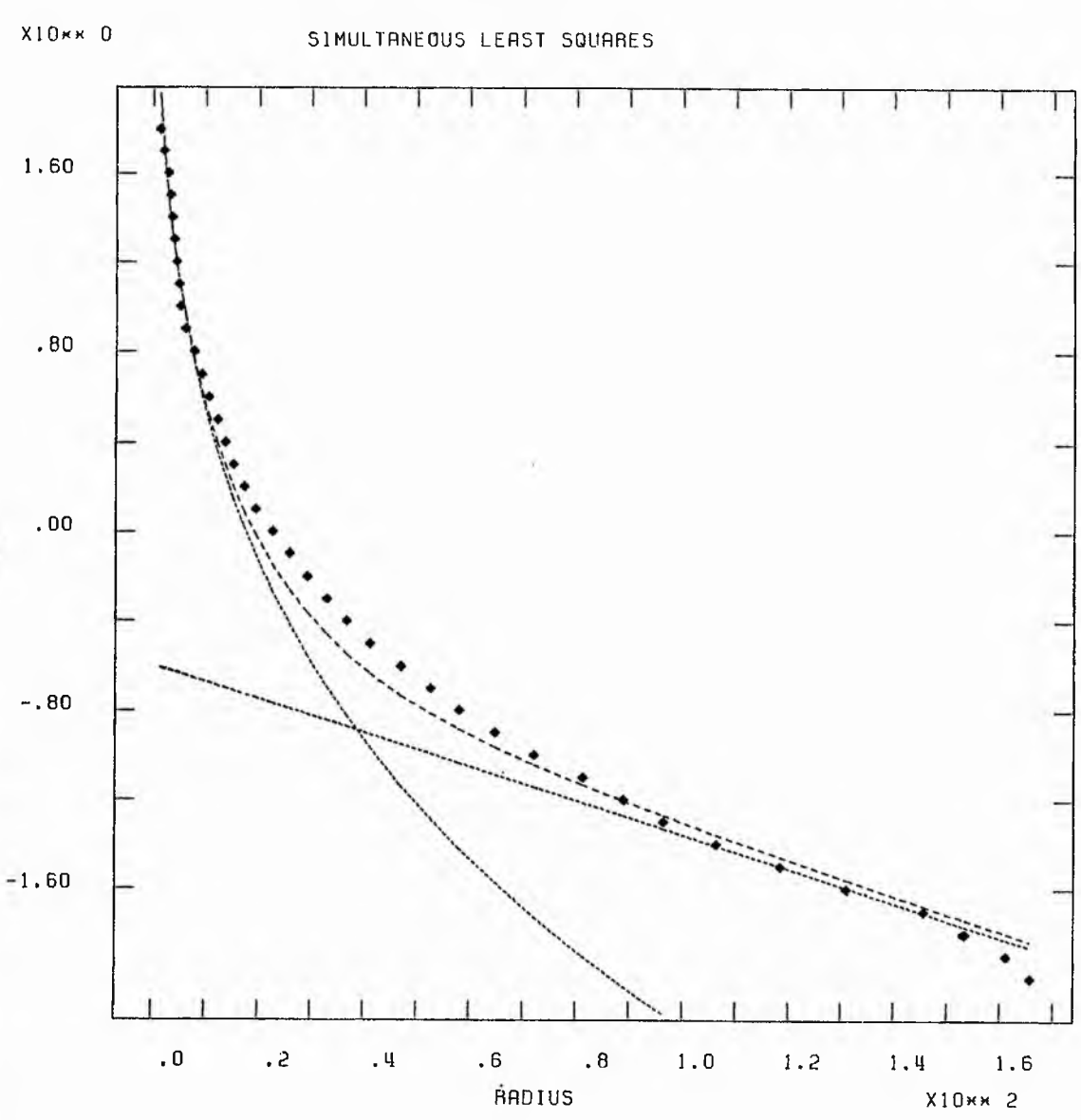
NGC 4371 I
SIMULTANEOUS LEAST SQUARES
X10** 0
1.60
.80
.00
-.80
-1.60
LOG I
.0
.2
.4
.6
.8
1.0
1.2
1.4
1.6
RADIUS
X10** 2

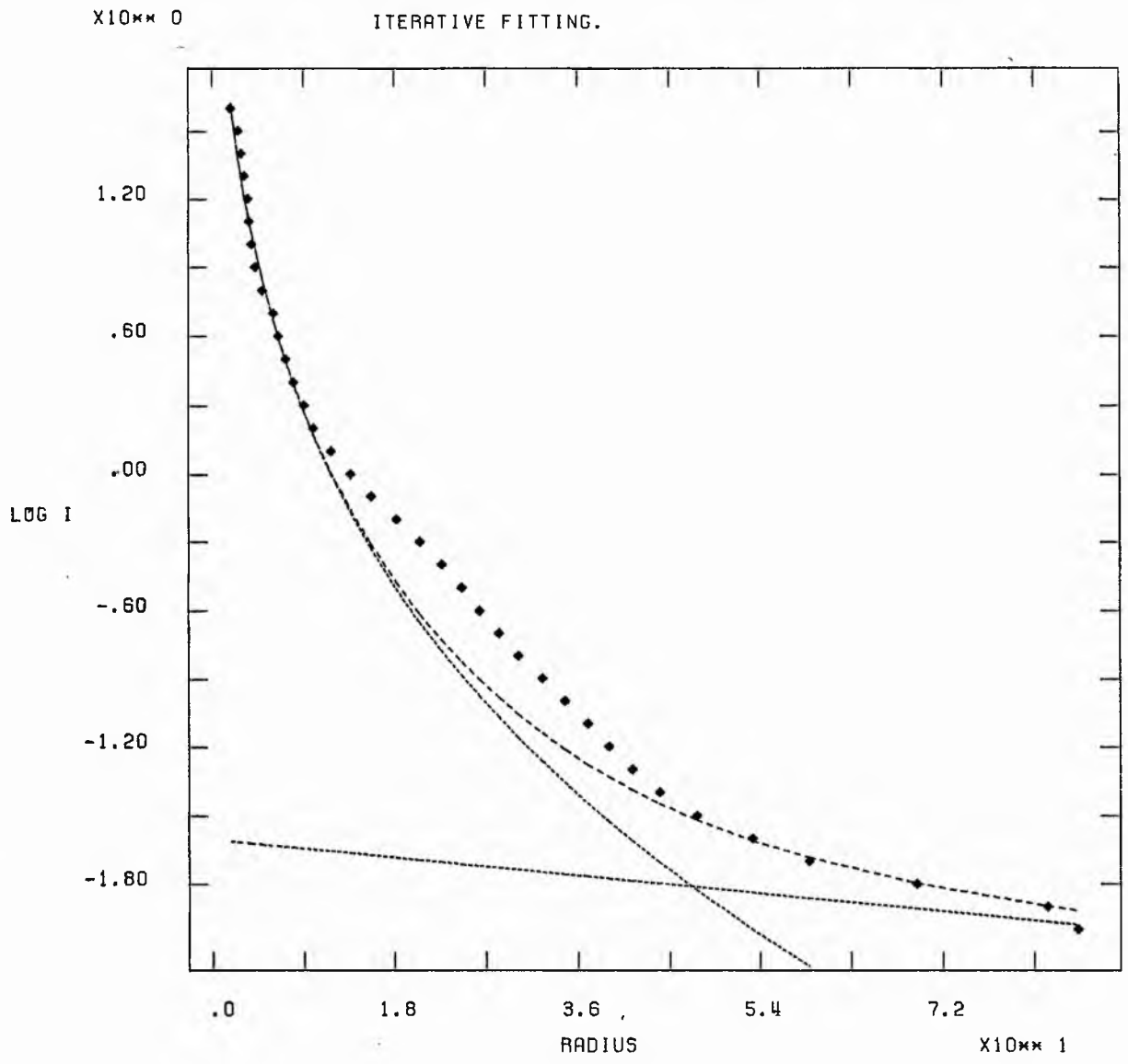
NGC 4377 I
ITERATIVE FITTING.
X10** 0
1.20
.60
.00
LOG I
-.60
-1.20
-1.80
.0
1.8
3.6
5.4
7.2
RADIUS
X10** 1

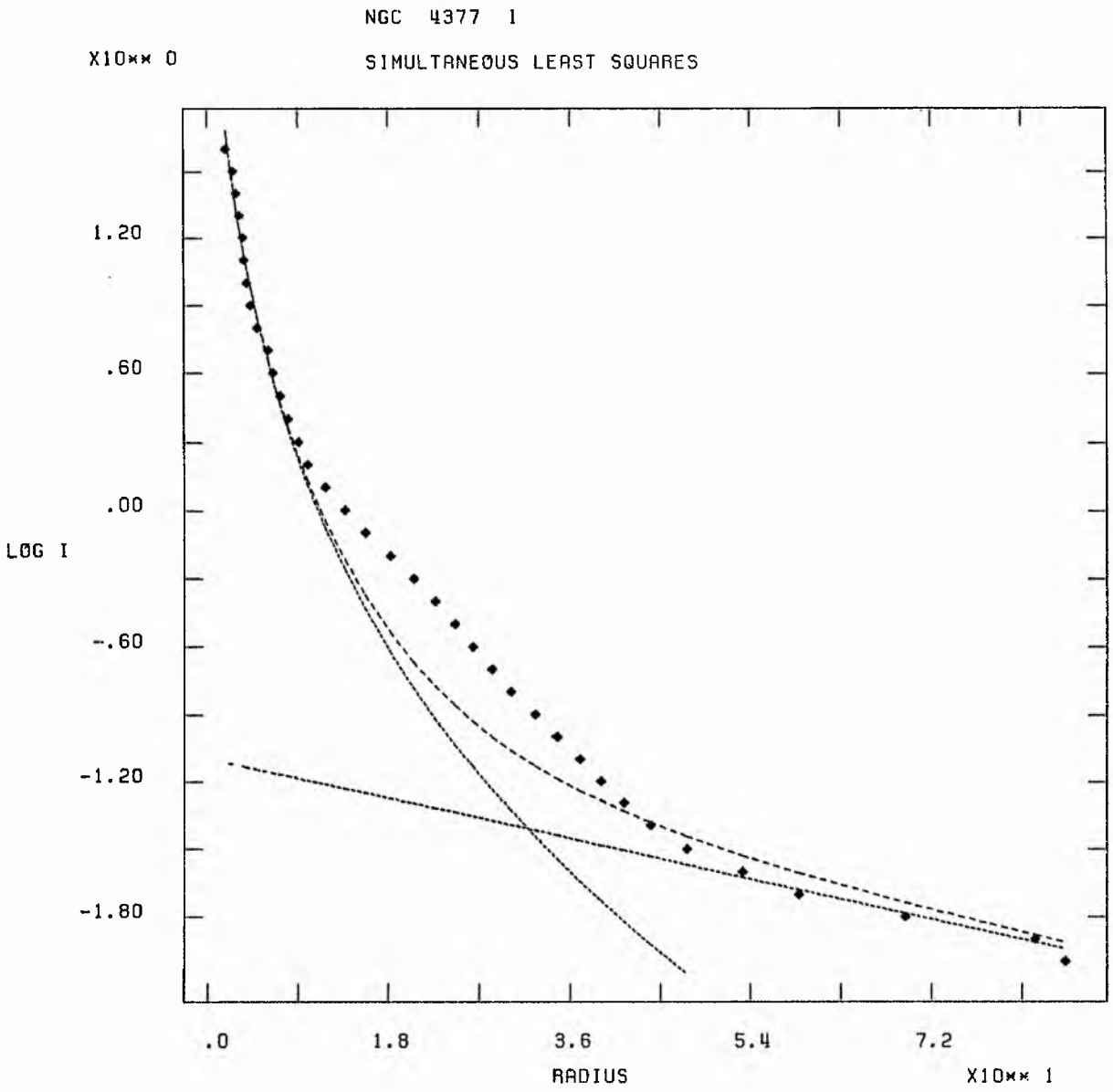
NGC 4377 I
SIMULTANEOUS LEAST SQUARES
X10** 0
1.20
.60
.00
LOG I
-.60
-1.20
-1.80
.0
1.8
3.6
5.4
7.2
RADIUS
X10** 1

NGC 4419 I

ITERATIVE FITTING.

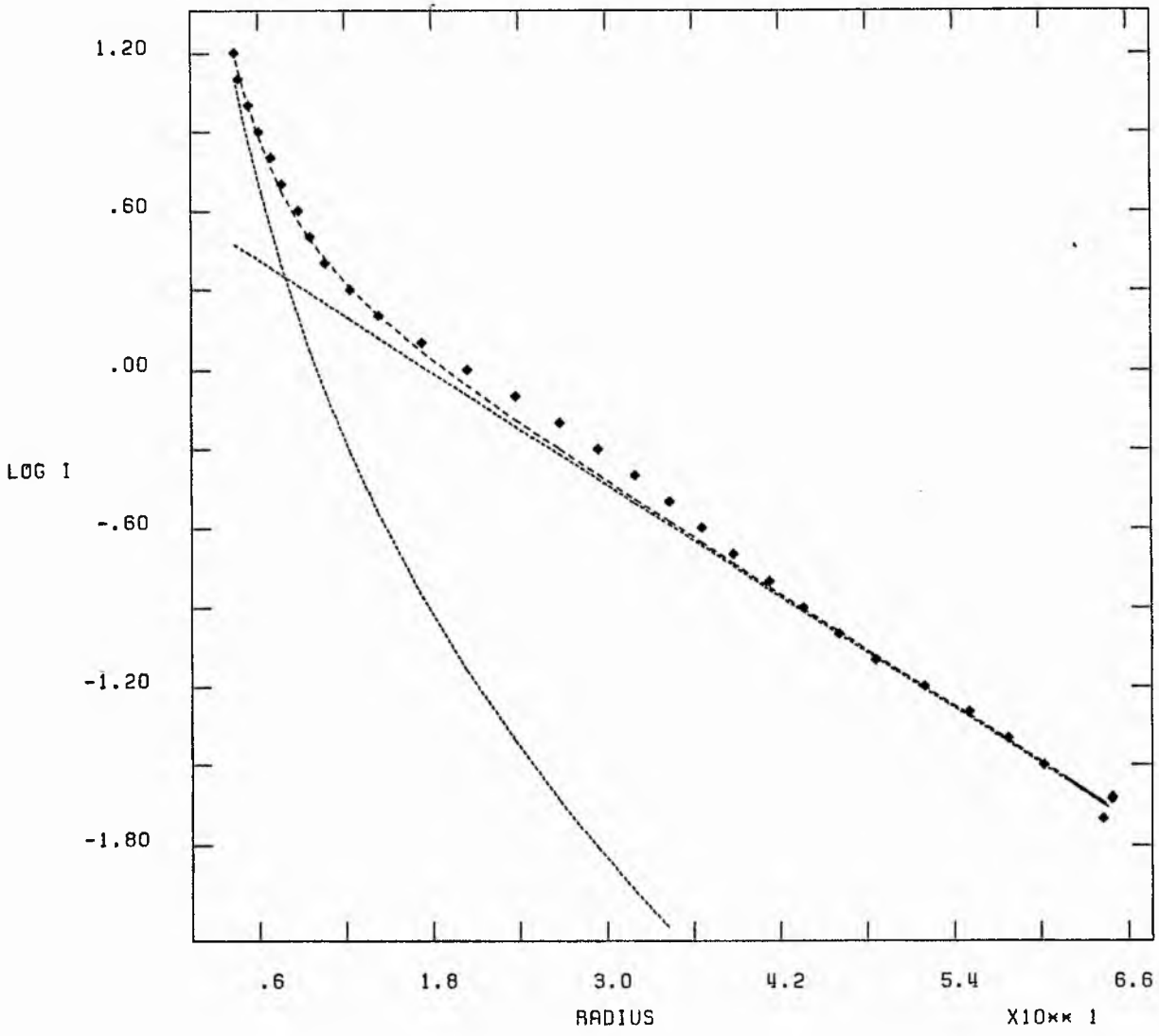

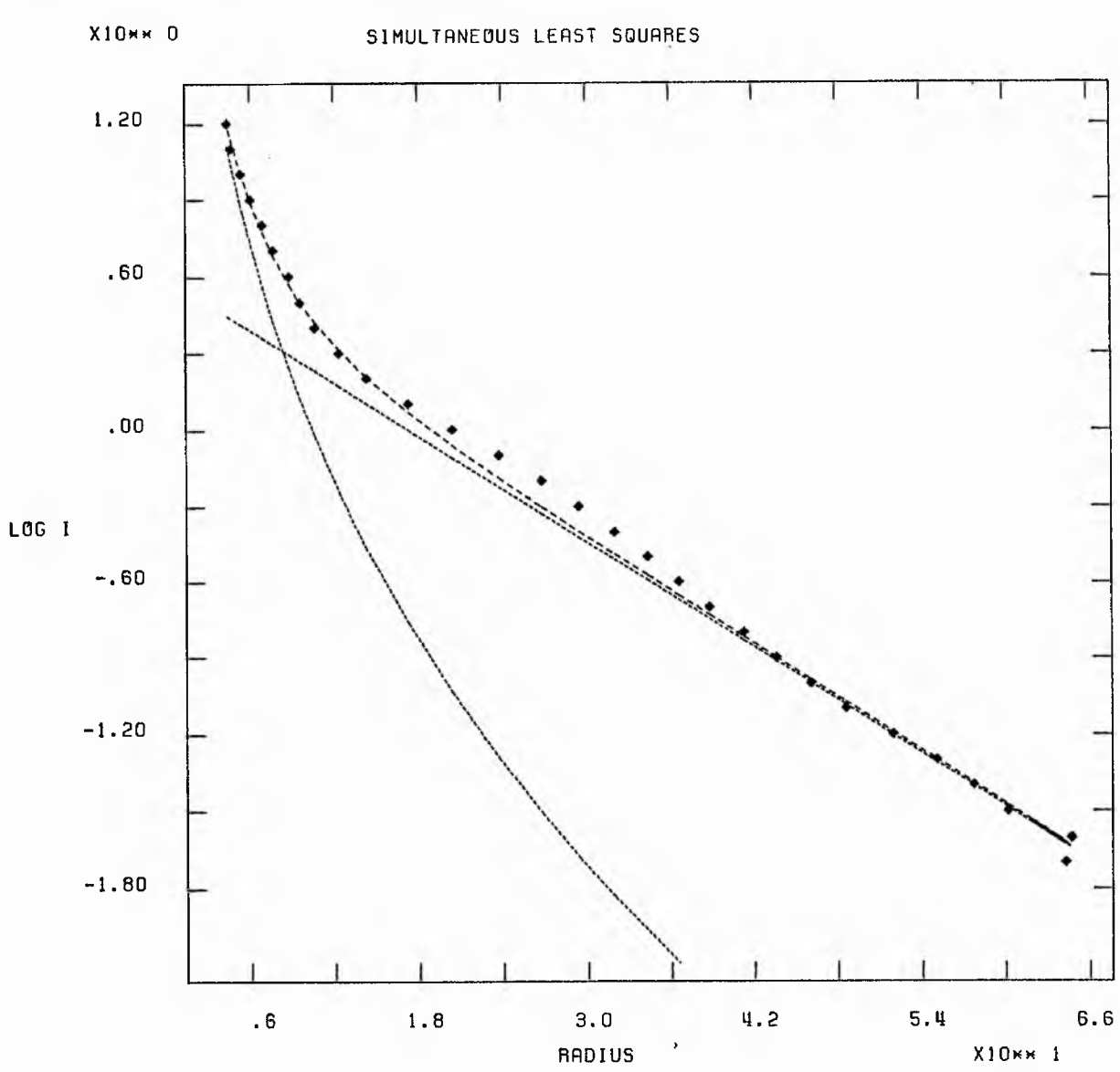
NGC 4419 I
SIMULTANEOUS LEAST SQUARES
X10** 0
1.20
.60
.00
LOG I
-.60
-1.20
-1.80
.6
1.8
3.0
4.2
5.4
6.6
RADIUS
X10** 1

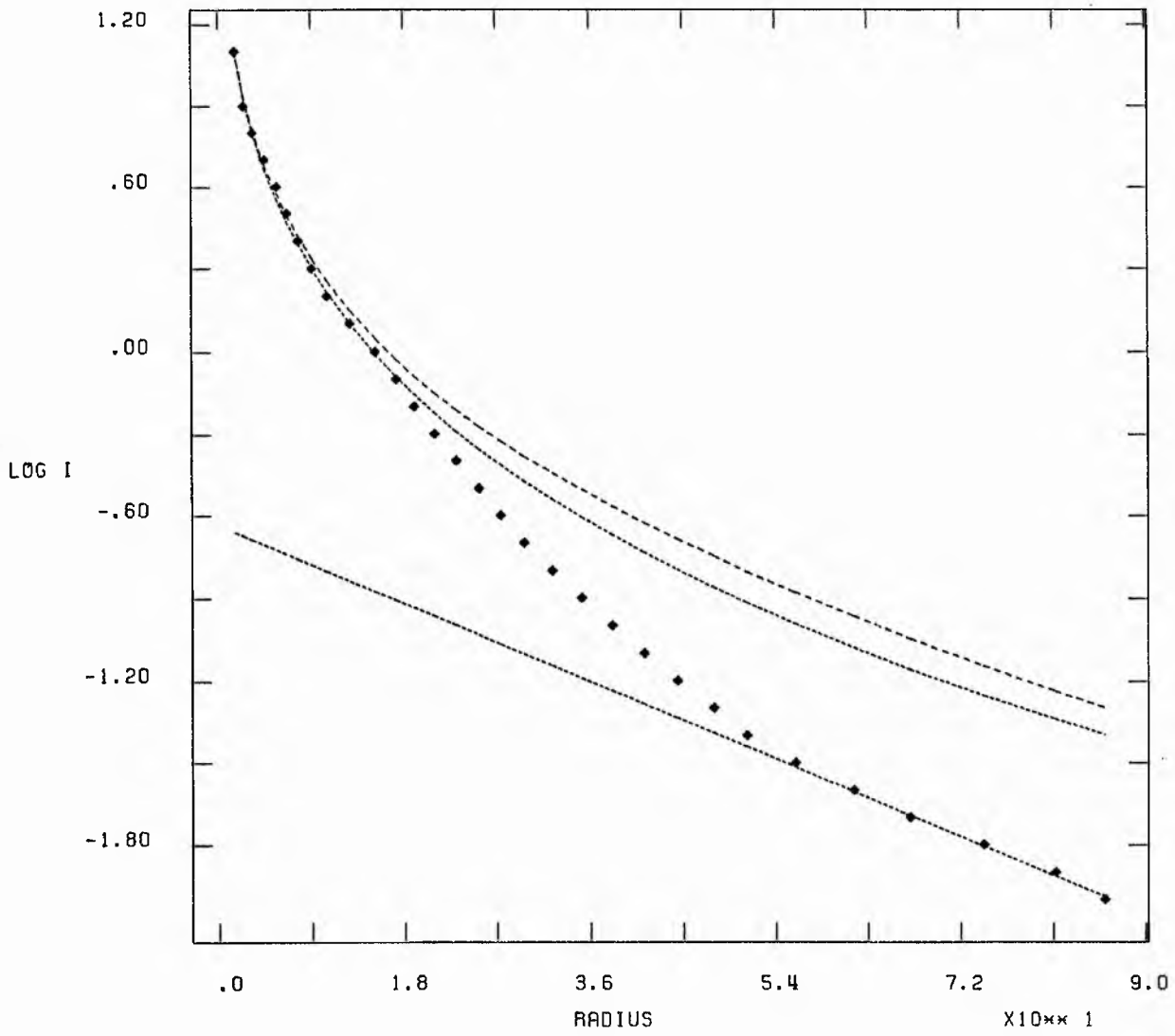
NGC 4425 I
SIMULTANEOUS LEAST SQUARES
X10** 0
1.20
.60
.00
LOG I
-.60
-1.20
-1.80
.0
1.8
3.6
5.4
7.2
9.0
RADIUS
X10** 1

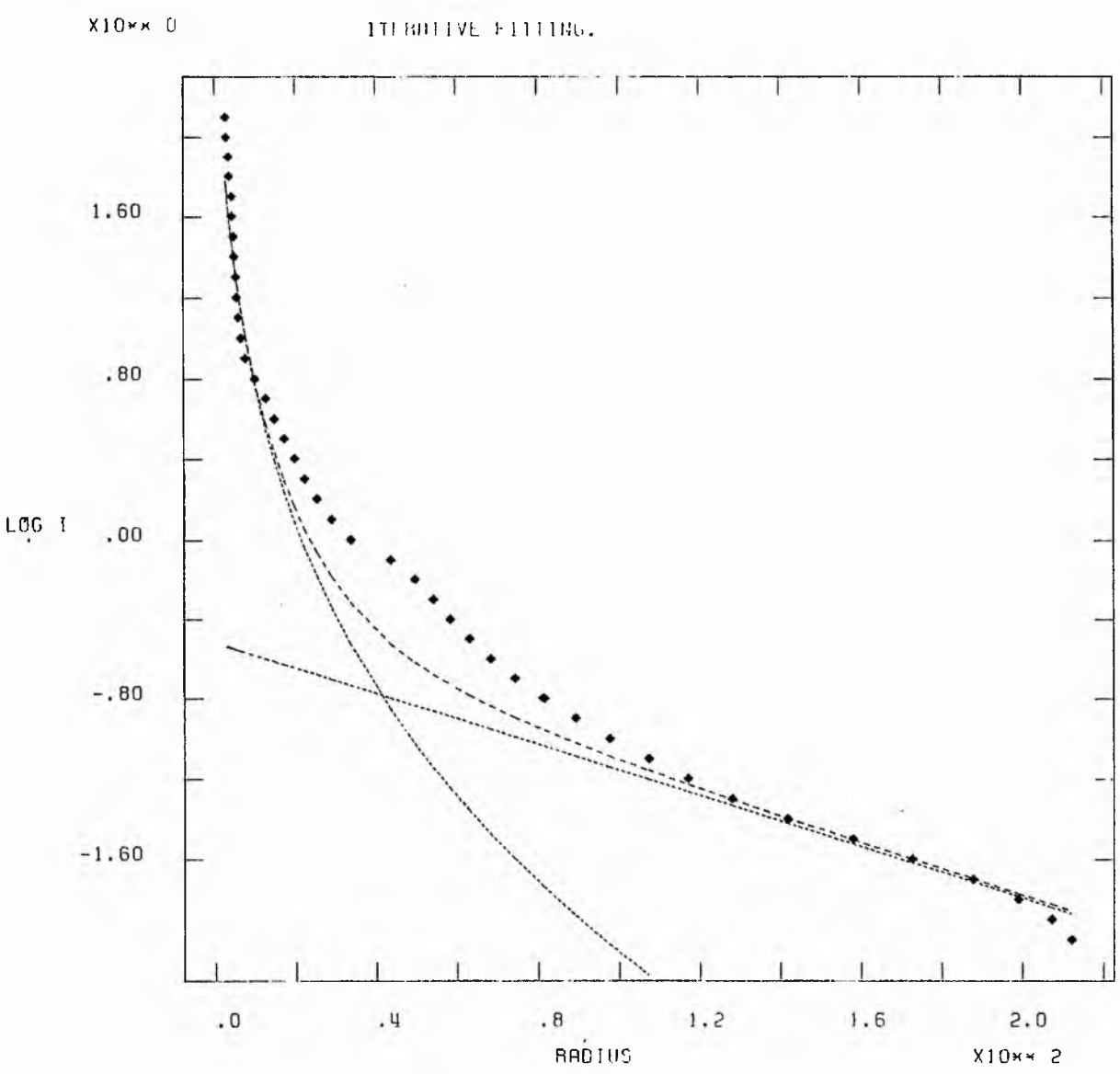
NGC 4929 I
X10** 0
ITERATIVE FITTING.
1.60
.80
LOG I
.00
-.80
-1.60
.0
.4
.8
1.2
1.6
2.0
RADIUS
X10** 2

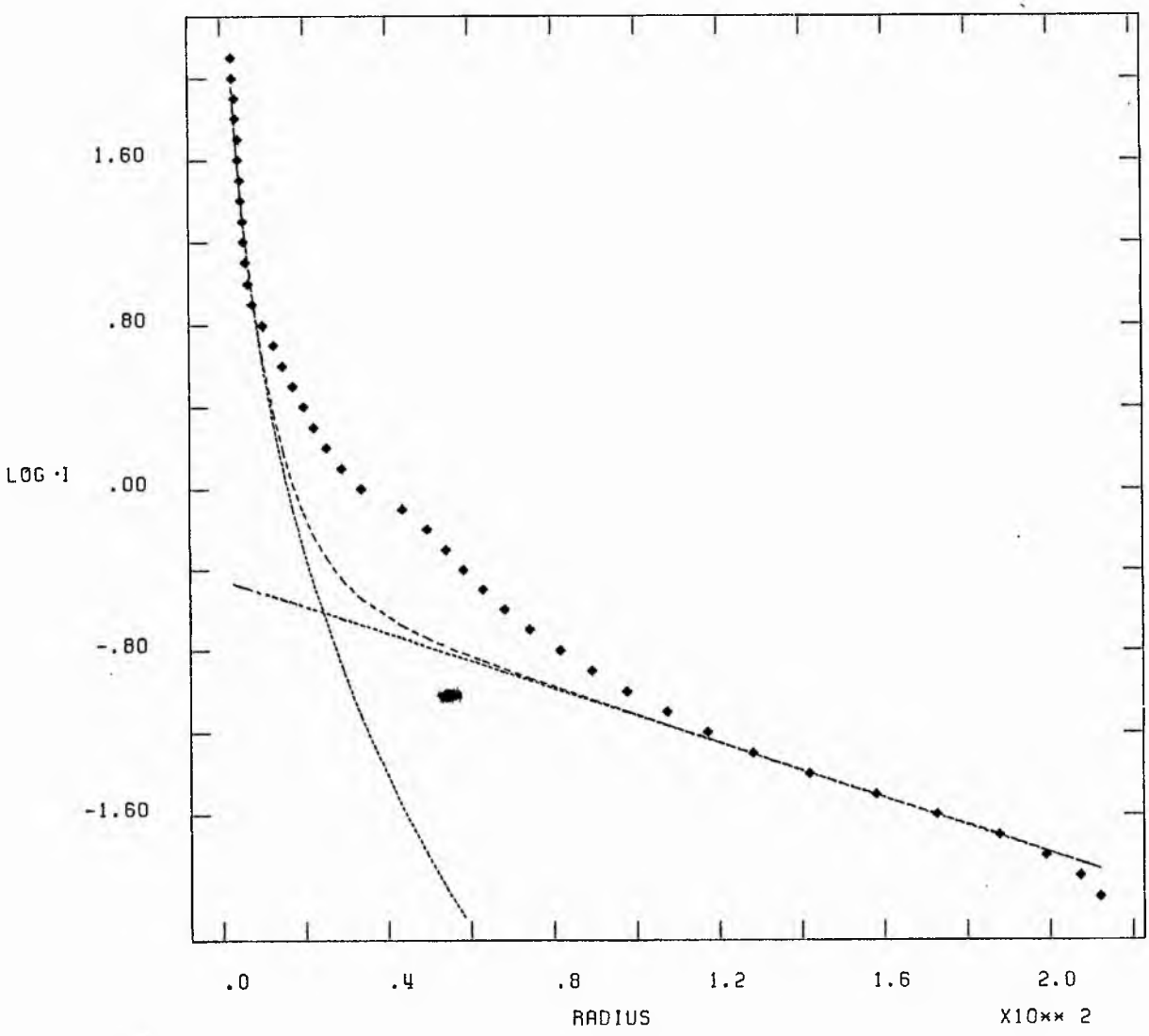
NGC 4429 1
SIMULTANEOUS LEAST SQUARES
X10** 0
1.60
.80
LOG I
.00
-.80
-1.60
.0
.4
.8
1.2
1.6
2.0
RADIUS
X10** 2

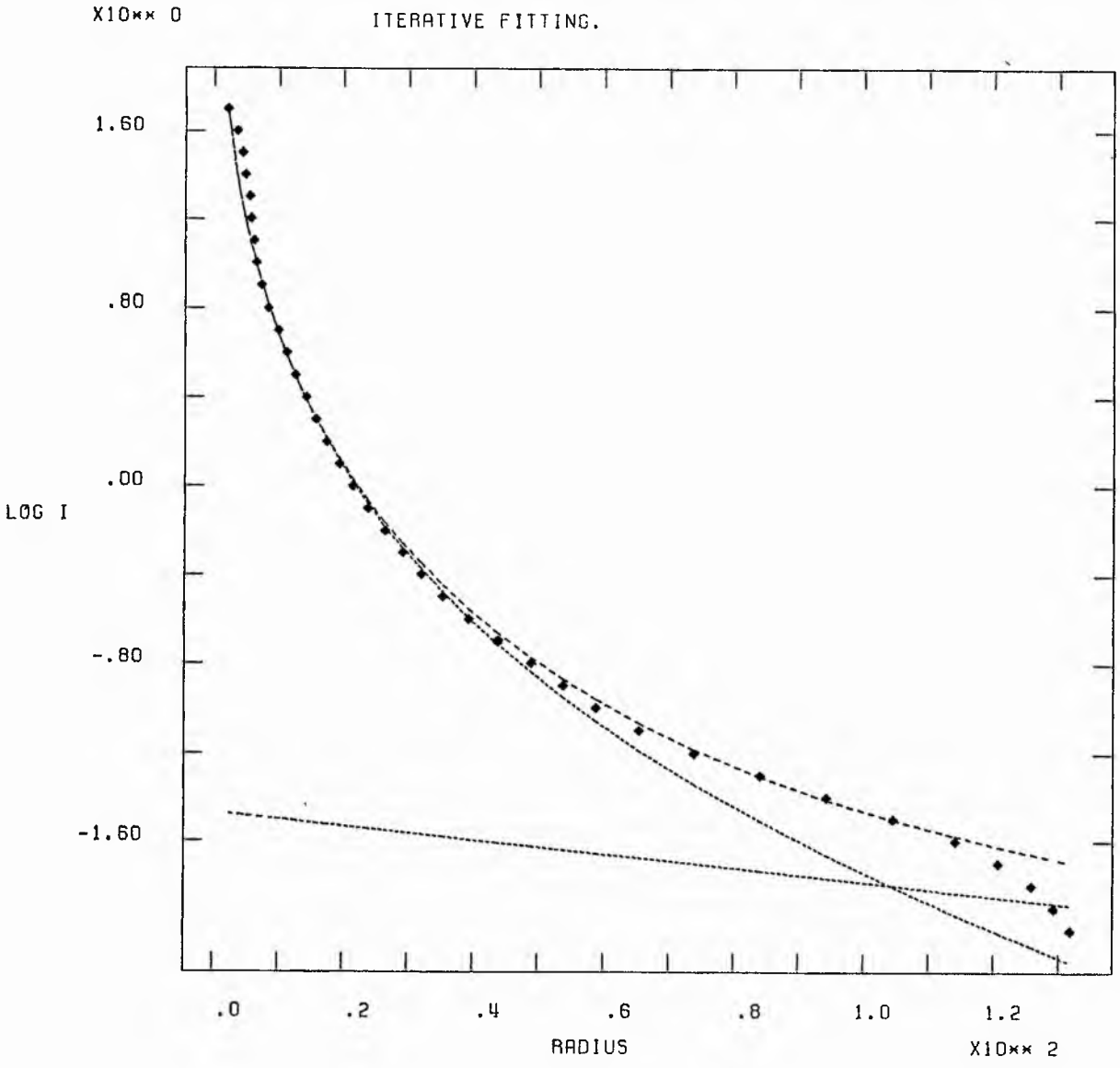
NGC 4435 I
ITERATIVE FITTING.
X10** 0
1.60
.80
.00
-.80
-1.60
LOG I
.0
.2
.4
.6
.8
1.0
1.2
RADIUS
X10** 2

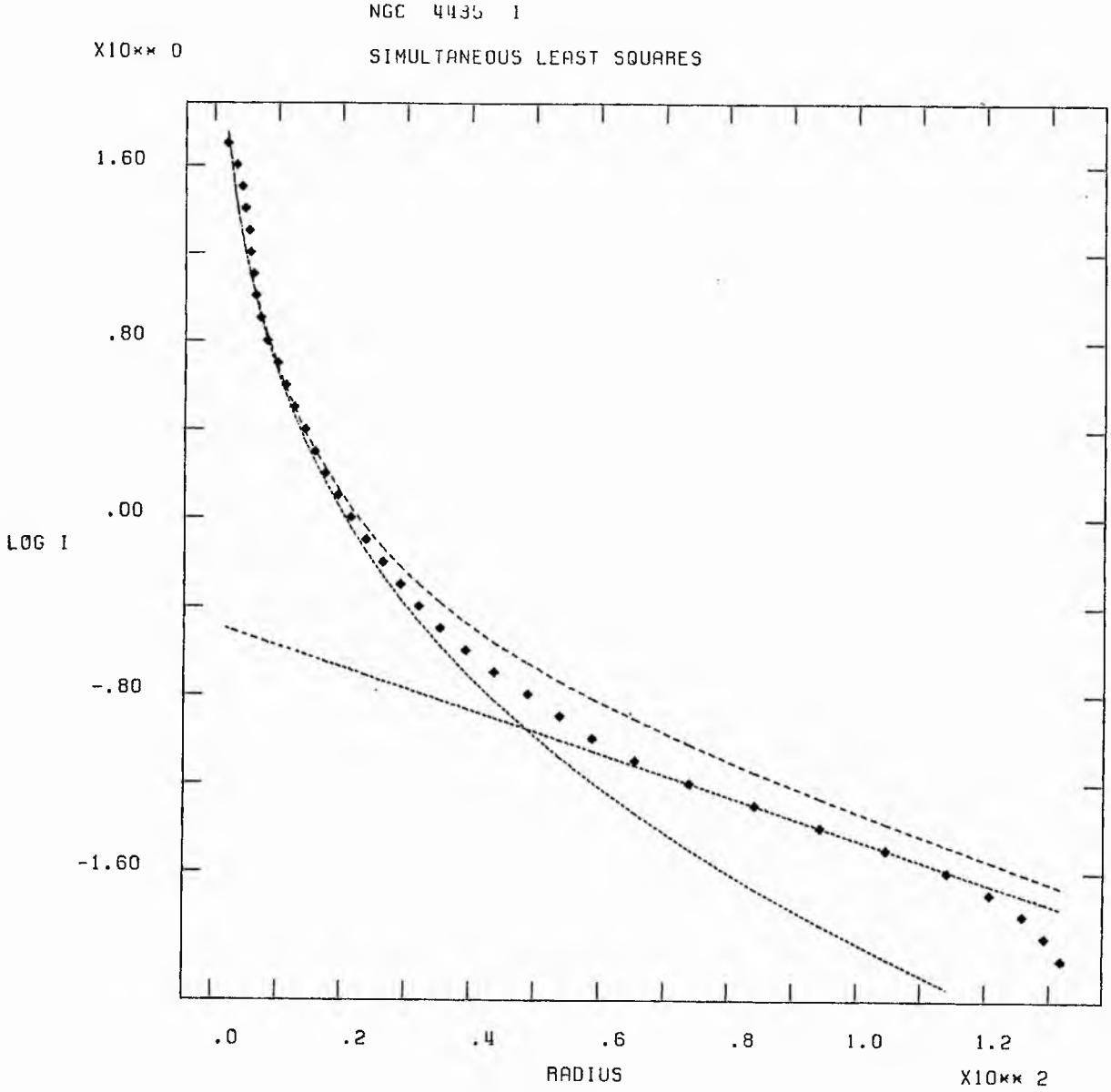
NGC 4435 I
SIMULTANEOUS LEAST SQUARES
X10** 0
1.60
.80
.00
LOG I
-.80
-1.60
.0
.2
.4
.6
.8
1.0
1.2
RADIUS
X10** 2

NGC 4438 I

SIMULTANEOUS LEAST SQUARES

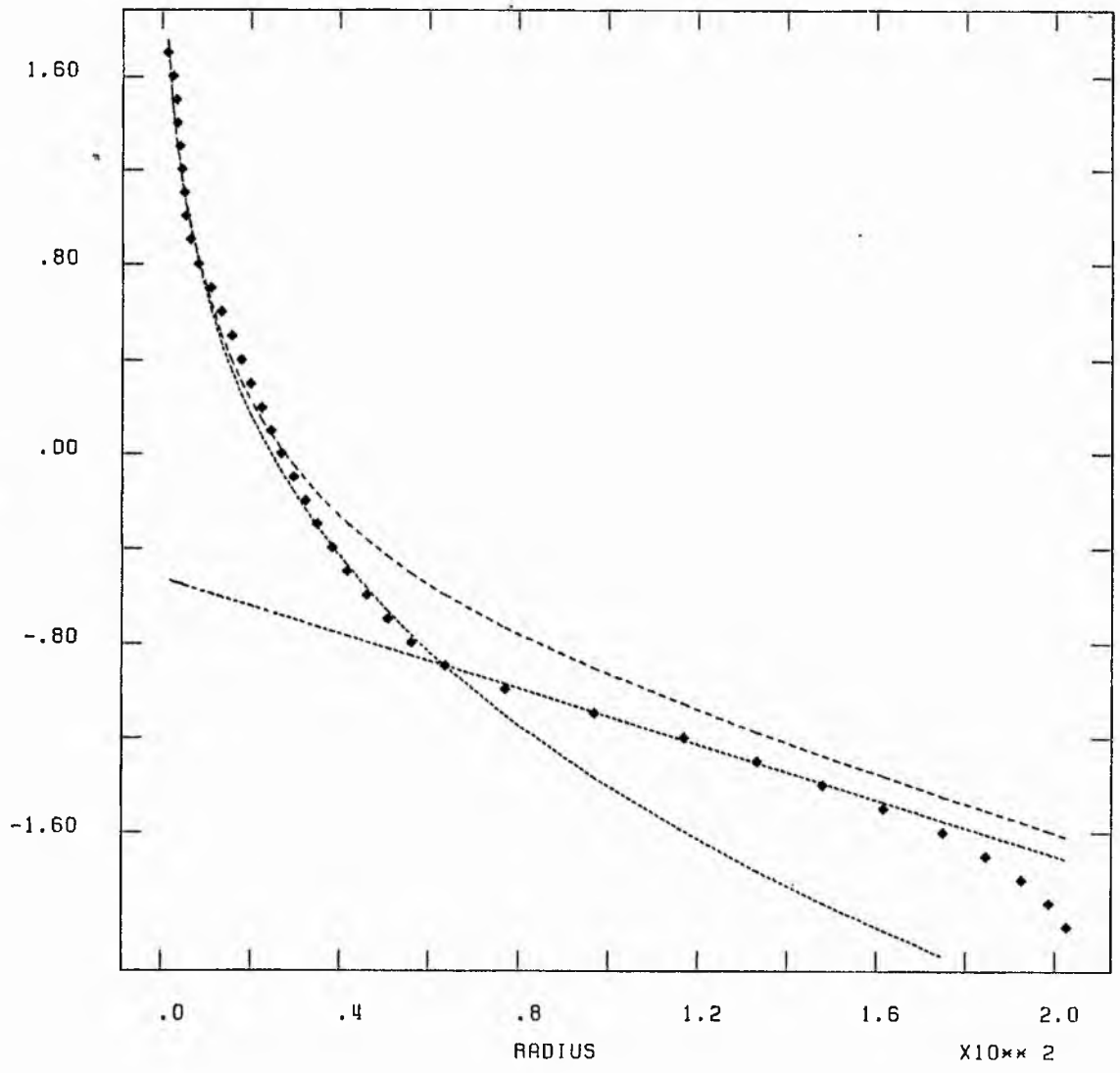

0G I

NGC 4459 1

ITERATIVE FITTING.

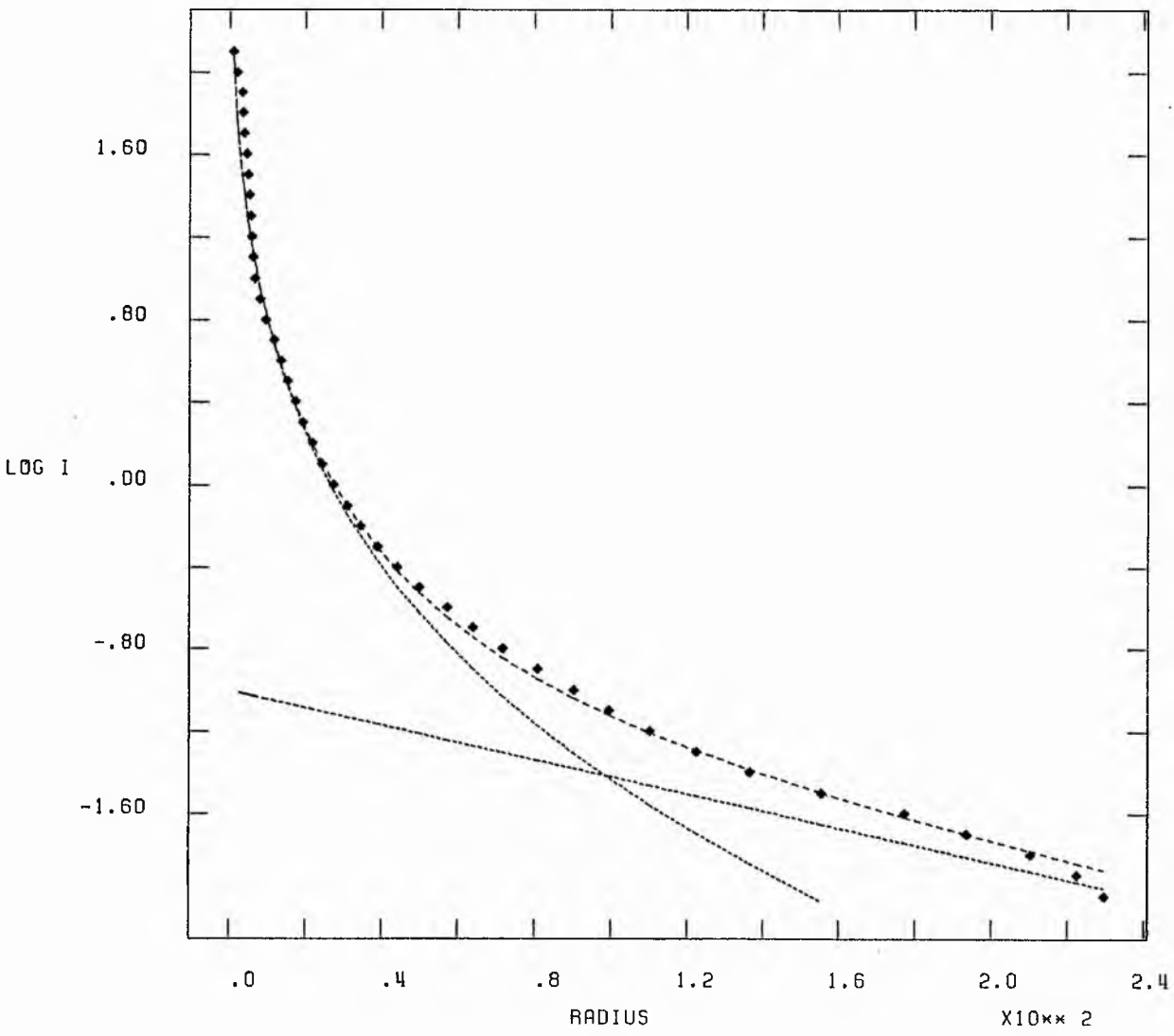

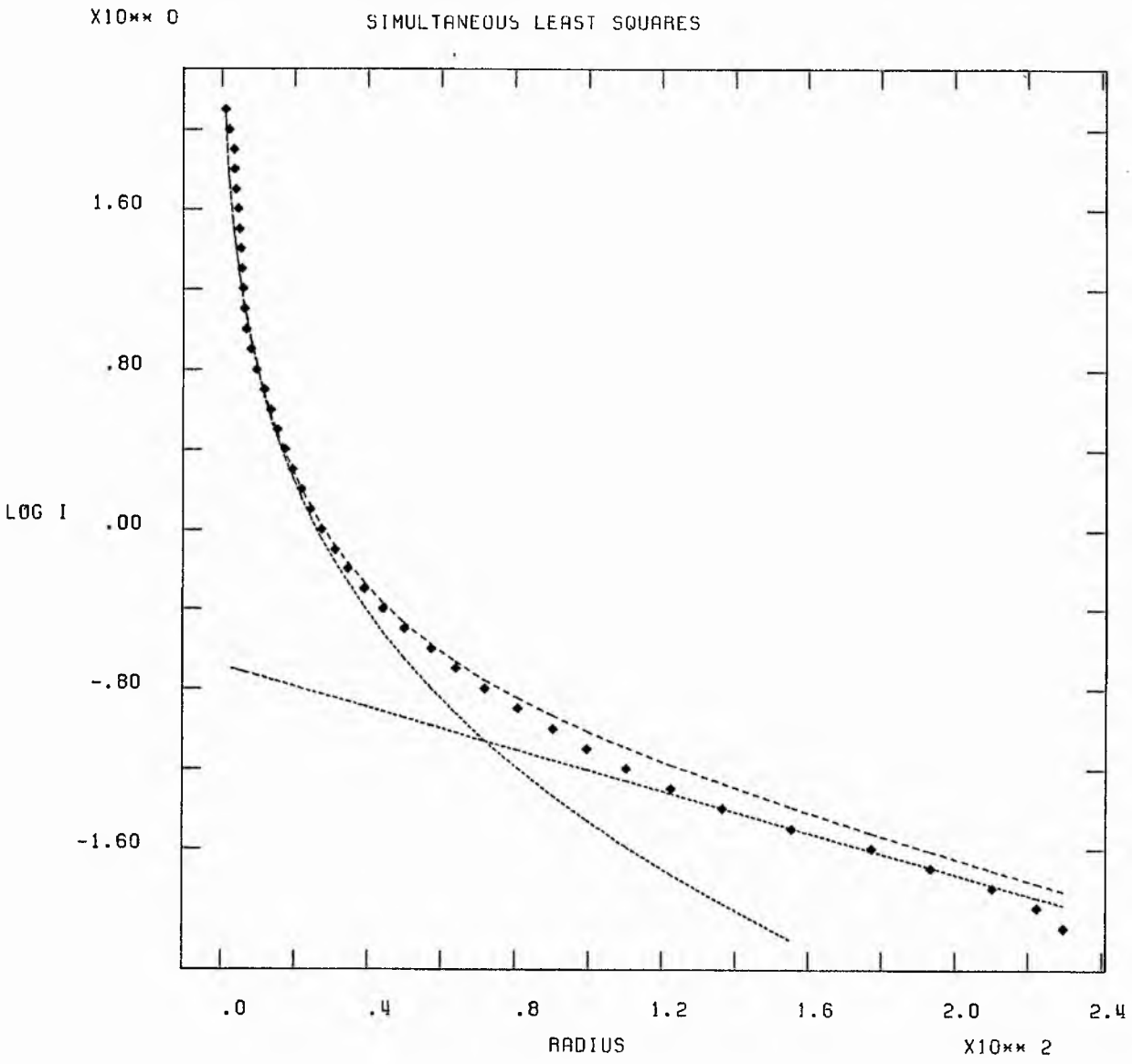
NGC 4459 I
SIMULTANEOUS LEAST SQUARES
X10** 0
1.60
.80
LOG I
.00
-.80
-1.60
.0
.4
.8
1.2
1.6
2.0
2.4
RADIUS
X10** 2

NGC 4461 1

ITERATIVE FITTING.

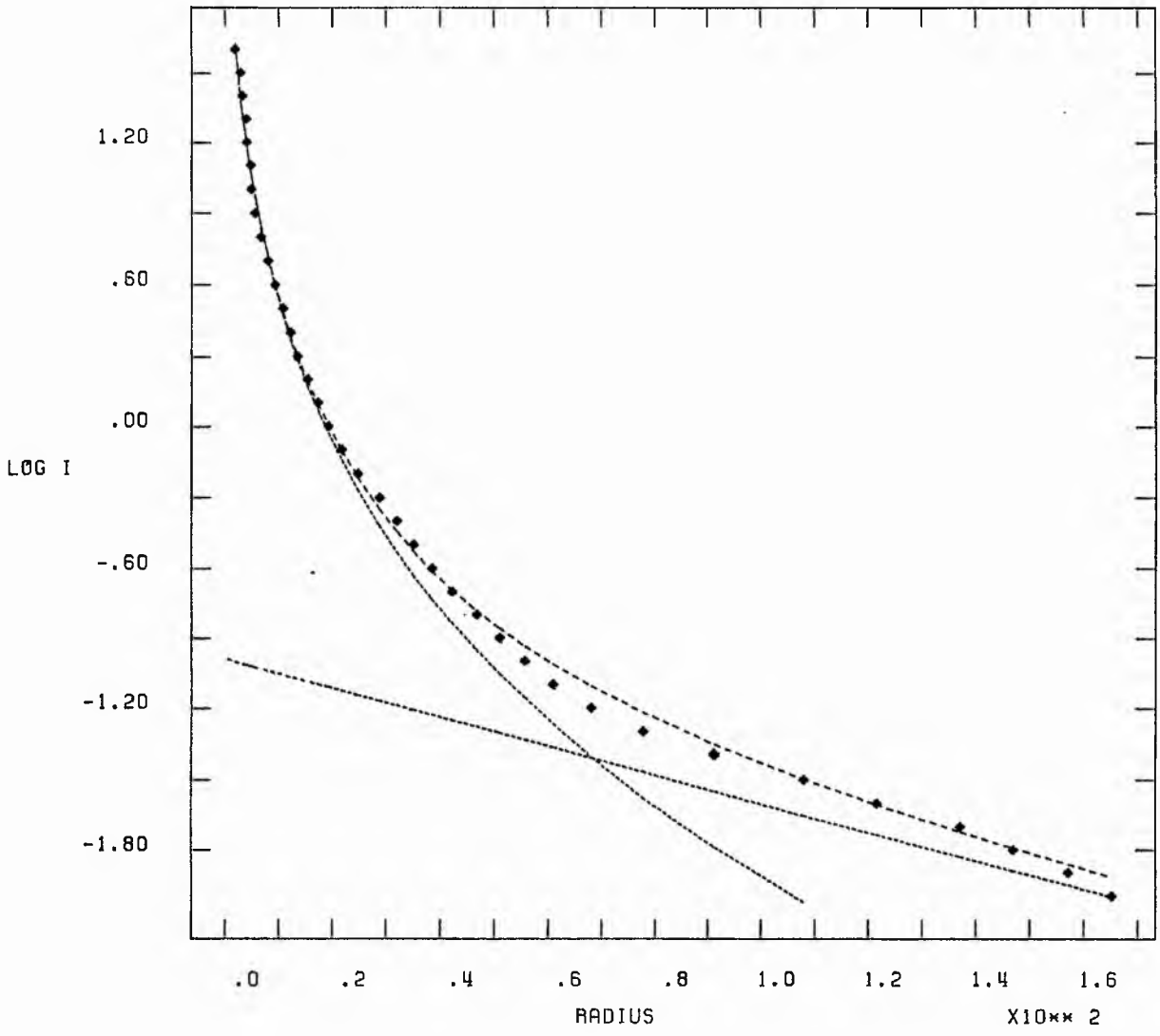

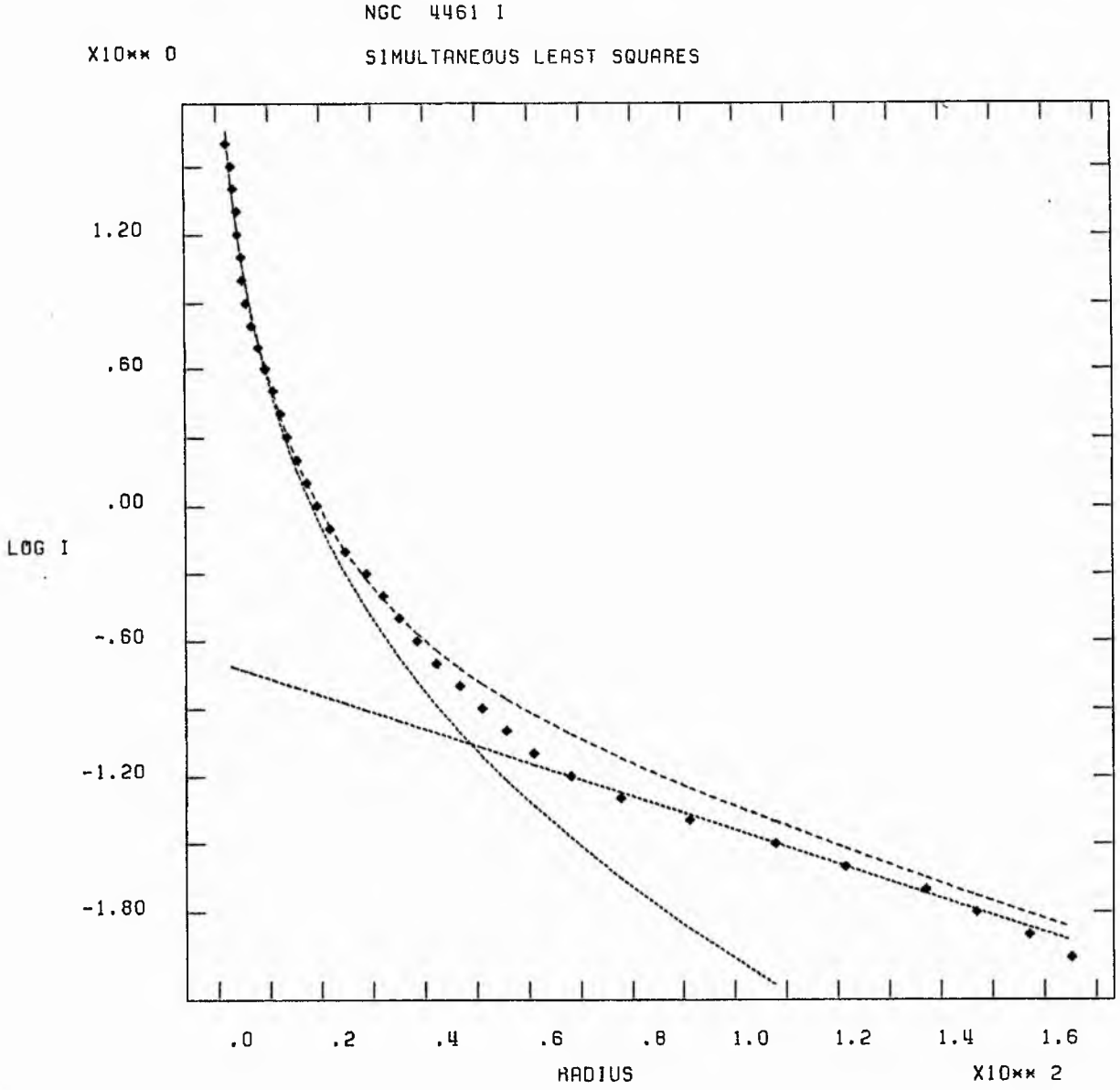
NGC 4461 I
SIMULTANEOUS LEAST SQUARES
X10** 0
1.20
.60
.00
LOG I
-.60
-1.20
-1.80
.0
.2
.4
.6
.8
1.0
1.2
1.4
1.6
RADIUS
X10** 2

NGC 4474 I

ITERATIVE FITTING.

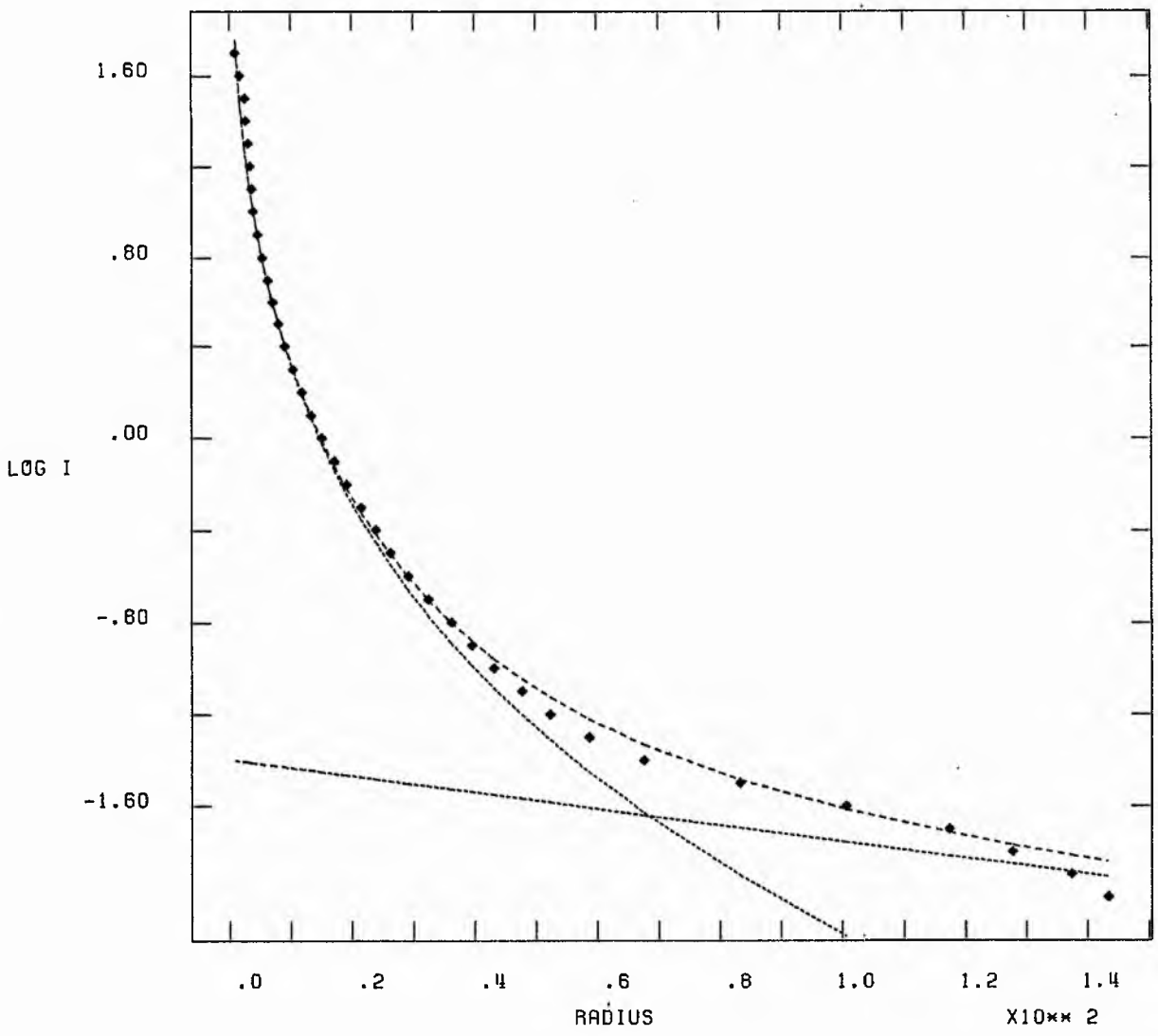

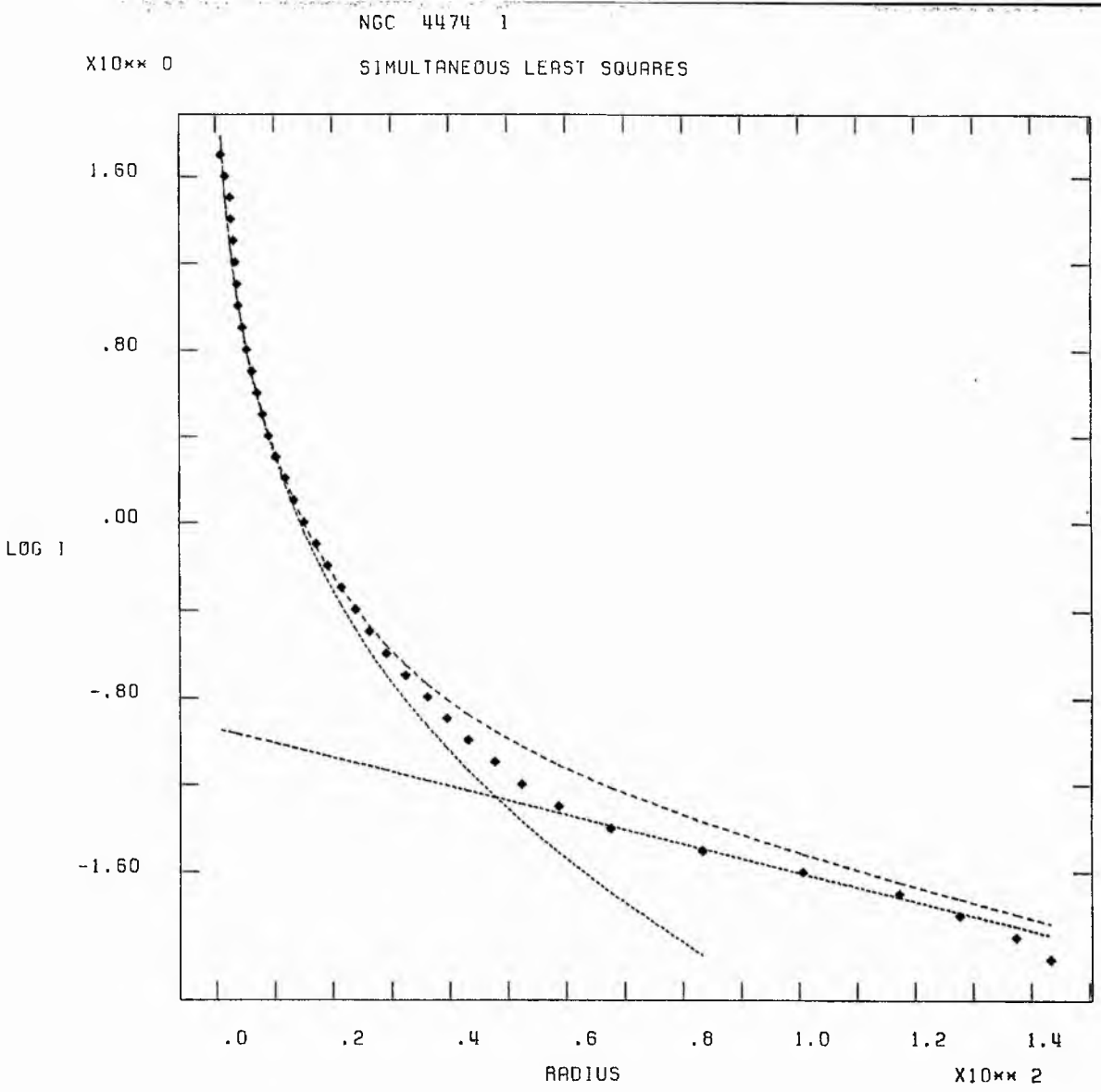
NGC 4474 1
SIMULTANEOUS LEAST SQUARES
X10** 0
1.60
.80
.00
LOG I
-.80
-1.60
.0
.2
.4
.6
.8
1.0
1.2
1.4
RADIUS
X10** 2

NGC 4477 I

ITERATIVE FITTING.

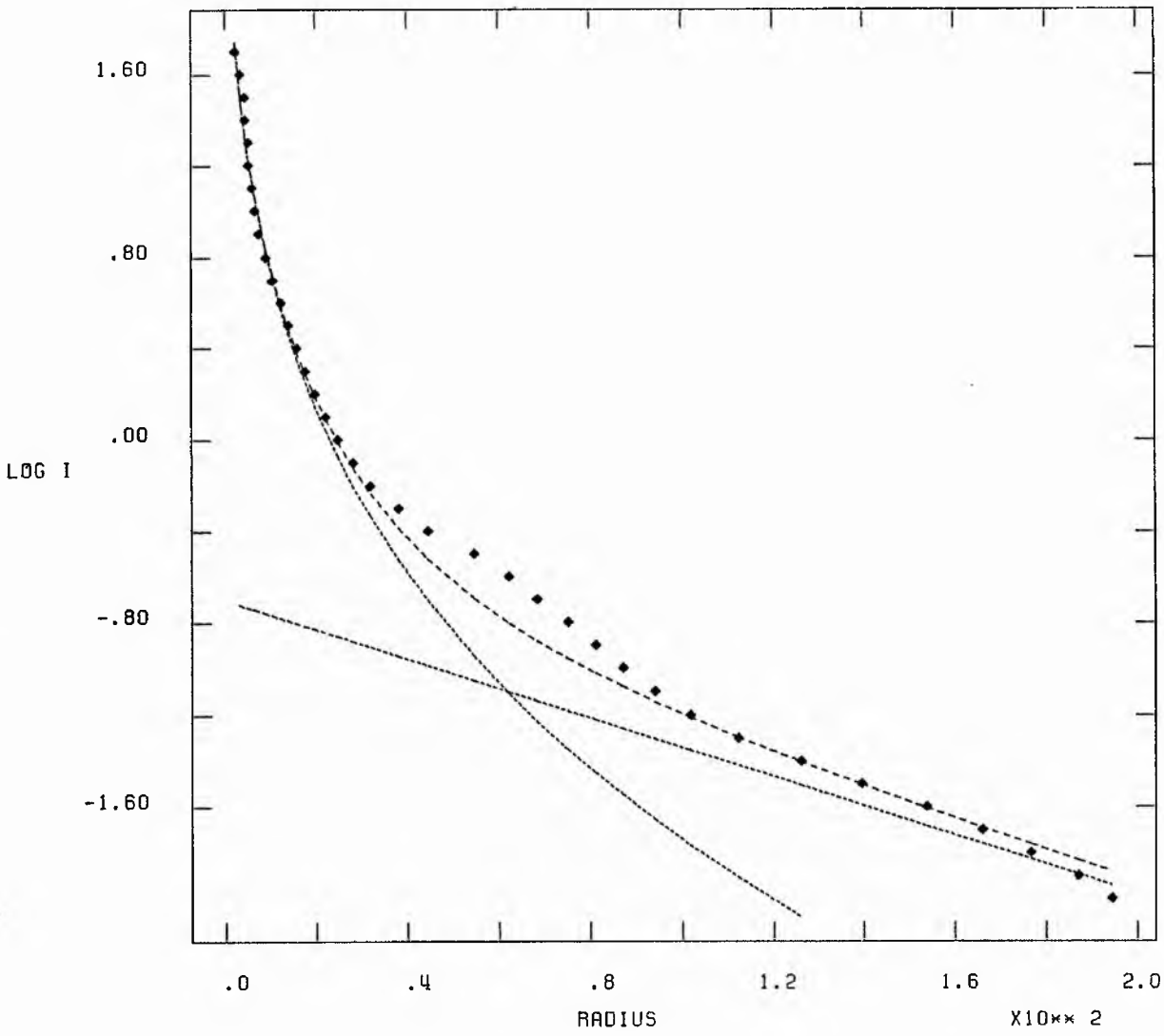

NGC 4477 1

SIMULTANEOUS LEAST SQUARES

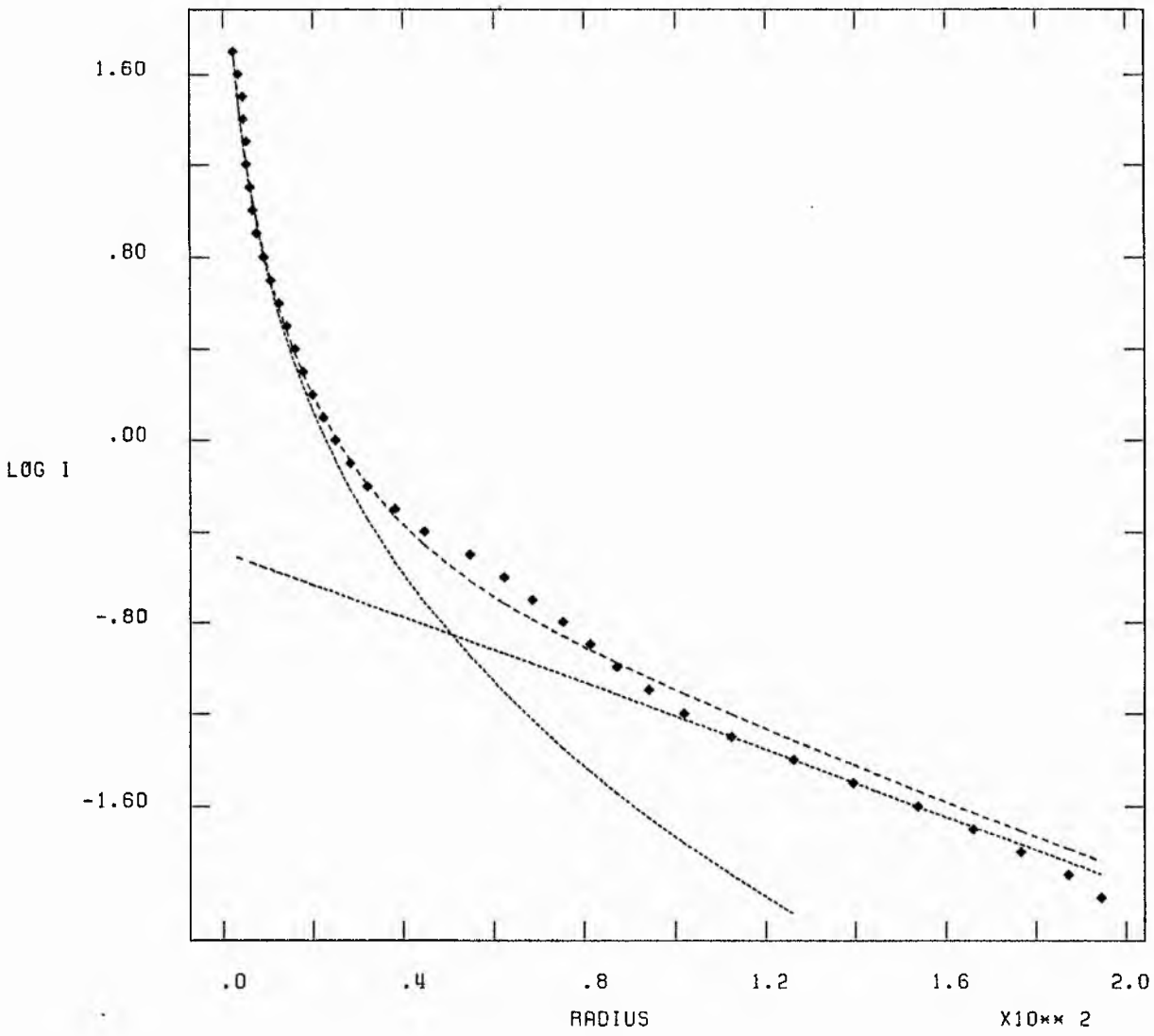

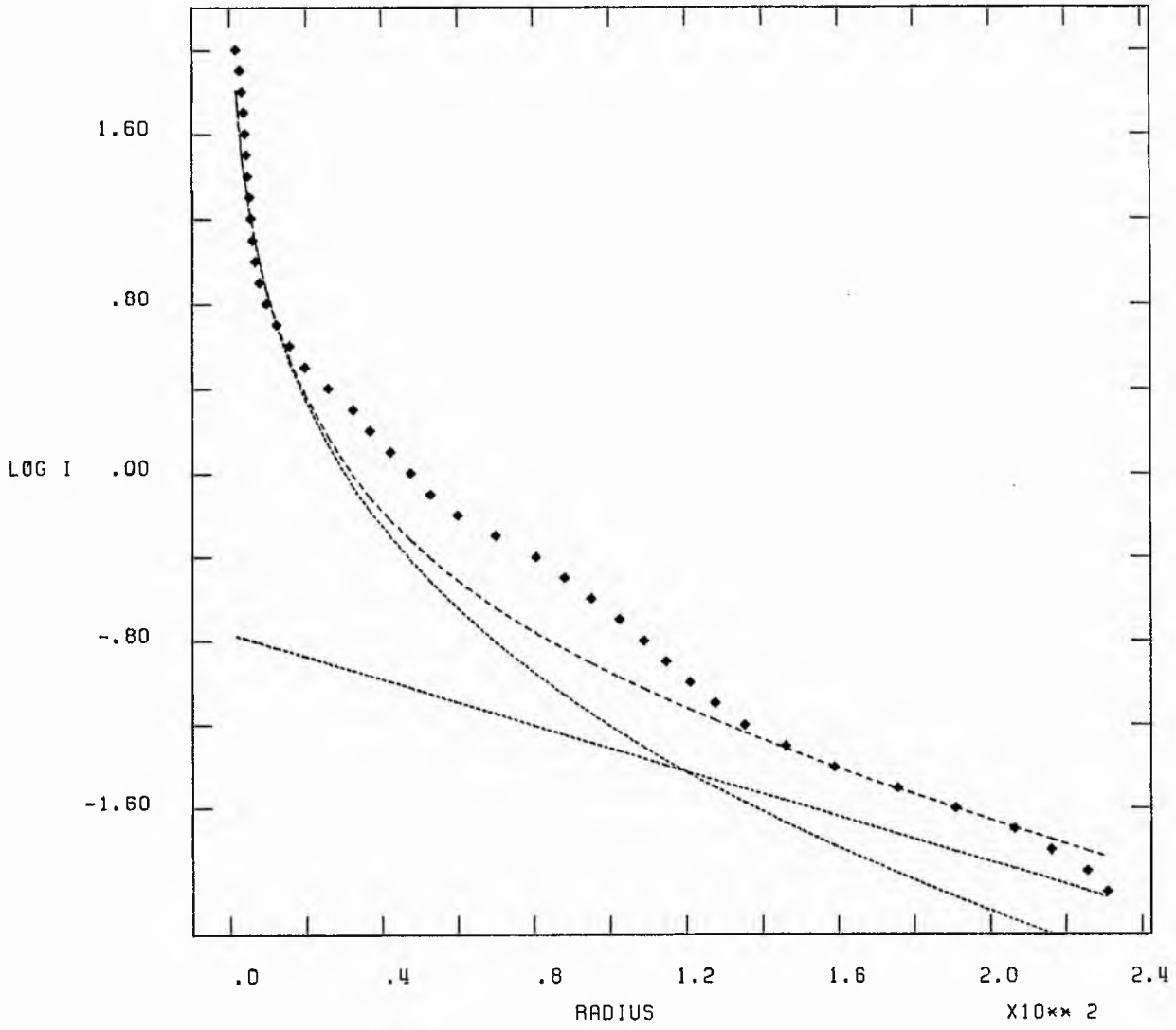
NGC 4501 I
ITERATIVE FITTING.
X10** 0
1.60
.80
LOG I .00
-.80
-1.60
.0
.4
.8
1.2
1.6
2.0
2.4
RADIUS
X10** 2

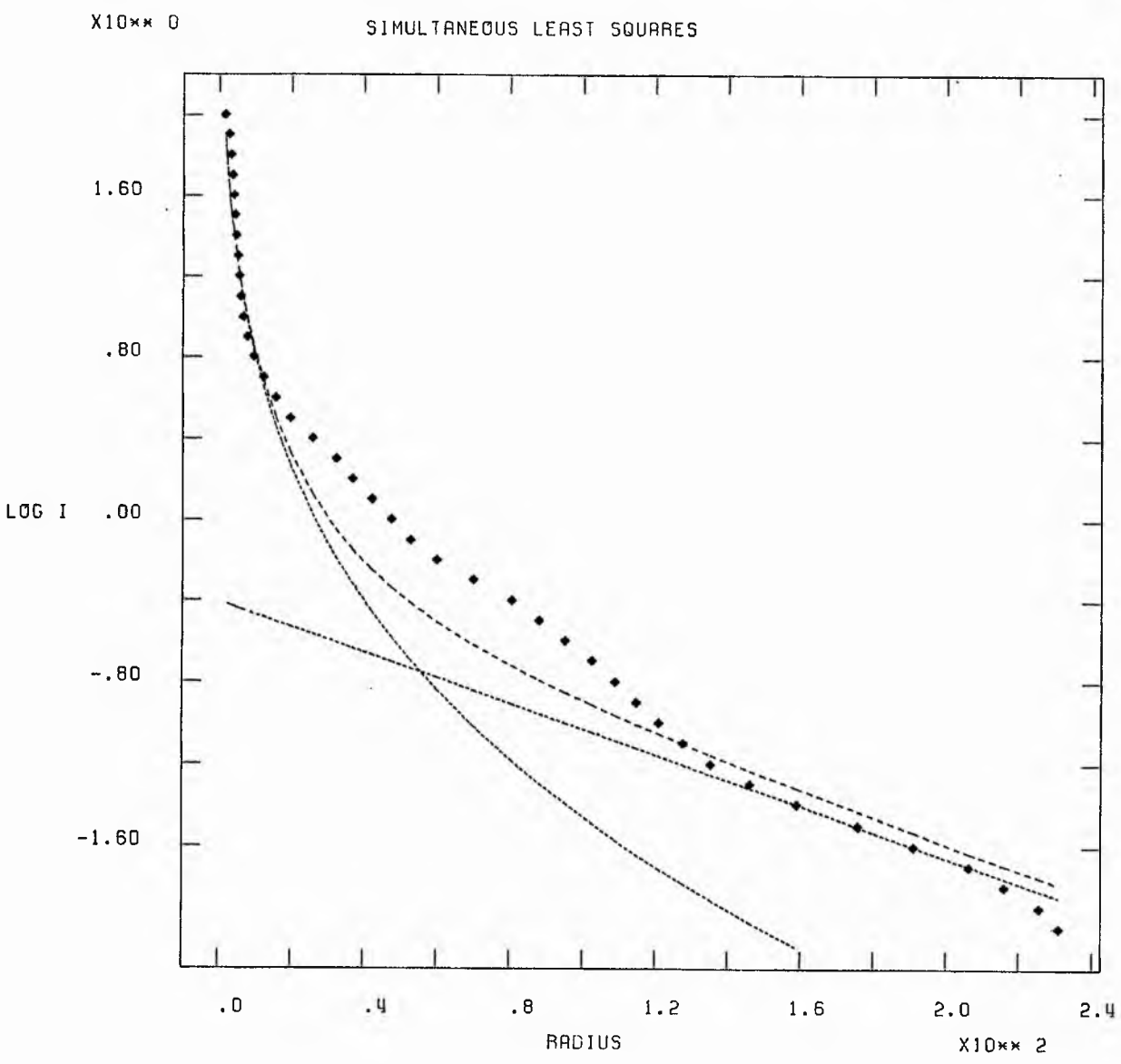
NGC 4501 I
SIMULTANEOUS LEAST SQUARES
X10** 0
1.60
.80
LOG I .00
-.80
-1.60
.0
.4
.8
1.2
1.6
2.0
2.4
RADIUS
X10** 2

NGC 4503 I

X10** 0

ITERATIVE FITTING.

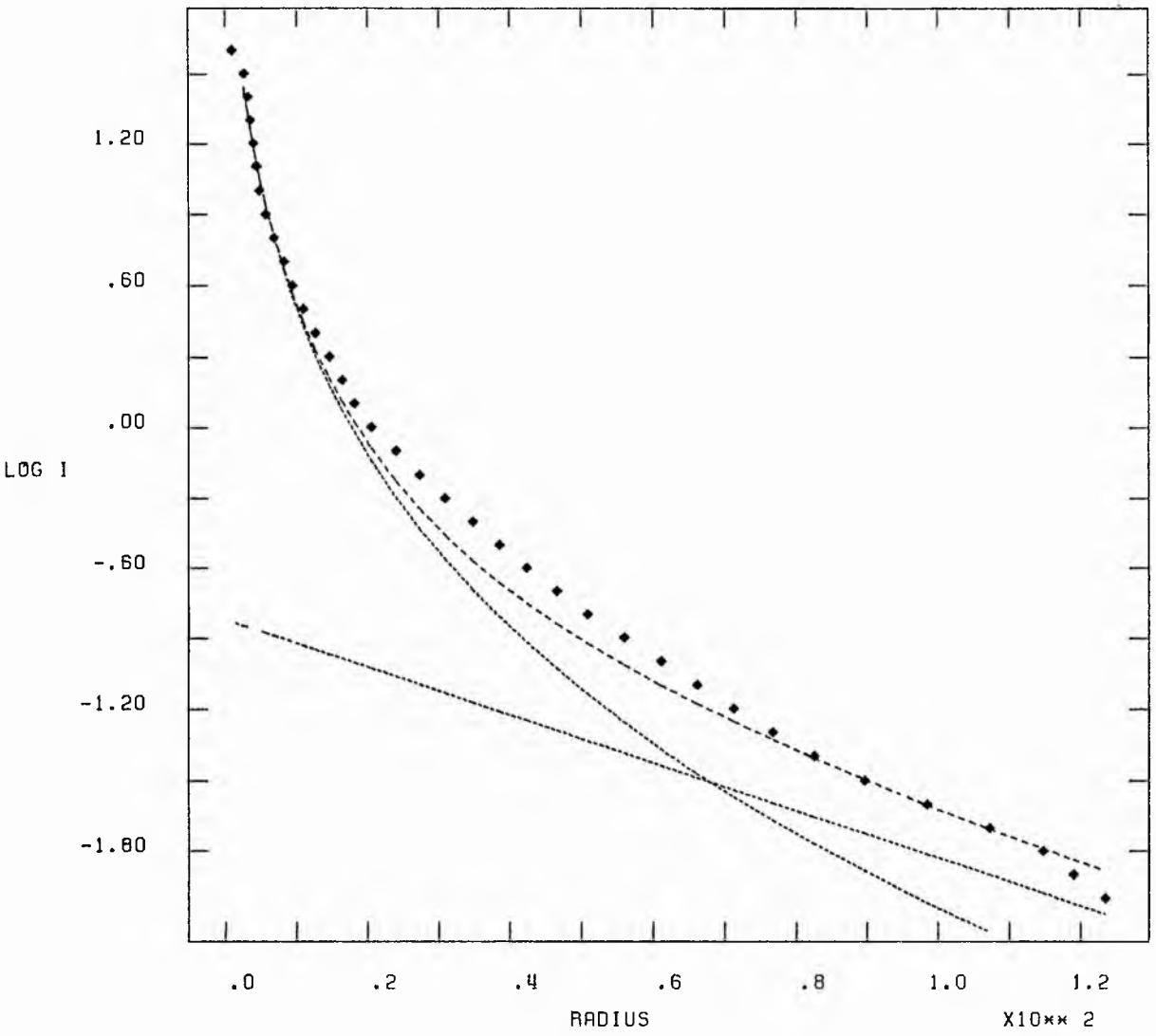

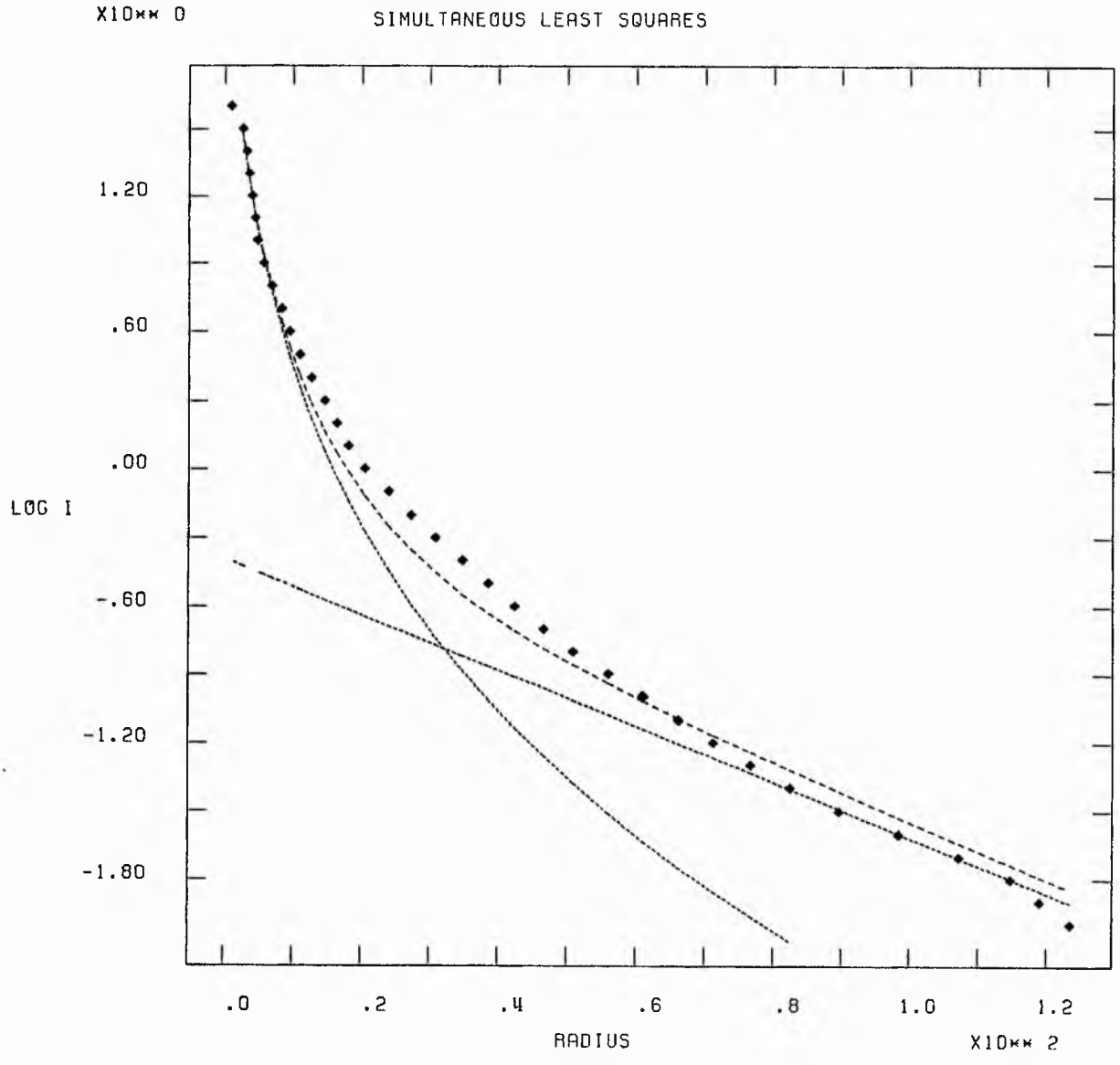
NGC 4503 I
SIMULTANEOUS LEAST SQUARES
X10** 0
1.20
.60
.00
LOG I
-.60
-1.20
-1.80
.0
.2
.4
.6
.8
1.0
1.2
RADIUS
X10** 2

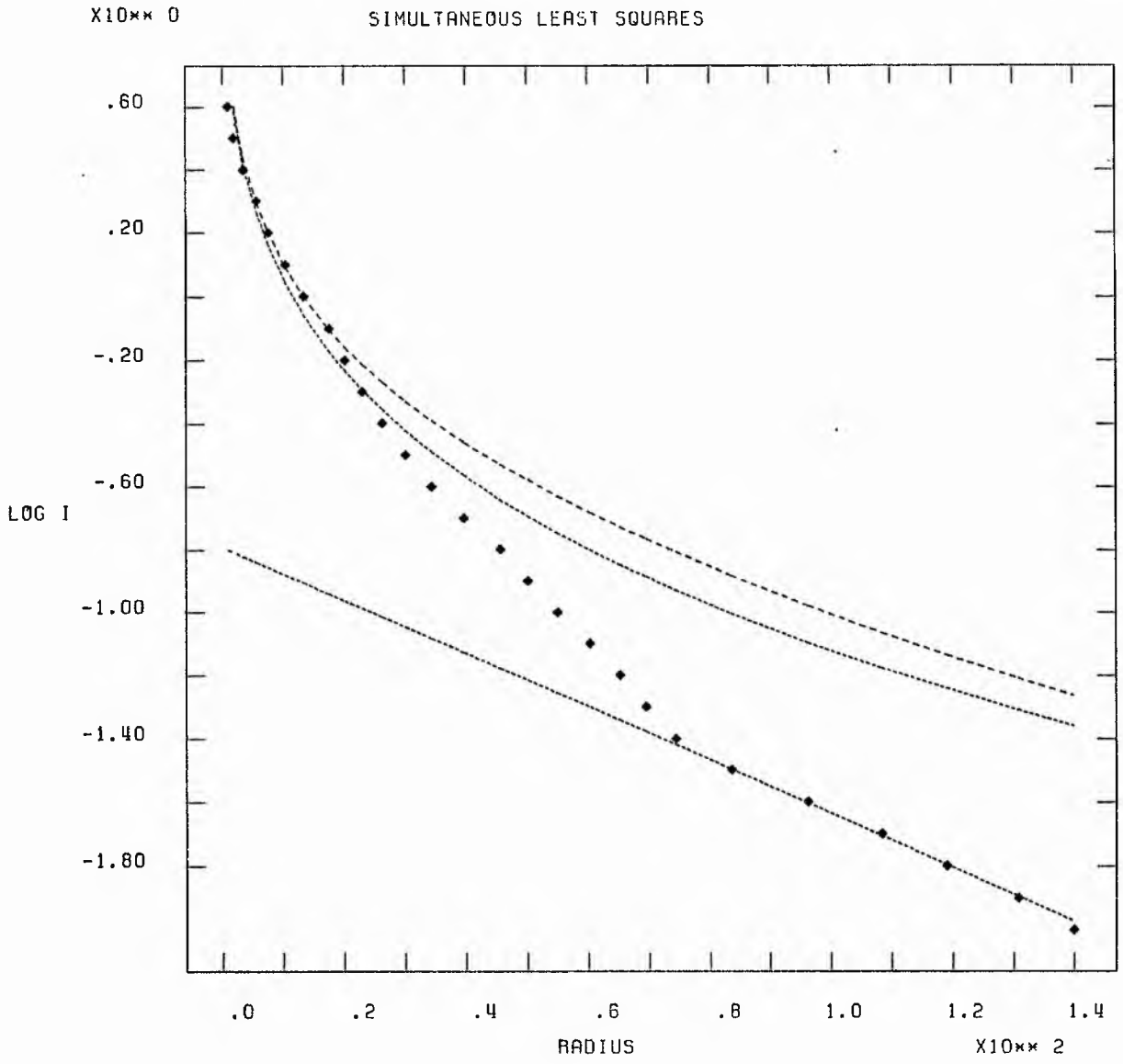
NGC 4531 I
SIMULTANEOUS LEAST SQUARES
X10** 0
.60
.20
-.20
-.60
LOG I
-1.00
-1.40
-1.80
.0
.2
.4
.6
.8
1.0
1.2
1.4
RADIUS
X10** 2

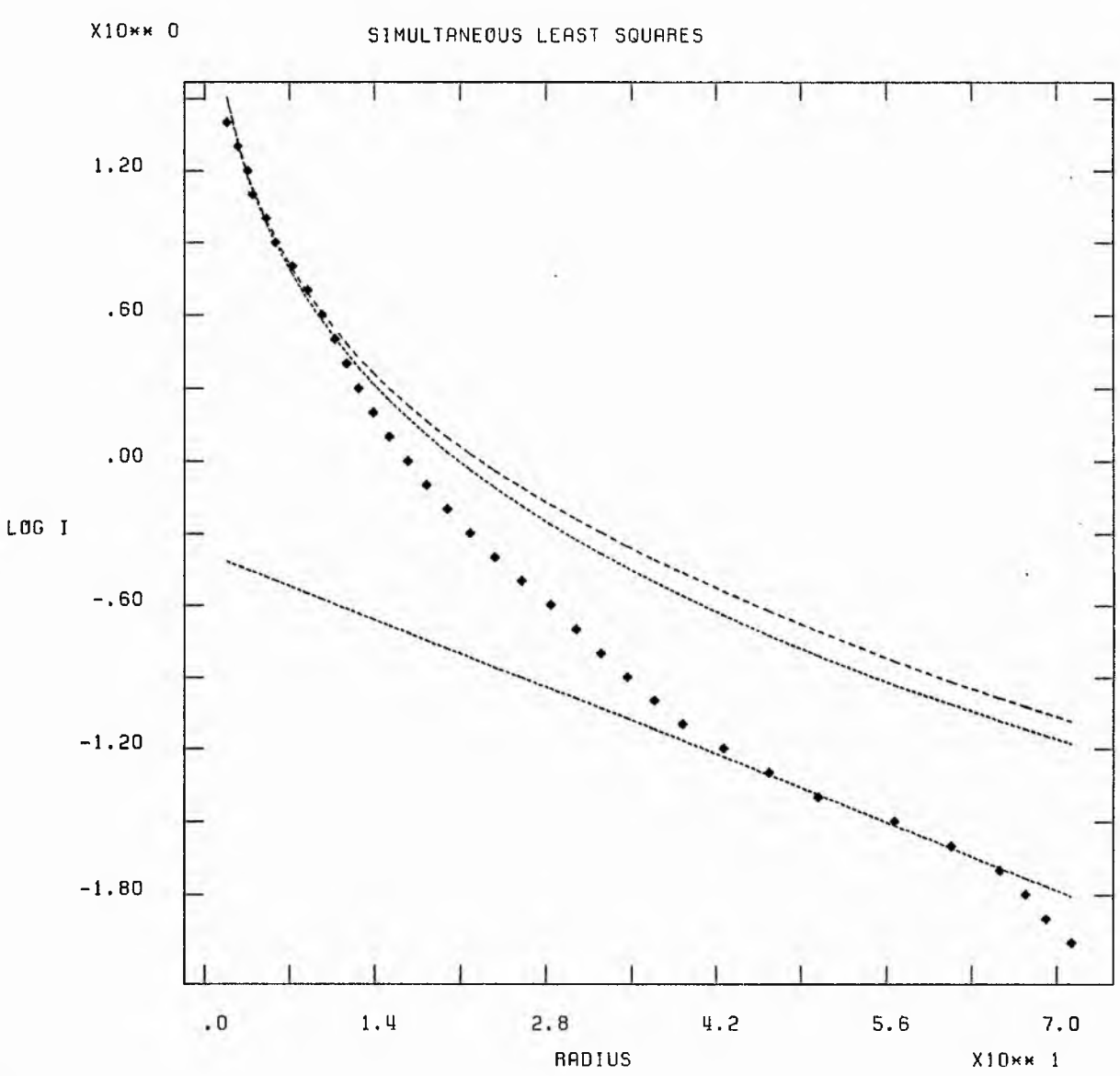
NGC 4550 I
SIMULTANEOUS LEAST SQUARES
X10** 0
1.20
.60
.00
LOG I
-.60
-1.20
-1.80
.0
1.4
2.8
4.2
5.6
7.0
RADIUS
X10** 1

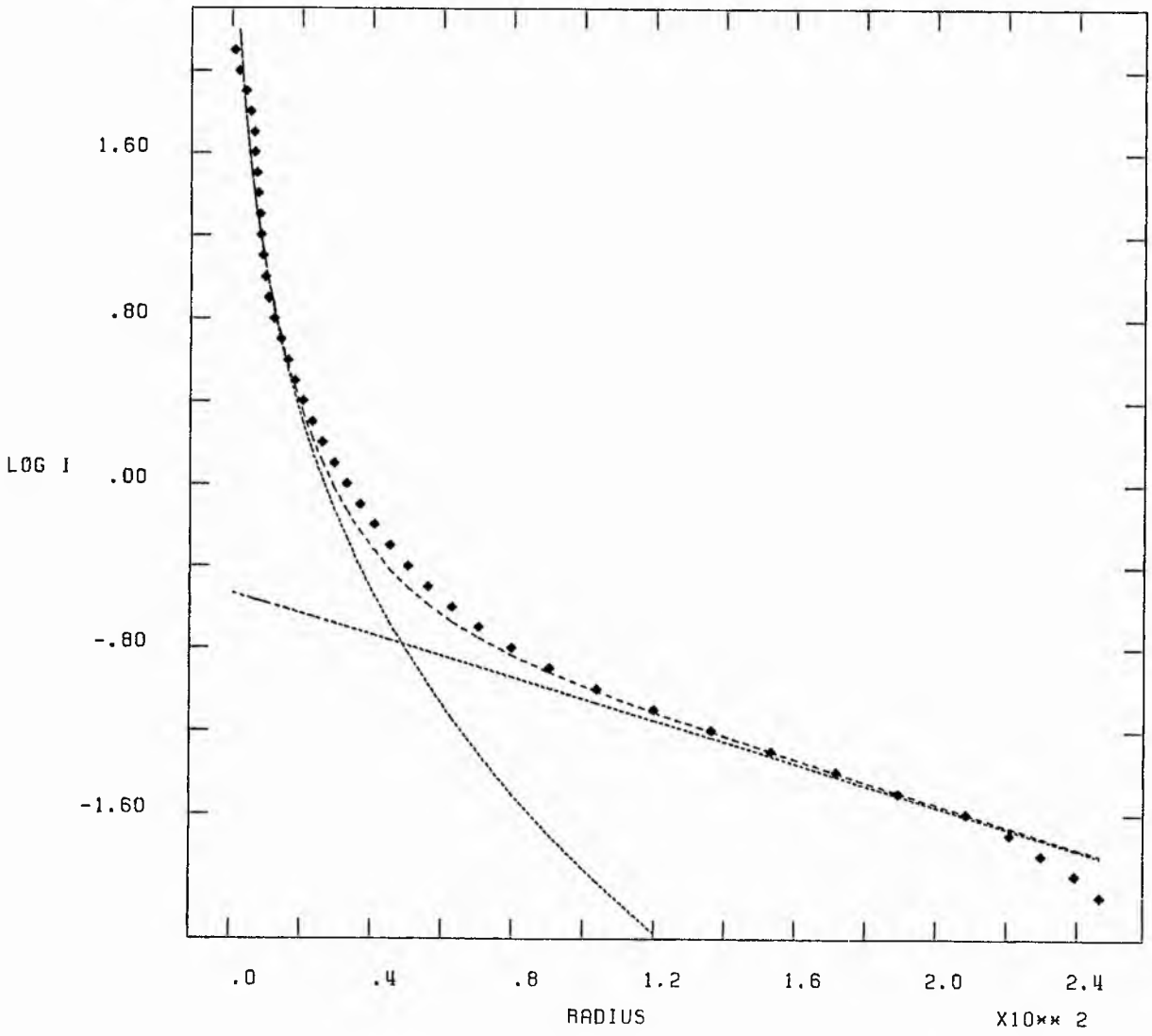
NGC 4552 I
ITERATIVE FITTING.
X10** 0
1.60
.80
LOG I
.00
-.80
-1.60
.0
.4
.8
1.2
1.6
2.0
2.4
RADIUS
X10** 2

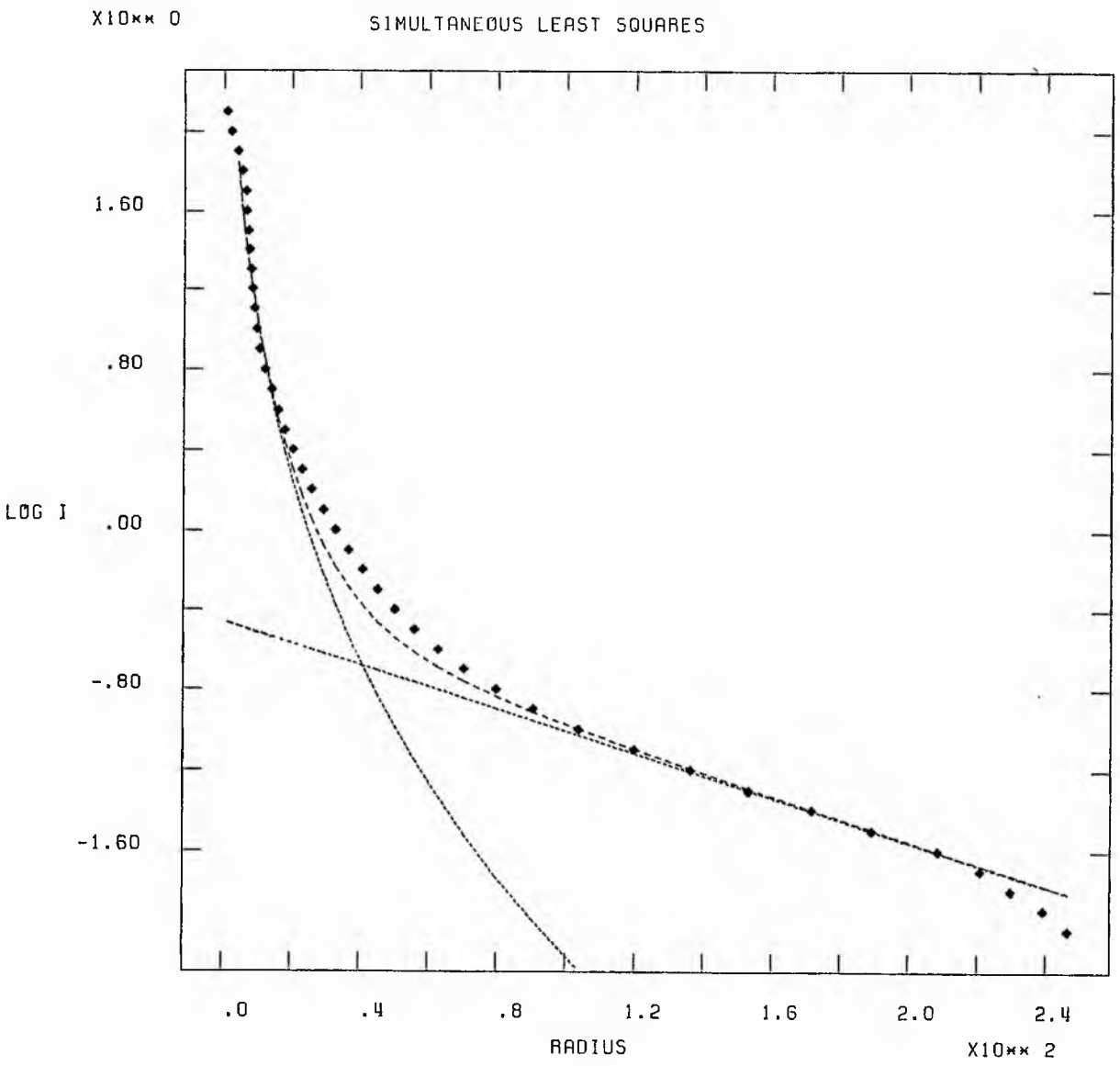
NGC 4552 I
SIMULTANEOUS LEAST SQUARES
X10** 0
1.60
.80
LOG I
.00
-.80
-1.60
.0
.4
.8
1.2
1.6
2.0
2.4
RADIUS
X10** 2

APPENDIX 'H'

Tabular Listing of Colour-Difference Profiles

N4267 (B - R) MAJOR AXIS

RADIUS arcsec	(B - R) Mag/#arcsec	RADIUS arcsec	(B - R) Mag/#arcsec
8.05	1.65	46.69	1.97
12.88	1.92	51.52	2.05
17.71	1.96	56.35	2.10
22.54	1.88	61.18	1.94
27.37	1.80	66.01	2.03
32.20	2.06	70.84	1.97
37.03	2.08	75.67	1.91
41.86	2.06		

N4267 (B - R) MINOR AXIS

RADIUS arcsec	(B - R) Mag/#arcsec	RADIUS arcsec	(B - R) Mag/#arcsec
8.05	1.71	51.52	2.02
12.88	1.87	56.35	2.15
17.71	1.80	61.18	2.20
22.54	2.04	66.01	2.19
27.37	2.01	70.84	2.01
32.20	1.87	75.67	1.92
37.03	2.02	80.50	2.00
41.86	1.92	85.33	2.07
46.69	2.00		

N4371 (B - R) LENS AXIS

RADIUS arcsec	(B - R) Mag/#arcsec	RADIUS arcsec	(B - R) Mag/#arcsec
8.05	1.79	70.84	2.09
12.88	2.17	75.67	1.99
17.71	2.25	80.50	2.07
22.54	1.98	85.33	2.14
27.37	2.01	90.16	2.04
32.20	2.05	94.99	2.01
37.03	2.05	99.82	2.05
41.86	1.96	104.65	2.13
46.69	1.95	109.48	2.22
51.52	1.88	114.31	2.17
56.35	1.91	119.14	2.28
61.18	1.98	123.97	2.30
66.01	2.08		

N4371 (B - R) BAR AXIS

RADIUS arcsec	(B - R) Mag/#arcsec	RADIUS arcsec	(B - R) Mag/#arcsec
8.05	1.95	37.03	1.98
12.88	2.17	41.86	1.92
17.71	1.88	46.69	1.91
22.54	1.89	51.52	2.09
27.37	1.86	56.35	2.35
32.20	1.91		

N4377 (B - R) MAJOR AXIS

RADIUS arcsec	(B - R) Mag/#arcsec	RADIUS arcsec	(B - R) Mag/#arcsec
8.05	2.15	27.37	1.74
12.88	2.10	32.20	1.88
17.71	1.87	37.03	1.72
22.54	1.62	41.86	1.71

N4377 (B - R) MINOR AXIS

RADIUS arcsec	(B - R) Mag/#arcsec	RADIUS arcsec	(B - R) Mag/#arcsec
8.05	1.86	22.54	1.53
12.88	1.86	27.37	1.85
17.71	1.51	32.20	1.88

N4419 (B - R) MAJOR AXIS

RADIUS arcsec	(B - R) Mag/#arcsec	RADIUS arcsec	(B - R) Mag/#arcsec
8.05	2.24	51.52	1.62
12.88	2.40	56.35	1.58
17.71	2.26	61.18	1.65
22.54	2.30	66.01	1.73
27.37	1.99	70.84	1.77
32.20	1.98	75.67	1.84
37.03	1.86	80.50	1.89
41.86	1.64	85.33	2.02
46.69	1.61		

N4419 (B - R) MINOR AXIS

RADIUS arcsec	(B - R) Mag/#arcsec	RADIUS arcsec	(B - R) Mag/#arcsec
8.05	2.86	22.54	1.74
14.49	1.87	27.27	1.97

N4425 (B - R) MAJOR AXIS

RADIUS arcsec	(B - R) Mag/#arcsec	RADIUS arcsec	(B - R) Mag/#arcsec
8.05	2.47	41.86	1.68
12.88	2.05	46.69	1.71
17.71	1.66	51.52	1.80
22.54	1.57	56.35	1.84
27.37	1.55	61.18	1.82
32.20	1.73	66.01	1.90
37.03	1.56	70.84	1.92

N4425 (B - R) MINOR AXIS

RADIUS arcsec	(B - R) Mag/#arcsec	RADIUS arcsec	(B - R) Mag/#arcsec
8.05	2.29	22.54	1.76
12.88	1.68	27.37	1.59
17.71	1.57		

N4429 (B - R) MAJOR AXIS

RADIUS arcsec	(B - R) Mag/#arcsec	RADIUS arcsec	(B - R) Mag/#arcsec
8.05	2.15	90.16	1.92
12.88	2.20	94.99	2.01
17.71	2.12	99.82	2.06
22.54	2.01	104.65	2.01
27.37	2.03	109.48	2.04
32.20	1.98	114.31	2.15
37.03	1.77	119.14	2.10
41.86	1.78	123.97	2.11
46.69	1.87	128.80	2.12
51.52	1.88	133.63	2.06
56.35	1.89	138.46	2.10
61.18	1.90	143.29	2.19
66.01	1.84	148.12	2.02
70.84	1.92	152.95	1.95
75.67	1.87	157.78	2.14
80.50	1.85	162.61	2.16
85.33	1.86	167.44	2.08

N4429 (B - R) MINOR AXIS

RADIUS arcsec	(B - R) Mag/#arcsec	RADIUS arcsec	(B - R) Mag/#arcsec
8.05	2.03	46.69	1.96
12.88	2.03	51.52	2.00
17.71	1.66	56.35	1.96
22.54	1.71	61.18	1.98
27.37	1.75	66.01	2.15
32.20	1.98	70.84	2.16
37.03	1.94	75.67	2.26
41.86	1.96		

N4435 (B - R) MAJOR AXIS

RADIUS arcsec	(B - R) Mag/#arcsec	RADIUS arcsec	(B - R) Mag/#arcsec
8.05	1.74	51.52	1.75
12.88	2.07	56.35	1.77
17.71	1.95	61.18	1.80
22.54	2.09	66.01	1.78
27.37	2.04	70.84	1.87
32.20	1.90	75.67	1.79
37.03	1.71	80.50	1.92
41.86	1.80	85.33	2.04
46.69	1.82		

N4435 (B - R) MINOR AXIS

RADIUS arcsec	(B - R) Mag/#arcsec	RADIUS arcsec	(B - R) Mag/#arcsec
8.05	1.74	41.86	1.86
12.88	1.72	46.69	1.84
17.71	1.74	51.52	1.92
22.54	1.81	56.35	2.16
27.37	1.77	61.18	1.96
32.20	1.89	66.01	1.91
37.03	1.98		

N4438 (B - R) MAJOR AXIS

RADIUS arcsec	(B - R) Mag/#arcsec	RADIUS arcsec	(B - R) Mag/#arcsec
8.05	2.20	-75.67	1.64
12.88	2.10	-80.50	1.51
17.71	2.12	-85.33	1.26
22.54	2.30	-90.16	1.50
27.37	2.28	-94.99	1.67
32.20	2.06	-99.82	1.61
37.03	2.04	-104.65	1.65
41.86	1.79	-109.48	1.70
46.69	1.76	-114.31	1.80
51.52	1.71	-119.14	1.70
56.35	1.60	-123.97	1.72
61.18	1.51	-128.80	1.83
66.01	1.78	-133.63	1.82
70.84	1.95	-138.46	1.77
75.67	2.01	-143.29	1.80
80.50	1.90	-148.12	1.68
85.33	1.96	-152.95	1.53
90.16	1.86	-157.78	1.63
94.99	1.78	-162.61	1.51
99.82	1.94	-167.44	1.52
104.65	1.67	-172.27	1.52
109.48	1.65	-177.10	1.58
114.31	1.56	-181.93	1.65
119.14	1.70	-186.76	1.69
123.97	1.50	-191.59	1.57
128.80	1.59	-196.42	1.66
141.68	1.82	-201.25	1.40
-8.05	1.89	-206.08	1.58
-12.88	1.84	-210.91	1.69
-17.71	1.87	-215.74	1.52
-22.54	2.20	-220.57	1.37
-27.37	2.04	-225.40	1.46
-32.20	1.92	-230.23	1.56
-37.03	1.75	-235.06	1.49
-41.86	1.24	-239.89	1.54
-46.69	1.57	-244.72	1.64
-51.52	1.39	-249.55	1.57
-56.35	1.44	-254.38	1.63
-61.18	1.55	-259.21	1.58
-66.01	1.48	-264.04	1.47
-70.84	1.50		

N4438 (B - R) BAR AXIS

RADIUS arcsec	(B - R) Mag/#arcsec	RADIUS arcsec	(B - R) Mag/#arcsec
8.05	2.52	-37.03	1.88
12.88	1.95	-41.86	2.00
17.71	1.94	-46.69	1.94
22.54	2.00	-51.52	1.74
27.37	1.85	-56.35	1.78
32.20	1.87	-61.18	1.66
37.03	1.85	-66.01	1.85
41.86	1.93	-70.84	1.79
46.69	1.83	-75.67	1.71
51.52	1.97	-80.50	1.75
56.35	1.92	-85.33	1.75
61.18	1.81	-90.16	1.57
-8.05	1.98	-94.99	1.94
-12.88	2.12	-99.82	2.07
-17.71	1.65	-104.65	1.93
-22.54	1.89	-109.48	1.65
-27.37	1.86	-125.58	1.68
-32.20	1.77		

N4459 (B - R) MAJOR AXIS

RADIUS arcsec	(B - R) Mag/#arcsec	RADIUS arcsec	(B - R) Mag/#arcsec
8.05	1.17	61.18	2.16
12.88	2.22	66.01	2.18
17.71	2.21	70.84	2.21
22.54	2.28	75.67	2.07
27.37	2.07	80.50	2.31
32.20	2.02	85.33	2.38
37.03	1.96	90.16	2.18
41.86	2.10	94.99	2.24
46.69	2.12	99.82	2.18
51.52	2.10	104.65	2.00
56.35	2.17	109.48	2.42

N4459 (B - R) MINOR AXIS

RADIUS arcsec	(B - R) Mag/#arcsec	RADIUS arcsec	(B - R) Mag/#arcsec
8.05	1.20	46.69	2.17
12.88	2.42	51.52	2.12
17.71	2.34	56.35	2.15
22.54	2.06	61.18	2.20
27.37	2.18	66.01	2.11
32.20	2.10	70.84	2.26
37.03	1.98	75.67	2.38
41.86	2.11	80.50	2.35

N4461 (B - R) MAJOR AXIS

RADIUS arcsec	(B - R) Mag/#arcsec	RADIUS arcsec	(B - R) Mag/#arcsec
8.05	2.03	56.35	1.87
12.88	2.16	61.18	2.00
17.71	1.90	66.01	2.00
22.54	1.69	70.84	2.13
27.37	1.78	75.67	2.02
32.20	1.58	80.50	2.08
37.03	1.94	85.33	2.01
41.86	1.84	90.16	2.06
46.69	1.96	94.99	2.01
51.52	1.96	99.82	1.94

N4461 (B - R) MINOR AXIS

RADIUS arcsec	(B - R) Mag/#arcsec	RADIUS arcsec	(B - R) Mag/#arcsec
8.05	2.06	27.37	1.79
12.88	1.76	32.20	2.01
17.71	1.57	37.03	2.23
22.54	1.67		

N4474 (B - R) MAJOR AXIS

RADIUS arcsec	(B - R) Mag/#arcsec	RADIUS arcsec	(B - R) Mag/#arcsec
8.05	1.66	37.03	1.72
12.88	1.94	41.86	1.71
17.71	1.75	46.69	1.64
22.54	1.77	51.52	1.72
27.37	1.70	56.35	1.91
32.20	1.61	61.18	1.92

N4474 (B - R) MINOR AXIS

RADIUS arcsec	(B - R) Mag/#arcsec	RADIUS arcsec	(B - R) Mag/#arcsec
8.05	1.88	27.37	1.71
12.88	1.61	32.20	1.74
17.71	1.73	37.03	1.75
22.54	1.73	41.86	1.75

N4477 (B - R) MAJOR AXIS

RADIUS arcsec	(B - R) Mag/#arcsec	RADIUS arcsec	(B - R) Mag/#arcsec
8.05	1.69	51.52	1.85
12.88	2.19	56.35	1.84
17.71	2.25	61.18	1.94
22.54	2.17	66.01	2.03
27.37	1.96	70.84	2.04
32.20	1.80	75.67	2.03
37.03	1.88	80.50	2.00
41.86	1.89	85.33	2.00
46.69	1.83	90.16	1.86

N4477 (B - R) MINOR AXIS

RADIUS arcsec	(B - R) Mag/#arcsec	RADIUS arcsec	(B - R) Mag/#arcsec
8.05	1.74	51.52	1.96
12.88	1.97	56.35	2.03
17.71	1.97	61.18	2.01
22.54	1.80	66.01	2.03
27.37	1.88	70.84	1.91
32.20	1.90	75.67	1.91
37.03	1.75	80.50	2.06
41.86	1.82	85.33	2.07
46.69	1.94	90.16	2.14

N4501 (B - R) MAJOR AXIS

RADIUS arcsec	(B - R) Mag/#arcsec	RADIUS arcsec	(B - R) Mag/#arcsec
8.05	1.87	94.99	1.74
12.88	2.00	99.82	1.63
17.71	2.19	104.65	1.57
22.54	2.01	109.48	1.72
27.37	2.03	114.31	1.59
32.20	1.95	119.14	1.57
37.03	1.79	123.97	1.54
41.86	1.81	128.80	1.53
46.69	1.89	133.63	1.54
51.52	1.75	138.46	1.55
56.35	1.73	143.29	1.58
61.18	1.82	148.12	1.59
66.01	1.75	152.95	1.57
70.84	1.70	157.78	1.52
75.67	1.75	162.61	1.47
80.50	1.74	167.44	1.55
85.33	1.82	172.27	1.64
90.16	1.64	177.10	1.64

N4501 (B - R) MINOR AXIS

RADIUS arcsec	(B - R) Mag/#arcsec	RADIUS arcsec	(B - R) Mag/#arcsec
8.05	2.48	46.69	1.64
12.88	2.29	51.52	1.67
17.71	1.91	56.35	1.52
22.54	1.94	61.18	1.58
27.37	1.73	66.01	1.56
32.20	1.62	70.84	1.50
37.03	1.59	75.67	1.51
41.86	1.60	80.50	1.57

N4503 (B - R) MAJOR AXIS

RADIUS arcsec	(B - R) Mag/#arcsec	RADIUS arcsec	(B - R) Mag/#arcsec
8.05	2.18	56.35	2.17
12.88	2.37	61.18	2.24
17.71	1.97	66.01	2.17
22.54	1.97	70.84	2.15
27.37	2.04	75.67	2.02
32.20	2.01	80.50	2.10
37.03	2.13	85.33	2.02
41.86	1.98	90.16	2.12
46.69	2.07	94.99	2.35
51.52	2.11	99.82	2.35

N4503 (B - R) MINOR AXIS

RADIUS arcsec	(B - R) Mag/#arcsec	RADIUS arcsec	(B - R) Mag/#arcsec
8.05	1.89	27.37	2.06
12.88	2.00	32.20	1.94
17.71	1.96	37.03	2.12
22.54	1.96	41.86	2.33

N4531 (B - R) MAJOR AXIS

RADIUS arcsec	(B - R) Mag/#arcsec	RADIUS arcsec	(B - R) Mag/#arcsec
8.05	1.86	51.52	1.81
12.88	1.75	56.35	1.90
17.71	1.65	61.18	2.01
22.54	1.62	66.01	1.88
27.37	1.75	70.84	1.80
32.20	1.79	75.67	1.93
37.03	1.80	80.50	1.91
41.86	1.83	85.33	1.88
46.69	1.76		

N4531 (B - R) MINOR AXIS

RADIUS arcsec	(B - R) Mag/#arcsec	RADIUS arcsec	(B - R) Mag/#arcsec
8.05	1.89	32.20	1.56
12.88	1.86	37.03	1.68
17.71	1.86	41.86	1.77
22.54	1.70	46.69	1.93
27.37	1.78	51.52	2.22

N4550 (B - R) MAJOR AXIS

RADIUS arcsec	(B - R) Mag/#arcsec	RADIUS arcsec	(B - R) Mag/#arcsec
8.05	1.71	46.69	1.80
12.88	2.06	51.52	1.72
17.71	1.94	56.35	1.63
22.54	1.94	61.18	1.67
27.37	1.88	66.01	1.68
32.20	1.50	70.84	1.70
37.03	1.75	75.67	1.77
41.86	1.69		

N4550 (B - R) MINOR AXIS

RADIUS arcsec	(B - R) Mag/#arcsec	RADIUS arcsec	(B - R) Mag/#arcsec
8.05	1.90	17.71	1.72
12.88	1.75	22.54	1.85

N4552 (B - R) MAJOR AXIS

RADIUS arcsec	(B - R) Mag/#arcsec	RADIUS arcsec	(B - R) Mag/#arcsec
8.05	1.35	70.84	2.14
12.88	1.78	75.67	2.08
17.71	2.31	80.50	1.94
22.54	2.09	85.33	2.16
27.37	2.10	90.16	2.27
32.20	1.87	94.99	2.00
37.03	1.98	99.82	1.98
41.86	2.09	104.65	2.03
46.69	2.07	109.48	2.04
51.52	2.18	114.31	1.97
56.35	2.08	119.14	1.93
61.18	2.10	123.97	1.92
66.01	2.11	128.80	2.00

N4552 (B - R) MINOR AXIS

RADIUS arcsec	(B - R) Mag/#arcsec	RADIUS arcsec	(B - R) Mag/#arcsec
8.05	1.61	66.01	2.19
12.88	2.12	70.84	2.26
17.71	2.40	75.67	2.16
22.54	2.03	80.50	2.21
27.37	1.91	85.33	2.14
32.20	1.82	90.16	2.14
37.03	2.04	94.99	2.08
41.86	2.18	99.82	2.21
46.69	2.16	104.65	2.18
51.52	2.03	109.48	2.32
56.35	1.93	114.31	2.40
61.18	2.11		

N4267 (B - I) MAJOR AXIS

RADIUS arcsec	(B - I) Mag/#arcsec	RADIUS arcsec	(B - I) Mag/#arcsec
8.05	1.72	37.03	2.20
12.88	2.04	41.86	2.14
17.71	2.17	46.69	2.13
22.54	2.06	51.52	2.20
27.37	2.03	56.35	2.18
32.20	2.14		

N4267 (B - I) MINOR AXIS

RADIUS arcsec	(B - I) Mag/#arcsec	RADIUS arcsec	(B - I) Mag/#arcsec
8.05	1.95	41.86	2.08
12.88	1.98	46.69	2.12
17.71	2.16	51.52	2.15
22.54	2.20	56.35	2.24
27.37	2.11	61.18	2.23
32.20	1.98	66.01	2.25
37.03	2.13	70.84	2.13

N4371 (B - I) LENS AXIS

RADIUS arcsec	(B - I) Mag/#arcsec	RADIUS arcsec	(B - I) Mag/#arcsec
8.05	3.10	56.35	2.19
12.88	2.48	61.18	2.22
17.71	2.53	66.01	2.38
22.54	2.40	70.84	2.33
27.37	2.33	75.67	2.23
32.20	2.32	80.50	2.37
37.03	2.32	85.33	2.33
41.86	2.28	90.16	2.16
46.69	2.28	94.99	2.16
51.52	2.14		

N4371 (B - I) BAR AXIS

RADIUS arcsec	(B - I) Mag/#arcsec	RADIUS arcsec	(B - I) Mag/#arcsec
8.05	2.27	32.20	2.36
12.88	2.40	37.03	2.20
17.71	2.27	41.86	2.13
22.54	2.33	46.69	2.13
27.37	2.31	51.52	2.22

N4377 (B - I) MAJOR AXIS

RADIUS arcsec	(B - I) Mag/#arcsec	RADIUS arcsec	(B - I) Mag/#arcsec
8.05	2.39	27.37	1.95
12.88	2.31	32.20	2.10
17.71	2.18	37.03	1.94
22.54	1.95		

N4377 (B - I) MINOR AXIS

RADIUS arcsec	(B - I) Mag/#arcsec	RADIUS arcsec	(B - I) Mag/#arcsec
8.05	2.00	22.54	1.76
12.88	2.10	27.37	1.87
17.71	1.83		

N4419 (B - I) MAJOR AXIS

RADIUS arcsec	(B - I) Mag/#arcsec	RADIUS arcsec	(B - I) Mag/#arcsec
8.05	2.74	46.69	1.88
12.88	2.42	51.52	1.90
17.71	2.14	56.35	1.84
22.54	2.23	61.18	1.81
27.37	2.22	66.01	1.88
32.20	2.04	70.84	1.93
37.03	2.01	75.67	2.08
41.86	1.91		

N4419 (B - I) MINOR AXIS

RADIUS arcsec	(B - I) Mag/#arcsec	RADIUS arcsec	(B - I) Mag/#arcsec
8.05	2.27	19.32	1.98
14.49	1.81	24.15	2.09

N4425 (B - I) MAJOR AXIS

RADIUS arcsec	(B - I) Mag/#arcsec	RADIUS arcsec	(B - I) Mag/#arcsec
8.05	2.48	41.86	1.97
12.88	2.23	46.69	2.00
17.71	2.01	51.52	1.99
22.54	1.89	56.35	2.06
27.37	1.93	61.18	2.07
32.20	2.11	66.01	2.11
37.03	1.86		

N4429 (B - I) MAJOR AXIS

RADIUS arcsec	(B - I) Mag/#arcsec	RADIUS arcsec	(B - I) Mag/#arcsec
8.05	3.46	80.50	2.16
12.88	2.29	85.33	2.15
17.71	2.27	90.16	2.21
22.54	2.28	94.99	2.25
27.37	2.32	99.82	2.29
32.20	2.22	104.65	2.22
37.03	2.15	109.48	2.27
41.86	2.16	114.31	2.38
46.69	2.17	119.14	2.32
51.52	2.21	123.97	2.30
56.35	2.25	128.80	2.33
61.18	2.27	133.63	2.31
66.01	2.20	138.46	2.30
70.84	2.29	143.29	2.46
75.67	2.18	148.12	2.35

N4429 (B - I) MINOR AXIS

RADIUS arcsec	(B - I) Mag/#arcsec	RADIUS arcsec	(B - I) Mag/#arcsec
8.05	3.46	37.03	2.14
12.88	2.23	41.86	2.11
17.71	2.07	46.69	2.18
22.54	2.15	51.52	2.38
27.37	2.07	56.35	2.30
32.20	2.21	61.18	2.18

N4435 (B - I) MAJOR AXIS

RADIUS arcsec	(B - I) Mag/#arcsec	RADIUS arcsec	(B - I) Mag/#arcsec
8.05	2.21	41.86	2.20
12.88	2.37	46.69	2.11
17.71	2.32	51.52	2.01
22.54	2.38	56.35	1.99
27.37	2.32	61.18	2.05
32.20	2.18	66.01	2.06
37.03	2.18		

N4435 (B - I) MINOR AXIS

RADIUS arcsec	(B - I) Mag/#arcsec	RADIUS arcsec	(B - I) Mag/#arcsec
8.05	2.10	33.81	2.14
19.32	2.19	38.64	2.20
24.15	2.12	43.47	2.00
28.98	2.14		

N4438 (B - I) MAJOR AXIS

RADIUS arcsec	(B - I) Mag/#arcsec	RADIUS arcsec	(B - I) Mag/#arcsec
8.05	2.77	-32.20	2.30
12.88	2.59	-37.03	2.10
17.71	3.07	-41.86	1.69
22.54	2.93	-46.69	1.91
27.37	2.72	-51.52	1.84
32.20	2.49	-56.35	1.86
37.03	2.31	-61.18	1.93
41.86	2.11	-66.01	1.86
46.69	1.92	-70.84	1.90
51.52	2.06	-75.67	1.98
56.35	1.99	-80.50	1.81
61.18	1.88	-85.33	1.50
66.01	2.14	-90.16	1.71
70.84	2.15	-94.99	2.01
75.67	2.17	-99.82	1.96
80.50	2.05	-120.75	2.08
85.33	1.95	-141.68	2.09
90.16	1.93	-183.54	1.96
-8.05	2.31	-188.37	1.82
-12.88	2.48	-193.20	1.76
-17.71	2.83	-198.03	1.62
-22.54	2.73	-202.86	1.49
-27.37	2.55	-207.69	1.71

N4438 (B - I) B.R AXIS

RADIUS arcsec	(B - I) Mag/#arcsec	RADIUS arcsec	(B - I) Mag/#arcsec
8.05	2.59	27.37	2.23
12.88	2.17	32.20	2.05
17.71	2.05	37.03	2.04
22.54	2.17	41.86	2.10

N4459 (B - I) MAJOR AXIS

RADIUS arcsec	(B - I) Mag/#arcsec	RADIUS arcsec	(B - I) Mag/#arcsec
8.05	1.88	56.35	2.59
12.88	2.35	61.18	2.52
17.71	2.38	66.01	2.50
22.54	2.28	70.84	2.55
27.37	2.39	75.67	2.43
32.20	2.39	80.50	2.61
37.03	2.30	85.33	2.64
41.86	2.41	90.16	2.57
46.69	2.46	94.99	2.60
51.52	2.42	99.82	2.53

N4459 (B - I) MINOR AXIS

RADIUS arcsec	(B - I) Mag/#arcsec	RADIUS arcsec	(B - I) Mag/#arcsec
8.05	1.81	41.86	2.48
12.88	2.38	46.69	2.59
17.71	2.37	51.52	2.58
22.54	2.31	56.35	2.64
27.37	2.50	61.18	2.62
32.20	2.42	66.01	2.50
37.03	2.41	70.84	2.63

N4461 (B - I) MAJOR AXIS

RADIUS arcsec	(B - I) Mag/#arcsec	RADIUS arcsec	(B - I) Mag/#arcsec
8.05	3.19	51.52	2.64
12.88	2.77	56.35	2.57
17.71	2.50	61.18	2.63
22.54	2.33	66.01	2.55
27.37	2.43	70.84	2.65
32.20	2.35	75.67	2.52
37.03	2.53	80.50	2.62
41.86	2.40	85.33	2.65
46.69	2.54		

N4461 (B - I) MINOR AXIS

RADIUS arcsec	(B - I) Mag/#arcsec	RADIUS arcsec	(B - I) Mag/#arcsec
8.05	3.50	22.54	2.31
12.88	2.77	27.37	2.47
17.71	2.18	32.20	2.70

N4474 (B -I) MAJOR XIS

RADIUS arcsec	(B - I) Mag/#arcsec	RADIUS arcsec	(B - I) Mag/#arcsec
8.05	2.27	37.03	2.13
12.88	2.22	41.86	2.11
17.71	2.01	46.69	2.09
22.54	2.11	51.52	2.17
27.37	2.03	56.35	2.29
32.20	2.00		

N4474 (B - I) MINOR AXIS

RADIUS arcsec	(B - I) Mag/#arcsec	RADIUS arcsec	(B - I) Mag/#arcsec
8.05	1.98	24.15	2.10
14.49	2.12	28.98	2.09
19.32	2.12		

N4477 (B - I) MAJOR AXIS

RADIUS arcsec	(B - I) Mag/#arcsec	RADIUS arcsec	(B - I) Mag/#arcsec
8.05	2.64	51.52	2.46
12.88	2.75	56.35	2.48
17.71	2.73	61.18	2.61
22.54	2.63	66.01	2.71
27.37	2.47	70.84	2.66
32.20	2.41	75.67	2.60
37.03	2.43	80.50	2.61
41.86	2.50	85.33	2.58
46.69	2.38		

N4477 (B - I) MINOR AXIS

RADIUS arcsec	(B - I) Mag/#arcsec	RADIUS arcsec	(B - I) Mag/#arcsec
8.05	2.67	46.69	2.53
12.88	2.57	51.52	2.53
17.71	2.57	56.35	2.56
22.54	2.38	61.18	2.59
27.37	2.47	66.01	2.68
32.20	2.49	70.84	2.57
37.03	2.38	75.67	2.62
41.86	2.37	80.50	2.78

N4501 (B - I) MAJOR AXIS

RADIUS arcsec	(B - I) Mag/#arcsec	RADIUS arcsec	(B - I) Mag/#arcsec
8.05	2.87	90.16	2.05
12.88	2.59	94.99	2.11
17.71	2.79	99.82	2.06
22.54	2.60	104.65	1.95
27.37	2.48	109.48	2.08
32.20	2.31	114.31	1.99
37.03	2.21	119.14	1.93
41.86	2.32	123.97	1.77
46.69	2.27	128.80	1.75
51.52	2.11	133.63	1.73
56.35	2.18	138.46	1.68
61.18	2.25	143.29	1.81
66.01	2.13	148.12	1.91
70.84	2.09	152.95	1.90
75.67	2.21	157.78	1.94
80.50	2.16	162.61	1.89
85.33	2.25		

N4501 (B - I) MINOR AXIS

RADIUS arcsec	(B - I) Mag/#arcsec	RADIUS arcsec	(B - I) Mag/#arcsec
8.05	3.62	46.69	2.00
12.88	2.87	51.52	2.05
17.71	2.62	56.35	1.89
22.54	2.38	61.18	2.00
27.37	2.35	66.01	2.00
32.20	2.08	70.84	1.92
37.03	1.94	75.67	2.01
41.86	2.06	80.50	2.06

N4503 (B - I) MAJOR AXIS

RADIUS arcsec	(B - I) Mag/#arcsec	RADIUS arcsec	(B - I) Mag/#arcsec
8.05	2.73	51.52	2.44
12.88	2.70	56.35	2.53
17.71	2.42	61.18	2.48
22.54	2.43	66.01	2.41
27.37	2.43	70.84	2.38
32.20	2.43	75.67	2.26
37.03	2.44	80.50	2.36
41.86	2.39	85.33	2.38
46.69	2.41		

N4503 (B - I) MINOR AXIS

RADIUS arcsec	(B - I) Mag/#arcsec	RADIUS arcsec	(B - I) Mag/#arcsec
8.05	2.67	27.37	2.43
12.88	2.39	32.20	2.32
17.71	2.43	37.03	2.44
22.54	2.38		

N4531 (B - I) MAJOR AXIS

RADIUS arcsec	(B - I) Mag/#arcsec	RADIUS arcsec	(B - I) Mag/#arcsec
8.05	2.35	41.86	2.15
12.88	2.13	46.69	2.07
17.71	1.95	51.52	2.07
22.54	2.03	56.35	2.10
27.37	2.06	61.18	2.23
32.20	2.13	66.01	2.10
37.03	2.15		

N4531 (B - I) MINOR AXIS

RADIUS arcsec	(B - I) Mag/#arcsec	RADIUS arcsec	(B - I) Mag/#arcsec
8.05	2.40	27.37	2.07
12.88	2.21	32.20	1.84
17.71	2.15	37.03	1.88
22.54	1.98	41.86	1.86

N4550 (B - I) MAJOR AXIS

RADIUS arcsec	(B - I) Mag/#arcsec	RADIUS arcsec	(B - I) Mag/#arcsec
8.05	2.28	37.03	2.06
12.88	2.31	41.86	1.97
17.71	2.33	46.69	2.08
22.54	2.33	51.52	2.00
27.37	2.27	56.35	1.93
32.20	1.95		

N4550 (B - I) MINOR AXIS

RADIUS arcsec	(B - I) Mag/#arcsec	RADIUS arcsec	(B - I) Mag/#arcsec
8.05	2.16	17.71	2.16
12.88	2.18		

N4552 (B - I) MAJOR AXIS

RADIUS arcsec	(B - I) Mag/#arcsec	RADIUS arcsec	(B - I) Mag/#arcsec
14.49	2.33	62.79	2.18
19.32	2.25	67.62	2.17
24.15	2.16	72.45	2.19
28.98	2.15	77.28	2.11
33.81	2.08	82.11	2.11
38.64	2.15	86.94	2.31
43.47	2.14	91.77	2.21
48.30	2.23	96.60	2.02
53.13	2.26	101.43	2.09
57.96	2.16	115.92	2.22

N4552 (B - I) MINOR AXIS

RADIUS arcsec	(B - I) Mag/#arcsec	RADIUS arcsec	(B - I) Mag/#arcsec
8.05	2.74	48.30	2.16
14.49	2.51	53.13	2.00
19.32	2.29	57.96	2.01
24.15	2.33	62.79	2.09
28.98	2.00	67.62	2.15
33.81	2.07	72.45	2.28
38.64	2.21	77.28	2.25
43.47	2.25	82.11	2.22

N4267 (R - I) MAJOR AXIS

RADIUS arcsec	(R - I) Mag/#arcsec	RADIUS arcsec	(R - I) Mag/#arcsec
8.05	0.06	37.03	0.12
12.88	0.12	41.86	0.10
17.71	0.20	46.69	0.16
22.54	0.19	51.52	0.16
27.37	0.22	56.35	0.08
32.20	0.09		

N4267 (R - I) MINOR AXIS

RADIUS arcsec	(R - I) Mag/#arcsec	RADIUS arcsec	(R - I) Mag/#arcsec
8.05	0.24	41.86	0.15
12.88	0.11	46.69	0.13
17.71	0.36	51.52	0.13
22.54	0.16	56.35	0.08
27.37	0.10	61.18	0.03
32.20	0.10	66.01	0.07
37.03	0.12	70.84	0.12

N4371 (R - I) LENS AXIS

RADIUS arcsec	(R - I) Mag/#arcsec	RADIUS arcsec	(R - I) Mag/#arcsec
8.05	1.31 :	56.35	0.27
12.88	0.32	61.18	0.24
17.71	0.28	66.01	0.31
22.54	0.42	70.84	0.24
27.37	0.32	75.67	0.25
32.20	0.27	80.50	0.29
37.03	0.28	85.33	0.19
41.86	0.31	90.16	0.12
46.69	0.34	94.99	0.15
51.52	0.27		

N4371 (R - I) BAR AXIS

RADIUS arcsec	(R - I) Mag/#arcsec	RADIUS arcsec	(R - I) Mag/#arcsec
8.05	0.31	32.20	0.44
12.88	0.23	37.03	0.23
17.71	0.39	41.86	0.22
22.54	0.44	46.69	0.22
27.37	0.45	51.52	0.13

N4377 (R - I) MAJOR AXIS

RADIUS arcsec	(R - I) Mag/#arcsec	RADIUS arcsec	(R - I) Mag/#arcsec
8.05	0.24	27.37	0.20
12.88	0.21	32.20	0.22
17.71	0.31	37.03	0.22
22.54	0.34		

N4377 (R - I) MINOR AXIS

RADIUS arcsec	(R - I) Mag/#arcsec	RADIUS arcsec	(R - I) Mag/#arcsec
8.05	0.14	22.54	0.23
12.88	0.23	27.37	0.02
17.71	0.32		

M4419 (R - I) MAJOR AXIS

RADIUS arcsec	(R - I) Mag/#arcsec	RADIUS arcsec	(R - I) Mag/#arcsec
8.05	0.50	46.69	0.27
12.88	0.02	51.52	0.27
17.71	-0.12	56.35	0.27
22.54	-0.06	61.18	0.16
27.37	0.23	66.01	0.15
32.20	0.06	70.84	0.16
37.03	0.15	75.67	0.25
41.86	0.27		

M4419 (R - I) MINOR AXIS

RADIUS arcsec	(R - I) Mag/#arcsec	RADIUS arcsec	(R - I) Mag/#arcsec
5.09	-0.31	24.15	0.29
10.10	0.08		

N4425 (R - I) M JCR KPNIS

RADIUS arcsec	(R - I) Mag/#arcsec	RADIUS arcsec	(R - I) Mag/#arcsec
8.05	0.02	41.86	0.29
12.88	0.18	46.69	0.29
17.71	0.34	51.52	0.18
22.54	0.32	56.35	0.22
27.37	0.38	61.18	0.26
32.20	0.38	66.01	0.21
37.03	0.30		

N4429 (R - I) MAJOR AXIS

RADIUS arcsec	(R - I) Mag/#arcsec	RADIUS arcsec	(R - I) Mag/#arcsec
8.05	1.31	80.50	0.32
12.88	0.10	85.33	0.29
17.71	0.15	90.16	0.28
22.54	0.28	94.99	0.25
27.37	0.30	99.82	0.22
32.20	0.25	104.65	0.21
37.03	0.39	109.48	0.23
41.86	0.38	114.31	0.23
46.69	0.30	119.14	0.22
51.52	0.32	123.97	0.20
56.35	0.36	128.80	0.20
61.18	0.37	133.63	0.24
66.01	0.37	138.46	0.20
70.84	0.38	143.29	0.27
75.67	0.31	148.12	0.32

N4429 (R - I) MINOR AXIS

RADIUS arcsec	(R - I) Mag/#arcsec	RADIUS arcsec	(R - I) Mag/#arcsec
8.05	1.44	37.03	0.21
12.88	0.20	41.86	0.15
17.71	0.41	46.69	0.21
22.54	0.44	51.52	0.38
27.37	0.32	56.35	0.32
32.20	0.23	61.18	0.20

N4435 (R - I) MAJOR AXIS

RADIUS arcsec	(R - I) Mag/#arcsec	RADIUS arcsec	(R - I) Mag/#arcsec
8.05	0.47	41.86	0.41
12.88	0.29	46.69	0.30
17.71	0.38	51.52	0.25
22.54	0.30	56.35	0.22
27.37	0.28	61.18	0.25
32.20	0.27	66.01	0.27
37.03	0.47		

N4435 (R - I) MINOR AXIS

RADIUS arcsec	(R - I) Mag/#arcsec	RADIUS arcsec	(R - I) Mag/#arcsec
8.05	0.37	28.98	0.34
14.49	0.43	33.81	0.22
19.32	0.48	38.64	0.27
24.15	0.34	43.47	0.13

N4438 (R - I) MAJOR AXIS

RADIUS arcsec	(R - I) Mag/#arcsec	RADIUS arcsec	(R - I) Mag/#arcsec
8.05	0.57	-32.20	0.38
12.88	0.49	-37.03	0.35
17.71	0.94	-41.86	0.45
22.54	0.63	-46.69	0.33
27.37	0.44	-51.52	0.45
32.20	0.43	-56.35	0.42
37.03	0.27	-61.18	0.38
41.86	0.32	-66.01	0.37
46.69	0.16	-70.84	0.40
51.52	0.35	-75.67	0.34
56.35	0.39	-80.50	0.30
61.18	0.37	-85.33	0.23
66.01	0.35	-90.16	0.21
70.84	0.20	-94.99	0.34
75.67	0.16	-99.82	0.35
80.50	0.15	-120.75	0.41
85.33	-0.01	-141.68	0.28
90.16	0.07	-183.54	0.25
-8.05	0.42	-188.37	0.21
-12.88	0.64	-193.20	0.13
-17.71	0.96	-198.03	0.04
-22.54	0.53	-202.86	0.07
-27.37	0.51	-207.69	0.06

N4438 (R - I) MINOR AXIS

RADIUS arcsec	(R - I) Mag/#arcsec	RADIUS arcsec	(R - I) Mag/#arcsec
8.05	0.34	27.37	0.38
12.88	0.14	32.20	0.23
17.71	0.25	37.03	0.18
22.54	0.23	41.86	0.13

N4459 (R - I) MAJOR AXIS

RADIUS arcsec	(R - I) Mag/#arcsec	RADIUS arcsec	(R - I) Mag/#arcsec
8.05	0.72	56.35	0.42
12.88	0.14	61.18	0.35
17.71	0.18	66.01	0.32
22.54	0.00	70.84	0.34
27.37	0.32	75.67	0.36
32.20	0.37	80.50	0.31
37.03	0.34	85.33	0.25
41.86	0.32	90.16	0.38
46.69	0.34	94.99	0.36
51.52	0.33	99.82	0.35

N4459 (R - I) MINOR AXIS

RADIUS arcsec	(R - I) Mag/#arcsec	RADIUS arcsec	(R - I) Mag/#arcsec
8.05	0.61	41.86	0.37
12.88	-0.04	46.69	0.42
17.71	0.03	51.52	0.46
22.54	0.25	56.35	0.49
27.37	0.33	61.18	0.42
32.20	0.33	66.01	0.39
37.03	0.43	70.84	0.38

N4461 (R - I) MAJOR AXIS

RADIUS arcsec	(R - I) Mag/#arcsec	RADIUS arcsec	(R - I) Mag/#arcsec
8.05	1.16	51.52	0.69
12.88	0.61	56.35	0.69
17.71	0.59	61.18	0.64
22.54	0.64	66.01	0.55
27.37	0.66	70.84	0.52
32.20	0.78	75.67	0.49
37.03	0.59	80.50	0.54
41.86	0.57	85.33	0.64
46.69	0.57		

N4461 (R - I) MINOR AXIS

RADIUS arcsec	(R - I) Mag/#arcsec	RADIUS arcsec	(R - I) Mag/#arcsec
8.05	1.44	22.54	0.64
12.88	1.00	27.37	0.68
17.71	0.61	32.20	0.69

N4474 (R - I) MAJOR AXIS

RADIUS arcsec	(R - I) Mag/#arcsec	RADIUS arcsec	(R - I) Mag/#arcsec
8.05	0.62	37.03	0.42
12.88	0.28	41.86	0.40
17.71	0.25	46.69	0.45
22.54	0.34	51.52	0.45
27.37	0.32	56.35	0.38
32.20	0.38		

N4474 (R - I) MINOR AXIS

RADIUS arcsec	(R - I) Mag/#arcsec	RADIUS arcsec	(R - I) Mag/#arcsec
8.05	0.11	24.15	0.39
14.49	0.50	28.98	0.38
19.32	0.38		

N4477 (R - I) MAJOR AXIS

RADIUS arcsec	(R - I) Mag/#arcsec	RADIUS arcsec	(R - I) Mag/#arcsec
8.05	0.95	51.52	0.62
12.88	0.56	56.35	0.63
17.71	0.48	61.18	0.68
22.54	0.47	66.01	0.68
27.37	0.51	70.84	0.62
32.20	0.61	75.67	0.57
37.03	0.55	80.50	0.61
41.86	0.61	85.33	0.58
46.69	0.56		

N4477 (R - I) MINOR AXIS

RADIUS arcsec	(R - I) Mag/#arcsec	RADIUS arcsec	(R - I) Mag/#arcsec
8.05	0.94	46.69	0.59
12.88	0.61	51.52	0.56
17.71	0.61	56.35	0.54
22.54	0.58	61.18	0.59
27.37	0.59	66.01	0.65
32.20	0.60	70.84	0.66
37.03	0.62	75.67	0.72
41.86	0.55	80.50	0.73

N4501 (R - I) MAJOR AXIS

RADIUS arcsec	(R - I) Mag/#arcsec	RADIUS arcsec	(R - I) Mag/#arcsec
8.05	1.06	90.16	0.40
12.88	0.59	94.99	0.38
17.71	0.59	99.82	0.43
22.54	0.59	104.65	0.38
27.37	0.46	109.48	0.36
32.20	0.36	114.31	0.40
37.03	0.42	119.14	0.36
41.86	0.51	123.97	0.24
46.69	0.38	128.80	0.21
51.52	0.34	133.63	0.19
56.35	0.45	138.46	0.14
61.18	0.43	143.29	0.22
66.01	0.38	148.12	0.33
70.84	0.39	152.95	0.34
75.67	0.46	157.78	0.41
80.50	0.43	162.61	0.42
85.33	0.43		

N4501 (R - I) MINOR AXIS

RADIUS arcsec	(R - I) Mag/#arcsec	RADIUS arcsec	(R - I) Mag/#arcsec
8.05	1.13	46.69	0.35
12.88	0.58	51.52	0.38
17.71	0.71	56.35	0.38
22.54	0.44	61.18	0.42
27.37	0.62	66.01	0.44
32.20	0.46	70.84	0.41
37.03	0.34	75.67	0.50
41.86	0.46	80.50	0.49

N4503 (R - I) MAJOR AXIS

RADIUS arcsec	(R - I) Mag/#arcsec	RADIUS arcsec	(R - I) Mag/#arcsec
8.05	0.55	51.52	0.33
12.88	0.34	56.35	0.36
17.71	0.45	61.18	0.23
22.54	0.46	66.01	0.23
27.37	0.39	70.84	0.22
32.20	0.43	75.67	0.25
37.03	0.31	80.50	0.26
41.86	0.43	85.33	0.36
46.69	0.34		

N4503 (R - I) MINOR AXIS

RADIUS arcsec	(R - I) Mag/#arcsec	RADIUS arcsec	(R - I) Mag/#arcsec
8.05	0.78	27.37	0.37
12.88	0.40	32.20	0.38
17.71	0.48	37.03	0.33
22.54	0.43		

N4531 (R - I) MAJOR AXIS

RADIUS arcsec	(R - I) Mag/#arcsec	RADIUS arcsec	(R - I) Mag/#arcsec
8.05	0.49	41.86	0.33
12.88	0.39	46.69	0.31
17.71	0.30	51.52	0.25
22.54	0.41	56.35	0.20
27.37	0.30	61.18	0.22
32.20	0.34	66.01	0.23
37.03	0.34		

N4531 (R - I) MINOR AXIS

RADIUS arcsec	(R - I) Mag/#arcsec	RADIUS arcsec	(R - I) Mag/#arcsec
8.05	0.51	27.37	0.29
12.88	0.35	32.20	0.28
17.71	0.29	37.03	0.20
22.54	0.29	41.86	0.09

N4550 (R - I) MAJOR AXIS

RADIUS arcsec	(R - I) Mag/#arcsec	RADIUS arcsec	(R - I) Mag/#arcsec
8.05	0.58	37.03	0.31
12.88	0.25	41.86	0.28
17.71	0.38	46.69	0.28
22.54	0.39	51.52	0.28
27.37	0.40	56.35	0.30
32.20	0.44		

N4552 (R - I) MAJOR AXIS

RADIUS arcsec	(R - I) Mag/#arcsec	RADIUS arcsec	(R - I) Mag/#arcsec
8.05	1.10	61.18	0.07
12.88	0.31	66.01	0.08
17.71	0.11	70.84	0.06
22.54	0.03	75.67	0.06
27.37	0.10	80.50	0.13
32.20	0.21	85.33	0.10
37.03	0.19	90.16	0.01
41.86	0.05	94.99	0.03
46.69	0.09	99.82	0.08
51.52	0.12	104.65	0.16
56.35	0.09		

N4552 (R - I) MINOR AXIS

RADIUS arcsec	(R - I) Mag/#arcsec	RADIUS arcsec	(R - I) Mag/#arcsec
8.05	1.15	48.30	0.03
14.49	0.08	53.13	0.05
19.32	0.06	57.96	0.01
24.15	0.17	62.79	-0.06
28.98	0.26	67.62	-0.06
33.81	0.15	72.45	0.05
38.64	0.14	77.28	0.06
43.47	0.06	82.11	0.04

APPENDIX 'I'

Tabular Listing of Luminosity Profiles

N4267 'B' MAJOR AXIS

NE WING

RADIUS arcsec	BRIGHTNESS Mag/#arcsec	RADIUS arcsec	BRIGHTNESS Mag/#arcsec
6.44	18.16	53.13	23.94
8.05	19.47	54.74	24.11
9.66	19.82	56.35	24.23
11.27	20.03	57.96	24.20
12.88	20.99	59.57	24.12
14.49	21.17	61.18	24.11
16.10	21.36	62.79	24.17
17.71	21.75	64.40	24.31
19.32	22.02	66.01	24.39
20.93	22.19	67.62	24.42
22.54	21.88	69.23	24.36
24.15	22.25	70.84	24.35
25.76	22.56	72.45	24.45
27.37	22.71	74.06	24.60
28.98	22.67	75.67	24.65
30.59	22.90	77.28	24.67
32.20	23.11	78.89	24.61
33.81	23.24	80.50	24.67
35.42	23.21	82.11	24.96
37.03	23.21	83.72	25.15
38.64	23.28	85.33	25.35
40.25	23.38	86.94	25.48
41.86	23.47	88.55	25.49
43.47	23.52	90.16	25.46
45.08	23.58	91.77	25.42
46.69	23.58	93.38	25.45
48.30	23.58	94.99	25.58
49.91	23.65	96.60	26.04
51.52	23.74		

N4267 'B' MAJOR AXIS

SW WING

RADIUS arcsec	BRIGHTNESS Mag/#arcsec	RADIUS arcsec	BRIGHTNESS Mag/#arcsec
6.44	19.26	67.62	24.23
8.05	19.35	69.23	24.30
9.66	19.82	70.84	24.36
11.27	20.65	72.45	24.49
12.88	21.19	74.06	24.56
14.49	21.53	75.67	24.55
16.10	21.51	77.28	24.54
17.71	22.20	78.89	24.49
19.32	21.79	80.50	24.48
20.93	22.29	82.11	24.54
22.54	22.29	83.72	24.60
24.15	22.43	85.33	24.71
25.76	22.14	86.94	24.86
27.37	22.53	88.55	24.98
28.98	22.71	90.16	25.04
30.59	22.80	91.77	25.05
32.20	22.94	93.38	25.04
33.81	23.04	94.99	25.03
35.42	23.16	96.60	25.06
37.03	23.28	98.21	25.17
38.64	23.37	99.82	25.30
40.25	23.37	101.43	25.39
41.86	23.30	103.04	25.37
43.47	23.24	104.65	25.31
45.08	23.28	106.26	25.31
46.69	23.42	107.87	25.36
48.30	23.60	109.48	25.44
49.91	23.74	111.09	25.52
51.52	23.77	112.70	25.60
53.13	23.72	114.31	25.62
54.74	23.67	115.92	25.65
56.35	23.71	117.53	25.69
57.96	23.81	119.14	25.80
59.57	23.81	120.75	25.99
61.18	23.79	122.36	26.11
62.79	23.82	123.97	26.27
64.40	24.00	125.58	26.52
66.01	24.17	127.19	26.69

N4267 'B' MINOR AXIS

SE WING

RADIUS arcsec	BRIGHTNESS Mag/#arcsec	RADIUS arcsec	BRIGHTNESS Mag/#arcsec
6.44	18.88	57.96	23.91
8.05	19.85	59.57	24.01
9.66	19.82	61.18	24.10
11.27	20.56	62.79	24.20
12.88	21.12	64.40	24.33
14.49	21.82	66.01	24.43
16.10	21.79	67.62	24.45
17.71	22.27	69.23	24.42
19.32	22.36	70.84	24.39
20.93	22.60	72.45	24.35
22.54	22.68	74.06	24.35
24.15	22.73	75.67	24.43
25.76	22.74	77.28	24.56
27.37	22.80	78.89	24.70
28.98	22.78	80.50	24.84
30.59	22.77	82.11	25.02
32.20	22.31	83.72	25.19
33.81	22.81	85.33	25.28
35.42	23.06	86.94	25.32
37.03	23.06	88.55	25.29
38.64	23.04	90.16	25.27
40.25	23.03	91.77	25.40
41.86	23.08	93.38	25.71
43.47	23.17	94.99	26.07
45.08	23.31	96.60	26.44
46.69	23.41	98.21	26.60
48.30	23.47	99.82	26.45
49.91	23.52	101.43	26.11
51.52	23.60	103.04	25.77
53.13	23.66	104.65	25.48
54.74	23.72	106.26	25.48
56.35	23.79	107.87	25.89

N4267 'B' MINOR AXIS

NW WING

RADIUS arcsec	BRIGHTNESS Mag/#arcsec	RADIUS arcsec	BRIGHTNESS Mag/#arcsec
6.44	19.01	66.01	24.01
8.05	20.14	67.62	23.94
9.66	19.82	69.23	23.93
11.27	20.37	70.84	24.00
12.88	20.99	72.45	24.17
14.49	21.66	74.06	24.23
16.10	22.07	75.67	24.23
17 71	22.02	77.28	24.21
19 32	22.29	78.89	24.27
20.93	22.33	80.50	24.42
22.54	22.57	82.11	24.46
24.15	22.68	83.72	24.49
25.76	22.74	85.33	24.48
27.37	22.79	86.94	24.49
28.98	22.81	88.55	24.68
30.59	22.80	90.16	24.83
32.20	22.89	91.77	25.05
33.81	23.03	93.38	25.29
35.42	23.13	94.99	25.47
37.03	23.12	96.60	25.53
38.64	23.14	98.21	25.48
40.25	23.17	99.82	25.38
41.86	23.26	101.43	25.17
43.47	23.31	103.04	25.01
45.08	23.37	104.65	24.96
46.69	23.39	106.26	25.01
48.30	23.37	107.87	25.10
49.91	23.37	109.48	25.23
51.52	23.47	111.09	25.37
53.13	23.59	112.70	25.51
54.74	23.72	114.31	25.69
56.35	23.81	115.92	25.85
57.96	23.92	117.53	26.01
59.57	23.97	119.14	26.22
61.18	24.01	120.75	26.50
62.79	23.99	122.36	26.63
64.40	24.00		

N4371 'B' BAR AXIS

S WING

RADIUS arcsec	BRIGHTNESS Mag/#arcsec	RADIUS arcsec	BRIGHTNESS Mag/#arcsec
6.44	18.86	48.30	23.62
8.05	19.52	49.91	23.85
9.66	20.39	51.52	24.08
11.27	20.65	53.13	24.29
12.88	20.71	54.74	24.53
14.49	21.15	56.35	24.82
16.10	21.20	57.96	25.02
17.71	21.52	59.57	25.17
19.32	21.67	61.18	25.30
20.93	21.83	62.79	25.44
22.54	21.61	64.40	25.71
24.15	21.77	66.01	25.99
25.76	21.88	67.62	26.17
27.37	21.96	69.23	26.25
28.98	22.02	70.84	26.26
30.59	22.14	72.45	26.15
32.20	22.15	74.06	26.00
33.81	22.04	75.67	25.81
35.42	22.30	77.28	25.66
37.03	22.05	78.89	25.60
38.64	22.15	80.50	25.68
40.25	22.39	82.11	25.88
41.86	22.80	83.72	26.12
43.47	23.09	85.33	26.41
45.08	23.26	86.94	26.97
46.69	23.42		

N4371 'B' B R AXIS

N WING

RADIUS arcsec	BRIGHTNESS Mag/#arcsec	RADIUS arcsec	BRIGHTNESS Mag/#arcsec
6.44	18.86	40.25	23.10
8.05	20.61	41.86	23.26
9 66	20.86	43.47	23.43
11 27	21.00	45.08	23.59
12.88	21 40	46.69	23.72
14.49	21 44	48.30	23.87
16.10	21.58	49.91	24.06
17.71	21.43	51.52	24.27
19.32	21.66	53.13	24.43
20.93	21.86	54.74	24.55
22.54	21.88	56.35	24 71
24.15	21.86	57.96	24.80
25.76	21.67	59.57	24.87
27.37	21.86	61.18	24.94
28.98	22.13	62.79	24 99
30.59	22.20	64.40	25.05
32.20	22.25	66.01	25.13
33.81	22.37	67.62	25.25
35.42	22.54	69.23	25.38
37.03	22.72	70.84	25.64
38.64	22.93	72.45	26.07

N4371 'B' LENS AXIS

W WING

RADIUS arcsec	BRIGHTNESS Mag/#arcsec	RADIUS arcsec	BRIGHTNESS Mag/#arcsec
6.44	18.86	80.50	24.15
8.05	19.47	82.11	24.15
9.66	19.74	83.72	24.14
11.27	20.09	85.33	24.22
12.88	20.47	86.94	24.28
14.49	20.71	88.55	24.27
16.10	21.20	90.16	24.19
17.71	21.45	91.77	24.10
19.32	21.57	93.38	24.09
20.93	21.73	94.99	24.17
22.54	21.90	96.60	24.30
24.15	22.06	98.21	24.39
25.76	22.22	99.82	24.46
27.37	22.39	101.43	24.54
28.98	22.49	103.04	24.61
30.59	22.64	104.65	24.65
32.20	22.82	106.26	24.65
33.81	22.96	107.87	24.60
35.42	23.01	109.48	24.54
37.03	23.00	111.09	24.45
38.64	23.00	112.70	24.48
40.25	23.12	114.31	24.67
41.86	23.29	115.92	24.79
43.47	23.41	117.53	24.94
45.08	23.45	119.14	25.05
46.69	23.47	120.75	25.15
48.30	23.44	122.36	25.22
49.91	23.31	123.97	25.26
51.52	23.20	125.58	25.28
53.13	23.20	127.19	25.31
54.74	23.31	128.80	25.34
56.35	23.41	130.41	25.33
57.96	23.46	132.02	25.33
59.57	23.49	133.63	25.39
61.18	23.52	135.24	25.47
62.79	23.59	136.85	25.56
64.40	23.67	138.46	25.57
66.01	23.75	140.07	25.65
67.62	23.81	141.68	25.73
69.23	23.86	143.29	25.73
70.84	23.90	144.90	25.68
72.45	23.89	146.51	25.79
74.06	23.89	148.12	25.90
75.67	23.91	149.73	25.93
77.28	24.00	151.34	25.97
78.89	24.11	152.95	26.26

M4371 'B' LENS AXIS

E TING

RADIUS arcsec	BRIGHTNESS Mag/#arcsec	RADIUS arcsec	BRIGHTNESS Mag/#arcsec
6.44	18.86	96.60	24.24
8.05	19.47	98.21	24.29
9.66	19.74	99.82	24.32
11.27	20.09	101.43	24.32
12.88	19.85	103.04	24.29
14.49	20.30	104.65	24.30
16.10	20.36	106.26	24.39
17.71	20.96	107.87	24.58
19.32	21.08	109.48	24.72
20.93	21.17	111.09	24.81
22.54	21.73	112.70	24.85
24.15	21.96	114.31	24.85
25.76	22.11	115.92	24.82
27.37	22.22	117.53	24.79
28.98	22.38	119.14	24.79
30.59	22.53	120.75	24.81
32.20	22.71	122.36	24.84
33.81	22.91	123.97	24.87
35.42	23.07	125.58	24.90
37.03	23.18	127.19	24.90
38.64	23.20	128.80	24.86
40.25	23.17	130.41	24.83
41.86	23.11	132.02	24.82
43.47	23.09	133.63	24.83
45.08	23.12	135.24	24.89
46.69	23.15	136.85	25.01
48.30	23.16	138.46	25.12
49.91	23.20	140.07	25.20
51.52	23.27	141.68	25.25
53.13	23.34	143.29	25.27
54.74	23.37	144.90	25.30
56.35	23.38	146.51	25.36
57.96	23.38	148.12	25.43
59.57	23.40	149.73	25.47
61.18	23.45	151.34	25.49
62.79	23.53	152.95	25.49
64.40	23.62	154.56	25.44
66.01	23.71	156.17	25.39
67.62	23.77	157.78	25.39
69.23	23.81	159.39	25.43
70.84	23.83	161.00	25.48
72.45	23.85	162.61	25.54
74.06	23.83	164.22	25.56
75.67	23.83	165.83	25.60
77.28	23.84	167.44	25.70
78.89	23.93	169.05	25.79
80.50	24.06	170.66	25.90
82.11	24.21	172.27	26.07
83.72	24.27	173.88	26.18
85.33	24.22	175.49	26.13
86.94	24.14	177.10	26.01
88.55	24.08	178.71	25.93
90.16	24.05	180.32	26.00
91.77	24.07	181.93	26.31
93.38	24.12	183.54	26.56
94.99	24.18		

N4377 'B' MAJOR AXIS

S WING

RADIUS arcsec	BRIGHTNESS Mag/#arcsec	RADIUS arcsec	BRIGHTNESS Mag/#arcsec
6.44	20.33	33.81	23.58
8.05	20.70	35.42	23.63
9.66	21.11	37.03	23.73
11.27	21.49	38.64	23.88
12.88	21.73	40.25	23.94
14.49	21.96	41.86	24.10
16.10	21.85	43.47	24.36
17.71	22.07	45.08	24.56
19.32	22.13	46.69	24.81
20.93	22.06	48.30	24.96
22.54	22.40	49.91	25.04
24.15	22.45	51.52	25.14
25.76	22.60	53.13	25.23
27.37	22.90	54.74	25.34
28.98	23.13	56.35	25.50
30.59	23.35	57.96	25.83
32.20	23.51		

N4377 'B' M'JOR 'YIS

N WING

RADIUS arcsec	BRIGHTNESS Mag/#arcsec	RADIUS arcsec	BRIGHTNESS Mag/#arcsec
6.44	19.83	33.81	23.67
8.05	20.12	35.42	23.81
9.66	20.51	37.03	23.93
11.27	21.22	38.64	24.08
12.88	21.40	40.25	24.25
14.49	21.42	41.86	24.42
16.10	21.89	43.47	24.59
17.71	22.11	45.08	24.77
19.32	22.26	46.69	24.99
20.93	21.95	48.30	25.20
22.54	22.33	49.91	25.35
24.15	22.45	51.52	25.46
25.76	22.51	53.13	25.57
27.37	22.63	54.74	25.72
28.98	22.93	56.35	25.89
30.59	23.23	57.96	26.12
32.20	23.50	59.57	26.51

N4377 'B' MINOR AXIS

W WING

RADIUS arcsec	BRIGHTNESS Mag/#arcsec	RADIUS arcsec	BRIGHTNESS Mag/#arcsec
6.44	20.33	28.98	23.71
8.05	20.70	30.59	23.90
9.66	21.11	32.20	24.07
11.27	21.49	33.81	24.24
12.88	21.73	35.42	24.41
14.49	21.96	37.03	24.58
16.10	21.85	38.64	24.70
17.71	22.07	40.25	24.82
19.32	22.13	41.86	24.92
20.93	22.06	43.47	24.99
22.54	22.26	45.08	25.08
24.15	22.67	46.69	25.26
25.76	23.08	48.30	25.66
27.37	23.43		

N4377 'B' MINOR AXIS

F WING

RADIUS arcsec	BRIGHTNESS Mag/#arcsec	RADIUS arcsec	BRIGHTNESS Mag/#arcsec
6.44	18.82	33.81	24.34
8.05	19.99	35.42	24.59
9.66	20.84	37.03	24.89
11.27	21.78	38.64	25.12
12.88	21.12	40.25	25.28
14.49	21.29	41.86	25.47
16.10	21.47	43.47	25.65
17.71	21.68	45.08	25.74
19.32	21.92	46.69	25.90
20.93	22.26	48.30	26.07
22.54	22.48	49.91	26.09
24.15	22.74	51.52	26.03
25.76	23.04	53.13	26.06
27.37	23.32	54.74	26.15
28.98	23.58	56.35	26.25
30.59	23.81	57.96	26.39
32.20	24.06	59.57	26.65

N4419 'B' MAJOR AXIS

SE WING

RADIUS arcsec	BRIGHTNESS Mag/#arcsec	RADIUS arcsec	BRIGHTNESS Mag/#arcsec
6.44	18.95	64.40	22.99
8.05	20.21	66.01	23.21
9.66	20 13	67.62	23.35
11.27	19.86	69.23	23.56
12.88	20.51	70.84	23.75
14.49	21.22	72.45	23.92
16.10	20.72	74.06	24.07
17.71	21.17	75.67	24.20
19.32	20.99	77.28	24.30
20.93	21.28	78.89	24.33
22.54	21.29	80.50	24.37
24.15	21.25	82.11	24.43
25.76	21.29	83.72	24.60
27.37	21.65	85.33	24.86
28.98	21.87	86.94	24.98
30.59	21.32	88.55	25.12
32.20	21.87	90.16	25.22
33.81	21.60	91.77	25.37
35.42	21.58	93.38	25.42
37.03	21.74	94.99	25.44
38.64	21.84	96.60	25.41
40.25	21.91	98.21	25.30
41.86	21.62	99.82	25.11
43.47	22.13	101.43	25.09
45.08	21.86	103.04	25.19
46.69	21.85	104.65	25.22
48.30	22.11	106.26	25.28
49.91	21.87	107.87	25.36
51.52	22.23	109.48	25.59
53.13	22.23	111.09	25.78
54.74	22.48	112.70	26.03
56.35	22.47	114.31	26.08
57.96	22.55	115.92	26.16
59.57	22.77	117.53	26.04
61.18	22.83	119.14	26.02
62.79	22.72	120.75	26.21

N4419 'B' MAJOR AXIS

NW WING

RADIUS arcsec	BRIGHTNESS Mag/#arcsec	RADIUS arcsec	BRIGHTNESS Mag/#arcsec
6.44	20.57	56.35	22.16
8.05	19.04	57.96	22.14
9.66	19.64	59.57	22.32
11.27	19.84	61.18	22.55
12.88	20.51	62.79	22.69
14.49	20.30	64.40	22.66
16.10	20.39	66.01	22.97
17.71	20.69	67.62	23.12
19.32	20.80	69.23	23 14
20.93	20.84	70.84	23.14
22.54	21.67	72.45	23.26
24.15	21.24	74.06	23 46
25.76	21.51	75.67	23 65
27.37	21.08	77.28	23.80
28.98	21.22	78.89	23.92
30.59	21.20	80.50	24.05
32.20	21.28	82.11	24.12
33.81	21.43	83.72	24.21
35.42	21.38	85.33	24.32
37.03	21.50	86.94	24.48
38.64	21.14	88.55	24.62
40.25	21.36	90.16	24.75
41.86	21.43	91.77	24.90
43.47	21.47	93.38	25.09
45.08	21.91	94.99	25.33
46.69	21.80	96.60	25.48
48.30	21.71	98.21	25.61
49.91	22.04	99.82	25.71
51.52	21.97	101.43	25.86
53.13	22.23	103.04	26.04
54.74	22.08	104.65	26.49

N4419 'B' MINOR AXIS

SW WING

RADIUS arcsec	BRIGHTNESS Mag/#arcsec	RADIUS arcsec	BRIGHTNESS Mag/#arcsec
5.44	20.57	25.76	23.98
8.05	20.21	27.37	24.26
9.66	20.96	28.98	24.52
11.27	21.53	30.59	24.90
12.88	21.89	32.20	25.15
14.49	21.80	33.81	25.34
16.10	22.34	35.42	25.45
17.71	22.84	37.03	25.47
19.32	23.13	38.64	25.55
20.93	23.23	40.25	25.74
22.54	23.39	41.86	26.03
24.15	23.67	43.47	26.42

N4419 'B' M'JOR AXIS

NE "ING

RADIUS arcsec	BRIGHTNESS Mag/#arcsec	RADIUS arcsec	BRIGHTNESS Mag/#arcsec
6.44	20.57	27.37	23.99
8.05	20.21	28.98	24.25
9.66	20.74	30.59	24.32
11.27	21.17	32.20	24.32
12.88	20.51	33.81	24.44
14.49	21.51	35.42	24.97
16.10	22.19	37.03	25.45
17.71	21.75	38.64	25.91
19.32	22.21	40.25	26.27
20.93	22.51	41.86	26.38
22.54	22.93	43.47	26.27
24.15	23.30	45.08	26.09
25.76	23.66	46.69	26.05

N4425 'B' MAJOR AXIS

SW WING

RADIUS arcsec	BRIGHTNESS Mag/#arcsec	RADIUS arcsec	BRIGHTNESS Mag/#arcsec
6.44	20.83	56.35	23.51
8.05	20.05	57.96	23.59
9.66	20.55	59.57	23.67
11.27	20.95	61.18	23.73
12.88	21.34	62.79	23.83
14.49	21.06	64.40	23.95
16.10	21.30	66.01	24.11
17.71	21.19	67.62	24.20
19.32	21.36	69.23	24.26
20.93	21.52	70.84	24.39
22.54	21.21	72.45	24.62
24.15	21.43	74.06	24.77
25.76	21.52	75.67	24.89
27.37	21.40	77.28	24.94
28.98	21.52	78.89	24.99
30.59	21.84	80.50	25.18
32.20	21.87	82.11	25.54
33.81	22.07	83.72	25.79
35.42	22.06	85.33	25.87
37.03	22.03	86.94	25.90
38.64	22.18	88.55	25.91
40.25	22.09	90.16	25.82
41.86	22.50	91.77	25.73
43.47	22.58	93.38	25.74
45.08	22.59	94.99	25.69
46.69	22.78	96.60	25.60
48.30	22.83	98.21	25.46
49.91	22.90	99.82	25.44
51.52	23.03	101.43	25.55
53.13	23.24	103.04	25.96
54.74	23.42	104.65	26.31

N4425 'B' MAJOR AXIS

NE WING

RADIUS arcsec	BRIGHTNESS Mag/#arcsec	RADIUS arcsec	BRIGHTNESS Mag/#arcsec
6.44	20.83	62.79	23.93
8.05	20.87	64.40	24.08
9.66	20.91	66.01	24.24
11.27	20.79	67.62	24.31
12.88	20.95	69.23	24.44
14.49	21.14	70.84	24.65
16.10	21.32	72.45	24.73
17.71	21.47	74.06	24.83
19.32	21.40	75.67	24.86
20.93	21.36	77.28	24.89
22.54	21.39	78.89	25.03
24.15	21.41	80.50	25.26
25.76	21.16	82.11	25.51
27.37	21.57	83.72	25.73
28.98	21.55	85.33	25.92
30.59	21.63	86.94	26.03
32.20	21.74	88.55	26.10
33.81	21.93	90.16	26.19
35.42	21.98	91.77	26.33
37.03	21.46	93.38	26.45
38.64	22.21	94.99	26.40
40.25	22.40	96.60	26.23
41.86	22.56	98.21	25.94
43.47	22.70	99.82	25.59
45.08	22.79	101.43	25.34
46.69	22.91	103.04	25.40
48.30	23.03	104.65	25.66
49.91	23.16	106.26	25.96
51.52	23.24	107.87	26.24
53.13	23.27	109.48	26.50
54.74	23.34	111.09	26.46
56.35	23.48	112.70	26.23
57.96	23.67	114.31	26.05
59.57	23.78	115.92	26.79
61.18	23.85		

N4425 'B' MINOR AXIS

SE WING

RADIUS arcsec	BRIGHTNESS Mag/#arcsec	RADIUS arcsec	BRIGHTNESS Mag/#arcsec
6.44	20.09	25.76	24.14
8.05	20.05	27.37	24.27
9.66	21.39	28.98	24.31
11.27	22.03	30.59	24.35
12.88	22.53	32.20	24.62
14.49	22.79	33.81	24.95
16.10	22.89	35.42	25.17
17.71	23.08	37.03	25.27
19.32	23.30	38.64	25.35
20.93	23.49	40.25	25.54
22.54	23.66	41.86	25.90
24.15	23.88	43.47	26.02

N4425 'B' MINOR AXIS

NW WING

RADIUS arcsec	BRIGHTNESS Mag/#arcsec	RADIUS arcsec	BRIGHTNESS Mag/#arcsec
6.44	20.83	27.37	24.43
8.05	20.77	28.98	24.66
9.66	20.91	30.59	24.83
11.27	21.89	32.20	25.12
12.88	22.27	33.81	25.28
14.49	22.59	35.42	25.51
16.10	22.89	37 03	25.70
17.71	23.23	38.64	25.99
19.32	23.58	40.25	26.16
20.93	23.96	41.86	26.41
22.54	24.24	43.47	26.68
24.15	24.40	45.08	26.69
25.76	24.34		

N4429 'B' MAJOR AXIS

W WING

RADIUS arcsec	BRIGHTNESS Mag/#arcsec	RADIUS arcsec	BRIGHTNESS Mag/#arcsec
6.44	19.41	103.04	23.34
8.05	19.70	104.65	23.38
9.66	20.09	106.26	23.48
11.27	19.51	107.87	23.59
12.88	20.35	109.48	23.67
14.49	19.83	111.09	23.71
16.10	20.26	112.70	23.75
17.71	20.38	114.31	23.80
19.32	20.32	115.92	23.85
20.93	20.76	117.53	23.88
22.54	20.91	119.14	23.91
24.15	20.57	120.75	23.95
25.76	21.11	122.36	23.98
27.37	21.24	123.97	24.00
28.98	21.29	125.58	24.03
30.59	21.52	127.19	24.09
32.20	21.44	128.80	24.14
33.81	21.37	130.41	24.16
35.42	21.55	132.02	24.15
37.03	21.75	133.63	24.17
38.64	21.47	135.24	24.21
40.25	21.61	136.85	24.26
41.86	21.92	138.46	24.32
43.47	21.99	140.07	24.37
45.08	22.09	141.68	24.44
46.69	22.10	143.29	24.50
48.30	22.13	144.90	24.54
49.91	22.19	146.51	24.54
51.52	22.14	148.12	24.51
53.13	22.31	149.73	24.44
54.74	22.31	151.34	24.40
56.35	22.35	152.95	24.43
57.96	22.38	154.56	24.52
59.57	22.44	156.17	24.64
61.18	22.37	157.78	24.66
62.79	22.29	159.39	24.70
64.40	22.27	161.00	24.70
66.01	22.27	162.61	24.88
67.62	22.31	164.22	24.94
69.23	22.38	165.83	24.98
70.84	22.35	167.44	25.01
72.45	22.30	169.05	24.98
74.06	22.26	170.66	24.96
75.67	22.16	172.27	25.02
77.28	22.29	173.88	25.16
78.89	22.31	175.49	25.33
80.50	22.19	177.10	25.44
82.11	22.27	178.71	25.50
83.72	22.21	180.32	25.53
85.33	22.32	181.93	25.51
86.94	22.48	183.54	25.49
88.55	22.51	185.15	25.52
90.16	22.58	186.76	25.60
91.77	22.73	188.37	25.67
93.38	22.87	189.98	25.71
94.99	22.97	191.59	25.78
96.60	23.10	193.20	25.86
98.21	23.25	194.81	25.88
99.82	23.34	196.42	25.93
101.43	23.34	198.03	26.08

N4429 'B' MAJOR AXIS

W WING

RADIUS arcsec	BRIGHTNESS Mag/#arcsec	RADIUS arcsec	BRIGHTNESS Mag/#arcsec
199.64	26.25	207.69	25.86
201.25	26.30	209.30	25.83
202.86	26.30	210.91	26.02
204.47	26.23	212.52	26.34
206.08	26.05	214.13	26.56

N4429 'B' MAJOR AXIS

E WING

RADIUS arcsec	BRIGHTNESS Mag/#arcsec	RADIUS arcsec	BRIGHTNESS Mag/#arcsec
6.44	19.41	103.04	23.47
8.05	19.70	104.65	23.57
9.66	20.09	106.26	23.62
11.27	20.71	107.87	23.61
12.88	20.42	109.48	23.64
14.49	20.06	111.09	23.71
16.10	20.75	112.70	23.81
17.71	20.32	114.31	23.90
19.32	20.70	115.92	23.97
20.93	20.63	117.53	24.02
22.54	21.17	119.14	24.04
24.15	21.13	120.75	24.07
25.76	21.39	122.36	24.13
27.37	21.15	123.97	24.19
28.98	21.39	125.58	24.26
30.59	21.51	127.19	24.31
32.20	21.69	128.80	24.35
33.81	21.75	130.41	24.38
35.42	21.77	132.02	24.42
37.03	21.74	133.63	24.44
38.64	21.97	135.24	24.44
40.25	21.86	136.85	24.45
41.86	22.04	138.46	24.52
43.47	22.16	140.07	24.64
45.08	22.01	141.68	24.76
46.69	22.12	143.29	24.85
48.30	22.14	144.90	24.86
49.91	22.21	146.51	24.82
51.52	22.33	148.12	24.77
53.13	22.32	149.73	24.63
54.74	22.27	151.34	24.67
56.35	22.22	152.95	24.77
57.96	22.24	154.56	24.86
59.57	22.35	156.17	25.01
61.18	22.40	157.78	25.12
62.79	22.37	159.39	25.18
64.40	22.38	161.00	25.23
66.01	22.33	162.61	25.26
67.62	22.24	164.22	25.19
69.23	22.27	165.83	25.13
70.84	22.41	167.44	25.14
72.45	22.39	169.05	25.19
74.06	22.09	170.66	25.27
75.67	22.26	172.27	25.34
77.28	22.33	173.88	25.38
78.89	22.29	175.49	25.36
80.50	22.27	177.10	25.28
82.11	22.37	178.71	25.18
83.72	22.51	180.32	25.12
85.33	22.51	181.93	25.15
86.94	22.49	183.54	25.27
88.55	22.68	185.15	25.40
90.16	22.88	186.76	25.54
91.77	22.99	188.37	25.66
93.38	23.09	189.98	25.73
94.99	23.17	191.59	25.70
96.60	23.25	193.20	25.65
98.21	23.30	194.81	25.68
99.82	23.34	196.42	25.79
101.43	23.39	198.03	25.84

M4429 'B' M JOR 'XIS

E WING

RADIUS arcsec	BRIGHTNESS Mag/#arcsec	RADIUS arcsec	BRIGHTNESS Mag/#arcsec
199.64	25.85	209.30	25.94
201.25	25.87	210.91	25.90
202.86	25.87	212.52	25.87
204.47	25.84	214.13	25.91
206.08	25.87	215.74	26.04
207.69	25.94	217.35	26.44

N4429 'B' MINOR AXIS

S WING

RADIUS arcsec	BRIGHTNESS Mag/#arcsec	RADIUS arcsec	BRIGHTNESS Mag/#arcsec
6.44	19.41	59.57	24.53
8.05	19.70	61.18	24 58
9.66	20.09	62.79	24.62
11.27	20.60	64.40	24.69
12.88	21.12	66.01	24.81
14.49	21.09	67.62	24.86
16.10	21.29	69.23	24.93
17.71	21.08	70.84	24.98
19.32	21.70	72.45	24.99
20 93	21.92	74.06	25.04
22.54	21.90	75.67	25.18
24.15	21.82	77.28	25.35
25.76	22.11	78.89	25.45
27.37	22.26	80.50	25.53
28.98	22.37	82.11	25.59
30.59	22.51	83.72	25.53
32.20	22.69	85.33	25.37
33.81	22.90	86.94	25.27
35.42	23.03	88.55	25.26
37.03	23.17	90.16	25.35
38.64	23.31	91.77	25.52
40.25	23.41	93.38	25.69
41.86	23.50	94.99	25.86
43.47	23.60	96.60	26.07
45.08	23.68	98.21	26.24
46.69	23.73	99.82	26.28
48.30	23.76	101.43	26.27
49.91	23.89	103.04	26.20
51.52	24.15	104.65	26.00
53.13	24.35	106.26	25.79
54.74	24.46	107.87	25.81
56.35	24.45	109.48	26.42
57.96	24.46		

N4429 'B' MINOR AXIS

N WING

RADIUS arcsec	BRIGHTNESS Mag/#arcsec	RADIUS arcsec	BRIGHTNESS Mag/#arcsec
6.44	19.41	69.23	24.77
8.05	19.70	70.84	24.88
9.66	20.09	72.45	25.01
11.27	20.10	74.06	25.10
12.88	20.58	75.67	25.19
14.49	20.66	77.28	25.31
16.10	21.00	78.89	25.40
17.71	20.54	80.50	25.42
19.32	21.43	82.11	25.43
20.93	21.65	83.72	25.41
22.54	21.74	85.33	25.38
24.15	21.93	86.94	25.46
25.76	21.84	88.55	25.67
27.37	22.23	90.16	25.81
28.98	22.46	91.77	25.89
30.59	22.76	93.38	25.90
32.20	22.83	94.99	25.84
33.81	22.82	96.60	25.71
35.42	22.86	98.21	25.67
37.03	22.98	99.82	25.70
38.64	23.09	101.43	25.74
40.25	23.17	103.04	25.78
41.86	23.24	104.65	25.82
43.47	23.33	106.26	25.87
45.08	23.47	107.87	25.92
46.69	23.63	109.48	25.98
48.30	23.79	111.09	26.06
49.91	23.93	112.70	26.19
51.52	24.02	114.31	26.33
53.13	24.03	115.92	26.49
54.74	23.98	117.53	26.64
56.35	23.92	119.14	26.72
57.96	23.92	120.75	26.66
59.57	23.92	122.36	26.56
61.18	24.04	123.97	26.51
62.79	24.23	125.58	26.55
64.40	24.46	127.19	26.59
66.01	24.58	128.80	26.59
67.62	24.63	130.41	26.63

N4435 'B' MAJOR AXIS

S.E. WING

RADIUS arcsec	BRIGHTNESS Mag/#arcsec	RADIUS arcsec	BRIGHTNESS Mag/#arcsec
6.44	18.27	91.77	24.89
8.05	19.52	93.38	24.86
9.66	19.85	94.99	24.91
11.27	19.70	96.60	25.00
12.88	19.85	98.21	25.09
14.49	20.57	99.82	25.10
16.10	20.47	101.43	25.07
17.71	20.26	103.04	25.03
19.32	20.57	104.65	25.01
20.93	20.97	106.26	25.04
22.54	21.27	107.87	25.14
24.15	21.22	109.48	25.30
25.76	21.65	111.09	25.47
27.37	21.19	112.70	25.63
28.98	21.72	114.31	25.73
30.59	21.58	115.92	25.73
32.20	21.81	117.53	25.71
33.81	21.99	119.14	25.66
35.42	22.11	120.75	25.55
37.03	22.14	122.36	25.43
38.64	22.55	123.97	25.36
40.25	22.69	125.58	25.34
41.86	22.78	127.19	25.31
43.47	22.90	128.80	25.35
45.08	23.02	130.41	25.47
46.69	23.13	132.02	25.55
48.30	23.19	133.63	25.59
49.91	23.19	135.24	25.68
51.52	23.18	136.85	25.88
53.13	23.23	138.46	26.00
54.74	23.37	140.07	26.05
56.35	23.49	141.68	26.08
57.96	23.60	143.29	26.04
59.57	23.66	144.90	25.84
61.18	23.70	146.51	25.60
62.79	23.72	148.12	25.46
64.40	23.79	149.73	25.38
66.01	23.87	151.34	25.32
67.62	23.92	152.95	25.27
69.23	23.98	154.56	25.29
70.84	24.05	156.17	25.31
72.45	24.13	157.78	25.32
74.06	24.16	159.39	25.33
75.67	24.18	161.00	25.37
77.28	24.25	162.61	25.43
78.89	24.35	164.22	25.46
80.50	24.45	165.83	25.46
82.11	24.49	167.44	25.53
83.72	24.57	169.05	25.73
85.33	24.79	170.66	25.84
86.94	24.86	172.27	25.79
88.55	24.90	173.88	25.71
90.16	24.91		

N4435 'B' MAJOR AXIS

NE WING

RADIUS arcsec	BRIGHTNESS Mag/#arcsec	RADIUS arcsec	BRIGHTNESS Mag/#arcsec
6.44	18.27	66.01	23.89
8.05	18.92	67.62	24.08
9.66	19.35	69.23	24.21
11.27	19.70	70.84	24.29
12.88	20.22	72.45	24.25
14.49	20.30	74.06	24.14
16.10	20.36	75.67	24.11
17.71	20.13	77.28	24.19
19.32	20.80	78.89	24.33
20.93	20.50	80.50	24.47
22.54	20.87	82.11	24.68
24.15	21.38	83.72	24.80
25.76	21.02	85.33	24.92
27.37	21.33	86.94	25.00
28.98	21.47	88.55	25.02
30.59	21.48	90.16	25.03
32.20	21.79	91.77	25.06
33.81	21.95	93.38	25.06
35.42	21.92	94.99	25.07
37.03	22.03	96.60	25.13
38.64	22.19	98.21	25.18
40.25	22.30	99.82	25.26
41.86	22.61	101.43	25.38
43.47	22.78	103.04	25.53
45.08	22.76	104.65	25.63
46.69	22.82	106.26	25.63
48.30	22.99	107.87	25.62
49.91	23.14	109.48	25.65
51.52	23.22	111.09	25.64
53.13	23.26	112.70	25.63
54.74	23.26	114.31	25.74
56.35	23.28	115.92	25.93
57.96	23.34	117.53	26.12
59.57	23.43	119.14	26.34
61.18	23.49	120.75	26.49
62.79	23.57	122.36	26.60
64.40	23.71	123.97	26.71

N4435 'B' MINOR AXIS

SE WING

RADIUS arcsec	BRIGHTNESS Mag/#arcsec	RADIUS arcsec	BRIGHTNESS Mag/#arcsec
6.44	18.27	103.04	24.68
8.05	19.40	104.65	24.58
9.66	19.86	106.26	24.59
11.27	19.70	107.87	24.92
12.88	21.32	109.48	25.10
14.49	21.55	111.09	25.25
16.10	21.52	112.70	25.31
17.71	21.83	114.31	25.26
19.32	21.87	115.92	25.13
20.93	22.30	117.53	25.00
22.54	22.34	119.14	24.93
24.15	22.26	120.75	24.87
25.76	22.40	122.36	24.83
27.37	22.55	123.97	24.86
28.98	22.68	125.58	24.92
30.59	22.81	127.19	25.00
32.20	22.90	128.80	25.06
33.81	22.97	130.41	25.05
35.42	23.12	132.02	24.97
37.03	23.27	133.63	24.85
38.64	23.33	135.24	24.71
40.25	23.35	136.85	24.53
41.86	23.45	138.46	24.54
43.47	23.63	140.07	24.63
45.08	23.78	141.68	24.66
46.69	23.85	143.29	24.68
48.30	23.85	144.90	24.65
49.91	23.84	146.51	24.56
51.52	23.90	148.12	24.54
53.13	24.05	149.73	24.54
54.74	24.28	151.34	24.49
56.35	24.42	152.95	24.33
57.96	24.45	154.56	24.15
59.57	24.46	156.17	24.03
61.18	24.51	157.78	23.93
62.79	24.61	159.39	23.90
64.40	24.68	161.00	23.95
66.01	24.71	162.61	24.05
67.62	24.72	164.22	24.06
69.23	24.75	165.83	23.96
70.84	24.78	167.44	23.86
72.45	24.80	169.05	23.83
74.06	24.88	170.66	23.90
75.67	24.94	172.27	24.01
77.28	24.95	173.88	24.11
78.89	24.98	175.49	24.19
80.50	24.99	177.10	24.27
82.11	24.92	178.71	24.32
83.72	24.85	180.32	24.27
85.33	24.81	181.93	24.19
86.94	24.78	183.54	24.20
88.55	24.81	185.15	24.33
90.16	24.86	186.76	24.51
91.77	24.94	188.37	24.62
93.38	25.01	189.98	24.72
94.99	25.03	191.59	24.77
96.60	24.99	193.20	24.79
98.21	24.95	194.81	24.81
99.82	24.90	196.42	24.85
101.43	24.79	198.03	24.90

N4435 'B' MINOR AXIS

SE WING

RADIUS arcsec	BRIGHTNESS Mag/#arcsec	RADIUS arcsec	BRIGHTNESS Mag/#arcsec
199.64	24.94	217.35	25.46
201.25	24.99	218.96	25.53
202.86	25.03	220.57	25.64
204.47	25.05	222.18	25.79
206.08	25.08	223.79	25.86
207.69	25.14	225.40	25.84
209.30	25.26	227.01	25.83
210.91	25.34	228.62	25.82
212.52	25.36	230.23	25.76
214.13	25.37	231.84	25.73
215.74	25.41	233.45	25.77

N4435 'B' MINOR XIS

NW WING

RADIUS arcsec	BRIGHTNESS Mag/#arcsec	RADIUS arcsec	BRIGHTNESS Mag/#arcsec
6.44	18.27	43.47	23.80
8.05	19.72	45.08	23.86
9.66	20.63	46.69	23.93
11.27	19.70	48.30	24.03
12.88	21.07	49.91	24.21
14.49	21.24	51.52	24.41
16.10	21.75	53.13	24.62
17.71	21.66	54.74	24.73
19.32	21.92	56.35	24.76
20.93	22.10	57.96	24.75
22.54	22.24	59.57	24.62
24.15	22.43	61.18	24.55
25.76	22.61	62.79	24.52
27.37	22.78	64.40	24.57
28.98	22.82	66.01	24.79
30.59	23.02	67.62	24.90
32.20	23.18	69.23	24.96
33.81	23.32	70.84	25.00
35.42	23.50	72.45	25.02
37.03	23.66	74.06	25.11
38.64	23.72	75.67	25.30
40.25	23.73	77.28	25.78
41.86	23.73	78.89	26.07

N4438 'B' MAJOR AXIS

SW WING

RADIUS arcsec	BRIGHTNESS Mag/#arcsec	RADIUS arcsec	BRIGHTNESS Mag/#arcsec
6.44	19.20	103.04	24.18
8.05	19.52	104.65	24.09
9.66	21.11	106.26	24.11
11.27	20.07	107.87	24.14
12.88	20.19	109.48	24.17
14.49	20.91	111.09	24.10
16.10	21.32	112.70	24.05
17.71	20.92	114.31	24.07
19.32	20.90	115.92	24.22
20.93	20.82	117.53	24.34
22.54	21.30	119.14	24.36
24.15	21.25	120.75	24.28
25.76	21.14	122.36	24.24
27.37	21.46	123.97	24.19
28.98	21.34	125.58	24.17
30.59	21.14	127.19	24.17
32.20	21.30	128.80	24.40
33.81	21.38	130.41	24.70
35.42	21.26	132.02	24.91
37.03	21.25	133.63	25.06
38.64	21.68	135.24	25.07
40.25	21.60	136.85	24.98
41.86	21.38	138.46	24.87
43.47	21.46	140.07	24.79
45.08	21.62	141.68	24.74
46.69	21.52	143.29	24.72
48.30	21.62	144.90	24.71
49.91	21.70	146.51	24.72
51.52	21.97	148.12	24.77
53.13	22.22	149.73	24.88
54.74	22.29	151.34	24.99
56.35	21.91	152.95	25.10
57.96	22.26	154.56	25.17
59.57	22.27	156.17	25.22
61.18	22.20	157.78	25.27
62.79	22.18	159.39	25.29
64.40	22.39	161.00	25.34
66.01	22.69	162.61	25.41
67.62	22.85	164.22	25.44
69.23	22.92	165.83	25.47
70.84	23.04	167.44	25.54
72.45	23.18	169.05	25.59
74.06	23.33	170.66	25.64
75.67	23.47	172.27	25.81
77.28	23.58	173.88	26.01
78.89	23.63	175.49	26.04
80.50	23.65	177.10	26.06
82.11	23.72	178.71	26.08
83.72	23.79	180.32	25.94
85.33	23.90	181.93	25.75
86.94	23.94	183.54	25.69
88.55	23.99	185.15	25.69
90.16	23.98	186.76	25.70
91.77	23.95	188.37	25.76
93.38	23.91	189.98	25.87
94.99	23.92	191.59	25.99
96.60	24.03	193.20	26.12
98.21	24.19	194.81	26.27
99.82	24.31	196.42	26.40
101.43	24.28	198.03	26.49

N4438 'B' MAJOR AXIS

SW WING

RADIUS arcsec	BRIGHTNESS Mag/#arcsec	RADIUS arcsec	BRIGHTNESS Mag/#arcsec
199.64	26.47	202.86	26.44
201.25	26.39	204.47	26.54

N4438 'B' MAJOR AXIS

NF WING

RADIUS arcsec	BRIGHTNESS Mag/#arcsec	RADIUS arcsec	BRIGHTNESS Mag/#arcsec
6.44	19.20	103.04	23.94
8.05	19.52	104.65	24.03
9.66	19.97	106.26	24.11
11.27	20.07	107.87	24.14
12.88	20.19	109.48	24.18
14.49	20.32	111.09	24.25
16.10	20.73	112.70	24.32
17.71	20.92	114.31	24.32
19.32	21.14	115.92	24.25
20.93	20.77	117.53	24.19
22.54	21.38	119.14	24.17
24.15	21.55	120.75	24.18
25.76	21.43	122.36	24.19
27.37	21.26	123.97	24.20
28.98	21.51	125.58	24.19
30.59	21.32	127.19	24.22
32.20	21.39	128.80	24.22
33.81	21.21	130.41	24.20
35.42	21.54	132.02	24.21
37.03	21.28	133.63	24.18
38.64	21.44	135.24	24.14
40.25	21.16	136.85	24.06
41.86	21.32	138.46	24.08
43.47	21.87	140.07	24.13
45.08	22.05	141.68	24.13
46.69	22.20	143.29	24.04
48.30	22.23	144.90	23.98
49.91	22.28	146.51	24.01
51.52	22.36	148.12	24.05
53.13	22.40	149 73	24.03
54.74	22.47	151.34	23.95
56.35	22.56	152.95	23.90
57.96	22.78	154.56	23.91
59.57	22.74	156.17	23.99
61.18	22.76	157.78	24.02
62.79	22.83	159.39	23.98
64.40	22.83	161.00	23.86
66.01	22.84	162.61	23.80
67.62	22.94	164.22	23.81
69.23	23.00	165.83	23.84
70.84	23.07	167.44	23.81
72.45	23.14	169.05	23.77
74.06	23.20	170.66	23.74
75.67	23.27	172.27	23.76
77.28	23.35	173.88	23.79
78.89	23.42	175.49	23.82
80.50	23.40	177.10	23.82
82.11	23.32	178.71	23.82
83.72	23.27	180.32	23.84
85.33	23.27	181.93	23.90
86.94	23.35	183.54	23.95
88.55	23.49	185.15	23.93
90.16	23.70	186.76	23.83
91.77	23.86	188.37	23.72
93.38	23.94	189.98	23.66
94.99	23.95	191.59	23.66
96.60	23.97	193.20	23.70
98.21	23.96	194.81	23.72
99.82	23.93	196.42	23.71
101.43	23.91	198.03	23.62

N4438 'B' MAJOR AXIS

NE WING

RADIUS arcsec	BRIGHTNESS Mag/#arcsec	RADIUS arcsec	BRIGHTNESS Mag/#arcsec
199.64	23.50	241.50	24.13
201.25	23.44	243.11	24.25
202.86	23.50	244.72	24.34
204.47	23.60	246.33	24.35
206.08	23.67	247.94	24.33
207.69	23.70	249.55	24.32
209.30	23.74	251.16	24.36
210.91	23.80	252.77	24.35
212.52	23.81	254.38	24.41
214.13	23.78	255.99	24.45
215.74	23.73	257.60	24.48
217.35	23.67	259.21	24.42
218.96	23.63	260.82	24.38
220.57	23.61	262.43	24.38
222.18	23.65	264.04	24.42
223.79	23.71	265.65	24.42
225.40	23.78	267.26	24.44
227.01	23.86	268.87	24.57
228.62	23.92	270.48	24.69
230.23	23.96	272.09	24.77
231.84	23.96	273.70	24.81
233.45	23.95	275.31	24.80
235.06	23.95	276.92	24.79
236.67	23.96	278.53	24.79
238.28	24.01	280.14	24.82
239.89	24.04		

N4438 'B' B'R 'XIS

SE WING

RADIUS arcsec	BRIGHTNESS Mag/#arcsec	RADIUS arcsec	BRIGHTNESS Mag/#arcsec
6.44	20.62	66.01	24.91
8.05	20.07	67.62	24.93
9.66	20.24	69.23	24.94
11.27	20.29	70.84	24.95
12.88	19.66	72.45	24.98
14.49	20.28	74.06	25.01
16.10	20.46	75.67	25.09
17.71	21.17	77.28	25.21
19.32	21.25	78.89	25.30
20.93	21.69	80.50	25.35
22.54	21.72	82.11	25.40
24.15	21.94	83.72	25.47
25.76	22.24	85.33	25.57
27.37	22.42	86.94	25.71
28.98	22.55	88.55	25.87
30.59	22.78	90.16	26.04
32.20	22.90	91.77	26.26
33.81	22.98	93.38	26.36
35.42	23.06	94.99	26.35
37.03	23.22	96.60	26.30
38.64	23.43	98.21	26.15
40.25	23.60	99.82	25.90
41.86	23.65	101.43	25.82
43.47	23.64	103.04	25.92
45.08	23.66	104.65	25.95
46.69	23.78	106.26	25.94
48.30	23.97	107.87	25.95
49.91	24.19	109.48	25.89
51.52	24.40	111.09	25.76
53.13	24.53	112.70	25.74
54.74	24.50	114.31	25.78
56.35	24.50	115.92	25.79
57.96	24.44	117.53	25.78
59.57	24.50	119.14	25.80
61.18	24.64	120.75	25.88
62.79	24.73	122.36	26.04
64.40	24.84	123.97	26.29

N4438 'B' B'R AXIS

NW WING

RADIUS arcsec	BRIGHTNESS Mag/#arcsec	RADIUS arcsec	BRIGHTNESS Mag/#arcsec
6.44	19.67	80.50	24.23
8.05	19.91	82.11	24.30
9.66	19.57	83.72	24.38
11.27	20.38	85.33	24.41
12.88	20.53	86.94	24.34
14.49	20.73	88.55	24.25
16.10	20.74	90.16	24.27
17.71	20.66	91.77	24.41
19.32	20.84	93.38	24.58
20.93	21.46	94.99	24.71
22.54	21.78	96.60	24.82
24.15	22.21	98.21	24.86
25.76	22.47	99.82	24.86
27.37	22.73	101.43	24.83
28.98	22.83	103.04	24.79
30.59	22.82	104.65	24.73
32.20	22.86	106.26	24.68
33.81	22.97	107.87	24.63
35.42	23.11	109.48	24.60
37.03	23.23	111.09	24.58
38.64	23.36	112.70	24.58
40.25	23.52	114.31	24.54
41.86	23.70	115.92	24.52
43.47	23.75	117.53	24.45
45.08	23.71	119.14	24.43
46.69	23.66	120.75	24.49
48.30	23.65	122.36	24.50
49.91	23.61	123.97	24.46
51.52	23.58	125.58	24.42
53.13	23.63	127.19	24.53
54.74	23.81	128.80	24.69
56.35	24.01	130.41	24.78
57.96	24.12	132.02	24.86
59.57	24.11	133.63	24.93
61.18	24.08	135.24	25.02
62.79	24.13	136.85	25.12
64.40	24.30	138.46	25.17
66.01	24.49	140.07	25.16
67.62	24.43	141.68	25.08
69.23	24.45	143.29	24.96
70.84	24.29	144.90	24.87
72.45	24.19	146.51	24.87
74.06	24.18	148.12	24.94
75.67	24.20	149.73	25.05
77.28	24.22	151.34	25.17
78.89	24.21	152.95	25.26

N4459 'B' M JCR AXIS

SE WING

RADIUS arcsec	BRIGHTNESS Mag/#arcsec	RADIUS arcsec	BRIGHTNESS Mag/#arcsec
6.44	18.30	85.33	24.42
8.05	18.86	86.94	24.42
9.66	19.28	88.55	24.51
11.27	19.65	90.16	24.65
12.88	20.45	91.77	24.71
14.49	20.43	93.38	24.65
16.10	20.89	94.99	24.55
17.71	21.22	96.60	24 50
19.32	20.85	98.21	24.52
20.93	20.98	99.82	24.55
22.54	21.32	101.43	24.53
24.15	21.58	103.04	24.50
25.76	21.49	104.65	24.54
27.37	21.70	106.26	24.67
28.98	21.93	107.87	25.03
30.59	21.94	109.48	25.32
32.20	22.01	111.09	25.49
33.81	22.34	112.70	25.57
35.42	22.37	114.31	25.58
37.03	22.07	115.92	25.52
38.64	22.36	117.53	25.44
40.25	22.49	119.14	25.45
41.86	22.77	120.75	25.52
43.47	22.88	122.36	25.58
45.08	22.90	123.97	25.61
46.69	22.94	125.58	25.61
48.30	23.05	127.19	25.56
49.91	23.14	128.80	25.48
51.52	23.23	130.41	25.40
53.13	23.31	132.02	25.37
54.74	23.40	133.63	25.41
56.35	23.45	135.24	25.57
57.96	23.42	136.85	25.88
59.57	23.45	138.46	26.07
61.18	23.53	140.07	26.14
62.79	23.67	141.68	26.18
64.40	23.75	143.29	26.25
66.01	23.82	144.90	26.27
67.62	23.94	146.51	26.32
69.23	24.05	148.12	26.42
70.84	24.10	149.73	26.47
72.45	24.07	151.34	26.43
74.06	24.04	152.95	26.39
75.67	24.06	154.56	26.36
77.28	24.16	156.17	26.29
78.89	24.34	157.78	26.21
80.50	24.53	159.39	26.19
82.11	24.58	161.00	26.33
83.72	24.51	162.61	26.43

N4459 'B' MAJOR AXIS

NW WING

RADIUS arcsec	BRIGHTNESS Mag/#arcsec	RADIUS arcsec	BRIGHTNESS Mag/#arcsec
6.44	18.30	72.45	24.07
8.05	18.86	74.06	24.05
9.66	20.08	75.67	24.04
11.27	20.75	77.28	24.09
12.88	20.24	78.89	24.22
14.49	20.28	80.50	24.35
16.10	20.98	82.11	24.45
17.71	20.84	83.72	24 55
19.32	20.83	85.33	24.60
20.93	21.06	86.94	24.52
22.54	21.29	88.55	24.32
24.15	21.41	90.16	24.18
25.76	21.80	91.77	24.23
27.37	21.97	93.38	24.51
28.98	22.18	94.99	24.85
30.59	22.25	96.60	24.99
32.20	22.27	98.21	25.05
33.81	22.34	99.82	25.01
35.42	22.43	101.43	24.78
37.03	22.55	103.04	24.76
38.64	22.69	104.65	24.81
40.25	22.88	106.26	24.96
41.86	22.92	107.87	25.15
43.47	22.99	109.48	25.28
45.08	23.12	111.09	25.39
46.69	23.23	112.70	25.46
48.30	23.28	114.31	25.44
49.91	23.29	115.92	25.37
51.52	23.29	117.53	25.39
53.13	23.40	119.14	25.51
54.74	23.59	120.75	25.69
56.35	23.79	122.36	25.90
57.96	23.92	123.97	26.02
59.57	23.96	125.58	25.96
61.18	23.92	127.19	25.78
62.79	23.88	128.80	25.61
64.40	23.88	130.41	25.52
66.01	23.91	132.02	25.64
67.62	23.92	133.63	25.91
69.23	23.97	135.24	26.28
70.84	24.03		

N4459 'B' MINOR AXIS

SW WING

RADIUS arcsec	BRIGHTNESS Mag/#arcsec	RADIUS arcsec	BRIGHTNESS Mag/#arcsec
6.44	18.30	77.28	24.86
8.05	18.86	78.89	24.90
9.66	19.63	80.50	24.95
11.27	20.26	82.11	25.01
12.88	20.69	83.72	25.07
14.49	20.28	85.33	25.12
16.10	21.14	86.94	25.13
17.71	21.21	88.55	25.15
19.32	21.05	90.16	25.19
20.93	21.54	91.77	25.23
22.54	21.84	93.38	25.24
24.15	22.07	94.99	25.29
25.76	22.19	96.60	25.38
27.37	22.30	98.21	25.43
28.98	22.42	99.82	25.46
30.59	22.57	101.43	25.55
32.20	22.77	103.04	25.74
33.81	22.91	104.65	25.83
35.42	22.91	106.26	25.84
37.03	23.05	107.87	25.88
38.64	23.14	109.48	25.98
40.25	23.14	111.09	26.04
41.86	23.24	112.70	26.16
43.47	23.39	114.31	26.37
45.08	23.57	115.92	26.53
46.69	23.68	117.53	26.54
48.30	23.75	119.14	26.52
49.91	23.81	120.75	26.42
51.52	23.82	122.36	26.24
53.13	23.89	123.97	26.09
54.74	24.00	125.58	25.96
56.35	24.18	127.19	25.77
57.96	24.35	128.80	25.61
59.57	24.49	130.41	25.55
61.18	24.51	132.02	25.59
62.79	24.43	133.63	25.82
64.40	24.37	135.24	26.12
66.01	24.36	136.85	26.40
67.62	24.40	138.46	26.65
69.23	24.47	140.07	26.77
70.84	24.58	141.68	26.68
72.45	24.72	143.29	26.56
74.06	24.76	144.90	26.69
75.67	24.81		

N4459 'B' MINOR AXIS

NE WING

RADIUS arcsec	BRIGHTNESS Mag/#arcsec	RADIUS arcsec	BRIGHTNESS Mag/#arcsec
6.44	18.30	67.62	24.35
8.05	18.86	69.23	24.52
9.66	19.79	70.84	24.77
11.27	20.30	72.45	24.93
12.88	20.59	74.06	25.01
14.49	21.41	75.67	25.02
16.10	21.12	77.28	25.04
17.71	21.43	78.89	25.07
19.32	21.55	80.50	25.13
20.93	21.71	82.11	25.20
22.54	21.57	83.72	25.28
24.15	22.04	85.33	25.32
25.76	22.31	86.94	25.31
27.37	22.46	88.55	25.26
28.98	22.63	90.16	25.21
30.59	22.68	91.77	25.15
32.20	22.72	93.38	25.11
33.81	22.65	94.99	25.09
35.42	22.72	96.60	25.11
37.03	22.92	98.21	25.18
38.64	23.10	99.82	25.31
40.25	23.25	101.43	25.42
41.86	23.39	103.04	25.55
43.47	23.54	104.65	25.65
45.08	23.61	106.26	25.70
46.69	23.59	107.87	25.68
48.30	23.61	109.48	25.68
49.91	23.68	111.09	25.68
51.52	23.77	112.70	25.73
53.13	23.82	114.31	25.86
54.74	23.88	115.92	25.98
56.35	23.95	117.53	26.07
57.96	23.97	119.14	26.06
59.57	23.96	120.75	25.99
61.18	23.99	122.36	25.90
62.79	24.13	123.97	25.88
64.40	24.28	125.58	26.09
66.01	24.29		

N4461 'B' MAJOR AXIS

S WING

RADIUS arcsec	BRIGHTNESS Mag/#arcsec	RADIUS arcsec	BRIGHTNESS Mag/#arcsec
6.44	19.26	66.01	23.63
8.05	19.46	67.62	23.76
9.66	19.79	69.23	23.90
11.27	19.97	70.84	24.02
12.88	20.66	72.45	24.01
14.49	20.67	74.06	23.97
16.10	20.81	75.67	23.94
17.71	21.25	77.28	24.04
19.32	20.97	78.89	24.15
20.93	21.25	80.50	24 20
22.54	21.35	82.11	24 16
24.15	21.43	83.72	24.13
25.76	21.66	85.33	24.18
27.37	21.74	86.94	24.35
28.98	22.08	88.55	24.58
30.59	22.02	90.16	24.65
32.20	21.93	91.77	24.69
33.81	22.24	93.38	24.69
35.42	22.38	94.99	24.58
37.03	22.44	96.60	24.61
38.64	22.44	98.21	24.78
40.25	22.43	99.82	24.95
41.86	22.45	101.43	25.15
43.47	22.49	103.04	25.33
45.08	22.52	104.65	25.47
46.69	22.56	106.26	25.52
48.30	22.69	107.87	25.54
49.91	22.85	109.48	25.57
51.52	22.98	111.09	25.60
53.13	23.08	112.70	25.56
54.74	23.15	114.31	25.54
56.35	23.25	115.92	25.56
57.96	23.39	117.53	25.59
59.57	23.54	119.14	25.65
61.18	23.61	120.75	25.81
62.79	23.59	122.36	26.12
64.40	23.59		

N4461 'B' MAJOR AXIS

N WING

RADIUS arcsec	BRIGHTNESS Mag/#arcsec	RADIUS arcsec	BRIGHTNESS Mag/#arcsec
6.44	19.39	78.89	23.88
8.05	20.05	80.50	24.02
9.66	20.21	82.11	24.14
11.27	20.39	83.72	24.20
12.88	20.80	85.33	24.21
14.49	21.14	86.94	24.16
16.10	21.16	88.55	24.14
17.71	21.18	90.16	24.17
19.32	21.35	91.77	24.34
20.93	21.46	93.38	24.51
22.54	21.52	94.99	24.58
24.15	21.24	96.60	24.61
25.76	21.79	98.21	24.56
27.37	21.71	99.82	24.51
28.98	21.68	101.43	24.60
30.59	21.85	103.04	24.77
32.20	21.86	104.65	24.95
33.81	22.13	106.26	25.19
35.42	22.26	107.87	25.45
37.03	22.35	109.48	25.58
38.64	22.40	111.09	25.64
40.25	22.35	112.70	25.61
41.86	22.33	114.31	25.44
43.47	22.20	115.92	25.22
45.08	22.59	117.53	25.13
46.69	22.74	119.14	25.14
48.30	22.82	120.75	25.24
49.91	22.92	122.36	25.42
51.52	22.98	123.97	25.62
53.13	22.99	125.58	25.80
54.74	23.05	127.19	25.93
56.35	23.16	128.80	26.04
57.96	23.30	130.41	26.11
59.57	23.43	132.02	26.12
61.18	23.53	133.63	26.02
62.79	23.61	135.24	25.88
64.40	23.64	136.85	25.72
66.01	23.66	138.46	25.60
67.62	23.68	140.07	25.59
69.23	23.75	141.68	25.70
70.84	23.85	143.29	25.89
72.45	23.92	144.90	26.06
74.06	23.90	146.51	26.13
75.67	23.83	148.12	26.22
77.28	23.80	149.73	26.82

N4461 'B' MINOR AXIS

W WING

RADIUS arcsec	BRIGHTNESS Mag/#arcsec	RADIUS arcsec	BRIGHTNESS Mag/#arcsec
6.44	19.02	33.81	24.44
8.05	19.79	35.42	24.58
9.66	20.21	37.03	24.79
11.27	20.39	38.64	25.08
12.88	21.23	40.25	25.43
14.49	20.88	41.86	25.67
16.10	21.28	43.47	25.80
17.71	21.73	45.08	25.85
19.32	21.86	46.69	25.86
20.93	22.20	48.30	25.88
22.54	22.56	49.91	25.93
24.15	22.93	51.52	25.96
25.76	23.16	53.13	25.97
27.37	23.29	54.74	25.85
28.98	23.47	56.35	25.68
30.59	23.73	57.96	25.82
32.20	24.09		

N4461 'B' MINOR AXIS

E WING

RADIUS arcsec	BRIGHTNESS Mag/#arcsec	RADIUS arcsec	BRIGHTNESS Mag/#arcsec
6.44	19.68	38.64	25.07
8.05	20.13	40.25	25.06
9.66	21.18	41.86	25.11
11.27	21.11	43.47	25.26
12.88	21.58	45.08	25.40
14.49	21.48	46.69	25.48
16.10	21.91	48.30	25.58
17.71	22.13	49.91	25.66
19.32	22.44	51.52	25.77
20.93	22.65	53.13	25.95
22.54	22.88	54.74	26.08
24.15	23.17	56.35	26.10
25.76	23.47	57.96	26.11
27.37	23.76	59.57	26.09
28.98	23.96	61.18	26.01
30.59	24.15	62.79	25.93
32.20	24.44	64.40	25.95
33.81	24.74	66.01	26.05
35.42	24.92	67.62	26.24
37.03	25.05	69.23	26.41

N4474 'B' M JCR 'XIS

SW WING

RADIUS arcsec	BRIGHTNESS Mag/#arcsec	RADIUS arcsec	BRIGHTNESS Mag/#arcsec
6.44	18.95	53.13	24.00
8.05	20.17	54.74	24.17
9.66	20.21	56.35	24.23
11.27	20.37	57.96	24.29
12.88	21.03	59.57	24.43
14.49	21.03	61.18	24.57
16.10	20.81	62.79	24.78
17.71	20.61	64.40	25.01
19.32	21.42	66.01	25.14
20.93	21.62	67.62	25.26
22.54	21.64	69.23	25.40
24.15	21.59	70.84	25.50
25.76	21.71	72.45	25.63
27.37	21.75	74.06	25.91
28.98	21.85	75.67	26.24
30.59	21.78	77.28	26.44
32.20	22.12	78.89	26.48
33.81	22.06	80.50	26.43
35.42	22.27	82.11	26.33
37.03	22.40	83.72	26.15
38.64	22.60	85.33	25.97
40.25	22.84	86.94	25.86
41.86	22.96	88.55	25.79
43.47	22.99	90.16	25.71
45.08	23.00	91.77	25.75
46.69	23.11	93.38	25.87
48.30	23.31	94.99	26.02
49.91	23.54	96.60	26.25
51.52	23.77	98.21	26.53

N4474 'B' MAJOR AXIS

NE WING

RADIUS arcsec	BRIGHTNESS Mag/#arcsec	RADIUS arcsec	BRIGHTNESS Mag/#arcsec
6.44	18.95	45.08	23.32
8.05	19.54	46.69	23.45
9.66	20.29	48.30	23.52
11.27	20.25	49.91	23.55
12.88	20.73	51.52	23.60
14.49	21.00	53.13	23.73
16.10	21.08	54.74	23.93
17.71	21.17	56.35	24.16
19.32	21.00	57.96	24.32
20.93	21.30	59.57	24.45
22.54	21.48	61.18	24.53
24.15	21.45	62.79	24.65
25.76	21.50	64.40	24.78
27.37	21.83	66.01	24.87
28.98	21.93	67.62	24.95
30.59	21.85	69.23	24.99
32.20	22.18	70.84	25.05
33.81	22.34	72.45	25.12
35.42	22.51	74.06	25.28
37.03	22.67	75.67	25.46
38.64	22.78	77.28	25.63
40.25	22.80	78.89	25.86
41.86	22.94	80.50	26.22
43.47	23.11	82.11	26.42

N4474 'B' MINOR 'XIS

SE WING

RADIUS arcsec	BRIGHTNESS Mag/#arcsec	RADIUS arcsec	BRIGHTNESS Mag/#arcsec
6.44	18.95	43.47	24.65
8.05	20.75	45.08	24.87
9.66	21.08	46.69	25.07
11.27	21.36	48.30	25.17
12.88	21.85	49.91	25.18
14.49	22.27	51.52	25.12
16.10	22.56	53.13	25.08
17.71	22.83	54.74	25.13
19.32	23.07	56.35	25.26
20.93	23.21	57.96	25.39
22.54	23.32	59.57	25.44
24.15	23.41	61.18	25.43
25.76	23.61	62.79	25.33
27.37	23.78	64.40	25.19
28.98	23.95	66.01	25.08
30.59	24.13	67.62	25.06
32.20	24.27	69.23	25.16
33.81	24.39	70.84	25.32
35.42	24.39	72.45	25.51
37.03	24.37	74.06	25.76
38.64	24.31	75.67	26.07
40.25	24.29	77.28	26.39
41.86	24.38		

N4474 'B' MINOR AXIS

NW WING

RADIUS arcsec	BRIGHTNESS Mag/#arcsec	RADIUS arcsec	BRIGHTNESS Mag/#arcsec
6.44	18.95	46.69	25.08
8.05	20.59	48.30	25.10
9.66	21.40	49.91	25.17
11.27	21.86	51.52	25.22
12.88	21.86	53.13	25.24
14.49	22.18	54.74	25.24
16.10	22.45	56.35	25.24
17.71	22.58	57.96	25.25
19.32	22.79	59.57	25.30
20.93	23.02	61.18	25.38
22.54	23.22	62.79	25.48
24.15	23.39	64.40	25.50
25.76	23.49	66.01	25.42
27.37	23.57	67.62	25.36
28.98	23.60	69.23	25.38
30.59	23.71	70.84	25.50
32.20	23.83	72.45	25.66
33.81	24.02	74.06	25.80
35.42	24.26	75.67	25.87
37.03	24.47	77.28	25.87
38.64	24.62	78.89	25.83
40.25	24.81	80.50	25.88
41.86	24.93	82.11	26.17
43.47	24.98	83.72	26.54
45.08	25.02		

N4477 'B' MAJOR AXIS

SW WING

RADIUS arcsec	BRIGHTNESS Mag/#arcsec	RADIUS arcsec	BRIGHTNESS Mag/#arcsec
6.44	19.27	64.40	23.87
8.05	19.79	66.01	23.88
9.66	19.59	67.62	23.99
11.27	20.31	69.23	24.09
12.88	20.42	70.84	24.11
14.49	20.40	72.45	24.05
16.10	20.81	74.06	24.08
17.71	21.65	75.67	24.15
19.32	20.86	77.28	24.19
20.93	21.13	78.89	24.22
22.54	21.55	80.50	24.29
24.15	21.28	82.11	24.40
25.76	21.25	83.72	24.49
27.37	21.72	85.33	24.53
28.98	21.78	86.94	24.50
30.59	22.03	88.55	24.47
32.20	22.15	90.16	24.57
33.81	22.29	91.77	24.86
35.42	22.53	93.38	25.10
37.03	22.69	94.99	25.36
38.64	22.68	96.60	25.57
40.25	22.71	98.21	25.76
41.86	22.95	99.82	25.80
43.47	23.04	101.43	25.80
45.08	23.07	103.04	25.76
46.69	23.09	104.65	25.83
48.30	23.13	106.26	25.82
49.91	23.20	107.87	25.76
51.52	23.28	109.48	25.70
53.13	23.41	111.09	25.60
54.74	23.51	112.70	25.33
56.35	23.53	114.31	25.18
57.96	23.52	115.92	25.25
59.57	23.58	117.53	25.37
61.18	23.73	119.14	25.53
62.79	23.84	120.75	25.92

N4477 'B' MAJOR AXIS

NE WING

RADIUS arcsec	BRIGHTNESS Mag/#arcsec	RADIUS arcsec	BRIGHTNESS Mag/#arcsec
6.44	18.74	69.23	24.03
8.05	19.25	70.84	24.00
9.66	19.59	72.45	24.02
11.27	20.09	74.06	24.07
12.88	21.05	75.67	24.10
14.49	20.40	77.28	24.04
16.10	20.61	78.89	23.95
17.71	20.57	80.50	23.99
19.32	20.82	82.11	24.09
20.93	21.18	83.72	24.15
22.54	21.02	85.33	24.10
24.15	21.33	86.94	24.12
25.76	21.49	88.55	24.22
27.37	21.36	90.16	24.38
28.98	21.55	91.77	24.50
30.59	21.75	93.38	24.61
32.20	21.83	94.99	24.65
33.81	21.78	96.60	24.76
35.42	22.21	98.21	24.99
37.03	22.42	99.82	25.19
38.64	22.62	101.43	25.41
40.25	22.75	103.04	25.53
41.86	22.83	104.65	25.58
43.47	22.85	106.26	25.56
45.08	22.85	107.87	25.54
46.69	22.94	109.48	25.51
48.30	23.02	111.09	25.53
49.91	23.10	112.70	25.61
51.52	23.20	114.31	25.70
53.13	23.32	115.92	25.78
54.74	23.40	117.53	25.83
56.35	23.43	119.14	25.99
57.96	23.46	120.75	26.08
59.57	23.54	122.36	26.05
61.18	23.61	123.97	26.07
62.79	23.65	125.58	26.24
64.40	23.69	127.19	26.44
66.01	23.82	128.80	26.48
67.62	23.95		

N4477 'B' MINOR AXIS

SE WING

RADIUS arcsec	BRIGHTNESS Mag/#arcsec	RADIUS arcsec	BRIGHTNESS Mag/#arcsec
6.44	19.27	72.45	23.74
8.05	19.64	74.06	23.80
9.66	19.91	75.67	24.00
11.27	20.31	77.28	24.26
12.88	20.84	78.89	24.48
14.49	20.96	80.50	24.62
16.10	21.60	82.11	24.65
17.71	21.47	83.72	24.71
19.32	21.60	85.33	24.93
20.93	21.95	86.94	25.06
22.54	22.11	88.55	25.16
24.15	22.14	90.16	25.32
25.76	22.18	91.77	25.46
27.37	22.30	93.38	25.47
28.98	22.46	94.99	25.44
30.59	22.61	96.60	25.46
32.20	22.65	98.21	25.40
33.81	22.55	99.82	25.25
35.42	22.53	101.43	25.18
37.03	22.58	103.04	25.17
38.64	22.64	104.65	25.17
40.25	22.75	106.26	25.16
41.86	22.96	107.87	25.22
43.47	23.06	109.48	25.29
45.08	23.11	111.09	25.33
46.69	23.10	112.70	25.37
48.30	23.18	114.31	25.41
49.91	23.23	115.92	25.47
51.52	23.22	117.53	25.55
53.13	23.20	119.14	25.69
54.74	23.24	120.75	25.87
56.35	23.31	122.36	26.02
57.96	23.36	123.97	26.09
59.57	23.39	125.58	26.13
61.18	23.44	127.19	26.13
62.79	23.48	128.80	25.99
64.40	23.54	130.41	25.95
66.01	23.67	132.02	26.09
67.62	23.83	133.63	26.28
69.23	23.87	135.24	26.39
70.84	23.81		

N4477 'B' MINOR AXIS

NW WING

RADIUS arcsec	BRIGHTNESS Mag/#arcsec	RADIUS arcsec	BRIGHTNESS Mag/#arcsec
6.44	19.27	64.40	23.59
8.05	19.25	66.01	23.58
9.66	19.59	67.62	23.49
11.27	20.31	69.23	23.46
12.88	21.00	70.84	23.60
14.49	21.15	72.45	23.78
16.10	21.36	74.06	23.93
17.71	21.65	75.67	24.03
19.32	21.82	77.28	24.10
20.93	21.95	78.89	24.17
22.54	22.03	80.50	24.32
24.15	21.71	82.11	24.46
25.76	22.34	83.72	24.52
27.37	22.41	85.33	24.46
28.98	22.45	86.94	24.36
30.59	22.55	88.55	24.35
32.20	22.61	90.16	24.37
33.81	22.67	91.77	24.54
35.42	22.74	93.38	24.79
37.03	22.64	94.99	24.98
38.64	22.57	96.60	25.19
40.25	22.58	98.21	25.36
41.86	22.72	99.82	25.47
43.47	22.96	101.43	25.54
45.08	23.08	103.04	25.57
46.69	23.10	104.65	25.58
48.30	23.12	106.26	25.56
49.91	23.15	107.87	25.51
51.52	23.16	109.48	25.48
53.13	23.18	111.09	25.40
54.74	23.21	112.70	25.34
56.35	23.29	114.31	25.38
57.96	23.31	115.92	25.54
59.57	23.33	117.53	25.87
61.18	23.36	119.14	26.23
62.79	23.48	120.75	26.64

N4501 'B' MAJOR AXIS

SE WING

RADIUS arcsec	BRIGHTNESS Mag/#arcsec	RADIUS arcsec	BRIGHTNESS Mag/#arcsec
6.44	19.30	103.04	22.61
8.05	19.40	104.65	22.66
9.66	19.49	106.26	22.75
11.27	19.81	107.87	22.82
12.88	20.26	109.48	22.84
14.49	20.19	111.09	22.87
16.10	20.44	112.70	22.84
17.71	20.27	114.31	22.77
19.32	21.03	115.92	22.69
20.93	20.88	117.53	22.68
22.54	21.25	119.14	22.72
24.15	21.38	120.75	22.75
25.76	21.43	122.36	22.74
27.37	21.29	123.97	22.78
28.98	21.38	125.58	22.78
30.59	21.05	127.19	22.79
32.20	20.90	128.80	22.83
33.81	21.13	130.41	22.86
35.42	21.08	132.02	22.87
37.03	21.05	133.63	22.88
38.64	20.75	135.24	22.89
40.25	20.93	136.85	22.92
41.86	21.00	138.46	22.94
43.47	21.05	140.07	22.96
45.08	21.26	141.68	22.98
46.69	21.07	143.29	22.99
48.30	21.15	144.90	23.00
49.91	21.02	146.51	23.03
51.52	21.05	148.12	23.07
53.13	20.95	149.73	23.15
54.74	20.99	151.34	23.22
56.35	21.23	152.95	23.26
57.96	21.43	154.56	23.26
59.57	21.73	156.17	23.29
61.18	21.84	157.78	23.35
62.79	21.63	159.39	23.41
64.40	21.59	161.00	23.44
66.01	21.51	162.61	23.49
67.62	21.25	164.22	23.58
69.23	21.47	165.83	23.70
70.84	21.36	167.44	23.83
72.45	21.50	169.05	23.91
74.06	21.76	170.66	24.01
75.67	21.91	172.27	24.04
77.28	22.07	173.88	24.18
78.89	22.22	175.49	24.24
80.50	22.24	177.10	24.30
82.11	22.33	178.71	24.37
83.72	22.21	180.32	24.55
85.33	22.18	181.93	24.67
86.94	21.98	183.54	24.76
88.55	22.02	185.15	24.77
90.16	21.91	186.76	24.77
91.77	22.06	188.37	24.80
93.38	22.07	189.98	24.87
94.99	22.20	191.59	24.98
96.60	22.32	193.20	25.06
98.21	22.41	194.81	25.12
99.82	22.59	196.42	25.14
101.43	22.61	198.03	25.18

SE WING

RADIUS arcsec	BRIGHTNESS Mag/#arcsec	RADIUS arcsec	BRIGHTNESS Mag/#arcsec
199.64	25.26	225.40	25.64
201.25	25.37	227.01	25.67
202.86	25.51	228.62	25.70
204.47	25.66	230.23	25.77
206.08	25.68	231.84	25.80
207.69	25.64	233.45	25.83
209.30	25.60	235.06	25.82
210.91	25.55	236.67	25.83
212.52	25.50	238.28	25.73
214.13	25.51	239.89	25.77
215.74	25.56	241.50	25.86
217.35	25.56	243.11	25.96
218.96	25.54	244.72	26.06
220.57	25.51	246.33	26.21
222.18	25.58	247.94	26.47
223.79	25.59	249.55	26.80

NW WING

RADIUS arcsec	BRIGHTNESS Mag/#arcsec	RADIUS arcsec	BRIGHTNESS Mag/#arcsec
6.44	19.64	103.04	22.12
8.05	19.70	104.65	22.19
9.66	19.93	106.26	22.00
11.27	19.99	107.87	22.23
12.88	20.48	109.48	22.35
14.49	20.52	111.09	22.47
16.10	21.12	112.70	22.52
17.71	20.95	114.31	22.40
19.32	20.90	115.92	22.17
20.93	21.30	117.53	22.58
22.54	20.51	119.14	22.64
24.15	20.88	120.75	22.55
25.76	20.79	122.36	22.56
27.37	20.99	123.97	22.61
28.98	20.69	125.58	22.65
30.59	20.69	127.19	22.69
32.20	20.97	128.80	22.75
33.81	20.92	130.41	22.86
35.42	21.00	132.02	22.95
37.03	20.79	133.63	22.95
38.64	21.15	135.24	22.97
40.25	21.27	136.85	23.02
41.86	21.10	138.46	23.08
43.47	21.41	140.07	23.18
45.08	21.23	141.68	23.28
46.69	21.50	143.29	23.42
48.30	21.56	144.90	23.54
49.91	21.63	146.51	23.57
51.52	21.62	148.12	23.56
53.13	21.55	149.73	23.50
54.74	21.77	151.34	23.50
56.35	21.93	152.95	23.53
57.96	22.02	154.56	23.59
59.57	21.96	156.17	23.59
61.18	21.91	157.78	23.67
62.79	21.83	159.39	23.67
64.40	21.92	161.00	23.77
66.01	22.12	162.61	23.77
67.62	22.21	164.22	23.83
69.23	22.33	165.83	23.89
70.84	22.37	167.44	23.99
72.45	22.29	169.05	24.11
74.06	22.37	170.66	24.24
75.67	22.31	172.27	24.44
77.28	22.41	173.88	24.53
78.89	22.20	175.49	24.60
80.50	21.86	177.10	24.63
82.11	22.07	178.71	24.64
83.72	22.37	180.32	24.63
85.33	22.57	181.93	24.75
86.94	22.64	183.54	24.83
88.55	22.57	185.15	24.96
90.16	22.46	186.76	25.08
91.77	22.43	188.37	25.23
93.38	22.51	189.98	25.35
94.99	22.47	191.59	25.53
96.60	22.46	193.20	25.61
98.21	22.43	194.81	25.68
99.82	22.30	196.42	25.72
101.43	22.24	198.03	25.86

N4501 'B' MAJOR AXIS

NW WING

RADIUS arcsec	BRIGHTNESS Mag/#arcsec	RADIUS arcsec	BRIGHTNESS Mag/#arcsec
199.64	25.84	215.74	25.87
201.25	25.82	217.35	26.03
202.86	25.84	218.96	26.12
204.47	25.83	220.57	26.17
206.08	25.69	222.18	26.25
207.69	25.65	223.79	26.26
209.30	25.66	225.40	26.26
210.91	25.69	227.01	26.29
212.52	25 72	228.62	26.50
214.13	25.76	230.23	26.60

N4501 'B' MINOR AXIS

SW WING

RADIUS arcsec	BRIGHTNESS Mag/#arcsec	RADIUS arcsec	BRIGHTNESS Mag/#arcsec
6.44	19.93	61.18	22.75
8.05	20.25	62.79	22.84
9.66	20.30	64.40	22.90
11.27	20.55	66.01	22.98
12.88	21.15	67.62	23.13
14.49	20.52	69.23	23.32
16.10	20.34	70.84	23.51
17.71	20.75	72.45	23.69
19.32	20.62	74.06	23.91
20.93	21.30	75.67	24.13
22.54	21.21	77.28	24.30
24.15	20.99	78.89	24.40
25.76	20.93	80.50	24.47
27.37	21.08	82.11	24.59
28.98	21.23	83.72	24.80
30.59	21.52	85.33	24.87
32.20	21.47	86.94	24.98
33.81	21.48	88.55	25.11
35.42	21.34	90.16	25.18
37.03	21.49	91.77	25.27
38.64	21.34	93.38	25.45
40.25	21.67	94.99	25.54
41.86	22.04	96.60	25.60
43.47	22.29	98.21	25.67
45.08	22.42	99.82	25.84
46.69	22.43	101.43	26.04
48.30	22.14	103.04	26.14
49.91	22.30	104.65	26.37
51.52	22.53	106.26	26.49
53.13	22.58	107.87	26.59
54.74	22.46	109.48	26.65
56.35	22.29	111.09	26.82
57.96	22.38	112.70	26.87
59.57	22.65		

N4501 'B' MINOR AXIS

NE WING

RADIUS arcsec	BRIGHTNESS Mag/#arcsec	RADIUS arcsec	BRIGHTNESS Mag/#arcsec
6.44	19.92	62.79	23.32
8.05	20.72	64.40	23.38
9.66	20.48	66.01	23.40
11.27	20.37	67.62	23.40
12.88	21.20	69.23	23.33
14.49	21.15	70.84	23.27
16.10	21.69	72.45	23.24
17.71	20.97	74.06	23.22
19.32	21.11	75.67	23.23
20.93	21.38	77.28	23.22
22.54	21.28	78.89	23.25
24.15	21.21	80.50	23.29
25.76	21.44	82.11	23.38
27.37	21.95	83.72	23.53
28.98	22.13	85.33	23.71
30.59	21.86	86.94	23.91
32.20	21.55	88.55	24.06
33.81	21.92	90.16	24.17
35.42	22.01	91.77	24.23
37.03	22.25	93.38	24.33
38.64	22.04	94.99	24.49
40.25	22.00	96.60	24.62
41.86	22.12	98.21	24.71
43.47	22.23	99.82	24.80
45.08	22.29	101.43	24.87
46.69	22.46	103.04	24.97
48.30	22.56	104.65	25.10
49.91	22.77	106.26	25.30
51.52	22.95	107.87	25.47
53.13	23.09	109.48	25.58
54.74	23.12	111.09	25.66
56.35	23.12	112.70	25.83
57.96	23.10	114.31	25.93
59.57	23.15	115.92	26.29
61.18	23.24		

N4503 'B' MAJOR AXIS

S WING

RADIUS arcsec	BRIGHTNESS Mag/#arcsec	RADIUS arcsec	BRIGHTNESS Mag/#arcsec
6.44	19.48	82.11	24.19
8.05	20.44	83.72	24.22
9.66	20.87	85.33	24.22
11.27	20.53	86.94	24.19
12.88	21.20	88.55	24.20
14.49	21.50	90.16	24.29
16.10	20.87	91.77	24.50
17.71	21.06	93.38	24.69
19.32	21.61	94.99	24.89
20.93	21.22	96.60	25.07
22.54	21.73	98.21	25.15
24.15	21.75	99 82	25.17
25.76	21.84	101.43	25.17
27.37	22.26	103.04	25.21
28.98	22.40	104.65	25.31
30.59	22.35	106.26	25.42
32.20	22.35	107.87	25.54
33.81	22.47	109.48	25.64
35.42	22.60	111.09	25.65
37.03	22.65	112.70	25.59
38.64	22.63	114.31	25.61
40.25	22.67	115.92	25.66
41.86	22.79	117.53	25.68
43.47	22.85	119.14	25.74
45.08	22.88	120.75	25.83
46.69	23.02	122.36	25.91
48.30	23.10	123.97	26.00
49.91	23.10	125.58	26.13
51.52	23.11	127.19	26.26
53.13	23.20	128.80	26.31
54.74	23.34	130.41	26.27
56.35	23.42	132.02	26.25
57.96	23.46	133.63	26.19
59.57	23.52	135.24	26.03
61.18	23.66	136.85	25.95
62.79	23.81	138.46	26.00
64.40	23.88	140.07	26.08
66.01	23.88	141.68	26.18
67.62	23.86	143.29	26.30
69.23	23.87	144.90	26.43
70.84	23.88	146.51	26.43
72.45	23.91	148.12	26.35
74.06	23.93	149.73	26.27
75.67	23.97	151.34	26.28
77.28	24.00	152.95	26.31
78.89	24.05	154.56	26.42
80.50	24.13	156.17	26.59

N4503 'B' MAJOR AXIS

N WING

RADIUS arcsec	BRIGHTNESS Mag/#arcsec	RADIUS arcsec	BRIGHTNESS Mag/#arcsec
6.44	19.48	78.89	24.09
8.05	19.72	80.50	24.13
9.66	20.03	82.11	24.13
11.27	20.46	83.72	24.15
12.88	20.60	85.33	24.19
14.49	20.91	86.94	24.30
16.10	20.82	88.55	24.46
17.71	21.00	90.16	24.56
19.32	21.26	91.77	24.64
20.93	21.38	93.38	24.72
22.54	21.59	94.99	24.76
24.15	21.65	96.60	24.81
25.76	21.87	98.21	24.84
27.37	21.87	99.82	24.85
28.98	21.64	101.43	24.83
30.59	22.02	103.04	24.82
32.20	22.24	104.65	24.90
33.81	22.37	106.26	24.99
35.42	22.43	107.87	25.09
37.03	22.51	109.48	25.28
38.64	22.52	111.09	25.50
40.25	22.43	112.70	25.63
41.86	22.53	114.31	25.76
43.47	22.66	115.92	25.93
45.08	22.65	117.53	26.15
46.69	22.72	119.14	26.36
48.30	22.91	120.75	26.44
49.91	23.00	122.36	26.43
51.52	23.04	123.97	26.37
53.13	23.12	125.58	26.18
54.74	23.26	127.19	25.90
56.35	23.39	128.80	25.73
57.96	23.46	130.41	25.64
59.57	23.51	132.02	25.64
61.18	23.53	133.63	25.76
62.79	23.55	135.24	25.91
64.40	23.56	136.85	25.99
66.01	23.60	138.46	25.98
67.62	23.69	140.07	25.88
69.23	23.85	141.68	25.72
70.84	23.98	143.29	25.63
72.45	23.98	144.90	25.72
74.06	23.91	146.51	26.03
75.67	23.91	148.12	26.52
77.28	24.01		

N4503 'B' MINOR AXIS

E WING

RADIUS arcsec	BRIGHTNESS Mag/#arcsec	RADIUS arcsec	BRIGHTNESS Mag/#arcsec
6.44	19.48	32.20	23.89
8.05	20.44	33.81	24.04
9.66	20.87	35.42	24.19
11.27	21.68	37.03	24.35
12.88	21.71	38.64	24.50
14.49	22.12	40.25	24.69
16.10	22.25	41.86	24.84
17.71	22.32	43.47	24.94
19.32	22.43	45.08	25.16
20.93	22.59	46.69	25.48
22.54	22.84	48.30	25.63
24.15	23.14	49.91	25.68
25.76	23.39	51.52	25.81
27.37	23.60	53.13	25.89
28.98	23.70	54.74	26.07
30.59	23.81		

N4503 'B' MINOR AXIS

W WING

RADIUS arcsec	BRIGHTNESS Mag/#arcsec	RADIUS arcsec	BRIGHTNESS Mag/#arcsec
6.44	19.48	33.81	23.52
8.05	19.88	35.42	23 81
9.66	20.53	37.03	24.04
11.27	20.44	38.64	24.14
12.88	20.84	40.25	24.25
14.49	21.75	41.86	24.47
16.10	22.06	43.47	24.94
17.71	22.22	45.08	25.32
19.32	22.37	46.69	25.63
20.93	22.51	48.30	25.85
22.54	22.73	49.91	25.91
24.15	22.93	51.52	25.81
25.76	23.03	53.13	25.63
27.37	23.07	54.74	25.65
28.98	23.09	56.35	25.85
30.59	23.16	57.96	26.02
32.20	23.29	59.57	26.24

N4531 'B' M JCR AXIS

SE WING

RADIUS arcsec	BRIGHTNESS Mag/#arcsec	RADIUS arcsec	BRIGHTNESS Mag/#arcsec
6.44	21.38	59.57	23.99
8.05	20.90	61.18	24.11
9.66	21.65	62.79	24.20
11.27	21.50	64.40	24.22
12.88	21.61	66.01	24.23
14.49	21.47	67.62	24.25
16.10	21.88	69.23	24.22
17.71	21.36	70.84	24.19
19.32	21.19	72.45	24.21
20.93	21.46	74.06	24.31
22.54	21.81	75.67	24.46
24.15	22.18	77.28	24.53
25.76	22.26	78.89	24.53
27.37	22.16	80.50	24.48
28.98	22.31	82.11	24.38
30.59	22.50	83.72	24.31
32.20	22.67	85.33	24.45
33.81	22.78	86.94	24.73
35.42	22.84	88.55	25.04
37.03	23.00	90.16	25.30
38.64	23.09	91.77	25.54
40.25	23.14	93.38	25.72
41.86	23.17	94.99	25.72
43.47	23.18	96.60	25.59
45.08	23.23	98.21	25.46
46.69	23.34	99.82	25.34
48.30	23.49	101.43	25.35
49.91	23.56	103.04	25.50
51.52	23.58	104.65	25.78
53.13	23.59	106.26	26.14
54.74	23.69	107.87	26.60
56.35	23.78	109.48	26.89
57.96	23.88		

N4531 'B' MAJOR AXIS

NW WING

RADIUS arcsec	BRIGHTNESS Mag/#arcsec	RADIUS arcsec	BRIGHTNESS Mag/#arcsec
6.44	21.38	56.35	23.83
8.05	21.53	57.96	24.00
9.66	21.42	59.57	24.16
11.27	21.50	61.18	24.23
12.88	21.59	62.79	24.19
14.49	21.88	64.40	24.13
16.10	21.65	66.01	24.11
17.71	21.57	67.62	24.12
19.32	21.88	69.23	24.17
20.93	22.08	70.84	24.26
22.54	21.99	72.45	24.37
24.15	22.01	74.06	24.46
25.76	22.14	75.67	24.61
27.37	22.23	77.28	24.70
28.98	22.71	78.89	24.72
30.59	22.80	80.50	24.76
32.20	22.76	82.11	24.68
33.81	22.77	83.72	24.80
35.42	22.88	85.33	24.94
37.03	23.01	86.94	25.20
38.64	23.17	88.55	25.52
40.25	23.33	90.16	25.76
41.86	23.42	91.77	25.91
43.47	23.42	93.38	25.93
45.08	23.38	94.99	25.88
46.69	23.43	96.60	25.88
48.30	23.52	98.21	25.97
49.91	23.60	99.82	26.06
51.52	23.60	101.43	26.37
53.13	23.62	103.04	27.23
54.74	23.70	104.65	27.97

N4531 'B' MINOR AXIS

SW WING

RADIUS arcsec	BRIGHTNESS Mag/#arcsec	RADIUS arcsec	BRIGHTNESS Mag/#arcsec
6.44	21.38	40.25	23.59
8.05	21.17	41.86	23.73
9.66	21.64	43.47	23.83
11.27	21.50	45.08	23.88
12.88	22.06	46.69	23.98
14.49	21.80	48.30	24.24
16.10	22.16	49.91	24.57
17.71	22.08	51.52	24.78
19.32	22.17	53.13	24.95
20.93	21.78	54.74	25.08
22.54	22.51	56.35	25.18
24.15	22.83	57.96	25.22
25.76	22.97	59.57	25.34
27.37	23.09	61.18	25.50
28.98	23.15	62.79	25.58
30.59	23.18	64.40	25.51
32.20	23.20	66.01	25.47
33.81	23.23	67.62	25.45
35.42	23.26	69.23	25.55
37.03	23.32	70.84	25.89
38.64	23.45		

N4531 'B' MINOR AXIS

NE WING

RADIUS arcsec	BRIGHTNESS Mag/#arcsec	RADIUS arcsec	BRIGHTNESS Mag/#arcsec
6.44	21.38	46.69	24.44
8.05	21.44	48.30	24.62
9.66	22.01	49.91	24.78
11.27	21.50	51.52	24.96
12.88	22.01	53.13	25.12
14.49	21.91	54.74	25.19
16.10	22.15	56.35	25.20
17.71	22.43	57.96	25.19
19.32	22.62	59.57	25.11
20.93	22.82	61.18	25.03
22.54	22.94	62.79	25.05
24.15	23.05	64.40	25.22
25.76	23.15	66.01	25.43
27.37	23.22	67.62	25.73
28.98	23.25	69.23	25.85
30.59	23.22	70.84	25.90
32.20	23.18	72.45	25.86
33.81	23.26	74.06	25.88
35.42	23.45	75.67	25.72
37.03	23.68	77.28	25.73
38.64	23.83	78.89	25.74
40.25	23.92	80.50	25.72
41.86	23.96	82.11	25.61
43.47	24.06	83.72	25.75
45.08	24.24	85.33	26.11

N4550 'B' MAJOR AXIS

S WING

RADIUS arcsec	BRIGHTNESS Mag/#arcsec	RADIUS arcsec	BRIGHTNESS Mag/#arcsec
6.44	18.56	53.13	23.07
8.05	19.31	54.74	23.22
9.66	19.45	56.35	23.34
11.27	19.76	57.96	23.44
12.88	19.66	59.57	23.59
14.49	19.93	61.18	23.75
16.10	19.82	62.79	23.89
17.71	20.31	64.40	23.95
19.32	21.09	66.01	23.97
20.93	21.24	67.62	24.03
22.54	21.36	69.23	24.13
24.15	21.15	70.84	24.24
25.76	21.53	72.45	24.37
27.37	21.62	74.06	24.51
28.98	21.67	75.67	24.64
30.59	21.35	77.28	24.74
32.20	21.83	78.89	24.79
33.81	21.92	80.50	24.75
35.42	22.02	82.11	24.69
37.03	22.24	83.72	24.60
38.64	22.46	85.33	24.58
40.25	22.57	86.94	24.70
41.86	22.51	88.55	24.85
43.47	22.59	90.16	25.13
45.08	22.82	91.77	25.46
46.69	22.97	93.38	25.68
48.30	22.99	94.99	25.77
49.91	22.96	96.60	25.82
51.52	22.97	98.21	26.00

N4550 'B' MAJOR AXIS

N WING

RADIUS arcsec	BRIGHTNESS Mag/#arcsec	RADIUS arcsec	BRIGHTNESS Mag/#arcsec
6.44	19.02	62.79	24.02
8.05	19.78	64.40	24.10
9.66	19.46	66.01	24.15
11.27	19.73	67.62	24.17
12.88	20.06	69.23	24.21
14.49	20.58	70.84	24.33
16.10	20.88	72.45	24.46
17.71	20.72	74.06	24.52
19.32	20.65	75.67	24.52
20.93	20.84	77.28	24.72
22.54	21.04	78.89	25.13
24.15	21.36	80.50	25.33
25.76	21.57	82.11	25.46
27.37	21.66	83.72	25.43
28.98	21.94	85.33	25.28
30.59	21.79	86.94	25.12
32.20	21.70	88.55	25.00
33.81	22.04	90.16	24.94
35.42	22.36	91.77	24.93
37.03	22.47	93.38	24.98
38.64	22.47	94.99	25.08
40.25	22.53	96.60	25.19
41.86	22.61	98.21	25.32
43.47	22.74	99.82	25.45
45.08	22.93	101.43	25.59
46.69	23.10	103.04	25.76
48.30	23.23	104.65	25.95
49.91	23.31	106.26	26.05
51.52	23.37	107.87	26.05
53.13	23.42	109.48	26.04
54.74	23.49	111.09	26.06
56.35	23.59	112.70	26.14
57.96	23.75	114.31	26.29
59.57	23.89	115.92	26.50
61.18	23.97		

N4550 'B' MINOR AXIS

W WING

RADIUS arcsec	BRIGHTNESS Mag/#arcsec	RADIUS arcsec	BRIGHTNESS Mag/#arcsec
6.44	19.46	17.71	23.25
8.05	21.03	19.32	23.60
9.66	21.32	20.93	23.95
11.27	21.75	22.54	24.36
12.88	22.19	24.15	24.56
14.49	22.55	25.76	24.87
16.10	22.91	27.37	25.81

N4550 'B' MINOR AXIS

E WING

RADIUS arcsec	BRIGHTNESS Mag/#arcsec	RADIUS arcsec	BRIGHTNESS Mag/#arcsec
6.44	19.98	17.71	23.16
8.05	20.97	19.32	23.44
9.66	20.94	20.93	23.75
11.27	21.65	22.54	24.12
12.88	22.10	24.15	24.61
14.49	22.54	25.76	26.04
16.10	22.86		

SE WING

RADIUS arcsec	BRIGHTNESS Mag/#arcsec	RADIUS arcsec	BRIGHTNESS Mag/#arcsec
6.44	18.57	103.04	24.34
8.05	18.95	104.65	24.31
9.66	19.00	106.26	24.20
11.27	19.18	107.87	24.17
12.88	19.91	109.48	24.22
14.49	20.57	111.09	24.40
16.10	20.81	112.70	24.50
17.71	20.68	114.31	24.60
19.32	20.86	115.92	24.61
20.93	21.12	117.53	24.66
22.54	21.44	119.14	24.67
24.15	21.24	120.75	24.73
25.76	21.29	122.36	24.79
27.37	21.67	123.97	24.81
28.98	21.76	125.58	24.80
30.59	21.67	127.19	24.81
32.20	21.90	128.80	24.83
33.81	21.53	130.41	24.90
35.42	22.14	132.02	24.98
37.03	22.24	133.63	25.07
38.64	22.21	135.24	25.17
40.25	22.23	136.85	25.25
41.86	22.36	138.46	25.27
43.47	22.53	140.07	25.24
45.08	22.56	141.68	25.23
46.69	22.70	143.29	25.24
48.30	22.81	144.90	25.28
49.91	23.02	146.51	25.36
51.52	23.16	148.12	25.52
53.13	23.19	149.73	25.64
54.74	23.15	151.34	25.65
56.35	23.14	152.95	25.60
57.96	23.23	154.56	25.52
59.57	23.33	156.17	25.46
61.18	23.38	157.78	25.41
62.79	23.37	159.39	25.45
64.40	23.42	161.00	25.47
66.01	23.50	162.61	25.56
67.62	23.57	164.22	25.63
69.23	23.63	165.83	25.67
70.84	23.66	167.44	25.67
72.45	23.68	169.05	25.66
74.06	23.67	170.66	25.58
75.67	23.67	172.27	25.50
77.28	23.67	173.88	25.44
78.89	23.65	175.49	25.44
80.50	23.70	177.10	25.56
82.11	23.84	178.71	25.66
83.72	24.03	180.32	25.69
85.33	24.12	181.93	25.74
86.94	24.21	183.54	25.81
88.55	24.23	185.15	25.87
90.16	24.32	186.76	25.89
91.77	24.26	188.37	25.91
93.38	24.14	189.98	25.90
94.99	23.98	191.59	25.83
96.60	23.99	193.20	25.66
98.21	24.07	194.81	25.55
99.82	24.21	196.42	25.50
101.43	24.29	198.03	25.44

N 4552 'B' MAJOR AXIS

SE WING

RADIUS arcsec	BRIGHTNESS Mag/#arcsec	RADIUS arcsec	BRIGHTNESS Mag/#arcsec
199.64	25.38	231.84	26.01
201.25	25.34	233.45	26.18
202.86	25.39	235.06	26.31
204.47	25.55	236.67	26.49
206.08	25.86	238.28	26.51
207.69	26.11	239.89	26.48
209.30	26.36	241.50	26.42
210.91	26.46	243.11	26.54
212.52	26.40	244.72	26.60
214.13	26.13	246.33	26.59
215.74	25.96	247.94	26.56
217.35	25.82	249.55	26.62
218.96	25.83	251.16	26.45
220.57	25.96	252.77	26.31
222.18	26.18	254.38	26.31
223.79	26.29	255.99	26.28
225.40	26.30	257.60	26.18
227.01	26.19	259.21	26.33
228.62	26.04	260.82	26.57
230.23	25.95	262.43	26.81

N4552 'B' M JCP XIS

N"" WIFG

RADIUS arcsec	BRIGHTNESS Mag/#arcsec	RADIUS arcsec	BRIGHTNESS Mag/#arcsec
6.44	18.08	103.04	24.37
8.05	18.56	104.65	24.50
9.66	19.00	106.26	24.57
11.27	19.76	107.87	24.69
12.88	19.08	109.48	24.62
14.49	20.18	111.09	24.59
16.10	20.55	112.70	24.51
17.71	20.44	114.31	24.48
19.32	20.74	115.92	24.47
20.93	20.75	117.53	24.50
22.54	20.93	119.14	24.49
24.15	20.70	120.75	24.50
25.76	21.51	122.36	24.41
27.37	21.47	123.97	24.44
28.98	21.47	125.58	24.47
30.59	21.71	127.19	24.60
32.20	21.59	128.80	24.64
33.81	21.85	130.41	24.70
35.42	21.90	132.02	24.75
37.03	21.91	133.63	24.78
38.64	22.27	135.24	24.86
40.25	22.28	136.85	24.94
41.86	22.41	138.46	24.98
43.47	22.56	140.07	25.00
45.08	22.57	141.68	25.03
46.69	22.70	143.29	25.00
48.30	22.79	144.90	24.98
49.91	22.88	146.51	24.98
51.52	22.95	148.12	24.98
53.13	23.01	149.73	25.02
54.74	23.04	151.34	25.06
56.35	23.09	152.95	25.07
57.96	23.18	154.56	25.08
59.57	23.29	156.17	25.13
61.18	23.39	157.78	25.17
62.79	23.46	159.39	25.18
64.40	23.50	161.00	25.24
66.01	23.49	162.61	25.30
67.62	23.48	164.22	25.31
69.23	23.54	165.83	25.26
70.84	23.66	167.44	25.30
72.45	23.78	169.05	25.30
74.06	23.82	170.66	25.37
75.67	23.81	172.27	25.52
77.28	23.84	173.88	25.69
78.89	23.84	175.49	25.75
80.50	23.87	177.10	25.81
82.11	23.89	178.71	25.81
83.72	24.02	180.32	25.87
85.33	24.18	181.93	25.89
86.94	24.32	183.54	25.95
88.55	24.35	185.15	26.08
90.16	24.31	186.76	26.14
91.77	24.21	188.37	26.04
93 38	24.20	189.98	25.95
94.99	24.24	191.59	25.84
96.60	24.28	193.20	25.77
98.21	24.29	194.81	25.76
99.82	24.28	196.42	25.75
101.43	24.31	198.03	25.77

N4552 'B' MAJOR AXIS

NW WING

RADIUS arcsec	BRIGHTNESS Mag/#arcsec	RADIUS arcsec	BRIGHTNESS Mag/#arcsec
199.64	25.80	209.30	25.92
201.25	25.73	210.91	25.85
202.86	25.72	212.52	25.85
204.47	25.80	214.13	25.93
206.08	25.92	215.74	26.39
207.69	25.94	217.35	26.64

M4552 'B' MINOR AXIS

NE WING

RADIUS (arcsec)	BRIGHTNESS (Magnitudes/#arcsec)	RADIUS (arcsec)	BRIGHTNESS (Magnitudes/#arcsec)
-6.44	18.60	-86.94	24.41
-8.05	18.85	-88.55	24.37
-9.66	19.00	-90.16	24.34
-11.27	19.14	-91.77	24.23
-12.88	20.32	-93.38	24.21
-14.49	20.24	-94.99	24.30
-16.10	20.71	-96.60	24.50
-17.71	21.23	-98.21	24.61
-19.32	20.87	-99.82	24.71
-20.93	20.62	-101.43	24.72
-22.54	21.15	-103.04	24.72
-24.15	21.40	-104.65	24.68
-25.76	21.75	-106.26	24.76
-27.37	21.48	-107.87	24.84
-28.98	21.52	-109.48	24.94
-30.59	21.69	-111.09	25.01
-32.20	21.99	-112.70	25.03
-33.81	21.96	-114.31	24.98
-35.42	22.10	-115.92	24.92
-37.03	22.19	-117.53	24.89
-38.64	22.40	-119.14	24.85
-40.25	22.61	-120.75	24.92
-41.86	22.63	-122.36	25.00
-43.47	22.66	-123.97	25.08
-46.69	22.89	-125.58	25.12
-48.30	22.92	-127.19	25.15
-49.91	22.92	-128.80	25.17
-51.52	22.91	-130.41	25.16
-53.13	22.80	-132.02	25.13
-54.74	22.81	-133.63	25.12
-56.35	23.02	-135.24	25.12
-57.96	23.25	-136.85	25.10
-59.57	23.42	-138.46	25.11
-61.18	23.53	-140.07	25.14
-62.79	23.59	-141.68	25.16
-64.40	23.60	-143.29	25.20
-66.01	23.62	-144.90	25.24
-67.62	23.76	-146.51	25.30
-69.23	23.98	-148.12	25.32
-70.84	24.15	-149.73	25.36
-72.45	24.14	-151.34	25.34
-74.06	24.03	-152.95	25.33
-75.67	23.96	-154.56	25.28
-77.28	24.03	-156.17	25.28
-78.89	24.20	-157.78	25.27
-80.50	24.35	-159.39	25.31
-82.11	24.44	-161.00	25.29
-83.72	24.44	-162.61	25.32
-85.33	24.41	-164.22	25.39

N4552 'B' MINOR AXIS

NE WING

RADIUS (arcsec)	BRIGHTNESS (Magnitudes/#arcsec)	RADIUS (arcsec)	BRIGHTNESS (Magnitudes/#arcsec)
-165.83	25.51	-186.76	26.03
-167.44	25.57	-188.37	26.02
-169.05	25.99	-189.98	26.06
-170.66	25.67	-191.59	26.19
-172.67	25.64	-193.20	26.24
-173.88	25.63	-194.81	26.34
-175.49	25.75	-196.42	26.38
-177.10	25.87	-198.03	26.45
-178.71	26.09	-199.64	26.46
-180.32	26.21	-201.45	26.62
-181.93	26.26	-202.86	27.35
-183.54	26.20	-204.47	28.10
-185.15	26.17		

SW WING

RADIUS (arcsec)	BRIGHTNESS (Magnitudes/#arcsec)	RADIUS (arcsec)	BRIGHTNESS (Magnitudes/#arcsec)
6.44	18.42	46.69	22.91
8.05	19.67	48.30	23.07
9.66	19.00	49.91	23.18
11.27	19.70	51.52	23.24
12.88	20.74	53.13	23.26
14.49	20.33	54.74	23.26
16.10	20.35	56.35	23.28
17.71	20.83	57.96	23.35
19.32	20.91	59.57	23.43
20.93	21.13	61.18	23.51
22.54	21.32	62.79	23.60
24.15	21.63	64.40	23.71
25.76	21.69	66.01	23.76
27.37	21.59	67.62	23.79
28.98	21.52	69.23	23.81
30.59	21.66	70.84	23.87
32.20	21.72	72.45	23.91
33.81	21.77	74.06	23.97
35.42	22.14	75.67	24.07
37.03	22.36	77.28	24.18
38.64	22.57	78.89	24.18
40.25	22.72	80.50	24.09
41.86	22.86	82.11	23.97
43.47	22.92	83.72	23.97
45.08	22.92	85.33	24.06
86.94	24.21	127.19	25.30
88.55	24.39	128.80	25.25
90.16	24.49	130.41	25.19
91.77	24.54	132.02	25.13
93.98	24.53	133.63	25.15
94.99	24.59	135.24	25.16
96.60	24.61	136.85	25.19
98.21	24.67	138.46	25.22
99.82	24.64	140.07	25.27
101.43	24.63	141.68	25.29
103.04	24.66	143.29	25.30
104.65	24.77	144.90	25.32
106.26	24.86	146.51	25.37
107.87	24.94	148.12	25.44
109.48	25.01	149.73	25.50
111.09	25.09	151.34	25.63
112.70	25.19	152.95	25.75
114.31	25.25	154.56	25.84
115.92	25.31	156.17	25.95
117.53	25.35	157.78	26.02
119.14	25.40	159.39	26.02
120.75	25.44	161.00	26.10
122.36	25.45	162.61	26.20
123.97	25.45	164.22	26.10
125.58	25.40	165.83	26.20

N4552 'B' MINOR AXIS

SW WING

RADIUS (arcsec)	BRIGHTNESS (Magnitudes/#arcsec)	RADIUS (arcsec)	BRIGHTNESS (Magnitudes/#arcsec)
167.44	26.33	178.71	25.70
169.05	26.25	180.32	25.85
170.66	26.10	181.93	25.99
172.27	25.95	183.54	26.21
173.88	25.86	185.15	26.90
175.49	25.89	186.76	27.18
177.10	25.64		

N4267 'R' MAJOR AXIS

SW WING

RADIUS arcsec	BRIGHTNESS Mag/#arcsec	RADIUS arcsec	BRIGHTNESS Mag/#arcsec
6.44	17.40	61.18	21.94
8.05	17.40	62.79	22.02
9.66	18.06	64.40	22.11
11.27	18.72	66.01	22.18
12.88	19.24	67.62	22.25
14.49	19.26	69.23	22.29
16.10	19.61	70.84	22.34
17.71	19.77	72.45	22.40
19.32	19.96	74.06	22.46
20.93	20.14	75.67	22.56
22.54	20.41	77.28	22.71
24.15	20.47	78.89	22.84
25.76	20.51	80.50	22.93
27.37	20.73	82.11	23.02
28.98	20.83	83.72	23.07
30.59	20.83	85.33	23.08
32.20	20.86	86.94	23.13
33.81	20.96	88.55	23.19
35.42	21.08	90.16	23.27
37.03	21.15	91.77	23.33
38.64	21.16	93.38	23.42
40.25	21.19	94.99	23.46
41.86	21.26	96.60	23.50
43.47	21.38	98.21	23.55
45.08	21.44	99.82	23.65
46.69	21.49	101.43	23.74
48.30	21.55	103.04	23.87
49.91	21.62	104.65	24.06
51.52	21.68	106.26	24.24
53.13	21.70	107.87	24.36
54.74	21.73	109.48	24.47
56.35	21.78	111.09	24.62
57.96	21.83	112.70	24.79
59.57	21.88		

N4267 'R' MAJOR AXIS

NE WING

RADIUS arcsec	BRIGHTNESS Mag/#arcsec	RADIUS arcsec	BRIGHTNESS Mag/#arcsec
6.44	17.40	54.74	21.87
8.05	17.71	56.35	21.93
9.66	18.02	57.96	21.99
11.27	18.58	59.57	22.06
12.88	18.98	61.18	22.12
14.49	19.26	62.79	22.17
16.10	19.62	64.40	22.22
17.71	19.71	66.01	22.27
19 32	20.18	67.62	22.33
20.93	20.25	69.23	22.41
22.54	20.30	70.84	22.50
24.15	20.52	72.45	22.59
25.76	20.71	74.06	22.69
27.37	20.85	75.67	22.80
28.98	20.88	77.28	22.91
30.59	20.95	78.89	23.06
32.20	21.00	80.50	23.20
33.81	21.08	82.11	23.36
35.42	21.16	83.72	23.48
37.03	21.21	85.33	23.51
38.64	21.27	86.94	23.48
40.25	21.31	88.55	23.46
41.86	21.38	90.16	23.46
43.47	21.45	91.77	23.51
45.08	21.54	93.38	23.59
46.69	21.60	94.99	23.75
48.30	21.64	96.60	23.87
49.91	21.70	98.21	24.00
51.52	21.76	99.82	24.22
53.13	21.83	101.43	24.53

N4267 'R' MINOR AXIS

SE WING

RADIUS arcsec	BRIGHTNESS Mag/#arcsec	RADIUS arcsec	BRIGHTNESS Mag/#arcsec
6.44	17.40	62.79	21.85
8.05	17.85	64.40	21.93
9.66	17.83	66.01	22.00
11.27	18.54	67.62	22.09
12.88	19.30	69.23	22.16
14.49	19.26	70.84	22.23
16.10	20.13	72.45	22.30
17.71	20.26	74.06	22.35
19.32	20.38	75.67	22.43
20.93	20.37	77.28	22.49
22.54	20.40	78.89	22.56
24.15	20.55	80.50	22.61
25.76	20.68	82.11	22.65
27.37	20.72	83.72	22.68
28.98	20.78	85.33	22.71
30.59	20.79	86.94	22.77
32.20	20.85	88.55	22.85
33.81	20.93	90.16	22.96
35.42	20.97	91.77	23.07
37.03	21.02	93.38	23.15
38.64	21.06	94.99	23.19
40.25	21.12	96.60	23.26
41.86	21.17	98.21	23.33
43.47	21.23	99.82	23.45
45.08	21.29	101.43	23.58
46.69	21.34	103.04	23.78
48.30	21.38	104.65	23.94
49.91	21.40	106.26	24.11
51.52	21.41	107.87	24.23
53.13	21.43	109.48	24.32
54.74	21.50	111.09	24.32
56.35	21.59	112.70	24.40
57.96	21.70	114.31	24.44
59.57	21.76	115.92	24.52
61.18	21.81	117.53	24.60

N4267 'R' MINOR AXIS

NW WING

RADIUS arcsec	BRIGHTNESS Mag/#arcsec	RADIUS arcsec	BRIGHTNESS Mag/#arcsec
6.44	17.40	62.79	21.92
8.05	18.16	64.40	21.97
9.66	18.65	66.01	22.01
11.27	19.26	67.62	22.06
12.88	19.68	69.23	22.11
14.49	19.26	70.84	22.16
16.10	20.20	72.45	22.24
17.71	20.42	74.06	22.32
19.32	20.59	75.67	22.40
20.93	20.67	77.28	22.48
22.54	20.69	78.89	22.56
24.15	20.70	80.50	22.64
25.76	20.77	82.11	22.70
27.37	20.82	83.72	22.79
28.98	20.88	85.33	22.89
30.59	20.91	86.94	23.00
32.20	20.92	88.55	23.11
33.81	20.97	90.16	23.24
35.42	21.05	91.77	23.32
37.03	21.15	93.38	23.35
38.64	21.20	94.99	23.35
40.25	21.26	96.60	23 39
41.86	21.32	98.21	23.44
43.47	21.36	99.82	23.51
45.08	21.38	101.43	23.60
46.69	21.43	103.04	23.74
48.30	21.52	104.65	23.86
49.91	21.59	106.26	23.96
51.52	21.62	107.87	24.02
53.13	21.63	109.48	24.10
54.74	21.66	111.09	24.09
56.35	21.71	112.70	24.11
57.96	21.77	114.31	24 10
59.57	21.83	115.92	24.19
61.18	21.88	117.53	24.33

N4371 'R' B'R AXIS

S WING

RADIUS arcsec	BRIGHTNESS Mag/#arcsec	RADIUS arcsec	BRIGHTNESS Mag/#arcsec
6.44	17.70	46.69	21.78
8.05	18.07	48.30	21.96
9.66	18.37	49.91	22.13
11.27	18.75	51.52	22.21
12.88	19.03	53.13	22.30
14.49	19.32	54.74	22.37
16.10	19.65	56.35	22.44
17.71	19.82	57.96	22.53
19.32	19.85	59.57	22.64
20.93	19.95	61.18	22.76
22.54	19.80	62.79	22.86
24.15	20.03	64.40	22.95
25.76	19.99	66.01	23.05
27.37	20.11	67.62	23.15
28.98	19.94	69.23	23.26
30.59	20.26	70.84	23.38
32.20	20.14	72.45	23.56
33.81	20.27	74.06	23.72
35.42	20.37	75.67	23.84
37.03	20.39	77.28	23.89
38.64	20.65	78.89	23.91
40.25	20.90	80.50	23.91
41.86	21.17	82.11	23.97
43.47	21.38	83.72	24.16
45.08	21.59	85.33	24.42

N4371 'R' B'R AXIS

N WING

RADIUS arcsec	BRIGHTNESS Mag/#arcsec	RADIUS arcsec	BRIGHTNESS Mag/#arcsec
6.44	17.20	46.69	21.57
8.05	17.88	48.30	21.69
9.66	18.16	49.91	21.81
11.27	18.58	51.52	21.92
12.88	18.65	53.13	22.06
14.49	18.98	54.74	22.21
16.10	19.36	56.35	22.34
17.71	19.67	57.96	22.47
19.32	19.41	59.57	22.58
20.93	19.78	61.18	22.68
22.54	19.86	62.79	22.80
24 15	20.06	64.40	22.93
25.76	20.08	66.01	23.07
27.37	20.13	67.62	23.18
28.98	20.13	69.23	23.27
30.59	20.32	70.84	23.32
32.20	20.31	72.45	23.34
33.81	20.39	74.06	23.36
35.42	20.32	75.67	23.38
37.03	20.45	77.28	23.40
38.64	20.65	78.89	23.48
40.25	20.84	80.50	23.63
41.86	21.03	82.11	23.84
43.47	21.24	83.72	24.16
45.08	21.43		

N4371 'R' LENS AXIS

W WING

RADIUS arcsec	BRIGHTNESS Mag/#arcsec	RADIUS arcsec	BRIGHTNESS Mag/#arcsec
6.44	17.50	88.55	22.08
8.05	17.76	90.16	22.13
9.66	17.82	91.77	22.17
11.27	18.12	93.38	22.20
12.88	18.16	94.99	22.22
14.49	18.43	96.60	22.28
16.10	18.68	98.21	22.37
17.71	18.98	99.82	22.42
19.32	19.34	101.43	22.46
20.93	19.71	103.04	22.46
22.54	19.84	104.65	22.46
24.15	20.23	106.26	22.47
25.76	20.03	107.87	22.49
27.37	20.42	109.48	22.52
28.98	20.52	111.09	22.56
30.59	20.64	112.70	22.60
32.20	20.78	114.31	22.63
33.81	20.88	115.92	22.66
35.42	20.98	117.53	22.68
37.03	21.04	119.14	22.69
38.64	21.12	120.75	22.70
40.25	21.21	122.36	22.72
41.86	21.29	123.97	22.74
43.47	21.35	125.58	22.78
45.08	21.37	127.19	22.81
46.69	21.38	128.80	22.83
48.30	21.36	130.41	22.83
49.91	21.35	132.02	22.87
51.52	21.35	133.63	22.92
53.13	21.38	135.24	22.96
54.74	21.43	136.85	23.02
56.35	21.49	138.46	23.09
57.96	21.53	140.07	23.15
59.57	21.54	141.68	23.22
61.18	21.57	143.29	23.29
62.79	21.63	144.90	23.34
64.40	21.68	146.51	23.37
66.01	21.70	148.12	23.38
67.62	21.71	149.73	23.38
69.23	21.74	151.34	23.37
70.84	21.80	152.95	23.39
72.45	21.89	154.56	23.43
74.06	21.95	156.17	23.47
75.67	21.97	157.78	23.48
77.28	21.97	159.39	23.49
78.89	21.98	161.00	23.50
80.50	22.02	162.61	23.56
82.11	22.08	164.22	23.68
83.72	22.12	165.83	23.85
85.33	22.11	167.44	24.02
86.94	22.08	169.05	24.19

N4371 'R' LENS AXIS

E AXIS

RADIUS arcsec	BRIGHTNESS Mag/#arcsec	RADIUS arcsec	BRIGHTNESS Mag/#arcsec
6.44	17.41	88.55	22.04
8.05	17.32	90.16	22.05
9.66	17.54	91.77	22.04
11.27	17.65	93.38	22.06
12.88	17.82	94.99	22.12
14.49	18.35	96.60	22.17
16.10	18.40	98.21	22.22
17.71	18.85	99.82	22.28
19.32	18.89	101.43	22.29
20.93	19.40	103.04	22.28
22.54	19.60	104.65	22.26
24.15	19.88	106.26	22.19
25.76	20.04	107.87	22.19
27.37	20.33	109.48	22.28
28.98	20.41	111.09	22.36
30.59	20.50	112.70	22.45
32.20	20.68	114.31	22.53
33.81	20.79	115.92	22.56
35.42	20.91	117.53	22.59
37.03	21.01	119.14	22.61
38.64	21.11	120.75	22.63
40.25	21.16	122.36	22.69
41.86	21.19	123.97	22.78
43.47	21.23	125.58	22.88
45.08	21.28	127.19	22.97
46.69	21.33	128.80	23.02
48.30	21.37	130.41	23.07
49.91	21.38	132.02	23.10
51.52	21.39	133.63	23.13
53.13	21.40	135.24	23.15
54.74	21.43	136.85	23.17
56.35	21.46	138.46	23.21
57.96	21.47	140.07	23.25
59.57	21.47	141.68	23.29
61.18	21.46	143.29	23.36
62.79	21.46	144.90	23.45
64.40	21.52	146.51	23.53
66.01	21.59	148.12	23.58
67.62	21.65	149.73	23.61
69.23	21.71	151.34	23.66
70.84	21.74	152.95	23.70
72.45	21.75	154.56	23.72
74.06	21.77	156.17	23.74
75.67	21.83	157.78	23.75
77.28	21.91	159.39	23.74
78.89	21.98	161.00	23.75
80.50	22.04	162.61	23.79
82.11	22.08	164.22	23.88
83.72	22.06	165.83	24.03
85.33	22.03	167.44	24.16
86.94	22.02	169.05	24.22

N4377 'R' MAJOR AXIS

S WING

RADIUS arcsec	BRIGHTNESS Mag/#arcsec	RADIUS arcsec	BRIGHTNESS Mag/#arcsec
6.44	17.82	37.03	22.24
8.05	18.40	38.64	22.38
9.66	18.87	40.25	22.52
11.27	19.50	41.86	22.65
12.88	19.52	43.47	22.77
14.49	19.89	45.08	22.89
16.10	20.04	46.69	23.01
17.71	20.32	48.30	23.12
19.32	20.41	49.91	23.26
20.93	20.64	51.52	23.40
22.54	20.79	53.13	23.49
24.15	20.91	54.74	23.56
25.76	20.97	56.35	23.65
27.37	21.11	57.96	23.75
28.98	21.27	59.57	23.89
30.59	21.47	61.18	24.06
32.20	21.70	62.79	24.27
33.81	21.92	64.40	24.52
35.42	22.10		

N4377 'R' MAJOR AXIS

N WING

RADIUS arcsec	BRIGHTNESS Mag/#arcsec	RADIUS arcsec	BRIGHTNESS Mag/#arcsec
6.44	17.95	35.42	21.83
8.05	18.16	37.03	22.02
9.66	18.46	38.64	22.18
11.27	18.82	40.25	22.35
12.88	19.22	41.86	22.51
14.49	19.68	43.47	22.65
16.10	19.73	45.08	22.79
17.71	20.20	46.69	22.93
19.32	20.42	48.30	23.06
20.93	20.32	49.91	23.18
22.54	20.55	51.52	23.30
24.15	20.74	53.13	23.46
25.76	20.85	54.74	23.63
27.37	20.96	56.35	23.81
28.98	21.10	57.96	24.01
30.59	21.31	59.57	24.25
32.20	21.50	61.18	24.51
33.81	21.67		

N4377 'R' MINOR AXIS

W WING

RADIUS arcsec	BRIGHTNESS Mag/#arcsec	RADIUS arcsec	BRIGHTNESS Mag/#arcsec
6.44	17.25	28.98	21.60
8.05	18.22	30.59	21.83
9.66	18.81	32.20	22.10
11.27	19.09	33.81	22.37
12.88	19.84	35.42	22.63
14.49	19.63	37.03	22.87
16.10	20.25	38.64	23.08
17.71	20.33	40.25	23.26
19.32	20.39	41.86	23.42
20.93	20.41	43.47	23.57
22.54	20.42	45.08	23.68
24.15	20.78	46.69	23.81
25.76	21.10	48.30	24.01
27.37	21.38	49.91	24.34

N4377 'R' MINOR AXIS

E WING

RADIUS arcsec	BRIGHTNESS Mag/#arcsec	RADIUS arcsec	BRIGHTNESS Mag/#arcsec
6.44	18.05	27.37	21.65
8.05	18.73	28.98	21.76
9.66	19.59	30.59	21.98
11.27	19.82	32.20	22.28
12.88	19.95	33.81	22.54
14.49	19.89	35.42	22.79
16.10	20.27	37.03	23.03
17.71	20.20	38.64	23.28
19.32	20.61	40.25	23.56
20.93	20.96	41.86	23.77
22.54	21.24	43.47	23.92
24.15	21.44	45.08	24.04
25.76	21.57	46.69	24.27

N4419 'R' MAJOR AXIS

SE WING

RADIUS arcsec	BRIGHTNESS Mag/#arcsec	RADIUS arcsec	BRIGHTNESS Mag/#arcsec
6.44	17.18	64.40	21.30
8.05	17.67	66.01	21.42
9.66	17.72	67.62	21.53
11.27	17.99	69.23	21.66
12.88	17.76	70.84	21.80
14.49	18.48	72.45	21.97
16.10	18.75	74.06	22.11
17.71	18.22	75.67	22.22
19.32	18.82	77.28	22.27
20.93	18.58	78.89	22.32
22.54	19.09	80.50	22.36
24.15	19.12	82.11	22.40
25.76	19.69	83.72	22.48
27.37	19.48	85.33	22.60
28.98	19.57	86.94	22.73
30.59	19.47	88.55	22.86
32.20	19.49	90.16	22.98
33.81	19.31	91.77	23.10
35.42	19.62	93.38	23.20
37.03	19.81	94.99	23.30
38.64	19.75	96.60	23.40
40.25	20.20	98.21	23.52
41.86	20.06	99.82	23.64
43.47	20.16	101.43	23.75
45.08	20.14	103.04	23.88
46.69	20.27	104.65	24.00
48.30	20.35	106.26	24.12
49.91	20.46	107.87	24.23
51.52	20.46	109.48	24.30
53.13	20.58	111.09	24.35
54.74	20.69	112.70	24.37
56.35	20.78	114.31	24.31
57.96	20.86	115.92	24.23
59.57	20.97	117.53	24.24
61.18	21.08	119.14	24.30
62.79	21.20	120.75	24.52

N4419 'R' MAJOR AXIS

NW WING

RADIUS arcsec	BRIGHTNESS Mag/#arcsec	RADIUS arcsec	BRIGHTNESS Mag/#arcsec
6.44	17.18	67.62	21.36
8.05	17.67	69.23	21.47
9.66	17.72	70.84	21.56
11.27	17.78	72.45	21.68
12.88	17.76	74.06	21.82
14.49	18.03	75.67	21.95
16.10	18.51	77.28	22.08
17.71	18.22	78.89	22.18
19.32	18.69	80.50	22.26
20.93	18.77	82.11	22.34
22.54	19.11	83.72	22.42
24.15	19.13	85.33	22.51
25.76	19.20	86.94	22.63
27.37	19.32	88.55	22.74
28.98	19.42	90.16	22.87
30.59	19.46	91.77	23.00
32.20	19.55	93.38	23.12
33.81	19.55	94.99	23.25
35.42	19.55	96.60	23.37
37.03	19.57	98.21	23.50
38.64	19.73	99.82	23.64
40.25	19.76	101.43	23.76
41.86	19.80	103.04	23.83
43.47	20.08	104.65	23.85
45.08	20.14	106.26	23.84
46.69	20.31	107.87	23.82
48.30	20.38	109.48	23.81
49.91	20.40	111.09	23.83
51.52	20.42	112.70	23.93
53.13	20.52	114.31	23.99
54.74	20.63	115.92	24.05
56.35	20.69	117.53	24.09
57.96	20.78	119.14	24.14
59.57	20.83	120.75	24.17
61.18	20.93	122.36	24.32
62.79	21.00	123.97	24.48
64.40	21.12	125.58	24.66
66.01	21.23		

N4419 'R' MINOR AXIS

SW WING

RADIUS arcsec	BRIGHTNESS Mag/#arcsec	RADIUS arcsec	BRIGHTNESS Mag/#arcsec
6.44	17.18	30.59	22.69
8.05	17.82	32.20	22.91
9.66	18.41	33.81	23.10
11.27	19.83	35.42	23.28
14.49	20.26	37.03	23.44
16.10	19.74	38.64	23.61
20.93	21.32	40.25	23.75
22.54	21.58	41.86	23.91
24.15	21.78	43.47	24.10
25.76	21.99	45.08	24.34
27.37	22.21	46.69	24.60
28.98	22.45		

N4419 'R' MINOR WING

NE WING

RADIUS arcsec	BRIGHTNESS Mag/#arcsec	RADIUS arcsec	BRIGHTNESS Mag/#arcsec
6.44	17.18	30.59	22.44
8.05	17.52	32.20	22.58
9.66	18.30	33.81	22.74
11.27	19.51	35.42	22.93
14.49	19.84	37.03	23.10
16.10	20.17	38.64	23.25
20.93	20.98	40.25	23.36
22.54	21.34	41.86	23.45
24.15	21.60	43.47	23.55
25.76	21.87	45.08	23.75
27.37	22.09	46.69	24.39
28.98	22.25		

N4425 'R' MAJOR AXIS

SW WING

RADIUS arcsec	BRIGHTNESS Mag/#arcsec	RADIUS arcsec	BRIGHTNESS Mag/#arcsec
6.44	17.84	54.74	21.61
8.05	18.46	56.35	21.73
9.66	18.46	57.96	21.85
11.27	18.87	59.57	21.95
12.88	19.16	61.18	22.06
14.49	18.94	62.79	22.16
16.10	19.64	64.40	22.22
17.71	19.73	66.01	22.27
19.32	19.72	67.62	22.38
20.93	19.66	69.23	22.50
22.54	19.78	70.84	22.63
24.15	19.83	72.45	22.77
25.76	20.00	74.06	22.92
27.37	20.08	75.67	23.06
28.98	19.84	77.28	23.20
30.59	20.16	78.89	23.31
32.20	20.13	80.50	23.42
33.81	20.22	82.11	23.50
35.42	20.34	83.72	23.57
37.03	20.52	85.33	23.63
38.64	20.60	86.94	23.69
40.25	20.74	88.55	23.74
41.86	20.91	90.16	23.83
43.47	21.04	91.77	23.93
45.08	21.13	93.38	24.04
46.69	21.19	94.99	24.22
48.30	21.24	96.60	24.39
49.91	21.30	98.21	24.52
51.52	21.38	99.82	24.66
53.13	21.47	101.43	24.80

N4425 'R' MAJOR AXIS

NE WING

RADIUS arcsec	BRIGHTNESS Mag/#arcsec	RADIUS arcsec	BRIGHTNESS Mag/#arcsec
6.44	17.84	61.18	21.92
8.05	18.17	62.79	22.02
9.66	18.46	64.40	22.11
11.27	18.88	66.01	22.21
12.88	19.12	67.62	22.31
14.49	18.97	69.23	22.42
16.10	19.45	70.84	22.56
17 71	19.70	72.45	22.68
19.32	19.84	74.06	22.79
20.93	19.80	75.67	22.92
22.54	19.91	77.28	23.04
24.15	19.91	78.89	23.16
25.76	19.72	80.50	23.26
27.37	19.84	82.11	23.41
28.98	19.98	83.72	23.55
30.59	20.07	85.33	23.67
32.20	19.92	86.94	23.74
33.81	20.21	88.55	23.81
35.42	20.29	90.16	23.85
37.03	20.40	91.77	23.89
38.64	20.41	93.38	23.91
40.25	20.54	94.99	24.01
41.86	20.68	96.60	24.12
43.47	20.83	98.21	24.22
45.08	20.96	99.82	24.29
46.69	21.06	101.43	24.37
48.30	21.11	103.04	24.40
49.91	21.19	104.65	24.38
51.52	21.29	106.26	24.31
53.13	21.40	107.87	24.21
54.74	21.51	109.48	24.11
56.35	21.59	111.09	24.09
57.96	21.70	112.70	24.19
59.57	21.80	114.31	24.43

N4425 'R' MINOR AXIS

SE WING

RADIUS arcsec	BRIGHTNESS Mag/#arcsec	RADIUS arcsec	BRIGHTNESS Mag/#arcsec
6.44	17.84	27.37	22.75
8.05	18.95	28.98	22.94
9.66	18.46	30.59	23.15
11.27	20.27	32.20	23.30
12.88	20.70	33.81	23.43
14.49	21.05	35.42	23.56
16.10	21.30	37.03	23.71
17.71	21.53	38.64	23.77
19.32	21.72	40.25	23.87
20.93	21.89	41.86	24.02
22.54	22.11	43.47	24.26
24.15	22.32	45.08	24.51
25.76	22.53		

N4425 'R' MINOR AXIS

NW WING

RADIUS arcsec	BRIGHTNESS Mag/#arcsec	RADIUS arcsec	BRIGHTNESS Mag/#arcsec
6.44	17.84	24.15	22.44
8.05	18.77	25.76	22.62
9.66	18.46	27.37	22.81
11.27	20.29	28.98	23.00
12.88	20.68	30.59	23.19
14.49	21.07	32.20	23.37
16.10	21.40	33.81	23.50
17.71	21.70	35.42	23.63
19.32	21.90	37.03	23.84
20.93	22.08	38.64	24.39
22.54	22.27		

N4429 'R' MAJOR AXIS

W WING

RADIUS arcsec	BRIGHTNESS Mag/#arcsec	RADIUS arcsec	BRIGHTNESS Mag/#arcsec
6.44	17.45	103.04	21.51
8.05	17.50	104.65	21.55
9.66	18.02	106.26	21.60
11.27	17.69	107.87	21.66
12.88	18.09	109.48	21.70
14.49	18.10	111.09	21.73
16.10	18.34	112.70	21.75
17.71	18.59	114.31	21.78
19.32	18.50	115.92	21.82
20.93	19.08	117.53	21.86
22.54	18.93	119.14	21.90
24.15	19.10	120.75	21.94
25.76	19.24	122.36	21.98
27.37	19.29	123.97	22.01
28.98	19.48	125.58	22.05
30.59	19.57	127.19	22.09
32.20	19.79	128.80	22.14
33.81	19.76	130.41	22.18
35.42	19.90	132.02	22.22
37.03	20.04	133.63	22.26
38.64	20.05	135.24	22.29
40.25	20.16	136.85	22.31
41.86	20.14	138.46	22.32
43.47	20.29	140.07	22.32
45.08	20.22	141.68	22.34
46.69	20.13	143.29	22.39
48.30	20.32	144.90	22.44
49.91	20.42	146.51	22.49
51.52	20.30	148.12	22.52
53.13	20.36	149.73	22.55
54.74	20.46	151.34	22.57
56.35	20.44	152.95	22.60
57.96	20.35	154.56	22.64
59.57	20.41	156.17	22.68
61.18	20.50	157.78	22.71
62.79	20.40	159.39	22.76
64.40	20.53	161.00	22.80
66.01	20.43	162.61	22.84
67.62	20.31	164.22	22.88
69.23	20.33	165.83	22.93
70.84	20.42	167.44	22.97
72.45	20.44	169.05	23.02
74.06	20.35	170.66	23.09
75.67	20.36	172.27	23.15
77.28	20.37	173.88	23.21
78.89	20.45	175.49	23.26
80.50	20.44	177.10	23.31
82.11	20.49	178.71	23.33
83.72	20.57	180.32	23.34
85.33	20.63	181.93	23.37
86.94	20.68	183.54	23.40
88.55	20.79	185.15	23.44
90.16	20.92	186.76	23.49
91.77	21.04	188.37	23.54
93.38	21.13	189.98	23.59
94.99	21.19	191.59	23.64
96.60	21.24	193.20	23.72
98.21	21.29	194.81	23.83
99.82	21.36	196.42	23.99
101.43	21.45	198.03	24.17

N4429 'R' MAJOR AXIS

W WING

RADIUS arcsec	BRIGHTNESS Mag/#arcsec	RADIUS arcsec	BRIGHTNESS Mag/#arcsec
199.64	24.31	207.69	24.57
201.25	24.46	209.30	24.46
202.86	24.59	210.91	24.34
204.47	24.65	212.52	24.32
206.08	24.62	214.13	24.55

E WING

RADIUS arcsec	BRIGHTNESS Mag/#arcsec	RADIUS arcsec	BRIGHTNESS Mag/#arcsec
6.44	17.45	103.04	21.32
8.05	17.50	104.65	21.39
9.66	17.55	106.26	21.47
11.27	17.84	107.87	21.52
12.88	17.74	109.48	21.54
14.49	18.27	111.09	21.53
16.10	18.01	112.70	21.55
17.71	18.15	114.31	21.60
19.32	18.42	115.92	21.69
20.93	18.53	117.53	21.77
22.54	18.65	119.14	21.86
24.15	18.85	120.75	21.93
25.76	19.06	122.36	21.95
27.37	19.18	123.97	21.97
28.98	19.18	125.58	21.99
30.59	19.38	127.19	22.04
32.20	19.28	128.80	22.10
33.81	19.64	130.41	22.14
35.42	19.75	132.02	22.18
37.03	19.83	133.63	22.23
38.64	20.08	135.24	22.28
40.25	19.90	136.85	22.31
41.86	20.17	138.46	22.34
43.47	20.19	140.07	22.40
45.08	20.18	141.68	22.49
46.69	20.22	143.29	22.55
48.30	20.30	144.90	22.60
49.91	20.33	146.51	22.65
51.52	20.32	148.12	22.68
53.13	20.44	149.73	22.70
54.74	20.35	151.34	22.71
56.35	20.38	152.95	22.71
57.96	20.46	154.56	22.72
59.57	20.48	156.17	22.74
61.18	20.49	157.78	22.77
62.79	20.52	159.39	22.82
64.40	20.60	161.00	22.86
66.01	20.41	162.61	22.90
67.62	20.52	164.22	22.93
69.23	20.53	165.83	22.97
70.84	20.45	167.44	23.01
72.45	20.44	169.05	23.07
74.06	20.40	170.66	23.12
75.67	20.33	172.27	23.16
77.28	20.38	173.88	23.19
78.89	20.37	175.49	23.23
80.50	20.39	177.10	23.30
82.11	20.46	178.71	23.36
83.72	20.47	180.32	23.41
85.33	20.50	181.93	23.44
86.94	20.50	183.54	23.46
88.55	20.56	185.15	23.46
90.16	20.71	186.76	23.45
91.77	20.82	188.37	23.45
93.38	20.89	189.98	23.46
94.99	20.95	191.59	23.48
96.60	21.02	193.20	23.49
98.21	21.09	194.81	23.52
99.82	21.18	196.42	23.55
101.43	21.25	198.03	23.57

N4429 'R' MAJOR AXIS

E WING

RADIUS arcsec	BRIGHTNESS Mag/#arcsec	RADIUS arcsec	BRIGHTNESS Mag/#arcsec
199.64	23.61	209.30	24.15
201.25	23.68	210.91	24.28
202.86	23.75	212.52	24.41
204.47	23.83	214.13	24.52
206.08	23.93	215.74	24.63
207.69	24.05	217.35	24.76

M4429 'R' MINOR AXIS

S WING

RADIUS arcsec	BRIGHTNESS Mag/#arcsec	RADIUS arcsec	BRIGHTNESS Mag/#arcsec
6.44	17.45	57.96	22.24
8.05	17.50	59.57	22.30
9.66	17.95	61.18	22.34
11.27	17.99	62.79	22.35
12.88	18.14	64.40	22.37
14.49	18.49	66.01	22.45
16.10	19.03	67.62	22.52
17.71	19.37	69.23	22.61
19.32	19.32	70.84	22.68
20.93	19.77	72.45	22.76
22.54	19.83	74.06	22.82
24.15	20.05	75.67	22.88
25.76	20.12	77.28	22.95
27.37	20.33	78.89	23.06
28.98	20.50	80.50	23.17
30.59	20.39	82.11	23.24
32.20	20.63	83.72	23.27
33.81	20.82	85.33	23.31
35.42	20.94	86.94	23.36
37.03	20.98	88.55	23.39
38.64	21.09	90.16	23.42
40.25	21.19	91.77	23.47
41.86	21.28	93.38	23.49
43.47	21.35	94.99	23.50
45.08	21.46	96.60	23.54
46.69	21.60	98.21	23.61
48.30	21.76	99.82	23.69
49.91	21.90	101.43	23.75
51.52	22.02	103.04	23.80
53.13	22.10	104.65	23.89
54.74	22.15	106.26	24.12
56.35	22.19	107.87	24.35

N4429 'R' MINOR AXIS

N WING

RADIUS arcsec	BRIGHTNESS Mag/#arcsec	RADIUS arcsec	BRIGHTNESS Mag/#arcsec
6.44	17.45	78.89	23.04
8.05	17.50	80.50	23.05
9.66	18.39	82.11	23.04
11.27	18.85	83.72	23.05
12.88	19.10	85.33	23.12
14.49	19.43	86.94	23.21
16.10	19.44	88.55	23.30
17.71	19.74	90.16	23.39
19.32	20.19	91.77	23.45
20.93	20.16	93.38	23.47
22.54	20.38	94.99	23.47
24.15	20.55	96.60	23.44
25.76	20.49	98.21	23.36
27.37	20.64	99.82	23.23
28.98	20.73	101.43	23.09
30.59	20.81	103.04	23.06
32.20	20.92	104.65	23.15
33.81	21.06	106.26	23.33
35.42	21.18	107.87	23.54
37.03	21.28	109.48	23.73
38.64	21.38	111.09	23.85
40.25	21.48	112.70	23.85
41.86	21.55	114.31	23.77
43.47	21.63	115.92	23.71
45.08	21.72	117.53	23.70
46.69	21.81	119.14	23.71
48.30	21.92	120.75	23.73
49.91	22.03	122.36	23.78
51.52	22.13	123.97	23.89
53.13	22.18	125.58	24.04
54.74	22.23	127.19	24.18
56.35	22.28	128.80	24.29
57.96	22.32	130.41	24.39
59.57	22.33	132.02	24.44
61.18	22.34	133.63	24.42
62.79	22.39	135.24	24.33
64.40	22.49	136.85	24.21
66.01	22.58	138.46	24.14
67.62	22.68	140.07	24.10
69.23	22.78	141.68	24.08
70.84	22.85	143.29	24.12
72.45	22.90	144.90	24.25
74.06	22.97	146.51	24.38
75.67	23.00	148.12	24.54
77.28	23.03		

N4435 'R' MAJOR AXIS

SW WING

RADIUS arcsec	BRIGHTNESS Mag/#arcsec	RADIUS arcsec	BRIGHTNESS Mag/#arcsec
6.44	17.06	99.82	23.08
8.05	17.31	101.43	23.10
9.66	17.54	103.04	23.13
11.27	17.86	104.65	23.18
12.88	17.96	106.26	23.24
14.49	18.14	107.87	23.28
16.10	18.38	109.48	23.33
17.71	18.51	111.09	23.39
19.32	18.63	112.70	23.40
20.93	18.67	114.31	23.39
22.54	18.88	115.92	23.42
24.15	19.27	117.53	23.49
25.76	19.30	119.14	23.59
27.37	19.38	120.75	23.66
28.98	19.53	122.36	23.70
30.59	19.82	123.97	23.71
32.20	19.92	125.58	23.68
33.81	19.94	127.19	23.63
35.42	20.43	128.80	23.64
37.03	20.49	130.41	23.69
38.64	20.72	132.02	23.74
40.25	20.86	133.63	23.76
41.86	20.97	135.24	23.77
43.47	21.04	136.85	23.77
45.08	21.17	138.46	23.75
46.69	21.29	140.07	23.77
48.30	21.38	141.68	23.84
49.91	21.45	143.29	23.93
51.52	21.49	144.90	23.98
53.13	21.56	146.51	23.98
54.74	21.61	148.12	23.97
56.35	21.66	149.73	23.99
57.96	21.72	151.34	23.97
59.57	21.79	152.95	23.94
61.18	21.85	154.56	23.91
62.79	21.93	156.17	23.83
64.40	22.00	157.78	23.72
66.01	22.10	159.39	23.60
67.62	22.21	161.00	23.57
69.23	22.28	162.61	23.58
70.84	22.35	164.22	23.60
72.45	22.42	165.83	23.57
74.06	22.42	167.44	23.54
75.67	22.42	169.05	23.49
77.28	22.45	170.66	23.47
78.89	22.49	172.27	23.47
80.50	22.53	173.88	23.51
82.11	22.64	175.49	23.56
83.72	22.74	177.10	23.62
85.33	22.81	178.71	23.63
86.94	22.85	180.32	23.63
88.55	22.87	181.93	23.62
90.16	22.84	183.54	23.62
91.77	22.84	185.15	23.61
93.38	22.87	186.76	23.59
94.99	22.90	188.37	23.55
96.60	22.95	189.98	23.54
98.21	23.02		

N4435 'R' MAJOR AXIS

NE WING

RADIUS arcsec	BRIGHTNESS Mag/#arcsec	RADIUS arcsec	BRIGHTNESS Mag/#arcsec
6.44	16.97	78.89	22.46
8.05	17.33	80.50	22.53
9.66	17.54	82.11	22.62
11.27	17.80	83.72	22.71
12.88	18.00	85.33	22.77
14.49	18.14	86.94	22.83
16.10	18.27	88.55	22.91
17.71	18.45	90.16	22.98
19.32	18.68	91.77	23.06
20.93	19.01	93.38	23.12
22.54	18.97	94.99	23.16
24.15	18.89	96.60	23.21
25.76	19.08	98.21	23.26
27.37	19.52	99.82	23.30
28.98	19.34	101.43	23.33
30.59	19.77	103.04	23.34
32.20	19.84	104.65	23.36
33.81	19.87	106.26	23.38
35.42	20.25	107.87	23.41
37.03	20.28	109.48	23.43
38.64	20.50	111.09	23.46
40.25	20.71	112.70	23.51
41.86	20.82	114.31	23.58
43.47	20.89	115.92	23.62
45.08	20.96	117.53	23.68
46.69	21.05	119.14	23.77
48.30	21.17	120.75	23.84
49.91	21.27	122.36	23.88
51.52	21.41	123.97	23.96
53.13	21.51	125.58	24.07
54.74	21.58	127.19	24.11
56.35	21.59	128.80	24.09
57.96	21.59	130.41	24.09
59.57	21.63	132.02	24.10
61.18	21.73	133.63	24.14
62.79	21.88	135.24	24.22
64.40	22.01	136.85	24.31
66.01	22.10	138.46	24.42
67.62	22.14	140.07	24.47
69.23	22.17	141.68	24.40
70.84	22.21	143.29	24.32
72.45	22.25	144.90	24.32
74.06	22.30	146.51	24.37
75.67	22.32	148.12	24.46
77.28	22.38		

SE WING

RADIUS arcsec	BRIGHTNESS Mag/#arcsec	RADIUS arcsec	BRIGHTNESS Mag/#arcsec
6.44	17.49	103.04	22.93
8.05	18.03	104.65	22.94
9.66	17.54	106.26	22.96
11.27	18.63	107.87	22.95
12.88	19.01	109.48	22.92
14.49	19.61	111.09	22.89
16.10	19.86	112.70	22.87
17.71	20.00	114.31	22.85
19.32	20.49	115.92	22.83
20.93	20.38	117.53	22.84
22.54	20.44	119.14	22.88
24.15	20.62	120.75	22.90
25.76	20.78	122.36	22.91
27.37	20.92	123.97	22.92
28.98	21.05	125.58	22.90
30.59	21.10	127.19	22.87
32.20	21.15	128.80	22.85
33.81	21.21	130.41	22.83
35.42	21.36	132.02	22.81
37.03	21.52	133.63	22.84
38.64	21.69	135.24	22.82
40.25	21.78	136.85	22.77
41.86	21.80	138.46	22.72
43.47	21.82	140.07	22.66
45.08	21.87	141.68	22.59
46.69	21.96	143.29	22.55
48.30	22.05	144.90	22.53
49.91	22.11	146.51	22.50
51.52	22.19	148.12	22.49
53.13	22.26	149.73	22.48
54.74	22.31	151.34	22.44
56.35	22.37	152.95	22.41
57.96	22.40	154.56	22.38
59.57	22.43	156.17	22.33
61.18	22.50	157.78	22.27
62.79	22.57	159.39	22.22
64.40	22.63	161.00	22.19
66.01	22.71	162.61	22.21
67.62	22.77	164.22	22.26
69.23	22.80	165.83	22.28
70.84	22.81	167.44	22.32
72.45	22.82	169.05	22.36
74.06	22.81	170.66	22.40
75.67	22.80	172.27	22.45
77.28	22.81	173.88	22.50
78.89	22.83	175.49	22.56
80.50	22.86	177.10	22.62
82.11	22.89	178.71	22.67
83.72	22.93	180.32	22.71
85.33	22.97	181.93	22.74
86.94	23.00	183.54	22.78
88.55	23.01	185.15	22.83
90.16	23.01	186.76	22.90
91.77	23.02	188.37	23.00
93.38	23.00	189.98	23.09
94.99	22.99	191.59	23.14
96.60	22.96	193.20	23.18
98.21	22.94	194.81	23.19
99.82	22.93	196.42	23.16
101.43	22.93	198.03	23.14

N4435 'R' MINOR AXIS

SE WING

RADIUS arcsec	BRIGHTNESS Mag/#arcsec	RADIUS arcsec	BRIGHTNESS Mag/#arcsec
199.64	23.15	231.84	23.77
201.25	23.17	233.45	23.72
202.86	23.18	235.06	23.67
204.47	23.25	236.67	23.64
206.08	23.33	238.28	23.61
207.69	23.39	239.89	23.58
209.30	23.42	241.50	23.59
210.91	23.45	243.11	23.62
212.52	23.48	244.72	23.66
214.13	23.52	246.33	23.72
215.74	23.59	247.94	23.82
217.35	23.67	249.55	23.94
218.96	23.74	251.16	24.07
220.57	23.78	252.77	24.18
222.18	23.80	254.38	24.25
223.79	23.83	255.99	24.32
225.40	23.84	257.60	24.41
227.01	23.82	259.21	24.54
228.62	23.81	260.82	24.74
230.23	23.81		

N4435 'R' MINOR AXIS

NW WING

RADIUS arcsec	BRIGHTNESS Mag/#arcsec	RADIUS arcsec	BRIGHTNESS Mag/#arcsec
6.44	17.41	59.57	22.57
8.05	17.74	61.18	22.66
9.66	17.54	62.79	22.78
11.27	18.56	64.40	22.88
12.88	19.17	66.01	22.94
14.49	19.30	67.62	22.99
16.10	19.60	69.23	23.04
17.71	19.99	70.84	23.07
19.32	20.19	72.45	23.11
20.93	20.35	74.06	23.15
22.54	20.43	75.67	23.24
24.15	20.61	77.28	23.34
25.76	20.73	78.89	23.44
27.37	20.82	80.50	23.49
28.98	20.93	82.11	23.55
30.59	21.05	83.72	23.57
32.20	21.12	85.33	23.59
33.81	21.23	86.94	23.55
35.42	21.30	88.55	23.52
37.03	21.41	90.16	23.51
38.64	21.49	91.77	23.51
40.25	21.60	93.38	23.54
41.86	21.70	94.99	23.64
43.47	21.83	96.60	23.74
45.08	22.00	98.21	23.83
46.69	22.17	99.82	23.92
48.30	22.21	101.43	23.95
49.91	22.28	103.04	23.98
51.52	22.29	104.65	24.04
53.13	22.34	106.26	24.14
54.74	22.37	107.87	24.28
56.35	22.44	109.48	24.46
57.96	22.52	111.09	24.57

N4438 'R' MAJOR AXIS

SW WING

RADIUS arcsec	BRIGHTNESS Mag/#arcsec	RADIUS arcsec	BRIGHTNESS Mag/#arcsec
6.44	17.25	103.04	22.44
8.05	18.03	104.65	22.45
9.66	17.95	106.26	22.47
11.27	17.73	107.87	22.47
12.88	19.01	109.48	22.47
14.49	18.14	111.09	22.51
16.10	18.33	112.70	22.53
17.71	20.00	114.31	22.55
19.32	18.44	115.92	22.57
20.93	18.58	117.53	22.60
22.54	18.93	119.14	22.63
24.15	18.96	120.75	22.66
25.76	18.83	122.36	22.67
27.37	19.21	123.97	22.69
28.98	19.07	125.58	22.73
30.59	19.08	127.19	22.78
32.20	19.11	128.80	22.82
33.81	19.45	130.41	22.90
35.42	19.30	132.02	23.00
37.03	19.30	133.63	23.07
38.64	19.48	135.24	23.11
40.25	19.52	136.85	23.13
41.86	19.61	138.46	23.11
43.47	19.94	140.07	23.04
45.08	19.72	141.68	22.96
46.69	19.98	143.29	22.95
48.30	19.78	144.90	22.99
49.91	20.24	146.51	23.06
51.52	20.19	148.12	23.15
53.13	20.33	149.73	23.24
54.74	20.48	151.34	23.30
56.35	20.58	152.95	23.34
57.96	20.60	154.56	23.39
59.57	20.68	156.17	23.44
61.18	20.72	157.78	23.47
62.79	20.73	159.39	23.50
64.40	20.78	161.00	23.50
66.01	20.85	162.61	23.53
67.62	20.95	164.22	23.59
69.23	21.03	165.83	23.69
70.84	21.08	167.44	23.77
72.45	21.18	169.05	23.83
74.06	21.32	170.66	23.82
75.67	21.46	172.27	23.80
77.28	21.57	173.88	23.76
78.89	21.67	175.49	23.76
80.50	21.77	177.10	23.81
82.11	21.86	178.71	23.89
83.72	21.89	180.32	23.93
85.33	21.91	181.93	23.92
86.94	21.96	183.54	23.89
88.55	22.05	185.15	23.82
90.16	22.12	186.76	23.77
91.77	22.17	188.37	23.75
93.38	22.18	189.98	23.78
94.99	22.17	191.59	23.82
96.60	22.18	193.20	23.89
98.21	22.25	194.81	23.90
99.82	22.32	196.42	23.91
101.43	22.39	198.03	23.92

N4438 'R' MAJOR AXIS

SW WING

RADIUS arcsec	BRIGHTNESS Mag/#arcsec	RADIUS arcsec	BRIGHTNESS Mag/#arcsec
199.64	23.97	209.30	24.39
201.25	24.02	210.91	24.39
202.86	24.11	212.52	24.40
204.47	24.20	214.13	24.45
206.08	24.29	215.74	24.60
207.69	24.35		

N4438 'R' MAJOR AXIS

NE WING

RADIUS arcsec	BRIGHTNESS Mag/#arcsec	RADIUS arcsec	BRIGHTNESS Mag/#arcsec
6.44	17.25	103.04	22.35
8.05	18.03	104.65	22.37
9.66	17.73	106.26	22.41
11.27	17.73	107.87	22.46
12.88	19.01	109.48	22.50
14.49	18.32	111.09	22.52
16.10	18.54	112.70	22.52
17.71	20.00	114.31	22 51
19.32	18.64	115.92	22.47
20.93	18.81	117.53	22.47
22.54	18.97	119.14	22.48
24.15	19.31	120.75	22.48
25.76	19.36	122.36	22.47
27.37	19.32	123.97	22.48
28.98	19.40	125.58	22.47
30.59	19.50	127.19	22.42
32.20	19.41	128.80	22.37
33.81	19.25	130.41	22.36
35.42	19.65	132.02	22.31
37.03	19.69	133.63	22.37
38.64	19.66	135.24	22.39
40.25	20.11	136.85	22.38
41.86	20.15	138.46	22.34
43.47	20.38	140.07	22.25
45.08	20.46	141.68	22.21
46.69	20.59	143.29	22.25
48.30	20.71	144.90	22.29
49.91	20.85	146.51	22.32
51.52	20.98	148.12	22.36
53.13	21.05	149.73	22.37
54.74	21.08	151.34	22.37
56.35	21.17	152.95	22.39
57.96	21.24	154.56	22.40
59.57	21.23	156.17	22.38
61.18	21.24	157.78	22.37
62.79	21.22	159.39	22.36
64.40	21.31	161.00	22.33
66.01	21.37	162.61	22.31
67.62	21.48	164.22	22.31
69.23	21.54	165.83	22.30
70.84	21.58	167.44	22.28
72.45	21.59	169.05	22.27
74.06	21.59	170.66	22.26
75.67	21.62	172.27	22.24
77.28	21.68	173.88	22.23
78.89	21.78	175.49	22.23
80.50	21.88	177.10	22.25
82.11	21.96	178.71	22.25
83.72	21.99	180.32	22.26
85.33	22.03	181.93	22.25
86.94	22.08	183.54	22.22
88.55	22.13	185.15	22.17
90.16	22.18	186.76	22.13
91.77	22.23	188.37	22.12
93.38	22.27	189.98	22.13
94.99	22.28	191.59	22.12
96.60	22.31	193.20	22.06
98.21	22.31	194.81	22.02
99.82	22.33	196.42	22.01
101.43	22.32	198.03	22.03

N4438 'R' MAJOR AXIS

NE WING

RADIUS arcsec	BRIGHTNESS Mag/#arcsec	RADIUS arcsec	BRIGHTNESS Mag/#arcsec
199.64	22.05	235.06	22.46
201.25	22.07	236.67	22.49
202.86	22.11	238.28	22.49
204.47	22.11	239.89	22.51
206.08	22.08	241.50	22.56
207.69	22.04	243.11	22.62
209.30	22.05	244.72	22.68
210.91	22.10	246.33	22.72
212.52	22.14	247.94	22.75
214.13	22.17	249.55	22.77
215.74	22.21	251.16	22.77
217.35	22.25	252.77	22.76
218.96	22.25	254.38	22.76
220.57	22.26	255.99	22.79
222.18	22.27	257.60	22.81
223.79	22.30	259.21	22.84
225.40	22.33	260.82	22.88
227.01	22.34	262.43	22.91
228.62	22.36	264.04	22.93
230.23	22.38	265.65	22.96
231.84	22.41	267.26	22.98
233.45	22.43		

N4438 'R' B R AXIS

SE AXIS

RADIUS arcsec	BRIGHTNESS Mag/#arcsec	RADIUS arcsec	BRIGHTNESS Mag/#arcsec
6.44	18.20	48.30	22.16
8.05	17.57	49.91	22.29
9 66	17.59	51.52	22.41
11.27	17.89	53.13	22.50
12.88	18.08	54.74	22 52
14.49	18.40	56.35	22.54
16.10	18.75	57.96	22.62
17 71	18.82	59.57	22.71
19.32	19.48	61.18	22.81
20.93	19.52	62.79	22.91
22.54	19.78	64.40	23.02
24.15	20.05	66.01	23.12
25.76	20.39	67.62	23.21
27.37	20.56	69.23	23 28
28.98	20.71	70.84	23 34
30.59	20.88	72.45	23 37
32.20	21.03	74.06	23.41
33.81	21.15	75.67	23.48
35.42	21.26	77.28	23.56
37.03	21.38	78.89	23.65
38.64	21.53	80.50	23.73
40.25	21.63	82.11	23.79
41.86	21.71	83.72	23.84
43.47	21.76	85.33	23.93
45.08	21.82	86.94	24.15
46.69	21.94		

N4438 'R' B:R AXIS

NW WING

RADIUS arcsec	BRIGHTNESS Mag/#arcsec	RADIUS arcsec	BRIGHTNESS Mag/#arcsec
6.44	17.44	88.55	22.74
8.05	17.59	90.16	22.75
9.66	18.19	91.77	22.74
11.27	18.23	93.38	22.74
12.88	18.34	94.99	22.76
14.49	18.71	96.60	22.78
16.10	18.64	98.21	22.78
17.71	19.13	99.82	22.78
19.32	19.51	101.43	22.77
20.93	19.60	103.04	22.77
22.54	19.82	104.65	22.80
24.15	20.36	106.26	22.85
25.76	20.69	107.87	22.90
27.37	20.87	109.48	22.96
28.98	20.90	111.09	23.01
30.59	21.01	112.70	23.06
32.20	21.11	114.31	23.11
33.81	21.22	115.92	23.14
35.42	21.27	117.53	23.13
37.03	21.34	119.14	23.10
38.64	21.44	120.75	23.07
40.25	21.55	122.36	23.04
41.86	21.68	123.97	23.01
43.47	21.75	125.58	23.01
45.08	21.75	127.19	23.06
46.69	21.72	128.80	23.10
48.30	21.72	130.41	23.09
49.91	21.78	132.02	23.09
51.52	21.86	133.63	23.10
53.13	21.96	135.24	23.02
54.74	22.08	136.85	22.93
56.35	22.21	138.46	22.94
57.96	22.32	140.07	23.02
59.57	22.40	141.68	23.12
61.18	22.45	143.29	23.26
62.79	22.50	144.90	23.42
64.40	22.54	146.51	23.53
66.01	22.56	148.12	23.55
67.62	22.56	149.73	23.53
69.23	22.54	151.34	23.49
70.84	22.52	152.95	23.44
72.45	22.50	154.56	23.38
74.06	22.49	156.17	23.31
75.67	22.49	157.78	23.22
77.28	22.50	159.39	23.15
78.89	22.50	161.00	23.09
80.50	22.48	162.61	23.08
82.11	22.51	164.22	23.14
83.72	22.57	165.83	23.28
85.33	22.63	167.44	23.44
86.94	22.68	169.05	23.51

N4459 'R' MAJOR AXIS

SE WING

RADIUS arcsec	BRIGHTNESS Mag/#arcsec	RADIUS arcsec	BRIGHTNESS Mag/#arcsec
6.44	17.66	90.16	22.16
8.05	17.82	91.77	22.27
9.66	18.00	93.38	22.37
11.27	18.23	94.99	22.45
12.88	17.93	96.60	22.48
14.49	18.22	98.21	22.53
16.10	18.64	99.82	22.59
17.71	18.81	101.43	22.65
19.32	18.94	103.04	22.71
20.93	19.09	104.65	22 78
22.54	19.25	106.26	22.82
24.15	19.45	107.87	22.86
25.76	19.70	109.48	22.91
27.37	19.66	111.09	22.96
28.98	19.88	112.70	23.02
30.59	19.95	114.31	23.08
32.20	20.28	115.92	23.14
33.81	20.40	117.53	23.21
35.42	20.32	119.14	23.28
37.03	20.49	120.75	23.34
38.64	20.51	122.36	23.39
40.25	20.63	123.97	23.45
41.86	20.74	125.58	23.53
43.47	20.78	127.19	23.62
45.08	20.87	128.80	23.69
46.69	20.95	130.41	23.75
48.30	21.06	132.02	23.81
49.91	21.13	133.63	23.87
51.52	21.19	135.24	23.88
53.13	21.25	136.85	23.87
54.74	21.33	138.46	23.83
56.35	21.43	140.07	23.75
57.96	21.50	141.68	23.65
59.57	21.54	143.29	23.59
61.18	21.56	144.90	23.59
62.79	21.61	146.51	23.63
64.40	21.66	148.12	23.70
66.01	21.70	149.73	23.79
67.62	21.73	151.34	23.91
69.23	21.79	152.95	23.98
70.84	21.86	154.56	24.02
72.45	21.94	156.17	24.05
74.06	21.98	157.78	24.09
75.67	22.00	159.39	24.13
77.28	22.03	161.00	24.22
78.89	22.07	162.61	24.35
80.50	22.08	164.22	24.45
82.11	22.06	165.83	24.51
83.72	22.02	167.44	24.54
85.33	21.99	169.05	24.56
86.94	21.98	170.66	24.60
88.55	22.03	172.27	24.68

N4459 'R' MAJOR AXIS

NW WING

RADIUS arcsec	BRIGHTNESS Mag/#arcsec	RADIUS arcsec	BRIGHTNESS Mag/#arcsec
6.44	17.40	90.16	22.35
8.05	17.82	91.77	22.40
9.66	18.00	93.38	22.42
11.27	18.00	94.99	22.43
12.88	17.92	96.60	22.45
14.49	18.22	98.21	22.48
16.10	18.53	99.82	22.53
17.71	18.52	101.43	22.57
19.32	18.94	103.04	22.59
20.93	18.77	104.65	22.64
22.54	18.33	106.26	22.69
24.15	19.11	107.87	22.73
25.76	19.58	109.48	22.80
27.37	19.87	111.09	22.89
28.98	19.95	112.70	22.96
30.59	19.91	114.31	22.98
32.20	20.18	115.92	23.02
33.81	20.32	117.53	23.07
35.42	20.40	119.14	23.12
37.03	20.49	120.75	23.19
38.64	20.50	122.36	23.32
40.25	20.64	123.97	23.41
41.86	20.77	125.58	23.47
43.47	20.81	127.19	23.54
45.08	20.91	128.80	23.60
46.69	20.97	130.41	23.65
48.30	21.05	132.02	23.69
49.91	21.11	133.63	23.73
51.52	21.18	135.24	23.74
53.13	21.24	136.85	23.72
54.74	21.33	138.46	23.66
56.35	21.42	140.07	23.59
57.96	21.50	141.68	23.52
59.57	21.54	143.29	23.49
61.18	21.57	144.90	23.51
62.79	21.60	146.51	23.55
64.40	21.64	148.12	23.64
66.01	21.69	149.73	23.77
67.62	21.73	151.34	23.90
69.23	21.77	152.95	24.01
70.84	21.80	154.56	24.07
72.45	21.86	156.17	24.11
74.06	21.92	157.78	24.15
75.67	22.00	159.39	24.19
77.28	22.07	161.00	24.27
78.89	22.11	162.61	24.37
80.50	22.14	164.22	24.48
82.11	22.18	165.83	24.55
83.72	22.22	167.44	24.59
85.33	22.23	169.05	24.61
86.94	22.26	170.66	24.66
88.55	22.30	172.27	24.73

SW WING

RADIUS arcsec	BRIGHTNESS Mag/#arcsec	RADIUS arcsec	BRIGHTNESS Mag/#arcsec
6.44	17.46	99.82	23.02
8.05	17.82	101.43	23.05
9.66	18.00	103.04	23.09
11.27	18.00	104.65	23.11
12.88	18.14	106.26	23.17
14.49	18.22	107.87	23.26
16.10	18.71	109.48	23.36
17.71	18.87	111.09	23.51
19.32	18.94	112.70	23.64
20.93	19.59	114.31	23.75
22.54	19.86	115.92	23.85
24.15	19.99	117.53	23.94
25.76	20.04	119.14	24.00
27.37	19.93	120.75	24.05
28.98	20.14	122.36	24.09
30.59	20.45	123.97	24.14
32.20	20.57	125.58	24.18
33.81	20.72	127.19	24.23
35.42	20.81	128.80	24.26
37.03	20.96	130.41	24.26
38.64	21.06	132.02	24.25
40.25	21.15	133.63	24.24
41.86	21.19	135.24	24.22
43.47	21.23	136.85	24.23
45.08	21.30	138.46	24.22
46.69	21.38	140.07	24.19
48.30	21.48	141.68	24.17
49.91	21.56	143.29	24.16
51.52	21.62	144.90	24.10
53.13	21.68	146.51	24.07
54.74	21.73	148.12	24.05
56.35	21.79	149.73	24.03
57.96	21.84	151.34	23.99
59.57	21.90	152.95	23.95
61.18	21.96	154.56	23.95
62.79	22.02	156.17	23.93
64.40	22.08	157.78	23.91
66.01	22.12	159.39	23.87
67.62	22.14	161.00	23.87
69.23	22.18	162.61	23.89
70.84	22.24	164.22	23.92
72.45	22.28	165.83	23.96
74.06	22.34	167.44	24.00
75.67	22.40	169.05	24.04
77.28	22.46	170.66	24.05
78.89	22.51	172.27	24.03
80.50	22.57	173.88	24.02
82.11	22.61	175.49	24.04
83.72	22.62	177.10	24.10
85.33	22.63	178.71	24.21
86.94	22.66	180.32	24.33
88.55	22.71	181.93	24.43
90.16	22.79	183.54	24.50
91.77	22.86	185.15	24.51
93.38	22.91	186.76	24.49
94.99	22.95	188.37	24.50
96.60	22.99	189.98	24.61
98.21	23.00		

N4459 'R' MINOR 'XIS

NE WING

RADIUS arcsec	BRIGHTNESS Mag/#arcsec	RADIUS arcsec	BRIGHTNESS Mag/#arcsec
6.44	17.47	72.45	22.63
8.05	17.82	74.06	22.65
9.66	18.00	75.67	22.68
11.27	18.22	77.28	22.71
12.88	18.21	78.89	22.76
14.49	18.22	80.50	22.83
16.10	18.85	82.11	22.89
17.71	19.16	83.72	22.95
19.32	18.94	85.33	23.03
20.93	19.28	86.94	23.10
22.54	19.70	88.55	23.15
24.15	19.99	90.16	23.22
25.76	20.28	91.77	23.28
27.37	20.39	93.38	23.30
28.98	20.47	94.99	23.31
30.59	20.49	96.60	23.31
32.20	20.67	98.21	23.30
33.81	20.82	99.82	23.30
35.42	20.94	101.43	23.31
37.03	21.06	103.04	23.35
38.64	21.12	104.65	23.43
40.25	21.17	106.26	23.52
41.86	21.24	107.87	23.63
43.47	21.35	109.48	23.76
45.08	21.46	111.09	23.85
46.69	21.54	112.70	23.91
48.30	21.61	114.31	23.97
49.91	21.66	115.92	24.03
51.52	21.73	117.53	24.06
53.13	21.83	119.14	24.10
54.74	21.94	120.75	24.14
56.35	22.02	122.36	24.19
57.96	22.07	123.97	24.20
59.57	22.10	125.58	24.22
61.18	22.13	127.19	24.23
62.79	22.17	128.80	24.25
64.40	22.26	130.41	24.28
66.01	22.36	132.02	24.31
67.62	22.45	133.63	24.34
69.23	22.54	135.24	24.41
70.84	22.59	136.85	24.58

N4461 'R' MAJOR AXIS

S WING

RADIUS arcsec	BRIGHTNESS Mag/#arcsec	RADIUS arcsec	BRIGHTNESS Mag/#arcsec
6.44	17.35	74.06	21.88
8.05	17.80	75.67	21.92
9.66	18.07	77.28	21.96
11.27	18.04	78.89	22.02
12.88	18.48	80.50	22.09
14.49	18.61	82.11	22.14
16.10	18.87	83.72	22.18
17.71	19.12	85.33	22.21
19.32	19.25	86.94	22.24
20.93	19.44	88.55	22.29
22.54	19.69	90.16	22.33
24.15	19.79	91.77	22.40
25.76	19.92	93.38	22.46
27.37	20.11	94.99	22.53
28.98	19.98	96.60	22.62
30.59	20.52	98.21	22.70
32.20	20.39	99.82	22.79
33.81	20.48	101.43	22.89
35.42	20.52	103.04	23.00
37.03	20.50	104.65	23.09
38.64	20.45	106.26	23.20
40.25	20.52	107.87	23.34
41.86	20.59	109.48	23.48
43.47	20.63	111.09	23.58
45.08	20.64	112.70	23.65
46.69	20.68	114.31	23.68
48.30	20.77	115.92	23.70
49.91	20.88	117.53	23.72
51.52	20.99	119.14	23.78
53.13	21.12	120.75	23.90
54.74	21.25	122.36	24.07
56.35	21.36	123.97	24.22
57.96	21.44	125.58	24.32
59.57	21.50	127.19	24.37
61.18	21.55	128.80	24.38
62.79	21.60	130.41	24.34
64.40	21.64	132.02	24.32
66.01	21.68	133.63	24.35
67.62	21.72	135.24	24.43
69.23	21.75	136.85	24.53
70.84	21.80	138.46	24.63
72.45	21.84		

N4461 'R' MAJOR AXIS

N WING

RADIUS arcsec	BRIGHTNESS Mag/#arcsec	RADIUS arcsec	BRIGHTNESS Mag/#arcsec
6.44	17.35	78.89	21.89
8.05	17.49	80.50	21.95
9.66	17.91	82.11	22.02
11.27	18.08	83.72	22.09
12.88	18.62	85.33	22.19
14.49	18.81	86.94	22.28
16.10	19.24	88.55	22.35
17.71	19.21	90.16	22.41
19.32	19.60	91.77	22.47
20.93	19.55	93.38	22.54
22.54	19.60	94.99	22.64
24.15	20.05	96.60	22.74
25.76	19.87	98.21	22.81
27.37	20.08	99.82	22.85
28.98	20.05	101.43	22.88
30.59	20.34	103.04	22.89
32.20	20.45	104.65	22.92
33.81	20.41	106.26	23.00
35.42	20.31	107.87	23.12
37.03	20.35	109.48	23.23
38.64	20.49	111.09	23.36
40.25	20.52	112.70	23.46
41.86	20.44	114.31	23.59
43.47	20.56	115.92	23.74
45.08	20.61	117.53	23.86
46.69	20.68	119.14	23.92
48.30	20.77	120.75	23.98
49.91	20.91	122.36	24.04
51.52	21.03	123.97	24.05
53.13	21.14	125.58	24.09
54.74	21.25	127.19	24.24
56.35	21.35	128.80	24.34
57.96	21.42	130.41	24.31
59.57	21.50	132.02	24.24
61.18	21.56	133.63	24.20
62.79	21.61	135.24	24.12
64.40	21.64	136.85	24.10
66.01	21.64	138.46	24.18
67.62	21.64	140.07	24.28
69.23	21.68	141.68	24.38
70.84	21.76	143.29	24.49
72.45	21.85	144.90	24.56
74.06	21.89	146.51	24.61
75.67	21.87	148.12	24.73
77.28	21.85		

N4461 'R' MINOR AXIS

W WING

RADIUS arcsec	BRIGHTNESS Mag/#arcsec	RADIUS arcsec	BRIGHTNESS Mag/#arcsec
6.44	17.35	43.47	23.26
8.05	18.14	45.08	23.37
9.66	17.96	46.69	23.47
11.27	18.49	48.30	23.54
12.88	19.56	49.91	23.59
14.49	19.52	51.52	23.61
16.10	19.88	53.13	23.65
17.71	20.18	54.74	23.67
19.32	20.29	56.35	23.67
20.93	20.69	57.96	23.71
22.54	20.98	59.57	23.79
24.15	21.16	61.18	23.90
25.76	21.37	62.79	24.00
27.37	21.61	64.40	24.12
28.98	21.89	66.01	24.21
30.59	22.10	67.62	24.22
32.20	22.25	69.23	24.20
33.81	22.39	70.84	24.18
35.42	22.52	72.45	24.19
37.03	22.68	74.06	24.22
38.64	22.83	75.67	24.34
40.25	22.99	77.28	24.55
41.86	23.14	78.89	24.67

N4461 'R' MINOR AXIS

E WING

RADIUS arcsec	BRIGHTNESS Mag/#arcsec	RADIUS arcsec	BRIGHTNESS Mag/#arcsec
6.44	17.35	37.03	22.69
8.05	18.19	38.64	22.84
9.66	18.68	40.25	22.98
11.27	19.07	41.86	23.12
12.88	19.54	43.47	23.24
14.49	19.92	45.08	23.35
16.10	20.44	46.69	23.45
17.71	20.45	48.30	23.54
19.32	20.69	49.91	23.63
20.93	20.94	51.52	23.73
22.54	21.21	53.13	23.81
24.15	21.42	54.74	23.88
25.76	21.64	56.35	23.97
27.37	21.84	57.96	24.04
28.98	22.00	59.57	24.14
30.59	22.14	61.18	24.29
32.20	22.27	62.79	24.45
33.81	22.40	64.40	24.50
35.42	22.54		

N4474 'R' MAJOR AXIS

SW WING

RADIUS arcsec	BRIGHTNESS Mag/#arcsec	RADIUS arcsec	BRIGHTNESS Mag/#arcsec
6.44	17.73	56.35	22.15
8.05	18.08	57.96	22.28
9.66	17.95	59.57	22.43
11.27	18.50	61.18	22.62
12.88	18.58	62.79	22.81
14.49	18.87	64.40	22.99
16.10	19.01	66.01	23.17
17.71	19.07	67.62	23.36
19.32	19.41	69.23	23.50
20.93	19.67	70.84	23.58
22.54	19.45	72.45	23.63
24.15	19.80	74.06	23.68
25.76	19.76	75.67	23.71
27.37	19.99	77.28	23.74
28.98	20.12	78.89	23.79
30.59	20.09	80.50	23.87
32.20	20.20	82.11	23.92
33.81	20.47	83.72	23.94
35.42	20.53	85.33	23.94
37.03	20.66	86.94	23.95
38.64	20.81	88.55	24.00
40.25	21.00	90.16	24.09
41.86	21.16	91.77	24.20
43.47	21.30	93.38	24.33
45.08	21.41	94.99	24.45
46.69	21.53	96.60	24.53
48.30	21.66	98.21	24.58
49.91	21.79	99.82	24.61
51.52	21.88	101.43	24.65
53.13	21.95	103.04	24.74
54.74	22.03		

N4474 'R' MAJOR AXIS

NE WING

RADIUS arcsec	BRIGHTNESS Mag/#arcsec	RADIUS arcsec	BRIGHTNESS Mag/#arcsec
6.44	17.73	53.13	22.14
8.05	18.08	54.74	22.25
9.66	18.61	56.35	22.41
11.27	18.82	57.96	22.51
12.88	18.99	59.57	22.61
14.49	19.00	61.18	22.68
16.10	19.22	62.79	22.73
17.71	19.27	64.40	22.79
19.32	19.57	66.01	22.87
20.93	19.54	67.62	22.95
22.54	19.98	69.23	23.03
24.15	20.04	70.84	23.11
25.76	20.14	72.45	23.22
27.37	19.96	74.06	23.37
28.98	20.38	75.67	23.52
30.59	20.52	77.28	23.67
32.20	20.64	78.89	23.82
33.81	20.74	80.50	23.93
35.42	20.87	82.11	24.03
37.03	20.98	83.72	24.17
38.64	21.10	85.33	24.29
40.25	21.19	86.94	24.34
41.86	21.31	88.55	24.34
43.47	21.43	90.16	24.28
45.08	21.58	91.77	24.18
46.69	21.75	93.38	24.11
48.30	21.91	94.99	24.11
49.91	22.03	96.60	24.20
51.52	22.09	98.21	24.40

N4474 'R' MINOR AXIS

SE WING

RADIUS arcsec	BRIGHTNESS Mag/#arcsec	RADIUS arcsec	BRIGHTNESS Mag/#arcsec
6.44	17.73	46.69	23.12
8.05	18.08	48.30	23.17
9.66	19.25	49.91	23.22
11.27	19.83	51.52	23.24
12.88	20.27	53.13	23.28
14.49	20.57	54.74	23.35
16.10	20.79	56.35	23.46
17.71	20.96	57.96	23.58
19.32	21.12	59.57	23.73
20.93	21.32	61.18	23.91
22.54	21.52	62.79	24.11
24.15	21.71	64.40	24.30
25.76	21.88	66.01	24.45
27.37	22.01	67.62	24.50
28.98	22.09	69.23	24.47
30.59	22.17	70.84	24.42
32.20	22.34	72.45	24.41
33.81	22.44	74.06	24.39
35.42	22.60	75.67	24.42
37.03	22.73	77.28	24.45
38.64	22.80	78.89	24.47
40.25	22.87	80.50	24.43
41.86	22.95	82.11	24.46
43.47	23.00	83.72	24.55
45.08	23.05	85.33	24.66

N4474 'R' MINOR AXIS

NW WING

RADIUS arcsec	BRIGHTNESS Mag/#arcsec	RADIUS arcsec	BRIGHTNESS Mag/#arcsec
6.44	17.73	43.47	23.02
8.05	18.08	45.08	23.15
9.66	19.59	46.69	23.27
11.27	20.01	48.30	23.35
12.88	20.37	49.91	23.39
14.49	20.66	51.52	23.40
16.10	20.81	53.13	23.40
17.71	21.03	54.74	23.40
19.32	21.20	56.35	23.41
20.93	21.39	57.96	23.48
22.54	21.56	59.57	23.61
24.15	21.70	61.18	23.77
25.76	21.80	62.79	23.91
27.37	21.91	64.40	24.04
28.98	22.05	66.01	24.12
30.59	22.21	67.62	24.12
32.20	22.33	69.23	24.09
33.81	22.44	70.84	24.09
35.42	22.52	72.45	24.13
37.03	22.59	74.06	24.24
38.64	22.67	75.67	24.37
40.25	22.78	77.28	24.49
41.86	22.90	78.89	24.64

N4477 'R' MAJOR AXIS

SW WING

RADIUS arcsec	BRIGHTNESS Mag/#arcsec	RADIUS arcsec	BRIGHTNESS Mag/#arcsec
6.44	17.45	72.45	22.08
8.05	17.71	74.06	22.09
9.66	17.84	75.67	22.12
11.27	18.10	77.28	22.17
12.88	18.27	78.89	22.22
14.49	18.40	80.50	22.25
16.10	18.41	82.11	22.26
17.71	18.87	83.72	22.29
19.32	18.87	85.33	22.35
20.93	18.85	86.94	22.42
22.54	19.10	88.55	22.54
24.15	19.44	90.16	22.68
25.76	19.44	91.77	22.82
27.37	19.50	93.38	22.95
28.98	19.87	94.99	23.07
30.59	20.07	96.60	23.17
32.20	20.09	98.21	23.25
33.81	20.38	99.82	23.32
35.42	20.50	101.43	23.38
37.03	20.65	103.04	23.44
38.64	20.77	104.65	23.50
40.25	20.82	106.26	23.58
41.86	20.95	107.87	23.66
43.47	21.04	109.48	23.74
45.08	21.16	111.09	23.77
46.69	21.21	112.70	23.74
48.30	21.24	114.31	23.61
49.91	21.28	115.92	23.51
51.52	21.36	117.53	23.48
53.13	21.50	119.14	23.48
54.74	21.61	120.75	23.55
56.35	21.67	122.36	23.71
57.96	21.69	123.97	23.85
59.57	21.69	125.58	23.91
61.18	21.70	127.19	23.96
62.79	21.75	128.80	24.03
64.40	21.82	130.41	24.09
66.01	21.91	132.02	24.19
67.62	22.00	133.63	24.35
69.23	22.06	135.24	24.54
70.84	22.09	136.85	24.68

N4477 'R' MAJOR AXIS

NE WING

RADIUS arcsec	BRIGHTNESS Mag/#arcsec	RADIUS arcsec	BRIGHTNESS Mag/#arcsec
6.44	17.45	72.45	22.00
8.05	17.63	74.06	22.00
9.66	17.99	75.67	22.02
11.27	18.11	77.28	22.05
12.88	18.10	78.89	22.07
14.49	18.54	80.50	22.06
16.10	18.35	82.11	22.09
17.71	18.61	83.72	22.19
19.32	18.71	85.33	22.28
20.93	19.16	86.94	22.38
22.54	18.78	88.55	22.50
24.15	19.15	90.16	22.60
25.76	19.25	91.77	22.71
27.37	19.57	93.38	22.83
28.98	19.75	94.99	22.92
30.59	19.98	96.60	23.01
32.20	20.20	98.21	23.09
33.81	20.33	99.82	23.17
35.42	20.52	101.43	23.24
37.03	20.66	103.04	23.30
38.64	20.78	104.65	23.35
40.25	20.89	106.26	23.43
41.86	20.99	107.87	23.54
43.47	21.08	109.48	23.63
45.08	21.11	111.09	23.72
46.69	21.16	112.70	23.78
48.30	21.25	114.31	23.80
49.91	21.38	115.92	23.78
51.52	21.45	117.53	23.79
53.13	21.49	119.14	23.80
54.74	21.53	120.75	23.82
56.35	21.61	122.36	23.85
57.96	21.68	123.97	23.88
59.57	21.72	125.58	23.90
61.18	21.73	127.19	23.92
62.79	21.73	128.80	23.98
64.40	21.72	130.41	24.05
66.01	21.74	132.02	24.12
67.62	21.81	133.63	24.25
69.23	21.90	135.24	24.42
70.84	21.97	136.85	24.58

N4477 'R' MINOR AXIS

SE WING

RADIUS arcsec	BRIGHTNESS Mag/#arcsec	RADIUS arcsec	BRIGHTNESS Mag/#arcsec
6.44	17.45	74.06	22.10
8.05	18.13	75.67	22.18
9.66	18.13	77.28	22.26
11.27	18.73	78.89	22.35
12.88	19.17	80.50	22.45
14.49	19.23	82.11	22.55
16.10	19.78	83.72	22.64
17.71	19.83	85.33	22.72
19.32	19.90	86.94	22.79
20.93	20.15	88.55	22.83
22.54	20.25	90.16	22.85
24.15	20.47	91.77	22.87
25.76	20.53	93.38	22.89
27.37	20.49	94.99	22.91
28.98	20.59	96.60	22.95
30.59	20.68	98.21	22.99
32.20	20.78	99.82	23.03
33.81	20.86	101.43	23.08
35.42	20.90	103.04	23.11
37.03	20.91	104.65	23.14
38.64	20.91	106.26	23.18
40.25	20.94	107.87	23.23
41.86	21.00	109.48	23.29
43.47	21.08	111.09	23.36
45.08	21.13	112.70	23.43
46.69	21.16	114.31	23.51
48.30	21.17	115.92	23.58
49.91	21.19	117.53	23.68
51.52	21.18	119.14	23.79
53.13	21.19	120.75	23.91
54.74	21.21	122.36	23.98
56.35	21.25	123.97	24.02
57.96	21.28	125.58	24.01
59.57	21.32	127.19	23.96
61.18	21.37	128.80	23.94
62.79	21.41	130.41	23.98
64.40	21.45	132.02	24.06
66.01	21.52	133.63	24.14
67.62	21.64	135.24	24.22
69.23	21.78	136.85	24.28
70.84	21.91	138.46	24.31
72.45	22.01	140.07	24.31

N4477 'R' MINOR AXIS

NW WING

RADIUS arcsec	BRIGHTNESS Mag/#arcsec	RADIUS arcsec	BRIGHTNESS Mag/#arcsec
6.44	17.45	74.06	21.90
8.05	17.56	75.67	22.06
9.66	17.76	77.28	22.18
11.27	18.28	78.89	22.26
12.88	18.49	80.50	22.35
14.49	18.88	82.11	22.41
16.10	19.17	83.72	22.46
17.71	19.40	85.33	22.50
19.32	19.63	86.94	22.51
20.93	19.98	88.55	22.54
22.54	20.01	90.16	22.58
24.15	20.23	91.77	22.63
25.76	20.32	93.38	22.72
27.37	20.40	94.99	22.84
28.98	20.53	96.60	22.95
30.59	20.49	98.21	23.05
32.20	20.68	99.82	23.15
33.81	20.76	101.43	23.22
35.42	20.78	103.04	23.27
37.03	20.80	104.65	23.33
38.64	20.88	106.26	23.42
40.25	20.95	107.87	23.50
41.86	21.04	109.48	23.57
43.47	21.11	111.09	23.61
45.08	21.17	112.70	23.64
46.69	21.20	114.31	23.68
48.30	21.23	115.92	23.75
49.91	21.26	117.53	23.85
51.52	21.28	119.14	23.94
53.13	21.27	120.75	24.02
54.74	21.26	122.36	24.09
56.35	21.27	123.97	24.13
57.96	21.32	125.58	24.17
59.57	21.37	127.19	24.22
61.18	21.45	128.80	24.28
62.79	21.54	130.41	24.29
64.40	21.62	132.02	24.28
66.01	21.65	133.63	24.30
67.62	21.65	135.24	24.33
69.23	21.66	136.85	24.32
70.84	21.68	138.46	24.34
72.45	21.76	140.07	24.41

SE WING

RADIUS arcsec	BRIGHTNESS Mag/#arcsec	RADIUS arcsec	BRIGHTNESS Mag/#arcsec
6.44	17.54	103.04	21.01
8.05	17.63	104.65	21.04
9.66	18.18	106.26	21.06
11.27	17.82	107.87	21.08
12.88	18.30	109.48	21.08
14.49	18.24	111.09	21.09
16.10	18.59	112.70	21.08
17.71	18.58	114.31	21.07
19.32	18.83	115.92	21.08
20.93	19.29	117.53	21.10
22.54	19.28	119.14	21.12
24.15	19.39	120.75	21.12
25.76	18.98	122.36	21.12
27.37	19.35	123.97	21.14
28.98	19.09	125.58	21.16
30.59	18.99	127.19	21.21
32.20	18.88	128.80	21.25
33.81	19.26	130.41	21.28
35.42	19.11	132.02	21.29
37.03	19.08	133.63	21.28
38.64	19.27	135.24	21.31
40.25	19.21	136.85	21.33
41.86	19.18	138.46	21.35
43.47	19.24	140.07	21.38
45.08	19.26	141.68	21.42
46.69	19.19	143.29	21.48
48.30	19.22	144.90	21.53
49.91	19.21	146.51	21.58
51.52	19.20	148.12	21.62
53.13	19.23	149.73	21.65
54.74	19.46	151.34	21.68
56.35	19.51	152.95	21.73
57.96	19.72	154.56	21.78
59.57	19.84	156.17	21.82
61.18	19.85	157.78	21.86
62.79	20.04	159.39	21.93
64.40	19.66	161.00	21.99
66.01	19.79	162.61	22.04
67.62	19.74	164.22	22.09
69.23	19.80	165.83	22.15
70.84	19.99	167.44	22.23
72.45	20.10	169.05	22.32
74.06	20.24	170.66	22.40
75.67	20.36	172.27	22.47
77.28	20.28	173.88	22.53
78.89	20.49	175.49	22.60
80.50	20.52	177.10	22.68
82.11	20.45	178.71	22.76
83.72	20.41	180.32	22.84
85.33	20.41	181.93	22.92
86.94	20.43	183.54	22.99
88.55	20.44	185.15	23.05
90.16	20.45	186.76	23.09
91.77	20.47	188.37	23.15
93.38	20.45	189.98	23.22
94.99	20.46	191.59	23.26
96.60	20.64	193.20	23.29
98.21	20.80	194.81	23.32
99.82	20.90	196.42	23.34
101.43	20.98	198.03	23.34

N4501 'R' MAJOR AXIS

SE WING

RADIUS arcsec	BRIGHTNESS Mag/#arcsec	RADIUS arcsec	BRIGHTNESS Mag/#arcsec
199.64	23.36	227.01	23.79
201.25	23.41	228.62	23.88
202.86	23.46	230.23	23.96
204.47	23.51	231.84	24.04
206.08	23.59	233.45	24.13
207.69	23.64	235.06	24.20
209.30	23.69	236.67	24.18
210.91	23.71	238.28	24.19
212.52	23.77	239.89	24.20
214.13	23.79	241.50	24.16
215.74	23.82	243.11	24.09
217.35	23.83	244.72	24.01
218.96	23.85	246.33	24.01
220.57	23.82	247.94	24.06
222.18	23.79	249.55	24.23
223.79	23.77	251.16	24.44
225.40	23.76		

N4501 'R' MAJOR AXIS

NW WING

RADIUS arcsec	BRIGHTNESS Mag/#arcsec	RADIUS arcsec	BRIGHTNESS Mag/#arcsec
6.44	17.54	103.04	20.65
8.05	17.63	104.65	20.57
9.66	17.74	106.26	20.58
11.27	18.25	107.87	20.57
12.88	18.30	109.48	20.67
14.49	18.35	111.09	20.76
16.10	18.25	112.70	20.84
17.71	18.56	114.31	20.87
19.32	18.72	115.92	20.91
20.93	18.79	117.53	20.98
22.54	18.71	119.14	21.07
24.15	18.67	120.75	21.14
25.76	18.97	122.36	21.16
27.37	18.86	123.97	21.16
28.98	19.15	125.58	21.17
30.59	18.92	127.19	21.22
32.20	18.90	128.80	21.29
33.81	19.04	130.41	21.36
35.42	19.23	132.02	21.42
37.03	19.13	133.63	21.47
38.64	19.28	135.24	21.51
40.25	19.33	136.85	21.54
41.86	19.46	138.46	21.59
43.47	19.47	140.07	21.65
45.08	19.59	141.68	21.72
46.69	19.54	143.29	21.77
48.30	19.63	144.90	21.80
49.91	19.85	146.51	21.81
51.52	19.94	148.12	21.83
53.13	19.84	149.73	21.87
54.74	20.08	151.34	21.90
56.35	20.12	152.95	21.93
57.96	20.13	154.56	21.96
59.57	19.98	156.17	22.00
61.18	20.18	157.78	22.07
62.79	20.07	159.39	22.17
64.40	20.21	161.00	22.26
66.01	20.28	162.61	22.31
67.62	20.40	164.22	22.36
69.23	20.39	165.83	22.41
70.84	20.37	167.44	22.48
72.45	20.48	169.05	22.57
74.06	20.52	170.66	22.64
75.67	20.40	172.27	22.73
77.28	20.55	173.88	22.81
78.89	20.51	175.49	22.89
80.50	20.28	177.10	22.95
82.11	20.28	178.71	23.01
83.72	20.49	180.32	23.08
85.33	20.61	181.93	23.12
86.94	20.69	183.54	23.17
88.55	20.73	185.15	23.19
90.16	20.74	186.76	23.23
91.77	20.73	188.37	23.25
93.38	20.68	189.98	23.31
94.99	20.68	191.59	23.36
96.60	20.71	193.20	23.42
98.21	20.72	194.81	23.49
99.82	20.73	196.42	23.52
101.43	20.68	198.03	23.53

N4501 'R' MAJOR AXIS

NW WING

RADIUS arcsec	BRIGHTNESS Mag/#arcsec	RADIUS arcsec	BRIGHTNESS Mag/#arcsec
199.64	23.52	217.35	23.91
201.25	23.51	218.96	23.96
202.86	23.49	220.57	24.00
204.47	23.53	222.18	24.07
206.08	23.57	223.79	24.12
207.69	23.65	225.40	24.21
209.30	23.71	227.01	24.29
210.91	23.76	228.62	24.37
212.52	23.82	230.23	24.39
214.13	23.85	231.84	24.45
215.74	23.88	233.45	24.57

N4501 'R' MINOR AXIS

SW WING

RADIUS arcsec	BRIGHTNESS Mag/#arcsec	RADIUS arcsec	BRIGHTNESS Mag/#arcsec
6.44	17.54	75.67	22.48
8.05	17.63	77.28	22.59
9.66	18.19	78.89	22.68
11.27	18.27	80.50	22.77
12.88	18.30	82.11	22.87
14.49	18.99	83.72	23.00
16.10	18.72	85.33	23.13
17.71	18.74	86.94	23.25
19.32	18.99	88.55	23.35
20.93	18.88	90.16	23.44
22.54	19.31	91.77	23.49
24.15	19.39	93.38	23.54
25.76	19.56	94.99	23.64
27.37	19.50	96.60	23.69
28.98	19.48	98.21	23.73
30.59	19.71	99.82	23.79
32.20	19.86	101.43	23.85
33.81	20.08	103.04	23.82
35.42	19.96	104.65	23.87
37.03	19.58	106.26	23.96
38.64	19.94	107.87	24.07
40.25	20.22	109.48	24.15
41.86	20.47	111.09	24.22
43.47	20.57	112.70	24.26
45.08	20.64	114.31	24.26
46.69	20.68	115.92	24.16
48.30	20.75	117.53	24.06
49.91	20.82	119.14	24.04
51.52	20.90	120.75	24.03
53.13	20.98	122.36	24.03
54.74	21.00	123.97	24.07
56.35	21.01	125.58	24.13
57.96	21.05	127.19	24.15
59.57	21.14	128.80	24.17
61.18	21.25	130.41	24.21
62.79	21.37	132.02	24.25
64.40	21.51	133.63	24.26
66.01	21.65	135.24	24.34
67.62	21.78	136.85	24.40
69.23	21.90	138.46	24.47
70.84	22.04	140.07	24.52
72.45	22.21	141.68	24.62
74.06	22.35	143.29	24.71

N4501 'R' MINOR AXIS

NE WING

RADIUS arcsec	BRIGHTNESS Mag/#arcsec	RADIUS arcsec	BRIGHTNESS Mag/#arcsec
6.44	17.54	70.84	21.73
8.05	17.63	72.45	21.80
9.66	18.16	74.06	21.85
11.27	18.53	75.67	21.86
12.88	18.30	77.28	21.82
14.49	18.84	78.89	21.81
16.10	19.17	80.50	21.87
17.71	19.11	82.11	21.97
19.32	19.29	83.72	22.09
20.93	19.37	85.33	22.22
22.54	19.32	86.94	22.33
24.15	19.44	88.55	22.45
25.76	19.66	90.16	22.53
27.37	19.98	91.77	22.63
28.98	20.22	93.38	22.72
30.59	20.21	94.99	22.82
32.20	20.09	96.60	22.88
33.81	20.14	98.21	22.99
35.42	20.46	99.82	23.06
37.03	20.45	101.43	23.14
38.64	20.52	103.04	23.21
40.25	20.43	104.65	23.31
41.86	20.47	106.26	23.39
43.47	20.59	107.87	23.44
45.08	20.70	109.48	23.53
46.69	20.79	111.09	23.65
48.30	20.91	112.70	23.79
49.91	21.04	114.31	23.85
51.52	21.18	115.92	23.93
53.13	21.31	117.53	23.95
54.74	21.38	119.14	23.96
56.35	21.44	120.75	23.95
57.96	21.49	122.36	23.96
59.57	21.55	123.97	23.94
61.18	21.58	125.58	23.93
62.79	21.59	127.19	23.95
64.40	21.63	128.80	24.04
66.01	21.64	130.41	24.25
67.62	21.66	132.02	24.45
69.23	21.67		

N4503 'R' MAJOR XIS

S WING

RADIUS arcsec	BRIGHTNESS Mag/#arcsec	RADIUS arcsec	BRIGHTNESS Mag/#arcsec
6.44	17.75	80.50	21.95
8.05	17.26	82.11	21.96
9.66	17.90	83.72	22.01
11.27	18.01	85.33	22.06
12.88	18.05	86.94	22.13
14.49	18.66	88.55	22.18
16.10	18.68	90.16	22.18
17.71	18.64	91.77	22.16
19 32	18.96	93.38	22.22
20.93	19.21	94.99	22.30
22.54	19.33	96.60	22 37
24.15	19.61	98.21	22.44
25.76	19.63	99.82	22.47
27 37	19.77	101.43	22.51
28.98	20.01	103.04	22.59
30.59	20.21	104.65	22.70
32.20	20.28	106.26	22.81
33.81	20.46	107.87	22.93
35.42	20.28	109.48	23.05
37.03	20.45	111.09	23.15
38.64	20.50	112.70	23.22
40.25	20.59	114.31	23.29
41.86	20.67	115.92	23.34
43.47	20.70	117.53	23.40
45.08	20.73	119.14	23.47
46.69	20.73	120.75	23.52
48.30	20.75	122.36	23.57
49.91	20.82	123.97	23.62
51.52	20.91	125.58	23.67
53.13	20.99	127.19	23.73
54.74	21.08	128.80	23 81
56.35	21.14	130.41	23.87
57.96	21.19	132.02	23 93
59.57	21.24	133.63	23.99
61.18	21.31	135.24	24.04
62.79	21.40	136.85	24.07
64.40	21.48	138.46	24 09
66.01	21.55	140.07	24.10
67.62	21.65	141.68	24 11
69.23	21.72	143.29	24 12
70.84	21.76	144.90	24 12
72.45	21.79	146.51	24.15
74.06	21.86	148.12	24 24
75 67	21.97	149.73	24.40
77.28	22.00	151.34	24.60
78.89	21.97		

N4503 'R' MAJOR AXIS

N WING

RADIUS arcsec	BRIGHTNESS Mag/#arcsec	RADIUS arcsec	BRIGHTNESS Mag/#arcsec
6.44	17.75	78.89	22.01
8.05	18.14	80.50	22.08
9.66	18.14	82.11	22.17
11.27	18.71	83.72	22.25
12.88	18.74	85.33	22.31
14.47	18.83	86.94	22.37
16.10	19.53	88.55	22.42
17.71	19.48	90.16	22.48
19.32	19.51	91.77	22.54
20.93	19.57	93.38	22.59
22.54	19.89	94.99	22.66
24.15	19.89	96.60	22.72
25.76	20.00	98.21	22.78
27.37	20.10	99.82	22.84
28.98	20.13	101.43	22.91
30.59	20.25	103.04	22.98
32.20	20.25	104.65	23.04
33.81	20.29	106.26	23.11
35.42	20.47	107.87	23.17
37.03	20.32	109.48	23.22
38.64	20.54	111.09	23.30
40.25	20.68	112.70	23.41
41.86	20.71	114.31	23.54
43.47	20.75	115.92	23.69
45.08	20.79	117.53	23.85
46.69	20.89	119.14	23.96
48.30	20.96	120.75	24.00
49.91	21.01	122.36	23.97
51.52	21.05	123.97	23.96
53.13	21.13	125.58	23.95
54.74	21.24	127.19	23.93
56.35	21.31	128.80	23.95
57.96	21.34	130.41	24.01
59.57	21.35	132.02	24.09
61.18	21.39	133.63	24.15
62.79	21.45	135.24	24.24
64.40	21.51	136.85	24.35
66.01	21.57	138.46	24.43
67.62	21.64	140.07	24.44
69.23	21.71	141.68	24.41
70.84	21.76	143.29	24.37
72.45	21.82	144.90	24.30
74.06	21.89	146.51	24.23
75.67	21.94	148.12	24.26
77.28	21.97	149.73	24.47

N4503 'R' MINOR AXIS

E WING

RADIUS arcsec	BRIGHTNESS Mag/#arcsec	RADIUS arcsec	BRIGHTNESS Mag/#arcsec
6.44	17.75	38.64	22.23
8.05	18.73	40.25	22.35
9.66	19.06	41.86	22.52
11.27	19.55	43.47	22.73
12.88	19.78	45.08	22.94
14.49	19.98	46.69	23.13
16.10	20.35	48.30	23.27
17.71	20.49	49.91	23.42
19.32	20.61	51.52	23.55
20.93	20.77	53.13	23.68
22.54	20.94	54.74	23.82
24.15	21.09	56.35	23.95
25.76	21.22	57.96	24.02
27.37	21.36	59.57	24.06
28.98	21.50	61.18	24.09
30.59	21.64	62.79	24.13
32.20	21.81	64.40	24.16
33.81	21.97	66.01	24.24
35.42	22.10	67.62	24.41
37.03	22.17	69.23	24.65

N4503 'R' MINOR AXIS

W WING

RADIUS arcsec	BRIGHTNESS Mag/#arcsec	RADIUS arcsec	BRIGHTNESS Mag/#arcsec
6.44	17.75	37.05	21.95
8.05	17.98	38.64	22.07
9.66	18.04	40.25	22.14
11.27	18.59	41.86	22.19
12.88	18.98	43.47	22.26
14.49	19.69	45.08	22.45
16.10	19.96	46.69	22.64
17.71	20.19	48.30	22.84
19.32	20.33	49.91	23.00
20.93	20.55	51.52	23.15
22.54	20.76	53.13	23.29
24.15	20.89	54.74	23.36
25.76	21.04	56.35	23.49
27.37	21.13	57.96	23.69
28.98	21.27	59.57	23.89
30.59	21.42	61.18	24.05
32.20	21.56	62.79	24.20
33.81	21.68	64.40	24.36
35.42	21.82	66.01	24.59

N4531 'R' MAJOR AXIS

SE WING

RADIUS arcsec	BRIGHTNESS Mag/#arcsec	RADIUS arcsec	BRIGHTNESS Mag/#arcsec
6.44	19.38	62.79	22.20
8.05	19.52	64.40	22.24
9.66	19.74	66.01	22.28
11.27	19.79	67.62	22.34
12.88	19.85	69.23	22.40
14.49	19.84	70.84	22.47
16.10	19.75	72.45	22.54
17.71	19.83	74.06	22.59
19.32	19.95	75.67	22.62
20.93	20.21	77.28	22.64
22.54	20.31	78.89	22.64
24.15	20.47	80.50	22.66
25.76	20.35	82.11	22.71
27.37	20.56	83.72	22.77
28.98	20.71	85.33	22.85
30.59	20.84	86.94	22.99
32.20	20.88	88.55	23.15
33.81	21.00	90.16	23.29
35.42	21.10	91.77	23.39
37.03	21.22	93.38	23.49
38.64	21.30	94.99	23.50
40.25	21.40	96.60	23.50
41.86	21.49	98.21	23.53
43.47	21.55	99.82	23.60
45.08	21.59	101.43	23.69
46.69	21.65	103.04	23.85
48.30	21.69	104.65	24.00
49.91	21.75	106.26	24.15
51.52	21.82	107.87	24.26
53.13	21.90	109.48	24.32
54.74	21.95	111.09	24.34
56.35	21.98	112.70	24.33
57.96	22.01	114.31	24.36
59.57	22.06	115.92	24.46
61.18	22.14	117.53	24.59

N4531 'R' MAJOR AXIS

NW WING

RADIUS arcsec	BRIGHTNESS Mag/#arcsec	RADIUS arcsec	BRIGHTNESS Mag/#arcsec
6.44	19.38	59.57	22.06
8.05	19.41	61.18	22.17
9.66	19.65	62.79	22.23
11.27	19.79	64.40	22.27
12.88	19.87	66.01	22.33
14.49	19.93	67.62	22.37
16.10	20.02	69.23	22.39
17.71	19.89	70.84	22.41
19.32	20.19	72.45	22.45
20.93	20.11	74.06	22.49
22.54	20.30	75.67	22.55
24.15	20.45	77.28	22.61
25.76	20.46	78.89	22.67
27.37	20.50	80.50	22.69
28.98	20.73	82.11	22.72
30.59	20.85	83.72	22.77
32.20	20.95	85.33	22.85
33.81	21.02	86.94	22.97
35.42	21.13	88.55	23.13
37.03	21.20	90.16	23.29
38.64	21.23	91.77	23.45
40.25	21.33	93.38	23.69
41.86	21.41	94.99	23.94
43.47	21.53	96.60	24.08
45.08	21.59	98.21	24.13
46.69	21.64	99.82	24.10
48.30	21.68	101.43	24.03
49.91	21.72	103.04	23.94
51.52	21.75	104.65	23.91
53.13	21.77	106.26	24.01
54.74	21.78	107.87	24.21
56.35	21.82	109.48	24.55
57.96	21.93		

N4531 'R' MINOR AXIS

SW WING

RADIUS arcsec	BRIGHTNESS Mag/#arcsec	RADIUS arcsec	BRIGHTNESS Mag/#arcsec
6.44	19.38	48.30	22.48
8.05	19.98	49.91	22.62
9.66	20.11	51.52	22.77
11.27	19.79	53.13	22.88
12.88	20.10	54.74	22.95
14.49	20.23	56.35	23.01
16.10	20.43	57.96	23.09
17.71	20.30	59.57	23.23
19.32	20.71	61.18	23.41
20.93	20.91	62.79	23.58
22.54	21.05	64.40	23.77
24.15	21.12	66.01	24.00
25.76	21.29	67.62	24.13
27.37	21.38	69.23	24.22
28.98	21.49	70.84	24.30
30.59	21.60	72.45	24.43
32.20	21.71	74.06	24.45
33.81	21.79	75.67	24.53
35.42	21.81	77.28	24.59
37.03	21.84	78.89	24.66
38.64	21.88	80.50	24.65
40.25	21.99	82.11	24.68
41.86	22.11	83.72	24.67
43.47	22.20	85.33	24.67
45.08	22.24	86.94	24.72
46.69	22.29	88.55	24.81

N4531 'R' MINOR AXIS

NE WING

RADIUS arcsec	BRIGHTNESS Mag/#arcsec	RADIUS arcsec	BRIGHTNESS Mag/#arcsec
6.44	19.38	48.30	22.36
8.05	19.48	49.91	22.43
9.66	19.34	51.52	22.52
11.27	19.79	53.13	22.64
12.88	19.62	54.74	22.78
14.49	20.14	56.35	22.92
16.10	20.13	57.96	23.04
17.71	20.37	59.57	23.13
19.32	20.53	61.18	23.20
20.93	20.74	62.79	23.28
22.54	20.88	64.40	23.39
24.15	21.07	66.01	23.52
25.76	21.18	67.62	23.65
27.37	21.33	69.23	23.81
28.98	21.47	70.84	23.95
30.59	21.55	72.45	24.14
32.20	21.61	74.06	24.31
33.81	21.67	75.67	24.45
35.42	21.74	77.28	24.53
37.03	21.81	78.89	24.57
38.64	21.86	80.50	24.52
40.26	21.95	82.11	24.52
41.86	22.06	83.72	24.58
43.47	22.17	85.33	24.64
45.08	22.23	86.94	24.75
46.69	22.27	88.55	24.80

N4550 'R' MAJOR AXIS

S WING

RADIUS arcsec	BRIGHTNESS Mag/#arcsec	RADIUS arcsec	BRIGHTNESS Mag/#arcsec
6.44	17.54	57.96	22.02
8.05	17.57	59.57	22.15
9.66	17.72	61.18	22.24
11.27	17.49	62.79	22.30
12.88	17.97	64.40	22.35
14 49	18.17	66.01	22.41
16.10	18 45	67.62	22.46
17.71	18.35	69.23	22.51
19.32	19.05	70.84	22.59
20.93	18.97	72.45	22.69
22.54	19.18	74.06	22.79
24.15	19.39	75.67	22.87
25.76	19.47	77.28	22.93
27.37	19.72	78.89	22.99
28.98	19.86	80.50	23.04
30.59	20.03	82.11	23.06
32.20	20.22	83.72	23.10
33.81	20.44	85.33	23.14
35.42	20.41	86.94	23.17
37.03	20.55	88.55	23.21
38.64	20.71	90.16	23.29
40.25	20.82	91.77	23.37
41.86	20.92	93.38	23.47
43.47	21.00	94.99	23.57
45.08	21.09	96.60	23.66
46.69	21.16	98.21	23.72
48.30	21.21	99.82	23.79
49.91	21.30	101.43	23.88
51.52	21.41	103.04	24.02
53.13	21.55	104.65	24.24
54.74	21.70	106.26	24.54
56.35	21.86		

N4550 'R' MAJOR AXIS

N WING

RADIUS arcsec	BRIGHTNESS Mag/#arcsec	RADIUS arcsec	BRIGHTNESS Mag/#arcsec
6.44	17.45	69.23	22.52
8.05	17.47	70.84	22.59
9.66	17.59	72.45	22.66
11.27	17.81	74.06	22.74
12.88	17.82	75.67	22.83
14.49	18.13	77.28	22.89
16.10	18.35	78.89	22.99
17.71	18.65	80.50	23.10
19.32	18.94	82.11	23.19
20.93	19.08	83.72	23.28
22.54	19.26	85.33	23.37
24.15	19.46	86.94	23.42
25.76	19.64	88.55	23.45
27.37	19.97	90.16	23.49
28.98	20.07	91.77	23.51
30.59	20.16	93.38	23.51
32.20	20.31	94.99	23.57
33.81	20.45	96.60	23.70
35.42	20.55	98.21	23.84
37.03	20.63	99.82	23.99
38.64	20.69	101.43	24.08
40.25	20.79	103.04	24.10
41.86	20.89	104.65	24.07
43.47	21.02	106.26	24.03
45.08	21.15	107.87	23.99
46.69	21.27	109.48	23.99
48.30	21.35	111.09	24.03
49.91	21.42	112.70	24.02
51.52	21.52	114.31	24.01
53.13	21.61	115.92	24.06
54.74	21.70	117.53	24.19
56.35	21.82	119.14	24.35
57.96	21.95	120.75	24.50
59.57	22.05	122.36	24.59
61.18	22.14	123.97	24.56
62.79	22.22	125.58	24.46
64.40	22.29	127.19	24.42
66.01	22.36	128.80	24.45
67.62	22.43	130.41	24.53

N4550 'R' MINOR AXIS

N WING

RADIUS arcsec	BRIGHTNESS Mag/#arcsec	RADIUS arcsec	BRIGHTNESS Mag/#arcsec
6.44	18.58	24.15	22.79
8.05	19.00	25.76	22.99
9.66	19.69	27.37	23.11
11.27	20.19	28.98	23.23
12.88	20.59	30.59	23.36
14.49	20.96	32.20	23.50
16.10	21.33	33.81	23.65
17.71	21.69	35.42	23.84
19.32	22.00	37.03	24.03
20.93	22.28	38.64	24.31
22.54	22.56		

N4550 'R' MINOR AXIS

E WING

RADIUS arcsec	BRIGHTNESS Mag/#arcsec	RADIUS arcsec	BRIGHTNESS Mag/#arcsec
6.44	17.74	25.76	22.91
8.05	18.45	27.37	23.18
9.66	18.84	28.98	23.40
11.27	19.79	30.59	23.56
12.88	20.11	32.20	23.69
14.49	20.63	33.81	23.82
16.10	21.03	35.42	23.94
17.71	21.30	37.03	24.00
19.32	21.58	38.64	24.03
20.93	21.87	40.25	24.06
22.54	22.20	41.86	24.32
24.15	22.59		

N4552 'R' MAJOR AXIS

SE WING

RADIUS arcsec	BRIGHTNESS Mag/#arcsec	RADIUS arcsec	BRIGHTNESS Mag/#arcsec
6.44	17.13	103.04	22.37
8.05	17.40	104.65	22.39
9.66	17.77	106.26	22.40
11.27	17.90	107.87	22.41
12.88	18.05	109.48	22.43
14.49	18.23	111.09	22.47
16.10	18.42	112.70	22.53
17.71	18.48	114.31	22.59
19.32	18.72	115.92	22.64
20.93	18.97	117.53	22.68
22.54	19.01	119.14	22.67
24.15	19.52	120.75	22.66
25.76	19.53	122.36	22.65
27.37	19.59	123.97	22.66
28.98	19.70	125.58	22.67
30.59	19.89	127.19	22.70
32.20	20.09	128.80	22.75
33.81	19.95	130.41	22.80
35.42	20.12	132.02	22.84
37.03	20.25	133.63	22.88
38.64	20.38	135.24	22.93
40.25	20.35	136.85	22.96
41.86	20.36	138.46	23.00
43.47	20.52	140.07	23.04
45.08	20.65	141.68	23.08
46.69	20.75	143.29	23.09
48.30	20.82	144.90	23.08
49.91	20.88	146.51	23.04
51.52	20.93	148.12	23.02
53.13	20.99	149.73	23.03
54.74	21.07	151.34	23.05
56.35	21.13	152.95	23.11
57.96	21.19	154.56	23.21
59.57	21.25	156.17	23.31
61.18	21.33	157.78	23.37
62.79	21.40	159.39	23.38
64.40	21.43	161.00	23.39
66.01	21.43	162.61	23.38
67.62	21.46	164.22	23.37
69.23	21.53	165.83	23.39
70.84	21.58	167.44	23.43
72.45	21.62	169.05	23.47
74.06	21.65	170.66	23.50
75.67	21.70	172.27	23.51
77.28	21.78	173.88	23.52
78.89	21.87	175.49	23.52
80.50	21.94	177.10	23.52
82.11	21.99	178.71	23.53
83.72	22.04	180.32	23.56
85.33	22.06	181.93	23.61
86.94	22.06	183.54	23.67
88.55	22.01	185.15	23.72
90.16	21.99	186.76	23.77
91.77	22.01	188.37	23.79
93.38	22.05	189.98	23.79
94.99	22.12	191.59	23.79
96.60	22.17	193.20	23.80
98.21	22.23	194.81	23.80
99.82	22.29	196.42	23.79
101.43	22.33	198.03	23.79

M4552 'R' MAJOR AXIS

SE WING

RADIUS arcsec	BRIGHTNESS Mag/#arcsec	RADIUS arcsec	BRIGHTNESS Mag/#arcsec
199.64	23.79	215.74	24.40
201.25	23.81	217.35	24.39
202.86	23.83	218.96	24.41
204.47	23.89	220.57	24.46
206.08	23.98	222.18	24.45
207.69	24.10	223.79	24.36
209.30	24.19	225.40	24.31
210.91	24.24	227.01	24.31
212.52	24.28	228.62	24.36
214.13	24.34	230.23	24.39

N4552 'R' MAJOR AXIS

NW WING

RADIUS arcsec	BRIGHTNESS Mag/#arcsec	RADIUS arcsec	BRIGHTNESS Mag/#arcsec
6.44	17.13	103.04	22.31
8.05	17.40	104.65	22.31
9.66	17.24	106.26	22.33
11.27	17.90	107.87	22.35
12.88	18.05	109.48	22.39
14.49	17.88	111.09	22.42
16.10	17.85	112.70	22.47
17.71	18.27	114.31	22.53
19.32	18.46	115.92	22.58
20.93	18.49	117.53	22.61
22.54	18.67	119.14	22.66
24.15	19.02	120.75	22.70
25.76	19.13	122.36	22.73
27.37	19.36	123.97	22.75
28.98	19.28	125.58	22.77
30.59	19.67	127.19	22.75
32.20	19.81	128.80	22.74
33.81	19.62	130.41	22.74
35.42	19.86	132.02	22.76
37.03	20.04	133.63	22.80
38.64	20.16	135.24	22.86
40.25	20.20	136.85	22.92
41.86	20.11	138.46	22.99
43.47	20.28	140.07	23.03
45.08	20.40	141.68	23.05
46.69	20.51	143.29	23.06
48.30	20.60	144.90	23.07
49.91	20.70	146.51	23.09
51.52	20.78	148.12	23.11
53.13	20.84	149.73	23.13
54.74	20.91	151.34	23.15
56.35	20.99	152.95	23.18
57.96	21.06	154.56	23.22
59.57	21.12	156.17	23.25
61.18	21.21	157.78	23.27
62.79	21.29	159.39	23.29
64.40	21.33	161.00	23.30
66.01	21.34	162.61	23.28
67.62	21.35	164.22	23.30
69.23	21.41	165.83	23.32
70.84	21.46	167.44	23.34
72.45	21.52	169.05	23.37
74.06	21.57	170.66	23.40
75.67	21.63	172.27	23.40
77.28	21.68	173.88	23.42
78.89	21.73	175.49	23.45
80.50	21.78	177.10	23.50
82.11	21.83	178.71	23.58
83.72	21.87	180.32	23.69
85.33	21.92	181.93	23.80
86.94	21.96	183.54	23.89
88.55	21.99	185.15	23.89
90.16	22.02	186.76	23.84
91.77	22.06	188.37	23.78
93.38	22.11	189.98	23.72
94.99	22.15	191.59	23.65
96.60	22.19	193.20	23.65
98.21	22.23	194.81	23.69
99.82	22.25	196.42	23.75
101.43	22.28	198.03	23.82

N4552 'R' MAJOR AXIS

NW WING

RADIUS arcsec	BRIGHTNESS Mag/#arcsec	RADIUS arcsec	BRIGHTNESS Mag/#arcsec
199.64	23.91	212.52	24.11
201.25	24.05	214.13	24.14
202.86	24.15	215.74	24.16
204.47	24.19	217.35	24.16
206.08	24.17	218.96	24.20
207.69	24.16	220.57	24.29
209.30	24.12	222.18	24.40
210.91	24.11	223.79	24.51

N4552 'R' MINOR AXIS

SW WING

RADIUS arcsec	BRIGHTNESS Mag/#arcsec	RADIUS arcsec	BRIGHTNESS Mag/#arcsec
6.44	17.13	103.04	22.59
8.05	17.40	104.65	22.61
9.66	17.55	106.26	22.63
11.27	17.90	107.87	22.64
12.88	18.05	109.48	22.65
14.49	18.07	111.09	22.67
16.10	18.36	112.70	22.70
17.71	18.77	114.31	22.76
19.32	19.01	115.92	22.83
20.93	19.05	117.53	22.89
22.54	19.12	119.14	22.90
24.15	19.67	120.75	22.92
25.76	19.72	122.36	22.92
27.37	19.84	123.97	22.94
28.98	19.87	125.58	22.98
30.59	19.97	127.19	23.05
32.20	20.21	128.80	23.11
33.81	20.22	130.41	23.15
35.42	20.24	132.02	23.18
37.03	20.37	133.63	23.21
38.64	20.46	135.24	23.23
40.25	20.52	136.85	23.25
41.86	20.61	138.46	23.31
43.47	20.71	140.07	23.35
45.08	20.78	141.68	23.37
46.69	20.85	143.29	23.37
48.30	20.93	144.90	23.36
49.91	21.02	146.51	23.33
51.52	21.10	148.12	23.33
53.13	21.18	149.73	23.35
54.74	21.24	151.34	23.41
56.35	21.30	152.95	23.48
57.96	21.38	154.56	23.53
59.57	21.46	156.17	23.56
61.18	21.51	157.78	23.56
62.79	21.51	159.39	23.55
64.40	21.50	161.00	23.54
66.01	21.53	162.61	23.55
67.62	21.62	164.22	23.58
69.23	21.73	165.83	23.63
70.84	21.81	167.44	23.67
72.45	21.85	169.05	23.70
74.06	21.90	170.66	23.73
75.67	21.95	172.27	23.77
77.28	21.97	173.88	23.84
78.89	21.98	175.49	23.95
80.50	22.02	177.10	24.08
82.11	22.09	178.71	24.20
83.72	22.14	180.32	24.28
85.33	22.19	181.93	24.31
86.94	22.22	183.54	24.34
88.55	22.25	185.15	24.34
90.16	22.28	186.76	24.31
91.77	22.30	188.37	24.27
93.38	22.33	189.98	24.22
94.99	22.37	191.59	24.13
96.60	22.40	193.20	24.05
98.21	22.45	194.81	24.05
99.82	22.50	196.42	24.11
101.43	22.55	198.03	24.28

N4552 'R' MINOR AXIS

NE WING

RADIUS arcsec	BRIGHTNESS Mag/#arcsec	RADIUS arcsec	BRIGHTNESS Mag/#arcsec
6.44	17.13	103.04	22.46
8.05	17.40	104.65	22.50
9.66	17.31	106.26	22.56
11.27	17.90	107.87	22.63
12.88	18.05	109.48	22.67
14.49	17.77	111.09	22.67
16.10	17.79	112.70	22.66
17.71	18.06	114.31	22.66
19.32	18.47	115.92	22.67
20.93	18.91	117.53	22.69
22.54	18.94	119.14	22.72
24.15	19.38	120.75	22.74
25.76	19.18	122.36	22.75
27.37	19.72	123.97	22.75
28.98	19.75	125.58	22.78
30.59	19.89	127.19	22.83
32.20	19.81	128.80	22.87
33.81	19.78	130.41	22.91
35.42	19.90	132.02	22.95
37.03	20.17	133.63	22.97
38.64	20.38	135.24	22.97
40.25	20.46	136.85	22.99
41.86	20.52	138.46	23.02
43.47	20.51	140.07	23.03
45.08	20.55	141.68	23.03
46.69	20.63	143.29	23.03
48.30	20.78	144.90	23.04
49.91	20.87	146.51	23.06
51.52	20.95	148.12	23.07
53.13	21.02	149.73	23.10
54.74	21.09	151.34	23.14
56.35	21.16	152.95	23.18
57.96	21.22	154.56	23.21
59.57	21.26	156.17	23.23
61.18	21.32	157.78	23.24
62.79	21.38	159.39	23.26
64.40	21.45	161.00	23.28
66.01	21.49	162.61	23.30
67.62	21.53	164.22	23.34
69.23	21.59	165.83	23.38
70.84	21.65	167.44	23.41
72.45	21.70	169.05	23.44
74.06	21.76	170.66	23.47
75.67	21.84	172.27	23.50
77.28	21.89	173.88	23.52
78.89	21.93	175.49	23.54
80.50	21.96	177.10	23.57
82.11	21.98	178.71	23.59
83.72	21.99	180.32	23.62
85.33	22.03	181.93	23.63
86.94	22.10	183.54	23.65
88.55	22.16	185.15	23.65
90.16	22.24	186.76	23.67
91.77	22.31	188.37	23.71
93.38	22.36	189.98	23.76
94.99	22.39	191.59	23.79
96.60	22.42	193.20	23.81
98.21	22.42	194.81	23.81
99.82	22.41	196.42	23.81
101.43	22.42	198.03	23.79

N4552 'R' MINOR AXIS

NE WING

RADIUS arcsec	BRIGHTNESS Mag/#arcsec	RADIUS arcsec	BRIGHTNESS Mag/#arcsec
199.64	23.81	210.91	23.96
201.25	23.84	212.52	23.99
202.86	23.85	214.13	24.02
204.47	23.85	215.74	24.01
206.08	23.88	217.35	24.08
207.69	23.93	218.96	24.20
209.30	23.95	220.57	24.39

N4267 'I' MAJOR AXIS

SW WING

RADIUS arcsec	BRIGHTNESS Mag/#arcsec	RADIUS arcsec	BRIGHTNESS Mag/#arcsec
6.44	17.06	49.91	21.52
8.05	17.74	51.52	21.56
9.66	18.32	53.13	21.61
11.27	18.66	54.74	21 66
12.88	19.09	56.35	21.72
14.49	19.07	57.96	21.79
16.10	19.52	59.57	21.87
17.71	19.66	61.18	21.91
19.32	19.90	62.79	21.96
20.93	20.11	64.40	22.01
22.54	20.21	66.01	22.07
24.15	20.35	67.62	22.12
25.76	20.47	69.23	22.15
27.37	20.63	70.84	22.10
28.98	20.74	72.45	22.01
30.59	20.86	74.06	21.91
32.20	20.95	75.67	21.91
33.81	21.02	77.28	22.02
35.42	21.05	78.89	22.26
37.03	21.09	80.50	22.55
38.64	21.12	82.11	22.85
40.25	21.17	83.72	23.05
41.86	21.23	85.33	23.19
43.47	21.29	86.94	23.34
45.08	21.35	88.55	23.45
46.69	21.40	90.16	23.59
48.30	21.46	91.77	23.76

N4267 'I' MAJOR AXIS

NE WING

RADIUS arcsec	BRIGHTNESS Mag/#arcsec	RADIUS arcsec	BRIGHTNESS Mag/#arcsec
6.44	17.06	57.96	21.94
8.05	17.26	59.57	22.05
9.66	18.14	61.18	22.14
11.27	18.52	62.79	22.20
12.88	18.90	64.40	22.25
14.49	19.07	66.01	22.31
16.10	19.28	67.62	22.37
17.71	19.53	69.23	22.41
19.32	19.75	70.84	22.44
20.93	19.95	72.45	22.45
22.54	20.11	74.06	22.47
24.15	20.24	75.67	22.53
25.76	20.35	77.28	22.61
27.37	20.45	78.89	22.69
28.98	20.55	80.50	22.79
30.59	20.66	82.11	22.88
32.20	20.78	83.72	22.92
33.81	20.87	85.33	22.98
35.42	20.95	86.94	23.10
37.03	21.02	88.55	23.24
38.64	21.10	90.16	23.37
40.25	21.18	91.77	23.46
41.86	21.24	93.38	23.47
43.47	21.28	94.99	23.40
45.08	21.32	96.60	23.30
46.69	21.35	98.21	23.18
48.30	21.42	99.82	23.15
49.91	21.49	101.43	23.14
51.52	21.54	103.04	23.15
53.13	21.63	104.65	23.19
54.74	21.73	106.26	23.30
56.35	21.83	107.87	23.47

N4267 'I' MINOR AXIS

SE WING

RADIUS arcsec	BRIGHTNESS Mag/#arcsec	RADIUS arcsec	BRIGHTNESS Mag/#arcsec
6.44	17.06	70.84	22.08
8.05	16.98	72.45	22.12
9.66	18.56	74.06	22.16
11.27	18.93	75.67	22.21
12.88	19.34	77.28	22.27
14 49	19.07	78.89	22.35
16.10	19.72	80.50	22.46
17.71	20.04	82.11	22 57
19.32	20.18	83.72	22.67
20.93	20.27	85.33	22.79
22.54	20.42	86.94	22.94
24.15	20.51	88.55	23.14
25.76	20.60	90.16	23.34
27.37	20.68	91.77	23.49
28.98	20.74	93.38	23.54
30.59	20.76	94.99	23.50
32.20	20.76	96.60	23.37
33.81	20.77	98.21	23.21
35.42	20.85	99.82	23.11
37.03	20.97	101.43	23.09
38.64	21.03	103.04	23.18
40.25	21.05	104.65	23.30
41.86	21.05	106.26	23.36
43.47	21 07	107.87	23.42
45.08	21.13	109.48	23.46
46.69	21.19	111.09	23.42
48.30	21.24	112.70	23.44
49.91	21.27	114.31	23.50
51.52	21.26	115.92	23.54
53.13	21.28	117.53	23.56
54.74	21.35	119.14	23.62
56.35	21.48	120.75	23.62
57.96	21.59	122.36	23.65
59.57	21.69	123.97	23.72
61.18	21.79	125.58	23.77
62.79	21.86	127.19	23.77
64.40	21.91	128.80	23.80
66.01	21.95	130.41	23.82
67.62	21.99	132.02	23.82
69.23	22.05	133.63	23.84

N4267 'I' MINOR AXIS

NW WING

RADIUS arcsec	BRIGHTNESS Mag/#arcsec	RADIUS arcsec	BRIGHTNESS Mag/#arcsec
6.44	17.06	53.13	21.54
8.05	17.68	54.74	21.60
9.66	18.50	56.35	21.68
11.27	18.88	57.96	21.74
12.88	19.35	59.57	21.81
14.49	19.07	61.18	21.86
16.10	19.68	62.79	21.89
17.71	20.05	64.40	21.91
19.32	20.17	66.01	21.93
20.93	20.28	67.62	21 96
22.54	20.40	69.23	22.01
24.15	20.52	70.84	22.08
25.76	20.59	72.45	22.15
27.37	20.68	74.06	22.24
28.98	20.74	75.67	22.30
30.59	20.78	77.28	22.36
32.20	20.82	78.89	22.42
33.81	20.87	80.50	22.49
35.42	20.94	82.11	22.55
37.03	20.96	83.72	22.67
38.64	20.99	85.33	22.79
40.25	21.05	86.94	22.89
41.86	21.14	88.55	22.99
43.47	21.22	90.16	23.17
45.08	21.28	91.77	23.33
46.69	21.35	93.38	23.50
48.30	21.40	94.99	23.66
49.91	21.46	96.60	23.89
51.52	21.50	98.21	24.06

N4371 'I' LENS AXIS

W WING

RADIUS arcsec	BRIGHTNESS Mag/#arcsec	RADIUS arcsec	BRIGHTNESS Mag/#arcsec
6.44	15.94	91.77	22.03
8.05	16.22	93.38	22.05
9.66	16.60	94.99	22.08
11.27	17.19	96.60	22.14
12.88	18.11	98.21	22.22
14.49	18.34	99.82	22.29
16.10	18.56	101.43	22.35
17.71	18.72	103.04	22.39
19.32	18.96	104.65	22.39
20.93	19.28	106.26	22.38
22.54	19.40	107.87	22.37
24.15	19.65	109.48	22.36
25.76	19.89	111.09	22.37
27.37	20.07	112.70	22.41
28.98	20.19	114.31	22.45
30.59	20.33	115.92	22.48
32.20	20.50	117.53	22.52
33.81	20.66	119.14	22.57
35.42	20.76	120.75	22.62
37.03	20.83	122.36	22.69
38.64	20.90	123.97	22.76
40.25	20.95	125.58	22.83
41.86	20.97	127.19	22.89
43.47	20.97	128.80	22.94
45.08	20.98	130.41	22.97
46.69	21.03	132.02	22.99
48.30	21.09	133.63	23.02
49.91	21.14	135.24	23.07
51.52	21.16	136.85	23.13
53.13	21.19	138.46	23.21
54.74	21.23	140.07	23.30
56.35	21.26	141.68	23.38
57.96	21.30	143.29	23.43
59.57	21.34	144.90	23.46
61.18	21.35	146.51	23.46
62.79	21.36	148.12	23.45
64.40	21.38	149.73	23.43
66.01	21.42	151.34	23.41
67.62	21.50	152.95	23.40
69.23	21.56	154.56	23.40
70.84	21.61	156.17	23.40
72.45	21.67	157.78	23.41
74.06	21.71	159.39	23.42
75.67	21.74	161.00	23.44
77.28	21.76	162.61	23.46
78.89	21.78	164.22	23.49
80.50	21.81	165.83	23.52
82.11	21.85	167.44	23.56
83.72	21.91	169.05	23.60
85.33	21.96	170.66	23.64
86.94	22.01	172.27	23.72
88.55	22.03	173.88	23.86
90.16	22.03		

N4371 'I' LENS AXIS

E WING

RADIUS arcsec	BRIGHTNESS Mag/#arcsec	RADIUS arcsec	BRIGHTNESS Mag/#arcsec
6.44	15.94	99.82	22.07
8.05	16.22	101.43	22.09
9.66	16.60	103.04	22.08
11.27	17.19	104.65	22.07
12.88	17.81	106.26	22.07
14.49	17.99	107.87	22.10
16.10	18.13	109.48	22.13
17.71	18.33	111.09	22.18
19.32	18.73	112.70	22.22
20.93	19.07	114.31	22.22
22.54	19.19	115.92	22.20
24.15	19.54	117.53	22.19
25.76	19.72	119.14	22.19
27.37	19.90	120.75	22.19
28.98	20.07	122.36	22.23
30.59	20.25	123.97	22.27
32.20	20.40	125.58	22.29
33.81	20.51	127.19	22.30
35.42	20.60	128.80	22.33
37.03	20.68	130.41	22.37
38.64	20.77	132.02	22 39
40.25	20.83	133.63	22 41
41.86	20.88	135.24	22.46
43.47	20.93	136.85	22.49
45.08	20.97	138.46	22.53
46.69	21.00	140.07	22.59
48.30	21.03	141.68	22.68
49.91	21.05	143.29	22.78
51.52	21.06	144.90	22.85
53.13	21.06	146.51	22.90
54.74	21.09	148.12	22.92
56.35	21.13	149.73	22.93
57.96	21.18	151.34	22.93
59.57	21.21	152.95	22.93
61.18	21.22	154.56	22.96
62.79	21.21	156.17	23.04
64.40	21.21	157.78	23.10
66.01	21.23	159.39	23.13
67.62	21.28	161.00	23.13
69.23	21.38	162.61	23.12
70.84	21.46	164.22	23.09
72.45	21.51	165.83	23.08
74.06	21.56	167.44	23.13
75.67	21.58	169.05	23.23
77.28	21.59	170.66	23.32
78.89	21.61	172.27	23.40
80.50	21.66	173.88	23.50
82.11	21.71	175.49	23.60
83.72	21.75	177.10	23.65
85.33	21.80	178.71	23.66
86.94	21.86	180.32	23.66
88.55	21.90	181.93	23.66
90.16	21.91	183.54	23.61
91.77	21.92	185.15	23.58
93.38	21.94	186.76	23.59
94.99	21.95	188.37	23.64
96.60	21.97	189.98	23.73
98.21	22.02	191.59	23.86

N4371 'I' BAR AXIS

S WING

RADIUS arcsec	BRIGHTNESS Mag/#arcsec	RADIUS arcsec	BRIGHTNESS Mag/#arcsec
6.44	16.93	45.08	21.35
8.05	17.96	46.69	21.58
9.66	18.28	48.30	21.77
11.27	18.62	49.91	21.93
12.88	18.83	51.52	22.04
14.49	19.02	53.13	22.11
16.10	19.31	54.74	22.19
17.71	19.18	56.35	22.31
19.32	19.39	57.96	22.47
20.93	19.56	59.57	22.65
22.54	19.50	61.18	22.81
24.15	19.53	62.79	22.97
25.76	19.59	64.40	23.13
27.37	19.67	66.01	23.19
28.98	19.68	67.62	23.20
30.59	19.64	69.23	23.23
32.20	19.84	70.84	23.28
33.81	19.96	72.45	23.34
35.42	20.01	74.06	23.44
37.03	20.17	75.67	23.60
38.64	20.38	77.28	23.73
40.25	20.69	78.89	23.82
41.86	20.94	80.50	23.91
43.47	21.16		

N4371 'I' BAR AXIS

N WING

RADIUS arcsec	BRIGHTNESS Mag/#arcsec	RADIUS arcsec	BRIGHTNESS Mag/#arcsec
6.44	16.93	48.30	21.52
8.05	17.49	49.91	21.69
9.66	17.89	51.52	21.87
11.27	18.24	53.13	22.04
12.88	18.50	54.74	22.18
14.49	18.72	56.35	22.35
16.10	18.93	57.96	22.51
17.71	19.10	59.57	22.63
19.32	19.52	61.18	22.73
20.93	19.32	62.79	22.80
22.54	19.44	64.40	22 83
24.15	19.50	66.01	22.83
25.76	19.49	67.62	22.84
27.37	19.61	69.23	22.84
28.98	19.64	70.84	22.86
30.59	19.75	72.45	22 93
32.20	19.86	74.06	23.04
33.81	19.98	75.67	23.16
35.42	20.13	77.28	23.24
37.03	20.31	78.89	23.32
38.64	20.48	80.50	23.33
40.25	20.65	82.11	23.29
41.86	20.82	83.72	23.28
43.47	21.00	85.33	23.40
45.08	21.18	86.94	23.57
46.69	21.34	88.55	23.69

N4377 'I' MAJOR AXIS

S WING

RADIUS arcsec	BRIGHTNESS Mag/#arcsec	RADIUS arcsec	BRIGHTNESS Mag/#arcsec
6.44	17.51	33.81	21.56
8.05	18.37	35.42	21.71
9.66	18.64	37.03	21.86
11.27	18.90	38.64	22.06
12.88	19.36	40.25	22.25
14.49	19.47	41.86	22.42
16.10	19.68	43.47	22.62
17.71	19.86	45.08	22.81
19.32	20.03	46.69	22.98
20.93	20.19	48.30	23.13
22.54	20.35	49.91	23.28
24.15	20.51	51.52	23.41
25.76	20.68	53.13	23 51
27.37	20.87	54.74	23.61
28.98	21.07	56.35	23.81
30.59	21.26	57.96	24.03
32.20	21.40		

N4377 'I' MAJOR AXIS

N WING

RADIUS arcsec	BRIGHTNESS Mag/#arcsec	RADIUS arcsec	BRIGHTNESS Mag/#arcsec
6.44	17.42	28.98	20.97
8.05	17.91	30.59	21.13
9.66	18.38	32.20	21.33
11.27	18.82	33.81	21.55
12.88	19.30	35.42	21.75
14.49	19.49	37.03	21.94
16.10	19.71	38.64	22.11
17.71	19.91	40.25	22.27
19.32	20.06	41.86	22.43
20.93	20.18	43.47	22.62
22.54	20.29	45.08	22.83
24.15	20.43	46.69	23.04
25.76	20.62	48.30	23.25
27.37	20.81	49.91	23.55

N4377 'I' MINOR AXIS

W WING

RADIUS arcsec	BRIGHTNESS Mag/#arcsec	RADIUS arcsec	BRIGHTNESS Mag/#arcsec
6.44	17.79	22.54	20.69
8.05	18.37	24.15	21.06
9.66	18.79	25.76	21.42
11.27	19.31	27.37	21.64
12.88	19.55	28.98	21.81
14.49	19.75	30.59	21.94
16.10	19.95	32.20	22.13
17.71	20.09	33.81	22.40
19.32	20.19	35.42	22.81
20.93	20.37	37.03	23.18

N4377 'I' MINOR AXIS

E WING

RADIUS arcsec	BRIGHTNESS Mag/#arcsec	RADIUS arcsec	BRIGHTNESS Mag/#arcsec
6.44	17.75	25.76	21.13
8.05	18.23	27.37	21.38
9.66	18.86	28.98	21.58
11.27	19.05	30.59	21.78
12.88	19.49	32.20	21.99
14.49	19.64	33.81	22.20
16.10	19.80	35.42	22.42
17.71	19.96	37.03	22.67
19.32	20.14	38.64	22.92
20.93	20.35	40.25	23.16
22.54	20.58	41.86	23.50
24.15	20.85		

N4419 'I' MAJOR AXIS

SE WING

RADIUS arcsec	BRIGHTNESS Mag/#arcsec	RADIUS arcsec	BRIGHTNESS Mag/#arcsec
6.44	16.96	61.18	20.99
8.05	17.20	62.79	21.09
9.66	17.21	64.40	21.19
11.27	17.89	66.01	21.34
12.88	18.17	67.62	21.50
14.49	18.47	69.23	21.63
16.10	18.71	70.84	21.77
17.71	18.86	72.45	21.86
19.32	18.84	74.06	21.95
20.93	18.87	75.67	22.04
22.54	19.10	77.28	22.14
24.15	19.24	78.89	22.24
25.76	19.38	80.50	22.34
27.37	19.24	82.11	22.44
28.98	19.28	83.72	22.51
30.59	19.36	85.33	22.57
32.20	19.41	86.94	22.63
33.81	19.57	88.55	22.70
35.42	19.46	90.16	22.80
37.03	19.49	91.77	22.93
38.64	19.63	93.38	23.02
40.25	19.73	94.99	23.06
41.86	19.82	96.60	23.07
43.47	19.91	98.21	23.05
45.08	20.00	99.82	23.04
46.69	20.06	101.43	23.08
48.30	20.14	103.04	23.15
49.91	20.20	104.65	23.19
51.52	20.27	106.26	23.28
53.13	20.36	107.87	23.35
54.74	20.46	109.48	23.43
56.35	20.58	111.09	23.52
57.96	20.73	112.70	23.70
59.57	20.87	114.31	23.80

N4419 'I' MINOR AXIS

NW WING

RADIUS arcsec	BRIGHTNESS Mag/#arcsec	RADIUS arcsec	BRIGHTNESS Mag/#arcsec
6.44	16.52	61.18	20.70
8.05	17.03	62.79	20.81
9.66	17.21	64.40	20.91
11.27	17.42	66.01	21.01
12.88	17.72	67.62	21.10
14.49	18.01	69.23	21.21
16.10	18.45	70.84	21.33
17.71	18.33	72.45	21.43
19.32	18.73	74.06	21.53
20.93	18.82	75.67	21.63
22.54	18.96	77.28	21.71
24.15	19.19	78.89	21.80
25.76	19.13	80.50	21.89
27.37	19.11	82.11	22.00
28.98	19.17	83.72	22.13
30.59	19.30	85.33	22.29
32.20	19.41	86.94	22.43
33.81	19.42	88.55	22.57
35.42	19.50	90.16	22.70
37.03	19.48	91.77	22.81
38.64	19.58	93.38	22.91
40.25	19.56	94.99	23.02
41.86	19.67	96.60	23.13
43.47	19.75	98.21	23.23
45.08	19.85	99.82	23.30
46.69	19.93	101.43	23.36
48.30	19.99	103.04	23.39
49.91	20.05	104.65	23.40
51.52	20.12	106.26	23.44
53.13	20.20	107.87	23.48
54.74	20.26	109.48	23.53
56.35	20.35	111.09	23.60
57.96	20.47	112.70	23.71
59.57	20.59	114.31	23.70

N4419 'I' MINOR AXIS

SW WING

RADIUS arcsec	BRIGHTNESS Mag/#arcsec	RADIUS arcsec	BRIGHTNESS Mag/#arcsec
6.44	17.88	22.54	21.43
8.05	18.79	24.15	21.67
11.27	19.46	25.76	21.88
12.88	19.81	27.37	22.11
14.49	20.14	28.98	22.30
16.10	20.40	30.59	22.48
17.71	20.68	32.20	22.86
19.32	20.94	33.81	23.26
20.93	21.17		

N4419 'I' MINOR AXIS

NE AXIS

RADIUS arcsec	BRIGHTNESS Mag/#arcsec	RADIUS arcsec	BRIGHTNESS Mag/#arcsec
6.44	17.37	24.15	21.14
8.05	18.27	25.76	21.39
11.27	18.86	27.37	21.74
12.88	19.51	28.98	22.02
14.49	19.67	30.59	22.29
16 10	19.85	32.20	22.54
17.71	20.07	33 81	22.77
19.32	20.33	35.42	23.00
20.93	20.62	37.03	23.24
22.54	20.89	38.64	23.58

N4425 'I' MAJOR AXIS

SW WING

RADIUS arcsec	BRIGHTNESS Mag/#arcsec	RADIUS arcsec	BRIGHTNESS Mag/#arcsec
6.44	17.95	46.69	20.85
8.05	18.25	48.30	20.93
9.66	18.41	49.91	21.06
11.27	18.60	51.52	21.20
12.88	18.83	53.13	21.31
14.49	18.98	54.74	21.39
16.10	19.08	56.35	21.48
17.71	19.29	57.96	21.56
19.32	19.46	59.57	21.65
20.93	19.25	61.18	21.74
22.54	19.35	62.79	21.83
24.15	19.55	64.40	21.94
25.76	19.43	66.01	22.05
27.37	19.43	67.62	22.14
28.98	19.50	69.23	22.23
30.59	19.62	70.84	22.30
32.20	19.67	72.45	22.36
33.81	19.84	74.06	22.44
35.42	20.02	75.67	22.53
37.03	20.18	77.28	22.61
38.64	20.31	78.89	22.72
40.25	20.43	80.50	22.88
41.86	20.56	82.11	23.15
43.47	20.69	83.72	23.44
45.08	20.79		

N4425 'I' M JCR AXIS

NE WING

RADIUS arcsec	BRIGHTNESS Mag/#arcsec	RADIUS arcsec	BRIGHTNESS Mag/#arcsec
6.44	17.95	46.69	20.79
8.05	18.18	48.30	20.87
9.66	18.41	49.91	21.00
11.27	18.60	51.52	21.13
12.88	18.78	53.13	21.25
14.49	19.08	54.74	21.33
16.10	19.34	56.35	21.41
17.71	19.31	57.96	21.51
19.32	19.53	59.57	21.61
20.93	19.59	61.18	21.71
22.54	19.56	62.79	21.81
24.15	19.66	64.40	21.92
25.76	19.59	66.01	22.04
27.37	19.61	67.62	22.16
28.98	19.58	69.23	22.30
30.59	19.67	70.84	22.43
32.20	19.78	72.45	22.55
33.81	19.87	74.06	22.69
35.42	19.99	75.67	22.86
37.03	20.07	77.28	22.99
38.64	20.20	78.89	23.11
40.25	20.31	80.50	23.19
41.86	20.45	82.11	23.27
43.47	20.58	83.72	23.34
45.08	20.71	85.33	23.52

N4425 'I' MINOR AXIS

SE WING

RADIUS arcsec	BRIGHTNESS Mag/#arcsec	RADIUS arcsec	BRIGHTNESS Mag/#arcsec
9.66	18.41	24.15	22.54
11.27	18.60	25.76	22.81
12.88	20.00	27.37	23.04
14.49	20.82	28.98	23.27
16.10	21.08	30.59	23.43
17.71	21.37	32.20	23.57
19.32	21.75	33.81	23.70
20.93	22.01	35.42	23.90
22.54	22.29		

N4425 'I' MINOR AXIS

NW WING

RADIUS arcsec	BRIGHTNESS Mag/#arcsec	RADIUS arcsec	BRIGHTNESS Mag/#arcsec
9.66	18.41	32.20	22.47
11.27	18.60	33.81	22.60
12.88	19.54	35.42	22.70
14.49	20.25	37.03	22.81
16.10	20.70	38.64	22 98
17.71	21.06	40.25	23.22
19.32	21.35	41.86	23.38
20.93	21.55	43.47	23.46
22.54	21.74	45.08	23.53
24.15	21.91	46.69	23.58
25.76	22.03	48.30	23.56
27.37	22.16	49.91	23.62
28.98	22.27	51.52	23.78
30.59	22.37		

N4429 'I' MAJOR AXIS

W WING

RADIUS arcsec	BRIGHTNESS Mag/#arcsec	RADIUS arcsec	BRIGHTNESS Mag/#arcsec
6.44	15.89	103.04	21.37
8.05	16.22	104.65	21.44
9.66	16.71	106.26	21.49
11.27	17.87	107.87	21.53
12.88	17.91	109.48	21.55
14.49	18.08	111.09	21.57
16.10	18.16	112.70	21.60
17.71	18.27	114.31	21.63
19.32	18.43	115.92	21.66
20.93	18.63	117.53	21.70
22.54	18.67	119.14	21.74
24 15	18.75	120.75	21.78
25.76	19.02	122.36	21.84
27.37	19.06	123.97	21.90
28.98	19.13	125.58	21.95
30.59	19.38	127.19	22.00
32.20	19.37	128.80	22.03
33.81	19.48	130.41	22.06
35.42	19.51	132.02	22.09
37.03	19.57	133.63	22.11
38.64	19.71	135.24	22.14
40.25	19.77	136.85	22.18
41.86	19.82	138.46	22.22
43.47	19.87	140.07	22.25
45.08	19.92	141.68	22.27
46.69	19.96	143.29	22.29
48.30	19.99	144.90	22.30
49.91	20.02	146.51	22.31
51.52	20.05	148.12	22.34
53.13	20.07	149.73	22.39
54.74	20.07	151.34	22.43
56.35	20.05	152.95	22.48
57.96	20.06	154.56	22.55
59.57	20.10	156.17	22.62
61.18	20.12	157.78	22.69
62.79	20.13	159.39	22.77
64.40	20.11	161.00	22.83
66.01	20.09	162.61	22.89
67.62	20.08	164.22	22.93
69.23	20.07	165.83	22.95
70.84	20.06	167.44	22.95
72.45	20.05	169.05	22.95
74.06	20.04	170.66	22.95
75.67	20.05	172.27	22.99
77.28	20.07	173.88	23.05
78.89	20.10	175.49	23.13
80.50	20.15	177.10	23.23
82.11	20.21	178.71	23.31
83.72	20.27	180.32	23.37
85.33	20.33	181.93	23.44
86.94	20.41	183.54	23.51
88.55	20.52	185.15	23.57
90.16	20.65	186.76	23.59
91.77	20.79	188.37	23.56
93.38	20.92	189.98	23.51
94.99	21.01	191.59	23.47
96.60	21.07	193.20	23.49
98.21	21.13	194.81	23.56
99.82	21.20	196.42	23.64
101.43	21.28	198.03	23.71

N4429 'I' MAJOR AXIS

W "ING

RADIUS arcsec	BRIGHTNESS Mag/#arcsec	RADIUS arcsec	BRIGHTNESS Mag/#arcsec
199.64	23.75	210.91	23.71
201.25	23.74	212.52	23.73
202.86	23.72	214.13	23.78
204.47	23.75	215.74	23.85
206.08	23.75	217.35	23.95
207.69	23.72	218.96	24.02
209.30	23.71	220.57	24.03

N4429 'I' MAJOR AXIS

E WING

RADIUS arcsec	BRIGHTNESS Mag/#arcsec	RADIUS arcsec	BRIGHTNESS Mag/#arcsec
6.44	15.89	103.04	21.03
8.05	16.22	104.65	21.09
9.66	16.71	106.26	21.16
11.27	17.60	107.87	21.22
12.88	17.81	109.48	21.24
14.49	17.87	111.09	21.23
16.10	17.98	112.70	21.24
17.71	18.09	114.31	21.30
19.32	18.19	115.92	21.41
20.93	18.28	117.53	21.51
22.54	18.51	119.14	21.58
24.15	18.63	120.75	21.63
25.76	18.71	122.36	21.66
27.37	18.84	123.97	21.70
28.98	18.90	125.58	21.75
30.59	19.15	127.19	21.78
32.20	19.26	128.80	21.80
33.81	19.30	130.41	21.82
35.42	19.46	132.02	21.85
37.03	19.52	133.63	21.88
38.64	19.58	135.24	21.93
40.25	19.60	136.85	22.00
41.86	19.74	138.46	22.06
43.47	19.78	140.07	22.09
45.08	19.84	141.68	22.10
46.69	19.92	143.29	22.11
48.30	19.98	144.90	22.12
49.91	20.02	146.51	22.14
51.52	20.04	148.12	22.20
53.13	20.04	149.73	22.25
54.74	20.04	151.34	22.29
56.35	20.04	152.95	22.31
57.96	20.04	154.56	22.32
59.57	20.06	156.17	22.32
61.18	20.08	157.78	22.35
62.79	20.10	159.39	22.41
64.40	20.10	161.00	22.47
66.01	20.11	162.61	22.52
67.62	20.10	164.22	22.55
69.23	20.08	165.83	22.54
70.84	20.06	167.44	22.51
72.45	20.06	169.05	22.49
74.06	20.06	170.66	22.48
75.67	20.06	172.27	22.51
77.28	20.05	173.88	22.56
78.89	20.05	175.49	22.61
80.50	20.07	177.10	22.65
82.11	20.11	178.71	22.65
83.72	20.16	180.32	22.65
85.33	20.20	181.93	22.65
86.94	20.24	183.54	22.65
88.55	20.31	185.15	22.65
90.16	20.39	186.76	22.67
91.77	20.48	188.37	22.69
93.38	20.58	189.98	22.72
94.99	20.66	191.59	22.78
96.60	20.73	193.20	22.85
98.21	20.79	194.81	22.94
99.82	20.88	196.42	23.02
101.43	20.97	198.03	23.08

N4429 'I' MAJOR AXIS

E WING

RADIUS arcsec	BRIGHTNESS Mag/#arcsec	RADIUS arcsec	BRIGHTNESS Mag/#arcsec
199.64	23.12	230.23	23.62
201.25	23.14	231.84	23.56
202.86	23.15	233.45	23.53
204.47	23.15	235.06	23.58
206.08	23.14	236.67	23.66
207.69	23.13	238.28	23.70
209.30	23.14	239.89	23.72
210.91	23.19	241.50	23.76
212.52	23.28	243.11	23.79
214.13	23.41	244.72	23.80
215.74	23.53	246.33	23.81
217.35	23.62	247.94	23.80
218.96	23.70	249.55	23.80
220.57	23.73	251.16	23.79
222.18	23.73	252.77	23.81
223.79	23.78	254.38	23.89
225.40	23.81	255.99	23.99
227.01	23.76	257.60	24.07
228.62	23.68		

N4429 'I' MINOR AXIS

S WING

RADIUS arcsec	BRIGHTNESS Mag/#arcsec	RADIUS arcsec	BRIGHTNESS Mag/#arcsec
6.44	15.89	61.18	21.97
8.05	16.22	62.79	22.07
9.66	16.71	64.40	22.17
11.27	18.02	66.01	22.25
12.88	18.18	67.62	22.35
14.49	18.56	69.23	22.48
16.10	18.73	70.84	22.62
17.71	18.93	72.45	22.72
19.32	19.16	74.06	22.81
20.93	19.46	75.67	22.86
22.54	19.56	77.28	22.87
24.15	19.69	78.89	22.87
25.76	19.86	80.50	22.90
27.37	20.03	82.11	22.96
28.98	20.18	83.72	23.05
30.59	20.30	85.33	23.14
32.20	20.42	86.94	23.21
33.81	20.54	88.55	23.25
35.42	20.66	90.16	23.28
37.03	20.78	91.77	23.30
38.64	20.90	93.38	23.28
40.25	21.02	94.99	23.26
41.86	21.14	96.60	23.24
43.47	21.27	98.21	23.22
45.08	21.36	99.82	23.25
46.69	21.40	101.43	23.35
48.30	21.43	103.04	23.48
49.91	21.47	104.65	23.66
51.52	21.53	106.26	23.83
53.13	21.59	107.87	23.93
54.74	21.66	109.48	23.95
56.35	21.74	111.09	24.09
57.96	21.82	112.70	24.28
59.57	21.90		

N4429 'I' MINOR AXIS

N WING

RADIUS arcsec	BRIGHTNESS Mag/#arcsec	RADIUS arcsec	BRIGHTNESS Mag/#arcsec
6.44	15.89	62.79	22.34
8.05	16.22	64.40	22.38
9.66	16.71	66.01	22.40
11.27	18.45	67.62	22.42
12.88	18.66	69.23	22.46
14.49	18.89	70.84	22.54
16.10	19.09	72.45	22.62
17.71	19.25	74.06	22.70
19.32	19.51	75.67	22.77
20.93	19.63	77.28	22.81
22.54	19.77	78.89	22.81
24.15	19.94	80.50	22.80
25.76	20.10	82.11	22.80
27.37	20.27	83.72	22.82
28.98	20.43	85.33	22.89
30.59	20.55	86.94	22.99
32.20	20.65	88.55	23.08
33.81	20.78	90.16	23.18
35.42	20.93	91.77	23.28
37.03	21.09	93.38	23.34
38.64	21.23	94.99	23.35
40.25	21.34	96.60	23.35
41.86	21.39	98.21	23.35
43.47	21.43	99.82	23.31
45.08	21.51	101.43	23.29
46.69	21.61	103.04	23.34
48.30	21.69	104.65	23.42
49.91	21.78	106.26	23.52
51.52	21.84	107.87	23.68
53.13	21.91	109.48	23.82
54.74	21.99	111.09	23.89
56.35	22.07	112.70	23.97
57.96	22.16	114.31	24.08
59.57	22.24	115.92	24.12
61.18	22.29		

N4435 'I' MAJOR AXIS

SW WING

RADIUS arcsec	BRIGHTNESS Mag/#arcsec	RADIUS arcsec	BRIGHTNESS Mag/#arcsec
6.44	16.46	91.77	22.49
8.05	16.49	93.38	22.45
9.66	17.26	94.99	22.46
11.27	17.51	96.60	22.52
12.88	17.69	98.21	22.59
14.49	17.85	99.82	22.66
16.10	17.93	101.43	22.77
17.71	18.14	103.04	22.91
19.32	18.34	104.65	23.01
20.93	18.41	106.26	23.03
22.54	18.72	107.87	23.00
24.15	18.77	109.48	22.98
25.76	18.98	111.09	22.96
27.37	19.03	112.70	22.95
28.98	19.23	114.31	22.96
30.59	19.50	115.92	22.98
32.20	19.63	117.53	22.99
33.81	19.73	119.14	22.98
35.42	19.85	120.75	22.95
37.03	19.96	122.36	22.94
38.64	20.12	123.97	22.92
40.25	20.28	125.58	22.88
41.86	20.42	127.19	22.87
43.47	20.56	128.80	22.88
45.08	20.72	130.41	22.86
46.69	20.85	132.02	22.88
48.30	20.96	133.63	22.94
49.91	21.07	135.24	22.99
51.52	21.21	136.85	22.99
53.13	21.32	138.46	23.00
54.74	21.40	140.07	22.97
56.35	21.45	141.68	22.92
57.96	21.47	143.29	22.85
59.57	21.49	144.90	22.81
61.18	21.52	146.51	22.79
62.79	21.59	148.12	22.78
64.40	21.68	149.73	22.81
66.01	21.79	151.34	22.89
67.62	21.87	152.95	23.00
69.23	21.92	154.56	23.12
70.84	21.96	156.17	23.22
72.45	22.00	157.78	23.29
74.06	22.05	159.39	23.32
75.67	22.10	161.00	23.33
77.28	22.18	162.61	23.30
78 89	22.26	164.22	23.27
80.50	22.35	165.83	23.26
82.11	22.45	167.44	23.28
83.72	22.55	169.05	23.33
85.33	22.60	170.66	23.39
86.94	22.60	172.27	23.40
88.55	22.55	173.88	23.38
90.16	22.51		

N4435 'I' MAJOR AXIS

NE WING

RADIUS arcsec	BRIGHTNESS Mag/#arcsec	RADIUS arcsec	BRIGHTNESS Mag/#arcsec
6.44	16.46	67.62	21.96
8.05	16.94	69.23	22.03
9.66	17.31	70.84	22.08
11.27	17.51	72.45	22.14
12.88	17.69	74.06	22.20
14.49	17.92	75.67	22.26
16.10	17.94	77.28	22.32
17.71	18.11	78.89	22.37
19.32	18.22	80.50	22.42
20.93	18.40	82.11	22.47
22.54	18.69	83.72	22.53
24.15	18.90	85.33	22.62
25.76	18.81	86.94	22.75
27.37	19.16	88.55	22.84
28.98	19.28	90.16	22.86
30.59	19.39	91.77	22.88
32.20	19.61	93.38	22.89
33.81	19.69	94.99	22.90
35.42	19.80	96.60	22.92
37.03	19.94	98.21	22.96
38.64	20.17	99.82	23.02
40.25	20.36	101.43	23.07
41.86	20.54	103.04	23.12
43.47	20.70	104.65	23.15
45.08	20.82	106.26	23.21
46.69	20.91	107.87	23.24
48.30	21.01	109.48	23.28
49.91	21.12	111.09	23.32
51.52	21.20	112.70	23.37
53.13	21.26	114.31	23.41
54.74	21.33	115.92	23.47
56.35	21.38	117.53	23.51
57.96	21.42	119.14	23.54
59.57	21.48	120.75	23.52
61.18	21.55	122.36	23.50
62 79	21.64	123.97	23.51
64.40	21.76	125.58	23.54
66.01	21.88	127.19	23.68

N4435 'I' MINOR AXIS

SE WING

RADIUS arcsec	BRIGHTNESS Mag/#arcsec	RADIUS arcsec	BRIGHTNESS Mag/#arcsec
6.44	16.46	104.65	22.91
8.05	17.48	106.26	22.92
9.66	17.99	107.87	22.91
11.27	18.32	109.48	22.89
14.49	18.87	111.09	22.88
16.10	19.26	112.70	22.88
17.71	19.51	114.31	22.88
19.32	19.75	115.92	22.88
20.93	19.93	117.53	22.88
22.54	20.16	119.14	22.86
24.15	20.33	120.75	22.81
25.76	20.45	122.36	22.78
27.37	20.53	123.97	22.74
28.98	20.61	125.58	22.67
30.59	20.73	127.19	22.60
32.20	20.89	128.80	22.58
33.81	21.02	130.41	22.59
35.42	21.10	132.02	22.62
37.03	21.15	133.63	22.67
38.64	21.23	135.24	22.69
40.25	21.37	136.85	22.70
41.86	21.49	138.46	22.69
43.47	21.63	140.07	22.66
45.08	21.76	141.68	22.61
46.69	21.86	143.29	22.59
48.30	21.93	144.90	22.58
49.91	21.96	146.51	22.58
51.52	21.99	148.12	22.56
53.13	22.02	149.73	22.59
54.74	22.07	151.34	22.58
56.35	22.14	152.95	22.51
57.96	22.24	154.56	22.42
59.57	22.30	156.17	22.35
61.18	22.36	157.78	22.29
62.79	22.41	159.39	22.22
64.40	22.51	161.00	22.17
66.01	22.60	162.61	22.15
67.62	22.65	164.22	22.11
69.23	22.68	165.83	22.08
70.84	22.75	167.44	22.07
72.45	22.80	169.05	22.11
74.06	22.88	170.66	22.16
75.67	23.01	172.27	22.22
77.28	23.13	173.88	22.29
78.89	23.20	175.49	22.39
80.50	23.18	177.10	22.49
82.11	23.18	178.71	22.58
83.72	23.19	180.32	22.62
85.33	23.17	181.93	22.64
86.94	23.12	183.54	22.63
88.55	23.15	185.15	22.60
90.16	23.19	186.76	22.63
91.77	23.17	188.37	22.73
93.38	23.13	189.98	22.87
94.99	23.10	191.59	22.96
96.60	23.01	193.20	23.02
98.21	22.90	194.81	23.07
99.82	22.83	196.42	23.08
101.43	22.84	198.03	23.05
103.04	22.87	199.64	23.02

N4435 'I' MINOR AXIS

SE WING

RADIUS arcsec	BRIGHTNESS Mag/#arcsec	RADIUS arcsec	BRIGHTNESS Mag/#arcsec
201.25	23.01		

N4435 'I' MINOR AXIS

NW WING

RADIUS arcsec	BRIGHTNESS Mag/#arcsec	RADIUS arcsec	BRIGHTNESS Mag/#arcsec
6.44	16.46	45.08	21.91
8.05	17.45	46.69	22.00
9.66	17.73	48.30	22.08
11.27	18.22	49.91	22.13
14.49	18.87	51.52	22.14
16.10	19.43	53.13	22.17
17.71	19.67	54.74	22.24
19.32	19.78	56.35	22.35
20.93	19.89	57.96	22.47
22.54	20.02	59.57	22.62
24.15	20.23	61.18	22.77
25.76	20.39	62.79	22.95
27.37	20.53	64.40	23.10
28.98	20.63	66.01	23.20
30.59	20.76	67.62	23.31
32.20	20.91	69.23	23.39
33.81	21.04	70.84	23.38
35.42	21.14	72.45	23.30
37.03	21.24	74.06	23.19
38.64	21.37	75.67	23.12
40.25	21.51	77.28	23.14
41.86	21.66	78.89	23.32
43.47	21.80		

N4438 'I' M JOR AXIS

SW WING

RADIUS arcsec	BRIGHTNESS Mag/#arcsec	RADIUS arcsec	BRIGHTNESS Mag/#arcsec
6.44	16.67	75.67	21.29
8.05	17.22	77.28	21.39
9.66	17.62	78.89	21.50
11.27	17.79	80.50	21.62
12.88	17.79	82.11	21.73
14.49	17.82	83.72	21.84
16.10	17.92	85.33	21.93
17.71	17.90	86.94	22.01
19.32	18.12	88.55	22.04
20.93	18.11	90.16	22.04
22.54	18.11	91.77	22.04
24.15	18.36	93.38	22.03
25.76	18.43	94.99	22.05
27.37	18.65	96.60	22.09
28.98	18.70	98.21	22.15
30.59	18.70	99.82	22.19
32.20	18.85	101.43	22.22
33.81	18.80	103.04	22.27
35 42	18.99	104.65	22.34
37.03	19.09	106.26	22.38
38.64	19.18	107.87	22.41
40.25	19.25	109.48	22.44
41.86	19.31	111.09	22.45
43.47	19.54	112.70	22.43
45.08	19.59	114.31	22.45
46.69	19.65	115.92	22.49
48.30	19.75	117.53	22.52
49.91	19.81	119.14	22.54
51.52	19.91	120.75	22.53
53.13	20.00	122.36	22.54
54.74	20.09	123.97	22.61
56.35	20.18	125.58	22.72
57.96	20.22	127.19	22.93
59.57	20.29	128.80	23.17
61.18	20.33	130.41	23.34
62.79	20.39	132.02	23.41
64.40	20.43	133.63	23.43
66.01	20.50	135.24	23.36
67.62	20.59	136.85	23.29
69.23	20.75	138.46	23.28
70.84	20.90	140.07	23.35
72.45	21.05	141.68	23.48
74.06	21.18	143.29	23.58

N4438 'I' MAJOR AXIS

NE WING

RADIUS arcsec	BRIGHTNESS Mag/#arcsec	RADIUS arcsec	BRIGHTNESS Mag/#arcsec
6.44	16.95	103.04	22.03
8.05	17.22	104.65	22.07
9.66	17.58	106.26	22.12
11.27	17.61	107.87	22.17
12.88	17.71	109.48	22.20
14.49	17.82	111.09	22.22
16.10	17.94	112.70	22.21
17.71	18.06	114.31	22.16
19.32	18.29	115.92	22.11
20.93	18.37	117.53	22.09
22.54	18.47	119.14	22.07
24.15	18.66	120.75	22.04
25.76	18.77	122.36	22.00
27.37	18.85	123.97	22.03
28.98	18.92	125.58	22.05
30.59	18.98	127.19	22.06
32.20	18.93	128.80	22.09
33.81	19.11	130.41	22.13
35.42	19.16	132.02	22.14
37.03	19.32	133.63	22.15
38.64	19.48	135.24	22.16
40.25	19.60	136.85	22.14
41.86	19.75	138.46	22.11
43.47	19.94	140.07	22.08
45.08	20.13	141.68	22.03
46.69	20.27	143.29	22.03
48.30	20.36	144.90	22.05
49.91	20.43	146.51	22.11
51.52	20.50	148.12	22.19
53.13	20.60	149.73	22.28
54.74	20.69	151.34	22.34
56.35	20.75	152.95	22.37
57.96	20.79	154.56	22.35
59.57	20.81	156.17	22.30
61.18	20.84	157.78	22.26
62.79	20.90	159.39	22.23
64.40	20.95	161.00	22.23
66.01	21.02	162.61	22.22
67.62	21.07	164.22	22.19
69.23	21.13	165.83	22.15
70.84	21.17	167.44	22.11
72.45	21.21	169.05	22.09
74.06	21.23	170.66	22.11
75.67	21.27	172.27	22.15
77.28	21.38	173.88	22.18
78.89	21.47	175.49	22.20
80.50	21.57	177.10	22.17
82.11	21.67	178.71	22.12
83.72	21.73	180.32	22.06
85.33	21.80	181.93	22.01
86.94	21.87	183.54	21.95
88.55	21.94	185.15	21.93
90.16	21.99	186.76	21.93
91.77	21.99	188.37	21.92
93.38	21.96	189.98	21.91
94.99	21.94	191.59	21.92
96.60	21.93	193.20	21.94
98.21	21.93	194.81	21.95
99.82	21.97	196.42	21.97
101.43	22.02	198.03	21.99

N4438 'I' MAJOR AXIS

NE WING

RADIUS arcsec	BRIGHTNESS Mag/#arcsec	RADIUS arcsec	BRIGHTNESS Mag/#arcsec
199.64	22.01	236.67	22.37
201.25	22.03	238.28	22.38
202.86	22.03	239.89	22.38
204.47	22.01	241.50	22.40
206.08	22.00	243.11	22.42
207.69	21.99	244.72	22.46
209.30	21.99	246.33	22.53
210.91	22.02	247.94	22.56
212.52	22.05	249.55	22.56
214.13	22.08	251.16	22.51
215.74	22.10	252.77	22.47
217.35	22.09	254.38	22.44
218.96	22.07	255.99	22.44
220.57	22.07	257.60	22.49
222.18	22.08	259.21	22.55
223.79	22.10	260.82	22.61
225.40	22.13	262.43	22.66
227.01	22.17	264.04	22.72
228.62	22.21	265.65	22.81
230.23	22.24	267.26	22.91
231.84	22.27	268.87	22.98
233.45	22.30	270.48	23.06
235.06	22.34		

N4438 'I' BAR AXIS

SE WING

RADIUS arcsec	BRIGHTNESS Mag/#arcsec	RADIUS arcsec	BRIGHTNESS Mag/#arcsec
6.44	17.36	45.08	21.95
8.05	17.22	46.69	22.00
9.66	17.69	48.30	22.09
11.27	17.93	49.91	22.18
12.88	18.22	51.52	22.29
14.49	18.47	53.13	22.44
16.10	18.59	54.74	22.65
17.71	18.91	56.35	22.85
19.32	19.26	57.96	22.95
20.93	19.53	59.57	23.00
22.54	19.82	61.18	23.08
24.15	20.04	62.79	23.13
25.76	20.21	64.40	23.16
27.37	20.42	66.01	23.23
28.98	20.63	67.62	23.35
30.59	20.81	69.23	23.44
32.20	20.93	70.84	23.51
33.81	21.05	72.45	23.56
35.42	21.21	74.06	23.58
37.03	21.38	75.67	23.57
38.64	21.53	77.28	23.55
40.25	21.66	78.89	23.54
41.86	21.78	80.50	23.55
43.47	21.89	82.11	23.72

N4438 'I' BAR AXIS

NW WING

RADIUS arcsec	BRIGHTNESS Mag/#arcsec	RADIUS arcsec	BRIGHTNESS Mag/#arcsec
6.44	17.36	80.50	22.65
8.05	17.22	82.11	22.69
9.66	17.69	83.72	22.79
11.27	17.93	85.33	22.88
12.88	18.22	86.94	22.90
14.49	18.05	88.55	22.82
16.10	18.40	90.16	22.70
17.71	18.74	91.77	22.60
19.32	18.93	93.38	22.54
20.93	19.28	94.99	22.54
22.54	19.42	96.60	22.60
24.15	19.68	98.21	22.70
25.76	19.95	99.82	22.78
27.37	20.21	101.43	22.83
28.98	20.44	103.04	22.85
30.59	20.62	104.65	22.86
32.20	20.76	106.26	22.88
33.81	20.85	107.87	22.95
35.42	20.93	109.48	23.02
37.03	21.01	111.09	22.99
38.64	21.12	112.70	22.95
40.25	21.23	114.31	22.88
41.86	21.32	115.92	22.74
43.47	21.40	117.53	22.62
45.08	21.48	119.14	22.60
46.69	21.57	120.75	22.61
48.30	21.64	122.36	22.65
49.91	21.73	123.97	22.72
51.52	21.84	125.58	22.82
53.13	21.94	127.19	22.95
54.74	21.99	128.80	23.05
56.35	22.03	130.41	23.07
57.96	22.06	132.02	23.06
59.57	22.08	133.63	23.07
61.18	22.12	135.24	23.05
62.79	22.20	136.85	23.02
64.40	22.28	138.46	23.00
66.01	22.35	140.07	22.99
67.62	22.40	141.68	22.97
69.23	22.42	143.29	22.95
70.84	22.46	144.90	22.96
72.45	22.54	146.51	23.02
74.06	22.63	148.12	23.09
75.67	22.65	149.73	23.18
77.28	22.64	151.34	23.27
78.89	22.64	152.95	23.39

N4459 'I' MAJOR AXIS

SE WING

RADIUS arcsec	BRIGHTNESS Mag/#arcsec	RADIUS arcsec	BRIGHTNESS Mag/#arcsec
6.44	16.47	80.50	21.76
8.05	17.12	82.11	21.79
9.66	17.61	83.72	21.81
11.27	17.80	85.33	21.83
12.88	18.01	86.94	21.84
14.49	18.26	88.55	21.86
16.10	18.40	90.16	21.89
17.71	18.66	91.77	21.92
19.32	18.83	93.38	21.97
20.93	18.97	94.99	22.02
22.54	19.02	96.60	22.07
24.15	19.37	98.21	22.10
25.76	19.37	99.82	22.13
27.37	19.50	101.43	22.17
28.98	19.64	103.04	22.20
30.59	19.78	104.65	22.23
32.20	19.80	106.26	22.28
33.81	19.72	107.87	22.32
35.42	19.95	109.48	22.36
37.03	20.14	111.09	22.43
38.64	20.26	112.70	22.51
40.25	20.35	114.31	22.59
41.86	20.43	115.92	22.67
43.47	20.50	117.53	22.74
45.08	20.54	119.14	22.79
46.69	20.60	120.75	22.82
48.30	20.68	122.36	22.86
49.91	20.78	123.97	22.90
51.52	20.86	125.58	22.93
53.13	20.91	127.19	22.95
54.74	20.95	128.80	22.99
56.35	20.98	130.41	23.05
57.96	21.04	132.02	23.13
59.57	21.12	133.63	23.19
61.18	21.22	135.24	23.22
62.79	21.30	136.85	23.22
64.40	21.35	138.46	23.19
66.01	21.38	140.07	23.18
67.62	21.42	141.68	23.24
69.23	21.46	143.29	23.33
70.84	21.52	144.90	23.40
72.45	21.57	146.51	23.48
74.06	21.62	148.12	23.54
75.67	21.67	149.73	23.62
77.28	21.70	151.34	23.72
78.89	21.74	152.95	23.84

N4459 'I' MAJOR AXIS

NW WING

RADIUS arcsec	BRIGHTNESS Mag/#arcsec	RADIUS arcsec	BRIGHTNESS Mag/#arcsec
6.44	16.47	75.67	21.63
8.05	17.32	77.28	21.68
9.66	17.40	78.89	21.76
11.27	17.72	80.50	21.86
12.88	17.82	82.11	21.92
14.49	18.09	83.72	21.93
16.10	18.32	85.33	21.91
17.71	18.45	86.94	21.85
19.32	18.64	88.55	21.81
20.93	18.48	90.16	21.82
22.54	18.90	91.77	21.89
24.15	19.25	93.38	22.01
25.76	19.18	94.99	22.15
27.37	19.43	96.60	22.24
28.98	19.59	98.21	22.27
30.59	19.78	99.82	22.29
32.20	19.83	101.43	22.29
33.81	19.89	103.04	22.29
35.42	19.98	104.65	22.32
37.03	20.11	106.26	22.36
38.64	20.23	107.87	22.41
40.25	20.31	109.48	22.46
41.86	20.38	111.09	22.50
43.47	20.47	112.70	22.56
45.08	20.56	114.31	22.64
46.69	20.65	115.92	22.76
48.30	20.74	117.53	22.89
49.91	20.81	119.14	23.02
51.52	20.88	120.75	23.12
53.13	20.92	122.36	23.15
54.74	20.97	123.97	23.15
56.35	21.02	125.58	23.15
57.96	21.07	127.19	23.14
59.57	21.15	128.80	23.16
61.18	21.24	130.41	23.25
62.79	21.31	132.02	23.38
64.40	21.34	133.63	23.48
66.01	21.35	135.24	23.53
67.62	21.38	136.85	23.54
69.23	21.43	138.46	23.53
70.84	21.50	140.07	23.54
72.45	21.52	141.68	23.65
74.06	21.57		

N4459 'I' MINOR AXIS

SW WING

RADIUS arcsec	BRIGHTNESS Mag/#arcsec	RADIUS arcsec	BRIGHTNESS Mag/#arcsec
6.44	16.47	80.50	22.28
8.05	17.11	82.11	22.31
9.66	17.51	83.72	22.34
11.27	17.84	85.33	22.37
12.88	18.04	86.94	22.39
14.49	18.42	88.55	22.41
16.10	18.58	90.16	22.45
17.71	18.80	91.77	22.52
19.32	19.08	93.38	22.60
20.93	19.17	94.99	22.68
22.54	19.45	96.60	22.74
24.15	19.53	98.21	22.78
25.76	19.58	99.82	22.83
27.37	19.79	101.43	22.87
28.98	19.93	103.04	22.90
30.59	20.07	104.65	22.93
32.20	20.20	106.26	22.97
33.81	20.31	107.87	22.99
35.42	20.41	109.48	23.00
37.03	20.49	111.09	22.99
38.64	20.60	112.70	22.96
40.25	20.70	114.31	22.92
41.86	20.78	115.92	22.91
43.47	20.82	117.53	22.94
45.08	20.88	119.14	23.01
46.69	20.95	120.75	23.09
48.30	21.04	122.36	23.18
49.91	21.09	123.97	23.24
51.52	21.13	125.58	23.29
53.13	21.18	127.19	23.34
54.74	21.25	128.80	23.40
56.35	21.32	130.41	23.43
57.96	21.39	132.02	23.45
59.57	21.48	133.63	23.46
61.18	21.53	135.24	23.48
62.79	21.59	136.85	23.49
64.40	21.67	138.46	23.51
66.01	21.75	140.07	23.53
67.62	21.83	141.68	23.55
69.23	21.90	143.29	23.56
70.84	21.96	144.90	23.57
72.45	22.02	146.51	23.59
74.06	22.07	148.12	23.66
75.67	22.12	149.73	23.74
77.28	22.18	151.34	23.83
78.89	22.23	152.95	23.88

M4459 'I' MINOR AXIS

NE WING

RADIUS arcsec	BRIGHTNESS Mag/#arcsec	RADIUS arcsec	BRIGHTNESS Mag/#arcsec
6.44	16.47	77.28	22.31
8.05	17.55	78.89	22.34
9.66	17.80	80.50	22.37
11.27	18.03	82.11	22.39
12.88	18.30	83.72	22.42
14.49	18.60	85.33	22.45
16.10	18.69	86.94	22.50
17.71	18.95	88.55	22.58
19.32	19.18	90.16	22.66
20.93	19.50	91.77	22.72
22.54	19.55	93.38	22.76
24.15	19.72	94.99	22.80
25.76	19.86	96.60	22.85
27.37	20.01	98.21	22.88
28.98	20.14	99.82	22.91
30.59	20.29	101.43	22.94
32.20	20.40	103.04	22.98
33.81	20.48	104.65	22.98
35.42	20.54	106.26	22.97
37.03	20.60	107.87	22.95
38.64	20.71	109.48	22.92
40.25	20.82	111.09	22.94
41.86	20.94	112.70	23.02
43.47	21.03	114.31	23.12
45.08	21.10	115.92	23.23
46.69	21.13	117.53	23.30
48.30	21.18	119.14	23.34
49.91	21.25	120.75	23.37
51.52	21.32	122.36	23.42
53.13	21.38	123.97	23.49
54.74	21.46	125.58	23.58
56.35	21.51	127.19	23.62
57.96	21.57	128.80	23.60
59.57	21.65	130.41	23.58
61.18	21.73	132.02	23.57
62.79	21.81	133.63	23.55
64.40	21.88	135.24	23.55
66.01	21.95	136.85	23.61
67.62	22.00	138.46	23.66
69.23	22.05	140.07	23.69
70.84	22.11	141.68	23.72
72.45	22.17	143.29	23.80
74.06	22.22	144.90	23.88
75.67	22.27	146.51	23.94

N4461 'I' MAJOR AXIS

S WING

RADIUS arcsec	BRIGHTNESS Mag/#arcsec	RADIUS arcsec	BRIGHTNESS Mag/#arcsec
6.44	16.24	61.18	21.00
8.05	16.48	62.79	21.09
9.66	16.80	64.40	21.15
11.27	17.24	66.01	21.22
12.88	18.04	67.62	21.29
14.49	18.28	69.23	21.36
16.10	18.41	70.84	21.41
17.71	18.58	72.45	21.47
19.32	18.91	74.06	21.51
20.93	19.13	75.67	21.55
22.54	19.12	77.28	21.58
24.15	19.12	78.89	21.61
25.76	19.37	80.50	21.63
27.37	19.47	82.11	21.65
28.98	19.54	83.72	21.66
30.59	19.64	85.33	21.70
32.20	19.79	86.94	21.75
33.81	19.88	88.55	21.82
35.42	19.90	90.16	21.91
37.03	19.91	91.77	22.00
38.64	19.94	93.38	22.07
40.25	19.97	94.99	22.14
41.86	19.99	96.60	22.19
43.47	20.02	98.21	22.21
45.08	20.11	99.82	22.24
46.69	20.22	101.43	22.26
48.30	20.31	103.04	22.31
49.91	20.36	104.65	22.38
51.52	20.43	106.26	22.47
53.13	20.53	107.87	22.55
54.74	20.66	109.48	22.64
56.35	20.78	111.09	22.74
57.96	20.87	112.70	22.86
59.57	20.94	114.31	23.07

N4461 'I' MAJOR AXIS

N WING

RADIUS arcsec	BRIGHTNESS Mag/#arcsec	RADIUS arcsec	BRIGHTNESS Mag/#arcsec
6.44	16.24	90.16	21.67
8.05	16.48	91.77	21.77
9.66	16.80	93.38	21.86
11.27	17.24	94.99	21.90
12.88	17.99	96.60	21.91
14.49	18.21	98.21	21.94
16.10	18.48	99.82	22.00
17.71	18.53	101.43	22.07
19.32	18.84	103.04	22.15
20.93	18.70	104.65	22.20
22.54	19.07	106.26	22.23
24.15	19.14	107.87	22.25
25.76	19.19	109.48	22.28
27.37	19.26	111.09	22.34
28.98	19.25	112.70	22.42
30.59	19.44	114.31	22.49
32.20	19.54	115.92	22.56
33.81	19.62	117.53	22.61
35.42	19.70	119.14	22.64
37.03	19.80	120.75	22.67
38.64	19.86	122.36	22.71
40.25	19.93	123.97	22.73
41.86	19.95	125.58	22.75
43.47	19.97	127.19	22.76
45.08	19.99	128.80	22.77
46.69	20.02	130.41	22.77
48.30	20.06	132.02	22.78
49.91	20.11	133.63	22.80
51.52	20.19	135.24	22.84
53.13	20.30	136.85	22.88
54.74	20.42	138.46	22.91
56.35	20.53	140.07	22.94
57.96	20.65	141.68	22.97
59.57	20.75	143.29	22.97
61.18	20.83	144.90	22.96
62.79	20.89	146.51	22.97
64.40	20.97	148.12	22.99
66.01	21.02	149.73	23.02
67.62	21.04	151.34	23.09
69.23	21.06	152.95	23.19
70.84	21.09	154.56	23.26
72.45	21.15	156.17	23.25
74.06	21.22	157.78	23.22
75.67	21.26	159.39	23.21
77.28	21.29	161.00	23.22
78.89	21.31	162.61	23.24
80.50	21.33	164.22	23.30
82.11	21.33	165.83	23.39
83.72	21.35	167.44	23.46
85.33	21.39	169.05	23.52
86.94	21.47	170.66	23.66
88.55	21.57		

N4461 'I' MINOR AXIS

W WING

RADIUS arcsec	BRIGHTNESS Mag/#arcsec	RADIUS arcsec	BRIGHTNESS Mag/#arcsec
6.44	16.24	56.35	23.09
8.05	16.48	57.96	22.99
9.66	16.80	59.57	22.87
11.27	17.24	61.18	22.80
12.88	18.86	62.79	22.79
14.49	19.13	64.40	22.77
16.10	19.45	66.01	22.76
17.71	19.75	67.62	22.81
19.32	20.05	69.23	22.86
20.93	20.30	70.84	22.89
22.54	20.50	72.45	22.91
24.15	20.67	74.06	22.89
25.76	20.85	75.67	22.83
27.37	21.02	77.28	22.80
28.98	21.16	78.89	22.81
30.59	21.29	80.50	22.85
32.20	21.41	82.11	22.95
33.81	21.55	83.72	23.08
35.42	21.68	85.33	23.21
37.03	21.78	86.94	23.34
38.64	21.92	88.55	23.40
40.25	22.13	90.16	23.39
41.86	22.39	91.77	23.38
43.47	22.69	93.38	23.34
45.08	22.97	94.99	23.25
46.69	23.19	96.60	23.19
48.30	23.31	98.21	23.21
49.91	23.35	99.82	23.25
51.52	23.34	101.43	23.30
53.13	23.27	103.04	23.38
54.74	23.17	104.65	23.51

N4461 'I' MINOR AXIS

E WING

RADIUS arcsec	BRIGHTNESS Mag/#arcsec	RADIUS arcsec	BRIGHTNESS Mag/#arcsec
6.44	16.24	35.42	21.94
8.05	16.48	37.03	22.04
9.66	16.80	38 64	22.16
11.27	17.24	40.25	22.33
12.88	18.68	41.86	22.53
14.49	18.92	43.47	22.72
16.10	19.37	45.08	22.83
17.71	19.71	46.69	22.92
19.32	19.94	48.30	22.98
20.93	20.14	49.91	23.00
22.54	20.35	51.52	22.99
24.15	20.58	53.13	23.01
25.76	20.82	54.74	22.98
27.37	21.10	56.35	22.95
28.98	21.35	57.96	22.98
30.59	21.55	59.57	23.11
32.20	21.73	61.18	23.27
33.81	21.86	62.79	23.38

N4474 'I' MAJOR 'XIS

SW WING

RADIUS arcsec	BRIGHTNESS Mag/#arcsec	RADIUS arcsec	BRIGHTNESS Mag/#arcsec
6.44	16.30	59.57	22.14
8.05	18.05	61.18	22.27
9.66	18.28	62.79	22.41
11.27	18.36	64.40	22.57
12.88	18.57	66.01	22.73
14.49	19.00	67.62	22.85
16.10	19.17	69.23	22.96
17.71	19.11	70.84	23.02
19.32	19.17	72.45	23.03
20.93	19.46	74.06	23.03
22.54	19.52	75.67	23.07
24.15	19.57	77.28	23.11
25.76	19.77	78.89	23.16
27.37	19.92	80.50	23.22
28.98	20.01	82.11	23.25
30.59	20.11	83.72	23.22
32.20	20.22	85.33	23.22
33.81	20.33	86.94	23.22
35.42	20.44	88.55	23.23
37.03	20.55	90.16	23.22
38.64	20.69	91.77	23.23
40.25	20.82	93.38	23.27
41.86	20.93	94.99	23.34
43.47	21.01	96.60	23.44
45.08	21.08	98.21	23.55
46.69	21.19	99.82	23.68
48.30	21.30	101.43	23.80
49.91	21.39	103.04	23.81
51.52	21.49	104.65	23.78
53.13	21.60	106.26	23.79
54.74	21.73	107.87	23.83
56.35	21.88	109.48	23.84
57.96	22.02		

N4474 'I' MAJOR AXIS

NE WING

RADIUS arcsec	BRIGHTNESS Mag/#arcsec	RADIUS arcsec	BRIGHTNESS Mag/#arcsec
6.44	16.30	45.08	21.07
8.05	17.59	46.69	21.21
9.66	17.99	48.30	21.32
11.27	18.15	49.91	21.45
12.88	18.35	51.52	21.57
14.49	18.66	53.13	21.68
16.10	18.71	54.74	21.81
17.71	18.79	56.35	21.91
19.32	19.09	57.96	22.00
20.93	19.14	59.57	22.10
22.54	19.32	61.18	22.23
24.15	19.43	62.79	22.35
25.76	19.40	64.40	22.46
27.37	19.63	66.01	22.59
28.98	19.67	67.62	22.69
30.59	19.78	69.23	22.74
32.20	19.88	70.84	22.75
33.81	20.02	72.45	22.80
35.42	20.13	74.06	22.89
37.03	20.26	75.67	23.01
38.64	20.40	77.28	23.11
40.25	20.57	78.89	23.24
41.86	20.75	80.50	23.36
43.47	20.91	82.11	23.53

N4474 'I' MINOR AXIS

SE WING

RADIUS arcsec	BRIGHTNESS Mag/#arcsec	RADIUS arcsec	BRIGHTNESS Mag/#arcsec
6.44	18.40	40.25	22.39
8.05	18.98	41.86	22.46
9.66	19.58	43.47	22.57
12.88	19.65	45.08	22.71
14.49	20.41	46.69	22.86
16.10	20.64	48.30	23.02
17.71	20.80	49.91	23.16
19.32	20.93	51.52	23.20
20.93	21.11	53.13	23.19
22.54	21.28	54.74	23.20
24.15	21.36	56.35	23.23
25.76	21.49	57.96	23.23
27.37	21.58	59.57	23.20
28.98	21.69	61.18	23.19
30.59	21.84	62.79	23.19
32.20	21.98	64.40	23.21
33.81	22.09	66.01	23.26
35.42	22.22	67.62	23.36
37.03	22.32	69.23	23.48
38.64	22.36	70.84	23.71

N4474 'I' MINOR AXIS

NW WING

RADIUS arcsec	BRIGHTNESS Mag/#arcsec	RADIUS arcsec	BRIGHTNESS Mag/#arcsec
6.44	16.30	35.42	22.06
8.05	17.97	37.03	22.16
9.66	18.59	38.64	22.28
12.88	19.53	40.25	22.43
14.49	19.95	41.86	22.53
16.10	20.26	43.47	22.59
17.71	20.46	45.08	22.63
19.32	20.64	46.69	22.69
20.93	20.84	48.30	22.80
22.54	21.06	49.91	22.98
24.15	21.27	51.52	23.17
25.76	21.41	53.13	23.35
27.37	21.58	54.74	23.50
28.98	21.71	56.35	23.57
30.59	21.81	57.96	23.58
32.20	21.90	59.57	23.63
33.81	21.98		

N4477 'I' MAJOR AXIS

SW WING

RADIUS arcsec	BRIGHTNESS Mag/#arcsec	RADIUS arcsec	BRIGHTNESS Mag/#arcsec
6.44	16.25	69.23	21.38
8.05	16.66	70.84	21.44
9.66	17.25	72.45	21.48
11.27	17.47	74.06	21.52
12.88	17.59	75.67	21.55
14.49	17.79	77.28	21.57
16.10	17.97	78.89	21.58
17.71	18.19	80.50	21.60
19.32	18.19	82.11	21.61
20.93	18.56	83.72	21.63
22.54	18.52	85.33	21.70
24.15	18.72	86.94	21.79
25.76	18.79	88.55	21.91
27.37	19.10	90.16	22.04
28.98	19.13	91.77	22.18
30.59	19.31	93.38	22.32
32.20	19.44	94.99	22.43
33.81	19.69	96.60	22.52
35.42	19.92	98.21	22.58
37.03	20.10	99.82	22.64
38.64	20.18	101.43	22.71
40.25	20.25	103.04	22.77
41.86	20.33	104.65	22.82
43.47	20.45	106.26	22.86
45.08	20.56	107.87	22.91
46.69	20.65	109.48	22.96
48.30	20.70	111.09	22.99
49.91	20.74	112.70	23.03
51.52	20.78	114.31	23.08
53.13	20.84	115.92	23.13
54.74	20.91	117.53	23.18
56.35	20.96	119.14	23.26
57.96	20.99	120.75	23.33
59.57	21.01	122.36	23.42
61.18	21.04	123.97	23.47
62.79	21.06	125.58	23.50
64.40	21.11	127.19	23.56
66.01	21.18	128.80	23.65
67.62	21.29	130.41	23.69

N4477 'I' MAJOR AXIS

NE WING

RADIUS arcsec	BRIGHTNESS Mag/#arcsec	RADIUS arcsec	BRIGHTNESS Mag/#arcsec
6.44	16.25	77.28	21.47
8.05	16.66	78.89	21.46
9.66	17.31	80.50	21.49
11.27	17.54	82.11	21.56
12.88	17.73	83.72	21.66
14.49	18.05	85.33	21.76
16.10	18.08	86.94	21.87
17.71	18.26	88.55	21.97
19.32	18.26	90.16	22.06
20.93	18.44	91.77	22.11
22.54	18.58	93.38	22.16
24.15	18.85	94.99	22.24
25.76	18.94	96.60	22.32
27.37	19.10	98.21	22.41
28.98	19.26	99.82	22.51
30.59	19.52	101.43	22.62
32.20	19.64	103.04	22.68
33.81	19.80	104.65	22.72
35.42	20.00	106.26	22.71
37.03	20.15	107.87	22.67
38.64	20.23	109.48	22.62
40.25	20.28	111.09	22.61
41.86	20.36	112.70	22.65
43.47	20.47	114.31	22.72
45.08	20.57	115.92	22.79
46.69	20.64	117.53	22.85
48.30	20.67	119.14	22.94
49.91	20.73	120.75	23.06
51.52	20.79	122.36	23.13
53.13	20.87	123.97	23.16
54.74	20.97	125.58	23.15
56.35	21.05	127.19	23.11
57.96	21.11	128.80	23.03
59.57	21.10	130.41	23.02
61.18	21.06	132.02	23.08
62.79	21.02	133.63	23.19
64.40	21.05	135.24	23.32
66.01	21.13	136.85	23.35
67.62	21.21	138.46	23.34
69.23	21.29	140.07	23.35
70.84	21.37	141.68	23.41
72.45	21.42	143.29	23.46
74.06	21.45	144.90	23.52
75.67	21.47		

N4477 'I' MINOR AXIS

SE WING

RADIUS arcsec	BRIGHTNESS Mag/#arcsec	RADIUS arcsec	BRIGHTNESS Mag/#arcsec
6.44	16.25	77.28	21.56
8.05	16.66	78.89	21.68
9.66	17.57	80.50	21.81
11.27	17.94	82.11	21.92
12.88	18.22	83.72	22.03
14.49	18.48	85.33	22.11
16.10	18.89	86.94	22.16
17.71	18.97	88.55	22.19
19.32	19.19	90.16	22.22
20.93	19.50	91.77	22.26
22.54	19.59	93.38	22.31
24.15	19.68	94.99	22.33
25.76	19.77	96.60	22.34
27.37	19.87	98.21	22.34
28.98	19.97	99.82	22.33
30.59	20.05	101.43	22.35
32.20	20.10	103.04	22.40
33.81	20.14	104.65	22.44
35.42	20.18	106.26	22.46
37.03	20.25	107.87	22.47
38.64	20.34	109.48	22.46
40.25	20.42	111.09	22.43
41.86	20.48	112.70	22.48
43.47	20.53	114.31	22.57
45.08	20.57	115.92	22.66
46.69	20.60	117.53	22.72
48.30	20.61	119.14	22.77
49.91	20.65	120.75	22.76
51.52	20.66	122.36	22.73
53.13	20.67	123.97	22.73
54.74	20.67	125.58	22.75
56.35	20.67	127.19	22.76
57.96	20.67	128.80	22.80
59.57	20.70	130.41	22.85
61.18	20.76	132.02	22.89
62.79	20.82	133.63	22.91
64.40	20.84	135.24	22.94
66.01	20.84	136.85	22.95
67.62	20.88	138.46	22.96
69.23	20.99	140.07	22.99
70.84	21.14	141.68	23.06
72.45	21.26	143.29	23.12
74.06	21.38	144.90	23.16
75.67	21.47		

N4477 'I' MINOR AXIS

NW WING

RADIUS arcsec	BRIGHTNESS Mag/#arcsec	RADIUS arcsec	BRIGHTNESS Mag/#arcsec
6.44	16.25	69.23	21.13
8.05	16.66	70.84	21.15
9.66	17.50	72.45	21.20
11.27	17.88	74.06	21.26
12.88	18.17	75.67	21.33
14.49	18.45	77.28	21.40
16.10	18.82	78.89	21.47
17.71	18.97	80.50	21.54
19.32	19.24	82.11	21.61
20.93	19.47	83.72	21.67
22.54	19.61	85.33	21.74
24.15	19.75	86.94	21.79
25.76	19.85	88.55	21.85
27.37	19.91	90.16	21.90
28.98	19.98	91.77	21.95
30.59	20.06	93.38	21.99
32.20	20.15	94.99	22.03
33.81	20.20	96.60	22.08
35.42	20.22	98.21	22.17
37.03	20.22	99.82	22.28
38.64	20.25	101.43	22.39
40.25	20.35	103.04	22.46
41.86	20.48	104.65	22.53
43.47	20.56	106.26	22.60
45.08	20.59	107.87	22.66
46.69	20.57	109.48	22.73
48.30	20.59	111.09	22.83
49.91	20.62	112.70	22.92
51.52	20.67	114.31	22.99
53.13	20.73	115.92	23.04
54.74	20.77	117.53	23.12
56.35	20.79	119.14	23.25
57.96	20.81	120.75	23.37
59.57	20.84	122.36	23.47
61.18	20.89	123.97	23.52
62.79	20.93	125.58	23.52
64.40	20.97	127.19	23.51
66.01	21.03	128.80	23.65
67.62	21.08		

N4501 'I' MAJOR AXIS

SE WING

RADIUS arcsec	BRIGHTNESS Mag/#arcsec	RADIUS arcsec	BRIGHTNESS Mag/#arcsec
6.44	16.39	103.04	20.53
8.05	16.63	104.65	20.56
9.66	16.94	106.26	20.61
11.27	17.73	107.87	20.65
12.88	17.50	109.48	20.64
14.49	17.98	111.09	20.64
16.10	18.20	112.70	20.61
17.71	17.84	114.31	20.61
19 32	18.45	115.92	20.61
20.93	18.56	117.53	20.64
22.54	18.67	119.14	20.72
24.15	18.84	120.75	20.83
25.76	18.70	122.36	20.95
27.37	18.90	123.97	21.04
28.98	18.81	125.58	21.10
30.59	18.70	127.19	21.16
32.20	18.79	128.80	21.20
33.81	18.70	130.41	21.25
35.42	18.70	132.02	21 29
37.03	18.66	133.63	21 33
38.64	18.72	135.24	21.37
40.25	18.79	136.85	21.39
41.86	18.72	138.46	21.42
43.47	18.81	140.07	21.44
45.08	18.87	141.68	21.41
46.69	18.83	143.29	21.40
48.30	18.97	144.90	21.32
49.91	18.92	146.51	21.26
51.52	18.98	148.12	21.24
53.13	19.03	149.73	21.27
54.74	19.12	151.34	21.31
56.35	19.33	152.95	21.34
57.96	19.37	154.56	21.35
59.57	19.39	156.17	21.38
61.18	19.50	157.78	21.44
62.79	19.55	159.39	21.52
64.40	19.60	161.00	21.59
66.01	19.55	162.61	21.66
67.62	19.52	164.22	21.70
69.23	19.61	165.83	21.75
70.84	19.73	167.44	21.79
72.45	19.81	169.05	21.83
74.06	19.86	170.66	21.89
75.67	19.91	172.27	21.97
77.28	19.96	173.88	22.05
78.89	20.01	175.49	22.11
80.50	20.04	177.10	22.16
82.11	20.09	178.71	22.19
83.72	20.11	180.32	22.20
85.33	20.11	181.93	22.21
86.94	20.08	183.54	22.27
88.55	20.07	185.15	22.35
90.16	20.08	186.76	22.43
91.77	20.09	188.37	22.52
93.38	20.12	189.98	22.61
94.99	20.17	191.59	22.66
96.60	20.27	193.20	22.66
98.21	20.38	194.81	22.69
99.82	20.46	196.42	22.74
101.43	20.51	198.03	22.77

M4501 'I' MAJOR AXIS

SE WING

RADIUS arcsec	BRIGHTNESS Mag/#arcsec	RADIUS arcsec	BRIGHTNESS Mag/#arcsec
199.64	22.76	236.67	22.90
201.25	22.78	238.28	23.04
202.86	22.76	239.89	23.11
204.47	22.73	241.50	23.16
206.08	22.69	243.11	23.16
207.69	22.72	244.72	23.10
209.30	22.73	246.33	23.03
210.91	22.75	247.94	23.03
212.52	22.77	249.55	23.08
214.13	22.81	251.16	23.16
215.74	22.84	252.77	23.26
217.35	22.86	254.38	23.32
218.96	22.87	255.99	23.38
220.57	22.89	257.60	23.36
222.18	22.91	259.21	23.35
223.79	22.97	260.82	23.33
225.40	23.01	262.43	23.34
227.01	22.99	264.04	23.32
228.62	22.92	265.65	23.36
230.23	22.84	267.26	23.41
231.84	22.75	268.87	23.52
233.45	22.72	270.48	23.61
235.06	22.76		

N4501 'I' MAJOR AXIS

NW WING

RADIUS arcsec	BRIGHTNESS Mag/#arcsec	RADIUS arcsec	BRIGHTNESS Mag/#arcsec
6.44	16.39	101.43	20.30
8.05	16.63	103.04	20.31
9.66	16.94	104.65	20.30
11.27	17.37	106.26	20.33
12.88	17.50	107.87	20.35
14.49	17.66	109.48	20.40
16.10	17.75	111.09	20.42
17.71	17.84	112.70	20.47
19.32	17.94	114.31	20.53
20.93	18.00	115.92	20.63
22.54	18.21	117.53	20.69
24.15	18.32	119.14	20.73
25.76	18.34	120.75	20.74
27.37	18.49	122.36	20.76
28.98	18.44	123.97	20.79
30.59	18.49	125.58	20.83
32.20	18.60	127.19	20.87
33.81	18.56	128.80	20.89
35.42	18.78	130.41	20.94
37.03	18.83	132.02	20.99
38.64	18.91	133.63	21.06
40.25	18.80	135.24	21.11
41.86	18.81	136.85	21.19
43.47	18.91	138.46	21.25
45.08	19.22	140.07	21.32
46.69	19.03	141.68	21.38
48.30	19.23	143.29	21.41
49.91	19.30	144.90	21.46
51.52	19.45	146.51	21.51
53.13	19.52	148.12	21.56
54.74	19.46	149.73	21.58
56.35	19.56	151.34	21.62
57.96	19.47	152.95	21.65
59.57	19.68	154.56	21.65
61.18	19.66	156.17	21.66
62.79	19.63	157.78	21.66
64.40	19.61	159.39	21.71
66.01	19.72	161.00	21.77
67.62	19.80	162.61	21.86
69.23	19.84	164.22	21.94
70.84	19.89	165.83	22.05
72.45	19.91	167.44	22.14
74.06	19.93	169.05	22.24
75.67	19.95	170.66	22.35
77.28	19.98	172.27	22.46
78.89	19.98	173.88	22.60
80.50	19.93	175.49	22.72
82.11	19.92	177.10	22.79
83.72	19.95	178.71	22.89
85.33	20.06	180.32	22.97
86.94	20.16	181.93	23.02
88.55	20.27	183.54	23.04
90.16	20.32	185.15	23.04
91.77	20.32	186.76	23.05
93.38	20.29	188.37	23.16
94.99	20.27	189.98	23.27
96.60	20.26	191.59	23.42
98.21	20.28	193.20	23.65
99.82	20.29	194.81	23.77

N4501 'I' MINOR AXIS

SW WING

RADIUS arcsec	BRIGHTNESS Mag/#arcsec	RADIUS arcsec	BRIGHTNESS Mag/#arcsec
6.44	16.39	86.94	22.33
8.05	16.63	88.55	22.38
9.66	16.94	90.16	22.46
11.27	17.83	91.77	22.57
12.88	17.50	93.38	22.69
14.49	18.16	94.99	22.85
16.10	18.26	96.60	22.97
17.71	17.84	98.21	23.01
19.32	18.33	99.82	23.03
20.93	18.49	101.43	23.05
22.54	18.64	103.04	23.12
24.15	18.69	104.65	23.24
25.76	18.74	106.26	23.31
27.37	18.97	107.87	23.29
28.98	18.90	109.48	23.22
30.59	19.14	111.09	23.13
32.20	19.40	112.70	23.02
33.81	19.59	114.31	23.05
35.42	19.58	115.92	23.12
37.03	19.68	117.53	23.24
38.64	19.68	119.14	23.31
40.25	19.59	120.75	23.34
41.86	19.87	122.36	23.32
43.47	20.08	123.97	23.32
45.08	20.18	125.58	23.34
46.69	20.25	127.19	23.34
48.30	20.28	128.80	23.35
49.91	20.31	130.41	23.35
51.52	20.36	132.02	23.32
53.13	20.46	133.63	23.28
54.74	20.58	135.24	23.28
56.35	20.68	136.85	23.25
57.96	20.69	138.46	23.19
59.57	20.71	140.07	23.25
61.18	20.77	141.68	23.27
62.79	20.89	143.29	23.27
64.40	21.00	144.90	23.28
66.01	21.11	146.51	23.36
67.62	21.26	148.12	23.32
69.23	21.46	149.73	23.37
70.84	21.64	151.34	23.24
72.45	21.78	152.95	23.26
74.06	21.86	154.56	23.36
75.67	21.90	156.17	23.48
77.28	21.96	157.78	23.57
78.89	22.01	159.39	23.64
80.50	22.08	161.00	23.69
82.11	22.17	162.61	23.73
83.72	22.26	164.22	23.79
85.33	22.32		

N4501 'I' MINOR AXIS

NE WING

RADIUS arcsec	BRIGHTNESS Mag/#arcsec	RADIUS arcsec	BRIGHTNESS Mag/#arcsec
6.44	16.39	70.84	21.32
8.05	16.63	72.45	21.34
9.66	16.94	74.06	21.37
11.27	18.18	75.67	21.42
12.88	17.50	77.28	21.46
14.49	18.58	78.89	21.52
16.10	18.63	80.50	21.59
17.71	17.84	82.11	21.67
19.32	18.86	83.72	21.76
20.93	18.94	85.33	21.85
22.54	18.98	86.94	21.96
24.15	19.34	88.55	22.07
25.76	19.21	90.16	22.17
27.37	19.55	91.77	22.26
28.98	19.31	93.38	22.34
30.59	19.55	94.99	22.39
32.20	19.76	96.60	22.45
33.81	19.89	98.21	22.49
35.42	19.95	99.82	22.55
37.03	19.96	101.43	22.62
38.64	19.99	103.04	22.70
40.25	20.04	104.65	22.80
41.86	20.15	106.26	22.90
43.47	20.25	107.87	22.97
45.08	20.36	109.48	22.99
46.69	20.53	111.09	23.03
48.30	20.72	112.70	23.09
49.91	20.88	114.31	23.25
51.52	20.95	115.92	23.38
53.13	20.97	117.53	23.47
54.74	20.99	119.14	23.47
56.35	21.05	120.75	23.39
57.96	21.11	122.36	23.21
59.57	21.17	123.97	23.14
61.18	21.21	125.58	23.17
62.79	21.24	127.19	23.24
64.40	21.25	128.80	23.30
66.01	21.27	130.41	23.36
67.62	21.31	132.02	23.41
69.23	21.33		

N4503 'I' MAJOR AXIS

S WING

RADIUS arcsec	BRIGHTNESS Mag/#arcsec	RADIUS arcsec	BRIGHTNESS Mag/#arcsec
6.44	16.79	72.45	21.61
8.05	17.23	74.06	21.65
9.66	17.65	75.67	21.68
11.27	17.84	77.28	21.70
12.88	18.12	78.89	21.70
14.49	18.23	80.50	21.71
16.10	18.50	82.11	21.72
17.71	18.73	83.72	21.74
19.32	18.63	85.33	21.75
20.93	18.85	86.94	21.79
22.54	19.15	88.55	21.84
24.15	19.16	90.16	21.89
25.76	19.45	91.77	21.97
27.37	19.51	93.38	22.07
28.98	19.64	94.99	22.16
30.59	19.72	96.60	22.22
32.20	19.83	98.21	22.26
33.81	19.96	99.82	22.30
35.42	20.07	101.43	22.33
37.03	20.16	103.04	22.37
38.64	20.20	104.65	22.44
40.25	20.22	106.26	22.52
41.86	20.25	107.87	22.60
43.47	20.30	109.48	22.71
45.08	20.36	111.09	22.82
46.69	20.44	112.70	22.91
48.30	20.53	114.31	22.98
49.91	20.63	115.92	23.02
51.52	20.69	117.53	23.05
53.13	20.74	119.14	23.08
54.74	20.80	120.75	23.14
56.35	20.86	122.36	23.19
57.96	20.95	123.97	23.23
59.57	21.04	125.58	23.22
61.18	21.11	127.19	23.17
62.79	21.16	128.80	23.14
64.40	21.23	130.41	23.20
66.01	21.31	132.02	23.34
67.62	21.41	133.63	23.54
69.23	21.48	135.24	23.69
70.84	21.56		

N4503 'I' MAJOR AXIS

N WING

RADIUS arcsec	BRIGHTNESS Mag/#arcsec	RADIUS arcsec	BRIGHTNESS Mag/#arcsec
6.44	16.79	67.62	21.41
8.05	17.23	69.23	21.47
9.66	17.96	70.84	21.53
11.27	17.94	72.45	21.59
12.88	18.36	74.06	21.65
14.49	18.51	75.67	21.71
16.10	18.58	77.28	21.77
17.71	18.72	78.89	21.80
19.32	18.90	80.50	21.81
20.93	19.08	82.11	21.83
22.54	19.13	83.72	21.85
24.15	19.36	85.33	21.89
25.76	19.44	86.94	21.95
27.37	19.54	88.55	22.03
28.98	19.71	90.16	22.13
30.59	19.84	91.77	22.22
32.20	19.90	93.38	22.29
33.81	19.94	94.99	22.31
35.42	20.01	96.60	22.30
37.03	20.11	98.21	22.28
38.64	20.18	99.82	22.28
40.25	20.21	101.43	22.31
41.86	20.25	103.04	22.39
43.47	20.33	104.65	22.50
45.08	20.43	106.26	22.60
46.69	20.50	107.87	22.70
48.30	20.55	109.48	22.82
49.91	20.58	111.09	22.93
51.52	20.62	112.70	23.03
53.13	20.69	114.31	23.12
54.74	20.77	115.92	23.21
56.35	20.86	117.53	23.25
57.96	20.95	119.14	23.25
59.57	21.05	120.75	23.27
61.18	21.15	122.36	23.32
62.79	21.22	123.97	23.38
64.40	21.29	125.58	23.47
66.01	21.36	127.19	23.65

N4503 'I' MINOR AXIS

W WING

RADIUS arcsec	BRIGHTNESS Mag/#arcsec	RADIUS arcsec	BRIGHTNESS Mag/#arcsec
6.44	16.79	35.42	21.59
8.05	17.23	37.03	21.72
9.66	18.29	38.64	21 86
11.27	18.77	40.25	22.00
12.88	18.92	41.86	22.13
14.49	19.36	43.47	22.23
16.10	19.56	45.08	22.37
17.71	19.84	46.69	22.55
19.32	20.07	48.30	22.73
20.93	20.24	49.91	22.92
22.54	20.41	51.52	23.12
24.15	20.58	53.13	23.32
25.76	20.74	54.74	23.46
27.37	20.86	56.35	23.54
28.98	20.98	57.96	23.57
30.59	21.11	59.57	23.55
32.20	21.27	61.18	23.51
33.81	21.43	62.79	23.54

N4503 'I' MINOR AXIS

E WING

RADIUS arcsec	BRIGHTNESS Mag/#arcsec	RADIUS arcsec	BRIGHTNESS Mag/#arcsec
6.44	16.79	37.03	21.73
8.05	17.23	38.64	21.82
9.66	18.30	40.25	21.94
11.27	18.70	41.86	22.09
12.88	19.05	43.47	22.28
14.49	19.36	45.08	22.54
16.10	19.64	46.69	22.79
17.71	19.88	48.30	22.95
19.32	20.05	49.91	23.02
20.93	20.23	51.52	23.07
22.54	20.40	53.13	23.13
24.15	20.59	54.74	23.22
25.76	20.76	56.35	23.38
27.37	20.91	57.96	23.56
28.98	21.04	59.57	23.68
30.59	21.18	61.18	23.74
32.20	21.33	62.79	23.80
33.81	21.48	64.40	23.86
35.42	21.62		

N4531 'I' MAJOR AXIS

SE WING

RADIUS arcsec	BRIGHTNESS Mag/#arcsec	RADIUS arcsec	BRIGHTNESS Mag/#arcsec
6.44	18.80	54.74	21.60
8.05	18.98	56.35	21.66
9.66	19.19	57.96	21.73
11.27	19.34	59.57	21.80
12.88	19.50	61.18	21.85
14.49	19.57	62.79	21.90
16.10	19.52	64.40	21.97
17.71	19.57	66.01	22.03
19.32	19.47	67.62	22.10
20.93	19.65	69.23	22.16
22.54	19.82	70.84	22.23
24.15	19.95	72.45	22.29
25.76	20.10	74.06	22.37
27.37	20.21	75.67	22.45
28.98	20.34	77.28	22.52
30.59	20.46	78.89	22.58
32.20	20.58	80.50	22.61
33.81	20.66	82.11	22.61
35.42	20.74	83.72	22.64
37.03	20.85	85.33	22.74
38.64	20.96	86.94	22.90
40.25	21.08	88.55	23.10
41.86	21.14	90.16	23.28
43.47	21.22	91.77	23.43
45.08	21.29	93.38	23.53
46.69	21.37	94.99	23.60
48.30	21.40	96.60	23.64
49.91	21.43	98.21	23.68
51.52	21.48	99.82	23.75
53.13	21.53		

N4531 'I' MAJOR AXIS

NW WING

RADIUS arcsec	BRIGHTNESS Mag/#arcsec	RADIUS arcsec	BRIGHTNESS Mag/#arcsec
6.44	18.93	49.91	21.50
8.05	18.98	51.52	21.58
9.66	19.31	53.13	21.65
11.27	19.40	54.74	21.70
12.88	19.50	56.35	21.75
14.49	19.43	57.96	21.83
16.10	19.68	59.57	21.91
17.71	19.80	61.18	21.99
19.32	19.80	62.79	22.07
20.93	19.88	64.40	22.12
22.54	19.98	66.01	22.13
24.15	20.09	67.62	22.13
25.76	20.19	69.23	22.15
27.37	20.27	70.84	22.18
28.98	20.38	72.45	22.24
30.59	20.49	74.06	22.31
32.20	20.60	75.67	22.38
33.81	20.68	77.28	22.45
35.42	20.76	78.89	22.52
37.03	20.87	80.50	22.59
38.64	20.96	82.11	22.72
40.25	21.03	83.72	22.89
41.86	21.10	85.33	23.04
43.47	21.18	86.94	23.18
45.08	21.25	88.55	23.31
46.69	21.30	90.16	23.46
48.30	21.36	91.77	23.67

N4531 'I' MINOR AXIS

SW WING

RADIUS arcsec	BRIGHTNESS Mag/#arcsec	RADIUS arcsec	BRIGHTNESS Mag/#arcsec
6.44	18.80	40.25	21.87
8.05	18.98	41.86	22.03
9.66	19.38	43.47	22.17
11.27	19.53	45.08	22.29
12.88	19.50	46.69	22.35
14.49	19.70	48.30	22.36
16.10	19.86	49.91	22.36
17.71	19.99	51.52	22.36
19.32	20.18	53.13	22.40
20.93	20.37	54.74	22.48
22.54	20.59	56.35	22.58
24.15	20.75	57.96	22.70
25.76	20.88	59.57	22.82
27.37	20.98	61.18	22.94
28.98	21.07	62.79	23.09
30.59	21.16	64.40	23.25
32.20	21.26	66.01	23.38
33.81	21.36	67.62	23.49
35.42	21.47	69.23	23.54
37.03	21.59	70.84	23.53
38.64	21.72	72.45	23.54

N4531 'I' MINOR AXIS

NE WING

RADIUS arcsec	BRIGHTNESS Mag/#arcsec	RADIUS arcsec	BRIGHTNESS Mag/#arcsec
6.44	19.09	40.25	21.80
8.05	18.98	41.86	21.96
9.66	19.39	43.47	22.11
11.27	19.58	45.08	22.27
12.88	19.50	46.69	22.44
14.49	19.75	48.30	22.57
16.10	20.00	49.91	22.64
17.71	20.22	51.52	22.70
19.32	20.46	53.13	22.76
20.93	20.64	54.74	22.79
22.54	20.79	56.35	22.86
24.15	20.90	57.96	22.96
25.76	21.01	59.57	23.05
27.37	21.15	61.18	23.12
28.98	21.30	62.79	23.23
30.59	21.41	64.40	23.33
32.20	21.50	66.01	23.42
33.81	21.54	67.62	23.51
35.42	21.58	69.23	23.60
37.03	21.64	70.84	23.69
38.64	21.70	72.45	23.82

N4550 'I' MAJOR AXIS

S WING

RADIUS arcsec	BRIGHTNESS Mag/#arcsec	RADIUS arcsec	BRIGHTNESS Mag/#arcsec
6.44	16.49	51.52	21.13
8.05	17.00	53.13	21.25
9.66	17.10	54.74	21.40
11.27	17.48	56.35	21.54
12.88	17.63	57.96	21.70
14.49	17.77	59.57	21.87
16.10	18.02	61.18	22.04
17.71	18.15	62.79	22.19
19.32	18.40	64.40	22.34
20.93	18.58	66.01	22.46
22.54	18.70	67.62	22.55
24.15	18.96	69.23	22.62
25.76	19.22	70.84	22.70
27.37	19.22	72.45	22.77
28.98	19.51	74.06	22.85
30.59	19.66	75.67	22.94
32.20	19.84	77.28	23.03
33.81	20.03	78.89	23.12
35.42	20.18	80.50	23.18
37.03	20.29	82.11	23.21
38.64	20.39	83.72	23.22
40.25	20.50	85.33	23.22
41.86	20.63	86.94	23.21
43.47	20.75	88.55	23.22
45.08	20.85	90.16	23.26
46.69	20.93	91.77	23.34
48.30	20.99	93.38	23.46
49.91	21.05	94.99	23.63

N4550 'I' MAJOR AXIS

N WING

RADIUS arcsec	BRIGHTNESS Mag/#arcsec	RADIUS arcsec	BRIGHTNESS Mag/#arcsec
6.44	16.81	62.79	22.03
8.05	17.14	64.40	22.04
9.66	17.34	66.01	22.01
11.27	17.58	67.62	22.01
12.88	17.68	69.23	22.08
14.49	17.77	70.84	22.23
16.10	18.07	72.45	22.41
17.71	18.29	74.06	22.58
19.32	18.61	75.67	22.65
20.93	18.77	77.28	22.65
22.54	18.95	78.89	22.62
24.15	19.04	80.50	22.65
25.76	19.23	82.11	22.76
27.37	19.54	83.72	22.93
28.98	19.66	85.33	23.05
30.59	19.59	86.94	23.08
32.20	19.83	88.55	23.03
33.81	20.02	90.16	22.90
35.42	20.16	91.77	22.73
37.03	20.28	93.38	22.64
38.64	20.39	94.99	22.64
40.25	20.51	96.60	22.65
41.86	20.63	98.21	22.67
43.47	20.73	99.82	22.69
45.08	20.82	101.43	22.72
46.69	20.92	103.04	22.76
48.30	21.05	104.65	22.84
49.91	21.16	106.26	22.93
51.52	21.22	107.87	23.01
53.13	21.29	109.48	23.05
54.74	21.39	111.09	23.07
56.35	21.53	112.70	23.08
57.96	21.67	114.31	23.18
59.57	21.83	115.92	23.36
61.18	21.96		

N4550 'I' MINOR AXIS

W WING

RADIUS arcsec	BRIGHTNESS Mag/#arcsec	RADIUS arcsec	BRIGHTNESS Mag/#arcsec
6.44	17.90	22.54	22.12
8.05	18.67	24.15	22.49
9.66	19.23	25.76	22.82
11.27	19.67	27.37	23.11
12.88	20.05	28.98	23.37
14.49	20.42	30.59	23.54
16.10	20.76	32.20	23.63
17.71	21.08	33.81	23.64
19.32	21.41	35.42	23.64
20.93	21.77	37.03	23.77

N4550 'I' MINOR AXIS

E WING

RADIUS arcsec	BRIGHTNESS Mag/#arcsec	RADIUS arcsec	BRIGHTNESS Mag/#arcsec
6.44	17.64	22.54	22.04
8.05	18.37	24.15	22.38
9.66	18.89	25.76	22.69
11.27	19.48	27.37	22.97
12.88	19.86	28.98	23.22
14.49	20.24	30.59	23.39
16.10	20.64	32.20	23.54
17.71	21.01	33.81	23.73
19.32	21.37	35.42	24.02
20.93	21.69		

N4552 'I' MAJOR AXIS

SE WING

RADIUS arcsec	BRIGHTNESS Mag/#arcsec	RADIUS arcsec	BRIGHTNESS Mag/#arcsec
6.44	15.67	98.21	22.02
8.05	15.91	99.82	22.06
9.66	17.15	101.43	22.09
11.27	17.31	103.04	22.10
12.88	17.65	104.65	22.10
14.49	17.77	106.26	22.12
16.10	17.92	107.87	22.15
17.71	18.21	109.48	22.19
19.32	18.30	111.09	22.26
20.93	18.61	112.70	22.31
22.54	18.73	114.31	22.33
24.15	18.97	115.92	22.34
25.76	18.98	117.53	22.36
27.37	19.17	119.14	22.40
28.98	19.52	120.75	22.44
30.59	19.42	122.36	22.46
32.20	19.54	123.97	22.49
33.81	19.71	125.58	22.52
35.42	19.81	127.19	22.54
37.03	19.84	128.80	22.61
38.64	19.94	130.41	22.69
40.25	20.06	132.02	22.75
41.86	20.17	133.63	22.78
43.47	20.30	135.24	22.80
45.08	20.41	136.85	22.82
46.69	20.49	138.46	22.84
48.30	20.55	140.07	22.87
49.91	20.60	141.68	22.93
51.52	20.69	143.29	22.97
53.13	20.76	144.90	22.98
54.74	20.83	146.51	22.96
56.35	20.88	148.12	22.94
57.96	20.95	149.73	22.92
59.57	21.02	151.34	22.91
61.18	21.09	152.95	22.92
62.79	21.14	154.56	23.00
64.40	21.18	156.17	23.09
66.01	21.22	157.78	23.16
67.62	21.26	159.39	23.22
69.23	21.30	161.00	23.29
70.84	21.34	162.61	23.35
72.45	21.40	164.22	23.47
74.06	21.45	165.83	23.62
75.67	21.49	167.44	23.76
77.28	21.52	169.05	23.79
78.89	21.57	170.66	23.77
80.50	21.62	172.27	23.66
82.11	21.67	173.88	23.57
83.72	21.73	175.49	23.53
85.33	21.77	177.10	23.56
86.94	21.79	178.71	23.63
88.55	21.84	180.32	23.71
90.16	21.87	181.93	23.77
91.77	21.90	183.54	23.85
93.38	21.92	185.15	23.94
94.99	21.96	186.76	24.02
96.60	21.98		

NW WING

RADIUS arcsec	BRIGHTNESS Mag/#arcsec	RADIUS arcsec	BRIGHTNESS Mag/#arcsec
6.44	15.67	103.04	22.37
8.05	15.91	104.65	22.37
9.66	17.15	106.26	22.38
11.27	17.71	107.87	22.41
12.88	17.91	109.48	22.42
14.49	17.77	111.09	22.42
16.10	18.14	112.70	22.42
17.71	18.38	114.31	22.40
19.32	18.62	115.92	22.34
20.93	18.96	117.53	22.30
22.54	19.03	119.14	22.28
24.15	19.17	120.75	22.32
25.76	19.24	122.36	22.38
27.37	19.45	123.97	22.47
28.98	19.62	125.58	22.55
30.59	19.63	127.19	22.63
32.20	19.69	128.80	22.66
33.81	19.76	130.41	22.67
35.42	19.91	132.02	22.66
37.03	20.03	133.63	22.65
38.64	20.12	135.24	22.67
40.25	20.22	136.85	22.66
41.86	20.33	138.46	22.69
43.47	20.42	140.07	22.75
45.08	20.52	141.68	22.80
46.69	20.58	143.29	22.84
48.30	20.64	144.90	22.92
49.91	20.69	146.51	23.00
51.52	20.78	148.12	23.10
53.13	20.89	149.73	23.17
54.74	20.99	151.34	23.20
56.35	21.06	152.95	23.17
57.96	21.13	154.56	23.10
59.57	21.23	156.17	23.01
61.18	21.32	157.78	22.96
62.79	21.33	159.39	22.95
64.40	21.35	161.00	22.95
66.01	21.39	162.61	22.99
67.62	21.46	164.22	23.01
69.23	21.53	165.83	22.99
70.84	21.59	167.44	22.96
72.45	21.64	169.05	22.94
74.06	21.70	170.66	22.95
75.67	21.73	172.27	22.99
77.28	21.76	173.88	23.08
78.89	21.79	175.49	23.18
80.50	21.83	177.10	23.25
82.11	21.88	178.71	23.30
83.72	21.95	180.32	23.30
85.33	22.01	181.93	23.29
86.94	22.05	183.54	23.28
88.55	22.10	185.15	23.27
90.16	22.13	186.76	23.26
91.77	22.16	188.37	23.26
93.38	22.20	189.98	23.28
94.99	22.24	191.59	23.30
96.60	22.27	193.20	23.35
98.21	22.30	194.81	23.41
99.82	22.32	196.42	23.44
101.43	22.34	198.03	23.47

N4552 'I' MAJOR AXIS

NW WING

RADIUS arcsec	BRIGHTNESS Mag/#arcsec	RADIUS arcsec	BRIGHTNESS Mag/#arcsec
199.64	23.45	215.74	23.76
201.25	23.41	217.35	23.77
202.86	23.37	218.96	23.83
204.47	23.32	220.57	23.87
206.08	23.31	222.18	23.90
207.69	23.36	223.79	23.95
209.30	23.44	225.40	24.00
210.91	23.54	227.01	24.01
212.52	23.67	228.62	24.03
214.13	23.73		

N4552 'I' MINOR AXIS

SW WING

RADIUS arcsec	BRIGHTNESS Mag/#arcsec	RADIUS arcsec	BRIGHTNESS Mag/#arcsec
6.44	15.67	96.60	22.15
8.05	15.93	98.21	22.18
11.27	17.38	99.82	22.26
12.88	17.71	101.43	22.35
14.49	17.77	103.04	22.41
16.10	18.06	104.65	22.45
17.71	18.39	106.26	22.47
19.32	18.53	107.87	22.50
20.93	18.79	109.48	22.54
22.54	18.84	111.09	22.57
24.15	19.13	112.70	22.60
25.76	19.30	114.31	22.61
27.37	19.41	115.92	22.61
28.98	19.58	117.53	22.57
30.59	19.64	119.14	22.58
32.20	19.76	120.75	22.62
33.81	19.80	122.36	22.71
35.42	19.97	123.97	22.80
37.03	20.10	125.58	22.87
38.64	20.23	127.19	22.93
40.25	20.33	128.80	22.95
41.86	20.42	130.41	22.93
43.47	20.51	132.02	22.91
45.08	20.59	133.63	22.90
46.69	20.69	135.24	22.90
48.30	20.77	136.85	22.95
49.91	20.82	138.46	22.99
51.52	20.90	140.07	23.04
53.13	21.00	141.68	23.08
54.74	21.11	143.29	23.15
56.35	21.21	144.90	23.23
57.96	21.27	146.51	23.32
59.57	21.32	148.12	23.37
61.18	21.39	149.73	23.41
62.79	21.51	151.34	23.42
64.40	21.54	152.95	23.38
66.01	21.61	154.56	23.36
67.62	21.61	156.17	23.35
69.23	21.66	157.78	23.34
70.84	21.68	159.39	23.35
72.45	21.71	161.00	23.40
74.06	21.75	162.61	23.45
75.67	21.80	164.22	23.51
77.28	21.83	165.83	23.60
78.89	21.87	167.44	23.67
80.50	21.89	169.05	23.71
82.11	21.89	170.66	23.72
83.72	21.86	172.27	23.71
85.33	21.88	173.88	23.71
86.94	21.93	175.49	23.72
88.55	22.02	177.10	23.74
90.16	22.09	178.71	23.75
91.77	22.15	180.32	23.90
93.38	22.17	181.93	24.00
94.99	22.17		

N4552 'I' MINOR AXIS

NE WING

RADIUS arcsec	BRIGHTNESS Mag/#arcsec	RADIUS arcsec	BRIGHTNESS Mag/#arcsec
6.44	15.67	80.50	22.02
8.05	15.57	82.11	22.10
11.27	17.73	83.72	22.18
12.88	18.00	85.33	22.25
14.49	17.77	86.94	22.34
16.10	18.32	88.55	22.41
17.71	18.53	90.16	22.46
19.32	18.70	91.77	22.49
20.93	18.95	93.38	22.52
22.54	19.06	94.99	22.55
24.15	19.26	96.60	22.59
25.76	19.40	98.21	22.65
27.37	19.57	99.82	22.67
28.98	19.58	101.43	22.69
30.59	19.71	103.04	22.69
32.20	19.84	104.65	22.70
33.81	19.86	106.26	22.68
35.42	20.02	107.87	22.68
37.03	20.17	109.48	22.69
38.64	20.31	111.09	22.75
40.25	20.42	112.70	22.80
41.86	20.51	114.31	22.86
43.47	20.58	115.92	22.89
45.08	20.66	117.53	22.89
46.69	20.76	119.14	22.83
48.30	20.88	120.75	22.77
49.91	20.97	122.36	22.75
51.52	21.05	123.97	22.80
53.13	21.07	125.58	22.86
54.74	21.14	127.19	22.93
56.35	21.22	128.80	23.03
57.96	21.31	130.41	23.14
59.57	21.38	132.02	23.27
61.18	21.46	133.63	23.42
62.79	21.55	135.24	23.57
64.40	21.58	136.85	23.66
66.01	21.62	138.46	23.69
67.62	21.66	140.07	23.70
69.23	21.69	141.68	23.70
70.84	21.73	143.29	23.67
72.45	21.75	144.90	23.69
74.06	21.79	146.51	23.78
75.67	21.83	148.12	23.86
77.28	21.88	149.73	23.91
78.89	21.94		

APPENDIX 'J'

Miscellaneous

UKSTU PROJECTION CALIBRATION

KPNO-type Stepwedge

Step	B-band log (Rel. Int.)	I-band log (Rel. Int.)	R-band log (Rel. Int.)
1	0.75	0.77	1.54
2	0.54	0.56	1.35
3	0.38	0.46	1.18
4	0.13	0.17	1.00
5	0.00	0.00	0.80
6	- 0.14	- 0.10	0.60
7	- 0.28	- 0.22	0.35
8	- 0.53	- 0.40	-
9	- 0.86	- 0.64	-
10	- 1.00	- 0.71	-
11	- 1.18	- 0.88	-
12	- 1.45	- 1.09	-
13	- 1.65	- 1.29	-
14	- 1.76	- 1.37	-
15	- 1.94	- 1.47	-
16	- 2.20	- 1.63	-

```
      program  axes
c
c
C     AXES is a program designed to read in two interactively
c     specified files and to modify the data depending upon
c     selected thresholds.
c
c     The data is expected to be held as (R,I) data pairs as
c     generated by VMSOUT when applied to PRIAXEASP output.
c     No more than 500 data pairs are expected.
c
c
c     All data values less than a minimum radius RMIN are
c     rejected, and intensity values above sky are unsmoothed.
c     Intensity values between sky and 20% sky are 3-point
c     averaged , while Intensity values between 20% and 2% sky
c     are 5-point averaged. When the Intensity falls below
c     2% of sky the process terminates. The data is output
c     to an interacively specifed file, and stored as (R,MAG)
c     data pairs .
c
c
c
c*****************************************************************
C
C                     DECLARATIONS
C
C*****************************************************************
C
      implicit none
      real r,int,mag,rfin,magfin,sky,rmin,thresh1,thresh2
      integer i,n,count,start
      character*80 rhsfil,lhsfil,newfil
      dimension r(500),int(500),mag(500),rfin(500),magfin(500)
c
c*****************************************************************
c
c       INTERACTIVELY SET SKY,RMIN,RHSFIL,LHSFIL,NEWFIL
C
C*****************************************************************
C
      write(*,01)
01    format(' ENTER PROFILE SKY (Magnitudes/sq.arcsec):'$)
      read(*,02) sky
02    format(f8.3)
      write(*,03)
03    format(' ENTER MINIMUM PROFILE RADIUS (arcsec):'$)
      read(*,04) rmin
04    format(f7.2)
      write(*,05)
05    format(' GIVE FILE NAME FOR RHS PROFILE:'$)
      read(*,06) rhsfil
06    format(a)
      write(*,07)
07    format(' GIVE FILE NAME FOR LHS PROFILE:'$)
      read(*,08) lhsfil
08    format(a)
      write(*,09)
09    format(' GIVE FILE NAME FOR OUTPUT PROFILE:'$)
      read(*,10) newfil
10    format(a)
```

```
c*****************SET***THRESHOLDS*****************************
      thresh1=(sky+1.75)
      thresh2=(sky+4.25)
c
c
c*************************************************************
c
c                   READ IN RHS PROFILE DATA
c
c*************************************************************
c
      open(1,status='old',file=rhsfil)
      do 15 i=1,500
            read(1,*,err=999,end=20) r(i),int(i)
            n=i
15    continue
20    continue
      close(1)
c
c*******CONVERT**INTENSITY**DATA**TO**SURFACE**MAGNITUDES**
c
      call magconv(int,mag,sky,n)
c
c**********MANIPULATE*AXIS*DATA*WITH*GIVEN*THRESHOLDS*********
c
      call thresher(r,mag,rfin,magfin,rmin,thresh1,thresh2,
     1sky,count,start,n)
c
C*************************************************************
C
c             WRITE OUT RHS DATA
c
c*************************************************************
c
      open(2,status='new',file=newfil)
      do 25 i=start,count
            write(2,21) rfin(i),magfin(i)
21          format(1h ,f8.2,f7.2)
25    continue
c*********************************************************
c
c             CLEAR R(I),MAG(I) DATA ARRAYS
c
c*********************************************************
      n=0.0
      do 30 i=1,500
            r(i)=0.0
            int(i)=0.0
30    continue
c
c*********************************************************
c
c             READ IN LHS PROFILE
c
c*********************************************************
      open(3,status='old',file=lhsfil)
      do 35 i=1,500
            read(3,*,err=999,end=40) r(i),int(i)
            n=i
35    continue
40    continue
      close(3)
c
```

```
c
      call magconv(int,mag,sky,n)
c
c********MANIPULATE**AXIS**DATA**WITH**GIVEN**THRESHOLDS***
c
      call thresher(r,mag,rfin,magfin,rmin,thresh1,thresh2,
     1sky,count,start,n)
c
c*********CONVERT**RADIUS**TO**NEGATIVE**VALUES**FOR**GRAPHICS*
c
      do 45 i=1,count
            rfin(i)=(rfin(i)*-1.0)
45    continue
C*************************************************************
c
c          WRITE OUT LHS DATA
c
c*************************************************************
      do 55 i=start,count
            write(2,50) rfin(i),magfin(i)
50          format(1h ,f8.2,f7.2)
55    continue
      close(2)
c
c*************************************************************
C
C           TERMINATION
C
C************************************************************
C
      stop ' NORMAL PROGRAM EXIT'
999   write(*,1000)
1000  format(' ERROR  READING IN DATA ')
      end
c
c
c
      subroutine magconv(int,mag,sky,n)
c
      implicit none
      real int,mag,sky

      dimension int(500),mag(500)
      integer i,n
c
      do 60 i=1,n
            if(int(i).gt.1.0)then
                  mag(i)=sky-(2.5*(alog10(int(i)-1)))
            else
                  mag(i)=30.00
            endif
60    continue
      return
      end
c
c
c
      subroutine thresher(r,mag,rfin,magfin,rmin,thresh1,
     1thresh2,sky,count,start,n)
      implicit none
      real r,mag,rfin,magfin,thresh1,thresh2,rmin,sky
      dimension r(500),mag(500),rfin(500),magfin(500)
      integer j,n,count,start
c
c
```

```
      count=0
      start=1
c
c
      do 100 j=1,n
            if(mag(j+2).eq.0.0) then
                  goto 101
            else
                  continue
            end if
            if(mag(j).lt.thresh2)then
                  count=count+1
                  if(r(j).gt.rmin)then
                        if(mag(j).lt.sky)then
                              magfin(j)=mag(j)
                              rfin(j)=r(j)
                        else
                            if(mag(j).le.thresh1)then
                                magfin(j)=
     1(mag(j-1)+mag(j)+mag(j+1))/3.0
                                rfin(j)=r(j)
                            else
                                magfin(j)=
     1(mag(j-2)+mag(j-1)+mag(j)+mag(j+1)+mag(j+2))/5.0
                                rfin(j)=r(j)
                            end if
                        endif
                  else
                        start=start+1
                  endif
            else
                  goto 101
            endif
100   continue
101   return
      end
```

```
      program colour
c
c
c     COLOUR is a program designed to read in two data files,
c     interactively specified with appropriate sky values,
c     containing galaxy luminosity profiles and to calculate
c     the difference (colour) between the profiles.
c
c     The data is expected as (R, MAG) data pairs in free
c     format; no more than 500 pairs are expected.
c     The program is designed to use the output generated by
c     AXES , which in turn uses VMSOUT decoded STARLINK data.
c
c
c     The program reads in PROFIL1 and looks for matching
c     radius values in PROFILE2. If the match is successful
c     the colour difference for this radius is calculated,
c     otherwise a warning is printed and the next R value is
c     examined. Whenever either MAG value falls below a
c     minimum threshold the procedure is terminated.
c
c
c     The colour profile generated is then smoothed in 3-point
c     bins, the data is then folded about radius=0.0
c      and the data written out to an interactively
c     specified data file as ( R, COLOUR ) data pairs.
c
c
c*****************************************************************
c
c                    DECLARATIONS
c
c*****************************************************************
c
      implicit none
      real r1,mag1,r2,mag2,colr,coldif,rfin,color
      real sky1,sky2,thresh1,thresh2
      dimension r1(500),mag1(500),r2(500),mag2(500)
      dimension colr(500),coldif(500)
      integer i,j,n1,n2,count,m,number
      character*80 prof1,prof2,newfil
c
c
c*****************************************************************
c
c       INTERACIVELY SPECIFY PROF1,SKY1,PROF2,SKY2 AND NEWFIL
c
c*****************************************************************
c
      write(*,01)
01    format(' GIVE FILE-NAME FOR "BLUEST" PROFILE:'$)
      read(*,02) prof1
02    format(a)
      write(*,03)
03    format(' GIVE SKY VALUE FOR PROFILE (Mags/sq.arcsec:'$)
      read(*,04) sky1
04    format(f8.3)
      write(*,05)
05    format(' GIVE FILE-NAME FOR "RED" PROFILE:'$)
      read(*,06) prof2
06    format(a)
      write (*,07)
```

```
07      format(' GIVE SKY VALUE FOR PROFILE (Mags/sq.arcsec):'$)
        read(*,08) sky2
0C      format(f8.3)
        write(*,09)
09      format(' GIVE OUTPUT FILE-NAME :'$)
        read(*,10) newfil
10      format(a)
C
C
C*****************SET**THRESHOLDS*****************************
C
        thresh1=(sky1+2.5)
        thresh2=(sky2+2.5)
C
C*****************************************************************
C
C               READ IN PROF1
C
C*****************************************************************
C
        open(1,status='old',file=prof1)
        do 11 i=1,500
                read(1,*,err=900,end=15) r1(i),mag1(i)
                n1=i
11      continue
15      close(1)
C
C*****************************************************************
C
C               READ IN PROF2
C
C*****************************************************************
C
        open(2,status='old',file=prof2)
        do 20 i=1,500
                read(2,*,err=901,end=25) r2(i),mag2(i)
                n2=i
20      continue
25      close(2)
C
C*****************************************************************
C
C               COLOUR DIFFERENCE CALCULATION
C
C*****************************************************************
C
        count=0
        do 60 i=1,n1
             do 50 j=1,n2
                  if(r2(j).ne.r1(i)) then
                       goto 40
                  else
                       if((mag1(i).gt.thresh1).or.
     1(mag2(j).gt.thresh2)) then
                            goto 60
                       else
                            count=count+1
                            coir(count)=r1(i)
                            coldif(count)=(mag1(i)-mag2(j))
                            GOTO 60
                       endif
                  endif
40                if(j.eq.n2) then
                       print*,' NO MATCH FOR R = ',r1(i)
                       GOTO 60
                  else
```

```
                    continue
                endif
50          continue
60      continue
c
c
c*****************************************************************
c
c               SMOOTHING COLOUR PROFILE
c
c*****************************************************************
c
        open(3,status='scratch')
        number=0
        m=1
        do 70 i=1,count
            if(i.lt.m) then
                goto 70
            else
                if((colr(i)*colr(i+1)).LE.0.0) then
                    m=m+1
                    goto 70
                else
                    continue
                end if
c
c
                if((colr(i+1)*colr(i+2)).LE.0.0) then
                    m=m+2
                    goto 70
                else
                    continue
                end if
c
c
                number=number+1
                rfin=colr(i+1)
                color=(coldif(i)+coldif(i+1)+coldif(i+2))/3.0
                write(3,65) rfin,color
65              format(1h ,f8.2,f7.2)
                m=m+3
            endif
70      continue
        rewind(3)
c*****************************************************
c
c               FOLDING DATA
c
c*****************************************************
c
        call fold(number,newfil)
c
c
c*****************************************************************
c
                        TERMINATION

c*****************************************************************
c
        stop ' NORMAL PROGRAM EXIT '
90      stop ' ERROR FROM READING DATA FILE 1 '
91      stop ' ERROR FROM READING DATA FILE 2 '
        END
        subroutine fold(number,newfil)
        implicit none
        integer number, i,j
```

```
      real r,col,fcol
      dimension r(500),col(500)
      character*80 newfil
c
c
      open(4,status='new',file=newfil)
c
      do 80 i=1,number
80        read(3,*,err=102,end=81) r(i),col(i)
81    close(3)
c
c
      do 100 i=1,number
          if(r(i).lt.0.0) then
              goto 101
          else
              continue
          end if
c
          do 90 j=i+1,number
              if(r(j).ne.(r(i)*-1.0)) then
                      goto 90
                  else
                      fcol=(col(i)+col(j))/2.0
                      write(4,85) r(i),fcol
85                    format(1h ,f8.2,f7.2)
                  end if
90        continue
c
c
100   continue
101   close(4)
102   return
      end
```

N4501 BLACKMANN'S I-BAND MAJOR AXIS

SE WING

RADIUS arcsec	BRIGHTNESS Mag/#arcsec	RADIUS arcsec	BRIGHTNESS Mag/#arcsec
10.00	18.17	155.00	21.30
27.50	18.80	180.00	21.92
55.00	19.42	210.00	22.55
82.50	20.05	270.00	23.17
120.00	20.67		

N4501 BLACKMANN'S I-BAND MAJOR AXIS

NW WING

RADIUS arcsec	BRIGHTNESS Mag/#arcsec	RADIUS arcsec	BRIGHTNESS Mag/#arcsec
15.00	18.17	165.00	21.92
25.00	18.80	180.00	22.55
50.00	19.42	200.00	23.17
80.00	20.05	230.00	23.80
120.00	20.67	260.00	24.42
140.00	21.30		

N4501 BLACKMANN'S I-BAND MINOR AXIS

SW WING

RADIUS arcsec	BRIGHTNESS Mag/#arcsec	RADIUS arcsec	BRIGHTNESS Mag/#arcsec
10.00	18.17	65.00	21.30
20.00	18.80	80.00	21.92
30.00	19.42	97.50	22.55
40.00	20.05	150.00	23.17
60.00	20.67		

N4501 BLACKMANN'S I-BAND MINOR AXIS

NE WING

RADIUS arcsec	BRIGHTNESS Mag/#arcsec	RADIUS arcsec	BRIGHTNESS Mag/#arcsec
10.00	17.55	80.00	21.30
15.00	18.17	95.00	21.92
25.00	18.80	112.50	22.55
30.00	19.42	145.00	23.17
45.00	20.05	180.00	23.80
60.00	20.67		

Multi-Aperture Photometry

GALAXY (NGC)	APERTURE (arcseconds)	B-MAGNITUDE
4267	244.4	12.07
"	131.3	11.74
"	255.9	11.69
"	345.3	11.57
"	143.9	12.06
"	203.3	11.93
"	203.3	12.00
"	287.2	11.97
4371	233.4	11.87
"	314.9	11.90
4377	161.5	12.91
"	208.0	12.56
4419	41.5	12.81
"	203.3	12.00
4425	64.3	13.22
"	134.3	13.22
"	131.3	12.97
"	233.4	13.22
"	165.3	12.91
4429	109.2	11.72
"	244.4	10.94
"	378.6	11.16
"	64.5	11.97
"	38.7	12.49
"	25.8	12.95
"	16.1	13.56
"	9.7	14.14
"	44	12.477 *1
"	59.9	12.178 *1
"	84.1	11.889 *1
4435	42.5	12.37
"	60.0	12.04
"	128.3	11.69
"	161.5	11.63
"	137.5	11.76
"	106.7	12.01
"	161.5	11.77
"	185.4	11.62
"	314.9	11.17
"	217.8	11.94
"	198.7	11.78
"	64.5	12.64
"	38.7	12.98
"	25.8	13.29
"	16.1	13.70
"	9.7	14.23
"	30.1	12.70
"	30.1	12.68
"	44.0	12.474 *1
"	44.0	12.485 *1
"	59.9	12.276 *1
"	84.1	12.091 *1

GALAXY (NGC)	APERTURE (arcseconds)	B-MAGNITUDE
4438	41.5	12.67
"	64.3	12.17
"	128.3	11.64
"	161.5	11.82
"	244.5	11.40
"	337.4	11.11
"	106.0	12.03
"	161.5	11.87
"	314.9	11.13
"	444.8	10.97
"	704.9	10.95
"	487.7	11.02
"	64.5	12.24
"	38.7	12.79
"	25.8	13.30
"	16.1	14.02
"	9.7	14.67
4458	64.3	13.18
"	137.5	13.17
"	104.3	13.21
"	109.2	13.29
"	185.4	12.83
"	198.7	12.90
"	45	13.65
"	32	13.93
4459	64.5	12.06
"	38.7	12.46
"	25.8	12.84
"	16.1	13.39
"	9.7	13.90
"	30.1	12.74
"	30.1	12.71
"	64.3	12.30
"	109.2	11.78
"	217.9	11.46
"	134.3	11.58
"	161.5	11.86
"	256.0	11.74
"	314.9	11.57
"	44.0	12.436 *1
"	44.0	12.444 *1
"	59.9	12.199 *1
"	84.1	11.984 *1
4461	128.3	12.25
"	161.5	12.15
"	244.4	12.02
"	106.7	12.44
"	233.4	12.01
"	314.9	11.87
"	370.0	11.67
"	203.3	12.15
"	300.7	12.04

GALAXY (NGC)	APERTURE (arcseconds)	B-MAGNITUDE
4461	59.7	12.63
"	75	12.576 *2
4474	143.9	12.62
"	161.5	12.62
4477	128.3	11.74
"	161.5	11.60
"	137.5	11.78
"	256.0	11.47
"	314.9	11.24
"	300.7	11.35
"	64.5	12.20
"	38.7	12.58
"	25.8	12.92
"	16.1	13.42
"	9.7	14.05
"	30.1	12.78
"	30.1	12.76
"	60.1	12.22
"	60.1	12.19
"	75	12.158
4501	42.5	12.62
"	128.3	11.08
"	161.5	11.14
"	280.6	10.55
"	12.0	14.17
"	250.1	10.52
"	161.5	10.85
"	238.9	10.50
"	185.4	10.31
"	455.2	10.18
"	190.8	10.74
"	109.2	11.26
"	61.2	11.97
"	36.0	12.69
"	21.6	13.29
"	64.5	11.89
"	38.7	12.56
"	25.8	13.09
"	16.1	13.71
"	9.7	14.34
"	31.1	12.973
"	59.9	12.073
"	84.1	11.633
4503	64	12.65
"	45	12.88
"	32	13.16
4550	64.3	12.78
"	244.4	12.53
"	64.5	12.76
"	38.7	13.03
"	25.8	13.34
"	16.1	13.85

GALAXY (NGC)	APERTURE (arcseconds)	B-MAGNITUDE
4550	9.7	14.48
4551	64.3	13.10
"	137.5	13.07
"	72.1	13.20
"	64	13.19
"	45	13.39
"	32	13.61
4552	64.3	11.60
"	143.9	11.18
"	203.3	11.11
"	131.3	11.08
"	256.0	10.92
"	314.9	11.00
"	287.2	11.00
"	64.3	11.60
"	143.9	11.18
"	203.3	11.11
"	131.3	11.08
"	256.0	10.92
"	314.9	11.00
"	287.2	11.00
"	64.5	11.64
"	38.7	11.99
"	25.8	12.29
"	16.1	12.74
"	9.7	13.29
"	30.1	12.20
"	60.1	11.70
"	84.6	11.50
"	31.1	12.178 *1
"	59.9	11.731 *1
"	84.1	11.536 *1

GALAXY (NGC)	APERTURE (arcseconds)	R (COUSINS) MAGNITUDE	
4429	44.0	10.82	*1
"	59.9	10.546	*1
"	84.1	10.282	*1
4435	44.0	10.847	*1
"	44.0	10.917	*1
"	59.9	10.714	*1
"	84.1	10.565	*1
4459	44.0	10.804	*1
"	44.0	10.806	*1
"	59.9	10.588	*1
"	84.1	10.367	*1
4461	75.0	10.973	*2
4477	75.0	10.572	*2
4501	31.1	11.192	*1
"	59.9	10.419	*1
"	84.1	10.031	*1

GALAXY (NGC)	APERTURE (arcseconds)	I (COUSINS) MAGNITUDE	
4429	44.0	10.14	*1
"	59.9	9.886	*1
"	84.1	9.662	*1
4435	44.0	10.007	*1
"	44.0	10.267	*1
"	59.9	10.064	*1
"	84.1	9.995	*1
4459	44.0	10.164	*1
"	44.0	10.146	*1
"	59.9	9.938	*1
"	84.1	9.727	*1
4461	75.0	10.344	*2
4477	75.0	9.896	*2
4501	31.1	10.494	*1
"	59.9	9.749	*1
"	84.1	9.394	*1
4552	31.1	9.910	*1
"	59.9	9.479	*1
"	84.1	9.306	*1

All data taken from de Vaucouleurs, de Vaucouleurs and Corwin (1974) and (1976) editions of "A reference Catalogue of Bright Galaxies" except where noted below:

*1: Kilkenny, D. 1982 Private Comm.

*2: Malcolm, G. 1983 (Unpublished data)